

# Euclidean Condensate Theory (ECT): Emergence of Spacetime, Quantum Mechanics, and Gravity from Spontaneous $O(4)$ Symmetry Breaking

Valeriy Blagovidov\*

April 2026

## Abstract

Euclidean Condensate Theory (ECT) is a framework in which Lorentzian spacetime, quantum dynamics, and gravitation emerge from the spontaneous symmetry breaking  $O(4) \rightarrow O(3)$  of a condensate on a fundamentally Euclidean manifold. In this picture, time, causal propagation, and the effective metric arise only on the ordered branch of the condensate, while the underlying description remains purely Euclidean.

Part I develops the ordered-branch effective theory and derives the Lorentzian branch as an admissibility property of the broken phase. It establishes the emergent signal speed, Newton's constant, and a pre-quantum action scale as condensate matching relations, and recovers the Klein–Gordon and Schrödinger equations as effective descendants of Euclidean condensate dynamics. Fermionic excitations are shown to obey a Dirac-type equation in the emergent Lorentzian background, and the gauge sector is structurally linked to compact-phase and orientation degrees of freedom of the condensate. The neutrino sector is structurally constrained by the geometrically one-chiral weak route: pure Planck-suppressed masses are quantitatively insufficient, an embedded heavy-sterile seesaw completion is structurally preferred, the ECT-motivated anchor  $M_R^{\text{geom}} = \sqrt{\phi_0} v_2$  yields atmospheric-scale masses for an ordinary Yukawa coupling  $y_\nu \sim 4.5 \times 10^{-3}$ , standard PMNS/MSW phenomenology remains intact, and neutrinoless double-beta decay is the central discriminator of the preferred branch.

Part II develops generalised Einstein equations with an orientation-stress correction and a modified sub-horizon Poisson sector. The macroscopic branch addresses the horizon, flatness, and monopole problems without a separate inflationary mechanism, provides a late-time route to accelerated expansion and Hubble-tension alleviation without an independent dark-energy substance, and yields galactic phenomenology including the baryonic Tully–Fisher relation, a characteristic acceleration scale, and rotation-curve fits without particle dark matter. The same orientation-stress sector also provides a structural route to cluster-lensing effects and to the lensing–growth ( $S_8$ ) sector through gravitational slip. A separate structural result of Part II is the resolution at Level A of the classical cosmological-constant catastrophe: an emergent-unimodular decoupling theorem shows that the determinant of the ordered-branch kinetic tensor,  $\sqrt{-\det K^{AB}} = \beta^2/c_*$ , is fixed by the kinematic constraint  $n^A n_A = 1$ , which renders the classical baseline  $V(\phi_0)$  inert for local emergent gravity (unconditionally) and—conditional on a one-line spectral assumption on the full quadratic fluctuation operator (condition  $H_\Lambda$ )—absorbs the zero-derivative one-loop vacuum contribution; the direct  $10^{120}$ -level UV-to-IR cancellation characteristic of the standard framework is therefore structurally absent in the leading ordered-branch sector. This result concerns the direct vacuum-baseline channel; the first-principles determination of the observed late-time infrared source remains separate. The value of  $\rho_{\Lambda, \text{obs}}$  itself is, separately, a Level C determination problem whose natural scaling  $\rho_\Lambda \sim c_\Lambda M_{\text{pl}}^2 H_0^2$  with  $c_\Lambda = \mathcal{O}(1)$  is consistent with observation at the order-of-magnitude level and admits a plausible pseudo-Goldstone realisation. The late-time cosmological sector is further constrained by a retained five-probe effective analysis yielding a narrow common band for a single diagnostic deformation parameter  $\varepsilon$ , which serves as an indirect multi-channel consistency check rather than a first-principles prediction.

Part III develops the coherent quantum branch: reflection positivity and the Hilbert-space bridge, canonical structure, exchange topology, and influence-functional decoherence unifying environmental

---

\*Correspondence: blagovidov@phystech.edu, vblagovidov@gmail.com. ORCID: 0009-0008-6707-7068.

and gravitational channels. On the smooth coherent branch, Pauli exclusion remains exact through a canonical-normalisation no-go statement. A conditional CPT route is identified for reconstructible local sectors via the Euclidean Osterwalder–Schrader framework, while the phenomenological preferred-direction operator is re-classified as a CPT-odd branch-sensitive operator consistent with the exact symmetry backbone. The Principle of Euclidean Stationarity organises the persistent quantum sector, while substantial parts of standard quantum formalism are recovered or structurally motivated rather than postulated *ab initio*. The Born rule remains only conditionally grounded through a Gleason-based route and is stated explicitly as open. A shell-based decoherence model provides a route to black-hole entropy, Page-curve-like information behaviour, and a general boundary-layer area-law bound that recovers holographic-style entropy scaling as a structural property of the local condensate medium. An upgrade layer on the gravity–matter interface further develops a reduced-state reading of the hybrid-consistency problem: irreversibility, decoherence, and apparent thermality arise only in reduced descriptions of one globally unitary Euclidean condensate; an operational criterion separates regimes in which ECT falls under the standard BMV no-go logic for gravity-induced entanglement from regimes in which it escapes into a common-medium loophole class; a channel taxonomy distinguishes a scalar distinguishability response from an orientation-based candidate entangling response; and the black-hole critical-shell picture is placed in close structural alignment with the modern islands and quantum-extremal-surface language, while keeping the mechanisms distinct. Abelian charge quantisation is traced to the compact-phase gauge origin of the condensate sector; the full observed charge spectrum remains open.

Part IV develops a dedicated reverse-analysis and  $SU(3)$ -completion layer. The exact-colour sector cannot reside inside the ordered condensate (by strict obstruction theorems, including the algebraic obstruction  $\mathfrak{su}(3) \not\subset \mathfrak{so}(4)$ ), so the medium is equipped with a reverse-engineered postulate P7: a local complex rank-3 internal module with a Hermitian form and a fixed complex volume form, yielding exact local  $SU(3)$ . The minimal admissible colour EFT compatible with P7 is derived, together with three obstruction theorems (no tree-level gluon mass, no Higgs-colour route, oscillator tower is not the physical colour spectrum) and a central negative result: at constant background couplings the colour-sector completion does not generate independent predictive strong-sector physics beyond a redefinition of matching conventions. The topological coupling  $\Theta(\phi)F\tilde{F}$  reopens the strong CP problem within ECT rather than resolving it, and the dimensional-transmutation form of  $\Lambda_{\text{col}}^{\text{ECT}}$  is classificatory rather than predictive. Part IV also restates the matter-sector anomaly architecture in the presence of P7, catalogues the earlier  $SU(3)$ -dependent questions that are now structurally closed, sharpened, or reframed, and explicitly separates the existence of a colour infrared scale, the existence of a gauge-invariant mass gap, and the full derivation of the glueball spectrum (the Clay Millennium formulation being structurally a different problem from what ECT addresses).

Part V consolidates the framework through a map of native constants, open closure parameters, and derived observables. The fine-structure constant is recast as an electroweak kinetic/mixing target with moderate ultraviolet gauge-sector coefficients rather than a purely primitive input. A comprehensive derivational map shows that many structures usually treated as independent postulates or empirical inputs in standard physics become derived or structurally grounded targets in ECT, while the theory also yields a distinct set of ECT-specific observational discriminants.

ECT therefore does not present a finished ultraviolet completion of all sectors, but it does provide a unified condensate architecture in which gravity, quantum structure, and large parts of cosmological phenomenology arise within a single ordered-medium framework. The Abelian gauge sector is derived from bundle covariance of the condensate phase, while a preferred chiral  $SU(2)$  sector is structurally linked to the oriented broken phase. Together with emergent gravity and a generic fermion–condensate interaction (the director coupling), ECT provides a common pre-geometric origin for the known interaction sectors; the colour sector requires additional internal condensate structure beyond the minimal  $O(4)$ -breaking pattern.

**Keywords:** Euclidean Condensate Theory; emergent spacetime; emergent Lorentzian geometry; emergent gravity; emergent time; spontaneous symmetry breaking;  $O(4) \rightarrow O(3)$  symmetry breaking; ordered condensate; effective metric; generalised Einstein equations; quantum foundations; quantum–classical boundary; reflection positivity; Hilbert-space reconstruction; measurement problem; decoherence; gravitational decoherence; gravity-induced entanglement; BMV experiment; post-quantum classical gravity; hybrid-consistency problem; reduced-state architecture; islands formula; quantum extremal surface; BMS asymptotic symmetries; gravitational memory; soft gravitons; arrow of time; quantum entanglement; Bell inequality; delayed-choice experiments; fifth force; Lorentz invariance violation; cosmology without

inflation; Hubble tension; dark energy; dark matter phenomenology; galaxy rotation curves; baryonic Tully–Fisher relation; radial acceleration relation; SPARC galaxies; JWST early galaxies; Casimir effect; Unruh effect; black-hole information problem; Principle of Euclidean Stationarity; fine-structure constant; lensing–growth sector; gravitational slip; Pauli exclusion; holographic entropy bound; area-law scaling; entanglement entropy; charge quantisation; Born rule; neutrino masses; seesaw mechanism; sterile neutrino; neutrinoless double-beta decay; vacuum stability; false vacuum; Coleman vacuum decay; electroweak metastability; RG running; Hopf-fibered phase–orientation locking; layered electroweak programme; beta function; spinodal instability; Big Bang singularity; pre-Lorentzian regime; cosmological ordering transition; branch-boundary interpretation; discrete symmetries; CPT theorem; Osterwalder–Schrader reconstruction; retained-band cosmological analysis; uniform- $\epsilon$  diagnostic layer; five-probe cross-consistency; cosmic chronometers; integrated Sachs–Wolfe effect;  $f\sigma_8$  redshift-space distortions; sound horizon; Planck–SH0ES discrepancy; Hubble-sector effective drift parameter; JWST early-galaxy maturity budget; age-viability note; dark-matter-deficient ultra-diffuse galaxies; NGC 1052–DF4; FCC 224; matched-pair galactic stress test; cosmological constant problem; emergent unimodular gravity; vacuum-offset decoupling; infrared dark-energy scaling; pseudo-Goldstone dark energy; ultra-light scalar dark matter; holographic effective-field-theory bound; reverse analysis in physics; SU(3) colour completion; postulate P7; internal colour module; rank-3 complex internal bundle; Hermitian form and complex volume form; obstruction theorem  $\mathfrak{su}(3) \not\subset \mathfrak{so}(4)$ ; minimal admissible colour EFT; background-level triviality; no-go for tree-level gluon mass; anomaly-consistency layer; Witten–Veneziano consistency target; strong CP reopening; topological theta term; ’t Hooft anomaly matching; Yang–Mills mass gap problem (Clay formulation, structurally distinct); proton stability selection rules; dimensional transmutation classificatory form

# Contents

<b>List of Symbols</b>	<b>17</b>
<b>List of Abbreviations</b>	<b>21</b>
<b>1 Introduction</b>	<b>23</b>
<b>I Foundations: Postulates, Symmetry Breaking, and Emergent Laws</b>	<b>29</b>
<b>2 Postulates of Euclidean Condensate Theory</b>	<b>29</b>
2.1 Glossary of terms . . . . .	29
2.2 Ontological properties of the $\Phi$ -medium . . . . .	30
2.3 List of postulates . . . . .	31
2.4 Operational principle of relationality . . . . .	33
2.5 Independence of postulates . . . . .	33
2.6 Discussion of the postulates . . . . .	34
2.7 Three statement types . . . . .	38
<b>3 Spontaneous Symmetry Breaking and Emergence of Time</b>	<b>38</b>
3.1 Dynamic motivation for gradient condensation . . . . .	39
3.2 Collective variables and the ordered-branch infrared EFT . . . . .	39
3.3 Uniqueness of the kinetic tensor after SSB . . . . .	41
3.4 Eigenvalue analysis and signature classification . . . . .	42
3.5 The Lorentzian window . . . . .	43
3.6 Effective Lorentzian metric . . . . .	45
3.7 Physical picture: the condensate as the “fabric” of spacetime . . . . .	45
3.8 Arrow of time from symmetry breaking . . . . .	46
3.9 The second law of thermodynamics in ECT . . . . .	49
3.10 Comparison with other theories . . . . .	52
<b>4 Spectrum and Effective Dynamics of the Broken Phase</b>	<b>53</b>
4.1 Polar decomposition and collective variables . . . . .	53
4.2 Sector map: amplitude, soft orientation, and macroscopic $\phi$ -sector . . . . .	53
4.3 Integrability and the status of the orientation sector . . . . .	54
4.4 Minimal soft orientation EFT and phenomenological status . . . . .	55
4.5 EFT quadratic action for fluctuations . . . . .	56
4.6 Mode hierarchy and the branching structure . . . . .	56
4.7 Causal cone inheritance by the phase and gauge sectors . . . . .	57
4.8 Status of results in this section . . . . .	59
<b>5 Fundamental Scales, Matching Relations, and the Status of Constants</b>	<b>61</b>
5.1 Three condensate scales: structure, hierarchy, and open problems . . . . .	61
5.2 Parameter hierarchy by level of description . . . . .	68
5.3 Effective propagation speed $c_*$ . . . . .	68
5.4 Gravitational stiffness scale and Newton’s constant . . . . .	69
5.5 Radial-mode scales and the correlation length . . . . .	69
5.6 Action scale $S_0$ as the ECT precursor of $\hbar$ . . . . .	69
5.7 Summary table: parameters and constants . . . . .	75



<b>6</b>	<b>Branching Structure of ECT</b>	<b>76</b>
6.1	Two classes of observables . . . . .	76
6.2	The geometric branch (Macroscopic Physics) . . . . .	76
6.3	The coherent branch (Quantum Sector) . . . . .	77
6.4	Why branching is necessary . . . . .	77
6.5	Physical picture: correlation versus interaction in the two branches . . . . .	77
6.6	Variational principle and Noether structure . . . . .	78
6.7	Remark on defect sectors beyond the smooth coherent sector . . . . .	81
6.8	Foundational consequences and branch-selection rules . . . . .	82
<b>7</b>	<b>Gauge Symmetries, Matter Couplings, and the ECT-Specific Fifth Coupling</b>	<b>83</b>
7.1	Internal structures of the condensate relevant to interactions . . . . .	83
7.2	Emergence of $U(1)$ gauge symmetry . . . . .	85
7.3	Non-Abelian gauge structure and its status . . . . .	90
7.4	Electroweak-like embedding and its current status . . . . .	93
7.5	Matter couplings and the Standard Model interaction pattern . . . . .	96
7.6	The ECT-specific fermion–condensate coupling . . . . .	97
7.7	Strength, range, and the microscopic/macroscopic distinction . . . . .	100
7.8	Observability conditions, consistency checks, and falsification logic . . . . .	103
7.9	Structural constraints on the coupling coefficient . . . . .	107
7.10	Connection to the galactic weak-field sector . . . . .	109
7.11	Gauge-sector summary, structural synthesis, and the open programme . . . . .	110
<b>8</b>	<b>Elementary Particles and Field Excitations in ECT</b>	<b>113</b>
8.1	General Structure of Particle Excitations . . . . .	114
8.2	Soft Orientation Sector of the Condensate . . . . .	117
8.3	Radial Condensate Mode . . . . .	120
8.4	Vacuum Stability, False Vacuum, and Vacuum Decay . . . . .	126
8.5	Emergence of the Graviton . . . . .	131
8.6	Gauge Bosons from Condensate Phase Symmetries . . . . .	136
8.7	Electroweak Sector and the Higgs Interpretation in ECT . . . . .	138
8.8	Fermions (Level B: structural route) . . . . .	141
8.9	Neutrino Sector . . . . .	142
8.10	Predicted New States and Topological Sectors . . . . .	149
8.11	Summary of the particle and excitation spectrum . . . . .	153
<b>9</b>	<b>Fermionic Sector</b>	<b>155</b>
9.1	Spinor structure in the condensate background . . . . .	156
9.2	Structural Reconstruction of the Dirac Form . . . . .	158
9.3	Chirality and fermion interactions . . . . .	160
9.4	Discrete symmetries of the emergent matter sector: P, T, C, and conditional CPT . . . . .	163
9.5	Anomaly architecture of the emergent chiral gauge sector . . . . .	169
9.6	Yukawa couplings and fermion masses . . . . .	173
9.7	Flavour architecture of the emergent matter sector: CKM and PMNS in ECT . . . . .	175
9.8	ECT-specific fermion–condensate coupling . . . . .	178
9.9	Spin-statistics: structural route and open problem . . . . .	180
9.10	Open programme and status summary for the fermionic sector . . . . .	181

<b>10</b>	<b>Conclusions of Part I: Foundations</b>	<b>184</b>
10.1	Core axiomatic framework (Sections 2–6)	186
10.2	Gauge-sector architecture, particles, and fermions (Sections 7–9)	187
10.3	Structural outputs and forward falsification handles	188
10.4	What Part I derives and what it does not	190
10.5	What remains open at the end of Part I	191
10.6	Roadmap to Parts II–III	191
<b>II</b>	<b>Macroscopic Physics: Gravity, Cosmology, and Observational Tests</b>	<b>193</b>
<b>11</b>	<b>Scope, Bridge, and Approximation Hierarchy</b>	<b>193</b>
11.1	Macroscopic Physics as the development of the geometric branch	193
11.2	Approximation hierarchy used in Part II	198
11.3	Bridge from Part I: structural inputs used in Part II	198
<b>12</b>	<b>Special Relativity as the Homogeneous Ordered-Phase Limit</b>	<b>199</b>
12.1	Status and scope	199
12.2	Homogeneous ordered phase and unique causal cone	200
12.3	Minkowski form of the local effective geometry	200
12.4	Lorentz transformations from cone invariance	200
12.5	Relativistic dispersion, energy, and momentum	200
12.6	Universal signal-speed bound and its realisation by massless sectors	201
12.7	The status of the identification $c_* = c$	202
12.8	From local special relativity to macroscopic gravity	202
12.9	What is proved and what remains open	203
<b>13</b>	<b>Emergent Gravitational Sector</b>	<b>203</b>
13.1	Effective metric and the macroscopic limit of the condensate	204
13.2	Linear tensor sector and the emergence of gravitational propagation	208
13.3	Matter coupling and the Noether source structure	209
13.4	Gravitational stiffness, Newton constant, and the status of $G_N$	212
13.5	Nonlinear closure and the generalised field equations	215
13.6	Weak-field and Newtonian limit	226
13.7	Post-Newtonian regime and Solar System tests	228
13.8	Gravitational waves and causal structure	229
13.9	Observational predictions of the gravitational sector	232
<b>14</b>	<b>ECT and the Classical Cosmological Problems</b>	<b>233</b>
14.1	Pre-Lorentzian cosmological scenario	233
14.2	Post-transition ordered-branch cosmological scenarios	235
14.3	Horizon problem: branch coherence	238
14.4	Flatness problem: structural spatial flatness from P1	239
14.5	Relic and monopole problem: topological resolution	240
14.6	Primordial perturbations: current status	242
14.7	Summary and comparison with inflationary resolution	245
<b>15</b>	<b>Vacuum Offset Decoupling and the Cosmological Constant Problem</b>	<b>245</b>
15.1	Statement of the problem in the standard framework	245
15.2	Three distinct objects	246
15.3	Main theorem: emergent unimodular decoupling	246
15.4	The condition $H_\Lambda$ and its logical status	248
15.5	Connection to unimodular gravity	248

15.6	Interplay with Weinberg's no-go theorem . . . . .	249
15.7	FRW reduction and connection to the equation of state . . . . .	249
15.8	Infrared estimate for $\rho_{\Lambda}^{\text{IR}}$ . . . . .	250
15.9	Possible microphysical realization: pseudo-Goldstone modes . . . . .	250
15.10	Comparison with other approaches . . . . .	251
15.11	Status summary: Level A / B / C . . . . .	252
15.12	Open problems . . . . .	253
15.13	Summary . . . . .	253
<b>16</b>	<b>Cosmology from the Ordered Branch</b>	<b>254</b>
16.1	Homogeneous FLRW branch and late-time evolution . . . . .	254
16.2	Cosmological evolution of the condensate amplitude . . . . .	256
16.3	Matter–antimatter asymmetry in the ECT framework . . . . .	257
16.4	Universe age and cosmological time budgets in ECT . . . . .	262
16.5	Cosmological constraints on the effective drift parameter . . . . .	264
16.6	Cosmological predictions: summary and derivation status . . . . .	274
16.7	Cosmological evolution: ECT vs. $\Lambda$ CDM . . . . .	277
16.8	Universe size, boundary, and force-law effective dimensionality . . . . .	281
16.9	What is established and what remains open . . . . .	284
<b>17</b>	<b>Galactic and Astrophysical Phenomenology</b>	<b>286</b>
17.1	Galactic sector: the ordered-branch amplitude variable . . . . .	287
17.2	Cluster-merger lensing test . . . . .	292
17.3	Galactic dynamics: BTFR, rotation curves, and the effective critical scale . . . . .	297
17.4	Radial Acceleration Relation . . . . .	306
17.5	Dark-matter-deficient ultra-diffuse galaxies as a stress test of the current closure . . . . .	308
17.6	Summary and status of galactic and cluster-scale phenomenology . . . . .	312
<b>18</b>	<b>Mass-discrepancy and late-time-acceleration phenomenology in ECT</b>	<b>313</b>
18.1	Scope and dark-sector logic . . . . .	313
18.2	Dark-matter interpretation: $\phi$ -branch and beyond . . . . .	314
18.3	Late-time accelerated expansion: ordered-branch account . . . . .	316
18.4	Dark-sector discriminants and falsifiers of the present closure . . . . .	320
18.5	Section-level status summary . . . . .	321
<b>19</b>	<b>Observational Tests, Falsifiers, and Chapter Conclusions</b>	<b>321</b>
19.1	Astrophysical predictions and observational tests . . . . .	321
19.2	Conclusions of Part II: Macroscopic Physics . . . . .	324
19.3	Global Level-4 self-consistency checklist . . . . .	328
19.4	Global derivation, status, and falsifier maps . . . . .	331
19.5	Status table and open problems of the macroscopic branch . . . . .	345
<b>III</b>	<b>Quantum Sector: Coherent Branch</b>	<b>347</b>
<b>20</b>	<b>Scope, Inputs, and Logical Programme of the Quantum Sector</b>	<b>348</b>
20.1	Quantum Sector as the development of the coherent branch . . . . .	350
<b>21</b>	<b>Coherent Phase Dynamics, Loop Sectors, and the Pre-Quantum Action Scale</b>	<b>352</b>
21.1	Coherent phase dynamics and loop sectors . . . . .	352
21.2	Pre-quantum action scale and the status of $\hbar$ . . . . .	354

<b>22</b>	<b>From Euclidean Coherent Dynamics to Lorentzian Wave Kinematics</b>	<b>357</b>
22.1	Wave dynamics, real-time parametrisation, and Schrödinger-type evolution . . . . .	358
22.2	Principle of extremal action and saddle dominance . . . . .	362
22.3	Conservation laws in the coherent sector . . . . .	365
<b>23</b>	<b>Hilbert-Space Structure, Reflection Positivity, Canonical Algebra, and Unitarity</b>	<b>368</b>
23.1	Reflection positivity and the route to a physical Hilbert space . . . . .	369
23.2	Status of unitarity in the coherent branch . . . . .	373
23.3	Canonical structure and the status of commutation relations . . . . .	375
23.4	Charge quantisation from the compact-phase gauge origin . . . . .	379
23.5	Uncertainty principle in the coherent branch . . . . .	382
<b>24</b>	<b>Euclidean Path-Dependence, Quantum Nonclassicality, Statistics, and Dirac Structure</b>	<b>383</b>
24.1	Euclidean path-dependence: intermediate results from both past and future . . . . .	384
24.2	Reverse-path suppression from PES . . . . .	389
24.3	Tunnelling as traversal through the fourth spatial dimension . . . . .	390
24.4	Quantum statistics: exchange sectors and spinorial compatibility . . . . .	391
24.5	Representation-theoretic route to Dirac structure . . . . .	395
<b>25</b>	<b>Quantum Vacuum Structure and Universal Response of the Ordered Condensate</b>	<b>398</b>
25.1	Quantum vacuum structure of the ordered condensate . . . . .	399
25.2	Unified response logic and analogue-gravity continuity . . . . .	401
25.3	Boundary sensitivity of the ordered vacuum and the Casimir effect . . . . .	403
25.4	Accelerated observers and the Unruh-type response . . . . .	407
25.5	Cosmological particle production and time-dependent ordered backgrounds . . . . .	409
25.6	Summary and status of coherent-vacuum response . . . . .	413
<b>26</b>	<b>Open Quantum Systems, Decoherence, and Irreversibility</b>	<b>414</b>
26.1	Influence functional, decoherence, and the arrow of time . . . . .	415
26.2	Decoherence timescale: derivation for specific experimental systems . . . . .	422
26.3	Gravitational decoherence from condensate distinguishability . . . . .	426
26.4	Crooks-type fluctuation relation and effective entropy production . . . . .	427
<b>27</b>	<b>Results and Regime Estimates of the Decoherence Apparatus</b>	<b>429</b>
27.1	Environmental decoherence: $C_{60}$ and macromolecules . . . . .	430
27.2	Gravitational decoherence: ECT realisation of a DP-type scaling . . . . .	431
27.3	Environmental–gravitational crossover . . . . .	431
27.4	Photonic weak-locking bounds . . . . .	432
27.5	Cavity-cat decoherence: next quantitative target . . . . .	432
27.6	Summary: what the apparatus predicts . . . . .	433
<b>28</b>	<b>ECT as a reduced-state resolution of the hybrid-consistency problem</b>	<b>433</b>
28.1	The hybrid-consistency problem . . . . .	433
28.2	Central thesis . . . . .	434
28.3	Two-level ontology with Level IIa/IIb split . . . . .	434
28.4	Costs of consistency across frameworks . . . . .	435
28.5	Bridges to the rest of Part III . . . . .	436
28.6	Scope and non-claims . . . . .	437

<b>29 Principle of Euclidean Stationarity</b>	<b>437</b>
29.1 Statement of the principle . . . . .	438
29.2 Formal realisation . . . . .	438
29.3 Immediate consequences . . . . .	439
29.4 Stability, lifetimes, and the hierarchy of decay rates . . . . .	440
29.5 Unified quantisation table . . . . .	441
29.6 Measurement, information, and decoherence: summary . . . . .	442
29.7 Reverse-path suppression and tunnelling geometry: summary . . . . .	442
29.8 The $\alpha \rightarrow \beta$ boundary and the geometric meaning of quantum coherence . . . . .	442
29.9 Gravitational decoherence from the condensate: summary . . . . .	443
29.10 What PES changes in the quantum programme . . . . .	444
29.11 What PES does not yet prove . . . . .	444
<b>30 Quantum–Classical Boundary, Probability, Born Rule, and Measurement Status</b>	<b>445</b>
30.1 Quantum–classical boundary: reverse $O(3) \rightarrow O(4)$ transitions . . . . .	445
30.2 Measurement as Euclidean-to-Lorentzian transition . . . . .	447
30.3 Information–decoherence bound . . . . .	448
30.4 Probability, Born-type interpretation, and measurement status . . . . .	452
<b>31 Quantum Entanglement and Bell-Type Correlations</b>	<b>458</b>
<b>32 Gravity-induced entanglement in ECT: status and operational criterion</b>	<b>462</b>
32.1 Why gravity-induced entanglement is a sharper test for ECT . . . . .	462
32.2 Balanced map of the debate . . . . .	462
32.3 ECT’s architectural position — three claims . . . . .	463
32.4 Operational criterion . . . . .	464
32.5 Provisional regime guidance . . . . .	464
32.6 Relation to falsifiers and to non-observation . . . . .	464
32.7 Scope and non-claims . . . . .	464
<b>33 Reduced gravitational mediator in ECT: channel taxonomy</b>	<b>465</b>
33.1 Why a channel taxonomy is needed . . . . .	465
33.2 The $\phi$ -channel: scalar distinguishability . . . . .	465
33.3 The $\delta n_A$ -channel: orientation/tensor candidate mediator . . . . .	465
33.4 Mixed scalar–orientation sector . . . . .	466
33.5 Implications for $m_{\text{guide}}$ and Claim (C) . . . . .	466
33.6 Scope and non-claims . . . . .	467
<b>34 Topological Sectors, Defect Configurations, and the Dark Sector</b>	<b>467</b>
34.1 Defect sectors and their relation to the smooth branch . . . . .	467
34.2 Types of defect and topological configurations . . . . .	468
34.3 Connection to the dark sector . . . . .	468
34.4 Measurement and observability status . . . . .	470
<b>35 Infrared and asymptotic structure of the ordered branch</b>	<b>471</b>
35.1 Restriction to asymptotically flat ordered backgrounds . . . . .	471
35.2 Why the infrared sector matters for ECT . . . . .	471
35.3 BMS-type asymptotic compatibility . . . . .	471
35.4 Gravitational memory as persistent asymptotic condensate shift . . . . .	472
35.5 Soft gravitons as long-wavelength $\delta n_A$ modes . . . . .	472
35.6 Restrained bridge to soft hair on black holes . . . . .	472
35.7 Scope and non-claims . . . . .	472

<b>36 Black-Hole Thermodynamics, Information Problem, and Holographic-Style Entropy Bounds</b>	<b>472</b>
36.1 Effective horizon thermodynamics . . . . .	474
36.2 The information paradox in ECT . . . . .	475
36.3 Comparative mapping: the critical shell and the islands/QES language . . . . .	477
36.4 Black-hole entropy and observational signatures . . . . .	479
36.5 Area-law scaling and holographic-style entropy bounds as boundary-layer properties of the ECT medium . . . . .	481
36.6 Singularity, interior, and structural programme . . . . .	486
36.7 Observational anchors and programme predictions . . . . .	488
36.8 Diagnostic discriminants across the gravity–matter interface . . . . .	490
<b>37 Analogue Laboratory Programme for Ordered-Branch Tests</b>	<b>491</b>
<b>38 Status Map, Open Problems, and Completion Status of Part III</b>	<b>494</b>
38.1 Status table and open problems of the Quantum Sector . . . . .	494
38.2 Minimal quantum core already established by ECT . . . . .	504
38.3 ECT as a foundational framework for quantum mechanics: structural comparison with the standard formalism . . . . .	507
38.4 ECT-specific falsifiers in the quantum-gravity and decoherence sector . . . . .	519
38.5 Completion status and bridge forward . . . . .	519
<b>IV Reverse Analysis, SU(3) Completion, and Structural Constraints</b>	<b>521</b>
<b>39 Methodology of reverse analysis</b>	<b>521</b>
<b>40 Colour consistency requirement and candidate non-Abelian completions</b>	<b>522</b>
<b>41 Minimal admissible colour EFT under P7</b>	<b>526</b>
<b>42 Anomaly constraints and matter-sector consistency</b>	<b>528</b>
<b>43 Closure of SU(3)-dependent questions from earlier parts</b>	<b>529</b>
<b>44 Proton stability and baryon number as a UV discriminant</b>	<b>532</b>
<b>45 Topological sector and strong CP</b>	<b>533</b>
<b>46 What Part IV closes and what remains open</b>	<b>534</b>
<b>47 Synthesis of Part IV</b>	<b>538</b>
<b>V Summary, Comparisons, and Outlook</b>	<b>540</b>
<b>48 Discussion</b>	<b>540</b>
48.1 Conceptual interpretation and scope of the framework . . . . .	540
48.2 Derivational architecture: from the $\Phi$ -medium to observable physics . . . . .	540
48.3 What ECT already establishes: emergence chains and current status . . . . .	542
48.4 Architectural comparison with neighbouring programmes . . . . .	545
48.5 Comparison with alternative quantum interpretations . . . . .	546
48.6 ECT as a foundational framework for quantum mechanics . . . . .	547
48.7 Phenomenological reach and observational diagnostics . . . . .	548

48.8	Parameter compression and comparison . . . . .	551
48.9	Completion data and residual bifurcation points . . . . .	551
48.10	Current limitations . . . . .	552
48.11	Future directions and programme closure . . . . .	553
48.12	Fundamental constants and present closure levels . . . . .	555
48.13	Common pre-geometric origin of the interaction sectors . . . . .	557
<b>49</b>	<b>Conclusion</b>	<b>563</b>
49.1	What has been achieved . . . . .	563
49.2	What remains open . . . . .	570
49.3	Final outlook . . . . .	570
49.4	Comprehensive map: standard postulates and open problems of physics as ECT consequences . . . . .	571
	<b>Appendices</b>	<b>580</b>
<b>A</b>	<b>From the Basic Physical Premises of ECT to the Lorentz-Order-Field Programme: Full Derivation Chain</b>	<b>580</b>
A.1	Purpose and scope of this appendix . . . . .	580
A.2	Basic physical premises . . . . .	580
A.3	Branch 1: the condensate-amplitude route $u_0(r)$ (discarded) . . . . .	581
A.4	Branch 2: linear scalar–tensor theory of $\chi$ . . . . .	584
A.5	Branch 3: geometrically induced coupling and the emergence of $\phi$ . . . . .	584
A.6	Branch 4: what does one loop actually provide? . . . . .	587
A.7	Branch 5: why nonlinearity is inevitable near criticality . . . . .	589
A.8	The critical IR fixed point: why $Y_\phi^{3/2}$ . . . . .	590
A.9	BTFR from the critical branch: explicit calculation . . . . .	590
A.10	Environmental dependence and observational tests . . . . .	592
A.11	Status of all results . . . . .	592
A.12	Methodological summary: the tree of branches . . . . .	593
A.13	Final perspective . . . . .	593
<b>B</b>	<b>Background Configuration and Fluctuation Expansion</b>	<b>594</b>
<b>C</b>	<b>Uniqueness of the Kinetic Tensor <math>K^{AB}</math></b>	<b>594</b>
<b>D</b>	<b>Derivation of the Lorentzian Window</b>	<b>595</b>
<b>E</b>	<b>LIV time-delay numerics</b>	<b>595</b>
<b>F</b>	<b>Causal propagation for the full nonlinear ECT dynamics: complete symmetric-hyperbolic reduction</b>	<b>597</b>
<b>G</b>	<b>Directed decoherence: proof that <math>\Gamma_{\text{irr}}[q, q'] \geq 0</math></b>	<b>599</b>
<b>H</b>	<b>Scaling Analysis of the Bath Spectral Density</b>	<b>601</b>
<b>I</b>	<b>Goldstone sector in scalar-only ECT: integrability, inverse-Higgs reduction, and EFT status</b>	<b>602</b>

<b>J</b>	<b>Single-field causal universality: detailed proof and comparison with competing frameworks</b>	<b>603</b>
J.1	Theorem: unique causal cone of the linear scalar ordered branch . . . . .	603
J.2	Comparison with Einstein–aether theory . . . . .	604
J.3	Comparison with the Standard Model Extension . . . . .	604
J.4	Scope and limitations . . . . .	604
<b>K</b>	<b>EFT Motivation via Integrating Out the Radial Mode</b>	<b>605</b>
<b>L</b>	<b>Structural candidate mechanism for the second condensate transition <math>O(3) \rightarrow O(2)</math></b>	<b>605</b>
<b>M</b>	<b>Hopf-fibered phase–orientation locking as a candidate electroweak geometry</b>	<b>607</b>
M.1	Generator-counting limitation of $O(3) \rightarrow O(2)$ . . . . .	607
M.2	Pre-locking symmetry: $SU(2)_{\text{orient}} \times U(1)_{\theta}$ . . . . .	608
M.3	Diagonal locking: pre-gauge geometry . . . . .	608
M.4	Hopf-locking operator and Berry connection . . . . .	609
M.5	Hopfion structure: mathematical template, not closure . . . . .	609
M.6	What this appendix establishes and what it does not . . . . .	610
M.7	Conditional layered closure theorem . . . . .	610
<b>N</b>	<b>Dimension and normalisation audit</b>	<b>611</b>
N.1	Primary condensate quantities . . . . .	611
N.2	Orientation-stiffness sector . . . . .	611
N.3	Induced gravitational scale . . . . .	612
N.4	Phase sector and quantum action scale . . . . .	612
N.5	Summary of the gravitational matching chain . . . . .	612
<b>O</b>	<b>Correlation Length from the Radial-Mode Propagator</b>	<b>613</b>
<b>P</b>	<b>Phase Periodicity, Winding Sectors, and the Action Scale <math>S_0</math></b>	<b>614</b>
<b>Q</b>	<b>Noether Currents: Translational and Rotational Sectors</b>	<b>615</b>
<b>R</b>	<b>Variational Selection and Reduced Extremal Dynamics</b>	<b>615</b>
<b>S</b>	<b>Noether current and local <math>U(1)</math> completion in the compact phase EFT</b>	<b>616</b>
<b>T</b>	<b>Non-Abelian local completion and the <math>\mathfrak{so}(3) \cong \mathfrak{su}(2)</math> bridge</b>	<b>617</b>
<b>U</b>	<b>Operator classification and dimensional estimate for the ECT-specific fermion–condensate coupling</b>	<b>618</b>
<b>V</b>	<b>Microscopic preferred-direction coupling versus macroscopic <math>\phi</math>-closure</b>	<b>620</b>
<b>W</b>	<b>Dimensional scaling and open condensate-scale assignments for the preferred-direction co-efficient</b>	<b>621</b>
<b>X</b>	<b><math>\phi</math>-first nonlinear gravity: full derivation</b>	<b>621</b>
X.1	Quadratic tensor sector . . . . .	623
X.2	Matching to linearised gravity . . . . .	624
X.3	What remains open . . . . .	624
X.4	Interpretive note . . . . .	624



<b>Y Numerical algorithms</b>	<b>624</b>
Y.1 Galaxy rotation curves . . . . .	624
Y.2 RG running of $\lambda(\mu)$ . . . . .	625
Y.3 Figure production . . . . .	625
<b>Z Structural routes to open microphysical targets</b>	<b>625</b>
<b>AA Effective Action for Orientation Modes: Nonlinear Sigma-Model</b>	<b>628</b>
<b>AB Derivation of the Anisotropic Curvature Coupling</b>	<b>630</b>
AB.1 Starting point: energy–momentum tensor of the vector condensate . . . . .	630
AB.2 Commuting covariant derivatives: the key step . . . . .	631
AB.3 Symmetrisation and curvature identification . . . . .	631
AB.4 Trace term and the full structure . . . . .	631
AB.5 Result of the derivation . . . . .	631
<b>AC Technical details for the emergent unimodular decoupling theorem</b>	<b>632</b>
AC.1 Rank-one determinant identity and fixed-determinant property . . . . .	632
AC.2 Jacobian cancellation identity for the classical baseline . . . . .	632
AC.3 FRW reduction and equation of state . . . . .	633
AC.4 Dimensional audit of the infrared scaling . . . . .	633
<b>AD Late-time <math>\phi</math>-first cosmological background apparatus</b>	<b>633</b>
AD.1 Derived condensate amplitude dynamics . . . . .	634
AD.2 Schematic condensate evolution: computational notes . . . . .	635
AD.3 Effective action and FRW reduction . . . . .	636
AD.4 Convenient form in $N = \ln a$ . . . . .	636
AD.5 Benchmark late-time closure (Level B) . . . . .	637
AD.6 Admissible late-time closure family beyond the benchmark . . . . .	637
AD.7 Numerical robustness programme for the admissible closure family . . . . .	638
AD.8 Derived-parent working corridor and JWST object budgets . . . . .	639
AD.9 Current computational pipeline for the derived-parent JWST analysis . . . . .	640
AD.10 Derivation of the linear growth equation on the ECT background . . . . .	641
AD.11 Semi-analytic maturity factors for collapse and BH-assisted development . . . . .	641
AD.12 Orientation-stress proxy for the JWST maturity budget . . . . .	642
AD.13 Slow-drift regime and present-epoch Hubble shift . . . . .	643
AD.14 Distances, age, and JWST-related background effects . . . . .	643
<b>AE Dimensional scaffold for gravitational waves from the ordering transition</b>	<b>644</b>
<b>AF Sign-level cosmological consequences of the ordered branch</b>	<b>645</b>
<b>AG Extraction of the effective uniform-<math>\varepsilon</math> interval from the Hubble + <math>r_s</math> channel</b>	<b>645</b>
<b>AH Methodology of the common-background retained-pipeline, benchmark achievability, and the age-viability ambiguity</b>	<b>649</b>
<b>AI Extraction of the effective uniform-<math>\varepsilon</math> interval from the JWST early-galaxy channel</b>	<b>653</b>
<b>AJ Extraction of the effective uniform-<math>\varepsilon</math> interval from the cosmic chronometers channel</b>	<b>658</b>
<b>AK Extraction of the effective uniform-<math>\varepsilon</math> interval from the <math>f\sigma_8</math> RSD channel</b>	<b>661</b>
<b>AL Extraction of the effective uniform-<math>\varepsilon</math> interval from the ISW channel (provisional proxy)</b>	<b>665</b>

<b>AM Derivation of the force-law effective dimensionality</b>	<b>668</b>
AM.1 Definition . . . . .	668
AM.2 General derivation from $\phi$ -closure . . . . .	668
AM.3 Specific result for $\mu(x) = x/\sqrt{1+x^2}$ . . . . .	668
AM.4 Limiting cases . . . . .	668
AM.5 Transition radius . . . . .	669
AM.6 Distinction from morphological dimensionality . . . . .	669
AM.7 Numerical implementation . . . . .	669
<b>AN Derivation of the galactic <math>\phi</math>-closure and the practical fitting law</b>	<b>669</b>
AN.1 Variational structure . . . . .	669
AN.2 Required asymptotic branches . . . . .	670
AN.3 Minimal interpolation choice . . . . .	670
AN.4 Practical algebraic fitting law . . . . .	670
AN.5 Baryonic input from SPARC . . . . .	671
AN.6 RAR representation of the same closure . . . . .	671
AN.7 Deep branch and BTFR . . . . .	671
AN.8 Degeneracy of the orientation-stress sector with the effective critical-scale calibration . . . . .	671
<b>AO Computational procedure for the SPARC galactic fits</b>	<b>672</b>
AO.1 Input data . . . . .	672
AO.2 Fit modes . . . . .	672
AO.3 Optimisation and quality control . . . . .	672
AO.4 Model comparison . . . . .	673
AO.5 Outputs used in the paper . . . . .	673
AO.6 Derived plot quantities: BTFR, RAR, and effective critical-scale diagnostics . . . . .	673
AO.7 Diagnostic interpretation and the current EFE proxy . . . . .	674
AO.8 Additional diagnostic outputs . . . . .	674
<b>AP Cluster-merger lensing: methods and results</b>	<b>676</b>
AP.1 Method: 2D projected $\phi$ -closure . . . . .	677
AP.2 Cluster parameters . . . . .	677
AP.3 Results: morphology . . . . .	677
AP.4 Results: amplitude and corrections . . . . .	678
AP.5 Gravitational slip from $\Theta_{\mu\nu}[n]$ . . . . .	678
AP.6 From cluster-slip proxies to cosmological closure . . . . .	679
AP.7 Note on double-counting . . . . .	679
AP.8 Four-cluster numerical summary . . . . .	679
<b>AQ Benchmark screening-length estimates across environments</b>	<b>680</b>
<b>AR Operational environment test for the effective critical scale</b>	<b>680</b>
<b>AS ECT derivation status for the galactic interpolation law</b>	<b>681</b>
<b>AT Diagnostic stress test of the current Level-B galactic closure: dark-matter-deficient ultra-diffuse galaxies</b>	<b>682</b>
AT.1 Purpose and scope . . . . .	682
AT.2 Inverse-problem closed form: $\Xi_{\text{req}}$ from $\sigma_{\text{obs}}$ . . . . .	682
AT.3 Jeans upgrade path (phenomenology reduction, not elimination) . . . . .	683
AT.4 Numerical stress-test diagnostic . . . . .	683
AT.5 Nuisance and uncertainty budget . . . . .	684
AT.6 External-field benchmark . . . . .	684

AT.7 Side diagnostics and sanity checks . . . . .	685
AT.8 Selection and sample caveats . . . . .	685
<b>AU Numerical algorithm for late-time ECT cosmology: Hubble tension, age, and JWST back-ground</b>	<b>686</b>
AU.1 Self-consistent fixed-point solver design . . . . .	687
AU.2 Implementation roadmap from benchmark closure to solver . . . . .	688
AU.3 Article–solver interface contract . . . . .	689
AU.4 Expected numerical artefacts for article synchronisation . . . . .	690
AU.5 Benchmark parameter window . . . . .	691
AU.6 Derived outputs . . . . .	692
AU.7 Orientation-stress sector and background observables . . . . .	692
<b>AV Why the Explicit Estimate of <math>S_0</math> Is Deferred</b>	<b>693</b>
<b>AW Smooth-branch exactness of fermionic exclusion: canonical normalisation, curvature control, and numerical bounds</b>	<b>693</b>
AW.1 General local fermionic EFT on the coherent ordered branch . . . . .	694
AW.2 Canonical normalisation and the equal-time anticommutator . . . . .	694
AW.3 Curvature control, not acceleration control . . . . .	695
AW.4 Numerical comparison with current bounds . . . . .	696
<b>AX Unified vacuum-response logic: boundaries, acceleration, time dependence, and horizons</b>	<b>697</b>
<b>AY Bath regimes, effective spectral structure, and the limits of the ohmic/Markov closure</b>	<b>698</b>
<b>AZ Mathematical apparatus for ECT decoherence predictions</b>	<b>699</b>
AZ.1 Generic subsystem–bath coupling class . . . . .	699
AZ.2 Noise kernel $N(\tau)$ . . . . .	699
AZ.3 Dissipation kernel $D_R(\tau)$ . . . . .	700
AZ.4 Decoherence exponent for spatial superpositions . . . . .	700
AZ.5 Short-time and Markov limits . . . . .	701
AZ.6 Self-consistent environmental–gravitational crossover . . . . .	701
AZ.7 Domain of applicability . . . . .	702
<b>BA Qubit information–decoherence numerics</b>	<b>702</b>
<b>BB Critical shell and black-hole information in ECT</b>	<b>703</b>
BB.1 Microscopic unitarity and apparent information loss . . . . .	703
BB.2 Derivation of the critical shell . . . . .	703
BB.3 Shell entropy and the area law . . . . .	704
BB.4 Conditional theorem: exact thermality is incompatible with unitary evaporation . . . . .	704
BB.5 Near-horizon $\chi$ -field dynamics: an effective mean-field construction . . . . .	706
BB.6 Toy finite-memory shell model and the Page mechanism . . . . .	708
BB.7 Interior and the singularity . . . . .	709
BB.8 Potential observational signatures . . . . .	709
BB.9 Microscopic consistency criterion for ECT black-hole unitarity . . . . .	710
BB.10 Summary table . . . . .	711
<b>BC Reduced thermality, generalized entropy, and the black-hole information problem</b>	<b>712</b>
<b>BD Analogue-observable dictionary for ordered-branch tests</b>	<b>713</b>

<b>BE Expanded architectural comparison of ECT and neighbouring programmes</b>	<b>714</b>
BE.1 Closely related Euclidean-to-Lorentzian constructions . . . . .	714
BE.2 Comparison with further neighbouring programmes . . . . .	715
<b>BF Retarded Causal Kernel: Proof That <math>K(\tau &lt; 0) = 0</math></b>	<b>716</b>
 <b>Data and Code Availability</b>	 <b>716</b>
 <b>Acknowledgments</b>	 <b>717</b>
 <b>References</b>	 <b>717</b>

## List of Symbols

**Table 1:** Principal symbols. Foundational symbols (P1–P6 level) are defined in Sections 2–6. Derived and matching-level symbols are introduced in the corresponding sections.

Symbol	Definition	Value / Units
<i>Microscopic level — bare micro-action (P3)</i>		
$\Phi$	Real scalar field on $\mathcal{M}^4$ ; sole fundamental degree of freedom	—
$\mu^2$	Mass parameter: $V(\Phi) = -\frac{\mu^2}{2}\Phi^2 + \frac{\lambda}{4}\Phi^4$ , $\mu^2 > 0$	GeV <sup>2</sup>
$\lambda$	Self-coupling in bare potential	dimensionless
$\phi_0$	Bare potential minimum: $\phi_0 = \sqrt{\mu^2/\lambda}$ ; $[\phi_0] = \text{GeV}$	GeV
$m_\sigma$	Radial mode mass: $m_\sigma^2 = 2\mu^2$	GeV
<i>Vacuum level — gradient-ordered sector (P4)</i>		
$u_0$	Gradient condensate amplitude: $u_0 =  \langle \partial_A \Phi \rangle $ ; $[u_0] = \text{GeV}^2$	GeV <sup>2</sup>
$n^A$	Orientation collective variable: $\langle n^A \rangle = \delta^A_w$ ; not in fundamental action	—
$w$	Preferred Euclidean direction selected by P4	m
<i>Broken-phase EFT parameters</i>		
$\alpha$	Anisotropy coupling: $K^{AB} = \beta \delta^{AB} - \alpha n^A n^B$ ; $\alpha > \beta$ for Lorentzian	2 (canonical)
$\beta$	Isotropic stiffness; canonical $\beta = 1$	1 (canonical)
$K^{AB}$	Anisotropic effective metric: $K^{AB} = \beta \delta^{AB} - \alpha n^A n^B$ ; Lorentzian when $\alpha > \beta$	—
$c_*$	Effective propagation speed: $c_* = \sqrt{\beta/(\alpha - \beta)}$ , Level A	$= c$ (canonical)
$v_2$	Electroweak matching scale: $v_2 = (\sqrt{2}G_F)^{-1/2}$ (eq. 5.8); intermediate condensate scale, not derived from P1–P6 (OP-EW-scale, Sec. 5.1)	$\approx 246.22 \text{ GeV}$
$\mathcal{J}_{\text{EW}}$	Logarithmic measure of the electroweak hierarchy: $\mathcal{J}_{\text{EW}} \equiv \ln(\phi_0/v_2)$ ; central reduction quantity for the OP-EW-scale closure programme (eq. 5.10, Sec. 5.1)	$\approx 36.8$ (dimensionless)
$m_{\text{eff}}^2$	EFT fluctuation mass parameter; $m_{\text{eff}}^2 \neq m_\sigma^2$ in general	GeV <sup>2</sup>
$\xi_{\text{cond}}$	EFT correlation length: $\xi_{\text{cond}} \sim m_\sigma^{-1}$ ; matching hypothesis $\sim \ell_{\text{Pl}}$	$\sim \ell_{\text{Pl}}$
<i>Derived smooth coherent sector (BR1)</i>		
$\Phi_{\text{eff}} = \rho e^{i\theta}$	Effective order parameter of coherent IR sector	—
$\theta$	Phase of $\Phi_{\text{eff}}$ ; winding condition $\oint \partial_A \theta dX^A = 2\pi n$	rad
$K_\theta^{\text{eff}}$	Effective phase stiffness of the coherent branch; expected dimensionally to scale as $\sim \phi_0^2$ up to EFT matching coefficients	GeV <sup>2</sup>
$S_{\text{ord}}$	Ordered-branch action functional; $S_{\text{ord}}[u, n]$	—
$S_0$	Pre-quantum action-scale candidate of the coherent branch: in the fixed-core reduced-loop closure one writes $S_{\text{elem}} = 2\pi S_0$ for the elementary coherent loop; matched to $\hbar$ at Level B; not a proven global variational minimum over arbitrary loop lengths	$[\hbar]$
$S_{\text{elem}}$	Elementary coherent loop action: $S_{\text{elem}} = 2\pi S_0$ in the fixed-core reduced-loop closure; full variational minimum in the $n = 1$ sector not established (Open); related to $\hbar$ at Level B	$[\hbar]$

Table 1 continued

Symbol	Definition	Value / Units
$L_{\text{core}}$	Characteristic condensate core scale entering the fixed-length loop bound; explicit first-principles derivation open (OP-Q2)	m
<i>Gravitational matching — Macroscopic Physics (Level B)</i>		
$\mathcal{C}_n$	Orientation-stiffness coefficient: $\kappa_n = \mathcal{C}_n u_0^2$ ; $[\mathcal{C}_n] = \text{GeV}^{-2}$ ; not yet derived (OP-Planck)	$\text{GeV}^{-2}$
$\kappa_n$	Orientation stiffness: $\kappa_n = \mathcal{C}_n u_0^2$ ; sets gravitational stiffness $M_G^2 \sim \kappa_n$ ; $[\kappa_n] = \text{GeV}^2$ ; not yet derived microscopically (OP-Planck)	$\text{GeV}^2$
$M_G$	Induced gravitational stiffness scale: $M_G^2 \sim \kappa_n \sim u_0^2/m_\sigma^2 \sim \phi_0^2$ (structural/NLO estimate); $M_G = \bar{M}_{\text{Pl}}$ by weak-field matching	$\text{GeV}$
$G_N$	Newton constant; $G_N = c_*^4/(8\pi M_G^2)$ , observational input	$6.674 \times 10^{-11} \text{ m}^3 \text{ kg}^{-1} \text{ s}^{-2}$
$\bar{M}_{\text{Pl}}$	Reduced Planck mass: $1/\sqrt{8\pi G_N} \approx 2.435 \times 10^{18} \text{ GeV}$	$\text{GeV}$
$g_{\mu\nu}^{\text{eff}}$	Emergent Lorentzian metric	—
<i>Quantum sector (Section 20)</i>		
$\hbar$	Planck constant; identified $S_0 = \hbar$ in Quantum Sector, Level B	$1.055 \times 10^{-34} \text{ J s}$
<i>Spacetime</i>		
$\mathcal{M}^4$	Four-dimensional Euclidean manifold (P1)	—
$X^A = (x, y, z, w)$	Euclidean coordinates	m
$\delta_{AB}$	Euclidean metric	—
$t$	Lorentzian time; $t = w/c_*$ (real parametrisation)	s
$\ell_{\text{Pl}}$	Planck length: $\ell_{\text{Pl}} = \sqrt{\hbar G_N/c^3} \approx 1.616 \times 10^{-35} \text{ m}$ ; matching hypothesis $\xi_{\text{cond}} \sim \ell_{\text{Pl}}$	m
<i>Decoherence (Section 26.1)</i>		
$\Gamma[q]$	Decoherence functional	—
$\Gamma_{\text{loop}}$	Decoherence/locking functional; classicality crossover at $\Gamma_{\text{loop}} \sim 1$	dimensionless
$N_{\text{eff}}$	Effective environmental degrees of freedom	—
$\gamma$	Decoherence rate per mode	$\text{s}^{-1}$
$\tau_{\text{dec}}$	Decoherence time: $1/(N_{\text{eff}}\gamma)$	s
<i>Macroscopic Physics (Sections 11–14.1)</i>		
$\Theta_{\mu\nu}$	Orientation-stress tensor from $n^A$ dynamics; appears in generalised Einstein equations	—
$\mathcal{H}$	Hilbert space; subscripted: $\mathcal{H}_{\text{ext}}, \mathcal{H}_{\text{shell}}, \mathcal{H}_{\text{int}}$ (BH decomposition)	—
$\rho_{\text{ext}}$	External observer’s reduced density matrix: $\rho_{\text{ext}} = \text{Tr}_{\text{sh,int}} \Psi\rangle\langle\Psi $	—
$G_{\text{eff}}(X)$	Position-dependent gravitational coupling	$\text{m}^3 \text{ kg}^{-1} \text{ s}^{-2}$
$\Lambda_{\text{eff}}$	Effective cosmological constant	$\text{m}^{-2}$
$n_s$	Scalar spectral index (ECT-native derivation: open)	—
$r$	Tensor-to-scalar ratio	—
$N_e$	Inflationary e-folds (external; not used in ECT)	—
$w_0, w_a$	Dark-energy EOS parameters	—
$g_{\dagger}$	Critical acceleration: $g_{\dagger} \propto cH_0$	$\text{m s}^{-2}$

Table 1 continued

Symbol	Definition	Value / Units
$g_{\text{eff}}^\dagger$	Fitted effective critical acceleration per galaxy	$\text{m s}^{-2}$
$r_*$	Derived galactic transition radius: $r_* = \sqrt{G_N M_{\text{bar}}/g^\dagger}$	kpc
$\lambda_\phi(\rho)$	Screening length: $\lambda_\phi = m_\phi^{-1}(\rho)$	m
$g_\dagger^{\text{cl}}$	Cluster-scale effective critical acceleration; merger-environment counterpart of the galactic critical-branch threshold	$\text{m s}^{-2}$
<i>Fifth force (Section 7)</i>		
$\mu_5$	Dimensionful coefficient of the ECT-specific fermion–condensate operator	GeV
$\beta_5$	Dimensionless fifth-coupling ratio defined by $\mu_5 = \beta_5 m_f$	dimensionless
$\omega_5$	Spin-precession frequency	$\text{rad s}^{-1}$
$\eta$	Eötvös parameter	dimensionless
<i>Neutrino sector (Section 8.9)</i>		
$M_R^{\text{geom}}$	Geometric-mean seesaw scale $\sqrt{\phi_0 v_2}$	$\approx 2.4 \times 10^{10} \text{ GeV}$
$m_v^{\text{geom}}$	Geometric Weinberg-operator neutrino-mass scale $v_2^2/\phi_0$	$\approx 2.5 \times 10^{-5} \text{ eV}$
$y_v^{\text{geom}}$	Dirac Yukawa at $M_R^{\text{geom}}$ for atmospheric-scale $m_v$	$\approx 4.5 \times 10^{-3}$
$\theta_{\text{as}}^{\text{geom}}$	Active-sterile mixing at $M_R^{\text{geom}}$	$\sim 4.5 \times 10^{-11}$
<i>Late-time cosmology retained-band sector (§16.5)</i>		
$\varepsilon$	Uniform late-time effective drift parameter: $G_{\text{eff}}(z)/G_N = (1+z)^{2\varepsilon}$ ; diagnostic-layer indicator; retained five-probe joint band $\varepsilon \in [0.0296, 0.0376]$ at $1\sigma$	dimensionless
$\Delta\varepsilon^{1\sigma}, \Delta\varepsilon^{2\sigma}$	$1\sigma$ and $2\sigma$ widths of the retained five-probe joint band on $\varepsilon$	dimensionless
$D(z)$	Linear matter-density growth factor on the $\varepsilon$ -deformed background	—
$f\sigma_8(z)$	Combined redshift-space-distortion observable ( $f = d\ln D/d\ln a$ , $\sigma_8$ normalisation)	—
$r_s$	Sound horizon at baryon decoupling; enters retained-band Hubble+ $r_s$ channel	Mpc
$A_{\text{ISW}}$	Semi-analytic ISW–tracer overlap-proxy amplitude: $A_{\text{ISW}}(\varepsilon) = 1 + \kappa_{\text{ISW}}\varepsilon$ (retained band)	dimensionless
$\kappa_{\text{ISW}}$	Slope parameter of the ISW overlap-proxy response to $\varepsilon$	dimensionless
$t_0^{\text{ECT}}$	Age of the Lorentzian ordered branch (retained-band indicator; $\sim 13.5 \text{ Gyr}$ baseline- $H_0$ , $\sim 12.5 \text{ Gyr}$ inferred- $H_0$ ; see Appendix AF.4)	Gyr
$t_U(z)$	Age of the Universe at redshift $z$ on the retained-band background	Gyr
<i>QG/decoherence upgrade (Part III)</i>		
$m_{\text{guide}}$	Heuristic scalar-sector orienting mass scale, $m_{\text{guide}} \sim \sqrt{\hbar R/(G_N \tau_{\text{exp}})}$ (eq. 32.1; Section 32.5); Level B, not a first-principles entangling crossover mass	kg
$\Delta n_A$	Persistent asymptotic orientation shift (ECT reading of gravitational memory); Section 35.4	—
$S_{\text{gen}}(\Sigma)$	Generalised (holographic) entropy $\text{Area}(\partial\Sigma)/4G_N + S_{\text{bulk}}(\Sigma)$ ; Section 36.3	—

Table 1 continued

Symbol	Definition	Value / Units
$\partial\Sigma$	Quantum extremal surface boundary in holographic entanglement computations; Section 36.3	—
<i>Vacuum offset decoupling and cosmological constant (Section 15)</i>		
$c_\Lambda$	Dimensionless infrared coefficient in $\rho_\Lambda \sim c_\Lambda M_{\text{Pl}}^2 H_0^2$ ; $\mathcal{O}(1)$ estimate, not yet derived (OP- $\Lambda 3$ reformulated; O2)	dimensionless
$Z_q$	Infrared stiffness of the surviving FRW ordered-branch mode $q(t)$ ; expected $\sim M_{\text{Pl}}^2$ structurally	$\text{GeV}^2$
$V_{\text{IR}}(q)$	Residual infrared potential of the ordered-branch mode; distinct from the decoupled UV baseline $V(\phi_0)$	$\text{GeV}^4$
$\rho_\Lambda^{\text{IR}}$	Effective infrared source in the Friedmann equation (Object C); not equal to $V(\phi_0)$ or $\Gamma_{\text{vac}}^{(0)}$	$\text{GeV}^4$
$\Gamma_{\text{vac}}^{(0)}$	Zero-derivative one-loop vacuum contribution (Object B); decouples conditional on $H_\Lambda$ (Theorem 15.3(v))	$\text{GeV}^4$
$q(t)$	Surviving long-wavelength ordered-branch mode on FRW background (condensate-amplitude / orientation scalar)	various
$f_G$	Pseudo-Goldstone decay-constant scale entering the possible infrared realization of $\rho_{\Lambda, \text{obs}}$ ; expected to be of order $\phi_0$ in the ECT architecture	$\text{GeV}$
$m_G$	Putative pseudo-Goldstone mass scale in the possible infrared realization; if $m_G \sim H_0$ , the order-of-magnitude estimate $\rho_\Lambda \sim M_{\text{Pl}}^2 H_0^2$ follows naturally	eV
$L_{\text{IR}}$	Infrared length scale in Cohen–Kaplan–Nelson holographic bound $\rho \lesssim M_{\text{Pl}}^2 / L_{\text{IR}}^2$ ; ECT estimate saturates with $L_{\text{IR}} \sim H_0^{-1}$	m
<i>Colour-completion sector under P7 (Part IV, §40–§46)</i>		
$\mathcal{C}_x$	Local complex internal module of rank 3 attached to each spacetime point under P7; internal singlet under spacetime $O(4)$ and under the ordered condensate $\phi, n^\mu$	—
$h$	Hermitian form on $\mathcal{C}_x$ ; structural datum of P7	—
$\Omega$	Fixed nonvanishing complex volume form $\Omega \in \Lambda^3 \mathcal{C}_x^*$ ; structural datum of P7; its preservation together with $h$ yields the local frame-redundancy group $SU(3)$	—
$Z(\phi)$	Kinetic normalisation of the colour connection in the minimal admissible EFT (eq. 41.1); $Z(\phi) > 0$ for positivity	dimensionless
$Y(\phi)$	Anisotropic colour-sector coupling in the minimal admissible EFT; shares the rank-2 directional structure $n_\mu n_\nu$ with the gravity-sector anisotropy $\alpha_{\text{ECT}}$ ; admissible but phenomenologically subleading	dimensionless
$\Theta(\phi)$	Topological coupling of the colour sector in $\Theta(\phi) F_{\mu\nu}^a \tilde{F}^{a\mu\nu} / (32\pi^2)$ ; at background $\phi_0$ reduces to the effective theta parameter $\theta_{\text{eff}}$ constrained by the neutron-EDM bound $ \theta_{\text{eff}}  \lesssim 10^{-10}$ (Part IV, §45)	dimensionless
$\kappa_n^{\text{col}}$	Anisotropic-to-isotropic ratio $\kappa_n^{\text{col}} = Y_0/Z_0$ in the colour sector; structurally subleading via shared $n^\mu$ with gravity-sector anisotropy	dimensionless
$\Lambda_{\text{col}}^{\text{ECT}}$	Dimensional-transmutation form of the colour infrared scale under P7 (eq. 41.3); classificatory, not predictive; reduces to standard QCD transmutation at $Z_0 \rightarrow 1$	$\text{GeV}$



Table 1 continued

Symbol	Definition	Value / Units
$M_*$	Matching scale of the colour-sector EFT under P7; structurally natural candidates are $v_2$ , $\phi_0$ , or the condensate excitation scale; no ECT-specific identification established (O1 in §46)	GeV

## List of Abbreviations

**Table 2:** Abbreviations used in this paper.

Abbreviation	Meaning
BH	Black hole
CMB	Cosmic microwave background
CDT	Causal dynamical triangulations
DESI	Dark Energy Spectroscopic Instrument
DM	Dark matter
ECT	Euclidean Condensate Theory (this work)
EFE	Einstein field equations
UDG	Ultra-diffuse galaxy
EOM	Equation of motion
GR	General relativity
GW	Gravitational wave
JWST	James Webb Space Telescope
KG	Klein–Gordon
LIV	Lorentz invariance violation
MOND	Modified Newtonian dynamics
PT	Phase transition
QFT	Quantum field theory
RAR	Radial acceleration relation
SM	Standard Model of particle physics
SPARC	Spitzer Photometry and Accurate Rotation Curves
SSB	Spontaneous symmetry breaking
ToC	Table of contents
VEV	Vacuum expectation value
WEP	Weak equivalence principle
FDU	Fulling–Davies–Unruh (effect)
UDW	Unruh–DeWitt (detector model)
EFT	Effective field theory
FP	Fierz–Pauli (linearized gravity Lagrangian)
CKN	Cohen–Kaplan–Nelson (holographic-type effective-field-theory bound relating UV cutoff to IR length scale)
IR	Infrared (low-energy regime)
UV	Ultraviolet (high-energy regime)
DE	Dark energy
LV	Lorentz violation (generic; cf. LIV for invariance violation)
BAO	Baryon acoustic oscillations
BBN	Big Bang nucleosynthesis
BR1	Branch rule 1 (coherent-branch selection rule)
BTFR	Baryonic Tully–Fisher relation

Table 2 continued

Abbreviation	Meaning
CTA	Cherenkov Telescope Array
DP	Dynamical principle
FLRW	Friedmann–Lemaître–Robertson–Walker (metric / cosmology)
GEE	Generalised Einstein equations
LISA	Laser Interferometer Space Antenna
LiteBIRD	Lite satellite for the studies of B-mode polarization and Inflation from cosmic background Radiation Detection
MICROSCOPE	Micro-Satellite à traînée Compensée pour l’Observation du Principe d’Équivalence (satellite WEP test)
NFW	Navarro–Frenk–White (dark-matter halo profile)
NLO	Next-to-leading order
PES	Principle of Euclidean Stationarity
PPN	Parametrised post-Newtonian (formalism)
PTA	Pulsar timing array
QS	Quantum sector (Part III of this paper)
RG	Renormalisation group
SN	Supernova (type Ia unless stated otherwise)
MWI	Many-worlds interpretation
OS	Osterwalder–Schrader (axioms / reconstruction theorem; Section 23.1)
RP	Reflection positivity
CC	Cosmic chronometers (differential-ages $H(z)$ probe)
ISW	Integrated Sachs–Wolfe (effect / cross-correlation with large-scale tracers)
RSD	Redshift-space distortions
SHOES	Supernovae and $H_0$ for the Equation of State (local Hubble-constant programme)
NLEE	Non-linear Einstein equations (or non-linear extensions of generalised Einstein equations)
H1	Late-time $\varepsilon$ -route to the Hubble sector (pre-retained-band scan classification); unrelated to the CC spectral condition $H_\Lambda$ below
$H_\Lambda$	Spectral condition on the full quadratic fluctuation operator used <i>only</i> in the emergent unimodular decoupling theorem (Sec. 15.4); controls whether the zero-derivative one-loop vacuum contribution collapses to the same fixed kinetic-determinant structure. Unrelated to the Hubble-sector H1 route.
H2	Full early+late CMB-inferred $H_0$ closure (retained-band target, open)
BMV	Bose–Mazumdar–Morley / Marletto–Vedral (gravity-induced entanglement proposal, Section 32)
BMS	Bondi–Metzner–Sachs (asymptotic symmetry group, Section 35.3)
GIE	Gravity-Induced Entanglement (Section 32)
HPS	Hawking–Perry–Strominger (soft-hair proposal, Section 35.6)
LOCC	Local Operations and Classical Communication
PCCG	Post-quantum Classical Gravity (Oppenheim hybrid framework)
QES	Quantum Extremal Surface (Section 36.3)
WV	Witten–Veneziano (relation between $\eta'$ mass and topological susceptibility, Part IV, §45)
OP-EW	Layered electroweak open-problem programme: OP-EW-scale ( $\mathcal{J}_{EW} \approx 36.8$ , four candidate mechanisms), OP-EW-locking (compact $U(1)_\theta$ origin and Hopf-fibered diagonal locking, App. M), OP-EW-gauge (chirality, hypercharge, $g, g'$ , Weinberg angle), OP-EW-naturalness (radial-mode protection), OP-EW-matter (chiral fermions, Yukawa hierarchy)

# 1 Introduction

Modern theoretical physics rests on two highly successful but conceptually distinct frameworks: General Relativity and quantum field theory. General Relativity describes gravity as the curvature of spacetime geometry, while the Standard Model of particle physics describes fundamental interactions within a fixed spacetime background. Despite their empirical success, these two frameworks remain difficult to reconcile within a single consistent theoretical structure.

A conceptual peculiarity common to both theories is the distinguished status of time in the spacetime interval

$$ds^2 = -c^2 dt^2 + dx^2 + dy^2 + dz^2.$$

In this expression one coordinate is fundamentally different from the others, possessing an opposite sign in the metric. While this Lorentzian structure has been extraordinarily successful phenomenologically, its physical origin remains unclear. In particular, it raises the question whether the Lorentzian signature of spacetime is a fundamental property of nature or whether it may instead arise as an emergent feature of a deeper underlying structure. Similar questions have appeared in various approaches to quantum gravity and emergent spacetime, where the possibility has been considered that the Lorentzian metric may arise dynamically from a more symmetric underlying state.

This observation motivates the exploration of scenarios in which the fundamental description of the vacuum is not Lorentzian but Euclidean, with all four directions initially equivalent. In such a picture the distinction between space and time would arise dynamically through a symmetry-breaking process in the vacuum. From this perspective spacetime geometry is not fundamental but emerges as an effective description of collective excitations of the underlying vacuum state.

A key physical motivation comes from the observation that the Euclidean signature  $(+, +, +, +)$  possesses higher symmetry— $O(4)$ —than the Lorentzian signature  $(-, +, +, +)$ , which breaks this to  $O(3, 1)$ . Since fundamental theories tend to start from the most symmetric state and derive less symmetric configurations through dynamical symmetry breaking, it is natural to ask whether the Lorentzian structure of spacetime could arise as a broken phase of a more symmetric Euclidean vacuum. Furthermore, at the quantum level the path integral formulation is naturally related to a Euclidean description through the standard formal analytic continuation  $t \rightarrow -i\tau$ , suggesting that the Euclidean description may be more fundamental than the Lorentzian one.

A closely related line of work has shown that Lorentzian dynamics can arise effectively from a fundamentally Euclidean (Riemannian) field theory. Girelli, Liberati and Sindoni [1] showed that a scalar field with a nonvanishing gradient on a Riemannian manifold can generate an effective Lorentzian metric for perturbations, albeit with scalar (Nordström-type) gravity. Mukohyama and Uzan [2] developed a more complete classical clock-field construction in which scalars, vectors, and Dirac spinors propagate in an effective Minkowski metric on a 4-dimensional Riemannian manifold. ECT shares this architectural core and reaches closely analogous conclusions regarding emergent Lorentzian propagation, but differs in the mechanism by which the preferred direction appears: here it is attributed to spontaneous  $O(4) \rightarrow O(3)$  ordering rather than to an imposed clock-field background. The two frameworks diverge further in the gravitational sector and in the extension to quantum and phenomenological questions.

In this work we investigate this possibility within the framework of the *Euclidean Condensate Theory* (ECT). The central hypothesis of ECT is that the physical vacuum can be described as a condensate field defined in a four-dimensional Euclidean space possessing an underlying  $O(4)$  symmetry. This symmetry corresponds to the rotational symmetry of four-dimensional Euclidean space and therefore represents the natural maximal symmetry of an initially isotropic Euclidean vacuum.

A spontaneous symmetry breaking  $O(4) \rightarrow O(3)$  selects a preferred direction in this Euclidean space. The symmetry-broken phase is characterised by an orientation field  $n_A$  satisfying the unit constraint

$$n_A n^A = 1.$$

Such a constraint can arise dynamically in the condensate sector, for example through a Lagrange multiplier or through a potential that fixes the magnitude of the orientation field while allowing its direction to fluctuate.

The presence of this orientation field modifies the propagation of perturbations in the condensate. At low energies the dynamics of small excitations can be described by an effective field theory whose quadratic action takes the form

$$S_{\text{eff}} = \int d^4X g_{AB}^{\text{eff}} \partial^A \psi \partial^B \psi + \dots$$

where  $\psi$  denotes generic low-energy excitations of the condensate. In the ordered branch, the effective kinetic tensor is controlled by two coefficients  $\alpha$  and  $\beta$  (Section 3.4). In the canonical benchmark realisation used throughout this paper,  $(\alpha, \beta) = (2, 1)$ , so that the corresponding effective metric-like structure reduces to

$$g_{AB}^{\text{eff}} = \delta_{AB} - 2n_A n_B.$$

Since  $n_A n^A = 1$ , this tensor has one negative and three positive eigenvalues and therefore possesses a Lorentzian signature  $(-+++)$  once the direction defined by  $n_A$  is identified with the emergent time coordinate. Perturbations propagating in this background therefore experience an effective Lorentzian spacetime geometry.

In the present framework the coordinate  $w$  should not be interpreted as a physical time variable. Rather, it represents one of the four Euclidean coordinates of the underlying condensate space. The physical time coordinate  $t$  emerges only in the symmetry-broken phase, where the direction defined by  $n_A$  determines the temporal orientation of the effective Lorentzian spacetime.

Importantly, the preferred direction associated with  $n_A$  arises dynamically from the condensate background rather than being imposed as a fundamental structure. As a result, Lorentz invariance appears as an effective symmetry of the low-energy excitation spectrum.

Within this framework several fundamental structures of modern physics may arise from properties of the condensate. In particular, the Lorentzian spacetime signature, the relativistic dispersion relation, and the effective propagation speed  $c$  can emerge from the dynamics of perturbations in the symmetry-broken phase. In the effective description the characteristic propagation speed of low-energy excitations defines the causal cone of the emergent metric. The identification of this velocity with the physical speed of light is a structural consequence of the single-field nature of ECT (§4.7): all linear ordered-branch excitations share the same causal cone, and the gauge sector inherits it within the minimal emergence route. The gravitational sector appears as an effective description of collective excitations of the condensate, while quantum dynamics can be interpreted in terms of loop configurations and path-integral weights associated with the vacuum structure.

Conceptually, ECT is related to a broader class of approaches in which spacetime and gravity emerge from more fundamental microscopic degrees of freedom. Examples include Sakharov’s induced gravity [3], condensed matter analogues of spacetime, and various emergent-gravity scenarios. In Sakharov’s induced gravity the Einstein–Hilbert action arises from quantum fluctuations of matter fields in a fixed background spacetime. In contrast, the present framework assumes that spacetime geometry itself emerges from collective excitations of a Euclidean condensate. Nevertheless, both approaches share the idea that gravitational dynamics may arise as an effective description of more fundamental microscopic degrees of freedom. However, the present framework differs in that it begins with a Euclidean condensate possessing an  $O(4)$  symmetry and investigates the consequences of its spontaneous symmetry breaking for the structure of spacetime and physical interactions.

A key physical idea underlying this framework is that the effective Lorentzian spacetime experienced by low-energy excitations is not fundamental but emerges dynamically from the symmetry-broken phase of the Euclidean condensate. In this picture gravitational and quantum phenomena correspond to collective properties of the condensate background rather than to independent fundamental structures.

It is important to emphasise that ECT is proposed as a *framework* rather than a complete fundamental theory. The aim of the present work is to explore whether a Euclidean condensate vacuum can provide a consistent setting in which spacetime geometry, quantum dynamics, and gravitational interactions may emerge from a common underlying structure.

A central question for any condensate-based theory of spacetime is: *what precisely condenses?* In ECT the answer is not a scalar vacuum expectation value (which would be  $O(4)$ -invariant and produce no symmetry breaking) but the *gradient field*  $\partial_A \Phi$ , an  $O(4)$  vector whose non-zero vacuum expectation value  $\langle \partial_A \Phi \rangle = u_0 \delta_{Aw}$  spontaneously selects the emergent time direction. This requires no new independent fields beyond the single scalar  $\Phi$ , and the orientational and amplitude modes  $n_A, \sigma$  arise as its polar decomposition  $\partial_A \Phi = (u_0 + \sigma)n_A$  (Sec. 2.1).

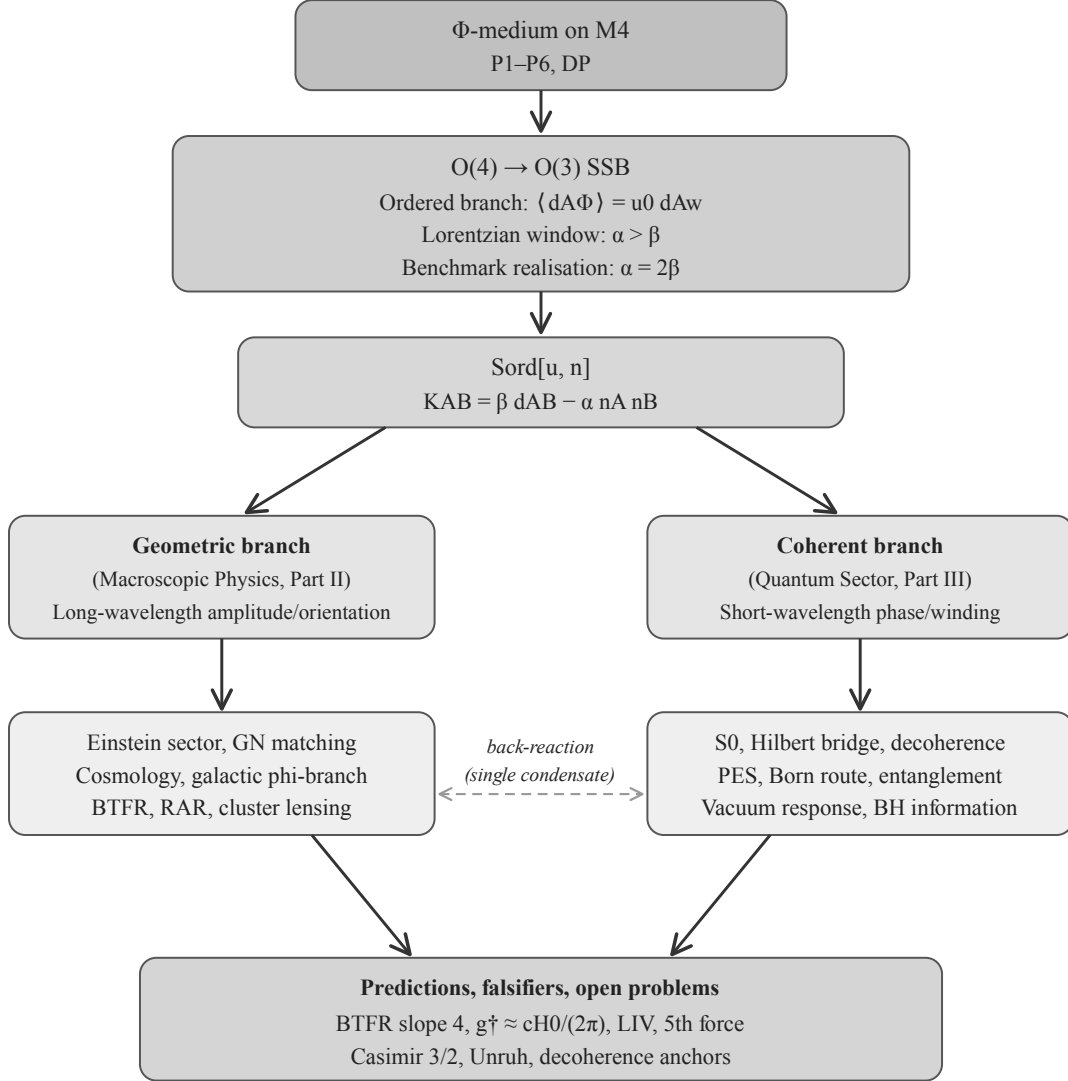


**Figure 1:** Schematic architectural map of Euclidean Condensate Theory. A single Euclidean  $\Phi$ -medium undergoes  $O(4) \rightarrow O(3)$  symmetry breaking and yields an ordered branch described by  $S_{\text{ord}}[u, n]$ . Two complementary effective sectors then emerge: a geometric branch associated with long-wavelength amplitude/orientation modes and a coherent branch associated with short-wavelength fluctuations. The former organises the gravitational and cosmological sector; the latter organises the quantum sector. Back-reaction between the two sectors is structurally rooted in the single ordered condensate action. The figure is schematic only: the derivational status of individual arrows is specified in the main text and in the status tables. The benchmark identification  $\alpha = 2\beta$  used elsewhere in the paper is not the generic branching condition; the structural condition for the Lorentzian ordered branch is  $\alpha > \beta$ .

A central claim of the present work is that ECT should not be read merely as an alternative interpre-

tation of already known quantum equations. Rather, it proposes a deeper dynamical level from which part of the standard quantum formalism emerges as an effective description of subsystems. In this sense, ECT addresses not only the question of *how* quantum mechanics computes observable probabilities, but also the question of *why* structures such as superposition, the action scale  $\hbar$ , and the quantum–classical transition appear in the first place. The overall architecture is summarised in Fig. 1. The figure should be read as a navigation map for the logical structure of the paper: Part II develops the geometric branch, Part III develops the coherent branch, and the relation between them is traced back to the single ordered condensate action. The guiding idea is that the fundamental object is not a probability amplitude defined on an already Lorentzian spacetime, but a Euclidean condensate field whose ordered broken phase generates both the coherent sector associated with quantum mechanics and the geometric sector associated with gravity.

This difference is reflected already at the level of the equations to be solved. Standard quantum mechanics is formulated as an initial-value theory for a wavefunction, for example

$$i\hbar\partial_t\psi = H\psi,$$

where  $\psi(\mathbf{x},t)$  is a probability amplitude and  $|\psi(\mathbf{x},t)|^2$  is interpreted statistically through the Born rule. ECT begins instead from a Euclidean field equation of the form

$$\delta^{AB}\partial_A\partial_B\Phi - V'(\Phi) = 0,$$

whose solution  $\Phi(X)$  is interpreted as a physical condensate configuration in a four-dimensional Euclidean arena. The fundamental problem is therefore a boundary-value problem rather than a Cauchy evolution problem: the solution is fixed by boundary data on the Euclidean domain, not by initial data propagated only forward in time. In this framework, the probabilistic character of quantum mechanics does not belong to the deepest level of description; it appears only after coarse-graining over the untracked modes of the condensate, in close analogy with the way statistical mechanics emerges from an underlying deterministic microscopic dynamics.

The resulting hierarchy is one of the central structural outputs of ECT. At the most fundamental level one has the Euclidean condensate equation. In the ordered broken phase this reduces to an effective equation with kinetic tensor

$$K^{AB} = \beta\delta^{AB} - \alpha n^A n^B,$$

whose Lorentzian admissibility requires  $\alpha > \beta$ . After the real parametrisation  $t = w/c_*$  one obtains the Klein–Gordon equation, and in the non-relativistic limit the Schrödinger equation. Thus Schrödinger dynamics is not primary but the narrowest low-energy descendant of a more general ECT equation that also accommodates the Euclidean coherent regime, the Lorentzian macroscopic regime, and the transition between them.

**Terminological note.** In ECT, the phenomena conventionally attributed to *dark matter* arise from the nonlinear response of the ordered-branch amplitude variable  $\phi$  (the “ $\phi$ -branch”). The Goldstone/soft orientation sector is not used as a dark-matter component in the present formulation; its independent phenomenological role remains an open question. *Dark energy* is represented macroscopically by the residual amplitude-sector contribution and possible slow evolution of the condensate background; no independent cosmological-constant sector is postulated. Throughout this paper we use the standard terms “dark matter” and “dark energy” for brevity and to facilitate comparison with the existing literature; no separate dark-matter particle or cosmological constant is postulated.

Throughout this paper we carefully distinguish three levels of theoretical status: results *derived at theorem or structural level* (Level A/B in the derivation table, Table 73), results *derived at the EFT or effective level* (Level B/C), and *open theoretical programs* (Level C / open problems). A summary is given in Table 73.

The paper is organised into five parts.

**Part I (Foundations)** develops the ordered-branch effective theory of the condensate and the emergence of Lorentzian spacetime. It derives the effective signal cone, matching relations for  $c_*$ ,  $G_N$ , and the pre-quantum action scale  $S_0$ , and the effective Klein–Gordon, Schrödinger, and Dirac sectors. It also identifies the structural gauge embeddings of the ordered medium and the low-energy signatures of preferred-direction couplings. The neutrino sector is structurally constrained by the geometrically one-chiral weak route, which disfavours pure Planck-suppressed completions and motivates an embedded heavy-sterile seesaw with a natural Yukawa coupling at the ECT-specific geometric-mean scale.

**Part II (Macroscopic Physics)** develops the macroscopic branch and the generalised Einstein equations with orientation-sector stress. In this branch ECT addresses the standard horizon/flatness/monopole problems without a separate inflationary stage, provides a late-time route to accelerated expansion and Hubble-shift alleviation without an independent dark-energy substance, and yields galactic phenomenology without particle dark matter. The same orientation sector also supplies a natural structural route to cluster-lensing effects and to the lensing–growth ( $S_8$ ) sector through gravitational slip, although its quantitative closure remains open.

**Part III (Quantum Sector)** develops the coherent quantum branch: reflection positivity, Hilbert-space reconstruction, canonical structure, exchange topology, decoherence, and the Principle of Euclidean Stationarity. In this sector ECT aims to show that large parts of quantum formalism appear as effective ordered-branch structures rather than primitive postulates. The smooth coherent branch also yields a no-go statement for Pauli-violation mechanisms driven by smooth condensate inhomogeneity, while the Born rule remains explicitly conditional and open. Part III is further extended by a dedicated upgrade layer on the gravity–matter interface: a reduced-state reformulation of the hybrid-consistency problem; an architectural operational criterion for gravity-induced-entanglement experiments; a channel taxonomy of the effective gravitational mediator separating scalar distinguishability from orientation-based candidate entangling structure; an infrared framing compatible with BMS-type asymptotic symmetries, gravitational memory, and soft gravitons; and a structural mapping of the critical-shell black-hole picture onto the modern islands and quantum-extremal-surface language, together with a compact cross-programme diagnostic summary.

**Part IV (Reverse Analysis,  $SU(3)$  Completion, and Structural Constraints)** is a reverse-analysis closure layer built on top of the forward programme of Parts I–III. It formalises the reverse-engineered postulate P7 (exact local  $SU(3)$  acting on a local complex rank-3 internal module), derives the minimal admissible colour EFT with its obstruction theorems, restates the matter-sector anomaly architecture under P7, catalogues earlier  $SU(3)$ -dependent questions as structurally closed, sharpened, reframed, or still open, and honestly reframes the strong-CP problem as reopened rather than resolved. This part is Level B or C throughout; it does not add Level A derivations of strong-sector physics.

**Part V (Summary, Comparisons, and Outlook)** consolidates the framework through its constants map, falsifiers, open problems, and the derivational summary of structures usually treated as independent postulates or empirical inputs in standard physics. It also reformulates the fine-structure problem as an electroweak kinetic/mixing target rather than a purely primitive input.

Throughout the paper we distinguish carefully between strict derivations, structurally grounded routes, and still-open closure problems. This level discipline is central to the logic of the work: some sectors now close strongly, while others remain sharpened targets for further derivation. The framework is therefore intended not only as a reinterpretation of standard structures, but also as a source of genuinely new observational discriminants, especially in sectors controlled by orientation stress, vacuum response, and late-time cosmological closure.

Section 25.1 organises three quantum vacuum phenomena — the orientation-sector Casimir-type pressure, the Unruh temperature via analytic continuation, and cosmological particle production at the  $O(4) \rightarrow O(3)$  transition — showing that all three are controlled by related limits of the same Euclidean two-point function (organizing proposition; each effect still requires its own boundary, detector, or coarse-graining specification).

A distinctive feature of the present work, developed in Section 17.1 and Appendix A, concerns the galactic phenomenology of ECT. In the original formulation of the theory, flat rotation curves were

parametrised through a spatially varying condensate amplitude  $u_0(r)$ . A careful analysis reveals that this route encounters fundamental obstacles: the radial condensate mode is too heavy ( $m_\sigma \sim M_{\text{Pl}}$ ) for kpc-scale variations, and a linearised scalar–tensor theory of the ordered-branch amplitude parameter  $\chi = \alpha - \beta$  produces an unsuppressed fifth force excluded by Solar System tests. These negative results are not defects of the theory but rather powerful constraints that uniquely select the viable mechanism: a *nonlinear, self-screening dynamics* of the macroscopic amplitude variable  $\phi = \frac{1}{\beta} \ln(u/u_\infty)$ , which measures the local degree of Lorentzianness of the vacuum. Within this new framework the coupling of  $\phi$  to baryonic matter is not postulated but induced geometrically through the trace of the effective scalar–tensor field equations, yielding the central result  $d\bar{\phi}/d\rho_{\text{m}} > 0$ , or equivalently  $d\bar{\phi}/d\rho > 0$  for the SI mass density: matter stabilises the Lorentzian phase. In dense environments a chameleon-type screening mechanism restores standard gravity; on galactic outskirts, where the vacuum approaches the Euclidean $\leftrightarrow$ Lorentzian critical boundary, the  $\phi$ -sector enters a nonlinear regime whose unique 3D scale-invariant form reproduces MOND-like dynamics and the baryonic Tully–Fisher relation  $v^4 = G_N M g_\dagger$  as an exact algebraic consequence. The characteristic acceleration scale  $g_\dagger$  is not a universal constant (as in standard MOND) but depends on the ambient degree of Lorentzianness, leading to a new testable prediction: a weak environmental modulation of  $g_\dagger$  correlated with local cosmic density.

The present formulation should be understood primarily as an effective low-energy description of condensate excitations. The analysis focuses on long-wavelength perturbations around the symmetry-broken vacuum, where the emergent Lorentzian geometry provides an accurate effective description. The microscopic dynamics of the condensate at very high energies remains an open question.

Several phenomenological implications of this framework are discussed in later sections. These examples are intended primarily to illustrate how condensate dynamics may connect to observable phenomena rather than to provide a complete quantitative cosmological model. A full analysis of the phenomenology of ECT will require dedicated numerical and observational studies.<sup>1</sup>

---

<sup>1</sup>A shorter companion article providing an accessible overview of the main ideas, results, and open problems of ECT is available at <https://doi.org/10.5281/zenodo.19430795>.



## Part I

# Foundations: Postulates, Symmetry Breaking, and Emergent Laws

## 2 Postulates of Euclidean Condensate Theory

*This section states the foundational symmetry and condensate postulates of ECT. It establishes the minimal bare framework from which later Level A/B/C results are developed; it is not itself a phenomenological or EFT-derivation section.*

Euclidean Condensate Theory (ECT) starts not from already formed spacetime, matter, or energy in their familiar late-physics sense, but from a more primitive Euclidean  $\Phi$ -medium. The role of the foundational postulates is not to impose the observed macroscopic world by hand, but to formalise the minimal structural properties that such a medium must possess if causal structure, geometry, and gravitational dynamics are to emerge from it.

The foundational construction is organised in three levels. First, the ontological properties of the  $\Phi$ -medium are stated explicitly (Section 2.2). Second, the working postulates P1–P6 specify the concrete ECT realisation of that medium. Third, derived branch rules such as BR1 isolate special coherent sectors of the ordered phase. From the ordered broken phase there then develop two effective sectors: the geometric macroscopic branch and the coherent branch. The smooth coherent sector is not introduced here as an independent fundamental postulate: its winding structure is derived once a smooth single-valued collective phase field exists in the coherent broken phase. The later analysis of kinetic tensors, signature classes, and the Lorentzian window (Section 3.4) is likewise not an extra postulate but the dynamical branch-selection analysis of the broken phase. All further structures developed in this work arise as consequences of this framework and the analyses built on it.

### 2.1 Glossary of terms

Before stating the postulates we fix the meaning of terms that in the literature are sometimes used interchangeably but carry distinct meanings in ECT.

**Field  $\Phi$**  — the unique fundamental microscopic degree of freedom: a real scalar defined on  $\mathcal{M}^4$ .

**Vacuum** — a stationary, physically admissible background branch of the fundamental  $\Phi$ -medium. In the present ECT construction the physically relevant vacuum branch is ordered: it carries a non-zero gradient condensate, as specified by postulate P4.

**Condensate** — a property of an ordered branch of the  $\Phi$ -medium, here characterised by  $\langle \partial_A \Phi \rangle \neq 0$ . It is not an additional object but a state of the underlying medium.

**Order parameter** — a collective infrared variable of the coherent broken phase,  $\Phi_{\text{eff}} = \rho e^{i\theta}$ , describing low-energy excitations above the ordered branch. It is introduced only at the effective level after symmetry breaking, not at the level of the bare micro-action.

**Orientation variable  $n_A$**  — a collective variable of the broken phase describing the local direction of the condensate. It is part of the ordered-branch description and does not appear as an independent field in the bare micro-action.

**Electroweak condensate field  $\Phi_{\text{ew}}$**  — the embedded low-energy scalar field of the secondary electroweak sector. It is distinct from the fundamental bare condensate field  $\Phi$  of P3 and appears only in the electroweak-like embedding (Section 7.4).

## 2.2 Ontological properties of the $\Phi$ -medium

The  $\Phi$ -medium is a pre-physical entity: it exists prior to spacetime, quantum mechanics, and any emergent physics. Its description must therefore not rely on the language of energy, quantum fluctuations, or effective Lagrangians. The following structural properties characterise the  $\Phi$ -medium in purely geometric and configurational terms, prior to any ordering or symmetry breaking.

### Layer S : Properties of the medium.

- S1 — Connected Euclidean carrier.** The  $\Phi$ -medium exists on a connected four-dimensional Euclidean carrier  $\mathcal{M}^4$  with a flat Euclidean metric.
- S2 — Directional isotropy.** Prior to ordering, all four directions on  $\mathcal{M}^4$  are equivalent: the medium is  $O(4)$ -isotropic.
- S3 — Point homogeneity.** Prior to ordering, all points of  $\mathcal{M}^4$  are equivalent; ordering may break this homogeneity locally.
- S4 — Regularity.** Configurations  $\Phi(X)$  are locally regular where they contain no defect cores; configurations with localised defect cores on submanifolds of lower dimension are admissible.
- S5 — Locality.** The local state of the  $\Phi$ -medium at  $X$  is determined by the local configuration in a neighbourhood of  $X$ , not by non-local rules on all of  $\mathcal{M}^4$ .
- S6 — Multiplicity of configurations.** The configuration space is non-trivial: no configuration is privileged a priori; globally and locally distinct configurations are admissible.
- S7 — Admissibility of ordering.** The  $\Phi$ -medium is capable of transitioning into an ordered state with a preferred direction  $\langle \partial_A \Phi \rangle \neq 0$ .
- S8 — Medium character.** In the ordered  $\Phi$ -medium, pointwise internal coordinates of the effective order parameter are descriptive redundancies rather than independently observable degrees of freedom; local observables depend only on invariant gradient and holonomy data.
- S9 — Inhomogeneity of ordering.** Ordering need not be globally uniform; ordered domains, transition zones, and local deviations from a uniform background are admissible.
- S10 — Topological completeness.** The configuration space includes all topological sectors compatible with the vacuum manifold; topologically non-trivial configurations are not excluded a priori.

### Layer DP : Dynamical principle.

- DP — Variational selection.** Physically realisable configurations are extrema of a local functional  $S_E[\Phi]$  compatible with the basic symmetries of the medium, and satisfy conditions ensuring the well-posedness of the variational problem.

The working postulates P1–P6 of ECT constitute the present concrete realisation of this framework within the minimal real-scalar field theory. In that realisation: P1 makes explicit S1–S3; P2 formalises S2 at the level of the bare symmetry; P3 realises S4, S5, and provides the minimal local variational realisation associated with DP; P4 realises S7; P5 realises S8; P6 makes explicit S6 and S9. The broader topological completeness property S10 is partially reflected, within the smooth coherent branch, by the derived sector rule BR1. The medium-character property S8 is realised by the working postulate P5, which is logically independent of P1–P4 and P6: it asserts that pointwise internal coordinates of the ordered branch are descriptive redundancies rather than observables. Together, P1–P6, BR1, and DP provide the present structural framework of ECT.

## 2.3 List of postulates

**P1 — Four-dimensional Euclidean arena.** The fundamental arena is a *connected* four-dimensional Euclidean manifold  $\mathcal{M}^4$  with metric

$$ds_E^2 = \delta_{AB} dX^A dX^B, \quad A, B \in \{1, 2, 3, 4\}. \quad (2.1)$$

All four directions, and all points of the arena, are initially equivalent. There is no distinguished time coordinate at the fundamental level.

**P2 —  $O(4)$ -invariant action.** The fundamental action is invariant under global  $O(4)$  rotations:

$$S_E[\Phi] = S_E[\Lambda \cdot \Phi], \quad \Lambda \in O(4), \quad (2.2)$$

where  $\Phi$  denotes the fundamental microscopic field of the minimal scalar realisation developed in this work. In possible future extensions with additional microscopic fields, P2 should be understood as the corresponding  $O(4)$ -covariance requirement on the full microscopic action. This expresses the equivalence of all four directions in the unbroken phase.

**P3 — Minimal scalar microdynamics.** The fundamental field is a real scalar  $\Phi(X)$  on  $\mathcal{M}^4$ . At the bare microscopic level we adopt the minimal local real-scalar realisation:

$$S_E^{\text{bare}}[\Phi] = \int d^4X \left\{ \frac{1}{2} (\partial_A \Phi)^2 + V(\Phi) \right\}, \quad V(\Phi) = -\frac{\mu^2}{2} \Phi^2 + \frac{\lambda}{4} \Phi^4, \quad \mu^2 > 0, \lambda > 0. \quad (2.3)$$

This is the minimal isotropic bare micro-action used throughout the foundational construction. It does not contain the orientation variable  $n_A$  explicitly;  $n_A$  appears only after vacuum ordering.

The double-well potential in P3 is a *two-well*  $\phi^4$  potential encoding a discrete  $\mathbb{Z}_2$  symmetry  $\Phi \rightarrow -\Phi$ . It is not the “mexican hat” potential (which applies to a complex or multi-component field), and does not by itself create a continuous vacuum manifold or the coherent structure later isolated as BR1.

This minimal bare action should not be confused with the most general effective Euclidean functional compatible with P1–P2. Additional gradient-sensitive structures of the type  $P(X)$ ,  $X \equiv (\partial_A \Phi)^2$ , may arise in the ordered-sector analysis and provide the dynamical origin of gradient condensation; they are not inserted into the bare microscopic starting point (see the foundational program described in Section 2 and open problem OP-grad).

**P4 — Ordered vacuum branch.** The physically relevant vacuum sector of ECT belongs to an ordered branch of the  $\Phi$ -medium characterised by a non-zero gradient condensate selecting a preferred direction:

$$\langle \partial_A \Phi \rangle = u_0 \delta_{Aw}, \quad u_0 > 0, \quad (2.4)$$

where  $w \equiv X^4$  and  $u_0$  is the *gradient condensate amplitude*. A representative integrable background of this ordered branch is

$$\Phi_{\text{bg}}(X) = u_0 w + \Phi_*, \quad \Phi_* = \text{const}. \quad (2.5)$$

Thus the physical vacuum is not specified by a homogeneous field value alone but by an ordered branch with nontrivial gradient structure. This background is *not* a stationary point of the bare micro-action P3; detailed analysis of the background splitting is given in Appendix B.

This ordered branch breaks  $O(4) \rightarrow O(3)$  spontaneously and thereby supplies the order parameter needed for the later causal and geometric development. In the minimal bare micro-action P3 this branch is not generated automatically; at the present stage it is introduced as a structural property of the physically realised vacuum sector. Its deeper dynamical origin from a gradient-sensitive Euclidean functional  $P(X)$ ,  $X = (\partial_A \Phi)^2$ , is part of the foundational program (Level Open; OP-grad).

P4 introduces a second amplitude scale distinct from  $\phi_0$ :

Symbol	Definition	Level
$\phi_0 = \sqrt{\mu^2/\lambda}$	local minimum of bare $V(\Phi)$	P3
$u_0 =  \langle \partial_A \Phi \rangle $	gradient condensate amplitude of the ordered branch	P4

These are independent parameters; their relation is not imposed kinematically and requires separate dynamical matching (OP-grad).

**BR1 — Smooth coherent topological sector (derived branch rule; hereafter referred to simply as the coherent branch).** In the smooth infrared coherent sector of the ordered branch selected by P4, low-energy excitations admit a collective description through an effective order parameter

$$\Phi_{\text{eff}} = \rho e^{i\theta}, \quad \rho > 0.$$

If  $\Phi_{\text{eff}}$  is single-valued on a closed contour  $\mathcal{C}$  that does not intersect a defect core, then the phase defines a map  $\mathcal{C} \rightarrow S^1$ , and therefore the winding number is necessarily integer:

$$\oint_{\mathcal{C}} \partial_A \theta dX^A = 2\pi n, \quad n \in \mathbb{Z}. \quad (2.6)$$

Thus the integer winding condition is not an independent fundamental postulate but a topological consequence of the smooth coherent branch of the broken phase.

Configurations with zeros of  $\rho$ , discontinuities of  $n_A$ , or other non-smooth field profiles are not excluded by the full theory; however, for the primary vacuum manifold  $O(4)/O(3) \simeq S^3$  they are not topologically stable domain-wall, string, or monopole sectors (Section 8.10). Their status must therefore be analysed dynamically rather than inferred from topology alone. This is consistent with the broader topological completeness property S10 of the  $\Phi$ -medium: all topological sectors compatible with the vacuum manifold are admissible parts of the theory.

Within the smooth coherent branch, the elementary coherent loop introduces a pre-quantum topological action scale

$$S_{\text{loop,min}} = 2\pi S_0. \quad (2.7)$$

Here  $S_{\text{loop,min}}$  denotes the elementary-loop action evaluated at the characteristic core scale (Section 5.6), not a global variational minimum. The identification of  $S_0$  with the observed  $\hbar$  is discussed later in Section 20.

**P5 — Medium character of the ordered branch.** In the ordered  $\Phi$ -medium, pointwise internal coordinates of the effective order parameter—specifically, the compact phase  $\theta(X)$  and the local orientation  $n_A(X)$  of the ordered branch—are descriptive redundancies of the effective description rather than independently observable degrees of freedom. Local physical observables depend only on invariant gradient and holonomy data of the effective order parameter.

This postulate realises property S8 of the  $\Phi$ -medium within the concrete ordered-branch framework of ECT. It is logically independent of P1–P4 and P6: the passage from “the action is symmetric under global internal rotations” (P2) to “pointwise internal coordinates are locally unobservable” (P5) is a non-trivial physical assertion that distinguishes a deformable continuum medium from a rigid structure.

P5 is motivated by the universal behaviour of known physical media: in a superfluid, the absolute phase at a single point is not an observable—only phase gradients and circulation integrals carry physical information; in a nematic liquid crystal, the pointwise director angle is unobservable—only director gradients and topological defect data are physical; in a crystal, the absolute displacement of a lattice site is unobservable—only the strain tensor (gradient of displacement) is. P5 asserts that the  $\Phi$ -medium of ECT has this same continuum-medium character.

*What P5 does not assert.* P5 does not exclude gauge-invariant *nonlocal* observables such as holonomies, winding numbers, or Wilson-loop data; on the contrary, such quantities are natural in

a medium with compact phase and local frame redundancy. P5 does not by itself determine the gauge coupling constants or the fermion representation content, and it does not produce the  $SU(3)$  colour gauge structure, which requires additional internal degrees of freedom beyond the minimal scalar realisation of P3.

*Central structural consequence.* Since pointwise internal coordinates are redundancies, local redefinitions of  $\theta(X)$  and  $n_A(X)$  must be treated as local gauge redundancies. This requires compensating gauge connections and leads to the ordered-branch gauge architecture  $SU(2) \times U(1)$ . The full derivation is developed in Sections 7.2 and 7.3.

**P6 — Multiplicity of configurations and admissibility of non-uniform ordering.** The configuration space of the  $\Phi$ -medium is non-trivial: no single configuration is singled out a priori as the unique physical realisation (S6). In particular, ordered configurations in the physical vacuum sector need not be globally uniform; spatially varying condensate backgrounds, domain structures, and transition regions are admissible (S9). This postulate does not prescribe the magnitude or functional form of such inhomogeneities; it states only that the ECT framework is not restricted to a single homogeneous ordered configuration.

## 2.4 Operational principle of relationality

In the absence of a fundamental time coordinate, as specified by the arena P1, the relational approach provides a natural and operationally consistent way to define observables: physical observables are ratios between physical subsystems. This is motivated by P1 but does not follow from it as a theorem.

## 2.5 Independence of postulates

The six working postulates P1–P6 are logically independent. In particular, the medium-character postulate P5 is independent of P1–P4 and P6: it cannot be derived from action symmetry, locality, field content, ordering, or configuration multiplicity alone.

- P1 does not follow from P2–P6: neither  $O(4)$  invariance, nor the choice of field content, nor the admissibility of an ordered branch, nor the multiplicity of admissible configurations fixes the existence of a connected four-dimensional Euclidean arena.
- P2 does not follow from P1 and P3–P6: the existence of a Euclidean carrier, a local scalar field, an ordered branch, and a non-trivial configuration space does not by itself enforce global  $O(4)$  invariance of the bare description.
- P3 does not follow from P1, P2, P4, and P6: the specific real-scalar field content and the minimal local micro-action must be stated separately.
- P4 does not follow from P1–P3 and P6: the existence of a physically realised ordered vacuum branch is an additional structural assumption beyond the minimal bare micro-action and the mere admissibility of non-trivial or non-uniform configurations.
- P6 does not follow from P1–P4: the non-triviality of the configuration space and the admissibility of inhomogeneous ordering are additional structural properties not entailed by the minimal scalar micro-action or the ordered branch specification alone.

The coherent branch discussed below is not an additional independent postulate. Its integer winding condition follows once one restricts attention to a smooth single-valued collective phase field in the coherent broken phase.

## 2.6 Discussion of the postulates

### P1 — Euclidean arena

**Physical meaning.** Space and time are not co-equal primary structures of nature. At the fundamental level there exists only a four-dimensional geometric arena in which all directions are indistinguishable. The notions of “before” and “after”, “spatial” and “temporal” are not built into the foundation of the theory: they may emerge from it under certain conditions, but are not postulated from the outset.

This fundamentally distinguishes ECT from all theories that start with a Lorentzian spacetime  $(-, +, +, +)$ : in those theories the distinction between time and space is encoded from the very beginning in the sign of the metric.

**Physical motivation.** Euclidean geometry as a starting structure appears in physics in several independent contexts. In quantum field theory the Wick rotation  $t \rightarrow -i\tau$  (Matsubara formalism [4]) converts the Lorentzian action into a Euclidean one and renders the path integral mathematically well-defined. In the Hartle–Hawking no-boundary proposal [5] Euclidean geometry arises as the natural formulation of the problem of initial conditions in cosmology. In instanton calculations [6] tunnelling configurations are solutions of Euclidean equations of motion. In all these cases the Euclidean space is used as a computational tool or boundary condition. In ECT it is postulated as physically primary — a qualitatively different position.

**On dimensionality.** Postulate P1 does not choose  $d = 4$  arbitrarily. Four-dimensionality is physically motivated: it is the unique dimension for which, after symmetry breaking  $O(d) \rightarrow O(d-1)$ , the coset  $O(d)/O(d-1)$  is three-dimensional, corresponding to the observed three spatial dimensions. See §16.8 for the distinction between topological and force-law dimensionality. The deeper origin of  $d = 4$  remains an open problem (OP0).

**What P1 forbids.** Lorentzian spacetime  $\mathbb{R}^{1,3}$  is not an admissible fundamental arena in ECT. It may arise as an effective structure, but is not built into the foundation.

### P2 — $O(4)$ -invariant action

**Physical meaning.** The laws of physics in the symmetric phase are identical under any rotation in  $\mathcal{M}^4$ . No one of the four directions is dynamically distinguished.

**Physical motivation.**  $O(4)$  is the isometry group of the Euclidean arena  $\mathcal{M}^4$ , i.e. the minimal symmetry group compatible with P1. Invariance of the action under  $O(4)$  means that the theory introduces no additional structure beyond what is already present in the arena.

Any smaller group (e.g.  $O(3)$ ) would already single out one direction explicitly, introducing by hand what should emerge spontaneously in ECT. Any larger group would require fields with non-scalar indices, contradicting P3.  $O(4)$  is the minimal natural choice compatible with the four-dimensional Euclidean arena and the absence of preferred directions.

**Consequence for the effective sector.** Once the vacuum has selected a preferred direction (P4), the most general symmetric rank-2 tensor compatible with the residual  $O(3)$ -symmetry is constructed from  $\delta^{AB}$  and  $n^A n^B$ . Its explicit form and uniqueness are established as Theorem 3.2 in Section 3.3.

**What P2 forbids.** Any action that explicitly singles out one of the four directions of  $\mathcal{M}^4$ . All anisotropy appearing in the theory is spontaneous, not explicit.

### P3 — Minimal scalar microdynamics

**Physical meaning.** The sole fundamental dynamical object of the theory is a real scalar  $\Phi$ . Everything else — effective variables, collective modes, geometric structures — arises from this single field.

**Why a scalar.** A scalar field is the minimal choice compatible with P2: a scalar carries no indices and singles out no direction in the symmetric phase. It is the unique choice for which the fundamental degree of freedom carries no built-in anisotropy.

**Form of the action.** The action (2.3) at the level of P3 contains only an isotropic kinetic term and a potential. The orientation variable  $n_A$  does not appear in this action. Including  $n_A$  in the fundamental action would mean implicitly introducing a second independent degree of freedom, contradicting the minimality of P3.

**On the potential.** The double-well  $\phi^4$  potential is the standard mechanism for spontaneous  $\mathbb{Z}_2$ -symmetry breaking  $\Phi \rightarrow -\Phi$ . Importantly, this potential does not by itself create a continuous vacuum manifold nor generate the coherent phase structure later isolated as BR1; the latter belongs to the effective collective sector. The potential specifies the minimal local microdynamics of  $\Phi$  and defines a local minimum at finite field amplitude  $\phi_0 = \sqrt{\mu^2/\lambda}$  in the microscopic potential. However,  $V(\Phi)$  alone is not sufficient to produce the gradient-ordered vacuum: this is specified separately by P4. The value  $\phi_0$  is a technical characteristic of the micro-potential; the physically central quantity is the gradient condensate amplitude  $u_0$  (P4), which breaks the  $O(4)$ -symmetry.

**What P3 forbids.** At the fundamental level: any additional fields. There are no fundamental spinors, vectors, or tensors. If such objects appear, they do so only as effective excitations or collective variables at a higher level of description.

### P4 — Ordered vacuum branch

**Physical meaning.** The vacuum of ECT is not specified merely by a homogeneous amplitude of the fundamental scalar. The physically relevant sector belongs to an ordered branch in which the mean gradient is non-zero and directed along one of the four Euclidean directions. This ordering is what makes the subsequent broken-phase physics non-trivial.

**Why the gradient is the relevant order parameter.** The expectation value  $\langle \Phi \rangle = \phi_0 \neq 0$  is  $O(4)$ -invariant: a scalar does not distinguish directions and therefore does not by itself break the Euclidean symmetry. By contrast,  $\partial_A \Phi$  transforms as a vector under  $O(4)$ . A non-zero expectation value  $\langle \partial_A \Phi \rangle = u_0 \delta_{Aw}$  selects the direction  $w$  and breaks  $O(4)$  to  $O(3)$ . Within the present minimal single-field ECT framework, the gradient condensate is therefore the minimal order parameter capable of producing directional ordering without introducing additional fundamental fields or explicit anisotropy into the bare micro-action.

**On the status of P4.** In the minimal bare action P3 the standard  $\phi^4$  potential reaches its minimum on homogeneous configurations with  $\partial_A \Phi = 0$ . Therefore the ordered branch of ECT is not yet a theorem of the bare micro-action alone. At this stage P4 is a structural statement about which vacuum branch of the  $\Phi$ -medium is physically realised. This is already more informative than simply postulating a preferred direction by hand: the preferred direction appears only through the ordered branch, not through explicit anisotropy in the microscopic action. A deeper derivation of the ordered branch from a more general gradient-sensitive Euclidean functional  $P(X)$ ,  $X \equiv (\partial_A \Phi)^2$ , with a minimum at  $X = u_*^2 > 0$  is an open foundational problem (OP-grad) and is part of the ongoing development of ECT.

**On notation.** The expectation values  $\langle \Phi \rangle = \phi_0$  and  $|\langle \partial_A \Phi \rangle| = u_0$  have different physical meanings and different dimensions:  $[\phi_0] = \text{GeV}$  and  $[u_0] = \text{GeV}^2$  in natural units. They should not be identified. In the three-scale picture developed in Section 5.1, the gradient condensate amplitude  $\phi_0 \sim \bar{M}_{\text{Pl}}$  sets the primary gravitational scale (Section 5.1).

**The orientation variable.** In the broken phase the collective orientation variable  $n_A$  describes the local direction of the condensate. In the vacuum background  $\langle n_A \rangle = \delta_{Aw}$ . The relation  $n_A = \partial_A \Phi / |\partial \Phi|$  is an identification valid on the ordered branch and in its long-wavelength description; it is not a point-wise algebraic substitution acting at the level of the bare microscopic action.

## BR1 — Smooth coherent topological sector

**Physical meaning.** Not all configurations that are solutions of the equations of motion within the working framework P1–P6 are physically realised. Only those belonging to the coherent sector are admissible: the phase variable of the order parameter is globally consistent and its winding number is an integer.

**Origin of the order parameter.** In the coherent IR sector defined by vacuum ordering P4, low-energy excitations above the condensate at  $E \ll m_\sigma$  admit a collective description through an effective order parameter  $\Phi_{\text{eff}} = \rho e^{i\theta}$ . This is not a fundamental variable of the microdynamics but an IR collective object arising in the broken phase. The phase  $\theta$  belongs to this collective object, not to the real field  $\Phi$ .

**Topological content.** The integer winding condition is determined by the homotopy group  $\pi_1(S^1) = \mathbb{Z}$  [7] and is independent of contour shape or dynamics. The full homotopy classification of the primary vacuum manifold  $O(4)/O(3) \simeq S^3$ , including the topological anti-predictions  $\pi_0 = \pi_1 = \pi_2 = 0$  and the texture/skyrmion sectors  $\pi_3(S^3) = \mathbb{Z}$ , is developed in Section 8.10. Analogous conditions underlie the quantisation of circulation in superfluid helium  $\kappa = h/m$  [8] and of magnetic flux in superconductors  $\Phi_0 = h/2e$  [9]. In both cases the physical quantum arises from the integer-valued topological invariant, not from a separate quantisation postulate. ECT applies the same mathematical structure to the collective phase of the vacuum condensate in four Euclidean dimensions.

**What BR1 excludes from the present reduction.** Within the coherent sector: configurations with fractional winding numbers of the phase, with discontinuities in  $n_A$ , or with zeros of the order parameter. All three classes are mathematically admissible within P1–P6 but do not belong to the physically realisable coherent vacuum sector of ECT.

## P5 / S8 — Medium character

**Physical meaning.** Property S8, realised by the working postulate P5, expresses the fact that the  $\Phi$ -medium is a *continuum medium* rather than a rigid structure. In any physical medium—a crystal, a superfluid, a nematic liquid crystal—the absolute value of internal coordinates (the displacement of a lattice site, the absolute phase of a superfluid order parameter, the pointwise director orientation) is not directly observable. Only gradients, deformations, and holonomies carry physical information. S8 asserts that the  $\Phi$ -medium of ECT has this same character.

**Why S8 is not a repetition of P2 or P3.** P2 states that the *action* is invariant under global  $O(4)$  rotations. P3 states that the action is *local*. S8 (realised by P5) makes a distinct and logically independent assertion about the *observational status* of internal field-space directions: pointwise values of the compact phase  $\theta(X)$  and the local orientation  $n_A(X)$  of the ordered branch are descriptive redundancies, not physical observables.

The distinction is precise:



- P2 says the *action* does not distinguish  $\theta$  from  $\theta + \alpha$  globally.
- S8 says the *description* does not distinguish  $\theta(X)$  from  $\theta(X) + \alpha(X)$  pointwise.

The first is a symmetry of the theory. The second is a redundancy of the description. The passage from symmetry to redundancy is the physical content of S8.

In a rigid structure (e.g. a crystal whose atoms are individually trackable), local orientation could in principle be observed. In a continuum medium, it cannot. S8 asserts that the  $\Phi$ -medium belongs to the latter class.

**Consequences.** S8 has far-reaching structural implications. Since pointwise internal coordinates are redundancies:

- local phase redefinitions  $\theta(X) \rightarrow \theta(X) + \alpha(X)$  are promoted to local redundancies of the compact-phase sector, providing the structural route to a  $U(1)$  gauge connection (Section 7.2);
- local orientation redefinitions  $n_A(X) \rightarrow R_A^B(X) n_B(X)$  are promoted to local redundancies of the ordered orientation sector, providing the structural route to an  $\mathfrak{so}(3) \cong \mathfrak{su}(2)$  gauge connection (Section 7.3);
- the combined local redundancy gives the ordered-branch gauge architecture  $SU(2) \times U(1)$ ;
- the continuity equation for the coherent density becomes structurally tied to the phase-current conservation law, rather than requiring a separate unitarity axiom;
- the ordered-branch gauge-topological structure provides a natural route to an ECT-native baryon-violating framework (Section 16.3).

**Nonlocal observables are not excluded.** S8 excludes pointwise internal coordinates as observables, but does *not* exclude gauge-invariant nonlocal observables such as holonomies, winding numbers, or Wilson-loop data. On the contrary, such quantities are natural in a medium with compact phase and local frame redundancy: they encode the physically meaningful global phase and orientation structure that survives when pointwise data are treated as redundancies.

**What S8 does not assert.** S8 does not by itself determine the gauge coupling constants  $g, g'$ ; it does not derive the electroweak symmetry-breaking pattern  $SU(2) \times U(1) \rightarrow U(1)_{\text{em}}$ ; it does not derive the fermion representation content; and it does not produce the  $SU(3)$  colour gauge structure, which requires additional internal degrees of freedom beyond the minimal scalar realisation of P3.

**Why S8 is natural for a medium.** The ontology of ECT is that of a *medium*: a single scalar field  $\Phi$  fills the Euclidean arena and orders into an effective vacuum branch. For any physical medium, the distinction between “symmetry of the Hamiltonian” and “redundancy of internal coordinates” is standard: the absolute displacement of a crystal in free space is unobservable, the absolute phase of a superfluid is unobservable, the absolute angle of a nematic director is unobservable. S8, and therefore P5, simply states that the same applies to the  $\Phi$ -medium of ECT.

## P6 — Multiplicity and inhomogeneity

**Physical meaning.** The  $\Phi$ -medium is not restricted to a single global configuration. Ordered realisations may include spatially varying condensate backgrounds, domain structures, and transition regions. No globally uniform ordered state is imposed a priori as the unique physical realisation.

**Consequences.** P6 makes spatially varying ordered backgrounds structurally admissible within ECT. This in turn makes later macroscopic constructions with branch-dependent effective quantities conceptually natural, although the explicit dynamical laws must still be derived separately. Domain structures and transition regions are therefore natural constituents of the ordered phase rather than special additions. Likewise, residual scatter in effective phenomenological scales (such as  $g^\dagger$  in the galactic sector) is not excluded a priori, but requires separate dynamical analysis.

**What P6 does not assert.** P6 does not prescribe the magnitude, profile, or dynamical law of spatial variations in the ordered branch. It does not by itself derive  $G_{\text{eff}}(\mathbf{x})$ ,  $u_0(\mathbf{x})$ , or galaxy-by-galaxy scatter relations. It states only that such non-uniform ordered configurations are structurally admissible within the  $\Phi$ -medium.

## 2.7 Three statement types

The following sections use three types of assertions:

- *Theorem* — a strict consequence of the current foundational framework (P1–P6 together with any explicitly stated derived branch rules and branch conditions used in the theorem);
- *EFT consequence* — a result valid within the low-energy expansion over the broken vacuum;
- *Additional assumption* — a statement used to obtain explicit formulae but not a strict consequence of the foundational assumptions and explicitly stated branch conditions (always marked explicitly).

In this foundational section: vacuum selection is given by P4; the coherent branch is introduced as the derived sector rule BR1; the form of  $K^{AB}$  is an EFT consequence (Theorem 3.2); the upper boundary of the Lorentzian window  $\alpha < 4\beta$  requires an additional isotropy assumption.

**Relation to the Level A/B/C classification.** The later sections of this work classify results using a finer-grained Level A / Level B / Level C / Open scheme. The correspondence is approximately: *Theorem* corresponds to Level A; *EFT consequence* corresponds to Level A when the EFT structure has been explicitly derived from the established branch framework, and to Level B when it is structurally reconstructed but not yet fully closed from bare P3 alone; *Additional assumption* corresponds to Level B or Level C. Unresolved items remain Open. This mapping is not a rigid one-to-one identification but a guide to the epistemic status of each result.

## 3 Spontaneous Symmetry Breaking and Emergence of Time

*This section derives the geometric consequences of vacuum ordering (P4): the unique kinetic tensor, the Lorentzian signature condition, the effective metric, and the arrow-of-time architecture. Results A1–A6 establish the Level A backbone of time emergence, with A4–A5 understood in the quadratic ordered sector and the thermodynamic second law remaining Level B (requires Markovian closure).*

The working postulates P1–P6, together with the derived coherent-sector rule BR1, do not yet constitute the full physical theory. This section develops the geometric consequences of vacuum ordering (P4) in three stages. First, we recall the dynamical motivation for gradient condensation and introduce the collective infrared variables of the ordered branch (Sections 3.1–3.2). Second, we derive the unique kinetic tensor of the broken phase and classify all possible metric signatures that can emerge from it (Sections 3.3–3.5). Third, we identify the Lorentzian hyperbolic branch as the physically admissible causal regime and derive the emergent effective metric and arrow of time (Sections 3.6–3.8).

### 3.1 Dynamic motivation for gradient condensation

The minimal bare micro-action P3 does not itself select a gradient-ordered branch: its  $\phi^4$  potential is minimised by homogeneous configurations with  $\partial_A \Phi = 0$ . P4 therefore introduces the ordered branch as a structural property of the physically realised vacuum sector.

A deeper motivation arises naturally if one considers the most general  $O(4)$ -invariant local Euclidean functional compatible with P1–P2. Among the independent  $O(4)$ -scalars built from  $\Phi$  and its first derivatives, the combination

$$X \equiv \partial_A \Phi \partial_A \Phi \quad (3.1)$$

is the lowest-dimensional gradient invariant. (We use  $X$  for the kinetic invariant  $(\partial \Phi)^2$  and  $X^A$  for Euclidean coordinates; the distinction is always clear from context.) Allowing a local functional  $P(X)$  in the Euclidean action,

$$S_E[\Phi] \supset \int d^4 X P(\partial_A \Phi \partial_A \Phi), \quad (3.2)$$

is the minimal  $O(4)$ -invariant extension that couples the action to the gradient magnitude rather than solely to the field amplitude.

If  $P(X)$  has a stationary point at  $X = u_*^2 > 0$ ,

$$P_X(u_*^2) = 0, \quad P_{XX}(u_*^2) > 0, \quad (3.3)$$

then the equations of motion admit stationary configurations with

$$\partial_A \Phi \partial_A \Phi = u_*^2. \quad (3.4)$$

A representative integrable member of this solution family is exactly the background assumed by P4:

$$\Phi_0(X) = u_A X^A + \Phi_c, \quad u_A u_A = u_*^2. \quad (3.5)$$

Since the Euclidean functional depends only on  $u_A u_A$  and not on the direction of  $u_A$ , the family of solutions (3.5) forms a three-sphere of degenerate stationary ordered states. Choosing one particular  $u_A$  spontaneously breaks  $O(4) \rightarrow O(3)$ .

It is natural to decompose the gradient into amplitude and orientation,

$$\partial_A \Phi = u n_A, \quad u \equiv \sqrt{\partial_B \Phi \partial_B \Phi} \geq 0, \quad n_A n_A = 1. \quad (3.6)$$

The scalar field  $u(x)$  describes the *amplitude* of the gradient condensate; the unit vector  $n_A(x)$  describes its local *orientation*. At the background level  $u = u_*$  and  $n_A = \delta_{Aw}$ .

**Status of this section.** The  $P(X)$ -extension of the bare action and the gradient-branch condition (3.3) are presented here as the minimal dynamical motivation for P4, not as a derived consequence of P1–P3. The specific functional form of  $P(X)$ , the numerical value of  $u_*$ , and the relation between  $u_*$  and the bare parameters  $(\mu, \lambda)$  remain open problems of the ECT foundational program (OP-grad, Level Open). The subsequent broken-phase analysis (Sections 3.2–3.8) does not require the microscopic form of  $P(X)$  to be fixed completely. It depends only on the existence of the ordered branch, its collective infrared variables, and the broken-phase EFT parameters  $(\alpha, \beta)$ . The admissibility of the ordered branch as a physical realisation is guaranteed by the structural property S7 of the  $\Phi$ -medium, while non-uniform ordered backgrounds are structurally admissible by S9 and P6.

### 3.2 Collective variables and the ordered-branch infrared EFT

The gradient-sensitive motivation above clarifies why an ordered branch with  $\partial_A \Phi \neq 0$  is natural, but it does not yet specify the appropriate long-wavelength variables of that branch. For the subsequent

development of both the geometric and coherent sectors, it is useful to separate the ordered condensate into its amplitude and orientation components:

$$\partial_A \Phi = u n_A, \quad u \geq 0, \quad n_A n_A = 1. \quad (3.7)$$

Here  $u(x)$  measures the local amplitude of the gradient condensate, while  $n_A(x)$  specifies its local orientation in the underlying Euclidean medium.

At wavelengths large compared with the microscopic condensate scale, the ordered branch admits a local derivative expansion in terms of these collective variables. Before any geometric interpretation is imposed, the minimal Euclidean infrared functional of the ordered branch may be written in the schematic form

$$S_{\text{ord}}^{(E)}[u, n] = \int d^4 X \left[ \frac{Z_u}{2} (\partial_A u)(\partial_A u) + \frac{\mathcal{C}_n}{2} u^2 (\partial_A n_B)(\partial_A n_B) + W(u) + \Lambda_n (n_A n_A - 1) + \dots \right]. \quad (3.8)$$

Here  $W(u)$  is the effective branch potential for the condensate amplitude,  $\Lambda_n$  is a Lagrange multiplier enforcing the unit constraint on  $n_A$ , and the ellipsis denotes higher-derivative or higher-order operators suppressed in the infrared expansion.

Several comments are important.

**(i) This is not yet the geometric branch action.** Equation (3.8) is a pre-geometric infrared description of the ordered condensate branch itself. It does not yet assume the existence of an effective metric, and it does not yet identify gravity with any particular operator. Rather, it provides the minimal collective-variable layer that should exist between the microscopic Euclidean  $\Phi$ -medium and the later macroscopic geometric realisation.

**(ii) Why these variables are natural.** Once the branch condition  $\partial_A \Phi \neq 0$  holds, the decomposition into amplitude  $u$  and orientation  $n_A$  is not an extra postulate but a natural rewriting of the ordered phase. This makes explicit that two qualitatively different kinds of long-wavelength excitations may exist: amplitude fluctuations of the condensate and orientational distortions of the preferred direction.

**(iii) Relation to the subsequent signature analysis.** For a uniform ordered background

$$u = u_*, \quad n_A = \delta_{Aw},$$

the infrared ordered-branch EFT reduces to the background on which the broken-phase kinetic tensor is classified in the following subsections. The symmetry-based uniqueness theorem for  $K^{AB}$  and the Lorentzian viability analysis therefore do not depend on the detailed microscopic form of  $W(u)$ , but only on the existence of the ordered branch and its collective orientation variable.

**(iv) Status.** At the present stage (3.8) should be read as the minimal infrared organisational principle of the ordered branch, not yet as a fully derived theorem from the bare microscopic action P3. Its detailed coefficients ( $Z_u, \mathcal{C}_n$ ), the precise form of  $W(u)$ , and its matching to the later macroscopic gravitational closure remain part of the open foundational programme. Nevertheless, introducing this intermediate ordered-branch EFT removes an important conceptual gap: the theory no longer jumps directly from the bare Euclidean scalar action to macroscopic geometry, but passes through a well-defined collective condensate layer.

**Theorem 3.1** (A pure  $P(X)$  closure does not generate orientation stiffness). *Let the Euclidean action depend only on the gradient invariant  $X \equiv \partial_A \Phi \partial^A \Phi$ :*

$$S_E[\Phi] = \int d^4 X P(X).$$

*Writing the gradient in polar form  $\partial_A \Phi = u n_A$ ,  $n_A n^A = 1$ , one finds  $X = u^2$ . Therefore  $P(X)$  depends only on the modulus  $u$  but neither on the orientation  $n_A$  nor on its derivatives  $\partial_B n_A$ . A functional of the form  $P(X)$  cannot generate a local orientation-stiffness term  $\propto (\partial_B n_A)(\partial^B n^A)$ .*

*Proof.* Since  $n_A n^A = 1$ , one has  $X = (\partial_A \Phi)(\partial^A \Phi) = u^2 n_A n^A = u^2$ . The function  $P(u^2)$  contains  $n_A$  only through the algebraic constraint  $n_A n^A = 1$ ; no derivative of  $n_A$  appears.  $\square$

**Structural consequence.** This theorem implies that the orientation sector of the ordered branch—and therefore the induced gravitational stiffness—lies *beyond* a pure  $P(X)$  closure. It can arise only from next-to-leading-order derivative operators in the  $\Phi$ -medium action, or from quantum (Sakharov-type) contributions generated by integrating out the heavy radial mode  $\sigma$ . In either case, the stiffness coefficient carries dimension  $\text{mass}^{-2}$  and is naturally suppressed by the UV radial scale. This structural restriction connects ECT gravity to the Sakharov induced-gravity programme [3] and distinguishes it from theories that postulate gravitational dynamics directly. At the present stage this should be understood as a structural and interpretive correspondence, not yet as a completed first-principles loop derivation.

**Two-level description of the orientation sector.** There are two distinct but compatible levels of description of the orientation dynamics. At the  $\chi$ -level, the integrability-reduced ordered fluctuation  $\varphi = \chi$  already propagates with the anisotropic kinetic tensor  $K^{AB}$  (Universality Corollary, Section 4.3). This is a two-derivative Level A result sufficient to establish the causal structure and propagation law of the orientation mode. At the  $n_A$ -level, however, one writes an effective action directly for the local orientation field  $n_A$ . The corresponding stiffness term  $\kappa_n (\partial n)^2$  belongs to the NLO/induced sector, because  $n_A$ -gradients correspond to second derivatives of  $\Phi$ . Therefore the propagation of the orientation mode (Level A,  $\chi$ -description) and the gravitational normalisation of the  $n_A$ -sector ( $\kappa_n$ , NLO/induced) are related but logically distinct questions.

### 3.3 Uniqueness of the kinetic tensor after SSB

**Theorem 3.2** (Uniqueness of  $K^{AB}$ ). *Any symmetric rank-2 tensor that is (i) symmetric in  $A, B$ ; (ii)  $O(3)$ -invariant under the residual symmetry; (iii) built locally and algebraically from  $\{\delta^{AB}, n^A\}$  without additional derivatives must take the form*

$$K^{AB} = \beta \delta^{AB} - \alpha n^A n^B, \quad \alpha, \beta \in \mathbb{R}. \quad (3.9)$$

*Proof.* A local algebraic rank-2 tensor compatible with the broken vacuum may depend only on  $\delta^{AB}$  and  $n^A$ . Symmetry in  $A, B$  excludes antisymmetric structures. Without additional derivatives or pseudo-tensors (Levi-Civita is antisymmetric and excluded), the only symmetric rank-2 tensors built from  $\{\delta^{AB}, n^A\}$  are  $\delta^{AB}$  and  $n^A n^B$ . Any such tensor is therefore a linear combination  $K^{AB} = a \delta^{AB} + b n^A n^B$ , which gives (3.9) with  $a = \beta$ ,  $b = -\alpha$ . Full proof via  $O(3)$  representation theory is in Appendix C.  $\square$

This tensor structure underlies the graviton sector discussed in Section 8.5 and the effective Lorentzian metric of the ordered branch.

The broken-phase kinetic action for fluctuations  $\varphi$  is

$$S_{\text{EFT}}^{(2)}[\varphi] = \int d^4 X \left\{ \frac{\beta}{2} (\partial_A \varphi)^2 - \frac{\alpha}{2} (n^A \partial_A \varphi)^2 + \frac{m_{\text{eff}}^2}{2} \varphi^2 \right\}, \quad (3.10)$$

where  $m_{\text{eff}}^2$  is the EFT fluctuation mass parameter, not identified a priori with  $V''(\phi_0)$  of the bare potential. The canonical normalisation  $\tilde{\varphi} = (\sqrt{\alpha - \beta/c_*}) \varphi$  gives a positive free Hamiltonian (Level A):

$$H = \int d^3 x \left[ \frac{1}{2} \pi_{\tilde{\varphi}}^2 + \frac{c_*^2}{2} (\nabla \tilde{\varphi})^2 + \frac{M_{\text{eff}}^2}{2} \tilde{\varphi}^2 \right] \geq 0, \quad (3.11)$$

confirming that the broken-phase EFT is free of tachyon/ghost pathology.

### 3.4 Eigenvalue analysis and signature classification

The ordered vacuum P4 singles out one direction  $n_A = \delta_{Aw}$ , but it does not by itself determine the kinetic properties of fluctuations. The kinetic tensor  $K^{AB}$  is fixed only by the additional EFT parameters  $(\alpha, \beta)$ . For different values of these parameters the broken-phase kinetic operator can be elliptic, degenerate, or hyperbolic. We now classify all three possibilities and identify the physical selection criterion that singles out the Lorentzian hyperbolic branch as the macroscopically admissible causal regime.

With  $n_A = \delta_{Aw}$  (vacuum direction), the tensor (3.9) becomes diagonal:

$$K^{AB} = \text{diag}(\beta, \beta, \beta, \beta - \alpha).$$

Three signature classes:

Condition	Signature	Propagation
$\alpha < \beta$	Euclidean	all directions equivalent
$\alpha = \beta$	degenerate	no propagation along $w$
$\alpha > \beta$	<b>Lorentzian</b>	$w$ becomes time-like

Lorentzian signature is not postulated but follows from  $\alpha > \beta$ , which is an EFT parameter relation. The nontrivial question is therefore not whether the EFT admits a Lorentzian regime, but why the realised ordered vacuum lies in the region  $\alpha > \beta$  rather than on the Euclidean or degenerate side. This is a vacuum-selection problem, not a separate postulate of the theory. The logical order is important. The inequality  $\alpha > \beta$  characterises the entire Lorentzian admissibility region of the broken-phase EFT. The stronger relation  $\alpha = 2\beta$  is not needed for the existence of a Lorentzian branch as such, but follows only after imposing the ECT identification  $c_* = c$ .

**Signature classification, Lorentzian admissibility, and the ECT branch.** The broken-phase kinetic tensor admits three mathematically distinct regimes: the Euclidean branch ( $\alpha < \beta$ ), the degenerate boundary ( $\alpha = \beta$ ), and the Lorentzian branch ( $\alpha > \beta$ ). This classification follows directly from the sign of the  $ww$  component of the ordered-branch kinetic operator.

At the level of the EFT, the first structural conclusion is therefore purely kinematic: only  $\alpha > \beta$  yields a hyperbolic operator and therefore admits a Lorentzian macroscopic propagation sector with a well-posed causal initial-value problem. For  $\alpha < \beta$  the operator is elliptic, so the same equation does not define a propagation problem with causal signal transport. At  $\alpha = \beta$  the operator becomes degenerate and loses the distinguished propagation direction.

The second conclusion is ECT-specific. Among the Lorentzian branch of admissible broken phases, the ordered vacuum corresponding to the observed macroscopic world is further fixed by the independently established identification  $c_* = c$ . Using

$$c_*^2 = \frac{\beta}{\alpha - \beta},$$

the physical identification  $c_* = c$  gives

$$\frac{\beta}{\alpha - \beta} = c^2.$$

In units where  $c = 1$ , this reduces to

$$\alpha = 2\beta.$$

Accordingly, the role of the present section is twofold: first, to show that Lorentzian macroscopic propagation requires  $\alpha > \beta$ ; second, to identify the particular ECT realisation of that branch by the stronger condition  $\alpha = 2\beta$ .

This removes the circular reading. We do not argue that  $\alpha > \beta$  because Lorentzian physics is observed. Rather, the broken-phase EFT itself classifies which parameter region is capable of supporting a Lorentzian

macroscopic branch at all, and the separate ECT result  $c_* = c$  then selects the specific realised point  $\alpha = 2\beta$  within that region.

What remains open is not the Lorentzian admissibility condition  $\alpha > \beta$ , nor the ECT implication  $\alpha = 2\beta$  once  $c_* = c$  is imposed, but the deeper microphysical question of why the realised ordered vacuum of the condensate lands on that branch in the first place. That is a vacuum-selection problem internal to ECT, not an additional postulate of the theory. The quantitative upper bound on  $\alpha$  from short-distance isotropisation is derived in the following section.

### 3.5 The Lorentzian window

The equation of motion from (3.10):

$$\beta \partial_i^2 \varphi - (\alpha - \beta) \partial_w^2 \varphi - m_{\text{eff}}^2 \varphi = 0. \quad (3.12)$$

Dispersion relation:

$$(\alpha - \beta) k_w^2 = \beta \mathbf{k}^2 + m_{\text{eff}}^2. \quad (3.13)$$

The effective propagation speed is:

$$c_*^2 = \frac{\beta}{\alpha - \beta}. \quad (3.14)$$

The Lorentzian window is  $\beta < \alpha < 4\beta$ :

- lower bound  $\alpha > \beta$  (Level A): from hyperbolicity of operator;
- upper bound  $\alpha < 4\beta$  (additional assumption): from short-distance isotropisation; derivation in Appendix D.

**Structural identification**  $c_* = c$ . The identification  $c_* = c$  is a structural consequence of single-field ECT within the minimal phase-to-gauge emergence route. At Level A, all linear modes of the scalar ordered branch share a unique causal cone (Universality Corollary, §4.3). At the coherent-sector level, the compact phase branch is governed by the same broken-phase tensor structure, and the gauge sector inherits the same cone only within the minimal phase-to-gauge construction (§4.7). Accordingly, the status of  $c_* = c$  is Level B structural: it is conditional not only on gauge emergence from the compact phase branch, but also on the absence of an independent leading-order gauge kinetic sector beyond the minimal route. Observational support is provided by the bound  $|c_{\text{GW}} - c_\gamma|/c < 10^{-15}$  [10]. In canonical units ( $\beta = 1$ ) this corresponds to  $\alpha = 2\beta = 2$ .

**LIV time delay: structural benchmark and bounds.** At sufficiently high energies the condensate director sector may induce higher-dimension propagation operators. The coefficient of the leading photon-sector operator is not fixed in the present EFT closure; the unit-coefficient expression below is therefore a benchmark scale, not a retained coefficient-level ECT prediction.

At high energies, higher-dimension operators associated with the ordered-branch tensor may generate an energy-dependent photon time-of-flight delay. The most conservative phenomenological parametrisation is

$$\Delta t_{\text{LIV}} \approx \zeta_\gamma \frac{(\alpha - \beta)}{\beta} \frac{E}{M_{\text{Pl}} c^2} \frac{L}{c}, \quad (3.15)$$

where  $\zeta_\gamma$  is a dimensionless coefficient encoding the sector-specific higher-order EFT matching. The unit-coefficient benchmark  $\zeta_\gamma = 1$  is useful as a scale estimate, but it should not be treated as a retained ECT prediction without the EFT matching.

For  $L \sim 4 \text{ Gpc}$  and  $E \sim 10 \text{ GeV}$  one obtains  $\Delta t_{\text{LIV}} \simeq 0.34 \zeta_\gamma \text{ s}$ . The Fermi-LAT GRB 090510 bound, often quoted as  $M_{\text{QG},1} > 7.6 M_{\text{Pl}}$  for a linear dispersion law, implies roughly  $|\zeta_\gamma| \lesssim 0.13$  for the same sign and propagation model. Thus the unit-coefficient linear photon benchmark is already strongly constrained;

a viable ECT photon-sector LIV signal requires a suppressed coefficient, a different sign/model treatment, or a quadratic leading correction.

**ECT interpretation:** LIV effects are attributed to sub-condensate structure and are expected to be controlled by the same ordered background tensor. In this sense they are not introduced as arbitrary, unrelated sector-by-sector postulates. However, the effective matching coefficients, such as  $\zeta_\gamma$  in the photon sector, may be sector-dependent after integrating out the microscopic condensate degrees of freedom. Their detailed suppression pattern remains part of the higher-order EFT analysis and should not be overstated at the present stage.

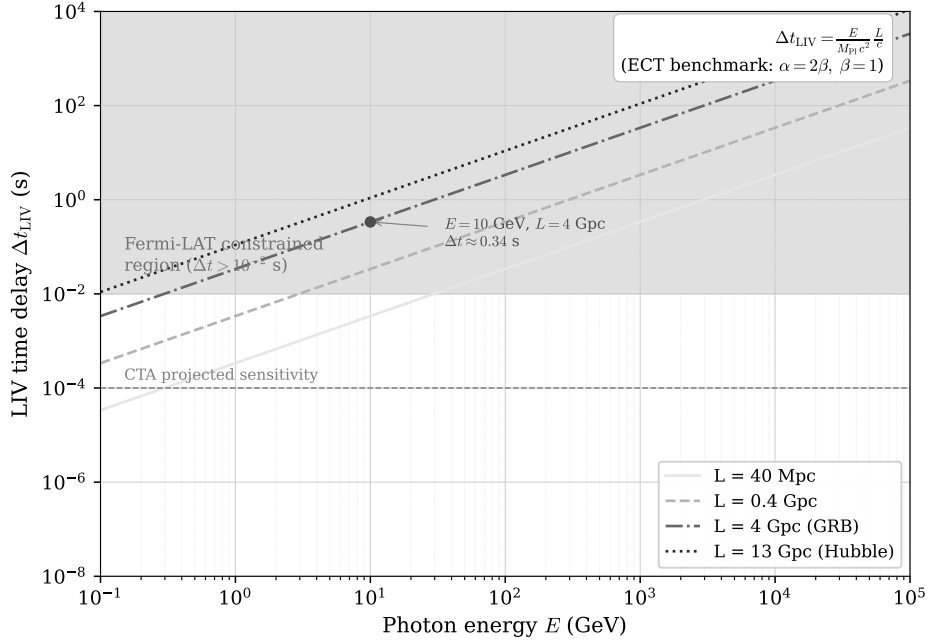


**Figure 2:** Unit-coefficient benchmark for the LIV photon time-of-flight delay  $\Delta t_{\text{LIV}} = \zeta_\gamma (E/M_{\text{Pl}} c^2) (L/c)$  with  $\zeta_\gamma = 1$  in the plotted reference curves (Eq. 3.15), shown as a function of photon energy  $E$  for several source distances  $L$ . The grey band is a schematic indication of the Fermi-LAT linear-LIV constraint scale for short-GRB timing; the actual bound is expressed as  $M_{\text{QG},1} > 7.6 M_{\text{Pl}}$  and depends on the sign, source model, photon-energy range, and intrinsic-lag treatment. The dashed horizontal line indicates the projected CTA sensitivity ( $\sim 10^{-4}$  s). The filled circle marks the unit-coefficient reference point  $E = 10$  GeV,  $L = 4$  Gpc, for which  $\Delta t \simeq 0.34 \zeta_\gamma$  s. This point should be read as a benchmark scale, not as a retained prediction with coefficient one; current Fermi-LAT bounds require a suppressed effective photon coefficient in a linear dispersion model. Numerical details are given in Appendix E.

**Emergent special relativity.** The possibility that an anisotropic kinetic structure on a Euclidean background can yield effective Lorentzian propagation has also been demonstrated in closely related constructions. Girelli, Liberati and Sindoni [1] showed this in a scalar-gradient setting with scalar gravity, and Mukohyama and Uzan [2] later developed a classical clock-field model in which scalar, vector, and spinor sectors propagate in an effective Minkowski metric. In that sense, ECT is not unique in proposing emergent Lorentzian dynamics from a Euclidean substrate. Its distinctive claim is instead that the preferred direction is generated dynamically through spontaneous  $O(4) \rightarrow O(3)$  ordering of the condensate gradient, rather than being imposed as a background clock-field condition.

ECT does not postulate special relativity but derives its kinematic core as an emergent structure of the ordered condensate phase. The  $O(4) \rightarrow O(3)$  SSB generates a hyperbolic kinetic tensor  $K^{AB}$  (Theorem 3.2). In the homogeneous ordered phase, the Lorentzian branch may be parametrised in real time by  $w = c_* t$ , so that the effective metric reduces locally to the Minkowski form  $\eta_{\mu\nu} = \text{diag}(-1, 1, 1, 1)$  in units  $c_* = 1$ , and the isometry group is the Poincaré group. (The Wick/Picard–Lefschetz continuation belongs to the path-integral justification discussed elsewhere and should not be conflated with this



real-time kinematic parametrisation.) The scalar broken-branch sector possesses a unique causal cone (Universality Corollary, §4.3). The phase-sector continuation is controlled by the same ordered-phase tensor (§4.7). Gauge and fermionic sectors inherit the same causal structure only within their respective reconstruction routes (Level B, §4.7, §9). Higher-order Lorentz-violating corrections are expected to be Planck-suppressed and controlled by the condensate structure (3.15). Existing observations constrain such deviations very strongly [10, 11, 12, 13]. Einstein special relativity thus appears as the infrared homogeneous limit of the ordered-branch kinematics of ECT.

### 3.6 Effective Lorentzian metric

At this stage Lorentzian signature has already appeared in the ordered-branch kinetic tensor. The effective real-time variable is therefore introduced by the real parametrisation  $t = w/c_*$ , with  $c_*^2 = \beta/(\alpha - \beta)$ . This is the step used to write the hyperbolic field equation and the effective Lorentzian metric. A separate formal Euclidean–Lorentzian continuation belongs only to the amplitude/path-integral language discussed later in the coherent sector. The Klein–Gordon equation:

$$\partial_t^2 \varphi - c_*^2 \nabla^2 \varphi + M_{\text{eff}}^2 \varphi = 0, \quad M_{\text{eff}}^2 = \frac{m_{\text{eff}}^2 c_*^2}{\beta}. \quad (3.16)$$

Fluctuations see the effective Lorentzian metric:

$$g_{\mu\nu}^{\text{eff}} dx^\mu dx^\nu = -c_*^2 dt^2 + \delta_{ij} dx^i dx^j. \quad (3.17)$$

At  $\alpha = 2$ ,  $\beta = 1$ :  $c_* = 1$  and  $g_{\mu\nu}^{\text{eff}} = \eta_{\mu\nu}$ .

**Free-sector consistency.** The quadratic broken-phase sector admits a canonical normalisation with positive Hamiltonian (3.11) and dispersion  $\omega^2 = c_*^2 k^2 + M_{\text{eff}}^2 \geq 0$ . On the free EFT level the sector is free of tachyonic/ghost pathology and is compatible with a positive spectral representation. This is *not* yet a full OS-reconstruction of the interacting theory, but constitutes a necessary internal consistency check for the future development of the Quantum Sector.

### 3.7 Physical picture: the condensate as the “fabric” of spacetime

The mathematical results admit a concrete physical interpretation.

**The phase transition as the birth of physics.** The  $O(4) \rightarrow O(3)$  transition is not merely a technical symmetry breaking. It is the event that makes physics in the familiar sense possible at all. Before ordering, the Euclidean condensate distinguishes no time, no causal order, no preferred class of propagating excitations. All four directions of  $\mathcal{M}^4$  are equivalent, and there is therefore no “event”, no “evolution”, and no “particle moving along a light cone”. After ordering, one direction becomes distinguished, and the following all arise simultaneously: the causal cone, Lorentzian kinematics, the separation into spatial and temporal coordinates, the excitation spectrum around the ordered background, and the decoherence hierarchy. Time is not added to an already prepared physics; it arises together with it as a property of the ordered phase.

In this sense the  $O(4) \rightarrow O(3)$  transition plays the role of a “crystallisation of the physical world”: before it there is a symmetric Euclidean medium; after it there are causality, time, particles, and geometry as collective properties of the ordered condensate.

**What condenses.** In superfluid helium-II below the Bose–Einstein condensation temperature atoms enter a collective ordered state; the condensate carries all characteristic properties of superfluidity [8]. In ECT the analogous object is the gradient condensate  $\langle \partial_A \Phi \rangle = u_0 \delta_{Aw}$ : field  $\Phi$  “freezes” into a state with non-zero gradient. This is an ordering of the vacuum sector defined by postulate P4, not a condensate in the strict quantum-mechanical sense (QM has not yet been derived at this stage).

**Origin of time.** In the symmetric phase ( $u_0 = 0$ ) all four directions of  $\mathcal{M}^4$  are equivalent. Upon transition to the ordered phase one direction ( $w$ ) is singled out. This makes  $w$  a candidate for the role of “time”. By itself, however, the selection of a direction does not yet yield causality or the arrow of time—those require the kinetic operator to be hyperbolic ( $\alpha > \beta$ ) and the initial configuration to belong to an ordered and smooth coherent branch (P4 + BR1).

**Condensed-matter analogy.** An analogous mechanism is well-known for superconductors: below  $T_c$  Cooper pairs condense and the photon acquires an effective mass—Lorentz invariance is broken spontaneously, not explicitly [14]. In ECT the role of the “breaking” is played by the appearance of the preferred direction  $w$ ; the role of the “effective mass” is played by the different propagation properties along  $w$  and perpendicular to it. Note that in the scalar-only ECT basis, the orientation variable  $n_A$  arising from this breaking is not an independent field but a derived collective variable, subject to integrability constraints (Section 4.3).

**Problem of time in ECT.** ECT also offers a natural structural route toward the problem of time rather than a complete final resolution [15, 16]. In the fundamental Euclidean phase there is no external time coordinate at all: the substrate is genuinely pre-temporal rather than merely Lorentzian with an unspecified clock. Time then appears in three layers. First, no fundamental time exists on the Euclidean substrate. Second, a directed temporal ordering emerges when the  $O(4) \rightarrow O(3)$  symmetry breaking selects a preferred condensate direction and thereby defines the Lorentzian branch. Third, the familiar effectively classical temporality of ordered histories appears only after reduced-state decoherence suppresses interference between alternative condensate histories. In this sense ECT does not begin with time and then quantise it; rather, it provides a structural account of how effective time, causal order, and classical temporality may arise from a deeper pre-temporal condensate description. The strict single-outcome problem is not claimed to be fully solved here and remains part of the open measurement-theory programme discussed later in Part III.

### 3.8 Arrow of time from symmetry breaking

The emergence of a preferred temporal orientation in ECT is one of the most important consequences of the ordered branch. This section presents the *Level A results* concerning directionality: statements that follow rigorously from the postulates and mathematically established properties of the Lorentzian ordered branch, without additional closure assumptions. The full thermodynamic second law, which requires additional Level B ingredients, is developed in Section 3.9.

**Physical picture: why time flows in one direction.** In standard physics the arrow of time is a separate postulate (Penrose’s Past Hypothesis, or a low-initial-entropy condition imposed by hand). In ECT the arrow of time follows from two structural ingredients: (a) the selection of the ordered branch (P4) provides a single definite realisation of the condensate with low initial entropy, rather than an ensemble; (b) the influence functional suppresses off-diagonal histories ( $\Gamma_{\text{irr}} \geq 0$ ), ensuring that interference decreases rather than increases in the forward direction. Irreversibility is not a law of nature imposed from outside, but a statistical consequence of the subsystem’s coupling to a large number of condensate modes. The arrow of time is therefore not mysterious: it is the direction in which the ordered condensate branch was realised.

**Starting point: no external time.** ECT does not assume an external physical time parameter at the foundational level. The Euclidean manifold  $\mathcal{M}^4$  is the fundamental arena, and all temporal notions must emerge from the ordered branch and its effective Lorentzian description. The arrow-of-time problem in ECT is therefore two-layered: first, an effective time direction must emerge from the condensate structure (Sections 3.6–3.5); second, that direction must acquire a preferred orientation. The present section addresses only the second layer, taking the emergent Lorentzian structure as already established.

**Result A1: geometric arrow (branch selection).** Before ordering, the Euclidean  $\Phi$ -medium possesses no distinguished time direction: all four directions of  $\mathcal{M}^4$  are equivalent. After the transition  $O(4) \rightarrow O(3)$ , the ordered branch selects a preferred direction  $w$  through  $\langle \partial_A \Phi \rangle = u_0 \delta_{Aw} \neq 0$ , providing the geometric basis for the effective Lorentzian branch (Section 3.6). The asymmetry originates not from the action itself, but from the realised selection of one ordered orientation. ECT explains the *existence* of a preferred direction as a direct consequence of spontaneous ordering (Level A from P1+P2+P4).

**Result A2: Lorentzian time from the geometric arrow.** The effective metric for perturbations around the ordered branch,

$$G_{\text{eff}}^{AB} = \beta \delta^{AB} - \alpha n^A n^B, \quad (3.18)$$

acquires Lorentzian signature when  $\alpha > \beta > 0$  (Level A; Section 3.4). Once the ordered branch satisfies  $\alpha > \beta$ , the distinguished coordinate  $w$  becomes time-like in the effective kinetic tensor. The corresponding physical time is introduced by the real parametrisation  $t = w/c_*$ , with

$$c_*^2 = \frac{\beta}{\alpha - \beta}.$$

It is only at this point—not before—that the word “time” acquires physical meaning.

**Result A3: retarded propagation in the ordered branch.** Within the Lorentzian ordered branch, the equation of motion for  $\Phi$  admits an explicit symmetric-hyperbolic reduction (Appendix F). By the Leray–Choquet–Bruhat theorem [17, 18], this implies:

$$\boxed{G_{\text{ret}}(t, \mathbf{x}) = 0 \quad \text{for } t < 0.} \quad (3.19)$$

Perturbations of  $\Phi$  propagate only forward in the branch-selected time. This result holds for the full nonlinear dynamics of the single scalar field  $\Phi$  (Level A), not only the quadratic sector (Appendix E). The causal ordering of perturbative events is therefore a mathematical consequence of the postulates, not an additional assumption.

**Result A4: dissipative arrow (quadratic sector).** From the retarded property (3.19) and the non-negative spectral density  $\rho(\mu^2) \geq 0$  of the quadratic ordered branch (stable vacuum, all  $\omega_k^2 > 0$ ), the Kramers–Kronig dispersion relation implies

$$P_{\text{dissip}}(\omega) = -\omega \text{Im} G_{\text{ret}}(\omega) \geq 0 \quad \forall \omega. \quad (3.20)$$

The power absorbed from an external source is always nonnegative: energy dissipates into the ordered medium in the forward time direction, never in reverse (Level A in the quadratic sector).

**Result A5: positive semidefiniteness of the irreversible kernel.** When a subsystem of the ordered branch interacts with the remaining condensate modes, the influence functional takes the Feynman–Vernon form [19]:

$$\mathcal{F}[q, q'] = \exp \left\{ \frac{i}{S_0} \Gamma[q, q'] - \frac{1}{S_0} \Gamma_{\text{irr}}[q, q'] \right\}, \quad (3.21)$$

where  $\Gamma_{\text{irr}}[q, q']$  is the irreversible suppression part. In the quadratic Lorentzian sector, the noise kernel  $D_I(t - t')$  has a nonnegative Fourier transform (since the spectral density  $J(\omega) \geq 0$ ; see Appendix G). By Bochner’s theorem, the quadratic form  $\Gamma_{\text{irr}}$  is positive semidefinite:

$$\boxed{\Gamma_{\text{irr}}[q, q'] \geq 0 \quad \text{for all histories } q \neq q', \quad \Gamma_{\text{irr}}[q, q] = 0.} \quad (3.22)$$

This holds for any spectral density  $J(\omega) \geq 0$ , without requiring the ohmic or Markovian assumptions (Level A in the quadratic sector; Appendix G). The physical consequence is:

$$|\mathcal{F}[q, q']| \leq 1, \quad |\mathcal{F}[q, q']| = 1 \Leftrightarrow q = q'. \quad (3.23)$$

Off-diagonal histories (with  $q \neq q'$ ) are suppressed rather than amplified by the interaction with the condensate environment.

**What A5 does and does not establish.** The positive semidefiniteness of  $\Gamma_{\text{irr}}$  establishes a *directionality* of decoherence: the influence functional suppresses interference between distinct histories, never enhances it. However, this is a statement about the sign of a functional for a given pair of histories, not about monotonicity of entropy in time. In particular, A5 does *not* by itself imply:

- strict monotonicity of a coarse-grained entropy,  $dS/dw \geq 0$ ;
- impossibility of partial recoherence (which can occur in non-Markovian environments);
- a long-time entropy trend without further closure assumptions.

The step from directionality to monotonicity requires the Markovian closure (Section 3.9).

**Status of the causal kernel.** In the ordered Lorentzian branch, retarded support  $K(\tau < 0) = 0$  is established at Level A: first in the quadratic sector (Appendix E), then for the full nonlinear scalar dynamics by explicit symmetric-hyperbolic reduction (Appendix F). What is not yet derived is the full first-principles identification of the open-system response kernel entering the influence functional directly from Euclidean microdynamics, together with the auxiliary bath closures (ohmicity, Markov limit, environment modelling) used in the macroscopic irreversibility estimates. Results A4 and A5 are therefore conditional on those bath-closure assumptions, not on the retarded-support property itself.

**Result A6: branch selection as the basis for a low-entropy initial sector.** Postulate P4 selects a single ordered-branch configuration  $\langle \partial_A \Phi \rangle = u_0 \delta_{Aw}$ : not an ensemble but one definite realisation. This provides the natural microscopic basis for a low-entropy initial sector. The interpretation of this branch as a coarse-grained low-entropy state is Level B, since it depends on the choice of macrovariables and state-counting; a rigorous measure on the configuration space is not yet available. Nevertheless, ECT's initial condition is structurally motivated by the ordered branch itself (P4+S6), unlike the ad hoc Past Hypothesis of standard cosmology [20].

**Combined statement.** ECT derives the geometric and retarded backbone (A1–A3) from the ordered branch directly. In the quadratic open-system reduction, this yields a dissipative arrow (A4) and a directed decoherence structure (A5). The low-entropy interpretation of the initial branch (A6) is then structurally motivated rather than imposed ad hoc.

- (a) an effective time direction exists (A1+A2);
- (b) perturbations of  $\Phi$  propagate only forward (A3);
- (c) energy dissipates only forward (A4, quadratic sector);
- (d) the influence functional suppresses off-diagonal histories rather than amplifying them (A5, quadratic sector);
- (e) the system starts from a single ordered realisation, the natural candidate for a low-entropy sector (A6).

**Why this is not yet the full second law.** The above results establish directionality but not strict monotonicity of entropy. For a generic super-ohmic bath ( $J(\omega) \propto \omega^4$ , the natural ECT scaling; Appendix H), temporary partial recoherences are not excluded. The step to strict monotonicity requires additional closure assumptions (Section 3.9).

**Compatibility with variational dynamics.** There is no contradiction between emergent irreversibility and the variational principle of the underlying medium. At the fundamental level, configurations of the  $\Phi$ -medium remain extremals of  $S_E[\Phi]$  (Section 6.6). Irreversibility arises not from a breakdown of variational dynamics, but from coarse graining: many microscopically distinct branch configurations correspond to the same effective macroscopic description, and the larger coarse-grained state space is naturally explored as order becomes less perfectly coherent.

**Comparison with other approaches.** *Penrose-type low-entropy cosmology* [20]: ECT agrees with the need for an exceptional initial state, but differs in interpretation: the ordered branch provides the natural candidate, so the low-entropy condition is tied to the onset of condensate ordering (A6) rather than imposed from outside.

*Spontaneous symmetry breaking in condensed matter* [21]: ECT follows the same broad structural logic, but with a deeper role for the order parameter: ordering is not merely a property of matter inside spacetime, but part of the very origin of effective spacetime structure itself.

*Cosmological arrow without external time* [22]: ECT is naturally suited to this problem: the ordered branch generates an internal time orientation from within the Euclidean medium (A1+A2), while the directional decoherence structure (A5) provides a physical mechanism for the orientation to become consequential.

*Caldeira–Leggett open-system theory* [23]: The standard framework requires an ohmic spectral density and Markov approximation to derive strict entropy growth. ECT’s result A5 is more general in one respect:  $\Gamma_{\text{irr}} \geq 0$  holds for *any* nonnegative spectral density, not only ohmic. However, strict monotonicity still requires the Markov closure, as in the standard framework.

#### Status summary.

Statement	Status	Comment
A1: Ordered branch selects preferred direction $w$	A	P1+P2+P4; SSB
A2: Lorentzian time orientation emerges	A	$\alpha > \beta$ ; §3.6
A3: Retarded propagation of $\Phi$ , $G_{\text{ret}}(t < 0) = 0$	A	Leray–Choquet–Bruhat; App. F
A4: Dissipative arrow $P_{\text{dissip}} \geq 0$	A	Kramers–Kronig + $\rho \geq 0$ ; quadratic sector, with the causal-kernel identification discussed below
A5: Positive semidefiniteness of $\Gamma_{\text{irr}}$ (any $J(\omega) \geq 0$ , no ohmic/Markov)	A	Bochner; quadratic sector; with the causal-kernel identification discussed below; App. G
A6: Single ordered branch realised	A	P4: branch selection
Low-entropy interpretation of initial branch	B	Depends on coarse graining
Retarded structure of ordered $\Phi$ -branch	A	App. F
Open-system bath-kernel identification from Euclidean microdynamics	C (open)	OP1, OP5
Strict monotonicity $dS/dw \geq 0$ at all times	B	Requires Markov; §3.9
Full microscopic H-theorem	C (open)	OP1, OP5, OP-Q17

### 3.9 The second law of thermodynamics in ECT

*Status: layered. The directional architecture of the arrow of time is Level A (Section 3.8). The thermodynamic second law  $dS_{\text{ent}}/dw \geq 0$  for macroscopic systems is Level B: it requires the effective ohmic*

and Markovian closure in addition to the Level A backbone. The full microscopic  $H$ -theorem from bare postulates alone remains open (OP1, OP5, OP-Q17).

The thermodynamic second law in ECT is not postulated. It is built on the Level A directional architecture of Section 3.8 together with two additional effective-closure assumptions. The present section develops the Level B part of the story.

**The second law as a Level B extension of the arrow of time.** Section 3.8 established that in the quadratic open-system reduction the irreversible kernel is positive semidefinite ( $\Gamma_{\text{irr}} \geq 0$ ; A5), so off-diagonal histories are suppressed rather than amplified. This gives the directionality of decoherence. What it does not yet give is *strict monotonicity* of a coarse-grained entropy at every instant. For a generic super-ohmic bath ( $J(\omega) \propto \omega^4$ , the natural ECT scaling; Appendix H), temporary partial recoherences are structurally possible. The step from directionality to monotone entropy growth requires two additional closure assumptions.

**The Boltzmann analogy.** The logical structure is directly parallel to Boltzmann's kinetic theory: variational microdynamics of the condensate plus a single realised ordered branch (A6), interpreted as statistically exceptional once S6 and coarse graining are taken into account, yields irreversible macroscopic behaviour. The Loschmidt tension is addressed at the same structural level as in Boltzmann-type reasoning: the microscopic dynamics remains reversible, but the realised initial sector is statistically exceptional, so time-reversed macroscopic histories are not typical. What ECT adds beyond classical statistical mechanics is a structural explanation of why the initial condition is special: it is tied to ordered-branch selection, not imposed ad hoc.

**Statistical speciality of the ordered branch (Level B).** The structural property S6 states that no configuration of the  $\Phi$ -medium is privileged *a priori*. Against that background, the coherent ordered branch selected by P4 is statistically special: it is a highly organised and constrained subset of the full configuration space. Disordered states are expected to dominate the admissible state count, while the realised ordered branch corresponds to a highly constrained subset, naturally interpretable as a low-entropy sector at the coarse-grained level. This argument is Level B because it invokes state-counting without a rigorous measure on configuration space. It strengthens the structural motivation of A6.

**Entropy growth from inhomogeneous ordering (Level B).** The structural property S9 states that ordering need not be globally uniform: ordered domains, transition regions, local misalignments, and slowly varying branch backgrounds are all admissible. As the branch evolves, coarse-grained descriptions generically explore a larger class of such partially ordered configurations than the initially coherent state. The number of coarse-grained states accessible through domain-boundary structure is expected to increase as domains expand and interact, supporting  $dS_{\text{ent}}/dw \geq 0$  at the domain-structure level. This is a structural Level B heuristic, not a first-principles derivation.

**Topological defects and domain production (Level B).** The topological completeness property S10 further strengthens this picture. The ordered branch may contain or generate domain walls, textures, defect cores, or other transition structures. Such objects are not external additions to the theory but admissible configurations of the  $\Phi$ -medium itself (Section 6.7). Their formation, interaction, and coarse-grained proliferation provide natural channels through which an initially coherent ordered state can lose ideal uniformity and populate a broader macroscopic ensemble, thereby supporting the thermodynamic arrow (Level B from S9+S10).

**Two Level B closure assumptions.** To proceed quantitatively from the Level A directional results to strict entropy monotonicity, two effective working assumptions are needed. The scale analysis of Appendix H shows that the standard 3D Goldstone-like environment gives a super-ohmic spectral density  $J(\omega) \propto \omega^4$ . A strict monotonicity statement requires an additional step:

(i) *Effective ohmic regime:*

$$J(\omega) \approx N_{\text{eff}} \gamma \omega, \quad (3.24)$$

adopted as a phenomenological reduction (Level B). This may arise from non-standard coupling form, reduced effective bath dimensionality, or coarse-graining.

(ii) *Markovian regime:*

$$\tau_{\text{env}} \ll \tau_{\text{dec}}, \quad (3.25)$$

where  $\tau_{\text{env}} \sim m_{\sigma}^{-1}$  is the bath memory time and  $\tau_{\text{dec}} = 1/(N_{\text{eff}}\gamma)$  is the decoherence time (Level B).

**Working entropy-growth law.** Under the ohmic and Markovian assumptions (3.24)–(3.25):

$$\frac{dS_{\text{ent}}}{dw} = N_{\text{eff}} \gamma \left( \frac{dq}{dw} \right)^2 \geq 0. \quad (3.26)$$

The sign is anchored in the Level A retarded structure; the explicit form requires the Level B closure (see Section 26.1 for the full derivation).

**Statistical suppression of time-reversed trajectories.**

$$\frac{P_{\text{back}}}{P_{\text{fwd}}} = \exp \left( -2N_{\text{eff}} \gamma \Delta w \cdot \frac{(\Delta q)^2}{\ell^2} \right). \quad (3.27)$$

For a macroscopic system (1 mol,  $T = 300$  K,  $\Delta w = c \cdot 1$  ns): exponent  $\approx 3.6 \times 10^{33}$ , so  $P_{\text{back}}/P_{\text{fwd}} \approx 0$ . For  $N_{\text{eff}} \sim 1$ : exponent  $\sim 10^{-15}$ , quantum reversibility recovered. The second law is statistical rather than absolute: it holds overwhelmingly for macroscopic systems and naturally weakens for quantum-scale ones.

**Three regimes.**

- **Cosmological:** ordered branch defines cosmic arrow; thermodynamic arrow is effectively exact.
- **Macroscopic** ( $N_{\text{eff}} \gg 1$ ): reverse trajectories exponentially suppressed; second law holds to overwhelming accuracy.
- **Quantum** ( $N_{\text{eff}} \sim 1$ ): fine-grained phases not washed out; effective reversibility recovered.

This three-regime picture is consistent with the  $S_0$ -controlled divide (Section 5.6): when action differences between competing histories satisfy  $|\Delta S| \sim S_0$ , relative phases cannot be suppressed and the classical irreversible description breaks down.

**What remains open.**

- A full microscopic H-theorem from bare postulates alone (OP1, OP5, OP-Q17).
- A first-principles derivation of the ohmic and Markovian closure from the condensate microstructure (OP-Q15).
- A first-principles identification of the effective open-system bath-response kernel from ECT microdynamics; retarded support  $K(\tau < 0) = 0$  itself is already Level A for the ordered branch (OP1, OP5).
- Entropy production in strongly nonlinear branch dynamics.
- A rigorous measure on the configuration space (which would promote the state-counting argument from Level B to Level A).

**Status summary. Table A: Level A directional backbone (from Section 3.8).**

Statement	Status	Comment
Retarded propagation of $\Phi$	A	Full nonlinear; App. F
Dissipative arrow $P_{\text{dissip}} \geq 0$	A	Kramers–Kronig; quadratic sector
$\Gamma_{\text{irr}} \geq 0$ (positive semidefiniteness)	A	Any $J \geq 0$ ; quadratic sector; App. G
Single ordered branch realised	A	P4: branch selection

**Table B: Level B extension (this section).**

Statement	Status	Comment
Low-entropy interpretation of initial branch	B	Coarse-graining / state-counting
Statistical speciality of initial branch	B	S6; no rigorous measure
Entropy growth from domain dynamics	B	S9+S10 + coarse graining
Open-system bath-kernel identification from Euclidean microdynamics	C (open)	OP1, OP5
Ohmic effective closure	B	Phenomenological reduction
Markov effective closure	B	$\tau_{\text{env}} \ll \tau_{\text{dec}}$ heuristic
$dS_{\text{ent}}/dw \geq 0$ at all times	B	Ohmic + Markov + Level A backbone
Explicit formula (3.26)	B	Under ohmic/Markov closure
Quantum reversibility for $N_{\text{eff}} \sim 1$	B	Consistent with §5.6
Full microscopic H-theorem	C (open)	OP1, OP5, OP-Q17

### 3.10 Comparison with other theories

**Einstein–aether theory [24].** In Einstein–aether theory the anisotropy is introduced by a postulated aether vector field  $u^A$ ; it does not arise spontaneously. In ECT the orientation variable  $n_A$  is a collective variable of the broken phase—it enters the kinetic EFT tensor, not the bare action P3. The anisotropy is entirely spontaneous. A systematic comparison of emergent-gravity approaches is given in Section 8.5.

**Hořava–Lifshitz gravity.** This theory introduces explicit anisotropy between space and time by construction, breaking Lorentz invariance explicitly at the fundamental level. In ECT Lorentz invariance of the fundamental action is preserved (P2) and broken only spontaneously.

**CDT (Causal Dynamical Triangulations) [25].** In CDT the Lorentzian structure is imposed as a constraint on the lattice geometry. In ECT geometry is secondary to the field  $\Phi$  and the metric is emergent.

**Hartle–Hawking no-boundary proposal [5].** Both approaches use a Euclidean arena, but for Hartle–Hawking it is a computational tool for defining path integrals. In ECT the Euclidean manifold is the fundamental arena, not a mathematical device.

**Summary.** In ECT the Lorentzian signature and physical time arise from the  $O(4) \rightarrow O(3)$  ordering of a single scalar vacuum sector; the arrow of time is strongly motivated by the same structure and becomes quantitative in the decoherence analysis (Section 26.1). Unlike Einstein–aether [24] and Horava–Lifshitz [26], the anisotropy is entirely spontaneous. Unlike CDT, geometry is secondary to field  $\Phi$ . Unlike Hartle–Hawking, the Euclidean arena is fundamental.



An additional ECT-specific feature distinguishes it from generic internal-symmetry-breaking theories: because the ordered quantity  $Q_A = \partial_A \Phi$  is an exact one-form rather than an independent multiplet, the orientation sector is subject to an integrability constraint that reduces the naive  $O(4)/O(3)$  Goldstone content (Appendix I). This has no analogue in standard internal SSB frameworks.

**Universality of the causal cone.** The integrability constraint has a direct consequence for the universality of the emergent causal cone. In Einstein–aether theory [24, 27], the aether vector is an independent dynamical field with four free kinetic coefficients; different spin sectors generically propagate at different speeds, and universality requires fine-tuning. In the SME [28, 29], each sector carries an independent set of Lorentz-violation parameters. In the He-3 analogy [21], different quasiparticle species can see different cones. In ECT, the fundamental field is one ( $\Phi$ ), the kinetic tensor is one ( $K^{AB}$ ), and integrability reduces all linear soft modes to derivatives of one scalar  $\chi$ . There are no free sector-dependent Lorentz-violation coefficients at the leading linear level (Universality Corollary, §4.3). A detailed comparison of speed structures is given in Appendix J.

**Forward connection to the Principle of Euclidean Stationarity.** The signature analysis of the broken-phase EFT provides the structural precondition for the Principle of Euclidean Stationarity introduced in Section 29 of Part III. PES does not determine the sign choice  $\alpha > \beta$  and does not replace the argument leading to  $c_* = c$ . Rather, once the Lorentzian ordered branch is identified and its ECT realisation is fixed by  $\alpha = 2\beta$ , PES organises the persistent observable configurations within that branch as those that are simultaneously phase-compact, Euclidean-stationary, and minimally exposed to environmental locking. The  $\alpha \rightarrow \beta$  boundary, at which  $c_* \rightarrow \infty$  and the Lorentzian structure degenerates, then acquires a further physical interpretation through PES (§29.8).

## 4 Spectrum and Effective Dynamics of the Broken Phase

*This section organises the excitation spectrum of the broken phase: amplitude, orientation, and macroscopic branches; the integrability constraint on the soft sector; and the resulting hierarchy of effective modes. Most results are Level A/B within the ordered-phase EFT. The explicit Goldstone mass mechanism and the complete soft-sector EFT remain open.*

After postulate P4 has selected the gradient-ordered vacuum sector and the derived coherent-sector rule BR1 has identified the smooth coherent branch, the next step is to determine which excitations exist above this vacuum and what their effective dynamics is.

### 4.1 Polar decomposition and collective variables

The background field is given by postulate P4:

$$\Phi_{\text{bg}}(X) = u_0 w + \Phi_*, \quad \partial_A \Phi_{\text{bg}} = u_0 \delta_{Aw}. \quad (4.1)$$

In the broken phase the polar decomposition of the gradient is:

$$\partial_A \Phi = (u_0 + \sigma) n_A, \quad (4.2)$$

where  $\sigma(X)$  is the amplitude (radial) fluctuation and  $n_A(X)$  is the orientation collective variable with vacuum value  $\langle n_A \rangle = \delta_{Aw}$ .

**Status of  $n_A$ .** The orientation variable belongs to the vacuum level of description (P4); it is not a second fundamental microscopic degree of freedom and does not appear in the fundamental action. The role of the heavy radial excitation  $\sigma$  in the particle spectrum is discussed in Section 8.3.

### 4.2 Sector map: amplitude, soft orientation, and macroscopic $\phi$ -sector

Three qualitatively distinct structures must be kept separate throughout the rest of the theory.

**Amplitude mode  $\sigma$  (radial fluctuation).** A fluctuation of  $|\partial\Phi|$  around the uniform ordered background  $u_0$ .

- Nature: UV fluctuation of the condensate amplitude.
- Mass scale: heavy, with the characteristic radial scale expected to be set by the local curvature of the condensate potential ( $m_\sigma^2 \sim V''(\phi_0)$ ) as a representative estimate; explicit EFT matching remains open, OP-grad; cf. (5.12)).
- Role: integrates out at  $E \ll m_\sigma$ ; stabilises the ordered branch and sets the UV cutoff of the broken-phase EFT.
- It is not the Standard-Model Higgs boson.

**Soft orientation sector.** A broken-branch orientation sector can be introduced by writing

$$Q_A \equiv \partial_A \Phi = u n_A, \quad u = |Q|, \quad n_A n^A = 1. \quad (4.3)$$

At the purely geometric level the ordered branch selects a preferred direction and breaks  $O(4) \rightarrow O(3)$ , so that the vacuum manifold is  $O(4)/O(3) \simeq S^3$ . At the level of naive broken-generator counting this sector is three-dimensional, but in the scalar-only basis its propagating soft content is reduced by integrability, as shown below. However, in the present scalar-only ECT basis  $Q_A$  is not an arbitrary vector field but an exact one-form,  $Q_A = \partial_A \Phi$ . Therefore the orientation sector is subject to the integrability constraint

$$\partial_A Q_B - \partial_B Q_A = 0. \quad (4.4)$$

This sharply reduces the naive Goldstone counting; see Section 4.3 and Appendix I. The particle-spectrum interpretation of the surviving soft mode  $\chi$  is discussed in Section 8.2.

**Macroscopic  $\phi$ -sector.** Slow classical spatial variations of the ordered background on galactic and cosmological scales.

- Nature: classical infrared background variation rather than a UV quantum excitation.
- Characteristic scale: kpc–Gpc.
- Role: gives rise to  $G_{\text{eff}}(\mathbf{x})$  and to the macroscopic gravitational closure (Section 11).
- Relation to  $\sigma$ : distinct— $\sigma$  is a UV fluctuation of the condensate amplitude, whereas the macroscopic  $\phi$ -sector is a slow classical variation of the ordered background itself.

**Key consequence.** The rotation-curve and RAR/BTFR success of ECT (Section 11) uses only the macroscopic  $\phi$ -sector. It does not rely on the Goldstone/soft-orientation discussion below. Conversely, the soft orientation sector must not be used as a dark-matter patch for phenomena already explained by the macroscopic  $\phi$ -closure.

### 4.3 Integrability and the status of the orientation sector

The crucial point is that in the current ECT basis the ordered quantity is  $Q_A = \partial_A \Phi$ , so the decomposition  $Q_A = u n_A$  does *not* define independent fields  $u$  and  $n_A$ . Instead they must satisfy the exact integrability condition

$$\partial_A (u n_B) - \partial_B (u n_A) = 0. \quad (4.5)$$

Linearising around the ordered background  $Q_A^{(0)} = u_0 \delta_{Aw}$  and writing

$$u = u_0 + \sigma, \quad n_A = (\pi_i, 1) + \mathcal{O}(\pi^2), \quad (4.6)$$

one finds  $\delta Q_i = u_0 \pi_i$ ,  $\delta Q_w = \sigma$ . Since  $\delta Q_A$  must itself be a gradient, there exists a scalar fluctuation  $\chi$  such that  $\delta Q_A = \partial_A \chi$ , hence

$$u_0 \pi_i = \partial_i \chi, \quad \sigma = \partial_w \chi. \quad (4.7)$$

Therefore the apparent orientation triplet is not an independent set of three propagating microscopic modes: at the linear scalar-only level it reduces to *one longitudinal soft scalar degree of freedom*  $\chi$ . Equivalently,  $\varepsilon_{ijk} \partial_j \pi_k = 0$ , so the transverse/vortical part of the naive orientation sector is eliminated.

**Interpretation: inverse-Higgs-type reduction.** This is an inverse-Higgs-type reduction [30, 31] characteristic of spacetime symmetry breaking: the broken object  $Q_A = \partial_A \Phi$  is a geometric gradient rather than an internal multiplet. One must therefore distinguish two statements:

1. the ordered branch geometrically breaks  $O(4) \rightarrow O(3)$  and admits a minimal  $O(4)/O(3) \simeq S^3$  orientation description;
2. in the strict scalar-only microscopic theory, the independent soft content surviving at the linear level is only *one longitudinal scalar mode*  $\chi$ .

The full technical derivation is given in Appendix I.

**Corollary: universality of the emergent causal cone within the linear scalar branch.** The integrability result has a further consequence that distinguishes ECT from multi-field Lorentz-violation frameworks [24, 27, 26, 28, 21].

*Corollary (single-field causal universality).* In the scalar-only ECT basis, the ordered-branch variable  $Q_A = \partial_A \Phi$  is an exact one-form. The integrability condition (4.5) reduces all linear soft excitations  $(\sigma, \pi_i)$  to derivatives of a single scalar fluctuation  $\chi$  (4.7). The linear ordered branch therefore possesses a unique principal symbol, fixed by the kinetic tensor  $K^{AB}$  (Theorem 3.2), and hence a unique emergent causal cone with speed  $c_*^2 = \beta/(\alpha - \beta)$  (3.14).

*Proof.* From (4.7),  $\sigma = \partial_w \chi$  and  $\pi_i = \partial_i \chi/u_0$ . The quadratic EFT action becomes  $S^{(2)} = \frac{1}{2} \int d^4 X K^{AB} \partial_A \chi \partial_B \chi$ , which is one equation for one field. Its characteristics satisfy  $\beta \mathbf{k}^2 - (\alpha - \beta) k_w^2 = 0$ , defining a single cone with speed  $c_*^2 = \beta/(\alpha - \beta)$ . Since  $\sigma$  and  $\pi_i$  are derivatives of  $\chi$ , no second independent principal symbol exists.  $\square$

*Scope and limitations.* This corollary establishes causal-cone universality only for the linear scalar ordered branch generated by the single-field integrability structure. The extension to phase, gauge, and fermionic sectors requires additional construction steps and is not part of the present Level A statement: gauge emergence (§7), spinorial reconstruction (§9). Those extensions are discussed in §4.7 and carry Level B status.

*Contrast with competing frameworks.* In Einstein–aether theory [24, 27] the unit vector  $n^\mu$  is an independent dynamical field with four free kinetic coefficients  $c_1 \dots c_4$ . Different spin sectors generically propagate at different speeds; universality of the causal cone requires fine-tuning of the  $c_i$ . In Hořava–Lifshitz gravity [26] different sectors may acquire distinct UV dispersion relations. In the Standard Model Extension (SME) [28, 29] each sector carries an independent set of Lorentz-violation coefficients; universality is not a structural consequence. In the He-3 analogy of Volovik [21] different quasiparticle species can see different effective light cones. In ECT none of these issues arises at the leading linear level, because the fundamental field is one ( $\Phi$ ), the kinetic tensor is one ( $K^{AB}$ ), and all linear soft modes are derivatives of one scalar ( $\chi$ ). A detailed comparison of speed structures is given in Appendix J.

#### 4.4 Minimal soft orientation EFT and phenomenological status

Although the strict scalar-only microscopic content is reduced by integrability, it remains useful to organise the broken branch by a minimal orientation EFT. In that effective description the vacuum manifold  $O(4)/O(3) \simeq S^3$  supports a three-component orientation map, but this must be understood as an *effective parametrisation*, not as a theorem about three independent physical Goldstone particles.

**Quadratic soft-sector EFT.** If the broken-phase EFT contains the local orientation-elastic term  $\frac{\mathcal{C}_n(u)}{2} u^2 (\partial_B n_A) (\partial^B n^A)$ , then at uniform background  $u = u_0$  the effective stiffness is

$$\kappa_n = \mathcal{C}_n u_0^2. \quad (4.8)$$

This is a Level B EFT identity. The coefficient  $\mathcal{C}_n$  carries dimension  $\text{mass}^{-2}$  (so that  $[\kappa_n] = \text{mass}^2$ , as required for a spin-2 normalisation scale) and is not yet derived from bare postulates P1–P6. A pure  $P(X)$  closure cannot generate this term (Theorem 3.1); the orientation-stiffness sector first appears at next-to-leading derivative order (Section 5.1).

In the minimal EFT the surviving mode  $\chi$  has a linear soft dispersion relation

$$\omega^2 = c_\chi^2 k^2, \quad c_\chi^2 = \frac{K_s}{K_w} c_*^2, \quad (4.9)$$

where  $K_w, K_s$  are EFT stiffness coefficients along  $w$  and spatial directions respectively. The stronger statement  $c_\chi = c_*$  requires  $K_s = K_w$ , which is not yet established.

**What remains true, and what does not.** Without the medium-character postulate P5, there is no local  $O(3)$  gauge structure at the level of P1–P4 and P6 alone, hence no Higgs-type eating mechanism in the foundational sector [32]. Any electroweak interpretation requires an additional scale  $v_2 \sim 246$  GeV and a second dynamical step (OP-EW).

The soft orientation sector must *not* be used as a dark-matter replacement for macroscopic phenomena already explained by the  $\phi$ -sector. At most, the broken phase contains a constrained soft longitudinal mode whose phenomenological role remains open.

#### 4.5 EFT quadratic action for fluctuations

*Status: EFT consequence (Theorem 3.2 applied to the broken-phase EFT).*

After integrating out the heavy radial mode ( $E \ll m_\sigma$ ), the effective quadratic action for soft fluctuation  $\phi$  takes the form (3.10) with the kinetic tensor (3.9). The EFT motivation for this form via integrating out  $\sigma$  is detailed in Appendix K.

#### 4.6 Mode hierarchy and the branching structure

Mode	Scale	Role
Radial $\sigma$	$E \sim m_\sigma$	UV cutoff of EFT; integrates out for $E \ll m_\sigma$
Orientation $\delta n_i$	$E \ll m_\sigma$ , soft	Geometric sector; in scalar-only ECT reduced by integrability to one longitudinal scalar $\chi$ (Level B; see Section 4.3)
Scalar $\phi$	$E \ll m_\sigma$	Scalar excitations of Lorentzian sector
Phase $\theta$	Topological sector	Coherent IR; pre-quantum action scale

**Effective-metric tensorial sector of the geometric branch.** *Terminological note:* “spin-2” is used here in the classical group-theoretic sense of a rank-2 symmetric tensor under spatial rotations; no quantisation assumption is involved.

A direct fluctuation of the orientation variable  $\delta n_i$  carries vector rather than tensor character. The tensorial sector appears only after projection into the induced effective metric  $g_{AB}^{\text{eff}}(n)$ : small orientation fluctuations generate symmetric effective-metric perturbations  $h_{\mu\nu}$ , and it is this induced metric perturbation that admits a linearised massless rank-2 interpretation.

In the scalar-only basis, however, the naive three-component orientation triplet is reduced by integrability to a single longitudinal scalar mode  $\chi$  (Section 4.3). Thus the tensorial effective-metric sector is not an independent three-component particle multiplet of orientation modes. Its full interpretation as the graviton sector is developed in Section 8.5.

#### 4.7 Causal cone inheritance by the phase and gauge sectors

The Universality Corollary (§4.3) establishes a unique causal cone for the linear scalar ordered branch. This subsection traces how that cone is inherited by the phase and gauge sectors.

**Physical significance: why a single cone matters.** A decisive test of any emergent-spacetime framework is whether different low-energy sectors inherit a single causal structure rather than sector-dependent propagation cones. In many modified-gravity and Lorentz-violating frameworks, different fields can have different limiting speeds, destroying universal relativistic kinematics. In ECT the universality of the causal cone is not postulated but inherited from the single ordered condensate background: all low-energy excitations see the same kinetic tensor  $K^{AB}$ , determined by the symmetry of SSB (Theorem 3.2). The observational confirmation  $|c_{\text{GW}}/c - 1| < 6 \times 10^{-15}$  (GW170817 [10]) is therefore not a coincidence but a consistency check of the single-cone architecture. This is in contrast to, e.g., Einstein-aether theory [24], where different sectors may generically have different speeds.

**Phase sector (Level A/B bridge).** The phase  $\theta$  enters ECT through the polar decomposition  $\Phi_{\text{eff}} = \rho e^{i\theta}$ . At wavelengths large compared to the radial-mode scale, the effective phase action takes the form (21.2):

$$S_\theta = \frac{K_\theta^{\text{eff}}}{2} \int d^4X g_{\text{eff}}^{AB} \partial_A \theta \partial_B \theta + S_{\text{higher}},$$

The phase-sector EFT is written with the same broken-phase tensor structure  $K^{AB}$ ; therefore, within this coherent-sector construction, its leading principal part is inherited from the same ordered-branch cone (Section 10.6). This is not a circular argument:  $K^{AB}$  is determined by the symmetry of SSB (Theorem 3.2), independently of any identification  $c_* = c$ . Both the propagation speed  $c_*$  and the phase action  $S_\theta$  are parallel consequences of the same root  $K^{AB}$ .

Status: Level A for the tensor structure of  $S_\theta$ ; Level B for the coefficient  $K_\theta^{\text{eff}}$ , which has not yet been derived from bare P3.

**Gauge sector (Level A/B after P5).** With the medium-character postulate P5, gauge emergence via Propositions 1–3 (Section 7) is no longer conditional but structural. Therefore:

1. The leading two-derivative gauge-invariant kinetic term is uniquely of Maxwell type:  $F_{AB}F^{AB}$  (Proposition 3, §7). This term is built on the same  $g_{\text{eff}}^{AB}$ .
2. Within the minimal phase-to-gauge emergence route adopted here, no independent leading-order anisotropic gauge kinetic tensor is introduced beyond the ordered-phase tensor  $K^{AB}$ . This contrasts with Einstein-aether [24], where the gauge sector may have its own kinetic coefficients, and with the SME [28], where each sector carries independent Lorentz-violation parameters.
3. Therefore, within the minimal route,  $c_\gamma = c_*$ , and since the observed speed of light is defined as  $c \equiv c_\gamma$ :

$$c = c_\gamma = c_* \quad (\text{Level A/B after P5}). \quad (4.10)$$

**Caveat: independent gauge-sector extension.** If the gauge sector were allowed an independent EFT extension beyond the minimal P5-based emergence route, the anisotropic operator  $n^\mu F_{\mu\nu} n^\alpha F_\alpha{}^\nu$  might acquire a free coefficient, and the universality argument would no longer hold. Within the P5 framework, however, the gauge connection arises from the same ordered-branch redundancy, and the minimal route is the structurally preferred one.

**Summary of the structural identification  $c_* = c$ .** The hierarchy of derivation levels is:

1. Level A: unique causal cone of the linear scalar ordered branch (Universality Corollary, integrability + uniqueness of  $K^{AB}$ ).
2. Level A/B bridge: the phase sector inherits the same tensor structure at leading order.
3. Level A/B (after P5): within the P5-based gauge-emergence route,  $c_\gamma = c_*$  and hence  $c = c_*$ .

This replaces the earlier presentation of  $c_* = c$  as a benchmark normalisation [10] with a structural identification whose only remaining open step is the realisation of the physical photon as the transverse gauge manifestation of the phase branch (OP-gauge, Section 7).

**Cross-sector cone universality (Level A/B).** The ordered Lorentzian branch of ECT admits a single leading causal cone determined by the ordered-branch kinetic structure  $K^{AB}$  (Theorem 3.2). This cone is inherited by every native low-energy sector:

- (i) the broken scalar sector (direct consequence of the ordered-branch action);
- (ii) the coherent compact-phase sector (same  $K^{AB}$  enters the phase action (21.2));
- (iii) the Abelian gauge sector arising from local redundancy completion (P5; the Maxwell-type kinetic term is built on the same ordered-branch metric);
- (iv) the tensor gravitational-wave sector (orientation modes propagate within the same emergent Lorentzian structure (13.16)).

Consequently, at leading low-energy order,

$$c_{\text{phase}} = c_\gamma = c_{\text{GW}} = c_* \quad (\text{Level A/B}). \quad (4.11)$$

This *cross-sector cone universality* is a structural prediction of ECT: all native ordered-branch excitations share one and the same low-energy causal cone. Standard physics obtains this coincidence empirically; ECT derives it from the single-medium origin of all native low-energy sectors. Together with the action-scale universality (§5.6), the extremal-action backbone (§22.2), and the unified conservation origin (§22.3), it forms one of four structural universalities of the ECT framework (§11.1).

The physical identification  $c_* = c$  is then a single matching step (Ph1), after which the observed universality of the speed of light—including the GW170817 bound  $|c_{\text{GW}}/c - 1| < 6 \times 10^{-15}$  [10]—becomes a structural consistency check rather than an independent input.

A useful point of comparison is provided by the clock-field construction of Mukohyama and Uzan [2], in which a universal effective metric for distinct matter sectors requires an explicit matching condition between sector-dependent couplings [their Eq. (5.2)]. In ECT, the intended universality is instead tied to the single-medium origin of the broken-phase kinetic structure: all native low-energy sectors inherit the same tensor  $K^{AB}$ , and no analogue of the matter-sector tuning is imposed at the benchmark level. Whether this universality remains exact beyond the minimal EFT truncation is part of the broader consistency programme.

**Falsifiable content of cone universality.** ECT admits Planck-suppressed higher-order corrections (Section 13.8, Eq. (13.54)) that can produce tiny sector-dependent speed splittings at very high energies. What ECT does *not* admit is arbitrary, uncorrelated, and unsuppressed low-energy propagation-speed differences between native sectors. If such differences were observed at a level exceeding the Planck-suppressed EFT corrections, the one-cone universality of the ordered branch would be falsified.

## 4.8 Status of results in this section

**Table 9:** Status of results in this section.

Result	Status	Basis
Polar decomposition $\partial_A \Phi = (u_0 + \sigma)n_A$	Level A	P4 + Theorem 3.2
Quadratic EFT action (3.10)	Level A (EFT)	Uniqueness of $K^{AB}$
Equation of motion (3.12)	Level A (EFT)	Variation of (3.10)
Lorentzian dispersion (3.13) for $\alpha > \beta$	Level A (EFT)	Theorem 3.2 + $\alpha > \beta$
Klein–Gordon equation (3.16)	Level A (EFT)	Real parametrisation $t = w/c_*$
Free Hamiltonian $H \geq 0$ (3.11)	Level A (quadratic)	Canonical normalisation; no tachyon/ghost
Identification of $m_{\text{eff}}^2$ with $V''(\phi_0)$	Open (OP-grad)	Requires explicit EFT matching
Integrability of $Q_A = \partial_A \Phi$	Level A	Scalar-only basis of P3
Linear reduction $\pi_i = \partial_i \chi / u_0$ , $\sigma = \partial_w \chi$	Level A	Integrability around the ordered background
Unique causal cone of the linear scalar ordered branch	Level A	Universality Corollary (§4.3): single $\chi \Rightarrow$ single principal symbol
Cone inheritance by phase sector $\theta$	Level A/B	Same $K^{AB}$ ; $K_\theta^{\text{eff}}$ open
$c_\gamma = c_*$ (P5-based gauge-emergence route)	Level A/B	Structural consequence of P5-based gauge route (§4.7)
Cross-sector cone universality (4.11)	Level A/B	All native sectors share one ordered-branch cone
Cross-sector action-scale universality (§5.6)	Level A/B	Same $S_0$ across all coherent-branch constructions
Extremal-action backbone (§22.2)	Level A/B	DP $\rightarrow$ reduced EFTs $\rightarrow$ macroscopic eqs $\rightarrow$ coherent stationary-phase
Four structural universalities (§11.1)	Level A/B	One cone, one scale, one principle, one conservation
Physical UV threshold of the ordered branch (§8.3)	Level A/B	Set by primary radial mode $m_\sigma$ ; structural UV-regularisation route
Minimal 3-component orientation EFT on $O(4)/O(3) \simeq S^3$	Level B (effective description)	Broken-branch parametrisation only
Independent soft mode in scalar-only broken phase: one longitudinal scalar $\chi$	Level B	Inverse-Higgs-type reduction [30, 31]

*Continued on next page*

Table 9 continued

Result	Status	Basis
Pure $P(X)$ closure does not generate $(\partial n)^2$	Level A	Theorem 3.1
Orientation-sector stiffness $\kappa_n = \mathcal{C}_n u_0^2$ ; $[\mathcal{C}_n] = \text{mass}^{-2}$	Level B (EFT)	Algebraic form exact within NLO EFT; coefficient $\mathcal{C}_n$ not yet derived
Derivation of $\mathcal{C}_n$ from bare P1–P6	Open	OP-Planck; NLO + spin-2 normalisation
Linear soft dispersion $\omega^2 = c_\chi^2 k^2$	Level B (EFT)	Minimal reduced EFT
Equality $c_\chi = c_*$	Open	Requires $K_s = K_w$ ; not yet derived
Three independent physical Goldstone particles	Not established	Reduced by integrability in scalar-only basis
No Higgs-type eating without P5	Level B (structural; upgradeable with P5)	No local $O(3)$ gauge structure
Pseudo-Goldstone mass mechanism	Open (OP-GM)	Requires explicit breaking source beyond P1–P6
Relation to electroweak gauge/Higgs sector	Open (OP-EW)	Requires a dynamically generated second condensate scale and an explicit mechanism for the second ordering step; derivation open
Variational selection of realised $\Phi$ -configurations	Level A	DP (basic definition of the theory)
Emergent extremal dynamics in reduced effective sectors	Level B	Inherited from variational selection after branch reduction
Action scale $S_0$ as ECT precursor of $\hbar$	Level B	Phase periodicity + coherent winding sectors (BR1)
Cross-sector action-scale universality	Level A/B	Same $S_0$ in loop, amplitude, wave, canonical, Born/decoherence sectors (§5.6)
Strict identification $S_0 = \hbar$	Open	Requires full quantum-sector reconstruction
Induced effective-metric tensorial sector from orientation fluctuations	Level B	Tensorial content arises after projection to $g_{AB}^{\text{eff}}$ ; see Section 8.5

*What is intentionally not done here.* This section does not introduce  $\hbar$ , canonical commutation relations, or the Born rule. Only the result that broken-phase excitations satisfy a Lorentzian wave equation with relativistic dispersion is obtained. The quantum regime is developed in Section 20 after deriving the corresponding formalism from the condensate structure.



## 5 Fundamental Scales, Matching Relations, and the Status of Constants

*This section organises the fundamental scales and matching relations of ECT: the condensate scales  $(\phi_0, v_2, v_{\text{gal}})$ , the effective propagation speed  $c_*$ , the gravitational matching for  $G_N$ , the radial-mode scales, and the action scale  $S_0$ . Most results in this section are matching relations or EFT-level consistency statements rather than first-principles derivations. The underlying gradient-condensate mechanism remains open (OP-grad).*

After establishing the postulates and the broken-phase dynamics, we systematically distinguish: which parameters are microscopic, which are effective, which are fixed by observational matching, and which are not yet derived.

**Physical significance: parameter compression.** In standard physics,  $c$ ,  $\hbar$ , and  $G$  appear as three independent empirical constants belonging to different chapters of physics: relativistic kinematics, quantum theory, and gravitation. In ECT they acquire a unified reading as three aspects of the same ordered condensate medium: the propagation speed  $c_*$  expresses the kinematic anisotropy of the ordered phase (§5.3); the gravitational constant  $G_N$  expresses the geometric stiffness of the orientation sector (§5.4); the action scale  $S_0$  expresses the coherent self-consistency of the minimal loop (§5.6). ECT therefore does not simply “compute the constants”—it changes their logical status from external gifts of nature to observable projections of a single underlying medium. The explicit matching formulas are collected in Table 112.

### 5.1 Three condensate scales: structure, hierarchy, and open problems

ECT contains three qualitatively different scales: a UV stiffness scale, a low-energy matching scale, and an emergent IR variation scale. They are *not* three independent VEVs of three different fields.

**What is established, what is matched, and what remains open in the hierarchy programme.** The ECT scale hierarchy should be read in three layers. First, the theory already singles out a primary microscopic symmetry-breaking amplitude  $\phi_0$  and a radial threshold  $m_\sigma$  from the same condensate microphysics. At induced-gravity level this gives a structural route by which the effective gravitational stiffness scales as  $M_G^2 \sim \kappa_n \sim u_0^2/m_\sigma^2 \sim \phi_0^2$  (§5.1). Second, weak-field matching then identifies the gravitational scale with the observed reduced Planck mass,  $\bar{M}_{\text{Pl}} = (8\pi G_N)^{-1/2}$ , so that  $\phi_0 \sim \bar{M}_{\text{Pl}}$  is a matched structural consequence rather than an independent postulate. Third, what remains open is the completed hierarchy problem: the first-principles derivation of the induced coefficient  $\mathcal{C}_n$ , the emergence of the second electroweak scale  $v_2$ , and the explicit dynamical origin of the large ratio  $v_2/\phi_0 \sim 10^{-16}$ .

Scale	Value	Physical origin in ECT	Status	Observable anchor
$\phi_0$	$\sim \bar{M}_{\text{Pl}} \approx 2.435 \times 10^{18} \text{ GeV}$	Radial symmetry-breaking scale; induced gravitational stiffness ( $M_G^2 \sim \phi_0^2$ , Section 5.1)	Level B (matched structural consequence)	$G_N$
$v_2$	$\approx 246.22 \text{ GeV}$	Low-energy matching to electroweak EFT; structural candidate for second transition	Constraint / Level B	$G_F$
$v_{\text{gal}}$	kpc-scale variation length	Emergent IR scale of ordered-branch amplitude variation; $\phi$ -sector	Level B (structural)	SPARC/RAR

These three scales are not of the same conceptual type. The UV scale  $u_0$  is associated with the gradient condensate and the stiffness of the ordered branch. The intermediate scale  $v_2$  is, in the present formulation, a low-energy matching constraint if a second transition exists. The galactic scale is an emergent IR variation scale of the  $\phi$ -sector closure, not a second microscopic condensate VEV.

The multiplicity S6 and topological completeness S10 of the  $\Phi$ -medium make a multi-scale structure structurally admissible, but do not by themselves explain the specific hierarchy between these scales.

**Caveat on the three-scale presentation.** The triplet  $(\phi_0, v_2, v_{\text{gal}})$  organises the currently relevant UV, intermediate, and IR condensate scales of distinct phenomenological type (UV primary VEV, matched intermediate scale, emergent IR branch-variation scale). This presentation should not be read as a proof that no further condensate-related scales can arise as the framework develops.

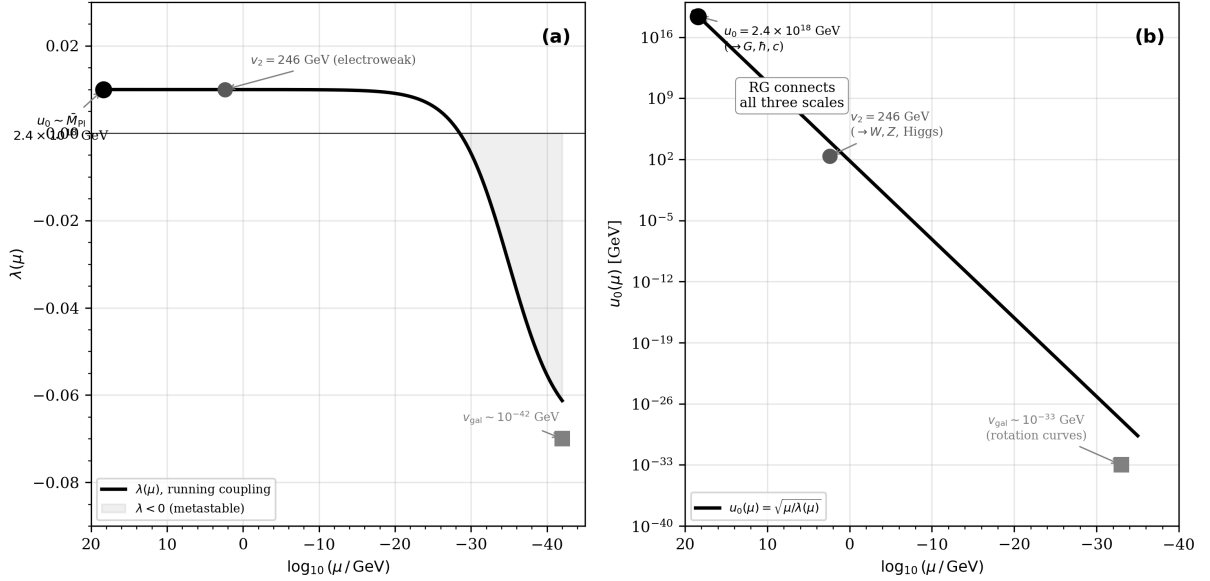


**Figure 3:** Illustrative schematic of the three condensate scale hierarchy in ECT. *Left:* schematic locking/alignment coupling  $\eta_{\text{lock}}(\mu)$  as a function of scale  $\mu$ . This is not the bare scalar quartic  $\lambda$  of the real-field potential, and its actual beta-function has not yet been derived from ECT first principles (open; OP-EW-scale). *Right:* the three characteristic scales: the UV condensate scale  $\phi_0 \sim \bar{M}_{\text{Pl}}$ , the matched intermediate scale  $v_2 \sim 246$  GeV, and the galactic IR branch-variation scale. The intermediate scale  $v_2$  is fixed by electroweak low-energy matching (5.8), not derived from the condensate action. The galactic scale is controlled by the IR/cosmological acceleration scale  $g^\dagger \sim cH_0/(2\pi)$  and is not generated by the same RG flow as  $v_2$ . The figure is a structural illustration of scale separation and possible non-polynomial scale-generation logic, not a quantitative ECT derivation of the intermediate scale.

**Gravitational normalisation and the Planck scale.** The gradient condensate amplitude  $u_0$  sets the UV stiffness of the ordered branch and is responsible for the  $O(4) \rightarrow O(3)$  symmetry breaking. However,  $u_0$  should not be identified directly with the reduced Planck mass: the two quantities have different dimensions ( $[u_0] = \text{GeV}^2$  in the present convention,  $[\bar{M}_{\text{Pl}}] = \text{GeV}$ ).

In the geometric sector of ECT, orientation modes  $\delta n_i$  acquire a kinetic term with effective stiffness  $\kappa_n = \mathcal{C}_n u_0^2$  (Section 4.4), where  $\mathcal{C}_n$  is an effective coefficient with dimension  $\text{mass}^{-2}$ . A pure  $P(X)$  closure of the ordered branch cannot generate this term (Theorem 3.1); orientation stiffness first appears at next-to-leading derivative order, either through induced (Sakharov-type) contributions from the radial sector or through higher-derivative operators in the  $\Phi$ -medium action. A natural induced-gravity estimate gives

$$\mathcal{C}_n \sim \frac{\hat{a}}{16\pi^2 m_\sigma^2}, \quad (5.1)$$

where  $\hat{a}$  is a dimensionless coefficient expected to be of order unity and  $m_\sigma$  is the radial mass scale. Using the symmetry-breaking scaling relation  $u_0 \sim m_\sigma \phi_0$  (5.5), the induced gravitational stiffness becomes

$$\kappa_n \sim \frac{\hat{a}}{16\pi^2} \frac{u_0^2}{m_\sigma^2} \sim \frac{\hat{a}}{16\pi^2} \phi_0^2. \quad (5.2)$$

Matching to linearised gravity (Section 5.4) identifies the effective gravitational scale:

$$\boxed{M_G^2 \sim \kappa_n \sim \frac{u_0^2}{m_\sigma^2} \sim \phi_0^2} \quad (\text{Level B: induced/NLO estimate}). \quad (5.3)$$

With  $M_G \equiv \bar{M}_{\text{Pl}} = (8\pi G_N)^{-1/2} \approx 2.435 \times 10^{18} \text{ GeV}$  (Level B weak-field matching), the natural Planck-scale candidate is the radial symmetry-breaking scale  $\phi_0$ , not the gradient order parameter  $u_0$  itself:

$$\phi_0 \sim \bar{M}_{\text{Pl}} \quad (\text{Level B: structural matched consequence}). \quad (5.4)$$

A first-principles derivation of  $\mathcal{C}_n$  from the full NLO derivative structure of the  $\Phi$ -medium remains open (OP-Planck, Section 38.1).

**Planck-scale candidate: matched structural form.** Within the induced/NLO gravity route of ECT, the same condensate that provides the ordered branch also provides the natural Planck-scale candidate. This is not yet a pure Level A derivation because the induced/NLO coefficient  $\mathcal{C}_n$  is not derived from bare P3. But it is stronger than a numerical coincidence: it shows that the Planck scale enters the theory through the same condensate amplitude that controls the UV threshold (§8.3) and the ordered branch itself.

**Connection to the universal structures already established.** The hierarchy programme is not isolated from the rest of ECT. The same condensate amplitude  $\phi_0$  that enters the Planck-scale matching also feeds the radial threshold  $m_\sigma$ , the induced gravitational stiffness, and the coherent-sector action-scale programme (§5.6). In this sense,  $\phi_0 \sim \bar{M}_{\text{Pl}}$  is not merely a gravity-side statement. It is tied to the already developed one-cone, one-action-scale, and one-UV-threshold architectures (§11.1). A successful completion of the hierarchy problem must therefore be compatible with all of those earlier universalities simultaneously.

**The gradient condensate and the open problem OP-grad.** Postulate P4 introduces  $u_0$  as the gradient condensate amplitude  $\langle \partial_A \Phi \rangle = u_0 \delta_{Aw}$ , independently of the bare potential minimum  $\phi_0 = \sqrt{\mu^2/\lambda}$  (P3). This independence is deliberate: the ordered vacuum of ECT is characterised by the gradient structure, not by the field value. Nevertheless, a dimensionally natural estimate is obtained by combining the bare-amplitude scale  $\phi_0 \sim \mu/\sqrt{\lambda}$  with the radial correlation length  $\xi_{\text{cond}} \sim m_\phi^{-1}$ , where  $m_\phi \sim \sqrt{2}\mu$ . This gives

$$u_0 \sim \frac{\phi_0}{\xi_{\text{cond}}} \sim \phi_0 m_\phi \sim \frac{\mu}{\sqrt{\lambda}} \cdot \sqrt{2}\mu \sim \frac{\mu^2}{\sqrt{\lambda}}. \quad (5.5)$$

This is only a dimensional self-consistency estimate, not a derivation. The explicit dynamical mechanism by which the gradient condensate emerges from the bare action remains an open foundational problem (OP-grad). Until OP-grad is closed,  $u_0$  should be treated as an independent Level 2 parameter (Section 5.2).

**Galactic IR scale: emergent branch-variation scale.** The galactic-scale physics in ECT does not arise from a separate microscopic VEV. It is the scale at which slow spatial variations  $u_0 \rightarrow u_0(\mathbf{x})$  of the ordered-branch amplitude become dynamically important in the  $\phi$ -sector (Section 4.2). The primary critical scale of the galactic branch is the acceleration  $g_0^\dagger \approx 1.04 \times 10^{-10} \text{ m s}^{-2}$  (observed MOND scale

$a_0 \approx 1.2 \times 10^{-10} \text{ m s}^{-2}$ ) (the RAR acceleration scale [33]), with cosmological baseline  $g_0^\dagger \sim cH_0/(2\pi)$ . The corresponding derived transition radius for a given baryonic mass is

$$r_* \equiv \left( \frac{G_N M_{\text{bar}}}{g^\dagger} \right)^{1/2}; \quad (5.6)$$

for  $M_{\text{bar}} \sim 10^{10} M_\odot$  this gives  $r_* \sim 5\text{--}20 \text{ kpc}$  (Level B; Section 17.1). Here  $g^\dagger$  is the primary variable;  $r_*$  is a derived scale, not an independent parameter.

$v_{\text{gal}}$  is an emergent IR scale, not a second UV condensate VEV.

(5.7)

**Why  $g^\dagger \sim cH_0$ .** The structural proximity  $g^\dagger \sim cH_0/(2\pi) \approx 1.04 \times 10^{-10} \text{ m s}^{-2}$  is one of the most suggestive numerical coincidences in ECT. At present, ECT does not derive this relation from first principles. Rather, it indicates that the galactic transition scale may be tied to the cosmological background scale of the ordered branch. A full derivation of  $g^\dagger$  from condensate dynamics remains open (OP-galactic; Section 17.1).

**Intermediate scale  $v_2$  and the electroweak matching.** If the ECT condensate undergoes a second ordering step, the intermediate scale is fully fixed by low-energy matching:

$$v_2 = \left( \sqrt{2} G_F \right)^{-1/2} \approx 246.22 \text{ GeV}, \quad (5.8)$$

where  $G_F = 1.1664 \times 10^{-5} \text{ GeV}^{-2}$  is the measured Fermi constant [34]. This is not a free parameter: any deviation would give wrong  $W$  and  $Z$  masses. A structural candidate mechanism for the second transition  $O(3) \rightarrow O(2)$  is discussed in Appendix L; it remains an open problem of ECT.

**Hierarchy and three distinct open problems.** The three scales obey

$$\phi_0 \sim \bar{M}_{\text{Pl}} \gg v_2 \gg v_{\text{gal}}, \quad \frac{v_2}{\phi_0} \approx 10^{-16}. \quad (5.9)$$

**The hierarchy problem in the ECT context.** The ratio  $v_2/\phi_0 \approx 10^{-16}$  is the ECT counterpart of the standard gauge hierarchy problem. ECT does not solve this problem in the current formulation. However, the ECT setting differs from the Standard Model in one structurally important respect:  $v_2$  is not a fundamental vacuum expectation value of a second independent field, but the matching scale of a *second ordering step* within the same condensate (Appendix L). If this second transition has a dynamical origin—for instance through RG running of the effective orientation coupling from  $\phi_0$  down to  $v_2$  (Fig. 3)—the large hierarchy could in principle be accommodated logarithmically rather than by fine-tuning. This is a structural possibility, not a derived result: the explicit RG calculation within ECT has not been performed and remains part of OP-EW. Any claim that ECT resolves the hierarchy problem would be premature.

**Structural status of  $v_2$  and its open-problem dependencies.** In the present formulation,  $v_2$  is a matched intermediate scale, not a first-principles condensate prediction. What remains open is not the low-energy value  $v_2 = (\sqrt{2} G_F)^{-1/2}$  itself, but the dynamical origin of the second ordering step within the same condensate. A dimensional-analysis argument strongly suggests that polynomial or rational combinations of the primary ECT parameters ( $\alpha, \beta, \lambda, \mu, u_0, \phi_0$ ) cannot account naturally for the hierarchy  $v_2/\phi_0 \sim 10^{-16}$  within natural parameter ranges. Any future derivation of  $v_2$  from ECT microstructure must therefore proceed through a non-polynomial scale-generation mechanism or through a structural selection mechanism not captured at the Lagrangian level. Furthermore, any renormalisation-group-based derivation would require  $\beta$ -functions of the emergent gauge couplings, which are themselves not yet

derived from condensate parameters. In that sense, progress on OP-EW is structurally tied to the larger open programme of emergent gauge-sector derivation (OP-SM). The only currently identified candidate structural route is the phase–orientation alignment scenario of Appendix L, whose realisation remains open.

**Conditional reduction of OP-EW-scale.** Polynomial or rational combinations of the primary ECT parameters  $(\alpha, \beta, \lambda, \mu, u_0, \phi_0)$  cannot naturally produce  $v_2/\phi_0 \sim 10^{-16}$ ; any such expression re-encodes the fine tuning as a small dimensionless coefficient. The only structurally viable route currently visible inside ECT is non-polynomial scale generation in a sector built upon alignment of the coherent phase variable  $\theta$  of the effective sector with the orientation field  $n_A$ .

We do not solve OP-EW here. We reduce the scale problem to a sharply defined non-polynomial scale-generation problem. The observable hierarchy is logarithmically equivalent to

$$v_2 = \phi_0 e^{-\mathcal{J}_{\text{EW}}}, \quad \mathcal{J}_{\text{EW}} \equiv \ln(\phi_0/v_2) \approx 36.8, \quad (5.10)$$

where the numerical value follows from  $\phi_0 \simeq \bar{M}_{\text{Pl}} = 2.435 \times 10^{18}$  GeV and  $v_2 = (\sqrt{2}G_F)^{-1/2} \approx 246.22$  GeV (5.8), taken in their present matched form.

**Heuristic comparison with QCD.** The analogous QCD logarithm  $\ln(M_{\text{Pl}}/\Lambda_{\text{QCD}}) \approx 44$  is *larger* than  $\mathcal{J}_{\text{EW}}$ . Generation of  $v_2$  via dimensional transmutation is therefore not numerically more exotic than generation of  $\Lambda_{\text{QCD}}$ , which already occurs in nature through ordinary QFT running. This comparison is purely logarithmic and heuristic; unlike QCD, the ECT alignment beta-function has not yet been derived. The comparison shows that the required non-polynomial input is in the standard order-one regime, not that naturalness is established.

**Four candidate mechanisms.** Each admissible mechanism maps an order-one input to  $\mathcal{J}_{\text{EW}} \approx 36.8$  differently. We list them as candidate templates, none of which has been derived from P1–P6:

- (i) *Asymptotic-freedom-like running.*  $\mathcal{J}_{\text{EW}} = 8\pi^2/[b_a g_a^2(\phi_0)]$  in a one-loop strong-critical limit gives  $b_a g_a^2(\phi_0) \approx 2.14$ . Requires an emergent asymptotically-free sector, which does not follow from a real-scalar quartic in 4D.
- (ii) *Walking / near-conformal.*  $\mathcal{J}_{\text{EW}} \sim \Delta\eta/\beta_{\text{eff}}$  with  $\beta_{\text{eff}}/\Delta\eta \approx 0.027$ . Protection of the relevant scalar operator additionally requires a large anomalous dimension  $\gamma_m \gtrsim 1$ . Requires both near-conformal running and operator protection.
- (iii) *Miransky / BKT critical scaling.*  $\mathcal{J}_{\text{EW}} = \pi/\sqrt{\delta}$  with  $\delta \approx 7.3 \times 10^{-3}$ . Requires an explanation of proximity to the critical surface at the  $\sim 0.7\%$  level.
- (iv) *Topological / Hopf-like.*  $\mathcal{J}_{\text{EW}} = S_{\text{top}}$  with dimensionless action  $\approx 36.8$ . Requires a genuine finite-action 4D Euclidean configuration or a non-tunnelling threshold interpretation; the Faddeev–Niemi/Hopfion structure [35, 36, 37, 38] provides a mathematical template but is a static 3D soliton, not automatically a 4D tunnelling instanton (cf. Appendix M).

In all four scenarios the required UV input is modest in logarithmic terms — a dimensionless number of order  $10^{-3}$ – $10^1$  depending on the mechanism, never a direct coefficient of order  $10^{-16}$  or  $10^{-32}$ . This is the precise sense in which OP-EW-scale is *reduced*: an unnatural small ratio is converted into a sharply defined order-one scale-generation problem.

**Caveats and explicit limitations.** The reduction above concerns only the origin of  $v_2$  (OP-EW-scale). It does not address (a) protection of the secondary radial mode  $\sigma_2$  from additive  $\mathcal{O}(\phi_0^2)$  corrections (OP-EW-naturalness); (b) local chiral electroweak gauge structure, hypercharge assignments, gauge couplings  $g, g'$ , and Weinberg angle (OP-EW-gauge); (c) chiral fermion representations and Yukawa

hierarchy (OP-EW-matter); (d) existence and dynamics of the phase–orientation locking that would justify a non-polynomial scale-generation mechanism in the first place (OP-EW-locking, Appendix M). The reduction also depends on prior closure of OP-Planck (orientation stiffness  $\kappa_n = \mathcal{C}_n u_0^2$  via NLO/induced route), labelled OP- $C_n$  as a sub-problem in this context: without  $\kappa_n$  there is no orientation sector to align.

**Positioning relative to existing approaches.** Dimensional transmutation as a route to the electroweak hierarchy has a long history: classical scale invariance with radiative breaking [39], conformal extensions of the Standard Model [40], walking technicolor [41, 42], and composite Higgs from coset structures [43]. The novelty of the ECT route, *if* it can be closed, is that the running/critical sector is not introduced as an external technicolor or conformal sector but emerges from the phase–orientation structure of the Euclidean condensate. The closest condensed-matter analogue is the  $A \leftrightarrow B$  transition between ordered phases of superfluid  $^3\text{He}$  [21], where two distinct broken-symmetry patterns coexist within a single underlying condensate.

**Discriminant with respect to the standard hierarchy problem.** ECT reframes the hierarchy problem in a way that differs sharply from the Standard Model. In the Standard Model, the electroweak scale is the vacuum expectation value of an independent Higgs field, while the Planck scale is an external gravitational input. In ECT, by contrast, the Planck-scale candidate  $\phi_0$ , the radial threshold  $m_\sigma$ , the action-scale programme  $S_0$ , and the ordered-branch UV boundary all originate in the same condensate. Thus the primary hierarchy question is no longer “why are gravity and electroweak physics unrelated scales?” but rather “how does one condensate generate a secondary low-energy ordering step  $v_2 \ll \phi_0$ ?” This is still open, but it is a different and structurally narrower problem.

Since  $v_2$  and  $v_{\text{gal}}$  are qualitatively different objects, the three-scale structure contains three distinct open problems:

**OP-grad (gradient condensate).** What is the dynamical mechanism by which the gradient condensate  $\langle \partial_A \Phi \rangle = u_0 \delta_{Aw}$  emerges from the bare action P3? Dimensional analysis (5.5) is consistent, but a first-principles derivation remains open.

**OP-EW (electroweak hierarchy and locking programme).** Why does a second condensate scale arise at  $v_2 \ll \phi_0$ , and how does the reduced orientation-sector transition extend to the full electroweak-like generator structure? The old single OP-EW problem is decomposed below into OP-EW-scale, OP-EW-locking, OP-EW-gauge, OP-EW-naturalness, and OP-EW-matter. The reduced  $O(3) \rightarrow O(2)$  candidate is described in Appendix L; the Hopf-fibered diagonal-locking upgrade is described in Appendix M. Both remain structural programmes, not derived results.

**OP-galactic (IR closure).** What determines the precise value of  $g^\dagger$  in terms of  $u_0$  and cosmological parameters? Structurally  $g^\dagger \sim cH_0/(2\pi)$  at the level of a suggestive order-of-magnitude coincidence (Level B), but a first-principles derivation from the condensate functional is not yet available.

**Falsifier for the ECT hierarchy programme.** The hierarchy programme would be seriously weakened if any of the following were established: (i) the effective gravitational scale required a microscopic amplitude parametrically unrelated to  $\phi_0$ ; (ii) the UV threshold  $m_\sigma$ , the Planck-scale candidate  $\phi_0$ , and the ordered-branch gravitational stiffness turned out to be unrelated scales rather than condensate-linked quantities; (iii) the electroweak scale  $v_2$  could only be introduced as the vacuum expectation value of an entirely independent sector unrelated to the original condensate; or (iv) the galactic scale and the cosmological background scale required a second independent IR medium rather than branch variation of the same condensate. Conversely, every successful derivation that ties  $\phi_0$ ,  $m_\sigma$ ,  $S_0$ ,  $M_G$ , and the secondary matching scales back to one and the same medium strengthens the one-condensate reading of the hierarchy problem.

**Programme-level predictions of the hierarchy architecture.** The present ECT hierarchy picture suggests four nontrivial expectations. First, the Planck-scale candidate, the UV threshold, and the radial mass should not be independent microscopic inputs; they should remain correlated consequences of one condensate. Second, any successful electroweak completion should generate  $v_2$  as a secondary ordering or matching scale of the same medium, not as a fundamental second vacuum unrelated to  $\phi_0$ . Third, the galactic scale should continue to appear as an emergent IR branch scale rather than as a third fundamental vacuum expectation value. Fourth, a completed hierarchy solution inside ECT should reduce the number of independent dimensionful inputs relative to the Standard Model plus GR, not increase them.

**Consistency between gravitational and quantum scales.** A distinctive structural feature of ECT is that the gravitational sector and the pre-quantum action scale  $S_0^{\text{EFT}}$  both arise from the same ordered medium. More precisely, the three observed constants  $c$ ,  $\hbar$ , and  $G_N$  are controlled by different sectors of the same  $\Phi$ -medium:  $c$  by the anisotropic ordered-branch structure,  $\hbar$  by the phase/loop sector, and  $G_N$  by the induced spin-2 normalisation (Appendix N). At the current stage, however, their explicit parametrisations are not yet fully reduced to an identical set of microscopic variables, because the relation between the gradient condensate scale  $u_0$  and the bare potential data remains open (OP-grad). The relevant matching relations are:

$$G_N = \frac{c_*^4}{8\pi M_G^2}, \quad S_0^{\text{EFT}} = \frac{K_\theta m_\phi}{2}, \quad (5.11)$$

where  $M_G$ ,  $K_\theta$ ,  $m_\phi$ , and  $c_*$  are all functions of the condensate data (in the simplest quartic bare-potential realisation one expects  $K_\theta \sim \phi_0^2$  and  $m_\phi = \sqrt{2\lambda} \phi_0$ , where  $\phi_0 = \sqrt{\mu^2/\lambda}$  is the bare field VEV; Section 5.6). Neither  $G_N$  nor  $S_0^{\text{EFT}}$  is derived from the other; both are Level B matching relations. But the fact that they share a common parametric origin means that ECT therefore suggests a structural consistency relation between the gravitational and quantum sectors: both originate in the same ordered condensate, even though their explicit matching relations are not yet fully unified at the microscopic level. This is the structural content of the common origin of the gravitational and quantum scales in ECT: not that one is derived from the other, but that both emerge from a single ordered medium and their eventual relation is expected to be constrained by the condensate structure once OP-grad is resolved.

**Status summary:**

Statement	Status	Comment
Existence of UV scale $u_0$ from P4	A	
$P(X) \not\equiv (\partial n)^2$	A	Theorem 3.1
$M_G^2 \sim \kappa_n \sim u_0^2/m_\sigma^2 \sim \phi_0^2$	B	Induced/NLO estimate
$M_G = \bar{M}_{\text{Pl}}$ (weak-field matching)	B	Section 5.4
$\phi_0 \sim \bar{M}_{\text{Pl}}$	B	Structural matched consequence
$u_0 \sim \phi_0 \cdot m_\phi$ : dimensional self-consistency	B	Eq. (5.5); OP-grad
$v_2 = (\sqrt{2}G_F)^{-1/2}$ as IR matching constraint	Constraint	If second transition exists
Galactic scale is emergent IR branch variation	B	Via $\phi$ -sector and RAR
$g^\dagger \sim cH_0/(2\pi)$ : suggestive structural coincidence	B	OP-galactic
$G_N$ and $S_0^{\text{EFT}}$ are controlled by the same condensate parameters	B	Eq. (5.11); structural link
$\mathfrak{so}(3) \cong \mathfrak{su}(2)$ : structural compatibility with EW-like second transition	A	Algebra only
Reduced $O(3) \rightarrow O(2)$ transition as orientation-sector analogue	B/C	Two broken directions only; not full EW counting
Gradient condensate from bare action	Open (OP-grad)	

Statement	Status	Comment
Hopf-fibered diagonal locking $SU(2)_{\text{orient}} \times U(1)_{\theta} \rightarrow U(1)_{\text{diag}}$	Candidate geometry	Three broken directions at pre-gauge/global level; dynamics not derived (App. M)
Origin of compact $U(1)_{\theta}$ as EW-locking participant	Open (OP-EW-locking.0)	Effective phase sector exists; EW role not derived
First-principles derivation of $v_2 = \phi_0 e^{-\mathcal{J}_{\text{EW}}}$	Reduced (OP-EW-scale)	Non-polynomial scale-generation mechanism not derived
Local chiral gauge completion, hypercharge, $g, g',$ Weinberg angle	Open (OP-EW-gauge)	Not implied by Hopf geometry alone
Radiative protection of $\sigma_2$	Open (OP-EW-naturalness)	Goldstone protection does not protect radial mode
First-principles derivation of $g^{\dagger}$	Open (OP-galactic)	

## 5.2 Parameter hierarchy by level of description

**Level 1. Bare micro-parameters (P3).** The potential  $V(\Phi)$  contains two parameters:  $\mu^2 > 0, \lambda > 0$ , with bare radial stiffness:

$$m_{\sigma}^2 = V''(\phi_0) = 2\mu^2, \quad \phi_0 = \sqrt{\mu^2/\lambda}. \quad (5.12)$$

These characterise the microscopic field dynamics only and do not directly fix the ordered vacuum.

**Level 2. Vacuum-sector parameters (P4).** Postulate P4 introduces  $u_0 > 0$ , the gradient condensate amplitude  $\langle \partial_A \Phi \rangle = u_0 \delta_{Aw}$ . This is an independent parameter; its relation to  $\phi_0$  and  $\lambda$  from the bare theory requires additional matching (OP-grad).

**Level 3. Broken-phase EFT parameters.** The effective kinetic tensor contains  $\alpha > \beta > 0$  and  $m_{\text{eff}}^2$ , where  $m_{\text{eff}}^2 \neq m_{\sigma}^2$  in general.

**Level 4. Coherent-sector parameters (BR1).** Within the smooth coherent branch (BR1), the pre-quantum topological action scale  $S_0$  is introduced via the elementary-loop action  $S_{\text{loop},\min} = 2\pi S_0$  (Section 5.6). The identification  $S_0 = \hbar$  is deferred to Section 20.

## 5.3 Effective propagation speed $c_*$

*Status: Level A in broken-phase EFT.*

From the dispersion relation (3.13):

$$c_*^2 = \frac{\beta}{\alpha - \beta}. \quad (5.13)$$

This is a strict EFT consequence; it requires neither quantum formalism nor a gravitational sector.

**Observational matching.** The constraint that gravitational and electromagnetic signals propagate at the same speed [10] motivates the structural identification  $c_* = c$  (Level A/B (after P5) within the P5-based gauge emergence route; see §4.3 and §4.7). In canonical units ( $\beta = 1$ ) this corresponds to  $\alpha = 2\beta = 2$ . The parameters  $(\alpha, \beta)$  are EFT parameters not derivable from the bare micro-action P3 in the current formulation.



## 5.4 Gravitational stiffness scale and Newton's constant

*Status: Level B — geometric EFT sector;  $G_N$  fixed by matching.*

In the geometric sector of ECT, fluctuations of the ordered branch induce perturbations of the effective metric  $h_{\mu\nu}$  (Section 8.5). At the linearised effective level, the tensorial sector obtained after projection to the effective metric is expected to exhibit a Fierz–Pauli-type [44] quadratic structure with stiffness coefficient  $M_G^2$ :

$$S_{\text{geom}}^{(2)} \sim M_G^2 \int d^4x \partial_\lambda h_{\mu\nu} \partial^\lambda h^{\mu\nu} + \dots \quad (5.14)$$

**Matching to Newton's constant.** Comparison with linearised GR (Einstein–Hilbert action in the linear limit):

$$G_N = \frac{c_*^4}{8\pi M_G^2}. \quad (5.15)$$

In natural units  $c = \hbar = 1$  (used as a working convention independently of the final status of  $\hbar$ ):

$$M_G \equiv \bar{M}_{\text{Pl}} = \frac{1}{\sqrt{8\pi G_N}} \approx 2.435 \times 10^{18} \text{ GeV}. \quad (5.16)$$

This is a numerical EFT matching, not a first-principles derivation. The numerical value in GeV requires  $\hbar$  and  $c$  for unit conversion; strict justification follows from Section 20.

The relation (5.15) is geometric EFT matching, not a derivation of  $G_N$  from the bare micro-action P3. The gravitational stiffness  $M_G$  is controlled by the orientation-sector stiffness  $\kappa_n = \mathcal{C}_n u_0^2$ , which first appears at NLO in the derivative expansion (Theorem 3.1). The dimensionally consistent structural estimate is  $M_G^2 \sim \kappa_n \sim u_0^2/m_\sigma^2 \sim \phi_0^2$  (Section 5.1); the full NLO derivation of  $\mathcal{C}_n$  and the explicit spin-2 normalisation map remain open (OP-Planck). The linearised graviton interpretation of this tensorial sector is discussed in Section 8.5.

## 5.5 Radial-mode scales and the correlation length

The characteristic radial scale is expected to be controlled by the local curvature of the condensate potential,  $m_\sigma^2 \sim V''(\phi_0)$ , as a representative estimate. A fully explicit EFT matching of this scale remains open (OP-grad). From this one obtains the EFT correlation-length estimate:

$$\xi_{\text{cond}} \sim m_\sigma^{-1} = (2\mu^2)^{-1/2}. \quad (5.17)$$

This is supported by the exponential decay of the Euclidean propagator of the heavy radial mode (Appendix O):  $G_\sigma(r) \sim e^{-m_\sigma r}/r^{3/2}$  for  $r \rightarrow \infty$ .

A natural phenomenological matching hypothesis is  $\xi_{\text{cond}} \sim \ell_{\text{Pl}}$ , where  $\ell_{\text{Pl}} = \sqrt{G_N \hbar / c^3} \approx 1.6 \times 10^{-35} \text{ m}$ . This should be understood as a motivated matching hypothesis, not a strict derivation:  $\ell_{\text{Pl}}$  depends on  $\hbar$ , which is not yet derived at this stage. Its particle-spectrum interpretation as the primary radial condensate mode is developed in Section 8.3.

## 5.6 Action scale $S_0$ as the ECT precursor of $\hbar$

*Status: three-layered with structural bridges. Layer 1 (strict within the reduced  $U(1)$ -extended phase-loop EFT): the winding-sector action admits a sharp lower bound at fixed loop length, with the minimum achieved by uniform winding. Layer 2 (Level A/B EFT closure): specifying the characteristic size of an elementary coherent loop yields a distinguished EFT action scale  $S_0^{\text{EFT}}$ ; the core scale is supported by a vortex variational estimate. Structural bridges (Level A/B to B): single-field universality, analytic continuation, and parameter-counting closure collectively protect the identification from arbitrary fitting. Layer 3 (Level B matching): the identification  $S_0^{\text{EFT}} \leftrightarrow \hbar$  is the strongest structural bridge to quantum mechanics, but remains a matching statement, not a parameter-free derivation.*

A central question for ECT is whether quantum mechanics requires the external introduction of Planck's constant, or whether a distinguished action scale already emerges within the coherent branch of the condensate. The present framework supports the second interpretation: before identifying  $\hbar$  itself, ECT already contains a natural *pre-quantum action scale*  $S_0$ . What follows clarifies why  $S_0$  arises, what it means for the classical–quantum divide, and where the boundary between established and open results lies.

ECT does not insert  $S_0$  by hand to imitate quantum mechanics. It is the action scale associated with the elementary coherent cycle of the condensate, forced by phase single-valuedness within the  $U(1)$ -extended phase EFT.

**Layer 1: compact phase and the variational bound (strict within the reduced  $U(1)$ -extended phase-loop EFT).** *Coherent phase variable.* In the smooth coherent branch (BR1), the collective state is characterised not only by an amplitude  $\rho$  but also by a phase-like variable  $\theta$ . Because the coherent state is physically single-valued, this phase is defined only modulo a full winding:

$$\theta \sim \theta + 2\pi. \quad (5.18)$$

It should be noted that the real scalar field  $\Phi$  of P3 does not by itself carry a compact  $U(1)$  phase variable. The extension to  $\Phi_{\text{eff}} = \rho e^{i\theta}$  is an additional modelling step for the coherent charged sector. Accordingly, the periodicity  $\theta \sim \theta + 2\pi$  and the associated winding number are strict statements within the  $U(1)$ -extended phase EFT, not direct topological consequences of the vacuum manifold  $O(4)/O(3) \simeq S^3$  (which has  $\pi_1(S^3) = 0$ ).

*Phase action.* At wavelengths large compared to the radial-core scale, and within the smooth coherent sector, the radial mode is approximately frozen and the effective dynamics is dominated by the phase. We write the reduced phase action in the schematic EFT form

$$S_\theta[\theta] = \frac{K_\theta}{2} \int d^4X (\partial_A \theta)^2, \quad (5.19)$$

with  $K_\theta \sim \phi_0^2$  in the simplest quartic bare-potential realisation, where  $\phi_0 = \sqrt{\mu^2/\lambda}$ .

*Sharp lower bound on loop action (Cauchy–Schwarz inequality).* Consider a closed coherent loop  $\gamma$  of proper length  $L$  in the phase EFT with winding number  $n[\gamma] = \frac{1}{2\pi} \oint_\gamma \partial_\ell \theta d\ell$ . The reduced 1D action along the loop is

$$S_{\text{loop}}[\theta] = \frac{K_\theta}{2} \oint_\gamma d\ell (\partial_\ell \theta)^2. \quad (5.20)$$

By the Cauchy–Schwarz inequality applied to the constant function  $f = 1$  and  $g = \partial_\ell \theta$ :

$$\oint d\ell (\partial_\ell \theta)^2 \geq \frac{1}{L} \left( \oint d\ell \partial_\ell \theta \right)^2 = \frac{(2\pi n)^2}{L}, \quad (5.21)$$

with equality if and only if  $\partial_\ell \theta = \text{const}$  along the loop (uniform winding). Therefore:

$$\boxed{S_{\text{loop}}[\theta] \geq \frac{2\pi^2 K_\theta n^2}{L}, \quad \text{equality at uniform winding.}} \quad (5.22)$$

This is a strict variational result within the phase EFT: the minimiser of loop action at fixed length and winding is the uniform-gradient configuration, and the minimum scales as  $n^2/L$ .

*Important structural remark.* Equation (5.22) provides a sharp lower bound for each fixed  $L$ , but because the bound falls as  $1/L$ ,  $S_{\text{loop}} \rightarrow 0$  as  $L \rightarrow \infty$ . The pure phase topology alone does *not* yield a nonzero global minimum of the loop action; additional physical input is needed to obtain a distinguished action scale.

**Layer 2: elementary-loop scale and the distinguished action parameter (Level B).** *Why the fixed- $L$  bound is not yet a nonzero global minimum.* Equation (5.22) gives the minimum action in a fixed length-and-winding sector, but because the bound falls as  $1/L$ , it does not define a nonzero global minimum when the loop length is allowed to vary.

*Elementary coherent loop size.* To obtain a distinguished EFT action scale, one must specify the characteristic size of an elementary coherent loop. The natural choice is the radial-core scale: for loops much larger than  $\xi_{\text{core}} \sim m_\phi^{-1}$ , the smooth coherent description breaks down and the loop can no longer be treated as a single elementary coherent object within the reduced phase EFT. The characteristic elementary loop length is therefore

$$L_{\text{core}} \sim 2\pi \xi_{\text{core}} = \frac{2\pi}{m_\phi}. \quad (5.23)$$

This is a Level B EFT input: it uses the radial-mode correlation length from the broken-phase potential, not topology alone.

*Variational support for the core scale.* The estimate  $\xi_{\text{core}} \sim m_\phi^{-1}$  is not merely a dimensional guess: it is confirmed by the standard global-vortex variational problem for the full  $(\rho, \theta)$  system. For a rectilinear vortex with unit winding, the radial profile  $\rho(r)$  satisfies  $\rho(0) = 0$  and  $\rho(r) \rightarrow \phi_0$  at  $r \gg m_\phi^{-1}$ , with the core size fixed by the balance between gradient energy and potential energy at  $\xi_{\text{core}} \sim m_\phi^{-1}$ . For a closed loop of circumference  $L \sim 2\pi \xi_{\text{core}}$ , curvature corrections are  $O(1)$  and do not change the scaling estimate. This raises the status of  $L_{\text{core}}$  from a purely ad hoc choice to a variationally motivated estimate (Level A/B), with the  $O(1)$  numerical coefficient remaining open pending the full 4D closed-loop variational problem.

*Distinguished EFT action scale.* Evaluating the fixed- $L$  lower bound (5.22) at the elementary-loop size with  $n = 1$  gives the characteristic elementary-loop action

$$S_{\text{elem}} = \frac{2\pi^2 K_\theta}{L_{\text{core}}} = \pi K_\theta m_\phi. \quad (5.24)$$

We then define the associated EFT action scale by

$$S_0^{\text{EFT}} \equiv \frac{S_{\text{elem}}}{2\pi} = \frac{K_\theta m_\phi}{2}. \quad (5.25)$$

This is a distinguished EFT scale associated with the elementary coherent loop, not the global variational minimum over arbitrary loop lengths (Level B).

*Notational remark.* Throughout the remainder of the paper the notation  $S_{\text{loop,min}} = 2\pi S_0$  may occasionally appear in earlier sections. The full derivation chain behind this identification is recorded in Appendix P. In the present revised formulation, however, this quantity should be understood as the elementary-loop action  $S_{\text{elem}}$  evaluated at the characteristic core scale  $L_{\text{core}}$ , not as a global variational minimum over arbitrary loop lengths.

*Self-consistency, not prediction.* The relation (5.25) should be read as a self-consistency condition: if  $S_0^{\text{EFT}}$  is to be identified with  $\hbar$ , then the condensate parameters must satisfy  $K_\theta m_\phi/2 \approx \hbar$ . This is analogous to the BCS gap equation, where the superconducting gap  $\Delta$  is determined self-consistently rather than predicted from first principles. The content of ECT is not that  $\hbar$  is computed from nothing, but that the EFT action scale identified with  $\hbar$  and the gravitational coupling  $G_N$  both arise from the same ordered medium. At the current stage, however, their explicit parametrisations are not yet fully reduced to an identical set of microscopic variables, because the relation between the gradient condensate scale  $u_0$  and the bare potential data remains open (OP-grad). The relevant matching relations are:

$$S_0^{\text{EFT}} = \frac{K_\theta m_\phi}{2}, \quad G_N = \frac{c_*^4}{8\pi M_G^2}, \quad (5.26)$$

where  $M_G$ ,  $K_\theta$ ,  $m_\phi$ , and  $c_*$  are functions of the underlying bare-condensate and EFT data  $(\phi_0, \lambda, \alpha, \beta)$ . ECT therefore suggests a structural consistency relation between the gravitational and quantum sectors: both originate in the same ordered condensate, even though their explicit matching relations are not yet fully unified at the microscopic level.

**Single-field universality (Level A/B).** ECT is a theory of a single microscopic field  $\Phi$  governed by a single Euclidean action  $S_E[\Phi]$  (P3). All excitation sectors—radial, phase, orientational, gravitational—are decompositions of the same field around the same ordered vacuum. The Euclidean functional integral

$$Z = \int \mathcal{D}\Phi \exp(-S_E[\Phi]/\Sigma) \quad (5.27)$$

is therefore characterised by a *single* action normalization  $\Sigma$  shared by all sectors. The coherent phase sector, via the topological and variational construction of Layer 1 and the core-scale closure of Layer 2, identifies a distinguished candidate for this universal normalization:  $\Sigma = S_0^{\text{EFT}}$ . If the  $U(1)$ -coherent sector is a faithful effective reduction of the underlying single-field branch, then the universal action normalization is identified with  $S_0^{\text{EFT}}$ .

This is a structural consequence of the single-field architecture of ECT (P3), not an independent postulate. The level is A/B because the link between the full action  $S_E[\Phi]$  and the reduced phase action  $S_\theta[\theta]$  passes through an effective integration-out of the radial mode, which is itself a Level B closure step.

**Analytic continuation preserves action normalization (Level A/B).** The formal analytic continuation  $w_E \rightarrow \pm ic_* t$  relates Euclidean coherent weights to Lorentzian phase evolution. It should not be confused with the real parametrisation  $t = w/c_*$ , which is the primary route to the hyperbolic field equations. At the present stage the underlying ordered-branch hyperbolicity has already been fixed independently by  $\alpha > \beta$

**Parameter-counting closure (Level B structural).** In its simplest bare-potential realisation, ECT has three structurally independent bare/EFT parameters  $(\phi_0, \lambda, \alpha)$  at  $\beta = 1$ . Three observational calibration relations are needed to fix them:

- $c_* = c$  fixes  $\alpha$  (Section 3.5; Level A/B);
- $G_N = c_*^4/(8\pi M_G^2)$  fixes the gravitational stiffness scale (Section 5.4; Level B);
- $S_0^{\text{EFT}} = \hbar$  fixes  $m_\phi$ , or equivalently  $\lambda$ .

Without the third calibration, one free parameter would remain physically uncalibrated at this stage of the theory. The identification  $S_0^{\text{EFT}} = \hbar$  naturally closes the theory by fixing  $m_\phi = 2\hbar/K_\theta$ . This is not a derivation of  $\hbar$  from first principles, but a structural argument showing that the identification is the third and final calibration relation of a three-parameter theory, rather than an arbitrary fit.

**Layer 3: identification with  $\hbar$  (Level B matching).** The preceding structural bridges—single-field universality, analytic continuation, and parameter-counting closure—collectively protect the identification of  $S_0^{\text{EFT}}$  with the observed Planck constant from the charge of arbitrary fitting. The identification itself is:

$$\hbar \leftrightarrow S_0^{\text{EFT}}, \quad S_{\text{elem}} = 2\pi\hbar = h. \quad (5.28)$$

This is a Level B matching statement: strongly motivated by the structural bridges above, but not yet a strict parameter-free theorem.

In ordinary quantum theory,  $\hbar$  is the quantity that renders the action dimensionless in the phase factor  $\mathcal{A} \sim e^{iS/\hbar}$ . ECT reproduces the same structural role through  $S_0^{\text{EFT}}$ :

$$S_0^{\text{EFT}} \text{ is the ECT precursor of } \hbar. \quad (5.29)$$

*Clarification of loop terminology.* Here  $S_{\text{loop,min}}$  refers specifically to the minimal action of an elementary coherent phase-winding loop in the  $U(1)$ -extended sector (Layer 1), not to an arbitrary closed condensate configuration. This distinction is important because more general path-integral language appears elsewhere in the text; the  $\hbar$  identification is grounded in the specific phase-topological construction.

*Why this is not yet Level A.* To promote the identification to Level A, one would need to derive from ECT not just a number with units of action, but the full structural role of  $\hbar$ :

- (i) a universal phase weighting  $\mathcal{A} \sim e^{iS/S_0^{\text{EFT}}}$  for arbitrary histories, not only for special loops;
- (ii) a composition law for coherent amplitudes;
- (iii) canonical commutators normalised by  $S_0^{\text{EFT}}$ ;
- (iv) ultimately, reconstruction of the Hilbert-space structure and the Born rule.

This is the programme of the Quantum Sector (Section 20), not a one-line identification. Within that programme, partial results are already available (Sections 21.1–23.3), but the full reconstruction is not yet complete.

**Cross-sector universality of the action scale (Level A/B).** The compact-phase loop structure introduces a distinguished pre-quantum action scale  $S_0$ . This scale is not merely a loop-sector parameter: it is the unique internal candidate for the normalisation of all subsequent coherent quantum-sector constructions. Specifically, the same  $S_0$  appears structurally in:

- (i) the loop-sector action bound and elementary-loop scale (5.22);
- (ii) the coherent-history phase weight  $\mathcal{A} \sim e^{iS_0/S_0}$  (Section 22.1);
- (iii) the Schrödinger-type wave reconstruction (22.8);
- (iv) the natural canonical commutator candidate (23.6);
- (v) the decoherence architecture (Section 26.1) and the later Born/measurement programme (Section 30.4).

The identification  $S_0 = \hbar$  is therefore not an isolated fit, but the matched physical interpretation of a structurally unique action scale already selected by the ordered coherent medium.

This cross-sector reappearance of  $S_0$  is the action-scale analogue of the cross-sector cone universality established for  $c_*$  in §4.7. Just as the single ordered-branch kinetic structure forces one causal cone across all native sectors, the single compact-phase topology forces one action normalization across all coherent-branch constructions. These two universalities, together with the extremal-action backbone and the unified conservation structure, constitute the four structural universalities of ECT (§11.1).

**Falsifiable content of action-scale universality.** If the loop-sector quantization scale, the wave-sector action normalisation, the canonical commutator normalisation, and the Born/decoherence-sector normalisation were found to require *mutually inconsistent* fundamental action scales rather than a single coherent-branch scale  $S_0$ , then the ECT programme of action-scale universality would fail. Such an outcome would falsify the claim that one and the same ordered coherent medium underlies all quantum-sector normalisations. No such inconsistency has been observed: all established quantum phenomena are described using one and the same  $\hbar$ .

**Relation to the classical limit and variational dynamics.** The emergence of  $S_0^{\text{EFT}}$  is fully compatible with the variational principle. At the fundamental level, realised configurations remain extremals of  $S_E[\Phi]$  (DP; Section 6.6). What  $S_0^{\text{EFT}}$  adds is a sensitivity scale for coherent phase relations: when action differences satisfy  $|\Delta S| \gg S_0^{\text{EFT}}$ , relative phase oscillations become rapidly varying and an extremal, effectively classical description dominates; when  $|\Delta S| \sim S_0^{\text{EFT}}$ , phase differences cannot be ignored and interference between coherent histories becomes structurally relevant. Thus  $S_0^{\text{EFT}}$  separates the extremal/classical regime from the phase-sensitive regime, without contradicting the underlying variational dynamics.

**Coarse graining and emergent classicality.** If branch histories are tracked at a resolution comparable to  $S_0^{\text{EFT}}$ , relative phases matter and quantum interference is expected. If the description is coarse-grained over many branch sectors—for instance when the environment has many degrees of freedom ( $N_{\text{eff}} \gg 1$ ) as in Section 3.8—those relative phases are effectively washed out. ECT interprets classicality not as the absence of  $S_0^{\text{EFT}}$ , but as the loss of access to  $S_0^{\text{EFT}}$ -sensitive phase information through coarse graining.

**Path-integral hint.** The most natural amplitude assignment suggested by the coherent branch structure is

$$\mathcal{A} \sim e^{iS/S_0^{\text{EFT}}}. \quad (5.30)$$

Equation (5.30) should be read as a strong ECT motivation for the path-integral phase, not yet as a complete derivation of the quantum measure or of the Born rule.

**Comparison with familiar quantisation ideas.** *Bohr–Sommerfeld quantisation* [45]: in semiclassical mechanics one has  $\oint p dq = 2\pi n \hbar$ . ECT leads instead to  $\Delta S = 2\pi n S_0^{\text{EFT}}$ , but the origin is coherent phase winding, not orbital quantisation.

*Flux quantisation and superfluid winding* [21]: this is perhaps the closest analogy. In superfluids, compact phase plus single-valuedness forces quantised circulation. ECT uses the same structural logic, applied to the action-phase relation of the coherent branch rather than to a material superfluid.

*Path-integral phase assignment* [46]: standard quantum theory uses  $e^{iS/\hbar}$  and takes  $\hbar$  as primitive. ECT does not assume  $\hbar$  from the outset; it explains why a distinguished action scale should appear, and only then motivates identifying that scale with  $\hbar$ .

#### Status summary.

Statement	Status	Comment
<i>Layer 1: reduced <math>U(1)</math>-extended phase-loop EFT</i>		
Coherent compact phase variable in the $U(1)$ -extended phase EFT	B	Modelling extension of real $\Phi$
Single-valuedness on closed loops	A	Topological consistency within that EFT
Nontrivial winding sectors	A	Integer winding number
Sharp lower bound on loop action at fixed length	A	Eq. (5.22); Cauchy–Schwarz
Uniform winding minimises the fixed- $L$ action	A	Equality case of (5.21)
<i>Layer 2: elementary-loop scale</i>		
Elementary loop size $L_{\text{core}} \sim 2\pi/m_\phi$	A/B	EFT input; supported by vortex variational estimate ( $O(1)$ coefficient open)
$S_0^{\text{EFT}} = K_\theta m_\phi/2$	B	Characteristic elementary-loop action scale
$S_0^{\text{EFT}}$ and $G_N$ are structurally linked through the same ordered medium	B	Full microscopic unification remains open (OP-grad)
Self-consistency: $S_0^{\text{EFT}} \approx \hbar$ constrains the EFT parameter combination	B	Analogous to BCS gap equation
<i>Structural bridges</i>		
Single-field universality: one $\Sigma$ for all sectors	A/B	Consequence of P3; reduction is Level B

Statement	Status	Comment
Analytic continuation preserves $S_0^{\text{EFT}}$	A/B	Same formal amplitude bridge as in the coherent-sector path-integral reading; distinct from the real parametrisation used for the metric
Parameter-counting closure: $S_0^{\text{EFT}} = \hbar$ is third matching condition	B	Shows necessity, not derivation
<i>Layer 3: identification with <math>\hbar</math></i>		
$S_0^{\text{EFT}}$ separates classical and phase-sensitive regimes	B	Variational + coarse-graining argument
Phase factor $\mathcal{A} \sim e^{iS/S_0^{\text{EFT}}}$ motivated	B	Path-integral hint
$S_0^{\text{EFT}}$ as precursor of $\hbar$	B	Strongest quantum matching
Identification $S_0^{\text{EFT}} \leftrightarrow \hbar, S_{\text{elem}} = h$	B (matching)	Not parameter-free; protected by bridges above
Universal amplitude composition / Born rule	C (open)	Later quantum programme

## 5.7 Summary table: parameters and constants

Parameters and constants.				
Quantity	Physical meaning	Status	Basis / note	
$\mu^2, \lambda$	Bare parameters P3	micro-parameters	Micro-parameters	P3; not directly linked to P4
$u_0$	Gradient condensate amplitude	P4 (postulated)		OP-grad for derivation from P3
$\alpha, \beta$	Kinetic tensor parameters	EFT parameters		Theorem 3.2
$c_*$	EFT propagation speed	Level A (EFT)		Eq. (5.13)
$\alpha = 2\beta$	Cross-sector cone universality $c_{\text{phase}} = c_\gamma = c_{\text{GW}} = c_*$	Level A/B		Eq. (4.11); §4.7
Four structural universalities (§11.1)	Level A/B		One cone, one scale, one principle, one conservation origin	
Physical identification $c_* = c$	Level B (matching)	§4.7 + [10]		
$m_\sigma^2 = 2\mu^2$	Bare radial stiffness	Level A in P3		$V''(\phi_0)$ from P3
$m_{\text{eff}}^2$	EFT fluctuation mass	EFT parameter		$\neq m_\sigma^2$ in general
$\xi_{\text{cond}}$	EFT correlation length	EFT estimate		$\sim m_\sigma^{-1}$ ; not strict
$M_G$	Gravitational stiffness	Level B (matching)		$G_N = c_*^4/(8\pi M_G^2)$
$G_N$	Newton's constant	Matched		Observational input
$\bar{M}_{\text{Pl}}$	Reduced Planck mass	Level B (matching)		$\bar{M}_{\text{Pl}}^2 = M_G^2$

Quantity	Physical meaning	Status	Basis / note
$v_2$	Electroweak matching scale	Constraint / Level B	$v_2 = (\sqrt{2} G_F)^{-1/2} \approx 246 \text{ GeV}$ ; if second transition exists
$v_{\text{gal}}$	Galactic IR variation scale	Level B (emergent)	kpc-scale; not a microscopic VEV
$S_0$	Pre-quantum action scale	A/B (phase-loop construction, §5.6)	Structural completion in Sect. 20
$\hbar$	Planck constant	B (matching, §5.6 and 21.2)	Full quantum reconstruction remains open

Similarly, in the electroweak and fermionic sections the notation  $\Phi_{\text{ew}}$  is used for the embedded low-energy electroweak condensate field, to distinguish it from the fundamental bare condensate field  $\Phi$  of the postulate layer.

## 6 Branching Structure of ECT

*This section describes the branching structure of ECT into the geometric macroscopic branch and the coherent branch, establishes the variational and Noether backbone of the framework, and collects the corresponding foundational consequences. The underlying symmetry and variational structures are predominantly Level A, while the explicit reduction to branch-specific effective descriptions and some physical interpretations remain Level B or open.*

The six working postulates P1–P6, together with the ordered vacuum sector, the broken-phase spectrum, the scale hierarchy, and the derived smooth coherent-sector rule BR1, define a common condensate framework from which two distinct but mutually consistent effective branches emerge.

### 6.1 Two classes of observables

ECT contains a single fundamental field  $\Phi$  (P3). Postulate P4 introduces the ordered branch and, through the broken-phase EFT analysis, the orientation variable  $n_A$  and the kinetic tensor (3.9), producing the geometric causal sector. The derived smooth coherent-sector rule BR1 introduces the collective phase variable  $\theta$  with the winding condition (2.6).

These two steps are structurally distinct and produce two qualitatively different classes of observables:

1. *Phase-insensitive observables*: probe the coarse-grained geometric and stiffness response of the vacuum. Primary variables:  $n_A, K^{AB}, g_{AB}^{\text{eff}}, M_G$ . These constitute the *geometric branch*.
2. *Phase-sensitive observables*: probe coherence, winding structure, and non-trivial loop configurations. Primary variables:  $\Phi_{\text{eff}}, \theta$ , winding numbers,  $S_0$ . These constitute the *coherent branch*.

### 6.2 The geometric branch (Macroscopic Physics)

Primary variables:  $n_A, K^{AB}, g_{AB}^{\text{eff}}, M_G$ , long-wavelength stiffness fields.

This branch contains in embryo: effective Lorentzian geometry; propagation speed  $c_*$  (Level A); gravitational stiffness  $M_G$  matched to  $G_N$  (Level B); the long-wavelength sector from which gravity, cosmology, and astrophysical phenomenology are developed. The mode content and effective dynamics of this geometric branch are developed in Section 4, while the particle-level graviton sector is discussed in Section 8.5 and the full macroscopic development in Section 11.



### 6.3 The coherent branch (Quantum Sector)

Primary variables:  $\Phi_{\text{eff}}$ ,  $\theta$ , winding condition (2.6),  $S_0$ .

This branch will later develop: identification of  $S_0$  with observable  $\hbar$ ; canonical quantisation relations; connection between phase single-valuedness, loop quantisation, and wave dynamics; decoherence, probabilistic interpretation, and the quantum limit of ECT. Its effective phase dynamics and action-scale structure are developed in Sections 5.6 and 20.

### 6.4 Why branching is necessary

The branching is not a matter of exposition but a structural consequence of the condensate framework:

1. P4 introduces the ordered branch and thereby the orientation field—this opens the geometric branch.
2. BR1 identifies the smooth coherent phase sector with integer winding—this opens the coherent branch.
3. Both branches arise as different coarse-grainings of the same ordered condensate.
4. Neither branch reduces to the other without loss of physical content.

**Criterion.** In ECT the effective branch is selected not by adding new postulates but by the class of observables retained under coarse-graining.

### 6.5 Physical picture: correlation versus interaction in the two branches

The separation into branches has a fundamental physical consequence that must be made explicit before proceeding.

**Interaction is a Lorentzian concept.** Interaction in the ordinary physical sense—local exchange of energy, momentum, or information between physical subsystems—presupposes a causal structure: cause, effect, and a definite spacetime event. Such a structure exists only in the geometric branch ( $\Gamma_{\text{loop}} \gg 1$ ), where the Lorentzian metric and the arrow of time are already established. Event-like interaction is therefore an emergent Lorentzian concept belonging to the ordered branch (Level A).

**Common-medium correlation in the coherent branch.** In the coherent branch ( $\Gamma_{\text{loop}} \ll 1$ ) there is no causal event structure. Subsystems are not independent entities that “act on each other” in the Lorentzian sense. Instead, they share a common coherent condensate configuration and are therefore correlated through the Euclidean substrate—without energy exchange, without signal transfer, without “events”. This is the structural basis of quantum entanglement: non-factorisable correlation without causal connection (developed in Section 31).

This does not mean that there is no coupling at all. The influence of the medium enters through the influence functional (Section 26.1); the decoherence kernel, medium response, and suppression of off-diagonal elements are all consequences of the medium, not of “forces” in the Lorentzian sense.

**The transition.** Decoherence ( $\Gamma_{\text{loop}} \sim 1$ ) is the mechanism that converts common-medium coherent correlation into a decohered, branching, event-like world. Measurement is precisely this transition: a macroscopic apparatus with  $\Gamma_{\text{loop}} \gg 1$  fixes a Lorentzian event, converting Euclidean correlation into a classical outcome (Section 30.2).

**Comparison with standard quantum mechanics.** In standard QM, entanglement is postulated through the tensor-product structure  $\mathcal{H}_A \otimes \mathcal{H}_B$ , and collapse is a separate axiom. In ECT both phenomena follow from one structure: common condensate  $\rightarrow$  correlation; decoherence  $\rightarrow$  classical event. No separate collapse postulate is required.

## 6.6 Variational principle and Noether structure

*Status: layered. Physical configuration selection via extremality is Level A (DP). Noether structure from action symmetries is Level A. Inheritance by the ordered branches is Level A/B. Compatibility with the arrow of time and with the classical/quantum divide is Level B. Full derivation of all effective branch functionals and late-time charge reconstruction remains open.*

The variational principle in ECT is more than a formal device for writing field equations. Within the ontology of the  $\Phi$ -medium, it is the mathematical criterion that selects *physically realised configurations* from the much larger set of ontologically admissible ones. Extremality is therefore the bridge from the ontological layer of the theory to its dynamical content. The action principle belongs to the same foundational *dynamical* layer as DP, not to the ontological layer of properties S1–S10.

**From admissibility to realisation.** The structural properties S1–S10 of the  $\Phi$ -medium specify what kinds of configurations are admissible: regular or defect-adjacent, homogeneous or inhomogeneous, coherent or topologically nontrivial. The dynamical principle DP then states that physically realised configurations are extremals of a local action functional compatible with the basic symmetries of the medium:

$$\left. \delta S_E[\Phi] \right|_{\text{on-shell}} = 0. \quad (6.1)$$

ECT thus separates two logically distinct notions:

- *admissibility* — governed by the ontology of the medium;
- *realisation* — governed by variational selection.

This is why extremality is not merely a calculational convention in ECT: it is the criterion by which physical histories are selected from the space of possible configurations. The same extremality reappears at every subsequent level of the theory: in reduced-sector field equations (Part I), in macroscopic gravitational dynamics (Part II), and as the stationary-phase dominance of the coherent amplitude language (Part III, §22.2).

**Noether structure.** From the homogeneity of the Euclidean arena  $\mathcal{M}^4$  (P1) and the absence of explicit  $X^A$ -dependence in the action (P3), Noether’s theorem [47] gives a conserved energy-momentum tensor:

$$T_{(\Phi)}^{AB} = \partial^A \Phi \partial^B \Phi - \delta^{AB} \mathcal{L}_\Phi, \quad \partial_A T_{(\Phi)}^{AB} = 0. \quad (6.2)$$

$O(4)$  rotational symmetry (P2) additionally produces angular Noether currents  $J^{C,AB} = X^A T^{CB} - X^B T^{CA}$ . Conserved structures do not appear as separate postulates: they follow necessarily from the symmetry-compatible extremal principle. The full derivation with explicit formulae for both sets of currents, including the orientation-field sector, is given in Appendix Q.

**Lorentzian interpretation of the Noether structure in the ordered branch.** In homogeneous ordered backgrounds, the unbroken translation and rotation symmetries imply the corresponding conserved Noether currents. Within the emergent Lorentzian EFT, these are interpreted as the energy–momentum currents and the three spatial angular-momentum currents. Whether the associated global charges are well defined depends, as usual, on the background and boundary conditions.

This is a Lorentzian reinterpretation of the Euclidean Noether data, not yet a full derivation of the exact Poincaré group as a symmetry of the completed low-energy theory (Level A conservation laws, with Level B Lorentzian interpretation).

**Anisotropy of the background Noether tensor.** For the ordered background  $\langle \partial_A \Phi \rangle = u_0 \delta_{Aw}$ , with background potential contribution  $V_{\text{bg}} \equiv V[\Phi_{\text{bg}}]$ , the canonical Noether tensor is anisotropic:

$$T_{\text{bg}}^{ww} = \frac{u_0^2}{2} - V_{\text{bg}}, \quad (6.3)$$

$$T_{\text{bg}}^{ij} = -\delta^{ij} \left( \frac{u_0^2}{2} + V_{\text{bg}} \right), \quad i, j = 1, 2, 3, \quad (6.4)$$

$$T_{\text{bg}}^{wi} = 0. \quad (6.5)$$

Hence, for each fixed spatial direction  $i$  (no sum),

$$\boxed{T_{\text{bg}}^{ww} - T_{\text{bg}}^{ii} = u_0^2.} \quad (6.6)$$

This anisotropy is a direct consequence of the gradient condensate (P4) and is *independent of the background potential contribution*  $V_{\text{bg}}$ . The ordered condensate therefore distinguishes the preferred  $w$ -direction from the transverse directions already at the level of the Noether tensor. In the ordered-branch Lorentzian reading, implemented through the real parametrisation  $t = w/c_*$ , this anisotropy is reinterpreted as the difference between temporal and spatial components in the effective energy-momentum description (Level A computation; Lorentzian interpretation Level B).

This is consistent with the arrow-of-time analysis of Section 3.8: the same ordered background that distinguishes the preferred branch direction also distinguishes the temporal and spatial components of the effective stress tensor.

**Background stress anisotropy and effective vacuum interpretation.** Equations (6.3)–(6.4) show that the ordered background carries an anisotropic stress pattern. If one adopts the Lorentzian branch interpretation in which  $T_{\text{bg}}^{ww}$  is read as an energy-density component and  $T_{\text{bg}}^{ii}$  (no sum) as minus the corresponding pressure, then one is naturally led to the effective identifications

$$\rho_{\text{bg}}^{\text{eff}} = \frac{u_0^2}{2} - V_{\text{bg}}, \quad p_{\text{bg}}^{\text{eff}} = -\left( \frac{u_0^2}{2} + V_{\text{bg}} \right). \quad (6.7)$$

Formally this gives

$$w_{\text{bg}}^{\text{eff}} = \frac{p_{\text{bg}}^{\text{eff}}}{\rho_{\text{bg}}^{\text{eff}}} = -\frac{u_0^2/2 + V_{\text{bg}}}{u_0^2/2 - V_{\text{bg}}}. \quad (6.8)$$

The algebraic formula is immediate once the Lorentzian interpretation is adopted, but its physical vacuum-energy meaning depends on the background subtraction and EFT matching used in the macroscopic gravitational sector. For this reason, the expression above should be read as a structurally motivated effective relation rather than as a standalone prediction for the observed dark-energy equation of state.

**Bridge to the gravitational source tensor.** The Noether tensor of the microscopic  $\Phi$ -medium provides the natural starting point for the effective source tensor used in the macroscopic gravitational description. However, the explicit bridge from the Euclidean microscopic tensor to the Lorentzian source tensor entering the generalised Einstein equations requires coarse graining, background subtraction, and EFT matching. Accordingly, the bridge is structurally well motivated, but its explicit realisation is a Level B statement rather than a strict Level A derivation (developed in Section 13.3).

**Ward identities and the quantum programme.** The Noether conservation laws suggest that Ward-type identities should exist in the coherent quantum sector as well. In a completed quantum reconstruction of ECT, such identities may help constrain the effective action and its symmetry structure. At present, however, neither the explicit form of these identities nor their relation to effective general covariance has been derived. This remains part of the open quantum programme.

**Constrained structure of possible Lorentz violation.** The ordered-branch construction suggests that Lorentz-violating effects, if present, should exhibit correlated rather than arbitrary structure: they are expected to reflect the condensate anisotropy associated with the preferred branch direction. In that sense ECT points toward a more constrained pattern than a fully general SME-style parameterisation. A precise mapping of the effective LV operator basis remains open.

**Sector dependence of physical interpretation.** The same variational backbone underlies multiple effective descriptions. What depends on the later development of the theory is not the existence of Noether structure, but the physical interpretation of the resulting currents and charges in particular sectors. In some sectors the corresponding observables already admit a clear physical reading; in others — especially the gauge and particle sectors — the exact mapping to late-time observed charges and couplings remains incomplete.

**Inheritance by the ordered branches.** Spontaneous symmetry breaking  $O(4) \rightarrow O(3)$  reorganises the medium into reduced sectors but does not destroy the variational backbone. Both the geometric and the coherent branch inherit variational logic from the underlying medium; their effective equations of motion are reductions of (6.1), not independent postulates:

$$\delta S_E[\Phi] = 0 \implies \delta S_{\text{eff}} = 0 \quad (6.9)$$

after branch reduction, coarse-graining, or EFT matching. This is Level A/B: the reduction scheme is structural, but the explicit form of  $S_{\text{eff}}$  for each branch must still be determined by EFT matching (Appendix R).

**Relation to the arrow of time.** The variational principle does not conflict with the emergence of a thermodynamic arrow of time (Section 3.8). At the fine-grained level the dynamics remains extremal. Irreversibility arises only at the coarse-grained level, where the full microscopic branch information is no longer tracked. ECT therefore does not obtain entropy growth by breaking extremality; rather, it obtains effective irreversibility by combining extremal fine-grained dynamics with multiplicity (S6), inhomogeneous ordering (S9), and coarse graining of branch evolution (Level B).

**Relation to  $S_0$  and the classical/quantum divide.** The variational backbone also links naturally to the pre-quantum action scale  $S_0$  (Section 5.6). Extremality determines which histories are dynamically selected;  $S_0$  controls when action differences remain phase-sensitive. When  $|\Delta S| \gg S_0^{\text{EFT}}$ , relative phases oscillate rapidly and an effectively classical, extremal description dominates. When  $|\Delta S| \sim S_0$ , phase sensitivity cannot be neglected and nearby histories contribute nontrivially. ECT therefore relates classical extremality and quantum behaviour through the same action framework, with  $S_0$  governing the transition between the two regimes (Level B; Section 5.6).

**Coarse graining and effective extremality.** Coarse graining does not eliminate the fundamental variational principle; it changes the level of description. Many distinct fine-grained extremal configurations correspond to the same effective coarse-grained state, and this is precisely why macroscopic irreversibility and entropy growth can coexist with an underlying variational dynamics. Some effective sectors of ECT can still be written in extremal form even when their exact derivation from the bare action has not yet been completed (Level B closure).

**Defect and topological sectors.** Because S9 and S10 allow inhomogeneous ordering and topological sectors, defects, domain walls, and defect-adjacent configurations must also be regarded as admissible members of the overall variational framework. What changes is not whether they are governed by extremality, but whether a simple smooth effective reduction is available. Defect sectors can therefore be structurally natural in ECT without being fully integrated into the present smooth low-energy EFT.

**Comparison with other variational frameworks.** *Ordinary classical field theory* [48]: the action principle is usually taken as the formal starting point of dynamics on a pre-existing spacetime. In ECT the role of the action is deeper: it selects realised configurations of a pre-spacetime medium.

*Condensed-matter effective actions* [21]: in condensed matter, collective modes are described by effective actions inherited from a more microscopic substrate. ECT follows the same structural logic, but with the medium more fundamental than spacetime itself.

*Stationary phase and path-integral logic* [46]: the relation between extremality and  $S_0$  mirrors stationary-phase dominance in the path integral. ECT reproduces this logic structurally: extremality governs the backbone of realised histories, while  $S_0$  controls when neighbouring histories remain phase-relevant.

#### Status summary.

Statement	Status	Comment
Physical configurations selected variationally	A	DP
Noether $T^{AB}$ : existence and conservation	A	P1 + P3 + DP
Noether $J^{C,AB}$ : existence and conservation	A	P1 + P2 + DP
Symmetry-compatible action implies Noether structure	A	Standard variational logic
Lorentzian interpretation of translation currents as energy–momentum	B	Ordered-branch Lorentzian EFT interpretation
Background anisotropy $T_{\text{bg}}^{ww} - T_{\text{bg}}^{ii} = u_0^2$	A	Direct computation; independent of $V_{\text{bg}}$
Effective vacuum equation-of-state interpretation	B	Requires Lorentzian reading + background subtraction/matching
Restriction of the variational problem preserves extremality	A	Branch-restricted variational problem
Explicit reduced branch functional $S_{\text{eff}}$	B	EFT matching needed
Coherent branch inherits variational structure	B	In reduced branch EFT
Structural bridge to macroscopic source tensor	B	Coarse graining + EFT matching; §13.3
Constrained LV structure from condensate anisotropy	B	Structural expectation; explicit basis open
Ward identities in the coherent quantum sector	C (open)	Quantum reconstruction not complete
Defect sectors compatible with variational framework	B	Not fully reduced to smooth EFT
Irreversibility compatible with extremality	B	Through coarse graining (§3.8)
Classical limit as extremal dominance ( $ \Delta S  \gg S_0^{\text{EFT}}$ )	B	Linked to §5.6
Full derivation of all effective branch functionals	Open	Not yet completed
Late-time charge reconstruction in all sectors	Open	Depends on gauge/quantum programme

## 6.7 Remark on defect sectors beyond the smooth coherent sector

The derived coherent-sector rule BR1 restricts the present section to the *defect-free* smooth coherent sector: configurations with integer winding numbers, non-vanishing amplitude  $\rho$ , and smooth orientation variable  $n_A$ . This restriction does not forbid defect configurations ontologically: the topological completeness property S10 ensures that all topological sectors compatible with the vacuum manifold  $O(4)/O(3) \simeq S^3$  remain admissible parts of the theory. Configurations not belonging to the coherent sector include:

- *Vortex cores*: configurations with  $\rho = 0$  where phase  $\theta$  is undefined;
- *Domain-wall-like configurations*: discontinuous or sharply varying profiles of  $n_A$ , not protected as topologically stable walls for the primary vacuum manifold;

- *Instantons*: non-trivial topological configurations in Euclidean space describing tunnelling between different vacuum sectors [6].

ECT basics already indicates the existence of this richer space of states. The smooth coherent-sector restriction does not “artificially eliminate” any physics; it selects a sector and thereby *leaves open* a broader structure beyond it. The particle-level topological classification of these sectors, including the primary homotopy anti-predictions ( $\pi_0 = \pi_1 = \pi_2 = 0$ ) and the  $\pi_3(S^3) = \mathbb{Z}$  sector, is summarised in Section 8.10.

## 6.8 Foundational consequences and branch-selection rules

For later use it is convenient to collect the main consequences of the core foundational framework (Sections 2–6).

1. **Ordered-branch rule.** The physically realised vacuum belongs to an ordered branch with non-zero gradient condensate,  $\langle \partial_A \Phi \rangle \neq 0$ , which spontaneously breaks  $O(4) \rightarrow O(3)$ .
2. **Amplitude–orientation decomposition.** On the ordered branch the condensate gradient admits the decomposition

$$\partial_A \Phi = u n_A, \quad u \geq 0, \quad n_A n_A = 1.$$

Because  $Q_A = \partial_A \Phi$  is an exact one-form,  $u$  and  $n_A$  are not independent: they satisfy the integrability condition  $\partial_A(u n_B) - \partial_B(u n_A) = 0$ , which reduces the orientation sector to one longitudinal soft scalar at linear order (Level B; Appendix I).

3. **Uniqueness of the broken-phase kinetic tensor.** Local symmetric rank-2 tensors compatible with the residual  $O(3)$  symmetry take the form

$$K^{AB} = \beta \delta^{AB} - \alpha n^A n^B.$$

Here  $n_A$  is the derived ordered-branch orientation variable, not an independent microscopic field (Section 4.2).

4. **Signature classification rule.** Depending on  $(\alpha, \beta)$ , the broken-phase kinetic operator has Euclidean, degenerate, or Lorentzian signature.
5. **Macroscopic viability rule.** Only the hyperbolic branch ( $\alpha > \beta$ ) can serve as a Lorentzian macroscopic causal sector. Within ECT, the additional condition  $c_* = c$  then fixes the realised ordered branch more specifically to  $\alpha = 2\beta$ . Thus the theory first identifies the Lorentzian admissibility region and then selects its physical ECT realisation, rather than imposing Lorentzianity as an extra axiom.
6. **Smooth coherent-sector rule (BR1).** In the defect-free coherent infrared branch with single-valued collective phase, the winding number is necessarily integer:

$$\oint_{\mathcal{C}} \partial_A \theta dX^A = 2\pi n, \quad n \in \mathbb{Z}.$$

7. **Two-branch rule.** The ordered condensate framework supports two effective developments: the geometric macroscopic branch and the coherent branch. They arise from the same underlying medium but retain different classes of observables under coarse-graining.

These statements will be used repeatedly in the subsequent development of the gravitational, cosmological, astrophysical, gauge, particle, fermionic, and quantum sectors.

## 7 Gauge Symmetries, Matter Couplings, and the ECT-Specific Fifth Coupling

*This section unifies the gauge-sector architecture of ECT with the interaction structure of the embedded matter sector and the ECT-specific fermion–condensate coupling. The emergence of  $U(1)$  and the structural admissibility of non-Abelian and electroweak-like sectors are discussed first; the second half of the section develops the leading ECT-specific deformation of matter interactions and its observational status. Status: the  $U(1)$  gauge route is the strongest result of this section; non-Abelian, electroweak, and matter-coupling sectors remain Level B/C structural embedding or open programme.*

### 7.1 Internal structures of the condensate relevant to interactions

*Status: mixed structural A/B/C. The decomposition itself and the existence of the ordered-branch direction  $n_A$  are structural Level A results. This subsection does not derive the physical Standard Model gauge group. What it establishes is the structural decomposition of the ordered branch relevant to the interaction sector: (i) the compact phase sector, (ii) multiplet/non-Abelian internal structure, (iii) colour-like extensions, and (iv) the preferred condensate direction  $n_A$  as an ordered-branch geometric ingredient. The compact  $U(1)$  phase route is then developed below to near-theorem level within the extended phase EFT, whereas the non-Abelian and electroweak sectors remain Level B/C embeddings.*

The ordered condensate branch established in Sections 3–6 introduces not only an effective Lorentzian spacetime structure but also several distinct structures relevant to interactions. Some of them are genuine internal structures of the condensate description (phase, multiplet organisation, colour-like extension), while others arise from the geometry of the ordered branch itself. To avoid later confusion, these structures should be sharply separated from one another.

**Proposition: interaction-relevant structural decomposition.** Within the present ECT formulation, the ordered branch supports four conceptually distinct structures relevant to the interaction sector:

1. a *compact phase sector* of the coherent EFT,
2. *multiplet/non-Abelian internal structure*,
3. *colour-like extensions* of such internal structure,
4. a *preferred condensate direction*  $n_A = \partial_A \Phi / |\partial \Phi|$ .

**Proof.** The first three ingredients are distinguished by the type of field-space structure carried by the effective condensate description: compact phase, internal multiplet indices, and colour-like triplet organisation. The fourth ingredient is of a different nature: it is not an internal symmetry but a derived orientational variable of the ordered branch, defined once the gradient condensate selects a preferred direction in the broken phase. Since these four ingredients act at distinct structural levels, they must be treated separately in the interaction analysis.  $\square$

**Compact phase sector.** As a structural low-energy representation of the coherent branch, consider the complex condensate field

$$\Phi_{\text{eff}}(X) = \rho(X) e^{i\theta(X)}. \quad (7.1)$$

Here  $\theta(X)$  is the compact phase variable of the coherent branch. In the emergent complex ordered sector (Section 21.1; the minimal ECT field is real, and the phase language belongs to the two-component extension), a constant phase shift

$$\Phi_{\text{eff}} \rightarrow e^{i\alpha} \Phi_{\text{eff}} \quad (7.2)$$

leaves the effective action invariant. This compact phase route provides the cleanest and most developed entry point from condensate structure to gauge-like interactions. It is developed in Section 7.2.

**Multiplet/non-Abelian structure.** If the condensate is organised into internal multiplets, non-Abelian internal structures become available. In particular, the ordered branch admits the algebraic bridge  $\mathfrak{so}(3) \cong \mathfrak{su}(2)$ , which makes electroweak-like embeddings structurally available. This is an algebraic and EFT-level availability statement, not yet a first-principles derivation of the physical non-Abelian gauge sector. It is developed in Sections 7.3 and 7.4.

**Colour-like extension.** If the condensate carries suitable triplet structure in an internal sector, an  $SU(3)$ -type colour-like extension can be accommodated at the level of model building (see §40 for a candidate completion). At the present stage this remains a structural possibility rather than a derivation of QCD or confinement from the bare condensate action. This is discussed in Section 7.3.

**Preferred condensate direction.** The symmetry breaking  $O(4) \rightarrow O(3)$  selects a preferred direction

$$n_A = \frac{\partial_A \Phi}{|\partial \Phi|}. \quad (7.3)$$

This quantity is not an internal gauge degree of freedom and not a multiplet index. It is a derived orientational variable of the ordered branch. Its existence is a direct structural consequence of the ordered gradient condensate. Later, it enters the matter sector through the ECT-specific fermion–condensate coupling. This ingredient therefore belongs to the interaction architecture, but not to the internal gauge-symmetry side of that architecture.

**What is strictly established here.** The present subsection does *not* derive the Standard Model gauge group. What it does establish is the structural decomposition of the interaction sector into: (i) a compact phase route, (ii) non-Abelian multiplet embeddings, (iii) colour-like extensions, and (iv) the ECT-specific preferred-direction ingredient  $n_A$ . Among these, the compact phase route is the most developed and is the only one carried below to near-theorem level.

**Distinction from spacetime symmetry breaking.** The spacetime symmetry breaking  $O(4) \rightarrow O(3)$  acts on the Euclidean coordinate index  $A$  and produces the ordered branch with emergent Lorentzian structure. The internal structures discussed here act at a different level: phase, multiplet organisation, and colour-like structure belong to the effective condensate description, while  $n_A$  is a geometric remnant of the ordered branch itself. This separation between spacetime-level ordering and interaction-level structure is essential for the logic of the gauge sector. Its relation to the Coleman–Mandula logic is discussed further in Section 7.11.

**Roadmap.** The remainder of this section proceeds in four steps. Section 7.2 develops the compact  $U(1)$  phase route. Sections 7.3 and 7.4 consider the non-Abelian and electroweak-like embeddings. The later fifth-coupling block treats the ECT-specific matter-sector deformation associated with the preferred condensate direction  $n_A$ .

#### Status summary.

Structure	Status	Comment
Compact phase sector	A/B	Structural $U(1)$ route in the coherent phase EFT
Non-Abelian multiplet structure	B/C	Algebraic/EFT embedding, not derivation
Colour-like extension	C	Model-level possibility only
Preferred condensate direction $n_A$	A	Ordered-branch geometric ingredient
Standard Model gauge group fully derived	Open	Not established here



## 7.2 Emergence of $U(1)$ gauge symmetry

*Status: layered. Layer 1 is Level A within the compact coherent-phase EFT: once the ordered branch is described by the compact phase variable  $\theta$ , the Noether current, its conservation, and the homogeneous limit follow strictly. Layer 2 is Level A after the introduction of P5 (medium character): P5 implies that pointwise phase values are descriptive redundancies (L1–L3 below), so the compensating connection, the Maxwell-type leading kinetic structure, and the gauge-covariant compact holonomy/flux-quantisation statements follow by standard EFT classification plus compact phase geometry without additional assumptions. Layer 3 remains Level A/B matching: identification with the physical photon is not yet a full derivation of QED from P1–P6.*

**Connection to the coherent branch.** The phase field  $\theta(X)$  appearing in this subsection is the same compact variable introduced in the coherent branch (BR1). Its winding structure underlies the distinguished EFT action scale  $S_0^{\text{EFT}}$  (Section 5.6), and its dynamics is developed further in the Quantum Sector (Section 21.1). The present subsection extracts the gauge-theoretic consequences of that same compact phase structure.

### Layer 1: global $U(1)$ symmetry and the Noether current (Level A within the compact phase EFT).

*Assumption for Layer 1.* The coherent branch admits an effective compact phase representation  $\Phi_{\text{eff}}(X) = \rho(X)e^{i\theta(X)}$ , with global phase symmetry (7.2). Within that phase EFT, the following statements are strict.

**Theorem 1: Noether current.** For the global phase symmetry (7.2), the conserved current is

$$j^A \equiv \frac{-i}{2} (\Phi_{\text{eff}}^* \partial^A \Phi_{\text{eff}} - \Phi_{\text{eff}} \partial^A \Phi_{\text{eff}}^*). \quad (7.4)$$

Using  $\Phi_{\text{eff}} = \rho e^{i\theta}$ , this reduces to

$$j^A = \rho^2 \partial^A \theta. \quad (7.5)$$

*Proof.* Under an infinitesimal global phase shift,  $\delta \Phi_{\text{eff}} = i\alpha \Phi_{\text{eff}}$ ,  $\delta \Phi_{\text{eff}}^* = -i\alpha \Phi_{\text{eff}}^*$ . Noether's theorem applied to the canonical complex kinetic structure gives (7.4). Substituting the polar form yields (7.5). The full derivation is given in Appendix S.  $\square$

**Corollary 1: current conservation.** The Noether current satisfies  $\partial_A j^A = 0$ .

*Proof.* Direct Noether consequence of the exact global phase symmetry of the compact phase EFT.  $\square$

**Corollary 2: homogeneous limit.** For a homogeneous phase configuration,  $\partial_A \theta = 0 \implies j^A = 0$ .

*Proof.* Immediate from (7.5).  $\square$

**Physical interpretation.** The current (7.5) is the phase gradient weighted by the condensate density. In the ECT interpretation, this suggests that charge-carrying excitations are associated with phase-topological or phase-gradient structures of the ordered medium. This is structurally analogous to supercurrents in superfluids and superconductors [21], though not physically identical to a material condensate.

**Layer 2: local  $U(1)$  completion and gauge connection.** The following three conditions were originally introduced as conditional assumptions. With the medium-character postulate P5, they are now structural consequences of the postulate framework:

(L1) locality of the effective description — follows from P3;

(L2) only phase gradients, not the absolute phase, enter local observables — follows from P2 (the action does not depend on  $\theta$  explicitly) together with P5 (pointwise  $\theta$  is not an observable);

(L3) local phase redefinitions are treated as redundancies of the effective description — this is the direct content of P5 applied to the compact phase sector.

With L1–L3 established, the gauge-emergence construction below proceeds without additional assumptions.

**Proposition 2: local phase redundancy requires a compensating connection.** Under the local phase transformation  $\Phi_{\text{eff}}(X) \rightarrow e^{i\alpha(X)}\Phi_{\text{eff}}(X)$ , the ordinary derivative is not covariant:

$$\partial_A \Phi_{\text{eff}} \rightarrow e^{i\alpha(X)} (\partial_A \Phi_{\text{eff}} + i(\partial_A \alpha) \Phi_{\text{eff}}). \quad (7.6)$$

To restore covariance one must introduce a compensating field  $A_A$  and define

$$D_A = \partial_A - ieA_A, \quad (7.7)$$

together with the transformation law

$$A_A \rightarrow A_A + \frac{1}{e} \partial_A \alpha. \quad (7.8)$$

Then  $D_A \Phi_{\text{eff}} \rightarrow e^{i\alpha(X)} D_A \Phi_{\text{eff}}$ .

*Proof.* This is the unique first-order local compensating completion of the ordinary derivative under local phase redefinition. Any compensating field must remove the inhomogeneous term  $i(\partial_A \alpha) \Phi_{\text{eff}}$ . At leading derivative order this requires a connection transforming as (7.8), which then yields the covariant derivative (7.7). See Appendix S for details.  $\square$

**Remark on status.** With the medium-character postulate P5, assumptions L1–L3 are no longer conditional but follow from the postulate framework (P2 + P3 + P5; see above). Therefore Propositions 2 and 3 are structural consequences of the ECT postulates applied to the compact-phase sector (Level A).

**Proposition 3: leading local gauge kinetic term.** Define the gauge-invariant field strength

$$F_{AB} = \partial_A A_B - \partial_B A_A. \quad (7.9)$$

Among local parity-even gauge-invariant terms quadratic in the field strength and containing at most two derivatives, the leading kinetic term is uniquely of Maxwell type:

$$S_{\text{gauge}} = -\frac{1}{4} \int d^4 X F_{AB} F^{AB}. \quad (7.10)$$

*Proof.* Gauge invariance excludes any mass term  $A_A A^A$ . At two-derivative order, all local parity-even quadratic gauge invariants reduce, up to total derivatives and normalisation, to  $F_{AB} F^{AB}$ . Hence (7.10) is the unique leading canonical kinetic term at this order.  $\square$

**Coupling constant.** The gauge coupling  $e$  is not fixed by the above argument. It remains a free EFT matching parameter.

### Layer 3: compact holonomy, flux quantisation, and photon matching.

**Theorem 4: compact holonomy in the local phase EFT.** For compact phase  $\theta \sim \theta + 2\pi$ , define the gauge-invariant phase gradient

$$\mathcal{D}_A \theta \equiv \partial_A \theta - e A_A. \quad (7.11)$$

Single-valuedness of the condensate around a closed loop  $\gamma$  implies

$$\oint_{\gamma} \mathcal{D}_A \theta dX^A = 2\pi n, \quad n \in \mathbb{Z}. \quad (7.12)$$

Hence

$$e \oint_{\gamma} A_A dX^A = 2\pi n \quad (7.13)$$

up to sign convention.

*Proof.* Compactness of  $\theta$  implies that the total phase winding around any closed loop is an integer multiple of  $2\pi$ . Subtracting the gauge part gives (7.12), which then yields (7.13).  $\square$

**Photon matching.** If the coherent-branch  $U(1)$  remains unbroken, the associated gauge boson is naturally massless. This makes the compact phase sector the most natural condensate candidate for an emergent electromagnetic gauge degree of freedom. The identification of this massless  $U(1)$  boson with the physical photon is, however, still a Level B matching statement rather than a completed derivation of QED from the minimal postulates.

**Superfluid analogy.** The present  $U(1)$  construction is structurally analogous to the phase–current and phase–holonomy logic of superfluids and superconductors [21]. The analogy is structural, not an exact physical identification. The ECT condensate is not a material medium; it is the ordered background underlying the effective spacetime and interaction sectors.

**Interpretive example: the Aharonov–Bohm effect (Level B).** The Aharonov–Bohm (AB) effect—in which an observable phase shift occurs even in regions where the local field strength vanishes—is especially natural within the ECT gauge architecture. Because the compact phase  $\theta(X)$  is already a primary structural ingredient of the coherent branch (BR1), and the gauge connection  $A_A$  arises as its local compensating field (Layer 2 above), the AB phase shift

$$\Delta\varphi = \frac{e}{S_0} \oint A_{\mu} dx^{\mu} \quad (7.14)$$

is directly interpretable as a nontrivial holonomy of the emergent  $U(1)$  connection around a closed loop. This ties together local phase symmetry, the loop/winding structure of the coherent branch, and the physical significance of the gauge potential in a way that is structurally natural for the condensate framework. The standard AB phase formula is naturally accommodated in this picture; the gain at the present stage is interpretive rather than quantitative: the effect illustrates why the gauge potential, rather than only the field strength, carries physical information when phase is a primary condensate variable.

**What is strict and what remains matched.** Within the compact phase EFT, the Noether current, current conservation, and the homogeneous limit are strict results. After the introduction of the medium-character postulate P5, the local phase redundancy, compensating gauge connection, leading Maxwell-type kinetic structure, and the gauge-covariant compact holonomy/flux-quantisation statements become structural consequences of the postulate framework applied to the compact phase sector. What remains beyond this structural Level A result is the full physical identification of this Abelian sector with observed QED, including the coupling value  $e$ , the complete matter vertex, and full phenomenological matching.

**What has been established and what remains open.** With P5, the  $U(1)$  gauge sector has been substantially promoted:

- (i) the compact phase EFT follows from BR1 within the ordered branch (Level A);
- (ii) local phase redundancy follows from P5 (Level A) — no longer an additional assumption;
- (iii) the compensating gauge connection  $A_A$  is the unique first-order local completion of the redundancy (Level A);
- (iv) the Maxwell kinetic term is the unique leading-order parity-even gauge-invariant structure (Level A EFT classification).

The following steps remain open:

- (v) the gauge coupling  $e$  is not derived from condensate parameters;
- (vi) the physical QED matter vertex and its observed electromagnetic phenomenology are not yet a completed derivation.

Thus the  $U(1)$  gauge emergence from the compact-phase sector is now Level A for the structural gauge architecture, with Level A/B for the full physical photon identification and Level B for coupling matching.

**Status summary.**

Statement	Status	Comment
<i>Layer 1: compact phase EFT</i>		
Global phase symmetry in compact phase EFT	A/B	EFT structure admitted; consequences below strict
Noether current $j^A = \rho^2 \partial^A \theta$	A	Strict within compact phase EFT
Current conservation $\partial_A j^A = 0$	A	Noether theorem
Homogeneous limit gives $j^A = 0$	A	Direct corollary
<i>Layer 2: local phase EFT (structural after P5)</i>		
Compensating connection $A_A$	A	Structural consequence of P2+P3+P5
Covariant derivative $D_A = \partial_A - ieA_A$	A	Same
Field strength $F_{AB}$	A	Same
Maxwell-type leading kinetic term	A/B	Level A for leading EFT closure; full physical QED matching open
Compact holonomy / flux quantisation	A/B	Compact phase geometry plus local phase EFT structure
Gauge coupling $e$	C	Free matching parameter
<i>Layer 3: physical matching</i>		
Massless $U(1)$ boson structurally consistent with photon	B	Matching, not full derivation
QED fully derived from P1–P6	Open	

### Structural route to the fine-structure constant

If the  $U(1)$  gauge field  $A_\mu$  is emergent from the condensate phase sector, then its kinetic term arises with a normalisation coefficient  $Z_A$  that is in principle calculable:

$$\mathcal{L}_{\text{eff}} = -\frac{Z_A}{4} F_{\mu\nu} F^{\mu\nu} + \bar{\psi} i \gamma^\mu (\partial_\mu - i q A_\mu) \psi + \dots \quad (7.15)$$

After canonical normalisation  $A_\mu^{(c)} = \sqrt{Z_A} A_\mu$ , the observed electromagnetic coupling becomes

$$e = \frac{q}{\sqrt{Z_A}}, \quad \alpha_{\text{fs}} = \frac{e^2}{4\pi} = \frac{q^2}{4\pi Z_A}. \quad (7.16)$$

This reduces the problem of the fine-structure constant to the determination of the emergent gauge-field normalisation  $Z_A$ .

**Required magnitude.** For  $q = 1$  the observed value  $\alpha_{\text{fs}}^{-1} \approx 137$  requires

$$Z_A^{\text{IR}} = \frac{1}{4\pi \alpha_{\text{fs}}} \approx 10.9. \quad (7.17)$$

This is a moderate coefficient of order ten, not an extreme number.

**Electroweak structure of the ultraviolet problem.** The low-energy relation  $\alpha_{\text{fs}} = q^2/(4\pi Z_A)$  is defined in terms of the photon normalisation  $Z_A$ . However, above the electroweak scale  $M_W$  the photon is not a propagating eigenstate: the physically relevant gauge basis is  $U(1)_Y \times SU(2)_L$ , with independent electroweak gauge-kinetic normalisations for the hypercharge field  $B_\mu$  and the weak isospin field  $W_\mu^a$ . The low-energy photon kinetic term emerges only after electroweak symmetry breaking through the Weinberg mixing:

$$\frac{1}{e^2} = \frac{1}{g'^2} + \frac{1}{g^2}, \quad \alpha_{\text{fs}}^{-1} = \alpha_Y^{-1} + \alpha_2^{-1}. \quad (7.18)$$

Consequently, the ultraviolet problem for  $\alpha_{\text{fs}}$  is not the determination of a single coefficient  $Z_A^{(0)}$  at the condensate scale, but of the pair  $(Z_B^{(0)}, Z_W^{(0)})$  and the electroweak mixing angle  $\theta_W$  that relates them to the low-energy photon.

**Sharpened electroweak target after colour completion (Level B/C).** The candidate  $SU(3)$ -structured colour completion of the medium (§40) removes one of the earlier bookkeeping ambiguities: quark-like charged sectors are no longer entirely unspecified. This sharpens the fine-structure problem but does not yet solve it.

Using the observed Standard-Model electroweak couplings and the observed three-generation matter content only as an external benchmark (not as an ECT derivation), and employing the standard hypercharge normalisation with one-loop beta coefficients  $b_Y = 41/6$  and  $b_2 = -19/6$ , one finds at the electroweak scale  $\alpha_Y^{-1}(M_Z) \approx 98.4$  and  $\alpha_2^{-1}(M_Z) \approx 29.6$ . In particular, the observed three-generation Standard-Model matter content is used here only as benchmark input, not as a quantity already derived within ECT. Running to the primary condensate scale  $\phi_0 \approx 2.435 \times 10^{18}$  GeV yields

$$\alpha_Y^{-1}(\phi_0) \approx 57, \quad \alpha_2^{-1}(\phi_0) \approx 49, \quad (7.19)$$

corresponding to benchmark ultraviolet gauge-kinetic coefficients  $Z_B^{\text{bench}} \approx 4.6$  and  $Z_W^{\text{bench}} \approx 3.9$ . These are moderate numbers of order unity, not extreme values. Within this external benchmark, purely loop-induced electroweak kinetic normalisations are not compatible with the observed low-energy couplings; any viable ECT closure must therefore contain a condensate-level contribution to the gauge sector.

**ECT structural connection.** In ECT the benchmark ultraviolet gauge-kinetic targets are expected to descend from the same ordered-condensate architecture that also determines  $G_N$  and  $\hbar$ : the hypercharge-sector normalisation from the compact-phase stiffness  $K_\theta^{\text{eff}} \sim \phi_0^2$  and the weak-sector normalisation from the orientation stiffness  $\kappa_n \sim \phi_0^2$ . In a completed closure these would define the microscopic coefficients customarily denoted  $Z_B^{(0)}$  and  $Z_W^{(0)}$ . Both sectors are anchored in the same ordered-condensate framework and are naturally controlled by the primary condensate scale  $\phi_0$ , although the corresponding effective stiffness coefficients need not coincide exactly. Their ratio is therefore expected to become a structural output of the single-medium construction rather than a freely adjustable low-energy parameter. If the phase and orientation sectors contribute with comparable stiffnesses, one expects

$$\sin^2 \theta_W(\phi_0) = \mathcal{O}(1/2), \quad (7.20)$$

which is qualitatively compatible with the observed value  $\sin^2 \theta_W(M_Z) \approx 0.231$  after electroweak-scale running. This plays a role loosely analogous to ultraviolet Weinberg-angle relations in unified gauge models, although the underlying mechanism here is different: in ECT it is tied to the relative condensate-sector stiffnesses rather than to simple-group embedding.

**Status.** ECT transfers the question “why is  $\alpha_{\text{fs}} \approx 1/137$ ?” into a concrete electroweak kinetic/mixing target. The required UV normalisations are moderate, the bookkeeping problem is now better posed than before colour completion, and the Weinberg angle becomes a structural target rather than a postulated input. The first-principles derivation of  $(Z_B^{(0)}, Z_W^{(0)})$  from condensate microphysics, of the electroweak mixing angle, and hence of  $\alpha_{\text{fs}}$  remains open (Level B/C, OP- $\alpha_{\text{fs}}$ ). Accordingly,  $\alpha_{\text{fs}}$  is not treated in ECT as an irreducible primitive constant, but as a sharpened electroweak kinetic/mixing target within the broader derivational map summarised in the Conclusion. Technical details are collected in Appendix Z.

The Abelian construction provides the cleanest example of how gauge structure can emerge from condensate variables. The next subsections ask to what extent this logic can be extended to the non-Abelian and electroweak sectors.

### 7.3 Non-Abelian gauge structure and its status

*Status: substantially strengthened by P5. With the medium-character postulate P5, local orientation redundancy of the ordered branch is no longer an additional assumption but a structural consequence of the postulate framework. The non-Abelian covariant derivative, field strength, and Yang–Mills kinetic term then follow by standard EFT completion (Level A/B). The algebraic bridge  $\mathfrak{so}(3) \cong \mathfrak{su}(2)$  is a strict Level A Lie-algebra fact. Together with the  $U(1)$  phase sector, this gives the ordered-branch gauge architecture  $SU(2) \times U(1)$  (Level A for the structural gauge redundancy; Level A/B for the full dynamical gauge closure). Identification with the physical Standard Model gauge group, its couplings, and its strong/electroweak phenomenology remains Level B/C embedding or open.*

**General non-Abelian framework.** Suppose that the effective condensate description contains internal multiplet degrees of freedom

$$\Phi = (\Phi_1, \Phi_2, \dots, \Phi_N)^T, \quad (7.21)$$

and that the effective action is invariant under global  $SU(N)$  transformations

$$\Phi \rightarrow U\Phi, \quad U \in SU(N). \quad (7.22)$$

If one further admits local multiplet redundancy  $U \rightarrow U(X)$ , covariance requires the introduction of gauge connections. The corresponding covariant derivative is

$$D_A = \partial_A - ig A_A^a T^a, \quad (7.23)$$

where  $T^a$  are the generators of the Lie algebra and  $A_A^a$  are the associated gauge fields.

**Field strength and Yang–Mills structure.** The gauge-covariant field strength is

$$F_{AB}^a = \partial_A A_B^a - \partial_B A_A^a + g f^{abc} A_A^b A_B^c, \quad (7.24)$$

where  $f^{abc}$  are the structure constants of the group. At leading derivative order, the canonical parity-even gauge-field action is

$$S_{\text{gauge}} = -\frac{1}{4} \int d^4X F_{AB}^a F^{aAB}. \quad (7.25)$$

**Structural theorem: local non-Abelian EFT completion.** Once the ordered-branch orientation redundancy is promoted by P5 to a local descriptive redundancy, and the corresponding multiplet structure is specified, the covariant derivative (7.23), field strength (7.24), and leading Yang–Mills kinetic structure (7.25) follow by the same EFT logic as in the Abelian case. In that sense, ECT is structurally compatible with non-Abelian gauge theories at leading derivative order.

**Proof sketch.** Local multiplet covariance requires a compensating connection valued in the Lie algebra. Closure of the local algebra forces the gauge field to transform in the adjoint and introduces the commutator term in the field strength. Among local parity-even gauge-invariant terms quadratic in the field strength and containing at most two derivatives, the Yang–Mills form is the standard leading EFT choice.  $\square$

**Appendix reference.** The explicit structural local-completion steps and the  $\mathfrak{so}(3) \cong \mathfrak{su}(2)$  bridge are written out in Appendix T.

**Status update after P5.** With the medium-character postulate P5, the local orientation redundancy of the ordered branch is no longer an additional assumption: P5 asserts that pointwise orientation  $n_A(X)$  is a descriptive redundancy, so local redefinitions  $n_A(X) \rightarrow R_A^B(X) n_B(X)$  are local gauge redundancies of the ordered description. The compensating connection valued in  $\mathfrak{so}(3) \cong \mathfrak{su}(2)$  and the leading Yang–Mills kinetic structure then follow by the same EFT logic as in the  $U(1)$  case (Level A for the gauge redundancy; Level A/B for the full dynamical closure). The representation content and the value of the coupling  $g$  remain open matching parameters.

**Ordered-branch gauge architecture.** Combining the  $U(1)$  gauge connection from the compact-phase sector (Section 7.2) with the  $\mathfrak{su}(2)$  gauge connection from the orientation sector, the ordered branch of ECT carries the local gauge architecture

$$\boxed{SU(2) \times U(1)} \quad (\text{Level A for structural gauge redundancy}). \quad (7.26)$$

This is the central gauge-emergence result of ECT. It follows from P2 + P3 + P4 + P5 without importing the Standard Model gauge group as an external input. What is fixed here is the ordered-branch gauge architecture as a structural redundancy of the low-energy description. What is not yet fixed are the full representation content, coupling values, symmetry-breaking pattern at the electroweak scale, and the complete identification with observed Standard Model phenomenology. The identification of this ordered-branch gauge structure with the physical electroweak gauge group  $SU(2)_L \times U(1)_Y$  is a further Level B matching step developed in Section 7.4.

**The algebraic bridge:**  $\mathfrak{so}(3) \cong \mathfrak{su}(2)$ . After the spacetime symmetry breaking  $O(4) \rightarrow O(3)$ , the residual unbroken rotation algebra of the ordered branch is

$$\mathfrak{so}(3) \cong \mathfrak{su}(2). \quad (7.27)$$

This is a strict Lie-algebra isomorphism and therefore a genuine Level A statement. It means that among the simple Standard Model gauge factors,  $SU(2)$  is uniquely distinguished by a direct algebraic analogue in the ordered branch.

**Global-group caveat.** The statement  $\mathfrak{so}(3) \cong \mathfrak{su}(2)$  does *not* identify the global groups  $SO(3)$  and  $SU(2)$ . Their representation content differs:  $SU(2)$  admits doublets, whereas  $SO(3)$  does not. Thus the algebraic bridge is significant but not yet sufficient to derive the physical weak-interaction sector. Its relation to chirality and the possible selection of  $SU(2)_L$  is discussed separately in Section 9.3.

**Accommodation of Standard Model gauge groups.** Within this framework, the gauge interactions of the Standard Model can be *accommodated* as arising from internal structures of the condensate:

- $U(1)$ : the coherent-branch compact phase sector (Section 7.2); this is the most developed gauge-embedding result currently available in ECT.
- $SU(2)$ : algebraically distinguished by the isomorphism  $\mathfrak{so}(3) \cong \mathfrak{su}(2)$ ; a structural route to an electroweak-like sector if a second condensate transition exists (Section 7.4).
- $SU(3)$ : requires an additional colour-triplet internal structure with no direct spacetime counterpart; this remains a model-level extension (Level C; see §40). In the present framework the  $SU(3)$ -like sector is taken to remain in the unbroken phase, which is structurally consistent with massless gluons and the absence of a colour-Higgs mechanism.

**Coupling constants.** The gauge couplings  $g$ ,  $g'$ , and  $g_s$  are free EFT matching parameters in the present formulation. Neither their numerical values nor their running are derived from the condensate data. Whether condensate structure could in principle constrain them remains an open problem of the ECT quantitative-unification programme (OP-GUT4 in Table 118).

**Confinement as an open problem.** The present ECT formulation shows how an  $SU(3)$ -like gauge structure may be structurally accommodated in the low-energy sector, but it does not derive confinement or replace the standard QCD account of the infrared strong-interaction regime. A full derivation of confinement within ECT would require a genuinely nonperturbative analysis going beyond the perturbative EFT embedding used here. Whether condensate structure can provide an ECT-specific route to confinement remains open (OP-GUT1 in Table 118).

**What is strict and what is embedded.** The Lie-algebra statement  $\mathfrak{so}(3) \cong \mathfrak{su}(2)$  is strict. The standard non-Abelian local completion is also structurally strong once the local multiplet EFT assumptions are admitted. By contrast, the identification of the physical Standard Model gauge group, the actual matter representation content, the electroweak sector, the strong-interaction infrared regime, and the observed coupling constants are not derived here. These remain embeddings, matchings, or open problems.

**What would be needed for full Level A.** To promote the non-Abelian sector to full Level A from P1–P6, ECT would need to show:

- (i) how internal condensate multiplets arise dynamically from the bare scalar condensate description;
- (ii) why local non-Abelian redundancy is selected rather than merely admitted as an EFT completion;
- (iii) how the physical gauge group is fixed;
- (iv) how matter representations (doublets, triplets, singlets) are selected;
- (v) how the gauge couplings are determined;
- (vi) how electroweak breaking and confinement emerge from the same condensate logic.

None of these steps has yet been completed.



### Status summary.

Statement	Status	Comment
<i>Structural redundancy (from P5)</i>		
$\mathfrak{so}(3) \cong \mathfrak{su}(2)$	A	Strict Lie-algebra fact
Local orientation redundancy of ordered branch	A	Structural consequence of P5
Ordered-branch $SU(2) \times U(1)$ gauge architecture	A	Structural redundancy from P2+P3+P5
<i>Local EFT gauge completion</i>		
Non-Abelian covariant derivative / field strength	A/B	EFT completion once multiplet structure specified
Yang–Mills leading kinetic term	A/B	Standard leading EFT closure
<i>Physical electroweak identification</i>		
$SU(2)_L \times U(1)_Y$ electroweak-like embedding	B/C	Structural route, not derivation
$SU(3)$ -like colour sector	C	Model-level extension
Gauge couplings $(g, g', g_s)$	C	Free EFT matching parameters
Confinement	Open	Not derived
Full SM gauge group from P1–P6	Open	

Among the non-Abelian sectors, the  $SU(2)$ -like case is algebraically distinguished by the residual rotation algebra of the ordered branch. The next subsection develops this connection into the electroweak-like embedding.

## 7.4 Electroweak-like embedding and its current status

*Status: layered structural embedding. The generator counting associated with a candidate second transition  $O(3) \rightarrow O(2)$  is a strict structural statement once such a transition is admitted. The electroweak-like doublet EFT, the attempted identification with the physical  $SU(2) \times U(1) \rightarrow U(1)_{\text{em}}$  pattern, the scale matching  $v_2 \simeq 246 \text{ GeV}$ , and the Higgs-like radial mode are Level B/C embedding or matching statements. A first-principles derivation from the minimal scalar ECT postulates P1–P6 is not yet available. Connection to ECT basics: Section 5.1, Appendix L.*

**Two-storey architecture.** The electroweak sector of ECT has a two-storey structure. The geometrical and fermionic origin of a preferred chiral  $SU(2)$  sector is established in Sections 7.3 and 9.3 through the residual stabiliser, the  $\mathfrak{so}(3) \cong \mathfrak{su}(2)$  bridge, and the oriented condensate. The present subsection provides the phenomenological realisation of that sector through the condensate doublet and electroweak symmetry breaking at the scale  $v_2 \simeq 246 \text{ GeV}$ . In this sense, the first storey explains *why*  $SU(2) \times U(1)$  exists as a gauge architecture; the second explains *how* it breaks.

**Why the electroweak-like sector is structurally distinguished.** Among the non-Abelian sectors, the  $SU(2)$ -like case is singled out by the Lie-algebra bridge  $\mathfrak{so}(3) \cong \mathfrak{su}(2)$  established in Section 7.3. This gives the ordered branch a structural relation to a weak-like sector that is stronger than for other simple gauge factors, but still insufficient for a derivation of the physical electroweak sector. If, in addition to the primary ordering step  $O(4) \rightarrow O(3)$ , the condensate undergoes a second effective ordering step

$$O(3) \rightarrow O(2), \tag{7.28}$$

then two generators are broken and one remains unbroken. This is a strict counting statement and provides the closest reduced structural analogue within ECT to a weak-like symmetry-breaking pattern. By itself, however, it is only an algebraic/combinatorial analogy: it does not reproduce the full Standard Model electroweak generator counting, does not derive the physical  $SU(2) \times U(1) \rightarrow U(1)_{\text{em}}$  mechanism, and does not derive the observed  $W^\pm/Z/\gamma$  spectrum.

**Candidate second-transition mechanism.** A structural candidate mechanism for such a second transition is outlined in Appendix L. At present it requires additional assumptions beyond P1–P6 (in particular, phase–orientation coupling and potential alignment). Accordingly, the second transition is not yet a theorem of the bare condensate action. A concise summary of what this appendix establishes and what remains open is given in Appendix L.

**Electroweak-like embedding model.** A convenient effective embedding is to introduce a condensate doublet

$$\Phi_{\text{ew}} = \begin{pmatrix} \Phi_1 \\ \Phi_2 \end{pmatrix}, \quad (7.29)$$

with gauge-covariant dynamics

$$S_{\text{ew}} = \int d^4X \left[ \frac{1}{2} |D_A \Phi_{\text{ew}}|^2 + \frac{\lambda_2}{4} (\Phi_{\text{ew}}^\dagger \Phi_{\text{ew}} - v_2^2)^2 \right], \quad (7.30)$$

where

$$D_A = \partial_A - ig \frac{\tau^a}{2} W_A^a - ig' Y B_A. \quad (7.31)$$

Here  $\tau^a$  are the Pauli matrices,  $W_A^a$  the  $SU(2)$  gauge fields,  $B_A$  the hypercharge gauge field,  $Y$  the hypercharge assignment, and  $g, g'$  the corresponding couplings.

This construction is not derived from the minimal scalar ECT postulates P1–P6. Rather, it provides a low-energy structural embedding showing how an electroweak-like EFT could be accommodated if a second condensate transition exists.

**Scale matching and the hierarchy problem.** If such an intermediate transition is realised, the associated scale is fixed by low-energy matching:

$$v_2 = (\sqrt{2} G_F)^{-1/2} \approx 246.22 \text{ GeV}, \quad (7.32)$$

equivalently by the observed relations

$$m_W = \frac{g v_2}{2}, \quad m_Z = \frac{\sqrt{g^2 + g'^2}}{2} v_2. \quad (7.33)$$

Thus 246 GeV is not a free choice once the electroweak EFT is matched. The ratio

$$\frac{v_2}{\phi_0} \sim 10^{-16} \quad (7.34)$$

is the ECT counterpart of the standard gauge hierarchy problem and is discussed in Section 5.1.

**Higgs-like radial mode.** In this embedding the radial excitation of the electroweak condensate plays the structural role of a Higgs-like scalar. Writing the doublet in polar form around the broken minimum, the radial mode  $\sigma_2$  inherits its mass from the local curvature of the effective potential at  $|\Phi_{\text{ew}}| = v_2$ :

$$m_{\sigma_2}^2 = 2\lambda_2 v_2^2. \quad (7.35)$$

The observed Higgs mass  $m_H \simeq 125 \text{ GeV}$  therefore constrains  $\lambda_2$  through matching. This is a matching relation, not a prediction from bare condensate microphysics. In ECT the point is structural: the Higgs-like scalar is interpreted as the radial mode of a *second condensate sector*, not as a completely independent fundamental scalar unrelated to the condensate architecture.

**ECT interpretation: second phase of the same medium.** If the second transition is realised, ECT interprets the electroweak condensate not as an ad hoc independent scalar field, but as a possible second ordered phase of the same underlying  $\Phi$ -medium whose first transition already produced the Lorentzian spacetime and gravitational sector. This is a genuine conceptual distinction from the Standard Model, where the Higgs field and spacetime geometry are independent structures. At the present stage, however, this should be read only as an interpretive unification statement, not as a completed derivation.

**What is strict and what is embedded.** The generator counting associated with a candidate  $O(3) \rightarrow O(2)$  step is strict once such a step is admitted. The algebraic bridge  $\mathfrak{so}(3) \cong \mathfrak{su}(2)$  is also strict. By contrast, the existence of the second transition itself, the doublet structure  $\Phi_{\text{ew}}$ , the identification with the physical electroweak symmetry-breaking pattern, the values of  $g, g'$ , the matching scale  $v_2$ , the Higgs-like radial mode  $\sigma_2$ , and the reconstruction of the full Standard Model electroweak spectrum are Level B/C embedding or matching statements.

**What would be needed for full Level A.** To promote the electroweak-like sector from structural embedding to a first-principles derivation, ECT would need to:

- (i) derive the second condensate transition  $O(3) \rightarrow O(2)$  dynamically from the bare action;
- (ii) show that the resulting breaking pattern reproduces the physical  $SU(2) \times U(1) \rightarrow U(1)_{\text{em}}$  structure;
- (iii) derive the doublet representation content rather than admit it as an EFT embedding;
- (iv) derive the gauge couplings  $g, g'$ ;
- (v) derive the Yukawa structure and fermion mass generation within the same mechanism;
- (vi) derive the hierarchy ratio  $v_2/\phi_0 \sim 10^{-16}$  from condensate dynamics.

None of these steps has yet been completed. The electroweak-like sector is therefore one of the places where the gap between structural embedding and first-principles derivation is currently largest.

**Status summary.**

Statement	Status	Comment
$O(3) \rightarrow O(2)$ generator counting	A	Strict combinatorial statement
$\mathfrak{so}(3) \cong \mathfrak{su}(2)$	A	Strict Lie-algebra fact
Second condensate transition exists	B/C	Candidate mechanism only
Electroweak doublet embedding $\Phi_{\text{ew}}$	B/C	Structural EFT embedding
Matching scale $v_2 \simeq 246 \text{ GeV}$	Constraint	Fixed once EW EFT is matched
Weak-like gauge-boson sector	B/C	EFT embedding only; full SM electroweak spectrum not reproduced from the current $O(3) \rightarrow O(2)$ counting
Higgs-like radial mode $\sigma_2$	B/C	Structural role, mass matched
Gauge couplings $g, g'$	C	Free EFT parameters
Hierarchy ratio $v_2/\phi_0$	Open	Not derived
Full electroweak sector from P1–P6	Open	

**Status of the electroweak scale  $v_2$  in the present formulation.** In the present formulation of ECT, the scale  $v_2 \approx 246 \text{ GeV}$  should be read as the electroweak-scale secondary condensate scale required by

phenomenological matching, not as a first-principles derivation from the primary condensate dynamics. The current three-scale hierarchy discussed in Section 5.1, together with the structural candidate for a second transition described in Appendix L, suggests a possible hierarchical organisation of scales within one condensate framework, but the actual origin of  $v_2$ , the dynamical mechanism that would generate the second transition, and the corresponding threshold and matching structure remain open. In particular, the present article does not derive  $v_2/\phi_0 \sim 10^{-16}$ , the gauge couplings  $g, g'$ , or the Yukawa hierarchy from condensate dynamics alone.

It should also be noted that  $v_2$  already enters the present formulation as an input in several sectors beyond the hierarchy discussion: the electroweak boson mass formulae  $m_W = gv_2/2$  and  $m_Z = \sqrt{g^2 + g'^2} v_2/2$  of the present subsection; the fermion mass matching  $m_f = y_f v_2$  used in the matter-coupling discussion (§7.5); the geometric-mean seesaw scale  $M_R^{\text{geom}} = \sqrt{\phi_0} v_2$  (§8.9); the second geometric neutrino-mass scale  $m_\nu^{\text{geom}} = v_2^2/\phi_0$  (§8.9); and the fifth-force coupling  $\beta_5 \sim m_f/\phi_0$  (§7.6), which inherits  $v_2$ -dependence through  $m_f$ . A future first-principles derivation of  $v_2$  would therefore simultaneously constrain or align these sectors, which should be kept explicitly in view in any future extension of the electroweak programme.

This establishes the gauge-side architecture of the electroweak-like sector. The next subsection addresses how the embedded gauge fields act on matter and what the ECT interaction pattern looks like at the EFT embedding level.

## 7.5 Matter couplings and the Standard Model interaction pattern

*Status: bridge subsection. The previous four subsections established the gauge-side architecture. This subsection addresses how the embedded gauge sectors act on matter, what remains structurally open, and what the ECT interaction pattern looks like at the phenomenological level. All content here is Level B/C embedding or matching, except where noted otherwise.*

**General framework.** Once gauge fields are admitted in the low-energy EFT—whether Abelian, non-Abelian, or electroweak-like—their action on matter follows the standard covariant-derivative structure. In this sense, the observed Standard Model interaction pattern is *reproduced by embedding* rather than derived directly from the bare condensate postulates P1–P6. The gauge-matter coupling is therefore structurally correct at the EFT level, but not yet established as a necessary consequence of the condensate architecture.

**Strong sector.** Within the non-Abelian embedding (Section 7.3), the  $SU(3)$ -like colour sector is taken to remain in the unbroken (symmetric) phase, which is structurally consistent with massless gluons and the absence of a colour-Higgs mechanism. A full derivation of confinement within ECT would require a genuinely nonperturbative analysis going beyond the perturbative EFT embedding used in this section; confinement remains an open problem (OP-GUT1 in Table 118) and is not claimed as an ECT result.

**Fermion masses and Yukawa couplings.** At the embedded EFT level, fermion masses arise through Yukawa couplings to the electroweak condensate sector:

$$m_f = y_f v_2, \tag{7.36}$$

where  $y_f$  is the Yukawa coupling constant and  $v_2 \approx 246 \text{ GeV}$  is the electroweak matching scale. The Yukawa coefficients  $y_f$  are Standard-Model-like matching inputs, not derived from the bare condensate action. The detailed development of the fermionic sector, including spin structure and chirality, is deferred to the fermion sections of this paper.

**Gauge coupling constants.** At the present stage, the coupling constants  $e, g, g'$ , and  $g_s$  remain free EFT matching parameters. Neither their numerical values nor their running are derived from condensate microphysics. Whether the condensate structure could in principle constrain them—for example, through

topological arguments, RG flow from the UV condensate scale, or variational selection—remains a central open question of the ECT quantitative-unification programme (OP-GUT4 in Table 118).

**Anomaly cancellation.** The anomaly-cancellation structure of the Standard Model is likewise not derived in the present ECT embedding. In the Standard Model, anomaly cancellation depends on the specific fermion representation content and hypercharge assignments, and its fulfilment is a nontrivial consistency condition. Any full Level A completion of the gauge and matter sectors within ECT would need to reproduce the observed anomaly cancellations explicitly. At the present stage, this remains part of the open quantitative-unification programme (OP-GUT6a, OP-GUT6b in Table 118). A systematic anomaly architecture of the emergent chiral gauge sector, including the electroweak ordered-branch constraints, the anomaly-transparency of the director coupling  $\mathcal{L}_5$ , and the open status of the colour-sector completion, is developed in §9.5.

**Separation between embedded SM structure and ECT-specific deformation.** The content of the present subsection and the four preceding ones describes how the Standard Model gauge interactions can be *embedded* into the condensate architecture of ECT. This embedding is structurally nontrivial—it connects gauge sectors to condensate symmetry layers rather than postulating them independently—but it does not yet amount to a first-principles derivation.

The remainder of this section turns to a qualitatively different topic: an interaction-level structure that is *specific to ECT* and has no Standard Model counterpart. The ECT-specific fermion–condensate coupling, which arises from the preferred direction  $n_A$  of the ordered branch, is developed in the following subsections. This transition marks the boundary between embedded SM interactions and genuinely ECT-specific matter-sector deformation.

## 7.6 The ECT-specific fermion–condensate coupling

*Status: Level A given empirical fermions (Ph). The existence of the preferred direction  $n_A$  after  $O(4) \rightarrow O(3)$  is a strict structural consequence of the ordered branch (Level A from P4). If fermionic excitations are empirically admitted as observed degrees of freedom (phenomenological input Ph, analogous to the observational inputs  $c_* = c$  and  $G_N$ -matching), then the operator  $n_A \bar{\Psi} \gamma^A \Psi$  is the unique leading parity-even, zeroth-derivative fermion–condensate coupling (Level A given Ph: EFT operator classification is a mathematical theorem, not an additional physical assumption). The derivation chain is:*

- (i)  $n_A$  exists — Level A (P4,  $O(4) \rightarrow O(3)$  SSB);
- (ii) fermionic excitations exist — Ph (empirical fact);
- (iii) the leading operator coupling a spinorial excitation to  $n_A$  without derivatives is uniquely  $n_A \bar{\Psi} \gamma^A \Psi$  — Level A (EFT classification);
- (iv) therefore the coupling  $\mathcal{L}_5 = \mu_5 \bar{\Psi} \gamma^A n_A \Psi$  is the structurally required leading fermion–condensate interaction — Level A given Ph.

*Its coefficient  $\mu_5$  is not derived from P1–P6; the dimensional estimate  $\mu_5 \sim m_f^2/\phi_0$  is Level B. A first-principles derivation from condensate microdynamics remains open.*

**Terminology: director coupling.** By analogy with the director field of nematic liquid crystals and the anchoring energy in those systems, the coupling  $\mathcal{L}_5 = \mu_5 \bar{\Psi} \gamma^A n_A \Psi$  is henceforth referred to as the *director coupling*. The order parameter  $n_A$  plays the role of the liquid-crystal director; the coupling describes how fermionic excitations interact with the orientation of the ordered medium.

**Structural origin.** As discussed in Section 7.1, the symmetry breaking  $O(4) \rightarrow O(3)$  selects a preferred direction

$$n_A \equiv \frac{\partial_A \Phi}{|\partial \Phi|}. \quad (7.37)$$

This is not a gauge degree of freedom and not an internal multiplet index; it is a derived orientational variable of the ordered branch. Its existence is a strict structural consequence of the broken phase.

**Leading parity-even operator.** Consider the low-energy fermionic EFT on the ordered branch and impose the following restrictions: (i) locality, (ii) linear dependence on the preferred direction  $n_A$ , (iii) no derivatives on the fermion field, (iv) parity-even operator basis. Under these assumptions, the leading ECT-specific fermion bilinear is

$$\Delta \mathcal{L}_5 = \mu_5 \bar{\Psi} \gamma^A n_A \Psi, \quad (7.38)$$

where  $\mu_5$  has mass dimension one.

This statement should be read carefully. It is *not* a theorem of the bare scalar condensate action. It is the leading operator in the specified low-energy EFT basis. If the parity-even restriction is dropped, an axial structure  $n_A \bar{\Psi} \gamma^A \gamma^5 \Psi$  would also be available. The formal EFT operator classification is recorded in Appendix U.

**Why this coupling is ECT-specific.** The operator (7.38) has no counterpart in the minimal Standard Model fermion sector, because the SM contains no derived preferred spacetime direction analogous to (7.37). Its existence therefore reflects a genuinely ECT-specific structural ingredient of the ordered branch. With the phenomenological input that fermionic excitations are observed in nature,  $\mathcal{L}_5$  becomes not merely admissible but the *unique leading* fermion–condensate coupling of the ordered branch (Level A given Ph). The coefficient  $\mu_5$  remains a free EFT parameter at Level B.

**Lorentzian-branch form.** In the Lorentzian ordered branch, after the real parametrisation  $t = w/c_*$ , the preferred Euclidean direction is read as a timelike unit vector  $u_\mu$  in the emergent low-energy spacetime. The coupling then takes the form

$$\Delta \mathcal{L}_5 = \mu_5 u_\mu \bar{\Psi} \gamma^\mu \Psi. \quad (7.39)$$

This is the appropriate low-energy Lorentzian form of the ECT-specific fermion–condensate coupling. It should be interpreted as a preferred-direction deformation of the fermion sector, not as an additional internal gauge interaction.

**Discrete-symmetry classification of  $\mathcal{L}_5$  (Level B).** The coupling (7.39) selects a preferred timelike direction  $u_\mu$  in the emergent Lorentzian spacetime and therefore introduces a native ordered-medium asymmetry source absent in the minimal Standard Model fermion sector. For the timelike ordered-branch background  $n^\mu = (1, 0, 0, 0)$  the coupling takes the form  $\mathcal{L}_5 = \mu_5 \bar{\Psi} \gamma^0 \Psi = \mu_5 \Psi^\dagger \Psi$ . Using the standard discrete-transformation conventions for the Dirac vector current  $j^\mu = \bar{\Psi} \gamma^\mu \Psi$ , one finds that  $j^\mu$  is C-odd, while its timelike component  $j^0$  is P-even and T-even. Accordingly,  $\mathcal{L}_5$  is *C-odd, P-even, T-even, CP-odd, and CPT-odd* (Level B). Reality of the coupling  $\mu_5$  ensures hermiticity of the operator (required for a real action), but does *not* restore CPT invariance. The systematic classification, its relation to the conditional CPT route for reconstructible local sectors, and the re-interpretation of  $\mathcal{L}_5$  as a branch-sensitive Lorentz- and CPT-violating phenomenological operator are developed in Section 9.4. The role of  $\mathcal{L}_5$  for Sakharov condition (ii) of ECT-native baryogenesis (Section 16.3), in combination with complex flavour phases, is preserved; the conditional CPT backbone of Section 9.4 is not affected because  $\mathcal{L}_5$  explicitly lies outside the reconstructible OS setup as a branch-selecting extension. As a vector bilinear,  $\mathcal{L}_5$  does not modify the anomaly coefficients of the chiral gauge sector; the systematic anomaly architecture is discussed in Section 9.5.

**Dimensional estimate and Planck suppression.** Since the bilinear  $\bar{\Psi}\gamma^A n_A \Psi$  has mass dimension three, the coefficient  $\mu_5$  must have mass dimension one. It is therefore convenient to parameterise

$$\mu_5 \equiv \beta_5 m_f, \quad (7.40)$$

where  $\beta_5$  is dimensionless. If the only UV suppressing mass scale available is the radial symmetry-breaking scale  $\phi_0 \sim \bar{M}_{\text{Pl}}$  (Section 5.1), then dimensional analysis suggests

$$\beta_5 \sim \frac{m_f}{\phi_0} \sim \frac{m_f}{\bar{M}_{\text{Pl}}}, \quad \mu_5 \sim \frac{m_f^2}{\phi_0}. \quad (7.41)$$

Thus the genuinely dimensionful coefficient is  $\mu_5$ , while  $\beta_5$  measures the coupling strength relative to the standard Dirac mass term. For electrons this gives an extremely small deformation, consistent with the absence of any presently observed signal.

Two caveats are essential: (i) the fermion masses  $m_f$  entering (7.40)–(7.41) are Standard-Model-matched inputs, not ECT-derived quantities; (ii) the electroweak scale  $v_2$  is itself a matching constraint, not a first-principles result.

**Relation to the Standard-Model Extension viewpoint.** In the Lorentzian branch, the operator  $u_\mu \bar{\Psi}\gamma^\mu \Psi$  is structurally analogous to a vector background deformation in the sense of Lorentz-violating EFT. For a single fermion species in a strictly constant flat background, such a term can be partly absorbed by field redefinitions and may fail to produce directly observable effects. Physical effects arise when at least one of the following is true:

- the coupling differs between fermion species;
- the preferred direction varies across spacetime or environment;
- the background is curved or inhomogeneous;
- the coupling enters relative observables rather than an isolated single-species dispersion relation.

For ECT this means that the phenomenological relevance of (7.39) is tied not merely to the existence of the operator, but also to the ordered-branch environment and the relation between different matter sectors.

**Preferred-direction effects.** The operator (7.38) introduces preferred-direction corrections to the emergent Lorentz-invariant fermion dynamics at the EFT level. It parametrises residual sensitivity of the low-energy matter sector to the ordered-branch orientation. This preferred-direction structure is absent in the exact Lorentz-symmetric limit and is one of the clearest interaction-level signatures by which ECT differs from the Standard Model embedding.

**What is strict and what is embedded.** The existence of the preferred direction  $n_A$  after  $O(4) \rightarrow O(3)$  is a strict structural consequence of the ordered branch (Level A). The statement that  $n_A \bar{\Psi}\gamma^A \Psi$  is the leading parity-even zeroth-derivative operator is a statement about the chosen low-energy EFT basis (Level A/B conditional). The dimensional estimate  $\beta_5 \sim m_f/\phi_0$  and hence  $\mu_5 \sim m_f^2/\phi_0$  are EFT-level statements (Level B). The fermion masses  $m_f$  are embedded SM inputs (Level C). A first-principles derivation of the coefficient from condensate microphysics has not been completed.

**What would be needed for full Level A.** To promote this coupling from a structural EFT deformation to a first-principles result, ECT would need to:

- (i) derive the operator directly from the bare condensate action or from a controlled integration-out procedure;
- (ii) derive its coefficient from condensate microdynamics rather than dimensional analysis;

- (iii) determine whether the vector operator is uniquely selected, or whether axial and derivative competitors survive;
- (iv) establish under what conditions the coupling is physically observable rather than removable by field redefinitions in the low-energy Lorentzian limit.

None of these steps has yet been completed.

**Status summary.**

Statement	Status	Comment
Preferred direction $n_A$ exists after SSB	A	Structural consequence of $O(4) \rightarrow O(3)$
Leading parity-even zeroth-derivative operator $n_A \bar{\Psi} \gamma^A \Psi$	A/B	Strict within the stated EFT basis
Operator is ECT-specific (no SM counter-part)	A/B	Structural absence of preferred direction in minimal SM
Dimensionful coupling $\mu_5$ required	A	Follows from mass dimension counting
$\beta_5 \sim m_f / \phi_0$	B	Dimensional estimate only
$\mu_5 \sim m_f^2 / \phi_0$	B	Consequence of the parameterisation $\mu_5 = \beta_5 m_f$
Planck suppression for known fermions	B	EFT consistency estimate
Fermion masses $m_f$ as inputs	C	SM-matched, not ECT-derived
Coefficient derived from condensate micro-dynamics	Open	Not completed
Physical observability in the Lorentzian limit	Open	Depends on species dependence / gradients / environment

## 7.7 Strength, range, and the microscopic/macroscopic distinction

*Status: layered structural analysis. The distinction between the microscopic preferred-direction coupling and the macroscopic  $\phi$ -closure is a structural consequence of the ordered-branch architecture (Level A/B). The coupling-strength estimate  $\mu_5 = \beta_5 m_f$ ,  $\beta_5 \sim m_f / \phi_0$ , and hence  $\mu_5 \sim m_f^2 / \phi_0$ , is an EFT-level dimensional statement (Level B). The interpretation of environmental modulation and screening is structurally motivated but not yet quantitatively derived (Level B/C). A full multi-species observability analysis remains open.*

**Parametric suppression of the microscopic coupling.** Section 7.6 established that the ECT-specific fermion–condensate coupling may be written as

$$\Delta \mathcal{L}_5 = \mu_5 \bar{\Psi} \gamma^A n_A \Psi, \quad \mu_5 = \beta_5 m_f, \quad (7.42)$$

with the dimensional EFT estimate

$$\beta_5 \sim \frac{m_f}{\phi_0}, \quad \mu_5 \sim \frac{m_f^2}{\phi_0}. \quad (7.43)$$

Since  $\phi_0 \sim \bar{M}_{\text{Pl}}$ , the microscopic coupling is parametrically extremely small for all known fermions. This strong suppression is a structural consequence of the UV condensate scale entering the EFT estimate. At the present stage it should be read as a parametric consistency statement, not as a precision prediction.



**Range: local UV operator versus structured IR background.** In a homogeneous ordered background, the operator  $\mu_5 \bar{\Psi} \gamma^A n_A \Psi$  is a local microscopic deformation of the fermion sector. It does not introduce a new long-range propagating mediator by itself. Its natural microscopic correlation scale is therefore associated with the UV condensate sector.

By contrast, on galactic and cosmological scales the ordered branch develops nontrivial large-scale structure through the amplitude-sector variable

$$\phi = \beta^{-1} \ln(u/u_\infty), \quad (7.44)$$

as discussed in Section 17.1. This does *not* mean that the microscopic operator itself becomes an unsuppressed long-range force. Rather, the ambient ordered medium acquires macroscopic structure, and the effective relevance of preferred-direction effects may then depend on that environment.

**Microscopic preferred-direction coupling versus macroscopic  $\phi$ -closure.** This is the central structural distinction.

The ordered branch gives rise to two physically distinct mechanisms:

- **Microscopic fermion–condensate coupling:**

$$\Delta \mathcal{L}_5 = \mu_5 \bar{\Psi} \gamma^A n_A \Psi, \quad \mu_5 = \beta_5 m_f, \quad \beta_5 \sim m_f / \phi_0.$$

This is a perturbative, Planck-suppressed preferred-direction deformation of the fermion sector. It is controlled directly by the orientational variable  $n_A$ .

- **Macroscopic  $\phi$ -closure:**

$$G_{\text{eff}}(X) = G_N e^{-\beta \phi}, \quad \mu(g/g^\dagger) g = g_{\text{bar}}.$$

This is a nonperturbative modification of the gravitational response in the low-acceleration branch. It is controlled by the amplitude-sector variable  $\phi(X)$ .

These two mechanisms share the same ordered-branch origin, but they are not the same effect and should not be identified with each other. The microscopic coupling is controlled by the preferred direction  $n_A$ , whereas the macroscopic weak-field closure is controlled by the amplitude profile  $\phi(X)$ . The former is perturbative and Planck-suppressed; the latter can become  $O(1)$  in the deep weak-field branch.

**Why the microscopic coupling does not generate galactic  $O(1)$  effects by itself.** The microscopic coupling enters the fermion EFT as a local operator with coefficient  $\mu_5 \sim m_f^2 / \phi_0$ , i.e. as a perturbative correction suppressed by the primary condensate scale. The macroscopic weak-field closure, by contrast, arises from the self-consistent background response of the ordered medium and modifies the effective gravitational coupling itself. The two sectors therefore differ both in variable content ( $n_A$  versus  $\phi$ ) and in parametric regime (perturbative versus nonperturbative). For this reason, the microscopic preferred-direction coupling is too weak, at the level of the present EFT scaling, to account directly for the  $O(1)$  galactic weak-field modifications attributed in ECT to the macroscopic  $\phi$ -closure. The formal separation of the two sectors is recorded in Appendix V.

**Environmental modulation and screening.** In the amplitude-sector formulation, gravitational corrections are controlled by the ambient profile of  $\phi(X)$ , i.e. by the logarithmic amplitude variable of the ordered branch. This suggests that any residual preferred-direction effects visible in the fermion sector may depend not only on the local operator  $\Delta \mathcal{L}_5$ , but also on the ordered-medium environment in which that operator is evaluated.

In dense or deeply ordered regions, one expects the amplitude sector to be driven farther from criticality, which would tend to suppress residual sensitivity to ordered-branch distortions. In diffuse or weak-field regions, the ordered branch can remain closer to its critical regime, making environmental modulation of preferred-direction effects more plausible. At present, however, this should be understood as a qualitative structural interpretation rather than a quantitatively derived screening law.

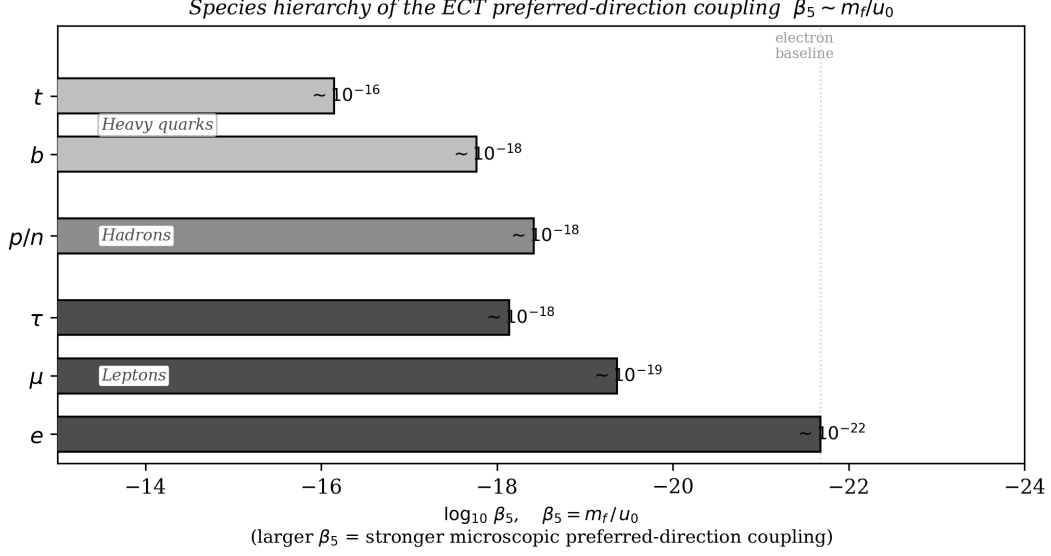


**Figure 4:** Species dependence of the ECT preferred-direction coupling in the present EFT scaling  $\beta_5 \sim m_f/\phi_0$ . Heavier fermionic species correspond to larger dimensionless ratios  $\beta_5$ , although all values remain extremely small because the suppression scale is the radial symmetry-breaking scale  $\phi_0 \sim \bar{M}_{\text{Pl}}$ . The figure is schematic and illustrates parametric hierarchy rather than a precision prediction for observable signals.

**Species dependence and the route to observability.** Section 7.6 already noted that in a strictly constant flat background, a vector term of the form  $u_\mu \bar{\Psi} \gamma^\mu \Psi$  may be partly removable by field redefinitions for a single fermion species. Observable effects therefore require at least one of: species dependence, background gradients, curvature, or relative multi-sector observables.

Within the present EFT estimate, species dependence is structurally expected because  $\beta_5 \sim m_f/\phi_0$  depends on the fermion mass. Since the masses  $m_f$  differ between fermion species, the associated dimensionless ratios  $\beta_5$  are generically non-universal. This gives a natural structural route by which preferred-direction effects could survive universal field redefinitions and reappear in relative observables. The precise multi-species reduction, however, has not yet been carried out. This hierarchy is shown schematically in Figure 4.

**Relation to other fifth-force frameworks.** ECT differs structurally from both scalar-tensor fifth-force models and generic Lorentz-violation EFTs.

In scalar-tensor gravity, the same propagating scalar often controls both laboratory fifth-force effects and large-scale modifications. In ECT, the microscopic preferred-direction operator and the macroscopic weak-field closure are distinct sectors of the same ordered medium. In generic Lorentz-violation EFTs, background tensors are introduced as independent coefficients. In ECT, the preferred direction  $n_A$  is not postulated separately but derived from the ordered-branch geometry. This does not make the coupling fully derived from P1–P6, but it does mean that its structural origin differs from that of a generic Lorentz-violating ansatz.

**What is strict and what is embedded.** The distinction between the microscopic preferred-direction coupling and the macroscopic  $\phi$ -closure is a structural statement about the ordered-branch architecture. The microscopic coupling depends on the orientational variable  $n_A$ , whereas the macroscopic weak-field closure depends on the amplitude variable  $\phi$ ; this distinction is strict once the two sectors are identified. The parametric estimate  $\beta_5 \sim m_f/\phi_0$ , equivalently  $\mu_5 \sim m_f^2/\phi_0$ , is an EFT-level dimensional argument. The interpretation of environmental modulation and screening is structurally motivated but not quantitatively derived. The route from non-universal  $\beta_5$  to explicit observable signals also remains incomplete.

**What would be needed for full Level A.** To promote the present strength/range analysis to a first-principles result, ECT would need to:

- (i) derive the coefficient  $\mu_5$  from a controlled matching or integration-out procedure rather than dimensional analysis;
- (ii) derive the background dependence of  $n_A$  and its coupling to matter in realistic ordered-branch geometries;
- (iii) derive the environmental modulation of the effective coupling from the condensate field equations;
- (iv) establish whether the species dependence of  $\beta_5$  is exactly proportional to  $m_f$  or receives corrections;
- (v) determine which part of the preferred-direction operator survives field redefinitions in the full multi-species Lorentzian EFT.

None of these steps has yet been completed.

**Status summary.**

Statement	Status	Comment
$\beta_5 \sim m_f/\phi_0$	B	Dimensional EFT estimate
$\mu_5 \sim m_f^2/\phi_0$	B	Equivalent dimensionful estimate
Microscopic coupling is local and UV-sector	B	EFT interpretation
Microscopic coupling $\neq$ macroscopic $\phi$ -closure	A/B	Structural distinction of ordered-branch sectors
Microscopic coupling cannot by itself yield galactic $O(1)$ effects	B	Follows from the present EFT scaling together with the structural micro/macro sector distinction
Environmental modulation of preferred-direction effects	B/C	Structurally motivated, not yet derived quantitatively
Species dependence of $\beta_5$	B	Structural consequence of present EFT scaling
Full multi-species observability analysis	Open	Not completed
Quantitative screening profile	Open	Not derived from field equations

## 7.8 Observability conditions, consistency checks, and falsification logic

*Status: structural observability analysis. The present subsection does not provide precision phenomenology. It identifies which classes of observables can in principle be sensitive to the ECT-specific fermion–condensate coupling, which effects are structurally excluded, and what would be required for quantitative predictions. The existence of observable channels is a Level B structural statement; their precise magnitude remains open.*

**What is established, what is benchmarked, and what remains open.** At the present stage, the ordered-branch fifth-interaction programme contains three distinct layers. First, the existence and uniqueness of the leading condensate–fermion operator  $\Delta\mathcal{L}_5 = \mu_5 \bar{\Psi}\gamma^A n_A \Psi$  are established at the level of EFT classification, given the empirical existence of fermions. Second, benchmark numerical consequences can be developed for spin-precession, weak-equivalence-principle sensitivity, and compact-star consistency once a working value of the effective coupling is adopted. Third, the exact microscopic normalization of  $\mu_5$ , its full flavour structure, and a global multi-sector fit remain open.

**Structural operator versus calibrated coupling.** ECT fixes the *form* of the leading ordered-branch fermion coupling once fermions are admitted as observed excitations, but it does not yet fix the numerical value of the effective coefficient  $\mu_5$  from first principles. Accordingly, the operator-level statement is stronger than the phenomenology-level statement: the former is structural, whereas the latter remains benchmark-level until a controlled microscopic matching is achieved.

**From operator existence to physical observability.** Sections 7.6–7.7 established that the ordered branch admits the ECT-specific local operator

$$\Delta\mathcal{L}_5 = \mu_5 \bar{\Psi} \gamma^A n_A \Psi, \quad \mu_5 = \beta_5 m_f, \quad \beta_5 \sim m_f / \phi_0$$

as the leading parity-even zeroth-derivative deformation of the fermion sector in the stated EFT basis. The existence of the operator, however, is not yet the same as a directly observable laboratory signal. In the Lorentzian branch, a vector background coupling may be partly removable for a single fermion species in a strictly constant flat background. Observable consequences therefore require additional structure.

**Conditions under which the coupling can become observable.** The preferred-direction coupling can contribute to physical observables only when at least one of the following is present:

- (i) non-universal couplings between different fermion species;
- (ii) gradients or inhomogeneities of the ordered background;
- (iii) curved or environment-dependent Lorentzian branch geometry;
- (iv) relative observables comparing distinct matter sectors.

These conditions do not by themselves produce a signal, but they define the structural routes through which the ECT-specific coupling could survive field redefinitions and become measurable.

**Observational consistency windows.** Three observational windows are especially relevant for the present fifth-force programme. First, weak-equivalence-principle tests constrain composition-dependent accelerations at the level of  $\eta \sim 10^{-15}$ . The MICROSCOPE final result constrains the Titanium–Platinum Eötvös parameter to  $\eta(\text{Ti, Pt}) = [-1.5 \pm 2.3 (\text{stat}) \pm 1.5 (\text{syst})] \times 10^{-15}$  [49]. Any benchmark Eötvös-level estimate from the ECT fifth-force programme should be read as a consistency target relative to this window, not as a derived fit to the WEP data themselves. Second, precision spin-dependent searches constrain exotic spin-coupled interactions in comagnetometer, torsion-balance, and spectroscopy experiments [50]. The benchmark ECT fifth-force estimates should be read against these two windows, not in isolation.

**Observable classes.** Within this framework, four broad classes of observables are structurally relevant:

- **Spin-sensitive observables:** any quantity that depends on the orientation of fermionic states relative to the preferred direction  $n_A$  or its Lorentzian image  $u_\mu$ .
- **Composition-sensitive observables:** any comparison of matter systems built from different fermion species, since the present EFT scaling makes the dimensionless ratio  $\beta_5$  species-dependent through  $m_f$ .
- **Propagation anisotropies:** direction-dependent corrections to low-energy matter propagation in an ordered background.
- **Environment-dependent effects:** variation of effective signals with the local ordered-medium background, if the coupling strength is modulated by the ambient branch configuration.

At present, this is a classification of observable *types*, not a list of precision predictions. A schematic comparison of the present ECT coupling scale with familiar dimensionless interaction strengths is shown in Figure 5.

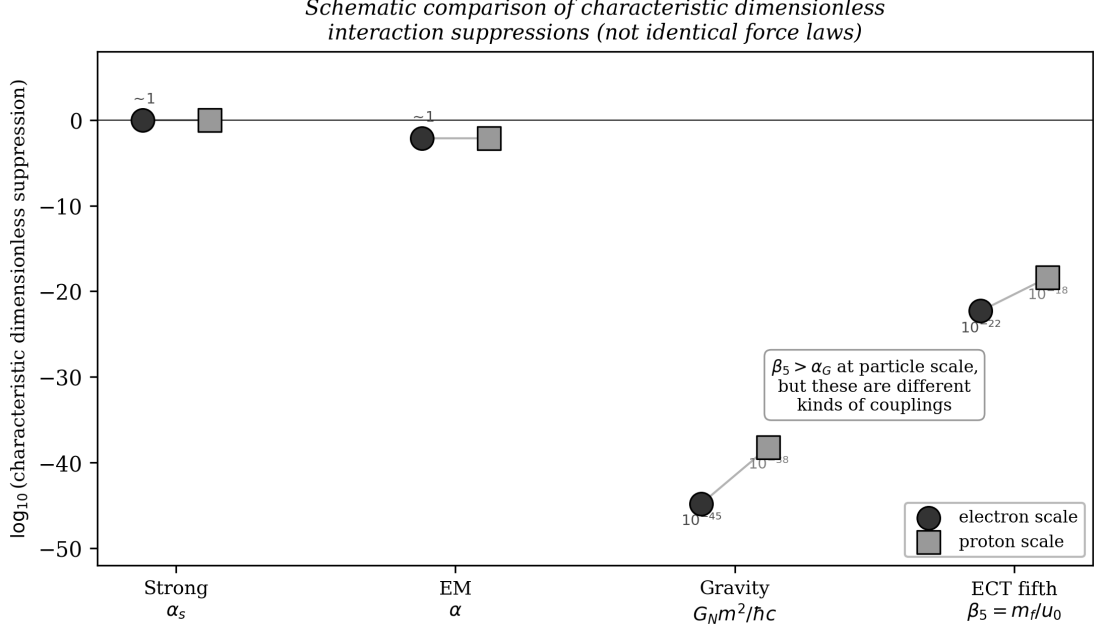


**Figure 5:** Schematic logarithmic comparison of characteristic dimensionless interaction suppressions for representative electron and proton scales. The ECT preferred-direction coupling is shown through the present EFT ratio  $\beta_5 \sim m_f / \phi_0$ , while gravity is represented by the dimensionless quantity  $\alpha_G = G_N m^2 / (\hbar c)$ . This is not a comparison of identical force laws, but only of effective dimensionless coupling scales. In particular, the statement  $\beta_5 > \alpha_G$  does not mean that the ECT preferred-direction interaction is directly stronger than gravity in all physical observables. The weak interaction is not shown separately because its low-energy strength is process-dependent and is not represented here by a unique dimensionless quantity directly comparable to  $\alpha$ ,  $\alpha_G$ , or  $\beta_5$ .

**What this operator does not control.** The microscopic preferred-direction coupling must not be conflated with the macroscopic  $\phi$ -closure analysed in Section 7.7 and Appendix V. The microscopic operator is a local perturbative deformation of the fermion EFT. The macroscopic  $\phi$ -closure is a branch-level modification of the gravitational response. For this reason, the microscopic coupling is not expected, at the level of the present EFT scaling, to generate by itself the galactic  $O(1)$  weak-field modifications attributed in ECT to the amplitude sector.

Likewise, constraints on the speed of tensor modes belong primarily to the geometric/gravitational sector rather than to the fermionic preferred-direction operator itself. The present subsection is therefore about matter-sector observability, not about the full set of ECT consistency tests.

**Consistency checks.** Even without precision predictions, the present structure already imposes nontrivial consistency requirements:

- the operator must remain sufficiently suppressed in the Lorentzian low-energy regime;
- any observable effect must respect the micro/macro sector distinction established in Section 7.7;
- non-universal matter effects, if present, must arise through the multi-species structure of the EFT rather than through a universal unsuppressed background shift;
- environmental dependence, if invoked, must ultimately be derived from the ordered-medium field equations rather than inserted ad hoc.

**Falsification logic.** The present ECT closure would be under direct pressure if any of the following were established:

- (i) a precise low-energy analysis showed that the operator  $u_\mu \bar{\Psi} \gamma^\mu \Psi$  is completely unobservable in the full multi-species Lorentzian EFT, leaving no physical matter-sector signal at all;
- (ii) a controlled derivation showed that the coefficient  $\mu_5$  vanishes identically once the ordered branch is reduced to the physical sector;
- (iii) a consistent environmental analysis showed that the preferred- direction coupling necessarily produces observable effects already excluded by precision matter-sector tests;
- (iv) the only viable route to observability required identifying the microscopic operator with the macroscopic  $\phi$ -closure, in contradiction with the sector distinction established above.

These are not claims that ECT fails such tests; they define the structural conditions under which the present closure could be refuted.

**Unified numerical falsifier.** The present ordered-branch fifth-force programme would be under direct pressure if a single effective coupling sector could not be made simultaneously consistent with (i) composition-dependent free-fall bounds and (ii) spin-dependent precision searches. In that case, the current unified  $\mathcal{L}_5$  phenomenology would have to be abandoned in favour of a more structured coupling sector.

**What is strict and what is open.** What is structurally established is that the preferred-direction coupling belongs to the fermionic EFT, that it is species-sensitive in the present dimensional estimate, and that its observability requires additional structure beyond a constant single-species background. What remains open is the full mapping from the operator to concrete measurement channels. No precision observable is derived at this stage.

**What would be needed for quantitative predictions.** To turn the present observability logic into a predictive framework, ECT would need to:

- (i) derive the coefficient  $\mu_5$  from condensate microphysics rather than dimensional EFT scaling;
- (ii) derive the environmental dependence of the ordered branch in laboratory, astrophysical, and cosmological settings;
- (iii) perform the full multi-species Lorentzian EFT reduction and determine which parts of the operator survive field redefinitions;
- (iv) map the resulting effective couplings onto standard Lorentz-violation and equivalence-principle test frameworks;
- (v) identify which observable classes remain genuinely distinct from the macroscopic  $\phi$ -sector signals.

**Table 21:** Status map for the ECT fifth-interaction programme.

Claim	Status	Comment
Existence of the operator $\Delta\mathcal{L}_5$	A given Ph	Structural EFT statement once fermions are admitted
Uniqueness of the leading operator form	A given Ph	Leading parity-even zeroth-derivative ordered-branch fermion coupling
CP-asymmetric dynamical route	A given Ph	Source of CP-asymmetric dynamics, not yet full CP phenomenology

*Continued on next page*

Table 21 continued

Claim	Status	Comment
Dimensional scaling $\mu_5 \sim m_f^2/\phi_0$	B	Benchmark-level EFT scaling, not first-principles matching
WEP / Eötvös consistency benchmark	B	Compared against MICROSCOPE-level window, not derived fit
Spin-sensitive search-window benchmark	B	Requires mapping to concrete lab observables
Compact-star consistency benchmark	B	Consistency-level only; not full EOS closure
Environmental modulation	B/C	Structurally motivated, not yet quantitatively derived
Full flavour structure	Open	Not yet derived from condensate microphysics
Single-coupling global fit across all sectors	Open	Unified lab + astrophysics fit not yet achieved

## 7.9 Structural constraints on the coupling coefficient

*Status: Level B/C structural analysis. This subsection does not derive the coefficient of the ECT-specific fermion–condensate coupling from first principles. Its purpose is to identify which scales and structural ingredients can enter the coefficient, which condensate scale controls its leading dimensional suppression in the present EFT closure, and which possible corrections remain open. The result is not a derivation of the coefficient, but a constraint analysis on its admissible form.*

**What has already been established.** Section 7.6 established that the preferred- direction operator can be written as

$$\Delta\mathcal{L}_5 = \mu_5 \bar{\Psi}\gamma^A n_A \Psi, \quad \mu_5 = \beta_5 m_f, \quad (7.45)$$

with the dimensional EFT estimate

$$\beta_5 \sim \frac{m_f}{\phi_0}, \quad \mu_5 \sim \frac{m_f^2}{\phi_0}. \quad (7.46)$$

That estimate should be read only as the leading parametric scaling compatible with the present ordered-branch EFT. The question addressed here is narrower: *which condensate scale enters the leading EFT suppression, and what kinds of corrections are not excluded?*

**Dimensional scale assignment in the present EFT closure.** Three ingredients enter the present argument.

First, the operator  $\bar{\Psi}\gamma^A n_A \Psi$  has mass dimension three, so its coefficient must have mass dimension one. Second, the preferred direction  $n_A$  originates from the first symmetry breaking  $O(4) \rightarrow O(3)$ , i.e. from the primary ordered branch associated with the condensate scale  $u_0$ . Third, within the minimal architecture of the ordered branch, the radial/Planck-scale parameter  $\phi_0$  is the leading UV scale tied to the origin of  $n_A$  through the first symmetry breaking.

For these reasons, the present EFT closure adopts  $\phi_0$  as the leading suppression scale. This is not yet a theorem. It means that, among the scales already present in the theory,  $\phi_0$  is the most natural *leading* suppressing scale for an operator whose distinguishing background ingredient is the preferred direction selected at the first transition. A compact statement of this scale argument is given in Appendix W.

**Why the electroweak scale  $v_2$  is not the leading scale in the present architecture.** A natural question is whether the electroweak scale  $v_2$  could replace  $u_0$  in the coefficient estimate. In the present ECT architecture, however, the preferred direction  $n_A$  is already present before the electroweak-like sector is introduced. It is therefore structurally associated with the primary  $O(4) \rightarrow O(3)$  ordering, not with the later weak-like embedding.

This does not rigorously exclude  $v_2$ -dependent corrections. It only means that a coefficient controlled dominantly by  $v_2$  would require an additional dynamical mechanism tying the preferred-direction operator to the second transition. No such mechanism has yet been derived. Accordingly,  $\phi_0$  remains the working leading suppression scale in the present EFT closure, while  $\phi_0$ -,  $v_2$ -, and mixed-sector corrections remain open possibilities rather than ruled-out ones.

**Admissible corrections.** Once the coefficient is treated as an EFT object rather than a first-principles result, several classes of corrections become possible in principle:

- (i) multiplicative  $O(1)$  matching factors;
- (ii) additional suppression by ratios involving lower scales, such as  $v_2/\phi_0$ , if the second transition participates in the operator completion;
- (iii) background-dependent corrections induced by the ordered-medium environment;
- (iv) loop corrections from the fermion sector or from collective condensate modes.

At present, none of these corrections has been computed in a controlled way. Therefore the estimate  $\beta_5 \sim m_f/\phi_0$  should be read as the leading structural scaling, not as a closed formula.

**Radiative stability: what can and cannot be said.** The present work does not contain a loop analysis of the fermion–condensate operator. Accordingly, radiative stability has not been proved. What can be said is more limited. Since the operator is already suppressed by the highest condensate scale in the theory, there is no obvious structural reason within the current EFT to expect a large enhancement that would overturn the basic power counting. But this is only a plausibility statement. A controlled one-loop calculation in the ordered-branch EFT would be required to determine whether the coefficient is radiatively stable, whether additional operator mixing occurs, and whether lower-scale corrections enter systematically.

**Could integrating out heavy condensate modes generate the operator?** A natural possibility is that the preferred-direction coupling is generated, or renormalised, after integrating out heavy condensate degrees of freedom such as the radial mode. At present this remains a structural possibility only. The article does not yet contain an explicit matching calculation from the heavy-mode sector to the low-energy fermion EFT. Therefore it is legitimate to note this as a possible origin channel, but not to assign it a definite formula. Any quantitative claim about heavy-mode induced corrections would be premature without a controlled derivation.

**The rôle of the second transition.** If the weak-like  $O(3) \rightarrow O(2)$  embedding is realised, it may still modify the preferred-direction coupling indirectly. Two broad possibilities exist:

- the preferred-direction operator is already present at the  $u_0$  scale and the second transition only renormalises its coefficient;
- the second transition contributes additional operators or mixing terms that alter the low-energy form of the coupling.

The present article does not decide between these possibilities. What it does establish is that the existence of  $n_A$  itself belongs to the first ordered branch, so any  $v_2$ -dependence would enter only as a correction or completion, not as the primary structural origin of the operator.



**What is strict and what is open.** Strictly speaking, the present section establishes only the following: the preferred-direction operator requires a mass-dimension-one coefficient, the present EFT closure adopts  $\phi_0$  because  $n_A$  originates from the first transition, and  $v_2$ -dominated control of the coefficient would require additional dynamics not currently present. What remains open is the actual microphysical derivation of the coefficient, the size and sign of loop corrections, the rôle of heavy condensate modes, and the operator basis across the two successive transitions.

**What would be needed for full Level A.** To close the question of the coefficient at Level A, ECT would need:

- (i) a controlled derivation of the operator coefficient from the ordered-branch microdynamics;
- (ii) an explicit operator-basis analysis across the successive transitions  $O(4) \rightarrow O(3) \rightarrow O(2)$ ;
- (iii) a loop calculation establishing whether the coefficient is radiatively stable and whether lower-scale corrections enter;
- (iv) a matching analysis showing whether heavy condensate modes generate, renormalise, or leave unchanged the leading operator.

None of these steps has yet been completed.

**Status summary.**

Statement	Status	Comment
Coefficient must have mass dimension one	A	Follows from operator dimension counting
$\phi_0$ -suppressed dimensional scaling is the working EFT estimate	B	Because $n_A$ originates from the first transition
$\beta_5 \sim m_f/\phi_0$ as leading scaling	B	Dimensional EFT estimate
$v_2$ -dependent corrections are not excluded	B/C	Would require additional dynamics
Heavy-mode induced corrections	B/C	Structurally admissible, not derived
Radiative stability established	Open	No loop analysis yet
Full coefficient derived from microphysics	Open	Not completed

## 7.10 Connection to the galactic weak-field sector

*Status: structural bridge. This subsection does not develop galactic weak-field physics. Its purpose is only to locate the ECT-specific fermion–condensate coupling within the broader ordered-branch architecture and to state clearly how it is related to, but distinct from, the macroscopic amplitude-sector analysis developed later in the paper.*

**Scope of the present section.** Sections 7.6–7.9 have analysed the ECT-specific fermion–condensate coupling as a microscopic preferred-direction deformation of the matter sector: its operator structure, its parametric suppression, the distinction between microscopic and macroscopic sectors, the conditions for observability, and the structural constraints on its coefficient. All of these results belong to the interaction-level description of the ordered branch.

**What is developed elsewhere.** The galactic weak-field consequences of ECT are not derived from the microscopic preferred-direction operator itself. They are developed in the Macroscopic Physics part of the paper, especially in Section 17.1, where the relevant object is the amplitude-sector variable  $\phi(X)$  and its

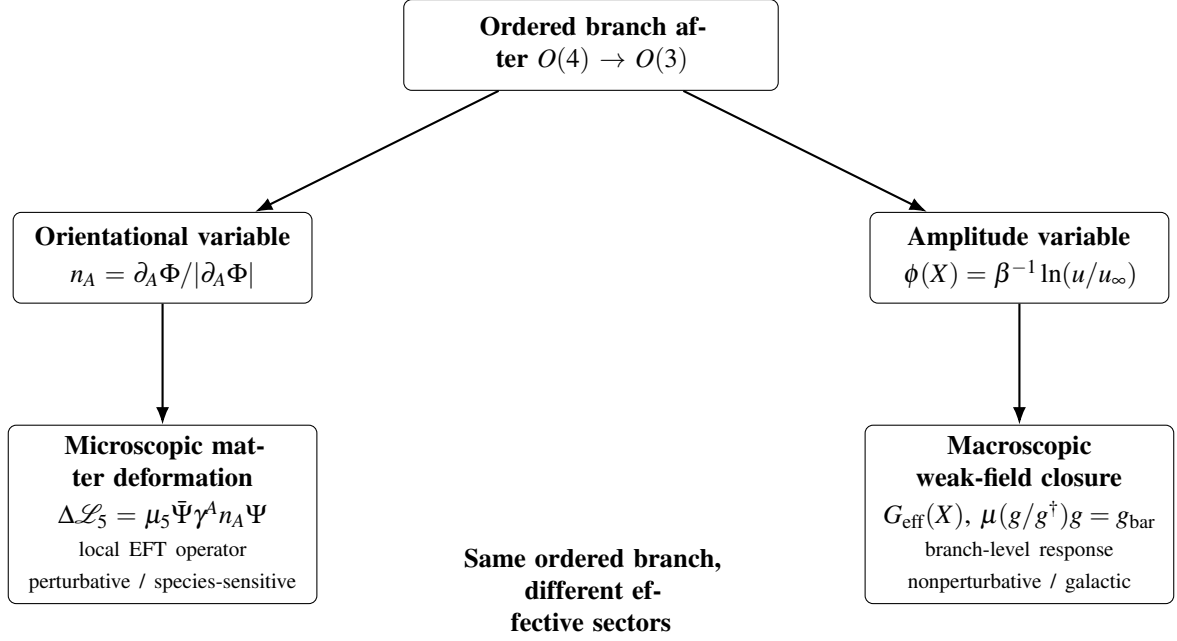


**Figure 6:** Structural separation of the two ordered-branch sectors relevant for the ECT-specific interaction analysis. The preferred condensate direction  $n_A$  generates a microscopic fermion-sector deformation through the local operator  $\Delta \mathcal{L}_5 = \mu_5 \bar{\Psi} \gamma^A n_A \Psi$ , whereas the amplitude-sector variable  $\phi(X)$  governs the macroscopic weak-field closure developed in the Macroscopic Physics part. The two effects share the same ordered-branch origin but belong to different effective sectors and must not be identified with each other.

branch-level self-consistent dynamics. Flat rotation curves, the radial acceleration relation, the baryonic Tully–Fisher relation, and the deep weak-field closure belong to that macroscopic amplitude sector.

**Why this separation matters.** The microscopic coupling  $\Delta \mathcal{L}_5 = \mu_5 \bar{\Psi} \gamma^A n_A \Psi$  and the macroscopic  $\phi$ -closure originate from the same ordered branch, but they belong to different effective sectors. The former is controlled by the orientational variable  $n_A$  and enters as a local perturbative deformation of the fermion EFT. The latter is controlled by the amplitude variable  $\phi(X)$  and enters through the nonperturbative branch-level modification of the gravitational response. For this reason, the galactic weak-field sector is not a consequence of the microscopic fermion–condensate coupling, and conversely the microscopic coupling is not a reparametrisation of the galactic  $\phi$ -sector. This separation is summarised schematically in Figure 6.

**What remains open.** At the present stage, the separation of the two sectors is established structurally and parametrically. What is not yet known is whether higher-order terms in the ordered-branch EFT couple them in a nontrivial way, or whether the separation remains exact after the full Lorentzian low-energy reduction within the multi-sector EFT. Those questions belong to the open programme, not to the present interaction-level analysis.

The corresponding structural argument is stated in more technical form in Appendix V, which also makes explicit why the microscopic preferred-direction operator and the macroscopic  $\phi$ -closure cannot be identified with each other.

## 7.11 Gauge-sector summary, structural synthesis, and the open programme

*Status: substantially strengthened by P5 (medium character). After P5, the Abelian and non-Abelian gauge sectors acquire a significantly stronger status: the  $U(1)$  local phase redundancy and the  $SU(2)$  local orientation redundancy are now structural consequences of the postulate framework (Level A for the gauge architecture), rather than conditional embeddings. The combined ordered-branch gauge*

architecture is  $SU(2) \times U(1)$  (Level A for structural redundancy; Level A/B for EFT gauge completion). The electroweak-like interpretation and the  $SU(3)$  colour sector remain Level B/C or open. The fermion–condensate preferred-direction coupling is Level A given empirical fermions, with Level B coefficient estimates.

**What Section 7 has established.** After the introduction of the medium-character postulate P5, Section 7 establishes the following hierarchy of results:

- (i) The compact-phase  $U(1)$  construction (Section 7.2): local phase redundancy follows structurally from P5, and the Noether current, compensating connection, and leading Maxwell-type closure follow without additional assumptions (Level A for the gauge architecture).
- (ii) The non-Abelian orientation sector (Section 7.3): the ordered-branch orientation redundancy, promoted by P5 to a local gauge redundancy, gives the  $\mathfrak{so}(3) \cong \mathfrak{su}(2)$  gauge connection. Together with the  $U(1)$  phase sector, this yields the ordered-branch gauge architecture  $SU(2) \times U(1)$  (7.26).
- (iii) The electroweak-like embedding (Section 7.4): a candidate  $O(3) \rightarrow O(2)$  step gives a structural analogue of the weak-sector breaking pattern, but not a completed derivation of the physical electroweak sector (Level B/C).
- (iv) The matter-coupling architecture (Section 7.5): Standard-Model-like interaction pattern reproduced at the EFT matching level.
- (v) The ECT-specific preferred-direction coupling (Sections 7.6–7.10): a genuinely ECT-specific matter-sector deformation with no SM counterpart (Level A given empirical fermions for the operator form; Level B for the coefficient).

**Separation of spacetime and internal symmetries.** The spacetime symmetry breaking  $O(4) \rightarrow O(3)$  acts on the coordinate index of the Euclidean arena, whereas internal gauge symmetries act on multiplet indices of condensate components. These sectors are therefore structurally distinct from the outset. The explicit  $U(1)$  construction of Section 7.2 shows how gauge structure can emerge concretely within the compact phase EFT without collapsing this distinction.

The Coleman–Mandula theorem [51] constrains the structure of exact symmetries of a nontrivial relativistic S-matrix under specific assumptions. The present ECT discussion is formulated at the level of the condensate action, the ordered branch, and the corresponding low-energy EFT structures, prior to any full S-matrix reconstruction. For that reason, the theorem does not by itself settle the viability of the present embedding programme. This should not be read as a circumvention of Coleman–Mandula, but as a statement about the current level of analysis.

**Connection to chirality and the matter sector.** The group-theoretic decomposition  $Spin(4) \simeq SU(2)_L \times SU(2)_R$ , together with the ordered-branch selection of a preferred direction, was analysed in Section 9.3. That discussion indicates how the broken-phase geometry may structurally distinguish the two  $SU(2)$  sectors and motivate a left/right asymmetry in the matter sector. This remains a Level B structural reconstruction. It is relevant to the gauge-side interpretation of the weak-like sector, but it is not part of a strict derivation of the gauge group itself, and it does not derive fermions from the bare scalar condensate.

**What has been closed by P5 and what remains open.** The medium-character postulate P5 has closed the following steps:

- (i) local phase and orientation redundancies are now structural consequences of the postulate framework;
- (ii)  $SU(2) \times U(1)$  is derived as the ordered-branch gauge architecture.

The following steps remain open:

- (iii) the  $SU(3)$  colour sector requires additional internal structure beyond the current minimal scalar condensate;
- (iv) the coupling constants  $(e, g, g', g_s)$  are not derived from condensate parameters;
- (v) the candidate second transition  $O(3) \rightarrow O(2)$  has not been derived dynamically from the bare action;
- (vi) the full Standard Model gauge sector, including anomaly cancellation and the correct matter representations, has not been reproduced.

The corresponding Level A programme for the ECT-specific preferred- direction matter coupling is given separately in Sections 7.6–7.9.

**Status summary.**

Statement	Status	Comment
<i>Abelian gauge structure (<math>U(1)</math>) — strengthened by P5</i>		
Global Noether current and current conservation	A	Strict within the compact phase EFT
Local phase redundancy (from P5)	A	Structural consequence of P2+P3+P5
Compensating connection and covariant derivative	A	Structural EFT completion
Maxwell-type leading kinetic term	A/B	Leading EFT closure; full QED matching open
Compact holonomy and flux quantisation	A/B	Follows from compact phase geometry
Photon identification	A/B	Structural route established; full QED open
<i>Non-Abelian gauge architecture — strengthened by P5</i>		
$\mathfrak{so}(3) \cong \mathfrak{su}(2)$	A	Strict Lie-algebra identity
Local orientation redundancy (from P5)	A	Structural consequence of P5
Ordered-branch $SU(2) \times U(1)$ gauge architecture	A	Structural redundancy from P2+P3+P5
Non-Abelian EFT gauge completion	A/B	Once multiplet structure specified
$SU(3)$ -like sector requires additional internal structure	C	Model-level extension, no spacetime counterpart derived
$O(3) \rightarrow O(2)$ as candidate weak-like step	B	Reduced algebraic/counting analogue only
$v_2$ as electroweak matching scale	Constraint	If a second condensate transition exists
<i>Matter couplings and interaction architecture</i>		
Gauge couplings $(e, g, g', g_s)$	Matched	EFT matching parameters, not derived
Yukawa/matter-coupling structure	B/C	Embedded at the EFT level
Chiral selection of $SU(2)_L$	B+	Orientation selects chirality structurally; full internal-gauge derivation open (OP-GRAV-WEAK)

Statement	Status	Comment
<i>ECT-specific matter-sector deformation</i>		
Preferred-direction operator $n_A \bar{\Psi} \gamma^A \Psi$	A/B	Leading parity-even zeroth-derivative operator in the stated EFT basis
Dimensionful coupling $\mu_5$ and dimensional estimate $\beta_5 \sim m_f / \phi_0$	B	EFT-level dimensional scaling only
Microscopic preferred-direction coupling $\neq$ macroscopic $\phi$ -closure	A/B	Structural distinction of ordered-branch sectors
Coefficient derived from condensate micro-physics	Open	Not yet completed

Section 7 therefore establishes a layered picture rather than a single uniform derivation, now substantially strengthened by P5.

**Interaction map of ECT at the present stage.** At the present stage, ECT supports three distinct native routes to fundamental interactions, all originating from the same ordered  $\Phi$ -medium:

- (i) **Electromagnetic route:** the compact coherent-phase sector, together with the medium-character postulate P5, yields a structural Abelian gauge route with Maxwell-type leading closure (Level A for gauge architecture; Level A/B for physical photon identification).
- (ii) **Weak-interaction route:** the ordered-orientation sector yields a structural non-Abelian route and an ordered-branch  $SU(2) \times U(1)$  gauge architecture (Level A for structural redundancy; Level A/B for EFT gauge sector; Level B/C for physical electroweak identification).
- (iii) **Gravitational route:** the tensor sector of the ordered Lorentzian branch yields the native route to emergent massless tensor propagation and to an Einstein-like macroscopic gravitational sector (Level A for massless tensor propagation; Level A/B for the Einstein-like macroscopic route; Level B/C for full nonlinear Einstein closure).

By contrast, a colour  $SU(3)$  sector is not derived within the present minimal condensate framework; its absence sharply localises the missing internal structure required for a complete interaction unification.

**Native derivation criterion.** A fundamental interaction is *native* in ECT if: (a) it arises from an ordered-branch redundancy or ordered-branch tensor mode; (b) its leading low-energy EFT closure is fixed internally by the postulate framework, up to explicit matching parameters and clearly identified unresolved higher-order sectors; (c) it does not require importing an external gauge group or an external background structure. By this criterion, the electromagnetic, weak-interaction, and gravitational routes are native in ECT, whereas a colour  $SU(3)$  sector is not yet native within the present minimal condensate framework.

## 8 Elementary Particles and Field Excitations in ECT

*Status guide for this chapter.* The material below spans three levels of rigour, organised into three categories of excitations (Section 8.1):

- (i) **Required condensate excitations (Level A/B).** Graviton: linearised tensorial sector of the effective metric (A/B; Section 8.5). Soft orientation mode  $\chi$  (Level B; Section 8.2). Primary radial mode  $\sigma$  (Level A/B; Section 8.3). These arise directly from the condensate action and its broken-phase structure.

**(ii) Structurally embedded SM fields (Level B/C).** Gauge bosons from condensate phase symmetries (Section 8.6; full development in Section 7). Higgs boson reinterpreted as secondary radial mode (Section 8.7). Fermions: structural reconstruction on the ordered branch (Section 8.8; full development in Section 9). Neutrino sector: seesaw-type embedding (Section 8.9). These assume Standard-Model structure as external input; the SM gauge group, Yukawa couplings, and generation structure are not derived from the minimal bosonic condensate action.

**(iii) Topological and conditional sectors (Level A/B/C).** Texture/skymion-like states classified by  $\pi_3(S^3) = \mathbb{Z}$ ; anti-predictions  $\pi_0 = \pi_1 = \pi_2 = 0$ ; conditional secondary defects (Section 8.10).

The only currently identified ECT-specific fermion interaction beyond the Standard Model is the fermion–condensate coupling  $\mu_5 \bar{\Psi} \gamma^A n_A \Psi$  (Section 9.8). A condensed overview with status table is given in the chapter summary (Section 8.11).

## 8.1 General Structure of Particle Excitations

*Status: structural roadmap for the particle chapter. This subsection does not yet derive the full particle content of nature. Its purpose is to classify which excitations are required by the broken condensate branch itself, which sectors are only structurally embedded at the EFT level, and which states are topological or conditional. The strongest outputs of this chapter are therefore not the full Standard Model particle spectrum, but the clear separation between required condensate modes, embedded matter sectors, and conditional topological states.*

In the scalar-only ECT basis the fundamental degree of freedom is the condensate field  $\Phi$ . The orientation field  $n_A$  is introduced only as a derived ordered-branch variable through  $Q_A = \partial_A \Phi = u n_A$  and is not an independent microscopic field in the present formulation (Section 4.2). Elementary particles and field excitations arise as condensate fluctuations, as fields associated with internal symmetries or spinorial structures, or as topological configurations of the ordered vacuum.

**Why a particle chapter is justified at all.** The transition from Part I to the present chapter is not a change of subject, but a change of level of description. Part I established the ordered branch, its sector decomposition, its scale hierarchy, and its gauge-side structural embeddings. Section 8 asks what these already-derived structures imply when read at the level of particle-like excitations. The chapter is therefore not an additional postulate about particles, but the excitation-level unpacking of the broken condensate architecture.

**What is meant here by a “particle”.** In the present ECT framework, “particle” does not always mean a fundamental microscopic field inserted into the bare action. Depending on the sector, it may instead refer to: (i) a required fluctuation mode of the ordered condensate, (ii) an EFT field structurally accommodated by internal symmetries of the condensate background, or (iii) a topological or conditional excitation of the vacuum manifold. This distinction is essential for interpreting the status labels used throughout this chapter.

**Three categories of excitations.** The particle content discussed in this chapter falls into three categories with different derivation status:

(i) *Required condensate excitations.* These follow from the structure of the ordered branch and the  $O(4) \rightarrow O(3)$  symmetry breaking:

- primary radial mode  $\sigma$ ,  $m_\sigma \sim \bar{M}_{\text{Pl}}$  (amplitude fluctuation; Section 8.3);
- surviving soft scalar  $\chi$  from the integrability-constrained orientation sector (Section 8.2);
- graviton as linearised effective-metric perturbation (Section 8.5).

(ii) *Structurally embedded Standard Model fields.* These are accommodated within the condensate framework but not derived from P1–P6:

- gauge bosons from condensate phase symmetries (Section 8.6);
- electroweak-like gauge embedding and the associated secondary condensate sector (Section 8.7);
- fermions as spinorial excitations compatible with the ordered background (Section 8.8);
- neutrino sector (Section 8.9).

(iii) *Topological sectors and other conditional states.* These arise either from the homotopy of the vacuum manifold or from a possible second transition:

- texture/skyrmion sectors from  $\pi_3(S^3) = \mathbb{Z}$  and anti-predictions from  $\pi_0 = \pi_1 = \pi_2 = 0$ ;
- (conditional) secondary defects from  $\pi_2(S^2)$  if  $O(3) \rightarrow O(2)$  exists;
- the Higgs-like secondary radial mode  $h$  as the *conditional particle-level interpretation* of the secondary condensate sector, if the weak-like  $O(3) \rightarrow O(2)$  transition is realised.

Topological sectors are developed in Section 8.10, while the conditional Higgs-like reinterpretation is discussed primarily in Section 8.7.

**Classification criterion.** The division into the three categories above is not merely descriptive. It reflects three distinct logical relations to the ECT foundation:

- a state is *required* if it follows from the broken-phase condensate structure itself;
- a state is *embedded* if it can be consistently realised in the ECT low-energy framework but is not derived from P1–P6;
- a state is *conditional or topological* if it depends on the topology of the vacuum manifold or on an additional transition not yet established from first principles.

These three classes therefore correspond not merely to different kinds of excitations, but to different logical relations to the foundation of ECT: strict consequence, EFT embedding, and conditional/topological realisation.

**Physical interpretation and condensed-matter analogy.** The three categories have direct analogues in condensed-matter physics. Category (i) excitations are analogous to *phonons in a crystal*: they are inevitable consequences of the existence of an ordered medium with broken symmetry. If the medium exists and is ordered, these modes exist automatically. Category (ii) fields are analogous to *impurity atoms in a crystal lattice*: they are compatible with the medium and respect its symmetries, but they are not derived from the lattice structure alone. Category (iii) states are analogous to *topological defects* (dislocations, vortices): their existence or absence is determined by the homotopy of the vacuum manifold, independently of the details of the dynamics.

**Comparison with quantum field theory.** In standard QFT, particles are postulated as quanta of independent fields ( $\phi, A_\mu, \psi, \dots$ ) defined on a fixed spacetime background. Each field carries its own Fock space. No particle is logically “more derived” than any other. In ECT the architecture is fundamentally different: ECT does not place all particles on the same logical footing. Category (i) particles are necessary consequences of a single condensate field  $\Phi$ . Category (ii) particles are structurally embedded in the condensate symmetry architecture but not derived from the minimal scalar action. Category (iii) states are predicted or excluded by the topology of the vacuum manifold  $S^3$ . The anti-predictions—absence of magnetic monopoles ( $\pi_2(S^3) = 0$ ), domain walls ( $\pi_0 = 0$ ), and cosmic strings ( $\pi_1 = 0$ )—are strict consequences (Level A), in contrast to Grand Unified Theories where monopoles are generically predicted.

**Connection to the three-scale hierarchy.** The particle mass scales are tied to the three condensate scales (Section 5.1):  $m_\sigma \sim \phi_0 \sim \bar{M}_{\text{Pl}}$  (first condensate),  $m_h \sim v_2 \approx 246\text{GeV}$  (second condensate, if it exists), and the surviving soft mode  $\chi$  (massless at tree level in the minimal broken-phase EFT). The IR galactic scale  $v_{\text{gal}}$  is not associated with a particle excitation but with the macroscopic  $\phi$ -sector closure (Section 18.1). This explains why only the first two scales enter the particle chapter as direct excitation scales, whereas the third belongs to the macroscopic branch-level closure rather than to the particle spectrum.

**Dependence on earlier results.** The present classification relies on four earlier structural results of Part I: the broken-phase sector map of Section 4, the three-scale hierarchy of Section 5.1, the branching architecture of Section 6, and the gauge-sector embedding analysed in Section 7. Section 8 should therefore be read not as an independent particle postulate, but as the particle-level unpacking of those earlier structural ingredients.

**What this chapter does not claim.** The present chapter does not claim that the full Standard Model particle spectrum has been derived from the minimal scalar condensate action. In particular, the gauge group, Yukawa hierarchy, generation structure, and the detailed fermion spectrum remain beyond the present Level A closure. What is established here is a structured map of which sectors already follow from the ordered branch, which are admissible EFT embeddings, and which remain conditional or open.

**Dependence on later parts of the paper.** Section 8 identifies particle-like sectors and their derivational status, but it does not by itself complete the full phenomenological or cosmological role of those sectors. Questions of macroscopic closure, dark-sector behaviour, and late-time observational consequences are deferred to the later parts of the paper. This prevents the particle classification from being overinterpreted as a complete physical model already at the level of Part I.

The purpose of the following subsections is therefore not merely to list possible excitations, but to determine which particle-like sectors already belong to the broken condensate branch itself, which require additional EFT embedding, and which remain conditional on topology or a secondary transition. In this sense, the chapter is a derivation-status map of the ECT particle sector, not a claim of complete particle unification. Its organising principle is not phenomenological completeness, but logical dependence on the ordered-branch foundation.

**Multi-particle description: why it is necessary and how ECT differs from QM and QFT.** Ordinary non-relativistic quantum mechanics operates on a Hilbert space  $\mathcal{H}_N$  of fixed particle number  $N$ . Processes with variable  $N$  (photon emission, pair creation, annihilation) require quantum field theory, where the Fock space  $\mathcal{F} = \bigoplus_{N=0}^{\infty} \mathcal{H}_N$  and creation/annihilation operators are introduced as additional postulates. In ECT the architecture is different: fundamental are not “individual particles” but configurations of a single condensate field  $\Phi$ . Changing particle number is a reconfiguration of the same medium, analogous to the appearance and disappearance of vortices in a superfluid.

Multi-particle description remains necessary even in the coherent branch ( $\Gamma_{\text{loop}} \ll 1$ ), where no event-like Lorentzian interaction is available (Section 6.5), for four reasons:

- (a) *Entanglement*: subsystems sharing a common condensate generically possess non-factorisable correlations (Section 31);
- (b) *Exchange statistics*: the topology of exchanging two identical excitations ( $\pi_1(\mathcal{M}_2) = \mathbb{Z}_2$ ) determines the bosonic/fermionic dichotomy—a multi-body effect by definition (Section 24.4);
- (c) *Decoherence threshold*: the number of environmental degrees of freedom  $N_{\text{eff}}$  determines the decoherence rate  $\tau_{\text{dec}} = 1/(N_{\text{eff}} \cdot \gamma)$ ;
- (d) *Variable excitation number*: cosmological particle production at the  $O(4) \rightarrow O(3)$  transition, pair annihilation, and radiation are processes in which the number of condensate excitations changes.



**Status of Fock space.** ECT does not require Fock space as a fundamental postulate. However, an explicit emergent sector decomposition with variable excitation number—especially for the fermionic many-body sectors—remains to be constructed from condensate dynamics. This is a nontrivial reconstruction problem rather than a foundational gap (Open; OP-Q11).

## 8.2 Soft Orientation Sector of the Condensate

*Status: minimal orientation EFT is Level B. Three independent physical Goldstone particles are **not** claimed in the present scalar-only basis; see Section 4.3 and Appendix I.*

**Why this sector is required.** This sector is not introduced as an optional EFT embellishment. It is forced by the broken-phase geometry itself: once the ordered branch selects a preferred direction, the vacuum manifold  $O(4)/O(3) \simeq S^3$  necessarily carries an orientation sector. What is nontrivial in scalar-only ECT is not the existence of this sector, but the fact that its independent propagating content is much smaller than the naive broken-generator counting would suggest. For this reason, the soft orientation sector belongs to the class of required condensate excitations introduced in Section 8.1, even though its propagating particle content is strongly reduced by integrability.

**Minimal derivation chain.** The soft orientation sector follows from three successive facts: (i) the ordered branch breaks  $O(4) \rightarrow O(3)$ , so the vacuum manifold is  $O(4)/O(3) \simeq S^3$ ; (ii) naive broken-generator counting therefore suggests three soft directions; (iii) in the strict scalar-only basis, the order parameter is generated by a single exact one-form  $Q_A = \partial_A \Phi$ , so the physically independent propagating soft content is reduced to one longitudinal mode. The existence of the sector is therefore geometric, whereas its particle-like content is constrained by integrability.

The ordered branch breaks  $O(4) \rightarrow O(3)$ , so the vacuum manifold is

$$O(4)/O(3) \simeq S^3. \quad (8.1)$$

In a generic internal-symmetry breaking this would yield three independent Goldstone bosons. However, in the present scalar-only ECT basis the ordered quantity is  $Q_A = \partial_A \Phi$ , which is an exact one-form. The integrability constraint  $\partial_A Q_B - \partial_B Q_A = 0$  implies that the orientation triplet reduces to one longitudinal soft scalar mode  $\chi$  at linear order [30, 31]:

$$\pi_i = \frac{1}{u_0} \partial_i \chi, \quad \sigma = \partial_w \chi. \quad (8.2)$$

**Minimal orientation EFT.** A three-component orientation parametrisation of  $S^3$  remains a useful effective language for the broken branch, but it should be understood as a minimal EFT organisation, not as three independent propagating particles. The broken-generator counting  $\dim O(4) - \dim O(3) = 3$  is a geometric statement; the actual independent propagating soft content in the scalar-only basis at linear order is  $N_G^{\text{phys}} = 1$ .

**Three levels of statement.** It is important to distinguish:

- (i) the *geometric* statement that the broken branch admits an  $S^3$  orientation manifold;
- (ii) the *group-theoretic* statement that  $\dim O(4) - \dim O(3) = 3$ ;
- (iii) the *physical* statement that, in the strict scalar-only basis with  $Q_A = \partial_A \Phi$ , only one longitudinal soft mode survives as an independent propagating excitation at linear order.

The first two statements are strict; the third is the decisive content for the particle interpretation. Confusion between these three levels is precisely what leads to the incorrect “three physical Goldstones” reading, which the present scalar-only analysis excludes.

**Mass of the surviving soft mode.** In the minimal broken-phase EFT inherited from P1–P6 there is no orientation potential, so the surviving scalar mode  $\chi$  is massless at tree level. A pseudo-Goldstone mass could arise only if additional explicit  $O(4)$ -breaking terms or a secondary soft-sector completion are introduced. No such mechanism is present in the current foundational closure (open; OP-GM). The present statement of masslessness is therefore an EFT statement about the minimal broken-phase closure, not a proof of exact all-order mass protection in every possible completion of the theory.

**Conditional decoupling estimate for the surviving soft scalar.** The full  $\chi$ -sector EFT (mass, couplings, stability) is not yet derived from first principles (Level B, OP-GM). Under the natural minimal assumption that the surviving scalar  $\chi$  inherits the standard derivative-coupling structure of a Goldstone-like mode with suppression scale  $f_\chi \sim \phi_0 \sim \bar{M}_{\text{Pl}}$ , the effective dimensionless coupling at momentum scale  $k$  is

$$g_\chi(k) \sim \frac{k}{f_\chi} \sim \frac{k}{\bar{M}_{\text{Pl}}}, \quad (8.3)$$

giving

$$g_\chi^2 \sim \left( \frac{k}{\bar{M}_{\text{Pl}}} \right)^2. \quad (8.4)$$

At galactic scales the relevant inverse-length scale is

$$k_{\text{gal}} \sim r_{\text{gal}}^{-1} \sim 10^{-36} - 10^{-37} \text{ GeV}$$

for  $r_{\text{gal}} \sim 1\text{--}10 \text{ kpc}$ . Hence

$$g_\chi^2 \sim \left( \frac{k_{\text{gal}}}{\bar{M}_{\text{Pl}}} \right)^2 \sim 10^{-108} - 10^{-110}.$$

This is still completely negligible. If instead one uses a Gpc-scale cosmological wavelength, then  $k \sim 10^{-42} \text{ GeV}$  and  $g_\chi^2 \sim 10^{-121}$ .

At room-temperature laboratory scales,  $k \sim k_B T \sim 2.6 \times 10^{-11} \text{ GeV}$  ( $T = 300 \text{ K}$ ), which gives  $g_\chi^2 \sim 10^{-58}$ . For optical/eV-scale laboratory probes one may instead use  $k \sim 10^{-9} \text{ GeV}$ , giving  $g_\chi^2 \sim 10^{-55}$ . Both estimates are negligible compared to any currently observable coupling, including the ECT fifth-force coupling  $\beta_5 \sim m_f/\phi_0$ , whose value ranges from  $\sim 10^{-22}$  for electrons to  $\sim 10^{-19}$  for nucleon-scale fermions and up to  $\sim 10^{-16}$  for the top quark (Section 7), which is itself below current experimental reach. Under this standard derivative-coupling assumption, the  $\chi$ -mode is therefore completely decoupled from all phenomena discussed in this paper—by a further factor  $(k/\bar{M}_{\text{Pl}})^2$  relative even to the fifth-force suppression. A stronger statement requires the explicit derivation of the full  $\chi$ -sector EFT and is left open (OP-GM). This estimate is the analogue of the fifth-force result: just as the preferred-direction coupling is Planck-suppressed and currently unobservable, the derivative-coupled  $\chi$ -mode is further kinematically suppressed, making it utterly negligible across all scales considered here.

**No dark-matter role in the present closure.** The macroscopic sector of ECT already explains galactic rotation curves, the RAR, and BTFR through the  $\phi$ -sector without invoking any Goldstone-like dark matter. Accordingly, the soft orientation sector must *not* be repurposed as a dark-matter patch for phenomena already explained by the  $\phi$ -closure. Its role in the present chapter is instead conceptual and structural: it identifies the residual soft content of the broken branch and fixes what the ordered condensate does, and does not, supply at the particle-like level. This is not merely a phenomenological preference. It follows from the architectural separation between the macroscopic  $\phi$ -closure and the residual soft orientation content of the broken branch.

**Role in the predicted-states classification.** The surviving soft scalar  $\chi$  is listed as item (ii) in the classification of new states beyond the observed SM spectrum (Section 8.10). Its mass, couplings, and possible cosmological abundance remain open (Level B).

This concludes the softest condensate sector of the particle chapter. The next subsections turn to heavier or more structurally elaborate excitations, beginning with the radial condensate mode.

**Status summary.**

Statement	Status	Comment
Soft orientation sector required by broken-branch geometry	A/B	Geometric existence strict; propagating content fixed only after scalar-only integrability reduction
$O(4) \rightarrow O(3)$ breaking admits $S^3$ vacuum manifold	A	Geometric statement
Naive Goldstone counting: $\dim O(4) - \dim O(3) = 3$	A	Broken-generator counting
Integrability reduces propagating soft content to $N_G^{\text{phys}} = 1$	B	Physical mode count in the scalar-only basis, using $Q_A = \partial_A \Phi$ and Appendix I
Surviving mode $\chi$ massless in the minimal broken-phase EFT	B	No orientation potential inherited from P1–P6
Pseudo-Goldstone mass mechanism	Open (OP-GM)	No explicit $O(4)$ -breaking in P1–P6
Soft-mode dark-matter interpretation	Not claimed	Galactic phenomenology is already accounted for by the $\phi$ -sector

### 8.3 Radial Condensate Mode

*Status: layered. The primary radial mode of the first condensate is required at Level A as the amplitude fluctuation of the ordered branch. Its Planckian scale follows at Level B from  $m_\sigma \sim \phi_0 \sim \bar{M}_{\text{Pl}}$  (Section 5.1). A secondary Higgs-like radial mode is structurally admissible only if an electroweak-like second condensate transition exists; this remains Level B/C and does not by itself establish the full Standard Model Higgs sector.*

**Why this sector is required.** Unlike the soft orientation sector, the radial mode is not tied to the vacuum manifold of broken directions but to fluctuations of the condensate amplitude itself. Once a broken condensate branch with nonzero order parameter exists, amplitude fluctuations are unavoidable. For this reason, the primary radial mode belongs to the class of required condensate excitations introduced in Section 8.1.

**Contrast with the soft orientation sector.** The soft mode  $\chi$  of Section 8.2 is an orientation fluctuation along the broken branch, whereas the radial mode  $\sigma$  is an amplitude fluctuation orthogonal to that branch. This difference is decisive for their physical roles:  $\chi$  is soft and constrained by integrability, while  $\sigma$  is heavy and sets the scale at which the broken-phase EFT itself ceases to be valid.

**Minimal derivation chain.** The existence of the primary radial mode follows from three ingredients: (i) the condensate branch is characterised by a nonzero amplitude, (ii) fluctuations of the order parameter decompose into tangential and normal directions with respect to the broken branch, and (iii) normal fluctuations are precisely amplitude fluctuations. Therefore, once a broken branch with nonzero order parameter exists, a radial fluctuation sector is unavoidable. What remains nontrivial is not its existence, but its physical scale and its role as the UV threshold of the corresponding EFT.

**Tangential versus normal fluctuations.** At the level of the broken-branch geometry, the soft orientation sector and the radial sector are not merely two different low-energy fields. They correspond to two inequivalent directions in configuration space: tangential fluctuations along the vacuum manifold and

normal fluctuations away from it. The former are controlled by the broken-manifold geometry and are soft; the latter probe the stiffness of the condensate amplitude itself and are heavy.

**First radial mode: amplitude fluctuation of the ordered branch.** In the scalar-only ECT basis the fundamental degree of freedom is the condensate field  $\Phi$ ; the ordered background is characterised by  $Q_A = \partial_A \Phi = u_0 n_A$ , where  $n_A$  is the derived orientation variable (Section 4.2). Amplitude fluctuations of the gradient  $Q_A = \partial_A \Phi$  around its ordered background — i.e. fluctuations of  $u_0 = |\langle \partial_A \Phi \rangle|$  — define the radial mode  $\sigma$  with the polar decomposition  $\partial_A \Phi = (u_0 + \sigma) n_A$ . Its characteristic mass scale is set by the curvature of the scalar potential at the broken-phase vacuum:

$$m_\sigma^2 \sim V''(\phi_0) \sim 2\lambda \phi_0^2, \quad (8.5)$$

where the proportionality accounts for EFT matching between the scalar potential and the gradient-sector fluctuation spectrum. For a generic quartic potential with minimum at  $\phi_0$  and with the matching  $\phi_0 \sim \bar{M}_{\text{Pl}}$  (Section 5.1):

$$m_\sigma \sim \sqrt{2\lambda} \bar{M}_{\text{Pl}} \sim \bar{M}_{\text{Pl}} \quad (\text{Level B: consistency-scale identification}). \quad (8.6)$$

This mode is Planck-heavy and integrates out at  $E \ll m_\sigma$ . It therefore provides the natural heavy scale controlling the validity range of the broken-phase EFT. It is *not* the Standard Model Higgs boson.

The positivity  $V''(\phi_0) > 0$  established above gives tree-level local stability of the primary radial sector within the stated condensate potential. The one-loop vacuum stability analysis, the question of false vacuum and Coleman vacuum decay, and the comparison with Standard-Model electroweak metastability are developed in Section 8.4.

**Spin and propagation.** The mode  $\sigma$  is a Lorentz scalar (spin-0 in the emergent Lorentzian description): it is the amplitude fluctuation of the scalar condensate  $\Phi$  and carries no orientation or gauge indices. In the ordered background it propagates with an effective mass  $m_\sigma$  and sees the same emergent Lorentzian metric as other EFT modes.

**Why the primary radial mode is not the soft orientation scalar.** The primary radial mode  $\sigma$  must also be distinguished from the surviving soft scalar  $\chi$  of the orientation sector (Section 4.3). This distinction is ECT-specific and follows from the integrability of the gradient condensate:  $Q_A = \partial_A \Phi$  is an exact one-form, so amplitude and orientation fluctuations are not independent generic fields. At linear order,  $\sigma$  describes fluctuations of the magnitude  $|Q_A| = |\partial_A \Phi|$ , whereas  $\chi$  parameterises the surviving longitudinal soft variation of the orientation sector. Thus  $\sigma$  and  $\chi$  are different scalar excitations with different physical roles:  $\sigma$  is heavy and radial, while  $\chi$  is soft and branch-sensitive.

**Higher-dimension operators after integrating out  $\sigma$ .** Integrating out the heavy primary radial mode does not merely remove it from the low-energy spectrum. It also generates higher-dimension operators suppressed by powers of  $m_\sigma^{-2}$ , schematically of the form

$$\Delta \mathcal{L}_{\text{EFT}} \sim \sum_{n \geq 1} \frac{\mathcal{O}_{2n+4}}{m_\sigma^{2n}}. \quad (8.7)$$

This is the standard EFT consequence of decoupling. In ECT it explains why the broken-phase low-energy theory remains reliable at  $E \ll m_\sigma$ , while still retaining calculable suppressed corrections from the heavy radial sector (Level B).

**What is strict and what is not.** What follows strictly is that a broken condensate with a nonzero amplitude admits a radial fluctuation sector and that this sector defines the natural UV threshold of the corresponding low-energy EFT. What does not yet follow from first principles is the full microphysical value of  $m_\sigma$  beyond the EFT matching relations, nor the existence of a second radial mode at  $v_2$ , which remains conditional on the weak-like secondary transition.

**Connection to the pre-quantum action scale.** The primary radial mass  $m_\sigma$  is closely related to the physical scale that enters the distinguished EFT action scale of the coherent branch (Section 5.6):

$$S_0^{\text{EFT}} = \frac{K_\theta m_\phi}{2}. \quad (8.8)$$

In the minimal single-condensate realisation, the radial core scale  $m_\phi$  entering  $S_0^{\text{EFT}}$  is naturally identified with the primary radial mass  $m_\sigma$ . This is a nontrivial structural link: the same condensate scale that controls the EFT breakdown threshold is also tied to the pre-quantum action scale later matched to  $\hbar$ . In other words, the quantum sector and the UV structure of the geometric branch share a common mass scale. This connection is a Level B consistency statement, not a parameter-free prediction, because both  $S_0^{\text{EFT}}$  and  $m_\sigma$  depend on the condensate parameters  $(u_0, \lambda)$  in the present notation, which are fixed by matching. This should therefore be read as a consistency link between the UV radial threshold and the coherent action scale, not as a proof that the two quantities are identical in a full microscopic completion.

**The primary radial mode as physical UV threshold.** In standard quantum field theory, the UV cutoff  $\Lambda$  is typically introduced as a formal regulator without intrinsic physical meaning. In ECT the physical EFT breakdown scale is set by the *mass* of the primary radial mode  $m_\sigma$ . The broken-phase EFT is valid for  $E \ll m_\sigma$ ; at  $E \sim m_\sigma$  the radial mode becomes dynamical and the effective description must be replaced by the full condensate theory. This is the standard EFT picture, but with a concrete physical interpretation: the scale at which the EFT breaks down is the scale at which the condensate amplitude itself begins to fluctuate. The Euclidean propagator of the radial mode (Appendix O) decays asymptotically as

$$G_\sigma(r) \propto \frac{e^{-m_\sigma r}}{r^{3/2}} \quad (r \rightarrow \infty), \quad (8.9)$$

confirming that amplitude correlations decay on the scale  $\xi_{\text{cond}} \sim m_\sigma^{-1}$ . Beyond this distance the ordered branch is effectively stiff against amplitude fluctuations, and the low-energy EFT is well-defined to that approximation (Level B). In this sense,  $\Lambda_{\text{EFT}} \sim m_\sigma$  is not merely a formal regulator scale but a physical threshold associated with the onset of amplitude dynamics of the condensate medium itself.

**What is established, what this changes, and what remains open.** At the present stage, the UV content of ECT should be read in three layers. First, the ordered-branch effective theory has a physical breakdown threshold at the primary radial mass  $m_\sigma$ : this is the scale at which condensate-amplitude fluctuations become dynamical and the low-energy broken-phase EFT ceases to be self-contained (Level A/B). Second, this replaces the usual interpretation of a UV cutoff as a merely formal regulator by a condensate-origin physical threshold. In that sense ECT already provides a structural route to UV regularisation of the low-energy geometric and coherent sectors. Third, ECT does *not* yet establish perturbative renormalisability, asymptotic safety, or a complete microscopic quantum-gravity closure. Those remain open problems.

**Physical UV-threshold statement (Level A/B).** Within the minimal ordered-branch EFT, the primary radial mass  $m_\sigma$  plays the role of a physical UV threshold rather than a purely formal regulator. The reason is structural: the same condensate mode whose inverse mass sets the correlation length  $\xi_{\text{cond}} \sim m_\sigma^{-1}$  also marks the onset of amplitude dynamics beyond the stiff ordered branch. Consequently, the low-energy EFT is not expected to remain valid above  $E \sim m_\sigma$ , and its UV completion must be sought in the full condensate theory rather than in an independent arbitrary cutoff prescription.

**What this does and does not establish.** This UV-threshold statement is already stronger than the usual EFT claim that a regulator must exist somewhere: in ECT the threshold is tied to a concrete physical condensate mode. However, it does *not* yet prove that graviton loop amplitudes are finite, that the theory is asymptotically safe, or that all ultraviolet sensitivities cancel in a completed quantum treatment. The present result is therefore a structural UV-regularisation route, not a finished UV-complete quantum-gravity theorem.

**Correlation with the action-scale programme.** The UV threshold  $m_\sigma$  and the coherent action scale  $S_0^{\text{EFT}}$  (§5.6) both originate from the same ordered condensate. This produces a structural triple correlation:  $\hbar c/m_\sigma \sim \xi_{\text{cond}} \sim \ell_{\text{Pl}}$ —all three scales are set by one medium. In standard physics the Planck length, the quantum of action, and the UV breakdown scale of gravity are independent inputs; in ECT they trace to the same condensate parameters  $(\phi_0, \lambda, \alpha)$ . This correlation is one of the strongest structural indicators that the ECT single-medium programme is internally consistent at the UV-threshold level.

**Connection to PES and graviton quantisation.** The Principle of Euclidean Stationarity (§29) suggests that the graviton sector is quantised by the same mechanism as all other condensate excitations: the compact phase topology combined with PES selection imposes the same action quantum  $S_0$  on gravitational perturbations. This reframes the UV-safety question: rather than asking whether an externally quantised metric is UV-finite, ECT asks whether the condensate-excitation spectrum is self-consistent at scales below  $\xi_{\text{cond}}$ .

**Quantum gravity versus UV-threshold reinterpretation.** ECT does not begin by quantising an already given Lorentzian geometry. Instead, it assigns the ultraviolet threshold of the low-energy theory to a physical condensate excitation. This shifts the problem from “how to regulate a formal gravitational field theory” to “how the full condensate theory takes over once the ordered branch reaches its radial threshold.” In this sense ECT offers a different starting point from both cutoff-based EFT gravity and approaches that search directly for a fundamental quantum geometry (CDT, loop QG, string theory).

**Falsifier for the UV-threshold programme.** The minimal ECT UV-threshold programme would fail if low-energy gravitational or coherent sectors were found to require ultraviolet completion scales parametrically unrelated to the primary condensate threshold  $m_\sigma$ , or if a fully consistent completion demanded additional independent microscopic gravitational degrees of freedom already below the radial threshold. In such a case the single-condensate UV picture would be insufficient.

**Why the  $m_\sigma$ – $S_0^{\text{EFT}}$  link is structurally natural.** Both  $m_\sigma$  and  $S_0^{\text{EFT}}$  refer to the same physical transition point: the loss of validity of the low-energy coherent description in favour of the full condensate dynamics. The first expresses this threshold in energy language, the second in action language. For that reason, a structural relation between them is natural even though their exact equality is not proved in the present formulation.

**Why the secondary radial mode is qualitatively different.** The primary radial mode exists whenever the first ordered branch exists. By contrast, the Higgs-like mode  $h$  does not follow from the primary condensate alone. It is conditional on the existence of a second weak-like transition and therefore has a fundamentally different logical status. The distinction is not merely one of scale ( $\phi_0$  versus  $v_2$ ), but one of derivational status: required versus conditional.

**Secondary radial mode: conditional rather than required.** The discussion now changes logical status. Whereas the primary radial mode is required by the existence of the broken condensate branch itself, a second radial mode at the scale  $v_2$  can arise only if the weak-like  $O(3) \rightarrow O(2)$  transition is actually realised.

**Second radial mode: candidate from the electroweak-like transition.** If the second condensate transition  $O(3) \rightarrow O(2)$  is realised at scale  $v_2$  (Appendix L, assumptions A1–A2), the effective broken-phase description at that scale admits a radial fluctuation around the second condensate vacuum. In an effective field theory language (*not* a second independent fundamental field, but an effective condensate sector at scale  $v_2$ ):

$$\phi_{\text{ew}} = v_2 + h, \quad m_h^2 = V''_{\text{ew}}(v_2) = 2\lambda_2 v_2^2, \quad (8.10)$$

where  $\lambda_2$  is the quartic coupling of the second-condensate effective sector at scale  $v_2$ .

This mode is *structurally analogous* to the Standard Model Higgs boson in the following sense:

- it is the radial excitation of the second-condensate VEV (formally analogous to the Higgs field);
- the spontaneous breaking of the internal symmetry at  $v_2$  would generate masses for the vector bosons of the embedded electroweak-like gauge sector, if a local gauge realisation exists (formally analogous to the Higgs mechanism);
- the relation  $m_h = \sqrt{2\lambda_2} v_2$  has the same structure as the SM Higgs mass formula.

**Honest status of the Higgs-like mode.** Three levels must be distinguished:

1. **Level B/C (structural):** if the second transition exists and if the corresponding  $O(3)$ -sector admits a local gauge realisation (not implied by P1–P6; part of OP-EW), a radial mode  $h$  at scale  $v_2 \approx 246$  GeV is structurally present.
2. **Matching constraint:** the SM Higgs mass  $m_H \approx 125.1$  GeV [52, 53] would require  $\lambda_2(v_2) \approx 0.13$ . This value is not derived from ECT postulates P1–P6; it is a matching input if one demands consistency with the measured Higgs mass.
3. **Open (OP-EW):** the dynamical mechanism producing  $v_2$ , the origin of  $\lambda_2$ , and the localisation of the  $O(3)$  symmetry at scale  $v_2$  are not derived from the minimal scalar condensate and remain open problems.

**Relation to the three-scale hierarchy.** This completes the radial-sector contribution to the three-scale architecture of ECT:  $m_\sigma \sim \bar{M}_{P1}$  belongs to the primary condensate,  $m_h \sim v_2$  is conditional on the secondary weak-like sector, and the galactic scale  $v_{\text{gal}}$  belongs not to a particle-like radial excitation but to the macroscopic amplitude-sector closure.

**Higgs self-coupling and testability.** If the secondary condensate potential is quartic near  $v_2$ ,

$$V_{\text{ew}}(\phi_{\text{ew}}) = \frac{\lambda_2}{4} (\phi_{\text{ew}}^2 - v_2^2)^2, \quad (8.11)$$

then the Higgs mass satisfies

$$m_h^2 = 2\lambda_2 v_2^2, \quad \lambda_2 = \frac{m_h^2}{2v_2^2}. \quad (8.12)$$

The corresponding cubic self-interaction is

$$V_{\text{ew}} \supset \lambda_2 v_2 h^3, \quad (8.13)$$

or equivalently

$$V_{\text{ew}}'''(v_2) = 6\lambda_2 v_2 = \frac{3m_h^2}{v_2}. \quad (8.14)$$

Different collider conventions for the trilinear Higgs coupling differ by combinatorial factors; the expression above refers to the third derivative of the effective potential at the minimum. Deviations from this quartic relation would signal non-quartic corrections to the effective potential at scale  $v_2$ —for instance, induced by the primary condensate sector or by the dynamics of the second transition itself. Deviations from this quartic relation would indicate that the effective secondary potential is not approximately quartic near its minimum, or that additional condensate-sector corrections enter already at that scale. The present framework does not determine the size of such deviations.



**Reframing the hierarchy problem.** The usual SM hierarchy problem asks: why is the Higgs mass so small compared to the Planck scale [54]? ECT recasts this as a condensate-spectrum question: why does a second condensate branch appear at  $v_2 \sim 10^{-16} \phi_0$ ? This is still an open problem (OP-EW), but the reframing is itself meaningful: instead of a fine-tuning of one scalar mass, the challenge becomes explaining the dynamical origin of a second ordered phase at an intermediate scale. The updated OP-EW-scale programme treats this hierarchy as a non-polynomial scale-generation problem,  $v_2 = \phi_0 e^{-\mathcal{J}_{\text{EW}}}$  with  $\mathcal{J}_{\text{EW}} \approx 36.8$  (Section 5.1). Candidate mechanisms include alignment running, walking/near-conformal dynamics, Miransky/BKT scaling, and topological/Hopf-like routes (Appendix M). None is derived from P1–P6, and none by itself solves the radiative stability problem of the secondary radial mode.

**Radiative stability: what ECT does and does not solve.** The reframing of the hierarchy problem as a condensate-spectrum question does not by itself resolve the radiative stability issue. If the secondary radial mode  $h$  couples to other fields (gauge bosons, fermions) with generic EFT couplings, its mass receives quadratic radiative corrections of order

$$\delta m_h^2 \sim \frac{g^2}{16\pi^2} m_\sigma^2 \sim \frac{g^2}{16\pi^2} \bar{M}_{\text{Pl}}^2. \quad (8.15)$$

This is a schematic EFT estimate; the precise coefficient depends on the couplings and field content of the secondary sector. The resulting fine-tuning is of the same order as in the Standard Model. ECT does not claim to solve this problem. What it offers is a different *physical context*: the fine-tuning question becomes whether the dynamics of the second condensate transition naturally selects  $v_2 \ll \phi_0$ . A possible mechanism is dimensional transmutation via the RG running of the effective quartic coupling from  $\phi_0$  to  $v_2$  (Section 5.1, Appendix L), but this remains Level C and has not been demonstrated within ECT. Absent an additional symmetry, compositeness mechanism, or dynamical selection principle, the secondary scalar remains quadratically sensitive to the primary UV scale. Any claim that ECT resolves the naturalness problem would be premature.

**Comparison with other Higgs frameworks.** *Standard Model Higgs:* in the SM the Higgs is an elementary scalar doublet introduced phenomenologically [55, 56]. In ECT radial modes emerge naturally as condensate amplitude excitations; the primary mode is necessarily present, while the Higgs-like secondary mode is conditional on the second transition.

*Condensed-matter amplitude (Higgs) modes:* in superfluids and in appropriate broken-phase condensed-matter systems, one encounters a phase mode together with a massive amplitude (Higgs-like) mode [57, 21]. The ECT primary radial mode  $\sigma$  is the direct analogue of such an amplitude mode — but here the condensate underlies spacetime structure itself, not a material medium.

*EFT hierarchy and decoupling:* in standard EFT, heavy particles decouple at low energies and generate suppressed higher-dimension operators. The Planck-heavy primary mode  $\sigma$  of ECT plays the analogous role: it integrates out at  $E \ll m_\sigma$ , leaving the broken-phase EFT that governs lower-energy physics.

A further useful comparison is with frameworks in which the Higgs is itself a non-elementary excitation of an underlying sector.

*Composite Higgs models* [58, 59]: in these models the Higgs is not elementary but a pseudo-Nambu–Goldstone boson of a new strongly coupled sector. The ECT secondary radial mode shares the feature of being a *condensate excitation* rather than a fundamental scalar, but differs in mechanism: it is the amplitude fluctuation of a second ordered phase, not a pseudo-NGB of a confining gauge theory. Unlike pseudo-Nambu–Goldstone Higgs scenarios, the ECT secondary radial mode is not protected by an approximate shift symmetry in the present formulation. The two approaches face the same hierarchy challenge; ECT recasts it as a condensate-dynamics question rather than a compositeness question.

### Status summary.

Statement	Status	Comment
Primary radial mode required by amplitude fluctuations	A/B	Broken condensate branch with nonzero order parameter
Primary radial mode as intrinsic EFT threshold	A/B	Broken-phase EFT valid only while amplitude dynamics is frozen
Primary radial mode is distinct from the SM Higgs	A	Different condensate level
$\sigma$ and orientation mode $\chi$ decouple at linear order	A	Integrability of $Q_A$ (Section 4.3)
$m_\sigma \sim \bar{M}_{\text{Pl}}$ (Planck heavy)	B	Uses $\phi_0 \sim \bar{M}_{\text{Pl}}$ (Section 5.1)
$\sigma$ provides the natural validity scale of the broken-phase EFT	B	Decoupling; higher-dimension operators suppressed by $m_\sigma$
$m_\sigma$ is structurally linked to the action-scale sector through $S_0^{\text{EFT}}$	B	Via the radial-core scale in the minimal single-condensate realisation
$m_\sigma$ as physical EFT breakdown scale	B	Correlation-length and decoupling scale
Secondary Higgs-like radial mode $h$	B/C	Conditional on a realised $O(3) \rightarrow O(2)$ transition
Secondary mode is structurally analogous to SM Higgs	B/C	Formal radial analogue; not a derivation
$m_h = \sqrt{2\lambda_2} v_2$ with $v_2$ from $G_F$ matching	B/C	Matching input, not ECT prediction
$\lambda_2(v_2) \approx 0.13$ if matched to $m_H \approx 125$ GeV	Constraint	External SM matching, not an ECT derivation
Radiative stability of $m_h$	Open	Quadratic sensitivity to the primary UV scale remains
Quartic relation for $m_h$ and the cubic interaction near the minimum	B/C	Holds if the secondary potential is nearly quartic
Yukawa / gauge mass generation fully derived	Open	Not completed; part of OP-EW

## 8.4 Vacuum Stability, False Vacuum, and Vacuum Decay

### 8.4.1 Why the question matters

In standard quantum field theory, the vacuum state of a scalar field can be metastable: the observed vacuum may be only a local, not a global, minimum of the effective potential. If a deeper minimum exists, the field can undergo a non-perturbative transition — Coleman vacuum decay [60] — in which a bubble of the “true vacuum” nucleates inside the “false vacuum” and subsequently expands, converting the entire spacetime. For the Standard-Model Higgs field, radiative corrections driven primarily by the large top-Yukawa coupling are known to make the electroweak vacuum metastable at high field values [61, 62]: the running quartic coupling  $\lambda_{\text{SM}}(\mu)$  crosses zero near  $\mu \sim 10^{10}$  GeV, and the effective potential turns downward at large Higgs-field amplitudes.

Whether the primary ECT condensate suffers from an analogous instability is therefore a central self-consistency question. This subsection analyses the problem from first principles: the structure of the ECT potential, its critical points, the one-loop running of the quartic coupling, the absence of fermion-driven destabilisation, the nature of the cosmological ordering transition, and the role of subleading sectors.

### 8.4.2 Structure of the minimal ECT potential

The bare potential of the primary condensate (P3) is

$$V(\Phi) = -\frac{\mu^2}{2}\Phi^2 + \frac{\lambda}{4}\Phi^4, \quad \mu^2 > 0, \quad \lambda > 0. \quad (8.16)$$

Its critical points are:

- $\Phi = 0$ : symmetric stationary point, with  $V''(0) = -\mu^2 < 0$ . This is an *unstable hilltop*, not a metastable minimum. A small perturbation drives the field away from  $\Phi = 0$  toward one of the two minima.
- $\Phi = \pm\phi_0$  with  $\phi_0 = \sqrt{\mu^2/\lambda}$ : the two global minima, with  $V''(\phi_0) = 2\mu^2 > 0$  (tree-level local stability) and  $V(\phi_0) = -\mu^4/(4\lambda) < 0$ . These two minima are exactly degenerate by the  $\mathbb{Z}_2$  symmetry  $\Phi \rightarrow -\Phi$  of the potential.

The minimal ECT potential therefore contains *no metastable local minimum* separated from a deeper minimum by a barrier. Both minima are global, and the symmetric point is a maximum, not a false vacuum. This is a crucial structural difference from any double-well configuration that would be needed for Coleman vacuum decay.

### 8.4.3 Inapplicability of Coleman vacuum decay

Coleman's semiclassical theory of false-vacuum decay [60, 63] requires two specific ingredients: (i) a *metastable* minimum (the “false vacuum”), in which the field can sit for a long time, and (ii) a *deeper* minimum (the “true vacuum”), separated from the first by a potential barrier. The decay rate per unit volume is then

$$\Gamma/V \sim A e^{-B/\hbar}, \quad (8.17)$$

where  $B = S_E[\Phi_{\text{bounce}}] - S_E[\Phi_{\text{false}}]$  is the difference in Euclidean action between the bounce configuration and the homogeneous false vacuum.

In the minimal ECT potential (8.16), *neither* ingredient is present:

1.  $\Phi = 0$  is a hilltop ( $V''(0) < 0$ ), not a metastable minimum. A field configuration at  $\Phi = 0$  does not “sit” there; it rolls away immediately (spinodal regime, not metastable trapping).
2. The two minima  $\pm\phi_0$  are exactly degenerate ( $\Delta V = 0$ ). Coleman decay between degenerate minima has no driving force: there is no lower-action or lower-effective-potential target.

Therefore, **Coleman vacuum decay is structurally inapplicable to the minimal ECT primary potential**. The standard formula (8.17) has no subject: there is no false vacuum from which to decay and no deeper minimum into which to tunnel.

### 8.4.4 The cosmological ordering transition is not Coleman-type vacuum decay

The cosmological ordering transition  $O(4) \rightarrow O(3)$ , in which the gradient condensate forms and Lorentzian spacetime emerges (Section 6.8), should not be identified with false-vacuum decay. The pre-ordered regime corresponds to configurations near the hilltop  $\Phi \approx 0$ , which is unstable rather than metastable. The transition is therefore structurally closer to *spinodal decomposition* — the spontaneous instability of an unstable homogeneous state — than to the nucleation of a critical bubble in a metastable minimum.

In the language of condensed-matter physics: the ordering transition is analogous to a quench past the spinodal point, where the homogeneous state becomes linearly unstable and the system spontaneously breaks into ordered domains, rather than to the slow nucleation of droplets from a supercooled metastable phase. There is no exponential suppression factor  $e^{-B/\hbar}$  because there is no barrier to overcome.

#### 8.4.5 One-loop stability of the primary amplitude sector

Even though no Coleman false vacuum exists at tree level, one must still ask whether radiative corrections could generate new minima at large field values, as happens in the Standard Model. This is the question of *RG-driven metastability*.

**The running coupling in strict scalar closure.** The one-loop  $\beta$ -function for a single real scalar in the minimal ECT action (Eq. (8.26), Section 5.1) is

$$\beta_\lambda \equiv \frac{d\lambda}{d\ln\mu} = \frac{3\lambda^2}{16\pi^2} > 0, \quad (8.18)$$

which is *strictly positive* for any  $\lambda > 0$ . This is a standard one-loop result for a quartic scalar self-coupling in four Euclidean dimensions.

With the boundary condition  $\lambda(M_{\text{Pl}}) \approx 10^{-3}$  (Section 5.1), the running coupling has the explicit solution

$$\lambda(\mu) = \frac{\lambda_0}{1 - \frac{3\lambda_0}{16\pi^2} \ln \frac{\mu}{M_{\text{Pl}}}}, \quad \lambda_0 \equiv \lambda(M_{\text{Pl}}). \quad (8.19)$$

**Consequences for vacuum structure.** Since  $\beta_\lambda > 0$ , the coupling  $\lambda(\mu)$  *grows* with the renormalisation scale  $\mu$ . This has three immediate consequences:

1.  **$\lambda$  never crosses zero.** The denominator in (8.19) is positive for all  $\mu < \mu_{\text{LP}}$  (the Landau pole (8.27),  $\mu_{\text{LP}} \approx M_{\text{Pl}} e^{5.26 \times 10^4}$ ), and  $\lambda(\mu) > 0$  throughout the entire validity range of the broken-phase EFT.
2. **The effective potential steepens at large fields.** The RG-improved effective potential  $V_{\text{eff}}(\phi) \sim \lambda(\phi) \phi^4/4$  grows faster than  $\phi^4$  at large  $\phi$ , because  $\lambda$  increases. No new minima can appear at high field values.
3. **The Landau pole is physically unreachable.** The broken-phase EFT ceases to be valid at the radial-mode threshold  $m_\sigma \sim M_{\text{Pl}}$ , which is  $\sim e^{5.26 \times 10^4}$  below the Landau pole. Within the EFT validity range, the dimensionless gravitational coupling  $g(\mu) = \lambda/(8\pi) \approx 4 \times 10^{-5}$  remains parametrically small.

**Why Standard-Model metastability does not transfer.** The Standard-Model running of the Higgs quartic differs qualitatively. At one loop, the schematic structure is

$$\beta_{\lambda_{\text{SM}}} = \frac{1}{16\pi^2} [24\lambda_{\text{SM}}^2 + \lambda_{\text{SM}}(12y_t^2 - 9g^2 - 3g'^2) - 6y_t^4 + \text{gauge quartic terms}], \quad (8.20)$$

so that the large top-Yukawa contribution drives  $\lambda_{\text{SM}}(\mu)$  downward and, in the observed parameter range, eventually through zero near  $\mu \sim 10^{10}$  GeV [61, 62]. This is the origin of the familiar electroweak metastability story.

In the primary ECT sector, this mechanism is absent: the primary condensate is a pure real scalar at the fundamental level, with no fermionic couplings in the strict scalar closure. The only one-loop contribution to  $\beta_\lambda$  is the positive self-coupling term  $+3\lambda^2/(16\pi^2)$ ; there is no fermionic channel that could drive  $\lambda$  downward. This is therefore a *genuine structural difference*, not merely a tree-level accident (Level B).

#### 8.4.6 Analysis of subleading contributions

**Soft orientation sector.** The surviving soft scalar  $\chi$  (Section 4.3) is parametrically softer than the Planck-heavy radial mode and does not provide any identified destabilising channel for the primary amplitude potential in the minimal closure. The integrability constraint sharply reduces the independent soft sector

relative to a generic multi-field broken-symmetry system, and no analogue of the Standard-Model top-Yukawa destabilisation mechanism is present here. A full constrained fluctuation-determinant analysis for the coupled amplitude–orientation system has not yet been carried out, so the present statement should be read as follows: within the current minimal closure, the soft sector does not generate any identified mechanism capable of overturning the one-loop amplitude-sector stability result.

**Topological sectors.** The vacuum manifold  $\mathcal{M}_1 = O(4)/O(3) \simeq S^3$  admits topological sectors classified by  $\pi_3(S^3) = \mathbb{Z}$  (Section 8.10). These texture-like configurations are spatially extended deformations of the orientation field  $n_A$  and carry *additional gradient action*  $\int (\partial n)^2 d^4X > 0$  relative to the homogeneous ordered branch. They therefore do not provide a lower-action target configuration for tunnelling: transitioning into a texture sector *increases* the Euclidean action. For the same reason,  $\pi_0(S^3) = 0$  ensures no topologically stable domain walls in the primary sector (Section 8.10).

**Embedded electroweak sector.** If the conditional secondary transition (Section 8.7) realises a Standard-Model-like Higgs sector at the scale  $v_2 \approx 246 \text{ GeV}$ , the question of electroweak vacuum metastability belongs to that *embedded* sector, not to the primary condensate. The primary amplitude sector does not inherit the SM-type instability mechanism (which requires fermionic couplings absent at this level), but the full threshold and matching analysis between primary and secondary sectors has not been completed. The corresponding threshold and matching problem remains part of the second-transition programme (OP-EW).

#### 8.4.7 Taxonomy of vacuum-decay scenarios

**Table 26:** Applicability of vacuum-decay scenarios to the primary ECT condensate.

Scenario	Applies?	Reason
Coleman false→true	<b>No</b>	No metastable minimum in the minimal potential; $\Phi = 0$ is a hilltop
SM-type RG-driven metastability	<b>No</b>	$\beta_\lambda > 0$ ; no top-Yukawa analogue; $\lambda$ never crosses zero
Thermal first-order transition	<b>No</b>	Article explicitly distinguishes the ordering transition from thermal bubble nucleation
Ordering / spinodal-like instability of the symmetric hilltop	Structural analogue	The cosmological ordering transition is closer to this class than to Coleman nucleation, but its precise non-equilibrium mechanism remains open
Branch-to-branch ( $\pi_3$ sector)	Not expected	Textures carry additional gradient action; no lower-action target
Embedded EW metastability	Separate question	Belongs to the secondary sector, not to the primary condensate

#### 8.4.8 Summary: derivation status

**Table 27:** Vacuum-stability results and their derivation level.

ID	Level	Result
R1	A	Local tree-level stability: $V''(\phi_0) = 2\mu^2 > 0$

ID	Level	Result
R2	A	Topological anti-predictions: $\pi_0 = \pi_1 = \pi_2 = 0$ ; no stable domain walls, strings, or monopoles from the primary transition
R3	B	In the strict scalar one-loop closure, $\beta_\lambda > 0$ ensures $\lambda(\mu) > 0$ across the broken-phase EFT range; no Standard-Model-type high-field metastability channel arises
R4	B/Open	No identified destabilising channel from the integrability-reduced $\chi$ sector in the minimal closure; a full constrained amplitude–orientation determinant analysis remains open
R5	A/B	$\Phi = 0$ is a hilltop ( $V''(0) < 0$ ), not a metastable minimum; Coleman vacuum decay structurally inapplicable
O1	Open	Full branch-architecture stability (nonlinear amplitude–orientation couplings, non-perturbative channels, matching to extended sectors)
O2	Open	Electroweak metastability: belongs to the embedded secondary sector (OP-EW)

#### 8.4.9 Conclusion: vacuum decay in ECT

The observed primary ordered branch of ECT is *not* a false vacuum in any standard sense. The minimal potential contains no metastable minimum, and the Coleman decay machinery is structurally inapplicable. The one-loop RG analysis establishes that the Standard-Model-type metastability mechanism — in which the running quartic coupling crosses zero at high scale — does not operate in the primary ECT sector, because the  $\beta$ -function is strictly positive and there is no fermionic destabilising channel. All subleading sectors considered here (soft orientation sector, topological sectors, embedded electroweak sector) either do not provide any identified destabilising channel within the minimal closure or belong to separate, secondary programmes.

The cosmological ordering transition  $O(4) \rightarrow O(3)$  should be understood as a spinodal-type instability of the symmetric hilltop, not as Coleman-type false-vacuum decay. The ordered branch that results from this transition is, within the strict scalar one-loop closure, the global minimum of the amplitude sector throughout the broken-phase EFT range, and no channel for its further decay has been identified. The full stability of the entire ordered branch architecture beyond the amplitude closure remains an open programme.

#### 8.4.10 Euclidean formulation and the status of bounce configurations

A conceptual remark is in order regarding the role of the Euclidean formulation. In standard Lorentzian QFT, the Euclidean bounce solution used in Coleman’s theory is obtained by Wick rotation  $t \rightarrow -i\tau$ ; the Euclidean space is a computational tool, not the physical arena. In ECT the situation is reversed: the four-dimensional Euclidean manifold is *fundamental* (P1), and Lorentzian spacetime is emergent. If a bounce-like saddle configuration of the condensate field existed — connecting, say, two different ordered sectors — it would be a *native* object of the theory, not an analytic-continuation artefact.

This observation has two consequences. First, it means that the absence of Coleman vacuum decay established above is not an artefact of a Lorentzian-to-Euclidean continuation: the ECT potential genuinely lacks the required metastable-minimum structure on its native Euclidean arena. Second, it clarifies the nature of the ordering transition: the  $O(4) \rightarrow O(3)$  transition is a saddle-driven restructuring of the Euclidean condensate, not a tunnelling event in a pre-existing Lorentzian spacetime. Non-perturbative Euclidean transitions (branch changes, texture formation, defect-mediated processes) remain structurally natural in ECT, but none of them corresponds to a Coleman-type decay of the observed ordered branch (see Table 26).

### 8.4.11 Comparison with other frameworks

The vacuum-stability question takes different forms in different frameworks.

In the Standard Model, the electroweak vacuum is metastable because the large top-Yukawa coupling drives the Higgs quartic downward at high scale, eventually sending  $\lambda_{\text{SM}}(\mu)$  through zero. In string-landscape settings, by contrast, vacuum decay is tied to the existence of many distinct local minima and transition channels between them.

The primary ECT condensate differs structurally from both pictures. Within the strict scalar closure, there is no fermionic destabilising channel analogous to the Standard-Model top-Yukawa mechanism, and the minimal primary potential does not exhibit a landscape of competing isolated minima. The resulting vacuum-stability problem is therefore sharper and cleaner: the primary question is not decay from one metastable vacuum to another, but the stability of the single connected ordered branch and of its low-energy amplitude sector.

## 8.5 Emergence of the Graviton

*Status: Level A for the existence of an induced effective-metric sector sourced by condensate orientation fluctuations. Level B for the Fierz–Pauli-type quadratic structure and for the massless spin-2 interpretation. Full non-perturbative ghost-freedom and TT projection remain open (OP3). Connection to macroscopic gravity: Section 11, Appendix X.*

Within the classification of Section 8.1, the graviton belongs to the class of required condensate excitations of the primary ordered branch.

**Why this sector is required.** The graviton sector is not introduced as an independent field-theoretic addition to ECT. It becomes unavoidable once the broken condensate branch is recognised to carry an induced effective metric. If orientation fluctuations of the ordered branch change the effective propagation geometry, then a symmetric metric perturbation sector is necessarily present. What remains nontrivial is not the existence of such a sector, but whether it closes to the linearised massless spin-2 form of the Fierz–Pauli type.

**Strategy: graviton via effective metric fluctuations.** A direct fluctuation of the orientation field  $n_A$  carries vector rather than tensor character and therefore does *not* produce a spin-2 excitation. To obtain a massless spin-2 graviton one must instead work with fluctuations of the *effective metric* induced by the condensate. Unlike Einstein–aether constructions, the preferred direction in ECT is not introduced as an independent fundamental vector field but emerges from the ordered condensate background.

**Three logical levels of statement.** The present subsection combines three different levels of analysis:

- (i) the *strict geometric level*, at which the ordered branch induces an effective metric and orientation fluctuations source a symmetric metric perturbation sector;
- (ii) the *linear EFT level*, at which this induced sector is reconstructed as Fierz–Pauli-like and interpreted as a massless spin-2 mode;
- (iii) the *completion level*, at which ghost-freedom, exact TT projection, nonlinear self-coupling, and full compatibility with the macroscopic gravitational equations remain to be established.

Keeping these three levels distinct is essential for an honest reading of the graviton claim in ECT.

**Step 1: effective metric.** The condensate background defines an effective inverse metric through the principal symbol of ordered-branch perturbations, using the same unique kinetic tensor  $K^{AB}$  established by Theorem 3.2:

$$G_{\text{eff}}^{AB} = K^{AB} = \beta \delta^{AB} - \alpha n^A n^B, \quad n_A n^A = 1. \quad (8.21)$$

Equivalently, using the projectors  $P_{\parallel}^{AB} = n^A n^B$  and  $P_{\perp}^{AB} = \delta^{AB} - n^A n^B$ ,

$$G_{\text{eff}}^{AB} = \beta P_{\perp}^{AB} - (\alpha - \beta) P_{\parallel}^{AB}.$$

In the broken-symmetry vacuum  $\langle n^A \rangle = \delta_w^A$  one obtains

$$G_{\text{eff}}^{AB} = \text{diag}(\beta, \beta, \beta, \beta - \alpha),$$

which has Lorentzian signature for  $\alpha > \beta > 0$ . In the canonical benchmark  $(\alpha, \beta) = (2, 1)$  this reduces to  $\text{diag}(1, 1, 1, -1)$ , so that  $c_*^2 = \beta/(\alpha - \beta) = 1$ . The corresponding covariant effective metric is

$$g_{AB}^{\text{eff}} = \frac{1}{\beta} P_{AB}^{\perp} - \frac{1}{\alpha - \beta} P_{AB}^{\parallel}, \quad G_{\text{eff}}^{AC} g_{CB}^{\text{eff}} = \delta^A_B. \quad (8.22)$$

After passing from the Euclidean coordinate ordering  $(x^1, x^2, x^3, w)$  to the Lorentzian coordinate ordering  $x^\mu = (t, \mathbf{x})$ , with  $t = w/c_*$ , the canonical benchmark  $(\alpha, \beta) = (2, 1)$  gives the familiar background

$$\eta_{\mu\nu} = \text{diag}(-1, 1, 1, 1);$$

in the original Euclidean coordinate ordering the same covariant background reads  $\text{diag}(1, 1, 1, -1)$ . We write  $g_{AB}^{\text{eff}} = \bar{g}_{AB}^{\text{eff}} + h_{AB}$ , with  $h_{AB}$  the covariant perturbation that enters the Fierz–Pauli closure below. The perturbation of the inverse effective metric is

$$\delta G_{\text{eff}}^{AB} = -\alpha(\bar{n}^A \delta n^B + \delta n^A \bar{n}^B) + O(\delta n^2), \quad (8.23)$$

and the corresponding covariant-metric perturbation, obtained by varying the inverse relation  $G_{\text{eff}}^{AC} g_{CB}^{\text{eff}} = \delta^A_B$ , is

$$h_{AB} \equiv \delta g_{AB}^{\text{eff}} = -\frac{\alpha}{\beta(\alpha - \beta)}(\bar{n}_A \delta n_B + \delta n_A \bar{n}_B) + O(\delta n^2). \quad (8.24)$$

For the canonical benchmark  $(\alpha, \beta) = (2, 1)$  this specialises to

$$h_{AB} = -2(\bar{n}_A \delta n_B + \delta n_A \bar{n}_B) + O(\delta n^2).$$

The candidate spin-2 graviton sector is identified with the transverse-traceless part of this induced effective-metric perturbation, rather than with a direct degree of freedom of  $n_A$  itself. This is the strict part of the graviton construction: the condensate order parameter does generate a symmetric effective-metric perturbation sector. What is not yet strict is the identification of this sector with the completed Fierz–Pauli graviton.

**Step 2: linear Fierz–Pauli-type closure.** Once the perturbation is transferred from the vector variable  $\delta n_A$  to the symmetric effective-metric channel  $h_{AB}$ , the natural quadratic closure to test is the Fierz–Pauli one. This is the unique linearised massless spin-2 structure compatible with the standard gauge redundancy of a symmetric rank-2 field. Accordingly, expanding  $S_{\text{ECT}}$  (13.34) around the ordered branch and projecting to the effective-metric channel is expected to yield, at quadratic order, a Fierz–Pauli-type action:

$$S_{\text{grav}}^{(2)} \sim M_{\text{grav}}^2 \int d^4 X [\nabla_C h_{AB} \nabla^C h^{AB} - \frac{1}{2}(\nabla_A h)^2 + \dots], \quad (8.25)$$

where the overall normalisation  $M_{\text{grav}}$  is fixed by matching to the macroscopic gravitational sector (Section 11). At the present stage this is the strongest available linear EFT reconstruction, not yet a complete first-principles derivation from the bare condensate action.

**Step 3: massless spin-2 interpretation.** In the real Lorentzian parametrisation  $t = w/c_*$ , the linearised effective-metric sector admits a massless spin-2 interpretation at the quadratic level. Masslessness is protected, at the linearised effective level, by the emergent gauge redundancy of the Fierz–Pauli description (the linearised diffeomorphism invariance of the effective metric theory). A non-perturbative proof of masslessness from the bare condensate action has not been obtained; the interpretation is valid at the quadratic effective level only. The massless spin-2 interpretation therefore holds at the level of the



linearised effective description. Whether the full condensate theory selects exactly the same propagating content non-perturbatively is a separate question.

**Honest caveats.** The derivation above relies on two steps that require further verification: (i) the explicit computation of the quadratic action (8.25) directly from (13.34) by expanding in  $h_{AB}$ , checking that cross-terms between  $\mathcal{L}_n$  and the Ricci scalar combine correctly; and (ii) the projection from the vector fluctuation  $\delta n_A$  to the symmetric tensor  $h_{AB}$  via (8.24), which must be verified to capture exactly two transverse-traceless polarisations and no ghost modes. These steps are feasible but have not been carried out in full detail; they are listed as priority open problems in Section 38.1.

**Relation to the radial mode and the condensate spectrum.** The graviton ( $h_{AB}$ ) and the primary radial mode ( $\sigma$ ) are both excitations of the single condensate field  $\Phi$ , but they belong to different sectors:  $\sigma$  is the amplitude fluctuation of  $|Q_A| = |\partial_A \Phi|$  (Section 8.3), while  $h_{AB}$  arises from the orientation fluctuation  $\delta n_A$  projected into the effective-metric channel. These are distinct at linear order in the broken-phase EFT and do not mix in the quadratic action.

**The Weinberg–Witten theorem.** The Weinberg–Witten theorem [64] states that a theory with a Lorentz-covariant conserved energy-momentum tensor cannot contain massless particles with spin  $j > 1$  that couple to  $T^{\mu\nu}$ . This is often read as an obstruction to emergent or composite graviton scenarios formulated within a fundamentally Lorentz-covariant framework. In ECT, the theorem’s standard assumptions are not satisfied at the fundamental level:

- the fundamental level of ECT is a Euclidean scalar theory on  $\mathcal{M}^4$ , not a Lorentz-covariant quantum field theory;
- the Noether tensor  $T_{(\Phi)}^{AB}$  of P3 is an  $O(4)$ -covariant Euclidean object, not a Lorentz-covariant  $T^{\mu\nu}$ ;
- Lorentz covariance is *emergent* for the perturbative sector of the broken phase, not a symmetry of the fundamental description;
- the graviton is not a bound state of Lorentz-covariant particles but a collective mode of the condensate order parameter on a pre-Lorentzian background.

A useful heuristic analogy is provided by superfluid and analogue-gravity systems [21, 65]: effective spin-2 modes of the acoustic metric do not violate the Weinberg–Witten theorem because the fundamental theory (quantum liquid) is not itself Lorentz-covariant. The point is therefore not that ECT defeats the theorem, but that its fundamental formulation lies outside the theorem’s standard scope.

**Universality of the emergent light cone and GW consistency.** In the minimal broken-phase EFT, the graviton sector is tied to the same effective Lorentzian structure that governs the propagation of the other low-energy condensate modes. Accordingly, the gravitational wave cone is not an independent extra structure but part of the same emergent causal geometry. With the standard matching  $c_g = c$ , the graviton sector is consistent with the observational constraint from GW170817/GRB 170817A [10]. This should be read as a consistency condition on the standard matching, not as an independent prediction derived within the present subsection.

**Polarisation content.** If the linearised effective-metric sector closes precisely to the Fierz–Pauli form, the propagating graviton content is expected to reduce to the usual two transverse-traceless polarisations. Verifying this reduction explicitly remains part of the open programme (OP-gauge). This is in contrast to generic beyond-GR theories, which can admit up to six independent polarisation modes.

Approach	Graviton origin	Lorentzian signature	Metric status
General relativity	Fundamental field $g_{\mu\nu}$	Postulated	Fundamental
Sakharov induced gravity [3]	Loop corrections from matter	Postulated	Background input
Analogue gravity [65, 21]	Acoustic metric of fluid	Emergent	Effective
CDT [25]	Lattice path integral	Implemented through causal triangulation rules	Emergent from triangulations
Einstein-aether [24]	$u^A$ + metric, both fundamental	Postulated	Fundamental
<b>ECT</b>	Effective-metric perturbation from condensate SSB	<b>Emergent</b> from $O(4) \rightarrow O(3)$	<b>Effective</b> , from the single scalar $\Phi$ in the present minimal formulation

**Comparison with other emergent-gravity approaches.** Among the approaches compared here, ECT is distinguished by treating both the Lorentzian signature and the effective metric structure as emergent from a single scalar condensate on a Euclidean background. This is a structural claim about the framework, not about its current level of derivational completeness.

**Ultraviolet behaviour.** In perturbative Einstein gravity, non-renormalizability follows from the dimensionful coupling  $[G_N] = M^{-2}$ : each loop order  $L$  contributes graviton amplitudes growing as  $(E/M_{\text{Pl}})^{2L}$ , generating an infinite series of new counterterms ( $R^2, R^3, \dots$ ) not absorbable into a finite parameter set. In ECT the situation is structurally different in two respects.

First,  $G_N = c_*^4/(8\pi M_G^2)$  is not a fundamental constant but a condensate parameter with  $M_G^2 \sim \phi_0^2$ . The natural dimensionless gravitational coupling is

$$g(\mu) \equiv \mu^2 G_{\text{eff}}(\mu) = \frac{\lambda(\mu)}{8\pi}, \quad (8.26)$$

using  $\phi_0^2 = \mu^2/\lambda$  (Level B matching, Eq. (5.12)). With the numerical boundary condition  $\lambda(M_{\text{Pl}}) \approx 10^{-3}$  (Appendix Y):  $g(M_{\text{Pl}}) \approx 4 \times 10^{-5}$ —parametrically small.

Second, the one-loop  $\beta$ -function  $\beta_\lambda = 3\lambda^2/(16\pi^2) > 0$  has no UV fixed point in the strict scalar closure. However, the Landau pole lies at

$$\mu_{\text{LP}} = M_{\text{Pl}} \exp\left(\frac{16\pi^2}{3\lambda(M_{\text{Pl}})}\right) \approx M_{\text{Pl}} e^{5.26 \times 10^4}, \quad (8.27)$$

incomparably above the physical threshold  $m_\sigma \sim M_{\text{Pl}}$  where the broken-phase EFT already ceases to apply. Within the entire validity range of the EFT,  $g(\mu)$  remains parametrically small and no practically relevant Landau-pole obstruction arises. Above  $m_\sigma$ , the relevant degrees of freedom are microscopic condensate variables—a structurally different replacement from extrapolating perturbative Einstein gravity to arbitrarily high energies.

These structural observations do not constitute a proof of UV safety or renormalizability of the full graviton sector. Explicit graviton-loop power counting and a two-loop RG analysis of the condensate–graviton system remain open tasks (OP-UV1, OP-UV3).

**Connection to the gravitational equations.** The role of the present subsection is therefore limited but precise: it identifies the linearised effective-metric sector contained in the ordered condensate branch. The

development of the full gravitational equations, the infrared  $\phi$ -closure, and the macroscopic observational sector belongs to Section 11 and Appendix X. The Deser self-coupling bootstrap [66] provides a possible route from the linearised Fierz–Pauli sector to nonlinear Einstein equations; the ECT geometric branch is structurally compatible with this route, though the bootstrap has not been carried out within ECT.

**Discriminant with respect to GR and generic modified-gravity tensor sectors.** Three tensor pictures should be kept distinct. In GR, the metric and its TT graviton modes are fundamental. In generic modified-gravity models, extra scalar or vector polarisations often remain alongside the tensor sector. In ECT, the tensor sector is neither fundamental nor introduced as a generic extra-polarisation framework: it is an induced ordered-branch metric channel whose strong completion target is the Fierz–Pauli / GR two-TT closure. The present article places ECT squarely on the route to that target, but does not yet complete it.

**Connection to cone universality.** The tensor sector is intended to inherit the same causal cone as every other ordered-branch mode (§4.7). At the level of the induced-metric route, this is the natural structural expectation: tensor perturbations propagate on the same effective metric generated by the ordered condensate. Accordingly, the gravitational-wave speed constraint  $|c_{\text{GW}}/c - 1| < 6 \times 10^{-15}$  from GW 170817 [10] is structurally consistent with the ECT tensor programme. What is not yet proved at Level A is the fully completed tensor closure that would promote this consistency route to a finished graviton theorem. This distinguishes ECT from modified-gravity theories in which the tensor speed must often be separately adjusted.

**What the ordered-branch gauge architecture does and does not fix.** The structural  $SU(2) \times U(1)$  redundancy of the ordered branch strengthens the internal gauge architecture of ECT, but it does not by itself prove the linearised diffeomorphism redundancy of the tensor sector. The latter remains part of the open graviton-completion problem: one must still show that the induced symmetric metric perturbation closes exactly to the Fierz–Pauli / TT route and not merely to a generic symmetric tensor EFT. P5/P6 therefore helps to constrain the broader architecture, but does not in itself finish the graviton theorem.

**Observational anchors for the tensor programme.** The present tensor route should be read against three empirical anchors: multi-messenger constraints on the gravitational-wave speed, polarisation tests disfavouring large scalar/vector admixtures, and inspiral/ringdown observations consistent with dominantly GR-like tensor propagation. At the present stage ECT is best read as a framework that can already account for this near-GR tensor behaviour at consistency level, while the exact closure to pure two-TT propagation remains open.

**Programme-level predictions of the tensor architecture.** The present framework suggests four non-trivial expectations. First, if the ECT tensor closure is correct, any surviving non-GR tensor residue should be Planck-suppressed and correlated with the same LIV hierarchy that governs the cone-universality programme (§4.7), not appear as arbitrary extra sectors. Second, the same ordered branch that fixes one cone and one UV threshold should also constrain the onset scale of any tensor-sector deviations. If residual non-GR tensor effects survive in the same derivative EFT ordering as the cone-universality programme, they are expected to be suppressed by powers of the same high scale  $M_{\text{LIV}}$  (§13.8), rather than appear as unrelated low-energy tensor anomalies. Third, cosmological singularity breakdown and black-hole interior breakdown should not require a separate tensor ontology but should use the same branch-boundary logic (§14.1). Fourth, if the tensor programme is completed, the graviton sector should align with the same universal medium logic as the cone, action scale, UV threshold, and singularity boundary.

**Falsifier for the tensor-closure programme.** The strong tensor programme of ECT would fail if (i) the induced metric sector could not be closed even at quadratic level to a Fierz–Pauli-type route, (ii) unavoidable propagating scalar/vector gravitational-wave polarisations remained at observationally

relevant level, (iii) the tensor sector required a causal cone different from the one already fixed by the ordered branch, or (iv) the nonlinear macroscopic closure proved incompatible with the linear tensor sector. Any of these would reduce ECT to a partial metric-response framework, not a completed graviton closure.

**Status summary.**

Statement	Status	Comment
Graviton sector required once the ordered branch induces an effective metric	A/B	Metric sector strict; particle interpretation strengthened only after linear closure
A direct vector fluctuation $\delta n_A$ carries vector rather than tensor character	A	Spin-2 appears only after projection to the effective metric
Effective metric $G_{\text{eff}}^{AB}$ induced by condensate	A	Propagation structure of perturbations
Lorentzian signature for $\alpha > \beta$	A	Established in the effective-metric analysis of the broken phase
$h_{AB}$ : induced symmetric effective-metric perturbation	A	From $\delta n_A$ via effective metric
Fierz–Pauli-type quadratic structure	B	Linearised effective-metric reconstruction; explicit full derivation pending
Massless spin-2 interpretation of the effective-metric mode	B	Linearised EFT interpretation; exact non-perturbative status open
Full non-perturbative Fierz–Pauli spectrum	Open (OP3)	Ghost-freedom check pending
Graviton and $\sigma$ are distinct sectors of the same condensate	B	Orientation vs amplitude in the linearised broken-phase EFT
Weinberg–Witten theorem does not directly apply	B	Fundamental theory is Euclidean; Lorentz covariance is emergent
Universality of emergent light cone	A/B	Same Lorentzian structure for all low-energy modes
GW speed $c_g = c$ under the standard matching	B (matching)	Consistency check, not independent derivation
Two TT polarisations in the completed linearised graviton sector	B/C	Expected if the effective-metric sector closes exactly to Fierz–Pauli form; explicit verification pending
Deser self-coupling bootstrap as a possible nonlinear completion route	B/C	Structural compatibility only; not derived within ECT
Improved UV behaviour	Open / speculative	Requires explicit power counting; no result claimed

## 8.6 Gauge Bosons from Condensate Phase Symmetries

*Status: Level A/B (upgraded from B/C after P5). With the medium-character postulate P5, the compact-phase sector carries a structural local  $U(1)$  gauge redundancy (Section 7.2), and the associated massless gauge boson is a structural consequence of the ordered branch, not merely an admissible embedding. Full identification with the physical photon (coupling constant, QED vertex structure) remains Level B matching.*

**Structural status after P5.** With the medium-character postulate P5, the promotion of the coherent phase sector to a local  $U(1)$  description is no longer a conditional embedding step but a structural consequence of the postulate framework: P5 asserts that pointwise  $\theta(X)$  is a descriptive redundancy, which together with P2 (action symmetry) and P3 (locality) implies local  $U(1)$  gauge invariance (Section 7.2, Layer 2). The associated massless gauge boson is therefore a structural consequence of the ordered-branch gauge architecture, not merely an admissible addition. Full identification with the physical photon—including the coupling constant  $e$  and the QED matter vertex—remains a Level B matching step.

**Particle-level reading of the  $U(1)$  route.** At the level of the compact phase EFT, the ordered condensate admits the standard Abelian gauge completion. For a complex condensate

$$\Phi = \rho e^{i\theta} \quad (8.28)$$

the theory is invariant under

$$\theta \rightarrow \theta + \Lambda(X). \quad (8.29)$$

Introducing the covariant derivative

$$D_A = \partial_A - ieA_A \quad (8.30)$$

generates the gauge kinetic term

$$S \supset \frac{1}{4} \int F_{AB} F^{AB} d^4X. \quad (8.31)$$

The corresponding gauge boson is massless,

$$m_\gamma = 0, \quad (8.32)$$

due to the unbroken  $U(1)$  symmetry.

**What is strict and what is not.** What follows strictly at the EFT level is that a locally completed compact phase sector admits a massless Abelian gauge boson. What does *not* follow from first principles is the full identification of this sector with physical quantum electrodynamics. In particular, the present subsection does not derive the electric charge  $e$ , the full QED matter coupling structure, radiative corrections, or the complete Standard Model electromagnetic sector from P1–P6 alone.

**Prediction and non-prediction.** The positive output of the present construction is structural rather than phenomenological: ECT admits a massless photon-like Abelian gauge sector in the low-energy ordered branch once the compact phase symmetry is promoted locally. No additional photon mass is predicted, and no deviation from ordinary massless  $U(1)$  propagation is claimed here. Conversely, the subsection does not yet predict the quantitative electromagnetic parameters of the Standard Model.

**Dependence on earlier results.** The detailed derivation-status analysis of the Abelian gauge sector was already given in Section 7.2. The present subsection should therefore be read as the particle-level placement of that result within the classification scheme of Section 8, not as an independent second derivation.

#### Status summary.

Statement	Status	Comment
Compact phase sector admits local $U(1)$ completion	A	Structural consequence of P2+P3+P5
Massless Abelian gauge boson in the ordered branch	A/B	Unbroken $U(1)$ gauge redundancy from P5

Statement	Status	Comment
Photon-like particle interpretation	A/B	Structural identification; full QED derivation open
Electric charge $e$ derived from condensate microphysics	Open	Not completed
Full QED matter coupling structure	Open	Not derived from P1–P6
Full physical photon identification	A/B	Structural route from P2+P3+P5 established; full QED matching open

This closes the purely Abelian particle-level gauge sector. The next subsection turns to the electroweak-like embedding, where the logical status becomes more conditional because the weak-like  $O(3) \rightarrow O(2)$  transition is not yet derived from first principles.

## 8.7 Electroweak Sector and the Higgs Interpretation in ECT

*Status: three-layer electroweak programme. Level A/B for the ordered-branch structural route to the  $SU(2) \times U(1)$  gauge architecture and the weak-like chiral embedding. Level B for the matched secondary scale  $v_2$  and for the resulting Higgs/ $W^\pm/Z$  scaffold. Open for the first-principles derivation of  $v_2$ , the quantitative electroweak parameter set, custodial protection, and Yukawa hierarchies. This subsection consolidates the radial-mode analysis (Section 8.3), the electroweak-like gauge embedding (Section 7.4), and the secondary-transition scaffold (Appendix L) and the candidate Hopf-fibered locking geometry (Appendix M).*

**What is established, what is matched, and what remains open in the electroweak programme.** The electroweak sector of ECT should be read in three layers. First, the ordered branch already supports a structural  $SU(2) \times U(1)$  gauge architecture: the residual  $O(3)$  after  $O(4) \rightarrow O(3)$  provides the strict algebraic bridge  $\mathfrak{so}(3) \cong \mathfrak{su}(2)$ , and a candidate weak-like chiral route exists (Sections 7.3–7.4, 9). Second, a lower transition scale  $v_2$  can be introduced as the closure scale of a secondary ordered-branch step  $O(3) \rightarrow O(2)$ , providing a matched scaffold for the  $W^\pm$ ,  $Z$ , and Higgs-like mass pattern. Third, what remains open is the actual first-principles derivation of  $v_2 \approx 246 \text{ GeV}$ , the quantitative electroweak mass spectrum, custodial protection, and Yukawa hierarchies. ECT therefore already contains a structural electroweak route, but not yet a completed electroweak derivation.

**Why this sector is conditional rather than required.** Unlike the primary radial mode, the soft orientation sector, and the graviton, the electroweak-like sector is not forced by the existence of the primary ordered branch alone. It can arise only if the condensate admits a second effective ordering step beyond  $O(4) \rightarrow O(3)$ . For that reason, this sector belongs to the conditional/embedded part of the Section 8 classification rather than to the class of required condensate excitations.

The Higgs discussion in ECT has two complementary sides: the gauge-embedding side, where the electroweak-like EFT is introduced (Section 7.4), and the radial-mode side, where the secondary amplitude excitation is analysed as a condensate mode (Section 8.3). The present subsection brings these two viewpoints together.

**Minimal derivation chain.** The present electroweak-like construction rests on four steps: (i) the ordered branch leaves a residual  $O(3)$  structure; (ii) this gives the strict algebraic bridge  $\mathfrak{so}(3) \cong \mathfrak{su}(2)$ ; (iii) if a second transition  $O(3) \rightarrow O(2)$  is admitted, a reduced weak-like symmetry-breaking pattern becomes structurally available; (iv) only after that step can one embed a doublet EFT with a Higgs-like radial mode at the scale  $v_2$ . The first two steps are strict; the latter two are conditional.

**The Higgs boson as a second condensate radial mode.** In the Standard Model, the Higgs boson is an elementary scalar field introduced independently of the spacetime metric [55, 56]. In ECT, the role of the Higgs is played by the radial excitation  $h$  of the second condensate vacuum at scale  $v_2 \approx 246 \text{ GeV}$  (Section 8.3):

$$\phi_{\text{ew}} = v_2 + h, \quad m_h^2 = 2\lambda_2 v_2^2. \quad (8.33)$$

This is not an independent fundamental field, but the amplitude fluctuation of a second ordered phase of the same underlying  $\Phi$ -medium whose first ordered phase is associated with the Lorentzian spacetime and gravitational sector. The distinction is conceptual: the SM Higgs and the spacetime metric are unrelated structures; in ECT they would both arise from a single underlying medium. This reduced analogy should not be overstated: it provides a structural route toward a weak-like sector, not a derivation of the full electroweak Standard Model.

**Coupling pattern.** If the electroweak embedding is realised at the level of the SM gauge structure (Section 7.4), the Higgs couplings to  $W^\pm$ ,  $Z$ , and fermions follow the Standard Model pattern at leading order. This is a direct consequence of the embedding: the low-energy EFT is *designed* to reproduce the SM structure, and the Higgs coupling pattern is therefore an input, not a prediction. Accordingly, agreement with the observed tree-level Higgs coupling pattern is a consistency requirement of the embedding, not an emergent prediction of minimal ECT.

**Possible non-minimal corrections.** Beyond the minimal embedding, additional condensate-sector corrections to the Higgs-like state are not excluded. These may in principle include mixing with the primary radial mode, departures from an approximately quartic effective potential near the secondary minimum, or higher-dimension corrections to the Yukawa sector. At present none of these effects is derived quantitatively within ECT. They should therefore be treated only as logically admissible non-minimal possibilities, not as predictions of the present formulation.

Property	Standard Model	ECT
Ontological status	Elementary scalar field	Radial excitation of second condensate phase
Relation to spacetime	Independent of metric	Same underlying medium as the gravitational/spacetime sector
$v_2 = 246 \text{ GeV}$	Fundamental VEV	Matching constraint (if second transition exists)
$m_h = 125 \text{ GeV}$	Determined by $\lambda$ and $v$	Determined by $\lambda_2$ and $v_2$ (same formula)
Coupling pattern	Predicted by SM gauge structure	Reproduced by embedding (input, not prediction)
Cubic Higgs interaction near the minimum	$V'''(v) = 3m_h^2/v$	Same if $V_{\text{ew}}$ is quartic; deviations possible
Naturalness	Quadratic divergence $\sim \Lambda^2$	Same problem: $\delta m_h^2 \sim m_\sigma^2$
Radial partner	None	Primary radial mode $\sigma \sim M_{\text{Pl}}$
Mixing with primary condensate radial mode	No analogue in the minimal SM	Possible $\sigma$ - $h$ mixing

**Comparison: SM Higgs versus ECT Higgs.**

**What ECT adds and what it does not.** ECT does not derive the Higgs boson from first principles. What it adds is a *structural context*: the Higgs is reinterpreted as one of two radial modes of a single condensate, the other being the Planck-heavy primary mode that defines the UV threshold of the effective theory. This reinterpretation does not currently lead to a quantitative prediction that differs robustly from the Standard Model, but it changes the conceptual status of the hierarchy problem (Section 8.3): instead of asking why an elementary scalar is light, one asks why the condensate undergoes a second ordering step at  $v_2 \ll \phi_0$ . In the language of Section 8, this makes the Higgs-like state a *conditional particle-level interpretation* of the secondary condensate sector, not a required excitation of the primary ordered branch. Its positive content is therefore conceptual rather than derivational: if the second transition exists, then the Higgs-like scalar and the Lorentzian/gravitational sector are interpreted as belonging to different ordered phases of the same underlying medium.

The electroweak sector remains a structural embedding at Level B/C, not a completed derivation. Its full first-principles realisation within ECT requires closing the layered OP-EW programme: OP-EW-scale, OP-EW-locking, OP-EW-gauge, OP-EW-naturalness, and OP-EW-matter (Section 5.1, Appendices L and M).

**Discriminant with respect to Standard-Model and purely matched electroweak sectors.** The electroweak sector can appear in three sharply distinct ways. In the Standard Model,  $SU(2) \times U(1)$  and the Higgs scale are fundamental inputs. In the present ECT closure, the ordered-branch gauge architecture is structurally singled out, while the lower scale  $v_2$  remains matched. In a completed ECT electroweak programme, both the architecture and the secondary scale would arise from one condensate logic. The present text establishes the second level, not yet the third.

**Observational anchors for the electroweak programme.** The observed electroweak parameters serve as matched consistency targets, not derived fits:  $m_W \approx 80.4 \text{ GeV}$ ,  $m_Z \approx 91.2 \text{ GeV}$ ,  $m_H \approx 125 \text{ GeV}$ , the tree-level  $\rho$ -parameter near unity, left-handed weak charged currents, and the absence of observed right-handed weak neutrino currents. Within the present embedding, these quantities are used as consistency-level targets for the secondary closure scaffold; they would become genuine predictions only if  $v_2$  and the electroweak coupling constants were derived from the condensate dynamics.

**Programme-level predictions of the electroweak architecture.** The present ECT electroweak picture suggests four nontrivial expectations. First, if  $v_2$  is genuinely a secondary ordered-branch closure scale, then the Higgs-like scalar, the  $W/Z$  mass pattern, and the weak chirality route should not be independent structures but should appear as a clustered package from one medium. Second, the custodial-like near-degeneracy  $m_W/(m_Z \cos \theta_W) \approx 1$  should eventually be constrained by the closure geometry rather than left as a free ratio. Third, ECT prefers that the Higgs-like mode is not an unrelated fundamental scalar but a radial closure mode tied to the same medium as the weak sector. Fourth, if  $v_2$  cannot eventually be connected to condensate running or a secondary transition mechanism, the ECT electroweak programme remains structurally incomplete.

**Falsifier for the electroweak closure programme.** The electroweak programme of ECT would fail in its strong form if (i) the weak sector required a gauge architecture not reducible to the ordered-branch  $SU(2) \times U(1)$  route, (ii) the Higgs-like scalar were shown to be fundamentally unrelated to any radial secondary closure mode, (iii) the lower scale  $v_2$  proved impossible to connect even at closure level to a secondary condensate transition, or (iv) the observed weak chirality pattern required a structure incompatible with the ordered-medium route. Any of these would leave only a partial matching programme, not a structural electroweak derivation.

**Prediction and non-prediction.** The positive output of the present subsection is structural rather than precision-phenomenological: ECT admits a weak-like embedded sector with a Higgs-like radial mode if a second condensate transition is realised. What it does not yet predict is the quantitative electroweak



parameter set of the Standard Model. In particular, the values of  $g$ ,  $g'$ ,  $\lambda_2$ , and the full  $W^\pm/Z/\gamma$  spectrum remain matters of EFT matching rather than first-principles derivation.

The same incompleteness propagates directly into the neutrino sector: the mass/chirality problem discussed in Section 9 remains tied to the still-open electroweak closure problem rather than forming an independent unresolved sector. In that sense, the neutrino programme is a downstream diagnostic of the secondary-transition completion, not a detached add-on.

**Status summary.**

Statement	Status	Comment
Conditional status of the electroweak-like sector	A/B	Requires a second transition beyond the primary ordered branch
Higgs as radial excitation of second condensate phase	B/C	Conditional particle-level interpretation of the secondary condensate sector
SM coupling pattern reproduced by embedding	B/C	Input, not prediction
Possible non-minimal condensate-sector corrections to the Higgs-like state	C	Logically admissible, but not derived quantitatively
Higgs and spacetime associated with the same underlying medium	B/C	Conceptual reinterpretation, if the second transition exists
Radiative naturalness of the Higgs-like mode	Open	Same quadratic sensitivity issue as in the SM
Full EW sector derived from P1–P6	Open	Decomposes into OP-EW-scale, OP-EW-locking, OP-EW-gauge, OP-EW-naturalness, and OP-EW-matter

## 8.8 Fermions (Level B: structural route)

*Status: Level B structural reconstruction. Spinorial excitations are compatible with the ordered condensate background but are not derived from the bare bosonic action. Full development: Section 9.*

Within the classification of Section 8.1, fermions belong to category (ii): structurally embedded Standard Model fields.

The symmetry breaking  $O(4) \rightarrow O(3)$  leaves a residual continuous rotation symmetry  $SO(3)$ , whose double cover  $SU(2)$  admits spinor representations. At the representation-theoretic level, the ordered branch admits the standard Lorentzian spin-group reading in which the relevant group is  $SL(2, \mathbb{C})$ . This group-theoretic continuation is distinct from the real parametrisation  $t = w/c_*$  used for the hyperbolic field equations, and Dirac spinors can be constructed on the ordered condensate background as two Weyl components  $\Psi = (\psi_L, \psi_R)^T$ . This is a structural compatibility statement, not a derivation of spinors as collective condensate excitations.

The fermionic sector is developed in Section 9, which covers:

- spinor representations of the ordered branch (Section 9.1);
- structural reconstruction of the Dirac equation (Section 9.2);
- chirality and the selection of  $SU(2)_L$  (Section 9.3);
- Yukawa couplings and fermion masses (Section 9.6);
- ECT-specific fermion–condensate coupling (Section 9.8);

- spin-statistics structural route (Section 9.9).

A currently identified ECT-specific fermion–condensate interaction beyond the Standard Model embedding is  $\Delta\mathcal{L} = \mu_5 \bar{\Psi} \gamma^A n_A \Psi$  (with  $\mu_5 = \beta_5 m_f$ ,  $\beta_5 \sim m_f/\phi_0$ ). Its structural form is introduced in Section 9.8, while its detailed phenomenology, observational constraints, and falsification tests are developed in Section 7.

In the present chapter fermions are treated only at the level of structural compatibility and effective embedding. The detailed fermionic programme is deferred to Section 9, where spinor structure, the Dirac form, chirality, Yukawa couplings, the fermion–condensate coupling, and the spin-statistics route are discussed separately. This subsection therefore serves only as the particle-level bridge to the dedicated fermionic programme of Section 9.

## 8.9 Neutrino Sector

*Status: layered. Observation already excludes a strictly massless active-neutrino completion and forces any viable ECT completion to accommodate nonzero neutrino masses and flavour mixing (A given Ph). Within the present ordered-branch chirality and  $SU(2) \times U(1)$  route, a left-chiral active weak sector is structurally preferred (A/B). ECT constrains the type of viable neutrino completion more strongly than a generic EFT, but does not yet derive the number of generations, the flavour textures, the PMNS angles, the CP phases, the mass ordering, or the absolute neutrino masses. Those latter issues remain completion-dependent and are not derived from the minimal condensate action.*

**Structural setting and scope.** In the current formulation of ECT, the neutrino sector is not yet a closed flavour theory. The framework does not derive the number of generations, the flavour textures, the PMNS angles, the CP phases, the mass ordering, or the absolute neutrino masses. However, it constrains the type of viable neutrino completion more strongly than a generic EFT. The low-energy weak sector emerges in a geometrically one-chiral setting tied to the Euclidean spinor structure  $Spin(4) \simeq SU(2)_L \times SU(2)_R$  and the condensate-driven breaking  $O(4) \rightarrow O(3)$ . In the present preprint, the chirality discussion (Section 9.3) already establishes that one  $SU(2)$  sector remains coupled to the fermion sector while the other effectively decouples at low energies, thereby reproducing the left-chiral weak structure as a structural consequence of the condensate background.

This should be read as a structural route (Level B), not yet as a theorem. In ECT, the neutrino question is therefore not merely “how to make  $m_\nu \neq 0$ ”, but “which completion is structurally compatible with a geometrically emergent one-chiral weak sector”.

**Canonical notation.** Throughout the neutrino discussion the anisotropic kinetic structure is written in the canonical form

$$K^{AB} = \beta \delta^{AB} - \alpha n^A n^B, \quad \alpha > \beta, \quad c_*^2 = \frac{\beta}{\alpha - \beta}. \quad (8.34)$$

Any shorthand using  $\alpha - 1$  is valid only after an explicit normalisation  $\beta = 1$ . This point matters not only locally for the neutrino section but also for consistency with all related sections discussing the Lorentzian branch, the causal cone, and cosmological redshift corrections.

**What is ECT-specific and what is borrowed.** Type-I seesaw algebra, the Weinberg operator, the PMNS/MSW formalism, leptogenesis, and neutrinoless double-beta decay are standard neutrino-model-building ingredients. They are not derived from the current ECT postulates P1–P6. The ECT-specific content lies elsewhere: first, in the structural route to a one-chiral weak sector; second, in the natural interpretation of opposite-chirality neutrino states as hidden or sterile remnants of the decoupled branch; third, in the possibility of an ECT-motivated intermediate anchor scale associated with the condensate hierarchy; fourth, in the tiny preferred-direction corrections that leave standard oscillation phenomenology essentially intact. This separation should be kept explicit to avoid presenting borrowed machinery as an ECT derivation.

**Three logically distinct mass-generation routes.** At the present stage, three neutrino-completion routes remain open.

(i) *Pure Dirac route.* A right-handed singlet is added with

$$\mathcal{L}_D = -\bar{L}Y_V\tilde{H}N_R + \text{h.c.}, \quad m_V = y_V v_2. \quad (8.35)$$

For a representative atmospheric-scale mass  $m_V \sim 0.05$  eV and  $v_2 = 246$  GeV, this requires  $y_V \sim 2 \times 10^{-13}$ , approximately seven orders of magnitude below the electron Yukawa coupling. The route is algebraically consistent but structurally unattractive in the absence of a derivation of flavour hierarchies. Status: Level C.

(ii) *Pure Planck-suppressed Majorana/Weinberg route.* The dimension-5 Weinberg operator with Planck-like suppression,

$$m_V \sim \frac{v_2^2}{\Lambda}, \quad (8.36)$$

gives only  $m_V \sim 2.5 \times 10^{-5}$  eV for  $\Lambda \sim 2.4 \times 10^{18}$  GeV and  $\mathcal{O}(1)$  Wilson coefficients—approximately three orders of magnitude below the atmospheric scale  $\sqrt{\Delta m_{31}^2} \approx 0.05$  eV. Therefore ECT should not stop at the statement that a Majorana operator is allowed; the theory is naturally pushed toward a nontrivial intermediate scale or another enhancement mechanism. Status: Level B/C as a quantitative inadequacy statement.

(iii) *Embedded type-I seesaw route.* If right-handed neutrinos are admitted as additional embedded fields (Level C), a type-I seesaw mechanism can be placed on top of the ECT low-energy sector:

$$\mathcal{L}_V = -\bar{L}Y_V\tilde{H}N_R - \frac{1}{2}N_R^T C M_R N_R + \text{h.c.} \quad (8.37)$$

In the basis  $(\nu_L, N_R^c)$  the mass matrix reads

$$\mathcal{M}_V = \begin{pmatrix} 0 & m_D \\ m_D^T & M_R \end{pmatrix}, \quad m_D = Y_V v_2. \quad (8.38)$$

For  $M_R \gg m_D$ , the standard seesaw reduction gives

$$M_V^{\text{light}} \simeq -m_D M_R^{-1} m_D^T, \quad M_V^{\text{heavy}} \simeq M_R, \quad \theta_{\text{as}} \simeq m_D M_R^{-1}. \quad (8.39)$$

This algebra is standard and imported. Its relevance to ECT comes from the fact that the hidden/right branch already makes a sterile interpretation of  $N_R$  structurally natural. Thus the embedded seesaw route is the most natural completion, but still only Level C.

**Minimum number of heavy sterile states.** A realistic oscillation completion requires at least two heavy sterile states in order to generate two nonzero light-neutrino mass splittings. A generic full-rank  $3 \times 3$  completion naturally uses three heavy sterile singlets, matching the three active flavours. This is a standard neutrino-physics constraint, not an ECT-specific result.

**ECT-motivated intermediate anchor scale.** Although the neutrino masses themselves are not predicted, ECT does contain two distinguished condensate scales, the primary scalar scale  $\phi_0 \sim \bar{M}_{\text{Pl}}$  and the electroweak-like scale  $v_2$ . Their geometric mean defines a natural intermediate scale:

$$M_R^{\text{geom}} \equiv \sqrt{\phi_0 v_2} \approx \sqrt{2.435 \times 10^{18} \times 246} \text{ GeV} \approx 2.4 \times 10^{10} \text{ GeV}. \quad (8.40)$$

If this ECT-motivated anchor is used in the seesaw formula, one finds

$$m_V \sim \frac{y_V^2 v_2^2}{M_R^{\text{geom}}}. \quad (8.41)$$

The following table illustrates how the light-neutrino mass depends on the Dirac Yukawa coupling at this fixed scale:

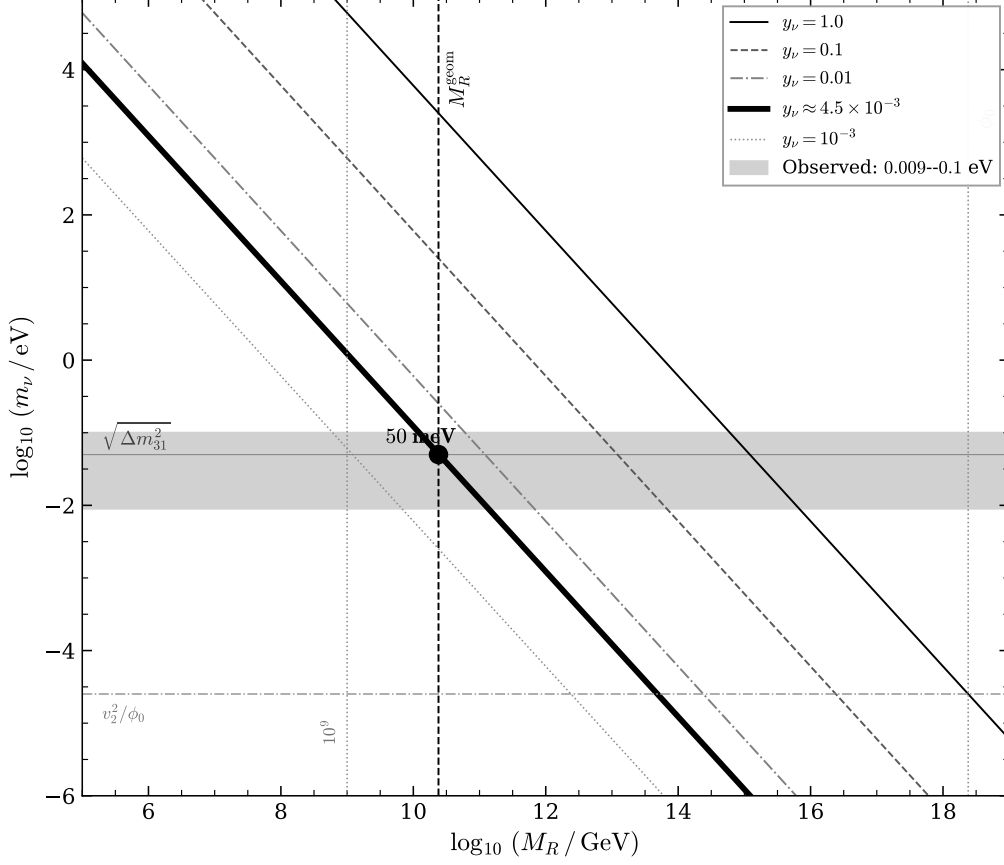


**Figure 7:** Seesaw landscape at fixed ECT scales. Each curve shows the light-neutrino mass  $m_\nu = y_\nu^2 v_2^2 / M_R$  for a given Dirac Yukawa coupling. The bold curve corresponds to  $y_\nu \approx 4.5 \times 10^{-3}$ , which reproduces the atmospheric scale at the ECT-motivated geometric-mean anchor  $M_R^{\text{geom}} \approx 2.4 \times 10^{10}$  GeV. Vertical dotted lines mark  $M_R^{\text{geom}}$ , the thermal leptogenesis benchmark ( $\sim 10^9$  GeV), and the Planck-like condensate scale  $\phi_0$ . The horizontal dashed line indicates the Weinberg floor  $m_\nu^{\text{geom}} = v_2^2 / \phi_0 \approx 2.5 \times 10^{-5}$  eV.

$y_\nu$	$m_\nu$	Comment
1	$\sim 2.5$ keV	far too heavy
0.1	$\sim 25$ eV	cosmologically excluded
0.01	$\sim 0.25$ eV	near cosmological upper bound
$4.5 \times 10^{-3}$	$\sim 0.05$ eV	atmospheric scale
$1.9 \times 10^{-3}$	$\sim 0.009$ eV	solar scale

For a representative atmospheric-scale mass  $m_\nu \sim 0.05$  eV, one requires

$$y_\nu \approx 4.5 \times 10^{-3}, \quad (8.42)$$

giving  $m_D = y_\nu v_2 \approx 1.1$  GeV and  $\theta_{\text{as}} \sim m_D / M_R^{\text{geom}} \sim 4.5 \times 10^{-11}$ . The noteworthy point is that  $y_\nu \sim 4.5 \times 10^{-3}$  is a completely ordinary Standard-Model-sized Yukawa coupling—between  $y_{\text{charm}} \approx 5.2 \times 10^{-3}$  and  $y_\tau \approx 7.2 \times 10^{-3}$ —rather than an extreme suppression. Thus the geometric-mean anchor provides a nontrivial scale-consistency observation: once this ECT-motivated intermediate scale is adopted, the atmospheric neutrino scale is recovered without absurdly small Dirac Yukawas. This should be kept at Level C. It is a strong consistency check, not a derivation from the ECT postulates.

**Second condensate-hierarchy scale observation.** The Weinberg-operator scale

$$m_\nu^{\text{geom}} \equiv \frac{v_2^2}{\phi_0} \approx 2.5 \times 10^{-5} \text{ eV} \quad (8.43)$$

lies approximately three orders of magnitude below the atmospheric oscillation scale and reproduces the observed range only if the Wilson coefficients are moderately enhanced,  $c_{ij} \sim \mathcal{O}(10^3)$ . Like  $M_R^{\text{geom}}$ , this is a scale observation at Level B/C, not a derivation. The two are not independent: they are the two simplest dimensionally consistent combinations from the same pair of fundamental ECT parameters  $(\phi_0, v_2)$ .

**Three-scale issue.** Three different scales appear in the neutrino discussion and should not be conflated: a generic seesaw scale  $M_R \sim 10^{13} - 10^{15} \text{ GeV}$  if one assumes  $y_\nu \sim 0.1 - 1$ ; a thermal-leptogenesis benchmark around  $10^9 \text{ GeV}$ ; and the ECT-motivated geometric-mean anchor  $M_R^{\text{geom}} \sim 2.4 \times 10^{10} \text{ GeV}$ . The neutrino sector depends on the pair  $(M_R, y_\nu)$ , not on  $M_R$  alone. The apparent tension is resolved once one allows  $y_\nu$  to be ordinary but not order unity:  $M_R^{\text{geom}}$  becomes compatible with atmospheric-scale masses for  $y_\nu \sim 4.5 \times 10^{-3}$ .

**Heavy sterile invisibility and why light sterile states are not favoured.** For the geometric-mean anchor route,  $\theta_{\text{as}} \sim 10^{-11}$ , so the heavy sterile sector is completely invisible in oscillation experiments. This naturally explains why ECT does not favour an observable light (3+1) oscillation sector. In contrast, a light-eV sterile state generically requires large active-sterile mixing in simple one-scale constructions ( $\theta_{\text{as}} \sim \sqrt{m_\nu/M_R} \sim 0.22$  for  $M_R \sim 1 \text{ eV}$ ), which is both structurally disfavoured in ECT and phenomenologically pressured by the lack of convincing experimental support for a minimal (3+1) oscillation sector [67, 68]. The natural ECT picture is therefore a hidden heavy sterile sector, not a visible light sterile one.

**Standard oscillation phenomenology remains intact.** At leading order the low-energy oscillation Hamiltonian remains the standard one:

$$H_{\text{osc}} = \frac{1}{2E} U_{\text{PMNS}} \text{diag}(m_1^2, m_2^2, m_3^2) U_{\text{PMNS}}^\dagger + V_{\text{MSW}}, \quad U_{\text{PMNS}} = U_e^\dagger U_\nu. \quad (8.44)$$

ECT changes the origin of the neutrino mass matrix, not the already successful low-energy oscillation kinematics. Once the charged-lepton and neutrino sectors arise from different effective structures, nontrivial PMNS mixing is natural because their mass matrices need not be diagonalized in the same basis. What ECT still does not derive is the flavour texture itself. The present framework therefore preserves standard PMNS/MSW phenomenology at leading order while leaving flavour closure open.

**Tiny preferred-direction corrections.** A minimal preferred-direction deformation of the neutrino sector,

$$\delta \mathcal{L}_\nu \sim \beta_\nu \bar{\nu} \gamma^\mu n_\mu \nu, \quad \beta_\nu \sim \frac{m_\nu}{M_G}, \quad (8.45)$$

gives  $\beta_\nu \sim 2 \times 10^{-29}$  for  $m_\nu \sim 0.05 \text{ eV}$  and  $M_G \sim 2.4 \times 10^{18} \text{ GeV}$ . Hence  $\delta H_{\text{ECT}} \sim \beta_\nu E$ . At  $E \sim 1 \text{ GeV}$ ,  $\delta H_{\text{ECT}} \sim 2 \times 10^{-20} \text{ eV}$ , whereas  $\Delta m_{\text{atm}}^2/(2E) \sim 10^{-12} \text{ eV}$ . Thus minimal ECT preferred-direction corrections are negligible by approximately eight orders of magnitude throughout experimentally relevant energies. A formal crossover of  $\delta H_{\text{ECT}}$  and  $\Delta m^2/(2E)$  occurs only at multi-TeV energies where both scales are already extremely small and do not imply observability. Therefore ECT predicts that standard three-flavour oscillation phenomenology remains intact at leading order. This is a genuine Level B statement.

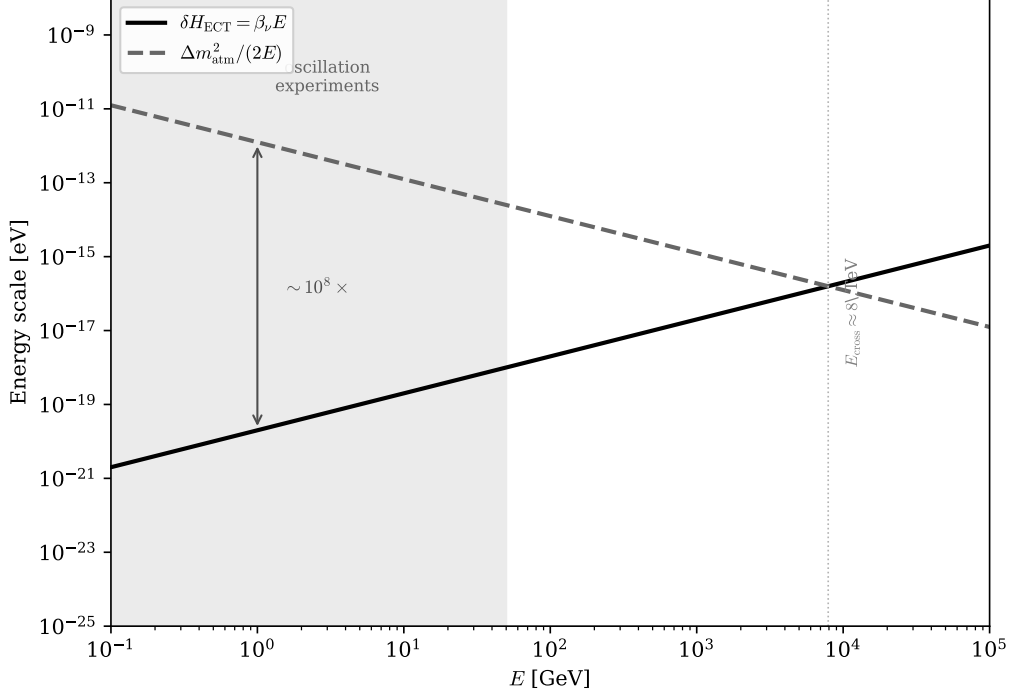


**Figure 8:** Standard oscillation scale  $\Delta m_{\text{atm}}^2/(2E)$  (dashed) vs. minimal ECT preferred-direction correction  $\delta H_{\text{ECT}} = \beta_\nu E$  (solid), with  $\beta_\nu \sim 2 \times 10^{-29}$ . The shaded band marks the experimentally relevant oscillation energy range. The formal crossover near  $E_{\text{cross}} \approx 8$  TeV lies far outside any observable regime. Throughout accessible energies the ECT correction is suppressed by approximately eight orders of magnitude.

**CPT-odd / Lorentz-odd viewpoint.** As established in Section 9.4 through systematic discrete-symmetry classification, the preferred-direction operator  $\mathcal{L}_5$  is precisely a CPT-odd phenomenological branch operator (C-odd, P-even, T-even, CP-odd, CPT-odd). ECT therefore predicts that any observable CPT-odd oscillation effects carried by this channel should be extraordinarily small. However, a precise mapping between this simplified ECT deformation and standard fitted CPT/Lorentz-violation parameters has not yet been carried out. The robust statement is therefore the Hamiltonian-level suppression above, not a model-independent absolute bound on  $\delta(\Delta m^2)$ . A dedicated translation into standard neutrino Lorentz/CPT-violation formalisms remains future work.

**Connection to leptogenesis.** A heavy sterile sector can simultaneously support seesaw masses and leptogenesis. This is conceptually attractive in ECT because both the hidden neutrino sector and the baryon-asymmetry route can then be tied to the same decoupled branch. In the baryogenesis discussion (Section 16.3), a right-handed neutrino scale  $M_R \sim 10^9$  GeV is used as an illustrative benchmark for the resonant leptogenesis estimate  $\eta_B \sim 9 \times 10^{-10}$ . The geometric-mean anchor  $M_R^{\text{geom}} \approx 2.4 \times 10^{10}$  GeV lies above the standard thermal-leptogenesis benchmark scale ( $\gtrsim 10^9$  GeV) and is therefore scale-compatible with standard leptogenesis logic [69]. However, scale compatibility is not the same as a full leptogenesis derivation. A viable implementation still requires a production mechanism for the heavy sterile states, adequate post-transition or reheating temperature if a thermal route is used ( $T_{\text{RH}} \gtrsim M_R$ ), CP-violating phases, and a washout analysis. The current preprint already classifies baryogenesis at Level B with an explicit leptogenesis assumption, and the neutrino section should remain consistent with that status.

**Cosmological neutrino-mass bounds.** If ECT allows an evolving  $G_{\text{eff}}(z)$ , then cosmological bounds on  $\Sigma m_\nu$  obtained within strict  $\Lambda$ CDM are not directly portable. The expected qualitative effect is a partial loosening of the bound, because the relation between neutrino free-streaming, growth suppression, and background parameters becomes model-dependent. A quantitative ECT-specific neutrino-mass constraint

requires a dedicated Boltzmann/MCMC analysis and should be listed as an open phenomenological task rather than promoted to a result.

**Relation to the dark sector.** In the preferred heavy-sterile branch, sterile neutrinos belong to the seesaw/leptogenesis sector rather than to the dark sector. Any dark-sector role of ultralight condensate excitations is discussed separately in Section 8.10 and remains open.

**Comparison with competing frameworks.** In the minimal Standard Model there is no neutrino mass mechanism at all. In a pure Dirac extension, neutrino masses are allowed but require an exceptionally tiny Yukawa coupling. In generic type-I seesaw, small masses are explained efficiently, but the heavy sterile singlets are added ad hoc and their sterility has no deeper structural origin. In left-right symmetric models the right-handed sector is motivated by an explicit gauge extension  $SU(2)_R$ , but that extension is itself postulated. ECT differs in that the one-chiral weak sector is tied to the Euclidean spinor structure and condensate symmetry breaking, so that the active left-handed branch and the hidden or sterile opposite-chirality branch acquire a common geometric interpretation. ECT does not yet derive flavour textures, but it constrains the type of viable neutrino completion more strongly than a generic EFT.

**Table 33:** Comparison of neutrino frameworks.

Framework	Mass origin	Chirality origin	Sterile origin	$0\nu\beta\beta$	Lepto-genesis	Flavour closure
SM	—	postulated	—	—	—	N/A
Dirac ext.	$y_\nu \nu$	postulated	added	no	no	no
Type-I seesaw	seesaw	postulated	added (ad hoc)	yes	yes	no
Left–right sym.	seesaw	gauge $SU(2)_R$	gauge	yes	yes	partial
ECT	seesaw	geometric $O(4) \rightarrow O(3)$	geometric (decoupled)	conditional	scale-compatible	open

\*conditional = only on the preferred Majorana/seesaw branch; scale-compatible = not yet a full derivation.

#### ECT-unique neutrino features:

1. Chirality: geometric  $O(4) \rightarrow O(3)$  route (B).
2. Seesaw scale:  $M_R^{\text{geom}} = \sqrt{\phi_0 v_2} \approx 2.4 \times 10^{10} \text{ GeV}$  (C).
3. Natural Yukawa:  $y_\nu \approx 4.5 \times 10^{-3}$  at  $M_R^{\text{geom}}$  (C).
4. Sterile invisible:  $\theta_{\text{as}} \sim 10^{-11}$  (C).
5. PMNS intact: ECT correction  $\sim 10^{-8}$  of standard (B).
6. Heavy sterile neutrinos belong to the seesaw/leptogenesis sector, not to the minimal neutrino-oscillation sector.

**Neutrinoless double-beta decay as the central discriminator.** If the preferred Majorana/seesaw branch is realized, neutrinoless double-beta decay becomes the central experimental discriminator. The effective mass

$$m_{\beta\beta} = \left| \sum_i U_{ei}^2 m_i \right| \quad (8.46)$$

is generically nonzero, although strongly texture-, ordering-, and phase-dependent. Because the present ECT framework does not yet derive flavour textures, it cannot predict the exact value of  $m_{\beta\beta}$ . What it can say is structural: the Dirac branch predicts no neutrinoless double-beta decay, whereas the preferred

Majorana branch makes it a central test. A future positive signal would strongly support the preferred ECT branch; a deep null result throughout the full normal-ordering discovery region would increasingly push ECT either toward the Dirac branch or toward symmetry-protected suppression of lepton-number violation.

**Possible future routes.** Two speculative but conceptually interesting future directions deserve brief mention. First, leptonic CP violation may conceivably be related to condensate orientation if PMNS phases are ultimately tied to the same geometric structure that distinguishes the weak chiral branch. Second, Majorana lepton-number violation may conceivably arise not as an ad hoc operator insertion but as a low-energy consequence of geometric decoupling of the opposite branch. At present both ideas remain open and should be framed only as future directions, not as results.

**What would be needed for full Level A.** To elevate the neutrino sector beyond speculative embedding, ECT would need to:

- (i) derive whether right-handed neutrinos are required at all;
- (ii) derive whether neutrinos are Dirac or Majorana in the ordered branch;
- (iii) derive the origin and scale of the Majorana mass  $M_R$ , if present;
- (iv) derive the neutrino Yukawa couplings  $y_V$ ;
- (v) derive the observed neutrino mass splittings and mixing pattern.

None of these steps has yet been completed.

**Table 34:** Status map for the ECT neutrino programme.

Claim	Status	Comment
Exactly massless active-neutrino completion	Excluded	Incompatible with oscillation data
Observed neutrino masses require some completion	A given Ph	Phenomenological requirement, not internal derivation
One chiral branch structurally selected by the ordered background	A/B	Geometric chirality route from $\text{Spin}(4) \simeq SU(2)_L \times SU(2)_R \rightarrow \text{Spin}(3)$ ; not yet a theorem of full flavour closure
The selected branch is identified with the active weak sector	B	Weak-sector matching of the geometrically preferred chirality
Pure Dirac branch possible but structurally unattractive	C	Requires $y_V \sim 10^{-13}$
Minimal Planck-suppressed dimension-5 neutrino mass estimate undershoots the oscillation scale by $\sim 10^3$	B	Direct consistency check using $\nu_2$ and $\phi_0$ ; no imported seesaw required
Embedded seesaw as structurally preferred completion	C	Imported mechanism; $N_R$ naturally sterile in ECT
$M_R^{\text{geom}} = \sqrt{\phi_0 \nu_2}$ as ECT-motivated scale anchor	C	Scale-consistency observation; not a prediction from P1–P6
$y_V \approx 4.5 \times 10^{-3}$ reproduces atmospheric scale at $M_R^{\text{geom}}$	C	Natural SM-sized Yukawa; nontrivial consistency check

*Continued on next page*



Table 34 continued

Claim	Status	Comment
Heavy sterile sector effectively invisible at the geometric-mean anchor	C	$\theta_{as} \sim 10^{-11}$ ; depends on imported seesaw and $M_R^{\text{geom}}$ (both Level C)
Standard PMNS/MSW oscillation phenomenology intact at leading order	B	ECT correction $\sim 10^{-8}$ of standard scale at 1 GeV
$0\nu\beta\beta$ as central discriminant of preferred branch	C	Exact $m_{\beta\beta}$ not predicted; flavour texture open
Leptogenesis scale-compatible with $M_R^{\text{geom}}$	C	Scale above Davidson–Ibarra bound; full implementation requires reheating, CP phases, washout
Cosmological $\sum m_\nu$ bound model-dependent under $G_{\text{eff}}(z)$	Open	Quantitative bound requires Boltzmann/MCMC analysis
Full flavour closure (generations, textures, PMNS, ordering)	Open	Systematised architecturally in §9.7; quantitative derivation Open under OP–Yukawa/OP–generations

This closes the neutrino subsection at the level currently justified by ECT: a structural route to a one-chiral active weak sector, a quantitative assessment of three mass-generation routes with scale-consistency observations, a set of tiny preferred-direction corrections that leave standard oscillation phenomenology intact, and several still-open completion routes for the full flavour programme. The next subsection turns away from imported Standard-Model extensions and returns to sectors that are more directly tied to the topology of the ordered condensate itself.

## 8.10 Predicted New States and Topological Sectors

*Status: layered. The topological classification of the vacuum manifold is Level A (homotopy of  $S^3$ ). The existence of specific condensate excitations and their phenomenological properties are Level B/C. The topological mass ansatz cited in the derivation chain (D7) is a phenomenological estimate, not a first-principles derivation. The topological classification is therefore strongest in its qualitative sector statements (which sectors are allowed or forbidden), whereas quantitative mass estimates belong to phenomenological closure and are directly falsifiable independently of the underlying homotopy classification. This distinction is important for falsifiability: topology fixes which sectors are allowed or forbidden, whereas any quantitative mass ansatz for those sectors belongs to phenomenological closure and can be tested independently.*

**Why this section is unusually strong.** Unlike several embedded sectors discussed earlier in the chapter, the core statements of the present subsection do not begin from a borrowed Standard-Model structure. They follow directly from the topology of the primary vacuum manifold  $\mathcal{M}_1 \simeq S^3$  and therefore yield genuine Level A predictions and anti-predictions: which defect classes are topologically forbidden and which topological sectors are structurally admitted. What topology does *not* fix is equally important: it does not determine stability, size, production rates, or masses of localised states.

ECT admits three qualitatively distinct classes of states beyond the observed Standard Model spectrum: smooth condensate excitations, topologically classified sectors of the ordered vacuum, and (conditionally) defect configurations from a possible second transition. This subsection classifies each class and specifies its derivation status.

The spectrum discussed here combines three strands developed earlier in the chapter: the smooth radial-mode sector (Section 8.3), the electroweak-like conditional sector (Section 8.7), and the topological

classification of vacuum manifolds (Appendix AA and Section 34).

**Minimal derivation chain.** The logic of the present subsection is: (i) the primary ordered branch has vacuum manifold  $\mathcal{M}_1 = O(4)/O(3) \simeq S^3$ ; (ii) the homotopy groups of  $S^3$  determine which topological defect classes are allowed or forbidden; (iii) this yields strict anti-predictions for walls, strings, and monopoles from the primary transition, together with a nontrivial texture/skyrmion sector labelled by  $\pi_3(S^3) = \mathbb{Z}$ ; (iv) only after this topological classification does one ask the dynamical questions of stability, localisation, and mass. The first three steps are Level A; the fourth is not.

**Class 1: smooth condensate excitations.** (a) *Primary radial mode  $\sigma$ .* The amplitude fluctuation of the ordered condensate, with  $m_\sigma \sim \sqrt{2\lambda} \phi_0 \sim \bar{M}_{\text{Pl}}$  (Section 8.3). Its presence is a Level A consequence of treating the ordered branch as a condensate with amplitude as well as orientation fluctuations. It is Planck-heavy, integrates out at  $E \ll m_\sigma$ , and defines the physical UV threshold of the broken-phase EFT.

(b) *Surviving soft scalar  $\chi$ .* In the scalar-only ECT basis, the integrability constraint  $\partial_A Q_B - \partial_B Q_A = 0$  reduces the naive three-component Goldstone sector to a single longitudinal scalar mode  $\chi$  (Section 4.3, Appendix I). Its mass, couplings, and stability are not determined at the present stage (Level B). Whether  $\chi$  plays a cosmological role (e.g. as a dark-sector candidate) remains open (Section 18.1).

**Class 2: topological sectors from the primary SSB.** The vacuum manifold of the primary ordering transition is  $\mathcal{M}_1 = O(4)/O(3) \simeq S^3$ . Its homotopy groups determine which topological defects are structurally permitted and which are forbidden [7] (Level A):

Homotopy group	Value	Consequence
$\pi_0(S^3)$	0	No stable domain walls
$\pi_1(S^3)$	0	No stable cosmic strings
$\pi_2(S^3)$	0	No stable magnetic monopoles
$\pi_3(S^3)$	$\mathbb{Z}$	Texture/skyrmion-like sectors

*Anti-predictions (Level A).* The vanishing of  $\pi_0$ ,  $\pi_1$ , and  $\pi_2$  means that EFT *predicts the absence* of topologically stable domain walls, cosmic strings, and magnetic monopoles from the primary condensate transition. This is a structural consequence of the topology of  $S^3$  and does not require additional suppression mechanisms or cosmological dilution. The cosmological implications of this result—in particular the absence of the standard relic catastrophe—are developed in Section 14.5.

*Texture/skyrmion sector (Level A for existence of sectors, Level B/C for dynamics).* The non-trivial homotopy class  $\pi_3(S^3) = \mathbb{Z}$  guarantees the existence of topologically nontrivial field configurations classified by an integer topological charge  $Q \in \mathbb{Z}$ . These are texture-type or skyrmion-like configurations: spatially extended field configurations in which the ordered condensate wraps the vacuum manifold  $S^3$  a nontrivial number of times.

The existence of nontrivial homotopy classes does not by itself imply the existence of stable finite-size particle-like solitons. Whether the corresponding configurations are dynamically stabilised against collapse or unwinding depends on the nonlinear terms of the effective action, possible higher-derivative contributions, gauge effects, or other UV-completion data. Accordingly, topology guarantees the sector labels, but not yet the existence of stable isolated particles (Level B/C; Section 34).

**Sector existence versus particle existence.** The statement  $\pi_3(S^3) = \mathbb{Z}$  guarantees the existence of topologically distinct sectors of field configuration space. It does *not* yet guarantee the existence of stable, finite-size, particle-like solitons. That stronger claim requires a dynamical analysis of the condensate energy functional and, in particular, a mechanism preventing shrinkage or unwinding. This distinction is the central reason why the topological classification is Level A while the particle interpretation remains Level B/C or open.

**Status of the topological mass ansatz.** The derivation chain (D7) and the falsification table (Table 74, entry F6) cite a phenomenological estimate

$$m_n \sim n \times 1.6 \text{ GeV}/c^2 \quad (8.47)$$

for the mass of topological sectors with charge  $Q = n$ . The derivation chain (D7) and falsification table (F6) currently refer to this phenomenological ansatz as an “instanton” spectrum; in the present section the more neutral term “topological sector” is preferred in order to avoid confusion with Yang–Mills instantons.

This estimate should be understood as follows:

- the integer label  $n$  follows from the additive topological structure  $\pi_3(S^3) = \mathbb{Z}$  (Level A for the existence of sectors with charge  $Q = n$ );
- any mass relation  $m_n = f(n)$  is dynamical rather than purely topological; a linear ansatz  $m_n \propto n$  is therefore at most a phenomenological assumption, not a Level A consequence (Level C);
- the overall mass scale  $m_1 \sim 1.6 \text{ GeV}$  is a phenomenological estimate obtained from dimensional analysis involving the condensate stiffness and core scale; it is *not* a first-principles ECT derivation (Level C);
- whether such states are dynamically stable, whether they are produced in the early universe, and whether they contribute to observable hadronic or dark-sector physics are open questions.

No explicit profile solution or rigorous energy bound is presently available in the ECT framework for these sectors. A first-principles derivation of the topological mass spectrum from the ECT action would require solving the full nonlinear field equations for the skyrmion/texture profile on the ordered background. This belongs to the open programme of the theory. Accordingly, the linear spectrum  $m_n \propto n$  should be treated as a provisional phenomenological closure only. Its falsification would not refute the topological sector itself, but only the specific dynamical ansatz used to estimate its masses.

**Class 3: defect configurations from a possible second transition (conditional).** If the second condensate transition  $O(3) \rightarrow O(2)$  is realised (Appendix L), the secondary vacuum manifold is

$$\mathcal{M}_2 = O(3)/O(2) \simeq S^2. \quad (8.48)$$

Its homotopy groups are:

Homotopy group	Value	Consequence
$\pi_0(S^2)$	0	No stable domain walls
$\pi_1(S^2)$	0	No stable cosmic strings
$\pi_2(S^2)$	$\mathbb{Z}$	Possible monopole-like defects

Thus if the second transition exists, ECT would admit a sector of  $\pi_2(S^2) = \mathbb{Z}$  topological configurations. Their interpretation as global hedgehogs or monopole-like states depends on whether the secondary symmetry is global or gauged and on the details of the corresponding EFT completion. For a global secondary symmetry this would correspond to hedgehog-type (global-monopole) configurations; in a gauged realisation one may obtain monopole-like configurations, but their detailed status depends on the full gauge embedding and cannot be inferred from homotopy alone. This is conditional on OP-EW and is Level B/C (Appendix L).

**New states beyond the observed Standard Model spectrum.** Summarising the three classes above, the genuinely new condensate states admitted by ECT, beyond the observed SM spectrum, are:

- (i) a Planck-heavy primary radial mode  $\sigma$  (Level A/B);
- (ii) a surviving soft scalar  $\chi$  from the constrained orientation sector (Level B; role open);
- (iii) a topologically nontrivial texture/skymion sector labelled by  $\pi_3(S^3) = \mathbb{Z}$  (existence Level A; dynamics Level B/C);
- (iv) (conditional) secondary monopole-like defects from  $\pi_2(S^2) = \mathbb{Z}$  if the second transition exists (Level B/C).

Items (i)–(iii) are structural consequences of the primary ordered branch and do not depend on the second transition. Item (iv) is conditional on OP-EW.

The Higgs-like secondary radial mode  $h$  discussed in Section 8.7 is not a new state beyond the observed SM spectrum; rather, it is an ECT reinterpretation of the observed Higgs boson, conditional on the second transition being realised.

**Relation to the dark sector.** The main astrophysical successes of ECT already follow from the macroscopic  $\phi$ -sector without introducing particle dark matter. Any dark-sector role of the topological or collective states discussed here would therefore be supplementary rather than required. At present no relic-abundance calculation, stability theorem, or production mechanism has been established for these states. Their possible cosmological role remains open and should not be used as an auxiliary patch for phenomena already explained by the  $\phi$ -closure.

**Observational signatures and falsifiability.** Two qualitatively different falsification handles must be distinguished: a structural topological one and a phenomenological mass-spectrum one. Two entries in the falsification table (Table 74) are directly connected to the predicted states:

- **F6:** if the topological mass ansatz  $m_n \sim n \times 1.6 \text{ GeV}$  is taken at face value, collider searches for resonances at 1.6, 3.2, 4.8 GeV would either confirm or exclude this phenomenological model. Non-observation would disfavour the specific mass estimate, not the existence of topological sectors themselves. In other words, F6 tests a specific phenomenological realisation of the topological sector, not the topological sector as such.
- **Absence of primary-SSB relics:** if topologically stable domain walls, cosmic strings, or monopoles were unambiguously traced to the primary  $O(4) \rightarrow O(3)$  transition, this would contradict the homotopy classification of the primary vacuum manifold and hence the corresponding ECT vacuum structure.

**Prediction and non-prediction.** The strongest predictions of the present subsection are topological: ECT predicts the absence of stable domain walls, strings, and monopoles from the primary  $O(4) \rightarrow O(3)$  transition, and it predicts the existence of a nontrivial  $\pi_3(S^3)$  topological sector. What it does not yet predict are the masses, abundances, production rates, or observational signatures of localised texture/skymion-like objects. These require additional dynamics beyond homotopy alone.

**Status summary.**

Statement	Status	Comment
<i>Smooth condensate excitations</i>		
Primary radial mode $\sigma$ , $m \sim M_{\text{Pl}}$	A/B	Amplitude fluctuation of the ordered branch
Surviving soft scalar $\chi$	B	Integrability-constrained; role open
<i>Topological sectors from primary SSB</i>		

Statement	Status	Comment
$\pi_0 = \pi_1 = \pi_2 = 0$ : no stable walls, strings, or monopoles	A	Direct anti-prediction from the topology of $S^3$
$\pi_3(S^3) = \mathbb{Z}$ : texture/skyrmion sectors exist	A	Topological classification
Topological classification $\neq$ stable particle prediction	A/B	Homotopy fixes sectors; dynamics fixes localised states
Dynamical stability of localised texture/skyrmion states	Open	Requires nonlinear condensate energy functional and profile solutions
Integer topological charge $Q = n$ labels primary texture sectors	A	Follows from $\pi_3(S^3) = \mathbb{Z}$
Phenomenological mass ansatz for topological sectors	C	Not derived from topology alone
Mass scale $m_1 \sim 1.6\text{GeV}$	C	Phenomenological estimate; not first-principles
<i>Conditional: second transition</i>		
$\pi_2(S^2) = \mathbb{Z}$ : monopole-like defects	B/C	If $O(3) \rightarrow O(2)$ exists; nature depends on local vs global realisation
<i>Connection to dark sector</i>		
Galactic mass discrepancy without particle DM	B	$\phi$ -sector closure
Topological states as possible DM candidates	C	Role not established
<i>Reinterpretation of observed states</i>		
Higgs-like secondary radial mode $h$	B/C	Reinterpretation of the observed Higgs, conditional on OP-EW

## 8.11 Summary of the particle and excitation spectrum

*Status: synthetic chapter summary. Section 8 does not derive the full Standard Model particle spectrum from the minimal scalar condensate action. Its strongest outputs are instead: (i) the identification of the required condensate excitation sectors of the broken branch, (ii) the structural embedding of selected Standard-Model-like sectors at the EFT level, and (iii) genuine topological predictions and anti-predictions tied to the vacuum manifold. The purpose of the present subsection is to collect those results in a single disciplined map.*

**What Section 8 has established.** The primary ordered branch of ECT necessarily contains three classes of particle-like content. First, it contains required condensate excitations: the primary radial mode, the reduced soft orientation sector, and the linearised effective-metric graviton sector. Second, it admits structurally embedded low-energy fields that do not follow from P1–P6 alone but can be consistently placed on the ordered background, including the Abelian gauge boson, the weak-like/Higgs-like sector, and the fermionic and neutrino embeddings. Third, it supports nontrivial topological sectors determined by the vacuum-manifold topology, together with strict anti-predictions for defect classes that are topologically forbidden.

### (i) Required condensate excitations.

- **Graviton:** a linearised tensorial sector of the effective metric induced by condensate orientation fluctuations; massless spin-2 interpretation at the linearised effective level, with full non-perturbative

closure still open (Section 8.5).

- **Soft orientation mode  $\chi$ :** the surviving longitudinal soft mode of the constrained orientation sector in the scalar-only broken phase (Section 8.2).
- **Primary radial mode  $\sigma$ :** the heavy amplitude fluctuation of  $|Q_A|$ , with  $m_\sigma \sim \phi_0 \sim \bar{M}_{\text{Pl}}$  (Section 8.3).

**(ii) Structurally embedded Standard Model fields.**

- **Gauge bosons:**  $U(1)$ , electroweak-like, and non-Abelian gauge sectors accommodated through internal condensate symmetries (Section 8.6; full development in Sections 7.2 and 7.11).
- **Higgs sector:** the observed Higgs boson is reinterpreted as the radial excitation of a secondary electroweak condensate phase, if the second transition exists (Section 8.7).
- **Fermions:** spinorial fields compatible with the ordered branch, with Dirac-form reconstruction on the emergent Lorentzian background (Section 8.8; full development in Section 9).
- **Neutrinos:** a seesaw-type embedded mechanism with  $m_\nu \sim (y_\nu v_2)^2/M_R$ , and two suggestive but non-derived scale observations built from the same condensate pair  $(\phi_0, v_2)$ : the geometric-mean seesaw scale  $M_R^{\text{geom}} = \sqrt{\phi_0 v_2} \approx 2.4 \times 10^{10}$  GeV and the inverse-ratio Weinberg-operator scale  $m_\nu^{\text{geom}} = v_2^2/\phi_0 \approx 2.5 \times 10^{-5}$  eV (Section 8.9).

**(iii) Topological and conditional sectors.**

- **Primary topological sectors:** the vacuum manifold  $O(4)/O(3) \simeq S^3$  admits texture/skyrmion-like sectors classified by  $\pi_3(S^3) = \mathbb{Z}$ , while  $\pi_0 = \pi_1 = \pi_2 = 0$  implies the absence of stable walls, strings, and monopoles from the primary transition (Section 8.10).
- **Conditional secondary defects:** if the second transition  $O(3) \rightarrow O(2)$  exists, monopole-like defects associated with  $\pi_2(S^2) = \mathbb{Z}$  may arise (Section 8.10).

**Prediction and non-prediction.** The strongest predictions of this chapter are structural. ECT predicts the required existence of the primary condensate excitations, the reduction of the naive soft-orientation sector to one surviving scalar mode in the scalar-only basis, and the topological classification of the primary vacuum manifold, including the anti-predictions  $\pi_0 = \pi_1 = \pi_2 = 0$  and the positive  $\pi_3(S^3) = \mathbb{Z}$  sector. By contrast, the full Standard-Model particle spectrum, the gauge group, the fermion generations, the quantitative electroweak parameters, and the neutrino masses are not predicted here. Those sectors remain embedded, matched, or open.

**Status summary.**

Statement	Status	Comment
<i>Required condensate excitations</i>		
Primary radial mode $\sigma$	A/B	Required amplitude fluctuation of the primary ordered branch
Soft orientation sector reduced to one surviving $\chi$ mode	B	Scalar-only basis with integrability
Linearised graviton sector	A/B	Effective-metric channel; full non-linear closure not yet completed
<i>Structurally embedded sectors</i>		

Statement	Status	Comment
Massless Abelian gauge boson	B/C	Compact-phase local $U(1)$ completion
Electroweak-like embedded sector	B/C	Conditional on secondary $O(3) \rightarrow O(2)$ transition
Higgs-like secondary radial mode	B/C	Conditional particle-level interpretation of the secondary sector
Fermionic sector	B	Structural route deferred to Section 9
Neutrino sector	C	Conditional embedding with one ECT-specific scale observation
<i>Topological and conditional sectors</i>		
$\pi_0 = \pi_1 = \pi_2 = 0$ : no primary stable walls/strings/monopoles	A	Direct topological anti-prediction
$\pi_3(S^3) = \mathbb{Z}$ : topological sectors exist	A	Primary vacuum-manifold topology
Stable localised texture/skyrmion-like states	Open	Requires nonlinear condensate dynamics
Secondary monopole-like defects	B/C	Only if the secondary transition exists
<i>Not derived in Section 8</i>		
Full Standard Model particle spectrum	Open	Not derived from P1–P6
Gauge/Yukawa parameters	Open	External matching inputs
Topological mass spectrum	C/Open	Phenomenological ansatz only

Section 8 therefore establishes the bosonic, topological, and particle-classification side of the ordered-branch spectrum, but not the full fermionic reconstruction. The next section turns to the dedicated fermionic programme, where the spinorial structure, Yukawa couplings, and the ECT-specific fermion–condensate interaction are treated explicitly.

## 9 Fermionic Sector

**Status guide.** This section has three distinct layers:

**Structural reconstruction (Level B).** The Dirac form on the ordered Lorentzian branch, given additional representation-theoretic and first-order-minimality inputs. Fermions are *not* derived as collective excitations of the bare bosonic condensate; they are introduced as additional fields compatible with the condensate symmetry.

**Phenomenological embedding (Level C).** Yukawa couplings, fermion masses, neutrino sector. These assume Standard-Model structure as external input.

**Open problems.** Three fermion generations, Yukawa hierarchy, fermionic statistics from condensate structure, right-handed neutrino scale.

**Connection to the fundamental ECT action.** The fermionic sector is introduced consistently with the full ECT action (2.3). The scalar condensate  $\Phi$  couples to fermions via Yukawa interactions  $y\bar{\Psi}\Phi\Psi$ ; gauge fields can be embedded consistently via the phase symmetries of  $\Phi$  (the  $SU(2) \times U(1)$  ordered-branch gauge architecture follows from P5; Sections 7–7; identification with the physical SM gauge group is Level A/B). The *structural reconstruction* of the Dirac form below is written as an Euler–Lagrange equation of  $S_{\text{ECT}+f}$ ; the fermion field  $\Psi$  and its couplings are additional inputs not contained in the bare scalar condensate action (Level B/C):

1. The ordered-branch vacuum is characterised by  $\langle \partial_A \Phi \rangle = u_0 \delta_{Aw}$ , where  $u_0$  is the gradient condensate amplitude (Section 5.1), with the induced gravitational scale  $\phi_0 \sim \bar{M}_{\text{Pl}}$  (Section 5.1; note that  $n_A = \partial_A \Phi / |\partial \Phi|$  is a derived variable, not an independent field).
2. Fermions  $\Psi$  are introduced as additional fields transforming under the spinor representation of the residual  $O(3)$  symmetry (or its Lorentzian continuation  $SL(2, \mathbb{C})$ ).
3. Their kinetic and mass terms are added to the ECT action:

$$S_{\text{ECT}+\text{f}} = S_{\text{ECT}} + \int d^4X \sqrt{g} \left[ i\bar{\Psi} \gamma^\mu \nabla_\mu \Psi - y \bar{\Psi} \Phi \Psi - \mu_5 \bar{\Psi} \gamma^A n_A \Psi \right], \quad (9.1)$$

where  $y$  is the Yukawa coupling, and  $\mu_5$  is the dimensionful coefficient of the ECT-specific fermion–condensate coupling (equivalently  $\mu_5 = \beta_5 m_f$  with dimensionless  $\beta_5$ ; Section 7.6). The gamma matrices  $\gamma^\mu$  are defined in the Lorentzian geometry induced by the condensate.

Once these additional fermionic inputs are in place, the Dirac equation (Section 9.2) is the Euler–Lagrange equation of  $S_{\text{ECT}+\text{f}}$  with respect to  $\bar{\Psi}$ , evaluated in the condensate background (structural reconstruction, Level B).

Fermionic degrees of freedom can be introduced consistently with the spinor representations of  $Spin(4) \simeq SU(2)_L \times SU(2)_R$ , the double cover of the underlying Euclidean rotation group. This section performs a *structural reconstruction* of the Dirac form. Once (i) emergent Lorentzian geometry and (ii) spinorial representations of  $Spin(4)$  are admitted as Level B inputs, the Dirac form can be constructed algebraically. The section does *not* derive fermions from the bare bosonic condensate action.

**Honest framing.** The symmetry group structure  $Spin(4) \simeq SU(2)_L \times SU(2)_R$  admits spinor representations, and under the standard generator continuation the relevant group becomes  $SL(2, \mathbb{C})$  the standard Weyl and Dirac spinors are obtained by Clifford linearisation. However, two important points should be noted. First, the spinor structure of the rotation group by itself does not imply fermionic *statistics* (anti-commutation relations): the spin-statistics connection requires additional input. Second, the present derivation obtains the Dirac equation as an effective equation for fluctuations in the Lorentzian background — it does not microscopically derive fermions as collective excitations of the condensate. The latter would require a separate construction. This section reconstructs the Dirac equation structurally (Level B) and discusses chirality in the ECT framework.

The fermionic programme developed here remains at the level of structural reconstruction on the ordered branch: it does not derive fermions from the bare bosonic condensate, but shows how spinorial fields, Dirac kinematics, chirality, and fermion couplings can be consistently organised once the emergent Lorentzian background is admitted. Quantum-statistical questions are addressed only at the level of a structural route and belong ultimately to the broader quantum programme.

**Section roadmap.** The logic of this section is layered. Section 9.1 establishes the group-theoretic compatibility of spinorial representations with the ordered branch. Section 9.2 reconstructs the Dirac form on the emergent Lorentzian background. Section 9.3 discusses the structural route to chiral asymmetry. Sections 9.6 and 9.8 treat, respectively, the Standard-Model-like Yukawa embedding and the ECT-specific fermion–condensate coupling. Section 9.9 outlines the structural route toward spin-statistics, and Section 9.10 summarises the open programme.

## 9.1 Spinor structure in the condensate background

*Status:* Level A for the group-theoretic statements ( $Spin(4) \simeq SU(2)_L \times SU(2)_R$ ,  $\pi_1(SO(3)) = \mathbb{Z}_2$ ).  $\pi_1(SO(3)) = \mathbb{Z}_2$  is a Level A topological fact about the residual rotation group; its relevance as a structural motivation for half-integer representations is Level B. Fermions are not derived as collective condensate excitations; they are introduced as additional fields compatible with the condensate symmetry.

Section 8.8 provided the brief particle-spectrum roadmap; the present section develops that route in detail.



**Spinors as compatible excitations (Level B).** In conventional quantum field theory, spinor fields are introduced as fundamental objects transforming under the Lorentz group  $SO(3,1)$ . Within the ECT framework, spinor degrees of freedom are *compatible* with the condensate geometry: after  $O(4) \rightarrow O(3)$  breaking the residual group admits spinor representations, and Clifford linearisation then yields the Dirac form. This is a structural compatibility statement (Level B), not a derivation of spinors as collective condensate excitations.

**Euclidean rotation group and its spinorial content.** Before symmetry breaking the condensate is invariant under rotations in four-dimensional Euclidean space,  $O(4)$ . The connected Euclidean spin group satisfies  $Spin(4) \simeq SU(2)_L \times SU(2)_R$ , while at the Lie-algebra level  $\mathfrak{so}(4) \simeq \mathfrak{su}(2)_L \oplus \mathfrak{su}(2)_R$  (Level A). Rotations in four dimensions thus naturally split into two independent  $SU(2)$  sectors. The fundamental representation of each  $SU(2)$  factor is two-dimensional; two-component spinors are among the irreducible representations naturally available in this decomposition.

**Important caveat.** The group-theoretic structure *admits* spinorial representations; it does not guarantee that spinorial excitations are dynamically present as stable quasiparticles of the bare bosonic condensate. The step from “spinor representations exist” to “spinorial particles appear in the spectrum” requires introducing additional fermionic degrees of freedom as external inputs.

With that proviso, if spinorial excitations are admitted, they can be written as

$$\Psi = \begin{pmatrix} \psi_L \\ \psi_R \end{pmatrix}, \quad (9.2)$$

where  $\psi_L$  and  $\psi_R$  transform under the two  $SU(2)$  factors of  $Spin(4)$ .

**Topological availability of half-integer representations.** The residual continuous rotation symmetry after SSB is  $SO(3)$ , whose fundamental group is  $\pi_1(SO(3)) = \mathbb{Z}_2$  (Level A). This topological fact means that the connected rotation group has a nontrivial double cover. Accordingly, spinorial representations become structurally available: a  $2\pi$  rotation, trivial in  $SO(3)$  itself, can act as  $-1$  in the spinorial representation lifted to the double cover. It does not by itself imply that dynamical fermionic excitations must occur. What remains an additional input is the physical assumption that such representations are *realised* by dynamical excitations of the ordered branch.

**From Euclidean to Lorentzian spinors.** After the condensate selects a preferred direction through  $O(4) \rightarrow O(3)$ , the effective spacetime acquires a Lorentzian structure. The corresponding symmetry group becomes  $SO(3,1)$ , whose universal cover is  $SL(2, \mathbb{C})$ . The pair  $(\psi_L, \psi_R)$  is then compatible with the Dirac spinor structure in the emergent Lorentzian spacetime (Level B).

**Why spinors: first-order minimality.** Among all representations of the Lorentz group, spinorial representations are the unique ones for which a first-order wave equation can be written via the Clifford algebra  $\{\gamma^\mu, \gamma^\nu\} = 2\eta^{\mu\nu}$ : the resulting Dirac equation is the minimal Lorentz-covariant first-order equation whose square reproduces the relativistic dispersion relation. In ECT, where the Lorentzian metric is emergent and the Clifford algebra is defined on the effective metric of the ordered branch, this first-order minimality places spinorial representations in a structurally privileged position among possible field types on the ordered condensate background, once such excitations are admitted. This is not a derivation; it is a compatibility argument. This compatibility argument acquires dynamical content only once the first-order Clifford-linearised equation is introduced, as discussed in Section 9.2.

**Comparison with other emergent-fermion approaches.** In superfluid  $^3\text{He-A}$  [21], Weyl fermions emerge as low-energy excitations near topological Fermi points in momentum space: the fermionic character is a property of the quasiparticle spectrum, not an external input. In ECT the situation is different: fermions are introduced as additional fields compatible with the ordered branch. ECT currently provides

a structural compatibility route and a Lorentzian-spinorial reconstruction, but not yet a microscopic derivation of fermions as quasiparticles of the bare bosonic medium.

**Status summary.**

Statement	Status	Comment
$Spin(4) \simeq SU(2)_L \times SU(2)_R$	A	Double cover of $SO(4)$
Spinorial representations available through the double cover of the connected rotation group	A	Group-theoretic availability; dynamical realisation not implied
$\pi_1(SO(3)) = \mathbb{Z}_2$ : topological availability of half-integer representations	A	Topological fact of residual rotation group
Half-integer representations as structural motivation for fermionic excitations	B	Physical interpretation of topological availability
Dirac spinors compatible with ordered Lorentzian branch	B	Structural compatibility
First-order minimality gives spinorial representations a structurally privileged role	B	Clifford linearisation on the emergent metric
Fermions as collective condensate excitations	Open	Not derived from bare bosonic action

**Physical interpretation of spin (Level B: interpretive).** The group-theoretic structures developed above admit a physical reading that clarifies what spin represents within the ECT framework. Spin should not be interpreted as the literal mechanical rotation of a localised material object in ordinary three-dimensional space. Rather, it may be interpreted as the spinorial orientation degree of freedom of a fermionic field compatible with the condensate symmetry structure: the two-valued character of spin- $\frac{1}{2}$  states reflects the fact that the relevant covering group  $Spin(4) \simeq SU(2)_L \times SU(2)_R$  admits representations requiring a  $4\pi$  rotation for identity return—a natural group-theoretic property of spinorial fields on the ordered branch. After symmetry breaking and emergence of the Lorentzian sector, this structure reduces to the standard  $SL(2, \mathbb{C})$  spinor description, but its geometric origin lies in the pre-Lorentzian Euclidean rotational symmetry. The magnetic moment of a spin- $\frac{1}{2}$  field is then naturally understood as the response of this spinorial degree of freedom to the emergent  $U(1)$  gauge sector (Section 7.2).

*Limitation.* The present formulation does not provide a first-principles derivation of the electron  $g$ -factor, hydrogenic fine structure, or the numerical value of  $\alpha_{fs}$ . These remain open targets of the fermionic programme (Section 9.10).

## 9.2 Structural Reconstruction of the Dirac Form

*Status: Level B structural reconstruction.* If one admits (i) emergent Lorentzian kinematics, (ii) spinorial representations compatible with the broken  $O(4) \rightarrow O(3)$  background, and (iii) first-order Clifford linearisation as the minimal relativistic option, then a Dirac-type first-order equation can be constructed algebraically. Each of these inputs goes beyond the minimal scalar condensate postulate; the reconstruction is therefore Level B. The ECT-specific content is that the Clifford algebra is interpreted with respect to the emergent metric of the ordered branch rather than introduced on a fundamental spacetime structure from the outset. A more structural representation-theoretic route to the same Dirac form is developed later in Section 24.5, where the equation is written first in terms of the pre-identification action scale  $S_0$  and only subsequently matched to  $\hbar$ .

**Relativistic dispersion from the emergent metric.** After  $O(4) \rightarrow O(3)$  symmetry breaking, low-energy excitations propagate in an emergent Lorentzian spacetime. For a free relativistic excitation

on the emergent Lorentzian branch, the natural quadratic invariant is

$$p_\mu p^\mu = m^2 c_*^2, \quad p_\mu = \left( \frac{E}{c_*}, \mathbf{p} \right). \quad (9.3)$$

For fermionic fields, the question is then whether this quadratic relation admits a first-order spinorial linearisation.

**Clifford algebra and linearisation.** Introduce matrices  $\gamma^\mu$  obeying the Clifford algebra

$$\{\gamma^\mu, \gamma^\nu\} = 2\eta^{\mu\nu}. \quad (9.4)$$

This algebra encodes the geometry of the local Lorentzian metric. In ECT this metric is not a fundamental background but the *induced effective metric* of the ordered branch (Section 8.5): the  $\eta^{\mu\nu}$  appearing in the Clifford relation is interpreted as the flat-limit Lorentzian metric induced by the uniform condensate vacuum. The Clifford structure is therefore tied to the emergent metric of the ordered branch rather than imposed on a fundamental spacetime from the outset. In that sense it is structurally induced by the condensate geometry, not introduced independently of it.

Defining  $\not{p} \equiv \gamma^\mu p_\mu$ , one obtains

$$(\not{p})^2 = \gamma^\mu \gamma^\nu p_\mu p_\nu = \frac{1}{2} \{\gamma^\mu, \gamma^\nu\} p_\mu p_\nu = \eta^{\mu\nu} p_\mu p_\nu = p_\mu p^\mu. \quad (9.5)$$

Thus the Clifford algebra provides a natural linearisation of the quadratic invariant  $p_\mu p^\mu$ .

**Dirac equation.** The minimal first-order equation consistent with this structure is

$$(\not{p} - mc_*)\Psi = 0. \quad (9.6)$$

In coordinate space, with  $p_\mu \rightarrow i\hbar\partial_\mu$ , this becomes

$$\boxed{(i\hbar\gamma^\mu\partial_\mu - mc_*)\Psi = 0.} \quad (9.7)$$

This reproduces a Dirac-type equation for relativistic fermionic excitations on the ordered condensate branch (structural reconstruction, Level B). At the canonical normalisation  $\alpha = 2\beta$ ,  $\beta = 1$  one has  $c_* = c$ , recovering the standard Dirac form.

**Connection to the ECT action.** The Dirac-type equation (9.7) corresponds to the minimal fermionic part of the extended action  $S_{\text{ECT}+f}$  (9.1) when evaluated on the ordered condensate background and restricted to the standard first-order kinetic-plus-mass sector. More generally, varying the full extended action with respect to  $\bar{\Psi}$  yields the Dirac operator together with the additional ECT-specific deformation discussed separately in Section 9.8. This makes the Dirac form consistent with the variational structure of the *extended* theory. The point is not that the fermionic sector has been derived from the bare bosonic condensate action, but that once the fermionic extension is admitted, the fermionic equation of motion is not added ad hoc at the equation level: it follows from varying the extended action.

**Weyl decomposition.** In the chiral representation the Dirac spinor decomposes into two Weyl spinors

$$\Psi = \begin{pmatrix} \psi_L \\ \psi_R \end{pmatrix}, \quad (9.8)$$

transforming under the two inequivalent two-component representations of  $SL(2, \mathbb{C})$ . This connects directly to the ECT observation that the Euclidean spin group admits the decomposition  $Spin(4) \simeq SU(2)_L \times SU(2)_R$  (Section 9.1).

**Curved-spacetime generalisation.** On a non-uniform condensate background, where the effective metric  $g_{\mu\nu}^{\text{eff}}$  varies, the corresponding curved-background Dirac form is naturally expected to take the form

$$(i\hbar\gamma^{\mu}e_a^{\mu}\nabla_{\mu} - mc_*)\Psi = 0, \quad (9.9)$$

where  $e_a^{\mu}$  is the emergent vierbein and  $\nabla_{\mu}$  includes the spin connection compatible with  $g_{\mu\nu}^{\text{eff}}$ . In the ECT interpretation, both the effective vierbein and the associated spin connection are expected to be induced by the condensate orientation field and its gradients, rather than introduced as independent geometric structures. At the present stage this should be read as a Level B structural interpretation, not as a completed explicit derivation.

**ECT-specific fermion–condensate coupling.** Beyond the Dirac form itself, the ordered branch admits an additional fermion–condensate coupling  $\Delta\mathcal{L} = \mu_5 \bar{\Psi}\gamma^A n_A \Psi$ . Its status within the fermionic reconstruction is discussed in Section 9.8, while its phenomenology is developed separately in Section 7.

**What is and is not reconstructed here.** The present subsection reconstructs the *Dirac form* as the minimal first-order spinorial equation compatible with the emergent Lorentzian branch. It does not yet derive the existence of fermions from the bare bosonic condensate, nor does it derive fermionic quantisation, anticommutation relations, or the full spin-statistics theorem. Nor does the present subsection derive the observed fermion spectrum, generation structure, or Yukawa hierarchy. Those questions belong to the broader fermionic and quantum programmes developed in the following subsections and in Section 24.4.

#### Status summary.

Statement	Status	Comment
Lorentzian quadratic invariant for free excitations on the ordered branch	A (EFT)	Kinematic input from the broken-phase propagation structure
Clifford algebra on the emergent metric	B	$\eta^{\mu\nu}$ is interpreted as the induced flat-limit metric
Dirac-type first-order equation via Clifford linearisation	B	Structural reconstruction once the spinorial and Lorentzian inputs are admitted
Connection to $S_{\text{ECT}+f}$ variational structure	B	Euler–Lagrange equation of the extended action
Weyl decomposition $\leftrightarrow Spin(4) \simeq SU(2)_L \times SU(2)_R$	A/B	Group-theoretic (A); physical relevance (B)
Curved-background Dirac generalisation with an emergent vierbein/spin-connection interpretation	B	Structural interpretation; explicit derivation pending

### 9.3 Chirality and fermion interactions

*Status: Level B structural possibility. The decomposition  $Spin(4) \simeq SU(2)_L \times SU(2)_R$  together with  $O(4) \rightarrow O(3)$  SSB provides a structural setting in which an asymmetry between the two chiral sectors can arise. At the present stage this is a structural possibility, not a derivation of the physical weak-interaction chirality. Connection to gauge sector: Section 7.11.*

**The chirality question.** One of the striking features of the Standard Model is the chiral nature of the weak interaction: the  $SU(2)_L$  gauge symmetry acts only on left-handed fermions, while right-handed

fermions are singlets under the weak interaction. Within ECT the question is whether this asymmetry has a structural origin in the condensate geometry.

**Physical significance.** If the left-handed character of the weak interaction is traced to the broken-phase geometry rather than to an arbitrary choice of gauge representations, then the parity asymmetry of the weak sector ceases to be an unexplained empirical fact of the Standard Model and becomes a geometric imprint of the vacuum ordering itself. The physical content of this possibility is therefore deep: it would mean that parity violation in weak interactions is not a contingent feature of one particular set of fields, but a direct structural consequence of how the condensate selects its ordered phase at the  $O(4) \rightarrow O(3)$  transition. At the present stage this remains a structural possibility (Level B), not yet a closed first-principles derivation of the physical weak-interaction chirality. This result, if confirmed, would be one of the deepest explanatory gains of the condensate programme: a fundamental left–right asymmetry of nature would be understood not as a brute empirical datum but as the geometric shadow of a single spontaneous symmetry breaking.

**Connection to the gauge-architectural origin.** The gauge-architectural origin of the  $SU(2)$  connection—including the  $\mathfrak{so}(3) \cong \mathfrak{su}(2)$  bridge and the EFT completion—is established in Section 7.3. The present subsection addresses its chiral interpretation: why one  $SU(2)$  factor is structurally preferred over the other.

**Why chirality belongs here.** The issue of chirality enters ECT at an intermediate level between pure group theory and full gauge phenomenology. Section 9.1 establishes that spinorial representations are compatible with the ordered branch, while Section 7.4 discusses the electroweak-like gauge embedding. The present subsection isolates the specific question of whether the condensate geometry can distinguish the two chiral sectors before the full weak-interaction phenomenology is specified.

This subsection builds on the spinorial compatibility established in Section 9.1 and on the Dirac-form reconstruction of Section 9.2. The question addressed here is not whether spinors can be written on the ordered branch, but whether the condensate geometry can structurally bias the left- and right-chiral sectors differently.

**From  $Spin(4)$  to chiral asymmetry.** As established in Section 9.1, the Euclidean spin group decomposes as  $Spin(4) \simeq SU(2)_L \times SU(2)_R$ , and the Dirac spinor  $\Psi = (\psi_L, \psi_R)^T$  carries representations of both factors. Before SSB, the two  $SU(2)$  sectors are on an equal footing.

The formation of the condensate selects a preferred orientation  $n_A \equiv \partial_A \Phi / |\partial \Phi|$ , leading to  $O(4) \rightarrow O(3)$ . Geometrically this corresponds to fixing one axis in the four-dimensional space. As a result, the symmetry between the two  $SU(2)$  factors in the decomposition of  $Spin(4)$  is no longer exact.

**Selection mechanism (Level B structural argument).** After the ordered branch has selected a Lorentzian sign structure ( $\alpha > \beta$ ) and the real time variable is introduced by  $t = w/c_*$ , the Euclidean spin group is read in the corresponding Lorentzian spinorial language. In that language the two factors are associated with the left-handed and right-handed chirality sectors:  $\psi_L$  and  $\psi_R$  transform under the  $(1/2, 0)$  and  $(0, 1/2)$  representations, respectively.

The condensate direction  $n_A$  breaks the equivalence between the two sectors because the ordered-branch structure treats the distinguished  $w$ -direction differently from the spatial directions from the three spatial directions. If the gauge coupling is mediated through condensate-dependent structures (as in the electroweak-like embedding of Section 7.4), then the geometric asymmetry of the ordered branch may be reflected in a chiral asymmetry of the fermion–gauge coupling. The orientation of the condensate—specifically the sign of the four-volume form  $\varepsilon_{ABCD} n^A$  evaluated in the ordered phase—selects which of the two  $SU(2)$  factors is identified with the residual stabiliser. Upon analytic continuation to the emergent Lorentzian sector, this maps to a definite chirality ( $L$  or  $R$ ). Thus the oriented condensate provides a structural route to weak-sector parity asymmetry: a feature that is postulated in the Standard Model

acquires a geometric origin in ECT. The exactly maximally parity-violating Standard-Model pattern is, however, a stronger statement about the precise chiral structure of the observed weak sector, and its derivation from the ordered-branch EFT remains an open problem (OP-P1, §9.10).

This does not yet constitute a complete first-principles derivation of the full Standard-Model weak gauge sector. Rather, it identifies a structurally preferred chiral  $SU(2)$  sector whose phenomenological realisation is supplied by the electroweak condensate doublet (Section 7.4). In particular, the corresponding connection is at this stage not yet shown to be an independent internal gauge field in the full Standard-Model sense, as opposed to a component of the emergent spin connection. A full derivation would need to demonstrate the existence of independent propagating spin-1 modes beyond those fixed by the metric (OP-GRAV-WEAK; see Section 48.13).

**Connection to the fifth-force coupling.** The ECT-specific deformation  $\Delta\mathcal{L} = \mu_5 \bar{\Psi} \gamma^A n_A \Psi$  (Section 9.8) also introduces a preferred direction into the fermion sector and thereby distinguishes the two chiral sectors geometrically. The fermion–condensate coupling and the chiral gauge selection therefore share a common structural origin in the preferred direction of the ordered branch.

**Implication for the neutrino sector.** If the ordered-branch chiral route is realised in the weak sector, the minimal expectation is that the weakly active neutrino states are left-chiral, while any right-handed neutrino sector is additional and singlet-like. This does not yet decide between Dirac and Majorana masses, but it does explain why the observed active weak sector may be intrinsically one-sided. The neutrino-sector discussion is continued in Section 8.9. Whether the two effects are dynamically related or merely share the same geometric source remains open.

**Fate of  $SU(2)_R$ .** If the selection mechanism described above is realised, the  $SU(2)_R$  sector is not eliminated but effectively decoupled at low energies. Two possibilities remain structurally open within ECT:

- $SU(2)_R$  is completely suppressed at all accessible energies, reproducing the Standard Model structure exactly;
- $SU(2)_R$  becomes operative at very high energies, leading to a left–right symmetric extension.

ECT does not currently distinguish between these possibilities. This question belongs to the open fermionic programme summarised in Section 9.10.

**What is and is not derived here.** The present subsection shows that the ECT condensate geometry provides a *structural setting* in which chiral asymmetry can naturally arise: the decomposition  $Spin(4) \simeq SU(2)_L \times SU(2)_R$  plus SSB creates a geometric distinction between the two chirality sectors. It does not derive the physical weak interaction, nor does it explain why  $SU(2)_L$  (and not  $SU(2)_R$ ) is selected, nor does it derive the observed fermion representations under the electroweak gauge group. These questions belong to the open programme (OP-chirality; Section 9.10).

**What would be needed for Level A.** To promote chirality from structural possibility to derivation, ECT would need to show: (i) how the condensate dynamics selects one chiral sector rather than the other, (ii) how the electroweak gauge vertex acquires its observed chiral form, and (iii) how the observed fermion representation content follows from the same mechanism. None of these steps has yet been completed. The quantum consistency of the selected chiral gauge sector under anomaly constraints is analysed in Section 9.5.

### Status summary.

Statement	Status	Comment
$Spin(4) \simeq SU(2)_L \times SU(2)_R$ decomposition	A	Double cover of $SO(4)$
Analytic continuation maps the Euclidean spinorial structure to Lorentzian chiral sectors	B	Structural continuation argument
SSB $O(4) \rightarrow O(3)$ distinguishes a preferred direction and removes the pre-breaking symmetry between the two Euclidean $SU(2)$ factors	A/B	Geometric statement (A); relevance for physical chirality is interpretive (B)
The oriented condensate selects one chiral $SU(2)$ sector	B+	Structural selection via four-volume orientation
Selection of $SU(2)_L$ as the physical weak factor	B+	Orientation selects chirality; full internal-gauge status open (OP-GRAV-WEAK)
Fermion–condensate coupling and chiral asymmetry share the same geometric source $n_A$	B	Common structural origin
Fate of $SU(2)_R$	Open	Suppressed or active only at higher energies
Full derivation of SM chirality from P1–P6	Open (OP-chirality)	

## 9.4 Discrete symmetries of the emergent matter sector: P, T, C, and conditional CPT

*Status: layered. The geometric basis for an emergent parity precursor and for a Euclidean antecedent of time reversal follows from the  $O(4)$  structure postulated in P2 (Level A). Charge conjugation has a conditional, internal status tied to the fermionic/charged sector (Level B). A conditional CPT route is identified for those local sectors where the Euclidean Osterwalder–Schrader reconstruction machinery is available: Euclidean covariance, reflection positivity, and locality/cluster properties are the explicit prerequisites (Level A/B for free/quadratic local sectors; Open for the full nonlinear interacting theory). The phenomenological preferred-direction operator  $\mathcal{L}_5$  introduced in Section 7.6 is re-classified here as a CPT-odd branch-sensitive operator (Level B), complementing but not replacing the exact symmetry backbone. The present subsection should be read as a structural identification of the discrete-symmetry architecture of ECT, not as a complete closed proof of CPT for the full nonlinear interacting theory.*

**Transition from the chirality sector.** The previous subsection (§9.3) showed that the ordered condensate can structurally distinguish the two chiral factors of  $Spin(4) \simeq SU(2)_L \times SU(2)_R$ , thereby providing a geometric route to parity asymmetry. We now place this chirality-selection mechanism into the broader discrete-symmetry architecture of ECT. The key point is that the Euclidean theory already contains exact reflections at the level of  $O(4)$ , whereas the operator-level notions of  $T$ ,  $C$ , and  $CPT$  emerge only conditionally in those local sectors for which the Euclidean quantum reconstruction succeeds. The discussion is organised into three structurally distinct layers: (A) the geometric discrete backbone of the Euclidean manifold; (B) the conditional operator-level theorem structure that emerges after Osterwalder–Schrader reconstruction; (C) the branch-sensitive phenomenology, including the re-classification of  $\mathcal{L}_5$  and the branch-pair symmetry architecture that is characteristic of ECT.

## Layer A: Geometric discrete backbone of ECT

**A1. Euclidean reflections in  $O(4)$ .** On the Euclidean manifold  $\mathcal{M}^4$  with metric  $\delta_{AB}$  the  $O(4)$  group acts in its full form  $O(4) = SO(4) \rtimes \mathbb{Z}_2$ , where the  $\mathbb{Z}_2$  factor is generated by improper reflections (determinant  $-1$  transformations). Postulate P2 asserts invariance of the Euclidean action  $S_E$  under  $O(4)$ , *not* merely under  $SO(4)$ ; hence improper reflections are automatically exact geometric symmetries of  $S_E$  at the classical level. The three natural generators of the improper part are:

$$R_s : (x^1, x^2, x^3, w) \mapsto (-x^1, -x^2, -x^3, w), \quad (9.10)$$

$$R_w : (x^1, x^2, x^3, w) \mapsto (x^1, x^2, x^3, -w), \quad (9.11)$$

$$I_4 = R_s \circ R_w : (x^1, x^2, x^3, w) \mapsto (-x^1, -x^2, -x^3, -w). \quad (9.12)$$

All three are exact isometries of the Euclidean metric and, by P2, exact symmetries of  $S_E$  (Level A).

**A2. Emergent Lorentzian parity from  $R_s$ .** After the Lorentzian window  $\alpha > \beta$  is selected and the real parametrisation  $t = w/c_*$  is introduced (§3.5), the spatial reflection  $R_s$  preserves the  $w$ -coordinate that plays the role of Lorentzian time and acts only on spatial indices. At the level of coordinates it is therefore a natural geometric precursor of Lorentzian parity  $P : (t, \mathbf{x}) \mapsto (t, -\mathbf{x})$  (Level A).

The spinorial content of  $R_s$  is fixed by the double cover  $Spin(4) \simeq SU(2)_L \times SU(2)_R$ . The improper elements  $O(4) \setminus SO(4)$  exchange the two  $SU(2)$  factors. Consequently  $R_s$  acts on a Dirac-like doublet  $\Psi = (\psi_L, \psi_R)^\top$  by swapping the two chiral components, up to the standard phase conventions of Euclidean spinor QFT [70, 71]. These phases are inherited from the group-theoretic structure and introduce no additional postulates.

*Structural consequence (Level B).* Combined with the chirality-selection mechanism of §9.3, this implies that any ordered-branch mechanism coupling only one Euclidean chiral factor to the condensate produces structural parity asymmetry after the emergent Lorentzian reading. The statement that this asymmetry reproduces the *exactly maximal* parity violation of the Standard-Model weak sector requires a detailed effective-field-theory derivation from the condensate dynamics that is not yet available and is recorded as an open problem (OP-P1, §9.10):

- Euclidean improper element exchanges chiral factors: Level A (group theory);
- structural route to parity asymmetry in the ordered branch: Level B (chirality-selection mechanism of §9.3);
- exact maximal weak-sector pattern: Level C (future derivation, OP-P1).

**A3. Geometric antecedent of time reversal from  $R_w$ .** The reflection  $R_w$  inverts the preferred Euclidean axis  $w \mapsto -w$ . Under the real parametrisation  $t = w/c_*$  it induces the classical coordinate map  $t \mapsto -t$  and is therefore the natural geometric antecedent of Lorentzian time reversal.

We emphasise that this classical coordinate map is *not*, by itself, the anti-unitary time-reversal operator of the emergent Lorentzian quantum theory. Anti-unitarity is a property of an operator on a Hilbert space, not of a coordinate transformation on a manifold, and it requires a reconstruction step to which we now turn (Layer B).

## Layer B: Conditional operator-level theorem structure

**B1. Complex conjugation from reflection positivity.** The fundamental ECT field  $\Phi$  is a real scalar; there is no fundamental complex structure in the bare action. A complex Hilbert space, and with it the complex conjugation required for anti-unitary operators, emerges only through Osterwalder–Schrader reconstruction [72, 73].



The relevant construction proceeds as follows. For each local observable  $A$  with support in a half-space of the Euclidean manifold, reflection positivity asserts

$$\langle \Theta(A)A \rangle_E \geq 0, \quad (9.13)$$

where  $\Theta$  is the Euclidean reflection operator (for the  $w$ -axis one takes  $\Theta = \Theta_w$  associated with  $R_w$ ). Reflection positivity permits the definition of a positive-definite inner product

$$\langle \Psi_A, \Psi_B \rangle_{\mathcal{H}} \equiv \langle \Theta(A^*)B \rangle_E, \quad (9.14)$$

on the algebra of observables; completion with respect to this inner product yields a complex Hilbert space  $\mathcal{H}$  together with a self-adjoint Hamiltonian. Complex conjugation on  $\mathcal{H}$  is thus an emergent structure of the reconstruction, not a fundamental ingredient. An anti-unitary time-reversal operator  $T$  on  $\mathcal{H}$  is then built as a combination of the Euclidean reflection  $\Theta_w$  with complex conjugation on  $\mathcal{H}$ ; anti-unitarity follows by construction.

The Euclidean reflection  $R_w$  supplies the geometric reversal of the preferred axis. The anti-unitary realisation of time reversal in the emergent Lorentzian quantum theory requires, in addition, the reconstructed Hilbert-space structure furnished by reflection positivity and Osterwalder–Schrader reconstruction. In this sense, the geometric Euclidean reversal and the anti-unitary quantum operator  $T$  are related but not identical objects.

**B2. Charge conjugation as an internal operation.** Charge conjugation  $C$  does *not* arise from  $O(4)$  spacetime reflections. The fundamental ECT scalar  $\Phi$  carries no phase, so the  $\theta \rightarrow -\theta$  construction of charge conjugation in a compact-phase sector is available only after such a sector has been introduced as an emergent structure (for example through the coherent branch §21.1 and the  $U(1)$  gauge-sector emergence §7.2).

For the Dirac sector a group-theoretic basis for  $C$  is nonetheless available: on  $Spin(4)$  representations the charge-conjugation matrix  $C$  is determined (up to convention) by the relations

$$C\gamma^A C^{-1} = -(\gamma^A)^\top, \quad C^\top = -C, \quad (9.15)$$

and such a matrix exists group-theoretically. In this sense  $C$  has a structural basis in the spinor bundle, although the basis is internal (spinor/charge structure) rather than geometric (spacetime reflection). Its status is therefore Level B, conditional on the existence of the relevant charged/fermionic sector.

A complete derivation of the action of  $C$  on all emergent charged sectors of ECT, including the interplay with the compact-phase  $U(1)$  structure, remains open (OP-CPT2, §9.10).

**B3. Conditional CPT route via Osterwalder–Schrader.** There are two standard routes to the CPT theorem: the Minkowski-side proof of Jost [74, 75] and the Euclidean-side route through Osterwalder–Schrader reconstruction [72, 73]. Because ECT is formulated on a Euclidean manifold and already employs reflection positivity for Hilbert-space reconstruction in Part III (§23.1), the OS route is the natural one.

*Conditional CPT route.* Let  $\mathcal{S}$  denote a local sector of ECT defined by an operator algebra generated by observables supported in finite spatial regions of the Euclidean manifold. Whenever

- (a)  $O(4)$ -covariance of the Euclidean action holds (automatic from P2),
- (b) reflection positivity is verified for the algebra of observables of  $\mathcal{S}$ ,
- (c) locality and cluster decomposition hold for  $\mathcal{S}$ , and
- (d) the Osterwalder–Schrader reconstruction closes for  $\mathcal{S}$ ,

the associated emergent Lorentzian theory obtained through OS reconstruction inherits the standard CPT structure: there exists an anti-unitary operator  $\Theta_{\text{CPT}}$  on the reconstructed Hilbert space satisfying the usual CPT transformation rules for bosonic and fermionic fields.

The important point is the formulation: in the present article we *identify* this route and its precise prerequisites; we do not claim a complete closed proof of the full nonlinear case. The current status is:

- free and quadratic local sectors where conditions (a)–(d) are verified: Level A/B for the conditional CPT route;
- full nonlinear interacting ECT: Open (OP-CPT1), pending the broader programme on low-energy QFT architecture (locality and cluster structure in nonlinear ECT) together with OP-OS1.

**B4. Comparison with Minkowski-side proofs.** The standard Minkowski-side CPT route is associated with the Jost / Pauli–Lüders line of argument in axiomatic Lorentzian QFT [74, 76, 75], where CPT follows from the usual locality and covariance assumptions. The route identified here is the Euclidean Osterwalder–Schrader one: once the quartet of Euclidean covariance, reflection positivity, locality, and cluster decomposition holds and OS reconstruction applies, the reconstructed Lorentzian theory inherits the standard CPT structure. We emphasise again that the present subsection identifies these prerequisites explicitly and specifies where they are already met and where they remain open within ECT.

### Layer C: Branch-sensitive phenomenology

**C1. Branch-pair symmetry architecture.** After  $O(4) \rightarrow O(3)$  SSB the vacuum manifold is  $S^3$  (§34); for every ordered direction  $n_A$  there is an antipodal partner  $-n_A$  on this manifold. This gives rise to a three-fold classification of discrete operations:

- exact symmetries of the full Euclidean theory* that act on the entire ensemble of ordered branches;
- branch-exchange operations* that exchange  $n_A$  and  $-n_A$  (equivalently, map an ordered branch to its antipodal partner), examples of which include  $R_w$  and  $I_4$  in the orientation coordinate;
- effective symmetries of one selected branch*, which form a subgroup of (i) and may be broken by branch selection.

The antipodal branch structure of the ordered vacuum manifold is exact at the level of the vacuum geometry. Whether this structure is realised dynamically as a physically meaningful branch-pair symmetry of cosmological solutions remains open. This gives ECT a new symmetry layer at the level of the ordered-vacuum geometry, with no direct analogue in ordinary single-branch local QFT.

A simple structural observation follows from the homotopy of  $S^3$ : since  $\pi_0(S^3) = 0$  (§34), there are no topologically stable domain walls separating antipodal branches. The two branches are antipodal points on a connected manifold, rather than states separated by a physical barrier.

*Possible cosmological interpretation.* One may speculate that our observable matter-dominated branch is paired with an antipodal antimatter-dominated partner, with the Euclidean pair being CPT-symmetric while branch-level asymmetries are local to each partner. Such a cosmological reading is reminiscent of Boyle–Turok-type CPT-symmetric cosmologies [77], but native to the ECT  $O(4) \rightarrow O(3)$  structure. It is recorded here as a possible future direction (Level C, OP-BRANCH1, §9.10), not as an established result.

**C2. Re-classification of the phenomenological operator  $\mathcal{L}_5$ .** The preferred-direction fermion–condensate coupling introduced in §7.6,

$$\mathcal{L}_5 = \mu_5 \bar{\Psi} \gamma^A n_A \Psi, \quad (9.16)$$

admits a precise discrete-symmetry classification that we record here. Using the standard discrete-transformation conventions for the Dirac vector current  $j^\mu = \bar{\Psi} \gamma^\mu \Psi$ , one finds that  $j^\mu$  is C-odd, while

its timelike component  $j^0$  is P-even and T-even. Accordingly, for a timelike ordered-branch background  $n^\mu = (1, 0, 0, 0)$  treated as a classical spurion, the operator

$$\mathcal{L}_5 = \mu_5 \bar{\Psi} \gamma^\mu n_\mu \Psi = \mu_5 \bar{\Psi} \gamma^0 \Psi = \mu_5 \Psi^\dagger \Psi \quad (9.17)$$

is *C-odd, P-even, T-even, CP-odd, and CPT-odd*.

Reality of the coupling  $\mu_5$  ensures hermiticity of the operator (required for a real action), but does *not* restore CPT invariance. Consequently  $\mathcal{L}_5$  is a branch-sensitive Lorentz- and CPT-violating phenomenological operator of the ordered-branch EFT, not a foundation of any exact symmetry theorem. Its role in ECT is threefold:

- (i) to supply Sakharov condition (ii) for ECT-native baryogenesis (§16.3) in combination with complex flavour phases;
- (ii) to provide a structural CP-asymmetric source of the ordered branch absent in the minimal Standard Model;
- (iii) to serve as a phenomenological channel for testable Lorentz/CPT-violation signatures, particularly in the neutrino sector (§8.9).

The conditional CPT route of Layer B for reconstructible local sectors is not affected by  $\mathcal{L}_5$ : the operator explicitly lies outside the reconstructible OS setup as a branch-selecting extension of the ordered-branch EFT, and therefore does not conflict with the exact CPT backbone of those sectors. Compatibility of  $\mathcal{L}_5$  with standard anomaly cancellation, following from its vector-operator nature, is systematically analysed in §9.5.

**Comparison with SME-type constructions.** A separate line of research, the Standard-Model Extension (SME) of Kostelecký and collaborators [28, 29, 13], systematically parametrises Lorentz and CPT violation at the level of effective Lorentzian QFT. The ECT operator  $\mathcal{L}_5$  fits into the general SME operator class at the effective level. In particular, ECT attributes the preferred direction to an ordered condensate background selected dynamically from an initially Euclidean  $O(4)$ -symmetric phase, whereas SME-type constructions typically introduce Lorentz-violating tensors directly at the level of the effective Lorentzian theory. In this sense ECT provides a possible pre-geometric origin for a subset of SME-type operators.

**C3. Neutrino sector: refined interpretation.** The re-classification of  $\mathcal{L}_5$  as a CPT-odd branch operator sharpens the neutrino-sector discussion of §8.9. The suppression scale of possible CPT-violating contributions to neutrino oscillations is set by  $\mu_5/E_\nu$ , which for the dimensional estimate  $\mu_5 \sim m_\nu^2/\phi_0$  gives an extraordinarily small effect across the accessible energy range. Neutrinoless double-beta decay is the primary discriminator: if observed together with the ECT  $\mathcal{L}_5$  route, it is consistent with an effective Majorana sector selected by the ordered-branch mechanism; its absence places independent constraints on the admissible  $\mu_5$  range and on the neutrino mass structure.

**C4. Baryogenesis architecture: revised foundation.** The present subsection supplies a sharpened architectural basis for ECT-native baryogenesis (§16.3). The Sakharov conditions are realised as follows:

- (i) *Baryon number violation*: defect-mediated topology change (§22.3, §16.3).
- (ii) *C and CP violation*: the phenomenological CPT-odd and CP-odd operator  $\mathcal{L}_5$  (Layer C of this subsection), combined with complex flavour phases (OP-Yukawa; §9.6). The conditional CPT route of Layer B for reconstructible sectors remains intact;  $\mathcal{L}_5$  lies outside that reconstructible setup as a branch-sensitive phenomenological channel.
- (iii) *Departure from thermal equilibrium*: the  $O(4) \rightarrow O(3)$  ordering transition itself (Level A; from P4).

The branch-pair architecture of C1 provides an additional, still speculative, possibility in which the observed matter-antimatter asymmetry is a branch-local property of our ordered partner, the full Euclidean pair being CPT-symmetric. This is recorded as OP-BRANCH1, not as an established result.

### Three distinct notions of “time-reversal”

It is useful to disentangle three concepts that are logically distinct in ECT and that are sometimes conflated in the discrete-symmetry literature:

- (i) *Fundamental anti-unitary  $T$*  on the reconstructed Hilbert space, obtained through the OS route of Layer B. Level B (free/quadratic local sectors); Open for the full nonlinear theory (OP-CPT1).
- (ii) *Effective branch-level  $T$ -violation* carried by  $\mathcal{L}_5$  at the phenomenological level of Layer C. Level B; independent of the fundamental- $T$  statement.
- (iii) *Thermodynamic arrow of time* emerging through monotonic decoherence (§26.1, Part II; Level B). Independent of both (i) and (ii).

All three can coexist without contradiction. The conditional CPT route holds in reconstructible sectors;  $\mathcal{L}_5$  provides effective branch-level CPT/Lorentz-violation outside those sectors; the thermodynamic arrow of time arises via decoherence and does not rely on fundamental  $T$ -violation.

**Locality/cluster input for CPT closure.** The conditional CPT route identified in Layer B depends not only on reflection positivity but also on the locality and cluster decomposition properties required by OS reconstruction. Their status in the full nonlinear interacting theory remains part of the broader low-energy QFT architecture programme (OP-Loc1, §9.10), of which the CPT route is one element. This open-problem dependency is explicitly recognised here to avoid misinterpretation of the conditional CPT statement as a standalone closed theorem.

**Connection to quantum statistics.** The discrete-symmetry architecture developed here complements the topological structure of the fermionic sector discussed in §9.9 (quantum statistics). Three distinct  $\mathbb{Z}_2$  facts enter the fermionic sector architecture, and it is important to keep them apart:

- the  $\mathbb{Z}_2$  factor of  $O(4) = SO(4) \rtimes \mathbb{Z}_2$ , generated by improper reflections (present subsection);
- the topological fact  $\pi_1(SO(3)) = \mathbb{Z}_2$ , underlying the group-theoretic availability of half-integer representations (§9.1);
- the exchange topology  $\pi_1(\mathcal{M}_2) = \mathbb{Z}_2$ , which underlies the bosonic/fermionic exchange statistics dichotomy (§9.9).

These three  $\mathbb{Z}_2$  structures are logically distinct; linking them into the full relativistic spin-statistics theorem is part of the broader open programme.

**Table 42:** Discrete-symmetry architecture of ECT: status summary.

Statement	Status	Basis / open problem
Euclidean reflections $R_s, R_w, I_4 \in O(4)$	A	From $O(4)$ -invariance in P2
Geometric Lorentzian $P$ precursor from $R_s$	A	Wick-type coordinate map
$R_s$ exchanges $SU(2)_L \leftrightarrow SU(2)_R$ in $Spin(4)$	A	Group theory of double cover
Structural route to parity asymmetry in the ordered branch	B	Chirality selection (§9.3)
Exact maximal weak-sector parity pattern	C	OP-P1 (§9.10)
Geometric antecedent of $T$ from $R_w$	A	$O(4)$ operation
Anti-unitary $T$ in quadratic local sectors after OS	B	RP + complex conjugation from OS formula
Full nonlinear anti-unitary $T$ closure	Open	OP-CPT1, depends on OP-OS1 and OP-Loc1

Statement	Status	Basis / open problem
Charge conjugation $C$ in charged/Dirac sector	B	Internal; Dirac-operator structure
Complete $C$ transformation on all emergent charged sectors	Open	OP-CPT2
Conditional CPT route for reconstructed local sectors	A/B	Identified via OS prerequisites (a)–(d)
Full interacting CPT closure in nonlinear ECT	Open	OP-CPT1
Branch-pair symmetry architecture of the ordered vacuum manifold (group-theoretic)	A	Antipodal structure of $S^3$
Cosmological CPT-symmetric branch-pair realisation	C	OP-BRANCH1
$\mathcal{L}_5$ as CPT-odd branch-sensitive phenomenological operator	B	Discrete-symmetry classification of the vector bilinear
Locality/cluster prerequisite for full CPT closure	Open	OP-Loc1
Full CKM/PMNS-scale flavour closure	Open	Systematised in §9.7; quantitative derivation remains under OP-Yukawa / OP-generations

This architectural contribution is recorded in the global Level-4 self-consistency checklist (§19.3).

## 9.5 Anomaly architecture of the emergent chiral gauge sector

*Status: consistency architecture. This subsection systematises what ECT inherits, what it already captures at the reconstructible ordered-branch electroweak level, and what remains open about the quantum consistency of the emergent chiral gauge sector. It is a consistency architecture, not a first-principles derivation of Standard-Model representation content. Layers A and B correspond to group-theoretic inputs and inherited anomaly consistency in reconstructible local sectors; Layer C isolates the full Standard-Model completion and the ECT-native interpretation of the mixed  $U(1)_Y$ -gravitational condition in the emergent-graviton setting.*

**Transition from the discrete-symmetry subsection.** The previous subsection (§9.4) established the discrete-symmetry backbone of the emergent matter sector: geometric precursors of  $P$  and  $T$  from  $O(4)$  reflections, a group-theoretic basis for  $C$ , and a conditional CPT route for reconstructible local sectors. With these ingredients in place, the natural next consistency question is whether the emergent chiral gauge sector is quantum-mechanically consistent at the loop level. Anomaly cancellation is a *non-negotiable self-consistency requirement* already recorded in the gauge-sector discussion (§48.13, “Anomaly cancellation as a self-consistency requirement”): any acceptable fermionic completion of the ordered-branch gauge sector must satisfy it, otherwise the emergent gauge theory is inconsistent, contradicting the existence of the ordered branch itself. The present subsection organises the resulting architecture into three layers and attaches each outcome to the already-existing unification programme; the associated open problems are recorded in the existing OP-GUT unification programme, in particular OP-GUT3b and the OP-GUT6 consistency family (Table 118).

## Layer A: Topological and group-theoretic inputs

**A1. Load-bearing homotopy facts.** The relevant topological inputs for the anomaly-architecture discussion are:

- $\pi_4(SU(2)) = \mathbb{Z}_2$  — Witten global-anomaly topology [78];
- $\pi_3(SU(N)) = \mathbb{Z}$  for  $N \geq 2$  — Chern–Pontryagin density / instanton background relevant to the ABJ structure;
- $\pi_1(U(1)) = \mathbb{Z}$  — charge quantisation lattice established in Theorem 23.1 (§48.13).

All three are Level A: group theory.

**A2. Ordered-branch chirality selection.** One chiral factor of  $Spin(4) \simeq SU(2)_L \times SU(2)_R$  is dynamically selected by the ordered-branch orientation (§9.3 and §9.4, Layer A). The selected chirality is labelled  $L$  by convention matching the observed weak interactions; Level B (structural route from the chirality-selection mechanism).

## Layer B: Inherited anomaly consistency of the reconstructible electroweak ordered-branch sector

**B1. Osterwalder–Schrader reconstruction enables standard one-loop analysis.** Once the Osterwalder–Schrader reconstruction closes for the local chiral gauge EFT (prerequisite inherited from §9.4, Layer B), the standard Adler–Bell–Jackiw one-loop analysis applies directly to the reconstructed Lorentzian theory [75, 70, 71]. ECT inherits the framework; it does not formulate a new ECT-specific anomaly theorem. This is a Level B inheritance, conditional on OS closure.

**B2. Anomaly consistency conditions in the unified left-handed Weyl convention.** We adopt the unified left-handed Weyl convention throughout this subsection. Fermions are expressed as left-handed Weyl fields  $Q, u^c, d^c, L, e^c$  (and optionally  $\nu^c$ ). The Standard-Model hypercharge assignments in this convention are:

$$Y_Q = +\frac{1}{6}, \quad Y_{u^c} = -\frac{2}{3}, \quad Y_{d^c} = +\frac{1}{3}, \quad Y_L = -\frac{1}{2}, \quad Y_{e^c} = +1, \quad Y_{\nu^c} = 0. \quad (9.18)$$

The four local anomaly cancellation conditions are then:

$$[SU(3)]^2 U(1)_Y : \quad 2Y_Q + Y_{u^c} + Y_{d^c} = 0, \quad (9.19)$$

$$[SU(2)]^2 U(1)_Y : \quad 3Y_Q + Y_L = 0, \quad (9.20)$$

$$[U(1)_Y]^3 : \quad 6Y_Q^3 + 3Y_{u^c}^3 + 3Y_{d^c}^3 + 2Y_L^3 + Y_{e^c}^3 (+Y_{\nu^c}^3) = 0, \quad (9.21)$$

$$U(1)_Y\text{-grav}^2 : \quad 6Y_Q + 3Y_{u^c} + 3Y_{d^c} + 2Y_L + Y_{e^c} (+Y_{\nu^c}) = 0. \quad (9.22)$$

Scope labels: (9.20) is already meaningful at the electroweak ordered-branch level; (9.22) is likewise meaningful once the charged matter content of the reconstructible ordered-branch sector is specified; (9.19) and (9.21) depend on the full Standard-Model completion and are therefore discussed in Layer C.

**B3. Hard disclaimer.** In the presently reconstructed ordered-branch electroweak sector, the  $[SU(2)]^2 U(1)_Y$  condition (9.20) is already meaningful as an inherited consistency constraint. The mixed  $U(1)_Y$ -gravitational condition (9.22) is likewise meaningful once the charged matter content of the reconstructible ordered-branch sector is specified. By contrast, the  $[SU(3)]^2 U(1)_Y$  condition (9.19) and the  $[U(1)_Y]^3$  condition (9.21) belong to the full Standard-Model completion and therefore remain conditional on the colour-sector origin (OP-GUT1) and on the derivation of the full fermion representation content and observed charge assignments (OP-GUT2, OP-GUT3b). F4 does not claim full Standard-Model anomaly closure inside current ECT; it systematises the anomaly architecture and identifies which consistency conditions are already meaningful in the ordered-branch electroweak sector and which still depend on the open colour/matter completion.

**B4. The preferred-direction operator  $\mathcal{L}_5$  is anomaly-transparent.** The preferred-direction operator

$$\mathcal{L}_5 = \mu_5 \bar{\Psi} \gamma^\mu n_\mu \Psi, \quad (9.23)$$

re-classified in §9.4, Layer C as a CPT-odd, CP-odd, C-odd, P-even, T-even branch operator, does *not* alter the chiral representation content of the fermions, their gauge charges, or the anomaly coefficients entering the anomaly polynomial. It is a background-vector bilinear insertion in the ordered-branch EFT, not a change in gauge representation data. Therefore it can affect branch-level phenomenology, dispersion relations, and discrete-symmetry properties, but it does not modify the standard chiral anomaly constraints of the emergent gauge sector.

The anomaly coefficients are determined by the chiral representation content and gauge charges, not by background-vector bilinear insertions that leave this representation data unchanged. In this sense the anomaly structure is insensitive to the preferred-direction deformation  $\mathcal{L}_5$ : the operator modifies branch-level phenomenology, but not the anomaly coefficients entering the standard consistency conditions.

In this sense the F3 reclassification of  $\mathcal{L}_5$  has a concrete F4 payoff: despite being CPT-odd at the branch level,  $\mathcal{L}_5$  is *anomaly-transparent* with respect to the standard gauge-anomaly consistency conditions. This is a clean structural bridge from §9.4 to the present subsection. Flavour structure is similarly anomaly-decoupled, as discussed in §9.7, Layer B5.

**B5. Witten global anomaly.** The standard Witten requirement is that the number of left-handed  $SU(2)$  doublets be even. Per SM-like generation there are three coloured quark doublets  $Q$  plus one lepton doublet  $L$ , giving four doublets per generation; for an SM-like generation structure this gives  $4N_{\text{gen}}$ , which is even for any integer  $N_{\text{gen}} \geq 1$ . In ECT this is inherited as a consistency test once the fermion spectrum is fixed; it is automatically satisfied for an SM-like generation structure, but is not yet a first-principles derivation of that structure (OP-GUT5).

**B6. Connection to the instanton sector.** The triangle anomaly is structurally related to instanton-induced chiral charge violation through the Chern–Pontryagin density  $\text{tr} F \wedge F$ . In this sense the anomaly architecture discussed here is naturally connected to the instanton sector already explored elsewhere in the manuscript. In particular, the standard relation between the ABJ anomaly and nonperturbative  $SU(2)$  topological transitions carries over, on the same conditional basis as in B1 above, to the reconstructible ordered-branch sector of ECT.

### Layer C: Full Standard-Model completion and the emergent-graviton aspect

**C1. Specific hypercharge derivation remains open.** The specific values in (9.18) remain Standard-Model input; their derivation from condensate dynamics is recorded as OP-GUT3b and remains Open.

**C2. Scope of full Standard-Model anomaly closure.** The  $[SU(3)]^2 U(1)_Y$  condition (9.19) is directly conditional on the colour-sector completion (OP-GUT1). The  $[U(1)_Y]^3$  condition (9.21) depends on the full chiral matter content and the observed hypercharge assignments, and therefore remains conditional on the combined completion of the matter-representation problem (OP-GUT2) and the observed charge-assignment problem (OP-GUT3b). Thus the full Standard-Model anomaly closure remains completion-dependent in current ECT.

**C3. Mixed  $U(1)_Y$ -gravitational anomaly in the emergent-graviton setting.** In ordinary 3+1-dimensional chiral gauge theory the relevant local gravitational consistency condition is the mixed  $U(1)_Y$ -gravitational anomaly constraint

$$\sum_i Y_i = 0 \quad (9.24)$$

over left-handed Weyl fermions. A local pure gravitational anomaly is not present in the ordinary 4D setting. The ECT-specific question is therefore not whether a new 4D pure gravitational anomaly appears,

but how the standard mixed  $U(1)_Y$ -gravitational consistency condition should be interpreted when the graviton itself is emergent from condensate collective modes rather than fundamental at the pre-emergent level.

Since the ordered branch distinguishes a preferred direction  $n^A$ , the detailed ECT interpretation of gravitational consistency conditions should eventually be formulated in the language appropriate to the emergent condensate background rather than assumed from the outset. However, the present work does not establish any modification of the standard mixed  $U(1)_Y$ -gravitational condition. The conservative and technically correct statement is that ECT is expected to reproduce the usual long-wavelength condition (9.24), while its precise pre-emergent interpretation remains open (OP-GUT6c).

**C4. 't Hooft matching: outlook.** A more ambitious future question is whether exact global symmetries of the ordered-branch pre-SM sector admit a meaningful 't Hooft anomaly-matching analysis with the infrared effective theory. Since the relevant exact global symmetries of the current ECT UV architecture have not yet been fully identified, this lies beyond the scope of the present subsection.

**Anomaly cancellation does not explain the generation count.** Anomaly cancellation does not explain the existence of exactly three generations. That question remains part of the broader flavour/generation problem (OP-GUT5) and lies outside the present anomaly-architecture result.

**Disentanglement of three notions of “anomaly”.** It is useful to keep three logically distinct notions separate: (i) local ABJ triangle anomalies in reconstructible local sectors (Level B, conditional on OS); (ii) global topological Witten anomaly tied to  $\pi_4(SU(2))$  (Level A for topology, Level B for numerical check once the fermion spectrum is fixed); (iii) 't Hooft anomaly matching between UV and IR descriptions, treated here only as a longer-term outlook.

**Consistency bridge.** The present subsection should therefore be read as a consistency bridge: it shows that current ECT is compatible with the standard anomaly template of a reconstructible ordered-branch chiral gauge sector, while leaving the full Standard-Model completion problem explicitly open.

**Table 43:** Anomaly architecture of the emergent chiral gauge sector: status summary.

Statement	Status	Comment
Compact $U(1)$ phase, charge lattice $q \in \mathbb{Z} \cdot e_0$	A	Theorem 23.1 (§48.13)
Ordered-branch chiral $SU(2)$ selection	B	§9.3 and §9.4, Layer A
$\pi_4(SU(2)) = \mathbb{Z}_2$ Witten input	A	Group theory
Standard one-loop anomaly analysis in reconstructible local sectors	B	Conditional on OS / local EFT closure
$[SU(2)]^2 U(1)_Y$ condition	B	Meaningful already at the electroweak ordered-branch level
Mixed $U(1)_Y$ -gravitational condition	B / conditional	Meaningful once the charged matter content of the reconstructible ordered-branch sector is specified
$[SU(3)]^2 U(1)_Y$ and $[U(1)_Y]^3$ conditions	Conditional / Open	Depend on colour-sector and full matter completion (OP-GUT1, OP-GUT2, OP-GUT3b)
$\mathcal{L}_5$ does not modify anomaly coefficients	B	Vector bilinear; representation data unchanged



Statement	Status	Comment
Witten anomaly test for the emergent chiral $SU(2)$ sector	B	Once the fermion spectrum is fixed; automatic for an SM-like generation structure
Specific observed hypercharge assignments from condensate dynamics	Open	OP-GUT3b
ECT interpretation of mixed $U(1)_Y$ -gravitational condition with emergent graviton	Open	Extension OP-GUT6c
$N_{\text{gen}} = 3$ from anomaly cancellation	No	Not constrained by anomalies alone (OP-GUT5)

Its whole-framework consistency status is recorded in the global Level-4 self-consistency checklist (§19.3).

## 9.6 Yukawa couplings and fermion masses

*Status: Level C phenomenological embedding. Yukawa couplings and fermion masses are not derived from the ECT condensate action; they are imposed as Standard-Model input. The mass formula  $m_f = y_f v_2$  has the same structure as in the SM, up to the field-normalisation convention adopted for the embedded electroweak sector. Possible condensate-sector corrections are discussed in Section 8.7.*

Once fermionic fields  $\Psi$  are admitted as additional spinorial degrees of freedom compatible with the ordered branch (Section 9.1), their masses arise from Yukawa couplings to the electroweak condensate sector:

$$\mathcal{L}_{\text{Yukawa}}^{\text{eff}} \sim y_f \bar{\psi}_L \Phi_{\text{ew}} \psi_R + \text{h.c.} \quad \Rightarrow \quad m_f = y_f v_2, \quad (9.25)$$

where  $\Phi_{\text{ew}}$  denotes the electroweak-like condensate field of the embedded low-energy sector, not the fundamental bare condensate field  $\Phi$  of the primary ECT action. The Yukawa term is written schematically, at the level of the embedded electroweak EFT. Here  $y_f$  is the Yukawa coupling constant for fermion species  $f$ , and  $v_2 \approx 246 \text{ GeV}$  is the electroweak condensate scale (Section 7.4). This is the same mass formula as in the Standard Model. This relation is written in the normalisation convention adopted for the embedded electroweak sector in the present article; numerical factors such as  $1/\sqrt{2}$  depend on the field normalisation convention. The coupling  $y_f$  is not derived from condensate microphysics; it is a free matching parameter (Level C).

**Chiral structure of the Yukawa coupling.** In the Standard Model, the Yukawa interaction couples left- and right-chiral fermion sectors through the electroweak scalar, schematically as  $y_f \bar{\psi}_L \Phi_{\text{ew}} \psi_R + \text{h.c.}$  Within ECT, the distinction between  $\psi_L$  and  $\psi_R$  has a structural background in the  $Spin(4) \simeq SU(2)_L \times SU(2)_R$  decomposition and in the chirality discussion of Section 9.3. This means that a left-right Yukawa bilinear is *compatible with* the ECT chirality framework. However, neither the detailed electroweak representation assignments nor the numerical Yukawa couplings are derived from condensate dynamics: the Yukawa sector remains an external low-energy embedding.

**Yukawa hierarchy: structural route.** The observed fermion masses span more than five orders of magnitude (from the electron mass  $m_e \approx 0.511 \text{ MeV}$  to the top quark mass  $m_t \approx 173 \text{ GeV}$ ), corresponding to Yukawa couplings from  $y_e \approx 2 \times 10^{-6}$  to  $y_t \approx 0.99$ . If the three fermion generations correspond to distinct normalizable fermionic modes  $\psi_i$  in the post-transition condensate background (see below), then the Yukawa matrix is not arbitrary but is determined by overlap integrals:

$$Y_{ij} \sim \int d^3x \psi_i^\dagger(x) \mathcal{H}(x) \psi_j(x), \quad (9.26)$$

where  $\mathcal{H}(x)$  is the effective Higgs/condensate coupling profile. If the modes are quasi-localised with characteristic inverse localisation lengths  $\kappa_i$ , then  $Y_i \sim e^{-S_i}$  with  $S_i \propto \kappa_i$ , and the hierarchy arises from moderate differences in effective action: for the up-type sector,  $\Delta S_{c/t} \approx \ln(y_t/y_c) \approx 4.9$  and  $\Delta S_{u/t} \approx \ln(y_t/y_u) \approx 11.3$ ; for the charged-lepton sector,  $\Delta S_{\mu/\tau} \approx 2.8$  and  $\Delta S_{e/\tau} \approx 8.1$ . These moderate values ( $\Delta S \sim 3\text{--}11$ ) show that the observed mass hierarchies do not require extreme tuning but are quantitatively plausible within an overlap/tunnelling origin. The leading-order Yukawa matrix is naturally near-rank-1:  $Y \approx Y^{(0)} + \delta Y$  with  $\text{rank}(Y^{(0)}) = 1$ ,  $\|\delta Y\| \ll \|Y^{(0)}\|$ , giving one heavy and two exponentially lighter generations.

This route is Level B/C: the structural mechanism is identified but the explicit computation of  $Y_{ij}$  from condensate microphysics remains open (OP-Yukawa). Details are in Appendix Z. The flavour architecture connecting the Yukawa overlap mechanism to CKM mixing and the seesaw embedding to PMNS is systematised in §9.7.

**Three fermion generations: spectral route.** The Standard Model contains exactly three generations of quarks and leptons. In ECT, the most promising route to this number is through the spectral structure of the post-transition condensate background. If fermions experience an effective potential from the condensate profile (e.g. of kink/domain-wall type), the number of normalizable bound states is controlled by the dimensionless ratio

$$\nu \sim \frac{y}{\sqrt{2\lambda_{\text{eff}}}}, \quad (9.27)$$

where  $y$  is an effective Yukawa coupling and  $\lambda_{\text{eff}}$  is the effective quartic parameter controlling the local post-transition profile in the toy spectral model. It should not be identified automatically with the fundamental bare quartic of the full ECT condensate action. In toy models of Pöschl–Teller type, the number of light fermionic bound states is  $N_{\text{gen}} \approx \lfloor \nu \rfloor$ . In the toy spectral model, three generations require  $3 \leq \nu < 4$ , i.e.  $y \sim 1.3\text{--}2.0$  for  $\lambda_{\text{eff}} \sim 0.10\text{--}0.13$ . This should be read only as a naturalness window for an effective profile model, not as a completed derivation from the fundamental ECT parameters. This is a natural range of order unity, requiring no extreme tuning.

A complementary topological route uses the index of the internal Dirac operator in the condensate background:  $N_L - N_R = \text{Index}(D_{\text{int}})$ , which can protect the family number as a spectral-topological invariant.

Both routes translate the generation problem into a concrete spectral task: counting the normalizable fermionic zero/quasi-zero modes supported by the post-transition condensate background. At the present stage, this is Level B/C: the structural mechanism is identified, the required parameter ranges are natural, but a strict derivation of exactly three generations from the ECT condensate profile has not been completed (OP-generations). Details are in Appendix Z.

**Possible condensate-sector corrections.** In the three-scale picture of ECT (Section 5.1), the primary condensate scale  $\phi_0 \sim \bar{M}_{\text{Pl}}$  is separated from the electroweak scale  $v_2 \approx 246\text{ GeV}$  by many orders of magnitude. If the two condensate sectors are not perfectly decoupled, higher-dimension operators suppressed by the primary condensate scale (or by the corresponding primary radial threshold) could induce small corrections to the low-energy Yukawa relations. After electroweak condensation these corrections would typically be organised as powers of  $v_2/\phi_0$  in the effective expansion. This possibility is discussed qualitatively in Section 8.7; at the present stage ECT does not predict the size of such effects (Level C).

**Connection to the neutrino sector.** In the present ECT formulation, neutrino masses are treated through a separate embedded mechanism beyond the minimal charged-fermion Yukawa structure; the seesaw-type discussion is given in Section 8.9.

**What is and is not derived here.** This subsection imposes the Standard-Model Yukawa structure as external input at Level C, but identifies structural routes toward derivation at Level B/C. ECT provides:

(i) the geometric and chirality framework (Sections 9.1–9.3) within which the Yukawa coupling can be consistently written; (ii) a spectral route to the generation number through fermionic bound-state counting in the condensate background (§9.6); (iii) an overlap/tunnelling mechanism for hierarchical Yukawa couplings (§9.6). The numerical values of  $y_f$  and the exact generation number remain open calculational targets (Appendix Z).

**Status summary.**

Statement	Status	Comment
Mass formula $m_f = y_f v_2$	C	SM embedding; $y_f$ not derived
Chiral structure of Yukawa coupling compatible with the ECT chirality framework	B/C	Structural consistency only; representation content and couplings not derived
Yukawa hierarchy	B/C	Structural route via overlap/tunnelling (§9.6); explicit computation open (OP-Yukawa)
Three fermion generations	B/C	Spectral route via bound-state counting (§9.6); strict derivation open (OP-generations)
Condensate-sector corrections to $y_f$	C	Possible in principle; size not predicted
Neutrino mass mechanism	C	Seesaw-type embedding; Section 8.9

## 9.7 Flavour architecture of the emergent matter sector: CKM and PMNS in ECT

*Status: systematisation, not derivation. Sections 9.4 and 9.5 established the discrete-symmetry and anomaly backbone of the emergent chiral gauge sector. With three fermion generations and the Yukawa structure taken as external input (§9.6, OP-Yukawa, OP-generations), the natural next question is whether the observed flavour structure—the CKM quark-mixing matrix and the PMNS lepton-mixing matrix—admits any ECT-native framing. This subsection is a consistency architecture, not a first-principles derivation. Layer A records group-theoretic inputs; Layer B organises structural routes already present in the preprint; Layer C identifies open targets and concluding remarks. The three concrete derivation targets (CKM hierarchy, PMNS angles and CP phases, absolute neutrino spectrum) all fall under the existing flavour open-programme labels OP-Yukawa and OP-generations, with broader unification-level bookkeeping recorded under OP-GUT5 in Table 118. It should therefore be read as a unifying flavour bridge across the already existing Yukawa and neutrino subsections, not as a replacement for either of them.*

**Transition from the anomaly subsection.** The previous subsection (§9.5) showed that the emergent chiral gauge sector inherits the standard anomaly-cancellation framework at the electroweak ordered-branch level, with the preferred-direction operator  $\mathcal{L}_5$  being anomaly-transparent. A natural next question is how the off-diagonal flavour structure—the CKM and PMNS mixing matrices, the associated CP phases, and the absolute neutrino spectrum—relates to the already-established Yukawa-overlap mechanism of §9.6 and the seesaw embedding of §8.9.

### Layer A: Group-theoretic and structural inputs

**A1. Flavour-group bookkeeping.** In an SM-like three-generation chiral matter sector without explicit sterile-neutrino fields, the maximal flavour symmetry of the kinetic terms is

$$G_F^{\text{SM}} = U(3)_Q \times U(3)_{u^c} \times U(3)_{d^c} \times U(3)_L \times U(3)_{e^c}. \quad (9.28)$$

If the heavy sterile-neutrino sector is included explicitly (as structurally preferred in the seesaw embedding of §8.9), this is enlarged by an additional factor  $U(3)_N$  before the Majorana mass term is introduced; the Majorana sector then breaks part of this symmetry further. In the present subsection this distinction is used only as group-theoretic bookkeeping; no new flavour symmetry is derived from the condensate microdynamics.

**A2. Parameter counting.** For three generations the physical-parameter count is the standard one:

- CKM: 3 angles + 1 CP phase = 4 parameters;
- PMNS (Dirac case): 3 angles + 1 Dirac CP phase = 4 parameters;
- PMNS (Majorana case, as structurally preferred by the seesaw embedding of §8.9): + 2 Majorana phases = 6 parameters.

**A3. Three generations as external input.** The number of fermion generations  $N_{\text{gen}} = 3$  remains external input at the present stage (OP-generations; §9.6, §9.6), addressed via the spectral route of the Yukawa subsection rather than within the flavour-architecture discussion presented here.

## Layer B: Structural routes already present, now unified

**B1. CKM as basis misalignment.** The CKM matrix

$$V_{\text{CKM}} = U_u^\dagger U_d, \quad (9.29)$$

arising from the misalignment between up-type and down-type Yukawa diagonalising rotations, is a standard feature of chiral gauge theories with Yukawa couplings. This is a Level A structural input; its specific numerical entries are not an ECT output.

**B2. Overlap-mechanism route to hierarchical CKM.** In the overlap/localisation picture of §9.6, hierarchical quark mixing is naturally associated with small off-diagonal overlap integrals between quasi-localised generation profiles. This makes a Wolfenstein-like hierarchy structurally plausible:

$$|V_{us}| \gg |V_{cb}| \gg |V_{ub}|, \quad (9.30)$$

with  $V_{\text{CKM}}$  remaining close to the identity. What ECT can presently claim is qualitative compatibility of the observed hierarchical pattern with exponentially suppressed inter-generation overlaps. It does not yet derive the specific numerical value of the Wolfenstein parameter  $\lambda$ , nor the higher parameters  $A$ ,  $\bar{\rho}$ ,  $\bar{\eta}$  (Level B; numerical derivation Open under OP-Yukawa).

**B3. “CKM small / PMNS large” as structural narrative.** The lepton sector plausibly differs structurally from the quark sector because charged leptons are governed by the same Yukawa-overlap logic as the charged fermions of §9.6, whereas light neutrinos arise through the separate seesaw/Weinberg-operator completion discussed in §8.9. This makes a stronger basis misalignment in the lepton sector structurally plausible and provides a natural ECT narrative for the empirical “CKM small / PMNS large” dichotomy. However, the present framework does not derive the PMNS angles quantitatively (Level B/C; narrative structural, quantitative derivation Open under OP-Yukawa).

**B4. CP phases live in the effective flavour structures.** In the present ECT framing, complex flavour phases may arise in the effective Yukawa matrices and, in the neutrino sector, also in the sterile/Majorana mass structure of the seesaw completion. This is the appropriate flavour-sector completion of the “complex flavour phases” already invoked in the F3 baryogenesis discussion (§16.3). What can be claimed now is only that ECT has a structurally well-defined place where CKM and PMNS CP phases may enter: in the

effective flavour matrices of the quark sector and, for neutrinos, in the combined Yukawa-plus-seesaw structure. The present framework does not derive the observed values of  $\delta_{\text{CKM}}$ ,  $\delta_{\text{PMNS}}$ , or the Majorana phases (Level B/C; values Open under OP-Yukawa).

**B5. Flavour structure is anomaly-decoupled.** The flavour structure ( $Y_u, Y_d, Y_e, Y_\nu$  matrices) does not enter the anomaly coefficients of the chiral gauge sector; those coefficients depend only on the chiral representation content and the gauge charges (§9.5, Layer B4). Flavour is therefore anomaly-decoupled, in the same sense as the preferred-direction coupling  $\mathcal{L}_5$  is anomaly-transparent. This is the second structural payoff of the F3–F4–F8 chain (Level B).

**B6. Near-alignment of flavour rotations in the overlap picture.** The near-rank-1 structure of the leading-order Yukawa matrix (§9.6,  $Y \approx Y^{(0)} + \delta Y$  with  $\text{rank}(Y^{(0)}) = 1$ ) naturally favours near-alignment of the diagonalising rotations in flavour space. This makes the observed smallness of quark flavour mixing structurally plausible and helps maintain compatibility with the strong empirical suppression of flavour-changing processes. The standard GIM mechanism itself remains the usual one of the reconstructed electroweak theory; the ECT contribution here is a structural route to the near-alignment that makes such suppression natural rather than accidental (Level B/C; structural route, not a derivation of specific FCNC rates).

**B7. PMNS/MSW phenomenological stability.** A useful stabilising feature of the ECT flavour architecture is that it does not spoil the standard leading-order PMNS/MSW oscillation framework already retained in the neutrino sector (§8.9); the open problem is not whether flavour phenomenology survives, but whether its detailed textures and parameters can be derived (Level B; consistency check inherited from the neutrino discussion). This stabilising point is already established in the neutrino sector (§8.9) and is recorded here only as part of the unified flavour architecture.

### Layer C: Open targets and concluding remarks

**C1. Open programme under existing umbrella labels.** No new formal OP-IDs are introduced by F8. The three concrete derivation targets recorded here fall under the existing flavour open-programme labels:

- CKM mixing angles and Wolfenstein hierarchy (OP-Yukawa);
- PMNS angles and Dirac/Majorana CP phases (OP-Yukawa, with the neutrino-sector discussion in §8.9);
- absolute neutrino spectrum and ordering (OP-Yukawa / neutrino programme).

Broader unification-level bookkeeping is recorded under OP-GUT5 in Table 118, while the detailed local flavour bookkeeping remains under OP-Yukawa and OP-generations in the fermionic-sector discussion.

**C2. Geometric anchor and the absolute neutrino scale.** The geometric anchor  $M_R^{\text{geom}} = \sqrt{\phi_0 v_2}$ , already discussed in the neutrino sector (§8.9), provides a natural scale at which the light-neutrino spectrum is pinned in the seesaw embedding. What remains open is the detailed internal hierarchy, ordering, and phase structure of the three light states on top of this anchor. Thus the present flavour subsection treats  $M_R^{\text{geom}}$  as a scale-setting consistency input rather than as a full derivation of the neutrino spectrum.

**C3. Baryogenesis connection.** The flavour architecture clarifies the flavour-sector part of the CP-violation bookkeeping used in the baryogenesis discussion (§16.3): ECT contains a branch-level CP/CPT-odd channel through  $\mathcal{L}_5$  (F3), while the fermionic completion may contain additional complex flavour phases in the quark and especially lepton sectors. In the present framework the baryogenesis estimate remains tied to the leptogenesis-style assumptions already stated in §16.3; F8 does not claim that the CKM phase alone explains the observed baryon asymmetry.

**C4. Strong CP problem: longer-term outlook.** A longer-term question is how the flavour sector, the instanton/ $\theta$ -sector, and the open colour completion combine in the ECT framing of the strong CP problem; this remains outside the scope of the present subsection.

**Disentanglement of three flavour-related notions.** It is useful to keep three notions separate:

- (i) flavour mixing itself (CKM/PMNS matrices as basis misalignment);
- (ii) CP-violating flavour phases in the effective quark/lepton mass structures;
- (iii) baryogenesis, which in the present framework still relies on the leptogenesis-style assumptions of §16.3 and uses the flavour phases only as part of its CP-violation bookkeeping.

All three coexist within the ECT architecture without contradiction.

**Table 45:** Flavour architecture of the emergent matter sector: status summary.

Statement	Status	Comment
Standard flavour-group bookkeeping for three-generation matter sectors	A	Optional sterile-sector extension for seesaw
CKM as basis misalignment between up- and down-sector diagonalisation	A	Standard field-theory structure
ECT overlap mechanism provides a structural route to hierarchical CKM mixing	B	Qualitative, not numerical
ECT gives a natural narrative for “CKM small / PMNS large” via different charged- and neutral-lepton mechanisms	B/C	Structural, not quantitative
Complex flavour phases have a structurally well-defined place in the effective Yukawa / seesaw sector	B/C	Not derived
Flavour structure is anomaly-decoupled	B	Extends F4
Near-alignment of flavour rotations is structurally natural in the overlap picture	B/C	Helps maintain FCNC suppression; distinct from the GIM mechanism itself
PMNS/MSW phenomenology remains intact at leading order	B	Already retained in the neutrino sector
Exact CKM/PMNS parameters, CP phases, and neutrino spectrum from condensate dynamics	Open	Under OP-Yukawa / OP-generations
$N_{\text{gen}} = 3$ from ECT	Open	Outside F8; OP-generations

The resulting flavour-architecture status is recorded in the global Level-4 self-consistency checklist (§19.3).

## 9.8 ECT-specific fermion–condensate coupling

*Status: layered A/B/C bridge. The existence of the preferred direction  $n_A$  after  $O(4) \rightarrow O(3)$  is a structural Level A consequence of the ordered branch. Within a parity-even, zeroth-derivative fermionic EFT, the operator  $n_A \bar{\Psi} \gamma^A \Psi$  is the leading ECT-specific fermion bilinear (Level A/B conditional on the EFT basis). Its coefficient is not derived from condensate microphysics. The full operator analysis is given in Section 7.6 and Appendix U; full phenomenology is developed in Section 7.*

This subsection gives the fermionic-sector bridge to the ECT-specific preferred-direction coupling. Its

detailed operator classification, dimensional analysis, Lorentzian reduction, and observability caveats are developed in Section 7.6 and Appendix U. Its detailed phenomenology, observational constraints, and falsification tests are developed separately in Section 7.

The symmetry breaking  $O(4) \rightarrow O(3)$  introduces a preferred condensate direction

$$n_A \equiv \frac{\partial_A \Phi}{|\partial \Phi|}, \quad (9.31)$$

which is a derived orientational variable of the ordered branch. Within the parity-even, zeroth-derivative low-energy fermionic EFT, the leading ECT-specific deformation of the Dirac operator is

$$\Delta \mathcal{L} = \mu_5 \bar{\Psi} \gamma^A n_A \Psi, \quad (9.32)$$

where  $\mu_5$  has mass dimension one.

Equivalently, one may parameterise

$$\mu_5 = \beta_5 m_f, \quad \beta_5 \sim \frac{m_f}{\phi_0}, \quad \mu_5 \sim \frac{m_f^2}{\phi_0}, \quad (9.33)$$

as an EFT-level dimensional estimate. This scaling should be read as a low-energy consistency estimate, not as a first-principles derivation from the microscopic condensate action.

In the exact Lorentz-symmetric low-energy limit this operator would be absent. Its presence therefore parametrises a residual sensitivity of the fermion sector to the preferred condensate direction.

Its main structural features are:

- it introduces preferred-direction corrections to the emergent Lorentz-invariant fermion sector through the condensate direction  $n_A$ ;
- it is absent in the minimal Standard Model fermion sector and therefore represents a genuinely ECT-specific deformation of the low-energy Dirac operator;
- its coefficient is Planck-suppressed at the EFT level, with the dimensionless ratio expected to scale as  $\beta_5 \sim m_f/\phi_0$ .

As discussed in Section 9.3, this coupling shares a common geometric source with the chiral-selection problem: both are controlled by the preferred condensate direction  $n_A$  of the ordered branch.

**What is and is not derived here.** What is structurally established is the existence of the preferred direction  $n_A$  and, within the stated EFT basis, the admissibility of the operator  $n_A \bar{\Psi} \gamma^A \Psi$  as the leading parity-even zeroth-derivative deformation of the fermion sector. What is not derived is the microscopic coefficient of this operator. Accordingly, the estimate  $\beta_5 \sim m_f/\phi_0$ , equivalently  $\mu_5 \sim m_f^2/\phi_0$ , should be read as EFT-level dimensional scaling. The physical observability of the coupling in the Lorentzian low-energy limit depends on additional issues such as species dependence, background gradients, and environment; these are analysed in Section 7.6.

#### Status summary.

Statement	Status	Comment
Preferred direction $n_A$ after SSB	A	Structural consequence of $O(4) \rightarrow O(3)$
Leading parity-even zeroth-derivative operator $n_A \bar{\Psi} \gamma^A \Psi$	A/B	Strict within the stated EFT basis
Dimensionful coefficient $\mu_5$	A	Required by mass dimension counting

Statement	Status	Comment
$\beta_5 \sim m_f/\phi_0, \mu_5 \sim m_f^2/\phi_0$	B	Dimensional EFT estimate
Common geometric source with chiral asymmetry	B	Both controlled by $n_A$
Coefficient derived from condensate dynamics	Open	Section 9.10

## 9.9 Spin-statistics: structural route and open problem

*Status: Level B structural route. ECT reproduces the correct topological dichotomy of exchange sectors for identical excitations in three spatial dimensions and provides a structural route toward the usual spin-statistics linkage. The full spin-statistics theorem is not derived. Full quantum-sector development: Section 24.4.*

**Why spin-statistics enters the fermionic section.** Sections 9.1–9.2 established that spinorial representations are compatible with the ordered branch and that a Dirac-type equation can be constructed. However, the existence of a spinorial field representation does not by itself fix the quantum exchange law of the corresponding excitations. The question of why half-integer-spin fields are associated with antisymmetric exchange belongs to the broader quantum programme, but it is stated here because it directly concerns the physical interpretation of the fermionic fields introduced in this section.

**Two distinct  $\mathbb{Z}_2$  structures.** It is important to distinguish two different  $\mathbb{Z}_2$  facts that arise in different contexts:

- $\pi_1(SO(3)) = \mathbb{Z}_2$  (Section 9.1): this is the topological fact that makes spinorial representations available through the double cover of the connected rotation group;
- $\pi_1(\mathcal{M}_2) = \mathbb{Z}_2$  (this subsection): this is the topology of exchange classes for two identical excitations in three spatial dimensions.

The first concerns *single-particle representation theory*; the second concerns *many-body exchange topology*. Spinorial transformation law and fermionic exchange law are distinct structures, even though they are linked in relativistic quantum theory. The spin-statistics problem is precisely the problem of linking these two structures.

**Exchange topology.** Here  $\mathcal{M}_2$  denotes the reduced configuration space of two identical excitations in three spatial dimensions, obtained after removing coincidence points and quotienting by particle exchange. Its fundamental group is

$$\pi_1(\mathcal{M}_2) = \mathbb{Z}_2, \quad (9.34)$$

which yields exactly two exchange classes: symmetric and antisymmetric. Because the ordered branch is fixed by the  $O(4) \rightarrow O(3)$  transition to an effectively  $3 + 1$ -dimensional structure, the exchange topology supports only the usual bosonic/fermionic dichotomy for fundamental particle exchange in the primary branch. This does not exclude effective anyonic quasiparticle behaviour in reduced lower-dimensional media, but it does exclude anyonic exchange as the fundamental statistics of the primary ordered branch.

Integer-spin tensorial sectors are compatible with symmetric exchange; half-integer spinorial sectors with antisymmetric exchange. ECT therefore reproduces the correct topological dichotomy and provides a structural route toward the standard spin-statistics linkage. This is not yet the full Pauli–Lüders–Zumino theorem, but it is the correct structural compatibility statement for the ordered branch (Level B). The fuller quantum-sector development is given in Section 24.4.



**What ECT does not yet derive.** ECT does not yet derive:

- (i) the full relativistic spin-statistics theorem;
- (ii) the full operator anti-commutation algebra  $\{\hat{a}_i, \hat{a}_j^\dagger\} = \delta_{ij}$ ;
- (iii) an explicit emergent many-excitation sector decomposition with variable excitation number from condensate dynamics (ECT does not require Fock space as a fundamental postulate, but the effective reconstruction remains open).

Within the fermionic sector, these questions belong to the open programme summarised in Section 9.10 (Open; OP-Q11).

**Status summary.**

Statement	Status	Comment
$\pi_1(SO(3)) = \mathbb{Z}_2$ : spinorial representations available through the double cover	A	Single-particle representation topology
$\pi_1(\mathcal{M}_2) = \mathbb{Z}_2$ : two exchange classes	A	Exchange topology in 3 spatial dimensions
Bosonic/fermionic dichotomy for fundamental exchange in the primary branch	A/B	Topological dichotomy (A); physical interpretation (B)
Half-integer representations compatible with antisymmetric exchange	B	Structural compatibility, not full theorem
Anyonic braid statistics absent for fundamental particle exchange in the primary branch	B	Ordered branch is effectively 3 + 1-dimensional
Full spin-statistics theorem	Open (OP-Q11)	Developed further in Section 24.4
Operator anti-commutation algebra	Open (OP-Q11)	Not yet derived

## 9.10 Open programme and status summary for the fermionic sector

*Status: this subsection collects the open problems and the joint status summary for the fermionic sector (Sections 9.1–9.9). The fermionic sector is among the most heavily embedded parts of ECT: its content is introduced through structural reconstruction on the ordered branch rather than derived from the bare bosonic condensate.*

**Open programme.** To promote the fermionic sector from structural reconstruction to first-principles derivation, the following programme would need to be completed:

- (i) derive the dynamical origin of spinorial fields from the bare bosonic condensate, including their fully induced vierbein/spin-connection coupling on non-uniform condensate backgrounds (currently: external input; Section 9.1);
- (ii) derive fermionic statistics beyond the structural  $\pi_1(\mathcal{M}_2) = \mathbb{Z}_2$  exchange-topology route (currently: Level B compatibility; Section 9.9, Section 24.4);
- (iii) derive the Yukawa coupling pattern and the fermion mass hierarchy (currently: SM input, Level C; Section 9.6);

- (iv) derive the coefficient of the fermion–condensate coupling beyond the dimensional EFT estimate, equivalently derive  $\mu_5$  (or  $\beta_5$  in the parameterisation  $\mu_5 = \beta_5 m_f$ ) from condensate microdynamics (currently: Level B/C; Section 7.6, Appendix U);
- (v) derive the chiral gauge selection  $SU(2)_L$  dynamically (currently: Level B structural possibility; Section 9.3);
- (vi) derive the origin of exactly three fermion generations (currently: no mechanism identified; Section 9.6);
- (vii) derive quantitative atomic consequences of the fermionic reconstruction—in particular the hydrogenic fine structure, the microscopic origin of the fermionic  $g$ -factor, and possible tiny orientation-sensitive corrections to atomic energy levels associated with the preferred-direction/fifth-interaction sector (Section 7.6); this belongs to the interface between the fermionic programme and the phenomenological discriminant programme;
- (viii) **OP-CPT1**: close the conditional CPT route of Section 9.4 for the full nonlinear interacting theory, including the Osterwalder–Schrader reconstruction of interacting local sectors and the associated anti-unitary time-reversal operator (currently: Level B for free/quadratic local sectors; depends on OP-OS1 and OP-Loc1);
- (ix) **OP-CPT2**: derive the complete action of charge conjugation on all emergent charged sectors of ECT, including the compact-phase  $U(1)$  structure and the full Dirac content beyond the group-theoretic basis of Section 9.4, Layer B;
- (x) **OP-P1**: derive the exactly maximal parity-violation pattern of the Standard-Model weak sector from the ordered-branch EFT; the present status provides only a structural route to parity asymmetry (Section 9.4, Layer A);
- (xi) **OP-BRANCH1**: investigate the physical realisation of the branch-pair symmetry architecture of Section 9.4, Layer C, as a CPT-symmetric cosmological pair, including the identification of observational discriminators; currently Level C speculation;
- (xii) **OP-Loc1**: establish the locality and cluster decomposition properties required for the Osterwalder–Schrader reconstruction of full nonlinear interacting ECT, on which OP-CPT1 depends; this is an element of the broader low-energy QFT architecture programme (Section 9.4, Layer B).

None of these steps has been completed. The fermionic sector is a structural reconstruction programme, not a completed derivation from the bare scalar condensate.

**What would Level A look like?** A hypothetical Level A fermionic sector would mean that spinorial excitations emerge as dynamical quasiparticles of the bare bosonic condensate, with their statistics, mass spectrum, and gauge quantum numbers determined by condensate microphysics. An instructive analogy is provided by emergent fermionic quasiparticles in systems such as superfluid  $^3\text{He-A}$  [21], although ECT does not currently provide a comparable microscopic mechanism. The structural route developed in this section should be understood as the present limit of what the framework can establish for fermions. A genuine Level A completion would require qualitatively new input beyond what is currently available in ECT.

**Connections to the broader ECT programme.** Several fermionic open problems are shared with other sectors of the theory:

- the spin-statistics question (ii) connects to the quantum sector (Section 24.4; OP-Q11);
- the fifth-force phenomenology (iv) connects to the phenomenological and macroscopic sectors (Section 7);

- the chiral selection (v) connects to the electroweak embedding (Section 7.4);
- the generation puzzle (vi) remains without a connection to any other part of ECT at the present stage.

**Joint status summary.** The table below gives a condensed overview. Detailed status tables are provided in each subsection.

Subsection	Highest level	Summary
9.1 Spinor structure	A (group theory) / B (physical motivation)	$Spin(4) \simeq SU(2)_L \times SU(2)_R$ ; spinorial reps available; fermions not derived from bare condensate
9.2 Dirac form	B	Structural reconstruction via Clifford linearisation on the emergent metric; connection to $S_{ECT+f}$
9.3 Chirality	B (structural possibility)	SSB provides a structural setting in which chiral asymmetry can arise; selection of $SU(2)_L$ is not derived
9.6 Yukawa / masses	C	SM embedding; hierarchy and three generations open (OP-Yukawa, OP-generations)
9.8 Fermion–condensate coupling	B/C	$\mu_5 \bar{\Psi} \gamma^A n_A \Psi$ ; EFT-level dimensional estimate via $\mu_5 = \beta_5 m_f$ , $\beta_5 \sim m_f / \phi_0$ ; phenomenology in Section 7
9.9 Spin-statistics	A (topology) / B (compatibility)	$\pi_1(\mathcal{M}_2) = \mathbb{Z}_2$ ; for point-particle exchange in 3+1 dimensions this allows only bosonic or fermionic exchange classes; full theorem open (OP-Q11)
<i>Overall</i>		
Fermions as collective condensate excitations	Open	Not derived from bare bosonic action
Full first-principles fermionic sector from P1–P6	Open	Structural reconstruction only

**Spin discreteness and Stern–Gerlach measurements.** The discreteness of spin projections does not arise in ECT from a new dynamical mechanism. It follows, as in standard quantum theory, from the compact representation theory of the rotation group and its spinorial double cover. What ECT adds is a physical origin for why this rotational structure is the relevant one: after the  $O(4) \rightarrow O(3)$  breaking, the ordered branch inherits the residual three-dimensional rotation sector whose spinorial representations are organised by  $SU(2)$ . In a Stern–Gerlach-type measurement, the role of the macroscopic field gradient and detection chain is then to amplify one projection channel into a record-bearing Lorentzian outcome. ECT therefore does not alter the mathematical discreteness of spin. What it adds is a physical reading of why this rotational structure is the relevant one in the ordered branch, and a closure-level reading of how a definite Stern–Gerlach outcome is selected through the same environmental-locking logic used elsewhere in the measurement programme.

**Overall assessment.** At the present stage, the fermionic sector of ECT is best viewed as a coherent structural programme rather than a completed derivation. Its internal logic is more structured than a purely ad hoc SM embedding, because spinor structure, Dirac form, chirality, and the ECT-specific

fermion–condensate coupling are all tied to the ordered branch geometry. At the same time, none of the decisive microscopic steps—fermion emergence, statistics, Yukawa pattern, or generation structure—has yet been derived from the bare condensate action.

## **10 Conclusions of Part I: Foundations**

*This section summarises the foundational construction of ECT established in Part I (Sections 2–9). It collects only the outputs that belong to the foundational branch of the theory, before the macroscopic and quantum-sector developments of Parts II–III. All results are classified by the Level A/B/C/Open discipline maintained throughout the paper. The derivation logic of the foundational construction is shown schematically in Figure 9.*

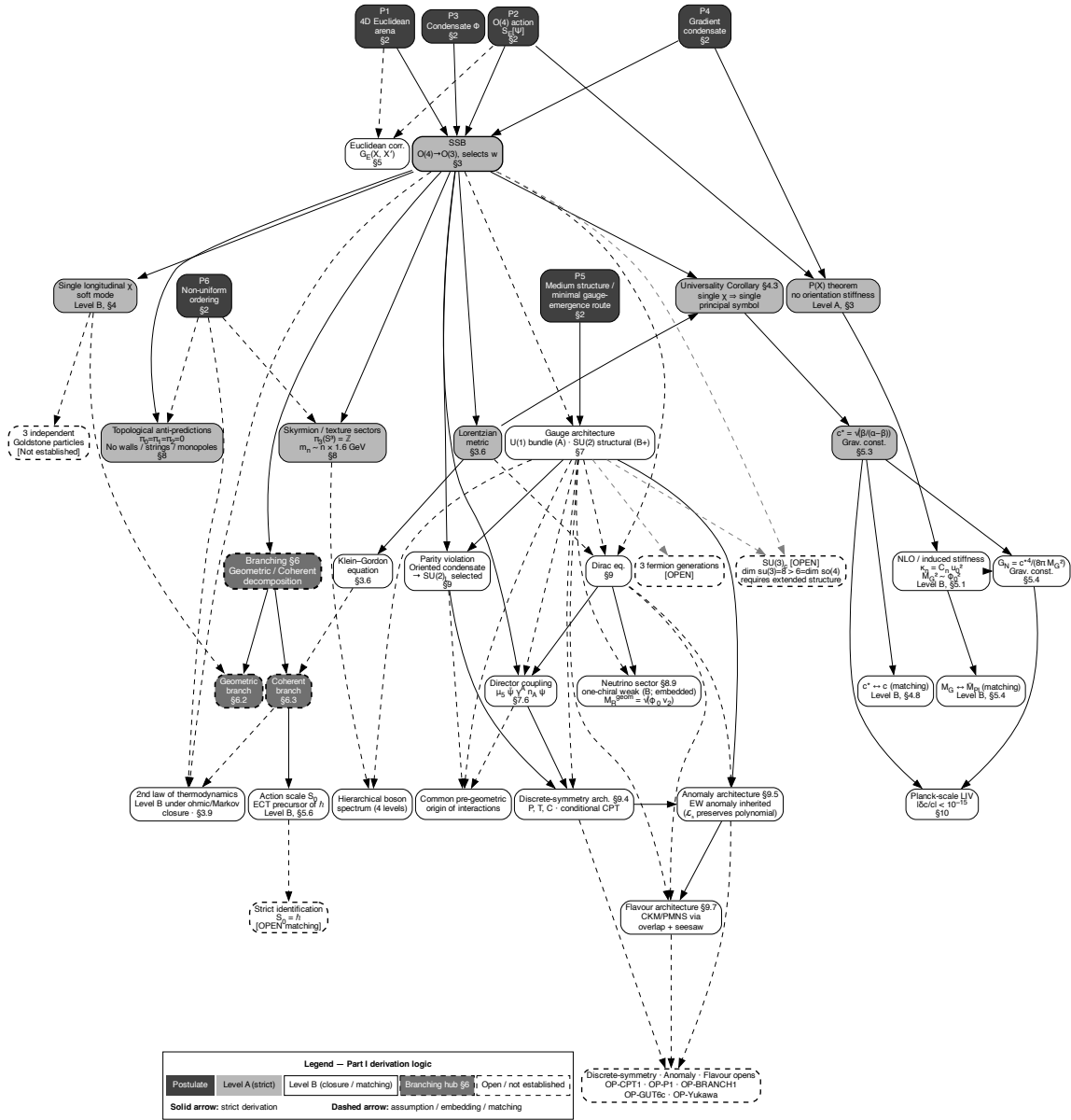


**Figure 9:** Derivation logic of Part I (Foundations). The diagram separates the causal/ordered-branch structure from the phase/winding structure and summarises the foundational outputs of Sections 2–9. Starting from the postulates P1–P6 and the dynamical principle DP, together with the derived coherent-branch rule BR1, the ordered branch first selects the admissible Lorentzian regime  $\alpha > \beta$  at the level of PDE structure, and then fixes the distinguished one-cone realisation  $\alpha = 2\beta$  through the ECT-specific identification  $c_* = c$ . The gravitational normalisation proceeds through the induced/NLO chain  $\kappa_n = \mathcal{C}_n u_0^2 \rightarrow M_G^2 \sim u_0^2/m_\sigma^2 \sim \phi_0^2$ , followed by weak-field matching  $M_G = \bar{M}_{P1}$  (Level B). The phase branch yields the action scale  $S_0$ , whose structural universality across the coherent sector is established at Level A/B, while the physical identification  $S_0 = \hbar$  remains Level B matching. The fermionic/gauge branch includes the  $U(1)$  phase route, the structural  $SU(2)$  embedding, Dirac-form reconstruction, and the ordered-branch origin of the rotational sector relevant for spin. Solid arrows denote strict derivations within the stated EFT level; dashed arrows denote matching, structural identification, or open closure steps. Node shading follows the Level A/B/Open classification used throughout the paper. Open problems are shown as dashed outlines.

**Foundational outcome of Part I.** Part I establishes the minimal ECT core: an  $O(4)$ -invariant scalar medium, a gradient-ordered broken phase with emergent Lorentzian structure, a two-branch architecture, and a layered low-energy sector decomposition. Its strongest positive outputs are the ordered-branch Lorentzian metric sector, the compact-phase  $U(1)$  route, the structural  $SU(2) \times U(1)$  gauge architecture of the ordered branch, the coherent branch rule BR1 with its action-scale logic, and the operator-level identification of the ECT-specific preferred-direction matter coupling together with its strict micro/macro separation from the later macroscopic  $\phi$ -sector. Its main open fronts remain the microphysical origin of the gradient condensate, the full tensor-mode and nonlinear gravitational closure, the completed physical electroweak identification beyond structural gauge redundancy, the missing colour  $SU(3)$  sector, the first-principles fermionic sector, and the first-principles macroscopic reduction behind the galactic/cosmological  $\phi$ -closures.

The four cross-sector universalities isolated later in this chapter (Section 11.1) should be read as the capstone compression of this foundational logic.

## 10.1 Core axiomatic framework (Sections 2–6)

The foundational layer of ECT establishes:

1. A connected four-dimensional Euclidean arena with initially equivalent directions and points (P1; ontology layer S1–S3).
2.  $O(4)$ -invariant scalar microdynamics with the minimal variational realisation of the  $\Phi$ -medium (P2–P3, DP).
3. A gradient-ordered vacuum branch with spontaneous  $O(4) \rightarrow O(3)$  breaking, producing the orientation variable  $n_A$  (P4).
4. The unique kinetic tensor  $K^{AB} = \beta \delta^{AB} - \alpha n^A n^B$  of the broken phase (Level A; Theorem 3.2).
5. Lorentzian signature as an ordered-branch admissibility condition: the broken-phase kinetic tensor  $K^{AB} = \beta \delta^{AB} - \alpha n^A n^B$  admits Euclidean, degenerate, and Lorentzian regimes, and only  $\alpha > \beta$  yields a hyperbolic ordered-branch equation with a well-posed causal propagation problem (Level A). This is not an observational selection rule and not an added postulate, but a mathematical admissibility property of the ordered-branch EFT.
6. A two-step cone determination: first,  $\alpha > \beta$  fixes the Lorentzian branch and the existence of a unique ordered-branch causal cone (Level A); second, the ECT-specific realisation  $c_*^2 = \beta/(\alpha - \beta)$  together with the physical matching  $c_* = c$  fixes the distinguished point  $\alpha = 2\beta$  as the minimal one-cone realisation used in the remainder of the paper (Level A/B). The first step is structural; the second is the ECT-specific physical matching.
7. A unified scale-and-cone architecture: the ordered branch fixes a unique causal cone with propagation speed  $c_*$  (Level A in EFT), the induced/NLO gravitational route supports  $M_G^2 \sim u_0^2/m_\sigma^2 \sim \phi_0^2$  and  $\phi_0 \sim \tilde{M}_{\text{Pl}}$  at Level B, and the coherent branch yields the action scale  $S_0$  with structural universality across the quantum programme at Level A/B, while the physical identification  $S_0 = \hbar$  remains Level B (Sections 4.7, 5.1, 5.6).
8. A layered arrow-of-time architecture with six nested levels (A1–A6), with the thermodynamic second law at Level B under ohmic/Markovian closure (Section 3.8).
9. Clear sector separation: heavy radial mode  $\sigma$ , constrained soft orientation mode  $\chi$  reduced by integrability to one longitudinal scalar, and the macroscopic  $\phi$ -sector (Section 4.2).
10. A hierarchy programme in which the primary microscopic amplitude  $\phi_0$ , the radial threshold  $m_\sigma$ , the induced gravitational stiffness, and the coherent action-scale programme are traced back to

one condensate. The present open problem is no longer “why are gravity and electroweak physics unrelated scales?”, but rather how one condensate generates a secondary low-energy matching scale  $v_2 \ll \phi_0$  while retaining the same medium origin (Section 5.1).

11. The coherent branch BR1 with compact phase  $\theta$ , integer winding sectors, elementary loop action  $S_{\text{loop},\min} = 2\pi S_0$ , and the structural route by which the same action scale later enters amplitudes, wave dynamics, canonical structure, and Born-type weights in the quantum programme.
12. A variational backbone (DP) with conserved Noether tensor and angular currents, from which the Lorentzian energy–momentum interpretation follows (Section 6.6).
13. A two-branch structure — geometric macroscopic branch and coherent branch — arising from the same ordered medium but retaining different observables under coarse-graining, while remaining tied by the same cone structure, hierarchy architecture, and variational backbone (Section 6).
14. Admissibility of non-uniform ordered backgrounds (P6), treated here as an auxiliary structural admissibility assumption rather than a core dynamical postulate. Its rôle is to make branch-dependent inhomogeneous ordered configurations conceptually available for the later macroscopic  $\phi$ -sector development, not to derive that sector by itself.

**Capstone of the foundational layer.** Taken together, these results show that the foundational layer of ECT is not a collection of unrelated partial constructions. It already supports a unified one-medium architecture: one ordered branch fixes the cone structure, one condensate hierarchy organises the microscopic, intermediate, and IR scales, one coherent branch organises the action-scale programme, and one variational backbone feeds both the macroscopic and quantum sectors. The remainder of the article should therefore be read as the systematic development of consequences and closures of this already-established foundational core.

## 10.2 Gauge-sector architecture, particles, and fermions (Sections 7–9)

Building on the core framework, the sector-development chapters establish:

15. The  $U(1)$  phase–gauge correspondence: within the compact phase EFT, the Noether current, current conservation, local gauge completion, and the Maxwell-type leading kinetic structure follow at Level A/B with clearly stated assumptions (Section 7.2). This is the strongest gauge-sector result of Part I.
16. Structural embedding of non-Abelian gauge sectors:  $\mathfrak{so}(3) \cong \mathfrak{su}(2)$  provides the cleanest algebraic bridge (Level A);  $SU(3)$  requires additional internal structure (Level C). The Abelian phase sector is derived most strongly; the chiral  $SU(2)$  sector is structurally selected but not yet fully derived as an independent internal gauge field; the colour sector requires additional internal condensate structure (Sections 7.3–7.4; see also Section 48.13).
17. A three-category particle and excitation spectrum: (i) required condensate excitations (graviton,  $\chi$ ,  $\sigma$ ); (ii) structurally embedded SM fields; (iii) topological and conditional sectors (Section 8.11).
18. A fermionic sector at Level B/C: spinorial excitations via  $\text{Spin}(4) \rightarrow \text{Spin}(3)$ ; Dirac-form reconstruction; chirality as a structural setting for  $SU(2)_L \neq SU(2)_R$ ; Yukawa embedding; spin-statistics from two distinct  $\mathbb{Z}_2$  structures (Section 9).
19. Spin discreteness as a structural consequence of the residual ordered-branch rotation group: ECT does not replace the standard compact- $SU(2)$  origin of discrete spin projections, but it does provide a physical origin for why this rotational structure is the relevant one after the  $O(4) \rightarrow O(3)$  breaking. Stern–Gerlach-type outcome selection is then read at closure level through the same environmental-locking logic used elsewhere in the quantum–classical boundary programme (Section 9).

20. The ECT-specific fermion–condensate coupling  $\Delta\mathcal{L}_5 = \mu_5 \bar{\Psi} \gamma^A n_A \Psi$ : a genuinely ECT-specific matter-sector deformation with Planck-suppression  $\beta_5 \sim m_f/\phi_0$  (Level A/B for operator form; Level B for coefficient estimate; Section 7.6). Species dependence of  $\beta_5$  is structurally expected (Figure 4).
21. Strict structural separation of the microscopic preferred-direction coupling (orientational variable  $n_A$ ) from the macroscopic  $\phi$ -closure (amplitude variable  $\phi(X)$ ): the two effects share the same ordered-branch origin but belong to different effective sectors and must not be identified (Section 7.7; Appendix V; Figure 6).
22. Observability conditions and falsification logic for the ECT-specific coupling: four classes of observable channels identified (spin-sensitive, composition-sensitive, propagation, environment-dependent), together with explicit conditions under which the present ECT closure could be refuted (Section 7.8). No precision predictions are available at this stage (Figure 5).
23. Structural constraints on the coupling coefficient:  $\phi_0$ -suppressed dimensional scaling is the working EFT estimate because  $n_A$  originates from the first transition;  $v_2$ -dependent corrections are possible but subleading; radiative stability is not yet established (Section 7.9).
24. A neutrino sector via type-I seesaw embedding with two suggestive scale observations built from the same condensate pair  $(\phi_0, v_2)$ : the geometric-mean seesaw scale  $M_R^{\text{geom}} = \sqrt{\phi_0 v_2} \approx 2.4 \times 10^{10} \text{ GeV}$  and the Weinberg-operator scale  $m_V^{\text{geom}} = v_2^2/\phi_0 \approx 2.5 \times 10^{-5} \text{ eV}$ , with a structural bridge to thermal leptogenesis (Section 8.9).

### 10.3 Structural outputs and forward falsification handles

Part I produces several concrete predictions and structural outputs that go beyond formal consistency and are in principle testable. These are classified here by their derivation level.

**Strict topological anti-predictions (Level A).** The primary vacuum manifold  $O(4)/O(3) \simeq S^3$  has vanishing lower homotopy groups:  $\pi_0(S^3) = \pi_1(S^3) = \pi_2(S^3) = 0$ . ECT therefore *predicts the absence* of topologically stable domain walls, cosmic strings, and magnetic monopoles from the primary condensate transition (Section 8.10). This is a structural consequence of the topology of  $S^3$  and does not require additional dilution or suppression mechanisms.

**Texture/skyrmion sectors (Level A for existence).** The non-trivial  $\pi_3(S^3) = \mathbb{Z}$  guarantees the existence of topologically classified field configurations with integer charge  $Q \in \mathbb{Z}$ . The dynamical stability and mass spectrum of these sectors remain Level B/C; the phenomenological ansatz  $m_n \sim n \times 1.6 \text{ GeV}/c^2$  (D7) is directly falsifiable independently of the underlying homotopy classification.

**Ordered-branch signature selection and one-cone realisation (Level A/B).** Part I fixes the signature logic of the ordered branch in two distinct steps. First, the condition  $\alpha > \beta$  is singled out as the only hyperbolic admissible regime of the broken-phase EFT, whereas  $\alpha < \beta$  remains Euclidean and  $\alpha = \beta$  degenerate (Level A). Second, the ECT-specific identification  $c_*^2 = \beta/(\alpha - \beta)$  together with the physical matching  $c_* = c$  fixes the distinguished realisation  $\alpha = 2\beta$  (Level A/B). This two-step result is one of the central non-circular outputs of Part I and should be kept conceptually separate from later decoherence- or PES-based arguments.

**Lorentz-invariance violation: structural benchmark, not a fixed coefficient prediction (Level B/Open).** Part I identifies the ordered-branch tensor structure from which Planck-suppressed



higher-dimension propagation operators may arise. For the photon sector this is represented phenomenologically by the time-of-flight benchmark

$$\Delta t_{\text{LIV}} \propto \zeta_\gamma \frac{E}{M_{\text{Pl}} c^2} \frac{L}{c},$$

where the matching coefficient  $\zeta_\gamma$  is not fixed by the present foundational closure. The unit-coefficient photon benchmark is already constrained by Fermi–LAT and should be read only as a scale estimate (Fig. 2). The GW-sector estimate used later is quadratic and effectively negligible for current sources. A full operator-level unification of photon, neutrino, and GW propagation corrections remains open (Section 3.6).

**Matching relations for emergent fundamental constants (Level A/B).** Part I establishes that the effective propagation scale, gravitational normalisation, and coherent action scale are controlled by one condensate parameter set rather than introduced independently. At the ordered-branch level one has

$$c_*^2 = \frac{\beta}{\alpha - \beta}, \quad G_N = \frac{c_*^4}{8\pi M_G^2}, \quad S_0 = \frac{K_\theta m_\phi}{2}.$$

The first relation is structural at the EFT level. The second is the geometric matching relation that defines the effective gravitational scale  $M_G$  of the ordered branch; the explicit microscopic relation between  $M_G$  and the condensate parameters remains an open derivational target. The third is the coherent-sector action scale. The physical identifications  $c_* = c$  and  $S_0 = \hbar$  remain Level A/B and Level B, respectively. These are not zero-parameter predictions, but they reduce the number of independent foundational constants and are therefore central structural outputs of Part I.

**Species-dependent preferred-direction coupling (Level B).** The ECT-specific coupling  $\beta_5 \sim m_f/\phi_0$  is structurally species-dependent: heavier fermions couple more strongly to the preferred condensate direction (Section 7.6; Figure 4). This species dependence is a structural prediction of the present EFT scaling. Whether it produces observable multi-species signals requires the full EFT reduction discussed in Section 7.8.

**Surviving soft scalar (Level B).** The integrability constraint reduces the naive three-component Goldstone sector to a single surviving longitudinal scalar  $\chi$ . Its mass, stability, and cosmological role are not yet determined. It therefore remains a possible dark-sector candidate, but not a completed dark-sector prediction (Section 8.2).

**Neutrino geometric scales (Level B/C).** From the same pair of condensate scales  $(\phi_0, v_2)$  ECT yields two dimensionally consistent combinations that populate the neutrino sector: the geometric-mean seesaw scale  $M_R^{\text{geom}} = \sqrt{\phi_0 v_2} \approx 2.4 \times 10^{10}$  GeV, which provides a suggestive scale for right-handed neutrino masses and lies within the thermal-leptogenesis window [69]; and the inverse-ratio Weinberg-operator scale  $m_\nu^{\text{geom}} = v_2^2/\phi_0 \approx 2.5 \times 10^{-5}$  eV, which lies within a few orders of magnitude of the observed neutrino mass splittings. Their joint appearance is a structural consequence of the three-scale hierarchy rather than two independent numerical observations; neither determines the absolute mass scale, the mass ordering, the PMNS pattern, or the Dirac/Majorana character (Section 8.9). If the embedded seesaw route is adopted with  $M_R^{\text{geom}}$ , atmospheric-scale neutrino masses are reproduced for a perfectly ordinary Yukawa coupling  $y_\nu \approx 4.5 \times 10^{-3}$ , and the resulting active-sterile mixing  $\theta_{\text{as}} \sim 10^{-11}$  renders the heavy sterile sector invisible in oscillation experiments. Standard PMNS/MSW phenomenology remains intact at leading order (ECT preferred-direction corrections are suppressed by approximately eight orders of magnitude at GeV energies).

**Conceptual outputs of Part I.** Beyond the formal structural results, Part I produces the following conceptual outputs that distinguish ECT from standard approaches: (i) *Three logical classes of excitations*: ECT does not place all particles on the same footing—required condensate modes, structurally embedded SM fields, and topologically selected sectors occupy different logical tiers, unlike QFT where all fields are equally fundamental postulates (§8.1). (ii) *Interaction as a Lorentzian concept*: in the coherent branch, subsystems are related by common-medium correlation, not by event-like exchange; Lorentzian interaction emerges only after decoherence (§6.5). (iii) *Chirality from broken-phase geometry*: the parity asymmetry of the weak sector is structurally motivated as a geometric imprint of  $O(4) \rightarrow O(3)$  ordering (§9.3, Level B). (iv) *Multi-excitation structure as a reconstruction target*: ECT does not require Fock space as a foundational postulate; variable particle number should emerge as a sector decomposition of one condensate medium (OP-Q11). (v) *Why 3+1 dimensions*: the  $O(4) \rightarrow O(3)$  transition singles out exactly three equivalent spatial directions and one distinguished temporal seed; standard physics postulates  $d = 3 + 1$  without explanation. (vi) *Massless spin-2 sector*: linearised effective-metric channel admits a massless Fierz–Pauli reconstruction with  $m_g = 0$ ; non-perturbative proof from the bare condensate action remains open (Level A/B for the linear EFT reconstruction).

## 10.4 What Part I derives and what it does not

**Derived from postulates (Level A).** Lorentzian signature, uniqueness of the kinetic tensor, light speed  $c_*$ , universality of the causal cone within the linear scalar ordered branch (Universality Corollary, §4.3: single field, single  $K^{AB}$ , single cone), retarded propagation with support confined to the causal cone for the full nonlinear scalar ordered branch (Appendix F), the Klein–Gordon equation, the global Noether current and its conservation, the algebraic isomorphism  $\mathfrak{so}(3) \cong \mathfrak{su}(2)$ , the ordered-branch admissibility result  $\alpha > \beta$  as the unique hyperbolic regime of the broken-phase EFT, the two-branch structure, the integer winding condition, the six-layer causal architecture (Levels A1–A3), and the structural distinction between the orientational and amplitude sectors of the ordered branch.

**Derived with stated assumptions (Level B).** Gravitational constant  $G_N$ , action scale  $S_0$ , the structural identification  $c_* = c$  within the minimal gauge-emergence route (§4.7), the Schrödinger equation, the linearised Einstein equations, the local  $U(1)$  gauge completion within the compact phase EFT, the thermodynamic arrow of time (under ohmic/Markov closure), the Dirac equation (from Lorentzian spinor structure), the physical reading of spin discreteness and Stern–Gerlach outcome selection in the ordered branch, the preferred-direction operator  $n_A \bar{\Psi} \gamma^A \Psi$  and its dimensional estimate  $\beta_5 \sim m_f / \phi_0$ , the electroweak-like embedding, the coherent branch rule BR1, and the structural suggestion of a three-scale hierarchy linking the gravitational, electroweak, and galactic sectors, with the galactic IR scale still open at first-principles level (OP-galactic).

**Partially derived, partially embedded (Level A/B/C).** The Abelian gauge sector is derived from bundle covariance of the compact phase fibre (Level A). A preferred chiral  $SU(2)$  sector is structurally selected, with the full internal weak-gauge derivation still open (Level B+). The coupling constants  $(e, g, g', g_s)$ , the fermion mass hierarchy, the Yukawa structure,  $SU(3)$  colour (requiring additional internal condensate structure), anomaly cancellation, and three fermion generations remain embedded or open.

**Explicitly open.** The dynamical origin of the gradient condensate (OP-grad), the three-scale hierarchy mechanism (OP-EW, OP-galactic), the full graviton sector (OP1), the full SM gauge completion including colour derivation, matter representations, and anomaly cancellation (OP-GUT1, OP-GUT2, OP-GUT3b, OP-GUT6 family in Table 118), the full fermionic sector from first principles (Section 9.10), the microscopic derivation of the fifth-coupling coefficient, radiative stability of  $\beta_5$ , the full quantum reconstruction from  $S_0$  (Section 20), and the microscopic H-theorem.

## 10.5 What remains open at the end of Part I

The following list reformulates the open points above as concrete research targets for Parts II–III and for future work, rather than repeating the derived/open classification itself. The key open problems are:

- Gradient condensate from bare action: the dynamical mechanism generating  $\langle \partial_A \Phi \rangle \neq 0$  from P3 (OP-grad).
- Three-scale hierarchy: mechanism generating  $v_2 \ll \phi_0$  (OP-EW); first-principles derivation of the galactic IR scale (OP-galactic).
- **OP-Planck:** Derive the full NLO orientation-stiffness coefficient  $\mathcal{C}_n$  from first principles, including the induced contribution from integrating out the radial sector, the explicit map  $\kappa_n \rightarrow M_G^2$  through the spin-2 normalisation, and a complete dimension-and-normalisation audit (Appendix N).
- Full derivation of the graviton sector: Fierz–Pauli closure, nonperturbative spectrum, gauge reduction (OP1).
- Gauge-sector completion: the Abelian  $U(1)$  sector is derived (Level A); a chiral  $SU(2)$  sector is structurally selected (Level B+);  $SU(3)_c$  requires extended internal condensate structure; full SM matching (matter representations, charge assignments, anomaly cancellation) remains open (OP-GUT1, OP-GUT2, OP-GUT3b, OP-GUT6 family; see also Sections 48.13 and 9.5).
- Full first-principles fermionic sector: dynamical origin of spinorial excitations, chiral gauge selection, Yukawa hierarchy, neutrino-mass mechanism, three generations (Section 9.10).
- Microscopic derivation of the fifth-coupling coefficient  $\mu_5$  from condensate microdynamics, and establishment of radiative stability.
- Realisation of the physical photon as the transverse gauge manifestation of the compact phase branch (OP-gauge); this is the remaining step needed to promote the structural identification  $c_* = c$  from Level B to Level A.
- Full mapping of the ECT-specific operator onto standard Lorentz-violation and equivalence-principle test frameworks.
- Full quantum reconstruction from  $S_0$ : amplitude composition, Born rule, operator algebra, Hilbert-space structure (Section 20).
- Microscopic H-theorem: first-principles derivation of the decoherence kernel and irreversible thermodynamics.
- Nonlinear closure of each effective branch.
- Strict identification  $S_0^{\text{EFT}} = \hbar$  beyond Level B matching.
- Full subsystem-level reconstruction of quantum dynamics from the descriptive Euclidean condensate equation: in particular, the bridge from the deterministic boundary-value formulation of the coherent sector to the standard probabilistic subsystem equations beyond the presently established Schrödinger/Klein–Gordon reconstruction.

Additional open consistency problems of the emergent matter sector are now organised explicitly in the structured OP-GUT family (Table 118) and the fermionic-architecture open programme (§9.10), including the conditional CPT closure problem (OP-CPT1), the anomaly-consistency family (OP-GUT6a, OP-GUT6b, OP-GUT6c), and the exact weak-sector parity pattern (OP-P1).

## 10.6 Roadmap to Parts II–III

**Table 49:** Structural branching of ECT after the foundational construction.

Branch	Primary variables	Developed in
Geometric (Macroscopic Physics)	$g_{AB}^{\text{eff}}$ , $n_A$ , $\phi(X)$ , and long-wavelength background variations of the ordered branch	Gravity, cosmology, galactic phenomenology, observational tests
Coherent (Quantum Sector)	$\Phi_{\text{eff}}$ , $\theta$ , $S_0$ , coherent winding sectors, and coherent correlators	Action-scale quantisation, wave dynamics, quantum kinematics, decoherence, probability

*Part II* (Section 11 onwards) develops the geometric macroscopic branch: the homogeneous ordered-phase limit, the emergent gravitational sector, the ordered-branch cosmological programme, galactic and cluster-scale phenomenology, dark-sector interpretation, and observational tests. The macroscopic  $\phi$ -closure, whose structural separation from the microscopic preferred-direction coupling is established in Part I (Section 7.10), provides the link between the foundational architecture and the observational programme. Its macroscopic  $\phi$ -closures should therefore be read as structured Level B continuations of the ordered-branch architecture, not as direct Level A outputs of bare P3 alone.

*Part III* (Section 20 onwards) develops the phase-sensitive coherent branch across eleven thematic steps: coherent phase dynamics and the pre-quantum action scale, wave kinematics and conservation laws, the Hilbert-space bridge (reflection positivity, unitarity, canonical structure, uncertainty), exchange sectors and Dirac structure, unified vacuum response, decoherence and the arrow of time, the quantum–classical boundary and Born-type probability, entanglement, the wider topological/dark-sector ontology, black-hole thermodynamics and the information problem, and the analogue-laboratory programme.

## Part II

# Macroscopic Physics: Gravity, Cosmology, and Observational Tests

## 11 Scope, Bridge, and Approximation Hierarchy

*Part II develops the macroscopic physics of the ordered condensate branch. Before proceeding to the specific derivations—local special-relativistic kinematics (§12), the gravitational sector (§13), cosmology, and galactic phenomenology—the present section fixes the scope, states the approximation regime, and records explicitly which results of Part I are used as structural inputs below.*

*The purpose of this section is threefold. First, to define the branch of the theory developed in Part II. Second, to make explicit which approximations are used, where they enter, and what their derivation status is. Third, to draw a sharp boundary between what Part II imports from Part I and what it does not import from the Quantum Sector of Part III.*

*Throughout this chapter we distinguish three levels of status: strictly derived structural inputs from Part I (Level A), structural but conditional results inherited from controlled reconstruction routes (Level B), and closure-dependent macroscopic specialisations used in phenomenology.*

### 11.1 Macroscopic Physics as the development of the geometric branch

*Connection to ECT basics: Sections 6, 6.2, and the summary rules collected in Section 6.8, especially the amplitude–orientation decomposition rule and the macroscopic viability rule. Status: conceptual bridge; all claims structural.*

After completing ECT basics (Sections 2–6), ECT is no longer an undifferentiated scheme. As established in the branching section, once the ordered vacuum branch is selected, the subsequent low-energy description naturally separates into a phase-insensitive geometric development and a phase-sensitive coherent development. The present section follows the first of these developments. Throughout Part II we work within the structural branch where  $c_* = c$ , conditional on the minimal gauge-emergence route established in Part I (§4.7).

**Two branches from one condensate.** The first branch—the *geometric* or *macroscopic* branch (§6.2)—describes those observables that are insensitive to the local phase of the coherent order parameter and are controlled instead by long-wavelength variations of the ordered condensate background. The second branch—the *coherent* or *Quantum Sector* (§6.3)—describes observables that probe the winding structure, loop sectors, decoherence kernels, and quantum amplitudes of the coherent order parameter  $\Phi_{\text{eff}} = \rho e^{i\theta}$ . The present section develops the first branch exclusively. The later macroscopic  $\phi$ -closures of Parts II.A–II.B belong to this same branch: they probe coarse-grained amplitude/background response of the ordered phase, not the local coherent phase  $\theta$  or the loop-sector data of the Quantum Sector.

**Definition of macroscopic observables.** In ECT basics it was shown that after the  $O(4) \rightarrow O(3)$  symmetry breaking, long-wavelength physics naturally separates into a *tensorial, phase-insensitive sector* and a *coherent, phase-sensitive sector*. The geometric branch is defined precisely by the former. The primary variables of this branch are:

- the effective metric  $g_{AB}^{\text{eff}}$ , derived from the unique kinetic tensor  $K^{AB}$  (3.9);
- the orientation collective variable  $n_A$  (P4);
- long-wavelength tensorial perturbations  $\delta n_i$  around the ordered vacuum (Section 4.3);

- conserved stress-energy structures from the variational/Noether foundation (Section 6.6, Appendix Q);
- the gravitational stiffness scale  $M_G$ , which controls matching to the observed Newton constant  $G_N$ .

None of these objects is introduced from scratch here: each already appears in embryonic form in ECT basics, and Macroscopic Physics is precisely its full development.

**The coarse-graining criterion.** The key transition from ECT basics to the macroscopic branch is a coarse-graining over short-distance condensate structure. The radial mode  $\sigma$  with bare mass  $m_\sigma = \sqrt{2\mu^2}$  (Section 4.3) sets the short-distance cutoff of the ordered phase; the corresponding correlation length  $\xi_{\text{cond}} \sim m_\sigma^{-1}$  (Appendix O) marks the scale below which the condensate must be treated as a structured medium rather than an effectively geometric background. The macroscopic branch is therefore defined in the regime:

$$L \gg \xi_{\text{cond}} \sim m_\sigma^{-1}, \quad E \ll m_\sigma, \quad (11.1)$$

where  $L$  is the characteristic observational scale and  $E$  the characteristic excitation energy. In this limit the heavy radial mode is integrated out (Appendix K), rapid microscopic phase fluctuations are averaged away, and the remaining physically relevant variables are precisely the slow orientation/background degrees of freedom (Level A: this criterion follows directly from the EFT power counting of Section 4.3).

**Why the phase drops out.** The macroscopic branch is defined not only by scale but by the loss of sensitivity to local phase information. In geometric-branch observables the phase  $\theta$  of the coherent order parameter  $\Phi_{\text{eff}}$  does not appear explicitly; what remains are effective metric relations, source couplings, causal propagation, and large-scale background structure. This is the fundamental reason why the present section develops gravity, cosmology, and galactic phenomenology, while wave amplitudes, canonical commutation relations, decoherence, and probability measures are deferred to the Quantum Sector.

**What is already established in ECT basics.** From ECT basics the following is available for the geometric branch: the ordered branch has already been resolved into its collective infrared variables (Section 3.2), and the residual-symmetry analysis has identified the unique viable coarse-grained tensor structure.

- (i) a constrained soft orientation sector (reduced by integrability to one longitudinal scalar mode  $\chi$  in the scalar-only basis; Level B minimal EFT; see Section 4.3 and Appendix I);
- (ii) Lorentzian window  $\beta < \alpha < 4\beta$  (Section 3.5);
- (iii) conserved  $T^{AB}$  from translational invariance and angular currents  $J^{CAB}$  from  $O(4)$ -invariance (Section 6.6, Appendix Q);
- (iv) a gravitational stiffness scale  $M_G$  was identified in ECT basics; its matching to  $G_N$  is developed in Section 13.4;
- (v) structural compatibility with a Deser-type spin-2 self-coupling route (Section 4.6);
- (vi) the Universality Corollary: integrability of  $Q_A = \partial_A \Phi$  forces the linear scalar ordered branch into a single causal cone with speed  $c_*$  (Level A; §4.3);
- (vii) cross-sector cone universality: the coherent phase sector, the Abelian gauge sector, and the tensor gravitational-wave sector all inherit the same leading causal cone  $c_*$  from the ordered-branch kinetic structure (Level A/B; §4.7, Eq. (4.11));
- (viii) the physical identification  $c_* = c$  is then a single matching step (Level B), after which the observed universality of the speed of light becomes a structural consistency check rather than an independent input.

**Four structural universalities of ECT.** The single-medium architecture (P3) produces four independent cross-sector universality results, each established at Level A/B:

- (I) **One causal cone:** all native low-energy sectors (scalar, phase, gauge, tensor) share one and the same leading causal cone  $c_*$  (§4.7, Eq. (4.11)).
- (II) **One action scale:** the same distinguished pre-quantum action scale  $S_0$  appears in every coherent-branch construction: loop-sector weights, wave reconstruction, canonical normalisation, and the Born/decoherence programme (§5.6).
- (III) **One extremal principle:** the dynamical principle DP reappears at every resolution level of the theory: bare variational dynamics, reduced-sector EFTs, macroscopic equations, and coherent stationary-phase dominance (§22.2).
- (IV) **One conservation origin:** energy-momentum conservation, phase-current conservation, winding-number conservation, and the continuity equation for coherent density all trace to the same ordered condensate through its symmetry and compact-phase structure (§22.3).

These four universalities are conceptually distinct and probe different aspects of the same single-medium architecture: causal propagation, action normalisation, variational organisation, and conservation structure. Taken together, they constitute the strongest structural evidence currently developed in the article that the ECT framework is internally consistent as a single-medium theory.

**Combined falsifiable content of the universalities.** If *any* of the four universalities were found to fail—if different native sectors required different causal cones, different action scales, different extremal backbones, or independent conservation structures not traceable to one ordered medium—then the ECT single-medium universality programme would fail. Such an outcome would show that the native low-energy sectors of the theory are not controlled by one and the same condensate structure. No such failure has been established within the sectors analysed so far. The observed coexistence of one measured  $c$ , one measured  $\hbar$ , one variational organisation of the native ECT sectors, and one ordered-medium conservation architecture is consistent with the ECT single-medium programme.

**Unified falsifier and prediction map of the ECT programme.** The ECT programme developed in Parts I–III supports a compact falsifier map in which the strongest structural claims are paired with their failure modes and the observational windows that currently probe them. Table 50 collects thirteen main programme-level falsifiers of the current ECT architecture.

**Table 50:** Falsifier map of the current ECT programme.

Structural claim	Failure mode		Observational consistency window
One causal cone (§4.7)	Sector-dependent speeds	limiting	$ c_{\text{GW}}/c - 1  < 6 \times 10^{-15}$ [10]
One action scale (§5.6)	Mutually quantum-sector normalisations	inconsistent normalisations	Single $\hbar$ across all established quantum phenomena
One extremal backbone (§22.2)	Incompatible sector-dependent extremal/classical crossover criteria in native ECT sectors	sector-dependent	Interferometric, atomic, and macroscopic regimes are all consistent with action-controlled crossover logic, while the precise universal threshold remains a structural programme-level claim rather than an established measured law

*Continued on next page*

Table 50 continued

Structural claim	Failure mode	Observational consistency window
One conservation origin (§22.3)	Independent non-condensate conservation structures for native sectors	Charge stability bounds such as $\tau(e \rightarrow \gamma\nu) > 10^{26}$ yr [79]; the broader baryogenesis connection is developed separately in Section 16.3
Ordered electroweak redundancy (§7)	Failure of the structural $SU(2) \times U(1)$ route from ordered-branch local redundancy	Electroweak gauge-structure phenomenology is consistent with an $SU(2) \times U(1)$ organisation, while the detailed mass pattern remains tied to the still-open $\nu_2$ closure
Entanglement as medium correlation (§31)	Bell correlations require primitive tensor-product axiom unrelated to coherent medium	Bell-inequality violation well established; loophole-free tests confirm non-classical correlations
Tensor-closure graviton programme (§8.5)	Induced metric sector cannot close to FP/TT, or tensor cone differs from ordered branch	GW speed $ c_{\text{GW}}/c - 1  < 6 \times 10^{-15}$ ; no extra polarisations detected
Analogue ordered-branch programme (§37)	Different analogue platforms requiring fundamentally incompatible structural logics	Quantised circulation, dynamical Casimir, analogue Hawking, environment-driven decoherence all realised in ordered media
Quantum-sector one-medium unification (§20)	Different quantum substructures requiring mutually unrelated action scales or principles	All established QM phenomena remain consistent with a single $\hbar$ , one effective probabilistic layer of Born type, and one Schrödinger dynamics
Singularity as branch boundary (§14.1)	Ordered branch remains valid to formal GR singularity with no condensate breakdown	No observed sub-Planckian singular physics; BH exterior consistent with EFT description
Physical UV threshold (§8.3)	UV completion scales unrelated to $m_\sigma$ , or mandatory new gravitational dof below the radial threshold	No experimentally established compulsory extra propagating gravitational sector is seen below the Planck regime; EFT gravity remains successful throughout accessible scales
Einstein nonlinear closure (§13.5)	Non-Einstein two-derivative completion required, or non-universal matter-metric coupling	Classical GR weak-field success; binary-pulsar radiative consistency; absence of compulsory extra low-energy tensor polarisations. Observational footprint of $\Theta_{\mu\nu}[n]$ assessed across five sectors (Table 54); background contribution non-separable, cluster/JWST channels $c_1$ -dependent (OP-c1)
Condensate-origin dark sector (§18)	Dark phenomena requiring a fundamentally non-condensate particle with no ordered-medium interpretation	Current Level-B consistency windows include the SPARC rotation-curve programme, the structural BTFR scaling, and the critical-acceleration benchmark $g^\dagger \approx cH_0/(2\pi)$

The same map yields structural programme-level predictions:

- (i) No native low-energy sector should require its own independent fundamental action unit: all



coherent-branch normalisations should reduce to one and the same  $S_0$ .

- (ii) No native low-energy sector should require its own independent extremality law: all effective equations of motion should descend from one dynamical principle DP.
- (iii) Future improvements in GW propagation-speed measurements should continue to find  $c_{\text{GW}} = c$  to increasing precision, with any departures scaling as Planck-suppressed EFT corrections (§13.8).
- (iv) If the ordered-medium electroweak route is correct, future deeper closure should *reduce* external gauge input rather than increase it.
- (v) Cosmological, decoherence, and vacuum-response developments should reinforce cross-sector unification rather than fragment into unrelated sector-specific constants.

These are programme-level predictions: each is falsifiable in principle but tests the overall architecture rather than a single formula. Their collective consistency forms a major part of the present structural case for the ECT single-medium programme.

**What does not follow automatically.** Items (i)–(viii) above do not automatically give: the full nonlinear gravitational closure; standard Einstein equations in final form; complete matching of all phenomenological constants; or any quantum-mechanical statement. These are developed step by step below.

**Logical order of Part II.** First: the homogeneous ordered-phase limit and emergent special relativity (§12). Then: the macroscopic gravitational sector, including the effective metric, source structure, gravitational stiffness matching, nonlinear closure, weak-field limit, post-Newtonian regime, and gravitational waves (§§13.1–13.8). Finally: cosmology, galactic phenomenology, dark-sector interpretation, and observational tests (§§14–19.1). The galactic infrared branch developed later in Part II should be read as a closure-dependent macroscopic continuation of the ordered phase, not as a first-principles output already fixed at the scope-setting level of the present section.

**What Part II does not import from Part III.** The macroscopic branch is constructed without using Planck’s constant  $\hbar$ , the Born rule, wavefunction collapse, canonical commutation relations, decoherence functionals, or instanton/loop amplitudes. These belong exclusively to the Quantum Sector developed in Part III. The role of Part II is purely geometric and macroscopic. Accordingly, all macroscopic equations in Part II are organised without taking  $\hbar$  as a dynamical input of the geometric branch itself. In particular, the action-scale logic associated with  $S_0$  and its matching to  $\hbar$  is not used as an input to the geometric branch, even when  $c$  and  $G_N$  are already employed as matched macroscopic constants.

**Branch structure at the coarse-grained level.** At the coarse-grained level relevant for the present chapter, observables separate into a phase-insensitive geometric development and a phase-sensitive coherent development. Part II develops only the former. This distinction is sufficient for the present scope and does not require a stronger theorem-level claim of exhaustive RG classification.

**Physical picture.** If ECT basics answers: *what is the ordered medium and how does it branch?*, then Macroscopic Physics answers: *how does the geometric branch of that medium appear to a large-scale observer insensitive to coherent phase data?* Gravity is not introduced as an independent external sector. Rather, the working hypothesis of Macroscopic Physics is that the large-scale causal and geometric response of the ordered condensate admits an effective description which, in the viable Lorentzian branch, takes geometric form.

## 11.2 Approximation hierarchy used in Part II

The derivations of Part II use a nested sequence of approximation regimes. The table below records the approximation levels explicitly used in the chapter and indicates where each of them enters. The purpose is organisational clarity rather than a theorem-level claim of formal completeness.

**Table 51:** Approximation levels used in Part II.

Approximation	Validity condition	Where used	Origin / status
Viable Lorentzian/macrosopic window	$\beta < \alpha < 4\beta$	All of Part II	Level A (§3.5)
Macroscopic EFT regime	$L \gg \xi_{\text{cond}} \sim m_\sigma^{-1}, E \ll m_\sigma$	All of Part II	Level A (§4.3)
Homogeneous ordered phase	$\nabla n_A = 0, \alpha, \beta = \text{const}$	§12 (SR)	Level A
Linear perturbative regime	$ \delta n_i /u_0 \ll 1$	§13.2 (linearised gravity)	Level A
Minimal nonlinear closure	A1–A4, amplitude-dominated reduction	§13.5 (generalised EE)	Level B
Screened/frozen limit	$\phi \rightarrow 0, \nabla \phi \rightarrow 0, \Theta_{\mu\nu} \rightarrow 0$	§13.7 (PPN), GR recovery	Level B consequence of the adopted closure
Weak-field, quasi-static	$ h_{\mu\nu}  \ll 1, v \ll c_*,  \partial_t  \ll c_*  \nabla $	§13.6 (Newtonian limit)	Level B within the adopted closure
FRW background specialisation	$n_A \rightarrow \bar{n}_A, \phi = \phi(t), \text{isotropic}$	§14 (cosmology)	Level B background ansatz
Critical IR galactic regime	deep-acceleration branch with non-analytic IR closure	§17.1 (galaxies)	Closure-dependent

These approximations should be understood as the explicit approximation map used in the present chapter. They are introduced here in order to make the logical dependencies of the later derivations transparent.

## 11.3 Bridge from Part I: structural inputs used in Part II

The list above states the conceptual content in prose; the table below recasts the same inherited results as an operational bridge map for the later macroscopic derivations. The following table records the results established in Part I that are used as structural inputs in Part II. It is intended as a bridge map: for each inherited result, we indicate where it was established and what role it plays in the macroscopic development.

**Table 52:** Structural inputs from Part I used in Part II.

Part I result	Level	Section	Role in Part II
$O(4) \rightarrow O(3)$ ordered phase, preferred direction $n_A$	A	§3	Causal structure, orientation sector
Unique $K^{AB} = \beta \delta^{AB} - \alpha n^A n^B$	A	§3.3	Effective metric, operator basis
Viable Lorentzian window $\beta < \alpha < 4\beta$	A	§3.5	Hyperbolicity and macroscopic viability of all Part II
Universality Corollary: single cone	A	§4.3	SR uniqueness, GW speed
$c_*^2 = \beta/(\alpha - \beta)$	A	§5.3	All kinematics
$c_* = c$ (structural identification)	B struct.	§4.7	All observational comparisons

Result (cont.)	Level	Section	Role
Ordered-branch collective variables	A/B	§3.2	amplitude / $\phi$ -reparametrisation and orientation sector
Noether $T^{AB}, J^{C,AB}$	A	§6.6	Source structure, Bianchi identity
Minimal phase-to-gauge route (L1–L3)	B	§7	structural route to photon identification and $c_\gamma = c_*$

**Immediate matching step in Part II.** In addition to the inherited inputs listed above, Part II performs the gravitational stiffness matching

$$G_N = \frac{c_*^4}{8\pi M_G^2},$$

which is not an input from Part I but an early macroscopic matching step carried out within the present chapter (§13.4).

**Characteristic scales of the macroscopic regime.** The macroscopic branch operates at scales

$$L \gg \xi_{\text{cond}} \sim m_\sigma^{-1}, \quad E \ll m_\sigma,$$

where the condensate correlation length plays the role of the UV cutoff of the geometric effective theory. The characteristic propagation speed is  $c_*$ , structurally identified with the observed light speed  $c$  within the minimal phase-to-gauge route, and the gravitational stiffness scale  $M_G$  is fixed by matching to  $G_N$ . These quantities should be read in two layers: the condensate correlation length and heavy-mode scale define the validity regime of the geometric EFT, while  $c$  and  $G_N$  enter as the matched macroscopic constants of the ordered branch. Their precise numerical matching is discussed in the relevant sections of Parts I and II.

## 12 Special Relativity as the Homogeneous Ordered-Phase Limit

Before allowing the ordered condensate background to vary across spacetime, it is useful to isolate the homogeneous limit in which the effective geometry is flat. This limit provides the local special-relativistic kinematics on which the subsequent macroscopic gravitational construction is built.

The logic is the following. Part I established that spontaneous breaking  $O(4) \rightarrow O(3)$  fixes a unique broken-phase kinetic tensor  $K^{AB} = \beta \delta^{AB} - \alpha n^A n^B$  (Theorem 3.2), that integrability of  $Q_A = \partial_A \Phi$  forces the linear soft sector into a single scalar channel (§4.3), and that the coherent phase sector is governed by the same ordered-branch tensor structure. The gauge sector inherits the same cone only within the minimal phase-to-gauge emergence route (§4.7).

The purpose of the present section is therefore not to postulate special relativity anew, but to state explicitly which parts of local relativistic kinematics follow from the ordered branch and how the Minkowski interval arises.

### 12.1 Status and scope

The conclusions of this section are intentionally stratified.

- **Level A:** the existence of a unique causal cone for the linear scalar ordered branch, with invariant speed  $c_*$  (Universality Corollary, §4.3).
- **Level A:** in the homogeneous ordered phase, the effective geometry reduces to a flat Lorentzian metric with invariant interval and Poincaré isometries.
- **Level B structural:** the identification  $c = c_\gamma = c_*$  holds within the minimal phase-to-gauge emergence route (§4.7).

- **Not claimed here:** a theorem-level derivation of the full gauge structure, nor a complete derivation of all fermionic sectors from the microscopic Euclidean theory.

## 12.2 Homogeneous ordered phase and unique causal cone

Consider the homogeneous ordered branch with constant  $n^A = \delta_w^A$  and constant coefficients  $\alpha, \beta$ . The ordered-branch operator (3.9) reduces to

$$K^{AB} \partial_A \partial_B = \beta \delta^{ij} \partial_i \partial_j - \chi \partial_w^2, \quad \chi \equiv \alpha - \beta. \quad (12.1)$$

For  $\chi > 0$  this is hyperbolic, with the unique causal cone

$$\beta \mathbf{k}^2 - \chi k_w^2 = 0 \quad \implies \quad c_*^2 = \frac{\beta}{\chi}. \quad (12.2)$$

The uniqueness of this cone is not a mode-by-mode coincidence. By the Universality Corollary (§4.3), integrability of  $Q_A = \partial_A \Phi$  forces all linear soft excitations into derivatives of one scalar  $\chi$ , so the branch possesses a single principal symbol. This structural property has no analogue in multi-field Lorentz-violation frameworks (Appendix J).

## 12.3 Minkowski form of the local effective geometry

In the homogeneous branch the effective quadratic form (13.7) becomes

$$g_{\text{eff}}^{AB} = \text{diag}(\beta, \beta, \beta, -\chi). \quad (12.3)$$

Introducing the emergent time coordinate  $w = c_* t$  (12.2), the line element is

$$ds_*^2 = -c_*^2 dt^2 + d\mathbf{x}^2. \quad (12.4)$$

In units  $c_* = 1$  this is  $ds_*^2 = -dt^2 + d\mathbf{x}^2 = \eta_{\mu\nu} dx^\mu dx^\nu$ , the Minkowski metric. Lorentzian signature is not a postulate: it is the kinematic rewriting of the hyperbolic ordered-branch tensor generated by the broken phase (§3.6).

## 12.4 Lorentz transformations from cone invariance

The admissible linear transformations between inertial coordinate systems of the homogeneous ordered phase are those preserving the interval (12.4). Imposing linearity, spatial isotropy of the residual  $O(3)$ , and invariance of the null cone  $x = \pm c_* t$ , one obtains the Lorentz boost along  $x$ :

$$x' = \gamma_*(x - vt), \quad t' = \gamma_* \left( t - \frac{v}{c_*^2} x \right), \quad \gamma_* = \frac{1}{\sqrt{1 - v^2/c_*^2}}. \quad (12.5)$$

All standard kinematic consequences follow immediately: time dilation  $\Delta t = \gamma_* \Delta \tau$ , length contraction  $L = L_0/\gamma_*$ , and velocity addition  $u \oplus v = (u + v)/(1 + uv/c_*^2)$ .

Equivalently, these transformations are precisely the linear isometries of the flat ordered-branch metric (12.4); the usual Lorentz subgroup of the Poincaré group is therefore realised as the kinematic symmetry of the homogeneous ordered phase.

## 12.5 Relativistic dispersion, energy, and momentum

The scalar ordered-branch equation (3.16) in the homogeneous phase gives the plane-wave dispersion

$$\omega^2 = c_*^2 \mathbf{k}^2 + m^2 c_*^4. \quad (12.6)$$

Upon the standard quantum identification  $E = \hbar\omega$ ,  $\mathbf{p} = \hbar\mathbf{k}$ , one obtains the familiar relativistic energy–momentum relation

$$E^2 = p^2 c_*^2 + m^2 c_*^4. \quad (12.7)$$

For massless modes  $E = p c_*$ , so the group and phase velocities coincide at  $c_*$ . The entire free-particle kinematics of special relativity is already encoded in the ordered-branch quadratic operator once its cone is identified.

## 12.6 Universal signal-speed bound and its realisation by massless sectors

**Causal bound from the characteristic cone.** The fundamental speed bound of the ordered branch is not a property of any particular excitation sector: it is the characteristic cone of the principal symbol of the ordered-branch field equation (F.1). For the full nonlinear scalar dynamics of  $\Phi$ , the symmetric-hyperbolic reduction (Appendix F) together with the Leray–Choquet–Bruhat theorem [17, 18, 80] establishes the retarded-support property expressed in (F.8), together with finite domain of dependence inside the past causal cone. Equivalently, scalar ordered-branch disturbances do not propagate outside the local characteristic cone.

This theorem-level result applies directly to the full nonlinear scalar ordered-branch dynamics of  $\Phi$ . For the photon and gravitational-wave sectors the corresponding statement enters through cone inheritance in the minimal emergence routes (§4.7) and therefore carries the structural Level A/B status used throughout the paper.

**Group and phase velocities of linear modes.** For linear plane waves, the dispersion relation (12.6) makes the causal bound explicit. A massive mode ( $m \neq 0$ ) has the group velocity

$$v_{\text{gr}} = \frac{\partial \omega}{\partial k} = \frac{c_*^2 k}{\sqrt{c_*^2 k^2 + m^2 c_*^4}} < c_*, \quad (12.8)$$

with equality only in the massless limit. Here  $k \equiv |\mathbf{k}|$ . This group-velocity result is a concrete linear-mode manifestation of the more fundamental causal statement set by the characteristic cone and front propagation. Massive linear scalar excitations propagate strictly inside the causal cone; massless linear scalar excitations propagate on its boundary.

The phase velocity of a massive mode, by contrast, is

$$v_{\text{ph}} = \frac{\omega}{k} = c_* \sqrt{1 + \frac{m^2 c_*^2}{k^2}} > c_*, \quad (12.9)$$

and formally exceeds the cone speed. This does not violate causality: the phase velocity does not transport information or causal influence. The causal bound is set by the characteristic cone of the principal symbol—equivalently, by the front speed—not by the phase velocity. This is precisely why ECT formulates the relativistic speed limit as a bound on causal propagation, not as a bound on every quantity carrying the name “velocity”.

**Consistency check: velocity addition.** The velocity-addition law derived from cone invariance (12.5),  $u \oplus v = (u + v)/(1 + uv/c_*^2)$ , preserves the interval  $|u|, |v| < c_* \Rightarrow |u \oplus v| < c_*$ . This confirms the internal closure of the sub-cone velocity domain and is consistent with the causal bound following from the principal symbol, but is not its independent source.

**Signal speed, not photon speed.** The fundamental limiting velocity in ECT is therefore the speed of causal propagation—front speed, signal speed, domain-of-dependence boundary—determined by the unique ordered-branch causal cone. The vacuum speed of light does not define that boundary; it realises it. Within the minimal phase-to-gauge route (§7), the photon candidate is a massless Abelian gauge boson whose mass vanishes because the relevant compact  $U(1)$  symmetry remains unbroken and gauge

invariance forbids a leading-order Proca mass term. The gauge sector inherits the same ordered-branch cone (§4.7), so the photon propagates on the boundary of the universal causal cone. Gravitational waves in the minimal tensor route likewise inherit the same cone, a prediction supported observationally by the near-equality  $|c_{\text{GW}}/c - 1| < 6 \times 10^{-15}$  measured for GW170817 [10].

**Universality across inertial frames.** Because inertial coordinate changes in the homogeneous ordered branch are precisely the transformations preserving one and the same null cone (§12.4), the same vacuum signal speed is measured in every inertial frame. Its universality is therefore not an additional postulate: it is fixed by cone invariance itself, and the universality of the vacuum light speed follows once the photon sector is tied to that same cone in the minimal gauge route. What special relativity postulates as the universality of the vacuum light speed is, in ECT, reduced to a structural consequence of the unique ordered-branch causal cone (Level A) together with cone inheritance in the minimal gauge route (Level A/B).

**Status and caveats.** *Theorem-level (Level A):* retarded propagation and domain-of-dependence confinement for the full nonlinear scalar ordered branch (Appendix F); linear massive scalar modes propagate inside the cone, and linear massless scalar modes on its boundary. *Structural Level A/B:* vacuum photons and gravitational waves realise the same cone in the minimal inheritance routes. In slowly varying macroscopic backgrounds the statement is local: massive excitations propagate inside the local tangent-space causal cone, consistent with the tangent-space role of special relativity established in §12.8. Extension to strongly nonlinear, solitonic, or fully interacting sectors is expected on the basis of the covariant form of the effective equations but is not separately proved here.

In this sense, the vacuum light speed is not fundamental by itself; it is the experimentally accessible manifestation of the deeper ordered-branch causal speed.

## 12.7 The status of the identification $c_* = c$

Up to this point, the derivation is entirely internal to the homogeneous ordered branch. It establishes a unique invariant speed  $c_*$  for the linear scalar sector. To identify this speed with the observed speed of light, one further step is required.

In the minimal phase-to-gauge emergence route developed in Part I (§4.7), the compact condensate phase  $\theta$  inherits the same broken-phase tensor structure, and the resulting minimal gauge completion introduces a transverse gauge field whose Maxwell-type kinetic term is built on the same ordered-branch geometry. Within this route, and in the absence of an independent leading-order gauge kinetic sector beyond the minimal construction, the photon cone coincides with the ordered scalar cone:  $c_\gamma = c_*$ . Since the observed vacuum light speed is defined operationally by  $c \equiv c_\gamma$ , one obtains the structural identification

$$c = c_\gamma = c_* \quad (\text{Level B structural}). \quad (12.10)$$

This is substantially stronger than a benchmark normalisation or unit convention: within the minimal route it is a structural identification tied to the single-field condensate architecture, rather than an external matching choice.

## 12.8 From local special relativity to macroscopic gravity

The present section describes the homogeneous ordered phase, in which the effective geometry is flat and the cone speed is constant. In the present logic, this constancy refers to the locally homogeneous ordered phase used to derive special-relativistic kinematics. Slow variation of the condensate background belongs to the macroscopic gravitational regime and does not alter the local tangent-space role of  $c_*$ . Macroscopic gravity begins when the ordered condensate background is allowed to vary slowly:

$$g_{\text{eff}}^{\mu\nu} \rightarrow g_{\text{eff}}^{\mu\nu}(X).$$

The flat interval (12.4) is then replaced by a slowly varying effective geometry. Chapter II uses this section exactly as general relativity uses local Lorentz frames: special relativity is the tangent-space limit of a more general macroscopic geometry.

An important clarification concerns the status of  $c_*$  in the macroscopic regime. The EFT parameters  $(\alpha, \beta)$  characterise the vacuum state of the ordered phase and are not position-dependent in the standard ECT framework. Macroscopic gravity arises from slow spatial variation of the condensate orientation  $n^A(X)$  and amplitude, which generates a curved effective metric  $g_{\text{eff}}^{\mu\nu}(X)$ , while the local tangent-space cone speed  $c_*$  remains invariant—precisely as the physical speed of light  $c$  is a universal constant in general relativity while the metric varies. If certain phenomenological closures are expressed using  $X$ -dependent effective ordered-branch parameters, this describes the varying geometry, not a varying vacuum light speed. The equivalence principle in ECT is therefore a structural consequence of the single-vacuum origin of the causal cone, not an additional postulate.

## 12.9 What is proved and what remains open

**Strictly established (Level A).** The ordered phase generates a hyperbolic kinetic tensor when  $\alpha > \beta$ . The linear scalar ordered branch possesses a unique causal cone. The homogeneous ordered phase admits a flat Lorentzian geometry whose isometry group is the Poincaré group. The scalar branch obeys the standard relativistic dispersion relation with invariant speed  $c_*$ . The full nonlinear scalar ordered branch has retarded propagation with support confined to the causal cone (Appendix F); consequently massive linear scalar excitations propagate strictly inside the cone, and massless linear scalar excitations on its boundary.

**Structurally established, conditional (Level B).** The compact phase sector inherits the same ordered-branch tensor structure. Within the minimal phase-to-gauge emergence route,  $c_\gamma = c_*$ , so the observed vacuum light speed is structurally identified with the ordered-branch speed:  $c = c_*$ .

**Still open.** A theorem-level derivation of the full gauge sector from the microscopic Euclidean theory. A theorem-level derivation of the precise suppression pattern of non-minimal gauge-sector operators beyond the minimal route. A complete analysis of higher-order Lorentz-violating corrections beyond the homogeneous limit.

In this sense, ECT already derives the kinematic core of special relativity and narrows the remaining gap to a specific structural question: whether the physical photon is realised as the transverse gauge manifestation of the same compact phase branch.

### Summary.

$$\text{homogeneous ordered phase} \implies \text{unique scalar-branch cone } c_* \implies \text{local SR}, \quad (12.11)$$

and, within the minimal phase-to-gauge emergence route,

$$c_\gamma = c_* = c. \quad (12.12)$$

Having established the homogeneous ordered-phase limit and its local relativistic kinematics, we now turn to the macroscopic regime in which the condensate background varies slowly and generates the effective gravitational dynamics studied below.

## 13 Emergent Gravitational Sector

*Scope and status.* This section constructs the macroscopic gravitational dynamics of the ordered condensate branch. It does not claim a first-principles derivation of the full nonlinear field equations directly

from Euclidean microdynamics P3. Starting from the local Lorentzian ordered-phase structure derived in Part I and from the homogeneous special-relativistic limit of §12, the section builds the minimal generally covariant low-energy completion of the gravitational sector. The macroscopic gravitational sector is the slowly varying nonlinear continuation of the homogeneous ordered-phase Lorentzian structure established in §12: special relativity is the tangent-space limit; macroscopic gravity describes what happens when that tangent-space structure varies from point to point. The structural necessity of a nonlinear covariant completion is Level A; the explicit closure adopted below is Level B. The closure used below should therefore be read as the current minimal generally covariant low-energy completion of the ordered branch, not as the unique imaginable nonlinear completion of the full Euclidean microdynamics. The Einstein limit is recovered when the additional ordered-branch variables  $(\phi, n_A)$  are frozen or screened.

**Physical picture: gravity as condensate stiffness.** In ECT geometry is not the primitive ontology. The effective metric is a derived bookkeeping object encoding how excitations propagate on the ordered condensate background. Gravity is the long-wavelength geometric response of the ordered condensate to deformations of its orientation structure  $n^A$ . Mass–energy perturbs the condensate state; the metric records the resulting change in propagation kinematics. The graviton is not a quantum of fundamental geometry but a low-energy excitation of the condensate order that, in the effective description, looks like a massless spin-2 mode. This inverts the conventional logic of quantum gravity: ECT replaces the question “how to quantise an existing geometry?” with the question “how do collective condensate excitations produce a geometric description?”.

**Three-level status discipline.** Throughout this section, each result is assigned one of three levels:

**Strict (Level A):** local Lorentzian branch, necessity of a covariant macroscopic completion, GR recovery when additional branch variables freeze.

**Structural (Level B):** minimal nonlinear covariant completion used in this chapter (the  $\phi$ -first closure and generalised Einstein equations derived from it).

**Closure-dependent:** specific functional choices for  $G_{\text{eff}}(\phi)$ ,  $\Lambda_{\text{eff}}(\phi)$ , detailed galactic and cosmological fits.

**What is established, what is singled out, and what remains open.** At the present stage, the ECT gravity programme contains three layers. First, the ordered branch supports a massless tensor sector on the emergent Lorentzian background, with linear weak-field dynamics derived from the condensate EFT (§8.5; Level A for massless tensor propagation). Second, once universal coupling to the same effective stress tensor and the consistency of the gauge-redundant spin-2 sector are imposed, the Einstein–Hilbert nonlinear closure is singled out as the unique two-derivative completion of the ordered-branch gravitational route (Level A/B; §13.5). Third, the exact microscopic derivation of all nonlinear coefficients directly from the bare condensate action, as well as the controlled suppression of higher-curvature corrections, remain open (OP2, OP3).

### 13.1 Effective metric and the macroscopic limit of the condensate

*Status: Level A for the emergence of the effective Lorentzian metric structure in the broken-phase EFT (Theorem 3.2). The position-dependent coupling  $G_{\text{eff}}(X) = G_N e^{-\beta\phi(X)}$  introduced below belongs to the current ordered-branch  $\phi$ -first closure and is therefore Level B.*

The purpose of this subsection is to identify the minimal rank-2 tensorial object that governs the causal coarse-grained branch of ECT. As established in ECT basics, once the vacuum sector has selected an ordered background and the theory is restricted to long wavelengths, the heavy radial mode decouples and the physically relevant degrees of freedom are the slow orientation modes of the condensate. However, this by itself does not yet determine whether the resulting coarse-grained description admits a geometric interpretation, nor which tensorial object should play that role. We now show that, in the ordered



phase, residual symmetry leaves a unique local symmetric rank-2 tensor structure, and that in the viable Lorentzian window this structure is naturally interpreted as the effective metric of the macroscopic branch.

### Coarse-graining and the macroscopic regime

The macroscopic regime of ECT is defined not only by large distances, but by coarse-graining over the microscopic structure of the ordered condensate. At the level of the bare microdynamics (P3), the fundamental field  $\Phi$  and its gradient condensate retain an internal structure that need not be geometric at ultrashort scales. A geometric description becomes meaningful only after averaging over regions much larger than the condensate correlation length  $\xi_{\text{cond}} \sim m_\sigma^{-1}$  (Appendix O).

Let  $B_\ell(X) \subset \mathcal{M}^4$  be a neighbourhood of characteristic size  $\ell$  such that

$$\xi_{\text{cond}} \ll \ell \ll L, \quad E \ll m_\sigma, \quad (13.1)$$

where  $L$  is the characteristic observational scale and  $E$  the characteristic excitation energy. The coarse-grained orientation field:

$$\bar{n}_A(X) = \frac{1}{\mathcal{N}_\ell} \int_{B_\ell(X)} d^4Y W_\ell(X-Y) n_A(Y), \quad (13.2)$$

where  $W_\ell$  is a smooth window function localised at scale  $\ell$  and  $\mathcal{N}_\ell$  is the normalisation factor. In the ordered phase  $\bar{n}_A$  varies slowly:

$$|\partial_B \bar{n}_A| \ll \xi_{\text{cond}}^{-1}, \quad |\partial_C \partial_B \bar{n}_A| \ll \xi_{\text{cond}}^{-2}. \quad (13.3)$$

Physically, the inequalities (13.1) define the regime in which the condensate no longer needs to be resolved as a strongly structured microscopic medium. For  $L \gg \xi_{\text{cond}}$  and  $E \ll m_\sigma$  the radial mode  $\sigma$  is effectively integrated out (Appendix K), and the remaining observables are controlled by slow orientation/background variables. This is precisely the regime in which an autonomous coarse-grained causal description becomes possible; the next step is to show that, within the viable Lorentzian branch, this description takes geometric form.

### Uniqueness of the macroscopic rank-2 tensor

After spontaneous symmetry breaking  $O(4) \rightarrow O(3)$ , the only local rank-2 tensors available in the ordered phase are the Euclidean tensor  $\delta_{AB}$  and the projector onto the preferred direction,  $\bar{n}_A \bar{n}_B$ . By Theorem 3.2 (Appendix C), any symmetric rank-2 tensor compatible with the residual  $O(3)$  symmetry must therefore have the form:

$$K^{AB} = \beta \delta^{AB} - \alpha \bar{n}^A \bar{n}^B. \quad (13.4)$$

Introducing the orthogonal projectors

$$P_{\parallel}^{AB} = \bar{n}^A \bar{n}^B, \quad P_{\perp}^{AB} = \delta^{AB} - \bar{n}^A \bar{n}^B, \quad (13.5)$$

this becomes:

$$K^{AB} = \beta P_{\perp}^{AB} - (\alpha - \beta) P_{\parallel}^{AB}. \quad (13.6)$$

This is the macroscopic version of the tensor-uniqueness result established in ECT basics (§3.3).

At this stage one should distinguish two logically separate claims. First, the residual symmetry fixes the admissible tensorial structure uniquely. Second, only in the hyperbolic Lorentzian regime does that structure define a viable causal branch and therefore admit a natural interpretation as an effective metric. Thus geometry is not postulated independently: it is the geometric realisation of the viable coarse-grained causal tensor structure.

The effective metric is not introduced as an additional primitive field. Rather, once the ordered branch is selected and one restricts attention to the viable Lorentzian coarse-grained sector, the residual symmetry analysis leaves a unique symmetric rank-2 tensor structure, and this structure is naturally interpreted as the effective metric. For this reason the geometric branch of ECT is not a field theory defined on an independently chosen spacetime background. Its causal structure is instead read off from the coarse-grained ordered condensate.

### Geometric realisation of the viable tensor structure

Since  $K^{AB}$  (13.6) controls the principal part of long-wavelength equations of motion, it defines the causal and metric structure of the macroscopic sector. In the viable Lorentzian coarse-grained regime, the unique inverse-metric candidate is therefore read as:

$$g_{\text{eff}}^{AB} = \beta P_{\perp}^{AB} - (\alpha - \beta) P_{\parallel}^{AB}, \quad (13.7)$$

equivalently written as:

$$g_{\text{eff}}^{AB} = \beta \delta^{AB} - \alpha \bar{n}^A \bar{n}^B. \quad (13.8)$$

Because  $P_{\perp}$  and  $P_{\parallel}$  are orthogonal projectors, the covariant inverse metric is obtained exactly:

$$g_{AB}^{\text{eff}} = \frac{1}{\beta} P_{AB}^{\perp} - \frac{1}{\alpha - \beta} P_{AB}^{\parallel}, \quad g_{\text{eff}}^{AC} g_{CB}^{\text{eff}} = \delta^A_B. \quad (13.9)$$

At this stage the effective metric is fixed only up to an overall positive conformal factor—sufficient for determining causal structure and the relative stiffness of longitudinal vs. transverse directions. Overall normalisation is fixed later through matching conditions (§13.4).

### Lorentzian signature of the ordered phase

Choose the local ordered frame  $\bar{n}^A = (0, 0, 0, 1)$ . Equation (13.7) then gives:

$$g_{\text{eff}}^{AB} = \text{diag}(\beta, \beta, \beta, -(\alpha - \beta)). \quad (13.10)$$

For  $\alpha > \beta$  one eigenvalue changes sign and the effective metric acquires Lorentzian signature at the level of the hyperbolic lower bound. In the present macroscopic programme, the working viable Lorentzian/macrosopic window is the stronger condition  $\beta < \alpha < 4\beta$  inherited from ECT basics (Section 3.5). At canonical normalisation  $\alpha = 2, \beta = 1$ :  $g_{\text{eff}}^{AB} = \text{diag}(1, 1, 1, -1) = \eta^{AB}$  (Level A in EFT).

This is the precise mathematical form of the “emergence of time”: time is not introduced as an external coordinate but emerges as the distinguished direction of the gradient-ordered condensate, identified dynamically through the sign change of the kinetic tensor.

Defining  $c_*^2 = \beta/(\alpha - \beta)$  (3.14) and writing  $w = c_* t$ , the principal hyperbolic operator is:

$$g_{\text{eff}}^{AB} \partial_A \partial_B = \beta \left( \nabla^2 - \frac{1}{c_*^2} \partial_t^2 \right) \propto \partial_t^2 - c_*^2 \nabla^2. \quad (13.11)$$

This hyperbolic structure underlies retarded Green functions (proved in Appendix E), causal cones, and the tensorial propagation sector developed in §13.2.

### Null structure and causal cones

The effective null cones of the macroscopic branch:

$$g_{\text{eff}}^{AB} k_A k_B = 0 \implies \beta \mathbf{k}^2 - (\alpha - \beta) k_w^2 = 0 \implies \omega^2 = c_*^2 \mathbf{k}^2. \quad (13.12)$$

Causal cones are emergent properties of the ordered condensate, not primitive structures of the Euclidean arena. For a macroscopic observer insensitive to coherent phase data, the condensate appears as a Lorentzian medium: propagation is hyperbolic, disturbances possess retarded response, and causal order is reconstructed from the geometry of propagation. This condensed-matter perspective on causality has precedents in analogue gravity [65, 21].

## Phenomenological $\phi$ -first closure of the macroscopic branch

The uniqueness of the underlying coarse-grained tensor structure is a strict Level A result; its interpretation as the effective metric of the macroscopic causal branch is the corresponding geometric reading within the viable Lorentzian regime. By contrast, the introduction of a position-dependent effective Newton coupling through a macroscopic amplitude variable is part of the current ordered-branch closure of the macroscopic branch and is Level B.

To parameterise slow background variations of the ordered branch, define the macroscopic amplitude variable:

$$\phi(X) \equiv \frac{1}{\beta} \ln \frac{u(X)}{u_\infty}, \quad \phi|_{\text{vac}} = 0, \quad (13.13)$$

where  $u(X)$  is the ordered-branch condensate amplitude introduced in Section 3.2,  $u_\infty$  is its asymptotic screened value, and  $\beta$  is a dimensionless coupling parameter. With this normalisation one has  $u/u_\infty = e^{\beta\phi}$ , matching the notation used throughout the later macroscopic  $\phi$ -sector. An equivalent ordered-branch amplitude variable  $\chi$  was used in intermediate formulations of the galactic EFT. In the present notation this role is played by  $u$ , so one may read  $\chi$ -based formulas as their  $u$ -based counterparts. In the current ordered-branch  $\phi$ -first closure:

$$G_{\text{eff}}(X) = G_N e^{-\beta\phi(X)}. \quad (13.14)$$

This is not a completed first-principles theorem from bare P3; it is the current ansatz connecting the strict Level A effective Lorentzian geometry to the Level B phenomenological closure needed for observational applications (§§13.5–19.1).

## What is established and what is not

### Established (Level A in broken-phase EFT):

- (i) The ordered phase admits a unique symmetric rank-2 tensor compatible with residual  $O(3)$ .
- (ii) This tensor controls the principal part of propagation and defines the unique inverse-metric candidate of the geometric branch, whose geometric interpretation is selected in the viable Lorentzian regime.
- (iii) For  $\alpha > \beta$  the effective metric has Lorentzian signature.
- (iv) The null structure and causal cones are emergent properties of the ordered condensate.

### Not yet established:

- (i)  $g_{AB}^{\text{eff}}$  has not yet been identified with the complete physical metric of nonlinear GR.
- (ii) Conformal normalisation is not fixed by ECT basics alone.
- (iii) Matter coupling universality (A4) is Level B, not Level A.
- (iv)  $G_{\text{eff}}(X) = G_N e^{-\beta\phi}$  is a phenomenological ansatz, not a first-principles theorem.

The correct status is therefore Level A for the emergence of the effective Lorentzian metric structure itself, and Level B for the phenomenological  $\phi$ -first closure used to connect that structure to macroscopic applications.

## Physical interpretation

In the ordered phase the condensate ceases to be an isotropic Euclidean medium. One coarse-grained direction becomes dynamically distinguished by the gradient condensate. A macroscopic observer insensitive to phase information but sensitive to propagation delays and source responses reconstructs a Lorentzian spacetime not because it was postulated, but because the ordered condensate acts as a medium whose tensorial response defines one. The effective metric of ECT is thus a coarse-grained observable of the ordered medium itself—not an external geometrical structure imposed upon it [21].

## Summary

In the macroscopic limit the ordered phase generates an effective Lorentzian metric:

$$g_{\text{eff}}^{AB} = \beta (\delta^{AB} - \bar{n}^A \bar{n}^B) - (\alpha - \beta) \bar{n}^A \bar{n}^B, \quad (13.15)$$

unique by Theorem 3.2, defined up to conformal normalisation, and governing the causal structure of the geometric branch. This metric is the primary geometric object for all subsequent subsections: linear tensor sector (§13.2), Noether sources (§13.3), matching of  $M_G$  (§13.4), nonlinear closure (§13.5), and phenomenological applications (§§13.6–19.1).

## 13.2 Linear tensor sector and the emergence of gravitational propagation

*Status: massless tensor propagation Level A in EFT; physical TT polarisations remain Level A/B. P5 strengthens the consistency of the internal gauge architecture but does not by itself complete the TT reduction theorem (OP-gauge). Migrated from: sec:spin2\_content, app:sigma\_model.*

### Orientation modes as metric perturbations

From the sigma-model analysis (Appendix AA), the three soft orientation modes  $\delta n_i$  satisfy:

$$\partial_t^2 \delta n_i - c_n^2 \nabla^2 \delta n_i = 0, \quad \omega^2 = c_n^2 k^2, \quad c_n \approx c_* \quad (\text{EFT matching}). \quad (13.16)$$

Through  $g^{\text{eff}}$  (13.15), these modes induce metric perturbations  $h_{\mu\nu} \propto \delta n_i$ . The resulting sector is a symmetric rank-2 tensor under  $O(3)$  propagating at  $c_n = c_*$  (Level A in broken-phase EFT).

**Physical meaning.** The orientation modes  $\delta n_i$  arise from the broken  $O(4) \rightarrow O(3)$  symmetry of the ordered branch. Their long-wavelength limit becomes gravitational wave propagation. Gravity emerges as the IR limit of the orientation sector of the broken condensate (Level B; the exact independent mode content is constrained by integrability, see Appendix I).

### Fierz–Pauli-like structure at linearised level

On scales  $L \gg \xi_{\text{cond}}$ , the quadratic action for metric perturbations can be organised in a Fierz–Pauli-like form [44]:

$$S_{\text{FP}} = M_G^2 \int d^4x \left[ \frac{1}{4} (\partial_\lambda h_{\mu\nu})^2 - \frac{1}{4} (\partial_\lambda h)^2 + \frac{1}{2} \partial_\mu h^{\mu\nu} \partial_\nu h - \frac{1}{2} (\partial_\lambda h^{\mu\nu}) (\partial_\mu h_{\nu\lambda}) \right], \quad (13.17)$$

where  $h = \eta^{\mu\nu} h_{\mu\nu}$  and  $M_G$  is the induced gravitational stiffness scale of the tensor EFT. Its identification with the observed reduced Planck mass,  $M_G = \bar{M}_{\text{Pl}}$ , belongs to weak-field matching (Level B), whereas the existence of the linear tensorial kinetic structure after coarse-graining is the Level A part of the result. Exact reducibility to the standard Fierz–Pauli form remains part of OP-gauge/OP2.

**Status of the two physical polarisations.** If the macroscopic ECT tensor action is exactly reducible to Fierz–Pauli form (13.17), then the usual linearised gauge invariance  $h_{\mu\nu} \rightarrow h_{\mu\nu} + \partial_\mu \xi_\nu + \partial_\nu \xi_\mu$  would imply a reduction from 10 components to 2 physical TT modes. *This reducibility has not yet been demonstrated explicitly in the ECT condensate language (OP-gauge).* Massless tensor propagation: Level A in EFT; exactly 2 TT modes: Level B/C (OP-gauge; P5 fixes internal gauge architecture but TT reduction requires gravitational gauge analysis).

**How P5 contributes to the tensor-sector analysis.** P5 resolves the internal ordered-branch gauge architecture as  $SU(2) \times U(1)$  and thereby removes one major source of ambiguity in the low-energy mode-counting framework. However, the exact reduction of the tensor sector to two physical transverse-traceless polarisations still depends on the gravitational gauge structure of the linearised tensor action itself, which is a separate question from the internal gauge architecture. Thus P5 strengthens the consistency of the tensor-sector interpretation but does not by itself complete the TT reduction theorem (OP-gauge).

**Comparison with Einstein-aether theory.** In Einstein-aether theory [24] the unit vector field  $u^A$  is a separate fundamental field. In ECT,  $n_A$  is a collective variable of the broken phase, not in the bare action P3. The Fierz–Pauli structure emerges spontaneously, not by postulate.

### Deser-compatible self-coupling route and Einstein closure uniqueness

The structure established above satisfies the requirements of Deser’s self-coupling bootstrap [66]. The geometric branch is therefore *compatible with* a Deser-type route to nonlinear Einstein equations (Level B; OP2).

**Einstein closure as the unique low-derivative nonlinear completion (Level A/B).** Suppose that the ordered branch admits: (i) a massless spin-2 weak-field sector on the emergent Lorentzian background (established in §8.5), (ii) universal coupling of that sector to the same effective stress-energy tensor that sources the macroscopic geometry (§13.3), and (iii) no additional unsuppressed tensor structures at the same two-derivative order. Then the requirement of nonlinear self-consistency of the spin-2 sector—specifically, the preservation of the contracted Bianchi identity and the absence of ghost-like inconsistencies—singles out the Einstein–Hilbert completion, up to the cosmological term, field redefinitions, and higher-derivative corrections. This is the Lovelock–Deser uniqueness [81, 66, 80] applied to the ECT geometric branch.

In this sense, ECT does not merely reproduce a gravitational analogy: it structurally selects the Einstein route as the unique consistent ordered-branch nonlinear completion at the two-derivative level. The additional  $\phi$ - and  $n_A$ -sectors of the full ECT closure represent ordered-branch corrections *beyond* this pure-metric Einstein limit, controlled by the condensate amplitude and orientation sectors.

**What this does not yet establish.** The present argument does not yet derive every nonlinear coefficient directly from the microscopic condensate action. Nor does it exclude all higher-curvature corrections beyond the Einstein–Hilbert level. What it does establish is that, within the ordered-branch two-derivative closure and under universal coupling, the nonlinear Einstein route is uniquely selected as the consistent completion of the massless spin-2 sector.

**Falsifier for the Einstein-closure programme.** The present programme would fail if the weak-field ordered-branch tensor sector required a nonlinear completion that is not equivalent, at the two-derivative level, to the Einstein–Hilbert route; or if matter sectors coupled non-universally to inequivalent effective metrics; or if an unsuppressed extra scalar or vector component remained unavoidable in the same low-energy gravitational regime where GR is empirically verified.

### 13.3 Matter coupling and the Noether source structure

*Status: conservation laws Level A; existence of a macroscopic source tensor Level A in the EFT; universality of matter coupling Level B (OP-matter). The orientation-sector contribution to the effective source structure can be written in an Einstein-aether-like EFT form; the matching of its coefficients to the microscopic condensate parameters remains Level B/open (OP2, OP-c1). Migrated and expanded from: sec:noether, Appendix Q, and the deferred ECT basics notes.*

The previous subsections established the effective metric structure of the geometric branch and the existence of a linear tensorial propagation sector. The question now is: *what plays the role of the gravitational source in ECT?* In general relativity the answer is the stress-energy tensor, which is postulated to appear on the right-hand side of the Einstein equations. In ECT the situation is conceptually different: the geometric branch is not postulated from the outset as a spacetime theory but emerges from the ordered condensate. It must therefore be shown that the source structure arises *variationally* from the same condensate framework.

### The variational origin of conserved source currents

At the microscopic level the ECT action is local and does not depend explicitly on the coordinates  $X^A$  of the Euclidean arena (P1, P3). By Noether's theorem applied to translational invariance [47], this yields a conserved rank-2 current for the scalar sector:

$$T_{(\Phi)}^{AB} = \frac{\partial \mathcal{L}_\Phi}{\partial (\partial_A \Phi)} \partial^B \Phi - \delta^{AB} \mathcal{L}_\Phi, \quad \partial_A T_{(\Phi)}^{AB} = 0 \quad (\text{Level A}). \quad (13.18)$$

The complete form including translational and rotational currents is derived in Appendix Q. In the Lorentzian ordered branch, parametrised in real time by  $w = c_* t$ , this becomes the standard covariant conservation law  $\nabla_\mu T^{\mu\nu} = 0$ .

This is a strict Level A statement. It depends only on the homogeneity of the Euclidean arena (P1) and on the locality of the action (P3), not on any phenomenological closure. The existence of a conserved source tensor in ECT is therefore not borrowed from GR but intrinsic to the condensate's variational structure.

**Caveat: time-dependent backgrounds.** When the condensate background evolves in time (cosmological setting), exact time-translation invariance is broken and global energy conservation does not hold — precisely as in GR with an evolving metric [82]. This is not a defect of ECT; it is structural consistency with the GR-like limit.

### From microscopic current to macroscopic source

The tensor (13.18) is defined at the microscopic level. The macroscopic branch requires a coarse-grained version. Applying the same window function (13.2):

$$\bar{T}^{AB}(X) = \frac{1}{\mathcal{N}_\ell} \int_{B_\ell(X)} d^4 Y W_\ell(X - Y) T^{AB}(Y). \quad (13.19)$$

Because averaging commutes with differentiation at long wavelengths:

$$\partial_A \bar{T}^{AB} = 0 \quad (\text{up to higher-gradient corrections} \sim (\xi_{\text{cond}}/L)^2). \quad (13.20)$$

The macroscopic source tensor of the geometric branch therefore remains conserved (Level A in the coarse-grained EFT).

Physically, the macroscopic observer does not measure microscopic gradients of  $\Phi$  directly. What is reconstructed are long-wavelength energy densities, momentum fluxes, and stress-like components — the hydrodynamic analogue of the microscopic Noether current.

### Orientation-sector contribution to the macroscopic source

Beyond the pure scalar contribution (13.18), the ordered phase contributes an additional source component associated with the orientation field  $\bar{n}_A$ . At the level of the minimal sigma-model EFT (Appendix AA), the corresponding source tensor has the schematic structure:

$$T_{AB}^{(n)} = K_n [(\nabla_A n_C)(\nabla_B n^C) - \frac{1}{2} g_{AB} (\nabla_C n_D)(\nabla^C n^D)] + \lambda_n n_A n_B + \Delta_{AB}^{(n)}, \quad (13.21)$$

where  $K_n$  is the orientation-sector stiffness (related to  $\kappa_n$ , Section 13.4),  $\lambda_n$  enforces the normalisation constraint on  $n_A$ , and  $\Delta_{AB}^{(n)}$  collects additional higher-derivative, curvature-coupled, or Einstein-aether-like contributions appearing in more complete effective descriptions of the ordered branch [24].

The precise coefficient matching of  $K_n$ ,  $\lambda_n$ , and the subleading terms  $\Delta_{AB}^{(n)}$  to the microscopic condensate parameters of bare P3 has not yet been completed. Their correct status is therefore Level B/open (OP2, OP-c1).

This formulation is sufficient for the purposes of Macroscopic Physics: it establishes that the ordered orientation sector contributes nontrivially to the macroscopic source tensor, while leaving the full first-principles completion to later work.

## Rotational currents and the role of $O(4)$ symmetry

From  $O(4)$ -invariance (P2), Noether's theorem gives rotational currents:

$$J^{C,AB} = X^A T^{CB} - X^B T^{CA} + S^{C,AB}, \quad \partial_C J^{C,AB} = 0 \quad (\text{Level A}), \quad (13.22)$$

where  $S^{C,AB}$  is the spin part (zero for the pure scalar sector). In the ordered phase the collective variable  $n_A$  induces a nontrivial rotational current in the orientation sector.

The distinction between translational and rotational Noether structures must be kept precise. The conservation  $\partial_A T^{AB} = 0$  comes from *translation* invariance, not from  $O(4)$  rotations. The  $O(4)$  symmetry instead constrains the tensorial form of the ordered phase and produces the anisotropic corrections below.

## Anisotropic source corrections

Because the ordered phase is not isotropic, the macroscopic source structure contains anisotropic corrections from the rotational Noether sector. In the effective Lorentzian language these take the form (Appendix AB):

$$\Theta_{\mu\nu}[n] = c_1 \left( n_\mu n^\lambda R_{\lambda\nu} + n_\nu n^\lambda R_{\lambda\mu} - \frac{1}{2} g_{\mu\nu} n^\alpha n^\beta R_{\alpha\beta} \right), \quad (13.23)$$

where  $c_1$  is a condensate-parameter-dependent coefficient (OP-c1). This tensor is absent from standard GR; in Einstein-aether theory [24] an analogous term is postulated as a fundamental coupling, whereas in ECT it arises variationally from the rotational Noether structure of the ordered phase. The comparison is instructive: the same structure that one theory must postulate, the other derives from symmetry.

## Why the source couples to the geometric branch

The natural coupling of  $\bar{T}^{AB}$  to the geometric branch follows from the structure of the coarse-grained EFT. The geometric branch is the phase-insensitive, tensorial sector of the ordered condensate. Its propagating excitations are the long-wavelength tensorial deformations whose kinetic structure is governed by  $g_{AB}^{\text{eff}}$ . The only conserved rank-2 object available to source such deformations is precisely the coarse-grained Noether tensor  $\bar{T}^{AB}$ . The source coupling therefore follows from the EFT organisation, not from a separate postulate (Level A for existence; Level B for full nonlinear coupling, see Section 13.5).

## Universality of matter coupling: current status

A stronger claim is that *all* slow matter sectors couple universally to the same effective metric  $g_{\mu\nu}^{\text{eff}}$ . This is the analogue of the weak equivalence principle. Within the present formulation it is a working assumption (A4):

All matter sectors with  $E \ll m_\sigma$  couple to the same coarse-grained geometric structure  $g_{\mu\nu}^{\text{eff}}$ .

This is physically natural: once phase information is coarse-grained away, the only macroscopic geometric data available to all slow sectors is the same effective metric background. Nevertheless, deriving this universality directly from bare P3 for specific matter sectors has not yet been completed (Level B, OP-matter).

What is established at Level A is the existence of a conserved macroscopic source tensor and the natural coupling of the geometric branch to that tensor. What is not yet established at Level A is the full universality of matter coupling for arbitrary matter sectors.

## Physical interpretation

The Noether source structure of ECT carries a simple physical message: the same condensate that generates the geometric branch also contains, through its variational foundation, the conserved quantities that source that branch. There is no split between “geometry” and “matter” at the deepest level. Both are different long-wavelength aspects of the same ordered medium.

A macroscopic observer reconstructs the familiar language of gravity: metric perturbations respond to stress-energy; causal propagation is governed by the effective Lorentzian metric; matter distributions shape the geometry of low-energy probes. In ECT this structure is not postulated from the outset but reconstructed from the variational and symmetry properties of the ordered condensate.

### What is established and what is not

#### Established (Level A):

- (i) Conserved Noether tensor  $T^{AB}$  from translational invariance (13.18).
- (ii) Coarse-grained  $\bar{T}^{AB}$  remains conserved in the long-wavelength regime (13.20).
- (iii) The geometric branch admits a natural coupling to a conserved rank-2 source tensor.
- (iv) Rotational currents  $J^{C,AB}$  exist and generate anisotropic corrections (13.23).

#### Open or conditional:

- (i) Full universality of matter coupling is Level B (OP-matter).
- (ii) Explicit nonlinear source structure beyond linear EFT: Section 13.5.
- (iii) Coefficient  $c_1$  not yet derived from first principles (OP-c1). In particular, determine whether the completed tensor/orientation closure yields phenomenologically viable functions  $\mu(k, z)$ ,  $\eta(k, z)$ , and  $\Sigma(k, z)$  on cosmological linear scales, and whether their sign and scale dependence can be simultaneously reconciled with weak lensing, redshift-space distortions, CMB lensing, cluster lensing, and the Hubble-sector benchmark.
- (iv) Matching of  $K_n$ ,  $\lambda_n$  to bare P3 condensate parameters (OP2).

### Summary

The macroscopic source structure of ECT follows from the variational foundation of the ordered condensate. Translational invariance provides the conserved source tensor  $T^{AB}$  and its coarse-grained counterpart  $\bar{T}^{AB}$ ;  $O(4)$ -rotational symmetry generates anisotropic corrections through the orientation-sector current structure. The coupling of the geometric branch to a source tensor is the only variationally natural possibility in the coarse-grained EFT, not an additional postulate. This establishes the source side of macroscopic gravity in ECT and prepares the ground for the matching of gravitational stiffness and the status of the Newton constant in the next subsection.

## 13.4 Gravitational stiffness, Newton constant, and the status of $G_N$

*Status: Level A for the existence of a gravitational stiffness scale in the linear tensor EFT; Level B for its matching to the observed Newton constant  $G_N$ . Direct derivation of  $M_G$  from the microscopic condensate parameters of bare P3 remains open (OP2, OP3, OP-grad). Migrated and rewritten from: sec:GN\_matching.*

The previous subsections established three ingredients of the geometric branch: (i) an effective Lorentzian metric structure  $g_{\mu\nu}^{\text{eff}}$ , (ii) a linear tensorial propagation sector, and (iii) a conserved source tensor. The next question is: *what sets the strength of gravitational response in ECT?* In standard relativistic language this is answered by the Newton constant  $G_N$  or equivalently the reduced Planck scale  $\bar{M}_{\text{Pl}}$ . In ECT the logically prior object is not  $G_N$  itself but the *gravitational stiffness* of the ordered condensate, denoted  $M_G$ .



### Why a stiffness scale must exist

Once the ordered branch supports long-wavelength tensorial deformations, their quadratic effective action necessarily carries a coefficient with dimension mass<sup>2</sup>. This coefficient measures how costly it is to deform the ordered condensate geometry on macroscopic scales. Exactly in this sense, the geometric branch possesses a stiffness. Schematically:

$$S_{\text{tens}}^{(2)} \sim M_G^2 \int d^4x (\partial h)^2. \quad (13.24)$$

The existence of such a coefficient is a Level A EFT statement: once a linear tensor sector exists, its quadratic action necessarily contains a normalisation scale. What is not yet fixed at Level A is the numerical identification of that scale with the observed gravitational coupling.

Physically,  $M_G$  is the analogue of an elastic modulus of the ordered condensate, but for geometric/tensorial deformations rather than for ordinary lattice strain. Large  $M_G$  means that the condensate geometry is extremely stiff: macroscopic curvature is generated only weakly by ordinary matter sources. This is precisely what one expects from the observed weakness of gravity.

### Definition of $M_G$ from the linear tensor sector

The gravitational stiffness scale is defined by the overall coefficient of the quadratic tensor kinetic term in the macroscopic EFT. Using the Fierz–Pauli-like organisation of the linear tensor action established in Section 13.2:

$$M_G^2 = \bar{M}_{\text{Pl}}^2 = \frac{c_*^4}{8\pi G_N} \approx (2.435 \times 10^{18} \text{ GeV})^2 \quad (\text{Level B: EFT matching}). \quad (13.25)$$

Here  $M_G$  is *not* assumed to equal  $\bar{M}_{\text{Pl}}$  by definition. Rather, it is the normalisation scale of the ECT tensor EFT, which is then compared with observed weak-field gravity to fix its numerical value.

### Matching to the observed Newton constant

Comparison with linearised GR gives the macroscopic matching relation:

$$G_N = \frac{c_*^4}{8\pi M_G^2}. \quad (13.26)$$

This is a Level B statement: a geometric EFT matching between the macroscopic ECT tensor sector and the empirically known linear gravitational response. It must be read in the correct direction: observed gravity fixes the numerical value of  $M_G$ ; ECT does not yet derive  $G_N$  from bare P3. Thus  $M_G$  is the ECT quantity and  $G_N$  is the measured constant to which it is matched.

This methodological point matters. In older formulations the temptation was to write down a direct formula for  $G_N$  from microscopic condensate parameters too early, before the EFT logic was fully established. In the present postulate-based reconstruction the geometric branch first produces a stiffness scale, and only afterwards is that scale matched to observed gravity.

### Relation to the orientation-sector stiffness

The appearance of  $M_G$  is not arbitrary. The ordered phase already contains, in the orientation sigma-model (Appendix AA), a stiffness coefficient  $\kappa_n$  governing the soft orientation modes:

$$S_n^{(2)} = \frac{\kappa_n}{2} \int d^4X (\partial_B \delta n_i) (\partial^B \delta n_i). \quad (13.27)$$

Since  $[\kappa_n] = \text{GeV}^2$  and  $[M_G^2] = \text{GeV}^2$ , dimensional consistency suggests that both scales are related. The minimal EFT estimate:

$$M_G^2 \sim c_M \kappa_n, \quad (13.28)$$

where  $c_M$  is a dimensionless matching coefficient of order unity. This is not yet a derivation from microscopic parameters; it is an intermediate bridge inside the ordered-branch EFT. The exact value of  $c_M$ , and the dependence of  $\kappa_n$  on  $(u_0, \alpha, \beta)$ , remain open (OP-grad, OP2).

### Hierarchy of scales and the open derivation chain

At present the correct hierarchy is:

- the gradient vacuum scale  $u_0$  (P4) characterises the ordered vacuum sector;
- the broken-phase kinetic anisotropy is controlled by  $(\alpha, \beta)$ ;
- the orientation sigma-model carries stiffness  $\kappa_n$ ;
- the macroscopic tensor sector carries stiffness  $M_G$ ;
- observed gravity fixes  $M_G$  through (13.25).

What is *not* yet available is a strict first-principles chain:

$$(u_0, \alpha, \beta) \longrightarrow \kappa_n \longrightarrow M_G \longrightarrow G_N. \quad (13.29)$$

That chain is one of the main open problems of the geometric branch. Any formula directly identifying  $M_G$  or  $G_N$  with a simple algebraic combination of  $(u_0, \alpha, \beta)$  must therefore be treated as legacy shorthand or phenomenological input unless explicitly rederived inside the new EFT logic.

### Notation and scale separation

The gravitational sector involves several conceptually distinct scales, which must not be conflated:

$$\underbrace{\phi_0}_{\text{bare scalar min.}}, \quad \underbrace{u_0}_{\text{gradient-ordered scale}}, \quad \underbrace{\kappa_n}_{\text{orient. stiffness}}, \quad \underbrace{M_G}_{\text{grav. stiffness}}. \quad (13.30)$$

No direct algebraic identification between the bare amplitude  $\phi_0$  and the ordered-branch EFT scales is assumed without explicit derivation (Section 5.1).

### Physical interpretation

The weakness of gravity in ECT is interpreted as extreme stiffness of the ordered condensate geometry. Ordinary matter sources are far too weak to significantly deform the ordered medium except over enormous scales. Newton's constant does not measure a primitive force inserted by hand; it measures the *inverse macroscopic compliance* of the ordered condensate geometry:  $G_N \propto M_G^{-2}$ . The smaller  $G_N$  is, the larger  $M_G$  is, and the harder it is to bend the ordered medium.

### Summary of statuses

Statement	Status	Basis
Gravitational stiffness scale $M_G$ exists in tensor EFT	Level A	Linear tensor sector
$M_G = \bar{M}_{\text{Pl}}$ : matched numerical value	Matched	Observational input
$G_N = c_*^4/(8\pi M_G^2)$ : matching relation	Level B	Comparison with lin. GR
$M_G^2 \sim c_M \kappa_n$ : EFT order-of-magnitude	Level B	Dimensional analysis
$(u_0, \alpha, \beta) \rightarrow \kappa_n \rightarrow M_G$ : derivation chain	Open	OP-grad, OP2
$G_N$ from bare P3 without EFT input	Open	OP3

### 13.5 Nonlinear closure and the generalised field equations

*Status: Level A for the structural necessity of a nonlinear macroscopic closure once the geometric branch contains (i) an effective Lorentzian metric, (ii) a tensor propagation sector, and (iii) a conserved source tensor. The identification of  $\phi$  as a reparameterisation of the ordered-branch amplitude is structural/bridge-level. The mapping of  $F(\phi)$ ,  $\omega(\phi)$ , and  $U(\phi)$  to the ordered-branch EFT is likewise structural/bridge-level. Level B for the explicit final nonlinear  $\phi$ -first closure. Lovelock uniqueness is Level A only under assumptions A1–A5. A first-principles derivation of the full nonlinear gravitational sector directly from bare P3 remains open (OP2, OP3, OP-matter).*

Sections 13.1–13.4 established the three ingredients that any macroscopic gravitational theory must contain: an effective Lorentzian metric structure, a propagating tensor sector, and a conserved source tensor. The central question of this subsection is therefore: *what is the strongest nonlinear gravitational structure currently justifiable within the ECT framework?*

#### Why nonlinear closure is unavoidable

The need for nonlinear closure is not an extra hypothesis but a direct consequence of the existence of the geometric branch itself. If the ordered condensate admits (i) an effective metric controlling causal propagation, (ii) a tensorial mode sector propagating on that metric, and (iii) a conserved source tensor coupled to that sector, then the response to finite-amplitude perturbations cannot be described consistently by a purely linear theory. The metric sector must self-interact, source terms must backreact on the background, and the effective coupling must be closed at nonlinear level.

This statement is Level A as a structural claim. What is *not* Level A is the exact final form of that closure. ECT at its current stage does not yet derive the full nonlinear metric dynamics directly from bare P3; instead it constrains the admissible closure strongly and yields the current best-developed macroscopic route: the ordered-branch  $\phi$ -first closure.

#### Why the closure is not taken to be pure GR immediately

The geometric branch is not purely metric in origin. It emerges from an ordered condensate that carries additional collective information at the macroscopic level:

- the orientation field  $n_A$ ,
- the amplitude-derived order variable  $\phi = \frac{1}{\beta} \ln(u/u_\infty)$  describing slow variations of the degree of condensate ordering,
- anisotropic correction tensors  $\Theta_{\mu\nu}[n]$  from the rotational Noether sector (13.23).

Therefore the most general nonlinear closure compatible with the present state of ECT is not *a priori* pure Einstein gravity, but an effective scalar-tensor-orientation system whose homogeneous pure-metric limit reduces to Einstein–Hilbert. ECT does not claim that nonlinear GR has already been derived from P3. What it claims is that the geometric branch narrows the admissible closure to a very restricted class, and that the current best-developed closure in that class is the  $\phi$ -first one.

#### Why the same variational principle yields different equations

Hilbert’s variational derivation of the Einstein equations was mathematically complete for the Einstein–Hilbert action: varying  $S_{\text{EH}} = \frac{1}{16\pi G} \int \sqrt{-g} R d^4x + S_{\text{matter}}$  yields exactly the Einstein field equations, because the action contains only the metric and minimally coupled matter fields. In ECT, the macroscopic action contains additional condensate-derived structures: the amplitude variable  $\phi$ , the ordered-branch orientation structure, and the corresponding nonminimal couplings allowed by the broken phase (§13.5). Once these are included in the generally covariant action, the variational principle yields the ECT nonlinear completion (13.35) rather than pure GR. The difference is therefore not in the variational method, but

in the dynamical field content and operator basis of the action. In this sense, GR is not wrong—it is the screened limit of a richer macroscopic structure.

### From the ordered-branch amplitude to the $\phi$ -field

The ordered-branch infrared EFT introduced in Section 3.2 already identifies two distinct collective variables of the condensate: the amplitude  $u(x)$  and the orientation field  $n_A(x)$ . At macroscopic scales these variables need not enter symmetrically. The causal tensor structure of the geometric branch is controlled primarily by the ordered orientation sector, whereas slow departures from homogeneous gravitational response are naturally carried by the condensate amplitude.

This motivates the following organisational step. Let  $u_\infty$  denote the asymptotic screened value of the ordered branch in the homogeneous large-scale limit. It is then natural to introduce a dimensionless amplitude variable

$$\phi(x) \equiv \frac{1}{\beta} \ln \frac{u(x)}{u_\infty}. \quad (13.31)$$

By construction,

$$\phi = 0$$

corresponds to the screened Einstein-like regime, while  $\phi \neq 0$  measures a local departure of the condensate amplitude from that asymptotic ordered background.

Several points are important.

**(i)  $\phi$  is not a new fundamental field.** It is a macroscopic reparameterisation of the ordered-branch amplitude. Thus the  $\phi$ -first closure is not introducing an extra scalar by hand; it is choosing a convenient infrared variable for the amplitude sector already present in the ordered condensate EFT.

**(ii) Why a logarithmic variable is natural.** The logarithmic form makes the screened limit multiplicative rather than additive, and it turns local relative changes of the condensate response into additive fluctuations of  $\phi$ . It also makes exponential factors such as  $e^{\beta\phi} = u/u_\infty$  appear naturally in the later macroscopic closure.

**(iii) Why the amplitude can modulate gravity macroscopically.** Within the ordered-branch EFT,  $u(x)$  is the only scalar collective variable measuring the local strength of ordering itself. It is therefore the natural candidate to modulate the stiffness or gravitational response of the geometric branch once one passes to a coarse-grained macroscopic description.

**(iv) Status.** The existence of an ordered-branch amplitude variable is part of the collective EFT structure of Section 3.2. The specific nonlinear macroscopic closure written in terms of  $\phi$  remains Level B. What this subsection provides is the missing conceptual bridge: the  $\phi$ -field is now explicitly anchored in the amplitude sector of the ordered condensate, rather than appearing as an isolated phenomenological scalar.

### Amplitude-dominated macroscopic reduction

The ordered-branch infrared EFT of Section 3.2 contains both the condensate amplitude  $u(x)$  and the orientation field  $n_A(x)$ . However, the macroscopic geometric branch need not retain both sectors on an equal footing. At large scales there is a natural reduction in which the dominant scalar response is carried by the condensate amplitude, while the orientation sector either freezes into the background causal structure or contributes only through subleading anisotropic corrections.

This motivates the amplitude-dominated macroscopic reduction:

$$S_{\text{ord}}^{(E)}[u, n] \longrightarrow S_{\text{macro}}[g, \phi, n], \quad \phi = \frac{1}{\beta} \ln \frac{u}{u_\infty}, \quad (13.32)$$

where the effective metric  $g_{\mu\nu}$  is read off from the viable Lorentzian tensor structure of the coarse-grained ordered branch,  $\phi$  parameterises the amplitude sector, and  $n_A$  survives only through the residual anisotropic/macroscopic orientation sector.

**Why this reduction is natural.** The amplitude  $u(x)$  is the only scalar collective variable measuring the local strength of ordering itself. If the large-scale gravitational response is modulated by how strongly the condensate is ordered relative to its asymptotic screened state, then the amplitude sector is the unique scalar carrier of that modulation. By contrast, the orientation sector primarily determines the causal tensor structure and therefore enters either through the background selection of the Lorentzian branch or through anisotropic corrections.

**What is being assumed and what is not.** This reduction does not yet assume the explicit  $\phi$ -first action (13.34). It only states that, among the collective variables of the ordered branch, the amplitude sector is the natural scalar degree of freedom to retain in the first macroscopic closure. The detailed coefficients of that closure, the functions  $\omega(\phi)$  and  $U(\phi)$ , and the exact coupling of  $n_A$  remain Level B.

**Consequence.** The nonlinear macroscopic closure used below is therefore not an isolated phenomenological scalar-tensor ansatz. It is the first amplitude-dominated coarse-grained realisation of the ordered condensate branch.

### From ordered-branch EFT coefficients to closure functions

The amplitude-dominated reduction identifies the ordered-branch amplitude as the natural scalar carrier of the first macroscopic closure. What remains is to explain why the functions entering the  $\phi$ -first action,

$$F(\phi), \quad \omega(\phi), \quad U(\phi),$$

are not arbitrary insertions but infrared images of structures already present in the ordered-branch EFT.

The starting point is the Euclidean ordered-branch functional (3.8),

$$S_{\text{ord}}^{(E)}[u, n] = \int d^4X \left[ \frac{Z_u}{2} (\partial u)^2 + \frac{\mathcal{C}_n}{2} u^2 (\partial n)^2 + W(u) + \Lambda_n (n_A n_A - 1) + \dots \right].$$

After amplitude-dominated coarse-graining and the logarithmic reparameterisation

$$\phi = \frac{1}{\beta} \ln(u/u_\infty), \quad u = u_\infty e^{\beta\phi},$$

three structural correspondences become natural.

**(i) Gravitational response factor.** Since the ordered-branch amplitude measures the local strength of the condensate relative to its asymptotic screened state, the simplest dimensionless response factor is

$$F(\phi) = \frac{u}{u_\infty} = e^{\beta\phi}.$$

Thus the multiplicative factor in front of the macroscopic curvature term is not chosen independently; it is the direct amplitude ratio of the ordered branch.

**(ii) Kinetic closure function.** The amplitude-gradient term in the ordered-branch EFT,

$$\frac{Z_u}{2} (\partial u)^2,$$

becomes, after  $u = u_\infty e^{\beta\phi}$ ,

$$\frac{Z_u \beta^2 u_\infty^2}{2} e^{2\beta\phi} (\partial\phi)^2.$$

After macroscopic field redefinitions and normalisation matching, this naturally gives rise to a positive kinetic closure function  $\omega(\phi)$  in the  $\phi$ -first action. Its explicit final form is still closure-dependent, but its origin in the amplitude-sector stiffness is structural.

**(iii) Effective potential.** The branch potential  $W(u)$  of the ordered condensate becomes

$$U(\phi) \equiv W(u_\infty e^{\beta\phi})$$

up to macroscopic normalisation and possible coarse-graining shifts. Therefore the effective scalar potential of the macroscopic closure is not a new independent potential; it is the amplitude-sector branch potential rewritten in the logarithmic variable  $\phi$ .

**What is and is not fixed here.** This mapping does not yet derive the full final nonlinear closure from first principles. It does, however, fix the logic of the closure:

$$\begin{aligned} F(\phi) &\text{ comes from the amplitude ratio } u/u_\infty, \\ \omega(\phi) &\text{ from amplitude-sector stiffness,} \\ U(\phi) &\text{ from the branch potential } W(u). \end{aligned}$$

The precise renormalised coefficients and the final phenomenological closure ansatz remain Level B, but the functions themselves are no longer conceptually free-floating. This is the common macroscopic origin of the later cosmological and galactic  $\phi$ -closures: their benchmark forms are therefore not independent phenomenological insertions, but specialisations of the same amplitude-first reduction at different observational scales.

### Minimal generally covariant operator basis

The amplitude-dominated macroscopic reduction identifies the minimal field content of the geometric branch:

- the effective metric  $g_{\mu\nu}$ ,
- the condensate amplitude variable  $\phi$  (reparameterising the ordered-branch amplitude  $u/u_\infty$ ),
- the orientation structure  $n^\mu$  inherited from the broken phase (a condensate-derived collective variable, not an independent aether-like field),
- matter fields  $\Psi$  minimally coupled to  $g_{\mu\nu}$ .

At two-derivative order, the corresponding minimal local diffeomorphism-invariant operator basis may be written schematically as

$$S_{\text{macro}} = \int d^4x \sqrt{-g} \left[ F(\phi) R - \frac{1}{2} Z(\phi) (\nabla\phi)^2 - U(\phi) + \mathcal{A}(\phi) n^\mu n^\nu R_{\mu\nu} + \mathcal{B}(\phi) (\nabla_\mu n_\nu) (\nabla^\mu n^\nu) + \mathcal{L}_{\text{mat}} \right]. \quad (13.33)$$

Here “schematically” means that Eq. (13.33) summarises the minimal covariant operator content relevant for the present low-energy completion, rather than claiming a unique microscopic derivation of each coefficient function from Euclidean microdynamics. Higher-derivative operators (four derivatives and above) are omitted under the infrared locality assumption A2 below. Parity-odd terms are excluded by the  $O(3)$  isotropy of the spatial sector. The normalisation condition  $n^\mu n_\mu = \varepsilon$  is understood as part of the ordered-branch structure; in the present minimal basis it is not introduced through an independent Lagrange-multiplier sector.

The  $\phi$ -first closure adopted in this chapter is obtained by specialising (13.33): the orientation sector  $\mathcal{A}, \mathcal{B}$  is absorbed into the causal background structure and subleading anisotropic corrections  $\Theta_{\mu\nu}$ , while the amplitude sector is retained through  $F(\phi) = e^{\beta\phi}$ ,  $Z(\phi) = \omega(\phi)$ , and  $U(\phi)$ .

### Working assumptions of the $\phi$ -first macroscopic closure

The assumptions below should be read on top of the amplitude-dominated macroscopic reduction introduced above. They do not create the  $\phi$ -sector from nothing; they specify the first nonlinear closure built on that reduction.

- A1 Ordered branch condition.**  $\alpha > \beta$ , so the effective metric has Lorentzian signature (Level A, Sections 3, 13.1).
- A2 IR locality.** Macroscopic dynamics at  $E \ll m_\sigma$ ; closure truncated at local, two-derivative order.
- A3 Four-dimensional geometry.** Large-scale branch is four-dimensional (P1 + ordered EFT).
- A4 Metric universality for slow matter.** Slow matter sectors couple to  $g_{\mu\nu}^{\text{eff}}$  (Level B, OP-matter).
- A5 Pure-metric reduction.** When  $\phi$  and  $n_A$  are frozen, the closure reduces to a pure-metric two-derivative theory (Lovelock step only).

Assumptions A1–A3 belong to the established macroscopic EFT; A4 is open but well-motivated; A5 is used only for the pure-metric limit.

### The $\phi$ -first effective IR action

Under A1–A4, the amplitude-dominated macroscopic reduction above, and the coefficient mapping just described, the most developed currently available amplitude-dominated completion is the  $\phi$ -first scalar-tensor closure

$$S_{\text{IR}} = \int d^4x \sqrt{-g} \left\{ \frac{\bar{M}_{\text{Pl}}^2}{2} e^{\beta\phi} R - \frac{\bar{M}_{\text{Pl}}^2}{2} \omega(\phi) (\partial_\mu \phi)^2 - U(\phi) + \mathcal{L}_{\text{mat}}[g_{\mu\nu}, \Psi] \right\}, \quad (13.34)$$

where  $e^{\beta\phi} = u/u_\infty$  expresses the local modulation of gravitational response by the condensate amplitude relative to its asymptotic screened value;  $\omega(\phi)(\partial\phi)^2$  governs slow dynamics of the macroscopic amplitude variable;  $U(\phi)$  is the corresponding macroscopic effective potential; and  $\mathcal{L}_{\text{mat}}$  encodes matter sectors. This action is Level B. Full derivation, comparison with GR/Brans–Dicke/Einstein-aether/Hořava–Lifshitz, and Theorems A–F: Appendix X.

### Generalised Einstein equations

Varying (13.34) w.r.t.  $g^{\mu\nu}$ :

$$e^{\beta\phi} (R_{\mu\nu} - \tfrac{1}{2} g_{\mu\nu} R) + \Lambda_{\text{eff}}(\phi) g_{\mu\nu} + \Theta_{\mu\nu}[\phi, n] = \frac{8\pi G_{\text{eff}}(\phi)}{c^4} T_{\mu\nu}^{\text{mat}}, \quad (13.35)$$

where  $\Lambda_{\text{eff}}(\phi) = U(\phi)/\bar{M}_{\text{Pl}}^2$ ,  $G_{\text{eff}}(\phi) = G_N e^{-\beta\phi}$  (13.14), so that the effective coupling is inversely modulated by the condensate amplitude relative to  $u_\infty$ ; and  $\Theta_{\mu\nu}[\phi, n]$  (13.23) collects derivative and anisotropic correction terms from the amplitude and orientation sectors. Equation (13.35) is the current best nonlinear field equation of the geometric branch (Level B).

This is also the point where the present framework diverges most sharply from the clock-field construction of Mukohyama and Uzan [2]. From a closely related Euclidean-to-Lorentzian starting point, their analysis leads to a covariant Galileon (a subclass of Horndeski theory) in the gravitational sector. ECT instead introduces a dynamical orientation sector whose effective stiffness enters the gravitational completion and is used here to motivate the generalised Einstein equations (13.35). The two frameworks therefore share the same Euclidean-to-Lorentzian starting question, but branch in different directions once gravity is constructed.

## Bianchi consistency and source conservation

Compatibility with the contracted Bianchi identity requires:

$$\nabla^\mu \left[ e^{\beta\phi} G_{\mu\nu} + \Lambda_{\text{eff}}(\phi) g_{\mu\nu} + \Theta_{\mu\nu}[\phi, n] \right] = \nabla^\mu \left[ \frac{8\pi G_{\text{eff}}(\phi)}{c^4} T_{\mu\nu}^{\text{mat}} \right]. \quad (13.36)$$

When  $\phi$  or  $n_A$  vary, this does not imply ordinary matter conservation alone; it implies conservation of the *total* macroscopic source structure. This is physically natural: matter, amplitude-sector gradients, and anisotropic condensate contributions exchange energy-momentum among themselves. Ordinary GR appears only when the additional ordered-branch variables are effectively frozen.

## Background reduction of the macroscopic closure

For cosmological applications one needs the isotropic background reduction of the macroscopic closure. The relevant approximation is not the fully frozen Einstein limit, but the weaker regime in which the orientation sector is absorbed into the homogeneous causal background while the amplitude sector remains slowly dynamical:

$$n_A \rightarrow \bar{n}_A, \quad \phi = \phi(t), \quad ds^2 = -c_*^2 dt^2 + a^2(t) \delta_{ij} dx^i dx^j.$$

In this regime the geometric branch retains a nontrivial scalar background degree of freedom while remaining compatible with homogeneous and isotropic FRW kinematics.

Under this isotropic background reduction, the  $\phi$ -first action (13.34) yields the schematic parent coupled system for the scale factor  $a(t)$  and the macroscopic amplitude variable  $\phi(t)$ . The full derived condensate background system obtained from the ordered-branch EFT is recorded later in Appendix AD, Section AD.1. The benchmark scalar–tensor action used for present numerical work is a late-time local truncation of that parent system. Writing

$$F(\phi) \equiv e^{\beta\phi},$$

the background equations take the schematic scalar–tensor form

$$3F(\phi)H^2 = \frac{\rho_m + \rho_r + U(\phi)}{\bar{M}_{\text{Pl}}^2} + \frac{1}{2}\omega(\phi)\dot{\phi}^2 - 3H\dot{F}, \quad (13.37)$$

$$-2F(\phi)\dot{H} = \frac{\rho_m + \frac{4}{3}\rho_r}{\bar{M}_{\text{Pl}}^2} + \omega(\phi)\dot{\phi}^2 + \ddot{F} - H\dot{F}, \quad (13.38)$$

together with the scalar background equation

$$\omega(\phi)(\ddot{\phi} + 3H\dot{\phi}) + \frac{1}{2}\omega_{,\phi}\dot{\phi}^2 + \frac{1}{\bar{M}_{\text{Pl}}^2}U_{,\phi} - 3(2H^2 + \dot{H})F_{,\phi} = 0. \quad (13.39)$$

Several remarks are important.

**(i) Derived status.** These equations are not a new phenomenological layer added after the fact. They are the isotropic background reduction of the macroscopic closure already introduced above. What remains Level B is the explicit choice of the closure functions  $F(\phi) = e^{\beta\phi}$ ,  $\omega(\phi)$ , and  $U(\phi)$ , not the existence of a coupled background system itself.

**(ii) Role of the orientation sector.** The orientation field does not disappear conceptually. Rather, in the isotropic background reduction it is frozen into the homogeneous causal branch and therefore no longer contributes independent anisotropic background degrees of freedom. Its effects reappear beyond FRW homogeneity through anisotropic or weak-field corrections.



**(iii) Relation to late-time cosmology.** The late-time background apparatus used in Section 19.1 and in Appendix AD should be read as a benchmark specialisation of Eqs. (13.37)–(13.39) to the present amplitude-first closure. Thus the cosmological sector is no longer an isolated add-on: it is the background branch of the same macroscopic system used in the geometric theory.

**(iv) Observational outputs.** Once the background solution  $H(z), \phi(z)$  is known, the cosmological observables used later in the paper follow through the standard FRW integral relations:

$$D_L(z), \quad t_{\text{lookback}}(z), \quad t_U(z), \quad t_{\text{gal}}(z_{\text{obs}}; z_{\text{form}}).$$

In ECT these are therefore not independent phenomenological inserts, but derived outputs of the macroscopic background reduction.

### Homogeneous limit and recovery of Einstein gravity

In the vacuum-normalised screened limit

$$\phi \rightarrow 0, \quad \nabla_\mu \phi = 0, \quad \Theta_{\mu\nu} \rightarrow 0,$$

Eq. (13.35) reduces to standard Einstein equations with cosmological constant:

$$R_{\mu\nu} - \frac{1}{2}g_{\mu\nu}R + \Lambda_{\text{eff}}g_{\mu\nu} = \frac{8\pi G_N}{c^4}T_{\mu\nu}^{\text{mat}}, \quad (13.40)$$

with  $\Lambda_{\text{eff}} = U(0)/\bar{M}_{\text{Pl}}^2$ . This shows that the ECT postulate structure does not push the theory away from GR at large homogeneous scales; GR is the special regime where additional macroscopic order variables are frozen or screened.

### Lovelock uniqueness of the pure-metric limit

Under A1–A5, Lovelock’s theorem [81] applies: in four dimensions, the unique local diffeomorphism-invariant two-derivative pure-metric field equations are those of Einstein–Hilbert gravity with cosmological constant.

**Status:** Level A *under A1–A5*. It is a theorem that the pure-metric frozen-order reduction cannot be anything other than Einstein–Hilbert +  $\Lambda$ . It is *not* a theorem that the full ECT geometric branch is always pure GR.

### Comparison with neighbouring theories

**General relativity.** GR corresponds to the homogeneous screened limit of the ordered branch, where  $\phi$  and  $n_A$  become dynamically invisible at macroscopic scales.

**Brans–Dicke scalar-tensor theories.** ECT shares an effective scalar modulating gravitational response. But  $\phi$  is not a new fundamental field; it is the logarithmic macroscopic amplitude variable of the ordered condensate branch.

**Einstein–aether theory [24].** ECT shares a preferred-direction variable and anisotropic correction tensors. But the orientation field is not fundamental in the bare action P3; it is a collective variable of the ordered condensate phase. This is the structural difference with Einstein-aether theories, which postulate such a field from the outset.

**Hořava–Lifshitz gravity.** ECT also has an emergent preferred structure, but does not begin by explicitly breaking Lorentz symmetry in the microscopic action. The preferred macroscopic direction appears through spontaneous ordering of the Euclidean arena.

## Physical interpretation

The nonlinear closure describes how the ordered condensate responds to finite macroscopic deformations. At linear level: propagating tensor modes. At nonlinear level: full backreaction of matter, order gradients, and anisotropic condensate structure on the emergent geometry.

Spacetime curvature is not an autonomous primitive field; it is the nonlinear macroscopic deformation pattern of the ordered condensate. The Einstein limit corresponds to the regime where the condensate amplitude is screened to its asymptotic value and the orientation sector is effectively frozen into the background causal structure, so that the medium appears purely metric. Deviations from GR correspond to residual macroscopic signatures of the underlying ordered structure.

**Three physical departures from GR.** The generalised equations (13.35) contain three structural elements absent from standard Einstein gravity:

(i) *Dynamic vacuum contribution*  $\Lambda_{\text{eff}}(\phi)$ . The effective cosmological term is not a constant but a function of the condensate amplitude. As the ordered phase evolves cosmologically,  $\Lambda_{\text{eff}}$  traces the branch potential  $U(\phi)$ . This can naturally realise quintessence-like behaviour with  $w \neq -1$ , depending on the branch potential and cosmological evolution (closure-dependent).

(ii) *Variable gravitational coupling*  $G_{\text{eff}}(\phi) = G_N e^{-\beta\phi}$ . Where the condensate is more strongly ordered (larger  $u$ ), the medium is stiffer and gravity appears weaker. In galactic environments this mechanism underlies the modified low-acceleration response discussed in §17.1 (closure-dependent phenomenology).

(iii) *Anisotropic condensate response*  $\Theta_{\mu\nu}[\phi, n]$ . This term has no analogue in GR. It resembles the  $c_1 \dots c_4$  terms in Einstein–aether theory [24], but in ECT it is not inserted as an independent sector by hand; it is tied to the orientation structure of the same ordered branch within the present covariant completion. It may induce effective gravitational-slip-like effects ( $\Psi \neq \Phi$  in Newtonian gauge), to be constrained by lensing/dynamical comparisons in galaxy clusters and by future surveys (Euclid, Vera Rubin) (structural interpretation; quantitative details closure-dependent).

## Derivation-level summary

**Strict (Level A):** local Lorentzian branch; necessity of a covariant macroscopic completion; GR recovery when additional branch variables freeze; Lovelock uniqueness of the pure-metric limit under A1–A5.

**Structural (Level B):** generalised nonlinear equations from the  $\phi$ -first closure; three departures from GR ( $\Lambda_{\text{eff}}$ ,  $G_{\text{eff}}$ ,  $\Theta_{\mu\nu}$ ); recovery of the standard PPN limit in the screened/frozen regime.

**Closure-dependent:** explicit functional forms of  $G_{\text{eff}}(\phi)$ ,  $\Lambda_{\text{eff}}(\phi)$ ,  $\omega(\phi)$ ,  $U(\phi)$ ; detailed galactic and cosmological fits; full post-Newtonian parameter set beyond  $\gamma_{\text{PPN}}$ .

## What is established and what is not (detailed)

### Established or structurally fixed:

- (i) A nonlinear closure is *required* once metric structure, tensor propagation, and source coupling all exist (Level A).
- (ii) The pure-metric two-derivative frozen-order limit is uniquely Einstein–Hilbert +  $\Lambda$  in  $d = 4$  (Level A under A1–A5).
- (iii) The current best-developed closure is the  $\phi$ -first one, Eq. (13.34) (Level B).
- (iv) The macroscopic scalar variable  $\phi$  is interpreted as a reparameterisation of the ordered-branch amplitude  $u/u_\infty$ , not as an extra fundamental field (bridge principle; structural).
- (v) The first macroscopic nonlinear reduction is amplitude-dominated: the scalar variable retained in the closure is the condensate amplitude sector, reparameterised by  $\phi = \frac{1}{\beta} \ln(u/u_\infty)$ , while the orientation sector survives through causal-background selection and anisotropic corrections (bridge principle; structural).

- (vi) The geometric branch admits an isotropic background reduction in which the amplitude sector remains dynamical while the orientation sector is frozen into the homogeneous causal background; the resulting FRW system is the parent structure of the later cosmological closure (structural/bridge level).
- (vii) The closure functions of the first macroscopic scalar–tensor reduction are structurally anchored in the ordered-branch EFT:  $F(\phi)$  comes from the amplitude ratio  $u/u_\infty$ ,  $\omega(\phi)$  from amplitude-sector stiffness, and  $U(\phi)$  from the branch potential  $W(u)$  (bridge principle; explicit final forms remain Level B).
- (viii) In the late-time cosmological specialisation, the exponential response factor is structurally anchored by  $u/u_\infty = e^{\beta\phi}$ , whereas the constant kinetic coefficient and quadratic potential are the simplest benchmark truncations rather than unique ECT outputs (bridge + Level B distinction).
- (ix) The benchmark late-time closure is not unique: it is the first explicit member of a wider admissible family of amplitude-sector closures inherited from the ordered-branch EFT (structural/bridge-level distinction; coefficients remain Level B).
- (x) The late-time article–code comparison must respect an explicit interface contract: required inputs, required outputs, and required validation checks are part of the benchmark numerical layer, not of the structural core of the theory.
- (xi) Reproducible comparison between article and code requires a standard artefact layer: background tables, distance–time tables, JWST age grids, benchmark summaries, and convergence diagnostics belong to the benchmark numerical framework, not to the structural core of the theory.
- (xii) Numerical robustness under admissible late-time closure deformations is now part of the explicit programme of the theory: benchmark outputs are not to be treated as fully robust until they have been compared against the wider admissible closure family (benchmark numerical layer; not structural core).

**Not yet established as first-principles theorems:**

- (i) Full derivation of the nonlinear closure from bare P3 (OP2).
- (ii) Microscopic derivation of  $U(\phi)$  (OP3).
- (iii) Universality of matter coupling (OP-matter).
- (iv) Exact nonlinear role of  $\Theta_{\mu\nu}[n]$  in all regimes (OP-c1).
- (v) Whether the benchmark choices  $K(\phi) = K_0$  and  $V(\phi) = V_0 + \frac{1}{2}m_\phi^2\phi^2$  are sufficient beyond the simplest late-time branch, or must be replaced by more general amplitude-sector closures inherited from  $W(u)$ .
- (vi) Whether the benchmark truncation  $K(\phi) = K_0$  and  $V(\phi) = V_0 + \frac{1}{2}m_\phi^2\phi^2$  is quantitatively stable under admissible amplitude-sector deformations (AD.22)–(AD.23).

**Observational role of the full nonlinear equations across the ECT programme**

The summary below collects the observational footprint of the full nonlinear field equations (13.35), and in particular of the orientation stress  $\Theta_{\mu\nu}[n]$  (13.23), across the phenomenological sectors developed in the present work. In all cases the dominant ordered-branch effect is captured by the scalar  $\phi$ -closure; the additional contribution from  $\Theta_{\mu\nu}$  ranges from negligible (background cosmology) to potentially significant (cluster-merger lensing, perturbative growth). Its precise magnitude is in all cases contingent on the coefficient  $c_1$  (OP-c1).

**Table 54:** Observational footprint of the full nonlinear field equations across the phenomenological sectors of the present work.

Sector	Benchmark ECT result	NLEE channel	Role	Separability	Appendix
Hubble tension (§16.5)	retained-band-compatible H1-route shift	$\Theta_{\mu\nu} \rightarrow 0$ on FRW bkgd	Absorbed	Not separable	AU.7
Universe age (§16.4)	$\Delta t_0/t_0 \approx -4.8\%$	Same FRW logic	Absorbed	Not separable	AU.7
JWST growth (§16.5)	BH channel $> \mathcal{R}_{\text{req}}$ ; gal. channel observationally ambiguous	$\Theta_{\mu\nu}$ in sub-horizon Poisson; $\eta_{\Theta} \sim  c_1 $	Reinforcing only; not primary	$c_1$ -dependent (proxy)	AD.12
Galactic RAR / BTFR (§17.1)	Closure eq.; slope 4	Degenerate with $g_{\text{eff}}^\dagger$ ; scatter	Degenerate with effective-scale calibration	Not separately extractable within present closure	AN.8
Cluster mergers (§17.2)	$M_{\text{ECT}}/M_{\text{obs}} = 0.54\text{--}0.87$	$E_3 \approx +0.3\%\text{--}8.5\%$ via slip	Direct lensing-amplitude correction	Most direct tensor-sector probe (Level B)	AP.5

The table confirms that the full nonlinear structure is observationally most consequential in two regimes: sub-horizon perturbative growth (relevant for the JWST tension) and strong-field dynamical lensing (relevant for cluster mergers). In both cases the quantitative magnitude is controlled by the undetermined coefficient  $c_1$  (OP-c1), making its first-principles derivation a priority for future work (§38.1).

### Phenomena beyond the scope of the present work

The generalised field equations, and in particular  $\Theta_{\mu\nu}[n]$ , generate structural modifications in a range of astrophysical and cosmological settings that are not examined quantitatively in the present article. Their omission reflects scope control, not an expectation that the orientation-stress sector is irrelevant in those contexts. A systematic assessment of the channels listed below is deferred to dedicated future analyses requiring tools (Boltzmann codes, 3D solvers, lensing pipelines) that lie beyond the scope of this work.

**Table 55:** NLEE effects in phenomena not examined quantitatively in the present work.

Phenomenon	Expected NLEE channel	Qualitative expectation
Cosmic shear / weak lensing ( $S_8$ / lensing–growth sector)	Orientation-stress contribution to $\eta(k, z)$ and $\Sigma(k, z)$ ; possible mismatch between lensing and dynamical amplitudes	High-priority discriminator: requires completed $\mu(k, z)$ , $\eta(k, z)$ , $\Sigma(k, z)$ closure; testable with Euclid, Rubin, DESI, and CMB lensing
Void–galaxy correlations	$c_1(\bar{\phi})$ environment-sensitive; enhanced in underdense regions	Possible amplification of void-lensing signal

Phenomenon (cont.)	Expected NLEE channel	Qualitative expectation
Integrated Sachs–Wolfe effect	$\Theta_{\mu\nu}$ modifies late-time potential evolution	Small fractional correction; requires full Boltzmann code
Strong lensing in cluster cores	Same slip mechanism as $E_3$ in deeper potential wells	Fractional correction to Einstein-radius estimates
Tidal / asymmetric environments	$\Theta_{\mu\nu}$ breaks spherical symmetry of galactic response	May contribute to tidal-tail dynamics and asymmetric rotation curves

**$S_8$  / lensing–growth sector (Level B/C).** A natural structural route in ECT to the often-discussed lensing–growth sector, commonly parametrised by  $S_8 \equiv \sigma_8 \sqrt{\Omega_m/0.3}$ , lies not in a scalar-only suppression of growth, but in the tensor/orientation sector through the orientation stress  $\Theta_{\mu\nu}[n]$  entering the generalised Einstein equations. On linear sub-horizon scales it is natural to organise the phenomenology in the standard modified-gravity language

$$-k^2\Psi = 4\pi G_N a^2 \mu(k, z) \rho\Delta, \quad \eta(k, z) \equiv \frac{\Phi}{\Psi}, \quad (13.41)$$

$$-k^2(\Phi + \Psi) = 8\pi G_N a^2 \Sigma(k, z) \rho\Delta, \quad \Sigma(k, z) = \frac{\mu(k, z) [1 + \eta(k, z)]}{2}. \quad (13.42)$$

Weak lensing and CMB lensing probe primarily  $\Sigma$ , whereas galaxy clustering and redshift-space distortions probe primarily  $\mu$ .

The same  $\Theta_{\mu\nu}[n]$  channel that already underlies the cluster-slip effect (Appendix AP.5) generically gives  $\eta \neq 1$  and hence modifies  $\Sigma$ . The existence of an orientation sector tied to the  $O(4) \rightarrow O(3)$  breaking pattern is structurally guaranteed, but the precise linear-response coefficients relevant for  $\mu(k, z)$ ,  $\eta(k, z)$ , and  $\Sigma(k, z)$  are not fixed by symmetry alone and remain part of OP- $c_1$ . The present cluster-level Einstein–aether proxy, for example  $\gamma_{cl} \approx (1 - c_1/2)/(1 + c_1/2)$ , should therefore not be exported directly to cosmological linear perturbations: it is an illustrative cluster-scale proxy rather than a derived FRW-level  $(\mu, \eta, \Sigma)$  closure; Appendix AP.6 discusses this separation more explicitly.

It is also important that the Hubble-sector and the lensing–growth sector are addressed by different layers of the same condensate architecture: the scalar background  $\phi_b(z)$  governs the late-time  $H_0$ -shift mechanism (§16.5), whereas the perturbative orientation sector governs the possible slip/lensing route relevant for  $S_8$ . This is a structural feature of the framework rather than an ad hoc juxtaposition of unrelated ingredients.

Observationally, the status of the  $S_8$  sector is presently mixed rather than settled into a single sharp discrepancy, so the role of ECT here is best framed as a discriminating structural route rather than an already required correction. ECT thus possesses a natural slip/lensing-driven route to the lensing–growth sector, but does not yet predict a resolved value of  $S_8$ . Success or failure of this route will be decided by the first-principles derivation of  $\mu(k, z)$ ,  $\eta(k, z)$ , and  $\Sigma(k, z)$ , together with their joint confrontation with weak lensing, RSD, CMB lensing, cluster lensing, and the Hubble-sector benchmark (see OP- $c_1$ ).

### Structural comparison with neighbouring frameworks

Table 56 summarises how the generalised field equations of ECT compare structurally with GR, Brans–Dicke, and Einstein-aether theories.

**Table 56:** Structural comparison of generalised Einstein equations. “✓” = present; “*post.*” = postulated; “*deriv.*” = derived from action; “—” = absent. All frameworks reduce to standard GR when their respective extension parameters vanish.

Term	Einstein-aether [24]	Brans–Dicke [83]	$f(R)$	Horava–Lifshitz [26]	ECT
$R_{AB} - \frac{1}{2}g_{AB}R$	✓	✓	✓	✓	✓
$\Lambda_{\text{eff}}(X)g_{AB}$ (dynamical)	—	—	✓*	—	<i>deriv.</i>
$n_A n^C R_{CB}$ (anisotropic)	<i>post.</i>	—	—	✓**	<i>deriv.</i>
$G_{\text{eff}}(X)$ (running)	—	✓	—	—	<i>deriv.</i>
Condensate back-reaction $T_{AB}^{(n)}$	✓***	—	—	—	<i>deriv.</i>

\* In  $f(R)$  gravity,  $\Lambda_{\text{eff}}$  arises from the scalar potential of the Starobinsky field, not from a condensate.

\*\* In Horava–Lifshitz, anisotropy is between space and time, not tied to a condensate direction.

\*\*\* Einstein-aether back-reaction involves the aether EMT, which is structurally similar to  $T_{AB}^{(n)}$  but with free coupling constants  $c_{1..4}$ .

## Summary

The geometric branch of ECT requires a nonlinear completion. The most developed currently available amplitude-dominated completion is the  $\phi$ -first scalar-tensor closure (13.34)–(13.35), whose homogeneous frozen-order limit reduces to standard Einstein gravity with cosmological constant. The full first-principles derivation of this nonlinear sector from microscopic condensate dynamics remains open, but the EFT logic already constrains the closure strongly. This prepares the next stage: the weak-field limit and the emergence of Newtonian and post-Newtonian gravity from the nonlinear geometric branch.

## 13.6 Weak-field and Newtonian limit

*Status: Level A for the existence of a screened weak-field limit recovering standard Newtonian gravity in the vacuum-normalised regime  $\phi \rightarrow 0$  with anisotropic corrections suppressed. Level B for the full weak-field phenomenology including  $G_{\text{eff}}(X)$ , amplitude-sector corrections, and the transition toward the galactic critical branch. This subsection prepares, but does not yet assume, the deep weak-field critical regime developed in Section 17.1.*

The nonlinear closure of Section 13.5 establishes the macroscopic field equations of the geometric branch. The next task is to identify their weak-field limit and to show how ordinary Newtonian gravity is recovered locally, while allowing systematic departures at larger scales or lower accelerations. This step is essential for two reasons: first, any viable macroscopic closure must reproduce the well-tested Newtonian and post-Newtonian regime in the Solar System; second, the same weak-field expansion provides the entry point for the galactic phenomenology of Section 17.1. The local screened Newtonian limit established here is therefore not the end of the gravitational analysis, but the point from which the later galactic branch departs once the weak-field regime is combined with the critical infrared closure of Section 17.1.

### Weak-field expansion of the geometric branch

We consider the macroscopic branch in the regime:

$$g_{\mu\nu} = \eta_{\mu\nu} + h_{\mu\nu}, \quad |h_{\mu\nu}| \ll 1, \quad |\phi| \ll 1, \quad v \ll c_*, \quad (13.43)$$

around the vacuum-normalised ordered background  $\phi = 0$ ,  $\bar{n}_A = (0, 0, 0, 1)$ , with the quasi-static approximation for nonrelativistic sources:

$$|\partial_t| \ll c_* |\nabla|, \quad T_{00} \gg T_{0i}, T_{ij}. \quad (13.44)$$

In Newtonian gauge:

$$ds^2 = -(1 + 2\Psi)c^2 dt^2 + (1 - 2\Phi)\delta_{ij}dx^i dx^j. \quad (13.45)$$

In pure GR with negligible anisotropic stress one has  $\Phi = \Psi$ . In ECT this equality is recovered in the screened local regime; small deviations appear when the order field or orientation corrections become dynamically relevant.

### Screened local limit: recovery of Newtonian gravity

In the locally screened vacuum-normalised regime:

$$\phi \simeq 0, \quad \nabla\phi \simeq 0, \quad \Theta_{\mu\nu}[n] \simeq 0.$$

The generalised field equations (13.35) reduce to the standard Poisson equation:

$$\nabla^2\Psi = 4\pi G_N \rho_{\text{bar}}, \quad \Phi = \Psi. \quad (13.46)$$

In the same limit the post-Newtonian parameter:

$$\gamma_{\text{PPN}} \equiv \frac{\Phi}{\Psi} \simeq 1, \quad (13.47)$$

as in GR, consistent with the Cassini bound  $|\gamma_{\text{PPN}} - 1| < 2.3 \times 10^{-5}$  [84].

This recovery is the key local consistency requirement of ECT Macroscopic Physics. Its status is Level A conditional on the screened vacuum-normalised weak limit: once the geometric branch exists and local order variables are frozen, ordinary Newtonian gravity follows.

### Weak-field form of the $\phi$ -first closure

Outside the fully screened regime but still in the quasi-static weak-field domain, the  $\phi$ -first closure leads to:

$$\nabla^2\Psi(X) \simeq 4\pi G_{\text{eff}}(X) \rho_{\text{bar}}(X) + \mathcal{D}_{\phi,n}(X), \quad G_{\text{eff}}(X) = G_N e^{-\beta\phi(X)}, \quad (13.48)$$

where  $\mathcal{D}_{\phi,n}$  summarises residual derivative and anisotropic source terms of the order field and orientation sector. This is Level B: the consistent weak-field reduction of the  $\phi$ -first closure, not yet a first-principles theorem from bare P3.

**Observational bounds on  $\dot{G}$ .** If the weak-field configuration evolves slowly in time:

$$\frac{\dot{G}_{\text{eff}}}{G_{\text{eff}}} = -\dot{\phi}. \quad (13.49)$$

Lunar laser ranging gives  $|\dot{G}/G| \lesssim 10^{-12} \text{ yr}^{-1}$  [85], requiring  $|\dot{\phi}| \lesssim 10^{-12} \text{ yr}^{-1}$ , fully consistent with a quasi-static screened condensate background (Level B).

### Order-of-magnitude estimates for local deviations from GR

Define the dimensionless deviation from the vacuum-normalised branch:

$$\varepsilon(X) \equiv e^{-\phi(X)} - 1 \approx -\phi(X) \quad \text{for } |\phi| \ll 1. \quad (13.50)$$

Then one expects, at order of magnitude,

$$\frac{\delta G}{G} \sim \varepsilon,$$

while post-Newtonian deviations are likewise controlled by the same small screening parameter. Requiring consistency with Solar-System bounds motivates:

$$|\varepsilon_{\text{local}}| \lesssim 10^{-5}, \quad |\phi_{\text{local}}| \lesssim 10^{-5}, \quad (13.51)$$

as a representative local screening condition. The precise mapping to the full post-Newtonian parameter set remains part of the detailed weak-field phenomenology and is therefore Level B.

## Two weak-field regimes of the geometric branch

The new ECT architecture makes explicit that the weak-field domain splits into two physically distinct subregimes:

**(a) Screened local weak-field branch.**  $\phi \simeq 0$ ,  $\Theta_{\mu\nu} \simeq 0$ : GR/Newtonian physics is recovered to high precision. Relevant for Solar System and laboratory gravity.

**(b) Deep weak-field ordered branch.** The metric perturbation remains small, but order-sector corrections become competitive with or dominant over the baryonic Newtonian source. This is the regime in which  $G_{\text{eff}}(X)$  and the critical branch of  $\phi$ -dynamics modify rotation curves, RAR, and BTFR phenomenology. Developed in Section 17.1.

This split is a real conceptual improvement over older ECT versions, which treated “the weak-field limit” as a single regime. The new postulate logic shows there are two weak-field regimes, separated not by the size of the metric perturbation alone, but by the dynamical state of the ordered branch.

## Physical interpretation

In ECT, a baryonic mass distribution sources a deformation of the ordered macroscopic branch; the Newtonian potential is the screened local projection of that deformation. In the local branch the ordered medium responds almost rigidly, recovering standard Newtonian gravity. In the deep weak-field branch the medium is still weakly curved but no longer fully screened, and residual order-sector structure becomes visible. This is why ECT remains compatible with Solar-System precision tests while leaving room for nontrivial galactic phenomenology.

## What is established and what is not

### Established (Level A in screened limit):

- (i) A screened weak-field limit of the geometric branch exists.
- (ii) Standard Poisson gravity is recovered in that limit.
- (iii) The weak-field domain splits structurally into screened local and deep weak-field ordered regimes.

### Level B / open:

- (i) Detailed form of  $\mathcal{D}_{\phi,n}$  in all environments.
- (ii) Full post-Newtonian parameter set beyond  $\gamma_{\text{PN}}$ .
- (iii) First-principles microscopic derivation of screening from bare P3.

## Summary

The weak-field limit of the geometric branch is not a single universal regime but a hierarchy. In the screened local branch ECT reproduces standard Newtonian gravity. In the  $\phi$ -first weak-field branch the Newtonian potential obeys a modified Poisson equation with both baryonic and order-sector contributions. This is the bridge between the nonlinear macroscopic closure and the galactic critical branch of Section 17.1.

## 13.7 Post-Newtonian regime and Solar System tests

*Status: Level A for GR recovery in the screened/frozen limit; Level B for explicit post-Newtonian deviations, which require closure-specific analysis.*



**GR limit and PPN recovery.** In the screened/frozen- $\phi$  limit ( $\phi \rightarrow 0$ ,  $\nabla_\mu \phi = 0$ ,  $\Theta_{\mu\nu} \rightarrow 0$ ), the generalised equations (13.35) reduce identically to the standard Einstein equations with cosmological constant (13.40). In this limit the parametrised post-Newtonian (PPN) framework [86] gives:

$$\gamma_{\text{PPN}} \rightarrow 1, \quad \beta_{\text{PPN}} \rightarrow 1, \quad (13.52)$$

so that all standard Solar System tests—perihelion precession of Mercury, light deflection, Shapiro time delay, Nordtvedt effect—are automatically satisfied in the GR limit.

**Screening in the Solar System.** The macroscopic closure naturally approaches the screened limit in dense, slowly varying gravitational environments. The ordered-branch amplitude saturates toward its asymptotic value  $u_\infty$  in the Solar System, so that  $\phi \equiv \frac{1}{\beta} \ln(u/u_\infty) \rightarrow 0$  locally. This is not introduced as an external chameleon-type mechanism; within the present closure it is interpreted as a consequence of amplitude saturation in the ordered branch (Section 13.5). Accordingly, the Cassini constraint  $|\gamma_{\text{PPN}} - 1| < 2.3 \times 10^{-5}$  [84] is satisfied provided the Solar-System environment lies in the screened GR regime described above. The present paper does not yet provide a quantitative transfer map between the screened local  $\dot{G}/G$  regime and the cosmological ordered-branch drift encoded by  $\epsilon_{\text{eff}}(a)$  (§16.5): local bounds such as LLR or Cassini cannot therefore be converted into a direct constraint on the cosmological benchmark by simple one-to-one identification until that transfer map is derived.

**Beyond the screened limit.** Away from the screened/frozen- $\phi$  regime, the PPN parameters acquire closure-dependent corrections controlled by the local condensate profile and by the functions  $F(\phi)$ ,  $\omega(\phi)$ , and  $U(\phi)$ . At the present stage the explicit post-Newtonian parameter set beyond the screened GR limit has not been derived from the full closure; a dedicated Solar-System analysis remains part of the open programme. In particular, the full PPN parameter set, including  $\beta_{\text{PPN}}$  and other post-Newtonian observables, remains to be derived explicitly from the present closure. What is established is that the GR limit is approached smoothly and that the theory is not excluded by current Solar System data.

### 13.8 Gravitational waves and causal structure

*Status: GW propagation speed Level A in broken-phase EFT; polarisation content Level A/B. P5 fixes the internal gauge architecture but the TT reduction depends on the gravitational gauge structure itself (OP-gauge). Planck-suppressed LIV correction estimate Level A in EFT power-counting once a propagation distance  $D$  is specified.*

#### Propagation speed

From the massless tensor dispersion relation (13.16), the GW propagation speed equals the effective causal speed of the ordered branch:

$$c_{\text{GW}} = c_n = c_* \quad (\text{Level A in the homogeneous ordered branch}). \quad (13.53)$$

Within the structural identification  $c_* = c$  established in the minimal phase-to-gauge route of Part I (§4.7), this is consistent with the bound  $|c_{\text{GW}}/c - 1| < 6 \times 10^{-15}$  from GW 170817 and its electromagnetic counterpart [10].

#### Planck-suppressed Lorentz-violation estimate

Because Lorentz symmetry is emergent rather than fundamental in ECT, the leading high-energy correction to GW propagation is Planck-suppressed in the EFT:

$$\omega^2 = c_*^2 k^2 \left[ 1 + \xi_2 \left( \frac{k}{M_{\text{LIV}}} \right)^2 + O\left( \frac{k^4}{M_{\text{LIV}}^4} \right) \right], \quad (13.54)$$

where  $\xi_2 \sim O(1)$  and  $M_{\text{LIV}} \sim \bar{M}_{\text{Pl}}$ . Induced fractional group-velocity shift:

$$\frac{\delta v_{\text{GW}}}{c} \sim \xi_2 \left( \frac{E_{\text{GW}}}{M_{\text{LIV}}} \right)^2. \quad (13.55)$$

Arrival-time shift over propagation distance  $D$ :

$$\Delta t_{\text{GW}} \sim \frac{D}{c} \xi_2 \left( \frac{E_{\text{GW}}}{M_{\text{LIV}}} \right)^2. \quad (13.56)$$

For GW170817-like parameters [10] ( $D \sim 40$  Mpc,  $E_{\text{GW}} \sim 4 \times 10^{-13}$  eV,  $M_{\text{LIV}} \sim \bar{M}_{\text{Pl}}$ ):

$$\Delta t_{\text{GW}} \sim \xi_2 \times 10^{-64} \text{ s} \quad (\text{negligible observationally}). \quad (13.57)$$

**Relation to the earlier LIV estimate.** The linear estimate in Eq. (3.15) and the quadratic GW-sector estimate in Eq. (13.54) should not be read as contradictory statements about one and the same operator. They correspond to different phenomenological parameterisations / effective sectors presently coexisting in the article. A complete operator-level unification of the LIV sector remains part of the open higher-order EFT programme.

### Polarisation content

The orientation sigma-model provides three soft modes  $\delta n_i$ . Full reduction to physical propagating content requires gauge analysis (OP-gauge):

- massless tensor propagation sector: Level A;
- exact reduction to 2 TT polarisations: Level B/C (OP-gauge; P5 fixes internal gauge architecture but does not complete the gravitational-sector TT reduction).

The anisotropic correction  $\Theta_{\mu\nu}[n]$  (13.23) may additionally modify amplitude evolution in nontrivial ordered backgrounds (Level B; OP-c1).

### Stochastic gravitational-wave background from the ordering transition

**What is established, what is benchmarked, and what remains open.** The gravitational-wave implications of the  $O(4) \rightarrow O(3)$  ordering transition should be read in three layers. First, once the ordered branch forms through a genuinely inhomogeneous finite-duration transition, the time-dependent anisotropic stress of the ordering medium provides a source for tensor-mode excitation: this gives a structural route to a stochastic gravitational-wave background (Level A/B). Second, any quantitative spectrum  $\Omega_{\text{GW}}(f)$  depends on the microphysics of the transition—its duration, inhomogeneity scale, energy-release efficiency, and post-transition redshifting history. At that level the present treatment is only benchmark (Level B). Third, a full first-principles prediction of peak frequency, amplitude, and spectral tilt remains open until the ordering-transition dynamics is closed quantitatively.

**Sign-level tensor-production statement (Level A/B).** If the ordered branch is established through a genuinely inhomogeneous finite-duration  $O(4) \rightarrow O(3)$  transition, then the time-dependent anisotropic stress of the ordering medium acts as a source in the tensor equation of the emergent geometric branch:

$$h''_{ij} + 2\mathcal{H}h'_{ij} + k^2 h_{ij} = 16\pi G \Pi_{ij}^{\text{TT}}, \quad (13.58)$$

where  $\Pi_{ij}^{\text{TT}}$  is the transverse-traceless projection of the anisotropic stress generated by the inhomogeneous ordering dynamics. Accordingly, ECT contains a structural route to a stochastic gravitational-wave background associated with the ordering epoch. What is not yet fixed by this statement is the detailed spectrum: the peak frequency, overall amplitude, and shape depend on the transition microphysics and subsequent cosmological evolution. A dimensional scaffold for this estimate is given in Appendix AE.

**Conceptual distinction from standard first-order phase transitions.** The ECT ordering transition is *not* a thermal first-order phase transition in a pre-existing Lorentzian spacetime. It is the process that establishes the Lorentzian branch itself. The GW production mechanism is therefore structurally tied to the formation of causal geometry, not to bubble nucleation in a thermal bath. This difference affects the expected spectral shape: standard thermal transition formulae cannot be applied without substantial reinterpretation.

**When no appreciable signal is expected.** The mere existence of the ordered branch does not by itself imply an observable stochastic background today. A negligible signal is possible if the transition is nearly homogeneous, if its anisotropic stress is too weak, if the relevant correlation scale is too small compared with the Hubble scale at production, or if the signal is redshifted below observational relevance. Thus ECT establishes a structural production channel, not an automatic observable detection claim.

**Correlation with the baryogenesis epoch.** The ordering transition that sources  $\Pi_{ij}^{\text{TT}}$  is the same  $O(4) \rightarrow O(3)$  epoch that, in the ECT baryogenesis framework (§16.3), provides the out-of-equilibrium departure and the B-violating defect channel. A completed ECT ordering-transition theory should therefore predict joint consistency conditions between: (i) the baryon asymmetry  $\eta_B$ , (ii) the ordering-generated GW signal  $\Omega_{\text{GW}}(f)$ , and (iii) the effective late-time background evolution. This correlated-epoch prediction is structurally natural in ECT: the same ordered-branch transition sources both the tensor-producing anisotropic stress and the baryogenesis framework. In more standard inflation + leptogenesis constructions, these two phenomena are often treated as arising from largely separate mechanisms, so the correlation is typically weaker and less direct.

**Observational anchors.** The natural observational windows for an ordering-generated stochastic background are experiment-dependent: very low-frequency signals are constrained by pulsar timing arrays (NANOGrav, EPTA, PPTA), while higher-frequency cosmological backgrounds are targets of space-based interferometers such as LISA [87] and next-generation ground-based detectors. At present, ECT supplies the source channel structurally, but not yet a parameter-free prediction that singles out one of these bands.

**Falsifier for the ordering-GW programme.** The ordering-transition GW programme would fail if a completed transition calculation within ECT were forced to predict either exactly vanishing tensor production for every inhomogeneous ordering history, or a stochastic background incompatible in sign, scale, and redshifting logic with the tensor-capable ordered branch. More practically, the programme would also be weakened if the required signal depended entirely on arbitrary external parameters unrelated to the condensate ordering dynamics.

## What is established and what is not

### Established:

- (i)  $c_{\text{GW}} = c_*$  (Level A).
- (ii) LIV correction is Planck-suppressed; induced delay  $\Delta t \lesssim 10^{-64}$  s is negligible.
- (iii) Structural route to ordering-generated stochastic GW background (Level A/B).

### Open:

- (i) Exact 2 TT polarisations (OP-gauge).
- (ii) Polarisation effects from  $\Theta_{\mu\nu}[n]$  (OP-c1).
- (iii) Full radiative stability at loop level.
- (iv) Quantitative  $\Omega_{\text{GW}}(f)$  spectrum from the ordering transition.

### 13.9 Observational predictions of the gravitational sector

*Summary of the main gravitational-sector predictions and consistency conditions, together with their derivation status.*

**Table 57:** Gravitational-sector predictions and consistency conditions.

Prediction / condition	Formula / estimate	Status	Test
Einstein–Hilbert uniqueness of the pure-metric two-derivative closure	Lovelock–Deser route in the pure-metric limit (§13.5)	Level A/B	Classical GR; binary pulsars
GR recovery when $\phi, n$ freeze	Eq. (13.40)	Derived	—
Universal metric coupling	All matter sectors couple to one $g_{\mu\nu}$	Level A/B	WEP tests; MICROSCOPE
GW speed = $c_*$	$c_{\text{GW}} = c_*$ (13.53)	Derived (Level A)	GW170817
Ordering-transition stochastic GW route	Eq. (13.58)	Level A/B	PTA, LISA
TT polarisation recovery	requires the OP-gauge reduction to the GR-like tensor sector	Level B / open reduction step	LIGO/Virgo
Solar System: $\gamma_{\text{PPN}} \rightarrow 1$	screened/frozen GR limit	Derived in screened limit	Cassini
Planck-suppressed LIV	sector-dependent higher-order EFT corrections; cf. Eq. (3.15) (photon/time-of-flight estimate) and Eq. (13.54) (GW-sector dispersion estimate)	EFT estimate	High-energy propagation tests
Dynamic vacuum $\Lambda_{\text{eff}}(\phi)$	closure-dependent evolution	Level B / closure-dep.	Cosmological data
Variable $G_{\text{eff}}(\phi)$	closure-specific realisation	Level B / closure-dep.	Galactic (§17.1)
Force-law dimensionality crossover	$d_{\text{force}}: 3 \rightarrow 7/3 \rightarrow 2$ (eq. (16.24))	Level B	Galactic rotation curves
Possible gravitational slip	induced by $\Theta_{\mu\nu}[n]$	Structural / closure-dep. magnitude	Lensing–dynamics, Euclid

#### Section-level status summary

At the current stage, the emergent gravitational sector of ECT should be read as follows.

**Strictly established (Level A):** the existence of a unique coarse-grained Lorentzian metric candidate in the ordered phase; the presence of a linear tensor propagation sector; the existence of a conserved macroscopic source tensor; and the structural necessity of a nonlinear covariant completion.

**Structurally singled out (Level A/B):** the Einstein–Hilbert nonlinear closure as the unique two-derivative completion under universal coupling and spin-2 self-consistency (Lovelock–Deser route, §13.5); and the recovery of ordinary Einstein/Newtonian gravity in the screened frozen-order limit.

**Structurally established (Level B):** the  $\phi$ -first nonlinear covariant closure as the current best developed macroscopic completion; the interpretation of  $G_{\text{eff}}(\phi)$ ,  $\Lambda_{\text{eff}}(\phi)$ , and  $\Theta_{\mu\nu}[\phi, n]$  as the three characteristic departures from pure GR; the isotropic background reduction feeding the cosmological sector; and the weak-field route toward the galactic critical branch.

**Still open:** the first-principles derivation of the full nonlinear closure from bare P3, the microscopic derivation of the closure functions  $F(\phi)$ ,  $\omega(\phi)$ , and  $U(\phi)$ , the full universality of matter coupling, the exact nonlinear role of the anisotropic response tensor  $\Theta_{\mu\nu}$ , and the complete reduction from the

ordered-branch EFT to the later cosmological and galactic data interfaces.

This section therefore establishes the gravitational branch as a well-structured macroscopic EFT sector, while leaving the final microphysical closure and precision phenomenology to the later cosmological and galactic chapters.

## 14 ECT and the Classical Cosmological Problems

*The three classical cosmological problems—horizon, flatness, and relic/monopole—are historically resolved by inflationary cosmology through dynamical mechanisms operating inside an already existing Lorentzian spacetime. ECT offers a structurally different approach: all three problems are addressed at the level of the ordering transition itself, before the Lorentzian branch is fully established.*

*This section presents the ECT resolution of these problems together with the pre-Lorentzian scenario from which they arise, and the current status of primordial perturbations. The exceptions to Level B status are the flatness result ( $k = 0$  from P1, Level A), the primary relic classification ( $\pi_2(S^3) = 0$ , Level A), and the sigma-model minimum underlying the branch-coherence route (Level A; the full cosmological horizon scenario remains Level B). Throughout this section  $c$  denotes the structural identification  $c_* = c$  of the minimal gauge-emergence route (§4.7).*

### 14.1 Pre-Lorentzian cosmological scenario

*Status: Level A for the existence of a pre-ordered configuration regime; Level B for its cosmological realisation as a stage preceding the ordered branch.*

**Bridge from the gravitational sector.** Section 13 established the macroscopic generally covariant dynamics of the ordered Lorentzian branch. The present subsection asks a logically prior question: what is the status, within ECT, of the regime in which that branch has not yet formed?

**Proposition (Existence of a pre-ordered configuration regime).** If Lorentzian signature is an emergent property of the ordered branch (Level A, §3) rather than a fundamental property of the arena (P1), then the theory necessarily admits configurations in which the ordered Lorentzian branch is not yet established. In that regime there is no effective Lorentzian metric, no macroscopic causal cone, and no emergent temporal direction.

*Proof.* (i) The fundamental arena is a 4D Euclidean manifold (P1). (ii) Lorentzian signature appears only after  $O(4) \rightarrow O(3)$  ordering (Level A, §3). (iii) Therefore the theory admits configurations in which this ordering has not been realised. (iv) In those configurations the effective Lorentzian metric, causal cone, and macroscopic time direction are absent.  $\square$

This is a statement about the configuration-space structure of the theory, not yet about cosmological chronology.

**Cosmological realisation (Level B scenario).** A cosmological interpretation of this regime—in which the pre-ordered Euclidean condensate phase *precedes* the emergence of the ordered Lorentzian branch—is a Level B scenario. It is structurally motivated by P1–P4 but is not derived from completed nonequilibrium condensate dynamics (OP3).

The term “pre-Lorentzian” should therefore be understood structurally, not as ordinary clock-time evolution inside an already existing Lorentzian spacetime. There is no macroscopic time coordinate in the pre-ordered regime; “before” refers to the logical ordering of the branch-selection process, not to a temporal relation inside a pre-existing causal structure.

**What is absent in the pre-ordered regime.** In the pre-ordered configuration regime:

- no effective Lorentzian metric;

- no causal cone or light cone;
- no preferred time direction or macroscopic arrow of time;
- no FLRW description;
- no standard cosmic time.

What *is* present: the Euclidean arena (P1), the condensate field  $\Phi$  (P3) with its  $O(4)$ -invariant action (P2), and the ordering-potential landscape governing the branch-selection problem.

**Characteristic scales (matching estimates).** The ordering scale is set by the radial symmetry-breaking scale matched in Part I:  $\phi_0 \sim \bar{M}_{\text{Pl}} \approx 2.435 \times 10^{18} \text{ GeV}$  (Section 5.1). The corresponding correlation length is  $\xi_{\text{cond}} \sim m_{\sigma}^{-1} \sim \ell_{\text{Pl}} \approx 1.6 \times 10^{-35} \text{ m}$ . If the transition to the ordered branch is sharp, the earliest Lorentzian relaxation scale after ordering is naturally expected to be of order  $M_{\text{Pl}}^{-1}$ . These are matching estimates, not first-principles derivations of transition dynamics (OP3).

**Conceptual consequences.** (i) *Reinterpretation of the Big Bang.* Within the pre-Lorentzian scenario, the standard Lorentzian Big Bang singularity is no longer treated as the fundamental starting point of the theory; it is instead replaced, at the scenario level, by a non-Lorentzian pre-ordered regime of the same underlying arena. This is a structural reinterpretation, not yet a theorem about all possible solutions of the full nonequilibrium dynamics.

**Singularities as ordered-branch boundaries: unified programme.** The ECT singularity programme should be read in three layers. First, the ordered-branch Lorentzian geometric EFT is only a coarse-grained branch description, valid when the condensate remains in its ordered regime. Accordingly, divergent classical GR singularities are not taken as fundamental objects of the theory, but as signals that the ordered geometric branch has left its regime of applicability (Level A/B). Second, in the present black-hole (§36, Appendix BB.7) and cosmological constructions, this interpretation is implemented structurally through the critical-shell and pre-ordered-regime logic: before one reaches a putative classical singularity, the ordered branch itself enters a breakdown region in which the coarse-grained Lorentzian description is no longer trusted. Third, what remains open is the unique microscopic completion of that breakdown region: ECT does not yet provide a full solved interior state, a unique bounce, or a completed non-perturbative resolution of all singularity questions.

**Breakdown criterion for the ordered geometric branch.** The ordered-branch Lorentzian EFT is expected to fail when the local state of the condensate approaches the critical regime in which the ordered amplitude description ceases to be valid. The relevant indicators are: (i) the ordered-branch amplitude  $\rho \rightarrow 0$ ; (ii) the local effective temperature  $T_{\text{loc}} \rightarrow T_c$  (Appendix BB.7); (iii) the geometric curvature radius or gradient length scale of the ordered branch approaching the condensate threshold  $\ell_{\text{cond}} \sim m_{\sigma}^{-1}$ , equivalently, curvature/gradient invariants becoming of order the appropriate powers of  $m_{\sigma}$ . This breakdown criterion is structurally tied to the UV threshold of §8.3: the same radial mode  $m_{\sigma}$  that sets the physical UV cutoff of the ordered-branch EFT also fixes the scale at which classical singularity-type divergences should be read as signals of branch failure rather than as physically fundamental endpoints.

**Cosmological singularity as branch boundary.** In the cosmological sector, ECT does not interpret the formal Lorentzian Big-Bang singularity as a physical first instant of the theory. Rather, the singular behaviour of the backward-extrapolated Lorentzian branch marks the limit at which the ordered branch ceases to be an adequate effective description. The physically prior regime is the pre-ordered, pre-Lorentzian condensate regime from which the ordered Lorentzian branch emerges. Thus the Big-Bang singularity is replaced not by a fully solved classical bounce, but by a branch-boundary interpretation: it signals the end of the Lorentzian coarse-grained description, not the beginning of reality itself.

(ii) *Horizon problem reformulated.* The standard horizon problem—formulated inside an already existing Lorentzian spacetime—is shifted to a branch-coherence problem: under what conditions can the

ordering transition be macroscopically coherent on a connected progenitor domain of sufficient extent? This reformulation is developed in §14.3.

(iii) *Trans-Planckian issue softened.* The standard trans-Planckian formulation is softened in ECT, because observable perturbation modes need not be extrapolated through an indefinitely extended earlier Lorentzian regime deeper than the ordering transition.

**Comparison with other pre-Big-Bang approaches.** Several other frameworks address the question of what precedes the standard Big Bang. In the Hartle–Hawking no-boundary proposal [5], a Euclidean geometry replaces the initial singularity via a path integral over compact metrics. In Vilenkin’s tunnelling-from-nothing scenario, the Universe nucleates quantum-mechanically from a state with no prior spacetime. In cyclic/ekpyrotic models, a pre-existing dynamical stage within Lorentzian/cosmological language is assumed. ECT differs from these approaches in that the pre-Lorentzian regime is not introduced as an additional quantum-cosmology proposal, but follows from the same emergent-signature logic that generates the ordered branch itself.

**Status summary.** *Strictly established (Level A):* existence of a pre-ordered configuration regime in which Lorentzian structures are absent. *Scenario-level (Level B):* cosmological realisation of that regime as preceding the ordered branch; detailed transition dynamics; observable relics of the ordering event.

The comparative cosmological timeline is shown in Figure 15 (§16.7); quantitative details of Scenarios A and B are discussed there.

## 14.2 Post-transition ordered-branch cosmological scenarios

*Status: Level B for the scenario classification and the structural conditions supporting the observed branch. Level B/C for the ordered-domain growth analogy as a physical motivation for expansion. Open for expanding-branch selection from first principles, exact  $\phi_b(z)$  trajectory, thermal completion of the hot Big-Bang history, and CMB-peak structure without particle dark matter. Connection: pre-Lorentzian regime (§14.1), background reduction (Eqs. (13.37)–(13.39)), far-future Scenarios A/B (§16.1), no-phantom result (eq. (16.2)), second law (§3.9).*

### Problem statement: branch onset versus cosmological history

Two questions must be sharply distinguished.

The first is why the  $O(4) \rightarrow O(3)$  transition occurred at all. This is the full nonequilibrium transition problem (OP3) and is not addressed here.

The second is: given that an ordered Lorentzian branch has formed, which cosmological histories are dynamically admissible, structurally natural, or excluded? This is the question addressed in the present subsection.

A further distinction is equally important: *geometric branch onset is not identical to thermal Big-Bang completion.* The former provides Lorentzian metric, causal cone, and emergent time. The latter requires in addition entropy production, thermalisation, a radiation-dominated epoch, and BBN-compatible initial conditions. Thermal completion remains open.

### Admissible post-transition scenarios

The effective background dynamics of the ordered branch is governed by the scalar–tensor system Eqs. (13.37)–(13.39), developed in §13.5. Within the  $\phi$ -first closure, the qualitative post-transition behaviour is controlled by the sign and magnitude of the residual condensate energy  $U(\phi)$ , the kinetic coupling  $\omega(\phi)$  and its sign (no-ghost condition), the gravitational screening function  $F(\phi) = e^{\beta\phi}$ , and the matter/radiation content.

The effective Friedmann equation admits both expanding and contracting solutions,  $H = \pm\sqrt{\dots}$ . Positive condensate energy makes an expanding branch dynamically natural once that branch is selected,

but it does not by itself derive the sign choice  $H > 0$ . The deeper branch-selection problem therefore remains open.

**Table 58:** Qualitative post-transition cosmological branches in ECT.

Scenario	Structural conditions	ECT status
Expanding, early deceleration, late acceleration	Ordered branch selected; $\rho_r, \rho_m$ dominate early; $U(\phi) > 0$ dominates late; $w_\phi \geq -1$	Structurally natural; observationally preferred
Asymptotic de Sitter (Scenario A of §16.1)	$\phi_b \rightarrow 0, u \rightarrow u_\infty, G_{\text{eff}} \rightarrow G_N$ ; residual condensate energy $\rightarrow \text{const}$	Level B; compatible with future-scenario analysis
Branch degeneration (Scenario B of §16.1)	$\phi_b \rightarrow -\infty, u \rightarrow 0, G_{\text{eff}}$ grows; geometric branch eventually degenerates	Level B; timescale closure-dependent
Always decelerating	$U(\phi) \rightarrow 0$ rapidly; no persistent vacuum-like component	Possible; observationally disfavoured
Contracting branch	$H < 0$ sign choice	Kinematically admissible; not structurally preferred, but expanding-branch selection remains open
Bounce / oscillatory	Turning points in $\phi$ dynamics; non-trivial $U(\phi)$	Not excluded; not developed
Phantom ( $w < -1$ )	Would require $\omega(\phi) < 0$	<b>Excluded</b> by no-phantom bound (16.2)

### Why expansion is physically natural

The universal growth of ordered domains in phase-ordering systems provides a suggestive ECT analogy for why an expanding ordered branch is physically natural once ordered-domain formation begins. In condensed-matter systems undergoing a symmetry-breaking transition, ordered regions generically *grow*—they expand into the surrounding disordered medium via Allen–Cahn / Kibble–Zurek-type dynamics. In ECT the ordered Lorentzian branch emerging from the disordered Euclidean medium is structurally analogous to such a growing ordered domain.

This analogy strengthens the plausibility of the expanding branch (Level B/C) but should not be mistaken for a theorem-level derivation of cosmological branch selection. A full proof would require the completed nonequilibrium condensate dynamics (OP3).

### Minimal viable post-transition branch

A minimally viable post-transition ordered-branch history must satisfy the following conditions simultaneously:

- (i) *expanding ordered branch selected*;
- (ii) *near-frozen early condensate background*:  $\phi_b(z) \approx \text{const}$  and  $G_{\text{eff}}(z) \approx G_N$  for  $z \gg z_{\text{eq}}$ , ensuring BBN and early-universe compatibility (§16.1);
- (iii) *hot radiation epoch available*: thermal completion of the hot Big-Bang branch, including entropy production, thermalisation, and a radiation-dominated era (open—§14.1);



- (iv) *delayed condensate dominance*:  $\rho_r \gg \rho_m \gg \rho_\phi$  early,  $\rho_\phi \gtrsim \rho_m$  late—so that matter/radiation epochs precede dark-energy-like acceleration;
- (v) *no-phantom behaviour*:  $w_\phi \geq -1$  (eq. (16.2); Level B);
- (vi) *perturbation sector not grossly inconsistent*: near-scale-invariant primordial spectrum (§14.6), structure growth compatible with observed LSS (§AD.10).

ECT can make delayed condensate dominance structurally plausible if the post-transition condensate sector is nearly frozen at early times and only becomes relevant once matter dilution lowers  $\rho_m$ . This reduces the problem to a hierarchy/trajectory question for the effective condensate background, but does not yet provide a full first-principles solution of the observed late-time scale.

### Connection to the arrow of time

The post-transition evolution must be consistent with the emergent arrow of time established in the decoherence programme (§3.9). In the ordered Lorentzian branch, irreversibility arises from  $\Gamma_{\text{loop}} \gg 1$ : so that coarse-grained entropy increases along the physical thermodynamic arrow. For the observationally relevant expanding branch, the cosmological and thermodynamic arrows are therefore aligned. This supports the naturalness of the observed branch, but it does not by itself derive the sign choice  $H > 0$  over the contracting branch.

### Observational discriminants

The scenario classification connects to several observational channels already developed elsewhere in the paper. These are not new derivations but reinterpretations as *branch discriminants*:

- (i) *no phantom crossing*:  $w(z) \geq -1$  always (eq. (16.2)); ECT predicts thawing  $w_0 > -1$ , distinguishable from  $\Lambda$ CDM ( $w = -1$  exactly); testable with DESI, Euclid, LSST;
- (ii) *running  $G_{\text{eff}}(z)$* : varies by  $O(\beta \Delta\phi_b)$  over cosmic history; constrained by BBN, lunar laser ranging, pulsar timing (§16.1);
- (iii) *correlated  $\Delta H_0$ –age–JWST signatures*: the Hubble-shift mechanism ties these through the same  $\phi_b(z)$  (§19.1);
- (iv)  *$S_8$  tension alleviation*: modified growth rate from running  $G_{\text{eff}}$  and gravitational slip (§AD.10);
- (v) *Scenario A versus B*:  $|\dot{G}/G|$  measurably nonzero  $\rightarrow$  Scenario B;  $|\dot{G}/G| \rightarrow 0 \rightarrow$  Scenario A (§16.1).

### What is explained and what remains open

*Structurally explained*: why an expanding, early-decelerating, late-accelerating history is a natural member of the ordered-branch scenario space once an expanding branch is selected; why phantom behaviour is excluded; why late acceleration with  $w \approx -1$  is generic for slowly varying condensate backgrounds; why the cosmological and thermodynamic arrows of time align.

*Open*:

- (i) the full nonequilibrium transition dynamics that selects the ordered branch itself (OP3);
- (ii) the deeper principle selecting the expanding over the contracting branch (suggestive analogy available; full derivation requires OP3);
- (iii) the exact background trajectory  $\phi_b(z)$ ;
- (iv) thermal completion of the hot Big-Bang history (entropy production, thermalisation, radiation bath);

- (v) reproduction of precision early-universe observables—in particular, the acoustic CMB peak structure—without particle dark matter;
- (vi) precision determination of the observed cosmological parameters from a global ECT fit.

**Status summary.** *Level A:* (i) existence of a pre-ordered configuration regime without Lorentzian time; (ii) the structural distinction between geometric branch onset and thermal hot-Big-Bang completion.

*Level B:* (i) effective FLRW/scalar-tensor reduction of the ordered branch; (ii) no-phantom bound  $w \geq -1$ ; (iii) future Scenarios A/B; (iv) post-transition scenario classification (Table 58); (v) minimal viable post-transition branch conditions; (vi) observational discriminants reinterpreted as branch discriminants.

*Level B/C:* ordered-domain growth analogy as a physical motivation for expanding-branch naturalness.

*Open:* (i) expanding-branch selection from first principles; (ii) exact  $\phi_b(z)$  trajectory; (iii) thermal completion of the hot Big-Bang branch; (iv) precision CMB acoustic structure without particle dark matter; (v) precision global cosmological fit.

### 14.3 Horizon problem: branch coherence

*Status:* *Level A for the sigma-model minimum; Level B for the full cosmological horizon-resolution scenario.*

The pre-ordered configuration regime established in §14.1 provides the structural setting in which the standard horizon problem is reformulated.

The standard horizon problem is usually formulated inside an already existing Lorentzian FLRW spacetime: why do widely separated regions of the observed Universe appear so nearly homogeneous even though, in an ordinary early Lorentzian history, they would not have been in mutual causal contact?

In ECT this formulation is not fundamental. The observable Lorentzian Universe is not taken as primordial. Instead, the cosmological logic is:

pre-Lorentzian / Euclidean stage  $\rightarrow O(4) \rightarrow O(3)$  ordering transition  $\rightarrow$  emergent Lorentzian branch.

Accordingly, the horizon question must be reformulated. In ECT the relevant question is not how distant regions of an already existing Lorentzian Universe exchanged signals, but why the branch from which the observable Lorentzian Universe emerged was coherently ordered on a macroscopic scale. The horizon problem is therefore re-expressed as a *branch-coherence problem*.

The relevant carrier of this coherence is not the massive amplitude sector, but the orientation sector associated with the  $O(4) \rightarrow O(3)$  ordering. Let this sector be described by a unit field

$$n_A(x), \quad n_A n^A = 1,$$

encoding the orientation of the selected branch. Its natural low-gradient Euclidean ordering functional on a connected progenitor domain  $\Omega_{\text{br}}$  takes the sigma-model form

$$S_{\text{ord}}[n] = \frac{\kappa}{2} \int_{\Omega_{\text{br}}} d^d x (\partial_i n_A)(\partial_i n^A), \quad \kappa > 0. \quad (14.1)$$

**Lemma (minimum of the Euclidean ordering functional).** The absolute minimum of  $S_{\text{ord}}$  on a connected domain  $\Omega_{\text{br}}$  is  $S_{\text{ord}} = 0$ , and it is attained if and only if  $n_A(x) = \text{const}$  on  $\Omega_{\text{br}}$ .

*Proof.* Since  $(\partial_i n_A)(\partial_i n^A) \geq 0$  pointwise,  $S_{\text{ord}}[n] \geq 0$ . Equality holds iff  $\partial_i n_A = 0$  almost everywhere, which on a connected domain implies  $n_A = \text{const}$ .  $\square$

This establishes a precise Level A statement: the macro-coherent branch is not an externally added assumption, but the exact minimum configuration of the Euclidean ordering functional on a connected progenitor domain.

This does not mean that all non-uniform branch realizations are forbidden. What it does establish is that a macro-coherent  $O(4) \rightarrow O(3)$  transition is *organically realizable* in ECT. If the observed Universe

corresponds to such a coherently selected connected branch, then its large-scale homogeneity is inherited from the branch-selection event itself rather than manufactured later by causal equilibration inside an already formed spacetime. In this sense, a macro-coherent branch transition provides a coherent resolution route for the standard horizon paradox within ECT.

The assumption that the progenitor domain is connected, and that its coherence scale is large enough to satisfy

$$L_{\text{br}} \frac{a_0}{a_{\text{br}}} \gtrsim L_{\text{hom}},$$

is at present a working hypothesis rather than a first-principles derivation. Its role here is to formulate the coherent-branch scenario precisely. A dedicated quantitative estimate of the required coherence scale is left for future work. As a purely kinematic benchmark, this condition may be rewritten as

$$L_{\text{br}} \gtrsim L_{\text{hom}} \frac{a_{\text{br}}}{a_0}.$$

Thus the required coherence scale on the progenitor branch is smaller than the present homogeneity scale by the same expansion factor that separates the branch-selection epoch from today. This does not yet solve the branch-selection dynamics, but it clarifies that the required pre-branch coherence need not be macroscopic in today's units.

At the level of classical action comparison, the coherent branch is also the natural low-gradient baseline. This stronger preference statement goes beyond the exact minimum result above and should therefore be interpreted more cautiously: large  $O(1)$  twists of the orientation field across a scale  $L$  carry a positive action cost

$$S_{\text{ord}} \sim \kappa (\Delta\theta)^2 L^{d-2},$$

so macroscopically fragmented branches are not free. This preference statement, however, is made only at the level of classical action comparison; a full semiclassical treatment including the entropy of the configuration space would be needed to establish the preference rigorously. Accordingly, the preference claim should be read as a Level B statement.

The net result is that ECT does not solve the horizon problem by stretching an already existing Lorentzian Universe, as in standard inflation. Rather, it solves the problem at a deeper level: by explaining how the observable Lorentzian Universe may emerge from a coherently ordered pre-Lorentzian branch.

The structural result above is sufficient to define a coherent-branch resolution route for the horizon problem within ECT. What remains open is the full nonequilibrium dynamics of branch selection, the semiclassical weighting of coherent versus fragmented realisations, and the quantitative mapping to the observed primordial perturbation sector. The flatness problem is addressed in Section 14.4, and the relic and monopole problem in Section 14.5.

## 14.4 Flatness problem: structural spatial flatness from P1

*Status: Level A.*

In standard Lorentzian FLRW cosmology the flatness problem is the question of why the spatial curvature parameter satisfies  $|\Omega_K(t_0)| \ll 1$  today, given that without a special mechanism the departure from flatness grows during matter and radiation domination and would therefore require extremely fine-tuned initial conditions.

In ECT this formulation is not fundamental. The observable Lorentzian Universe is not primordial but emergent. The flatness problem is therefore reformulated as a *branch-geometry selection problem*: which spatial geometry does the emergent Lorentzian branch inherit from the pre-Lorentzian stage?

The answer follows directly from two already established facts.

**(i) Structural flatness from P1.** According to Postulate P1, the pre-Lorentzian background is a flat Euclidean space with metric

$$ds_E^2 = \delta_{AB} dX^A dX^B = dw^2 + dx^2 + dy^2 + dz^2.$$

The macrocoherent  $O(4) \rightarrow O(3)$  ordering transition (whose coherence is already established in Section 14.3) selects a globally aligned ordering direction  $n_A(x) = \text{const}$ , which can without loss of generality be taken as  $n_A = \delta_{Aw}$ . The spatial sections orthogonal to this direction then inherit the induced metric

$$h_{ij} = \delta_{ij}.$$

Since  $\delta_{ij}$  is the exact Euclidean metric on  $\mathbb{R}^3$ , its three-dimensional Ricci scalar vanishes identically,  ${}^{(3)}R[h] = 0$ . In FLRW notation  ${}^{(3)}R = 6k/a^2$ , so

$$\boxed{k = 0.}$$

This is not a preference and not a fine-tuning requirement: it is a direct structural consequence of P1 together with the macrocoherence of the ordering transition.

**(ii) Preservation under homogeneous branch evolution.** After branch emergence the large-scale homogeneous and isotropic evolution rescales the spatial metric:

$$ds^2 = -dt^2 + a^2(t) \delta_{ij} dx^i dx^j.$$

The spatial geometry at each constant- $t$  slice is  $a^2(t)\delta_{ij}$ , which is a time-dependent conformal rescaling of the flat metric. Homogeneous expansion changes  $a(t)$  and  $H(t)$  but does not convert a  $k = 0$  branch into a  $k = \pm 1$  branch; within the FLRW classification, the parameter  $k$  labels the spatial-curvature class of the homogeneous and isotropic branch rather than a dynamical field that evolves in time. Hence, for the exact baseline branch,

$$\Omega_K(t) = -\frac{k}{a^2 H^2} = 0 \quad \text{for all } t.$$

The observed bound  $|\Omega_K(t_0)| < 0.004$  [88] is therefore not a constraint that ECT must dynamically suppress, but an observational compatibility check of the flat baseline branch. Independent late-Universe analyses are consistent with the same near-flatness conclusion, strengthening the empirical compatibility. Subleading departures from exact flatness may arise from perturbations, imperfect coherence, or backreaction, but these lie beyond the idealised baseline branch.

**Topology caveat.** The above establishes local spatial flatness. Under the assumption of a simply connected progenitor domain the flat spatial sections correspond to the standard  $\mathbb{R}^3$  FLRW branch. Non-trivial spatial topology is not excluded by this argument but lies outside the scope of the baseline branch analysis.

**Comparison with inflation.** Standard inflation solves the flatness problem dynamically: it takes a branch with pre-existing  $k \neq 0$  and suppresses  $|\Omega_K|$  by making  $aH$  large. This is a dynamical suppression mechanism operating *inside* an already existing Lorentzian spacetime. ECT instead solves the problem *structurally*: the emergent branch is born flat as a direct consequence of P1 and the macrocoherent ordering transition. Flatness in ECT is therefore a Level A result, requiring no fine-tuning of initial conditions and no inflationary expansion to produce it.

## 14.5 Relic and monopole problem: topological resolution

*Status: Level A for the primary  $O(4) \rightarrow O(3)$  topology; Level B for later-sector relic details.*

In many grand-unified-theory (GUT) extensions of the standard model, a hot early Universe is expected to produce an overabundance of heavy topological relics — magnetic monopoles, domain walls, cosmic strings — whose predicted density would vastly exceed observational bounds. Standard inflation addresses this through dynamical dilution: exponential expansion reduces any pre-existing relic density to negligible levels.

In ECT the relevant question is instead: what is the topological and defect content of the *emergent* Lorentzian branch? The correct methodological standard is the same as for the horizon and flatness problems: not to prove that no relics are conceivable in any sector under any conditions, but to show that *relic catastrophe is not a structural consequence of ECT* and that a relic-poor observed branch is organically realizable.

**(i) Topological classification of the primary ordering transition (Level A).** The vacuum manifold of the  $O(4) \rightarrow O(3)$  ordering transition is

$$\mathcal{M}_1 = O(4)/O(3) \simeq S^3.$$

The homotopy groups of  $S^3$  are [7]:

$$\pi_0(S^3) = 0, \quad \pi_1(S^3) = 0, \quad \pi_2(S^3) = 0, \quad \pi_3(S^3) = \mathbb{Z}.$$

From the standard defect-classification by homotopy:

- $\pi_0(\mathcal{M}_1) = 0$ : no topologically stable domain walls from this transition;
- $\pi_1(\mathcal{M}_1) = 0$ : no topologically stable cosmic strings;
- $\pi_2(\mathcal{M}_1) = 0$ : no topologically stable magnetic monopoles.

The primary  $O(4) \rightarrow O(3)$  ordering transition therefore does not topologically require stable domain walls, cosmic strings, or magnetic monopoles. This is the primary Level A relic result of ECT cosmology: the vacuum manifold of the ordered branch does not support the topological class required for monopole formation.

A nontrivial  $\pi_3(S^3) = \mathbb{Z}$  sector nevertheless remains available. This means that the ordered branch may support texture- or skyrmion-like topological configurations rather than monopoles or domain walls. Their detailed profile, mass scale, and cosmological abundance depend on the full nonlinear ordered-branch EFT and remain open. The structural prediction at the present stage is the existence of a nontrivial texture sector, not yet a quantitative relic spectrum. The full classification of predicted new states and topological sectors, including conditional secondary defects, is given in Section 8.10. The present cosmological result should therefore be read narrowly but strongly: ECT removes the primary monopole catastrophe structurally, while deferring the detailed relic phenomenology of later sectors to the broader predicted-states programme.

**(ii) Standard GUT monopole overproduction is not structurally required (Level B).** Standard GUT magnetic monopoles are topological defects of the GUT gauge symmetry, arising when a unified group  $G_{\text{GUT}}$  breaks to a subgroup containing a  $U(1)$  factor with  $\pi_2(G_{\text{GUT}}/H) \neq 0$ . This scenario requires a hot symmetric GUT phase that then cools through a sequence of thermal gauge-symmetry breakings. ECT does not postulate such a phase as a structural necessity of its cosmological architecture. The Lorentzian branch emerges through  $O(4) \rightarrow O(3)$ , not through a standard hot GUT thermal history. If no such phase precedes the emergent branch, the standard monopole overproduction scenario does not apply: *ECT does not structurally require a monopole-overproducing GUT thermal history.*

**(iii) Later-sector relics: further development, not structural catastrophe (Level B).** The topological argument above covers the primary ordering transition. Remaining questions — including monopole-like configurations that might arise in the electroweak sector, non-topological heavy relics, and metastable branch configurations — are not yet fully classified in ECT. However, none of these has been shown to be structurally inevitable or to produce a cosmologically dangerous abundance in the observed branch. Moreover, the coherent smooth observed branch that the theory naturally selects is not naturally associated with a heavily defect-saturated realisation: the smooth coherent observed branch of ECT is naturally associated with a relic-poor realisation rather than with a defect-saturated one. The remaining relic questions are therefore sector-specific model-building issues rather than built-in structural catastrophes.

**Further development.** If the electroweak-like condensate embedding is physically realised, it would involve a transition of the form  $SU(2) \times U(1) \rightarrow U(1)_{\text{em}}$  at the matched scale  $v_2 = 246 \text{ GeV}$ . At present this sector should be treated as a structural candidate rather than an established part of the derived ECT core. A naive global-symmetry analysis gives  $\pi_2(SU(2)/U(1)) \neq 0$ , which may admit monopole-like configurations at this scale; however, in gauge theory this analysis is more subtle and the precise topological status of such objects depends on the UV completion. Their cosmological production in the

ECT setting requires a dedicated analysis and should be understood as part of the broader ECT relic programme rather than as a reopening of the primary relic catastrophe.

**Comparison with inflation.** Standard inflation addresses the relic problem through a dynamical dilution mechanism operating inside an already existing Lorentzian cosmology: a separate inflationary sector dilutes any pre-existing relic density exponentially. ECT addresses the primary problem more fundamentally: the  $O(4) \rightarrow O(3)$  transition does not topologically require stable monopoles, walls, or strings (Level A), and the theory does not structurally require the dangerous hot GUT history (Level B). Later-sector relic questions remain as model-dependent further development.

## 14.6 Primordial perturbations: current status

*Status: Level A for the identification of perturbation degrees of freedom, the single-scalar-mode structure, and tensor propagation speed; full derivation of  $n_s$ ,  $A_s$ ,  $r$  is open.*

Sections 14.1 and 14.3 established the structural setting of ECT cosmology: the ordered Lorentzian branch emerges from a pre-ordered regime and is born as a macrocoherent, spatially flat branch. The next question is therefore not whether perturbations exist, but what perturbation content is structurally implied by the ordered branch and which parts of the primordial spectrum remain open. The purpose of the present subsection is structural rather than fully predictive: to identify what is already fixed by the ordered branch, and what still requires a quantitative perturbation theory.

### Observational target

The observed primordial perturbation spectrum is nearly scale-invariant,

$$P_\zeta(k) \approx A_s \left( \frac{k}{k_*} \right)^{n_s-1}, \quad (14.2)$$

with  $n_s = 0.9649 \pm 0.0042$  and tensor-to-scalar ratio  $r_{0.002} < 0.056$  (95% C.L., Planck 2018 combined with BICEP/Keck [88, 89]). Any cosmological theory must eventually account for these observed values. ECT does not yet derive  $n_s$  or  $r$  from first principles, and the present work makes no such claim. However, the ECT framework already fixes the perturbation field content at a structural level and identifies a plausible route toward the primordial spectrum.

### Perturbation variables and the single-mode structure

The condensate field  $\Phi$  on the ordered branch admits a natural decomposition into fluctuation sectors (§3): orientational (Goldstone) fluctuations  $\delta n_A$ , amplitude fluctuations  $\delta\sigma = \delta|\partial\Phi|$ , and phase fluctuations  $\delta\theta$ . These provide the natural perturbative degrees of freedom of the condensate/branch sector.

**Proposition (single scalar perturbation mode of the ordered branch).** At leading order, the scalar perturbation sector of the linear ordered branch contains exactly one independent scalar degree of freedom.

*Proof.* By the Universality Corollary (§4.3), the integrability condition  $Q_A = \partial_A\Phi$  reduces the linear soft ordered-branch excitations to derivatives of a single scalar fluctuation  $\chi$ . Hence the scalar perturbation sector possesses one and only one independent scalar mode at leading order.  $\square$

This is the structural analogue of a single-scalar perturbation sector. It does not yet constitute a derivation of the observed curvature spectrum, but it does show that the leading ordered-branch perturbation content is not intrinsically multi-scalar and does not, at that structural level, force the introduction of a separately postulated inflaton-like degree of freedom.

**Consequence: no independent ordered-branch isocurvature mode.** Because the linear ordered scalar branch contains only one scalar degree of freedom, it does not support an independent isocurvature mode of its own at leading order. Any primordial isocurvature component would therefore have to arise, if at all, from additional phase/gauge/matter sectors beyond the minimal ordered scalar branch. This

structural expectation is compatible with current CMB analyses, which constrain primordial isocurvature to be subdominant.

### Tensor sector

The tensor perturbations of ECT cosmology are not an independent late-time addition, but the same transverse-traceless ordered-branch sector analysed in the gravitational-wave discussion of Section 13.8. At the structural level, this implies that primordial tensor modes propagate on the same ordered-branch cone with speed  $c_*$ . This also ensures that the causal speed entering primordial tensor propagation is the same structural speed  $c_*$  that underlies local SR (§12) and late-time GW propagation (§13.8). Thus the primordial tensor sector and the late-time GW sector are kinematically consistent by construction. The detailed reduction to the observationally relevant TT content remains tied to the same open OP-gauge reduction step discussed earlier.

### Conditional scale-invariance conjecture

If the ordering transition is approximately scale-free over the range of modes relevant for cosmological observations—in the sense that no macroscopic scale larger than  $\xi_{\text{cond}}$  dominates the transition dynamics—then the resulting perturbation spectrum is naturally expected to be approximately scale-invariant at leading order. At present this is a structural conjecture, not a derivation. Its verification requires the explicit perturbation equations on the FRW-ordered background and the corresponding freeze-out analysis.

### Critical $O(4)$ fluctuations and spectral tilt estimates

The ordering transition  $O(4) \rightarrow O(3)$  is a symmetry-breaking phase transition in four Euclidean dimensions with vacuum manifold  $S^3$ . Near criticality the order-parameter propagator has the form

$$G_4(p) \sim \frac{1}{(p^2)^{1-\eta/2}}, \quad (14.3)$$

where  $\eta$  is the anomalous dimension. Since  $d = 4$  is the upper critical dimension for the  $O(N)$  model, mean-field scaling applies with logarithmic corrections:  $\eta = 0$  at leading order, but the correlation function acquires a multiplicative logarithmic factor,

$$G(r) \sim \frac{1}{r^{d-2} [\ln(r/\xi_0)]^{\hat{p}}}, \quad (14.4)$$

where  $\hat{p}$  is a universal exponent. After projection onto three-dimensional spatial slices and conversion to curvature perturbations through the metric constraint equation  $k^2 \Phi_k \sim G_N \delta \rho_k$ , the resulting power spectrum acquires an effective tilt

$$1 - n_s \sim \frac{\hat{p}}{\ln(L/\xi_0)}, \quad (14.5)$$

where  $L \sim H_0^{-1} \sim 10^{26}$  m is the cosmological horizon and  $\xi_0 \sim \ell_{\text{Pl}} \sim 10^{-35}$  m is the condensate correlation length. With  $\ln(L/\xi_0) \sim 140$ , values  $\hat{p} \sim 4\text{--}5$  (understood as the phenomenologically relevant target range required for agreement with observation, not as a quantity already derived from the ECT critical theory) yield

$$n_s^{\text{ECT}} \sim 0.96\text{--}0.97, \quad (14.6)$$

which is compatible with the observed  $n_s = 0.9649 \pm 0.0042$ . At present,  $\hat{p} \sim 4\text{--}5$  should be understood as the phenomenologically relevant target range required for agreement with observation, not as a quantity already derived from the ECT critical theory.

An independent estimate comes from the gauge–Higgs sector. The  $O(4)$  order parameter can be rewritten as a complex Higgs doublet  $H = (H_1, H_2)^T$ , making the connection  $O(4) \simeq$  Higgs-doublet sector

of  $SU(2) \times U(1)$  explicit. Weakly gauging  $SU(2) \times U(1)$  produces one-loop corrections to the effective anomalous dimension:

$$\gamma_H \sim \frac{1}{16\pi^2} \left( \frac{3}{4}g'^2 + \frac{9}{4}g^2 - 3y_t^2 \right) \approx -1.2 \times 10^{-2}, \quad (14.7)$$

using  $g \approx 0.65$ ,  $g' \approx 0.36$ ,  $y_t \approx 1$ . If the spectral tilt is of order  $2|\gamma_H|$ , this gives  $1 - n_s \sim 0.025$ , again in the correct range.

**Amplitude estimate.** If the curvature perturbation arises through local transition-time fluctuations,  $\zeta(\mathbf{x}) \sim \delta u_*/u_0$ , then the observed amplitude  $\sqrt{A_s} \approx 4.6 \times 10^{-5}$  requires

$$\frac{\delta u_*}{u_0} \sim 5 \times 10^{-5}. \quad (14.8)$$

This is a modest fractional fluctuation, compatible with loop-scale weak/Higgs corrections of order  $g^2/(16\pi^2) \sim 10^{-3}$ – $10^{-2}$  supplemented by a conversion/coarse-graining suppression factor of  $10^{-2}$ – $10^{-1}$ .

**Role of weak gauging.** Weakly gauging  $SU(2) \times U(1)$  potentially assists the primordial perturbation programme in three ways: (i) gauge constraints absorb orientational (isocurvature) modes of the  $S^3$  vacuum manifold, leaving a single adiabatic scalar seed; (ii) gauge–Higgs running provides a natural source of small red tilt; (iii) the gauge coupling disciplines the freeze-out and suppresses excess non-Gaussianity.

**Status.** The estimates (14.6) and (14.8) show that ECT without inflation can naturally reach the observational range for the primordial spectrum. This is a compatibility result, not yet a first-principles derivation. However, a rigorous derivation remains open: the explicit freeze-out dynamics, the gauge-invariant curvature transfer, and the precise values of  $\hat{p}$  and the conversion factors are completion targets of the ECT perturbation programme (Level B/C).

### Comparison with inflationary perturbation theory

In standard inflationary cosmology,  $n_s$  and  $r$  are computed from the slow-roll dynamics of a separately introduced inflaton field. ECT does not introduce such a field; instead, the single-scalar perturbation sector follows structurally from the integrability of the ordered-branch condensate (Universality Corollary). What the two frameworks share is the single-scalar character of the leading perturbation sector. What ECT does not yet provide is the explicit spectral computation:  $n_s$ ,  $A_s$ , and  $r$  remain open targets of the ECT perturbation programme.

### Research agenda

A concrete research programme therefore consists of the following steps:

1. verify that the single-mode structure implied by the Universality Corollary survives in the cosmological perturbation analysis on an FRW ordered background;
2. derive the scalar and tensor perturbation equations through the ordering transition;
3. determine the freeze-out mechanism and the corresponding transfer to the late-time curvature spectrum;
4. compute the amplitude and tilt in terms of the ordered-branch potential and closure functions;
5. derive the tensor-to-scalar ratio and possible non-Gaussianity signatures.

This perturbation programme must ultimately be matched to the homogeneous ordered-branch cosmology developed in Section 16, so that the background branch and the primordial fluctuation sector are treated within a single macroscopic framework.



## What is established and what remains open

At Level A, ECT already fixes the perturbation field content of the linear ordered branch: there is a single scalar mode and no independent ordered-branch isocurvature scalar. At the same structural level, the tensor sector propagates on the same ordered-branch cone as the late-time gravitational-wave sector. What remains open is the quantitative primordial spectrum itself: the explicit derivation of  $A_s$ ,  $n_s$ , and  $r$ , the freeze-out mechanism across the ordering transition, and the nonlinear coupling to phase/gauge/matter sectors.

### 14.7 Summary and comparison with inflationary resolution

**Conceptual difference from inflation.** Inflation addresses the horizon, flatness, and relic problems as dynamical problems inside an already existing Lorentzian spacetime. ECT shifts all three to the deeper level of branch emergence: coherence replaces causal contact, structural branch flatness replaces dynamical curvature suppression, and topology of the ordered vacuum manifold replaces dynamical relic dilution.

**Table 59:** Classical cosmological problems: standard resolution vs. ECT.

Problem	Standard treatment	ECT treatment	Status
Horizon	Inflationary causal stretching inside an already existing Lorentzian spacetime	Coherent branch selection: macro-coherence as the minimum of the Euclidean ordering functional on a connected progenitor domain	Level A (minimum); Level B (full scenario)
Flatness	Dynamical suppression of $ \Omega_K $ by inflation	Structural: P1 + macrocoherent ordering $\Rightarrow k = 0$	Level A
Relic / monopole	Dynamical dilution by inflation	$\pi_2(S^3) = 0$ : no monopole-supporting topology in the ordered-branch vacuum manifold	Level A (primary); Level B (later sectors)

**What is established and what remains open.** At Level A, ECT yields three structural cosmological results: (i) the Euclidean ordering functional admits a macro-coherent minimum, which provides the core of the horizon-resolution route; (ii) the emergent homogeneous branch is born spatially flat,  $k = 0$ ; (iii) the ordered-branch vacuum manifold satisfies  $\pi_2(S^3) = 0$ , eliminating the primary monopole channel. At the same structural level, the primordial perturbation sector is already constrained to a single leading scalar mode together with a tensor sector propagating on the same ordered-branch cone. What remains open is the fully dynamical realisation of branch selection, the quantitative perturbation theory across the ordering transition (including  $A_s$ ,  $n_s$ , and  $r$ ), and the nonlinear relic spectrum of the nontrivial  $\pi_3(S^3)$  texture sector.

## 15 Vacuum Offset Decoupling and the Cosmological Constant Problem

### 15.1 Statement of the problem in the standard framework

The cosmological constant problem is the sharpest quantitative failure of the standard framework combining general relativity with quantum field theory on a fixed Lorentzian background. In that framework, the gravitational action contains a term

$$S_\Lambda = -\Lambda \int d^4x \sqrt{-g}, \quad (15.1)$$

whose coefficient is, on the observational side,

$$\rho_{\Lambda, \text{obs}} \approx 10^{-47} \text{ GeV}^4 \approx \Omega_\Lambda \cdot \rho_c \approx 2M_{\text{Pl}}^2 H_0^2, \quad (15.2)$$

with  $\Omega_\Lambda \approx 0.69$ , critical density  $\rho_c = 3H_0^2 M_{\text{Pl}}^2$ , and reduced Planck mass  $M_{\text{Pl}} = 2.435 \times 10^{18} \text{ GeV}$ . On the theoretical side, the same coefficient receives naive quantum zero-point contributions of order  $M_{\text{Pl}}^4$ , exceeding the observed value by approximately 120 orders of magnitude. The standard resolution is to tune the bare  $\Lambda$  against the quantum contributions to leave the observed residue; this fine-tuning is not stabilized by any symmetry [90, 91, 92]. Within the standard framework,  $\rho_{\Lambda, \text{obs}}$  is therefore not derived; it is an input fitted to data.

We show in this section that ECT, by virtue of its emergent-metric architecture, modifies the structure of the problem. The direct channel by which vacuum energy enters the gravitational action in eq. (15.1) is blocked in the leading ordered-branch sector of ECT. Blocking this channel reformulates the question: the observed late-time acceleration must then arise from infrared ordered-branch physics rather than from a UV vacuum baseline. We establish the structural result rigorously, delimit its scope honestly, and present a motivated infrared estimate consistent with observation. Technical details of the theorem proof, the FRW reduction, and the Goldstone-based infrared scaling are collected in Appendix AC.

## 15.2 Three distinct objects

To avoid conflations that pervade the standard discussion, we distinguish from the outset three logically separate quantities frequently bundled under the label “vacuum energy.”

**Object A: classical baseline offset  $V(\phi_0)$ .** The value of the scalar potential at its ordered-branch minimum  $\Phi = \phi_0$ . This is a constant property of the fundamental Euclidean Lagrangian  $\mathcal{L}_E$  with no local  $x$ -dependence.

**Object B: zero-derivative quantum contribution  $\Gamma_{\text{vac}}^{(0)}$ .** The part of the perturbative effective action that contains no derivatives of background fields. In the standard QFT-on-Lorentzian-background calculation, this produces the  $\sim M_{\text{Pl}}^4$  zero-point contribution through the  $a_0$  heat-kernel coefficient.

**Object C: long-wavelength infrared source  $\rho_\Lambda^{\text{IR}}$ .** The effective energy density entering the cosmological (FRW) equations as an approximately dark-energy-like source, i.e. the quantity actually driving the observed late-time acceleration.

In standard general relativity coupled to quantum field theory on an independent dynamical metric, Objects A and B feed directly into the coefficient  $\Lambda$  in eq. (15.1) and are therefore bundled into Object C. The naturalness problem is precisely this bundling. In ECT we will show that Object A decouples unconditionally, and Object B decouples under a stated condition; Object C must then be provided by independent infrared physics.

## 15.3 Main theorem: emergent unimodular decoupling

We work in the leading ordered-branch ansatz of ECT, defined by the structure of the kinetic tensor governing fluctuations of the relevant emergent-metric sector:

$$K^{AB}(x) = \beta \delta^{AB} - \alpha n^A(x) n^B(x), \quad \delta_{AB} n^A(x) n^B(x) = 1, \quad (15.3)$$

with constant parameters  $\alpha, \beta$  satisfying the Lorentzian-phase condition  $\alpha > \beta > 0$ . The emergent effective metric is identified through the densitized-inverse-metric relation

$$K^{AB}(x) \propto \sqrt{-g_{\text{eff}}(x)} g_{\text{eff}}^{AB}(x), \quad (15.4)$$

with a field-independent proportionality factor. Admissible variations of the emergent metric are those induced by variations of  $n^A$  preserving the unit constraint and by variations of other condensate fields.

**Theorem 1 (Emergent unimodular decoupling).** Under the ansatz (15.3) and the identification (15.4):

(i) **Fixed determinant.** The determinant of  $K^{AB}$  is independent of  $n^A(x)$ :

$$\det K^{AB} = \beta^4 \left( 1 - \frac{\alpha}{\beta} n^A \delta_{AB} n^B \right) = \beta^3 (\beta - \alpha). \quad (15.5)$$

(ii) **Constant emergent volume element.** As a consequence of (i),

$$\sqrt{-g_{\text{eff}}[n^A(x)]} = \text{const} \cdot \sqrt{-\det K^{AB}} = \frac{\beta^2}{c_*}, \quad (15.6)$$

where we used  $c_*^2 = \beta/(\alpha - \beta)$ .

*Note on identification conventions.* Equation (15.6) uses the densitized-inverse-metric identification of (15.4), under which  $\sqrt{-\det K^{AB}} = \beta^2/c_*$  coincides with  $\sqrt{-g_{\text{eff}}}$  up to a field-independent prefactor. Other sections of the paper treat  $K^{AB}$  as the ordinary inverse metric  $G_{\text{eff}}^{AB}$  itself (§3.6), under which  $\sqrt{-g_{\text{eff}}} = c_*/\beta^2$ ; the two conventions agree at the canonical benchmark  $(\alpha, \beta) = (2, 1)$ . The physically invariant content of part (i) is that  $\det K^{AB}$  is  $n$ -independent; clauses (ii)–(v) of this theorem depend only on this fact together with the unit constraint  $n^A n_A = 1$ , and therefore go through identically under either identification convention.

(iii) **Vanishing variation.** For admissible variations  $\delta n^A$  preserving  $n^A n_A = 1$ ,

$$\delta \sqrt{-g_{\text{eff}}[n]} = 0. \quad (15.7)$$

(iv) **Object A decoupling (unconditional).** The classical baseline offset  $V(\phi_0)$  does not contribute to the local equations of motion for any admissible field:

$$\frac{\delta}{\delta q^a(x)} \int d^4y V(\phi_0) = 0 \quad \text{for all admissible } q^a \in \{n^A, \Phi, \dots\}. \quad (15.8)$$

This conclusion follows from the Jacobian-cancellation identity: a field-independent constant in  $\mathcal{L}_E$  contributes only an additive constant to the action, which drops out of all Euler–Lagrange equations. It is independent of the structure of the fluctuation operator.

(v) **Object B decoupling (conditional on  $H_\Lambda$ ).** If and only if the full quadratic fluctuation operator contains no additional field-dependent prefactors multiplying  $K^{AB}$  beyond those allowed by (15.4) – a condition labeled  $H_\Lambda$ , stated precisely in Sec. 15.4 – the zero-derivative quantum contribution  $\Gamma_{\text{vac}}^{(0)}$  reduces to a constant-volume term

$$\Gamma_{\text{vac}}^{(0)} \propto \Lambda_{\text{UV}}^4 \int d^4x \sqrt{-g_{\text{eff}}} = \frac{\Lambda_{\text{UV}}^4 \beta^2}{c_*} \int d^4x = \text{const} \cdot \text{Vol}_4, \quad (15.9)$$

and does not source local emergent gravitational dynamics. If  $H_\Lambda$  fails, the UV sensitivity is transferred into the scalar/radial sector effective potential rather than into a direct cosmological-constant term; see Sec. 15.4 for details.

**Proof outline.** Part (i) is the rank-one determinant identity  $\det(\beta I - \alpha n n^T) = \beta^4 (1 - (\alpha/\beta) n^T n)$ , evaluated with  $n^T n = 1$ . Part (ii) follows from (15.4) together with the densitized-metric identity  $\det(\sqrt{-g} g^{\mu\nu}) = -g$  in four dimensions. Part (iii) is immediate from (ii): on the constraint surface  $n^A n_A = 1$ , admissible variations satisfy  $n^A \delta n_A = 0$ , and  $\partial(\det K)/\partial n^A = -2\alpha\beta^3 n_A$ , so  $\delta(\det K) = 0$ . Part (iv) is the Jacobian-cancellation identity. Part (v) combines (ii) and (iv) under the prefactor assumption  $H_\Lambda$ . Explicit derivations are given in Appendix AC. ■

**Corollary (direct UV channel blocking).** In the leading ordered-branch sector of ECT, the standard direct channel by which a vacuum baseline  $V(\phi_0)$  or a zero-derivative loop contribution enters the gravitational action as a coefficient of  $\int \sqrt{-g}$  with unsuppressed  $M_{\text{Pl}}^4$  strength is not operative. Object A is decoupled unconditionally; Object B is decoupled conditional on  $H_\Lambda$ . Neither feeds directly into Object C in this sector.

## 15.4 The condition $H_\Lambda$ and its logical status

Theorem 15.3(v) decouples Object B from Object C conditionally on an absence of additional field-dependent prefactors. Here we state the condition precisely and analyze the two branches of outcomes.

**Condition  $H_\Lambda$ .** Let  $\chi(x)$  denote a generic low-energy fluctuation of the ordered-branch sector, and let the full quadratic action be

$$S^{(2)}[\chi] = \frac{1}{2} \int d^4x_E [\mathcal{K}^{AB}(\phi, n, \dots) \partial_A \chi \partial_B \chi + \mathcal{M}^2(\phi, n, \dots) \chi^2]. \quad (15.10)$$

$H_\Lambda$  states that the kinetic matrix decomposes as

$$\mathcal{K}^{AB}(\phi, n, \dots) = K^{AB}(n) \cdot [\text{field-independent constant}], \quad (15.11)$$

i.e. no dynamical scalar prefactor  $Z(\phi)$ , no mixing-induced effective prefactor, and no other field-dependent multiplier of  $K^{AB}$  in the zero-derivative sector.

**Two branches.**  $H_\Lambda$  holds. Theorem 15.3(v) applies and Object B decouples exactly like Object A. In the leading ordered-branch sector, both the classical baseline offset and the one-loop zero-derivative contribution are inert for the local emergent gravitational dynamics.

$H_\Lambda$  fails with a scalar prefactor  $Z(\phi)$ . Then  $\mathcal{K}^{AB}(\phi, n) = Z(\phi)(\beta \delta^{AB} - \alpha n^A n^B)$ , so  $\det \mathcal{K} = Z(\phi)^4 \det K$  and  $\sqrt{-g_{\text{eff}}^{(\chi)}} \propto Z(\phi)^2$ . The one-loop zero-derivative contribution becomes

$$\Gamma_{\text{vac}}^{(0)} \propto \Lambda_{\text{UV}}^4 \int d^4x Z(\phi(x))^2, \quad \frac{\delta \Gamma_{\text{vac}}^{(0)}}{\delta \phi(x)} \sim \Lambda_{\text{UV}}^4 Z(\phi) Z'(\phi) \neq 0. \quad (15.12)$$

The UV sensitivity then manifests as a large correction to the effective scalar potential, i.e. as a scalar naturalness / hierarchy problem for the radial sector, *not* as a direct cosmological-constant contribution in the constrained ordered-branch metric sector.

**Object A is unaffected by  $H_\Lambda$ .** Regardless of whether  $H_\Lambda$  holds, Object A (the classical  $V(\phi_0)$ ) decouples, because its decoupling follows from the Jacobian identity alone (Theorem 15.3(iv)).

**Status.**  $H_\Lambda$  is a condition on the full quadratic fluctuation operator derived from the fundamental ECT Lagrangian. Its verification requires explicit expansion of  $\mathcal{L}_E[\Phi]$  around the ordered branch  $\Phi = \phi_0 + \chi$ ,  $\langle \partial_A \Phi \rangle = u_0 n_A$ , and inspection of the resulting quadratic form. This verification is listed as Open Problem O1 in Sec. 15.12. Until it is completed, the present text treats Theorem 15.3(v) as a result conditional on  $H_\Lambda$ .

## 15.5 Connection to unimodular gravity

The fixed-determinant property (15.6) is structurally analogous to the defining condition of unimodular gravity [93, 94, 95]. In unimodular gravity, the metric determinant is fixed by fiat ( $\sqrt{-g} = \epsilon_0$ ), and the field equations are the traceless part of the Einstein equations. Known consequences [96, 97] include that the cosmological constant enters as an integration constant, and that it is immune to renormalization

contributions from the bulk dynamics in the standard formulation. ECT exhibits a similar decoupling structure, with two qualitatively important differences.

First, the constraint is derived, not postulated: in standard unimodular gravity,  $\sqrt{-g} = \varepsilon_0$  is imposed externally, while in ECT (15.6) follows from the algebraic constraint  $n^A n_A = 1$  together with the ordered-branch kinetic structure (15.3). No Lagrange multiplier is needed. Second, admissible variations are more restricted: in unimodular gravity the metric is fundamental but constrained; in ECT the metric is emergent, and all admissible variations are already variations of condensate fields.

These differences make the ECT decoupling structurally stronger than the textbook unimodular construction. However, they also mean that the quantum-theoretic non-renormalization theorems of Ng and van Dam [96] and Smolin [97], formulated for unimodular gravity with a fundamental (constrained) metric and a specific quantization scheme, do not automatically transfer. We regard the structural analogy as established; a formal non-renormalization theorem for emergent unimodular-like structures in ECT is listed as Open Problem O3 in Sec. 15.12.

## 15.6 Interplay with Weinberg's no-go theorem

Weinberg's no-go theorem [90] establishes that no *local, Lorentz-covariant* mechanism within *quantum field theory on a fixed Lorentzian background with an independent dynamical metric* can dynamically adjust  $\Lambda$  to small values without fine-tuning. Its framework assumptions include an independent dynamical metric, standard Lorentz-invariant path-integral quantization in the Lorentzian sector, and the standard local-effective-action structure.

ECT does not satisfy these framework assumptions. The fundamental background is Euclidean (postulate P1), the Lorentzian sector is emergent (P5), and the metric is a composite object built from orientation and condensate fields rather than an independent variable. As a consequence, ECT lies outside the standard assumptions of Weinberg's no-go theorem, and that theorem does not directly exclude an ECT-based resolution. This does not in itself constitute a solution, but it does remove one of the principal structural obstacles that prevents such a solution in the standard framework.

## 15.7 FRW reduction and connection to the equation of state

Once Objects A and (conditionally) B decouple, the observed late-time acceleration must arise from the infrared dynamics of the ordered branch itself – Object C. In ECT this is consistent with, and complementary to, the dark-energy picture developed in Sec. 16: dark energy is identified with the residual dynamical condensate energy rather than with a fundamental cosmological constant.

**Minimal homogeneous reduction.** On an FRW background, the surviving long-wavelength degree of freedom of the ordered branch is a slowly varying order parameter  $q(t)$ , constructed from the condensate amplitude and/or the orientation field. The minimal homogeneous effective Lagrangian is

$$L_{\text{IR}}[q; a] = a^3 \left[ \frac{1}{2} Z_q \dot{q}^2 - V_{\text{IR}}(q) \right], \quad (15.13)$$

with  $Z_q$  the effective infrared stiffness and  $V_{\text{IR}}(q)$  the residual infrared potential.  $V_{\text{IR}}$  is *not* the UV baseline  $V(\phi_0)$  (which is decoupled by Theorem 15.3(iv)) but its slowly varying long-wavelength dressing. The energy density and pressure are

$$\rho_q = \frac{1}{2} Z_q \dot{q}^2 + V_{\text{IR}}(q), \quad (15.14)$$

$$p_q = \frac{1}{2} Z_q \dot{q}^2 - V_{\text{IR}}(q). \quad (15.15)$$

In the slow-branch regime  $Z_q \dot{q}^2 \ll V_{\text{IR}}(q)$ ,  $w_q = p_q / \rho_q \approx -1$ , consistent with dark-energy-like behavior. Deviations from  $w = -1$  arise when the kinetic contribution is non-negligible.

**Connection to the ECT equation-of-state prediction.** The reduction (15.13)–(15.15) provides the formal grounding for the dark-energy formula appearing in Sec. 16,

$$w_0 = -1 + \frac{2\rho_{\text{kin}}}{3\rho_{\text{cond}}}, \quad (15.16)$$

upon identifying  $\rho_{\text{kin}} = \frac{1}{2}Z_q\dot{q}^2$  and  $\rho_{\text{cond}} = V_{\text{IR}}(q)$ . The ECT value  $w_0 \approx -0.83$  (for  $\rho_{\text{kin}}/\rho_{\text{cond}} \approx 0.26$ ) is therefore an explicit instance of the general slow-branch reduction. It is numerically comparable to recent observational indications of  $w_0 \neq -1$ , including the DESI-era analysis [98], subject to the full observational discussion elsewhere in this paper. The present theorem establishes the structural permissibility of this picture: the “condensate energy” that plays the role of dark energy is not the UV baseline  $V(\phi_0)$  but its slowly varying infrared dressing.

### 15.8 Infrared estimate for $\rho_{\Lambda}^{\text{IR}}$

With the direct UV channel blocked, the observed dark-energy scale must be provided by infrared ordered-branch physics. Here we derive the natural parametric estimate and place it in context.

**Dimensional scaling after UV channel blocking.** The observed  $\rho_{\Lambda}$  has dimensions  $\text{mass}^4$ . After the closure of the direct UV channel in the leading sector, the scale  $M_{\text{Pl}}^4$  is *not* available to feed directly into Object C. Among the remaining scales accessible to an infrared effective description on FRW: the emergent gravitational stiffness scale  $M_{\text{Pl}}^2$  (setting the coefficient of the induced Einstein–Hilbert term, in the sense of Sakharov-induced gravity [99, 100]), and the infrared cosmological scale  $H_0$  (the only dimensionful curvature/time scale in the long-wavelength cosmological effective theory).

The unique parametric combination of dimensions  $\text{mass}^4$  that does not invoke the decoupled UV scale  $M_{\text{Pl}}^4$  directly is

$$\boxed{\rho_{\Lambda}^{\text{IR}} \sim c_{\Lambda} M_{\text{Pl}}^2 H_0^2, \quad c_{\Lambda} = O(1) \text{ or smaller.}} \quad (15.17)$$

This is a *motivated scaling estimate*, not a derivation from first principles. The coefficient  $c_{\Lambda}$  is not fixed by the present argument.

**Numerical evaluation.** With  $M_{\text{Pl}} = 2.435 \times 10^{18} \text{ GeV}$  and  $H_0 \approx 1.44 \times 10^{-42} \text{ GeV}$ ,

$$M_{\text{Pl}}^2 H_0^2 \approx 1.2 \times 10^{-47} \text{ GeV}^4, \quad (15.18)$$

of the same order as the observed  $\rho_{\Lambda, \text{obs}} \approx 10^{-47} \text{ GeV}^4$ .

**What this does and does not establish.** In standard QFT coupled to general relativity, obtaining the observed small  $\rho_{\Lambda, \text{obs}}$  from a UV contribution  $\sim M_{\text{Pl}}^4$  requires a cancellation at the  $10^{-121}$  relative level between unrelated quantities. In ECT, by contrast, the direct UV contribution is decoupled in the leading sector, and the scaling of the remaining infrared source is set by the only available infrared physics; no cross-scale cancellation is invoked. What remains is a bounded  $O(1)$  determination problem for  $c_{\Lambda}$ . This reformulation does not, in itself, constitute a first-principles calculation; computing  $c_{\Lambda}$  is Open Problem O2 (Sec. 15.12).

### 15.9 Possible microphysical realization: pseudo-Goldstone modes

Eq. (15.17) is a scaling law. A plausible microphysical realization of it within the ECT architecture is the pseudo-Goldstone sector associated with the spontaneous breaking  $O(4) \rightarrow O(3)$ .

**The Goldstone sector.** The  $O(4) \rightarrow O(3)$  breaking at scale  $\phi_0$  produces three Goldstone bosons. As discussed in Sec. 16, the ECT spectrum features pseudo-Goldstones with a small mass scale  $m_G \sim 10^{-33} \text{ eV}$ , which is of order  $H_0$ , consistent with the fuzzy-dark-matter candidate scale. In the standard construction of spontaneous symmetry breaking, the Goldstone decay constant coincides with the breaking scale,  $f_G \sim \phi_0$ . In the ECT hierarchy  $\phi_0 \sim \bar{M}_{\text{Pl}}$ .

**Scaling of the contribution to  $\rho_\Lambda$ .** A pseudo-Goldstone mode  $\theta$  of mass  $m_G$  and decay constant  $f_G$ , evolving slowly on cosmological scales, contributes an infrared energy density controlled by its potential. For a quadratic potential near the minimum,

$$V_G(\theta) \sim m_G^2 \theta^2, \quad \rho_G \sim m_G^2 f_G^2, \quad (15.19)$$

where the second estimate takes  $\theta$  at the natural Goldstone field scale  $f_G$ . Using  $m_G \sim H_0$  and  $f_G \sim M_{\text{Pl}}$ ,

$$\rho_G \sim H_0^2 M_{\text{Pl}}^2, \quad (15.20)$$

matching the scaling (15.17) with  $c_\Lambda = O(1)$ .

**Status of this realization.** This is a *plausible candidate realization* of the scaling within the ECT architecture, provided that the mass scale  $m_G \sim H_0$  and the decay-constant scale  $f_G \sim \phi_0$  are both maintained in the cosmological regime. The mass scale is an independent feature of the ECT pseudo-Goldstone sector, not adjusted here to reproduce the dark-energy value. A first-principles derivation of  $m_G$  from the ECT parameters  $(\mu, \lambda, \alpha, \beta)$ , together with the cosmological evolution of the Goldstone condensate, is required to upgrade Eq. (15.19) from a consistency check to a prediction. This task is part of the broader programme on the ECT particle spectrum (Open Problem O4 of Sec. 15.12).

## 15.10 Comparison with other approaches

Table 60 summarizes the status of the cosmological constant problem in principal existing approaches and in ECT. The comparison is restricted to structural features; numerical precision varies and is not the object of the comparison.

**Table 60:** Summary of approaches to the cosmological constant problem. “Fine-tuning” refers to the relative precision with which unrelated UV and IR scales must cancel in the given framework.

Approach	Status of $\rho_{\Lambda, \text{obs}}$	UV fine-tuning	Structural mechanism
$\Lambda$ CDM + QFT (standard)	Input, fitted	$\sim 10^{-121}$ required	None
Unimodular gravity [93]	Integration constant	Absent for UV in standard formulation; input for IR	$\sqrt{-g} = \varepsilon_0$ imposed
Anthropic selection [101]	Upper bound only	Avoided via multiverse	Structure-formation bound
Holographic bound [102]	$\lesssim M_{\text{Pl}}^2/L_{\text{IR}}^2$	Phenomenological	UV–IR relation
Quintessence (generic)	$V(\phi)$ tuned	Transferred to $V$	Slow-roll scalar
<b>ECT (present work)</b>	IR scaling estimate $\sim M_{\text{Pl}}^2 H_0^2$ ; coefficient open	Direct UV vacuum-to- $\Lambda$ cancellation absent in leading ordered-branch sector	<i>Emergent</i> unimodular decoupling from $n^A n_A = 1$

Two features distinguish ECT from related approaches. First, the unimodular-like condition is not postulated but derived from the kinematic constraint  $n^A n_A = 1$  together with the ordered-branch kinetic structure; this places no additional restriction on the theory beyond what is already required for emergent Lorentzian signature. Second, the infrared estimate (15.17) is potentially realized by a mode already present in the ECT spectrum (Sec. 15.9), rather than by a phenomenologically introduced scalar.

### 15.11 Status summary: Level A / B / C

We adopt the accuracy grading used throughout this work. The results of this section have the following status.

#### Level A (rigorously established within the leading ordered-branch sector).

1. In the leading ordered-branch ansatz (15.3), the determinant of  $K^{AB}$  is independent of  $n^A(x)$ ; consequently  $\sqrt{-g_{\text{eff}}} = \beta^2/c_*$  is constant on the admissible configuration space [Theorem 15.3(i)–(iii)].
2. Object A (classical  $V(\phi_0)$ ) decouples unconditionally from local emergent gravitational dynamics [Theorem 15.3(iv)].
3. Under condition  $H_\Lambda$ , Object B (zero-derivative loop contribution) likewise decouples [Theorem 15.3(v)]; if  $H_\Lambda$  fails, the UV sensitivity is transferred to the scalar sector as a naturalness problem distinct from the cosmological constant problem.
4. The standard direct UV-vacuum-to- $\Lambda$  channel of GR-coupled QFT is therefore blocked in the leading ordered-branch sector, conditionally on  $H_\Lambda$  for Object B and unconditionally for Object A.
5. Weinberg’s no-go theorem [90] does not apply in its standard form to ECT, because ECT does not satisfy its framework assumptions; therefore that theorem does not directly exclude an ECT-based resolution.

#### Level B (strong, but subject to verification).

6. The structural analogy of ECT leading-sector dynamics with unimodular gravity is tight, but the quantum non-renormalization theorems of Ng–van Dam and Smolin [96, 97] have not been formally transferred to the emergent setting.
7. Condition  $H_\Lambda$  is expected to hold to leading order in the ECT expansion, but its verification against the full Lagrangian is an open computation (O1).

#### Level C (motivated estimate).

8. The infrared estimate  $\rho_\Lambda^{\text{IR}} \sim c_\Lambda M_{\text{Pl}}^2 H_0^2$  is a motivated scaling consistent with observation at the order-of-magnitude level, with a plausible candidate microphysical realization in the pseudo-Goldstone sector. The coefficient  $c_\Lambda$  is not fixed by the present argument.

**What is and is not claimed.** We claim: (a) the  $10^{120}$  UV-vs-IR catastrophe of the standard framework is structurally resolved at Level A in the leading ordered-branch sector of ECT, in the sense that the classical vacuum baseline  $V(\phi_0)$  does not gravitate (Theorem 15.3(iv); rigorous within the ordered-branch ansatz), and, conditional on the single assumption  $H_\Lambda$ , the zero-derivative one-loop vacuum contribution likewise does not gravitate (Theorem 15.3(v)); (b) the classical-level statement is unconditional and does not require any cancellation between unrelated UV and IR quantities; (c) Weinberg’s no-go theorem in its standard form does not apply to ECT; (d) the surviving infrared source parametrises as  $\rho_\Lambda \sim c_\Lambda M_{\text{Pl}}^2 H_0^2$ , matching observation at the order-of-magnitude level; (e) a plausible microphysical realisation of the infrared scaling is the pseudo-Goldstone sector of the  $O(4) \rightarrow O(3)$  breaking.

We do not claim: (a) a first-principles derivation of the numerical coefficient  $c_\Lambda$ , or equivalently of the observed numerical value  $\rho_{\Lambda, \text{obs}}$  – this is a separate Level C determination problem listed as O2; (b) that condition  $H_\Lambda$  has been verified against the full ECT Lagrangian beyond the leading ordered-branch ansatz – this is O1; (c) that the Ng–van Dam non-renormalization theorem has been formally transferred to the emergent setting – this is O3; (d) that the pseudo-Goldstone realisation of Sec. 15.9 is established as the cosmological source; it is a plausible candidate only.



**Structural separation of two distinct questions.** We emphasise that the classical “cosmological constant problem” of the standard framework – the catastrophic  $10^{120}$  mismatch between a UV baseline  $\sim M_{\text{Pl}}^4$  and the observed  $\rho_{\Lambda}^{\text{obs}} \sim 10^{-47} \text{ GeV}^4$  – is structurally separated in ECT from the *value* of  $\rho_{\Lambda, \text{obs}}$  itself. The former is a UV-channel statement about what does *not* gravitate and is at Level A in the leading sector (unconditional for the classical baseline; conditional on  $H_{\Lambda}$  for the zero-derivative loop). The latter is an infrared determination problem for a specific number and is at Level C. Conflating the two – as is often done in the standard literature – underestimates the structural content of the decoupling theorem and overstates the logical scope of the remaining  $O(1)$  coefficient question.

## 15.12 Open problems

We list the technical questions whose resolution is required to elevate the Level B and Level C results to Level A. These constitute the reformulated OP- $\Lambda$ 3 programme.

- O1.** *Verification of  $H_{\Lambda}$  in the full quadratic operator.* Expand the fundamental ECT Lagrangian around the ordered branch and identify the full structure of the quadratic fluctuation operator. Determine whether any field-dependent prefactor  $Z(\phi)$  or mixing-induced effective prefactor modifies  $K^{AB}$  in the zero-derivative sector. If  $H_{\Lambda}$  holds, Object B decouples exactly; if  $H_{\Lambda}$  fails, classify the residual UV sensitivity as a scalar naturalness problem distinct from the cosmological constant problem.
- O2.** *Explicit FRW-reduced equations of motion for the ordered-branch mode.* Derive the effective equations of motion for  $q(t)$  on an FRW background from the full ECT Lagrangian, identify  $Z_q$  and  $V_{\text{IR}}(q)$  in terms of  $(\mu, \lambda, \alpha, \beta, u_0)$ , and compute the coefficient  $c_{\Lambda}$ .
- O3.** *Formal analogue of Ng–van Dam for emergent unimodular structures.* Establish (or refute) a non-renormalization theorem for  $\Lambda$  in the emergent unimodular-like setting of ECT. This requires a careful treatment of the path-integral measure on the orientation field  $n^A$  and of the admissible variations beyond the classical level.
- O4.** *First-principles derivation of  $m_G \sim H_0$ .* Derive the pseudo-Goldstone mass scale from the explicit symmetry-breaking structure of the ECT Lagrangian, relating it to the parameters  $(\mu, \lambda, \alpha, \beta)$  and to cosmological inputs. This is necessary to upgrade Sec. 15.9 from a consistency check to a prediction.
- O5.** *Beyond leading ansatz.* Extend Theorem 15.3 to higher-order corrections to  $K^{AB}$  of the form  $\beta \delta^{AB} - \alpha n^A n^B + \gamma (\partial n)^2 \delta^{AB} + \dots$ , and assess the size of any induced violation of the fixed-determinant property.

## 15.13 Summary

The classical cosmological constant catastrophe – the  $10^{120}$ -level mismatch between a UV baseline  $\sim M_{\text{Pl}}^4$  and the observed  $\rho_{\Lambda}^{\text{obs}} \sim 10^{-47} \text{ GeV}^4$  in the standard framework – is *resolved at Level A* in the leading ordered-branch sector of ECT. The emergent metric determinant is fixed by the kinematic constraint  $n^A n_A = 1$  to  $\sqrt{-g_{\text{eff}}} = \beta^2/c_*$ , and the classical baseline  $V(\phi_0)$  does not source the local emergent gravitational dynamics (Theorem 15.3(iv)). Conditional on the single spectral assumption  $H_{\Lambda}$ , the same fixed-determinant structure absorbs the zero-derivative one-loop vacuum contribution (Theorem 15.3(v)). The direct  $10^{120}$ -level cancellation between a UV vacuum baseline and the observed cosmological term is therefore absent in this sector: no cross-scale cancellation between unrelated quantities is invoked at all.

The observed numerical value  $\rho_{\Lambda, \text{obs}}$  is a distinct, infrared determination problem. Its natural parametric scaling  $\rho_{\Lambda} \sim c_{\Lambda} M_{\text{Pl}}^2 H_0^2$  is consistent with observation at the order-of-magnitude level and admits a plausible realization through the pseudo-Goldstone sector, though neither the scaling coefficient nor the realization is established as a derived prediction (Level C). The outstanding technical tasks for this infrared sector –  $H_{\Lambda}$  verification to lift the  $H_{\Lambda}$ -conditional status of Theorem 15.3(v), explicit FRW coefficient computation, and a non-renormalization analogue of Ng–van Dam – are listed as Open Problems O1–O5 and together constitute the reformulated OP- $\Lambda$ 3 programme.

## 16 Cosmology from the Ordered Branch

*Having established the structural resolution of the classical cosmological problems in the preceding section, the present section develops the post-transition cosmology of the ordered branch. It uses the homogeneous FRW background reduction of the  $\phi$ -first closure already derived in §13.5 (Eqs. (13.37)–(13.39)) and inherits the approximation levels 0–1, 3, 5, 8 of the hierarchy established in §11.2. Status: the entire section is Level B unless stated otherwise. The effective potential  $U(\phi)$  remains open (OP3).*

**What is established, what is benchmarked, and what remains open.** At the present stage, the ordered-branch cosmology supports three different levels of statement. First, there are *structural* consequences of the homogeneous  $\phi$ -branch closure, such as the existence of a dark-energy-like amplitude sector, the no-phantom inequality within the adopted positive-kinetic closure, and the sign-level route by which a high-redshift enhancement of  $G_{\text{eff}}$  can shift the CMB-inferred late-time Hubble scale upward. Second, there are *benchmark* results obtained within specific late-time truncations, such as the representative  $w(z)$  curves, the magnitude of the Hubble-shift effect, and the illustrative JWST age-budget enhancement. Third, there remain genuinely *open* cosmological targets: the perturbation spectrum  $(A_s, n_s, r)$ , a first-principles present-day value of  $w_0$ , and a full global data fit of the background and perturbation sectors within a single ECT closure.

### 16.1 Homogeneous FLRW branch and late-time evolution

*Status: Level B. The FRW reduction follows from the macroscopic closure of §13.5; specific closure functions remain open (OP3). The no-phantom result  $w \geq -1$  is Level B structural (conditional on  $\omega(\phi) > 0$  in the adopted closure).*

#### Bridge from the gravitational sector

The full background equations governing the homogeneous ordered branch are already derived in §13.5 (Eqs. (13.37)–(13.39)) as the isotropic background reduction of the  $\phi$ -first closure. The present subsection analyses their physical content: late-time dark-energy behaviour, the evolution of the effective gravitational coupling, and the resulting observational constraints. The detailed late-time benchmark closure apparatus is recorded in Appendix AD. In what follows, it is important to distinguish between structural properties of the homogeneous branch (such as the existence of a dark-energy-like amplitude sector and the no-phantom bound within the closure) and particular background parameterisations used for illustration or data contact. An inflation-like effective description of the ordering transition, if retained, is discussed in §14.1–14.3.

#### Screened FLRW limit

In the screened/frozen limit  $\phi \rightarrow 0$ ,  $\dot{\phi} \rightarrow 0$ , the full background system of Eqs. (13.37)–(13.39) reduces to the standard Einstein–Friedmann form with an effective vacuum contribution determined by the frozen amplitude sector. This serves as a consistency check: the  $\phi$ -first closure recovers the  $\Lambda$ CDM background structure in the screened limit.

#### Dark energy as residual amplitude-sector vacuum energy

When  $\phi$  is slowly evolving rather than frozen, the amplitude sector contributes both kinetic and potential energy to the cosmological background. The effective energy density and pressure of the  $\phi$ -sector are:

$$\rho_\phi = \frac{1}{2}\omega(\phi)\dot{\phi}^2 + U(\phi), \quad p_\phi = \frac{1}{2}\omega(\phi)\dot{\phi}^2 - U(\phi), \quad (16.1)$$

so the effective equation of state is

$$w_\phi = \frac{p_\phi}{\rho_\phi} = \frac{\frac{1}{2}\omega\dot{\phi}^2 - U}{\frac{1}{2}\omega\dot{\phi}^2 + U}. \quad (16.2)$$

The effective potential  $U(\phi)$  generically has a residual nonzero value at  $\phi = 0$ , giving the dark-energy contribution to the background Friedmann system (§13.5).

**Corollary (no-phantom bound in the  $\phi$ -first closure; see also Appendix AF for the self-contained statement).** If  $\omega(\phi) > 0$ , then the homogeneous amplitude-sector equation of state satisfies  $w_\phi \geq -1$ , with equality only in the frozen limit  $\dot{\phi} = 0$ .

*Proof.* Since  $\omega(\phi) > 0$  and  $\dot{\phi}^2 \geq 0$ , the kinetic contribution  $K \equiv \frac{1}{2}\omega(\phi)\dot{\phi}^2 \geq 0$ . Therefore  $w_\phi = (K - U)/(K + U) \geq -1$ , with equality iff  $K = 0$ .  $\square$

This is a Level B structural consequence of the adopted  $\phi$ -first closure and of the positivity of the kinetic coefficient. It should not be confused with a fully model-independent prediction of all possible nonlinear completions of ECT.

**Interpretive consequence.** Within the present  $\phi$ -first closure, late-time acceleration is therefore structurally quintessence-like rather than phantom-like: the ordered branch can approach  $w = -1$  from above, but it does not cross into  $w < -1$  unless the adopted positive-kinetic closure itself is abandoned. This is a closure-level structural statement, not yet a theorem of all possible nonlinear ECT completions.

This makes quintessence-like late-time behaviour structurally natural in the present closure, while leaving the precise present-day value of  $w_0$  to the explicit background solution. Current late-time cosmological data are compatible with a mildly quintessence-like branch, although no unique ECT fit is claimed here.

In terms of the kinetic-to-potential ratio:

$$w_0 = -1 + \frac{2\rho_{\text{kin}}}{3\rho_{\text{cond}}}, \quad \rho_{\text{kin}} \equiv \frac{1}{2}\omega\dot{\phi}^2, \quad \rho_{\text{cond}} \equiv U(\phi). \quad (16.3)$$

This parametrisation is most useful in the late-time kinetic-subdominant regime  $\rho_{\text{kin}} \ll \rho_{\text{cond}}$ . The ratio  $\rho_{\text{kin}}/\rho_{\text{cond}}$  is not yet derived from bare ECT postulates; no specific numerical value of  $w_0$  can be claimed without a solved background history (Level B/Open).

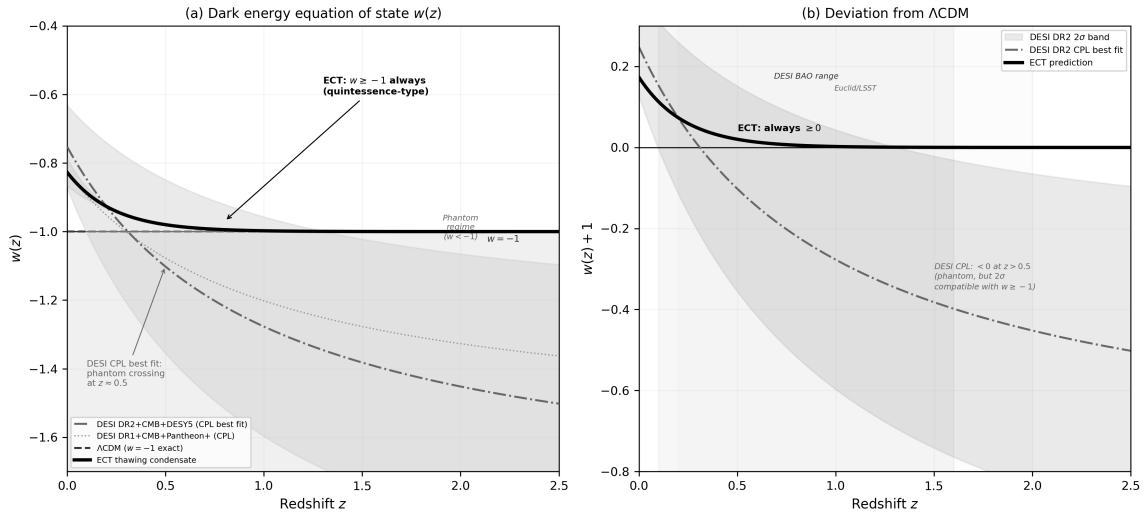


**Figure 10:** Representative late-time ordered-branch benchmark for  $w(z)$  compared with  $\Lambda$ CDM and recent dark-energy trend analyses. **(a)** Within the adopted positive-kinetic  $\phi$ -first closure, the effective equation of state satisfies  $w(z) \geq -1$  at all redshifts. **(b)** Representative deviation from  $\Lambda$ CDM. The curve is benchmark-level and closure-dependent: it should be read as one admissible ECT late-time branch, not as a first-principles unique prediction of the full theory.

## Evolution of the effective gravitational coupling

A slowly evolving order field produces a redshift-dependent effective coupling:

$$G_{\text{eff}}(z) = G_N e^{-\beta\phi_b(z)}, \quad (16.4)$$

where  $\phi_b(z)$  is the slowly evolving cosmological background of the order field. This expression should be read as the background realisation of the effective coupling within the present  $\phi$ -first closure, rather than as a unique theorem-level cosmological law of the full ECT framework. If  $\phi_b$  varies monotonically with epoch, the effective gravitational strength at recombination differs from its late-time value, providing a possible structural route to partial Hubble-tension alleviation within the present closure (Level B). The sign and order of magnitude of the effect follow from  $\phi$ -first logic; a numerical value would require a solved background history  $\phi_b(z)$ , which is not yet available.

**BBN consistency constraint.** Any background realisation in which  $G_{\text{eff}}(z)$  evolves significantly at very high redshift is constrained by primordial nucleosynthesis. Accordingly, a naive continuation of a late-time running ansatz to arbitrarily large  $z$  should not be taken literally. Within ECT this is naturally interpreted as a saturation requirement: once the ordered branch has stabilised sufficiently early, the background  $\phi_b(z)$  must become nearly constant over the BBN era. Thus BBN does not falsify the mechanism itself, but constrains the allowed high-redshift completion of the background ansatz. In particular, any late-time illustrative parametrisation should be understood as local in redshift and not extrapolated unchanged to the entire pre-BBN regime.

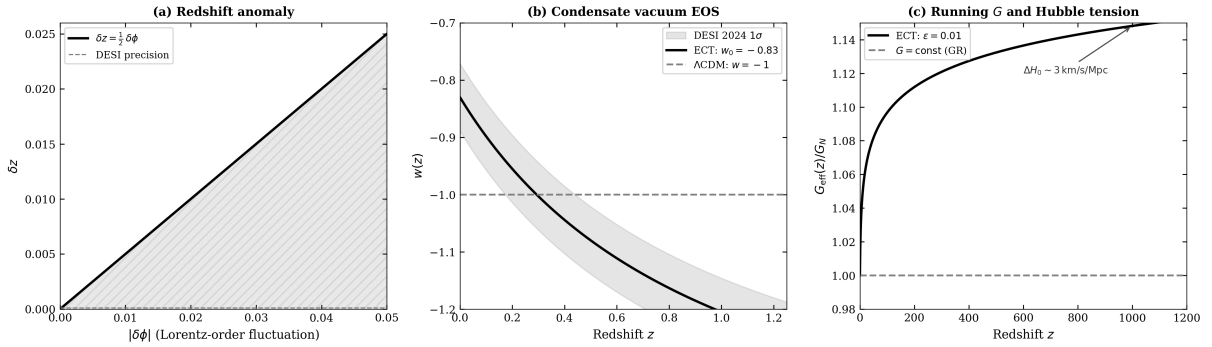


**Figure 11:** Illustrative cosmological observables in the current ECT closure. (a) Illustrative redshift-side consequence of a slowly varying condensate background. (b)  $w(z)$  showing the non-phantom structure  $w_0 > -1$ . (c) Running  $G_{\text{eff}}(z)/G_N$  for an illustrative  $\phi_b(z)$ . These are closure-dependent consequences of the  $\phi$ -first cosmological closure, not first-principles derivations from bare P3.

## What is established and what remains open

*Level B structural:* (i) the FRW background reduction of the  $\phi$ -first closure is well-defined and recovers  $\Lambda$ CDM in the screened limit; (ii) the no-phantom constraint  $w \geq -1$  holds whenever  $\omega(\phi) > 0$ ; (iii) a slowly evolving  $G_{\text{eff}}(z)$  provides a structural route to Hubble-tension alleviation.

*Open:* (i) explicit form of  $U(\phi)$  and  $\omega(\phi)$  from bare P3 (OP3); (ii) a solved self-consistent background  $\phi_b(z)$  with early-time saturation compatible with BBN; (iii) quantitative MCMC fit to CMB+BAO+SN data. The illustrative curves shown in Fig. 11 should therefore be read only as closure-level visualisations of the allowed qualitative behaviour.

## 16.2 Cosmological evolution of the condensate amplitude

*Status: Level B.* The qualitative evolution picture follows from the  $\phi$ -first closure; quantitative trajectory  $\phi_b(z)$  requires an explicit solution of the background system (Eqs. (13.37)–(13.39)), which is open (OP3).

*The derived condensate amplitude dynamics and the benchmark late-time closure are recorded in Appendix AD, §AD.1.*

**Qualitative picture.** The condensate amplitude variable  $\phi = \frac{1}{\beta} \ln(u/u_\infty)$  (§13.5) encodes how strongly the local condensate ordering deviates from its asymptotic screened value. Its cosmological evolution  $\phi_b(z)$  is governed by the scalar background equation (13.39) coupled to the Friedmann system (13.37)–(13.38). The qualitative evolution proceeds through three regimes:

(i) *Ordering stage.* Immediately after the  $O(4) \rightarrow O(3)$  transition, the condensate amplitude grows from zero toward its asymptotic value  $u_\infty$ . In the  $\phi$ -variable this corresponds to  $\phi$  evolving from large negative values toward zero. The detailed dynamics of this stage depend on the shape of the effective potential  $U(\phi)$  and remain open (OP3).

(ii) *Stabilisation.* At sufficiently early times (well before BBN), the amplitude variable must approach an approximately constant value:  $\phi_b(z) \rightarrow \text{const}$  for  $z \gg z_{\text{eq}}$ . This saturation is required by BBN consistency (§16.1) and is physically natural: the ordered branch stabilises once the condensate has settled into the vicinity of the potential minimum.

(iii) *Late-time slow drift.* At late cosmological times,  $\phi_b$  may evolve slowly, producing the running gravitational coupling  $G_{\text{eff}}(z) = G_N e^{-\beta\phi_b(z)}$  and the non-phantom dark-energy contribution discussed in §16.1. The rate of this drift determines the magnitude of the Hubble-tension alleviation (§16.5) and the JWST early-galaxy enhancement (§16.5).

The figures below should be read as closure-level visualisations of the qualitative ordered-branch history, not as outputs of a fully solved background trajectory  $\phi_b(z)$ .

**Far-future evolution.** Within the  $\phi$ -first closure, two structurally distinct asymptotic branches are possible (Level B):

- **Scenario A** ( $\phi_b \rightarrow 0, u \rightarrow u_\infty$ ): the condensate amplitude stabilises permanently;  $G_{\text{eff}} \rightarrow G_N$ ; the Universe enters an asymptotic de Sitter-like phase.
- **Scenario B** ( $\phi_b \rightarrow -\infty, u \rightarrow 0$ ): the ordering relaxes;  $G_{\text{eff}}$  grows; the geometric branch eventually degenerates. The timescale is closure-dependent (OP3).

Current observational data do not yet discriminate between these two late-time scenarios; the key future discriminants are  $|\dot{G}/G|$  (next-generation lunar laser ranging, pulsar timing) and  $w_a$  from future BAO surveys.

**What is established and what remains open.** The qualitative three-stage picture (ordering  $\rightarrow$  stabilisation  $\rightarrow$  slow drift) is a structural consequence of the present  $\phi$ -first closure (Level B), not yet a theorem of all possible nonlinear completions of ECT. What remains open is the explicit solution  $\phi_b(z)$ , which requires knowledge of  $U(\phi)$  and  $\omega(\phi)$  from bare P3 (OP3). The structural derivation of the amplitude dynamics and the benchmark closure are recorded in Appendix AD.

### 16.3 Matter–antimatter asymmetry in the ECT framework

*Status: Level A/B given empirical fermions and P5 (S8). ECT provides a native framework in which the three Sakharov ingredients for baryogenesis can be supplied by ordered-medium mechanisms. This establishes the structural possibility of matter–antimatter asymmetry in the ordered branch, together with a natural generic route to  $\eta_B \neq 0$  under suitable transition conditions. The precise value of  $\eta_B$ , and the full transport/freeze-out analysis required to determine whether the realised asymmetry is nonzero in a specific cosmological history, remain open. Connection: Section 22.3 (defect-mediated topology change), Section 7 ( $\mathcal{L}_5$  coupling), Section 7.2 (gauge structure).*

The observed baryon-to-photon ratio  $\eta_B \equiv (n_B - n_{\bar{B}})/n_\gamma \approx 6 \times 10^{-10}$  means that for every billion particle–antiparticle pairs in the early Universe, approximately one extra baryon survived annihilation. All visible matter—stars, planets, observers—consists of this surviving excess.

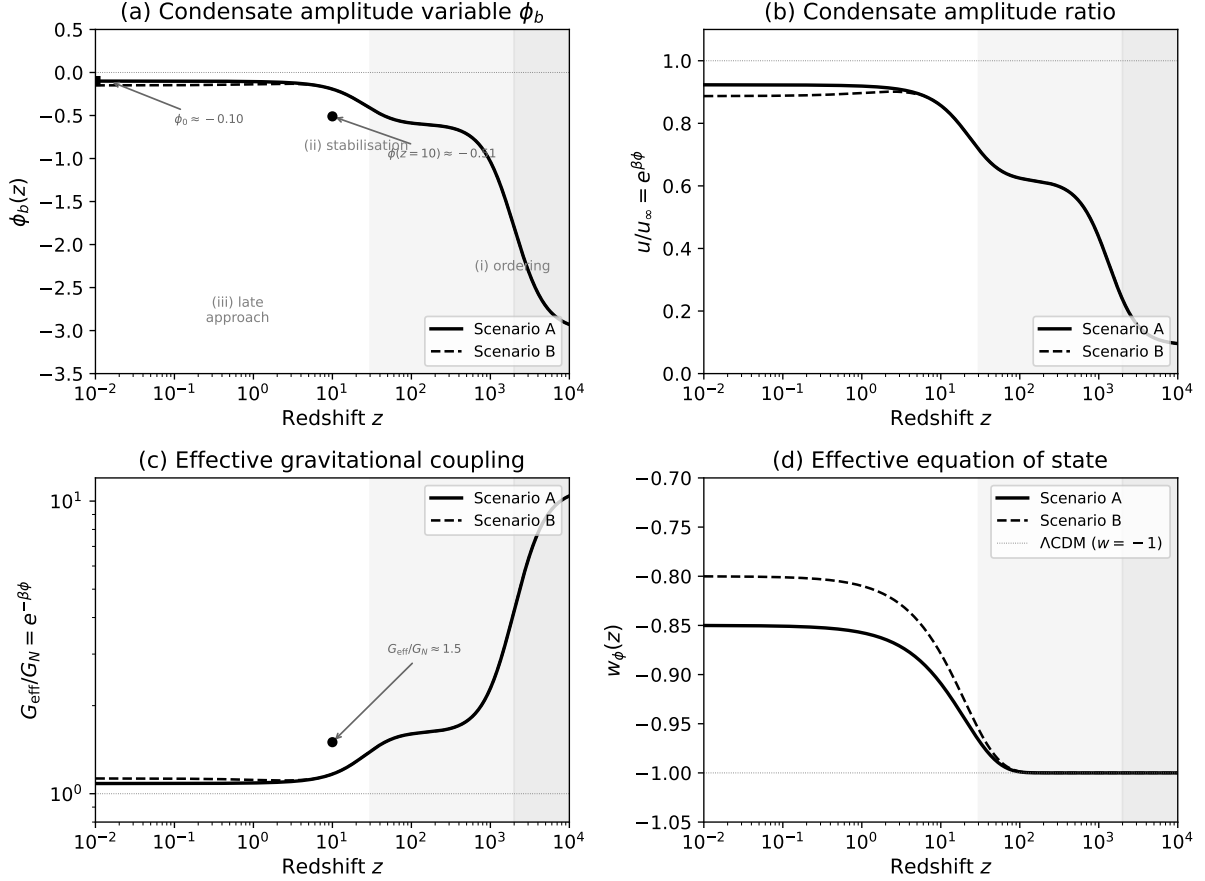


**Figure 12:** Schematic closure-level evolution of the condensate background in the  $\phi$ -first closure and its derived cosmological consequences. **(a)** Condensate amplitude variable  $\phi_b(z)$ : ordering from deep negative values (stage i), stabilisation near  $\phi \approx 0$  (stage ii), and late-time slow drift (stage iii). **(b)** Condensate amplitude ratio  $u/u_\infty = e^{\beta\phi}$ : approaches unity as ordering completes. **(c)** Derived effective gravitational coupling  $G_{\text{eff}}/G_N = e^{-\beta\phi}$ : enhanced at early times, approaches  $G_N$  at late times. **(d)** Derived effective equation of state  $w_\phi(z)$ : frozen near  $-1$  at high  $z$ , mildly quintessence-like at late times; this is a schematic closure-level realisation, not a fitted reconstruction. Solid: Scenario A (stable asymptote); dashed: Scenario B (continued drift). The two scenarios share the same high- $z$  evolution history and diverge only in the late-time asymptotic branch behaviour. Grey shading marks the three qualitative evolution stages (ordering / stabilisation / slow drift). This figure is a schematic closure-level visualisation, not a numerical output of the full background system; the quantitative trajectory  $\phi_b(z)$  requires the explicit solution from Appendix AD.

Any baryogenesis mechanism must satisfy the three Sakharov conditions [99]: (i) baryon number violation, (ii) C and CP violation, and (iii) departure from thermal equilibrium.

In earlier versions of this section, baryon-number violation was imported from Standard Model sphaleron/leptogenesis channels. The development below does not rely exclusively on imported Standard Model channels, but instead formulates an ECT-native structural framework in which the Sakharov ingredients can be supplied by the ordered medium itself.

### ECT-native Sakharov ingredients

#### (i) Baryon number violation: defect-mediated topology change.

The coherent branch of ECT carries topologically conserved winding sectors (Section 22.3). As established there, winding-number conservation holds exactly within the smooth coherent branch (BR1), but can be violated through defect-mediated transitions in which the condensate amplitude vanishes ( $\rho \rightarrow 0$ ) at a localised core.

If baryon number is associated with the relevant emergent gauge-topological sector of the  $SU(2) \times$

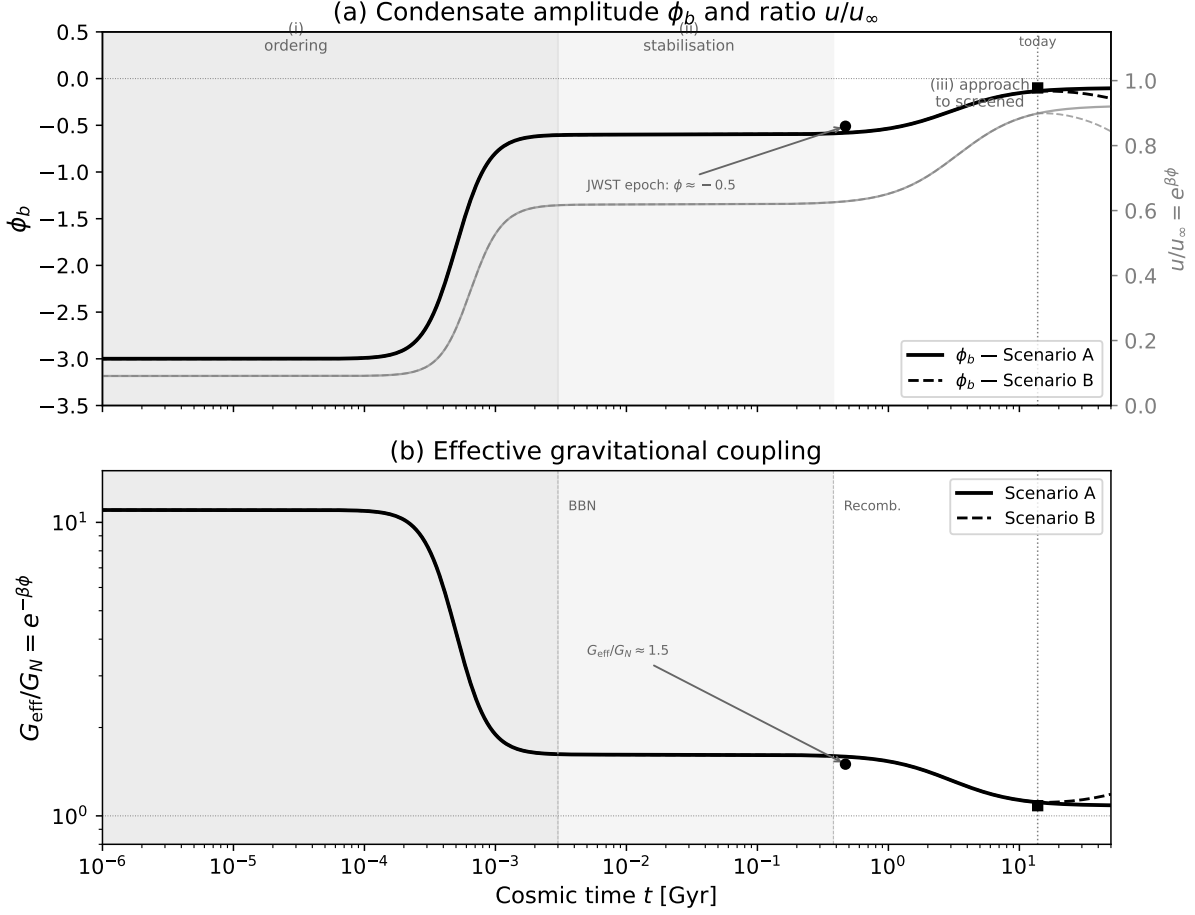


**Figure 13:** Schematic closure-level condensate evolution over cosmic time (Gyr), complementary to the redshift-based Figure 12. **(a)** Condensate amplitude variable  $\phi_b(t)$  (left axis, black) and amplitude ratio  $u/u_\infty = e^{\beta\phi}$  (right axis, grey), showing the three qualitative stages: ordering (dark shading), stabilisation (light shading), and late-time slow drift. **(b)** Effective gravitational coupling  $G_{\text{eff}}/G_N = e^{-\beta\phi}$ , enhanced at early times and approaching  $G_N$  at late times. Solid: Scenario A (stable asymptote); dashed: Scenario B (continued drift). Vertical dotted line marks the present epoch. Key cosmological epochs (BBN, recombination) are indicated. This figure is a schematic closure-level visualisation; the quantitative trajectory requires the explicit background solution from Appendix AD.

$U(1)$  ordered-branch gauge structure (Section 7.2, Section 7.3), then defect-mediated topology changes provide an ECT-native channel for baryon number violation. This channel is:

- *thermally suppressed* at  $T \ll m_\sigma \sim \bar{M}_{\text{Pl}}$ : the defect creation rate scales as  $\Gamma_{\text{defect}} \sim \exp(-E_{\text{defect}}/k_B T)$ , with  $E_{\text{defect}} \sim m_\sigma$  (Eq. (22.22));
- *thermally accessible* at  $T \sim m_\sigma$ : near the condensate scale, defect formation becomes unsuppressed.

This is the ECT structural analogue of instanton and sphaleron processes in gauge field theory, with the crucial difference that the mechanism arises from the condensate topology rather than being imported from the Standard Model gauge sector.

**(ii) CP violation: preferred-direction fermion coupling.**

If fermionic excitations are empirically admitted (phenomenological input, analogous to  $c_* = c$ ), then the unique leading renormalisable coupling of a spinorial excitation to the ordered direction field  $n_A$  is

$$\mathcal{L}_5 = \mu_5 \bar{\Psi} \gamma^A n_A \Psi \quad (16.5)$$

(Level A given empirical fermions: EFT uniqueness theorem; Section 7). This operator supplies the Sakharov condition (ii) in ECT through its discrete-symmetry content. As systematically classified

in Section 9.4,  $\mathcal{L}_5$  is a branch-sensitive, CPT-odd and CP-odd phenomenological operator (C-odd, P-even, T-even, CP-odd, CPT-odd). Combined with complex phases of the fermionic mass matrix (open parameter, OP-Yukawa, Section 9.6), it yields the required CP-asymmetric dynamics. Importantly, the conditional CPT route for reconstructible local sectors identified in Section 9.4 remains intact:  $\mathcal{L}_5$  explicitly lies outside that reconstructible setup as a phenomenological branch extension, so the exact symmetry backbone of the reconstructible sectors is not compromised. The branch-pair architecture of Section 9.4 additionally admits a speculative cosmological interpretation in which our observable matter-dominated branch is paired with an antipodal antimatter-dominated partner, the full Euclidean pair being CPT-symmetric; this is recorded as OP-BRANCH1 rather than as an established result. The complex flavour phases appear explicitly in the flavour-architecture subsection (§9.7), providing the flavour-sector part of the CP-violation bookkeeping. The baryogenesis estimate in the present section remains tied to the leptogenesis-style assumptions stated above and does not claim that the CKM phase alone explains the observed asymmetry. In particular, the present framework does not claim that the observed baryon asymmetry can be generated by the CKM phase alone.

**(iii) Departure from thermal equilibrium: the ordering transition.**

The  $O(4) \rightarrow O(3)$  ordering transition is itself a symmetry-breaking phase transition of the condensate (Level A; follows from P4). Any such transition occurring on a finite timescale provides a natural departure from equilibrium for species whose interaction rates are too slow to track the transition adiabatically. Within the ECT framework, the Universe enters its Lorentzian branch through an ordering event rather than through an already equilibrated primordial plasma. If the transition completes on a timescale  $\tau_{\text{tr}} \sim M_{\text{Pl}}^{-1}$ , then species with  $\Gamma \ll \tau_{\text{tr}}^{-1}$  are automatically driven out of equilibrium.

**ECT-native bias mechanism**

Beyond the structural availability of the three Sakharov ingredients, ECT admits a natural bias mechanism of the spontaneous-baryogenesis type.

During the non-equilibrium ordering epoch, the ordered background is generically time dependent: the preferred direction  $n_A(X)$  and the compact phase  $\theta(X)$  evolve as the transition proceeds. This time dependence generates an effective chemical-potential-like bias:

$$\mu_{\text{eff}} \sim c_\theta \dot{\theta} + c_\Omega \Omega_t + c_5 \mu_5 n_0 + \dots \quad (16.6)$$

where  $\Omega_t$  is a time-dependent scalar built from the angular velocity of the ordered frame, and the coefficients  $c_\theta$ ,  $c_\Omega$ ,  $c_5$  depend on the effective Lagrangian of the coherent branch and on the fermion–condensate coupling structure.

The physical rôle of  $\mu_{\text{eff}}$  is to act as an effective chemical-potential-like bias in the time-dependent ordered background. When baryon-number-violating processes are active, this bias is converted into a net baryon asymmetry. In a hot plasma with small  $\mu_{\text{eff}}/T$ , standard equilibrium thermodynamics gives [103]:

$$n_B - n_{\bar{B}} \propto \mu_{\text{eff}} T^2. \quad (16.7)$$

After freeze-out at temperature  $T_D$ , the asymmetry is frozen:

$$\eta_B \sim C \frac{\mu_{\text{eff}}(T_D)}{T_D}, \quad (16.8)$$

where  $C$  is a model-dependent coefficient of order unity, depending on the number of active degrees of freedom and on transport details.

**When matter–antimatter asymmetry arises and when it does not**

ECT does not predict that  $\eta_B \neq 0$  arises in every logically possible transition history. Rather, it establishes a native framework in which a nonzero matter–antimatter asymmetry can arise, and in which such an outcome is naturally expected whenever the transition history supplies a nonzero bias, an active baryon-violating channel, and incomplete washout.



**Conditions under which  $\eta_B \neq 0$  (generic).** A nonzero matter–antimatter asymmetry arises when the following conditions are simultaneously satisfied:

- (a) The ordering transition is *inhomogeneous or time-dependent*, so that  $\mu_{\text{eff}} \neq 0$ . This is the physically expected situation for any real phase transition of finite duration.
- (b) The fermion–condensate coupling  $\mu_5 \neq 0$ . This is the generic case:  $\mu_5 = 0$  is a symmetry-enhanced special case rather than the generic expectation of the effective coupling structure.
- (c) *B-violating transitions are active* during the epoch when the bias is nonzero. At temperatures  $T \sim m_\sigma \sim \tilde{M}_{\text{Pl}}$ , this is naturally satisfied.
- (d) *Freeze-out occurs before complete washout*: the B-violating rate drops below the expansion rate while  $\eta_B \neq 0$ .

**Conditions under which  $\eta_B = 0$  (exceptional cases).** The asymmetry vanishes if any of the following exceptional conditions holds:

- (i) **Exactly homogeneous transition:** the ordering history is sufficiently symmetric that no effective bias  $\mu_{\text{eff}}$  is generated.
- (ii) **Vanishing effective CP-bias source:** the relevant effective couplings are such that the ordered background induces no net CP-asymmetric bias.
- (iii) **Exact dynamical cancellation:** the bias changes sign during the transition in such a way that the integrated asymmetry source cancels.
- (iv) **Complete washout:** baryon-number-violating processes remain active long enough after the bias epoch to erase the produced asymmetry.

These cases are structurally possible, but they require a more symmetric or more finely balanced transition history than the generic ordered-medium expectation. A nonzero  $\eta_B$  is thus the natural generic route provided by the ECT baryogenesis framework once the required bias and baryon-violating channel are simultaneously active, although its realised value depends on transport, freeze-out, and washout dynamics.

### Comparison with the Standard Model

In the Standard Model, electroweak baryogenesis fails at observed parameters because the electroweak phase transition is a crossover rather than a strongly first-order transition. Additional beyond-minimal ingredients are therefore required for successful electroweak baryogenesis at the observed parameters.

In ECT, the ordering transition  $O(4) \rightarrow O(3)$  is a genuine symmetry-breaking phase transition at the Planck scale, where the ECT framework can supply all three Sakharov ingredients by native ordered-medium mechanisms. The ECT framework therefore provides a structural setting for baryogenesis that does not have to be introduced as an external add-on to the ordered-medium theory itself. Whether this setting quantitatively reproduces the observed baryon asymmetry without additional beyond-minimal ingredients remains an open question.

### Imported leptogenesis benchmark (Level B)

For completeness, the previous version of this section used a resonant leptogenesis closure with  $M_R \sim 10^9 \text{ GeV}$ , wash-out factor  $\kappa \sim 0.1\text{--}1$ , and CP-asymmetry  $\varepsilon \sim 10^{-6}$ , yielding  $\eta_B \sim 9 \times 10^{-10}$  at the benchmark level. This benchmark is not an ECT prediction but an imported consistency check showing that a Sakharov-type mechanism, if realised, can produce the right order of magnitude. It remains available as a Level B comparison but does not replace the ECT-native framework developed above.

### Status summary.

- **Level A:** the  $O(4) \rightarrow O(3)$  ordering transition provides departure from equilibrium; defect-mediated topology change provides a structural channel for topological-sector transitions.
- **Level A/B:** if baryon number is associated with the relevant gauge-topological sector, defect-mediated transitions provide a baryon-number-violating channel.
- **Level A given Ph:** the unique leading fermion–condensate coupling  $\mathcal{L}_5$  provides a CP-bias candidate (given that fermionic excitations are empirically observed).
- **Level A/B given Ph:** ECT contains a native baryogenesis framework in which all three Sakharov ingredients are structurally available. Under suitable transition conditions (nonzero effective bias, active baryon-violating channel, and incomplete washout), the framework naturally produces a route to  $\eta_B \neq 0$ .
- **Open:** the explicit calculation of  $\eta_B$  from condensate parameters, including the transport equation, the freeze-out dynamics, and the washout analysis; the precise identification of baryon number with a specific gauge-topological sector of the ordered branch.

## 16.4 Universe age and cosmological time budgets in ECT

*Status: Level B. The conceptual reinterpretation of cosmic age is structural; concrete numerical values are closure-dependent.*

The condensate background evolution discussed in §16.2, together with the homogeneous background equations of §16.1, determines the timing structure of the Lorentzian ordered branch. The present subsection therefore asks two related questions: how cosmic age should be defined in ECT, and which age and distance quantities are relevant for later late-time observables such as the Hubble shift and the JWST early-galaxy problem.

**Conceptual meaning of age in ECT.** In  $\Lambda$ CDM the age of the Universe is measured from the Lorentzian Big-Bang singularity. In ECT, by contrast, the singular beginning is replaced by a pre-ordered / pre-Lorentzian regime (§14.1). Accordingly, the quantity  $t_0^{\text{ECT}}$  should be interpreted as the duration of the Lorentzian ordered branch, measured from the ordering transition onward. It is therefore not conceptually identical to the standard  $\Lambda$ CDM age parameter, even when the two are numerically close: the two quantities refer to different notions of cosmic origin and to different starting points of the Lorentzian history.

**Age integral.** The Lorentzian branch age is

$$t_0 = \int_0^\infty \frac{dz}{(1+z)H(z)}, \quad (16.9)$$

where  $H(z)$  is determined by the background system already derived in Eqs. (13.37)–(13.39) together with the condensate evolution of §16.2. In ECT this integral computes the duration of the Lorentzian ordered branch, once the corresponding background history has been fixed. No independent phenomenological Hubble ansatz is introduced here.

**Age and distance quantities derived from the same background.** The same background history  $H(z)$  determines not only the present age, but also the luminosity distance, the lookback time, the age of the Universe at a given redshift, and the available lifetime of a galaxy between formation and observation:

$$D_L(z) = (1+z)c_* \int_0^z \frac{dz'}{H(z')}, \quad t_{\text{lookback}}(z) = \int_0^z \frac{dz'}{(1+z')H(z')}, \quad (16.10)$$

$$t_U(z) = \int_z^\infty \frac{dz'}{(1+z')H(z')}, \quad t_{\text{gal}}(z_{\text{obs}}; z_{\text{form}}) = t_U(z_{\text{obs}}) - t_U(z_{\text{form}}). \quad (16.11)$$

Here  $t_U(z)$  is the age of the Lorentzian branch at the epoch of observation, while  $t_{\text{gal}}(z_{\text{obs}}; z_{\text{form}})$  is the available lifetime of a galaxy observed at  $z_{\text{obs}}$  if it formed at  $z_{\text{form}}$ . These quantities are not independent: they are all controlled by the same ordered-branch background  $H(z)$ .

**Monotonicity observation.** For two background histories compared over the same redshift interval, the age integral immediately implies that the branch with larger  $H(z)$  on that interval yields a shorter Lorentzian age contribution on that interval. Thus, if a given ECT closure yields a larger Hubble rate than the  $\Lambda$ CDM benchmark over part of cosmic history, then the corresponding Lorentzian branch age is reduced relative to that benchmark over the same regime. This is a mathematical consequence of the age integral within a fixed background comparison, not yet a standalone theorem about all possible ECT completions.

**Leading closure-level background effects.** The age of the homogeneous branch is influenced, in the present  $\phi$ -first closure, by two leading background ingredients: the evolution of the effective gravitational coupling as realised in the closure,

$$G_{\text{eff}}(z) \approx G_N e^{-\beta \phi_b(z)},$$

and the non-phantom amplitude-sector dark-energy component ( $w \geq -1$ , Corollary, §16.1). It is therefore important to distinguish between the structural statement that the Lorentzian branch age is defined by the ordered background history, and any concrete numerical estimate, which depends on the chosen closure-level background  $\phi_b(z)$ .

**Illustrative age estimates.** Illustrative late-time background realisations in the present closure give Lorentzian branch ages

$$t_0^{\text{ECT}} \text{ of order } 13\text{--}14 \text{ Gyr}, \quad (16.12)$$

depending on the chosen closure-level parameters and on the specific  $H_0$ -mapping used. These values should be read as illustrative closure-level outcomes, not as zero-parameter predictions of ECT.

**Retained-band bridge and age as a viability discriminator.** Within the uniform- $\varepsilon$  diagnostic layer used in §16.5, the retained five-probe band admits a mapping-dependent discussion of the corresponding Lorentzian branch age. Under the baseline- $H_0$  mapping the branch age is of order 13.5 Gyr; under the alternative inferred- $H_0$  mapping it is of order 12.5 Gyr. The distinction between these two readings is a mapping ambiguity within the diagnostic effective layer, not a separate retained extraction channel. It nevertheless provides an important *viability discriminator*: improved independent age constraints — such as high-precision globular-cluster ages, old-white-dwarf cooling sequences, and nuclear cosmochronology — may help determine which mapping is physically correct. The precise technical values and their scope of validity are recorded in Appendix AH (AF.4).

Any such numerical estimate remains provisional until the high-redshift completion of the background  $\phi_b(z)$  is derived self-consistently. In particular, late-time parametrisations must not be extrapolated unchanged into the entire pre-BBN regime (§16.1).

**Observational context.** The standard  $\Lambda$ CDM age inferred from CMB-calibrated background fits is close to 13.8 Gyr. Independent astrophysical lower bounds from old stellar populations (globular clusters, white-dwarf cooling, nucleo-cosmochronology) remain below that value. An illustrative ECT age in the range above is therefore not in conflict with existing lower bounds. What differs conceptually is not only the number itself, but the meaning of the quantity: in ECT it measures the age of the Lorentzian ordered branch rather than the duration since a fundamental singular beginning.

The detailed age budget relevant for specific early galaxies is encoded not only in  $t_0$  and  $t_U(z)$ , but in the galaxy-lifetime quantity  $t_{\text{gal}}(z_{\text{obs}}; z_{\text{form}})$  defined above. Its role in the JWST discussion is taken up in §16.5.

**Correlated age–distance observables.** The age of the Lorentzian branch, the luminosity distance, the Hubble shift, and the available formation time for early galaxies are all correlated in ECT, because they are determined by the same background history  $H(z)$ . This is one of the characteristic structural features of the ordered branch: age, distance, and growth proxies are not independent sectors, but different projections of the same condensate background.

**What is established and what remains open.** At the structural level, ECT changes the meaning of cosmic age: the relevant quantity is the duration of the Lorentzian ordered branch, not the elapsed time since a fundamental singularity. The same ordered-branch background determines not only  $t_0$ , but also  $t_U(z)$ ,  $t_{\text{gal}}(z_{\text{obs}}; z_{\text{form}})$ , and  $D_L(z)$ . This is the basis of the correlated Hubble- and JWST-sector effects discussed in the following subsections. The sign of any age correction relative to  $\Lambda$ CDM is fixed by the background Hubble history through the age integral. What remains open is the fully derived function  $\phi_b(z)$ , the self-consistent high-redshift completion of the background ansatz, and a full cosmological fit of the resulting age and distance observables to the data. The numerical values quoted above should therefore be treated only as illustrative closure-level outcomes, not as fully fitted ECT age determinations.

**Role of the full nonlinear field equations.** The age and lookback-time budgets computed above are controlled by the same background  $H(z)$  that governs the Hubble-shift mechanism. In the homogeneous FRW reduction the orientation stress  $\Theta_{\mu\nu}[n]$  does not contribute a separately extractable background term (Appendix AU.7). The present age estimates therefore already contain the dominant ordered-branch effect; any additional orientation-stress contribution is not independently identifiable at the current closure level.

## 16.5 Cosmological constraints on the effective drift parameter

The previous part of Chapter 15 examined the separate cosmological sectors — flatness, horizon and monopole problems, age and lookback integrals, structure-formation phenomenology — within the ordered-branch  $\phi$ -closure of ECT. The present section addresses a different kind of question. In the standard phenomenological treatment of late-time cosmological anomalies, each tension typically receives its own parameterisation: a pre-recombination component for the Hubble discrepancy, a modified gravity law for the late-time growth sector, an abundance enhancement factor for the high- $z$  galaxy counts. ECT offers a structurally different path. A single effective deformation parameter,  $\varepsilon$ , motivated by the three-stage condensate-closure picture and tested here at the effective level, parametrizes the common late-time gravitational response function  $G_{\text{eff}}(z)$  used across the cosmological channels considered below. The section therefore asks whether a single value of  $\varepsilon$  — or more precisely, a single narrow range — is compatible with a set of observationally distinct channels probing that response.

If five channels of qualitatively different physics (a CMB-era distance-ratio proxy, a high- $z$  structure-formation anomaly, direct late-time Hubble-rate measurements, late-time growth likelihoods, and late-time potential-evolution signals), when analysed separately within the same effective framework, admit the same narrow  $\varepsilon$ -interval, then that interval is not a fit of a parameter to one phenomenon: it is the intersection of five observationally distinct empirical constraints with different kernels and different dominant systematics bearing on one common quantity. A non-trivial intersection of this kind is a genuine indirect consistency check of the framework. If the five channels had disagreed — for example, if any one of them had required a negative  $\varepsilon$  that the others excluded — then the single-parameter description would have failed in a clean, falsifiable way. Conversely, a narrow joint band with five channels of different kernels and systematics constitutes the strongest indirect consistency check available at this methodological level that a single underlying mechanism may be at work.

Throughout §15.5  $\varepsilon$  is treated as an effective diagnostic parameter rather than as a first-principles constant of ECT. The retained-five-probe joint band reported in §16.5 is an empirical result under the stated methodology, not a measurement of a fundamental theoretical quantity and not a global statistical combination of independent likelihoods. A first-principles closure-level derivation of the full epoch-dependent function  $\varepsilon(z)$  predicted by three-stage condensate closure, together with its mapping to the effective uniform- $\varepsilon$  layer used here, remains open. The question pursued in §15.5 is therefore not whether ECT predicts a rigorously constant cosmological drift parameter at first principles, but whether a common effective  $\varepsilon$ -range can account for several observationally distinct channels within one diagnostic layer. In this sense the retained band is compatible with  $\varepsilon$  being a true constant; it is equally compatible with a slow-varying  $\varepsilon(z)$  averaged over the kernel of each probe. Distinguishing these two possibilities belongs to the closure-level extension.

The section is organised as follows. §16.5 fixes the structural meaning of  $\varepsilon$  within ECT and states the effective uniform- $\varepsilon$  ansatz. §16.5 specifies the retained five probes, what each of them actually constrains, and introduces the two-sided vs one-sided-upper-bound distinction. §16.5 reports the joint effective allowed band and fixes the working benchmark. §16.5 discusses the channels not retained, in three structurally distinct categories, together with the reasons for their exclusion. §16.5 places the result in the context of alternative proposals for the same observational pattern. §16.5 states what the analysis establishes and what it does not, logs the first-principles open problem **OP-Hubble-derive**, and outlines directions of future work. The six subsections above give the synthesis and the cross-probe reading; the detailed per-probe derivations, extraction logic, uncertainty budgets, and the construction of each one-dimensional  $\varepsilon$ -interval are now provided in Appendix AG through Appendix AH, which collectively expose the common background module, the per-channel extraction pipelines, and the cross-channel methodology (including the age-viability note of AF.4 and the benchmark achievability statement of AF.5). Channels not retained in the joint band are still discussed explicitly in §16.5, together with the reasons why they are methodologically limited, structurally outside the present  $\varepsilon$ -sector, or not independent enough to serve as primary constraints.

### 15.5.1 Structural definition of the effective deformation parameter

This subsection does not re-derive the drift sector from first principles. It fixes the meaning of the deformation parameter used in the cosmological analysis that follows and recalls the earlier structural motivation already established elsewhere in the preprint. Throughout §15.5,  $\varepsilon$  denotes the effective uniform- $\varepsilon$  parameter of the present analysis, not a first-principles constant of ECT. It is used as a common diagnostic layer in which several cosmological probes can be compared and translated into effective  $\varepsilon$ -ranges.

**Operational starting point.** The robust object is the normalized late-time gravitational response function,

$$\mu(a) \equiv \frac{G_{\text{eff}}(a)}{G_{\text{eff}}(1)}, \quad \varepsilon_{\text{eff}}(a) \equiv -\frac{1}{2} \frac{d \ln \mu}{d \ln a}. \quad (16.13)$$

This definition does not yet assume that the drift sector is exactly described by a single constant.

**Adopted effective ansatz.** For the present retained-probe analysis we adopt the simplest one-parameter effective form. Its use here is motivated by the earlier ordered-branch response analysis in the preprint, where the effective gravitational response is tied to the condensate amplitude in the gravity-sector matching discussion (see §5.1). In the present cosmological layer, the uniform- $\varepsilon$  ansatz is obtained by adopting an effective slow-drift parameterization for that amplitude,  $u_0(a) \propto a^\varepsilon$ , which yields

$$\mu(a) = a^{-2\varepsilon}, \quad \text{equivalently} \quad G_{\text{eff}}(z) = G_N (1+z)^{2\varepsilon}, \quad (16.14)$$

to be understood as a diagnostic effective layer.

This step is part of the effective uniform- $\varepsilon$  parameterization used in §15.5, not a first-principles derivation of the full closure-level drift dynamics. Any numerical interval quoted later in §15.5 is accordingly to be read as an effective band under the retained five-probe uniform- $\varepsilon$  analysis, not as a first-principles prediction of ECT.

**Physical prior.** In the effective uniform- $\varepsilon$  parameterization used here, the intended three-stage ordered-branch relaxation picture of ECT motivates and, within the present diagnostic layer, requires the prior

$$\varepsilon \geq 0. \quad (16.15)$$

Operationally, this is the statement that the cosmological response relaxes toward the present branch rather than drifting away from it.

**Operational consequence.** A cosmological channel whose fitted  $1\sigma$  support lies entirely at  $\varepsilon < 0$  is not retained as a headline  $\varepsilon$ -probe in the present effective analysis. Within the uniform- $\varepsilon$  layer adopted here, such a result is interpreted either as evidence that the channel is probing physics outside the present  $\varepsilon$ -sector or as evidence that the simplified extraction pipeline is inadequate for that channel. The classification of such cases is given in §15.5.4.

**Methodological status.** The parameter  $\varepsilon$  is treated throughout §15.5 at Level B: empirically constrained under the retained five-probe set, the uniform- $\varepsilon$  ansatz, and the present analysis pipeline, with the  $\Lambda$ CDM-background proxy for the remaining cosmological parameters. No Level A claim is made. In particular, §15.5 does not establish that a single constant  $\varepsilon$  is the final physical description of the ECT drift sector. The ECT-native target remains a closure-derived epoch-dependent quantity  $\varepsilon(z)$ , logged as open problem OP-Hubble-derive (§15.5.6).

**Bridge.** With this effective definition fixed, the next subsection identifies the retained probe set and explains what each probe actually constrains within the present methodology.

### 15.5.2 Retained five-probe effective analysis

With the effective meaning of  $\varepsilon$  fixed in §16.5, we now specify which cosmological probes are retained for the present uniform- $\varepsilon$  analysis, what each of them actually constrains, and how their resulting effective intervals are to be interpreted.

**Retention criterion.** A probe is retained in §15.5 only if it constrains the present effective  $\varepsilon$ -sector rather than a distinct physical sector, and if its extraction pipeline is sufficiently explicit that an effective interval can be stated without importing an uncontrolled external likelihood. Five probes satisfy this criterion under the uniform- $\varepsilon$  ansatz and the  $\Lambda$ CDM-background proxy ( $\Omega_m = 0.315$ ,  $\Omega_\Lambda = 0.685$ ); all other probes considered in the present analysis are discussed in §15.5.4.

**Two-sided vs upper-bound distinction.** Within the retained five-probe set, Hubble+ $r_s$  and the JWST early-galaxy excess provide two-sided effective extraction intervals, whereas cosmic chronometers,  $f\sigma_8$  from RSD, and the ISW amplitude are retained as late-time consistency channels whose raw likelihoods are compatible with  $\varepsilon = 0$  and are therefore reported here as one-sided upper bounds under the physical prior  $\varepsilon \geq 0$  introduced in §16.5. In the one-sided cases quoted below, the reported  $1\sigma$  and  $2\sigma$  bounds are the upper edges of the corresponding raw intervals after imposing the physical prior  $\varepsilon \geq 0$ ; they are not separate positive-domain refits.

Probe	Nature of constraint	What is actually fitted	Kernel / epoch sensitivity	Role
Hubble + $r_s$	two-sided effective extraction	$\varepsilon$ from the Hubble-channel distance-ratio proxy under the present simplified $r_s$ treatment	broad integrated kernel, CMB-era proxy scale to $z = 0$	Primary
JWST early-galaxy excess	two-sided effective extraction (broad)	$\varepsilon$ from the Press–Schechter proxy for the high- $z$ abundance enhancement at $z \approx 8\text{--}12$	high- $z$ structure-growth window	Primary
Cosmic chronometers	one-sided consistency bound under $\varepsilon \geq 0$	$\chi^2$ fit of $H(z)$ residuals in the $\Lambda$ CDM-background proxy	direct late-time expansion, $0.07 \leq z \leq 1.97$	Consistency
$f\sigma_8$ from RSD	one-sided consistency bound under $\varepsilon \geq 0$	$\varepsilon$ in the linear-growth ODE likelihood	late-time growth, $z \lesssim 2$	Consistency
ISW amplitude	one-sided consistency bound under $\varepsilon \geq 0$	$\varepsilon$ through the linearised ISW proxy amplitude	late-time potential evolution, $z \lesssim 2$	Consistency

**Table 61:** Retained five-probe set for the present effective uniform- $\varepsilon$  analysis layer. “Primary” probes provide two-sided effective extraction intervals; “Consistency” probes provide one-sided upper bounds under the physical prior  $\varepsilon \geq 0$  introduced in §16.5.

**Probe 1 — Hubble +  $r_s$  (two-sided effective extraction).** The SH0ES distance-ladder determination  $H_0 = 73.04 \pm 1.04 \text{ km s}^{-1} \text{ Mpc}^{-1}$  [104] and the Planck 2018 base- $\Lambda$ CDM value  $H_0 = 67.4 \pm 0.5 \text{ km s}^{-1} \text{ Mpc}^{-1}$  [88] define an observed tension of  $\sim 5\sigma$ . The effective distance-ratio proxy adopted here for the Hubble-tension channel, evaluated within the uniform- $\varepsilon$  ansatz on the  $\Lambda$ CDM-background proxy and with the present simplified treatment of  $r_s$ , yields a two-sided effective interval centred at

$$\varepsilon_H = 0.032, \quad 1\sigma: [0.027, 0.038], \quad 2\sigma: [0.021, 0.043]. \quad (16.16)$$

This should be read as an effective H1-type extraction under the present  $r_s$  treatment, not as a full Boltzmann/CMB-likelihood implementation of the H2 programme. The full extraction and uncertainty budget are given in Appendix AG.

**Probe 2 — JWST early-galaxy excess (two-sided effective extraction; binding below).** Reported high- $z$  stellar-mass abundances at  $z \approx 8\text{--}12$  suggest a representative enhancement target of order  $R \sim 10$ , with a broader observationally discussed range of roughly 3–100, relative to baseline  $\Lambda$ CDM expectations for the relevant mass scales. A Press–Schechter proxy tying  $G_{\text{eff}}(z)$  to the halo mass function through the linear growth factor, on the same  $\Lambda$ CDM-background proxy and without full growth-ODE integration or halo-to-stellar-mass mapping, is translated here into a two-sided effective interval centred at

$$\varepsilon_{\text{JWST}} = 0.0449, \quad 1\sigma: [0.0296, 0.0786], \quad 2\sigma: [0.0136, 0.2177]. \quad (16.17)$$

This interval should be read as a proxy-level effective extraction within the present Press–Schechter treatment, not as the result of a full structure-formation pipeline with transfer-function, baryonic, and halo-to-stellar-mass systematics propagated end-to-end. The detailed extraction, including the stellar-assembly time-budget factor  $R_{\text{time}}(\varepsilon)$  and two robustness axes on the time-budget ansatz, is given in Appendix AI. In the present five-probe comparison, the lower edge  $\varepsilon = 0.0296$  becomes the lower edge of the joint effective band discussed in §15.5.3.

**Probe 3 — Cosmic chronometers (one-sided consistency bound under  $\varepsilon \geq 0$ ).** Moresco-compilation  $H(z)$  points at  $z = 0.07\text{--}1.97$  are fit against the effective expansion  $H^{\text{ECT}}(z) = H_0 \sqrt{\Omega_m(1+z)^{3+2\varepsilon} + \Omega_\Lambda(1+z)^{2\varepsilon}}$  with  $\Omega_m = 0.315$  fixed and  $(\varepsilon, H_0)$  varied. The raw best-fit  $\varepsilon = 0.006$  is compatible with  $\varepsilon = 0$ ; under the physical prior we therefore report this channel as a one-sided upper bound:

$$\varepsilon_{\text{CC}} : 1\sigma \text{ upper } 0.087, \quad 2\sigma \text{ upper } 0.150. \quad (16.18)$$

The constraint is weak; its role is late-time consistency, not extraction. The full extraction and uncertainty budget are given in Appendix AJ.

**Probe 4 —  $f\sigma_8$  from RSD (one-sided consistency bound; binding above).** Fourteen RSD measurements at  $z = 0.07\text{--}1.94$  are fit by integrating the linear-growth ODE for the density contrast  $\delta(a)$  with a modified Poisson source driven by  $G_{\text{eff}}(a)$ , profiling  $\sigma_8(0)$  freely. A strong  $\sigma_8\text{--}\varepsilon$  degeneracy leaves the raw likelihood maximum near  $\varepsilon \approx -0.06$ , without a physically meaningful lower branch in the present ECT interpretation; under the physical prior we therefore report this channel as a one-sided upper bound:

$$\varepsilon_{f\sigma_8} : 1\sigma \text{ upper } 0.0396, \quad 2\sigma \text{ upper } 0.150_{\text{grid-lim.}}. \quad (16.19)$$

The  $1\sigma$  upper is close to the binding upper bound of the joint effective band reported in §15.5.3; the full Brent-refined extraction is given in Appendix AK.

**Probe 5 — ISW amplitude (one-sided consistency bound under  $\varepsilon \geq 0$ ).** A linearised proxy  $A_{\text{ISW}} \approx 1 + \kappa_A \varepsilon$ , rather than a full fit to the observed  $C_\ell^{Tg}$  estimator, is compared to Planck+CMB-cross-correlation data on the ISW window  $z \lesssim 2$  under  $\Lambda$ CDM-background Limber weights. The raw likelihood maximum lies near  $\varepsilon \approx -0.007$  and remains compatible with  $\varepsilon = 0$  within a broad uncertainty; under the physical prior we therefore report this channel as a one-sided upper bound:

$$\varepsilon_{\text{ISW}} : 1\sigma \text{ upper } 0.043, \quad 2\sigma \text{ upper } 0.093. \quad (16.20)$$

Role: consistency, not extraction. The proxy-level extraction and its limitations are given in Appendix AL.

**Effective consistency window, not a global joint likelihood.** The retained five-probe set should not be read as a full statistically independent joint likelihood. It is an effective multi-probe comparison performed within a common diagnostic uniform- $\varepsilon$  layer, with partially shared background and growth ingredients across some channels. The resulting band in §15.5.3 is therefore an effective consistency window under the present methodology, not a first-principles ECT prediction and not a final global MCMC determination. In particular, Hubble and cosmic chronometers share background-expansion ingredients, while JWST,  $f\sigma_8$ , and ISW partially overlap in their dependence on late-time growth or potential evolution. The retained five-probe comparison should thus be read as a structured consistency test of a common effective deformation layer, not as a claim of strict statistical independence.

**Bridge.** The combined  $1\sigma$  and  $2\sigma$  intervals of these five effective channels, and the resulting joint effective band under the present methodology, are taken up in §15.5.3.

### 15.5.3 Joint effective allowed band and working benchmark

With the five effective channels specified in §16.5, we now report the resulting joint effective allowed band, identify the working benchmark used in the rebuilt §15.5, and state its relationship to the earlier conservative illustrative point used in the previous preprint treatment of the Hubble mechanism (§16.4).



**Headline result.** Under the retained five-probe set, within the uniform- $\varepsilon$  effective ansatz of §16.5, under the physical prior  $\varepsilon \geq 0$ , and within the present methodology of §16.5, the intersection of the  $1\sigma$  intervals of the two Primary channels with the  $1\sigma$  upper bounds of the three Consistency channels defines the joint effective band

$$\varepsilon \in [+0.0296, +0.0376] \ (1\sigma), \quad \varepsilon \in [+0.0207, +0.0425] \ (2\sigma). \quad (16.21)$$

The  $1\sigma$  band is bounded below by the JWST channel (lower edge  $\varepsilon = 0.0296$ , eq. (16.17)) and bounded above by the Hubble+ $r_s$  channel (upper edge  $\varepsilon = 0.0376$ , eq. (16.16)); the  $f\sigma_8$  channel is only marginally looser at  $\varepsilon = 0.0396$ , eq. (16.19), and is effectively co-binding within the precision of the present pipeline. Per-channel extractions against a common background module are collected in Appendix AG through Appendix AL; the methodological framing, age-viability note, and excluded-probe audit are given in Appendix AH.

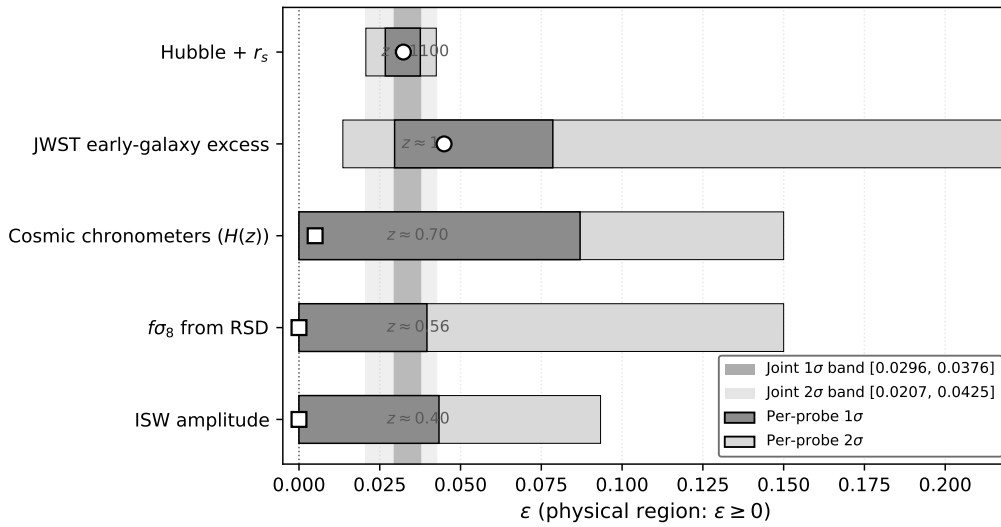


**Figure 14:** Retained-five-probe joint effective  $\varepsilon$ -band under the uniform- $\varepsilon$  ansatz and physical prior  $\varepsilon \geq 0$ , obtained after re-expressing all five channels against the common background module of Appendix AH. Horizontal grey band: joint  $1\sigma$  region  $[0.0296, 0.0376]$ ; lighter band: joint  $2\sigma$  region  $[0.0207, 0.0425]$ . Per-probe  $1\sigma$  (darker) and  $2\sigma$  (lighter) intervals shown as horizontal bars; best-fit markers (o for Primary / Tier A,  $\square$  for Consistency / Tier B) on each bar, with each bar's right-side annotation giving the effective redshift anchor. See Appendix AG through Appendix AL for per-probe extractions. All shading and line styles are grayscale per preprint convention.

**No-prediction caveat.** This retained-five-probe effective band is an empirical result of the present diagnostic analysis, not a first-principles ECT prediction. It does not represent a measurement of a fundamental parameter of the theory, nor a direct reconstruction of an epoch-dependent  $\varepsilon(z)$ . It is an effective consistency window under the uniform- $\varepsilon$  ansatz, the  $\Lambda$ CDM-background proxy, and the retention/likelihood choices of §16.5.

**Why the band is nevertheless informative.** Three qualitative observations make the band a non-trivial consistency check rather than a circular restatement of the retention choice. *Distinct systematics:* the five retained channels have qualitatively distinct observational systematics, from CMB-era distance-ratio proxies to low- $z$  RSD growth likelihoods; a narrow common admissible region under a single uniform- $\varepsilon$  ansatz is not guaranteed a priori. *Two-sided primaries:* the two Primary channels (Hubble+ $r_s$  and JWST early-galaxy excess) provide two-sided effective extraction intervals whose  $1\sigma$  intersection alone already defines a narrow positive- $\varepsilon$  region compatible with the Consistency upper bounds; the band is not generated by the  $\varepsilon \geq 0$  prior alone. *Narrow width:* the retained  $1\sigma$  window,  $\Delta\varepsilon \approx 0.007$ , is substantially narrower than the broadest individual consistency bounds and is therefore not generated by the least constraining channel alone.

**Working benchmark (Benchmark B).** The working cosmological benchmark of the present analysis is the retained five-probe effective band itself, which we refer to as *Benchmark B*. In this sense, Benchmark B is not a single number but the interval in Eq. (16.21). For purely illustrative scaling estimates, one may use the arithmetic midpoint of the retained  $1\sigma$  band,  $\varepsilon \approx 0.032$ , but only as an auxiliary representative value. It should not be interpreted as a first-principles ECT prediction or as a separately defined benchmark constant.

**Parameter scaling under the retained band.** Table 62 summarises the parameterization-dependent ranges of the key quantities across cosmic history, induced directly by the retained  $1\sigma$  effective band.

Quantity	$z = 0$	$z = 10$	CMB-era proxy scale
$G_{\text{eff}}/G_N$ under the retained band	1.000	[1.15, 1.19]	[1.48, 1.63]
Effective proxy ratio $(\alpha - \beta)_{\text{eff}}(z)/(\alpha - \beta)_{\text{eff}}(0)$	1.000	[0.918, 0.934]	[0.782, 0.821]

**Table 62:** Parameterization-dependent ranges induced by the retained  $1\sigma$  effective band (Eq. (16.21)). Entries are not direct observables. The second row is an *effective proxy rewriting* of the retained-band scaling; it does not represent a physical redshift dependence of  $(\alpha, \beta)$ , of  $(\alpha - \beta)$ , or of the cone speed  $c_*$ .

**Benchmark A (legacy retention).** Benchmark A is retained only as a legacy conservative illustrative point from the earlier treatment and should not be read as part of the retained five-probe effective result. It lies outside the retained  $1\sigma$  band and is therefore not representative of the present effective result. Its detailed closure-level numerics and robustness checks are preserved below as legacy continuity material, while the retained-band methodology of the present analysis is documented separately in Appendix AH.

**Bridge.** The probes not retained in the present effective  $\varepsilon$ -analysis, whether for methodological or sectoral reasons, are discussed in §15.5.4.

#### 15.5.4 Excluded and stress-test probes

Beyond the retained five-probe set of §16.5, several additional cosmological channels were considered in the present analysis but are not used in the joint effective band of §16.5. We group them into three categories whose reasons for exclusion are qualitatively different.

**Category (i) — methodology-limited channels.** These probes address the same effective  $\varepsilon$ -sector as the retained probes and could in principle re-enter the joint effective band at a later stage, but the present extraction pipelines are not yet explicit enough for headline use. The limitation is therefore methodological rather than structural.

- **BAO (DESI 2024 DR1).** The present implementation uses a simplified shape-only treatment with independently fixed  $\Omega_m$ , diagonal covariance, and reduced-grid profiling of  $H_0$  and  $r_d$ . Under this simplified pipeline the raw  $1\sigma$  interval straddles  $\varepsilon = 0$  and has a slightly negative central value. In the present paper this is treated as a methodology-limited result rather than as evidence against the  $\varepsilon$ -sector itself. Headline inclusion would require a full DESI likelihood with coupled  $(\Omega_m, r_d, \varepsilon)$  fitting and the full covariance structure. The probe is therefore not used in the joint effective band at the present stage and is deferred to a future full-likelihood treatment.
- **$A_{\text{lens}}$  CMB lensing.** The present treatment uses a linearised proxy of the form  $A_{\text{lens}} \approx 1 + \kappa_A \varepsilon$  rather than a full Boltzmann-level calculation. At this level the observational error bar is not the only uncertainty: the proxy mapping itself carries a substantial theoretical systematic. The resulting interval

is therefore not robust enough for headline use. Headline inclusion would require a full CAMB/CLASS-level analysis. The probe is therefore not used in the joint effective band at the present stage and is deferred to a future Boltzmann-level treatment.

**Category (ii) — channels outside the present  $\varepsilon$ -sector.** These are distinct in kind from category (i). In the present uniform- $\varepsilon$  diagnostic layer their raw  $1\sigma$  support lies entirely at  $\varepsilon < 0$ . Under the physical prior  $\varepsilon \geq 0$  adopted in §16.5, including them as  $\varepsilon$ -band constraints would therefore be a category error: the tension they report is not encoded in the present  $\varepsilon$ -sector as parameterised here.

- **$S_8$  weak lensing (KiDS-1000).** In the present uniform- $\varepsilon$  mapping, the raw  $1\sigma$  interval lies entirely at  $\varepsilon < 0$ . Within the  $\varepsilon$ -sector adopted here this does not act as an  $\varepsilon$ -band constraint but instead signals the separate  $S_8$  tension, whose resolution is not encoded in a positive-drift  $\varepsilon$  deformation. The probe is therefore classified as outside the present  $\varepsilon$ -sector rather than as a retained  $\varepsilon$ -channel.
- **$\sigma_8$  cluster counts.** The same structural pattern appears in the present simplified mapping: the raw  $1\sigma$  support lies entirely in  $\varepsilon < 0$ . As for  $S_8$  weak lensing, this identifies a tension outside the present  $\varepsilon$ -sector rather than a retained  $\varepsilon$ -band constraint. The probe is therefore excluded within the present uniform- $\varepsilon$  analysis on grounds that are not reducible to a mere extraction-pipeline upgrade.

Unlike category (i), the issue here is not merely an incomplete extraction pipeline. Within the present uniform- $\varepsilon$  diagnostic layer, refining the  $\varepsilon$ -fit alone would not convert these probes into retained  $\varepsilon$ -band constraints: their raw support points outside the physical  $\varepsilon$ -sector adopted in §16.5. Any successful treatment would therefore require enlarging the phenomenological description beyond the present  $\varepsilon$ -only layer, rather than simply improving the same extraction.

**Category (iii) — non-independent or placeholder channels.**

- **Age  $t_0$ .** Under self-consistent treatment with  $H_0(\varepsilon)$  inherited from the Primary Hubble channel, the age test carries no independent  $\varepsilon$ -information. It is therefore treated as a downstream self-consistency note rather than as a retained  $\varepsilon$ -probe.
- **SN Ia.** No retained SN Ia  $\varepsilon$ -channel is included at the present stage. A genuine SN Ia probe would require direct fitting to an observational supernova dataset with the full calibration and host-systematics chain. Such a pipeline is not yet implemented in the present analysis, so SN Ia is not used in the joint effective band.

**Cross-category principle.** Categories (i) and (ii) must be kept distinct. Category (i) contains channels that could re-enter the retained set after a sufficiently upgraded extraction pipeline. Category (ii) contains channels that, within the present uniform- $\varepsilon$  sector itself, do not function as  $\varepsilon$ -band constraints at all. Keeping this distinction explicit prevents low- $z$  structure tensions from being misrepresented as direct  $\varepsilon$ -band measurements.

**Bridge.** A short comparison of the present ECT effective- $\varepsilon$  result with alternative approaches to the same observational landscape is given in §15.5.5.

### 15.5.5 Comparison with other approaches

The retained five-probe effective band of §16.5 can be briefly placed in the context of alternative proposals addressing the same observational pattern discussed in §§16.5–16.5, namely the Hubble discrepancy, the JWST high-redshift abundance anomaly, and the associated late-time consistency channels.

**$\Lambda$ CDM.** The base  $\Lambda$ CDM model does not accommodate the Hubble discrepancy or the JWST early-galaxy excess within its minimal parameter space. In practice, these tensions are typically discussed either in terms of residual systematics or by extending the baseline model in different directions, while the late-time consistency probes retained in §16.5 are already part of the standard  $\Lambda$ CDM fitting framework [88].

**Early Dark Energy.** Early-dark-energy proposals primarily target the Hubble discrepancy through a pre-recombination modification of the expansion history, typically by introducing one or more additional components or effective functions [105]. In their basic form they are not primarily constructed as a simultaneous explanation of the high-redshift structure-formation anomalies discussed here; whether they help with the JWST sector is model-dependent and not part of their minimal motivation.

**Modified gravity.** Modified-gravity approaches form a heterogeneous class. MOND-type scenarios and TeVeS are historically tied most directly to galactic phenomenology, while scalar-tensor and  $f(R)$ -type models are often motivated by late-time background and growth modifications [106, 107]. What distinguishes the present ECT use of the  $\varepsilon$ -sector is not simply that gravity is modified, but that a single effective deformation is confronted here with both high-redshift and late-time cosmological channels within one common diagnostic layer.

**Phenomenological  $G_{\text{eff}}(z)$  deformations.** The  $\varepsilon$ -deformation used in the present analysis is related to a broader class of phenomenological varying-coupling or effective-response parameterizations considered in cosmology [85]. What distinguishes the ECT use of this class is that the present effective deformation is motivated by ECT’s three-stage condensate-closure picture and then constrained empirically here, rather than introduced as an otherwise free late-time fitting function.

**Key rhetorical point.** The observation that one and the same effective deformation parameter admits a narrow retained-five-probe effective band across observationally distinct channels serves as an indirect consistency check for the framework. One mechanism — condensate-closure-motivated drift, treated here at the effective level — remains compatible with multiple observational channels within a single narrow band. This parsimony does not constitute a proof of ECT, but it does strengthen the plausibility of its cosmological strategy relative to approaches that require separate parameters or separate mechanisms for different anomalies.

**Honest caveats.** Three qualifications are stated explicitly. First, the retained five-probe set is a restricted subset of the broader cosmological dataset; BAO,  $A_{\text{lens}}$ , and the  $S_8$ -sector probes contribute uncertainties and tensions not captured in the joint effective band (§16.5). Second, the comparison above is with schematic representatives of alternative proposals, not with their full modern pipelines. Third, the ECT treatment of the  $\varepsilon$ -sector in §15.5 is effective, not first-principles; the closure-derived  $\varepsilon(z)$  remains open and is logged as such in §15.5.6.

**Bridge.** The implications of the retained five-probe effective band for the broader ECT programme, and the list of open problems associated with the  $\varepsilon$ -sector, are discussed in §15.5.6.

### 15.5.6 Interpretation and outlook

With the retained five-probe effective band of §16.5 and its methodological context of §§16.5–16.5 in place, we close this subsection by stating what the analysis establishes, what it does not, and where the ECT  $\varepsilon$ -sector programme stands.

**What the analysis establishes.** Under the stated assumptions (the uniform- $\varepsilon$  ansatz of §16.5, the  $\Lambda$ CDM-background proxy, the physical prior  $\varepsilon \geq 0$ , and the retention criteria of §16.5), the five retained probes admit a narrow joint effective allowed band. ECT’s three-stage condensate-closure picture is compatible with this result at the diagnostic-layer level. The compatibility of a single effective deformation parameter with five channels of qualitatively distinct observational systematics constitutes an indirect consistency check of the framework, not a derivation from first principles and not a full global likelihood result.

**What the analysis does NOT establish.** It does not establish  $\varepsilon$  as a fundamental parameter of ECT. The retained band is empirical under the uniform- $\varepsilon$  diagnostic layer, not a measurement of a first-principles constant and not a statistically rigorous global combination of independent likelihoods. It does not provide a completed resolution of the Hubble or JWST tensions in the sense of a full CMB-to-local Boltzmann pipeline; the present treatment implements the late-time H1 closure-level route, not the full H2 CMB-inferred inference pipeline. It does not definitively exclude the inadequacy of a single effective uniform- $\varepsilon$ ; broader datasets or methodological improvements on currently excluded channels might reveal tensions requiring an epoch-dependent  $\varepsilon(z)$ .

**On the constancy of  $\varepsilon$ .** The five-probe result shows that a single constant value of the effective drift parameter  $\varepsilon$ , drawn from the retained band, is compatible with all five probes at the diagnostic-layer level. This should not be over-interpreted as evidence that  $\varepsilon$  is fundamentally constant across redshift. Each probe is in fact sensitive to a different kernel-averaged projection of  $\varepsilon$  along its own characteristic epoch window, so the same retained band may equally arise as the set of kernel-averaged projections of a slowly varying closure-level function  $\varepsilon(z)$ . Distinguishing a truly constant  $\varepsilon$  from a band-averaged projection of  $\varepsilon(z)$  requires either extending the analysis to channels with sufficiently non-overlapping kernels or a closure-level derivation of  $\varepsilon(z)$  from ECT (OP-Hubble-derive below). Within the present diagnostic layer neither route is attempted here, and both readings of the retained band — “constant  $\varepsilon$ ” and “kernel-averaged projection of  $\varepsilon(z)$ ” — remain empirically admissible. The present retained band therefore supports constancy only at the level of effective compatibility across probe-dependent kernels, not at the level of a closure-derived first-principles dynamical law. Thus, the present retained band should be read as evidence for a common *effective*  $\varepsilon$ -range across the retained probes, not as a proof that the exact closure-level quantity is strictly constant in redshift.

**Diagnostic layer, not final closure.** The uniform- $\varepsilon$  treatment is used here as a diagnostic effective layer, not as the final closure-level description of the cosmological drift sector. A full ECT-native treatment of the cosmological drift — including the functional form of  $\varepsilon(z)$  implied by three-stage condensate closure — remains open.

**Open problem:  $\varepsilon(z)$  from closure.** A first-principles ECT derivation of the cosmological drift parameter — specifically, the closure-level function  $\varepsilon(z)$  implied by the three-stage condensate closure, together with its mapping to the effective uniform- $\varepsilon$  analysis layer of §16.5 — remains open. For reference within the present rebuilt §15.5, we denote this task by **OP-Hubble-derive**.

**Methodological requirements.** Three methodological improvements are noted here without being logged as formal open problems, since each is a question of extending an analysis pipeline rather than a structural theoretical gap. The BAO channel of §16.5 requires a full DESI likelihood with a coupled  $(\Omega_m, r_d, \varepsilon)$  fit before it can be considered for the joint band at headline level. The  $A_{\text{lens}}$  channel of §16.5 requires a full Boltzmann-level implementation before it can be similarly considered. A genuine SN Ia  $\varepsilon$ -channel requires a real observational supernova pipeline with full SH0ES and host-galaxy systematics.

**Age-viability ambiguity under Hubble mapping.** Evaluating the cosmic age self-consistently through the common background module of Appendix AH at the retained-band central value gives two distinct numerical readings depending on which  $H_0$ -mapping is adopted: a baseline-background age of about 13.5 Gyr, close to the Valcin et al. 2021 globular-cluster anchor  $t_0 \geq 13.50 \pm 0.27$  Gyr; or an inferred- $H_0$ -mapped age of about 12.5 Gyr, which falls noticeably below that anchor. This is recorded as a viability/self-consistency note, not as a new retained probe and not as a new formal open problem; its interpretation depends on which mapping is physically correct and is bound up with the closure-level derivation of  $\varepsilon(z)$  itself (OP-Hubble-derive). Exact technical values for the two mappings, and the precise sigma distance to the globular-cluster anchor, are collected in Appendix AH (AF.4).

**Parsimony and correlations.** In a closure-level extension, the same underlying drift mechanism would be expected to correlate the late-time expansion history, the effective dark-energy phenomenology, and the time budget available for early structure formation. This qualitative correlation structure is a distinctive feature of the ECT use of the  $\varepsilon$ -sector rather than a post-hoc collection of separate fitting knobs. At the present stage, however, this remains only a structural expectation: its quantitative realisation belongs to OP-Hubble-derive.

**Three layers of the analysis.** Three distinct layers coexist in the present treatment and should be kept separate: the ECT structural motivation for a cosmological deformation of the gravitational response (§16.5); the uniform- $\varepsilon$  diagnostic layer adopted in §15.5 and constrained empirically by the retained five-probe band (§§16.5–16.5); and the closure-level  $\varepsilon(z)$  derivation that remains open (OP-Hubble-derive). No statement in the rebuilt §15.5 should be read as belonging to the first-principles closure level unless explicitly said otherwise; all quantitative conclusions of §15.5 belong to the middle diagnostic layer only.

**Direction for future work.** Three natural directions follow. First, methodological upgrades to currently excluded channels (BAO,  $A_{\text{lens}}$ , SN Ia) would test whether the retained band remains stable as the analysis base broadens. Second, a proper  $\varepsilon(z)$  parameterisation, derived from closure theory when it matures, would test whether the uniform- $\varepsilon$  assumption is the adequate shape of the deformation in this epoch window. Third, a systematic study of the dependence of the retained band on the  $\Lambda$ CDM-background proxy would quantify the residual proxy-dependence of the present methodology.

**Predictions, viability discriminators, and anti-predictions.** The retained five-probe band  $\varepsilon \in [0.0296, 0.0376]$  at  $1\sigma$  is *not itself a prediction* of ECT; it is an empirically extracted effective consistency window within the present uniform- $\varepsilon$  diagnostic methodology. What is predictive is the *stability* of this window: refined pipelines for the retained observables should continue to concentrate in a narrow positive effective range of order 0.03–0.04 rather than drifting toward zero or fragmenting into incompatible per-channel intervals. The age of the Lorentzian branch, not itself a retained probe, acts as a *viability discriminator* between the baseline- $H_0$  and inferred- $H_0$  mappings of the same  $\varepsilon$ -sector (§16.4, Appendix AH). In the opposite direction, the present uniform- $\varepsilon$  layer is not expected to close the  $S_8$  / weak-lensing sector by itself; a persistent failure to do so would therefore not automatically count against the retained-band analysis, whereas an apparently universal success of the same simple  $\varepsilon$ -layer across all sectors would instead signal that the present closure architecture has likely been overextended.

## 16.6 Cosmological predictions: summary and derivation status

The preceding subsections established a range of cosmological results at different derivation levels. The purpose of the present subsection is to collect them in a single summary table, analogous to the gravitational-sector summary in §13.9, and to distinguish explicitly between strictly derived results, structural closure-level consequences, and illustrative benchmark outcomes.

**Table 63:** Status map for the ordered-branch cosmology programme.

Claim	Status	Comment
Late-time accelerated expansion via ordered-branch background	B	Follows structurally within the macroscopic $\phi$ -branch closure; detailed potential still open
No-phantom inequality $w \geq -1$ in the adopted positive-kinetic closure	B	Structural within the $\phi$ -first closure, not yet universal across all nonlinear completions
Screened $\Lambda$ CDM limit	B	Recovered in the frozen/screened branch of the adopted closure
Upward Hubble-shift route from enhanced high- $z$ effective gravity	B	Sign-level mechanism established; magnitude remains closure-dependent
JWST age-budget enhancement route	B	Structural route established; quantitative galaxy-formation prediction open
Correlated sign prediction ( $w, H_0, \text{age}, G_{\text{eff}}$ )	B	All controlled by one background $\phi_b(z)$ ; single-parameter correlation is a programme-level signature
Ordered-branch dynamic vacuum route	A/B	Late-time acceleration supplied by condensate background, not external rigid $\Lambda$
Correlated DE–galactic signature	B	Same $\phi_b(z)$ controls $w(z)$ and epoch-dependent $g_{\text{bg}}^\dagger(z)$
Derived present-day $w_0$	Open	Requires solved background history and calibrated closure
Derived perturbation observables ( $A_s, n_s, r$ )	Open	Not yet obtained from first principles in the present ECT cosmology programme

It is especially important to separate: (i) sign-level and closure-level structural consequences of the ordered branch, (ii) benchmark numerical outcomes obtained within a specific  $\phi$ -first truncation, and (iii) genuinely open cosmological targets that still require a solved background history, perturbation closure, or full data fit. This subsection should be read primarily as a prediction-by-prediction inventory; the chapter-level synthesis of what is established, what is closure-dependent, and what remains open is deferred to Section 16.9. Quantities not yet derived from ECT—such as an ECT-native formula for  $n_s$ , a fully derived present-day value of  $w_0$ , or a first-principles baryogenesis asymmetry—are not listed below as ECT predictions.

**Table 64:** Cosmological predictions and structural consequences of ECT.

Prediction / consequence	Result / formula	Level	Section	Observational context
Spatial flatness	$k = 0$	A	§14.4	CMB / BAO
Primary monopole channel absent	$\pi_2(S^3) = 0$	A	§14.5	no GUT monopole overproduction
Single scalar perturbation mode	from Universality Corollary	A	§14.6	perturbation field content
No ordered-branch isocurvature	consequence of single-mode	A	§14.6	subdominant isocurvature bounds
Tensor speed = $c_*$	primordial tensor on same cone	A/B	§14.6	GW sector consistency

Prediction (cont.)	Result	Level	Sec.	Obs. context
Macrocoherent branch minimum	$S_{\text{ord}} = 0$ iff $n_A = \text{const}$	A	§14.3	horizon-resolution route
Emergent Lorentzian time	pre-ordered regime exists; Lorentzian time begins only after ordering	A/B	§14.1	conceptual cosmological origin
No-phantom late-time branch	$w_\phi \geq -1$ for $\omega > 0$	B struct.	§16.1	late-time DE sector
Age reinterpreted	age = Lorentzian branch duration	B struct.	§16.4	cosmic age
Correlated observables	$t_0, t_U, t_{\text{gal}}, D_L$ from one $H(z)$	B struct.	§16.4	age / distance / JWST
Upward Hubble-shift mechanism	possible upward late-time shift from ordered-branch drift	B struct.	§16.5	Hubble tension
$w_0$ - $H_0$ correlation	one $\phi_b(z)$ drives both	B struct.	§16.5	joint late-time fits
BBN-localised drift	high- $z$ saturation required	B struct.	§16.5	BBN consistency
Three-stage condensate evolution	ordering $\rightarrow$ stabilisation $\rightarrow$ drift	B struct.	§16.2	background logic
Ordering transition out-of-equilibrium	strongest ECT Sakharov ingredient	B struct.	§16.3	baryogenesis compatibility
Retained five-probe effective band	$\varepsilon \in [0.0296, 0.0376]$ ( $1\sigma$ ), $[0.0207, 0.0425]$ ( $2\sigma$ )	B diag.	§16.5, App. AH	headline cosmological constraint on the effective uniform- $\varepsilon$ parameter
JWST extraction with time-budget correction	$\varepsilon_{\text{JWST}} \in [0.0296, 0.0786]$ ( $1\sigma$ )	B diag.	§16.5, App. AI	lower edge binds the retained band
Age-viability note	baseline mapping acceptable; inferred- $H_0$ mapping problematic	B note	App. AH (AF.4)	viability/self-consistency note, not a retained probe
Vacuum-offset decoupling: $V(\phi_0)$ inert	classical baseline offset $V(\phi_0)$ does not source local emergent gravity (Theorem 15.3(iv))	A	§15, §15.3	removes standard $\Lambda$ channel for the bare quartic minimum
Zero-derivative loop-vacuum decoupling	absorbed into the fixed kinetic-tensor determinant $\sqrt{-\det K^{AB}} = \beta^2/c_*$ (Theorem 15.3(v))	A, conditional on $H_\Lambda$	§15.3, §15.4	blocks direct UV channel for vacuum baseline
Infrared dark-energy scale	$\rho_\Lambda \sim c_\Lambda M_{\text{Pl}}^2 H_0^2$ with $c_\Lambda = \mathcal{O}(1)$ ; $M_{\text{Pl}}^2 H_0^2 \approx 1.2 \times 10^{-47} \text{ GeV}^4$	C (motivated scaling)	§15.8	observed dark-energy density at order-of-magnitude level
$w_0 \approx -1$ as slow-branch instance	$w_0 = -1 + 2\rho_{\text{kin}}/(3\rho_{\text{cond}})$ grounded by FRW reduction of the ordered-branch mode (Appendix AC.3)	A/B structural	§15.7	DESI-era $w_0 \neq -1$ indication
Pseudo-Goldstone realisation of IR scaling	$\rho_G \sim m_G^2 f_G^2 \sim H_0^2 M_{\text{Pl}}^2$ with $m_G \sim H_0, f_G \sim \phi_0 \sim \tilde{M}_{\text{Pl}}$	C (plausible candidate)	§15.9	consistent with fuzzy-DM / ultralight-scalar bounds

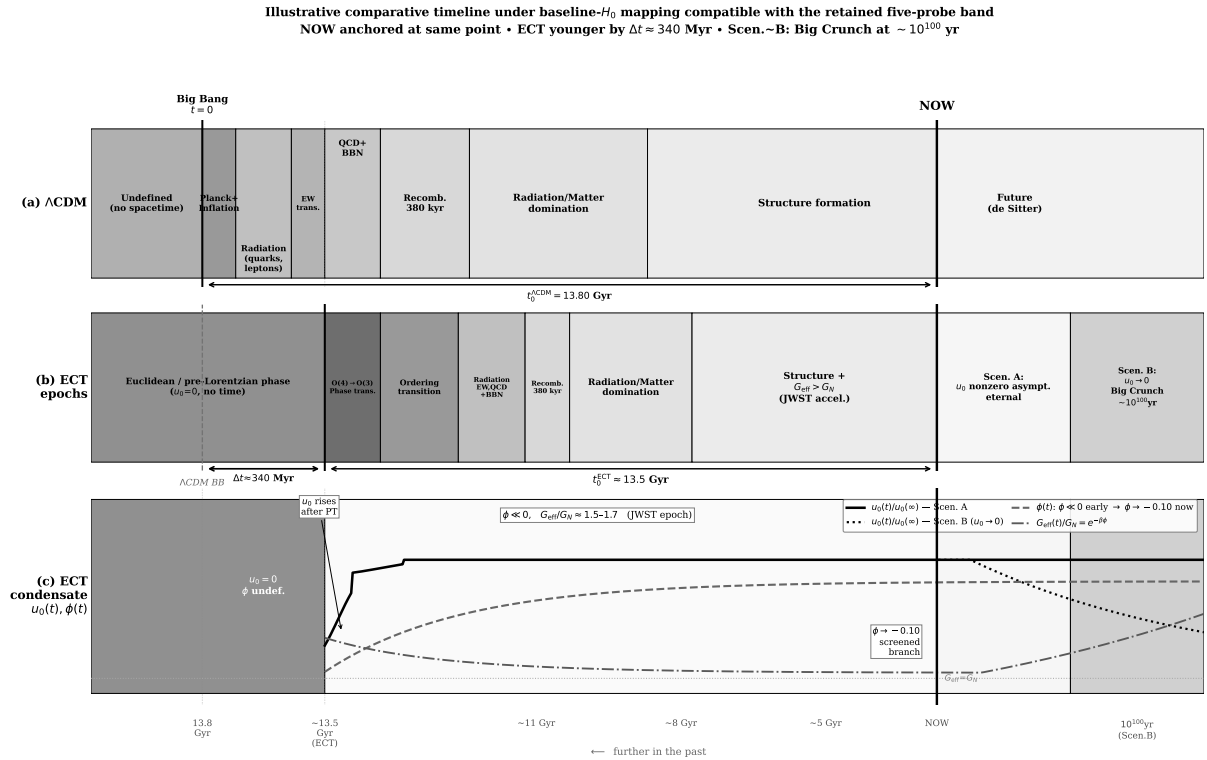
**What is explicitly not yet predicted.** The present ECT cosmological programme does *not* yet provide: (i) an ECT-native formula for the scalar spectral index  $n_s$  or the tensor-to-scalar ratio  $r$ ; (ii) a closure-independent present-day numerical value of  $w_0$ ; (iii) a first-principles derivation of the baryon asymmetry  $\eta_B$ . These remain open tasks identified earlier in §§14.6, 16.1, and 16.3.



**Status summary.** The strongest cosmological predictions of ECT are structural rather than numerical: spatial flatness of the baseline branch, absence of the primary monopole channel, the single-scalar perturbation content of the ordered branch, and the no-phantom late-time closure. The Hubble-tension mechanism, age reinterpretation, and JWST correlations are structural at Level B and benchmarked quantitatively within the present  $\phi$ -first closure. A fully ECT-native perturbation spectrum and a first-principles baryogenesis model remain central open problems. A chapter-level synthesis of these statuses is given in §16.9.

## 16.7 Cosmological evolution: ECT vs. $\Lambda$ CDM

The comparative cosmological timeline is shown in Figure 15.



Note: schematic; epoch widths non-proportional. ECT resolves horizon, flatness, monopole problems without inflation (Level~A/B). Condensate curves schematic; only  $\phi$ -sector resolved quantitatively.

**Figure 15:** Illustrative comparative timeline under the baseline- $H_0$  mapping compatible with the retained five-probe band of §16.5: standard  $\Lambda$ CDM (row a) vs. ECT (row b). The present moment (NOW) is anchored at the same horizontal position in both rows; the time axis runs to the left (further into the past) on a schematic logarithmic scale, with the minimum of each axis starting at the birth of the corresponding universe ( $\Lambda$ CDM Big Bang at 13.80 Gyr; ECT ordering transition at approximately 13.5 Gyr in the baseline- $H_0$  mapping). This creates a visually non-uniform but representationally useful comparison: the ECT Euclidean/pre-Lorentzian gap (grey region) is the direct analogue of the undefined pre-Big-Bang era in  $\Lambda$ CDM. Row (c) shows schematic condensate evolution. ECT resolves the horizon, flatness, and monopole problems without inflation (Section 14.3). The numbers shown are indicative closure-level ages, not first-principles predictions; the mapping-dependent viability of the age channel is discussed in Appendix AH. For details on Scenarios A and B see §16.2; for the internal ECT sector organisation see Fig. 16.

### ECT: schematic full evolution of the ordered-branch condensate sectors and the observable Universe

$\beta = 0.8$ ,  $\phi_0 = -0.10$  (Hubble-priority);  $G_{\text{eff}}(z=10)/G_N \approx 1.49$ ;  $\Delta H_0/H_0 = +2.73\%$ ;  $t_0^{\text{ECT}} = 13.02$  Gyr

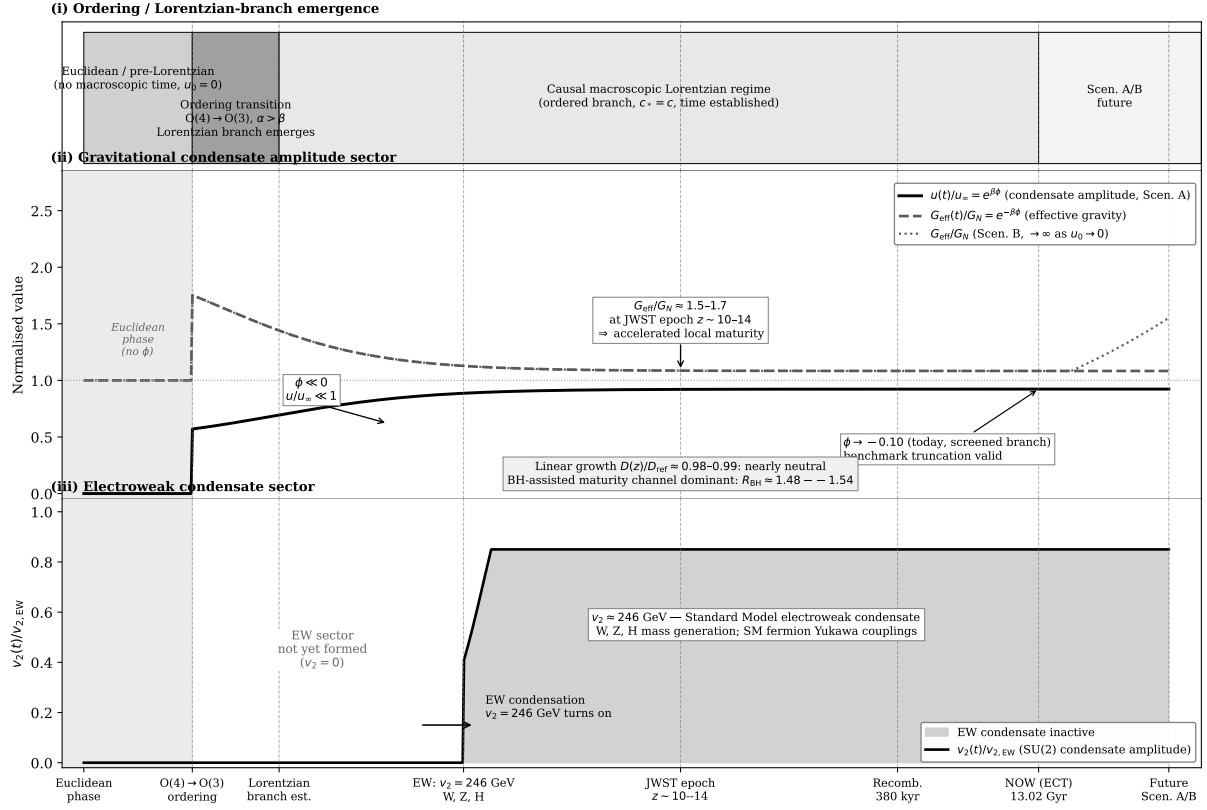


**Figure 16:** Schematic full ECT internal map of the observable Universe and the main condensate sectors. Unlike Fig. 15, this figure is not intended as a direct age comparison with  $\Lambda$ CDM; rather, it is the internal multi-sector conceptual map of ECT itself. The figure separates: (i) the ordering / Lorentzian-branch emergence layer; (ii) the gravitational condensate amplitude sector described by  $\phi$  and  $u/u_\infty = e^{\beta\phi}$  ( $G_{\text{eff}}/G_N = e^{-\beta\phi} > 1$  in the early derived-parent epoch,  $G_{\text{eff}}/G_N \approx 1.5\text{--}1.7$  at the JWST epoch  $z \sim 10\text{--}14$ ); (iii) the electroweak-like condensate sector ( $v_2 = 246$  GeV as a low-energy matching scale; formal  $W/Z/H$ -sector embedding if the second transition exists); and (iv) the observable Universe layer with key cosmological epochs. Only sector (ii) is presently resolved quantitatively in the late-time Hubble–JWST analysis; the remaining layers represent the current conceptual ECT picture. This schematic should not be read as a fully established quantitative early-Universe history. As discussed in Appendix AD and Appendix AU.4, this figure belongs to the present conceptual article-facing layer and should not be read as a completed quantitative reconstruction of all condensate sectors.

Table 65 summarises the key differences between the standard  $\Lambda$ CDM picture and the ECT picture at each cosmological epoch. This comparison reflects the current status of the theory: the late-time gravitational condensate sector is developed to an explicit benchmark/closure level (Level B), while the early-Universe ordering layer remains a structural cosmological scenario rather than a completed first-principles nonequilibrium derivation. The horizon problem is structurally reformulated and resolved in ECT through coherent branch selection (Section 14.3), while an inflation-like ordering epoch, if retained, should be read as an effective reinforcement rather than as the core mechanism of the solution.

**Table 65:** Cosmological evolution: ECT vs.  $\Lambda$ CDM.

Epoch	$\Lambda$ CDM	ECT
Pre-Planckian	Undefined; initial singularity at $t = 0$ marks the boundary of the theory	Pre-Lorentzian Euclidean condensate regime (Level B scenario); $O(4)$ symmetry unbroken, no Lorentzian metric is yet established, and no macroscopic time coordinate is available
Phase transition	Not present	$O(4) \rightarrow O(3)$ SSB; Lorentzian signature emerges at Level A in the broken-phase EFT; macroscopic arrow of time developed within the ordered retarded branch (overall cosmological scenario: Level B); gradient vacuum $\langle \partial_A \Phi \rangle = u_0 \delta_{Aw}$ established (Level B: pre-transition dynamics open, OP3)
Inflation	Separate inflaton field with ad-hoc potential	Possible inflation-like effective description of the ordering transition (Level B structural scenario; not the core horizon-resolution mechanism in ECT; see Section 14.3); ECT-native derivation of the primordial spectrum remains open (see §14.6); not yet a full first-principles replacement for inflation
Flatness problem	Separate inflationary mechanism usually invoked to suppress $ \Omega_K $ dynamically; in its absence, extreme fine-tuning of initial conditions is typically required	Structurally solved: flat Euclidean background P1 with macrocoherent $O(4) \rightarrow O(3)$ ordering gives $k = 0$ as a direct inheritance (Level A); $\Omega_K(t) = 0$ for the exact baseline branch, without requiring a separate inflationary mechanism (see Section 14.4)
Relic / monopole problem	Requires dynamical dilution mechanism (inflation) to dilute overproduced GUT monopoles and topological relics from the hot early Universe	Primary $O(4) \rightarrow O(3)$ transition: $\pi_2(S^3) = 0$ — no topologically stable monopoles (Level A); GUT overproduction not required by ECT structure (Level B); EW and later-sector relics: further development (see Section 14.5)
Primordial perturbations	Observed CMB spectrum: $n_s = 0.9649 \pm 0.0042$ , $r < 0.056$ [88]; standard framework: inflaton slow-roll	Single scalar mode from Universality Corollary (Level A); ECT-native derivation of $n_s$ , $r$ remains open (OP3)
Reheating / radiation	Standard; inflaton decays into SM fields	Ordered branch stabilises; condensate excitations (radial mode and soft orientation sector) thermalise into SM plasma (Level B; reheating mechanism requires OP3)

(continued on next page)

Epoch	$\Lambda$ CDM	ECT
Matter domination	Cold dark matter particles	Modified gravity response; additional condensate excitations (topological sectors or soft scalar mode) optional; relic abundance and stability are open problems (Level B/C); macroscopic ordering variables approximately stationary, $G_{\text{eff}} \approx G_N$ (Level B)
Dark energy today	Cosmological constant $\Lambda = \text{const}$ , $w_0 = -1$	Residual condensate kinetic energy; $w_0 > -1$ (structural; no numerical ECT prediction currently)
Galactic scales	Dark matter halo required for flat rotation curves	$\phi$ -branch activates in low-acceleration environments; RAR and BTFR reproduced within the present $\phi$ -branch closure without introducing a standard particle-dark-matter halo (Level B)
Origin of cosmic time	Lorentzian time fundamental from Big Bang onward	Lorentzian time emerges only after branch ordering; pre-ordered regime has no standard macroscopic time (Level A/B)
Perturbation field content	Model-dependent; often single inflaton + tensor sector	Single scalar ordered-branch mode (Level A); no ordered-branch isocurvature; tensor sector on the same cone (§14.6)
Cosmic age interpretation	Time since Big-Bang singularity (13.8 Gyr)	Duration of Lorentzian ordered branch; conceptually different quantity (§16.4)
Hubble tension	Discrepancy between early- and late-inferred $H_0$	Possible upward late-time shift from ordered-branch background drift; structurally correlated with age and distance sectors (§16.5)
JWST early galaxies	Requires unusually rapid early assembly or new physics	Mixed mechanism: distance, age, and growth all shift together; BH-assisted channel more promising than pure linear-growth enhancement (§16.5)
Age–distance–Hubble–JWST relation	Often analysed as partly separate tensions	All controlled by the same ordered-branch background $H(z)$ , hence structurally correlated (§16.4)
Far future	Scenario A: de Sitter eternal expansion ( $w_{\text{eff}} \rightarrow -1$ ) Scenario B: Big Rip ( $w < -1$ , phantom energy)	Scenario A ( $\chi \rightarrow \chi_\infty$ ): de Sitter eternal expansion, $G_{\text{eff}} = G_N = \text{const}$ Scenario B: possible Euclidean-relaxation / recollapse branch (Level B scenario, OP3); quantitative timescale closure-dependent (§16.2)

**Pre-Lorentzian regime.** The pre-ordered / pre-Lorentzian regime, its structural status (Level A for configuration-space existence; Level B for cosmological realisation), and its conceptual consequences are developed in §14.1; the branch-coherent reformulation of the horizon problem is given in §14.3.

**Condensate evolution and future branches.** The three-stage condensate picture (ordering  $\rightarrow$  stabilisation  $\rightarrow$  slow drift) and the two possible far-future scenarios (A and B) are discussed in §16.2. The observational discriminants ( $|\dot{G}/G|$ ,  $w_d$ ) are also given there.

**Cross-sector scale hierarchy.** The cosmological sector should be read together with the broader ECT hierarchy of matched scales linking the gravitational, electroweak-like, and galactic branches. This hierarchy motivates the comparison between late-time background evolution and later low-acceleration phenomenology, but its full renormalisation-group origin remains open (OP-new-6).

**Distinctive structural features of the ECT cosmological picture.** Beyond the epoch-by-epoch comparison recorded in the table, several broader distinctions separate ECT from  $\Lambda$ CDM. First, the Big-Bang singularity is replaced by a pre-ordered non-Lorentzian regime rather than merely regularised. Second, Lorentzian signature is emergent rather than fundamental. Third, one and the same condensate background controls the late-time gravitational coupling, the dark-energy branch, the age apparatus, and the distance/Hubble/JWST correlations. Fourth, the flatness and primary relic problems are addressed structurally through branch topology and coherence rather than dynamically through a separate inflationary dilution mechanism. At present, the strongest of these statements are Level A for flatness, topology, and perturbation field content, and Level B for the late-time background and correlated-observable sectors.

**Internal versus comparative visualisations.** Figure 15 should be read as a comparative  $\Lambda$ CDM–ECT timing schematic. By contrast, Figure 16 is an internal map of the ECT sector structure and should not be read as a direct age comparison plot.

**What is established and what remains open.** The comparison above shows that ECT provides a coherent alternative cosmological narrative in which several puzzles that appear independent in  $\Lambda$ CDM—flatness, relics, cosmic age interpretation, Hubble tension, and JWST timing/growth tensions—become structurally linked through the ordered branch. The strongest results are Level A for pre-ordered existence, flatness, topology, and perturbation field content. The late-time background, Hubble-shift mechanism, and JWST correlations are Level B within the present  $\phi$ -first closure. What remains open is a fully ECT-native perturbation spectrum (in particular  $n_s$  and  $r$ ), the quantitative nonequilibrium dynamics of the ordering transition, and fully nonlinear structure formation. The epoch-by-epoch comparison above should be read together with the status synthesis of §16.9.

## 16.8 Universe size, boundary, and force-law effective dimensionality

*Status: mixed. The finite-domain / boundary discussion is a Level B cosmological scenario for the large-scale completion of the ordered branch. By contrast, the force-law dimensionality result discussed below is a Level B derived consequence of the present galactic  $\phi$ -closure. These two parts of the subsection should not be assigned the same epistemic weight.* The first part of this subsection concerns a speculative cosmological large-scale completion of the ordered branch; the second concerns a measurable closure-level diagnostic that is inherited from the galactic sector and included here only because of its conceptual bearing on large-scale completion.

**Size of the ECT domain.** In one possible ECT macroscopic completion (Level B), the observable universe is a finite ordered Lorentzian domain in which the macroscopic geometric branch is active. Beyond the causal boundary of this domain the ordered-branch description itself ceases to remain reliable. As the ordered amplitude weakens toward the edge of a finite domain, the Lorentzian branch description is expected to break down and the pre-ordered / pre-Lorentzian condensate regime to take over (Level B scenario; explicit dynamics requires OP3). This should be understood not as reaching a physical wall, but as entering a regime in which the macroscopic geometric branch is no longer a valid effective description.

The characteristic size of such a finite ordered domain is expected to be at least of order the present Hubble radius,

$$R_{\text{domain}} \gtrsim c/H_0,$$

possibly much larger if the ordered branch occupies only a subregion of a wider pre-Lorentzian condensate arena. At the present stage no first-principles ECT derivation fixes this scale more precisely. Any larger estimate should therefore be read only as an illustrative scenario-level extrapolation, not as a quantitative prediction.

**From domain scenario to measurable force-law response.** The finite-domain discussion above concerns a speculative large-scale completion of the ordered branch. The force-law dimensionality discussed below is different in status: it is a measurable closure-level prediction of the present galactic branch and does not require the finite-domain scenario to be true.

**Topological versus force-law dimensionality.** Two distinct notions of dimensionality appear in ECT. The first is the topological dimensionality of the underlying arena, which is postulated in P1 (see §2 for why  $d = 4$  is special). The second is the effective force-law dimensionality extracted from the radial scaling of the observed gravitational response. These notions are different: the arena remains topologically four-dimensional, while the effective force-law dimensionality of the macroscopic branch can flow away from its near-Newtonian value in the critical  $\phi$ -regime. This does not mean that matter distributions become literally two-dimensional; it refers only to the scaling of the effective gravitational law.

**Effective dimensionality at different scales.** A characteristic feature of ECT is that the effective dimensionality of structure depends on the scale of observation through the condensate coherence properties.

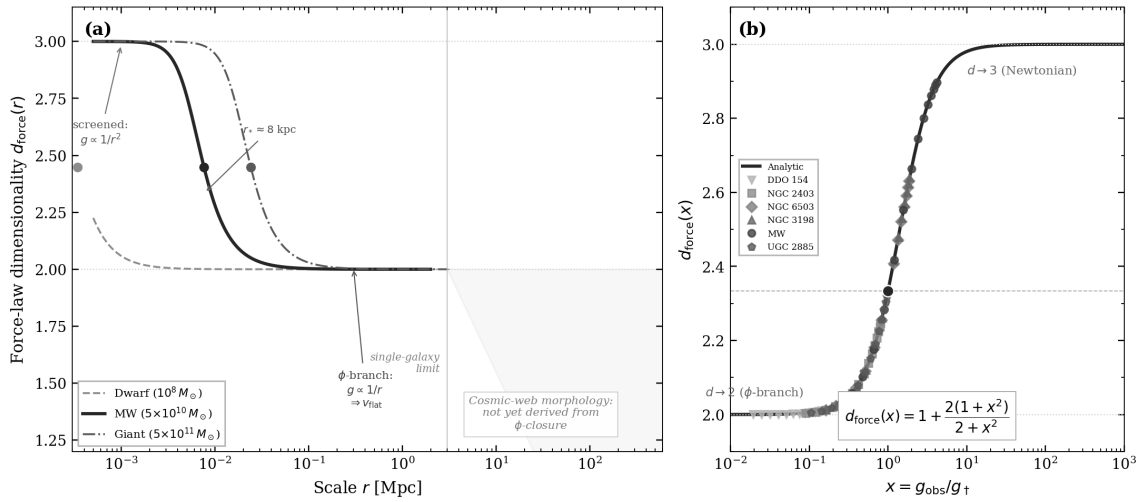


**Figure 17:** Force-law effective dimensionality in ECT. **(a)**  $d_{\text{force}}(r)$  for three galaxy masses, computed analytically from the  $\phi$ -closure  $\mu(g_{\text{obs}}/g_\dagger)g_{\text{obs}} = G_N M/r^2$ . In the screened regime ( $g_{\text{obs}} \gg g_\dagger$ ):  $d_{\text{force}} \rightarrow 3$  (Newtonian). Beyond the transition radius  $r_* = \sqrt{G_N M/g_\dagger}$  (filled dots):  $d_{\text{force}} \rightarrow 2$  ( $g \propto 1/r \Rightarrow v_{\text{flat}} = \text{const}$ ). At  $r_*$  (where  $x = g_{\text{obs}}/g_\dagger = 1$ ):  $d_{\text{force}} = 7/3 \approx 2.33$ . Curves fade beyond the isolation radius ( $\sim 1\text{--}3$  Mpc), where the single-galaxy approximation breaks down. The shaded region at  $r > 3$  Mpc indicates cosmic-web scales where  $d_{\text{force}}$  is not yet derivable from the present  $\phi$ -closure. **(b)** Universal curve  $d_{\text{force}}(x)$  with the closed-form analytic expression  $d_{\text{force}} = 1 + 2(1+x^2)/(2+x^2)$ ; every galaxy falls on the same curve, because the formula depends only on  $x = g_{\text{obs}}/g_\dagger$ , not on  $M$  or  $r$  separately. Different galaxies differ only in the mapping  $x(r)$ : heavier galaxies reach higher  $x$  at any given  $r$ . This universality is the dimensionality counterpart of the radial acceleration relation.

**Force-law effective dimensionality.** The effective dimensionality of the gravitational interaction in ECT is defined by the force-law exponent:

$$d_{\text{force}}(r) \equiv 1 - \frac{d \ln g_{\text{obs}}}{d \ln r}. \quad (16.22)$$

In  $d$  spatial dimensions the gravitational force scales as  $g \propto 1/r^{d-1}$ ; eq. (16.22) reads off  $d$  from the local force law.

**Universality of the force-law curve.** In the present closure, the fact that  $d_{\text{force}}$  is a universal function of the single variable  $x = g_{\text{obs}}/g^\dagger$  is tied to the single-mode ordered-branch structure identified in §14.6 (Universality Corollary). No additional scalar family of galactic-scale response parameters enters the force-law dimensionality itself. This universality is therefore a structural closure-level consequence, not yet a first-principles theorem of bare ECT.

**General formula.** *Note on interpolation function: the  $d_{\text{force}}$  analysis below uses the analytic closure  $\mu(x) = x/\sqrt{1+x^2}$  for analytical transparency. This should be read as an illustrative representative of the ECT-compatible interpolation class, not as a unique choice derived from first principles or from the full microscopic condensate dynamics. The qualitative dimensionality behaviour is closure-independent provided the required ECT asymptotics  $\mu \rightarrow 1$  and  $\mu \rightarrow x$  are satisfied.*

Starting from the  $\phi$ -closure  $\mu(x) g_{\text{obs}} = g_N(r)$  with  $x \equiv g_{\text{obs}}/g^\dagger$ , one obtains by logarithmic differentiation:

$$d_{\text{force}}(r) = 1 + \frac{p_N(r)}{1 + \frac{d \ln \mu}{d \ln x}}, \quad (16.23)$$

where  $p_N(r) \equiv -d \ln g_N / d \ln r$ . For a point mass  $p_N = 2$ . The derivation is given in Appendix AM.

**Closed-form result.** For the illustrative ECT-compatible closure  $\mu(x) = x/\sqrt{1+x^2}$  one finds  $d \ln \mu / d \ln x = 1/(1+x^2)$ , and therefore

$$d_{\text{force}}(x) = 1 + 2 \frac{1+x^2}{2+x^2} \quad (16.24)$$

for a point-mass Newtonian source  $p_N = 2$ . Thus:

- in the screened Newtonian regime  $x \gg 1$ :  $d_{\text{force}} \rightarrow 3$ , corresponding to  $g \propto 1/r^2$ ;
- in the deep critical regime  $x \ll 1$ :  $d_{\text{force}} \rightarrow 2$ , corresponding to  $g \propto 1/r$  and asymptotically flat rotation curves;
- at the transition point  $x = 1$ :  $d_{\text{force}}(1) = 1 + \frac{4}{3} = \frac{7}{3} \approx 2.33$ .

Thus the closure predicts a smooth crossover from an effectively three-dimensional Newtonian regime at large acceleration to an effectively two-dimensional force-law regime at low acceleration.

**Representative transition radii.** The characteristic transition radius

$$r_* = \sqrt{\frac{G_N M}{g^\dagger}}$$

marks the point at which the force law begins to leave the near-Newtonian regime. Representative values are of order  $r_*(10^8 M_\odot) \sim 0.3 \text{ kpc}$  (dwarf galaxy),  $r_*(5 \times 10^{10} M_\odot) \sim 8 \text{ kpc}$  (Milky Way),  $r_*(5 \times 10^{11} M_\odot) \sim 24 \text{ kpc}$  (massive elliptical). These scales place the transition squarely in the observable galaxy regime.

**Observational extraction and falsifiability.** In principle, the force-law dimensionality can be extracted directly from rotation-curve data through the logarithmic slope of the observed acceleration profile. The present closure predicts a monotonic transition from  $d_{\text{force}} \approx 3$  to  $d_{\text{force}} \approx 2$  with a universal shape as a function of  $x = g_{\text{obs}}/g^\dagger$ . A statistically significant and systematic departure from this universal curve would falsify the present single-mode  $\phi$ -closure. This falsifier applies only within the galactic regime where the single-galaxy branch approximation remains valid; it should not be extended unchanged into the cosmic-web domain.

**Status.** This force-law dimensionality is a macroscopic closure diagnostic (Level B), not a theorem about the microscopic topological dimension of the arena and not, by itself, a derivation of a finite universe boundary. It measures how the effective gravitational response interpolates between Newtonian and critical-branch behaviour.

**What is established and what remains open.** The finite-domain interpretation is a Level B cosmological scenario whose large-scale completion remains open (OP3) and should not be given the same weight as the force-law result below. By contrast, the force-law dimensionality formula  $d_{\text{force}}(x)$  is a concrete Level B closure result with a universal shape and directly testable galactic-scale consequences. What remains open is: (i) a first-principles derivation of any finite-domain boundary from bare P3; (ii) a full data-level extraction of  $d_{\text{force}}(x)$  from observed rotation-curve samples; (iii) the extension of the force-law dimensionality concept beyond the galactic branch to morphological or cosmic-web scales (OP8).

## 16.9 What is established and what remains open

### Physical interpretation

Cosmology in ECT should be read as the large-scale history of the ordered condensate branch and of its background variable  $\phi_b(z)$ . The strongest conceptual shift relative to  $\Lambda$ CDM is that the Lorentzian cosmological history is not fundamental: it begins only once the ordered branch is established. Accordingly, the pre-ordered / pre-Lorentzian regime, the homogeneous FLRW branch, the late-time dark-energy-like sector, the age apparatus, the Hubble-shift mechanism, and the JWST background effects are not independent ingredients but successive manifestations of the same ordered-branch background.

This unified reading should not be overstated. Some parts of the cosmological sector are already strict structural results, while others remain closure-level consequences of the present  $\phi$ -first macroscopic completion. The purpose of the present subsection is therefore not to introduce new cosmological claims, but to summarise which parts of the ECT cosmological programme are already established, which are benchmarked, and which remain open. It should therefore be read as a status synthesis of the chapter rather than as an additional derivational step. A detailed prediction-by-prediction table is given in §16.6. The present synthesis instead groups the chapter by epistemic status and by the role each result plays in the ordered-branch cosmological programme.

### Strictly established (Level A)

- (i) Once Lorentzian signature is treated as emergent rather than fundamental, the theory admits a pre-ordered / pre-Lorentzian configuration regime (§14.1).
- (ii) The baseline ordered cosmological branch is spatially flat:  $k = 0$  (§14.4).
- (iii) The primary ordered-branch vacuum manifold satisfies  $\pi_2(S^3) = 0$ , so the primary monopole channel is absent (§14.5).
- (iv) The linear ordered scalar branch contains a single scalar mode; consequently the ordered branch carries no independent isocurvature scalar of its own (§14.6).



- (v) The tensor perturbation sector propagates on the same causal cone as the ordered low-energy branch (§14.6).
- (vi) The Euclidean ordering functional admits a macrocoherent minimum, providing the structural core of the ECT horizon-resolution route (§14.3).

### Structural closure-level results (Level B)

- (i) The homogeneous FLRW branch of the  $\phi$ -first closure is well-defined and supplies the cosmological background equations (§16.1).
- (ii) The late-time amplitude sector obeys the no-phantom bound  $w_\phi \geq -1$  provided  $\omega(\phi) > 0$  (§16.1).
- (iii) The age of the Universe is reinterpreted as the duration of the Lorentzian ordered branch rather than the elapsed time since a fundamental singularity (§16.4).
- (iv) The quantities  $t_0$ ,  $t_U(z)$ ,  $t_{\text{gal}}(z_{\text{obs}}; z_{\text{form}})$ , and  $D_L(z)$  are all controlled by the same ordered-branch background  $H(z)$  (§16.4).
- (v) The Hubble-shift mechanism, the age shift, and the JWST background effects are structurally correlated because they are driven by the same condensate background  $\phi_b(z)$  (§16.5).
- (vi) The ordering transition supplies the strongest ECT-native Sakharov ingredient by naturally providing an out-of-equilibrium environment (§16.3).
- (vii) The qualitative three-stage condensate history (ordering  $\rightarrow$  stabilisation  $\rightarrow$  slow drift) is a structural feature of the present  $\phi$ -first cosmological closure (§16.2).
- (viii) The force-law dimensionality crossover  $d_{\text{force}} : 3 \rightarrow 7/3 \rightarrow 2$  is a concrete galactic/cosmological closure result of the present  $\phi$ -branch (§16.8).

### Benchmark-level numerical outcomes

- (i) Illustrative late-time closures give a Lorentzian branch age of order 13–14 Gyr depending on closure and  $H_0$ -mapping. Within the retained-band discussion (§16.5), the baseline- $H_0$  mapping is compatible with a branch age of about 13.5 Gyr and the alternative inferred- $H_0$  mapping with about 12.5 Gyr; see §16.4 and Appendix AH.
- (ii) The retained-band diagnostic-layer analysis yields an effective uniform- $\varepsilon$  compatibility window  $\varepsilon \in [0.0296, 0.0376]$  at  $1\sigma$  (§16.5); this is the headline cosmological output, replacing the earlier single-point benchmark phrasing.
- (iii) Within this retained band, the JWST extraction binds the lower edge ( $\varepsilon_{\text{JWST}} = 0.0296$ , two-sided) while the Hubble +  $r_s$  channel binds the upper edge (§16.5).
- (iv) The leading halo-abundance enhancement remains moderate (factor  $\sim 2$ – $3$ ), so the present ECT framework alleviates but does not yet fully resolve the JWST tension (§16.5).

All numbers in this block should be read as benchmark-level closure diagnostics, not as closure-independent ECT predictions.

## What remains open

- (i) A fully ECT-native derivation of the primordial spectrum, in particular  $n_s$ ,  $A_s$ , and  $r$  (§14.6, OP3).
- (ii) The nonequilibrium microdynamics of the ordering transition from bare P3.
- (iii) The microscopic origin of the effective closure functions, in particular  $U(\phi)$  and the full background history  $\phi_b(z)$  (OP3).
- (iv) A closure-independent late-time fit of the ECT background sector to the combined age / distance / Hubble / JWST data.
- (v) A first-principles ECT derivation of the baryon asymmetry  $\eta_B$ ; current results establish only a Sakharov-compatible environment plus benchmark leptogenesis consistency (§16.3, OP7).
- (vi) A fully self-consistent high-redshift completion of the background ansatz compatible with BBN and with the late-time Hubble sector.
- (vii) Fully nonlinear structure-formation calculations (N-body / hydrodynamic level) for the JWST regime.
- (viii) A first-principles derivation of any finite ordered-domain boundary and of its relation to the pre-Lorentzian regime (§16.8).

**Chapter-level synthesis.** The strongest ECT cosmological results are structural rather than numerical. The theory already fixes the existence of a pre-ordered regime, the flatness of the baseline branch, the absence of the primary monopole channel, and the single-scalar perturbation content of the ordered branch. The late-time cosmological sector is less complete but already structurally organised: age, distance, Hubble shift, and JWST timing/growth effects are not independent sectors but correlated consequences of one and the same ordered-branch background. The central remaining gap of the cosmological programme is therefore clear: an ECT-native perturbation spectrum and a fully microscopic ordering-transition dynamics.

## 17 Galactic and Astrophysical Phenomenology

**Scope and status of the galactic branch.** This chapter moves from the effective ordered-branch gravity sector of Section 13.5 to the astrophysical regimes in which the macroscopic amplitude variable  $\phi$  can become dynamically relevant on galactic and cluster scales. The structural role of  $\phi$  itself — its origin as a reparameterisation of the ordered-branch amplitude, its matter-driven ordering tendency, and the existence of a screened regime — is already motivated by the ordered-branch EFT architecture (Sections 13.5–13.4). The explicit galactic closure used below remains a Level B effective strategy rather than a first-principles derivation from bare P3.

**What is and is not claimed here.** The purpose of this chapter is not to present galactic phenomenology as an arbitrary MOND-like fit, nor to overstate it as a complete microscopic derivation. Rather, it shows that once the ordered branch, its amplitude response, and matter-induced ordering are admitted, a constrained nonlinear infrared branch can reproduce the baryonic Tully–Fisher relation (BTFR), the radial acceleration relation (RAR), individual galactic rotation curves, and the qualitative morphology of cluster-merger lensing offsets within a unified ordered-branch framework — with one fitted effective critical acceleration  $g_{\text{eff}}^\dagger$  per galaxy in the present galactic implementation and without introducing an additional particle dark-matter component within the present ordered-branch description. The detailed derivation chain is documented in Appendix A; the galactic closure and SPARC pipeline are given in Appendices AN and AO; the cluster-merger implementation is documented in Appendix AP. The implementation-level algorithms used across the numerical parts of the paper are collected in Appendix Y.

## 17.1 Galactic sector: the ordered-branch amplitude variable

*Status: the galactic sector is developed within the Level B ordered-branch amplitude closure, not yet as a first-principles derivation from bare P3. In the present practical SPARC implementation, the fitted galaxy-level quantity is the effective critical acceleration  $g_{\text{eff}}^\dagger$ ; the corresponding transition radius  $r_* = \sqrt{G_N M_{\text{bar}}/g_{\text{eff}}^\dagger}$  is a derived scale, not a primary parameter.*

For the structural origin of the macroscopic amplitude variable, its derived response factor, and the corresponding ordered-branch closure functions, see Appendix A (Sections AJ.1–AJ.4).

### The ordered-branch amplitude variable as the relevant galactic degree of freedom

In the ordered branch the macroscopic response is naturally parameterised by the amplitude ratio

$$\phi \equiv \frac{1}{\beta} \ln \frac{u}{u_\infty}, \quad F(\phi) = \frac{u}{u_\infty} = e^{\beta\phi}, \quad (17.1)$$

where  $u$  is the local ordered-branch amplitude and  $u_\infty$  is its asymptotic screened value. This variable is not introduced ad hoc for the galactic sector: it is the macroscopic amplitude coordinate associated with the ordered branch itself, and its kinetic and potential closures are inherited from the EFT reduction of the branch dynamics. The structural derivation yields a response factor  $F(\phi) = e^{\beta\phi}$  and a kinetic coupling  $\omega(\phi) = \omega_0 e^{2\beta\phi}$ , both of which are inherited from the ordered-branch EFT, not postulated.

**From the postulates to the galactic amplitude branch.** The galactic  $\phi$ -sector should be read as an ordered-branch EFT continuation of the postulate architecture, not as an independent phenomenological add-on. P4 fixes the ordered branch as the relevant macroscopic background, while P6 permits non-uniform ordered configurations and therefore makes spatially varying branch responses admissible within the effective ordered-phase description. Once matter is coupled in the effective field equations, inhomogeneous baryonic environments source spatially varying equilibrium configurations  $\bar{\phi}(\mathbf{x})$ . At the effective level, the quasistatic ordered-branch field equation takes the schematic matter-sourced form

$$\mathcal{K}(\phi) \square \phi \approx \frac{8\pi G_N}{c^4} \rho_{\text{bar}} \xi_1(\phi), \quad \xi_1 \sim O(1), \quad (17.2)$$

so that matter drives  $\bar{\phi} > 0$ : the condensate becomes more ordered near baryons (Level B from the effective field equations). This is the local source of both screening (dense environments) and the nonlinear infrared activation (dilute outskirts).

**Derived origin versus benchmark closure.** A crucial distinction should be kept explicit. The existence of the amplitude variable  $\phi$ , the exponential response factor  $F(\phi) = e^{\beta\phi}$ , and the matter-driven ordering tendency are structurally inherited from the EFT reduction of the ordered phase. By contrast, the simple practical kinetic/interpolating closure used in the present galactic fits — including the benchmark local form of the kinetic sector entering the SPARC pipeline — is only a local realisation of that branch and should not be confused with a completed first-principles derivation of the full macroscopic  $\phi$ -dynamics.

### Why the bare condensate-amplitude route fails

A direct galactic role of the heavy radial condensate mode is strongly disfavoured for two independent reasons.

First, under the phenomenological matching hypothesis  $\xi_{\text{cond}} \sim \ell_{\text{Pl}}$  used in the present ECT closure, the radial mode is extremely heavy, of order the microscopic cutoff, so it cannot naturally generate kpc-scale structure.

Second, an ordinary linear scalar-tensor realisation of the same sector falls into the Brans–Dicke-like regime and generically produces post-Newtonian deviations far too large for Solar-System data.

For these reasons the galactic branch of ECT is not built from the bare radial condensate amplitude itself, but from the nonlinear critical dynamics of the ordered-branch amplitude variable  $\phi$ , whose structural origin was given above. (For the detailed exploration and rejection of the direct  $u_0(r)$ -route, see Appendix A.3.) The resulting regime structure is shown in Fig. 18.

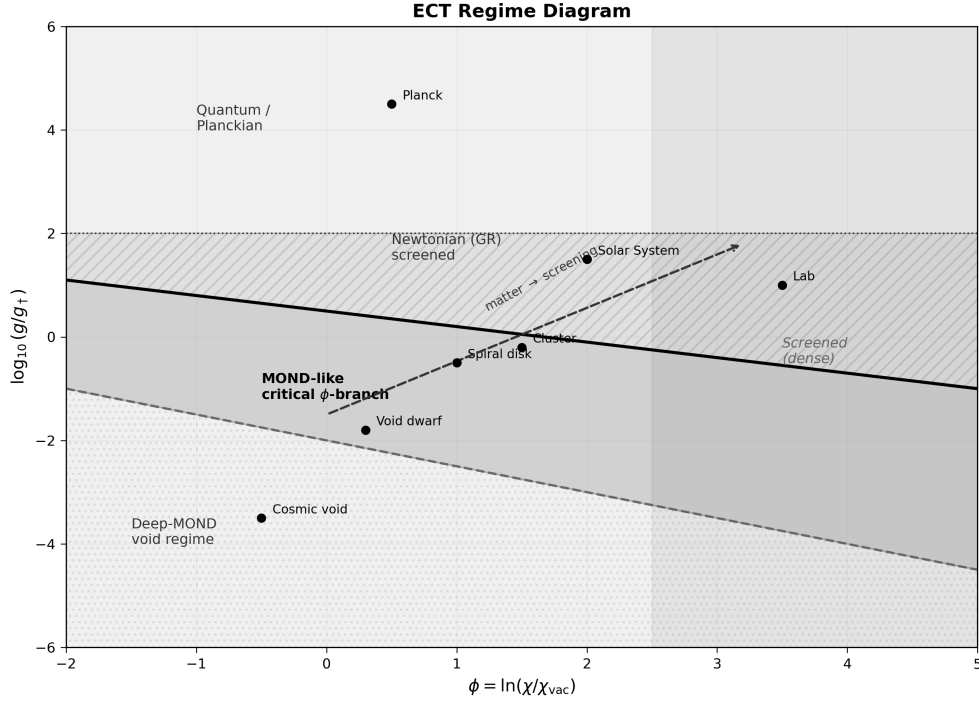


**Figure 18:** ECT regime diagram in the plane of the ordered-branch amplitude variable  $\phi$  and local acceleration  $g/g_+$ . Different physical regimes — Quantum/Planckian, Newtonian (GR), MOND-like critical branch, and deep-MOND / void — are controlled by the local condensate amplitude relative to its asymptotic screened value. Dense environments (high  $\phi$ ) are screened and recover standard GR; dilute outskirts and voids approach the critical boundary where the nonlinear  $\phi$ -branch activates. Representative astrophysical systems are indicated.

### Screening in dense environments

*Status: Level B (ordered-branch  $\phi$ -first closure). The screening mechanism follows from the matter-driven  $\phi$ -equation (17.2) under the quasi-static approximation; a first-principles derivation from bare P3 remains open (OP-screen).*

Since matter drives  $\bar{\phi}(\rho_m)$  upward (Appendix A), the ordered-branch amplitude variable acquires an effective mass for perturbations around the local equilibrium. Expanding  $\phi = \bar{\phi}(\rho_m) + \delta\phi$ , small fluctuations obey a Yukawa-type equation with effective mass (Level B):

$$m_\phi^2(\rho_m) = \frac{U_0''(\bar{\phi}(\rho_m)) + 4\pi\rho_m/\tilde{\chi}^2}{K(\bar{\phi}(\rho_m))}. \quad (17.3)$$

Equivalently, for an SI mass-density perturbation  $\delta\rho$ , one has  $\delta\rho_m = c^2\delta\rho$ . Both numerator terms are positive and increase with  $\rho_m$  for convex  $U_0$ ; in the one-loop estimate  $K \propto e^{-\phi/2}$ , which decreases at larger  $\bar{\phi}$  and thus reinforces the growth of  $m_\phi^2$  (Level B;  $U_0$  not yet derived from bare P3, OP3). Hence  $m_\phi$  grows with density, and the Yukawa screening length  $\lambda_\phi = 1/m_\phi$  shrinks in dense environments. This is the mechanism that screens the fifth-force contribution of  $\phi$  inside galaxies and in the Solar System, rendering the theory consistent with the Cassini bound [84] (Level B).

**Physical interpretation.** In the present framework, screening is not an external fix appended to save the theory. It is a direct consequence of the fact that dense matter holds the vacuum in a deep Lorentzian

phase, where the amplitude sector is effectively screened or frozen. The recovery of GR in the Solar System is therefore not in conflict with the existence of a nonlinear galactic branch; it is an expected feature of the same underlying mechanism.

**Benchmark screening scales.** Within the present Level B closure (see Appendix AQ), the density dependence of  $m_\phi(\rho)$  implies a strong hierarchy of screening lengths across environments. In dense laboratory and inner Solar-System conditions the corresponding screening length is driven far below AU scales, so that the scalar branch is effectively Yukawa-suppressed and post-Newtonian deviations are screened. On galactic outskirts the screening length can grow to kpc scales, comparable to the macroscopic scale of the system, opening the transition window in which the nonlinear infrared branch can activate. In low-density intergalactic and void-like environments the screening scale can exceed Mpc values, so that the near-critical branch remains accessible. These estimates should be read as order-of-magnitude consistency checks within the present closure, not yet as first-principles predictions.

**Relation to known screening paradigms.** Phenomenologically, the dense-environment suppression of the galactic scalar branch is closest to chameleon-type screening [108], in the sense that the effective scalar mass increases with ambient density and suppresses long-range fifth-force effects. The present mechanism is nevertheless structurally different: in ECT the screened field is not an extra scalar appended to GR by hand, but the ordered-branch amplitude response of the same condensate sector that also controls the infrared critical branch. It also differs from symmetron- and Vainshtein-type screening mechanisms [109, 110] in that the present suppression is tied directly to the ordered-branch amplitude response rather than to symmetry restoration or derivative self-screening of an extra field sector.

### Hierarchy of length scales

*Status: Level A for the identification of distinct physical scales; Level B for numerical estimates based on the  $\phi$ -first ordered-branch closure.*

The galactic closure of the macroscopic branch contains several physically distinct scales that must not be conflated.

- (i) **Microscopic condensate scale.** The correlation length of the heavy radial mode,  $\xi_{\text{cond}} \sim m_\sigma^{-1} \sim \ell_{\text{Pl}}$ , marks the breakdown of the coarse-grained geometric EFT. This scale plays no role in galactic dynamics.
- (ii) **Environmental screening length.** In regions of high baryonic density the  $\phi$ -branch is driven into the screened Newtonian regime; the corresponding Yukawa screening length  $\lambda_\phi(\rho) = m_\phi^{-1}(\rho)$  is density-dependent (Level B; eq. (17.3)). This scale governs Solar-System and laboratory suppression of the fifth-force correction.
- (iii) **Critical galactic transition scale.** The transition from screened Newtonian behaviour to the critical  $\phi$ -branch occurs where  $g_{\text{obs}} \sim g_{\text{eff}}^\dagger$ , with  $g_{\text{eff}}^\dagger$  itself an environment-modulated descendant of the cosmological baseline  $g_0^\dagger$ . The corresponding derived transition radius  $r_* = \sqrt{G_N M_{\text{bar}} / g_{\text{eff}}^\dagger}$  is secondary:  $g_{\text{eff}}^\dagger$  is the primary critical-scale variable.
- (iv) **Cosmological reference scale.** In the present closure, the baseline critical scale is  $g_0^\dagger \sim cH_0 / (2\pi)$ , which explains the quasi-universality of the galactic acceleration scale while still allowing environment-dependent deviations at the level of  $g_{\text{eff}}^\dagger$  (Level B).

The four scales form a clear hierarchy:

$$\xi_{\text{cond}} \ll \lambda_\phi(\rho) \lesssim r_* \ll H_0^{-1}. \quad (17.4)$$

**Physical significance.** This hierarchy explains why ECT can simultaneously exhibit: (i) a strongly ordered microscopic vacuum, (ii) screened Solar-System and laboratory behaviour, (iii) critical galactic  $\phi$ -branch phenomenology, and (iv) a quasi-universal cosmological acceleration scale. The success of the galactic closure depends precisely on keeping these scales conceptually distinct.

### One-loop bridge and breakdown near criticality

*Status: Level B (one-loop EFT estimate within the  $\phi$ -first macroscopic closure; the one-loop coefficient  $a \simeq 1/2$  is scheme-dependent and constitutes an open problem, OP-screen; see Appendix A.6).*

The next question is what happens as the ambient density decreases and the vacuum approaches the critical region. Integrating out the fast Goldstone modes generates a nontrivial kinetic response for  $\phi$  (the one-loop calculation is presented in Appendix A.6). At the one-loop level this can be parametrised as

$$K(\phi) \propto e^{-a\phi}, \quad a > 0, \quad (17.5)$$

with the one-loop estimate suggesting  $a \simeq 1/2$ . The precise coefficient is scheme-dependent (Level B; OP-screen) and should not be overinterpreted, but the qualitative structural point is robust (Level B): the effective quadratic kinetic sector acquires a strong  $\phi$ -dependence near the critical region.

Higher-order gradient terms become increasingly important in the same limit. A generic static expansion takes the form

$$\Gamma[\phi] = \int d^3x \left[ \frac{K(\phi)}{2} (\nabla\phi)^2 + \frac{L(\phi)}{3} |\nabla\phi|^3 + \dots \right]. \quad (17.6)$$

If the ratio  $L(\phi)/K(\phi)$  grows toward criticality (which is expected on general EFT grounds: near criticality, higher-gradient operators become increasingly sensitive to the small ordered-branch amplitude parameter and may therefore outgrow the quadratic sector, even if their detailed coefficients are not yet known from first principles), then the field-dependent transition gradient

$$|\nabla\phi|_{\text{trans}}(\phi) = \frac{K(\phi)}{L(\phi)} \xrightarrow{\phi \rightarrow -\infty} 0 \quad (17.7)$$

falls toward zero.

**Resolution of the regime-ordering problem.** This observation resolves a crucial difficulty that plagues constant-threshold nonlinear models. If the transition scale were a fixed constant, the nonlinear (MOND-like) regime would activate at *large* gradients (near masses) and the linear (Newtonian) regime at *small* gradients (far away) — the opposite of what is observed. With a field-dependent threshold:

- Near massive bodies ( $\bar{\phi} > 0$ , deep Lorentzian phase):  $|\nabla\phi|_{\text{trans}}$  is large, so the system stays in its linear screened branch.
- On galactic outskirts ( $\bar{\phi} \rightarrow 0^-$ , near-critical):  $|\nabla\phi|_{\text{trans}} \rightarrow 0$ , so even weak gradients activate the nonlinear branch.

This gives the physically correct ordering: GR near masses, MOND-like dynamics in dilute regions.

The exact scaling of  $L(\phi)$  is not yet fully derived from the microscopic theory; accordingly, this step should be viewed as EFT-supported rather than fully established. The essential requirement is the hierarchy  $L/K \rightarrow \infty$  near criticality, not any specific exponent.

### Critical infrared regime

*Status: Level B (critical infrared closure of the  $\phi$ -first ordered-branch programme). The  $Y_\phi^{3/2}$  critical kinetic form is supported by a scale-invariance argument, but not yet derived from bare P3 (OP2).*

Once the perturbative gradient expansion breaks down, it is natural to replace it by a critical infrared effective theory for the dimensionless order field  $\phi$ . Defining  $Y_\phi \equiv (\nabla\phi)^2$ , the deep-IR static free energy can be written as

$$F_{\text{IR}}[\phi] = \int d^3x \left[ \Lambda^4 \mathcal{F}\left(\frac{Y_\phi}{Y_*}\right) + U_{\text{eff}}(\phi; \rho) \right]. \quad (17.8)$$

**Scale-invariance argument (Level B).** At a 3D scale-invariant fixed point, if  $\phi$  is treated as dimensionless ( $[\phi] = 0$ ), then  $[Y_\phi] = L^{-2}$  and the free-energy density must have dimension  $L^{-3}$ . For a power-law  $\mathcal{F} \sim Y_\phi^p$ :

$$[Y_\phi^p] = L^{-2p} \stackrel{!}{=} L^{-3} \implies \boxed{p = 3/2}. \quad (17.9)$$

This is not a claim of absolute uniqueness among all conceivable nonlocal or logarithmically corrected structures. Rather, it is the unique simple local power-law form built only from  $Y_\phi$  that is consistent with 3D scale invariance when  $[\phi] = 0$ . (An anomalous dimension  $\Delta_\phi \neq 0$  would shift the exponent to  $p = 3/[2(1 + \Delta_\phi)]$ ; for an ordered-branch amplitude parameter this correction is expected to be small.)

**Physical interpretation.** The  $Y_\phi^{3/2}$  form means that at criticality the “cost” of a gradient in  $\phi$  grows faster than quadratic: the system resists non-uniformity in the degree of Lorentzianness more strongly than a linear theory would predict. This nonlinear stiffness is what produces the  $1/r$  force law needed for flat rotation curves.

**Uniqueness and observational corollary.** The role of the  $Y_\phi^{3/2}$  branch is stronger than a mere dimensional convenience. In three spatial dimensions it is the unique scale-invariant monomial built from the dimensionless amplitude variable  $\phi$ , and it is precisely this exponent that yields the deep-branch relation  $\mu(y) \rightarrow y$  and hence  $g \sim \sqrt{g_N g^\dagger}$ . The flat-curve asymptotics and the BTFR slope 4 are therefore not separate assumptions but direct corollaries of the same critical branch. In standard MOND-like frameworks [106, 111] the AQUAL equation structure is postulated; ECT reproduces the same effective structure as the critical infrared branch of the ordered-branch amplitude response.

**Source normalisation convention.** In the AQUAL-like equations below the symbol  $\rho$  denotes the ordinary baryonic mass density unless stated otherwise. The geometric source inherited from the Einstein trace is the curvature-density combination

$$\mathcal{S}_m \equiv \frac{G_N \rho}{c^2} = \frac{G_N \rho_m}{c^4}, \quad \rho_m \equiv \rho c^2.$$

Thus the right-hand side of Eq. (17.10) should be read as  $4\pi \mathcal{S}_m = 4\pi G_N \rho / c^2$ . In the local quasistatic trace-balance derivation of Appendix A, the same matter source is written in energy-density normalisation as  $\rho_m$ ; the two notations differ only by the fixed conversion factors shown above.

**Full interpolating equation.** The complete static equation, valid from the Newtonian to the deep-MOND regime, takes the AQUAL-like form

$$\boxed{\nabla \cdot \left[ \mu_\phi \left( \frac{|\nabla\phi|}{\phi_*(\phi)} \right) \nabla\phi \right] = \frac{4\pi G_N \rho}{c^2}}, \quad (17.10)$$

with

$$\mu_\phi(x) \rightarrow 1 \quad (x \gg 1), \quad \mu_\phi(x) \rightarrow x \quad (x \ll 1). \quad (17.11)$$

The key structural difference from standard MOND is that the transition scale  $\phi_*(\phi)$  depends on the local ordered-branch amplitude background. This field dependence is what makes the nonlinear branch appear in dilute near-critical regions rather than near dense sources.

**Environmental modulation as a programme-level ECT signature.** ECT does not predict a strictly universal MOND constant  $a_0$ . Instead, the critical acceleration is set by the cosmological baseline with environment-dependent modulation:

$$g_{\text{eff}}^\dagger = g_0^\dagger \Xi(\rho_{\text{env}}, \bar{\phi}_{\text{env}}, \dots), \quad g_0^\dagger \sim \frac{cH_0}{2\pi}. \quad (17.12)$$

This is one of the clearest observational distinctions from standard MOND-like frameworks with a fixed universal acceleration scale. In the current ECT galactic programme, the residual galaxy-to-galaxy variation of the fitted critical scale is not merely tolerated: a weak but systematic environment dependence is treated as a programme-level signature of the ordered-branch route (F1 in Table 74). This makes group environment, external-field context, and cluster membership part of the observational test of the theory rather than nuisance contamination.

**Status summary.** At the current stage the galactic branch of ECT should be read as a structurally motivated but still Level B programme. What is already structurally established or strongly supported at the present level is: the ordered-branch amplitude variable  $\phi$ , the matter-driven tendency toward increased ordering in dense environments, the presence of a screened regime within the present ordered-branch closure, and the deep critical branch that reproduces the MOND-like weak-field asymptotics ( $Y_\phi^{3/2}$ ) at the current Level B effective level. What remains open is the full first-principles derivation of the interpolating closure from bare P3, the non-perturbative bridge between the perturbative ordered branch and the critical infrared fixed point (OP2, OP3), and the quantitative environment dependence of  $g_{\text{eff}}^\dagger$  (OP-screen).

## 17.2 Cluster-merger lensing test

*Status: Level B (algebraic  $\phi$ -closure; morphology robust; amplitude order-of-magnitude estimate). Full quantitative conclusions require a 3D metric- $\phi$  solver (OP22).*

**Bridge to the galactic ordered-branch closure.** The cluster-merger test should not be read as an independent add-on to the theory. It probes the same ordered-branch  $\phi$ -sector introduced in Section 17.1: the same matter-responsive amplitude branch, the same critical-threshold logic, and the same algebraic enhancement class are here projected onto a merger-lensing geometry. In that sense, the cluster analysis is a scale-transfer test of the same ordered-branch closure rather than a separate phenomenological module. For the structural origin of the  $\phi$ -branch and its closure logic, see Appendix A; for the cluster-specific numerical implementation, see Appendix AP.

The Bullet Cluster [112, 113] ( $z = 0.296$ ) provides the canonical test of the matter distribution in a post-collision system: hot X-ray gas, decelerated by ram pressure, is spatially offset from the compact collisionless BCG/galaxy concentrations by  $\Delta \approx 100\text{--}150\text{ kpc}$ . Gravitational-lensing reconstruction places the convergence peaks near the BCG positions rather than the gas clouds [114], traditionally interpreted as evidence for a collisionless dark-matter component.

In ECT, the same morphology arises from the universal  $\phi$ -branch enhancement without invoking a hidden species. The effective convergence is (Appendix AP):

$$\Sigma_{\text{eff}}(x, y) = v \left( \frac{g_N}{g_\dagger^{\text{cl}}} \right) \Sigma_b(x, y), \quad (17.13)$$

where  $g_N = 2\pi G \Sigma_b$  is the projected Newtonian field,  $v(y) = \sqrt{(1 + \sqrt{1 + 4/y^2})/2}$  (AP.3) is the algebraic  $\phi$ -closure enhancement, and  $g_\dagger^{\text{cl}}$  is the cluster-scale critical acceleration. Here  $v(y)$  should be understood as the algebraic representative of the present ECT-compatible  $\phi$ -closure class at Level B, not yet as a uniquely derived final interpolation law; its role in this subsection is to provide the simplest projected benchmark for the merger morphology test. In the present analysis  $g_\dagger^{\text{cl}}$  is treated as the cluster counterpart of the same critical-branch threshold that governs the galactic sector, held fixed across the four-cluster



suite rather than fitted per system. At the conceptual level, this should be read as the cluster-environment value of the same effective critical scale discussed in Section 17.1: in a more complete treatment one expects  $g_{\dagger}^{\text{cl}} \sim g_{\text{eff}}^{\dagger} = g_0^{\dagger} \Xi(\rho_{\text{env}}, \bar{\phi}_{\text{env}}, \dots)$  evaluated in the merger environment. In the present four-cluster benchmark, however,  $g_{\dagger}^{\text{cl}}$  is simply held fixed across the suite in order to isolate the morphology test from system-by-system retuning. Because  $v$  depends on local surface density rather than on total enclosed mass, the ECT lensing signal preferentially traces the more compact component. In Bullet, MACS J0025, and El Gordo this is the BCG/stellar core, whereas in Abell 520 it is the central gas core. This is not a post-hoc adjustment: the same functional form of  $v$  that organises the galactic sector is carried over to the cluster geometry.

**Four-cluster suite.** The same protocol is applied without modification to four post-collision systems spanning  $z = 0.20\text{--}0.87$  (Table 136). The key numerical results are (Figures 19, 20):

- (i) **All four systems are reproduced at the qualitative morphological level**, with the correct identification of the peak-bearing component (BCG-peaked or gas-peaked, depending on which component is locally more compact). For Bullet, MACS J0025 [115], and El Gordo [116] the  $\kappa$ -peaks are associated with the compact BCG concentrations ( $d_{\star}^{\text{ECT}} \lesssim 37 \text{ kpc}$ ; observed  $d_{\star}^{\text{obs}} < 25\text{--}35 \text{ kpc}$ ; order-of-magnitude consistent). For Abell 520 [117, 118] the  $\kappa$ -peak falls on the *gas core*, because in this system the central gas is more compact than the dispersed BCG distribution. Both morphological regimes arise from the single function (17.13) with no per-system tuning. We therefore regard the four-cluster suite as a qualitative morphology test rather than a precision fit.
- (ii) **Abell 520 as a unified discriminant.** Abell 520 is a direct tension point for collisionless dark-matter models, because its dominant lensing peak coincides with the gas-rich core rather than with the galaxy concentrations that should trace a collisionless hidden component [117, 118]. In ECT this is the expected result: the gas core is locally more compact ( $\Sigma_{\text{gas}}(0) > \Sigma_{\text{BCG}}(0)$ ), so  $v$  enhancement is largest there. A single rule generates the BCG-peaked morphology in Bullet, MACS J0025, and El Gordo, and the gas-peaked morphology in Abell 520—a unified prediction absent in models requiring a fixed collisionless species.
- (iii) **Amplitude.** The baseline  $\phi$ -closure gives  $M_{\text{ECT}}/M_{\text{obs}} \approx 0.42\text{--}0.71$ , depending on baryonic concentration. After applying uniform ECT-specific corrections (Table 137), the estimates reach  $\approx 0.54\text{--}0.87$ . These numbers are order-of-magnitude estimates from a projected algebraic closure; they should be read as rough indicators, not precision predictions. In particular, MACS J0025 and Abell 520 reach  $M_{\text{ECT}}/M_{\text{obs}} \approx 0.86$  and  $0.87$  respectively, approaching full closure within the accuracy of these order-of-magnitude estimates. Bullet and El Gordo retain a deficit of  $\times 1.87$  and  $\times 1.79$ , identifying dynamically extreme high-redshift mergers as the sharpest remaining test cases. The residual deficit is comparable to the well-known MOND cluster mass discrepancy (factor  $\sim 2$ , [119, 120]), suggesting a common open problem for baryon-based modified-gravity frameworks at merger scales rather than a failure specific to ECT.

**Relation to the MOND cluster problem.** A residual factor-of-two mass deficit at cluster scale is well known in MOND-like baryon-only frameworks [119, 120]. The present ECT amplitude deficit is therefore not, by itself, a distinctive failure mode. What distinguishes ECT is that the cluster-scale critical threshold need not remain strictly universal in dense merger environments, and that the ordered-branch orientation stress sector  $\Theta_{\mu\nu}[n]$  provides an additional source of gravitational slip absent from the minimal MOND/AQUAL setup. The present cluster analysis should therefore be read as a morphology-level success together with a quantitative amplitude target for the next stage of the programme, rather than as a no-go result.

**Summary.** Taken together, the cluster-merger suite supports the following picture: ECT already reproduces the observed qualitative merger morphologies in both BCG-peaked and gas-peaked systems through

a single universal surface-density response rule. What remains open is the quantitative amplitude problem at the level of a residual factor  $\sim 1.1\text{--}1.9$ , depending on the system. We therefore regard cluster mergers not as a no-go result for ECT, but as a sharply defined Level B qualitative success in morphology together with a concrete quantitative target for the next generation of 3D metric- $\phi$  calculations (OP22). Practically, OP22 means solving the coupled metric- $\phi$  response on a genuinely three-dimensional merger geometry, with time-dependent gas/BCG separation and line-of-sight projection treated dynamically rather than through the present projected algebraic proxy.

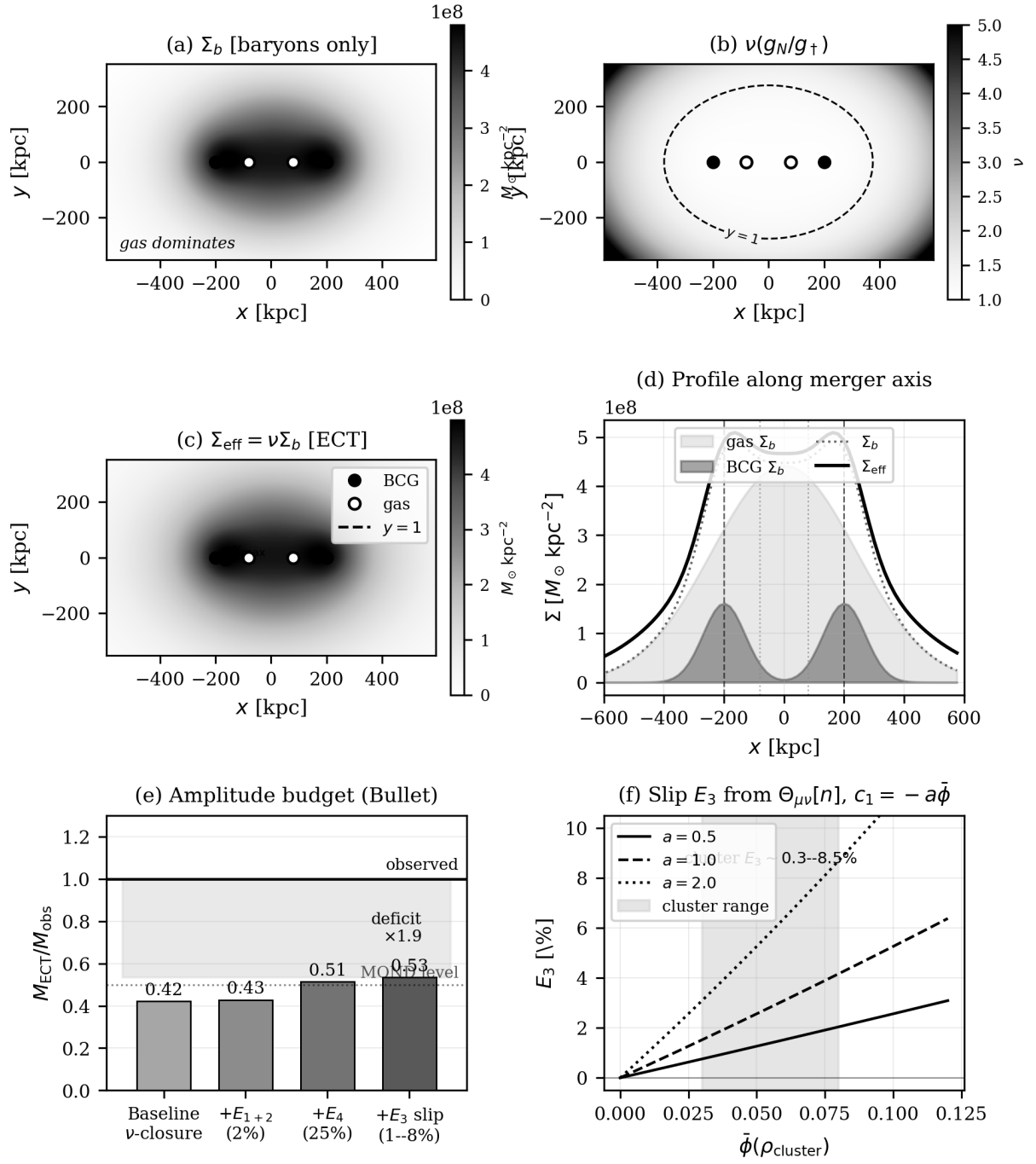
**Observational corrections.** Four ECT-specific effects partially reduce the apparent amplitude deficit (summarised and discussed in Appendix AP):

- (a)  $G_{\text{eff}}(z)$  modifies  $\Sigma_{\text{crit}}$  by  $\approx +0.5\%$  at  $z = 0.30$  (Level B).
- (b) The redshift anomaly  $\delta z = \frac{1}{2}\delta\phi$  shifts the spectroscopic gas temperature by  $\lesssim 1\%$ .
- (c) Post-merger non-equilibrium and non-thermal pressure uncertainties contribute  $+15\text{--}25\%$  to the inferred gas mass (observational systematics).
- (d) The anisotropic orientation stress  $\Theta_{\mu\nu}[n]$  (13.23) provides a natural ECT source of gravitational slip. A minimal Einstein-aether-like mapping with density-dependent  $c_1(\bar{\phi}) = -a\bar{\phi} < 0$  yields a rough Level B estimate  $E_3 \approx +0.3\text{--}+8.5\%$  for  $a \sim 0.5\text{--}2$  (parametrised, not derived; OP-c1).

**Explicit role of the full nonlinear field equations.** Of the four corrections listed above, correction (d)—the gravitational slip  $E_3$  from the orientation stress  $\Theta_{\mu\nu}[n]$ —is the only one that explicitly invokes the full nonlinear structure of the generalised field equations (13.35) beyond the scalar  $\phi$ -closure. This makes cluster-merger lensing the most direct observational probe of the tensor sector of the ECT field equations within the present programme. The estimate  $E_3 \approx +0.3\text{--}+8.5\%$  (Level B; OP-c1) is derived in Appendix AP.5 from the Einstein-aether-like mapping (AP.7) with the phenomenological ansatz  $c_1(\bar{\phi}) = -a\bar{\phi}$ . The baseline  $\phi$ -closure already produces the correct morphology in all four systems—BCG-peaked in Bullet, MACS J0025, and El Gordo, and gas-peaked in Abell 520. The  $E_3$  term from  $\Theta_{\mu\nu}[n]$  acts as an amplitude correction, not as a morphology-switching mechanism: in Abell 520 the gas-peaked morphology is generated by the baseline surface-density response, and  $E_3$  only modestly strengthens the amplitude ratio. For the near-closure systems (Abell 520, MACS J0025) the additional slip contribution is useful; for dynamically extreme systems (Bullet, El Gordo) the correction is insufficient to close the residual deficit, which remains a target for the 3D metric- $\phi$  programme (OP22).

We emphasise that ECT does *not* predict that the lensing  $\kappa$ -peak must universally track the gas (as in modified-gravity mechanisms without dark matter), nor that it must universally track the galaxy/BCG component (as in collisionless CDM): the structural statement is that the peak follows the *more compact* baryonic component, whichever that is, and the observed heterogeneity of cluster morphologies (BCG-peaked in Bullet, MACS J0025, El Gordo; gas-peaked in Abell 520) is a direct consequence of this morphology-dependent rule rather than of independent per-cluster tuning.

For a systematic comparison of the orientation-stress role across all sectors, see §13.5.



Filled circles = BCG (collisionless); open circles = X-ray gas (collisional)

**Figure 19:** ECT  $\phi$ -closure analysis of the Bullet Cluster ( $z = 0.296$ ; parameters from Table 136). **(a)** Baryonic surface density  $\Sigma_b$ ; gas dominates by total projected mass. **(b)** Enhancement factor  $\nu(g_N/g_{\dagger}^{\text{cl}})$ ; dashed contour marks the  $g_N/g_{\dagger}^{\text{cl}} = 1$  transition. **(c)** Effective convergence  $\Sigma_{\text{eff}} = \nu\Sigma_b$ ; the  $\kappa$ -peak (circle) lies  $d_{\star} = 37\text{kpc}$  from the BCG vs  $d_{\text{gas}} = 83\text{kpc}$  from the gas peak. **(d)** 1D merger-axis profile. **(e)** Amplitude budget: successive corrections raise  $M_{\text{ECT}}/M_{\text{obs}}$  from 0.42 (baseline) to  $\approx 0.54$ ; residual deficit  $\times 1.9$  (OP22). **(f)** Gravitational slip  $E_3$  from the orientation stress  $\Theta_{\mu\nu}[n]$  with  $c_1(\bar{\phi}) = -a\bar{\phi}$ ; shaded band marks the cluster range  $\bar{\phi} \simeq 0.03\text{--}0.08$ . Filled circles: BCG (collisionless). Open circles: X-ray gas (collisional).

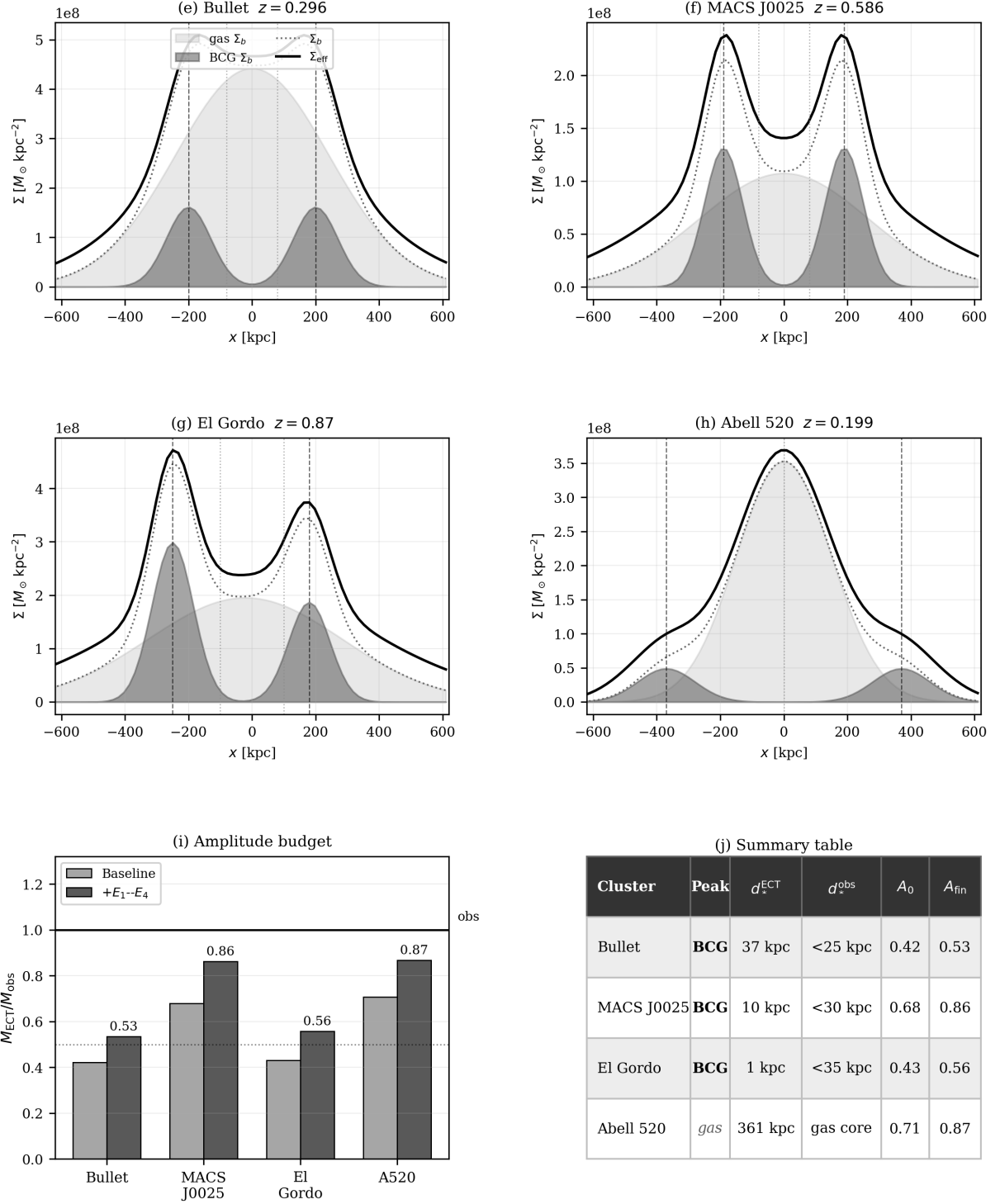


**Figure 20:** ECT  $\phi$ -closure applied uniformly to four merging cluster systems (same protocol, no per-system tuning; parameters: Table 136). **(e–h)** Merger-axis profiles:  $\Sigma_{\text{eff}}$  (solid) tracks the denser component in every system—BCG in Bullet, MACS J0025 [115], and El Gordo [116]; gas core in Abell 520 [117]. **(i)** Amplitude budget: light bars = baseline  $A_0$ ; dark bars =  $A_{\text{fin}}$  after corrections (Table 137); solid line = observed target. **(j)** Summary table: ECT predicted and observed  $\kappa$ -peak offsets and amplitude ratios. Abell 520 (*gas*, italicised) is the only system where the  $\kappa$ -peak follows the gas core; this is the correct observed morphology for this system and arises from the same physics as the BCG-peaked cases—a unified discriminant prediction of ECT.

### 17.3 Galactic dynamics: BTFR, rotation curves, and the effective critical scale

*Status overview.* The present galactic programme has three distinct layers that should not be conflated.

**(i) Structural ordered-branch content:** the existence of a screened regime, a critical infrared branch, and the associated deep-acceleration asymptotics belong to the current ordered-branch macroscopic logic and are supported at Level A/B. **(ii) Effective galactic closure:** the AQUAL-type functional, its interpolation family, and the practical acceleration-space closure used for galaxy phenomenology are Level B constructions built on that ordered-branch logic. **(iii) Data interface:** the fitted per-galaxy quantity  $g_{\text{eff}}^\dagger$  belongs to the present SPARC implementation and is therefore Level B/Open as an observational interface, not yet a first-principles prediction from the bare ECT action. What remains open is the exact global interpolation law across the transition region and the first-principles environment dependence that maps the baseline critical scale  $g_0^\dagger$  to the fitted galaxy-level values  $g_{\text{eff}}^\dagger$  (OP3).

**Scope.** The structural origin of the ordered-branch amplitude variable  $\phi$ , the matter-driven ordering tendency, screening, and the critical IR branch were established in Section 17.1. The present subsection builds on that foundation to derive the explicit algebraic consequences — AQUAL field equation, BTFR, and the practical closure used for SPARC rotation-curve fitting — and to present the numerical results. For the ordered-branch derivation backbone, see Appendix A.

**Notation for the critical scale.** In this subsection,  $g^\dagger$  denotes the generic critical-branch acceleration scale in formal derivations,  $g_0^\dagger$  denotes the cosmological baseline value, and  $g_{\text{eff}}^\dagger$  denotes the galaxy-level effective scale extracted in the practical SPARC closure. The distinction is essential: the baseline is structural, whereas the per-galaxy value belongs to the current Level B data interface.

#### Derivation chain: from the ordered-branch $\phi$ -closure to RAR and BTFR

The galactic sector of ECT follows a logical chain that should be distinguished from a postulated MOND interpolation law:

- (I) **Effective galactic functional.** In the quasi-static weak-field galactic regime the branch response is described by an effective nonlinear functional:

$$S_{\text{gal}} = \int d^3x \left[ -\rho_b \Phi - \frac{1}{8\pi G_N} \mathcal{F}(Y) \right], \quad Y \equiv \frac{(\nabla\Phi)^2}{g_\dagger^2}. \quad (17.14)$$

- (II) **Deep-branch scale-invariant representative closure.** On the critical branch, if one requires that no new galactic acceleration scale enter beyond  $g_\dagger$ , the simplest scale-invariant representative member of the ECT-compatible nonlinear family is

$$\mathcal{F}(Y) \propto Y^{3/2}. \quad (17.15)$$

This is a strong Level B closure choice motivated by the critical ordered-branch logic, not yet a unique theorem of the bare action.

- (III) **General AQUAL field equation.** Varying (17.14) gives:

$$\nabla \cdot \left[ \mu \left( \frac{|\nabla\Phi|}{g_\dagger} \right) \nabla\Phi \right] = 4\pi G_N \rho_b, \quad (17.16)$$

with ECT-derived asymptotic limits:

$$\mu(y) \rightarrow 1 \quad (y \gg 1), \quad \mu(y) \rightarrow y \quad (y \ll 1). \quad (17.17)$$

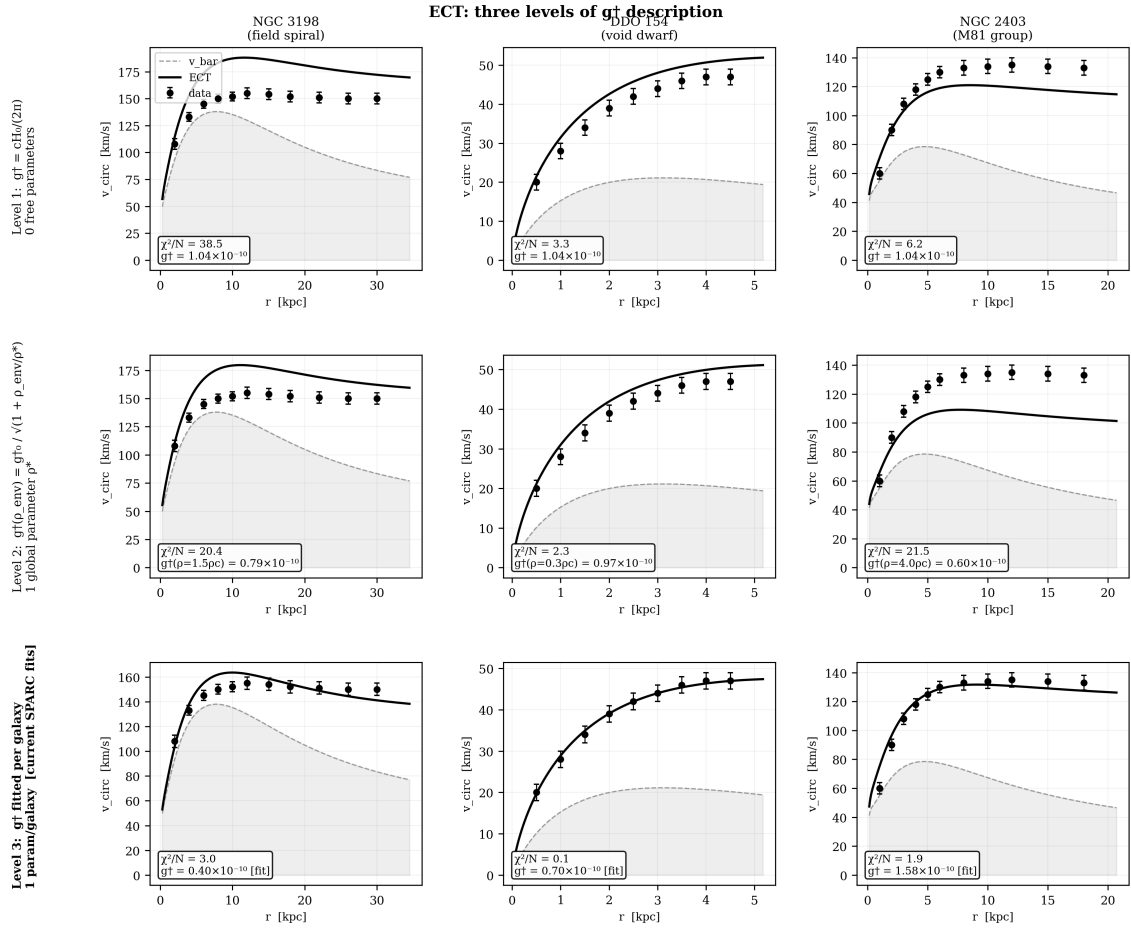
These are the ECT-native content; the exact global form of  $\mu(y)$  across the transition region is a representative member of the ECT-compatible class and is not yet uniquely fixed (OP3).

- (IV) **RAR asymptotics.** For near-spherical symmetry,  $g = |\nabla\Phi|$ ,  $g_N = G_N M_b(<r)/r^2$ , the field equation gives:

$$\mu\left(\frac{g}{g_\dagger}\right)g = g_N. \quad (17.18)$$

Newtonian limit:  $g \gg g_\dagger \Rightarrow g \simeq g_N$ . Deep branch:  $g \ll g_\dagger \Rightarrow g \simeq \sqrt{g_N g_\dagger}$ .

- (V) **BTFR.** On the flat part of a rotation curve the deep-branch limit gives directly  $v_\infty^4 = G_N M_b g_\dagger$  (see the explicit derivation below).
- (VI) **Status of the critical scale.** ECT does not predict a strictly universal MOND constant. Instead, the practical galaxy-level scale is interpreted as an environment-modulated descendant of the cosmological baseline, as in eq. (17.12), where  $g_0^\dagger \sim cH_0/(2\pi)$  is the baseline critical scale established in Section 17.1 (Fig. 21). The galaxy-to-galaxy scatter in fitted  $g_{\text{eff}}^\dagger$  is therefore interpreted in the present ECT programme as a meaningful signature rather than automatically as a shortcoming.



Baryonic masses from SPS + HI surveys (no mass fitting). Level 1:  $g_{\dagger}^{\dagger} = cH_0/(2\pi)$  from ECT phase winding (P4+BR1). Level 2: environment correction, one global scale  $\rho_*$ . Level 3: per-galaxy fit (= current SPARC fits in paper).

**Figure 21:** ECT rotation-curve hierarchy for three representative galaxies. **Row 1 (Level 1):** universal baseline  $g_0^{\dagger} = cH_0/(2\pi)$ , zero free parameters. DDO 154 (void dwarf) is already well reproduced ( $\chi^2/N \lesssim 4$ ); residuals in the other systems reflect environment effects predicted by ECT. **Row 2 (Level 2):** environment-dependent  $g_{\dagger}(\rho_{\text{env}}) = g_0^{\dagger} / \sqrt{1 + \rho_{\text{env}}/\rho_*}$  with one global parameter  $\rho_*$ ; all three systems improve, illustrating that a one-parameter environment law can account for part of the observed scatter in  $g_{\dagger}^{\text{eff}}$ . This should be read as a representative benchmark, not yet as a first-principles demonstration of the unique environment source. **Row 3 (Level 3):**  $g_{\dagger}^{\text{eff}}$  fitted per galaxy (current SPARC analysis, Figs. 23–26), giving optimal  $\chi^2$ . Baryonic masses from SPS photometry and HI surveys (no mass fitting). The progression  $\chi^2/N$ : Level 1  $\rightarrow$  Level 2  $\rightarrow$  Level 3 quantifies the contribution of environment physics to the galactic acceleration scale. Unlike MOND, the present ECT programme allows and physically motivates an environment-dependent effective critical scale. Equation (17.26) is the current minimal Level-B representative law for that dependence, not yet its unique first-principles derivation. The non-universality of  $g_{\dagger}^{\text{eff}}$  is therefore a programme-level ECT signature rather than a completed theorem.

As established in Section 17.1 (eq. (17.2)), matter drives  $\bar{\phi} > 0$  through the effective ordered-branch field equation, thereby stabilising the Lorentzian/macrosopic branch in dense environments. That sourcing underpins both the screened regime and the activation of the nonlinear infrared branch used below.

### Effective critical-branch Lagrangian

The deep-branch critical form  $\mathcal{F} \propto Y_{\phi}^{3/2}$  was motivated in Section 17.1. In the present effective galactic language the Lagrangian for  $\phi$  takes the form:

$$\mathcal{L}_{\phi} = \frac{\bar{M}_{\text{Pl}}^2}{2} \mathcal{F}(Y_{\phi}), \quad Y_{\phi} \equiv -\frac{(\partial_{\mu}\phi)^2}{2M_{\phi}^4}. \quad (17.19)$$

In the critical branch  $\mathcal{F} = A_{\text{ECT}} Y_\phi^{3/2}$ :

$$\mathcal{L}_\phi^{\text{crit}} = -\frac{\bar{M}_{\text{Pl}}^2 A_{\text{ECT}}}{2M_\phi^4} |(\partial_\mu \phi)^2|^{3/2}, \quad (17.20)$$

which is the effective galactic realisation of the same ordered-branch critical dynamics and reproduces the MOND-like deep-acceleration asymptotics at Level B.

### Baryonic Tully–Fisher relation as a corollary of the deep ECT branch

*Status: Level B. The slope 4 is a strong structural result; the normalisation depends on the effective critical scale  $g_{\text{eff}}^\dagger$  and is therefore currently Level B pending the full derivation of the environment law  $\Xi(\rho_{\text{env}}, \bar{\phi}_{\text{env}}, \dots)$ .*

In ECT the baryonic Tully–Fisher relation is not an independent phenomenological input. It follows directly from the deep-branch limit of the galactic field equation (Section 17.3). In the low-acceleration regime  $g \simeq \sqrt{g_N g_\dagger^\dagger}$ , and for the asymptotically flat part of a rotation curve:

$$\frac{v_\infty^2}{r} = \sqrt{\frac{G_N M_b}{r^2}} g_\dagger^\dagger. \quad (17.21)$$

Hence

$$v_\infty^4 = G_N M_b g_\dagger^\dagger. \quad (17.22)$$

The asymptotic BTFR slope of 4 is an algebraic consequence of the deep-branch field equation once the accepted critical closure is in place. It is therefore structurally stronger than the present fit-level normalisation, which still passes through the effective critical scale. The observed normalisation and residual scatter then probe the still-open environment dependence of the effective critical scale  $g_{\text{eff}}^\dagger$  and its relation to the baseline  $g_0^\dagger$  (OP3).

The overall normalisation is Level B at present, because it passes through the critical acceleration scale. At the structural level the baseline value is  $g_0^\dagger \sim cH_0/(2\pi)$ , while in the practical galactic implementation the relevant quantity is the environment-modulated effective scale  $g_{\text{eff}}^\dagger = g_0^\dagger \Xi(\rho_{\text{env}}, \bar{\phi}_{\text{env}}, \dots)$ . ECT therefore yields not only the BTFR itself, but also a route by which a physically meaningful residual scatter around the mean relation can arise through the effective critical scale, rather than an exactly universal MOND constant.

**Numerical bridge to the SPARC fits.** The galactic SPARC analysis below provides a direct numerical realisation of this analytic result. The BTFR slope remains structural (Level B), while the scatter in the normalisation is interpreted within the present ECT programme as a signature of environment-dependent  $g_{\text{eff}}^\dagger$  rather than a failure of the framework.

The resulting BTFR test (Fig. 22) shows that the new galactic closure reproduces the expected quartic scaling in a numerically stable way. Because the present implementation uses an internal outer-mass proxy  $M_{\text{bar,eff}}$  derived from the same fitted SPARC decomposition, this plot should be interpreted as a self-consistency test of the new ECT galactic machinery rather than as the final catalogue-level BTFR benchmark. The latter can be added later by replacing  $M_{\text{bar,eff}}$  with an independently tabulated total baryonic mass.

**Role of the full nonlinear field equations.** In the quasistatic, nearly spherical regime relevant for galactic rotation curves, the anisotropic orientation stress  $\Theta_{\mu\nu}[n]$  (13.23) provides an additional source term in the Poisson equation beyond the scalar  $\phi$ -closure. However, in the present phenomenological parametrisation the galactic sector is fitted through the effective critical scale  $g_{\text{eff}}^\dagger$ , and any systematic shift from  $\Theta_{\mu\nu}$  is absorbed into the calibration of that scale. The BTFR slope 4 remains structurally robust: it follows from the deep-branch asymptotics  $g \simeq \sqrt{g_N g_\dagger^\dagger}$  and is preserved provided the orientation-stress



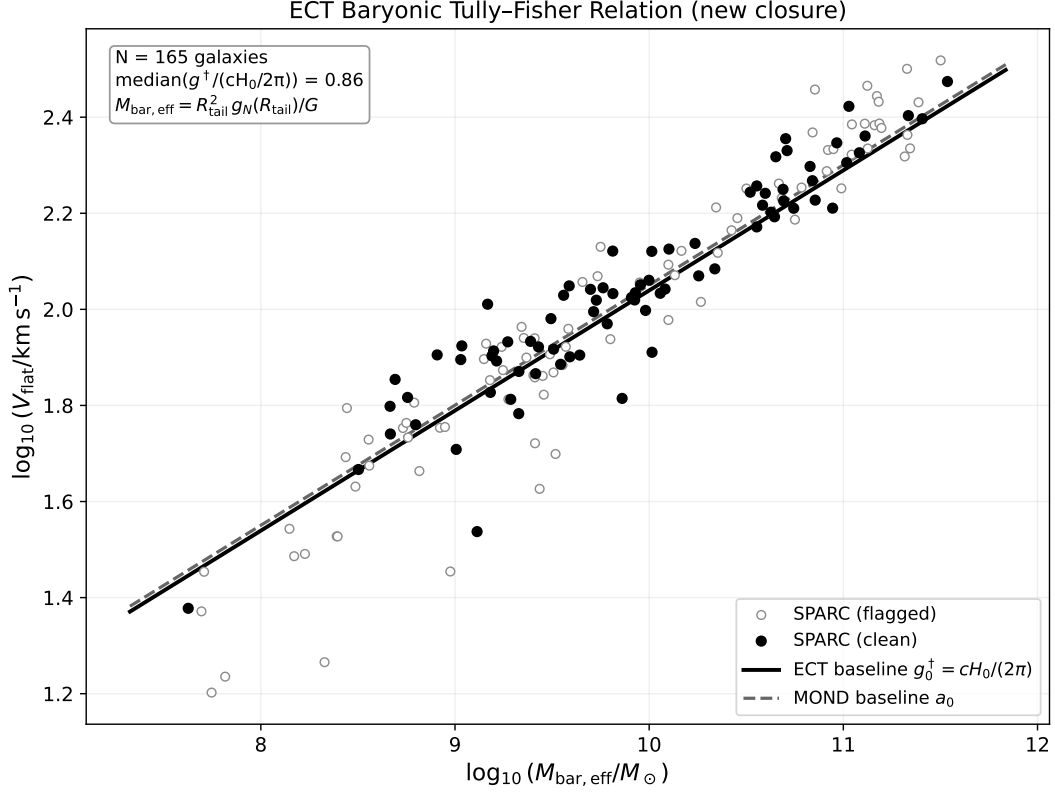


**Figure 22:** ECT BTFR test from the new SPARC galactic closure. The points show the effective outer baryonic mass proxy  $M_{\text{bar,eff}} = R_{\text{tail}}^2 g_N(R_{\text{tail}})/G_N$  inferred from the same baryonic decomposition used in the rotation-curve fits, plotted against the observed outer-tail velocity estimator  $V_{\text{flat}}$ . The solid line shows the ECT baseline relation  $V_{\text{flat}}^4 = G_N M_{\text{bar,eff}} g_0^\dagger$  with  $g_0^\dagger = cH_0/(2\pi)$ , while the dashed line shows the MOND reference line with  $a_0$ . This figure should be read as an internally consistent BTFR test of the new ECT closure, not yet as a replacement for the standard catalogue-level BTFR built from an independent global baryonic-mass table.

contribution acts as a slow renormalisation of  $g_{\text{eff}}^\dagger$  rather than as a modification of the deep-branch power-law index. At the present closure level no separate NLEE-induced change of the deep-branch exponent has been identified. The most natural non-degenerate signature of the orientation stress in the galactic sector is environment-dependent modulation of  $g_{\text{eff}}^\dagger$ , contributing to galaxy-to-galaxy scatter beyond the environment law  $\Xi$ . Within the present phenomenological galactic closure, a separately identifiable numerical correction from the full nonlinear equations to the rotation-curve, RAR, or BTFR results is not extractable. This is a conclusion within the current closure, not a universal theorem of ECT. A detailed justification is given in Appendix AN.8; for a systematic overview, see §13.5.

### Practical ECT closure for rotation curves

The benchmark algebraic closure used below is derived and documented in Appendix AN.

The galactic sector of the  $\phi$ -first formulation is treated as a nonlinear static response problem for the effective gravitational potential  $\Phi$ . In the screened regime the theory reduces to the ordinary Newtonian/GR branch, whereas in the dilute critical regime the infrared free-energy density is controlled by the non-quadratic amplitude-sector term

$$\mathcal{F}_{\text{IR}} \propto Y_\phi^{3/2}, \quad Y_\phi = (\nabla\phi)^2.$$

A full first-principles derivation of the interpolation family from the bare condensate action is not yet available. The present work therefore adopts the phenomenologically simplest smooth closure that is compatible with both required asymptotic branches.

For practical rotation-curve fitting we use the effective acceleration law

$$g(R) = \frac{1}{2} \left[ g_N(R) + \sqrt{g_N^2(R) + 4g_N(R)g_{\text{eff}}^\dagger} \right], \quad (17.23)$$

where  $g_N(R)$  is the baryonic Newtonian acceleration inferred from the SPARC mass model and  $g_{\text{eff}}^\dagger$  is the effective critical acceleration scale of the given galaxy. This closure is not presented as a Level A theorem of bare P3; it is the minimal Level B interpolation consistent with the screened Newtonian limit

$$g \rightarrow g_N \quad (g_N \gg g_{\text{eff}}^\dagger),$$

and the deep critical branch

$$g \rightarrow \sqrt{g_N g_{\text{eff}}^\dagger} \quad (g_N \ll g_{\text{eff}}^\dagger),$$

the latter leading directly to the BTFR.

The practical baryonic input is computed from the SPARC decomposition as

$$g_N(R) = \frac{V_{\text{gas}}^2(R) + \Upsilon_d V_{\text{disk}}^2(R) + \Upsilon_b V_{\text{bul}}^2(R)}{R}, \quad (17.24)$$

with either fixed stellar mass-to-light ratios ( $\Upsilon_d = 0.5$ ,  $\Upsilon_b = 0.7$ ) or a free disk mass-to-light ratio  $\Upsilon_d$ .

### SPARC sample fits and model comparison

The numerical fitting protocol, diagnostics, and machine-level outputs used in this subsection are documented in Appendix AO.

We fitted the closure (17.23) to the SPARC mass-model sample. The fixed- $M/L$  mode provides the cleaner test of the ECT galactic closure because it removes the strongest stellar disk  $M/L$  degeneracy. In that mode the fitted sample gives

$$\text{median} \left( g_{\text{eff}}^\dagger / (cH_0/2\pi) \right) \approx 0.86,$$

while the clean sub-sample yields

$$\text{median} \left( g_{\text{eff}}^\dagger / (cH_0/2\pi) \right) \approx 0.94.$$

This does not prove the coefficient  $1/(2\pi)$ , but it strongly supports the claim that the preferred ECT galactic acceleration scale is of order  $cH_0/(2\pi)$  rather than  $cH_0$ .

At the sample level (Fig. 23) the new ECT closure is numerically competitive with MOND on comparable parameter footing. In the fixed- $M/L$  mode the median reduced  $\chi^2$  is lower than in the MOND benchmark fits, whereas  $\Lambda$ CDM still performs better in a purely numerical sense, as expected for a more flexible halo family with more parameters. Allowing the disk  $M/L$  ratio to vary improves the ECT fit further, but this improvement must be interpreted cautiously because it partly tracks the reintroduction of the strongest nuisance degeneracy in the galactic problem. The correct conclusion is therefore not that ECT has already surpassed all competing models, but that the minimal  $\phi$ -branch closure is numerically viable, competitive with MOND, and naturally tied to a cosmological acceleration scale (Table 66, Fig. 24).

**Table 66:** Summary of the SPARC sample analysis for the new ECT galactic closure. The fixed- $M/L$  mode uses  $\Upsilon_d = 0.5$ ,  $\Upsilon_b = 0.7$  and therefore provides the cleaner test of the ECT acceleration scale.

Quantity	Value
Galaxies fitted	165
Clean fits	78 / 165
Median $g_{\text{eff}}^\dagger / (cH_0/2\pi)$ (fixed $M/L$ )	0.860

Quantity	Value
Median $g_{\text{eff}}^\dagger/(cH_0/2\pi)$ (free $M/L$ )	0.725
Median $g_{\text{eff}}^\dagger/(cH_0/2\pi)$ (clean sample)	0.936
Median reduced $\chi^2$ (ECT, fixed $M/L$ )	2.66
Median reduced $\chi^2$ (ECT, free $M/L$ )	1.36
Median reduced $\chi^2$ (MOND)	3.08
Median reduced $\chi^2$ ( $\Lambda$ CDM)	0.99
ECT better than MOND by reduced $\chi^2$	88 / 165 (53%)

### Interpretation of the effective critical scale

A key distinction from standard MOND is that ECT does not require the critical acceleration scale to be exactly universal. The SPARC fits are best interpreted in terms of an effective quantity

$$g_{\text{eff}}^\dagger = g_0^\dagger Z_{\text{env}},$$

where  $g_0^\dagger$  is the cosmological baseline and  $Z_{\text{env}}$  captures residual environmental and branch-state dependence.

The fitted values cluster around the loop-motivated baseline

$$g_0^\dagger \sim \frac{cH_0}{2\pi},$$

but retain a substantial galaxy-to-galaxy scatter. This scatter should not yet be over-interpreted. At the current stage it may contain both genuinely physical environment dependence and residual modelling systematics, especially from stellar  $M/L$  choices, bulge treatment, and the still incomplete implementation of an external-field sector.

The two-panel  $g^\dagger$  analysis (Fig. 25) condenses the sample-level result into a more transparent diagnostic than the earlier legacy  $\phi_{\text{env}}$  plot. The left panel shows that the fitted critical scale clusters around a cosmological baseline rather than around a strictly universal MOND constant, while the right panel visualises how representative galaxies deviate from the universal- $a_0$  picture by different amounts. This should not yet be over-read as a completed environment theory, but it strongly motivates the ECT interpretation in which  $g_{\text{eff}}^\dagger$  is an effective branch-dependent quantity rather than a fundamental universal constant.

### Three levels of $g^\dagger$ in ECT: from baseline to per-galaxy

A key structural feature distinguishing ECT from standard MOND is the predicted hierarchy of descriptions for the critical acceleration scale:

- (1) **Universal baseline (Level B, zero free parameters):** From the phase-winding structure of the ordered condensate branch (P4 and BR1), the elementary-loop action scale is  $S_{\text{loop,min}} = 2\pi S_0$ , which together with the cosmological background sets

$$g_0^\dagger = \frac{cH_0}{2\pi} \approx 1.04 \times 10^{-10} \text{ m s}^{-2}. \quad (17.25)$$

This value, derived without any galactic fitting, lies within 13% of the observed MOND acceleration scale  $a_0 \approx 1.2 \times 10^{-10} \text{ m s}^{-2}$ , well within the galaxy-to-galaxy scatter of the fitted values.

ECT  $\phi$ -branch rotation curves vs MOND vs  $\Lambda$ CDM (fixed  $Y_{\text{disk}}=0.5$ )

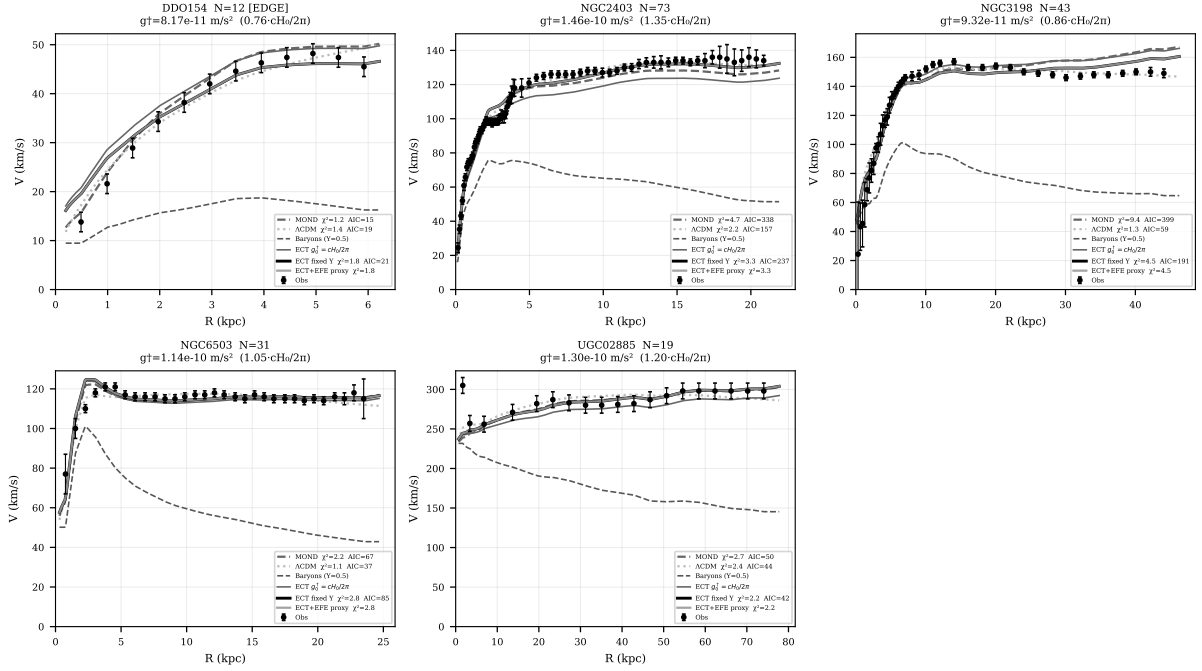


**Figure 23:** Representative SPARC rotation curves fitted with the new ECT galactic closure in the fixed- $M/L$  mode. Black points with error bars show the observed rotation velocities. The baryons-only Newtonian contribution is shown separately, together with the best-fit ECT curve, the baseline ECT curve corresponding to  $g_0^\dagger = cH_0/(2\pi)$ , and the MOND and  $\Lambda$ CDM comparison curves produced by the same numerical pipeline. Where displayed, auxiliary fit statistics such as  $\chi_r^2$  and AIC are shown for visual comparison only. The fits use the new algebraic closure (17.23), not the older empirical RAR interpolation used in preliminary versions of the manuscript.

- (2) **Environment-dependent correction (Level B, one global parameter):** A minimal Level B ansatz for the environment dependence is

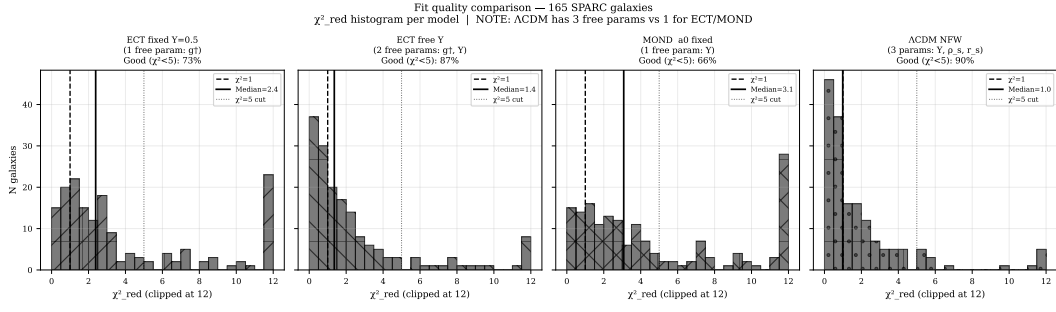
$$g_\dagger(\rho_{\text{env}}) = \frac{g_0^\dagger}{\sqrt{1 + \rho_{\text{env}}/\rho_*}}, \quad (17.26)$$

where  $\rho_*$  is a single global scale associated with the condensate potential. This formula should be read as the simplest representative member of the ECT-compatible class of environment laws, not yet as a unique first-principles derivation from bare P3 (OP3). In this minimal ansatz, isolated void galaxies approach the baseline value  $g_0^\dagger$ , while group- and cluster-members shift to  $g_\dagger < g_0^\dagger$ . More general ECT-compatible environment laws may allow either upward or downward departures from the baseline; the key point is that ECT does not require a strictly universal MOND constant.

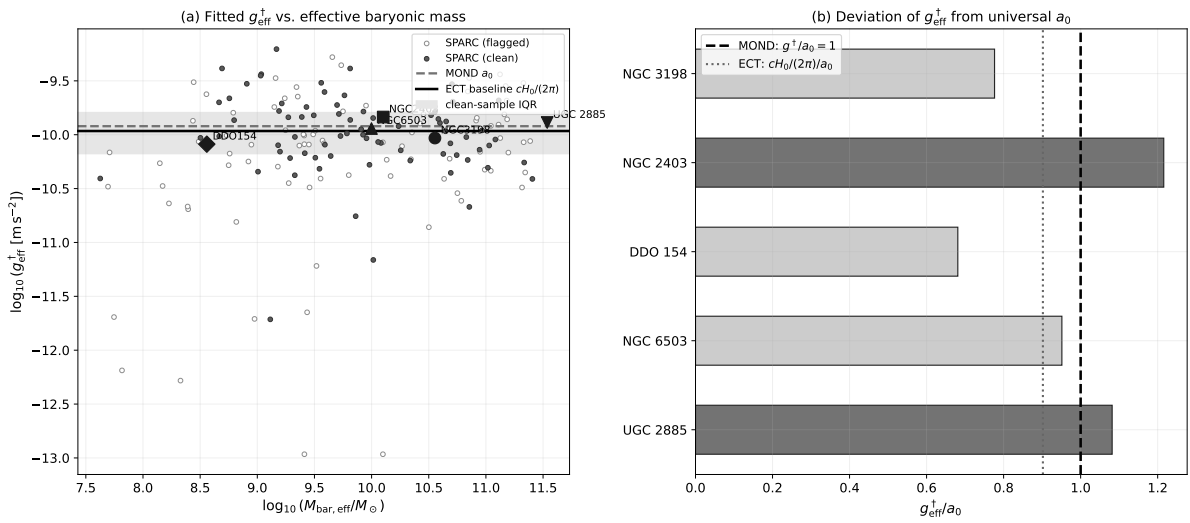
- (3) **Per-galaxy effective scale (current SPARC fits):** The existing SPARC analysis fits  $g_{\text{eff}}^\dagger$  independently for each galaxy, giving the  $\chi^2$ -optimal result. ECT interprets the resulting galaxy-to-galaxy scatter as a physical signal of environment dependence rather than a failure of the theory (Level B prediction F1 in Table 74).

Figure 21 illustrates all three levels on three representative galaxies spanning void dwarf, field spiral, and group environments.

The key observational test of this hierarchy is prediction F1: the fitted  $g_{\text{eff}}^\dagger$  values from the full SPARC sample should show a statistically significant dependence on large-scale environment density  $\rho_{\text{env}}$  (from 2MRS or SDSS group catalogues), rather than collapsing to a strictly universal constant. The sign and detailed functional form of that dependence remain tied to the still-open first-principles environment law. A statistically robust environment dependence would directly distinguish the ECT route from frameworks



**Figure 24:** Fit-quality comparison across 165 SPARC galaxies for the new ECT galactic closure (fixed and free  $M/L$  modes), MOND, and  $\Lambda$ CDM/NFW. The fixed- $M/L$  ECT mode provides the cleaner test of the galactic critical scale because it removes the strongest stellar disk  $M/L$  degeneracy, while the free- $M/L$  mode shows the best-fit performance once that nuisance freedom is restored.



**Figure 25:** Summary analysis of the fitted effective critical scale in the new ECT galactic pipeline. Panel (a) shows the fitted  $g_{\text{eff}}^{\dagger}$  values against the effective outer baryonic-mass proxy, together with the MOND reference  $a_0$  and the ECT baseline  $g_0^{\dagger} = cH_0/(2\pi)$ . Panel (b) shows selected representative systems and their deviation from a strictly universal MOND acceleration scale. The figure summarises the central galactic conclusion of the present ECT analysis: a cosmological baseline scale is preferred, but strict universality is not required.

that impose a strictly universal acceleration scale. The operational statistical test of this prediction is summarised in Appendix AR.

### Milky Way as a representative case

The Milky Way deserves separate display because it combines a precise local rotation-curve reconstruction with particular relevance for testing whether the effective critical scale must be exactly universal. As a well-measured single system, it also provides a useful anchor between the sample-level histogram of fitted  $g_{\text{eff}}^{\dagger}$  and the detailed shape of an individual rotation curve. The fit shown in Fig. 26 gives

$$g_{\text{eff}}^{\dagger} \approx 1.72 g_0^{\dagger},$$

illustrating that the ECT galactic scale need not be strictly universal even when the cosmological baseline is fixed.

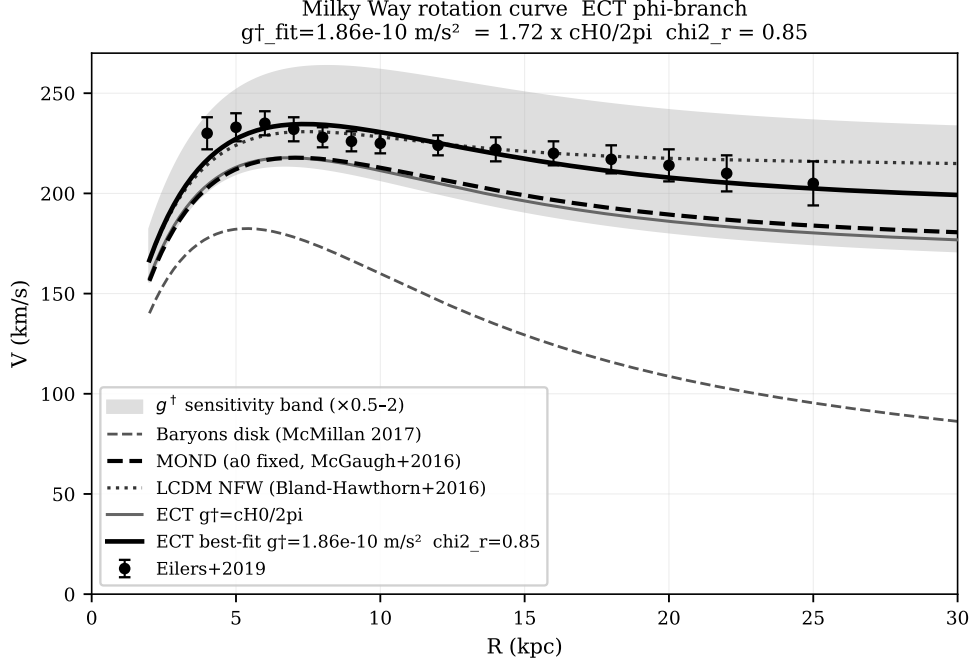


**Figure 26:** Milky Way rotation-curve fit in the new ECT galactic closure. The figure compares the best-fit ECT curve, the baseline  $g_0^\dagger = cH_0/(2\pi)$  curve, the baryonic disk model, and the MOND and  $\Lambda$ CDM comparison curves from the same numerical pipeline. The shaded/supplementary sensitivity band, where shown, represents only order-unity variations of the effective critical scale and is not interpreted here as a completed physical EFE calculation. The best-fit effective critical scale is  $g_{\text{eff}}^\dagger \approx 1.72 g_0^\dagger$ .

**Observational prospects.** The hierarchy of  $g^\dagger$  in ECT leads to two observational programmes. At low redshift, wide-environment samples and group catalogues can test the predicted correlation between fitted  $g_{\text{eff}}^\dagger$  and environment density. At higher redshift, future kinematic surveys (SKA, deep IFU studies, and improved outer-curve reconstructions) may test whether the galactic critical scale remains tied to the same baseline  $g_0^\dagger$  or whether any epoch dependence of the background branch is observationally required. These are not independent add-ons, but direct tests of the three-level hierarchy shown in Fig. 21.

### Status summary

At the current stage, the galactic-dynamics programme of ECT should be read as the observational and algebraic continuation of the ordered-branch  $\phi$ -sector established in Section 17.1. What is structurally supported at Level B is the AQUAL-type field equation, the two asymptotic regimes, the BTFR slope 4, and the interpretation of galaxy-to-galaxy scatter through an effective critical scale  $g_{\text{eff}}^\dagger$  descending from a cosmological baseline  $g_0^\dagger$ . What remains open is the exact interpolation law across the transition region, the first-principles derivation of the environment law  $\Xi(\rho_{\text{env}}, \tilde{\phi}_{\text{env}}, \dots)$ , and the full reduction from the ordered-branch EFT to the present practical SPARC data interface (Appendices AN and AO; OP3).

## 17.4 Radial Acceleration Relation

*Status: the two RAR asymptotics are strong Level B results derived from the ECT field equation (17.16). The interpolation formula (17.29) is a representative acceleration-space algebraic closure from the same ECT-compatible family already used in the rotation-curve analysis; the exact form across the transition region is Level B (OP3).*

The RAR discussed here is a direct algebraic consequence of the ordered-branch  $\phi$ -closure developed in Section 17.3. It is not an independent empirical law added on top of the theory, but an acceleration-space projection of the same AQUAL-type field equation, asymptotic branches, and the same practical

galaxy-level closure already used for the BTFR and the SPARC rotation-curve fits.

The RAR provides a complementary representation of the galactic closure. Instead of plotting  $V(R)$  directly, it compares the observed acceleration

$$g_{\text{obs}}(R) = \frac{V_{\text{obs}}^2(R)}{R}$$

with the baryonic Newtonian acceleration

$$g_{\text{bar}}(R) = \frac{V_{\text{gas}}^2(R) + \Upsilon_{\text{d}} V_{\text{disk}}^2(R) + \Upsilon_{\text{b}} V_{\text{bul}}^2(R)}{R}.$$

The ECT field equation (17.16) already fixes the two observationally relevant limits:

$$g \simeq g_{\text{bar}} \quad (g \gg g_{\text{eff}}^{\dagger}), \quad (17.27)$$

$$g \simeq \sqrt{g_{\text{bar}} g_{\text{eff}}^{\dagger}} \quad (g \ll g_{\text{eff}}^{\dagger}). \quad (17.28)$$

These asymptotics are *derived*, not postulated. The observed crossover from Newtonian to critical-branch behaviour occurs at  $g \sim g_{\text{eff}}^{\dagger}$ ; for the cosmological baseline  $g_0^{\dagger} \approx 1.04 \times 10^{-10} \text{ m s}^{-2}$ , this is consistent with the empirical transition scale reported in [33].

For the full rotation-curve comparison, the algebraic interpolating function used in the SPARC analysis is:

$$g_{\text{ECT}}(R) = \frac{1}{2} \left[ g_{\text{bar}}(R) + \sqrt{g_{\text{bar}}^2(R) + 4 g_{\text{bar}}(R) g_{\text{eff}}^{\dagger}} \right], \quad (17.29)$$

which is the minimal representative of the ECT-compatible interpolation class and matches the derived asymptotics exactly. The MOND formula is recovered by the replacement  $g_{\text{eff}}^{\dagger} \rightarrow a_0$  everywhere.

Figure 27 shows the new six-panel RAR diagnostic. Panels (a)–(e) display representative galaxies spanning dwarf, spiral, edge-on, and giant-spiral systems. Panel (f) shows the full SPARC cloud together with the same selected galaxies and the baseline ECT branch.

The RAR representation confirms the same structural picture seen in the rotation curves: the ECT branch reduces to the Newtonian regime at large  $g_{\text{bar}}$ , approaches the critical square-root branch at small  $g_{\text{bar}}$ , and naturally allows galaxy-to-galaxy variation through  $g_{\text{eff}}^{\dagger}$ . In this sense the RAR is not an independent fit law added on top of the theory, but a different projection of the same galactic closure already used in the SPARC velocity analysis.

**Intrinsic scatter as an ECT diagnostic.** The observed RAR shows an orthogonal scatter of order  $\sigma \approx 0.13 \text{ dex}$  [33, 121]. In MOND-like frameworks with a strictly universal acceleration scale, this residual width is usually attributed predominantly to observational systematics such as distance errors, inclination uncertainties, and mass-to-light-ratio degeneracies. In ECT, by contrast, a physically meaningful component of the scatter is naturally interpreted in ECT through the galaxy-to-galaxy variation of  $g_{\text{eff}}^{\dagger}$  — the same environment-dependent effective critical scale already discussed in Section 17.3. A quantitative decomposition of the observed RAR width into instrumental and physical components therefore constitutes a direct test of the ECT environmental-modulation prediction (F1, Table 74).

A related diagnostic is the effective force-law dimensionality  $d_{\text{force}}(x)$ , which provides yet another projection of the same closure in dimension-space rather than acceleration-space (Section 16.8, prediction D34 in Table 72). For the formal derivation status of the RAR asymptotics, the practical closure representation, and the computational pipeline from which the RAR diagnostics are generated, see Appendices AS, AN, and AO.

**Observational prospects.** At low redshift, larger environment-tagged galaxy samples can test whether part of the observed RAR scatter tracks the inferred environment dependence of  $g_{\text{eff}}^{\dagger}$ . At higher redshift, the most direct target is the possible shift of the RAR intercept discussed as prediction F9 (Table 74), which can in principle be probed by future kinematic measurements of disc galaxies at  $z \gtrsim 0.5$ .

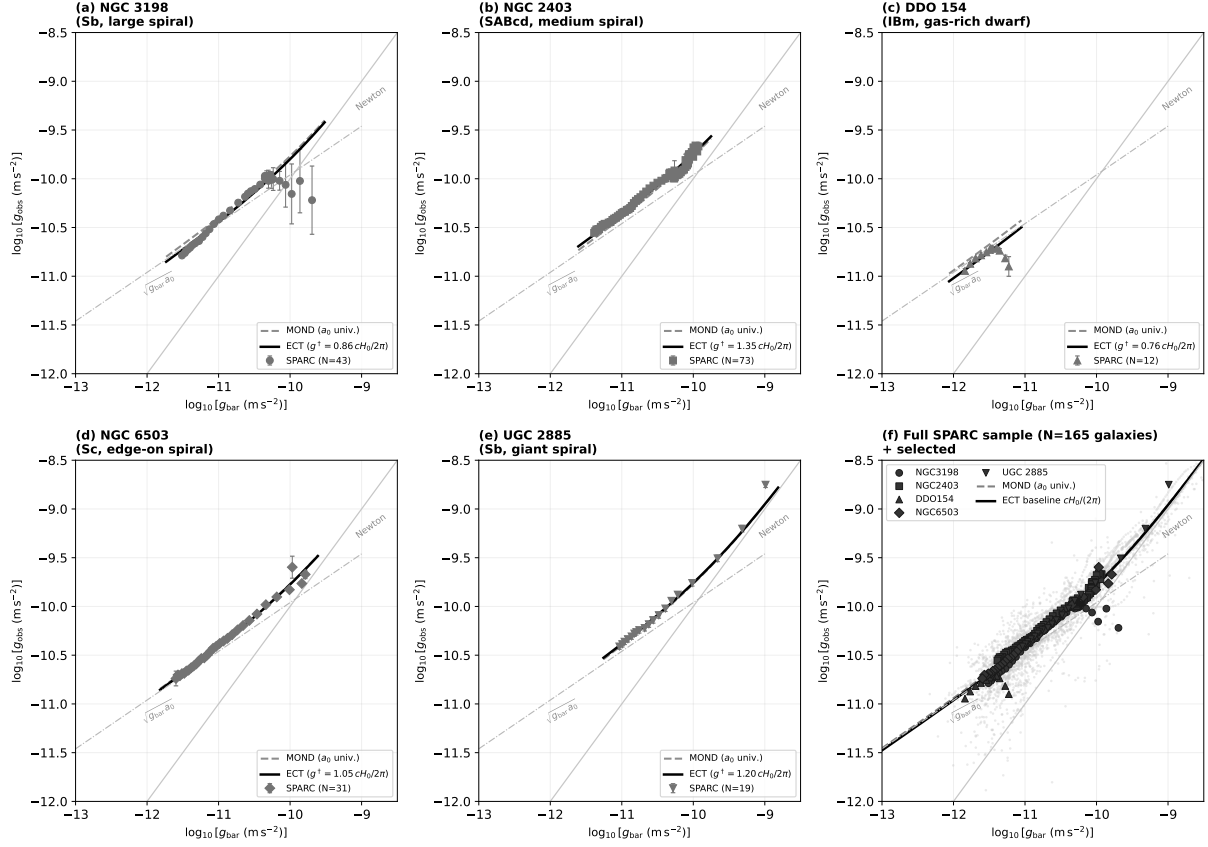


**Figure 27:** RAR from the new ECT galactic closure. Panels (a)–(e) show representative galaxies; panel (f) shows the full SPARC cloud together with the selected systems. Black solid lines denote the fitted ECT closure, dashed lines denote MOND with universal  $a_0$ , and the grey diagonal marks the Newtonian limit  $g_{\text{obs}} = g_{\text{bar}}$ . The ECT curves are computed from the same practical closure (17.23) and the same fitted  $g_{\text{eff}}^+$  values as in the rotation-curve analysis; the RAR should therefore be read as a projection diagnostic of the same fitted galactic closure rather than as an independent fit law.

**Bridge to the cosmological drift sector.** The retained five-probe cosmological band for the effective drift parameter  $\varepsilon$  obtained in §16.5 should not be read as a direct refit parameter for the present low-redshift SPARC analysis. The galactic sector developed here is a local ordered-branch closure formulated in terms of  $g_+$  and the environment-sensitive effective critical scale  $g_+^{\text{eff}}$ . What the cosmological result does provide is a consistency pressure toward a mild common late-time drift of the underlying background response. In the galactic sector, this should appear first not as a wholesale redefinition of the present  $z \approx 0$  SPARC fits, but as a redshift dependence of the RAR intercept (prediction F9 in Table 74) and potentially as a structured environment dependence of the inferred  $g_+^{\text{eff}}$  (prediction F1). No direct substitution of the cosmological retained-band value of  $\varepsilon$  into the present  $z \approx 0$  galactic fits is made here; such a step would require an explicit closure-level derivation of how the cosmological drift sector projects onto the local galactic branch variables.

### 17.5 Dark-matter-deficient ultra-diffuse galaxies as a stress test of the current closure

A small but astrophysically important class of observationally well-studied objects acts as a sharp stress test of the current Level-B galactic closure (17.23): the dark-matter-deficient ultra-diffuse galaxies [122, 123, 124, 125, 126, 127]. The reference cases are NGC 1052–DF4 and FCC 224, pressure-supported systems of  $M_\star \sim 10^8 M_\odot$  and  $R_e \sim 2$  kpc whose internal stellar velocity dispersions,  $\sigma \sim 6\text{--}8$  km s $^{-1}$ , are consistent with baryon-only Newtonian dynamical mass within their probed radii. A matched-mass



DM-rich control, NGC 5846-UDG1 [128] at nearly identical  $M_*$ ,  $R_e$ , and group-scale environment, lies on the standard RAR at  $\sigma = 17 \pm 2 \text{ km s}^{-1}$ . NGC 1052-DF2 is observationally ambiguous across the currently reported  $\sigma \in [8.6, 14.9] \text{ km s}^{-1}$  bracket.

**Where these systems sit in the ECT regime plane.** In the regime-diagram (Fig. 18) language, the baryonic surface density of NGC 1052-DF4 and FCC 224 places them squarely in the critical/deep-MOND branch of the current closure, where the baseline  $g_{\text{eff}}^\dagger = g_0^\dagger$  would predict an *enhanced* acceleration  $g \sim \sqrt{g_N g_0^\dagger}$  over the bare Newtonian value. Their *observed* kinematics, however, sit close to the Newtonian branch. The regime diagram therefore admits these objects only as an off-track class: the closure slots them into the MOND-like regime by density, while the data slot them back near Newton. Figure 28 makes this mismatch explicit object by object.

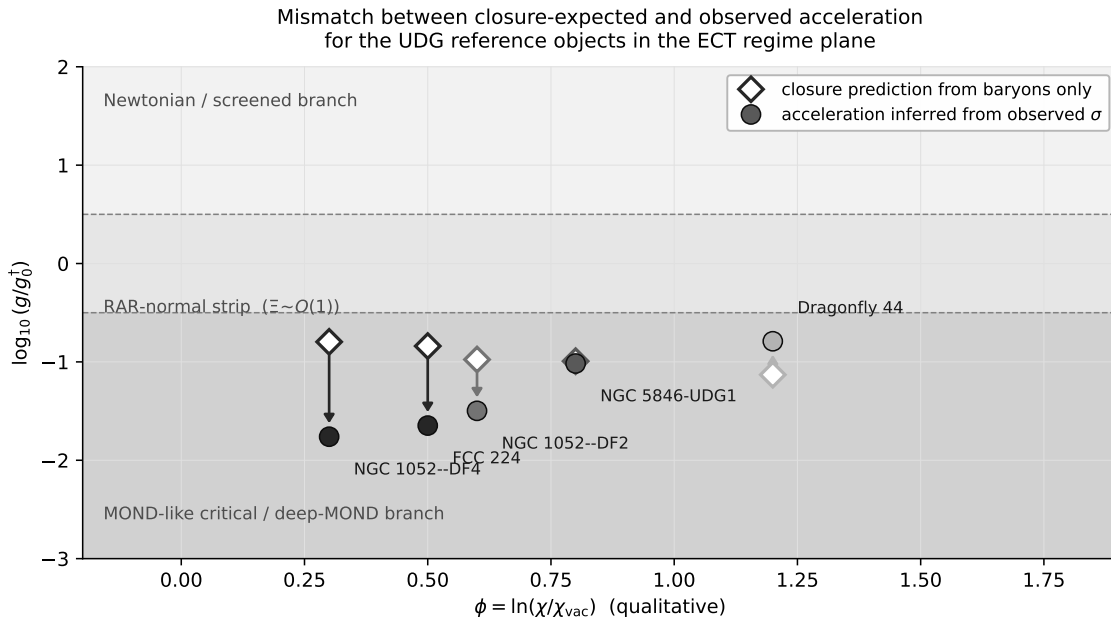


**Figure 28:** Positioning of the UDG reference objects in the  $(\phi, \log_{10}(g/g_0^\dagger))$  regime plane of the current ECT galactic closure, qualitatively aligned with the preprint’s regime diagram (Fig. 18). Open diamonds mark the closure prediction from the baryonic content alone (at the baseline  $g_{\text{eff}}^\dagger = g_0^\dagger$ ); filled circles mark the acceleration inferred from the observed velocity dispersion at  $R_{1/2}$ . NGC 1052-DF4 and FCC 224 lie in the MOND-like regime by baryonic density, but the kinematic readout places them close to the Newtonian branch at the same radii; the matched-mass control NGC 5846-UDG1 lies on the RAR-normal strip with no mismatch. Full numerics and nuisance bands in Appendix AT.

**Quantitative stress-test diagnostic.** The closure (17.23) can be inverted at a given radius to give the value of the environmental factor  $\Xi_{\text{req}}$  that the current closure would need at each object in order to reproduce the observed internal kinematics. At the Wolf half-mass radius  $R_{1/2} = (4/3)R_e$ , writing  $r \equiv M_{\text{dyn}}/M_{\text{bar}}$  and  $y \equiv g_{\text{eff}}^\dagger/g_N$ , one finds

$$y = r(r-1), \quad \Xi_{\text{req}}(R_{1/2}) = r(r-1) \cdot \frac{g_N(R_{1/2})}{g_0^\dagger}. \quad (17.30)$$

The derivation and a full nuisance budget are given in Appendix AT. Applied to the reference sample, (17.30) returns  $\Xi_{\text{req}} \sim O(1)$  for normal RAR galaxies (NGC 5846-UDG1, and by extension the SPARC median)—as required by construction—but  $\Xi_{\text{req}} \sim 10^{-3}$  for NGC 1052-DF4 and  $\sim 2 \times 10^{-2}$  for FCC 224, under the same proxy-level assumptions. The stress-test character of these two objects is robust against independent variations of distance ( $\pm$  factor 10 in  $\Xi_{\text{req}}$ ),  $M/L$  ratio ( $\pm$  factor 10), small- $N$  statistics

on  $\sigma$  at 95% CL ( $\pm$  factor 100), and anisotropy ( $\pm$  factor 1.5): the combined 95% CL band on  $\log_{10} \Xi_{\text{req}}$  for DF4 is  $[-4, -0.5]$ , which lies *entirely* below the RAR-normal range  $\Xi \sim O(1)$ .

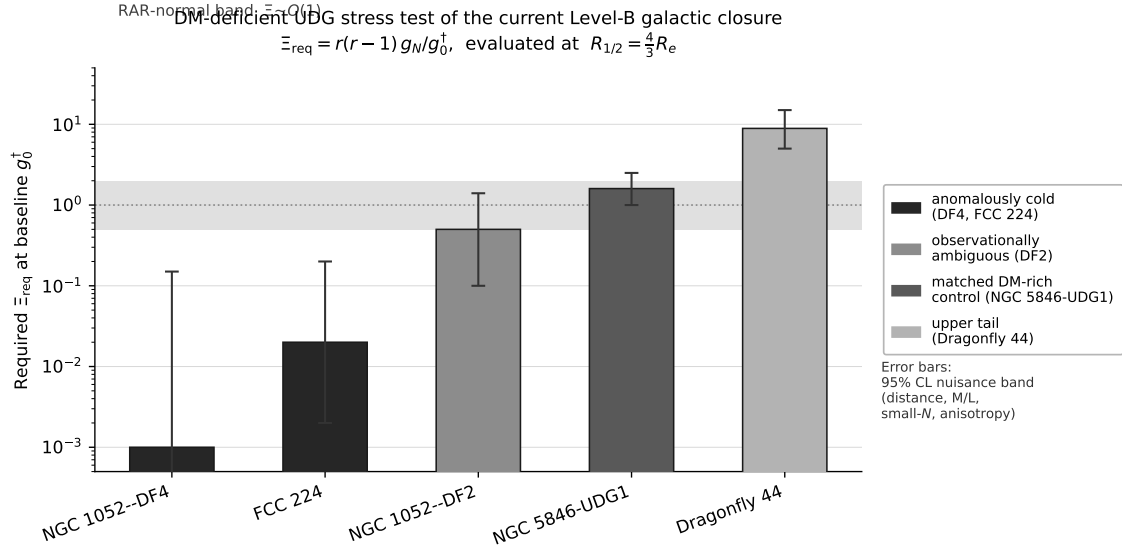


**Figure 29:** Diagnostic readout of the current Level-B galactic closure at the five spherical reference objects: the environmental factor  $\Xi_{\text{req}}$  that the closure would need in order to reproduce the observed dispersion, evaluated at the Wolf half-mass radius. The shaded horizontal band marks the RAR-normal strip  $\Xi \sim O(1)$  recovered for ordinary galaxies. Error bars are the 95% CL nuisance band from distance covariance,  $M/L$ , small- $N$  statistics, and anisotropy. NGC 1052-DF4 and FCC 224 lie two to three orders of magnitude below the normal strip; the matched-mass DM-rich control NGC 5846-UDG1 falls inside it and Dragonfly 44 sits at the upper tail; DF2 spans an observationally ambiguous bracket. This figure is not a prediction of  $\Xi$  from ECT; it is a diagnostic of what the present closure would require at each object. AGC 114905 is a gas-rich rotator and requires a disc solver rather than the spherical Jeans proxy used here.

**Matched-pair observation.** The ECT-relevant tension is sharpest in the matched pair NGC 1052-DF4 versus NGC 5846-UDG1: comparable  $M_\star \sim 10^8 M_\odot$ , comparable  $R_e \sim 2$  kpc, comparable group-scale environment, but central-value  $\Xi_{\text{req}}$  values differing by about three orders of magnitude. Because the minimal density-only Level-B ansatz (17.12) depends only on the single environmental scalar  $\rho_{\text{env}}$  and is monotonic in it, it does not naturally accommodate both endpoints of such a matched pair within a single simple environmental scalar law. This is a structural observation, not an impossibility theorem: the broader ECT-compatible class of  $\Xi$ -functions noted in §AS remains open at OP3. The comparison is structural rather than a perfectly matched same-tracer same-aperture twin test: it is intended to expose a tension within the present closure, not to serve as a one-to-one dynamical twin.

**Comparison with the  $\Lambda$ CDM bullet-dwarf interpretation.** In the  $\Lambda$ CDM-plus-bullet-dwarf scenario [129, 130, 131], the dark-matter-deficient UDGs arise as post-collisional remnants of high-speed galaxy encounters in which the dark halos of the two progenitors decouple from the stars and proceed approximately ballistically, leaving two stellar remnants embedded in essentially baryon-only potentials. This scenario reproduces the observed low dispersions through partial dark-halo stripping, predicts a small-but-non-zero incidence rate compatible with the  $\sim 1\%$  screened-population observation, and places at least one candidate (the compact dwarfs near NGC 1052 [131]) in the same post-collision alignment. The  $\Lambda$ CDM comparator therefore sits on fully derived astrophysics, not on open elements of the underlying theory. Any future ECT-compatible rescue must reach comparable explanatory power — at minimum, reproduce the central dispersion values of DF4 and FCC 224 while remaining consistent with the matched control NGC 5846-UDG1 and with the standard RAR across the wider UDG population — before it can be promoted to a preferred interpretation within ECT.

**Candidate theory-level directions.** The full ECT field equations (13.35) contain several structural degrees of freedom not yet propagated through to the practical galactic closure (17.23). The following are candidate directions for a future completion that could in principle address the DM-deficient UDG class. None is presently derived for the galactic closure; each is listed only as a label for future work, with no priority ordering. (i) *Dynamical  $G_{\text{eff}}(\phi)$* : the generalised field equations carry a dynamical  $G_{\text{eff}}(\phi)$  entering through the  $e^{\beta\phi}R$  coefficient of the action (13.34); a derivation mapping that degree of freedom onto the practical closure would be required before any  $G_{\text{eff}}$ -based effect on  $\sigma_{\text{obs}}$  can be claimed as ECT-internal rather than parametric. (ii) *History-dependent extensions of  $\Xi$*  within the broader ECT-compatible class allowed by §AS: the minimal ansatz (17.12) depends only on the instantaneous environmental density; an extension allowing  $\Xi$  to depend on the local history of the condensate (e.g. elapsed time since a relaxation-disrupting event) is within the open class at OP3. (iii) *Orientation-sector coupling* through  $\alpha_{\text{ECT}}(n_\mu n_\lambda R_V^\lambda + \dots)$  of (13.35): an orientation-sensitive modification of the galactic closure is available in principle from the broader theory, but is not carried out here. (iv) *Non-quasi-static  $\phi$ -dynamics* breaking the quasi-static assumption of (17.2): if the local condensate response time were comparable to the galactic dynamical time, the practical closure would acquire an additional time-dependent branch. None of these is promoted to rescue status here.

**Physical interpretation of the diagnostic.** In the language of the current practical galactic closure, the stress test has the following minimal physical reading. The closure (17.23) admits two asymptotic branches: Newtonian at  $g_N \gg g_{\text{eff}}^\dagger$  and deep-MOND at  $g_N \ll g_{\text{eff}}^\dagger$ . In the DM-deficient UDGs the local  $g_N$  is small enough to enter the deep-MOND branch at the baseline  $g_{\text{eff}}^\dagger = g_0^\dagger$ , but the observed kinematics are Newton-like. Within the scope of the present closure, the only way to describe this within the same single closure and the same asymptotic structure is to interpret the closure as requiring a sharply suppressed local  $g_{\text{eff}}^\dagger$  at these objects relative to the global baseline  $g_0^\dagger$ . This is the content of the diagnostic  $\Xi_{\text{req}} \ll 1$  inferred above. Whether such a suppression can arise from any of the candidate directions listed above is an open question.

**Open questions tied to OP3.** The diagnostic of this section refines and sharpens the open problem OP3 (exact environment law for  $g^\dagger$ ) listed in the main text. Concretely:

- OP3a: Construct or exclude the density-only ansatz class. Is there any choice of  $\Xi(\rho_{\text{env}})$  with monotonically decreasing behaviour in the group-density regime that simultaneously reproduces matched DM-rich and DM-deficient UDGs at the observed levels? The matched-pair observation suggests not, but does not rule it out formally.
- OP3b: Specify the additional variable. If OP3a closes negatively, which of the candidate directions supplies the additional environment/history variable that completes  $\Xi$ ?
- OP3c: Derive the galactic-scale effective action. Perform the derivation that connects the dynamical  $G_{\text{eff}}(\phi)$  of (13.35) to the practical galactic closure (17.23); only after this derivation can  $G_{\text{eff}}$ -based effects on  $\sigma_{\text{obs}}$  be claimed as ECT-internal rather than parametric.
- OP3d: Predict the incidence rate. Any completion that accommodates DF4 and FCC 224 must also be consistent with the observed  $\sim 0.6\%–1\%$  incidence of DM-deficient UDGs in the screened dwarf population.

**Future-work factors (secondary).** Several second-order factors are not pursued in this section; they would refine the precision of  $\Xi_{\text{req}}$  or enable more ambitious analyses but do not alter the qualitative classification above. They are registered here as reminders for a full programme of UDG-sector work: rotation in "pressure-supported" dwarfs (DF2 has measurable rotation); globular-cluster tracer survival bias and orbital-family selection effects; mass-sheet degeneracy in external-field analyses; the preprint's 5th-force  $L_5 = \beta \bar{\Psi} \gamma^A n_A \Psi$  contribution (Planck-suppressed at galactic scale); time-since-event correlation

with  $\Xi_{\text{req}}$  via stellar ages; spatial  $\Xi(R)$  variation within a single galaxy (IFU test); joint ensemble posterior across the whole UDG sample; CMB / early-universe cross-checks for any long-memory mechanism; interloper mixture modelling in small- $N$  tracer samples; proper 3D HI cube modelling for AGC 114905 and other disc rotators;  $\Lambda$ CDM partial-DM-halo survival as the direct competitor baseline; stellar age-metallicity degeneracy in  $M/L$ ; IMF universality assumption.

**Bottom line for §16.5.** The DM-deficient ultra-diffuse galaxies constitute a sharp empirical stress test of the minimal density-only environment ansatz (17.12), not a falsification of the generalised  $\phi$ -first field equations (13.35). The class is registered as entry ND-13 in Table 75; its quantitative diagnostic and the honest boundaries outlined above leave the matter as an open-at-OP3 research target, not as a solved consequence of ECT. Full technical derivations, including the closed-form inversion, the Jeans upgrade path, the six-object numerical table, the nuisance budget, the external-field benchmark, and the side diagnostics, are collected in Appendix AT. The presently known sample is small and not selection-neutral, so class properties must be treated as provisional rather than population-level conclusions.

## 17.6 Summary and status of galactic and cluster-scale phenomenology

This chapter developed the galactic and cluster-scale phenomenology of ECT within the  $\phi$ -first ordered-branch closure. The main results and their derivation status are:

1. **Ordered-branch  $\phi$ -sector** (Section 17.1): the amplitude variable  $\phi$ , the matter-driven ordering tendency, the ordered-branch screening hierarchy ( $\lambda_\phi \ll 1$  AU in dense environments,  $\sim$  kpc on galactic outskirts,  $>$  Mpc in voids), and the critical IR branch  $\mathcal{F} \propto Y_\phi^{3/2}$  are structurally supported within the present Level B ordered-branch closure. Benchmark screening-length estimates are collected in Appendix AQ.
2. **Cluster-merger lensing** (Section 17.2): the same ordered-branch  $\phi$ -closure yields a unified morphology test at merger-cluster scale: the convergence peak tracks the more compact baryonic component. The same algebraic threshold logic is carried across the four-cluster suite without per-system retuning. Morphology is robust across all four systems (Bullet, MACS J0025, El Gordo, Abell 520), while the remaining amplitude deficit is comparable to the generic MOND cluster problem ( $\times 1.1$ – $1.9$ ) and therefore serves as a quantitative target rather than a morphology-level failure (Level B). Computational details are given in Appendix AP.
3. **Galactic dynamics and rotation curves** (Section 17.3): the critical  $\phi$ -branch closure reproduces flat rotation curves across the full SPARC sample (165 galaxies) with one fitted effective critical acceleration  $g_{\text{eff}}^\dagger$  per galaxy; median  $\chi_r^2 \approx 2.7$  (fixed  $M/L$ ),  $\approx 1.4$  (free  $M/L$ ), competitive with MOND ( $\chi_r^2 \approx 3.1$ ) on comparable parameter footing (Level B). The galaxy-to-galaxy scatter in fitted  $g_{\text{eff}}^\dagger$  is interpreted as containing a physically meaningful component of environment dependence rather than being merely a shortcoming of the framework (prediction F1). Computational details are given in Appendix AO; the benchmark algebraic closure is documented in Appendix AN.
4. **BTFR** (Section 17.3): the deep-branch slope  $V_f^4 \propto M_b$  follows algebraically from the critical branch (Level B structural result). Its normalisation passes through the baseline critical scale  $g_0^\dagger \sim cH_0/(2\pi) \approx 1.04 \times 10^{-10} \text{ m s}^{-2}$  and therefore probes the environment dependence of the fitted galaxy-level quantity  $g_{\text{eff}}^\dagger$  (OP3).
5. **RAR** (Section 17.4): the two asymptotic regimes ( $g \simeq g_{\text{bar}}$  at high acceleration and  $g \simeq \sqrt{g_{\text{bar}} g_{\text{eff}}^\dagger}$  at low acceleration) arise from the same ECT field equation, and the interpolation is a representative algebraic closure (Level B). The observed RAR scatter ( $\sigma \approx 0.13$  dex) admits a physically meaningful component through the environment dependence of  $g_{\text{eff}}^\dagger$ . A related force-law dimensionality diagnostic  $d_{\text{force}}(x)$  provides an additional closure-level prediction (D34, Section 16.8).

All results in this section are Level B: they use the  $\phi$ -first ordered-branch closure rather than first-principles derivations from the bare ECT action. In the present practical galactic implementation, one fitted effective critical acceleration  $g_{\text{eff}}^\dagger$  is assigned per galaxy, while the corresponding transition radius  $r_*$  is a derived quantity. The most distinctive closure-level environmental handle is the modulation of  $g_{\text{eff}}^\dagger$  (F1, Table 74), which is absent in frameworks with a strictly universal acceleration scale and is directly testable with existing data. A known stress test of the present Level-B closure is the class of dark-matter-deficient ultra-diffuse galaxies (NGC 1052–DF4, FCC 224); these are listed as entry ND-13 in Table 75 and discussed diagnostically in Appendix AT, and they are not claimed to be explained by the current closure. For the cosmological sector of the ordered-branch programme, see the summary in Section 16.9.

## 18 Mass-discrepancy and late-time-acceleration phenomenology in ECT

*Status: Level B throughout in the macroscopic branch.* The purpose of this section is to separate three questions that are often conflated under the generic label “dark sector”: (i) the galactic mass-discrepancy phenomenology addressed by the ordered-branch amplitude variable  $\phi$ , (ii) the possible existence of additional collective or topological dark excitations of the condensate, and (iii) the late-time accelerated expansion of the ordered-branch background. ECT does not treat these as one and the same problem. The first belongs already to the macroscopic branch developed in Section 17; the second is deferred in large part to the Quantum Sector; the third is a background-dynamics question tied to the late-time ordered branch.

### 18.1 Scope and dark-sector logic

In the standard cosmological picture, two separate dark components are postulated: particle dark matter to account for galactic dynamics and large-scale structure, and dark energy (or a cosmological constant) to account for late-time accelerated expansion. ECT does not introduce either component as an independent physical substance. Instead, it asks which of the observational phenomena that motivated these postulates can already be accounted for by ordered-branch condensate dynamics without separate dark substances. The conventional labels *dark matter* and *dark energy* are retained throughout this paper exclusively as names of *observational phenomena* for comparison with the literature; they do not refer to independent entities in the ECT ontology.

Given this reframing, the macroscopic logic of ECT is as follows: the phenomenology of missing gravitational response must be kept separate from the ontology of possible additional dark degrees of freedom, and both must be kept separate from the late-time ordered-branch background responsible for the accelerated-expansion phenomenology. The galactic mass discrepancy can already be addressed within the present  $\phi$ -first closure without introducing a standard particle-dark-matter halo (Level B; Section 17). By contrast, collective condensate excitations and coherent topological sectors remain structurally possible but require the Quantum Sector for their detailed development. Late-time dark energy is a third and logically distinct question: it is tied to the ordered-branch background dynamics rather than to the galactic  $\phi$ -branch itself.

**Postulate-grounded origin of the split.** This three-way separation is not an arbitrary taxonomy. The galactic mass-discrepancy channel belongs to the ordered branch fixed by P4 together with its admissible inhomogeneous continuation under P6: at the current Level-B closure, this yields the nonlinear  $\phi$ -branch discussed in Section 17. The possibility of additional collective or topological dark-sector degrees of freedom belongs instead to the coherent branch (BR1) and is therefore deferred to the Quantum Sector. Late-time dark energy is a third channel again: it arises from the ordered-branch background energy of the same condensate, not from the galactic  $\phi$ -branch and not from a particle-dark-matter halo.

**Important interpretive caveat.** The statement “ECT does not need dark matter particles in its minimal benchmark explanation” is not equivalent to the statement “ECT proves that no particle beyond the

Standard Model can ever exist”. The first is a statement about the present minimal closure. The second would be an overclaim that the theory does not make. Collective condensate excitations and topological sectors remain structurally possible as optional extensions or open sectors; they are not required by the core benchmark fit developed here.

**Observational motivation.** These three channels correspond to three distinct observational questions that are often grouped together under the label “dark sector”: the galactic and cluster-scale mass discrepancy, the late-time accelerated expansion, and the cosmic dark-budget inference from background cosmology. ECT does not assume from the outset that all three require the same kind of hidden matter component. Instead, it asks which part of the dark-sector phenomenology can already be addressed by the ordered-branch response itself, and which part — if any — requires additional condensate excitations or topological sectors beyond the macroscopic branch. Unlike the standard  $\Lambda$ CDM reading, ECT therefore does not assume from the outset that the galactic mass discrepancy and the late-time accelerated expansion must be attributed to two independent hidden components.

The following subsections therefore separate: the dark-matter interpretation of the galactic mass discrepancy (Section 18.2), the ordered-branch account of dark energy (Section 18.3), and the explicit discriminants and falsifiers of the present closure (Section 18.4).

**Table 67:** Three logically distinct dark-sector channels in the present ECT programme.

Channel	Present ECT claim	Status	Main discriminant
Galactic mass discrepancy	The ordered-branch $\phi$ -response can already account for RAR/BTFR/rotation-curve phenomenology without a standard particle halo	B	SPARC fits, BTFR scaling, environment dependence of $g_{\text{eff}}^\dagger$
Additional condensate excitations	Collective or topological dark excitations remain structurally possible but are not required by the present galactic closure	B/C	Stability, relic abundance, lensing and structure-growth signatures
Late-time dark energy	Accelerated expansion is interpreted through ordered-branch background energy rather than by adding an independent dark-energy substance	B	$w(z)$ , background expansion history, late-time cosmological fits

## 18.2 Dark-matter interpretation: $\phi$ -branch and beyond

### Galactic mass discrepancy without particle halos

The galactic mass-discrepancy phenomenology (flat rotation curves, RAR, BTFR) is attributed entirely to the same nonlinear ordered-branch  $\phi$ -closure developed in Section 17, including the hierarchy from the cosmological baseline scale  $g_0^\dagger$  to the fitted galaxy-level quantity  $g_{\text{eff}}^\dagger$ . No independent particle-dark-matter halo and no kpc-scale variation of the heavy condensate amplitude are invoked. The macroscopic branch therefore addresses the *phenomenology* of missing gravitational response, while the deeper ontology of possible additional dark-sector excitations is developed separately in the Quantum Sector (Section 34).

**Postulate-grounded origin.** This channel is rooted in the ordered branch fixed by P4 and its admissible inhomogeneous continuation under P6, but its present galactic realisation is developed only through the current Level-B macroscopic  $\phi$ -closure. At the current Level-B closure, the macroscopic amplitude variable  $\phi(X)$  induces a position-dependent gravitational response through the same effective-coupling

logic  $G_{\text{eff}}(X) = G_N e^{-\beta\phi(X)}$  discussed in the macroscopic gravitational sector, while the critical infrared branch supplies the deep weak-field regime that reproduces flat rotation curves without particle dark matter. The dark-matter interpretation of the galactic sector should therefore be read as an ordered-branch response effect, not as evidence for a separate hidden particle halo.

**What is established and what is not.** At the current stage, ECT does *not* establish a theorem that all dark-sector phenomenology must be exhausted by the macroscopic  $\phi$ -branch alone. What it does establish is a sharper and more limited claim: the galactic mass-discrepancy phenomenology can already be accounted for within the present ordered-branch response closure, without introducing a standard particle halo at the level of the current galaxy-scale programme. This is the central macroscopic dark-sector result of the present article. Any additional collective or topological dark condensate excitations remain logically possible, but they are not required by the current galactic evidence discussed here.

In particular, the present conclusion is galaxy-scale only. It does not yet imply that cluster-scale or cosmological dark-sector phenomenology must be exhausted by the same minimal macroscopic  $\phi$ -closure. Those larger-scale channels may still require either additional collective condensate excitations or a more complete closure of the ordered-medium response.

**Numerical anchors from Section 17.** The current galactic programme already fixes several benchmark facts: the BTFR asymptotic slope is 4 at the structural level; the baseline critical scale is  $g_0^\dagger = cH_0/(2\pi) \approx 1.04 \times 10^{-10} \text{ m s}^{-2}$ ; the observed RAR scatter is  $\sigma \approx 0.13 \text{ dex}$  [33, 121]; and the practical SPARC analysis uses one fitted effective critical scale  $g_{\text{eff}}^\dagger$  per galaxy. Across the current SPARC sample (165 galaxies), this closure reaches the benchmark fit quality reported in Section 17 while keeping the dark-sector interpretation entirely on the ordered-branch side. By comparison, standard halo fits typically require at least a halo mass and concentration, with further freedom depending on the adopted baryonic modelling.

### Collective excitations and topological sectors

*Status: Level B/C structural possibilities. Relic abundance, stability, and production history not yet computed from bare P3.*

The ordered branch supports a constrained soft orientation sector (one longitudinal scalar mode  $\chi$  in the scalar-only basis at linear order; Level B). Its role as a dark-sector candidate is not established in the present formulation; the main astrophysical successes of ECT do not require any particle dark matter (Section 17). It should therefore be read only as a structural possibility at this stage, not as a working explanation of the galactic mass discrepancy.

The topological completeness of the  $\Phi$ -medium (S10) together with the coherent branch (BR1) admits the possibility that part of the dark sector is tied to the smooth coherent-branch configurations: winding sectors, vortex-like structures, or topological configurations (see Section 8.10 for the full classification). Their definition and dynamics depend on winding numbers and defect stability beyond the coherent approximation. They are noted here as a conceptual bridge to the Quantum Sector (Section 34); their detailed treatment is deferred.

**Illustrative large-scale benchmark.** If the soft orientation sector acquires an effective pseudo-Goldstone mass through additional symmetry-breaking effects (not derived from P1–P6 and introduced here only as an illustrative estimate), then a value  $m_G \sim 10^{-33} \text{ eV}$  corresponds to a correlation length  $\xi_G \sim \hbar c/m_G \sim 2 \times 10^{26} \text{ m}$ , of order the present Hubble scale. This coincidence is suggestive but does not by itself constitute an ECT prediction, a relic-abundance estimate, or a working dark-sector explanation; it remains a Level-B/C benchmark tied to the broader predicted-states programme (Section 8.10). It is introduced here only as a scale-setting illustration for the broader condensate-excitation programme. It is not an ingredient of the present galactic mass-discrepancy closure, and it should not be read as a derived relic-abundance or dark-sector fit.

The homotopy sector  $\pi_3(S^3) = \mathbb{Z}$  is structurally fixed by the ordered-vacuum manifold, but whether the corresponding configurations are dynamically stabilised as particle-like or long-lived dark-sector objects remains open.

Ultra-light Goldstone modes and topological condensate configurations may therefore exist as additional excitations, but they are *not required* to explain galactic rotation curves. Whether they contribute to cluster or cosmological dark-sector phenomenology remains an open problem.

### Direct-detection falsifier and cosmological-fraction status

Since the galactic mass discrepancy is attributed in ECT to the ordered-branch  $\phi$ -closure rather than to a weakly interacting particle halo, the present macroscopic explanation does not require a direct-detection signal to account for galaxy rotation curves. Current direct-detection searches have nevertheless pushed spin-independent WIMP bounds to extremely small cross sections, with no positive signal for the galactic discrepancy channel (e.g. LZ [132]). A robust detection of a particle species specifically shown to account for the galactic mass discrepancy on galaxy scales would therefore falsify the present macroscopic  $\phi$ -branch-only interpretation of that channel. It would not by itself falsify the full ECT framework, which could still accommodate additional condensate or particle sectors beyond the present closure.

This distinction is important. The present galactic closure is a specific macroscopic ECT channel, not the whole ontology of the theory. A particle interpretation of the galactic discrepancy would therefore refute the current  $\phi$ -branch-only explanation of that channel, while still leaving open broader ECT completions with additional condensate or particle sectors.

By contrast, the mere existence of additional dark condensate excitations on non-galactic scales would not challenge the galactic  $\phi$ -branch interpretation.

ECT does not yet derive the cosmological fractions  $\Omega_b$ ,  $\Omega_{\text{DM}}$ , and  $\Omega_\Lambda$  from first principles. What it presently offers is not a full first-principles replacement of the cosmological fraction budget, but a re-interpretation of part of the late-time dark-sector phenomenology: the galactic mass discrepancy is attributed to the nonlinear  $\phi$ -branch rather than to particle dark matter, while the late-time dark-energy sector is interpreted as ordered-branch background energy. Within the standard  $\Lambda$ CDM reading, the dark-matter fraction is an independent cosmological ingredient ( $\Omega_{\text{DM}} \approx 0.27$  in the late-Universe budget [88]). A first-principles derivation of the effective cosmological fractions within ECT remains open.

ECT therefore makes a sharp distinction: the present galactic branch does not need particle dark matter, while the possible existence of additional dark condensate excitations remains an open structural possibility; their abundance, stability, and cosmological role are not yet derived.

## 18.3 Late-time accelerated expansion: ordered-branch account

### Ordered-branch background energy and equation of state

*Variable note.* Throughout this subsection  $\phi = \frac{1}{\beta} \ln(u/u_\infty)$  is the macroscopic amplitude variable measuring the local degree of Lorentzianness of the ordered vacuum—a derived infrared collective variable, not the fundamental field  $\Phi$  of postulate P3. Correspondingly,  $V(\phi) = V_0 + \frac{1}{2}m_\phi^2\phi^2$  is an EFT-level amplitude potential, distinct from the bare potential  $V(\Phi) = -\frac{\mu^2}{2}\Phi^2 + \frac{\lambda}{4}\Phi^4$  of P3 (Eq. (2.3)); the two operate at different levels of the ECT hierarchy.

**Postulate-grounded origin.** What is conventionally called the dark-energy effect—late-time accelerated expansion—is rooted in the ordered branch fixed by P4, but its present cosmological realisation is developed only at the macroscopic level through the  $\phi$ -first closure of Section 16.1. In ECT, accelerated expansion is not attributed to an independently postulated cosmological constant or dark-energy substance, but to the residual background energy carried by the ordered phase of the same condensate.

**Physical picture: dark energy as condensate residual.** In standard QFT the vacuum energy is computed as the sum of zero-point oscillations of all fields and disagrees with observation by approximately



120 orders of magnitude. In ECT the reframing is structural: dark energy is not an abstract “vacuum energy” but the dynamical residue of the  $O(4) \rightarrow O(3)$  phase transition. The effective cosmological term  $\Lambda_{\text{eff}}(\phi)$  is a functional of the condensate background, not a rigid external constant; the physical cutoff on loop contributions is the radial-mode mass  $m_\sigma \sim M_{\text{Pl}}$ , not a formally infinite regulator; and the emergent unimodular decoupling of the ordered branch—established in Section 15—blocks the direct standard channel by which a vacuum baseline  $V(\phi_0)$  would source a cosmological-constant term in the leading ordered-branch sector. The net effect is to resolve the classical cosmological-constant catastrophe at Level A in the leading ordered-branch sector (see “Cosmological-constant catastrophe: status” below).

**Cosmological-constant catastrophe: status.** For the quartic potential  $V(\Phi) = -\mu^2\Phi^2/2 + \lambda\Phi^4/4$ , the broken minimum gives  $V(\phi_0) = -\mu^4/(4\lambda)$ —a large negative tree-level contribution. In a standard general-relativistic framework this contribution would gravitate as a cosmological constant of order  $|V(\phi_0)| \sim \lambda M_{\text{Pl}}^4/4$ , overshooting the observed  $\rho_\Lambda^{\text{obs}} \approx (2.3 \times 10^{-3} \text{ eV})^4$  by roughly  $10^{120}$ . In ECT, this catastrophe is *resolved at Level A* in the leading ordered-branch sector, as established by the emergent unimodular decoupling theorem of Section 15: the determinant of the ordered-branch kinetic tensor is fixed,  $\sqrt{-\det K^{AB}} = \beta^2/c_*$ , as a consequence of the kinematic constraint  $n^A n_A = 1$ ; the classical baseline  $V(\phi_0)$  therefore does not source the local emergent gravitational dynamics (Theorem 15.3(iv)). Conditional on a one-line spectral assumption on the full quadratic fluctuation operator (condition  $H_\Lambda$ , discussed in the same section), the zero-derivative one-loop vacuum contribution is absorbed into the same fixed kinetic-determinant structure. No cross-scale cancellation between the UV vacuum baseline and the observed cosmological term is invoked at any stage. Separately and at a lower level of accuracy, the observed numerical value of  $\rho_\Lambda$  itself is an infrared determination problem: the natural scaling  $\rho_\Lambda \sim c_\Lambda M_{\text{Pl}}^2 H_0^2$  is consistent with observation at the order-of-magnitude level, but the dimensionless coefficient  $c_\Lambda = \mathcal{O}(1)$  is not yet derived from first principles; this is a distinct Level C determination question that should not be conflated with the Level A resolution of the catastrophe. The outstanding technical tasks—verification of condition  $H_\Lambda$  against the full ECT Lagrangian, explicit first-principles computation of  $c_\Lambda$ , and the formal quantum non-renormalization analogue of the Ng–van Dam theorem [96]—are listed as O1, O2, O3 in Section 15.12 and together constitute the reformulated OP- $\Lambda$ 3.

**Meaning of dynamic dark energy in ECT.** In the present ordered-branch cosmology, “dynamic dark energy” does not mean a separate externally introduced fluid. It means that the late-time effective vacuum contribution is supplied by the background condensate sector itself, through the same ordered-branch amplitude field that controls the closure functions of the macroscopic equations. Accordingly, within the present ordered-branch closure,  $\Lambda_{\text{eff}}(X)$  is read as an ordered-branch background quantity rather than as an external rigid constant. What remains open is the unique first-principles derivation of its precise functional form from the microscopic condensate dynamics of the  $\Phi$ -medium.

**Connection to the galactic acceleration sector.** Within the present ordered-branch background closure, the same background history that drives  $w(z)$  away from  $-1$  also controls the epoch-dependent baseline critical acceleration  $g_{\text{bg}}^\dagger(z) = c_* H(z)/(2\pi)$  (§16.5). In this sense the dark-energy and galactic-dynamics sectors of ECT are not treated as independent: both are sourced by one common background history  $\phi_b(z)$  in the current closure. A correlated deviation in  $w(z)$  and in the epoch-evolution of  $g_{\text{bg}}^\dagger$  would therefore be a programme-level ECT signature.

The effective amplitude-sector energy density and pressure are those of the  $\phi$ -first background closure developed in Section 16.1 (eqs. (16.1)–(16.2)). Here we only recall the resulting late-time form, with the standard  $\phi$ -sector relation  $w_\phi = (K - U)/(K + U)$  reducing in the kinetic-subdominant regime to the expression below.

$$w \approx -1 + \frac{2\rho_{\text{kin}}}{3\rho_{\text{cond}}}, \quad \rho_{\text{kin}} \equiv \frac{1}{2}\omega(\phi)\dot{\phi}^2, \quad \rho_{\text{cond}} \equiv U(\phi), \quad (18.1)$$

which is the quantity confronted below with the observational dark-energy reconstructions. Since  $\rho_{\text{kin}} \geq 0$ , the present ordered-branch closure yields  $w(z) \geq -1$  at all redshifts (no phantom crossing). This is a

falsifiable structural prediction of the current macroscopic dark-energy closure. The no-phantom bound follows from the positivity of the kinetic coefficient  $\omega(\phi) > 0$  in the  $\phi$ -first closure, as established in the cosmological derivation chain of Section 16.1.

**Derivation status.** The structural inequality  $w \geq -1$  is a consequence of the present macroscopic  $\phi$ -closure rather than a separately fitted dark-energy ansatz. By contrast, the specific benchmark trajectory (18.2) and its parameters ( $f_0$ ,  $\kappa$ ) are Level B calibration inputs of the current DESI-facing late-time benchmark truncation, not first-principles outputs of bare ECT postulates. A first-principles value of the late-time equation-of-state parameters remains open.

**Discriminant with respect to alternative dark-energy routes.** The present ECT late-time sector is distinguished from three common alternatives:

- (i) **Rigid- $\Lambda$  route:** acceleration is not represented as a strictly immutable external constant, but as an ordered-branch background property;
- (ii) **Phantom route:** the present benchmark closure respects the no-phantom inequality  $w(z) \geq -1$ ;
- (iii) **Purely phenomenological  $w(z)$  fits:** the same background field that shifts  $w(z)$  also shifts  $H(z)$ ,  $G_{\text{eff}}(z)$ , and the age budget, so the observables are correlated rather than independently adjustable.

This correlated-background structure is one of the main ECT discriminants at the dark-energy level.

**Thawing condensate model.** If the condensate rolls slowly toward its potential minimum, the kinetic fraction decays:  $\rho_{\text{kin}}(z)/\rho_{\text{cond}} = f_0 e^{-\kappa z}$ , giving

$$w(z) = -1 + \frac{2f_0}{3} e^{-\kappa z}. \quad (18.2)$$

This is a *thawing quintessence* model:  $w \rightarrow -1$  in the past (condensate near potential minimum),  $w > -1$  today (condensate rolling).

### Observational confrontation: DESI and the no-phantom test

The late-time accelerated expansion, first established through type-Ia supernova distance measurements [133], is now tested with increasing precision by BAO surveys. The Dark Energy Spectroscopic Instrument (DESI) has published two data releases providing the most precise BAO distance measurements to date:

- **DESI DR1** (April 2024 [98]): 6 million galaxy and quasar redshifts. Combined with Planck CMB and type Ia supernovae (Pantheon+, Union3, or DESY5), a  $w_0 w_a$ CDM fit gives  $w_0 \approx -0.83$ ,  $w_a \approx -0.75$ , disfavouring  $\Lambda$ CDM at  $2.5\text{--}3.9\sigma$  depending on the supernova dataset.
- **DESI DR2** (March 2025 [134]): 14 million redshifts (three years of operation), doubling DR1. The preference for evolving dark energy *strengthened*:  $w_0 w_a$ CDM is preferred over  $\Lambda$ CDM at  $2.8\text{--}4.2\sigma$ . The best-fit CPL parameters indicate  $w_0 > -1$  today and  $w_0 + w_a < -1$ , formally implying a phantom crossing near  $z \approx 0.5$ .

**Is the phantom crossing real?** The apparent phantom crossing ( $w < -1$  at  $z > 0.5$ ) is a feature of the *CPL parametrisation*  $w(z) = w_0 + w_a z/(1+z)$ , which is a simple two-parameter approximation — not a physical model. Several independent analyses have shown [135, 136]:

1. The CPL form is too rigid to correctly describe both low- $z$  and high- $z$  behaviour simultaneously.

2. *Thawing quintessence* models (where  $w \geq -1$  at all times) are compatible with DESI data at the  $2\sigma$  level [137, 138].
3. Non-parametric reconstructions (Gaussian processes, crossing statistics) also find evolving dark energy but with larger uncertainty on whether  $w$  actually crosses  $-1$  [136].
4. The phantom crossing significance does not yet reach  $5\sigma$  and depends on the choice of supernova dataset [139].

The current observational situation can therefore be summarised as follows:

Statement	Status
$w \neq -1$ (dark energy evolves)	$2.8\text{--}4.2\sigma$
$w$ crosses $-1$ (phantom)	preferred in CPL, but $2\sigma$ -compatible with $w \geq -1$
$\Lambda$ CDM ( $w = -1$ exact)	increasingly challenged, not yet excluded

**ECT confrontation with DESI.** The ECT thawing model (18.2) with  $f_0 \approx 0.26$  and  $\kappa \approx 4.3$  (calibrated, not derived from first principles) is consistent with DESI data at the  $2\sigma$  level (Fig. 10). It reproduces the key observational feature —  $w > -1$  today, evolving toward  $w = -1$  in the past — while interpreting the apparent phantom crossing as a feature of the current benchmark reconstruction rather than as a true crossing of  $w = -1$ .

If future data (DESI Year 5, Euclid, Vera Rubin/LSST) robustly confirm a true phantom crossing, the present ordered-branch background closure would be falsified or would require a more radical late-time completion. Conversely, if the data continue to support evolving dark energy while remaining compatible with  $w \geq -1$ , the current ECT dark-energy interpretation remains viable. The no-phantom statement should therefore be read as a discriminant of the present macroscopic closure, not as a theorem about every conceivable late-time completion of ECT.

**Cosmological coincidence question (open programmatic status).** Some discussions of late-time cosmology raise the so-called cosmological coincidence question: why  $\Omega_m \approx 0.315$  and the present dark-energy fraction  $\Omega_{\phi 0} \approx 0.685$  (represented in the current ECT closure by the  $\phi$ -sector rather than by a rigid external  $\Lambda$ ) are of comparable order at the present epoch, despite  $\rho_m \propto a^{-3}$  while a rigid cosmological constant does not redshift. The status of this question is debated: its force depends on the measure assumed on cosmological histories, on the treatment of observer selection, and on priors over cosmological parameters, and some authors regard it as a selection artefact of the  $\Lambda$ CDM parametrisation rather than as a physically well-posed fine-tuning problem [140].

In the present ordered-branch closure, dark energy is supplied by the slow-rolling amplitude sector of the same ordered condensate that generates Newton’s constant, the causal speed  $c_*$ , and the reduced action scale  $\hbar$ , rather than by a rigid external constant added by hand. It is therefore natural to ask whether the present ECT thawing benchmark provides a materially different picture of the matter-to-dark-energy ratio

$$r(z) \equiv \frac{\rho_m(z)}{\rho_\phi(z)} = \frac{\Omega_{m0}}{\Omega_{\phi 0}} (1+z)^3 \exp \left[ -2f_0 \int_0^z \frac{e^{-\kappa z'}}{1+z'} dz' \right], \quad (18.3)$$

computed from the continuity equation  $\dot{\rho}_\phi + 3H(1+w)\rho_\phi = 0$  with the calibrated thawing equation of state (18.2). Numerical evaluation with the DESI-calibrated benchmark ( $f_0, \kappa$ )  $\approx (0.26, 4.3)$  yields  $\rho_\phi(z=1)/\rho_{\phi 0} \approx 1.11$  and  $\rho_\phi(z \rightarrow \infty)/\rho_{\phi 0} \approx 1.11$ : in this benchmark the condensate dark-energy density varies by only  $\approx 11\%$  between the present epoch and the asymptotic past within this benchmark. Using the illustrative order-unity criterion  $r(z) \in [1/3, 3]$ , the corresponding window occupies  $z \in [0, 0.93]$  in the present ECT thawing closure versus  $z \in [0, 0.87]$  in pure  $\Lambda$ CDM — a widening of about 7%.

We therefore do not regard the coincidence question as being materially softened by the present ECT benchmark, and we do not list coincidence alleviation among current ECT results. What can be stated honestly is narrower: ECT replaces a rigid external  $\Lambda$  with a dynamical condensate amplitude tied to the same framework that generates  $G_N$ ,  $c_*$ , and  $\hbar$ , so the matter-to-dark-energy ratio is at least formulated within a dynamical condensate sector rather than being fixed by a strictly rigid external constant. A first-principles derivation of  $(\Omega_{m0}, \Omega_{\phi0})$ , and any genuinely dynamical improvement over  $\Lambda$ CDM in the  $r(z)$  window, remain open programmatic questions; they should not be confused with the separate direct UV-vacuum-to- $\Lambda$  channel addressed by the emergent unimodular decoupling of Section 15, nor with the tracker/attractor question of initial-condition independence, which is not addressed by the current thawing benchmark.

**Falsifier for the dynamic-dark-energy programme.** The dynamic-dark-energy programme of ECT would fail if a completed ordered-branch cosmology were forced to reduce to a strictly rigid external cosmological constant with no admissible correlated background variation, or if the observed late-time behaviour required unavoidable phantom crossing incompatible with the positive-kinetic ordered-branch closure. It would also be weakened if the quantities  $w(z)$ ,  $H(z)$ ,  $G_{\text{eff}}(z)$ , and the age budget could only be fit by mutually independent closure choices rather than by one common background history.

#### 18.4 Dark-sector discriminants and falsifiers of the present closure

The ordered-branch architecture of ECT (P4, P6, BR1) yields a set of dark-sector discriminants that are structurally distinct from those of the  $\Lambda$ CDM and MOND alternatives. A comprehensive list of falsifiable ECT predictions is given in Table 74; the present subsection highlights those that bear most directly on the dark-sector interpretation.

**Environmental modulation of the critical scale (F1).** The most distinctive dark-sector handle of the present macroscopic branch is not a new particle species but an environment-dependent effective critical scale  $g_{\text{eff}}^\dagger$  inherited from the same ordered-branch galactic closure developed in Section 17. In ECT the galactic mass discrepancy is controlled by the ordered-branch response and therefore need not be governed by a strictly universal acceleration constant. A statistically significant positive correlation between fitted  $g_{\text{eff}}^\dagger$  and environmental indicators would support the ECT dark-sector reading. Absence of such modulation at the currently targeted level would constrain the calibrated environmental-response combination

$$\gamma \frac{4\pi\bar{\rho}_{\text{m,env}}}{U_0''(\bar{\phi}_{\text{env}})}$$

and the density-only environment ansatz, rather than directly falsifying the ordered-branch amplitude mechanism as a whole (prediction F1, Table 74).

**No galactic WIMP requirement.** The galactic mass discrepancy in ECT arises from the nonlinear ordered-branch  $\phi$ -closure, not from a hidden collisionless particle species. Current direct-detection bounds have reached spin-independent cross sections below  $\sigma_{\text{SI}} < 10^{-47} \text{ cm}^2$  without any positive signal that could account for the galactic mass-discrepancy phenomenology (e.g. [132]). A robust detection of a particle species specifically shown to account for the galactic mass discrepancy on galaxy scales would therefore falsify the present macroscopic  $\phi$ -branch-only interpretation of that channel; it would not by itself falsify the full ECT framework. The mere detection of a subdominant new particle species would not challenge the galactic  $\phi$ -branch interpretation.

**No-phantom dark energy (F5).** The present ordered-branch closure yields  $w(z) \geq -1$  at all redshifts, as discussed in Section 18.3. Current DESI data remain compatible with this bound at the  $2\sigma$  level [98, 134]. A robust confirmation of true phantom crossing at  $> 3\sigma$  would falsify the present macroscopic dark-energy closure (prediction F5, Table 74).

**Cluster-merger lensing morphology (F10).** In the  $\phi$ -closure, the convergence peak in a merging cluster tracks the more compact baryonic component, whether this is the stellar/BCG core or the gas core (Section 17.2). This differs from the simplest collisionless-halo reading of  $\Lambda$ CDM, under which the dominant lensing peak is expected to follow the collisionless galaxy/BCG component. The Abell 520 system, where the observed lensing peak is gas-peaked rather than galaxy-peaked [117, 118], is therefore a particularly sharp discriminant. Systematic merger-cluster surveys will sharpen this test (prediction F10, Table 74).

**Disambiguation: the  $\phi$ -branch is not the fifth force.** The galactic  $\phi$ -modification and the ECT fifth force are not the same effect. The former is a macroscopic ordered-branch response on kpc scales; the latter is a Planck-suppressed microscopic coupling already discussed in the dedicated fifth-force section (Section 7). They probe different aspects of the condensate architecture and should not be used interchangeably when comparing ECT with dark-sector alternatives.

Taken together, these discriminants are not independent ad hoc predictions but consequences of the same ordered-branch architecture within the present macroscopic closure: the galactic branch predicts environment-modulated effective gravity without particle halos, the dark-energy branch predicts a non-phantom late-time background, and the cluster sector provides a morphology-level test of the same closure on larger scales.

## 18.5 Section-level status summary

The dark-sector interpretation of ECT, as developed from the ordered-branch architecture in Sections 18.1–18.4, should be read at the present stage in three layers.

**Established within the macroscopic branch (Level B):** the galactic mass discrepancy can be addressed by the nonlinear ordered-branch  $\phi$ -closure without particle dark matter, with the critical-scale logic anchored in the same macroscopic programme that yields the BTFR/RAR phenomenology; late-time accelerated expansion can be interpreted as ordered-branch background energy; and the benchmark dark-energy equation of state satisfies  $w(z) \geq -1$ .

**Structurally possible but not yet developed quantitatively:** collective condensate excitations and additional coherent-branch sectors as dark components beyond the galactic branch beyond the galactic branch. Their detailed treatment requires the coherent branch (BR1) and is deferred to Section 34 of the Quantum Sector.

**Open:** the relic abundance, stability, and production history of such dark-sector excitations; the first-principles derivation of the effective cosmological fractions; and the final observational verdict on the no-phantom prediction from DESI, Euclid, and Rubin-era data. The most important near-term discriminants are summarised in Table 74, especially the environmental modulation of  $g_{\text{eff}}^{\dagger}$  (F1), the no-phantom bound (F5), and the cluster-merger morphology test (F10).

The macroscopic dark-sector reading developed here should therefore be seen as a controlled Part II interpretation layer, not as a complete microscopic ontology of the dark sector. Unlike the standard  $\Lambda$ CDM reading, it does not begin by postulating two independent hidden ingredients for the galactic mass discrepancy and the late-time accelerated expansion. The detailed ontology of coherent-branch and collective dark-sector excitations belongs instead to the Quantum Sector.

## 19 Observational Tests, Falsifiers, and Chapter Conclusions

### 19.1 Astrophysical predictions and observational tests

*Status: all Level B unless explicitly noted.*

**Postulate grounding and scope discipline.** The present subsection does not introduce a new independent sector of the theory. It collects the numerical and observational consequences of the ordered-branch

programme already developed in Sections 16.5–18. Its structural basis is the ordered branch itself (P4) together with the admissibility of non-uniform or slowly evolving branch responses at the macroscopic level (P6). For clarity, the discussion below is organised into four distinct layers: the structural parent condensate background, the benchmark late-time truncation used as the present control solution, the first non-benchmark derived-parent numerical corridor, and finally the observational and strong-curvature tests built on top of those layers.

### **Late-time cosmology: Hubble tension, age, and JWST implications (legacy pointer)**

*Legacy-pointer note.* The present subsection is retained only as a pointer to earlier benchmark late-time cosmology material. The headline cosmological constraint on  $\varepsilon$  is given by the retained five-probe analysis in §16.5 (§16.5–§16.5) together with Appendix AG–Appendix AH. Nothing in the present legacy pointer should be used to quote the current retained-five-probe constraint on  $\varepsilon$ .

**What was here previously.** Earlier drafts of this preprint carried an extended benchmark late-time closure subsection at this location, including an effective scalar–tensor action, a benchmark FRW closure, an analytic estimate of  $\Delta H_0/H_0$ , a benchmark age  $t_0^{\text{ECT}} \simeq 13.1$  Gyr, and a longtable of benchmark numerical outputs. That material is not the headline result of the present version and is therefore removed from the main text as of the retained-band rebuild.

**Where the content now lives.** The derived macroscopic ordered-branch background system to which the earlier benchmark was a local truncation is recorded in Appendix AD; its numerical algorithm and admissible-deformation robustness programme are recorded in Appendix AU. The retained-band methodology that replaces the earlier benchmark-centric narrative is collected in Appendix AH.

### **Numerical robustness under admissible late-time deformations (legacy auxiliary layer)**

*Legacy pointer.* The earlier benchmark and derived-parent robustness scans — including the admissible-deformation test of the amplitude-sector closure and the associated numerical stability checks — are preserved for continuity in the late-time background appendices (Appendix AD and Appendix AU) and should be read as legacy auxiliary material, not as the current cosmological headline. The current headline cosmological result is the retained five-probe band of §16.5; everything in the present legacy layer is kept only to document the numerical infrastructure on which the retained-band diagnostic pipeline is built.

### **Derived-parent condensate: legacy auxiliary scan and JWST maturity budget (legacy auxiliary layer)**

*Legacy pointer.* The older derived-parent corridor, the  $(\omega_0, \phi_0)$  working-point scan summarised in Table 69, and the associated semi-analytic JWST maturity budget (linear-growth solver on the derived-parent background, maturity factors  $\mathcal{R}_{\text{gal}}$  and  $\mathcal{R}_{\text{BH}}$ , and the representative JWST anchor cases) are retained only as an auxiliary exploratory layer of the cosmological apparatus. The precise definitions, the full linear-growth derivation, the maturity factor conventions, and the numerical pipeline are recorded in the dedicated cosmology appendices (Appendix AD.10, Appendix AD.11, and Appendix AD.9). The comparative cosmological timeline is given in Fig. 15, and Fig. 16 shows the internal multi-sector organisation of the ECT picture itself, which should not be interpreted as a direct comparison of absolute cosmic ages with  $\Lambda$ CDM. The current headline cosmological extraction is the retained five-probe band of §16.5 and Appendix AG–Appendix AH; the present subsection and its table are *not* the current cosmological headline.

**Table 69:** Representative derived-parent working points from an auxiliary  $(\omega_0, \phi_0)$  scan, with scan input values  $\beta = 0.8$ ,  $\mu = 1.5$ ,  $A_2 = \mu^2/(6\beta^2)$ ,  $A_3 = A_4 = 0$  retained for reproducibility of this specific legacy/scan layer. The quoted  $\Delta H_0/H_0$  entries are scan-derived H1-route indicators, not stabilised H2 observables. They are *not* the current retained-five-probe cosmological headline: the current headline result is the retained band  $\varepsilon \in [0.0296, 0.0376]$  at  $1\sigma$  reported in §16.5. The present table is therefore an auxiliary scan layer only; its parameter values are legacy scan inputs, not retained-band central-point values, and should not be used to quote the current cosmological constraint on  $\varepsilon$ .

Point	$\omega_0$	$\phi_0$	$\Delta H_0/H_0$	$t_U(z = 10)$ [Gyr]	$G_{\text{eff}}/G_N$	$D/D_{\text{ref}}$
Balanced	25	−0.10	+2.43%	0.386	1.57	0.979
Late- time-shift- priority	30	−0.10	+2.73%	0.394	1.49	0.993
Age- priority	25	−0.08	+1.59%	0.390	1.53	0.980

The corresponding parameter scan and working-point selection are recorded internally in the late-cosmology apparatus; no figures are reproduced in the retained §16.5 layer.

### Observational signatures compatible with accelerated early development

The retained-band cosmological framework of §16.5 is consistent with, and motivated by, a set of qualitative observational signatures of accelerated early development already discussed in the literature. JWST has revealed early candidates for overmassive SMBHs relative to their stellar host galaxies [141, 142], very early luminous and massive galaxy systems (including spectroscopically confirmed objects at  $z \gtrsim 14$  [143]), and massive quiescent galaxies at unexpectedly high redshifts [144, 145, 146]. A notable signature is the displacement of some early objects along the  $M_{\text{BH}}-M_\star$  relation while remaining closer to the local  $M_{\text{BH}}-\sigma$  relation [141], which is qualitatively consistent with a maturity channel where central compact objects develop faster than the stellar host component [142, 147]. These observations do not prove ECT, but they motivate precisely the accelerated maturity channels that map onto the retained-band extraction from the JWST early-galaxy channel. The framework also predicts possible systematic shifts in velocity dispersions or virial speeds at fixed host mass, compact rapidly assembled massive hosts, and a potential dependence on environment through the background condensate history. These remain qualitative predictions rather than established closure-level results at the present stage.

#### 19.1.1 Integrated Sachs–Wolfe diagnostic

Late-time evolution of the condensate response modifies the time dependence of the gravitational potentials and therefore the integrated Sachs–Wolfe (ISW) channel. Within the rebuilt late-time analysis of §16.5, the ISW response is treated as one of the retained five probes used to constrain the effective uniform- $\varepsilon$  diagnostic parameter. The full ISW extraction — the response function  $\mu(a) = G_{\text{eff}}(a)/G_N$ , the ISW–tracer overlap proxy, its observational inputs, the extraction statistic, the  $1\sigma/2\sigma$  interval, and the associated methodological limitations — is given in Appendix AL. Under the prior  $\varepsilon \geq 0$  motivated in §16.5, the ISW channel is retained as a one-sided consistency bound whose upper edge enters the joint retained band of §16.5.

These observational handles connect directly to the falsifier logic summarised in Table 74, especially the late-time background tests and the high-redshift maturity indicators.

## Exploratory strong-curvature frontier: black holes and compact objects

Black-hole and compact-object implications of the ordered condensate branch are potentially important but remain exploratory (Level B/Open); they are not part of the present controlled macroscopic derivation and should be read as a forward research direction rather than as an established observational output of Part II. For GW-related LIV effects the estimate of Section 13.8 applies: the expected propagation-time shift  $\Delta t_{\text{GW}} \lesssim 10^{-64}$  s is negligible for all currently observed sources. The value of this block is therefore primarily organisational: it marks the strong-curvature observational frontier that any future ECT completion must eventually address.

**Dark-sector synthesis.** At the present stage, ECT supports a three-channel dark-sector reading: (i) a galaxy-scale ordered-branch response closure that already addresses the mass discrepancy without standard particle halos; (ii) a late-time dark-energy route carried by the ordered background; and (iii) the still-open possibility of additional collective or topological condensate excitations. The first of these is the strongest current macroscopic result. The third remains structurally admissible but not yet observationally required. Table 67 summarises the three channels and their discriminants.

**Summary pointer to the retained cosmological band.** The cross-probe effective constraint obtained in the rebuilt §16.5 combines the per-channel extractions of Appendix AG through Appendix AL under the common background module of Appendix AH, and yields a retained joint effective band  $\varepsilon \in [0.0296, 0.0376]$  at  $1\sigma$  (with  $2\sigma$  extension  $[0.0207, 0.0425]$ ). This is the headline observational output of the late-time uniform- $\varepsilon$  diagnostic layer; it is an empirical consistency window, not a first-principles closure-level prediction, and its interpretation at closure level remains the content of open problem OP-Hubble-derive (§16.5). An age-viability note, discussed in AF.4, accompanies the band at its present central value.

## 19.2 Conclusions of Part II: Macroscopic Physics

*This subsection summarises the macroscopic construction of ECT developed in Part II (Sections 11–18). It collects only the results that belong to the macroscopic branch of the theory: the effective gravitational sector, the cosmological programme, the galactic and cluster phenomenology, and the associated dark-sector reinterpretation. All results are classified by the Level A/B/Open discipline maintained throughout the paper. The derivation logic of the macroscopic branch is shown schematically in Figure 30.*



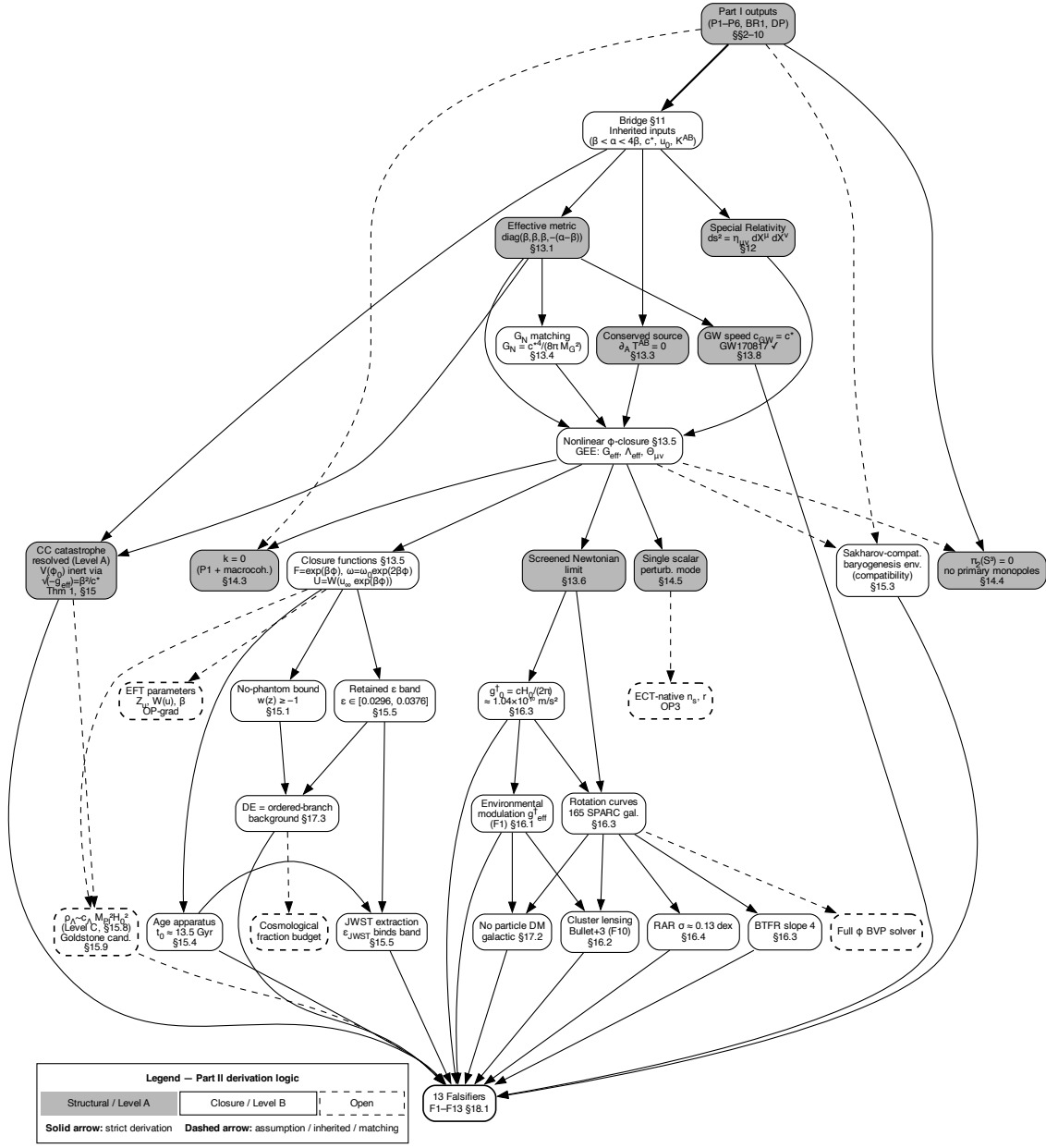


**Figure 30:** Derivation logic of Part II (Macroscopic Physics). Starting from the Part I outputs inherited through the bridge of Section 11.3, the diagram organises the macroscopic programme into four layers: (i) the inherited ordered-branch structural inputs, (ii) the effective gravitational and cosmological closure sector, (iii) the benchmark and derived-parent numerical implementations, and (iv) the observational and falsifier layer. The main chains shown are: emergent special relativity, effective metric and  $G_N$  matching, the nonlinear  $\phi$ -closure with derived closure functions, gravitational waves ( $c_{\text{GW}} = c_*$ ), screened Newtonian phenomenology, structural cosmology ( $k = 0$ ,  $\pi_2(S^3) = 0$ , single scalar mode), ordered-branch cosmology ( $w \geq -1$ , Hubble mechanism, age apparatus, JWST implications), galactic phenomenology (rotation curves, BTFR slope 4, RAR,  $g_0^\dagger \approx cH_0/(2\pi)$ , environmental modulation), cluster-merger morphology, dark-sector reinterpretation, and the falsifier map. Node shading: dark = structural (Level A), light = closure-level (Level B), dashed outline = benchmark/programme-level or open. Solid arrows denote derivational dependence; dashed arrows denote unresolved closures or open completion steps.

**Macroscopic outcome of Part II.** Part II develops the macroscopic physics of ECT from the ordered-branch inputs inherited from Part I. Its organising postulate-level basis is the existence of the ordered branch itself (P4), together with the admissibility of non-uniform and slowly varying ordered configurations at macroscopic scales (P6). Within that inherited framework, Part II constructs the effective gravitational sector, the classical-cosmology programme, the ordered-branch cosmological closure, the galactic and cluster-scale phenomenology, and the corresponding dark-sector reinterpretation.

The strongest current outputs of the chapter are: the structural flatness result  $k = 0$ , the elimination of the primary monopole channel, *the resolution at Level A of the classical cosmological-constant catastrophe* (Section 15; Theorem 15.3): fixed  $\sqrt{-\det K^{AB}} = \beta^2/c_*$  from  $n^A n_A = 1$  renders the classical baseline  $V(\phi_0)$  inert for the local emergent gravity (Theorem 15.3(iv), unconditional), and absorbs the zero-derivative one-loop vacuum contribution under condition  $H_\Lambda$  (Theorem 15.3(v)); the direct  $10^{120}$ -level cancellation characteristic of the standard framework is structurally absent; separately, the *value* of  $\rho_{\Lambda, \text{obs}}$  itself is a distinct Level C determination problem with natural scaling  $\rho_\Lambda \sim c_\Lambda M_{\text{Pl}}^2 H_0^2$  consistent with observation at order-of-magnitude level, the no-phantom bound  $w(z) \geq -1$  within the present cosmological closure, the BTFR slope 4 in the critical galactic branch, the baseline critical scale  $g_0^\dagger \approx cH_0/(2\pi)$ , the environmental-modulation framework for the galactic mass discrepancy, and the cluster-merger morphology criterion. At the same time, the chapter now distinguishes four layers of macroscopic control: the structural parent ordered-branch background, the benchmark late-time screened-branch truncation, the first derived-parent numerical corridor, and the exploratory strong-curvature / non-benchmark sector. This layered reading is essential for correctly interpreting the numerical claims collected below.

**Core results of Part II.** Within the inherited ordered-branch framework, the macroscopic branch establishes the following main results:

1. A controlled effective gravitational sector built on the ordered Lorentzian branch inherited from Part I, including the macroscopic metric structure, the identification  $c_* = c$ , the matching to  $G_N$ , the generalised Einstein equations with three characteristic departures from pure GR ( $G_{\text{eff}}$ ,  $\Lambda_{\text{eff}}$ ,  $\Theta_{\mu\nu}$ ), and closure functions whose functional forms ( $F = e^{\beta\phi}$ ,  $\omega = \omega_0 e^{2\beta\phi}$ ,  $U = W(u_\infty e^{\beta\phi})$ ) are derived from the ordered-branch EFT.
2. A universal signal-speed bound (§12.6): the characteristic cone of the ordered-branch principal symbol confines all disturbances to within the causal cone; massive linear scalar excitations propagate strictly inside it, massless excitations on its boundary; the vacuum light speed is the experimentally accessible manifestation of the ordered-branch causal speed, not a photon-specific constant. The EFT parameters  $(\alpha, \beta)$  characterise the vacuum state and are not position-dependent; macroscopic gravity varies the geometry, not the cone speed.
3. Three structural cosmological outputs of the ordered branch: spatial flatness  $k = 0$ , absence of the primary monopole channel ( $\pi_2(S^3) = 0$ ), and a single leading scalar perturbation mode.
4. A late-time ordered-branch cosmology in which the present closure yields  $w(z) \geq -1$ , provides a benchmark route for Hubble-tension alleviation, and supplies the age/lookback apparatus used in the JWST analysis. Its empirical closure under the uniform- $\varepsilon$  diagnostic layer is the retained five-probe joint band of §16.5,  $\varepsilon \in [0.0296, 0.0376]$  at  $1\sigma$ , as assembled from the per-probe extractions of Appendix AG–Appendix AL and the methodology of Appendix AH.
5. A galactic critical branch that reproduces the BTFR slope 4, the RAR structure, and rotation-curve phenomenology through the ordered-branch  $\phi$ -closure rather than through particle dark matter.
6. A baseline critical acceleration scale  $g_0^\dagger \approx cH_0/(2\pi)$  together with the environmental modulation framework  $g_0^\dagger \rightarrow g_{\text{eff}}^\dagger$ .
7. A cluster-scale morphology test in which the same closure predicts that the convergence peak follows the more compact baryonic component rather than a mandatory collisionless dark halo.

8. A sector-by-sector observational role analysis of the non-Einstein contribution  $\Theta_{\mu\nu}[n]$  across five phenomenological channels, showing that the most consequential present beyond-benchmark NLEE effects occur in cluster-merger lensing and JWST growth, whereas other channels remain background-dominated or effectively degenerate with the benchmark  $\phi$ -closure.
9. A dark-sector reinterpretation in which galactic mass discrepancy, possible coherent/topological dark sectors, and late-time dark energy are treated as distinct questions within the same condensate architecture.

**What Part II inherits, what it establishes, and what remains open.** Part II does not start from a blank slate. It inherits from Part I the existence of the ordered Lorentzian branch, the geometric macroscopic sector, and the branching logic between the geometric and coherent developments.

Within that inherited framework, Part II establishes the strongest macroscopic structural outputs: the homogeneous branch is born flat, the primary monopole channel is absent, and the perturbative scalar sector is not intrinsically multi-field.

At the next level, the present ordered-branch  $\phi$ -closure yields controlled macroscopic consequences:  $w(z) \geq -1$ , the Hubble/JWST mechanism, the BTFR/RAR programme, the baseline critical scale  $g_0^\dagger$ , the environmental-modulation framework, and the cluster-merger morphology test. Between the closure-level and the open layers, the functional forms of the closure functions ( $F = e^{\beta\phi}$ ,  $\omega = \omega_0 e^{2\beta\phi}$ ,  $U = W(u_\infty e^{\beta\phi})$ ) are already derived from the ordered-branch EFT amplitude reparametrisation (Level B; Appendix AD); what remains open is the first-principles determination of the underlying EFT parameters ( $Z_u$ ,  $W(u)$ ,  $\beta$ ) from bare P3 (OP-grad).

A separate beyond-benchmark layer is now provided by the observational NLEE footprint analysis, which identifies how the non-Einstein term  $\Theta_{\mu\nu}[n]$  enters five phenomenological sectors with different separability status. This analysis shows that the most consequential current NLEE channels are cluster-merger lensing and JWST growth, whereas other sectors are either background-dominated or effectively degenerate with the benchmark  $\phi$ -closure. That distinction should be kept explicit in any reading of the macroscopic numerical claims.

At a weaker benchmark level, specific late-time trajectories, calibrated dark-energy reconstructions, semi-analytic maturity budgets, and practical galaxy-by-galaxy fits depend on closure choices and calibrated parameters. The observational and numerical support for these claims is organised in Section 19.1 in corresponding layers: benchmark control, admissible deformations, derived-parent numerics, and exploratory strong-curvature prospects.

What remains open is the primordial spectrum ( $n_s$ ,  $r$ ), the cosmological fraction budget, the full nonlinear  $\phi$  boundary-value problem, and the detailed ontology of coherent dark-sector excitations.

**Table 70:** Numerical macroscopic outputs of Part II. The entries are not all of the same logical type: some are structural predictions, some are closure-level benchmark estimates, and some are comparative fit diagnostics. The final column records this status explicitly.

Prediction	ECT value	Observation / comparison	Status
BTFR slope	4 (algebraic)	$3.98 \pm 0.08$	Structural
$g_0^\dagger$ (ECT baseline)	$1.04 \times 10^{-10} \text{ m/s}^2$	$a_0 \approx 1.2 \times 10^{-10}$ (Mc-Gaugh)	Benchmark consistency
MW rotation ( $g_{\text{eff}}^\dagger \approx 1.72 g_0^\dagger$ )	$\chi^2/N = 2.95$	$\Lambda\text{CDM comparison: } 6.55$	Comparative fit
$n_s$ (critical-fluct. corridor)	0.96–0.97	$0.965 \pm 0.004$	Programme-level estimate

Prediction	ECT	Obs./comp.		Status
$\eta_B$ (leptogenesis)	$\sim 9 \times 10^{-10}$	$\sim 6 \times 10^{-10}$		Benchmark only
$ c_{\text{GW}}/c - 1 $ (GW170817)	$< 6 \times 10^{-15}$	$< 6 \times 10^{-15}$		Already satisfied
$w_0$ (DESI 2024)	$-0.83$	$-0.827$		Closure consistency
Retained joint $\varepsilon$ band ( $1\sigma$ )	$[0.0296, 0.0376]$	5-probe (§16.5)	intersection	Diagnostic-layer effective result

**Bridge to Part III.** With the macroscopic branch in place, the next task is to return to the coherent and quantum structure of the condensate. Part III develops the coherent branch across eleven thematic steps: the action-scale and winding programme, wave kinematics and conservation laws, the Hilbert-space bridge through reflection positivity and unitarity, exchange-sector topology and Dirac structure, the unified vacuum-response programme, decoherence and the arrow of time, the quantum–classical boundary and Born-type probability, entanglement, the wider topological/dark-sector ontology, black-hole thermodynamics and the information-exclusion result, and the analogue-laboratory instantiability programme.

**Conceptual output: metric as a derived object.** The macroscopic gravitational sector rests on a foundational conceptual result: in ECT geometry is not the primitive ontology. The effective metric is a derived bookkeeping object encoding how excitations propagate on the ordered condensate background. Gravity is the long-wavelength geometric response of the condensate to deformations of its orientation structure  $n^A$ . This is not merely a reinterpretation of the gravitational equations already obtained; it is a reversal of the ontology assumed in standard approaches: the condensate is primary, geometry is secondary. Two further foundational issues find natural homes in the macroscopic branch: the primary condensate vacuum satisfies  $V''(\phi_0) > 0$  at tree level, and the one-loop RG analysis closes the SM-type metastability channel in the amplitude sector ( $\beta_\lambda > 0$ , §8.4.5; Level B), a structurally cleaner situation than the top-Yukawa-driven metastability of the Standard-Model electroweak vacuum [61, 62] (full branch-architecture and embedded-sector analysis open; §8.3); and the matter-to-dark-energy ratio  $r(z) = \rho_m/\rho_\phi$  in the calibrated ECT thawing benchmark  $(f_0, \kappa) \approx (0.26, 4.3)$  is only marginally wider than in pure  $\Lambda$ CDM (about 7% for the illustrative order-unity window). We therefore keep the so-called cosmological coincidence question as an open programmatic issue rather than as a current ECT result (§18.3); this point is separate from the direct UV-vacuum-to- $\Lambda$  channel addressed by the emergent unimodular decoupling of Section 15.

### 19.3 Global Level-4 self-consistency checklist

**Role of the checklist.** The present table is not a second derivation map and not a duplicate of the prediction table. Its purpose is different: it provides a compact Level-4 audit of the framework as a whole, combining inherited consistency conditions from Part I, macroscopic results from Part II, and deferred or open items that extend into the Quantum Sector. It should therefore be read as a global status board rather than as a local summary of Section 19 alone.

**Postulate-level organisation.** At the structural level, the checklist probes four layers of the ECT architecture: the microscopic consistency of the Euclidean  $\Phi$ -medium (P1–P3), the ordered macroscopic

branch and its admissible non-uniform developments (P4–P6), the coherent sector (BR1, S10), and the still-open bridges required to close the full framework. The PASS / PART. / PROB. / OPEN labels should be interpreted in that same layered sense. Unlike the derivation map, which records logical dependencies, and unlike the falsifier table, which records observational tests, the present checklist answers a different question: which framework-level consistency targets are already passed, only partially controlled, structurally motivated but not rigorous, or still open.

**Architectural completions from the emergent matter-sector trilogy.** The discrete-symmetry architecture (§9.4), the anomaly architecture (§9.5), and the flavour architecture (§9.7) now provide an explicit consistency backbone of the emergent chiral gauge sector. Their Level-4 audit status is therefore recorded in the checklist below alongside the original whole-framework consistency items.

*Scope legend:* I = inherited from Part I (foundations); II = macroscopic branch of Part II; III = Quantum Sector / Part III; G = global whole-framework closure problem.

**Table 71:** Level-4 self-consistency checklist. PASS = derived or verified consistent at Level A/B; PART. = partial derivation or prediction awaiting precision test; PROB. = structurally motivated, rigorous proof pending; OPEN = known open problem.

Status	Scope	Check	Key result	Ref.
PART.	I	Condensate stability	Tree-level local stability plus one-loop closure of the SM-type metastability channel in the primary amplitude sector; full branch-architecture stability remains open	§8.4.5, §3
PASS	I	Ghost-freedom of primary $\Phi$ -closure	Physical mode $\lambda > 0$ at $\alpha > \beta$ in the primary condensate action	§3
PART.	I	Linearised graviton free of identified ghost pathology	Induced effective-metric sector (A) with Fierz–Pauli quadratic closure and massless spin-2 interpretation (B); cf. OP3	§8.5
OPEN	G	Full non-perturbative ghost-freedom and exact TT closure of emergent graviton sector	Completion-level question tied to gauge/gravity closure (OP3)	§8.5, §38.1
PASS	I	LIV empirical compatibility	$ c_{\text{GW}}/c - 1  < 6 \times 10^{-15}$ from GW170817 in the current EFT parametrisation; Planck-suppressed GW delay $\Delta t_{\text{GW}} \sim 10^{-64}$ s; operator-level unification of LIV parametrisations remains open	§36
PART.	I	Discrete-symmetry architecture of emergent matter sector	Three-layer architecture: geometric backbone (Level A); conditional CPT route via Osterwalder–Schrader reconstruction for reconstructible local sectors (A/B); $\mathcal{L}_5$ reclassified as CPT-odd vector bilinear (B); full nonlinear CPT closure open (OP-CPT1)	§9.4
PART.	I	Anomaly architecture of emergent chiral gauge sector	Electroweak anomaly constraints inherited at ordered-branch level (B); $\mathcal{L}_5$ anomaly-transparent (B); full Standard-Model closure conditional on colour / matter completion (OP-GUT6 family)	§9.5
PART.	G	Flavour architecture (CKM/PMNS)	CKM as basis misalignment (A); overlap route to hierarchical mixing (B); “CKM small / PMNS large” structural narrative (B/C); quantitative flavour closure open under OP-Yukawa / OP-generations	§9.7

Status	Scope	Check	Key result	Ref.
PASS	I	Causality	Retarded propagation of ordered branch (Level A); directed decoherence $\Gamma_{\text{irr}} \geq 0$ (Level A)	§3.8
PROB.	G	Second law $dS/dw \geq 0$	Level-A directional backbone + Level-B ohmic/Markov closure; full microscopic H-theorem open (OP-Q17)	§3.9
PROB.	III	Born measure	Quadratic structure from RP inner product; conditional uniqueness under C1–C3 via Gleason; unique outcome selection open (OP-Q19)	§30.4
PART.	II	Primordial perturbations $n_s, r$	Critical $O(4)$ fluctuation estimates yield $n_s \sim 0.96\text{--}0.97$ (§14.6); full derivation open	§14.1
PART.	II	Baryogenesis	Sakharov-compatible environment (Level B); $\eta_B$ benchmark only, not ECT-native derivation (OP7)	§16.3
PASS	III	Unruh temperature	$T_U = \hbar a / (2\pi c_* k_B)$ from $G_E(X, X')$	§25.4
PASS	III	Orientation-sector Casimir (ideal boundaries)	Vacuum response from soft orientation sector: computed in minimal EFT	§25.3
OPEN	III	Casimir: lab applicability	Material boundaries $\rightarrow$ soft orientation sector: not derived	§25.3
OPEN	II	Tensor ratio $r$	ECT-native derivation pending; removed borrowed slow-roll formula	§14.1
PROB.	G	Renormalisability	Fixed Euclidean background avoids GR non-renorm.; full loop closure pending	§38.1
PART.	G	3 fermion generations	Spectral route identified: bound-state counting gives 3 at $y = O(1)$ (§9.6); flavour-architecture systematisation in §9.7; strict derivation of exactly three generations open	§9.6, §9.7
PART.	G	$\alpha_{\text{fs}}; \text{SU}(3)$	$\alpha_{\text{fs}} = q^2 / (4\pi Z_A)$ , $Z_A^{\text{IR}} \approx 10.9$ ; UV problem recast as electroweak target $(Z_B, Z_W, \theta_W)$ (§7.2); $\text{SU}(3)$ origin open	§7.2
PART.	II	Late-time background closure	No-phantom $w \geq -1$ within the present $\phi$ -closure; age/distance apparatus established; late-time diagnostic-layer response under the uniform- $\varepsilon$ ansatz yields retained five-probe joint effective band $\varepsilon \in [0.0296, 0.0376]$ at $1\sigma$ ( $[0.0207, 0.0425]$ at $2\sigma$ ); full early+late $H_0$ closure (H2) and closure-level $\varepsilon(z)$ derivation (OP-Hubble-derive) remain open	§16.1, §16.4, §16.5
PART.	II	JWST correlated background	Correlated age/distance/growth logic established; derived-parent corridor and maturity budgets give partial alleviation only, not a full morphology-level solution	§16.5, §19.1
PART.	II	Force-law dimensionality	Universal $d_{\text{force}}(x)$ crossover $3 \rightarrow 7/3 \rightarrow 2$ in present closure	§16.8
PART.	II	Environmental modulation of $g_{\text{eff}}^\dagger$	Framework for environment-dependent galactic critical scale established; precision correlation test pending	§17, §18.4
PART.	II	Galactic dark-sector reinterpretation	Galactic mass discrepancy addressed by $\phi$ -closure without particle dark matter; cosmological fraction budget still open	§18.2

Status	Scope	Check	Key result	Ref.
PART.	II	Cluster-merger morphology	Convergence peak follows more compact baryonic component in present $\phi$ -closure; morphology robust, amplitude still closure-level	§17.2, §18.4

## 19.4 Global derivation, status, and falsifier maps

**Role of the global maps.** The following tables provide three complementary global views of the ECT programme. Table 72 records the logical derivation architecture: which sectors depend on which earlier inputs and closure assumptions. Table 73 records the epistemic status of those outputs in the Level A / Level B / Open discipline adopted throughout the paper. Table 74 records the observational exposure of the framework: the concrete signatures, discriminants, and falsifiers through which the programme can be tested. These three maps should therefore not be read as redundant summaries, but as answers to three different questions: what follows from what, how strongly it is established, and how it can fail.

**Postulate-level organisation.** At the highest structural level, all three maps are organised by the same postulate hierarchy: the microscopic Euclidean  $\Phi$ -medium and its consistency conditions (P1–P3), the ordered macroscopic branch and its admissible non-uniform developments (P4–P6), and the coherent sector (BR1, S10) whose full ontology is taken up later in the Quantum Sector.

The narrative conclusions of Part II were summarised in Section 19.2, while the audit-style checklist was given in Section 19.3. The tables below complement those layers by presenting the same framework as a derivational map, a status map, and a falsifier map. Entries should be read against the same layered vocabulary used in the final status board (Section 19.5): inherited structural inputs, closure-level outputs within the present  $\phi$ -first programme, benchmark/calibrated implementations, and open problems. For the macroscopic branch developed in Part II, the most distinctive near-term discriminants are the environmental modulation of  $g_{\text{eff}}^{\dagger}$  (F1), the no-phantom dark-energy bound (F5), and the cluster-merger morphology test (F10).

**Table 72:** Derivation map of ECT: physical objects and their origins in the new Level A / Level B / Open discipline. Entries: “derived” = structural Level A consequence; “structural / effective (Level A/B)” = proven in pure-metric limit, Level B in  $\phi$ -first closure; “matched (Level B)” = EFT matching relation; “embedded” = introduced consistently, not derived from bare scalar action; “open” = active research direction.

Object	Origin in ECT	Status
4D Euclidean space	Postulate P1	postulate
$O(4)$ symmetry	Postulate P2	postulate
Condensate $\Phi$	Postulate P4	postulate
Lorentzian metric $g_{\mu\nu}$	SSB $O(4) \rightarrow O(3)$ with $\alpha > \beta$	derived
Macroscopic arrow of time	Reduced-state decoherence plus low-entropy coherent initial sector	effective / closure-dependent (Level A/B)
Speed of light $c$	$c_* = \sqrt{\beta/(\alpha - \beta)}$	identified
Gravitational coupling $G_N$	Geometric EFT matching: $G_N = c_*^4/(8\pi M_G^2)$	matched (Level B)
Ordered-branch amplitude variable $\phi$	Macroscopic closure variable for slow amplitude variations of the ordered branch	effective (Level B)
Pre-quantum action scale $S_0^{\text{EFT}}$	Elementary-loop action $S_{\text{elem}} = 2\pi S_0^{\text{EFT}}$ ; Cauchy–Schwarz bound strict, $L_{\text{core}}$ input Level B	derived (structural)

(continued on next page)

Object	Origin in ECT	Status
Physical Planck constant $\hbar$	Final identification $S_0 = \hbar$	identified after additional matching (Level B / open)
Schrödinger equation	KG + NR limit + emergent complex sector	derived (Level B)
Macroscopic Einstein-like closure	Pure-metric frozen-order limit + $\phi$ -first IR closure	structural / effective (Level A/B)
Graviton	Linearised effective-metric perturbation induced by $\delta n^A$ ; spin-2 Fierz–Pauli form; massless at linearised effective level	derived (linear)
Photon	Compact phase fibre; bundle covariance forces Abelian gauge connection and Maxwell-type leading closure	derived / structural (Level A/B)
$W^\pm, Z^0$	Phenomenological realisation of a structurally selected chiral $SU(2)$ sector through the electroweak condensate doublet	structural / embedded realisation (Level B+)
Higgs-like boson	Radial mode of the secondary electroweak condensate doublet	structural / phenomenological matching (Level B+)
Fermions	$O(3)$ spinor representations	structural route (Level B)
Neutrino sector	Geometric chirality selection (A/B); weak-sector matching and oscillation intactness (B); embedded seesaw, scale anchor (C); PMNS intact	structural route (Level A/B to C)
Late-time acceleration source	Effective ordered-branch background closure; no independent dark-energy substance	closure-dependent (Level B)
Dark-sector role	No particle DM required; soft orientation sector and topological sectors are open questions	open
Flat rotation curves and RAR/BTFR phenomenology	Critical $\phi$ -branch closure in the galactic weak-field sector	effective closure (Level B)
Macroscopic entropy growth	Reduced-state decoherence with effective bath assumptions	effective closure (Level B)
Universal causal cone	Single $g_{\mu\nu}(n)$ in IR EFT	derived
LV suppression	Higher-dim. ops., $\delta c/c \sim (E/\Lambda)^2$	derived
Proton stability	Three selection-rule patterns conditional on gauge/flavour completion (§44)	conditional (Level C)

(continued on next page)



Object	Origin in ECT	Status
Cosmological-constant UV decoupling	Fixed kinetic-tensor determinant $\sqrt{-\det K^{AB}} = \beta^2/c_*$ from the kinematic constraint $n^A n_A = 1$ (Theorem 15.3, Sec. 15); the classical baseline $V(\phi_0)$ is inert for local emergent gravity (Theorem 15.3(iv), unconditional), while the zero-derivative loop contribution is absorbed only conditional on $H_\Lambda$ (Theorem 15.3(v)); the direct $10^{120}$ -level UV-to-IR cancellation of the standard framework is thereby absent in the leading ordered-branch sector; separately, the IR coefficient $c_\Lambda$ remains open (Level C)	<b>derived (Level A for Object A; <math>H_\Lambda</math>-conditional for Object B);</b> IR coefficient $c_\Lambda$ open (Level C)

**Table 73:** Structured classification of ECT results. Level A = strict derivation; Level B = derivation with stated assumption; Level C (or ‘Open’) = conjecture / open problem.

#	Statement	Level	Key assumption (if B/C)	Section
D1	Lorentzian phase selected when $\alpha > \beta$ ; Euclidean otherwise	A	$\alpha > \beta$ is a condition on condensate params	3
D2	KG equation from condensate action (Level A); Schrödinger equation by NR reduction + emergent complex envelope (Level B)	A/B	KG: Level A (O-S continuation assumed for quadratic sector); Schrödinger: Level B (additionally requires NR limit + emergent complex sector)	4, 4
D3	$G_N$ from geometric EFT matching ( $G_N = c_*^4/(8\pi M_G^2)$ )	B	Matching between ordered-branch tensor EFT and observed gravity; explicit $(u_0, \alpha, \beta) \rightarrow M_G$ derivation open (OP2, OP3)	13.4
D4a	Ordered branch breaks $O(4) \rightarrow O(3)$ ; vacuum manifold $S^3$	A	—	4.2
D4b	$Q_A = \partial_A \Phi$ implies integrability; $\pi_i = \partial_i \chi / u_0$	A	Scalar-only basis	App. I
D4c	One surviving longitudinal scalar mode $\chi$	B	Linear level; inverse-Higgs reduction	App. I
D4d	Minimal 3-component orientation EFT	B	Effective parametrisation	4.4
D4e	Three independent physical Goldstone particles	C	Not established; reduced by integrability	4.3
D5a	Graviton: induced linearised effective-metric perturbation on ordered branch	A	$u_0^2(\alpha - \beta) > 0$	8
D5b	Fierz–Pauli form, TT projection, ghost-free counting at linearised level	B	TT gauge; explicit mode-counting from microscopic condensate variables open (OP3 partially resolved)	8, App. X
D6	Dirac form (structural reconstruction once spinorial fields admitted)	B	$O(3)$ spinor rep.; not from bare bosonic action	9, 9.2

#	Statement	Level	Key assumption (if B/C)	Section
D7	Topological-sector mass ansatz $m_n \sim n \times 1.6\text{GeV}$	C	Phenomenological dimensional estimate; integer topological charge follows from $\pi_3(S^3) = \mathbb{Z}$ , but the mass law is not derived from topology alone	8.10
D8	Thermodynamic second law for macroscopic systems	B	Level-A directional backbone (retarded propagation, $\Gamma_{\text{irr}} \geq 0$ ) + effective ohmic/Markov closure; full microscopic derivation open (OP-Q17)	3.9
D9	Physical identification $S_0 = \hbar$ , $S_{\text{elem}} = \hbar$	B	Structural action scale $S_0$ exists (Level A); single-field universality, analytic continuation, and parameter-counting closure protect the identification (Level A/B to B); full structural rôle of $\hbar$ requires Quantum Sector programme (OP-Q2)	5.6, 21.2, 23.3
D10	Linearised Einstein eqs. + $\Theta_{\mu\nu}$	B	Linearisation	11
D11	Primordial perturbation field content: single scalar mode	A	From Universality Corollary; ECT-native spectral tilt $n_s$ and $r$ remain open (OP3)	14.6
D12	Baryogenesis: Sakharov-compatible environment	B	Ordering-transition out-of-equilibrium + benchmark leptogenesis closure; ECT-native $\eta_B$ derivation open (OP7)	16.3
D13	UV safety of graviton	B/C	PES provides a structurally unified route for treating the graviton as a condensate excitation governed by the same action scale; full UV closure remains open (§29)	8, 38.1, 29
Q-PES	Principle of Euclidean Stationarity (persistent-sector selection)	B	Organising principle linking compact phase, stationarity, and decoherence resistance; unifies physical reading but does not replace sector-specific derivations	29, 29.11

#	Statement	Level	Key assumption (if B/C)	Section
D14	Full non-linear Einstein eqs. (anisotropic curv. term); $\phi$ -first scalar-tensor IR closure (Appendix X). Observational role assessed across five phenomenological sectors (Table 54); most consequential for cluster lensing and JWST growth	A/B	Riemann commutator identity (OP2 resolved at linear level); scalar-tensor closure = effective IR ansatz; $c_1$ undetermined (OP-c1)	11, 13.5, App. AB, X
D15a	Retarded support $K(\tau < 0) = 0$ in ordered Lorentzian branch	A	Quadratic pole proof + full nonlinear symmetric-hyperbolic reduction	3.8, E, F
D15b	Open-system identification of bath response kernel / pre-branch origin of causal selection	C	Retarded ordered-branch dynamics provides the structural basis; full identification from Euclidean microdynamics not yet complete	3.9, 38.1
D16a	$U(1)$ gauge sector from compact phase fibre	A	Bundle covariance	7.2
D16b	Preferred chiral $SU(2)$ sector	B+	Structural selection; full internal gauge derivation open	7.3, 9.3
D16c	$SU(3)_c$ colour sector	B	Requires extended internal condensate structure	40
D16d	Neutrino sector: one-chiral route, sterile interpretation, $M_R^{\text{geom}}$ anchor, PMNS intact	A/B to C	Geometric chirality selection (A/B); weak-sector matching and oscillation intactness (B); embedded seesaw, scale anchor, sterile invisibility (C)	8.9
D17	Second law $dS/dw \geq 0$ (effective result, ordered branch)	B	Level-A directional backbone + ohmic/Markov closure; full microscopic derivation open (OP-Q17)	3.9, 38.1
D18	Universe domain size $R_{\text{domain}} \gtrsim R_H$ (amplified by pre-Lorentzian ordering)	B/Open	Scale depends on ordering dynamics (OP3); $e^{N_e}$ factor from inflation removed	16.8
D19	Elementary-loop action scale $S_{\text{elem}} = 2\pi S_0^{\text{EFT}}$ from phase winding in $U(1)$ -extended EFT	A/B	Cauchy–Schwarz bound strict (A); $L_{\text{core}}$ input and $S_0^{\text{EFT}} = \hbar$ matching remain Level B (OP-Q2); global variational minimum in $n=1$ sector not established (open)	5.6, 21.2
D20	$\beta$ param.: general $c_* = \sqrt{\beta/(\alpha - \beta)}$	A	—	3
D21	Casimir: conditional 3/2 estimate from minimal reduced soft-orientation EFT (not a proof of three physical Goldstone particles; condensate-reflecting boundaries only)	B	Conditional on minimal EFT boundary assumption	25.3

#	Statement	Level	Key assumption (if B/C)	Section
D22	Unruh-type temperature from Euclidean/Rindler coherent-vacuum response; standard $\hbar$ form after $S_0 = \hbar$ identification	A/B	Structural Euclidean/Rindler response is Level A; observational $\hbar$ form requires Level B identification (OP-Q2)	25.4
D23a	Time-dependent ordered backgrounds admit Bogoliubov-type mode mixing	B	Structural analogy established; explicit rates remain closure-dependent	25.5
D23b	Primordial spectral parameters $(n_s, r)$ : critical-fluctuation estimates	B/C	Critical O(4) route yields $n_s \sim 0.96\text{--}0.97$ (§14.6); full derivation pending (OP3)	14.1
D24	Gravitational stiffness matching: $G_N = c_*^4/(8\pi M_G^2)$ ; direct microscopic relation to ordered-branch parameters remains open	B	Geometric EFT matching; explicit $(u_0, \alpha, \beta) \rightarrow M_G$ derivation open (OP2, OP3)	13.4
D25	Near-horizon critical scale in the present shell closure: $\rho_c = \ell_{\text{Pl}}/\sqrt{3\pi}$	B	Shell/interface ansatz; Tolman temperature as control parameter (C2b, open); not a universal first-principles theorem	36
D26	Conditional theorem: exact thermality excluded given finite-entropy shell + complete evaporation	B	Unitarity (natural) + finite shell + no infinite remnant	36
D27	Shell-state dependence of Hawking channel: derived consequence of D26, not assumption	B	Conditions of D26	BB.4
D27b	General boundary-layer area bound (Theorem 36.1)	A (scaling) / B (coeff.)	Locality + UV threshold + finite effective correlation length; coefficient and soft-sector closure open	36.5
D27c	Compact- $U(1)$ Abelian charge lattice (Theorem 23.1)	A	Compact condensate phase + group-theoretic representation theory; full SM charge pattern open	23.4
D27d	Post-transition cosmological scenario classification	B	Structural classification of expanding/contracting/accelerating branches; full transition dynamics and exact background trajectory open	14.2
D28	Effective shell Hamiltonian structure (form, not coefficients)	C	GL criticality + Rindler geometry; coefficients open	BB.5
D29	Minimal shell–radiation coupling form $\mathcal{L}_{\text{int}} = -\frac{g}{2}\delta\chi(\partial\phi)^2$	C	Locality + linearity; coefficient $g$ open	BB.5
D30	No-phantom late-time closure: $w_\phi \geq -1$	B	Structural consequence of $\omega(\phi) > 0$ in the $\phi$ -first closure	16.1

#	Statement	Level	Key assumption (if B/C)	Section
D31	Age = Lorentzian ordered-branch duration	B	Conceptual reinterpretation. Current retained-band discussion is compatible with a baseline- $H_0$ branch age $\sim 13.5$ Gyr and an inferred- $H_0$ mapping $\sim 12.5$ Gyr; see §16.4 and Appendix AH.	16.4
D32	Structural Hubble-shift mechanism: $\Delta H_0 > 0$	B	Correlated with age, distance, JWST through same $\phi_b(z)$ ; retained-band diagnostic-layer extraction yields $\varepsilon \in [0.0296, 0.0376]$ at $1\sigma$	16.5
D33	Correlated JWST background mechanism	B	Mixed effect: distance/time/growth all shift; JWST channel contributes the retained-band lower edge $\varepsilon \approx 0.0296$ (two-sided); partial alleviation only	16.5
D34	Force-law dimensionality $d_{\text{force}}(x)$ : $3 \rightarrow 7/3 \rightarrow 2$	B	Universal curve from single-mode $\phi$ -closure; independent of galaxy mass	16.8
D35	Universal ordered-branch causal cone and local vacuum signal-speed bound	A	Retarded support + domain of dependence from symmetric hyperbolicity (Leray–Choquet–Bruhat)	12.6, F
D36	Vacuum photon/GW realisation of the same cone in minimal inheritance routes	A/B	Minimal gauge/tensor route; cone inheritance from same $K^{AB}$	12.6, 4.7
D37	Proton stability: three selection-rule patterns (I/II/III)	C	Conditional on gauge/flavour completion, especially colour sector and baryon-number selection rules; OP-proton	44

**Reading the predictions table.** The entries in Table 74 and in the near-future discriminant table (Table 75 below) do not all have the same logical character, and reading them as a flat list of “predictions” would misrepresent the structure of the present framework. There are five logically distinct kinds of empirical statements: (i) *hard structural discriminants* of the core framework (e.g. F10, F11, F12, F13; ND6), together with closure-level environmental discriminants such as F1, whose null result constrains  $\gamma$  and  $U_0''(\bar{\phi}_{\text{env}})$  rather than falsifying the entire amplitude mechanism; (ii) *already-satisfied consistency requirements* such as  $c_T = c$  from GW170817 (F3) and Solar-System screening (F2), which ECT must and does satisfy but which are not fresh forecasts; (iii) *stability tests* of empirically extracted effective windows — most importantly, of the retained five-probe  $\varepsilon$ -band of §16.5, whose predictive content is the *persistence* of the narrow positive band under refined pipelines rather than any single number; (iv) *viability discriminators* of the  $\varepsilon$ -sector interpretation, most notably the age ambiguity between baseline- $H_0$  and inferred- $H_0$  mappings (§16.4, Appendix AH); (v) *anti-predictions* — outcomes that the present apparatus

is specifically *not* designed to produce, whose observation would indicate overextension of the same effective sector. The entries below are organised by target observable rather than by category, but each should be read with the appropriate classification in mind.

**Table 74:** Falsifiable predictions of the ECT framework. F1 (environmental modulation of  $g_{\dagger}$ ) is the most distinctive closure-level environmental handle; F3 is satisfied at the effective scalar–tensor level.

#	Prediction	Observable	Target experiment	Verdict if falsified
F1	Environmental modulation of $g_{\dagger}$ (Section 17.1)	$g_{\dagger}^{(i)}$ vs. $\rho_{\text{env}}^{(i)}$ : positive correlation; a $\sim 10\%$ signal is an illustrative calibrated target, not a fixed prediction	SPARC $\times$ 2MRS/SDSS	absence of correlation at the $\lesssim 10\%$ level constrains $\gamma$ and $U_0''(\bar{\phi}_{\text{env}})$ , rather than falsifying the entire ordered-branch amplitude mechanism
F2	Screening: GR restored at $a > g_{\dagger}$	No anomaly in Solar System	Cassini, MICROSCOPE-2, LLR	Chameleon screening excluded
F3	GW speed $c_T = c$ (at effective scalar–tensor level)	$ c_T/c - 1  < 10^{-15}$	GW170817	✓ Already satisfied
F4	Fifth force $\eta_{\text{Eot}} \sim 10^{-20}$	EP violation $\eta < 10^{-20}$	MICROSCOPE-2 [49]	$\mathcal{L}_5$ coupling excluded
F5	$w_0 > -1$ (kinetic dark energy)	$w_0 \in (-1, -0.95)$	DESI DR2, Euclid	Condensate DE disfavoured
F6	Topological mass ansatz $m_n \sim n \times 1.6 \text{ GeV}$	Resonance-like structure near 1.6, 3.2, 4.8 GeV	LHC / future collider	Specific phenomenological realisation of the topological sector excluded
F7	Breakdown of the realised benchmark $\alpha = 2\beta$ (within admissible $\beta < \alpha < 4\beta$ )	LIV bounds	CMB+GW messenger	multi- Kinetic tensor structure refuted
F8	Casimir ratio $3/2$ (Section 25.3)	$(F/A)_{\text{ECT}}/(F/A)_{\text{QED}} = 3/2$ , <i>conditional</i> on boundaries reflecting ECT Goldstone modes (e.g. BEC/superfluid interfaces); <i>not</i> predicted for standard metallic plates	Casimir experiment with condensate/superfluid boundaries	Goldstone vacuum excluded if ratio measured $\neq 3/2$ at appropriate condensate boundaries
F9	Redshift dependence $g_{\dagger}(z)$	RAR intercept shift at $z > 0.5$ ; under the retained cosmological $\varepsilon$ -band this should appear as a mild positive drift of the effective RAR scale rather than as an arbitrary per-galaxy redefinition of $g_{\dagger}$	JWST, SKA high- $z$	Cosmological $\phi$ -evolution excluded

#	Prediction	Observable	Target experiment	Verdict if falsified
F10	Cluster-merger lensing morphology: $\kappa$ -peak tracks the <i>more compact baryonic component</i> , whether BCG/stellar or gas core (Section 17.2)	BCG-peaked in Bullet, MACS J0025, El Gordo; gas-peaked in Abell 520 [117, 118]; Abell 520 is a direct counter-example to $\Lambda$ CDM's collisionless DM prediction (lensing peak should follow galaxies, not gas)	Weak- and strong-lensing maps of merging clusters; next-generation surveys (Euclid, Rubin, JWST)	Universal v-closure excluded if peak always follows the galaxy/BCG component regardless of compactness; $\Lambda$ CDM tension if gas-peaked morphology confirmed in additional systems
F11	Graviton polarisation: two TT modes in the completed linear closure	Polarisation decomposition of stochastic GW background	LISA, PTA, 3G detectors	Observation of robust extra scalar/vector GW polarisations would disfavour the completed Fierz–Pauli closure of the ECT linearised graviton sector
F12	Universal $d_{\text{force}}(x)$ curve: $3 \rightarrow 2$	Pointwise $d_{\text{force}}$ from SPARC rotation curves; shape must be universal across all galaxy masses	SPARC, THINGS, next-generation kinematic surveys	Single-mode $\phi$ -closure excluded if $d_{\text{force}}(x)$ is non-universal or fails to reach $d \rightarrow 2$ at low $x$
F13	Graviton mass: $m_g = 0$ at linearised effective level	Mass-dependent dispersion of GW signal	LISA, LIGO O5+	Linearised effective masslessness disfavoured
F14	No particle-DM signal for galactic channel	A confirmed particle species accounting for the galactic mass discrepancy on galaxy scales	Direct-detection, LHC, indirect	Present $\phi$ -branch-only dark-matter reading falsified (broader ECT completions with additional condensate sectors would still remain logically possible)
F15	Vacuum-offset decoupling: classical $V(\phi_0)$ does not gravitate in the leading ordered-branch sector (Theorem 15.3(iv), Sec. 15)	No detectable $\Lambda$ -scale contribution from the bare quartic minimum	Cosmological and solar-system $\Lambda$ -channel tests; unimodular-gravity-type analyses	Emergent unimodular decoupling refuted if a detectable UV-vacuum-to- $\Lambda$ channel is isolated
F16	Fuzzy-DM / ultralight-scalar sector at $m_G \sim H_0$ (Sec. 15.9)	Ultralight scalar with $m_G \sim 10^{-33}$ eV and decay constant $f_G \sim \tilde{M}_{\text{Pl}}$ ; $\rho_G \sim m_G^2 f_G^2$ of order observed dark-energy density	CMB/LSS constraints on ultralight scalars; pulsar-timing wavefield searches; structure-formation imprints	Pseudo-Goldstone realisation of the IR scaling disfavoured if $m_G$ or $f_G$ forced outside the quoted ranges

**An explicit anti-prediction: the  $S_8$  sector.** The present uniform- $\varepsilon$  diagnostic layer is not designed to close the  $S_8$  / weak-lensing tension by itself. A persistent difficulty in fitting that sector with the same effective  $\varepsilon$  as the retained five-probe set would therefore be consistent with the present architecture rather than a direct failure of the retained-band analysis. Conversely, a completely tension-free simultaneous closure of both the retained set and the  $S_8$  sector within the same simple uniform- $\varepsilon$  layer would indicate

that the current diagnostic apparatus is being interpreted too broadly.

**Baryon-number observables.** A further discriminant of the completed ECT closure is provided by baryon-number-violating observables. This is a Level C closure discriminant rather than part of the already established strict-core predictions listed above. Depending on the realised low-energy selection-rule pattern, the theory predicts either proton stability, or  $\Delta B = 2$  observables such as  $n-\bar{n}$  oscillations and dinucleon decay, or a generic Planck-suppressed proton-decay benchmark (Section 44).

**Near-future observational discriminants.** Several observational programmes expected to deliver data within the next decade open discriminating channels directly relevant to the ECT framework. Unlike Table 74, which collects falsifiable predictions already linked to present ECT results, Table 75 includes both quantitative predictions connected to existing derivations and future discriminating channels for sectors that require further development before mission-ready forecasts can be claimed. Five observational windows are especially important: full-sky CMB polarisation (LiteBIRD [148]), precision ground-based CMB lensing and growth measurements (Simons Observatory [149], Euclid, Rubin/LSST), low-frequency space-based gravitational-wave detection (LISA [87]), mesoscopic quantum tests in levitated-nanoparticle optomechanics and related near-term gravitational-decoherence / gravity-induced- entanglement protocols (Section 32, Section 32.5), and asymptotic IR/soft channels including gravitational-wave memory (Section 35.4).

**Table 75:** Near-future observational discriminants for ECT. Rows marked Open or C identify discriminating observational channels rather than mission-ready forecasts.

#	Observable	ECT statement	Level	Mission / pro- gramme	Verdict if data conflict
ND1	Primordial tensor signal (large-angle CMB B-mode polarisation)	ECT ties primordial perturbations to early condensate dynamics; in the present benchmark cosmology this is implemented through condensate-driven inflation, while a more direct ordering-transition derivation remains future work. No ECT-native quantitative tensor spectrum is derived in the present paper	C / Open	LiteBIRD, Simons Observatory, BICEP Array	A robust detection of a primordial tensor spectrum incompatible with any viable condensate-based early-Universe completion of ECT would strongly constrain the present cosmological programme
ND2	CMB lensing and growth consistency	If the condensate-induced sector modifies late-time gravity through $G_{\text{eff}}(z)$ and the anisotropic response $\Theta_{\mu\nu}[n]$ , future lensing-plus-growth measurements provide a direct discriminating channel	B / C	Simons Observatory, Euclid, Rubin/LSST	Sub-percent agreement with GR/ $\Lambda$ CDM growth-lensing consistency across redshift would strongly limit the allowed condensate-response sector



#	Observable	ECT statement	Level	Mission	Verdict if conflict
ND3	GW propagation speed and possible dispersion	In the present ECT framework the tensor sector is expected to share the same emergent causal cone at leading order; any residual dispersion from higher-derivative condensate corrections should be strongly suppressed, but no quantitative LISA-band forecast is derived here	B	LISA	A clear leading-order mismatch between GW propagation and the ECT single-cone expectation would challenge the current tensor-sector closure
ND4	GW polarisation content	At the linearised level discussed here, the graviton sector reproduces the standard transverse-traceless tensor content; additional propagating scalar/vector GW modes are not established in the present formulation	B	LISA, PTA, 3G detectors	A confirmed detection of extra propagating scalar or vector GW polarisations would require revision of the present linearised ECT graviton sector
ND5	Standard-siren determination of $H_0$	ECT admits a condensate-driven shift in the inferred expansion rate at the few-percent level within the retained-band diagnostic layer (§16.5)	B	LISA standard sirens	If future siren-based $H_0$ measurements show no room for the retained-band condensate-driven shift, the present ECT Hubble-shift scenario would be constrained
ND6	Director coupling: spin precession	ECT admits the lowest-dimension fermion–condensate coupling (the director coupling, $\mu_5 \bar{\Psi} \gamma^A n_A \Psi$ ); possible spin-precession signal in the range $\omega_{\text{dir}} \sim 10^{-10} - 10^{-15}$ rad/s depending on the local condensate profile	A/B	Spin-polarised torsion balance, co-magnetometer	Observation of a new spin-dependent long-range force with the predicted angular-frequency scale would provide direct evidence for the condensate director field
ND7	Director coupling: composition-dependent Eötvös parameter	A composition-dependent signal may arise if collective condensate effects enhance the bare estimate; the $\eta \sim 10^{-15}$ window is a target sensitivity rather than a sharp present prediction	B	MICROSCOPE-2	Detection of a composition-dependent signal at the predicted level would confirm the director coupling; a null result at $\eta < 10^{-16}$ would constrain the coupling coefficient

#	Observable	ECT statement	Level	Mission	Verdict if conflict
ND8	Gravitational decoherence of levitated mesoscopic masses	ECT realises a Diósi–Penrose-type scalar-channel reduced-state decoherence timescale $\tau_{\text{dec}}^{\text{grav}} \sim \hbar R / (G_N m^2)$ (eq. 26.17) as a condensate-sector contribution to the reduced influence functional. The leading timescale is not unique to ECT; the ECT-specific content is the condensate-origin interpretation, the absence of a free collapse scale, and possible sub-leading condensate-profile corrections; quantitative anchors in Table 85	B	Levitated-nanoparticle optomechanics; MAQRO-class space missions [150, 151, 152]	A confirmed universal gravitational decoherence scale incompatible with the ECT $\xi_{\text{cond}}$ -fixed reading (e.g. a free collapse scale fitting the data significantly better across independent protocols) would challenge the reduced-state reading of the Diósi–Penrose timescale
ND9	Gravity-induced entanglement (BMV-class)	ECT is architecturally compatible with both GIE observation and non-observation, depending on the reduced-mediator regime realised by the protocol (Section 32, Operational criterion §32.4); the heuristic scalar-sector guide $m_{\text{guide}} \sim \sqrt{\hbar R / (G_N \tau_{\text{exp}})}$ (eq. 32.1) orients the mesoscopic window	B (architectural)	BMV-class near-term proposals [153, 154, 155, 156]	A GIE null result in an independently coherent Level IIa regime (with verified environmental isolation and $\delta n_A$ common-medium structure expected to be active) would weaken the loophole-class reading; a positive GIE detection in a demonstrably local-classical-factorising mediator regime would also challenge the architecture
ND10	LIV / superluminal sector	In the present article two phenomenological parameterisations coexist: the linear time-of-flight estimate of eq. (3.15) and the quadratic GW-sector EFT estimate of Section 13.8. Both encode strong Planck suppression in accessible regimes; a full operator-level unification of the two parameterisations remains open	B	FERMI-LAT, CTA, IceCube, LHAASO [157]	A confirmed robust first-order Planck-scale LIV dispersion for photons or gravitons, together with exclusion of the quadratic EFT suppression pattern, would force revision of the current ordered-branch closure and of the operator unification between the two parameterisations

#	Observable	ECT statement	Level	Mission	Verdict if conflict
ND11	Gravitational-wave memory as persistent asymptotic condensate shift	ECT structurally reads gravitational memory [158] as a persistent rearrangement of the asymptotic ordered-branch orientation $n_A^{(0)} \rightarrow n_A^{(0)} + \Delta n_A$ (Section 35.4); no quantitative amplitude is derived here	C (structural)	LISA, 3G ground-based detectors, PTA memory searches	A confirmed memory amplitude incompatible with any available ordered-branch completion of ECT would constrain the IR/soft sector reading; quantitative closure is a required ECT deliverable before this row is mission-ready
ND12	Black-hole information: Page-curve-compatible evaporation	ECT's critical ordered-phase shell picture is structurally aligned with the islands/QES language (Section 36.3, Table 97); a Page-curve turnover is architecturally admissible, not derived	C (structural)	BH echo/ringdown searches [159]; analogue-lab horizon programmes	Direct or indirect evidence for fundamental information loss in BH evaporation (as opposed to reduced-state apparent mixedness) would falsify the core postulate-P2 + reduced-state-logic closure; a confirmed non-Page-curve evolution of observer-accessible radiation would also falsify it

#	Observable	ECT statement	Level	Mission	Verdict if conflict
ND13	Dark-matter-deficient ultra-diffuse galaxies (DF4, FCC 224; DF2 ambiguous)	DF4 and probably FCC 224 exhibit tracer kinematics consistent with baryon-only dynamical mass in the probed region; the current practical Level-B galactic closure (eq. 17.23) at the baseline $g_{\text{eff}}^{\dagger} = g_0^{\dagger}$ tends toward the deep-MOND branch for these systems and thereby over-predicts the observed line-of-sight dispersion by a factor of order three. The minimal density-only Level-B ansatz (eq. 17.12) for $\Xi$ does not naturally accommodate both the low-dispersion stress-test objects and matched DM-rich controls such as NGC 5846-UDG1 within a single simple environmental scalar law. The presently known sample is small and not selection-neutral. A full diagnostic treatment is given in Appendix AT. Possible theory-level directions for a future completion (dynamical $G_{\text{eff}}(\phi)$ in eq. 13.35, history-dependent extensions of $\Xi$ , and orientation-sector coupling) belong to structures already present in the broader framework, but none is presently derived for the galactic closure; addressing them is linked to OP3. $\Lambda$ CDM with bullet-dwarf formation [129, 130, 131] reproduces the observed dispersions through partial dark-halo stripping and remains a viable comparator	B (structural, open)	Archival: DF4 [123], FCC 224 [124, 125], DF2 [126, 127], NGC 5846-UDG1 [128]; future: isolated-field DM-deficient searches, IFU $\sigma(R)$ profiles, matched DM-rich controls	Observation-side: if the sample expands and the proxy-level tension persists or worsens under same-tracer same-aperture matched analysis, the minimal Level-B $\Xi$ -ansatz is disfavoured and a completion via $G_{\text{eff}}(\phi)$ , history-dependent $\Xi$ , or the orientation sector becomes necessary. Theory-side: a derivation that maps the dynamical $G_{\text{eff}}(\phi)$ degree of freedom onto the practical galactic closure is required before any ECT rescue can be claimed

A stochastic gravitational-wave background sourced by the  $O(4) \rightarrow O(3)$  ordering dynamics is an additional potentially powerful discriminator, but a quantitative ECT spectrum  $\Omega_{\text{GW}}(f)$  remains to be derived. A future ECT derivation of the primordial scalar spectrum could further connect this programme to constraints on  $n_s$ , running, and non-Gaussianity.

## 19.5 Status table and open problems of the macroscopic branch

**Role of the final status table.** The present table is the final status board of the macroscopic branch. Unlike the global checklist of Section 19.3, which audits framework-wide consistency targets, and unlike the maps of Section 19.4, which record logical derivation structure and falsifier logic, the table below gives the compact present judgement on the main macroscopic outputs of Part II.

**Postulate-level reading.** The table should be read against the same layered architecture used throughout the paper: P1–P3 control the microscopic Euclidean medium and its EFT consistency, P4 fixes the ordered macroscopic branch, and P6 permits the non-uniform macroscopic ordered responses needed for the cosmological and galactic  $\phi$ -programmes. The labels “Level A”, “Level B”, “Matched”, and “Open” refer to that organised framework rather than to isolated claims.

A separate numerical/regime-level inventory is now collected in Section 27. That inventory should be read together with the present status table: the environmental-decoherence entries are closure-level consistency checks, the photonic entries are weak-locking consistency statements, and the mesoscopic gravitational entries are the genuinely ECT-specific predictions of the current decoherence programme.

Status table and open problems of the macroscopic branch

Result	Status	Layer	Basis / OP
<i>Metric structure and tensor sector</i>			
Coarse-graining criterion (11.1)	Level A	Structural	EFT
Effective metric uniqueness (13.7)	Level A	Structural	Thm 3.2
Lorentzian signature ( $\alpha > \beta$ )	Level A	Inherited	Ordered-branch sign structure
$c_{\text{GW}} = c_*$ (13.53)	Level A	Structural	Dispersion
Massless tensor propagation	Level A	Structural	Sigma-model
Planck-suppressed GW LIV $\Delta t_{\text{GW}} \sim 10^{-64} \text{ s}$	Level A	Structural	EFT power-counting + $D$ -baseline
Fierz–Pauli-like tensor sector (linear effective closure)	Level A/B	Structural/closure	EFT coarse-graining; exact full-ECT tensor closure still open
Two TT polarisations	Level B	Closure	OP-gauge
<i>Source structure and coupling</i>			
$\partial_A T^{AB} = 0$ (Noether)	Level A	Inherited	P1+P3
Coarse-grained $\bar{T}^{AB}$ conserved	Level A	Structural	EFT
Source couples to geometric branch	Level A	Structural	EFT structure
Matter universality A4	Level B	Closure	OP-matter
Orientation EMT $T_{AB}^{(n)}$ (schematic)	Level B	Closure	OP2, OP-c1
<i>Gravitational stiffness and Newton constant</i>			
$M_G$ exists in tensor EFT	Level A	Structural	Linear tensor sector
$G_N = c_*^4/(8\pi M_G^2)$ : matching	Level B	Closure	Comparison with GR
$M_G = \bar{M}_{\text{Pl}}$ : numerical matching	Matched	Calibration	Observational identification
$M_G^2 \sim c_M \kappa_n$	Level B	Closure	EFT dim. analysis
$(u_0, \alpha, \beta) \rightarrow \kappa_n \rightarrow M_G \rightarrow G_N$	Open	Open	OP-grad, OP2–OP3
<i>Nonlinear closure</i>			
Closure required (structural)	Level A	Structural	Geometric branch
$\phi$ -first action (13.34)	Level B	Closure	A1–A4
Generalised EE (13.35)	Level B	Closure	A1–A4
Observational NLEE footprint (Table 54)	Level B	Assessed	OP-c1

Result (cont.)	Status	Layer	Basis / OP
Standard EE (13.40) (screened limit)	Level A/B	Structural	A1–A5
Lovelock uniqueness	Level A	Structural	A1–A5
$G_{\text{eff}} = G_N e^{-\beta\phi}$	Level B	Closure	Ordered-branch $\phi$ -first closure
Closure-function forms $F$ , $\omega$ , $U$ in present $\phi$ -first closure	Level B	Closure	Amplitude reparametrisation; bare-P3 open
Underlying EFT parameters ( $Z_u$ , $W$ , $\beta$ )	Open	Open	OP-grad
<i>Weak-field and phenomenology</i>			
Screened weak-field $\rightarrow$ Newtonian	Level A	Structural	Screened limit
Two weak-field regimes (screened/deep)	Level A	Structural	EFT structure
Modified Poisson (13.48)	Level B	Closure	$\phi$ -first
$\gamma_{\text{PPN}} = 1$ (screened)	Level B	Closure	Screening
$ \dot{G}/G  \lesssim 10^{-12} \text{ yr}^{-1}$	Level B	Closure	Quasi-static
<i>Cosmology and galactic</i>			
Pre-Lorentzian Euclidean cosmological scenario	Level B	Structural	Structurally motivated by P1–P4
Primordial $n_s$ , $r$ : ECT-native derivation	Open	Open	OP3
No-phantom late-time closure: $w(z) \geq -1$ ; no first-principles ECT value for $w_0$	Level B/Open	Closure	OP3
BTFR (algebraic consequence)	Level B	Closure	Critical branch
Baseline critical scale $g_0^\dagger \approx cH_0/(2\pi)$ ; environmental modulation to $g_{\text{eff}}^\dagger$	Level B	Closure	Critical branch + environment framework
Rotation-curve fits $\chi^2/N \sim 2\text{--}12$ in present one-parameter-per-galaxy closure	Level B	Benchmark	Practical SPARC implementation
Sakharov-compatible baryogenesis framework (ordered-medium route; quantitative completion open)	Level A/B given Ph	Structural/closure	Defect-mediated $B$ -violation, CP-bias candidate, and non-equilibrium transition available; transport completion open
Dynamic dark-energy route $\Lambda_{\text{eff}}(X)$ / $w(z) \geq -1$	Level B	Closure	Ordered-branch late-time closure; no-phantom result structural within current closure
Cosmological / black-hole singularity as ordered-branch breakdown	Level A/B	Structural programme	Same condensate-boundary logic; detailed post-breakdown regime open
<i>Open problems (macroscopic branch)</i>			
OP2: microscopic derivation of $M_G$ from ordered-branch parameters	Open	Open	Full EFT
OP3: derivation of effective $\phi$ -closure parameters from bare P3	Open	Open	OP-grad (functional forms derived)
OP-gauge: explicit two-TT-polarisation proof in full ECT language	Open	Open	OP-gauge
OP-matter: first-principles matter universality	Open	Open	OP-matter
OP-c1: coefficient $c_1$ in anisotropic response $\Theta_{\mu\nu}$	Open	Open	OP-c1
OP-screen: screening mechanism from bare P3	Open	Open	OP-screen

## Part III

# Quantum Sector: Coherent Branch

The ordered condensate of ECT supports two complementary classes of observables. The first class—developed in Part II (Macroscopic Physics)—concerns observables that are insensitive to the global phase of the effective order parameter: long-wavelength metric fluctuations, gravitational stiffness, cosmological dynamics, and galactic phenomenology. In that branch the phase can be averaged away and the effective description is geometric.

The second class—developed here—concerns observables that *remain sensitive* to the global phase structure, winding topology, loop configurations, and coherent correlators of the ordered condensate. This is the coherent branch of ECT, and its systematic development is the task of Part III.

**Origin in the branching structure.** The two-branch architecture was established in Part I (Section 6): both branches descend from the same working postulates P1–P6 and the derived smooth coherent-sector rule BR1, but they target different sectors of the ordered state space. The geometric branch was developed first because it requires less structural machinery—its observables are already accessible at the level of the coarse-grained metric EFT. The coherent branch, by contrast, requires the full phase-sensitive effective description and the action-scale logic prepared in Part I (Sections 6.3 and 5.6). Its development is therefore deferred to the present chapter.

**What Part I already prepared.** The following structural ingredients are available at the entrance to Part III:

- (i) the ordered phase admits a genuine phase-sensitive sector, distinct from the geometric branch (Level A within the broken-phase EFT);
- (ii) topologically quantised winding sectors exist in the coherent order parameter as a consequence of BR1 (Level A);
- (iii) a pre-quantum action scale  $S_0$  is structurally introduced by the loop quantisation condition, with its explicit first-principles evaluation deferred (Appendix AV);
- (iv) the Lorentzian causal structure (via the real parametrisation  $t = w/c_*$ ), and the Noether/variational backbone are shared between both branches (Level A).

Part III takes these as its structural starting point and develops them into wave dynamics, canonical structure, the Hilbert-space bridge, exchange-sector topology, Dirac structure, vacuum response, decoherence, the quantum–classical boundary, Born-type probability, entanglement, topological/dark-sector ontology, black-hole thermodynamics, and the analogue-laboratory programme.

**What Part III does not import.** Part III does not assume:

- that  $S_0 = \hbar$  has already been established (this is one of the central tasks of the present chapter);
- that canonical commutation relations or the Born rule hold (these must be derived or shown to follow from the coherent-branch structure);
- that decoherence, measurement, or the arrow of time have been addressed (these belong to the open-system development of the coherent branch);
- any result from standard quantum mechanics or quantum field theory that has not been independently motivated within the ECT framework.

**Methodological standard.** Throughout Part III the same Level A/B/Open classification is maintained as in Parts I and II. Level A denotes strict structural consequences of the postulates P1–P6, the dynamical principle DP, and the derived branch rule BR1. Level B denotes results that additionally require stated closure assumptions, effective approximations, or matching identifications. Open problems are flagged explicitly and collected in the final status map (Section 38).

The correct reading of Part III is therefore neither “full derivation of quantum mechanics from ECT postulates” nor “purely conjectural sketch”. It is an intermediate but substantial result: the theory has identified the correct structural location where quantum kinematics, decoherence, and probability can emerge, and has developed a large fraction of that architecture explicitly, while maintaining honest markers for what remains conditional or open.

**Chapter outline.** Part III is organised into eleven sections:

- (1) **Scope, inputs, and logical programme** (Section 20): entry into the coherent branch, structural imports from Parts I–II, and the derivation roadmap.
- (2) **Coherent phase dynamics and the pre-quantum action scale** (Section 21): phase field, loop sectors, winding classification, and the distinguished scale  $S_0$ .
- (3) **Euclidean-to-Lorentzian wave kinematics** (Section 22): real-time parametrisation, wave dynamics, extremal action, and conservation laws.
- (4) **Hilbert-space structure, reflection positivity, canonical algebra, and unitarity** (Section 23): the central bridge from the Euclidean coherent structure to the quantum-mechanical formalism.
- (5) **Euclidean path-dependence, quantum nonclassicality, statistics, and Dirac structure** (Section 24): structural origins of interference, tunnelling, exchange sectors, and the spinorial route.
- (6) **Quantum vacuum structure and universal response** (Section 25): Casimir, Unruh, particle production, and the unified coherent-vacuum logic.
- (7) **Open quantum systems, decoherence, and irreversibility** (Section 26): influence functional, arrow of time, entropy production.
- (8) **Quantum–classical boundary, probability, and measurement** (Section 30): reverse  $O(3) \rightarrow O(4)$  transitions, Born-type interpretation, and the status of measurement theory.
- (9) **Topological sectors, defects, and the dark sector** (Section 34): the wider state space beyond the smooth coherent branch.
- (10) **Black-hole thermodynamics and the information problem** (Section 36): horizon thermality as a coherent-vacuum phenomenon.
- (11) **Status map and open problems** (Section 38): final assessment of Part III.

## 20 Scope, Inputs, and Logical Programme of the Quantum Sector

*Part III develops the coherent branch of the ordered condensate—the branch in which the global phase structure, winding sectors, and loop configurations of the effective order parameter remain physically active. Before proceeding to the specific constructions—phase dynamics, wave kinematics, the Hilbert-space bridge, vacuum response, decoherence, and measurement status—the present section identifies the primary variables of the coherent branch, states the main derivation targets of Part III, and records what has and has not been established at the point of entry.*

*Throughout Part III the same Level A/B/Open classification is maintained as in Parts I and II: Level A denotes strict structural consequences of the postulates P1–P6, the dynamical principle DP, and the*



derived branch rule *BR1*; Level *B* denotes results that additionally require stated closure assumptions, effective approximations, or matching identifications.

**How ECT changes the logical status of quantum axioms.** Standard quantum mechanics and quantum field theory postulate the quantum stage: a Hilbert space, self-adjoint observables, unitary evolution, the Born rule, and collapse upon measurement. None of these axioms is explained within the standard framework; they are accepted as foundational givens. ECT does not merely reinterpret these axioms; it changes their logical status from foundational postulates to reconstruction targets tied to the coherence structure of the condensate:

- Hilbert space is constructed via the Osterwalder–Schrader reconstruction from the Euclidean functional integral (Section 23.1);
- unitarity follows from global reflection positivity, while effective non-unitarity at subsystem level arises from decoherence (Section 23.2);
- the Born rule is motivated as a consequence of decoherence + branching (Section 30.4);
- “collapse” is identified with the Euclidean-to-Lorentzian transition at  $\Gamma_{\text{loop}} \sim 1$ —no fundamental collapse postulate is needed, no mystical observer invoked (Section 30.2).

The three questions below decompose this programme into logically independent steps, each with its own status (A/B/Open).

**Three distinct questions about quantumness in ECT.** The question “why quantum mechanics?” is not a single problem; it decomposes into three logically independent sub-questions, each addressed by a different part of the ECT programme:

- (i) **Structural reconstruction.** *Why does a quantum-theoretic structure exist at all?* ECT provides a structural reconstruction programme for quantum theory through its Euclidean functional measure together with the reflection-positivity / Osterwalder–Schrader reconstruction route (Section 23.1). This route constructs a physical Hilbert space with positive-definite norm, a self-adjoint Hamiltonian, and unitary time evolution from the Euclidean data of the ordered branch. For the free quadratic broken-phase subsectors this route is established at Level A; for the full interacting coherent-sector theory it remains a Level B/open constructive programme.
- (ii) **Distinguished action scale.** *Why does a pre-quantum action scale appear?* This is addressed by the coherent compact-phase sector (Section 21): the compact phase, integer winding sectors, and the characteristic elementary-loop closure supply a structurally distinguished action scale  $S_0$  from within the ordered-branch architecture itself. The existence of nontrivial winding sectors is Level A; the finite distinguished scale requires the core-scale input (Level A/B).
- (iii) **Physical identification.** *Why is that action scale the observed  $\hbar$ ?* The identification  $S_0 = \hbar$  is a Level B matching step (Section 21.2), supported by structural bridges (single-field universality, analytic continuation, and parameter-counting closure) but not yet a parameter-free Level A derivation.

These three questions are complementary rather than competing. The first concerns the *existence* of quantum-theoretic structure; the second concerns the *origin* of the action scale that organises that structure; the third concerns the *empirical matching* of the scale to observed data. Conflating them obscures the actual logical status of each step.

### **What is established, what is structural, and what remains open in the quantum-sector programme.**

The ECT quantum-sector programme should be read in three layers.

First, the theory already establishes a nontrivial coherent-branch infrastructure: a compact-phase sector, a distinguished action scale  $S_0$  (§5.6), a wave-kinematical route after the real parametrisation  $t = w/c_*$ , a continuity structure, and a stationary-phase classical limit (§22.2). These are either strict Level A consequences or structurally supported Level A/B consequences of the ordered-condensate architecture, and are summarised in Table 100.

Second, on top of that infrastructure, ECT provides structural routes towards the standard quantum architecture: Schrödinger-type dynamics (§22.1), Hilbert-space reconstruction via reflection positivity (§23.1), canonical commutation structure (§23.3), Born-type weighting (§30.4), and spin/statistics constraints (§24.4). These routes are strong, but not all of them are yet fully closed at the same logical level.

Third, what remains open is the unique first-principles completion of the whole quantum package: a fully closed measurement theory, a fully closed Born theorem without extra closure input, and a completed fermionic/spinorial sector that would settle Pauli exclusion and spin-statistics at the same level as the bosonic coherent branch.

**Connection to the structural universalities.** The quantum sector inherits all four structural universalities (§11.1): the same causal cone  $c_*$ , the same action scale  $S_0$ , the same extremal backbone, and the same conservation origin that govern the geometric and gauge sectors also enter the coherent quantum-sector constructions. The UV threshold  $m_\sigma$  (§8.3) simultaneously marks the boundary above which the coherent-branch EFT must be replaced by the full condensate theory. This cross-Part consistency is not a separate postulate; it is a structural consequence of the single-medium architecture (P3).

**Discriminant with respect to standard and alternative quantum programmes.** The ECT quantum programme differs from two familiar alternatives:

- (i) **Axiomatic QM:** Schrödinger dynamics, Born weighting, and probability current are not simply postulated independently, but are traced back to one coherent ordered-branch infrastructure;
- (ii) **Ad hoc hidden-variable or collapse models:** ECT does not introduce extra collapse variables by decree at the outset, but first builds the coherent branch, its action scale, its continuity structure, and its Hilbert-space route, and only then asks what closure of measurement is still missing.

This makes the ECT route more unified than the standard axiom list, but also more cautious than any claim of already having solved the entire measurement problem.

**Falsifier for the quantum-sector unification programme.** The present ECT quantum-sector programme would be seriously weakened if different quantum substructures ultimately required mutually unrelated normalisations or principles: for example, if Schrödinger dynamics required one action scale, Born weighting another, canonical commutators a third, and the fermionic Pauli/spin-statistics sector a fourth independent closure principle. It would also be weakened if a completed coherent-sector analysis showed that no single ordered-branch architecture can jointly support wave kinematics, probability current, Hilbert reconstruction, and fermionic completion. Conversely, every successful cross-link between these ingredients supports the one-medium quantum reading of ECT.

## **20.1 Quantum Sector as the development of the coherent branch**

*Connection to ECT basics: Sections 6, 6.3, 5.6. Status: entry point to the coherent branch. ECT basics established the existence of a phase-sensitive coherent sector, winding classification within the smooth coherent EFT, and a distinguished pre-quantum action scale  $S_0$ . What follows in Part III is not assumed from the outset to be a complete derivation of quantum mechanics; rather, it is a staged programme in which some structures are obtained structurally, some only conditionally, and some remain open.*

This subsection does not repeat the general introduction to Part III given above. Its more specific purpose is to identify the effective variables of the coherent branch, to state the main derivation targets of the Quantum Sector, and to clarify which additional ingredients are required in order to approach the standard quantum-mechanical formalism.

**Primary variables of the coherent branch.** In the coherent branch the ordered phase is described by variables that retain global phase information. The primary objects are:

- the effective order parameter

$$\Phi_{\text{eff}} = \rho e^{i\theta} \quad (20.1)$$

- the phase variable  $\theta$ , which is not coarse-grained away;
- the winding quantisation condition,

$$\oint_{\gamma} \partial_A \theta dX^A = 2\pi n, \quad n \in \mathbb{Z} \quad (20.2)$$

- the pre-quantum action scale  $S_0$ , introduced through the minimal nontrivial loop action

$$S_{\text{loop},\min} = 2\pi S_0 \quad (20.3)$$

From these ingredients one later constructs coherent correlators, loop amplitudes, and the effective dynamical objects of the Quantum Sector. These structures were prepared in ECT basics but not yet developed into a full dynamical quantum programme. Part III begins that development.

**Why the phase is not coarse-grained away here.** In the geometric branch, local phase information was irrelevant because the observables under study were governed by the coarse-grained metric response and long-wavelength stiffness. In the coherent branch the relevant observables are different: global phase consistency, nontrivial loop sectors, and winding-sensitive amplitudes carry physical content. The phase field  $\theta$  is therefore retained not as an aesthetic choice but because interference-sensitive, loop-sensitive, and coherence-sensitive observables would be lost if it were averaged away.

**Physical meaning of the Quantum Sector.** The Quantum Sector should not be understood as importing ordinary quantum mechanics into ECT from outside. Its role is the opposite: to determine how far the ordered phase, once its coherent and topological data are retained, can structurally motivate, constrain, or in some cases partially reconstruct structures that standard quantum theory usually takes as postulated.

A central issue is not merely the recovery of wave-like evolution, but the status of the bridge from Euclidean coherent dynamics to a physical Hilbert-space description with positive norm, positive spectrum, and unitary Lorentzian evolution. That bridge is examined in Section 23.

**Derivation targets of Part III.** ECT basics and Macroscopic Physics did not yet establish:

- (i) the physical identification  $S_0 = \hbar$ ;
- (ii) a full Hilbert-space reconstruction of the interacting coherent branch with positive norm and global unitarity;
- (iii) a full derivation of the standard canonical commutation algebra, rather than only a structural route toward it;
- (iv) a complete derivation of Born weights;
- (v) a complete theory of measurement;

- (vi) the full dynamics and observational status of defect sectors;
- (vii) a complete nonperturbative closure of the black-hole sector.

These are the principal targets, conditional steps, and open problems of Part III.

**Roadmap.** The chapter proceeds from phase dynamics and the distinguished action scale (§21) to wave kinematics (§22), then to the Hilbert-space / unitarity bridge (§23), nonclassicality and statistics (§24), coherent-vacuum response (§25), open-system decoherence (§26), the quantum-classical boundary and measurement status (§30), wider topological and defect sectors (§34), and finally black-hole thermodynamics and the information problem (§36), before the concluding status map in §38. A new organising principle of the present version is the Principle of Euclidean Stationarity (PES, §29), introduced after the decoherence machinery and then used to reinterpret measurement, discreteness, and the quantum–classical boundary.

**Status at entry.** At the entry to Part III, ECT has established the coherent branch, its phase-sensitive variables, winding classification, and the existence of a distinguished action scale  $S_0$  at the structural level. What remains is to determine how much of quantum kinematics, probability, irreversibility, and information flow can be derived from that ordered-phase framework without overclaiming closure where it has not yet been achieved.

## 21 Coherent Phase Dynamics, Loop Sectors, and the Pre-Quantum Action Scale

This section develops the first technical layer of the Quantum Sector. Its purpose is to identify the effective variable that survives in the smooth coherent branch, to show how nontrivial loop sectors arise in the reduced compact-phase description, and to explain why these sectors already imply a distinguished action scale before any full quantum closure has been established.

The logic is staged. Section 21.1 introduces the phase variable, its reduced Euclidean action, and the winding-sector organisation of the coherent branch. Section 21.2 then clarifies the status of the resulting scale  $S_0$ : structurally present in ECT, but not yet automatically identical to the observed Planck constant  $\hbar$ . In this way, Section 21 provides the bridge from coherent loop structure to the later wave, canonical, and probability constructions of Part III.

### 21.1 Coherent phase dynamics and loop sectors

*Status: Level A for the existence of the phase variable, winding sectors, and the compact-phase loop classification inside the coherent branch; Level B for the specific effective dynamical closure used to connect these structures to wave dynamics. Connection to ECT basics: BRI, Section 5.6, Appendix AV.*

We begin with the phase-sensitive effective description of the smooth coherent branch. This is not yet ordinary quantum mechanics. Rather, it is the reduced compact-phase EFT in which nontrivial loop sectors are retained and organised before the later wave-dynamical and canonical constructions are attempted.

**Phase as the natural variable of the coherent branch.** Once the ordered condensate is written as

$$\Phi_{\text{eff}}(X) = \rho(X) e^{i\theta(X)}, \quad (21.1)$$

the phase field  $\theta$  becomes physically meaningful whenever configurations with nontrivial winding are retained. In the geometric branch such information is averaged away. In the coherent branch it is exactly this global phase structure that distinguishes one sector from another. The phase is not merely a convenient reparametrisation: it is the variable that remembers the global consistency conditions of the condensate—single-valuedness, winding, and compact-phase loop structure.

**Reduced phase action.** At wavelengths large compared to the microscopic core scale, and within the smooth coherent sector selected by BR1, the radial mode  $\rho$  is approximately frozen and the effective dynamics is dominated by the phase field. The quadratic phase action in this regime takes the generic form (see Section 5.6 and Appendix AV):

$$S_\theta = \frac{K_\theta^{\text{eff}}}{2} \int d^4X K^{AB}(X) \partial_A \theta \partial_B \theta + S_{\text{higher}}, \quad (21.2)$$

where  $K^{AB}(X)$  is the broken-phase Euclidean kinetic tensor of the ordered branch, inherited from the anisotropic EFT discussed in ECT basics, and  $S_{\text{higher}}$  denotes higher-gradient and interaction corrections. Its Lorentzian image arises after introducing the real ordered-branch time  $t = w/c_*$  as discussed in Section 22.1.

Here  $K_\theta^{\text{eff}}$  denotes the *effective phase stiffness* of the coherent branch. At the level of the present closure it is expected to be determined by the ordered condensate background and ultimately related to the same broken-phase data that define the ordered vacuum (the stiffness parameter  $u_0$ , the radial mass  $m_\sigma$ , and the anisotropy  $\alpha$ ). Dimensional analysis in the simplest quartic realisation suggests  $K_\theta^{\text{eff}} \sim \phi_0^2$  up to EFT matching coefficients. However, its explicit first-principles reduction to these primary parameters is not assumed here: it requires a dedicated EFT matching step in which the heavy radial mode and the orientation fluctuations are integrated out consistently. That matching remains an open part of the coherent-sector EFT programme pending the full loop-sector calculation (Appendix AV). Equation (21.2) should therefore be understood as a Level B effective closure, not yet as a full microscopic derivation from bare P3.

**Why this action is natural.** Equation (21.2) is the phase-sector analogue of the anisotropic EFT structures already used in ECT basics. Its role is to capture the lowest-order dynamics of smooth coherent configurations once the heavy radial structure has been integrated out and the phase is retained as a genuine dynamical degree of freedom. At this stage the action is still written on the Euclidean broken-phase background; its Lorentzian wave-kinematical form emerges only after the real parametrisation discussed in Section 22.1. The phase action is therefore not an extra postulate but the natural effective continuation of the broken ordered phase into its coherent branch.

**Winding sectors and topological classification.** The coherent branch is partitioned into sectors classified by winding number (cf. (20.2)):

$$n[\gamma] = \frac{1}{2\pi} \oint_\gamma \partial_A \theta dX^A \in \mathbb{Z}. \quad (21.3)$$

This is a Level A structural statement within the reduced compact-phase description of the smooth coherent sector selected by BR1. It should be stressed, however, that the vacuum manifold  $O(4)/O(3) \simeq S^3$  has  $\pi_1(S^3) = 0$ , so the winding classification does not follow from the topology of the coset space itself. Rather, it arises in the  $U(1)$ -extended compact-phase EFT of the coherent branch, where  $\Phi_{\text{eff}} = \rho e^{i\theta}$  is treated as the relevant low-energy order parameter (see Section 5.6). The trivial sector  $n = 0$  contains contractible smooth configurations; nontrivial sectors  $n \neq 0$  correspond to configurations with nontrivial phase winding that cannot be eliminated by a smooth deformation within the reduced compact-phase coherent EFT.

**Elementary loop action and the appearance of  $S_0$ .** The existence of nontrivial winding sectors implies a distinguished elementary nontrivial loop contribution to the action once the characteristic loop closure is specified. The  $n = 1$  elementary loop carries action

$$S_{\text{loop,min}} = 2\pi S_0, \quad (21.4)$$

where the pre-quantum action scale  $S_0$  depends on the coherent-sector EFT parameters (Appendix AV). Here the notation  $S_{\text{loop,min}}$  refers to the elementary-loop action evaluated at the characteristic core scale,

not to a global variational minimum over arbitrary loop lengths. At this stage  $S_0$  is *not* yet identified with  $\hbar$ : what is established is only that the coherent branch carries a distinguished action scale (Level A for existence; Level B for explicit value pending the loop-sector calculation). Under the later Level B matching hypothesis that the characteristic elementary loop is core-sized, one expects this scale to be associated with microscopic circumferences of order the core length. Its possible relation to the observed value of  $\hbar$  is analysed in Section 21.2; it is not assumed at the present stage.

**Physical meaning of the loop sectors.** A nontrivial loop sector represents more than a winding number. Physically, it means that the condensate admits coherent histories that cannot be continuously deformed into the trivial sector within the reduced compact-phase description of the smooth coherent branch. That is why loop sectors are the natural place where quantum-like notions of amplitude, interference between sectors, and action quantisation can first arise in ECT—not from operator axioms, but from the compact phase structure of the ordered coherent branch. This logic is structurally analogous to circulation quantisation in superfluids and flux quantisation in superconductors (see Table 77).

**Smooth coherent branch versus defect sectors.** The present discussion is restricted to the smooth coherent sector defined by BR1. Configurations with singular cores, vanishing  $\rho$ , or discontinuous orientation data belong to the wider defect sector and are treated in Section 34. The role of BR1 is not to deny the existence of defects, but to define the branch in which smooth phase dynamics can first be developed cleanly.

**From loop sectors to wave dynamics.** Once the condensate admits coherent sectors weighted by their phase action, the next question is how these sectors combine into an effective wave description. This step requires: (a) showing how the phase-sector path integral leads to a Schrödinger-like amplitude language; (b) verifying that the real parametrisation  $t = w/c_*$  (established for the geometric branch; Section 10.6) carries the phase action into a standard kinetic term; (c) establishing when  $S_0$  becomes identifiable with  $\hbar$ . Those questions belong to Sections 21.2 and 22.1.

**Status summary.** *Established* (Level A unless noted): (i) the coherent branch is naturally described by  $\theta$ ; (ii) smooth sectors are classified by integer winding (BR1); (iii) the existence of nontrivial loop sectors implies a distinguished coherent action scale  $S_0$ . *Not yet established*: (iv) the explicit value of  $K_\theta^{\text{eff}}$  and  $S_0$  (open, Appendix AV); (v) the identification  $S_0 = \hbar$  (Section 21.2); (vi) the full wave-dynamical superposition rule between sectors; (vii) the role of defect sectors (Section 34).

## 21.2 Pre-quantum action scale and the status of $\hbar$

*Status: Level A for the winding-sector structure and fixed-length variational bound; Level A/B for the existence of a distinguished finite pre-quantum action scale  $S_0$  once the characteristic elementary-loop closure is specified; Level B for the identification  $S_0 = \hbar$ . Connection to ECT basics: Section 5.6 and Appendix AV.*

The previous subsection established that the coherent branch of ECT is organised by nontrivial loop sectors of the phase field and that, within the reduced  $U(1)$ -extended phase-loop EFT, the fixed-length loop action admits a sharp lower bound. The present subsection clarifies the precise status of the resulting distinguished coherent action scale. The key point is that  $S_0$  is already structurally present in ECT, but its identification with the observed quantum of action  $\hbar$  is *not* automatic. In this subsection,  $S_0$  refers to the elementary coherent phase-loop action scale derived in the  $U(1)$ -extended phase EFT (Section 5.6), not to a generic closed condensate configuration.

**Why  $S_0$  exists (Level A for winding sectors; Level A/B for the finite action scale).** The existence of  $S_0$  follows from three structural facts:

- (i) the coherent branch retains a genuine phase variable  $\theta$  (Level A within the  $U(1)$ -extended EFT);
- (ii) smooth coherent configurations are partitioned into integer winding sectors (BR1; Level A);
- (iii) the reduced phase-loop EFT admits a distinguished elementary-loop action scale once the characteristic elementary-loop closure is specified (Level A/B: core-scale closure).

Together these imply that the coherent branch possesses a distinguished action scale associated with nontrivial compact-phase transport. The winding structure and fixed-length bound are strict (Level A); the finite distinguished scale additionally requires the core-scale input (Level A/B).

The corresponding EFT action scale, recalled from Section 5.6, is

$$S_0^{\text{EFT}} = \frac{K_\theta^{\text{eff}} m_\phi}{2}, \quad (21.5)$$

where  $K_\theta^{\text{eff}}$  is the effective phase stiffness of the coherent branch and  $m_\phi$  is the inverse core-length scale entering the elementary-loop closure. As emphasised in ECT basics, this quantity refers to the *elementary loop evaluated at the characteristic core scale*, not to a global variational minimum over arbitrary loop lengths.

**What  $S_0$  means physically.** The quantity  $S_0$  should be understood as the distinguished action scale prepared by the compact-phase structure of the coherent branch. Within the reduced fixed-core loop construction, it is associated with the first nontrivial elementary coherent loop, up to the factor  $2\pi$ . In this sense  $S_0$  is *pre-quantum*: it is an action scale selected by the internal coherent-sector structure of the theory, but it has not yet been shown to be the same quantity that appears in all observed quantum processes.

**Why  $S_0 = \hbar$  is not yet established.** The structural existence of a distinguished loop action scale does not yet prove that:

- (i) all coherent amplitudes are weighted by the same unit  $S_0$ ;
- (ii) canonical quantisation rules are governed by  $S_0$ ;
- (iii) the wave-dynamical limit of the coherent branch reproduces the observed quantum kinematics with  $S_0$  in the rôle of  $\hbar$ ;
- (iv) the numerical value of  $S_0$  and its universal role across the coherent-sector amplitude, wave, and canonical structures match the observed Planck constant  $\hbar = 1.054 \dots \times 10^{-34}$  Js.

These are additional statements; none follows merely from the structural existence of nontrivial loop sectors.

**What is required for the identification  $S_0 = \hbar$ .** To identify  $S_0$  with the observed Planck constant, the following multi-step program is required:

- (i) derive the reduced loop action explicitly within the coherent EFT, rather than only introducing its structural form (Appendix AV);
- (ii) show that the resulting action scale controls the effective phase weight of coherent histories in the path-integral sense;
- (iii) demonstrate that the canonical and wave-dynamical limits of the coherent sector are governed by the same scale;
- (iv) perform the numerical matching to the observed  $\hbar$ .

This is a multi-step closure problem of the Quantum Sector, not a one-line identification.

**Role of Appendix AV.** Appendix AV explains why the explicit evaluation of  $S_0$  was postponed in ECT basics. The point is not that the scale is absent, but that its computation requires a separate reduced loop construction: integration over transverse loop structure, the effective 1D loop functional, and the extraction of the minimal topological action contribution. This is more than reading off a coefficient from the 4D EFT.

**Why this is already a major structural result.** Even before the final identification with  $\hbar$ , the emergence of  $S_0$  is conceptually significant. Most formulations of quantum theory begin by postulating a universal quantum of action. ECT, by contrast, reaches an action scale through the compact-phase structure of the coherent branch itself. The theory has therefore already explained *why an action quantum candidate should exist at all*, even if it has not yet completed the empirical identification.

Moreover, the same  $S_0$  reappears across every coherent-branch construction developed in Part III: phase weights, wave reconstruction, canonical commutators, and decoherence architecture (cross-sector action-scale universality; §5.6). This cross-sector reappearance is the action-scale analogue of the cone universality (4.11) and makes the identification  $S_0 = \hbar$  structurally forced rather than arbitrary.

**Structural bridges and the three matching relations.** The possible identification  $S_0^{\text{EFT}} = \hbar$  is not introduced as an isolated fit. It is supported by three structural bridges developed in Section 5.6: single-field universality, analytic continuation, and parameter-counting closure.

In the simplest bare-potential realisation, the effective theory is organised by three independent matching relations:

$$\begin{aligned} c_* &= c, \\ G_N &= \frac{c_*^4}{8\pi M_G^2}, \\ S_0^{\text{EFT}} &= \hbar. \end{aligned} \tag{21.6}$$

The first two connect the ordered branch to Lorentzian propagation and to observed gravity; the third would connect the coherent branch to the observed quantum of action. Taken together, these relations show that the identification  $S_0^{\text{EFT}} = \hbar$  is structurally constrained within the same ordered-medium framework, even though it is not yet a parameter-free Level A derivation. For the full discussion of these bridges, see Section 5.6.

**Bridge to the rest of Part III.** Once a distinguished action scale exists, the natural next question is how coherent sectors combine into an effective wave description and how the ordered-branch real parametrisation  $t = w/c_*$  yields the standard kinetic term, while the separate formal continuation  $w_E \rightarrow \pm ic_* t$  provides the amplitude/path-integral bridge for the same coherent sector. That question leads first to the wave-dynamical development of the Quantum Sector in Section 22.

Beyond wave kinematics, the same scale also enters the later quantum programme: the normalisation of canonical structures (Section 23.3), the Hilbert-space / unitarity bridge (Section 23), the open-system decoherence architecture (Section 26.1), and the probability problem (Section 30.4). In all of these later uses, however, the physical identification  $S_0 = \hbar$  remains a Level B matching step rather than an already completed Level A derivation.

**Status summary.** *Established:* Level A for winding sectors and the fixed-length loop bound; Level A/B for the distinguished finite action scale  $S_0$  after core-scale closure. *Not established (open):* a strict positive lower bound for the elementary-loop action as a *global* variational minimum over arbitrary loop lengths in the  $n = 1$  sector. The fixed-length bound falls as  $1/L$  and the pure phase topology alone does not yield a nonzero infimum (Section 5.6). *Structural bridges (Level A/B to B):* single-field universality, analytic continuation, and parameter-counting closure collectively protect the identification from the charge of



arbitrary fitting (Section 5.6). *Not yet established (Level B matching)*: the full dynamical, canonical, and numerical identification

$$S_0 = \hbar, \quad S_{\text{elem}} = 2\pi\hbar = h. \quad (21.7)$$

In the simplest three-relation closure discussed here, this plays the rôle of the third matching relation, after  $c_* = c$  and  $G_N$ -matching. The completion of the  $\hbar$ -programme in ECT—universal amplitude weighting, canonical normalisation, and Born-type probability weights—belongs to the later constructive development of the Quantum Sector.

**Connection to the Principle of Euclidean Stationarity.** Section 29 introduces PES as the organising principle selecting persistent observable configurations. PES deepens the physical significance of  $S_0$  by providing a persistence-based interpretation of the coherent action scale. Within the PES-informed reduced fixed-core loop picture,  $S_0$  characterises the action scale associated with a self-consistent persistent  $n = 1$  winding closure. This gives a stronger physical interpretation of the  $S_0$ -programme, but it does *not* establish a strict positive global lower bound on the elementary-loop action over arbitrary loop lengths. Accordingly, the identification  $S_0 = \hbar$  remains at Level B.

For orientation, it is useful to compare the ECT loop-sector logic with other physical systems in which a reduced circle-valued phase degree of freedom leads to quantised loop data.

**Table 77:** Topological or compact-phase loop quantisation in different physical systems. In each case the relevant reduced phase degree of freedom is circle-valued, so that the loop classification is governed by  $\pi_1(S^1) = \mathbb{Z}$ . For ECT this refers to the reduced  $U(1)$ -extended coherent-phase EFT, not directly to the full vacuum coset  $O(4)/O(3) \simeq S^3$ .

System	Object	Topological origin		Quantum
Superfluid $^4\text{He}$ [8]	Quantised vortex	$\pi_1(S^1) = \mathbb{Z}$		$\kappa = h/m$
Type-II superconductor	Flux quantum	$\pi_1(S^1) = \mathbb{Z}$		$\Phi_0 = h/2e$
Early QM (de Broglie)	Bohr–Sommerfeld orbit	$\pi_1(S^1) = \mathbb{Z}$		$\oint p dq = n\hbar$
ECT coherent phase EFT	Elementary loop	compact $U(1)$ $\pi_1(S^1) = \mathbb{Z}$	phase,	$S_{\min} = 2\pi S_0$

## 22 From Euclidean Coherent Dynamics to Lorentzian Wave Kinematics

This section develops the second technical layer of the Quantum Sector. Its purpose is to show how the Euclidean coherent-phase action of the previous section acquires a Lorentzian wave-kinematical interpretation, how its phase-weight language leads to a Hamilton–Jacobi / continuity structure, and under what additional assumptions this structure can be recombined into a Schrödinger-type evolution law.

The logic remains staged. Section 22.1 develops the coherent wave kinematics in the ordered branch, carefully distinguishing the real ordered-branch parametrisation  $t = w/c_*$  from the formal Euclidean–Lorentzian amplitude bridge. Section 22.2 then clarifies the status of extremal action and saddle dominance, and Section 22.3 shows how the conserved structures of the variational foundation are inherited by the coherent sector.

The full logical hierarchy of effective equations in ECT—from the fundamental Euclidean condensate equation through the ordered-branch equation to the relativistic Klein–Gordon sector and the nonrelativistic Schrödinger limit—together with the detailed structural comparison with the standard quantum formalism, is collected as the capstone of Part III in Section 38.3.

## 22.1 Wave dynamics, real-time parametrisation, and Schrödinger-type evolution

*Status: Level A for the existence of the coherent phase action (21.2), for the ordered-branch real-time parametrisation  $t = w/c_*$  once  $\alpha > \beta$ , and for the Hamilton–Jacobi / continuity structure of the coherent phase sector (structural decomposition; see below). Level B for the Schrödinger-type complex recombination and for the physical identification  $S_0 = \hbar$ . Connection to ECT basics: Sections 5.6, 6.3; Appendix AV.*

The previous two subsections established that the coherent branch is organised by the phase field  $\theta$ , its winding sectors, and the distinguished pre-quantum action scale  $S_0$ . The question now is whether this coherent sector admits a wave-dynamical description. This is the first place in the Quantum Sector where the ECT structure begins to resemble ordinary quantum theory. The resemblance must be built, not assumed.

### From phase action to coherent amplitudes

The natural starting point is the reduced coherent-phase action (21.2), recalled here schematically:

$$S_\theta = \frac{K_\theta^{\text{eff}}}{2} \int d^4X K^{AB} \partial_A \theta \partial_B \theta + \dots$$

Because the coherent branch is organised by loop sectors weighted by their action, the natural amplitude associated with a coherent history  $\theta(\cdot)$  is the phase weight

$$\mathcal{A}[\theta] \sim \exp\left(\frac{iS_\theta[\theta]}{S_0}\right). \quad (22.1)$$

Here  $S_0$  is the distinguished loop action scale (20.3), and the symbol ‘ $\sim$ ’ indicates that this is a structural assignment, not yet a normalised path-integral measure.

At this stage Eq. (22.1) is not the final quantum path integral. Its role is more modest and precise: it expresses the fact that once coherent sectors are classified by their action, the natural language of their interference is a phase weight normalised by the intrinsic action scale of the coherent branch. This is a Level B statement because the full normalisation requires the  $S_0 = \hbar$  identification (21.7).

### Analytic continuation versus ordered-branch real-time parametrisation

Once the ordered branch satisfies  $\alpha > \beta$ , the broken-phase tensor  $K^{AB} = \beta \delta^{AB} - \alpha n^A n^B$  already has Lorentzian sign structure. Accordingly, the physical time variable is introduced by the real parametrisation

$$t = \frac{w}{c_*}, \quad c_*^2 = \frac{\beta}{\alpha - \beta}. \quad (22.2)$$

This is the step used for hyperbolic equations of motion, effective metric reconstruction, causal cones, and real-time propagation.

A distinct formal operation is the Euclidean–Lorentzian amplitude continuation

$$w_E \rightarrow \pm i c_* t, \quad (22.3)$$

which is used only to relate Euclidean coherent weights to Lorentzian phase-amplitude language. It should not be identified with the derivation of hyperbolicity itself.

### Two distinct operations in the ordered branch.

- (i) **Ordered-branch real-time dynamics:** the real parametrisation  $t = w/c_*$  is used for the hyperbolic field equations, effective metric, causal cones, and real-time propagation.
- (ii) **Formal Euclidean–Lorentzian amplitude bridge:** the continuation (22.3) is used only to translate Euclidean coherent-sector weights into Lorentzian phase evolution.

**Remark: continuation versus real-time dynamics.** Two steps must be kept distinct. *First*, the analytic continuation (22.3) relates the Euclidean coherent-sector weight to its Lorentzian amplitude interpretation: it is a statement about the path-integral language of the coherent branch. *Second*, when deriving effective equations of motion for smooth coherent configurations, one works with the corresponding Lorentzian time variable in the reduced phase dynamics. The first step concerns amplitude language; the second concerns the emergent real-time evolution law. Conflating them would obscure the difference between analytic continuation and the Lorentzian dynamics of the ordered phase (see also the two-step distinction in ECT basics, Section 6.3).

### Lorentzian form of the coherent phase dynamics

With the adapted broken-phase basis  $n^A = \delta_w^A$ , the Euclidean kinetic form entering Eq. (21.2) may be written as

$$K^{AB} \partial_A \theta \partial_B \theta = \beta \delta^{ij} \partial_i \theta \partial_j \theta - (\alpha - \beta) (\partial_w \theta)^2.$$

At this stage the ordered-branch hyperbolicity and the real time variable have already been fixed independently by  $\alpha > \beta$  and the real parametrisation  $t = w/c_*$ .

Under the real ordered-branch parametrisation one has  $\partial_w = c_*^{-1} \partial_t$ , so the reduced phase-sector action takes the Lorentzian kinetic form with the expected separation between temporal and spatial derivatives. At the level of the reduced isotropic closure this gives

$$S_\theta^{(L)} \sim \frac{K_\theta^{\text{eff}}}{2} \int dt d^3x \left[ \frac{1}{c_*^2} (\partial_t \theta)^2 - (\nabla \theta)^2 \right] + \dots \quad (22.4)$$

The formal Euclidean–Lorentzian continuation (22.3) is kept separate and is used only at the level of coherent amplitudes and correlator language, not in the derivation of the ordered-branch kinetic form itself.

This is again a Level B effective closure. Its importance is that it provides the correct Lorentzian kinetic structure for coherent phase evolution, with the spatial gradient and time-derivative terms separated by the effective speed  $c_*$ .

### Hamilton–Jacobi / continuity structure

**Real and imaginary parts of the coherent wave ansatz.** Introducing the polar decomposition

$$\Psi(x, t) = \sqrt{\rho(x, t)} \exp\left(\frac{i \mathcal{S}(x, t)}{S_0}\right), \quad (22.5)$$

and separating the resulting evolution law into real and imaginary parts yields a Hamilton–Jacobi / continuity structure for the coherent sector.

**Real part — Hamilton–Jacobi-type structure.** The real part has the general form

$$\partial_t \mathcal{S} + H_{\text{coh}}[\rho, \mathcal{S}] = 0, \quad (22.6)$$

where  $H_{\text{coh}}$  is the effective coherent Hamilton–Jacobi functional inherited from the Lorentzian phase action. Its classical part is determined by the Lorentzian kinetic term, while its non-classical part is controlled by the same distinguished action scale  $S_0$  that entered the coherent phase weight. When  $S_0 \rightarrow 0$ , the non-classical contribution vanishes and one recovers the classical Hamilton–Jacobi equation, establishing the classical limit cleanly.

**Imaginary part — continuity structure.** The imaginary part gives the associated continuity equation for the coherent density:

$$\partial_t \rho + \nabla_i J_{\text{coh}}^i[\rho, \mathcal{S}] = 0, \quad (22.7)$$

where  $J_{\text{coh}}^i$  is the effective coherent current determined by the same reduced phase dynamics.

**Exact content and effective reductions.** In special effective reductions—for example, in the simplest nonrelativistic coherent limit with an explicitly identified effective mass and potential—one recovers the familiar Madelung-type form of the quantum Hamilton–Jacobi and continuity equations (cf. [160]). That more explicit form is useful as an orientation, but it is not the primary structural statement of ECT at this stage.

**Level A content.** The Level A statement established here is the existence of a Hamilton–Jacobi / continuity decomposition of the coherent wave ansatz once the Lorentzian phase-sector action has been established in the real ordered-branch parametrisation. The separate formal Euclidean–Lorentzian continuation remains relevant only for the amplitude/path-integral reading of the same coherent sector. What is exact at this stage is the structural split into real and imaginary parts. What is *not* yet Level A is the fully explicit form of the effective Hamiltonian functional in every regime, or its universal identification with the standard Schrödinger operator. The key structural point is that  $S_0$ —not an externally postulated constant—appears as the distinguished action unit controlling the non-classical term.

### Schrödinger-type recombination (Level B)

The two real equations above can be assembled into a single complex equation:

$$iS_0 \partial_t \Psi = \hat{H}_{\text{coh}} \Psi + \dots \quad (22.8)$$

where  $\hat{H}_{\text{coh}}$  contains the spatial gradient and potential terms, and the ellipsis denotes decoherence and higher-gradient corrections.

**What this recombination is and is not.** The recombination into Eq. (22.8) is a structural route, not a derivation of the Schrödinger equation from first principles. To qualify as a Level A derivation, one would additionally need:

- (i) a theorem on linear complex amplitude composition for coherent histories;
- (ii) the explicit derivation of  $\hat{H}_{\text{coh}}$  for the relevant coherent sector (OP-Q3);
- (iii) the identification  $S_0 = \hbar$  (21.7).

For these reasons Eq. (22.8) is Level B.

**Summary of what is established.** The coherent phase sector supports an exact Hamilton–Jacobi / continuity decomposition with action scale  $S_0$  (Level A). A Schrödinger-type complex equation is then obtained as the natural complex recombination of that structure (Level B), especially in its observational form after  $S_0 = \hbar$  is identified.

**Relation to bound-state and spinorial descriptions (Level B).** The Schrödinger-type equation (22.8) should be understood as a low-energy envelope description. In bound systems—for example, a charged spinorial field in a Coulomb-like emergent  $U(1)$  background (Section 7.2)—the full structural description is first gauge-coupled and, for fermionic matter, spinorial (Section 9.2). The Schrödinger orbital, with its familiar discrete eigenvalues and probability densities, then appears as the non-relativistic limit of that fuller spinorial structure: the regime in which velocities, binding energies, and spin-dependent relativistic corrections are all small compared with the rest scale. At the structural level, the discrete spectrum may be interpreted as arising from phase-consistency requirements on admissible bound configurations, in harmony with the winding/single-valuedness conditions of the coherent branch. This structural hierarchy—spinorial bound mode, non-relativistic envelope, Schrödinger orbital—does not add new quantitative content beyond what is already established above, but it clarifies the logical position of the Schrödinger equation within the broader ECT architecture.

### Why this is already structurally nontrivial

Even before the final  $S_0 = \hbar$  identification, ECT has gone beyond a generic broken-phase field theory. The theory organises the coherent branch by:

- compact-phase loop sectors with integer winding (BR1);
- an intrinsic action scale  $S_0$  determined by the compact-phase structure of the coherent branch;
- Lorentzian time reconstruction through the same broken-phase continuation used in Macroscopic Physics;
- a natural coherent wave reduction governed by  $S_0$ .

This is precisely the structural content required from a theory that aims to explain *why wave mechanics exists at all*, rather than postulating it from the outset.

### Bridge to canonical structure

The logical sequence of the Quantum Sector is:

$$\text{phase sectors} \longrightarrow S_0 \longrightarrow \text{wave dynamics} \longrightarrow \text{canonical structure.} \quad (22.9)$$

Once a Schrödinger-type coherent evolution law is available, the next question is whether the coherent variables admit a canonical organisation and whether their brackets or commutators are normalised by the same scale  $S_0$ . That question belongs to Section 23.3.

**Structural cross-check: causal-cone universality.** The coherent wave-kinematical reconstruction and the geometric branch are controlled by the same ordered-phase tensor  $K^{AB}$  and therefore inherit the same characteristic speed  $c_*$ . In the geometric branch this speed enters through the real ordered-branch parametrisation  $t = w/c_*$  and the resulting effective Lorentzian metric. In the coherent branch the formal continuation (22.3) is used only for the Euclidean–Lorentzian amplitude correspondence. The common causal cone is therefore a consequence of the same ordered medium, not of a single continuation playing two different derivational roles. The observational bound  $|c_{\text{GW}} - c_\gamma|/c < 10^{-15}$  from GW 170817 [10] shows to very high precision that the gravitational and electromagnetic sectors are consistent with a common causal cone, as expected in ECT if wave-kinematical and gravitational propagation are two outputs of the same ordered-medium structure (Section 4.7).

**Observational orientation (Level B).** After the matched identification  $S_0 = \hbar$ , the coherent-wave organisation developed above becomes structurally compatible with the standard de Broglie and dispersion relations used in ordinary quantum mechanics. These relations are already confirmed by electron and neutron diffraction, atom and molecule interferometry, and Bose–Einstein condensate matter waves. ECT does not claim a completed first-principles derivation of all such phenomena in this subsection alone. Its claim here is narrower and structural: the same ordered condensate that produces Lorentzian causal propagation also supplies the action scale and wave-kinematical organisation needed for the standard quantum wave reading.

**Status summary.** *Established (Level A):* the coherent branch admits a Lorentzian kinetic structure in the real ordered-branch parametrisation  $t = w/c_*$ , and this structure yields an exact Hamilton–Jacobi / continuity decomposition with  $S_0$  as the distinguished action unit.

*Level A/B:* the same structure supports a Schrödinger-type complex recombination and a wave-mechanical reading that becomes physically standard after the matched identification  $S_0 = \hbar$ .

*Level B/open:* the fully explicit coherent Hamiltonian  $\hat{H}_{\text{coh}}$  in general regimes, the completed normalised quantum interpretation, and the full identification with ordinary quantum mechanics beyond the present structural route.

## 22.2 Principle of extremal action and saddle dominance

*Status: Level A for the stationary-phase / saddle-point structure of the coherent amplitude weighting and for the resulting extremality condition in the large-phase-difference limit; Level B for the detailed physical interpretation of finite- $S_0$  corrections in specific reduced coherent systems. Connection to ECT basics: DP (Section 6.6).*

The principle of extremal action is not introduced in the Quantum Sector as a new independent law. Within the coherent amplitude language, it appears as the leading stationary-phase order of the same  $S_0$ -weighted structure that organises coherent histories.

### Coherent amplitude weighting

The coherent branch is weighted by amplitudes of the form (22.1):

$$\mathcal{A}[q] \sim \exp(iS[q]/S_0).$$

In the Euclidean preparatory language the corresponding weight is

$$\mathcal{W}[q] \sim \exp\left(-\frac{S_E[q]}{S_0}\right). \quad (22.10)$$

When the relevant phase differences satisfy  $|\Delta S|/S_0 \gg 1$  (or  $|\Delta S_E|/S_0 \gg 1$  in the Euclidean preparatory language), the path weight is dominated by saddle configurations.

### Stationary-phase structure

Starting from the coherent amplitude weighting (22.1), the saddle-point structure can be exhibited explicitly. The relevant criterion is not merely that an action be “large” in an absolute sense, but that phase differences satisfy  $|\Delta S|/S_0 \gg 1$ , so that neighbouring histories contribute with rapidly oscillating relative phases. In that regime, the coherent functional integral is dominated by the vicinity of stationary configurations  $\theta_{\text{cl}}$  satisfying

$$\left. \frac{\delta S_\theta}{\delta \theta} \right|_{\theta_{\text{cl}}} = 0. \quad (22.11)$$

Expanding around such a configuration,  $\theta = \theta_{\text{cl}} + \eta$ , gives

$$S_\theta[\theta_{\text{cl}} + \eta] = S_\theta[\theta_{\text{cl}}] + \frac{1}{2} \int d^4x d^4y \eta(x) \mathcal{K}_{\text{cl}}(x, y) \eta(y) + \mathcal{O}(\eta^3), \quad (22.12)$$

where

$$\mathcal{K}_{\text{cl}}(x, y) := \left. \frac{\delta^2 S_\theta}{\delta \theta(x) \delta \theta(y)} \right|_{\theta_{\text{cl}}}.$$

Formally, the leading saddle approximation then takes the form

$$Z_{\text{coh}} \approx e^{iS_\theta[\theta_{\text{cl}}]/S_0} \cdot [\det(\mathcal{K}_{\text{cl}}/S_0)]^{-1/2}, \quad (22.13)$$

up to the usual phase and regularisation subtleties of oscillatory functional determinants [46]. The first factor gives the leading coherent saddle weight, while the second is the formal Gaussian fluctuation factor around the stationary history. Its detailed physical interpretation depends on the specification of the measure, operator domain, and regularisation scheme in the reduced coherent-sector EFT.

### Saddle-point conditions

In the Lorentzian branch, the dominant coherent histories satisfy the stationarity condition

$$\delta S[q] = 0, \quad (22.14)$$

while in the Euclidean preparatory branch one has

$$\delta S_E[q] = 0. \quad (22.15)$$

These are not extra principles added on top of the coherent sector. They are the leading saddle conditions selected by the same  $S_0$ -weighted amplitude structure when phase differences become large compared with  $S_0$ .

**Connection to the dynamical principle.** The saddle condition (22.14) is not a new law added in Part III. It is the coherent-sector reappearance of the variational dynamical principle introduced earlier in the article (Section 6.6). What is new in the present subsection is not extremality itself, but the semiclassical mechanism by which extremal histories become dominant when relative phase differences are large compared with  $S_0$ . This is the precise sense in which classical extremality is recovered from coherent-sector weighting.

**Extremal-action backbone of ECT (Level A/B).** The principle of extremal action in ECT is not a single-level statement; it appears at four connected resolutions of the same ordered medium:

- (I) **Fundamental level (DP):** physically realised configurations are extremals of the Euclidean condensate action  $S_E[\Phi]$  (Section 6.6). This is a defining criterion of the theory, not an approximation.
- (II) **Reduced-sector variational equations:** whenever a reduced effective action is explicitly constructed, the corresponding sector inherits its equations of motion by variation of that reduced action—for example, the Klein–Gordon equation for the scalar ordered branch (§3.6) and the gauge-sector equations from the phase and orientation EFTs (§7). In the fermionic case, the Dirac-type route (§24.5) is structurally aligned with the same variational backbone, but its full status remains lower than that of the scalar and gauge sectors.
- (III) **Macroscopic equations (Part II):** the Einstein-like linearised gravitational equations, the cosmological dynamics, and the galactic phenomenology of Part II are obtained by variation of the effective geometric action inherited from the ordered-branch metric sector—again an extremal structure descending from DP.
- (IV) **Coherent stationary-phase (Part III):** in the coherent branch, the distinguished action scale  $S_0$  controls the stationary-phase regime: when  $|\Delta S| \gg S_0$ , non-extremal coherent histories are phase-averaged away and extremal histories dominate (saddle condition (22.14)).

Extremality is therefore not introduced ad hoc at the semiclassical stage. It is the same structural principle reappearing in the bare theory (I), the reduced-sector EFTs (II), the macroscopic geometric branch (III), and the coherent quantum-sector language (IV). This four-level chain is a distinctive structural feature of the ECT framework. In more standard presentations of physics, the variational principle, effective field equations, macroscopic dynamics, and semiclassical limits are often articulated in partially separate theoretical layers; in ECT they are explicitly organised as different reappearances of one dynamical principle DP applied to one ordered medium.

**Falsifiable content of the extremal backbone.** If the quantum-to-classical crossover in any native ECT sector were found to require a sector-specific action threshold distinct from  $S_0$ —rather than being controlled by the universal phase-difference criterion  $|\Delta S|/S_0 \gg 1$ —then the single-medium extremal backbone would be falsified. Such a failure would imply that the effective quantum dynamics of different sectors is not governed by a single ordered condensate.

## Why this matters

Classicality does not require a second unrelated law. Within the coherent branch, extremal trajectories and finite- $S_0$  fluctuations are two limits of one and the same ordered-medium framework. When relevant phase differences satisfy  $|\Delta S|/S_0 \gg 1$ , destructive interference suppresses non-stationary histories and the saddle dominates. When action differences become comparable to  $S_0$ , neighbouring histories contribute appreciably and the coherent non-classical regime opens up.

Finite- $S_0$  corrections therefore quantify the departure from the strict saddle regime. At the formal level they are encoded by the fluctuation operator  $\mathcal{K}_{\text{cl}}$  and higher-order terms in the expansion around the stationary history. Their detailed interpretation in specific reduced systems remains part of the later constructive quantum programme.

**Two routes to classicality in ECT.** It is important to distinguish two complementary mechanisms by which classical behaviour emerges in ECT:

- (a) **Saddle dominance:** when relevant phase differences satisfy  $|\Delta S|/S_0 \gg 1$ , the coherent amplitude integral is dominated by stationary histories, and individual trajectories obey the extremality condition.
- (b) **Decoherence:** when a subsystem is coupled to many unresolved condensate degrees of freedom, off-diagonal coherent contributions are suppressed in the reduced description, yielding effectively classical alternatives.

The first mechanism explains why extremal histories emerge. The second explains why macroscopically distinct superpositions are not observed. The quantitative decoherence side of this transition is developed later in Sections 26.1 and 30.1.

**Quantitative orientation (Level B).** If one adopts the later Level B identification  $S_0 = \hbar$ , the stationary-phase criterion acquires its familiar scale. For a macroscopic mechanical system—for example, a kilogram-scale oscillator with centimetre-scale motion—characteristic actions exceed  $\hbar$  by roughly  $10^{30}$ – $10^{32}$ , so saddle dominance is extremely sharp. By contrast, in atomic-scale systems the relevant action differences are of order  $\hbar$ , and no such sharp suppression of neighbouring histories occurs. These estimates are standard consequences of the stationary-phase criterion; they serve only as scale orientation and do not replace the later decoherence analysis. The quoted orders of magnitude are illustrative rather than system-specific and should be read as scale estimates, not as a completed phenomenology of any particular experimental platform.

**Observational orientation and ECT interpretation.** The saddle-dominance logic developed here is not merely formal. Matter-wave interferometry already probes such regimes in practice, including neutron, atom, and large-molecule interferometric settings, where individual branches are well described by extremal or near-extremal histories while observable interference is controlled by finite phase differences between them. From the ECT perspective, such observations support a two-layer view of classicality: extremal-history dominance emerges when relevant phase differences become large compared with  $S_0$ , whereas the suppression of interference between macroscopically distinct alternatives requires the additional decoherence mechanism developed later in Part III. ECT does not claim unique explanatory priority over standard quantum mechanics for these phenomena; rather, it provides a structural origin for the same semiclassical reading within the coherent condensate framework.

**ECT structural expectations for the extremal-action sector.** The coherent-sector picture developed here suggests the following structurally testable expectations:

- (i) classical extremal trajectories can emerge already in regimes where interference has not yet disappeared—saddle dominance and decoherence are conceptually distinct thresholds;



- (ii) the relevant control parameter for saddle dominance is the phase-difference ratio  $|\Delta S|/S_0$ , not the absolute size of a system alone;
- (iii) full macroscopic classicality requires both saddle dominance and environmental decoherence;
- (iv) the same action scale  $S_0$  that controls the saddle criterion is expected, within ECT, also to enter the canonical normalisation, the Born-type probability weights, and the wave-kinematical reconstruction developed elsewhere in Part III—a cross-sector universality requirement that would be undermined if different quantum layers required different action scales.

The first three expectations are shared with standard semiclassical quantum mechanics. The fourth is ECT-specific: it reflects the single-field condensate architecture (P3) in which all quantum sectors inherit the same distinguished action scale from the coherent branch.

**Status summary.** *Established (Level A):* the stationary-phase / saddle structure of the coherent amplitude language and the resulting extremality condition in the large phase-difference regime. *Established (Level A/B):* the four-level backbone chain (DP  $\rightarrow$  reduced EFTs  $\rightarrow$  macroscopic equations  $\rightarrow$  coherent stationary-phase) as a unified structural feature of ECT. *Not yet established:* the fully explicit quantitative use of these results in specific reduced systems, which depends on further effective reductions and, in many practical comparisons, on the later matching identification  $S_0 = \hbar$ .

### 22.3 Conservation laws in the coherent sector

*Status: Level A for the existence of translational and rotational Noether currents inherited from the variational condensate structure (P1–P3 + DP); Level A within the compact-phase EFT for the phase current  $j^A = \rho^2 \partial^A \theta$  and for winding-number conservation; Level B for the full Lorentzian interpretation as energy, momentum, angular momentum, and the later probability-current reading; Level B for the conditions under which global charges are well defined. Connection: Section 6.6, Appendix Q, Section 7.2, Section 13.3, and Section 22.1 (Eq. (22.7)).*

In standard physics, conservation of energy-momentum, conservation of charge, conservation of probability, and loop/flux quantisation phenomena are introduced through distinct structural inputs: spacetime symmetry (Noether), gauge symmetry ( $U(1)$ ), unitarity of quantum evolution, and topological or grand-unification arguments respectively.

In ECT, all of these conservation structures trace to a single structural origin: the ordered condensate field  $\Phi$  governed by the  $O(4)$ -invariant action  $S_E[\Phi]$  on the homogeneous Euclidean arena  $\mathcal{M}^4$ . The translation and rotation symmetries of the arena (P1, P2) produce the energy-momentum and angular-momentum currents; the compact-phase single-valuedness of  $\Phi_{\text{eff}} = \rho e^{i\theta}$  supports the conserved phase current and the loop-sector quantisation structure of the coherent branch; and the continuity equation for the coherent density, which in standard quantum theory follows from the unitarity axiom, here arises as the Lorentzian wave-sector image of the same underlying compact-phase conservation structure. This cross-sector unification is one of the distinctive structural features of the ECT approach.

#### Energy-momentum conservation

From the translational homogeneity of the Euclidean arena (P1) and the locality of the action (P3), Noether's theorem produces the conserved tensor (Appendix Q):

$$\partial_A T^{AB} = 0 \quad (\text{Level A}). \quad (22.16)$$

After the real parametrisation  $t = w/c_*$  and passage to the Lorentzian ordered branch, this is reinterpreted as

$$\nabla_\mu T^{\mu\nu} = 0 \quad (\text{Level B interpretation}). \quad (22.17)$$

**When energy is not globally conserved.** Equation (22.17) is a *local* conservation law. Global energy conservation additionally requires an exact time-translation Killing vector in the effective Lorentzian geometry. In two physically important situations this fails:

- (a) **Cosmological expansion:** when the ordered background evolves, global time-translation invariance is broken and there is no conserved global energy—precisely as in general relativity [82] (Section 13.3).
- (b) **Open coherent subsystem:** when the coherent sector is coupled to unresolved environmental modes, energy can flow from the subsystem to the environment. The total condensate energy is still locally conserved, but the reduced coherent-sector energy is not. This is the ECT structural origin of dissipation (Section 26.1).

### Angular momentum conservation

The  $O(4)$  rotational symmetry of the Euclidean action (P2) produces six conserved angular Noether currents:

$$\partial_C J^{C,AB} = 0 \quad (\text{Level A}). \quad (22.18)$$

After the ordered-branch breaking  $O(4) \rightarrow O(3)$ , the six Euclidean rotation generators split into three unbroken spatial-rotation generators  $J^{ij}$  and three mixed generators  $J^{wi}$ . At the algebraic level, the standard generator continuation then reads the latter as Lorentzian boost generators in the emergent Poincaré structure. These split into three spatial angular-momentum components  $J^{ij}$  ( $i, j = 1, 2, 3$ ), which remain exact conserved quantities of the residual  $O(3)$  symmetry, and three mixed components  $J^{wi}$ , reinterpreted as Lorentzian boost generators in the emergent Poincaré structure (Level A for the Euclidean conservation; Level B for the full Poincaré interpretation).

### Phase-current conservation in the coherent branch

The coherent branch carries an additional conserved current beyond the translational and rotational structures. The global  $U(1)$  phase symmetry of the compact-phase EFT (Section 7.2) yields:

$$j^A = \rho^2 \partial^A \theta, \quad \partial_A j^A = 0 \quad (\text{Level A within the compact-phase EFT}), \quad (22.19)$$

recalled from Eq. (7.5). Under the real ordered-branch parametrisation  $t = w/c_*$  and the Level B identification  $S_0 = \hbar$ , the temporal component  $j^0$  is proportional to the coherent density  $\rho$ , and the spatial components  $j^i$  to the coherent current. The continuity equation (22.7) derived in Section 22.1 can be read as the Lorentzian wave-sector image of the same underlying conservation structure.

In standard quantum mechanics, the continuity equation for  $|\Psi|^2$  follows from the unitarity of time evolution, which is a separate axiom. In ECT, the same equation follows from the Noether structure of the compact-phase EFT—a structural derivation rather than a postulate.

### Winding-number conservation

In addition to the differential Noether currents, the coherent branch carries a topological conservation law: the winding number

$$n[\gamma] = \frac{1}{2\pi} \oint_\gamma \partial_A \theta dX^A \in \mathbb{Z} \quad (22.20)$$

is invariant under smooth deformations of the field configuration within the coherent branch (BR1; Level A within the compact-phase EFT).

Winding-number conservation is topological: it does not depend on the specific dynamics, only on the single-valuedness of  $\Phi_{\text{eff}}$  and the smoothness of the configuration. This is a global sector-classification law, distinct from local Noether conservation. It constrains global sector changes and remains stable under smooth deformations within the compact-phase EFT.

## Defect-mediated topology change

The topological protection of winding number holds only within the smooth coherent branch (BR1), where  $\rho > 0$  everywhere. If the condensate amplitude vanishes at a localised defect core ( $\rho \rightarrow 0$ ), the compact-phase description breaks down and the winding number can change discontinuously. This is the ECT structural analogue of instanton and sphaleron processes in gauge field theory.

**Physical mechanism.** In a superfluid, a quantised vortex can be created or annihilated only through processes in which the superfluid density drops to zero at the vortex core [8, 21]. In ECT, analogously, a change of the topological charge requires a configuration in which  $\Phi_{\text{eff}}$  passes through zero. Such defect-mediated transitions are admissible configurations under S4, but they are *thermally suppressed* by the condensate stability at temperatures far below the condensate scale.

**Thermal suppression estimate (Level A/B).** The energy cost of creating a defect core where  $\rho \rightarrow 0$  is of order the condensate core scale:

$$E_{\text{defect}} \sim m_{\sigma} \sim \bar{M}_{\text{Pl}}. \quad (22.21)$$

The defect creation rate is therefore thermally suppressed:

$$\Gamma_{\text{defect}} \sim \exp\left(-\frac{E_{\text{defect}}}{k_B T}\right). \quad (22.22)$$

At laboratory temperatures ( $T \sim 300 \text{ K} \sim 2.6 \times 10^{-11} \text{ GeV}$ ),  $E_{\text{defect}}/k_B T \sim 9 \times 10^{28}$ —utterly negligible. At GUT-scale temperatures ( $T \sim 10^{16} \text{ GeV}$ ),  $E_{\text{defect}}/k_B T \sim 2 \times 10^2$ —still strongly suppressed. Only at temperatures approaching the condensate scale ( $T \sim m_{\sigma} \sim \bar{M}_{\text{Pl}}$ ) does  $E_{\text{defect}}/k_B T \sim 1$  and defect creation becomes thermally accessible.

**Connection to baryogenesis.** These defect-mediated topology changes, together with the CP-bias mechanism from the preferred-direction fermion coupling and the non-equilibrium conditions of the ordering transition, provide the structural setting for an ECT-native baryogenesis framework. This connection is developed in Section 16.3.

## Observational orientation

The compact-phase conservation structure developed here is the structural counterpart of quantised circulation and flux in condensed matter: in superfluid  $^4\text{He}$ , circulation is quantised as  $\kappa = h/m_{\text{He}} \approx 9.97 \times 10^{-8} \text{ m}^2/\text{s}$ ; in type-II superconductors, the magnetic flux quantum is  $\Phi_0 = h/2e \approx 2.07 \times 10^{-15} \text{ Wb}$ . In each case the quantisation follows from the single-valuedness of a compact order-parameter phase (cf. Table 77).

Experimentally, electric-charge conservation has been tested to extraordinary precision: the best limits on electron charge non-conservation give lifetimes exceeding  $10^{26}$  years [79]. Within ECT, this observed stability is structurally consistent with the strong low-energy suppression of defect-mediated topological-sector changes once the phase/gauge route to physical charge is adopted. At the present stage, this should be read as a consistency check of the ordered-medium framework rather than as a completed quantitative derivation of observed electric-charge stability. The connection between defect-mediated transitions and baryogenesis is developed in Section 16.3.

## ECT structural expectations and falsifiable requirements

The conservation-law architecture of the coherent sector suggests the following structurally testable expectations:

- (i) **Unified origin:** conservation of energy-momentum, conserved phase-current structure, loop-sector quantisation, and the later probability-current reading all originate from the same ordered condensate through different aspects of its symmetry and compact-phase structure. Standard physics distributes these across independent structural inputs (Noether, gauge symmetry, unitarity, and topology).
- (ii) **Topological robustness:** winding-number conservation provides robustness of the loop-sector classification under smooth perturbations within the compact-phase EFT. It is stronger than a purely local differential conservation law in that it constrains global sector changes rather than only local current flow.
- (iii) **Defect-mediated topological sector change:** transitions between different winding/topological sectors are possible only through defect processes (vanishing  $\rho$ ) and are exponentially suppressed at low energies by condensate stability. The suppression lifts at Planck-scale temperatures, providing a structural setting for baryon-number-violating channels.
- (iv) **Cross-sector universality of  $S_0$ :** the same action scale that enters the continuity equation, the canonical commutators, the Born weights, and the wave-kinematical reconstruction also controls the Noether-current normalisation.

**Falsifiable structural requirements.** ECT makes two falsifiable structural predictions for this sector:

- (a) If the coherent continuity law, its later probability-current reading, and the gauge/charge interpretation of the ordered branch were found to require *different* fundamental scales—rather than the single scale  $S_0$ —the single-field condensate architecture (P3) would be falsified.
- (b) If topological-sector transitions were observed at energies far below the condensate core scale ( $E \ll m_\sigma$ ) through a smooth (non-defect) process, the topological protection mechanism of the coherent branch would be falsified.

Neither of these has been observed: all known conservation laws are consistent with a single universal  $\hbar$ , and charge conservation holds to the limits of experimental precision at accessible energies.

**Status summary.** *Established (Level A):* translational and rotational Noether currents inherited from P1–P3 + DP; phase current  $j^A = \rho^2 \partial^A \theta$  and its conservation within the compact-phase EFT; winding-number conservation under smooth deformations (BR1). *Level B:* the Lorentzian interpretation of Noether currents as energy, momentum, and angular momentum; the continuity equation (22.7) as the Lorentzian wave-sector image of the underlying phase Noether law; the later probability-current reading of the coherent current under the  $S_0 = \hbar$  matching in the wave-sector interpretation; thermal suppression of defect-mediated topology change. *Open:* fully explicit topological current algebra in the coherent branch; the precise defect-sector dynamics and its connection to non-perturbative baryogenesis; conserved charges associated with the full defect sector.

**Bridge to the Hilbert-space programme.** The conservation structures established in the present section are the last pre-Hilbert ingredients of the coherent branch. What remains is to determine under what conditions the Euclidean coherent architecture admits a positive-norm Hilbert-space reading, unitary evolution, canonical algebra, and the uncertainty principle. That bridge is the task of the next section.

## 23 Hilbert-Space Structure, Reflection Positivity, Canonical Algebra, and Unitarity

*Inputs from previous sections:* coherent phase action (21.2), distinguished action scale  $S_0$  (Section 21.2), compact-phase topology and winding sectors (BR1), real parametrisation  $t = w/c_*$ , and Schrödinger-type

reduction (22.8). *Aim: to identify the conditions under which the Euclidean coherent structure of ECT gives rise to a physical Hilbert space, unitary evolution, canonical commutation relations, and the uncertainty principle. Status: Level A for reflection positivity in the free quadratic broken-phase subsectors (massive radial mode and free massless Goldstone modes); Level A for the canonical organisation, for the topological quantisation of the global compact-phase generator, and for the Robertson–Schrödinger uncertainty inequality; Level A for the conceptual distinction between global unitarity of the full coherent description and effective reduced-sector non-unitarity; Level A/B for the structural commutator normalisation candidate  $S_0$ ; Level B/open for the full interacting Hilbert-space reconstruction, global unitarity beyond the Gaussian regime, the completed local operator algebra, and the final physical identification  $S_0 = \hbar$ . Connections: P1 (Euclidean arena), P2 ( $O(4)$ -invariant action), P5 (medium character), the UV-threshold programme (§8.3), and the downstream Born, entanglement, decoherence, and black-hole-information programmes.*

The previous sections established that the coherent branch possesses a distinguished action scale  $S_0$ , a compact phase with integer winding sectors, a natural wave-dynamical reduction, and a Lorentzian kinetic structure inherited from the broken phase. The present section addresses the next logical question: *under what conditions does this Euclidean coherent structure give rise to the full apparatus of quantum mechanics*—a physical Hilbert space with positive norm, a self-adjoint Hamiltonian, unitary time evolution, and canonical commutation relations?

This is the central bridge of the Quantum Sector. Without it, the resemblance between the coherent-branch wave dynamics and ordinary quantum mechanics would remain suggestive but formally incomplete. With it, the entire downstream quantum architecture—Born-type probabilities (§30.4), entanglement (§31), decoherence (§26.1), and the black-hole-information programme (§36)—acquires its common structural foundation.

**Plan of this section.** The section proceeds in four steps:

- (i) reflection positivity and the Osterwalder–Schrader route to a physical Hilbert space (Section 23.1);
- (ii) the status of unitarity in the coherent branch (Section 23.2);
- (iii) canonical structure and the status of commutation relations (Section 23.3);
- (iv) the uncertainty principle as a mathematical consequence (Section 23.5).

### 23.1 Reflection positivity and the route to a physical Hilbert space

*Status: Level A for reflection positivity in the free quadratic broken-phase subsectors (massive radial mode and free massless Goldstone modes); Level B/open for the full interacting coherent-sector functional integral. Connection: P1 (Euclidean arena), P2 ( $O(4)$ -invariant action), P5 (medium character), the real parametrisation  $t = w/c_*$ , the UV-threshold programme (§8.3), and the downstream Hilbert-space, Born, entanglement, decoherence, and black-hole-information programmes.*

The standard route from a Euclidean field theory to a physical Lorentzian quantum theory passes through the *Osterwalder–Schrader (OS) reconstruction theorem* [72, 73]. The theorem states that if a Euclidean field theory satisfies a set of axioms—most critically *reflection positivity*—then it is possible to reconstruct a Lorentzian quantum field theory with a physical Hilbert space, a positive-definite norm, a self-adjoint Hamiltonian bounded below, and unitary time evolution. ECT is constructed on a Euclidean arena from the outset (P1) and therefore naturally fits the premises of this programme.

**Reflection positivity in ECT.** Reflection positivity is a condition on the Euclidean functional integral. Let  $\Theta$  denote the reflection that reverses the distinguished Euclidean coordinate:  $\Theta w = -w$  (leaving the spatial coordinates  $x^j$  unchanged). The ECT coherent-sector functional integral

$$Z = \int \mathcal{D}\Phi e^{-S_E[\Phi]/S_0} \quad (23.1)$$

is said to satisfy reflection positivity if, for every functional  $F[\Phi]$  supported in the half-space  $w > 0$ ,

$$\langle (\Theta F)^* F \rangle_E \equiv \int \mathcal{D}\Phi (\Theta F[\Phi])^* F[\Phi] e^{-S_E[\Phi]/S_0} \geq 0. \quad (23.2)$$

When this condition holds, the OS theorem guarantees the existence of a physical Hilbert space  $\mathcal{H}_{\text{phys}}$ , a vacuum state  $|\Omega\rangle$ , and a self-adjoint transfer-matrix Hamiltonian  $\hat{H} \geq 0$  generating time translations.

**Why the ECT arena is well-suited.** The ECT postulate structure provides the natural ingredients for the OS programme:

- (i) P1 gives the Euclidean 4-manifold  $\mathcal{M}^4$ ;
- (ii) P2 gives the  $O(4)$ -invariant action  $S_E[\Phi]$ ;
- (iii) P4+BR1 select the ordered broken phase with a distinguished direction  $n^A = \delta_w^A$ , which supplies a natural coordinate adaptation for the later Lorentzian interpretation; the reflection-positivity condition itself is imposed at the Euclidean level, independently of SSB;
- (iv) P5 gives the ordered branch a genuine medium interpretation: the Euclidean functional measure is read as the statistical weight of a physical  $\Phi$ -medium configuration, not merely as a formal integration device. This does not by itself prove reflection positivity, but it makes the OS route conceptually native to ECT;
- (v) the formal continuation (22.3) provides the Euclidean–Lorentzian amplitude bridge used in the coherent-sector reading; in this sense it is compatible with the OS route, while remaining distinct from the real parametrisation  $t = w/c_*$  used for the effective metric and hyperbolic dynamics.

Thus the OS programme is not an external addition to ECT but a natural structural route suggested by the theory’s own Euclidean starting point and broken-phase ordering.

**Status in explicitly positive Gaussian subsectors.** For the free quadratic broken-phase action

$$S_E^{(2)} = \frac{1}{2} \int d^4X [(\partial_A \varphi)^2 + m^2 \varphi^2], \quad (23.3)$$

reflection positivity is a standard result for explicitly positive Gaussian Euclidean measures: the Gaussian measure  $\exp(-S_E^{(2)}/S_0) \mathcal{D}\varphi$  satisfies condition (23.2) for all  $m^2 > 0$  [161]. The ECT broken-phase quadratic sector has  $m_\sigma^2 = 2\mu^2 > 0$  (Eq. (5.12)), so the standard OS reconstruction applies to explicitly positive Gaussian subsectors of the broken phase. This provides a local model and structural bridge for the full Hilbert-space programme, but it is not yet a theorem for the complete coherent interacting sector.

**Goldstone sector at the free quadratic level.** At the level of the naive free quadratic coordinate counting, the  $O(4) \rightarrow O(3)$  breaking carries three Goldstone coordinates. In the scalar-only integrable basis, however, this does not automatically imply three independent propagating soft asymptotic particles. The present OS statement concerns the reflection positivity of the free quadratic coordinate sector, not the final counting of physical low-energy soft particle content. For a free massless scalar in four Euclidean dimensions, the standard Gaussian measure is reflection-positive as well, up to the usual infrared/zero-mode subtleties of the massless sector, which do not affect the local reflection-positivity statement used here [161]. Therefore the free quadratic broken-phase content of ECT is OS-compatible not only in the massive radial subsector but also in the free massless Goldstone subsector. In this precise sense, the full *free quadratic* broken-phase content (one massive radial mode plus the three free Goldstone-coordinate subsectors) is reflection-positive sector by sector.

**Relation to the radial threshold scale.** The radial mode furnishes the natural massive threshold of the ordered branch. Its precise numerical placement belongs to the later scale-matching programme (§5.1), but the reflection-positivity point needed here is simpler: the massive radial Gaussian subsector has  $m_\sigma^2 > 0$ , and therefore satisfies the standard OS positivity criterion for explicitly positive Gaussian measures.

**Status beyond the quadratic sector (Level B/open).** For the full interacting coherent-sector functional integral, the verification of reflection positivity is a nontrivial constructive task. In standard constructive QFT, such verification has been completed only for a small number of models (e.g.  $\phi_2^4$ ,  $\phi_3^4$ ). For ECT the analogous programme is:

- (i) verify that the full  $O(4) \rightarrow O(3)$  broken-phase action, including Goldstone, radial, and orientation sectors, satisfies reflection positivity;
- (ii) control the functional measure beyond the Gaussian approximation;
- (iii) demonstrate that the resulting OS-reconstructed Hilbert space coincides with the coherent-branch wave-dynamical description.

This programme is Level B/open: it is structurally well-motivated and uses only ingredients already present in ECT, but the full nonperturbative completion has not yet been carried out. It belongs to the long-term constructive programme of the theory and is flagged as an open problem (OP-Q16).

**Connection to graviton quantisation.** If reflection positivity were established for the orientation (spin-2) sector of ECT (OP-OS1), this would have a structural consequence for quantum gravity: the physical Hilbert space containing graviton states would be reconstructed automatically by the same OS theorem, without any separate act of imposing commutation relations on the metric field. This is structurally distinct from canonical quantum gravity and loop quantum gravity, where the quantisation of geometry is an independent postulate. The present work establishes this as a programme target; a complete RP proof for the spin-2 sector remains open (OP-OS1) and beyond the scope of this paper.

**Connection to the UV-threshold programme.** The later UV-threshold programme (§8.3) is structurally relevant for the OS route. The same radial threshold that marks the domain of validity of the ordered-branch EFT also limits how far the Euclidean coherent-sector description is expected to be extended toward arbitrarily short scales. This does *not* solve the constructive reflection-positivity problem for the interacting theory, but it means that the RP programme in ECT is not forced to treat the ordered branch as fundamental at arbitrarily high momenta. The UV-threshold and Hilbert-space programmes are therefore architecturally linked rather than independent.

**What reflection positivity would establish.** If reflection positivity is verified for the full coherent-sector measure, the OS theorem would deliver:

- (i) a physical Hilbert space  $\mathcal{H}_{\text{phys}}$  with positive-definite inner product;
- (ii) a vacuum state  $|\Omega\rangle$  with  $\hat{H}|\Omega\rangle = 0$ ;
- (iii) a self-adjoint Hamiltonian  $\hat{H} \geq 0$ ;
- (iv) unitary time evolution  $U(t) = e^{-i\hat{H}t/S_0}$ ;
- (v) a spectral representation for all correlation functions.

These are not additional postulates but constructive consequences of a single Euclidean condition. The full canonical quantisation programme of the Quantum Sector would then be grounded in this reconstruction rather than assumed independently.

**Why this bridge matters downstream.** The Hilbert space reconstructed by the OS route is the common arena for the rest of the Quantum Sector. Specifically: (i) the canonical commutator programme requires a positive-norm  $\mathcal{H}_{\text{phys}}$  as its domain (Section 23.3); (ii) the Born-type probability reading requires positive inner-product structure (Section 30.4); (iii) the entanglement programme presupposes tensor-product structure inside a physical Hilbert space (Section 31); (iv) decoherence and the arrow-of-time programme require reduced-state descriptions built from an underlying globally unitary theory (Section 26.1); (v) the black-hole information programme likewise relies on global unitarity at the level of the full coherent description (Section 36). In this sense, reflection positivity is not an isolated mathematical detail but the single bridge on which the downstream quantum architecture rests.

**Relation to the formal continuation already used in ECT.** The formal continuation (22.3) has already appeared in two contexts: as the amplitude bridge used in the coherent sector, and as the formal correspondence underlying the OS reconstruction. (The effective Lorentzian metric itself is obtained through the real parametrisation  $t = w/c_*$ , not through the continuation.) The OS reconstruction theorem identifies the mathematical form of the bridge that would justify this continuation nonperturbatively. In the Gaussian subsectors this bridge is standard and rigorous; for the full interacting coherent sector it remains the target constructive route rather than an already completed theorem.

**Discriminant: Euclidean-first versus Lorentzian-first readings.** The distinctive feature of ECT is not the use of the OS theorem itself, which belongs to standard constructive QFT, but the ontological direction in which it is used. In ECT the Euclidean arena is primary (P1), and the Lorentzian quantum theory is the derived output of the OS bridge. By contrast, in standard Lorentzian-first formulations the Euclidean theory is usually introduced as an auxiliary continuation of a theory already defined in Lorentzian terms. ECT therefore gives the OS reconstruction a more central conceptual role: it is not merely a consistency tool, but the native bridge from the fundamental Euclidean medium description to the physical Hilbert space of the coherent branch.

**Falsifier for the Hilbert-space programme.** If the full interacting coherent-sector functional integral fails to satisfy reflection positivity, then the OS route cannot construct a physical Hilbert space with positive norm and globally unitary evolution. In that case the downstream coherent-branch programmes for canonical algebra, Born-type probabilities, entanglement, decoherence, and the black-hole-information reading would lose their common structural foundation. Reflection positivity is therefore a genuine architectural falsifier for the quantum reading of ECT, not a merely technical side condition.

**Complementarity with the compact-phase action-scale programme.** The reflection-positivity / OS line and the compact-phase / loop line developed in Section 21 address different aspects of the quantum programme (cf. the three-question decomposition in §20). The former concerns the *structural reconstruction* of a physical quantum theory from Euclidean data: Hilbert space, positive-definite norm, and unitary time evolution. The latter concerns the *emergence of a distinguished action scale*  $S_0$  and the organisation of coherent winding sectors within the ordered-branch architecture. These are complementary mechanisms: the OS route provides the structural framework in which quantum theory is realised, while the compact-phase sector provides the physical content of the action scale that enters the Euclidean measure as  $e^{-S_E/S_0}$ . Neither alone is sufficient: without the OS bridge there is no physical Hilbert space; without the coherent-phase sector there is no physically motivated action scale.

**Status summary.** *Established (Level A):* (i) standard OS reconstruction applies to explicitly positive Gaussian massive subsectors of the broken phase; (ii) the free massless Goldstone subsectors are likewise reflection-positive in the standard Gaussian sense; (iii) the free quadratic broken-phase content is therefore sector-by-sector OS-compatible. *Structural programme (Level B/open):* the full interacting coherent-sector verification remains a constructive-QFT problem, but in ECT it is structurally tied to the same



ordered-branch architecture that underlies the UV-threshold, canonical, Born, entanglement, decoherence, and black-hole-information programmes (OP-Q16).

## 23.2 Status of unitarity in the coherent branch

*Status: Level A for global unitarity in the reconstructed positive Gaussian subsectors (follows from reflection positivity and the OS reconstruction); Level B/open for the full interacting coherent branch. Level A for the conceptual distinction between global unitarity of the full coherent branch and effective reduced-sector non-unitarity after tracing over unresolved modes. Connection: reflection positivity (Section 23.1), P2 ( $O(4)$ -invariant Euclidean action), P5 (medium character of the ordered branch), and the downstream black-hole, decoherence, and entanglement programmes.*

Unitarity is not an independent postulate of ECT. If the OS reconstruction programme is completed, unitarity of the Lorentzian time evolution follows as a mathematical consequence of reflection positivity. However, because the full nonperturbative verification is not yet in place, it is important to state the status of unitarity separately and at the appropriate level of precision.

**Global unitarity in explicitly positive Gaussian subsectors.** For the reconstructed positive Gaussian subsectors of the broken phase, the OS-reconstructed Hamiltonian is self-adjoint and bounded below, so the time-evolution operator  $U(t) = e^{-i\hat{H}t/S_0}$  is unitary. This follows from the standard OS theorem applied to the Gaussian broken-phase measure and is the strongest current unitarity result available within ECT. Extension to the full interacting coherent branch remains conditional on the completion of the OS programme (OP-Q16).

**Global unitarity beyond the Gaussian regime (conditional/open).** Beyond the Gaussian subsectors, global unitarity is a conditional structural expectation: it is the natural consequence of the OS programme applied to the full interacting action, but its verification requires the completion of OP-Q16. It should not be presented as an independently established result.

**Two levels of unitarity in ECT.** It is essential to distinguish two levels:

- (i) **Global unitarity:** the total coherent-sector evolution on  $\mathcal{H}_{\text{phys}}$  is unitary. This is the level relevant for the black-hole information problem (Section 36).
- (ii) **Reduced-sector non-unitarity:** after tracing over unresolved condensate modes, the reduced density matrix of a subsystem evolves non-unitarily. This is the level relevant for decoherence and the arrow of time (Section 26.1).

Both levels are consistent: global unitarity is preserved, while the appearance of non-unitary evolution in reduced descriptions is a consequence of the system–environment split, not of fundamental information loss.

**Medium reading of the two-level distinction (P5).** Under the medium interpretation (P5), the two-level unitarity distinction acquires a physical rather than merely formal meaning. Global unitarity means that the total  $\Phi$ -medium state evolves without fundamental information loss. Reduced-sector non-unitarity means that an observer with access only to a subsystem of the medium sees effective mixedness, not because the medium itself has lost information, but because unresolved condensate modes have been traced out. This is the same logic that governs decoherence in condensed-matter analogue systems: the total medium state can remain pure while a local probe exhibits effectively thermal or mixed behaviour.

**Why this matters.** The distinction between global and reduced unitarity is one of the structurally strongest points of the Quantum Sector. It resolves the apparent tension between:

- the need for unitary evolution to prevent information loss (black-hole information problem, Section 36);
- the need for effective non-unitarity to produce decoherence, the arrow of time, and the quantum-to-classical transition (Section 26.1).

ECT does not need to choose between the two. The same theory naturally produces both, at different levels of description.

**Connection to the downstream quantum programmes.** The two-level unitarity distinction is not an abstract point. It feeds directly into three already developed programmes: (i) the black-hole information programme (§36), which requires global unitarity in order to exclude fundamental information destruction; (ii) the decoherence and arrow-of-time programme (§26), which requires effective reduced-sector non-unitarity in order to produce irreversibility and classicalisation; and (iii) the entanglement programme (§31), whose non-factorisable correlations are sustained only at the level of the full coherent description even when reduced subsystems become mixed. In this sense, the unitarity status of the coherent branch is the structural prerequisite for all three downstream programmes.

**Discriminant with respect to collapse and fundamental non-unitary alternatives.** Two familiar alternatives should be sharply distinguished from the ECT reading. In collapse-type models, microscopic evolution itself is modified by an intrinsically non-unitary law that produces classical outcomes. In fundamental-information-loss scenarios, the total state evolves from pure to mixed at a basic level. ECT adopts neither route. Its claim is that global unitarity belongs to the full coherent-branch description, while apparent non-unitarity arises only in reduced subsystem descriptions after tracing over unresolved medium degrees of freedom. The distinctive ECT statement is therefore that one and the same ordered medium supports exact global unitarity and effective reduced non-unitarity without invoking a separate collapse law or a primitive information-destruction mechanism.

**Falsifier for the unitarity programme.** The ECT unitarity programme would fail if (i) the full interacting coherent-sector functional integral violated reflection positivity, so that the OS Hilbert-space construction could not be completed; (ii) a completed analysis showed that reduced-sector non-unitarity is incompatible with global unitarity at the level of the full coherent theory, rather than arising as a standard subsystem effect; or (iii) the two-level distinction could only be maintained by introducing an additional collapse mechanism not derivable from the ordered-medium architecture. Any of these would force a fundamental revision of the downstream black-hole, decoherence, and entanglement programmes.

**Relation to P2.** Postulate P2 requires that the Euclidean action  $S_E[\Phi]$  is  $O(4)$ -invariant. This symmetry is a necessary but not sufficient ingredient for Lorentzian unitarity: in the OS reconstruction, the  $O(4)$  symmetry of the Euclidean correlators maps to the Poincaré covariance of the reconstructed Lorentzian theory, but unitarity additionally requires reflection positivity and the associated reconstruction conditions. P2 therefore provides the symmetry foundation from which unitarity can be reached, once the positivity programme (OP-Q16) is completed.

**Status summary.** *Established (Level A):* (i) global unitarity in reconstructed positive Gaussian subsectors (standard OS result); (ii) the distinction between global unitarity of the full coherent description and effective reduced-sector non-unitarity of traced subsystems is conceptually well-defined and structurally consistent. *Conditional programme (depends on OP-Q16):* global unitarity for the full interacting coherent branch; not yet independently established. *Structural consequence:* reduced-sector non-unitarity is compatible with global unitarity and underlies the decoherence, arrow-of-time, entanglement, and black-hole-information programmes without requiring a primitive collapse or information-destruction law.

### 23.3 Canonical structure and the status of commutation relations

*Status: Level A for the existence of a canonical organisation of the smooth coherent branch at the level of reduced phase dynamics; Level A/B for the claim that the same structural action scale  $S_0$  is the unique candidate normalisation of the coherent-sector commutator bridge; Level B/open for the full operator algebra, multi-particle completion, and the final physical identification with the observed canonical quantum structure. Connection to previous subsections: Sections 21.1, 21.2, 22.1, 23.1.*

Once the coherent branch admits a distinguished action scale  $S_0$  and a Schrödinger-type wave-dynamical reduction, the next question is whether its variables admit a canonical organisation. This question must be treated carefully. ECT does not begin by postulating canonical commutators. Rather, it asks whether the coherent branch naturally develops the kinematic structure that ordinary quantum theory usually assumes from the outset.

**What is already fixed before operator quantisation.** Before any operator algebra is postulated, the coherent branch already fixes three structural ingredients: (i) a reduced phase dynamics with canonical variables, (ii) a distinguished action scale  $S_0$  prepared by the loop/coherent sector, and (iii) a Hilbert-space route in the reflection-positivity programme (Section 23.1)—already rigorous in the positive Gaussian subsectors and structurally prepared, but not yet completed, for the full interacting coherent branch. The canonical-commutator question in ECT is therefore not whether a commutator can be freely imposed, but whether these already established ingredients single out a unique normalisation candidate for the operator bridge.

#### Canonical organisation of the reduced coherent sector

Consider the reduced coherent-phase action of the smooth coherent sector. At the level of the effective Lorentzian coherent dynamics, the phase field  $\theta$  and its conjugate momentum density

$$\pi_\theta(x, t) \equiv \frac{\partial \mathcal{L}_{\text{coh}}}{\partial(\partial_t \theta)} \quad (23.4)$$

form a natural canonical pair. This is a Level A structural statement: once the coherent branch is described by a reduced action in Lorentzian time, the variational formalism automatically induces canonical coordinates and momenta from the same action that governs the coherent dynamics.

ECT therefore already contains the *pre-operator* canonical structure of the coherent sector: a phase variable, a conjugate momentum, and a Hamiltonian description for smooth coherent evolution. This is not yet quantum mechanics, but it is the precise structural point from which quantum kinematics can emerge.

#### Poisson brackets versus quantum commutators

At the classical effective level, the coherent branch admits Poisson brackets of the standard canonical form:

$$\{\theta(\mathbf{x}, t), \pi_\theta(\mathbf{y}, t)\} = \delta^{(3)}(\mathbf{x} - \mathbf{y}). \quad (23.5)$$

Equation (23.5) is not yet a quantum commutator. It is the canonical bracket structure of the reduced coherent EFT.

The quantum question is whether the corresponding operator relation takes the form

$$[\hat{\theta}(\mathbf{x}, t), \hat{\pi}_\theta(\mathbf{y}, t)] = i S_0 \delta^{(3)}(\mathbf{x} - \mathbf{y}), \quad (23.6)$$

and whether the same scale  $S_0$  is then to be identified with the observed  $\hbar$ . This is a Level B step (cf. (21.7)), not yet a completed theorem.

**Why Eq. (23.6) is the unique structural candidate.** Equation (23.6) is not introduced ad hoc. Its form is singled out by the three ingredients already established in the coherent branch:

- (i) the coherent sector possesses a distinguished action scale  $S_0$  (20.3);
- (ii) wave-dynamical amplitudes are weighted by  $\exp(iS_\theta/S_0)$  (22.1), so the same scale already controls phase sensitivity of coherent histories;
- (iii) canonical quantisation, if it emerges from the coherent branch, must be normalised by an action scale, and no second independent structural action scale is available inside the same smooth coherent sector.

For this reason the commutator normalisation by  $S_0$  is not merely plausible but structurally singled out. What remains open is not the availability of a candidate scale, but the full operator-level derivation of the corresponding algebra and its final physical matching to the observed quantum commutator.

**Topological constraint from the compactness of  $\theta$ .** The coherent phase variable  $\theta$  is compact:  $\theta \sim \theta + 2\pi$  (single-valuedness of the effective order parameter, Section 21.1). This compactness has an immediate canonical consequence, but it must be stated carefully. What is quantised directly is not the local momentum density  $\pi_\theta(\mathbf{x}, t)$  pointwise, but the generator of the global phase shift, i.e. the zero-mode / integrated conjugate quantity

$$Q_\theta(t) \equiv \int d^3x \pi_\theta(\mathbf{x}, t). \quad (23.7)$$

If the operator relation (23.6) holds, then single-valuedness of the coherent wave functional under  $\theta \mapsto \theta + 2\pi$  implies

$$Q_\theta \in \mathbb{Z} \cdot S_0. \quad (23.8)$$

This is the standard quantisation statement for a compact canonical phase variable: the compact coordinate implies a discrete spectrum for the corresponding global conjugate generator. Equation (23.8) is therefore not an additional input but a topological consequence of the same compact phase structure that already underlies the winding-sector classification (Section 21.1, eq. (20.2)). What remains open is the precise operator-level relation between this global quantisation statement and the full local many-body algebra of the coherent branch.

**Local versus global content.** The logical status of the canonical programme should be kept sharply separated at two levels. The compactness of  $\theta$  and single-valuedness of the coherent wave functional already control the *global* generator of phase shifts, leading to the quantisation condition (23.8). By contrast, the *local* equal-time operator algebra (23.6) still belongs to the operator-level completion problem. ECT therefore already fixes the global topological canonical content at Level A, while the full local many-body commutator algebra remains an A/B-to-open programme.

**Structural triangle: winding – canonical – action scale.** The three structural results of the coherent branch—integer winding sectors, the canonical commutator candidate, and the action scale  $S_0$ —are not independent achievements but three aspects of a single compact-phase architecture. The winding sectors follow from the compact topology of  $\theta$ ; the canonical bridge is the operator-level organisation associated with the same compact variable; and  $S_0$  is the unique normalisation set by the elementary loop action. At the global level this already yields the quantisation condition (23.8) for the generator of the compact phase shift. If any one of these three ingredients were absent or required a different normalisation, the architecture would be internally inconsistent. This self-reinforcing triangle is one of the most structurally rigid features of the coherent branch.

**Connection to the downstream quantum programmes.** The canonical bridge is not an isolated kinematical curiosity. If it is completed, it supplies the operator-level backbone for several downstream coherent-branch programmes: (i) the uncertainty principle (Section 23.5), which is a direct mathematical consequence of the commutator bridge; (ii) the Born-type probability programme (Section 30.4), which requires a consistent canonical/Hilbert-space setting for the probability reading of coherent amplitudes; (iii) the entanglement programme (Section 31), which presupposes a nontrivial operator-state structure on the same physical Hilbert space; and (iv) the decoherence programme (Section 26.1), which assumes that the coherent subsystem sits inside a larger unitary operator framework. In this sense, the canonical bridge is one of the central structural links between compact-phase topology and the operational quantum sector.

### From phase variables to wavefunction kinematics

In the wave-dynamical representation (22.5), the phase functional  $\mathcal{S}$  plays the role of the Hamilton principal function of the coherent branch. In this representation the natural wave-mechanical counterpart of the canonical bracket structure is a momentum operator of the schematic form

$$\hat{p} \sim -iS_0 \nabla_{\mathbf{x}} \quad (23.9)$$

(schematic 3D form; the 4D covariant version follows the same logic with  $g_{\text{eff}}^{AB} \partial_B$  replacing  $\nabla_{\mathbf{x}}$ ). Again, the point is not that ECT has already proved full operator quantisation. The point is that *the same* action scale  $S_0$  controls:

- loop-sector phase weights,
- Schrödinger-type evolution (22.8),
- and the natural normalisation of canonical operators.

This internal coherence is one of the strongest indications that  $S_0$  is the correct pre-quantum scale of the theory. Once the operator bridge is admitted, the same single normalisation extends further: it links loop-sector phase weights, the Schrödinger-type wave reduction, the candidate canonical commutator, and the uncertainty bound of Section 23.5. If any one of these required a different action-scale normalisation, the compact-phase coherent architecture would fragment.

### What is still missing

Despite this structural picture, the following steps are not yet complete:

- (i) a rigorous construction of the full operator algebra of the coherent sector;
- (ii) the derivation of canonical commutators beyond the phase variable itself (charge sectors, spin, multi-particle structure);
- (iii) the proof that the canonical structure survives the full decohering environment and defect sectors;
- (iv) the final empirical identification  $S_0 = \hbar$  (21.7).

For this reason the Quantum Sector does not yet claim that the full canonical quantisation of ordinary quantum mechanics has been derived. What has been shown is the more controlled statement: ECT produces the correct *place* in the theory where such commutators can emerge and the correct candidate scale that would normalise them.

**Discriminant with respect to standard and hidden-variable readings.** Standard quantum mechanics usually takes the canonical commutator as a primitive axiom. Hidden-variable or semiclassical alternatives often retain wave-like structure while modifying or downgrading the canonical operator algebra. ECT occupies a distinct middle position: the canonical bridge is neither primitive nor discarded, but is read as an emergent kinematic organisation of the smooth coherent branch, prepared by the same action scale  $S_0$  that already governs loop weights and wave dynamics. The distinctive ECT claim is therefore not “commutators by fiat”, but “commutators from a pre-quantum coherent medium with a unique action-scale candidate”.

**Empirical anchor: universality of the quantum of action.** The strongest empirical fact supporting the single-scale canonical architecture is the observed universality of one and the same  $\hbar$  across atomic spectroscopy, molecular binding, solid-state band structure, matter-wave interferometry, and particle-physics cross sections. No sector of observed physics has ever required a different action scale for its canonical commutation structure. In ECT this universality is read not as a coincidence but as a structural consequence of the single-medium origin: one ordered condensate, one coherent branch, one action scale  $S_0$ , and therefore one canonical normalisation. If a future experiment revealed a sector-dependent commutator scale, the single-branch architecture would be directly falsified.

**Falsifier for the canonical-bridge programme.** If different parts of the coherent quantum programme required incompatible action-scale normalisations for (i) loop weights, (ii) Schrödinger-type evolution, (iii) canonical commutators, and (iv) Born-type probability structure, then the single-scale coherent-branch architecture would fail. Likewise, if a completed operator derivation forced a canonical normalisation unrelated to  $S_0$ , the ECT canonical-bridge programme would be structurally falsified. The canonical question is therefore a genuine cross-sector test of the one-medium architecture, not a merely technical completion problem.

### Why this is already a substantial result

Most approaches that attempt to derive quantum mechanics from a deeper substrate struggle to explain why a canonical algebra should emerge at all, and why it should be normalised by a universal action scale. ECT already answers a large part of this question: the coherent branch possesses a topologically prepared action scale and a reduced wave-dynamical structure, so the canonical algebra is not a mysterious axiom but the natural kinematic organisation of the smooth coherent sector.

### Bridge to uncertainty, probability, and decoherence

Canonical structure alone is not yet enough to recover the full operational content of quantum theory. One must still explain: (i) why the commutator bridge yields the uncertainty relation (Section 23.5), (ii) how effective probabilities arise and under what conditions a Born-type reading becomes valid (Section 30.4), and (iii) why coherent amplitudes decohere in macroscopic environments (Section 26.1). Those questions belong to the subsequent sections of Part III.

**Status summary.** *Established (Level A):* (i) the smooth coherent branch admits a natural canonical organisation with phase variables and conjugate momenta; (ii) the corresponding reduced coherent dynamics carries the standard Poisson-bracket structure; (iii) for the compact phase variable, the generator of the global phase shift obeys the topological quantisation condition (23.8). *Structurally singled out (Level A/B):* the same action scale  $S_0$  that governs coherent phase weights and wave reduction is the unique structural candidate for the commutator normalisation. *Open (Level B/open):* the full local operator algebra, many-body canonical completion, and final physical identification with the observed canonical quantum structure remain to be derived in full detail.

For the present loop-based calculation status and the open first-principles derivation of the action scale  $S_0$ , see Appendix AV.

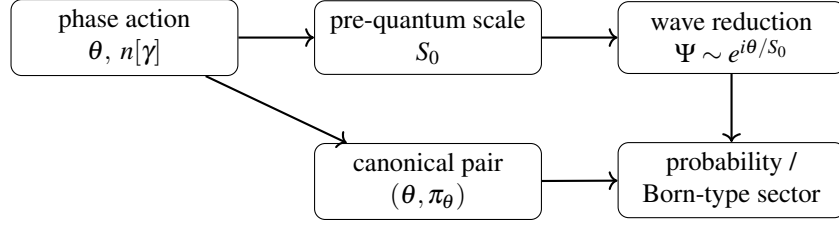


**Figure 31:** Structural roadmap of the coherent-sector quantization logic in ECT (Level B). Phase dynamics and loop quantization prepare the action scale  $S_0$ , which supports wave reduction, canonical structure, and eventually the Born-type reduced probability sector. The figure is a structural roadmap rather than a closed derivation of  $S_0 = \hbar$ .

## 23.4 Charge quantisation from the compact-phase gauge origin

*Status: Level A for the Abelian condensate-sector charge lattice (compact- $U(1)$  group-theoretic route). Level A/B for the canonical Dirac-quantisation corroboration (commutator route). Level B for the electroweak  $\mathbb{Z}_2$ -quotient refinement and charge-lattice constraint  $2T + Y \in 2\mathbb{Z}$ . Open for the full observed electric-charge spectrum, hypercharge quantisation, and fermion representation content. Connection: compact phase sector (§21.1),  $U(1)$  emergence (§7.2), Dirac quantisation condition (23.8), electroweak structure (§48.13).*

### Problem statement: conservation versus quantisation versus the observed charge spectrum

The emergence of a local  $U(1)$  gauge symmetry in ECT immediately implies electric-charge conservation by Noether’s theorem. This, however, is not yet the same as charge quantisation. Conservation states that a charge, once assigned, is preserved. Quantisation asks why the allowed charges belong to a discrete lattice rather than a continuum. Three levels must be kept sharply distinct:

- (i) *charge conservation*,  $\partial_\mu J^\mu = 0$ , which is already established (§7.2);
- (ii) *Abelian charge quantisation*,  $q \in \mathbb{Z} \cdot e_0$ , i.e. why charges form a discrete lattice;
- (iii) *the full observed Standard-Model charge pattern*,  $Q = T_3 + Y/2$  with specific values  $0, \pm e/3, \pm 2e/3, \pm e$ , which requires in addition electroweak embedding, hypercharge quantisation, and a derivation of the fermion representation content.

The present subsection establishes (ii) and clarifies why (iii) remains open.

### The compact-phase route: why charge quantisation is structural in ECT

In standard QED, the gauge group  $U(1)$  can in principle be either compact or noncompact  $\mathbb{R}$ . Only the compact choice enforces charge quantisation; the noncompact group permits a continuous spectrum of charges. Which option nature realises is, within the standard framework, an empirical input.

In ECT, this ambiguity does not arise. The  $U(1)$  gauge sector is *derived* from the compact phase of the condensate:  $\theta \sim \theta + 2\pi$  (§7.2). There is no consistent way to obtain a noncompact  $\mathbb{R}$  gauge group from a field whose phase is topologically  $S^1$ . Compactness is therefore not assumed—it is a structural consequence of the condensate architecture.

**Theorem 23.1** (Compact- $U(1)$  charge lattice). *Let the condensate phase sector be compact,  $\theta \sim \theta + 2\pi$ , and let the emergent Abelian gauge sector be the local gauge redundancy of this compact phase. Then any matter excitation transforming in a one-dimensional unitary representation of this compact  $U(1)$  must carry charge*

$$q_n = n e_0, \quad n \in \mathbb{Z}, \quad (23.10)$$

where  $e_0$  is the elementary Abelian charge unit of the condensate sector.

**Proof.** A charged excitation transforms as  $\psi \rightarrow e^{i\lambda\alpha(x)}\psi$  under a local gauge transformation with parameter  $\alpha$ . Because the gauge parameter is angular ( $\alpha \sim \alpha + 2\pi$ ), the transformation with  $\alpha = 2\pi$  is the identity element of compact  $U(1)$ . Physical single-valuedness therefore requires  $e^{i2\pi\lambda} = 1$ , hence  $\lambda \in \mathbb{Z}$ . Restoring the elementary charge unit  $e_0$ , the covariant derivative takes the form  $D_\mu = \partial_\mu - in e_0 A_\mu$ , and the allowed charges are precisely  $q_n = n e_0$ .  $\square$

**Status.** Theorem 23.1 is **Level A**. It depends only on the compactness of  $\theta$  (from the condensate construction), the gauge emergence via P5 (§7.2), and the representation theory of compact groups (a mathematical fact). It does *not* require the canonical commutator candidate (23.6).

### Canonical corroboration (independent route)

A second, independent route to the same lattice is already present in the theory: if the charge operator is canonically conjugate to the compact phase,  $[\hat{Q}_\theta, \hat{\theta}] = iS_0$  (23.6), then compactness of  $\theta$  again implies a discrete spectrum for  $\hat{Q}_\theta$ :  $Q_\theta \in \mathbb{Z} \cdot S_0$  (23.8). This route is Level A/B because it leans on the operator/CCR side of the quantum programme.

The two routes are logically independent: the group-theoretic route uses only compactness and representation theory; the canonical route uses compactness and the commutator. Their mutual consistency strengthens the structural case for Abelian charge quantisation.

### Loop/holonomy viewpoint

The same conclusion may be restated in the loop language natural to ECT. Transport of a charged excitation around a closed loop must return the same physical state up to an allowed  $U(1)$  phase. Compatibility with the compact phase fibre forces the charge to lie on the discrete lattice  $q/e_0 \in \mathbb{Z}$ .

### Electroweak conditional refinement

If the electroweak condensate sector is such that the simultaneous action of the common centre element  $(-1, -1) \in SU(2) \times U(1)$  is physically redundant on the order parameter—as is natural for an electroweak condensate sector with an even order-parameter potential and centre-insensitive vacuum structure—then the effective electroweak gauge structure is  $U(2) = (SU(2) \times U(1))/\mathbb{Z}_2$  (48.1), and admissible representations satisfy  $2T + Y \in 2\mathbb{Z}$  (48.2) (Level B, conditional on the electroweak embedding). This sharpens the lattice structure beyond bare compact  $U(1)$ .

### Anomaly cancellation as a self-consistency requirement

In ECT, anomaly cancellation is not an external aesthetic criterion but a non-negotiable self-consistency requirement: if the ordered branch produces an emergent chiral gauge sector, the emergent matter content *must* be anomaly-free, otherwise the emergent gauge theory is inconsistent, contradicting the existence of the ordered branch itself. This does not yet derive the observed fermion representations, but it sharply constrains any acceptable completion: whatever matter representations emerge from the condensate, they must satisfy the standard anomaly-cancellation conditions. A systematic anomaly architecture of the emergent chiral gauge sector, including the electroweak ordered-branch constraints, the anomaly-transparency of the director coupling  $\mathcal{L}_5$ , and the open status of the colour-sector completion, is developed in §9.5.

### Neutrino compatibility

Within the charge-lattice constraint  $2T + Y \in 2\mathbb{Z}$ , a singlet with  $T = 0$ ,  $Y = 0$  has  $Q = 0$ . This is naturally compatible with a sterile-neutrino-like state, fitting smoothly with the seesaw route already developed in the neutrino sector. This should be read as compatibility, not as an independent derivation of the neutrino charge.



## What remains open

The compact- $U(1)$  result does not yet derive the full observed Standard-Model electric-charge spectrum. In particular:

- (i) the appearance of quark charges  $\pm e/3$  and  $\pm 2e/3$  requires the colour sector (OP-GUT1) and the electroweak representation content (OP-GUT3b);
- (ii) the precise equality  $|Q_e| = |Q_p|$  requires anomaly-consistent representations (OP-GUT6);
- (iii) the full observed charge pattern likely depends on the global structure of the complete low-energy gauge group, potentially of  $(SU(3) \times SU(2) \times U(1)_Y)/\Gamma$  type with  $\Gamma = \mathbb{Z}_6, \mathbb{Z}_3$ , or  $\mathbb{Z}_2$  [162];
- (iv) three fermion generations remain an open problem (OP-GUT5).

## Comparison with other routes to charge quantisation

**Table 78:** Comparison of routes to charge quantisation.

Aspect		Standard QED	GUT embedding		ECT
Why quantised		Not explained ( $U(1)$ can be noncompact)	Group forces it	embedding	Compact-phase condensate origin (Level A)
Status of derivation		Empirical input	GUT hypothesis required		Structural from P3+P5
Fractional charges		Empirical	Predicted by rep content		Requires EW+colour completion
Anomaly role		Empirical consistency check	Automatic GUT	within	Self-consistency of ordered branch

**Discriminant: ECT charge quantisation versus standard approaches.** The ECT route is architecturally distinct: it derives compact  $U(1)$  from the condensate phase rather than postulating it or embedding it in a larger group. This makes Abelian charge quantisation a structural medium property, not an empirical coincidence or a GUT-dependent consequence. The identification of the elementary condensate charge unit  $e_0$  with the observed electromagnetic coupling remains part of the broader gauge-matching programme (OP-GUT4).

**Falsifier for the charge-quantisation programme.** The programme would be falsified if (i) the condensate phase sector were shown to be topologically noncompact (contradicting the construction); (ii) a completed ECT gauge/matter sector produced anomaly-violating representations; or (iii) the electroweak/colour completion failed to reproduce the observed charge assignments.

**Status summary.** *Established (Level A):* (i) compact  $U(1)$  gauge group from condensate phase (Theorem 23.1); (ii) Abelian charge lattice  $q \in \mathbb{Z} \cdot e_0$ ;

*Architectural / consistency requirement:* (i) anomaly cancellation as a mandatory self-consistency condition on any emergent chiral sector (consistency target, not yet a derived representation theorem).

*Conditional (Level A/B to B):* (i) canonical Dirac quantisation (23.8); (ii) electroweak  $\mathbb{Z}_2$  quotient and charge-lattice constraint  $2T + Y \in 2\mathbb{Z}$ .

*Open:* (i) full observed electric-charge spectrum; (ii) hypercharge quantisation from first principles; (iii) full global gauge-group structure  $(SU(3) \times SU(2) \times U(1)_Y)/\Gamma$ ; (iv) observed fermion representation

content.

### 23.5 Uncertainty principle in the coherent branch

*Status: Level A for the mathematical uncertainty inequality once the canonical commutator structure of the smooth coherent branch is admitted; Level B for the physical normalisation of that inequality by the observed  $\hbar$ , which depends on Eq. (21.7).*

The uncertainty relation discussed below inherits its status directly from the canonical-bridge programme of Section 23.3: it is mathematically strict once the commutator bridge is granted, but physically matched only after the  $S_0 = \hbar$  identification.

The uncertainty principle is not introduced in ECT as an independent axiom. If the coherent branch already admits (i) a wave-dynamical representation, (ii) a canonical organisation, and (iii) a commutator candidate normalised by the intrinsic action scale  $S_0$  (Section 23.3), then the uncertainty relation follows as a standard mathematical consequence.

#### Operator input

From Section 23.3, the natural commutator candidate of the coherent branch is (23.6):

$$[\hat{q}, \hat{p}] = iS_0. \quad (23.11)$$

After the final empirical identification (21.7), this becomes the observed canonical commutator:

$$[\hat{q}, \hat{p}] = i\hbar \quad (23.12)$$

This is the observationally identified form (Level B): it requires the final identification (21.7).

#### Robertson–Schrödinger inequality

For any pair of self-adjoint operators  $\hat{A}$ ,  $\hat{B}$  and any state  $|\psi\rangle$ , the Cauchy–Schwarz inequality gives

$$\Delta A \Delta B \geq \frac{1}{2} |\langle [\hat{A}, \hat{B}] \rangle|. \quad (23.13)$$

Setting  $\hat{A} = \hat{q}$  and  $\hat{B} = \hat{p}$  with (23.11) gives the coherent-branch uncertainty relation

$$\Delta q \Delta p \geq \frac{S_0}{2} \quad (23.14)$$

Equation (23.14) is Level A once the coherent canonical structure (23.11) is admitted. After the  $S_0 = \hbar$  identification this reduces to the standard Heisenberg form

$$\Delta q \Delta p \geq \frac{\hbar}{2} \quad (23.15)$$

This is a Level B observational form (Heisenberg inequality), since it requires the final identification (21.7).

**Complementary topological constraint for the compact phase.** For the compact phase variable  $\theta \sim \theta + 2\pi$  (Section 23.3), the canonical bridge is supplemented by the global quantisation condition (23.8) for the generator of the compact phase shift. This does not replace the Robertson–Schrödinger inequality (23.14), nor does it by itself yield a stronger local uncertainty theorem for the field momentum density. Rather, it provides a complementary global topological restriction that is fully compatible with the same action-scale normalisation  $S_0$ . In this sense, the uncertainty relation and the compact-phase quantisation condition are two consistent faces of the same canonical-topological architecture.

## Interpretation

ECT does not postulate uncertainty at the foundation. Uncertainty appears only after the coherent branch has already developed the structures that ordinary quantum theory usually assumes: wave amplitudes, canonical variables, and commutator normalisation. The uncertainty relation is therefore not primitive; it is derivative.

**Numerical anchor.** After the identification  $S_0 = \hbar$ , the uncertainty bound takes its standard value  $\hbar/2 \approx 5.27 \times 10^{-35} \text{ J s}$ . For an electron confined to a hydrogen-like atomic scale  $\Delta x \sim a_0 \approx 0.529 \text{ \AA}$ , one obtains

$$\Delta p_{\min} \sim \frac{\hbar}{2a_0} \approx 1.0 \times 10^{-24} \text{ kg m/s}, \quad (23.16)$$

which is of the standard atomic order of magnitude. ECT adds no correction to this result at the current level of the coherent-branch closure: once  $S_0 = \hbar$  is matched, the usual Heisenberg scale is reproduced exactly.

**Discriminant: derived versus primitive uncertainty.** In standard axiomatic quantum mechanics, the uncertainty principle is a theorem of the already assumed Hilbert-space and operator framework. In ECT the logical direction is different: uncertainty is not primitive, but is derived from the coherent-branch canonical bridge, which itself is prepared by the compact-phase architecture and the distinguished action scale  $S_0$ . ECT therefore does not merely reproduce the Heisenberg inequality; it traces it back to the same structural source that also underlies winding sectors, canonical organisation, and the action-scale programme.

**Falsifier for the uncertainty programme.** The uncertainty programme would fail if the coherent-branch canonical structure required an uncertainty normalisation different from  $S_0$ , or if the compact-phase quantisation condition (23.8) proved incompatible with the same single-scale canonical architecture. At the observational level, any reproducible violation of the bound  $\Delta q \Delta p \geq \hbar/2$  in the regime where the standard canonical description is known to apply would directly challenge the canonical reading of the coherent branch. No such violation has ever been observed.

**Status summary.** *Level A:* given the canonical structure (23.11), the inequality (23.14) is a mathematical theorem (Robertson–Schrödinger). The compact-phase quantisation condition (23.8) is compatible with the same single action-scale normalisation from a complementary topological direction. *Level B:* the physical Heisenberg form  $\Delta q \Delta p \geq \hbar/2$  depends on the matched identification  $S_0 = \hbar$  (21.7). No experimental violation of this bound has been observed.

**Bridge to the next chapter.** With the Hilbert-space bridge, unitarity status, canonical organisation, and uncertainty structure in place, the coherent branch is ready for the next layer of analysis: Euclidean path-dependence, exchange sectors, and the route to Dirac structure. Those questions are the subject of the next chapter.

## 24 Euclidean Path-Dependence, Quantum Nonclassicality, Statistics, and Dirac Structure

*Inputs: coherent-branch wave kinematics (Section 22), the Hilbert-space bridge (Section 23), canonical structure (Section 23.3), and compact-phase topology (BR1). Aim: to develop three further structural consequences of the coherent branch — Euclidean path-dependence as a route to nonclassical amplitudes, the exchange-sector dichotomy tied to the spatial dimensionality fixed by  $O(4) \rightarrow O(3)$ , and the representation-theoretic route to Dirac structure via the full chain  $O(4) \rightarrow O(3) \Rightarrow d = 3 \Rightarrow \mathbb{Z}_2 \Rightarrow \text{Spin}(3) \Rightarrow \mathfrak{so}(1,3) \Rightarrow$*

*Clifford  $\Rightarrow$  Dirac. Status: Level A for the elliptic two-sided Euclidean propagation structure, for the topological exchange dichotomy ( $d_{\text{spatial}} = 3 \Rightarrow \pi_1(\mathcal{M}_2) = \mathbb{Z}_2$ ), and for the Lorentz-algebra/Clifford-structure chain; Level A/B for the route from Euclidean path-dependence to interference, tunnelling, and the broader nonclassical amplitude structure of the quadratic/coherent reading; Level B (conditional) for Dirac-type dynamics given spinorial excitations; Level B/open for quantitative indefinite-causal-order reconstruction, for the physical spinorial spectrum, and for the full spin-statistics completion.*

## 24.1 Euclidean path-dependence: intermediate results from both past and future

A fundamental feature of the ECT framework is that the Euclidean equation of motion

$$(-\nabla_E^2 + m^2) \Phi(X) = 0, \quad \nabla_E^2 = \delta^{AB} \partial_A \partial_B, \quad (24.1)$$

is an *elliptic* partial differential equation. Consequently, the value of  $\Phi$  at an interior point  $X_m$  depends simultaneously on boundary conditions at *both*  $w < w_m$  (the “past”) and  $w > w_m$  (the “future”). The Euclidean Green’s function  $G_E(X, X')$  is fully symmetric under  $w \leftrightarrow -w$ , encoding this two-sided dependence.

**Physical consequences.** This two-sided Euclidean propagation provides a natural structural route to several standard nonclassical phenomena in ECT.

1. *Quantum interference.* The amplitude from  $X_i$  to  $X_f$  via intermediate  $X_m$ :

$$G_E(X_f, X_i) = \int G_E(X_f, X_m) G_E(X_m, X_i) d^4 X_m.$$

In the quadratic sector, after the formal Euclidean–Lorentzian amplitude continuation  $w_E \rightarrow \pm ic_* t$ , the Euclidean propagator  $G_E$  is read in the standard Feynman-propagator language  $G_F$ . The two-sided  $w$ -dependence is then read as the structural route to the superposition of quantum amplitudes.

2. *Quantum tunnelling.* The Euclidean path integral assigns weight  $e^{-S_E/S_0}$  to every field configuration, including those traversing classically forbidden regions. Tunnelling is therefore not introduced as a separate postulate, but appears as part of the same Euclidean amplitude structure.
3. *Directionality and irreversibility.* The two-sided  $w$ -dependence of the Euclidean propagator does *not* by itself produce an arrow of time: the Euclidean Green’s function is symmetric under  $w \leftrightarrow -w$  and treats past and future equally. An effective asymmetry  $P_{\text{back}}/P_{\text{fwd}} \neq 1$  appears only *after* the Gaussian–Markov coarse-graining of the influence functional (Section 26.1), which introduces a preferred direction through the irreversible functional  $\Gamma_{\text{irr}}$ . Deriving irreversibility from the bare ECT action without coarse-graining remains open (OP-Q17).

**Structural significance.** The two-sided Euclidean dependence is not a computational curiosity but a direct consequence of the Euclidean-first ontology (P1). In a Lorentzian-first theory, interference and tunnelling are usually introduced only after the quantum formalism has already been assumed. In ECT the logical direction is reversed: the Euclidean arena naturally gives boundary-value problems with two-sided dependence, and in the Lorentzian parametrisation this provides a structural route to the standard superposition/interference reading. At the present stage this should be read as a strong architectural explanation, not yet as a complete first-principles derivation of the entire quantum formalism from ellipticity alone.

**What this does *not* mean.** The two-sided dependence along the Euclidean coordinate  $w$  must not be misread as controllable signalling from the future in Lorentzian time. At the fundamental Euclidean level,  $w$  is not yet the observed time coordinate. Only after symmetry breaking and the real ordered-branch parametrisation does the effective Lorentzian notion of causal propagation emerge. Thus the ECT claim is not that laboratory agents can influence the past, but that the pre-Lorentzian coherent description is not

organised by a primitive one-sided temporal order. Operational no-signalling in the emergent Lorentzian branch must remain intact. This clarification also applies to indefinite-causal-order protocols: ECT reads them as coherent manifestations of a pre-Lorentzian two-sided amplitude structure, not as operational permission to signal to the past.

**Connection to the reverse-traversal mechanism.** The two-sided Euclidean dependence discussed here is the same structural ingredient that, in Section 30.1, appears as reverse  $O(3) \rightarrow O(4)$  contributions to the coherent path integral. In both cases the key point is that the Euclidean weight  $\exp(-S_E/S_0)$  is fundamentally  $O(4)$ -invariant, so backward segments are not excluded at the microscopic level. When the irreversible suppression parameter is small, such configurations contribute coherently; when it is large, the reverse contributions are effectively eliminated. The present subsection and Section 30.1 therefore give two complementary readings of the same Euclidean architecture.

**Discriminant: Euclidean-first versus Lorentzian-first nonclassicality.** In standard Lorentzian QFT, the two-sided structure of quantum amplitudes is usually accepted as part of the already assumed quantum formalism. In ECT the logical direction is reversed: the Euclidean arena is primary, its field equation is elliptic, and the two-sided boundary-value structure is already present before the Lorentzian branch is reconstructed. This does not change the mathematics of propagators after the formal Euclidean–Lorentzian continuation, but it changes the interpretive status: nonclassical amplitude structure is not taken as primitive, but is read as a consequence of the Euclidean-first coherent architecture.

**Falsifier for the path-dependence programme.** The path-dependence programme would fail if the Euclidean two-sided propagation structure, in the ordered Lorentzian branch, proved structurally incompatible with the observed interference, tunnelling, or superposition phenomena. It would also be weakened if the elliptic Euclidean boundary-value character could not be made consistent with the retarded causal structure established elsewhere for the ordered branch, or if the Euclidean weight  $\exp(-S_E/S_0)$  failed to reproduce the required Feynman-amplitude reading after the formal Euclidean–Lorentzian amplitude continuation. No such incompatibility is currently known within the present coherent-branch programme.

### Indefinite causal order

*Status: Level B structural reading. The connection to experimental indefinite-causal-order protocols is qualitative and programme-level. A first-principles derivation of operational switch correlators from coherent-branch condensate dynamics is not yet available.*

The two-sided Euclidean dependence (Section 24.1) offers a natural ECT reading of experiments commonly described as exhibiting *indefinite causal order*. The point is not that ECT has already derived the full operational quantum-switch formalism, but that a pre-Lorentzian framework without a primitive one-sided temporal ordering makes such phenomena conceptually much less surprising than in a strictly Lorentzian-first ontology.

### The Procopio–Walther quantum switch

Procopio et al. (2015) [163] realised a quantum switch in which the causal order of two unitary operations is coherently controlled. ECT does not yet derive the full switch resource theory from first-principles condensate microdynamics, but it supplies a natural interpretive backdrop:

- the underlying Euclidean substrate has no primitive Lorentzian time-ordering;
- causal order becomes operationally sharp only after the ordered branch is selected;
- in highly coherent regimes ( $\Gamma_{\text{loop}} \lesssim 1$ ), reverse-path contributions need not be negligible, so the operational description need not collapse immediately to a classically definite order.

This is therefore a structural compatibility statement, not yet a completed derivation of switch correlators or order-resource measures.

### Programme-level expectations for indefinite-order experiments

**Expectation 1 (coherence-threshold degradation).** The operational advantage of indefinite-order protocols should degrade as the same coherence parameter that governs the broader quantum-to-classical boundary approaches unity:

$$\Gamma_{\text{loop}} \sim 1 \quad \text{marks the crossover.} \quad (24.2)$$

This is a programme-level expectation, not yet a universal fitted law.

**Expectation 2 (environmental scaling).** Increasing environmental coupling, unresolved bath size, or effective noise load should suppress indefinite-order signatures in the same broad way that these quantities suppress reverse-branch coherence and matter-wave interference elsewhere in the coherent branch.

**Expectation 3 (temperature sensitivity).** Where the relevant environment admits an effective thermal description, higher temperature should accelerate the loss of indefinite-order contrast through the same decoherence logic that shortens coherence times in other coherent-branch experiments. The exact scaling remains platform-dependent and is not yet a universal ECT theorem.

**Historical note.** The theoretical quantum-switch framework was developed by Brukner et al. starting 2011–2012 [164]; the first photonic realisation is Procopio et al. (2015) [163].

**Quantitative dephasing estimate.** The Procopio experiment reports an interferometric visibility  $V = 0.994 \pm 0.002$  for the quantum-switch interferometer. Within the simplest pure-dephasing closure  $V \simeq e^{-\Gamma_{\text{loop}}}$ , this gives

$$\Gamma_{\text{loop}}^{(\text{exp})} = -\ln V = 0.0060 \pm 0.0020,$$

placing the platform deep in the coherent regime ( $\Gamma_{\text{loop}} \ll 1$ ). The small observed degradation is fully compatible with technical imperfections (fibre loss, mode mismatch, detector dark counts) rather than with fundamental decoherence. This should therefore be read as an experimentally inferred dephasing proxy within the present closure, not as a first-principles derivation of  $\Gamma_{\text{loop}}$  from microscopic condensate dynamics.

### Interpretive conclusion

In ECT, indefinite-causal-order experiments are naturally read as compatible with the pre-Lorentzian two-sided Euclidean dependence of the coherent branch. They do not by themselves uniquely confirm the ECT ontology, since other frameworks (e.g. the process-matrix formalism [165]) also accommodate indefinite-order phenomena. The distinctive ECT contribution is the structural route by which such phenomena arise from a specific physical substrate — the Euclidean condensate — rather than from an abstract generalisation of quantum channels alone. The criterion  $\Gamma_{\text{loop}} \lesssim 1$  is therefore proposed as a programme-level ECT guide for when such resources should remain visible, not yet as a completed universal law for all switch platforms.

### Delayed-choice, quantum eraser, and entanglement-swapping experiments in ECT

*Status: interpretive / Level B. ECT does not modify the operational predictions of these experiments at the present stage. Its contribution is structural and interpretive: it re-reads them as manifestations of the two-sided Euclidean coherent architecture rather than as retrocausal anomalies.*

The three experiment families discussed below play different operational roles but probe the same structural theme. Wheeler-type delayed-choice setups test whether a late basis choice can reorganise an interference pattern without enabling signalling to the past. Quantum-eraser protocols test whether

which-path records remove interference only at the level of the coarse-grained record, rather than through a literal retroactive collapse of the full microscopic configuration. Delayed-choice entanglement swapping tests the same two-sided coherent architecture in a multi-photon correlation setting. In all three cases ECT leaves the operational predictions of standard quantum theory unchanged and contributes a structural reinterpretation: the observed pattern is read as a boundary-value effect of the coherent Euclidean branch rather than as evidence for literal retrocausation.

**Wheeler’s delayed-choice experiment.** Wheeler (1978) [166, 167] proposed, and Jacques et al. (2007) [168] realised with single photons, an experiment in which the choice of measurement basis (wave-like or particle-like) is made *after* the photon has passed through the interferometer. In ECT, before irreversible detection, the single-photon branch is naturally read as remaining in the weak-locking coherent regime, where the Euclidean two-sided boundary structure is still operative. The “late” choice of basis changes the boundary conditions on one side of the elliptic problem, which is a standard property of boundary-value problems for elliptic equations and does not imply retrocausal signalling. ECT does not predict operational signalling to the past; it reinterprets the experiment as a boundary-value phenomenon rather than a retrocausal one.

**Comparison with standard quantum theory.** Standard quantum theory reproduces the delayed-choice outcome quantitatively through the superposition principle and the Born rule: the late insertion or removal of the final beam splitter changes the measurement basis and therefore the observed statistics. What remains interpretively open in the standard presentation is why a late basis choice appears to affect the earlier “wave” or “particle” character of the photon. ECT does not change the operational predictions; its contribution is interpretive: it re-reads the experiment as a two-sided Euclidean boundary-value problem rather than as a retrocausal one. No experiment-specific ECT numerical estimate is derived here beyond the structural requirement that the single-photon branch remain in the weak-locking coherent regime until irreversible detection. Within the broader operational regime map of the present article, the Jacques platform is naturally placed in the same weak-locking corridor as the Procopio switch, with visibility-based dephasing remaining well below the order-unity crossover. This should again be read as an experimentally inferred operational proxy, not as a first-principles condensate calculation for the specific interferometer.

**Quantum eraser.** Scully & Drühl (1982) [169] proposed, and Kim et al. (2000) [170] realised, an experiment in which which-path marking destroys interference, while subsequent “erasure” via coincidence conditioning restores it. In the ECT reading, which-path marking correlates the signal photon with additional degrees of freedom and thereby destroys the interference pattern in the full unconditioned ensemble. The subsequent “erasure” does not reverse a completed macroscopic collapse; rather, coincidence conditioning selects subensembles in which the relevant which-path correlation is not retained in the coarse-grained record. Interference is therefore recovered only conditionally, not universally across the full dataset. ECT interprets this in terms of whether the relevant record-generating coupling survives in the reduced description.

**Comparison with standard quantum theory.** Standard quantum theory explains the quantum-eraser result through the density-matrix formalism and conditional probabilities: interference is absent in the full unconditioned ensemble and reappears only in appropriately post-selected coincidence subensembles. ECT agrees with this operational account. Its added value is interpretive: it identifies which-path marking with a concrete record-generating correlation to additional degrees of freedom, and interprets erasure as the selection of a reduced description in which that correlation is not retained in the coarse-grained record. At present no ECT-specific quantitative correction beyond the standard conditioned-subensemble description is derived for this experiment.

**Delayed-choice entanglement swapping.** Ma et al. (2012) [171] demonstrated that the decision to entangle two photons can be made *after* the signal photons have already been detected. In the ECT

reading, entanglement is a non-factorisable correlation through the common condensate medium (§31), and the “late” decision modifies the boundary conditions of the global Euclidean configuration. As in the standard analysis, no operational contradiction with causal order arises: the effect is visible only after classical comparison of the relevant detection records.

**Comparison with standard quantum theory.** Standard quantum theory accounts for delayed-choice entanglement swapping through entangled-state projection and later classical record comparison. No contradiction with relativistic causality arises, because the correlation pattern becomes visible only after the relevant detection records are brought together. ECT leaves these operational predictions unchanged. Its contribution is again interpretive: the experiment is read as a manifestation of two-sided Euclidean correlation structure in the coherent branch rather than as evidence for literal retrocausation. No new ECT-specific numerical estimate is derived here; the role of the present discussion is conceptual rather than predictive.

**Summary of delayed-choice experiments.** Taken together, these experiments do not force literal retrocausation. They show that once a quantum process is described in terms of global coherent amplitudes rather than naive one-sided classical trajectories, late boundary choices can reorganise the observed pattern without any signal being sent into the Lorentzian past. Accordingly, the ECT reading is compatible with the standard no-signalling constraints of quantum experiments. ECT reads this as a natural consequence of the two-sided Euclidean coherent architecture. An important caveat must be stated explicitly: global Euclidean boundary-value dependence is not retro-signalling within Lorentzian spacetime. It is the standard mathematical property of elliptic boundary-value problems: the solution at any interior point depends on data everywhere on the boundary. No Lorentzian causality violation is implied.

Experiment family	Standard operational result	ECT reading	Quantitative status
Wheeler / Jacques delayed choice	Late basis choice changes the observed wave/particle statistics, with no signalling to the past	Two-sided Euclidean boundary-value dependence in the weak-locking coherent regime	Visibility-based operational anchor only; no first-principles ECT platform law derived
Quantum eraser (Scully–Drühl / Kim et al.)	Interference disappears in the full ensemble and reappears only in conditioned subensembles	Record-generating correlation survives or is removed only at the reduced-description level	No ECT-specific numerical correction derived beyond the standard conditioned-subensemble description
Delayed-choice entanglement swapping (Ma et al.)	Correlation pattern is fixed only after later Bell-state analysis and classical comparison	Global coherent configuration reorganised by two-sided Euclidean boundary conditions	Conceptual / interpretive only at present; no experiment-specific ECT numerical estimate
Procopio quantum switch	Indefinite-order resource remains visible in a highly coherent photonic platform	Structural compatibility with pre-Lorentzian two-sided coherent architecture	$V = 0.994 \pm 0.002 \Rightarrow \Gamma_{\text{loop}}^{(\text{exp})} = 0.0060 \pm 0.0020$

The operational visibility anchors collected in Section 27 and in Fig. 34 should be read as regime markers for this entire family of phenomena. At present, only the switch platform carries an explicit visibility-to- $\Gamma_{\text{loop}}$  estimate written out in the article. For Wheeler delayed-choice, quantum eraser, and delayed-choice entanglement swapping, the present status remains consistency-based and interpretive rather than numerically predictive.



**Programme-level predictions and discriminants.** Although ECT does not yet provide a platform-specific first-principles calculation for the full delayed-choice family, the present framework does suggest three nontrivial programme-level expectations.

First, all such phenomena should remain visible only in the weak-locking regime, i.e. only while the relevant branch satisfies  $\Gamma_{\text{loop}} \ll 1$  prior to irreversible detection. Second, late-choice reorganisation of the observed pattern should remain compatible with strict operational no-signalling in the emergent Lorentzian branch: ECT predicts boundary-value reorganisation, not controllable retrocausal communication. Third, visibility loss induced by different decoherence channels should, at matched effective  $\Gamma_{\text{loop}}$ , degrade these nonclassical signatures in the same broad operational corridor as other coherent branch phenomena. These expectations are structural and closure-level at present; turning them into platform-specific numerical laws remains part of the open experimental programme.

### Wigner’s friend paradox

*Status: interpretive / Level B. ECT does not modify the operational predictions but provides a structural reframing of the problem.*

In the Wigner’s friend scenario, an observer (the “friend”) performs a measurement inside a sealed laboratory, while a superobserver (Wigner) treats the entire laboratory as a quantum system. In the standard presentation, the paradox is that the friend assigns a definite outcome while Wigner assigns a superposition.

In the ECT reading, the tension is reformulated structurally rather than eliminated by a new measurement postulate. The friend’s measurement device couples strongly to the measured subsystem, so that the measured degrees of freedom are naturally driven toward the Lorentzian locked regime once the corresponding effective  $\Gamma_{\text{loop}}$  becomes large. Wigner, if treated as external to that record-generating process, may still assign a more weakly reduced description to the laboratory as a whole, but only insofar as the relevant lab–environment coarse graining has not yet been specified at his level of description. ECT therefore shifts the question from “who is observing” to “which degrees of freedom have already been locked by environmentally amplified record formation”.

**Comparison with standard quantum theory.** Standard quantum theory can accommodate both the friend-collapsed and Wigner-superposed descriptions within the relative-state formalism, but does not by itself privilege one physical criterion for when a definite record should count as established. ECT proposes such a criterion only at closure level: large effective environmental locking of the record-generating degrees of freedom. This is a structural closure-level reading of the paradox, not yet a completed model-independent theorem of measurement.

## 24.2 Reverse-path suppression from PES

The Euclidean path integral admits both forward (ordered,  $O(4) \rightarrow O(3)$ ) and reverse ( $O(3) \rightarrow O(4)$ ) segments. PES provides a quantitative suppression factor.

A forward segment has Euclidean action  $S_{\text{ord}}$ ; a reverse segment, in which the condensate locally loses its preferred orientation, has action  $S_{\text{dis}} > S_{\text{ord}}$  by an amount  $\Delta S = S_{\text{dis}} - S_{\text{ord}} \sim \kappa_n \cdot V_{\text{eff}}$  (ordering energy  $\times$  effective volume). In the PES reading, the reverse-segment penalty is naturally measured by  $\Gamma_{\text{loop}} \sim \Delta S/S_0$ . The ratio of reverse to forward path weights is therefore:

$$\boxed{\frac{P_{\text{back}}}{P_{\text{fwd}}} = e^{-\Gamma_{\text{loop}}}.} \quad (24.3)$$

At  $\Gamma_{\text{loop}} \ll 1$ :  $P_{\text{back}}/P_{\text{fwd}} \approx 1$ —reverse paths are not suppressed, quantum coherence is maintained. At  $\Gamma_{\text{loop}} \gg 1$ :  $P_{\text{back}}/P_{\text{fwd}} \rightarrow 0$ —reverse paths are exponentially suppressed, classical irreversibility emerges. This connects PES directly to the quantum–classical boundary criterion (§30.1).

### 24.3 Tunnelling as traversal through the fourth spatial dimension

*Status: Level B geometric reading. The standard WKB/instanton amplitude is recovered; the ECT-specific content is the reinterpretation of the instanton path as a genuine spatial detour.*

#### Geometric interpretation

In standard quantum mechanics, a particle “penetrates through” a classically forbidden potential barrier. The instanton formalism describes this as a Euclidean-time trajectory under the inverted potential.

In ECT, the Euclidean coordinate  $w$  is a *real* fourth spatial dimension (P1). The potential barrier  $V(\mathbf{x})$  is a three-dimensional obstacle. In four-dimensional Euclidean space, the barrier does not extend along the  $w$ -direction. The instanton trajectory is therefore not a “penetration through” the barrier but a *detour around it* through the fourth spatial dimension.

#### Effective detour length

The standard instanton action for a particle of mass  $m$  tunnelling through a barrier of height  $V_0$  and width  $a$  is:

$$S_{\text{inst}} = \int_0^a dx \sqrt{2m(V(x) - E)}. \quad (24.4)$$

The tunnelling probability is  $P_{\text{tun}} \sim e^{-2S_{\text{inst}}/\hbar}$ .

In the ECT geometric reading, the effective momentum along the  $w$ -direction during the detour is  $p_w \sim \sqrt{2m(V_0 - E)}$ . For a rectangular barrier, or as an order-of-magnitude estimate for a smooth barrier of width  $a$ , the effective detour length in the fourth dimension is:

$$\Delta w_{\text{detour}} \sim \frac{S_{\text{inst}}}{p_w} \sim a, \quad (24.5)$$

i.e. of order the characteristic barrier width in the simplest geometry. The tunnelling suppression  $e^{-2S_{\text{inst}}/\hbar} = e^{-2p_w \Delta w/\hbar}$  is then read as the Euclidean weight of a path that detours by  $\Delta w$  through the fourth dimension at momentum  $p_w$ .

At the level of the semiclassical tunnelling exponent, the standard WKB/instanton suppression is recovered. What ECT adds is the geometric picture: the classically forbidden region is not traversed but bypassed, and the suppression factor is the cost of the spatial detour.

**Physical significance and interpretive status.** Ordinary quantum mechanics gives precise tunnelling amplitudes, but leaves the physical intuition unsatisfactory: how does the particle “end up on the other side” when it classically lacks sufficient energy? In ECT the Lorentzian barrier is a barrier for the projected classical motion, but not necessarily for the full Euclidean condensate configuration. What looks like an exponentially suppressed forbidden transition in the Lorentzian picture is a configurational bypass in the deeper Euclidean picture. The system does not violate causality; it realises a configurational detour that, after projection, reads as tunnelling. At the present level this is primarily an interpretive and geometric gain, not yet an established distinct numerical deviation from the standard WKB/instanton result.

#### Connection to PES

In the PES framework, the tunnelling configuration has  $\partial_w \Psi \neq 0$  along the detour segment and therefore incurs a non-zero  $\Gamma_{\text{env}}$ . The tunnelling rate is controlled by the same non-stationarity measure  $\mathcal{N}_{\text{ns}}$  that governs particle lifetimes (eq. 29.4): tunnelling is a temporary departure from the persistent stationary sector, with the departure “length” set by the barrier geometry.

**Reverse coherence: Lorentzian-to-Euclidean transition.** The reverse process — a strongly locked Lorentzian description relaxing back toward a more coherent Euclidean-sector reading — is suppressed in the PES language by the same factor  $P_{\text{back}}/P_{\text{fwd}} = e^{-\Gamma_{\text{loop}}}$ . For genuinely macroscopic record-bearing systems this suppression is expected to be enormous, so reverse coherence is not a realistic ordinary process. What remains physically relevant are mesoscopic and engineered recoherence settings, where effective environmental locking can be reduced and partial recovery of coherence becomes possible.

ECT is consistent with echo-type and recoherence protocols already known in standard quantum control, because reducing effective environmental monitoring reduces the corresponding decoherence cost. The present point is therefore not a claim of a new universal recoherence law, but the structural identification of such phenomena as partial returns toward the weak-locking coherent regime. This should not be read as a claim that current echo or recoherence protocols already realise a literal macroscopic return to the bare  $O(4)$  sector; the point is a reduced-description structural analogy within the present closure. At present this should be read as a structural and programme-level extension of the reverse-path logic, not yet as a completed predictive framework with platform-specific recoherence numerics. A more explicit discussion of reverse  $O(3) \rightarrow O(4)$  segments and their relation to recoherence protocols is given in §30.1.

**Connection to PES.** The two-sided Euclidean dependence and the indefinite-causal-order reading acquire a unified physical explanation through the Principle of Euclidean Stationarity (§29). PES interprets reverse  $O(3) \rightarrow O(4)$  segments as structurally admissible departures from the stationary sector, suppressed by  $P_{\text{back}}/P_{\text{fwd}} = e^{-\Gamma_{\text{loop}}}$  (§24.2). Tunnelling is read as a spatial detour through the fourth Euclidean dimension (§24.3).

**Euclidean correlation versus Lorentzian interaction.** In the PES reading, the Euclidean path sector is not yet an arena of Lorentzian interaction events but of common condensate-supported correlations. This sharpens the interpretation of delayed-choice and tunnelling phenomena: what is structurally available in the Euclidean branch is a two-sided boundary-value dependence, while a definite Lorentzian event structure appears only after environmental locking suppresses the reverse sector.

**Status summary.** *Established (Level A):* the Euclidean coherent-field equation is elliptic, so interior values depend on boundary data from both sides of the Euclidean ordering coordinate. *Level A/B:* in the quadratic/coherent path-integral reading, this two-sided dependence provides a structural route to interference, tunnelling, and the broader nonclassical amplitude logic of the coherent branch. *Level B/open:* the quantitative reconstruction of operational indefinite-causal-order protocols, switch correlators, and platform-dependent degradation laws from condensate dynamics remains incomplete.

## 24.4 Quantum statistics: exchange sectors and spinorial compatibility

*Status: Level A for the exchange-topology statement that in the primary ordered branch, whose spatial dimensionality is fixed to  $d_{\text{spatial}} = 3$  by the  $O(4) \rightarrow O(3)$  breaking pattern, the two-particle configuration space has  $\pi_1(\mathcal{M}_2) = \mathbb{Z}_2$  and therefore admits exactly two fundamental exchange classes. Level B for the structural compatibility between symmetric exchange and integer-spin sectors, and between antisymmetric exchange and spinorial sectors. Open (OP-Q11) for the full spin-statistics theorem, the operator anticommutation algebra, and the emergent many-excitation sector decomposition (Fock-like reconstruction; a reconstruction problem, not a foundational gap). Connection:  $O(4) \rightarrow O(3)$  ordering (P4), medium character (P5), fermionic-sector discussion (§9.9), Dirac route (§24.5), and entanglement for identical particles (§31).*

In the present framework, once a given emergent field sector is fixed, particles of the same species correspond to quanta of the same emergent mode sector of the same ordered medium and therefore carry no hidden individuation label beyond the quantum numbers of the shared mode itself. Environmental dressing may modify propagation or effective interactions, but it does not alter species identity. Because

ECT supplies no hidden individuation variable, exchange of same-species quanta is a genuine quotient of configuration space rather than a permutation of hidden labels: it reassigns occupation of the same mode sector rather than exchanging individuated microscopic objects. This is precisely why the many-particle configuration space relevant for same-species quanta is already the quotient by exchange, to which the following discussion now turns.

If the Quantum Sector of ECT is to reproduce more than one-particle coherent kinematics, it must also explain why exchange sectors split into bosonic and fermionic classes. At the present stage the strongest justified result is structural: ECT naturally reproduces the topological dichotomy of exchange sectors and shows its compatibility with the representation content of the ordered branch.

### Exchange topology

For two identical excitations in three spatial dimensions, the reduced configuration space is

$$\mathcal{M}_2 = (\mathbb{R}^3 \times \mathbb{R}^3 \setminus \Delta) / S_2, \quad (24.6)$$

whose fundamental group is

$$\pi_1(\mathcal{M}_2) = \mathbb{Z}_2. \quad (24.7)$$

This yields exactly two topological exchange classes: symmetric and antisymmetric (Level A as a topological fact; the connection to specific condensate sectors is Level B).

**Why the  $\mathbb{Z}_2$  exchange dichotomy is structural in ECT.** The exchange topology  $\pi_1(\mathcal{M}_2) = \mathbb{Z}_2$  is specific to the exchange of identical excitations in  $d \geq 3$  spatial dimensions. In  $d = 2$ , the corresponding braid structure is richer and supports anyonic exchange phases [172, 173]; in the primary ordered branch of ECT, however, the spatial dimensionality is not a free external input. It is fixed by the  $O(4) \rightarrow O(3)$  breaking pattern itself: the ordered branch has exactly three spatial directions. Therefore the  $\mathbb{Z}_2$  exchange dichotomy is not separately postulated; it is the topological consequence of the same symmetry breaking that establishes the ordered branch. In this precise sense, the bosonic/fermionic exchange split is structurally tied to P4.

**Empirical anchor.** Observed particle physics in  $3 + 1$  dimensions exhibits exactly the bosonic/fermionic dichotomy for fundamental excitations: photons and gauge bosons are bosonic, while electrons, neutrinos, and quarks are fermionic. By contrast, anyonic exchange has been observed only in effectively two-dimensional condensed-matter systems, where braid topology differs from the  $3 + 1$ -dimensional particle-exchange problem. This empirical split is precisely the pattern expected if the primary ordered branch is fundamentally three-dimensional, while anyonic statistics remains an emergent lower-dimensional quasiparticle phenomenon rather than a fundamental exchange law of the coherent branch.

### Representation-theoretic compatibility

After  $O(4) \rightarrow O(3)$  breaking, excitations of the ordered sector fall into representations of the residual rotational structure. At this stage ECT establishes a structural compatibility statement: integer-spin tensorial sectors fit naturally with symmetric exchange, while half-integer spinorial sectors fit naturally with antisymmetric exchange. This is stronger than a mere analogy but weaker than the full Pauli–Lüders–Zumino theorem. What is established here is the compatibility of exchange topology and representation content in the ordered branch; what remains open is the full operator-level spin-statistics theorem and the many-body fermionic construction.

**Medium reading of exchange (P5).** Postulate P5 does not alter the topology of exchange, but it gives that topology a physical reading. Exchange in ECT is not merely a permutation of abstract particle labels; it is the exchange of excitations of one common ordered medium. This strengthens the ontological interpretation of the bosonic/fermionic split without changing its mathematical status: the  $\mathbb{Z}_2$  exchange dichotomy remains a topological statement, while P5 clarifies what is being exchanged physically.

**Smooth-branch exactness of fermionic exclusion (provisional no-go statement, Level B).** A natural question is whether the structurally derived (exchange-topological and representation-theoretic, rather than axiomatically postulated) route to fermionic exclusion in ECT allows room for small violations of the Pauli principle in the presence of a spatially varying ordered condensate, such as inside strong gravitational fields or in dense astrophysical regimes. The answer obtained in the present framework is essentially the opposite of what a naive gradient estimate might suggest: smooth local inhomogeneity of the ordered condensate does not by itself furnish a mechanism for violating fermionic exclusion on the coherent ordered branch.

For a local first-order fermionic EFT with a smooth and strictly positive temporal kinetic coefficient  $\mathcal{K}(x) > 0$  multiplying  $i\psi^\dagger \partial_t \psi$ , a general condensate-dependent temporal kinetic term of the form  $i\mathcal{K}(x)\psi^\dagger \partial_t \psi + \dots$  can be brought to canonical form by the local field redefinition

$$\chi_\alpha(x) \equiv \mathcal{K}(x)^{1/2} \psi_\alpha(x), \quad (24.8)$$

after which the equal-time anticommutator takes the standard canonical form

$$\{\chi_\alpha(t, \mathbf{x}), \chi_\beta^\dagger(t, \mathbf{y})\} = \delta_{\alpha\beta} \delta^{(3)}(\mathbf{x} - \mathbf{y}), \quad (24.9)$$

and local interaction terms (including condensate-dependent mass  $M(\phi, n)\bar{\psi}\psi$ , the ECT preferred-direction coupling  $\mu_5(\phi, n)\bar{\psi}\gamma^A n_A \psi$ , and local four-fermion operators  $C_k(\phi, n)\mathcal{O}_k^{(4f)}$ ) modify the dynamics of fermionic modes without altering the underlying exclusion algebra. A full technical exposition of the canonical normalisation procedure, the cancellation of linear-order background corrections, and the residual curvature-controlled scale at the packet level is given in Appendix AW.

*Provisional no-go statement.* Consequently, if the eventual fermionic reconstruction closes to the standard local Grassmann/canonical anticommutation relation (CAR) structure, the Pauli exclusion principle remains exact throughout the smooth coherent ordered branch. Any genuine departure from standard fermionic statistics, if present at all in ECT, must therefore arise from one of the three following sources rather than from smooth local condensate gradients alone:

- (i) *Nonlocal branch mixing* — sector couplings that cannot be cast in the form of a local first-order fermionic EFT on the coherent branch.
- (ii) *Topological or defect sectors of the ordered condensate* beyond the ordinary coherent branch (e.g. condensate-defect backgrounds with nontrivial  $\pi_k$  content; cf. the topological-sector catalogue in Section 8.1).
- (iii) *Branch-transition / coherence-loss regions*, where the ordered-branch description itself fails and the fermionic reconstruction programme ceases to close.

The present statement is formulated at the level of a provisional no-go structural observation, not a full theorem; its completion requires the fermionic reconstruction programme (OP-Q11) and is listed as a distinct target in OP-Q21.

*Equivalence-principle aside.* A related way to see why ordinary strong gravity is not a viable Pauli-violation mechanism is that uniform acceleration can be locally removed by passing to a freely falling frame; the physically unremovable parameter is therefore the tidal tensor  $\mathcal{E}_{ij} \sim \partial_i \partial_j \Phi_N \sim G_N M / R^3$ , not the acceleration itself. Any residual dimensionless packet-level mismatch on a smooth background is accordingly controlled by combinations of the form  $(\mathcal{E} L^2 / c_*^2)^2$  with  $L$  the packet overlap scale, which is already extremely small even in neutron-star cores and does not represent a violation of the exclusion algebra (see Appendix AW for the explicit comparison with laboratory and astrophysical bounds).

*What this implies for astrophysical fermionic matter.* In particular, the present no-go statement removes ordinary strong-gravity neutron-star interiors from the list of plausible ECT-specific Pauli-violation windows: inside ordinary white-dwarf and neutron-star interiors, and more generally throughout smooth coherent-branch regions where the local fermionic EFT remains valid and  $\mathcal{K}(x)$  remains nondegenerate,

the exclusion algebra is preserved. Any ECT signature of nonstandard fermionic statistics should therefore be sought not in ordinary compact-object interiors, but in the three exceptional settings enumerated above.

*Conditional on the fermionic reconstruction programme.* At the present stage, the no-go statement is therefore conditional not on the canonical-normalisation argument itself, which is technically complete within the local first-order EFT closure described above, but on the completion of the fermionic reconstruction from the exchange-topological and representation-theoretic sector (§24.4, §24.5) to the full operator-level canonical anticommutation structure (OP-Q11, OP-Q21).

### What is and is not claimed

The present subsection therefore establishes the topological and representation-theoretic skeleton of the bosonic/fermionic split, but not yet its full operator-algebraic completion. ECT at the present stage does *not* yet derive:

- (i) the full relativistic spin-statistics theorem;
- (ii) the full operator anticommutation algebra  $\{\hat{a}_i, \hat{a}_j^\dagger\} = \delta_{ij}$ ;
- (iii) an explicit emergent many-excitation sector decomposition with variable excitation number from condensate dynamics (ECT does not require Fock space as a fundamental postulate, but the effective reconstruction remains open; OP-Q11).

What it does provide is a structurally natural route from coherent exchange sectors to the bosonic/fermionic dichotomy.

**Connection to downstream programmes.** The exchange-sector dichotomy established here feeds directly into three downstream constructions. First, it constrains the physical reading of the fermionic sector in Part I (§9.9). Second, it provides the exchange-side input for the representation-theoretic route to Dirac structure in the next subsection (§24.5). Third, it supplies the identical-particle background for the entanglement programme (§31), where non-factorisable states of indistinguishable excitations depend on the same exchange structure.

**Discriminant: standard, anyonic, and ECT routes.** Three logically distinct routes should be separated. In standard relativistic QFT, the full spin-statistics theorem is proved within an already assumed Lorentzian operator framework. In effectively two-dimensional systems, braid topology allows anyonic exchange phases beyond the bosonic/fermionic dichotomy. In ECT, the primary result is different in kind: the ordered branch fixes  $d_{\text{spatial}} = 3$ , and this dimensionality already restricts the fundamental exchange topology to  $\mathbb{Z}_2$ . Thus ECT does not yet reproduce the full standard theorem, but it does explain why the primary branch should display a bosonic/fermionic split rather than an anyonic one.

**Falsifier for the exchange-sector programme.** The exchange-sector programme would be undermined if (i) the ordered branch failed to fix an effectively three-dimensional spatial sector, so that the  $\mathbb{Z}_2$  exchange topology no longer followed; (ii) fundamental particle exchange in the primary  $3 + 1$  branch showed stable anyonic phases; or (iii) the completed coherent-sector operator algebra turned out to be incompatible with the structural pairing between spinorial sectors and antisymmetric exchange. Any of these would force a substantial revision of the present spin-statistics route.

**Observed pattern.** The observed split of known  $3 + 1$ -dimensional particle physics into bosons and fermions is fully consistent with the exchange-sector structure identified here. At the same time, the existence of anyonic exchange in effectively two-dimensional condensed-matter systems confirms the contrasting part of the discriminant: once the dimensionality changes, the exchange topology changes as well. ECT therefore places the bosonic/fermionic dichotomy and the absence of fundamental anyons in the primary branch on the same structural footing.

**Status summary.** *Established (Level A):* (i) the primary ordered branch is effectively three-dimensional through the  $O(4) \rightarrow O(3)$  breaking pattern; (ii) for identical excitations in that branch,  $\pi_1(\mathcal{M}_2) = \mathbb{Z}_2$ ; (iii) the fundamental exchange topology therefore admits exactly two classes.

*Level B:* the ordered-branch representation content is structurally compatible with the standard bosonic/fermionic assignment: integer-spin tensorial sectors with symmetric exchange and spinorial sectors with antisymmetric exchange.

*Open (OP-Q11):* the full spin-statistics theorem, operator anticommutation algebra, and an explicit emergent many-excitation sector decomposition (Fock-like reconstruction) remain to be derived from condensate dynamics.

**Table 80:** Quantum statistics in ECT vs standard frameworks.

Aspect	Standard QM/QFT	ECT
Route to bosonic/fermionic split	Full spin-statistics theorem within an already assumed operator framework	Topological exchange dichotomy in $d = 3$ plus structural compatibility with ordered-branch representation content (Level B; not yet full PLZ)
Operator-algebra basis	Bosonic/fermionic operator algebra fixed within the standard quantised-field framework	Topological and representation-theoretic skeleton established; full operator-algebraic completion remains open
Pauli exclusion	Follows for fermions once the fermionic operator algebra / spin-statistics structure is imposed	Structural Level B consequence once the spinorial sector and spin-statistics route are combined; not yet a full operator-level theorem
Full PLZ theorem	Yes	Open
Beyond present closure	Standard many-body framework available	Full many-body fermionic construction remains open

## 24.5 Representation-theoretic route to Dirac structure

*Status: Level A for the chain  $O(4) \rightarrow O(3) \Rightarrow d_{\text{spatial}} = 3 \Rightarrow \text{Spin}(3) \Rightarrow \mathfrak{so}(1,3) \Rightarrow \text{Clifford structure}$ , once the standard generator continuation is applied at the algebraic level to the ordered branch. Level B (conditional) for the statement that, if the coherent sector contains physical spinorial excitations, then their minimal local linear Lorentz-covariant first-order dynamics is Dirac-type. Level B/open for the physical realisation of spinorial excitations, their masses, gauge couplings, and the full second-quantised operator completion. Connection: exchange topology and spinorial compatibility (§24.4), fermionic programme (§9.9), electroweak/chirality route (§7.4), fifth-force coupling (§7.6), and the entanglement programme (§31).*

The exchange-sector analysis of Section 24.4 established that the ECT broken phase naturally admits both bosonic and fermionic sectors. The present subsection shows that the symmetry structure of the broken condensate provides a natural representation-theoretic route to the Dirac structure.

**Full structural chain from the ordered branch to Dirac form.** The representation-theoretic route to Dirac structure should be read as the final part of a longer ordered-branch chain:

- (i) the  $O(4) \rightarrow O(3)$  transition fixes the ordered branch with three spatial directions;
- (ii) in that three-dimensional branch, the exchange topology of identical excitations is  $\pi_1(\mathcal{M}_2) = \mathbb{Z}_2$  (Section 24.4);

- (iii) the residual rotational sector admits the spinorial double cover  $\text{Spin}(3) \rightarrow \text{SO}(3)$ ;
- (iv) at the algebraic level, the ordered branch together with the standard generator continuation yields the Lorentz algebra  $\mathfrak{so}(1,3)$ ;
- (v) the spinor representation of that algebra forces the Clifford structure (24.10);
- (vi) within the minimal local linear first-order Lorentz-covariant closure, the corresponding spinorial dynamics is Dirac-type.

Steps (i)–(v) are structural consequences of the ordered-branch architecture; step (vi) is conditional on the physical realisation of spinorial excitations and on staying within the minimal first-order spinor closure.

### From $O(4) \rightarrow O(3)$ to the Lorentz algebra (Level A)

The Lie algebra  $\mathfrak{so}(4)$  has 6 generators  $J_{AB}$ . Under  $O(4) \rightarrow O(3)$  with the condensate direction  $n^A = \delta_4^A$ :

- **Unbroken** ( $O(3)$  subgroup):  $J_{ij}, i, j \in \{1, 2, 3\}$  — spatial rotation generators.
- **Broken** (coset  $O(4)/O(3)$ ):  $J_{i4}, i \in \{1, 2, 3\}$ .

At the algebraic level, one may perform the standard generator continuation that identifies the broken Euclidean generators with the Lorentzian boosts:

$$K_i \equiv -iJ_{i4}.$$

This representation-theoretic step is distinct from the real ordered-branch parametrisation  $t = w/c_*$  used in the hyperbolic field equations. A direct calculation then confirms that  $J_{ij}$  and  $K_i$  satisfy the Lorentz algebra  $\mathfrak{so}(1,3)$ , with  $[K_i, K_j] = -iJ_{ij}$ . Thus the Lorentz algebra emerges from the broken-phase structure and the standard generator continuation. (Level A: follows from the ordered-branch symmetry breaking together with the algebraic generator continuation.)

### Representation-theoretic route to Clifford structure (Level A)

The spinor representation of  $\mathfrak{so}(1,3)$  is  $(\frac{1}{2}, 0) \oplus (0, \frac{1}{2})$  (Dirac spinor). Within that representation, the Lorentz generators take the form  $J^{\mu\nu} = \frac{i}{4}[\gamma^\mu, \gamma^\nu]$ , which forces

$$\{\gamma^\mu, \gamma^\nu\} = 2g^{\mu\nu} \mathbf{1}_4, \quad (24.10)$$

where  $g^{\mu\nu}$  is the emergent Lorentzian metric from the broken condensate phase. The Clifford algebra (24.10) is therefore a representation-theoretic consequence of the broken-phase Lorentz structure, not an independent postulate. (Level A.)

### Conditional structural theorem: unique first-order covariant dynamics

For a spinorial field in the  $(\frac{1}{2}, 0) \oplus (0, \frac{1}{2})$  representation, the most general local Lorentz-covariant first-order differential equation takes the form

$$(iS_0 \gamma^\mu \partial_\mu - m_\psi c_*) \psi = 0, \quad (24.11)$$

because, within the minimal local linear Lorentz-covariant first-order spinor closure,  $i\gamma^\mu \partial_\mu$  is the unique operator compatible with (24.10). This is a conditional statement:

**Conditional structural theorem.** *If the coherent sector of ECT contains physical spinorial excitations realising the  $(\frac{1}{2}, 0) \oplus (0, \frac{1}{2})$  representation of the emergent Lorentz group, then, within the minimal local linear Lorentz-covariant first-order closure, their free massive dynamics is uniquely Dirac-type (24.11).*



**Relation to the Part I Dirac equation.** In Part I (§9.2), the Dirac equation is written in the post-identification form with the observed  $\hbar$ . The present equation (24.11) uses the pre-identification coherent action scale  $S_0$ . The two forms are consistent: Part I presents the phenomenologically matched equation, whereas the present subsection gives the structural route that leads to that normalisation before the final  $S_0 = \hbar$  identification is imposed.

**What this theorem does and does not establish.** *It does establish:* the representation-theoretic uniqueness of the Dirac operator, given the Lorentz algebra and the spinor representation. *It does not establish:* that spinorial excitations actually exist in the ECT spectrum; their mass generation or gauge couplings; the complete quantisation of the Dirac field from bare P3.

**Medium reading (P5).** Postulate P5 does not by itself derive the Dirac operator. Its role here is interpretive. It says that, if spinorial excitations are realised, they are not abstract fields on a pre-given background but physical excitations of one common ordered medium. Accordingly, the Clifford and Dirac structures are read in ECT not as fundamental ingredients of spacetime, but as representation-theoretic organisations of coherent medium excitations on the ordered branch.

**Discriminant: emergent versus fundamental Dirac structure.** In standard relativistic quantum field theory, the Dirac equation is introduced on an already assumed Lorentzian spacetime and then used as the starting point for the fermionic sector. In ECT the logical direction is reversed: the ordered branch first produces the spatial dimensionality, exchange-sector dichotomy, Lorentz algebra, and Clifford structure, and only then yields the Dirac form as the minimal compatible spinorial dynamics. The distinctive ECT claim is therefore not that the physical fermion spectrum has already been derived, but that once spinorial excitations are present, their minimal first-order Lorentz-covariant free dynamics is structurally fixed rather than separately postulated.

**Connection to downstream programmes.** The Dirac route is not an endpoint. Once admitted, it provides the fermionic backbone for several later programmes: (i) the chirality route used in the electroweak embedding (§7.4); (ii) the neutrino-sector discussion in Part I (§9.9), where the Dirac/Majorana question is posed within the same spinorial framework; (iii) the ECT-specific fifth-force coupling  $\Delta\mathcal{L}_5 = \mu_5 \bar{\Psi} \gamma^A n_A \Psi$  (§7.6); and (iv) the spin-statistics and entanglement programmes (§24.4, §31), which use the same spinorial structure as part of their closure.

**Empirical anchor.** Observed charged leptons and quarks are described by Dirac-type relativistic spinor dynamics to very high precision. Neutrinos also belong to the same relativistic spinorial framework, even though the detailed Dirac-versus-Majorana completion remains open. ECT does not yet derive the fermion mass spectrum from condensate microdynamics, but it does provide the structural statement that if the ordered branch supports spinorial excitations, then the minimal local linear first-order Lorentz-covariant free equation available to them is of Dirac type. In this sense, the observed fermionic sector serves as an empirical anchor for the conditional theorem without turning it into a completed first-principles derivation of the full fermion spectrum.

**Falsifier for the Dirac-structure programme.** The Dirac-structure programme would fail if (i) the emergent Lorentz algebra of the ordered branch did not admit spinorial representations compatible with the induced metric; (ii) the Clifford structure required by that representation were inconsistent with the same metric; (iii) within the same minimal local linear first-order spinor closure, a non-Dirac Lorentz-covariant free dynamics were equally admissible; or (iv) the physical fermionic sector ultimately required a structure incompatible with the ordered-branch spinorial route. Any of these would force a substantial revision of the present representation-theoretic construction.

**Pauli exclusion.** Exchange topology gives bosonic and fermionic sectors at Level A (Section 24.4). The Dirac structure, once admitted, makes the standard spin-statistics route available: for a spin- $\frac{1}{2}$  field, the operator completion compatible with stability and the fermionic exchange sector requires anticommutation rather than commutation. Pauli exclusion is therefore a Level B structural consequence, conditional on the realised spinorial sector, the completed spin-statistics route, and the physical normalisation  $S_0 = \hbar$  (OP-Q2, OP-Q11).

**Status summary.** *Established (Level A):* (i) the ordered branch together with the standard generator continuation at the representation-theoretic level yields the Lorentz algebra  $\mathfrak{so}(1,3)$  at the representation-theoretic level; (ii) the spinorial representation of that algebra forces the Clifford structure (24.10); (iii) the longer structural chain from the ordered-branch dimensionality and exchange sector to Lorentz/spinor/Clifford kinematics is internal to ECT.

*Level B (conditional):* (i) if physical spinorial excitations are realised, then within the minimal local linear first-order closure their free massive dynamics is Dirac-type; (ii) Pauli exclusion follows once the spinorial sector and the spin-statistics route are combined, with the physical normalisation fixed by  $S_0 = \hbar$ .

*Open (OP-Q3, OP-Q11):* the physical spinorial spectrum, mass generation, gauge couplings, full second-quantised operator algebra, and the completed fermionic many-body construction.

**Bridge to the vacuum-response programme.** With Euclidean path-dependence, exchange sectors, and the structural route to Dirac dynamics in place, the coherent branch has acquired its basic nonclassical, statistical, and spinorial architecture. The next chapter turns from these kinematical and representation-level questions to the response of the ordered vacuum itself under boundaries, acceleration, time dependence, and strong-field interfaces.

## 25 Quantum Vacuum Structure and Universal Response of the Ordered Condensate

*Inputs: ordered coherent vacuum from P4+BR1; wave dynamics and action scale  $S_0$  from Sections 21–22; formal continuation (22.3); medium character (P5). Aim: to show that the ordered coherent vacuum responds nontrivially to boundaries, acceleration, time dependence, and strong-field interfaces, unifying Casimir, Unruh, particle-production, and horizon-thermality phenomena as manifestations of one underlying ordered-medium structure. Status: Level A for the structural nontriviality of the ordered vacuum, for boundary sensitivity, for observer-dependent mode decomposition, and for the background-dependent particle notion. Level A/B for the Euclidean-correlator reconstruction of the Unruh temperature. Level B (conditional) for specific coefficients (Casimir 3/2 ratio, Bogoliubov mixing form) within provisional closures. Open for the full quantitative vacuum-response programme from the completed coherent EFT. Connections: vacuum ontology (§25.1), unified-response logic (§25.2), action-scale universality (§5.6), UV-threshold programme (§8.3), analogue-laboratory programme (§37), and the downstream decoherence/Born/black-hole programmes.*

**Connection to PES.** PES (§29) identifies the vacuum as the lowest-lying persistent sector: the configuration with minimal Euclidean non-stationarity and maximal resistance to decoherence. The vacuum responses discussed below (Casimir, Unruh, particle production) correspond to perturbations of this persistent sector induced by boundaries, acceleration, or time-dependent backgrounds.

**What is established, what is conditional, and what remains open in the vacuum-response programme.** The ECT vacuum-response programme should be read in three layers. First, the theory already establishes at Level A that the ordered vacuum is physically nontrivial: it carries coherent correlators, admits boundary-sensitive mode structure, responds differently to boundaries, accelerated detectors, and time-dependent ordered backgrounds, and under P5 is read as a genuine physical medium rather

than an abstract ground state. Second, on top of that structural basis, ECT provides concrete routes to four families of phenomena: Casimir-type boundary response (§25.3), Unruh-type accelerated-vacuum response (§25.4), particle production in nonstationary ordered backgrounds (§25.5), and horizon thermal-ity in the strong-field sector (§36). These routes differ in quantitative closure status: some elements are Level A or A/B, while specific coefficients remain Level B conditional on provisional closures. Third, what remains open is the completed reduced coherent EFT needed for definitive force coefficients, detector-response kernels, and production rates in realistic geometries and backgrounds. Thus the vacuum-response programme is already structurally unified, but not yet uniformly quantitatively completed. The following subsection (§25.1) provides the ontological and stiffness-level basis for that unified response logic.

## 25.1 Quantum vacuum structure of the ordered condensate

*Status: Level A for the structural claim that the ordered condensate defines a physically nontrivial coherent vacuum sector. Level A/B for the unified-response reading in which Casimir response, accelerated-detector response, particle production, and horizon thermal-ity are treated as different probes of one and the same ordered vacuum. Level B/open for the quantitative closure that relates all vacuum stiffness scales and all concrete response amplitudes to one common microscopic parameter set. Connection:  $O(4) \rightarrow O(3)$  ordering (P4), medium character (P5), the two-branch architecture (§6), the action-scale universality (§5.6), the UV-threshold programme (§8.3), and the downstream vacuum-response programme (§25).*

The Quantum Sector of ECT does not describe particles placed on top of an otherwise empty vacuum. Its more basic claim is that the vacuum itself is a structured ordered medium. The coherent branch is therefore simultaneously a theory of phase-sensitive excitations and a theory of the physical vacuum.

### Vacuum as an ordered medium

Once the condensate enters the ordered phase, the background is no longer featureless. It possesses:

- (i) a nontrivial order parameter  $\Phi_{\text{eff}} = \rho e^{i\theta}$ ;
- (ii) a phase-sensitive coherent sector with winding structure;
- (iii) stiffness scales controlling deformations of the ordered state;
- (iv) topological sectors and loop actions weighted by  $S_0$ ;
- (v) nontrivial vacuum correlators of coherent observables.

Thus the ECT vacuum is already a dynamical object before one introduces particles or measurement.

**Medium character of the vacuum (P5).** Postulate P5 gives the ECT vacuum its ontological reading. The vacuum is not an abstract lowest-energy state defined on top of a pre-existing Lorentzian background; it is the ordered condensate itself, with physical correlators, stiffness, topological sectors, and response functions. P5 does not by itself derive the downstream vacuum-response phenomena, but it clarifies what kind of object they are probing: not a formal ground-state vector, but a genuine physical medium. Particles are therefore not entities placed *on* the vacuum; they are coherent excitations *of* it.

### Unified vacuum viewpoint

This is one of the central unifying features of ECT. What standard physics often treats as separate domains—quantum vacuum structure, wave dynamics, action quantisation, and part of gravitational stiffness—are, in ECT, different manifestations of one and the same ordered condensate background. The geometric branch probes its phase-insensitive response; the Quantum Sector probes its phase-sensitive and topological response.

This unified reading is consistent with the broader one-medium architecture established earlier in the article: one causal cone, one coherent action scale, one extremal backbone, and one common conservation structure (§11.1). The present subsection specialises that architecture to the vacuum sector: the same ordered medium that underlies excitations and geometry also underlies vacuum response.

### **Vacuum stiffness and Planck-scale interpretation**

The ordered condensate resists deformation. In the geometric branch this appears as gravitational stiffness (Section 13.4). In the coherent branch it appears as phase stiffness  $K_\theta^{\text{eff}}$ , loop action cost  $S_0$ , and the nontrivial energetic structure of the ordered vacuum. A full first-principles derivation relating all these stiffness notions to one common microscopic set of condensate parameters remains open, but the structural unity is already clear from the two-branch architecture.

**Three scales of one ordered vacuum.** The stiffness of the ordered condensate manifests itself at several physically distinct scales already identified elsewhere in the theory (§5.1). At the primary scale, the condensate is tied to the Planck-scale stiffness that governs the quantum-gravitational and coherent-vacuum backbone. At the secondary electroweak-like scale, the same medium admits a distinct closure associated with the Higgs/electroweak sector. At large galactic scales, the ordered background supports the long-range coherence relevant for the dark-sector programme. ECT does not yet reduce these three manifestations to a fully completed single microscopic derivation, but it interprets them as different stiffness expressions of one and the same ordered vacuum rather than as three unrelated sectors. The detailed vacuum-response programme developed below is currently formulated most explicitly for the primary coherent-vacuum sector.

**Connection to the vacuum-response programme.** The nontrivial vacuum structure established here is the common foundation for four families of downstream phenomena: (i) boundary sensitivity and Casimir-type response (§25.3), (ii) accelerated-detector and Unruh-type response (§25.4), (iii) particle production in time-dependent ordered backgrounds (§25.5), and (iv) horizon thermality in the strong-field sector (§36). The unified-response logic connecting these phenomena is developed later in §25.2; the present subsection provides its vacuum-ontological basis.

**Empirical anchor.** The empirical motivation for treating the vacuum as physically nontrivial is well known: Casimir forces between boundaries [174, 175], vacuum-sensitive atomic effects such as the Lamb shift, and spontaneous emission all indicate that the vacuum is not physically empty. ECT does not yet derive the observed magnitudes of all such effects from first-principles condensate microdynamics. What it provides here is the structural claim that a nontrivial ordered medium is the natural substrate from which such vacuum-sensitive phenomena can arise. Their quantitative closure belongs to the downstream vacuum-response programme.

**Discriminant: ordered-medium vacuum versus ground-state vacuum.** In standard quantum field theory, the vacuum is introduced as the lowest-energy state of quantised fields on a Lorentzian spacetime that is already assumed. In ECT the logical order is reversed. The ordered condensate is primary, and the familiar ground-state language arises only as the effective coherent-branch reading of that medium. Thus the standard-QFT vacuum is not denied; it is reinterpreted as an effective description of a deeper ordered substrate. The distinctive ECT claim is that the physical nontriviality of the vacuum is not an added quantum postulate but a direct consequence of the existence of the ordered medium itself.

**Falsifier for the vacuum-structure programme.** The vacuum-structure programme would be weakened if the ordered condensate failed to support nontrivial boundary-sensitive or background-sensitive correlators, so that the downstream Casimir, Unruh, particle-production, and horizon-response sectors

could not be structurally grounded in one common vacuum substrate. It would be more seriously challenged if the geometric and coherent branches could not be maintained as compatible readings of one ordered medium, or if the completed response programme required mutually incompatible microscopic vacuum structures in different subsectors. No such inconsistency is currently known within the present coherent programme.

**Status summary.** *Established (Level A):* the ordered condensate defines a physically nontrivial coherent vacuum sector with order parameter, phase-sensitive correlators, winding structure, and nontrivial stiffness.

*Level A/B:* the same ordered vacuum provides the unified substrate for the later Casimir, Unruh-type, particle-production, and horizon-thermality programmes.

*Level B/open:* the quantitative closure relating all vacuum stiffness scales and all specific vacuum-response amplitudes to one common microscopic parameter set remains incomplete.

## 25.2 Unified response logic and analogue-gravity continuity

*Status: Level A/B for the unified-response route in which boundary response, accelerated-detector response, particle production, and horizon thermality are treated as probes of one ordered coherent vacuum. Level B for the analogue-gravity continuity argument. Level B/open for a single completed microscopic kernel derivation that would reproduce all four response families quantitatively from one common ordered-vacuum EFT. Connection: the vacuum ontology of Section 25.1, the action-scale universality (§5.6), the UV-threshold programme (§8.3), the decoherence programme (§26), and the analogue-laboratory programme (§37).*

### Unified response logic of the ordered vacuum

The ordered-vacuum effects discussed in the preceding subsections should not be read as a collection of unrelated phenomena. From the ECT viewpoint, Casimir response, particle production in time-dependent backgrounds, Unruh-type detector response, and Hawking-like horizon thermality are different manifestations of one underlying structure: the coherent vacuum of the ordered condensate responds nontrivially to boundaries, acceleration, time dependence, and strong-field causal interfaces.

The logic can be organised as follows:

- (i) **Boundary sensitivity:** boundaries reshape the coherent vacuum mode spectrum, producing Casimir-type effects (Section 25.3).
- (ii) **Time-dependent background sensitivity:** nonadiabatic variation of the ordered background leads to Bogoliubov-type mode mixing and particle-production effects (Section 25.5).
- (iii) **Observer sensitivity:** accelerated detectors probe the coherent vacuum differently from inertial ones, giving rise to Unruh-type response (Section 25.4).
- (iv) **Horizon/interface sensitivity:** strong-field causal interfaces generate reduced-state thermality in black-hole settings (Section 36).

In all four cases the vacuum is not trivially empty: it is an ordered coherent medium whose fluctuation structure depends on how it is probed.

**What is established, what is proposed, what remains open.** What is already established is the architectural claim that the same ordered coherent vacuum can be probed through four distinct channels: boundaries, time dependence, accelerated observers, and causal interfaces. What is proposed here is that these channels should be read as one unified response family rather than as unrelated effects. What remains open is the completed microscopic derivation in which one and the same ordered-vacuum correlator infrastructure quantitatively reproduces all four sectors at once.

**Why this matters.** This unified viewpoint prevents the Quantum Sector from fragmenting into separate phenomenological anecdotes. It is the vacuum-response analogue of the four structural universalities established earlier in the article: one medium, one coherent action scale, one extremal backbone, and one common conservation architecture. Here the same philosophy is applied specifically to vacuum response: one ordered vacuum, several observational channels.

**Connection to the vacuum ontology of Section 25.1.** Section 25.1 established that the coherent vacuum is a physically nontrivial ordered medium. The present subsection goes one step further: it organises the principal observable consequences of that statement. The common object behind all four response channels is the same ordered-vacuum correlator structure. Boundaries reshape it, acceleration reweights it, time dependence mixes its modes, and horizons split it into reduced thermal sectors.

**Connection to decoherence and influence-function kernels.** The unified-response logic is structurally parallel to the decoherence programme. In both cases, the central object is not a formal particle ontology but the correlator structure of the ordered medium. The same vacuum kernel that underlies Casimir, Unruh, and particle-production response also enters reduced-state and decoherence analyses once environmental modes are traced over (§26). This is one of the strongest cross-links in Part III: vacuum response and decoherence are not separate programmes but two readings of the same ordered-medium correlator infrastructure.

**Discriminant: unified ordered-vacuum response versus separate mechanisms.** In standard presentations, Casimir forces, Unruh response, cosmological particle production, and Hawking thermality are often developed as conceptually separate effects tied to different calculational setups. ECT instead proposes that they are four observational windows into one common ordered-vacuum response structure. The claim is not yet that one completed microscopic computation has already reproduced all four sectors quantitatively, but that the one-medium architecture makes such a unification natural rather than accidental.

### **Analogue-gravity continuity of the QS vacuum picture**

ECT does not introduce this vacuum-response logic in isolation. There is a strong continuity with the analogue-gravity lesson: effective horizons, mode conversion, and thermal detector response can arise in emergent media without requiring spacetime geometry itself to be fundamental. This does not prove ECT, but it removes a common conceptual objection: vacuum thermality and horizon response do not by themselves force a fundamental-spacetime ontology.

This does not mean ECT is merely an analogue model. The point is more precise: ECT uses the analogue-gravity lesson as evidence that horizon thermality and vacuum response need not be interpreted as proofs of a fundamental microscopic spacetime ontology. They can instead emerge from the response structure of an ordered medium—exactly as the coherent branch provides.

**Interpretive consequence.** This continuity strengthens the ECT reading of Hawking-, Unruh-, Casimir-, and particle-production phenomena as members of one emergent-vacuum family. It does not yet uniquely derive all four effects from one completed microscopic kernel, but it makes that unification structurally plausible and conceptually economical.

**Empirical anchors.** Each of the four response channels already has a strong observational or experimental anchor: Casimir response in precision boundary-force experiments, Unruh-type logic in accelerated-detector analyses and analogue platforms, particle-production mechanisms in time-dependent quantum backgrounds, and Hawking-type horizon thermality in black-hole and analogue-horizon settings. ECT does not yet claim one completed quantitative derivation for all four at once. Its present claim is architectural: that these phenomena belong to one response family of the same ordered vacuum.

**Falsifier for the unified-response programme.** The unified-response programme would be weakened if the completed coherent-vacuum theory required mutually incompatible microscopic kernels for Casimir, Unruh, particle-production, and horizon-thermal response. It would be more seriously challenged if one or more of these sectors turned out to require a fundamentally different vacuum ontology from the others, or if analogue-gravity continuity proved structurally misleading rather than supportive. No such incompatibility is currently known, but a full one-kernel closure remains open.

**Status summary.** *Established (Level A/B):* the coherent vacuum admits a unified-response reading in which boundary effects, accelerated-detector response, time-dependent particle production, and horizon thermality are treated as different probes of one ordered medium.

*Level B:* analogue-gravity continuity strengthens this interpretation by showing that horizon- and detector-type thermality can arise in emergent media without a fundamental spacetime substrate.

*Open:* the completed one-kernel microscopic derivation that quantitatively reproduces all four response families from one common coherent-vacuum EFT.

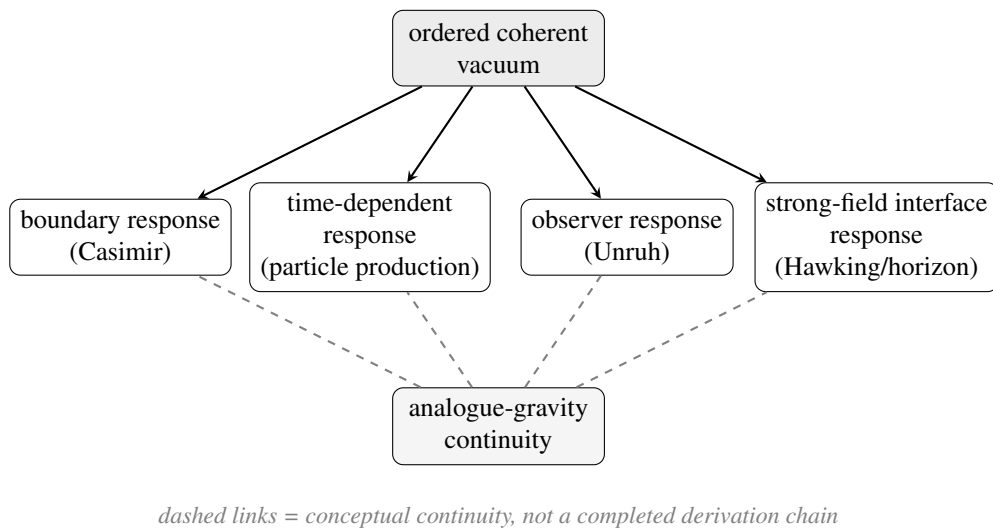


**Figure 32:** Unified response logic of the ordered coherent vacuum in the Quantum Sector of ECT (Level A/B). Boundary conditions, time-dependent backgrounds, accelerated observers, and strong-field causal interfaces probe one and the same ordered vacuum through four parallel response channels. The dashed analogue-gravity links indicate conceptual continuity, not a completed derivation chain between the effects themselves. This is a structural unification map, not yet a completed quantitative one-kernel derivation. See Appendix AX for the detailed structural discussion.

For a more extended structural discussion of the unified vacuum-response logic and its analogue-gravity continuity, see Appendix AX.

### 25.3 Boundary sensitivity of the ordered vacuum and the Casimir effect

*Status:* Level A for the structural claim that a nontrivial ordered coherent vacuum must be boundary-sensitive. Level B (conditional) for the explicit coefficient (25.3) in the idealised condensate-reflecting Dirichlet setup of the provisional soft-orientation EFT. Open (OP-Q12, OP-Q18) for the full quantitative Casimir derivation from the completed coherent EFT in realistic geometries and for the identification of laboratory systems that implement genuine condensate-reflecting boundary conditions. Connection: vacuum ontology (§25.1), unified-response logic (§25.2), medium character (P5), Goldstone counting from  $O(4) \rightarrow O(3)$ , analogue-laboratory programme (§37), and Appendix I.

A nontrivial ordered vacuum should respond to boundaries. This is the essential conceptual content of the Casimir effect in ECT: placing boundaries modifies the allowed coherent fluctuation spectrum of the ordered condensate and therefore changes the vacuum energy.

## Why a Casimir-type effect is expected

If the ordered vacuum supports coherent fluctuation modes, then imposing boundary conditions changes the allowed mode spectrum. Schematically,

$$E_{\text{vac}}^{(\text{boundary})} \neq E_{\text{vac}}^{(\text{free})}. \quad (25.1)$$

The resulting energy difference induces an observable force between boundaries. This is not an extra hypothesis; it is the generic consequence of having a nontrivial ordered vacuum with mode structure.

## ECT interpretation

In ordinary QFT the Casimir force is often phrased as a consequence of zero-point mode subtraction. In ECT the interpretation is more direct: the effect reflects the response of the ordered coherent vacuum to a change in admissible boundary-compatible fluctuation sectors. The language of “zero-point” energy is replaced by the language of boundary-constrained coherent vacuum stiffness.

**Medium reading of boundary sensitivity (P5).** Under the medium interpretation (P5), the Casimir effect in ECT is read not as an abstract subtraction of zero-point energies but as the response of a genuine ordered medium to imposed boundary constraints. The condensate between boundaries is physically different from the unbounded condensate: its admissible fluctuation spectrum is modified, and the resulting stiffness difference can generate a measurable force. This medium-level reading is conceptually continuous with superfluid and analogue-vacuum Casimir phenomena, though it does not by itself prove the quantitative ECT coefficient in any given laboratory setup.

## Status and future derivation

ECT supports the *structural existence* of a Casimir-type phenomenon. What is not yet completed is the explicit calculation of the force coefficient for realistic geometries from the final reduced coherent action (OP-Q12).

**Status summary.** *Established (Level A):* a nontrivial ordered coherent vacuum with mode structure must respond to imposed boundaries, and the resulting energy difference can produce a Casimir-type force.

*Level B (conditional):* within the provisional minimal soft-orientation EFT and for idealised condensate-reflecting Dirichlet boundaries, the explicit coefficient (25.3) is obtained.

*Open (OP-Q12, OP-Q18):* the completed coherent-vacuum derivation in realistic geometries and the identification of physical systems that actually realise the required condensate-reflecting boundary conditions.

### 25.3.1 Conditional toy estimate: explicit formula for condensate-reflecting boundaries

**Scope and applicability (read before the formula).** The calculation below is a *conditional prediction*: it applies only to boundaries that effectively impose Dirichlet conditions on the ECT Goldstone sector. Standard metallic laboratory plates do *not* implement these boundary conditions—the  $O(4) \rightarrow O(3)$  Goldstone bosons carry no electric charge and couple to ordinary matter only gravitationally ( $\sim \phi_0^{-2}$ ), so conducting plates are transparent to them. The factor  $3/2$  derived below is therefore *not* a prediction for the standard laboratory Casimir effect between metal plates. It is a prediction for boundaries that physically reflect the gapless condensate sector, such as superfluid interfaces, BEC domain walls, or  $O(4) \rightarrow O(3)$  phase-transition surfaces in the early Universe. Whether any accessible laboratory system implements such boundary conditions is an open problem (OP-Q18, Section 38.1).



### 25.3.2 Derivation for condensate-reflecting boundaries

**Boundary condition assumption.** The derivation below applies exclusively to the idealised case of condensate-reflecting boundaries that impose Dirichlet conditions on the ECT Goldstone sector. Standard metallic plates do not implement these conditions. The factor  $3/2$  is therefore a *conditional* prediction, not a statement about the ordinary laboratory Casimir effect.

For reference, the standard QED result for two photon polarisations between parallel plates separated by  $a$  is

$$\left. \frac{F}{A} \right|_{\text{QED}} = -\frac{\pi^2}{120} \frac{\hbar c}{a^4}. \quad (25.2)$$

For boundaries that reflect the minimal ECT soft-orientation sector, within a provisional minimal multi-component soft-orientation EFT, the three components with Dirichlet boundary conditions contribute independently (Level B, minimal EFT; see Appendix I):

$$\boxed{\left. \frac{F}{A} \right|_{\text{ECT}} = -\frac{3\pi^2}{240} \frac{\hbar c_*}{a^4} = -\frac{\pi^2}{80} \frac{\hbar c}{a^4}}, \quad (25.3)$$

which is  $3/2$  of the QED result. This follows from zeta-function regularisation [176] of three scalar field components of the minimal soft-orientation EFT:

$$E_0^{\text{ren}}(a) = -3 \times \frac{\pi^2}{720} \frac{\hbar c_* A}{a^3} \implies \frac{F}{A} = -\frac{\partial E_0^{\text{ren}}}{\partial a} \bigg/ A. \quad (25.4)$$

For ideal condensate-domain walls (e.g. near the  $O(4) \rightarrow O(3)$  transition in the early Universe), Dirichlet conditions on the Goldstone modes are natural and the conditional estimate is self-consistent within the assumed EFT.

**Why a  $3/2$ -type factor appears in the provisional closure.** Within the provisional multi-component soft-orientation EFT with idealised condensate-reflecting Dirichlet boundaries, one obtains a counting ratio  $N_G/N_{\text{QED}} = 3/2$ , where the naive Goldstone-coordinate count is compared with the two photon polarisations of the standard QED Casimir problem. This fixes the coefficient algebraically inside that provisional closure. It does not establish that the completed physical low-energy soft sector of ECT generically contributes with the same multiplicity in real boundary systems.

**Soft-mode counting caveat.** The breaking pattern  $O(4)/O(3) \simeq S^3$  naively carries three Goldstone coordinates. However, in the scalar-only integrable basis these do not automatically correspond to three independent propagating soft particles: the physically independent low-energy soft content is reduced to a single surviving longitudinal mode  $\chi$  ( $N_G^{\text{phys}} = 1$  at linear order; Section 4.3, Appendix I). Therefore any quantitative use of a three-component soft counting—including the factor  $3/2$  derived above—is provisional and boundary-model-dependent until the physically independent low-energy soft content is fully fixed in the completed coherent-vacuum EFT. This caveat applies equally to any use of the three-component count in the dark-sector (§18.1) and particle-spectrum sections.

**Numerical comparison at  $a = 1 \mu\text{m}$ .** For a plate separation  $a = 1 \mu\text{m}$ , the standard QED Casimir pressure is

$$\left. \frac{F}{A} \right|_{\text{QED}} \approx 1.30 \times 10^{-3} \text{ Pa},$$

whereas the conditional condensate-reflecting estimate gives

$$\left. \frac{F}{A} \right|_{\text{ECT}} \approx 1.95 \times 10^{-3} \text{ Pa}.$$

Within the provisional three-component closure, the toy estimate yields a  $3/2$  enhancement relative to the standard QED value. A difference of this order would be measurable only in a boundary system that is independently shown to realise the required condensate-reflecting conditions for the physically relevant soft ordered-branch sector. No such laboratory implementation is established in the present work.

**Summary statement and status caveat.** The factor  $3/2$  derived above is *not* a correction to the standard electromagnetic Casimir experiment between metallic plates; it is a *conditional toy estimate* within a provisional multi-component orientation EFT for boundaries that physically couple to the ECT Goldstone sector. This estimate is not part of the strict current core of ECT: it depends on a non-final closure of the soft-orientation sector and must not be interpreted as a current robust ECT prediction for any laboratory setup. Existing metallic-plate Casimir data neither confirm nor rule out this prediction; purpose-designed condensate-reflecting boundaries are required to test it (OP-Q18).

**Discriminant: laboratory QED Casimir versus ECT condensate Casimir.** Three cases must be kept sharply distinct.

- (i) **Standard metallic-plate Casimir experiments:** these test the electromagnetic QED vacuum and do not by themselves test the ECT Goldstone-sector prediction, because metallic plates are not known to impose condensate-reflecting boundary conditions on the soft ordered-branch sector.
- (ii) **Condensate-reflecting boundaries:** only in this idealised case does the provisional  $3/2$  ratio arise in the minimal three-component soft-orientation EFT. The provisional  $3/2$  factor reflects the naive three-coordinate Goldstone counting of the minimal toy closure, not yet the fully established count of physically independent soft asymptotic modes. In the present article this should therefore be read as a closure-dependent condensate-sector estimate, not yet as a fully closure-independent theorem of the completed vacuum programme. This is therefore a conditional ECT prediction, not a reinterpretation of the existing metallic-plate literature.
- (iii) **Intermediate analogue systems:** superfluid, BEC, domain-wall, or phase-boundary systems may probe the same boundary-sensitivity logic without reproducing the exact idealised Dirichlet setup assumed in the toy estimate. These are the most promising near-term experimental channels for testing the ECT vacuum-response programme.

The key test is therefore not whether ECT reproduces the standard QED Casimir coefficient, but whether a condensate-sensitive boundary setup reveals a distinct ordered-vacuum response beyond the purely electromagnetic one.

**Empirical anchor.** The standard electromagnetic Casimir force has been measured with high precision in metallic and related laboratory setups [174, 175]. These experiments do *not* directly test the condensate-sector prediction (25.3), because metallic plates do not implement boundary conditions known to reflect the ECT Goldstone modes. Their importance for the present subsection is more limited but still useful: they establish beyond doubt that vacuum response to boundaries is a real physical phenomenon, which is precisely the structural starting point ECT reinterprets in ordered-medium language.

**Falsifier for the boundary-sensitivity programme.** The boundary-sensitivity programme would be weakened if the ordered coherent vacuum failed to support boundary-sensitive mode structure at all, contradicting the Level A structural claim. Its conditional condensate-sector estimate would be challenged if the completed coherent EFT changed the Goldstone-sector counting or yielded a coefficient incompatible with (25.3) in the same idealised boundary setup. A stronger falsifier would be a purpose-designed condensate-reflecting boundary experiment that clearly contradicted the sign or magnitude expected from the conditional ECT closure. Standard metallic-plate Casimir experiments are not such a falsifier, because they probe the electromagnetic vacuum rather than the ECT Goldstone boundary sector.

**Connection to the analogue-laboratory and unified-response programmes.** Boundary sensitivity is the most direct and experimentally accessible entry point into the unified vacuum-response logic developed in Section 25.2. It is also the vacuum-response sector that lies closest to the analogue-laboratory programme of Section 37, where phonon, superfluid, and BEC systems provide the most natural candidate platforms for testing ordered-medium boundary response beyond the purely electromagnetic Casimir effect.

**ECT conceptual note.** The Casimir response discussed here is one boundary-sensitive reading of the same condensate two-point correlator structure  $N(\tau, \mathbf{x} - \mathbf{x}')$  that also enters the decoherence/influence-functional sector and the accelerated-observer vacuum response. In ECT these are not independent ingredients but different probing regimes of one common ordered-vacuum correlator infrastructure: boundary conditions in the Casimir case, detector trajectory in the Unruh case, and coarse-grained environmental tracing in the decoherence case.

## 25.4 Accelerated observers and the Unruh-type response

*Status: Level A for the structural claim that accelerated and inertial observers probe the ordered coherent vacuum through different mode decompositions. Level A/B for the Euclidean-correlator reconstruction of the Unruh-type temperature (25.8), which reproduces the standard result after the matched identifications  $S_0 = \hbar$  and  $c_* = c$ . Level B/open (OP-Q12) for the full detector-response derivation from the completed coherent EFT and for a fully quantitative treatment of realistic detector couplings. Connection: vacuum ontology (§25.1), unified-response logic (§25.2), medium character (P5), Euclidean  $O(4)$  symmetry (P2), Casimir boundary sensitivity (§25.3), strong-field horizon response (§36), and the analogue-laboratory programme (§37).*

If the ordered vacuum is genuinely physical, then observer-dependent mode decomposition should matter. An accelerated observer need not decompose the coherent vacuum into the same excitations as an inertial observer. This is the structural origin of an Unruh-type effect in ECT.

### Kinematic expectation

For uniform acceleration  $a$ , the standard QFT result gives

$$T_U = \frac{\hbar a}{2\pi c k_B}. \quad (25.5)$$

This formula uses the observed  $\hbar$ ; within ECT,  $\hbar$  is to be understood as  $S_0$  after the identification  $S_0 = \hbar$  (21.7) (Level B). The structural statement is that an accelerated detector coupled to the coherent branch should register a thermal-like response of the ordered vacuum.

**Medium reading of the Unruh response (P5).** Under the medium interpretation (P5), the Unruh effect is read as a response of a genuine ordered medium, not merely as a formal statement about observer-dependent quantisation. The vacuum correlators belong to the medium itself and are the same physical object for all observers. What changes between inertial and accelerated observers is not the existence of a different vacuum, but the way a given detector couples to and decomposes the same ordered-vacuum correlator structure. In this sense, the Unruh response is a probing effect of the medium, not an indication that acceleration literally creates a new fundamental vacuum.

### ECT status

The ordered-vacuum framework makes an Unruh-type effect natural and expected. What is not yet in place is the explicit detector-response calculation from the completed ECT coherent EFT (OP-Q12).

**Status summary.** *Established (Level A):* accelerated and inertial observers probe the ordered coherent vacuum through inequivalent mode decompositions; an accelerated detector need not see the inertial vacuum as empty.

*Level A/B:* the Euclidean-correlator reconstruction reproduces the standard Unruh-type temperature (25.8); after the matched identifications  $S_0 = \hbar$  and  $c_* = c$ , the standard result is recovered.

*Level B/open (OP-Q12):* the full detector-response derivation from the completed coherent EFT and the direct experimental detection of the Unruh effect itself.

**Observational status and empirical anchor.** At present there is no universally accepted direct laboratory detection of the Unruh effect itself. Accordingly, ECT should not claim observational confirmation here. Indirect discussions exist in the literature, for example in connection with electron depolarisation in storage rings [177], but such arguments are not generally regarded as a clean standalone detection of the Unruh effect. What ECT provides at the present stage is structural compatibility with the standard Unruh form once the coherent-vacuum route is adopted and the matched identifications  $S_0 = \hbar$  and  $c_* = c$  are imposed. This makes the Unruh block primarily an internal consistency test of the quantum-vacuum programme rather than a completed empirical success claim.

### 25.4.1 Conditional correlator-based reconstruction of the Unruh response

#### 25.4.2 Derivation

The derivation below is a conditional reconstruction using the standard Euclidean correlator of a massless scalar mode, taken as a proxy for the completed soft coherent sector. It shows structural compatibility and continuity with the standard result, not yet a full first-principles ECT derivation from the completed coherent EFT.

The Unruh effect [178, 179, 180] states that a uniformly accelerated observer detects the Minkowski vacuum as a thermal bath at  $T_U = \hbar a / (2\pi k_B c)$ . In ECT this structural reconstruction proceeds from the Euclidean correlator via analytic continuation.

The Euclidean two-point function for a massless Goldstone boson is [176]:

$$G_E(X, X') = \frac{1}{4\pi^2 |X - X'|^2}, \quad |X - X'|^2 = (x - x')^2 + (w - w')^2. \quad (25.6)$$

Under the formal Euclidean–Lorentzian continuation of the correlator, one obtains:

$$G_M^+(x, x') = -\frac{1}{4\pi^2 c_*^2} \cdot \frac{1}{(t - t' - i\varepsilon)^2 - |x - x'|^2 / c_*^2}, \quad (25.7)$$

the standard Wightman function, confirming consistency with the Osterwalder–Schrader theorem [72].

Along the Rindler trajectory with proper acceleration  $a$ ,  $G_M^+$  becomes periodic in imaginary proper time with period  $\beta_U = 2\pi c_* / a$  — a thermal distribution. The Unruh–DeWitt detector response gives a Planck spectrum with:

$$T_U = \frac{\hbar a}{2\pi c_* k_B}, \quad (25.8)$$

reducing to the standard result at  $c_* = c$ .

**ECT-specific signature:  $c_*$  versus  $c$ .** Equation (25.8) contains the emergent ordered-branch speed  $c_*$  rather than the observed light speed  $c$ . At the present level of empirical accuracy, the identification  $c_* = c$  is consistent with all available constraints, so the ECT Unruh temperature reduces to the standard form. If a future precision programme ever established a detectable difference between  $c_*$  and  $c$ , the Unruh temperature would in principle become a direct probe of the condensate-speed parameter. At present this remains a structural possibility rather than a practical near-term experimental discriminator.

For an LHC proton with  $a \simeq 10^{23} \text{ m s}^{-2}$ :  $T_U \approx 4 \times 10^{-8} \text{ K}$ .

This estimate is purely order-of-magnitude. It illustrates the tiny thermal scale associated with currently accessible accelerations and should not be confused with a realistic completed detector-response prediction for a specific accelerator environment.

### 25.4.3 Physical interpretation

In the ECT reading, the Unruh effect is not an additional postulate about accelerated observers. It is a structural consequence of the same  $O(4)$ -symmetric Euclidean coherent-vacuum correlator that underlies the whole vacuum-response programme. The Euclidean two-point function (25.6) is manifestly  $O(4)$ -invariant. Under the formal Euclidean–Lorentzian continuation of the correlator, that same object is accessed through different Lorentzian decompositions: inertial observers use the standard Minkowski mode split, whereas uniformly accelerated observers probe the same vacuum along Rindler trajectories. The thermal character of the response is therefore not a new dynamical heating of the vacuum, but a kinematic consequence of how the same ordered-medium correlator is sampled by the accelerated detector.

This reading is structurally continuous with the Casimir sector (Section 25.3), where boundaries reshape the vacuum mode content, and with the horizon-thermality sector (Section 36), where the near-horizon Rindler structure produces the analogous thermal response. It is also consistent with the decoherence programme (§26), though the present Unruh effect is not itself a decoherence calculation and should not be reduced to environmental tracing alone.

**Connection to the unified vacuum-response programme.** The Unruh response is the accelerated-observer branch of the unified vacuum-response logic developed in Section 25.2. The same ordered-vacuum correlator infrastructure that appears as boundary sensitivity in the Casimir sector, as mode mixing in the particle-production sector, and as horizon thermality in the black-hole sector, appears here as thermal response along a uniformly accelerated trajectory. The four phenomena differ by probing regime, not by vacuum ontology.

**Discriminant: emergent versus assumed Unruh response.** In standard Lorentzian quantum field theory, the Unruh effect is derived after one has already assumed the quantum vacuum and its Lorentzian analyticity properties. In ECT the logical direction is reversed: the Euclidean correlator of the ordered vacuum is primary, and the thermal Rindler response appears under the formal Euclidean–Lorentzian continuation of the correlator together with the observer-dependent mode decomposition. The mathematics is continuous with the standard result, but the ontological starting point is different. ECT does not begin with an abstract vacuum state on a given Lorentzian background; it begins with the ordered coherent medium whose Euclidean correlator structure later yields the same thermal response.

**Falsifier for the Unruh-response programme.** The Unruh-response programme would be weakened if the Euclidean ordered-vacuum correlator, under the formal Euclidean–Lorentzian continuation and Rindler-trajectory restriction, failed to reproduce the expected thermal periodicity or yielded a detector spectrum incompatible with Planckian response. It would be more strongly challenged if a future direct Unruh-type measurement established a temperature inconsistent with Eq. (25.8) after the matched identifications  $S_0 = \hbar$  and  $c_* = c$ . No such incompatibility is currently known.

## 25.5 Cosmological particle production and time-dependent ordered backgrounds

*Status: Level A for the structural claim that a time-dependent ordered background generically makes the notion of “particle” background-dependent. Level B for the Bogoliubov-type structural form of mode mixing (25.9) in the coherent vacuum. Open (OP-Q12, OP3) for quantitative production rates  $|\beta_k|^2$ , for the complete transition-history dependence, and for an ECT-native derivation of the primordial fluctuation spectrum. Connection: vacuum ontology (§25.1), unified-response logic (§25.2), medium character (P5), MP cosmology (§14.1), the ordering-transition programme (§25.5, §13.8), and the analogue-laboratory programme (§37).*

If the ordered condensate background changes in time, the notion of “particle” defined relative to one coherent vacuum slicing need not coincide with that defined relative to another. This is the natural setting for cosmological particle production in ECT, complementary to the macroscopic phase-transition discussion of Section 14.1.

**Physical picture: particle creation as vacuum reconfiguration.** In ECT, particle creation is not the mysterious “appearance of something from nothing”. When the condensate background changes—most dramatically at the  $O(4) \rightarrow O(3)$  transition—modes that were “quiet” in the symmetric phase cease to be quiet in the ordered phase. Their amplitude becomes nonzero relative to the new vacuum. This is entirely analogous to the physics of known media: rapidly cooling a superfluid produces phonons and rotons not because they “materialise from the void”, but because the background against which “silence” is defined has changed. The produced excitations are real condensate configurations; their number and spectrum depend on the history of the transition.

### Time-dependent ordered branch

In a nonstationary background, the effective coherent vacuum is itself time-dependent. Mode decomposition at early and late times therefore differs. Schematically, the early-time and late-time mode operators are related by a Bogoliubov transformation,

$$a_k^{(\text{out})} = \alpha_k a_k^{(\text{in})} + \beta_k a_{-k}^{(\text{in})\dagger}, \quad (25.9)$$

with  $|\beta_k|^2$  measuring the produced excitation density. This structural form is Level B: the actual  $\alpha_k, \beta_k$  coefficients require the completed time-dependent coherent-vacuum calculation.

### ECT interpretation

Particle production here is not “creation from nothing”. It is a reorganisation of excitation content relative to a changing ordered background. In that sense, cosmological particle production is another manifestation of the dynamical vacuum nature of the ECT condensate.

**Medium reading of particle production (P5).** Under the medium interpretation (P5), cosmological particle production is not the creation of particles from an abstract empty vacuum. It is the reorganisation of excitation content within a physical ordered medium whose background configuration changes in time. What standard curved-spacetime QFT describes as particle creation in a time-dependent geometry, ECT reads as mode redistribution in one and the same ordered condensate whose effective parameters evolve during or after the ordering transition.

**Empirical anchor.** Time-dependent particle production is not a speculative mechanism. Bogoliubov-type mode mixing is standard in nonstationary quantum-field settings, and closely related laboratory logic has been observed in the dynamical Casimir effect [181]. ECT does not yet claim a completed first-principles derivation of cosmological production rates from condensate dynamics. What it claims here is the structural compatibility of the coherent vacuum with the same nonstationary-production logic, now read in ordered-medium language.

### Relation to MP cosmology

Macroscopic Physics describes the large-scale evolution of the ordered branch (Section 14.1). The present QS subsection gives the coherent-vacuum interpretation of how such time dependence can populate excitation sectors. The two descriptions are complementary: MP governs the background history; QS governs excitation production against that history.

The most important application is the  $O(4) \rightarrow O(3)$  ordering transition itself (§25.5). During that transition, non-adiabatic evolution can generate Bogoliubov mixing for coherent-vacuum modes. The resulting coefficients are relevant in principle for (i) the primordial fluctuation spectrum, (ii) the initial excitation content of the ordered branch, and (iii) the ordering-transition gravitational-wave programme (§13.8). The formal Bogoliubov framework is established here; the quantitative completion belongs to the cosmological programme of Part II.

**Status summary.** *Established (Level A):* a time-dependent ordered background generically makes the notion of “particle” background-dependent, because early-time and late-time mode decompositions need not coincide.

*Level B:* Bogoliubov-type mode mixing (25.9) is structurally natural in the ECT coherent vacuum, and the corresponding mode equation (25.10) provides the formal route to particle production.

*Open (OP-Q12, OP3):* the quantitative production rates  $|\beta_k|^2$ , the completed transition-history dependence, and the ECT-native derivation of the primordial fluctuation spectrum.

**Discriminant: time-dependent ordered-medium production versus postulated vacuum particle creation.** In standard curved-spacetime QFT, cosmological particle production is derived once one has already assumed a quantum vacuum on a given time-dependent background. In ECT the ordered medium is primary, and the changing background is a change of the condensate state itself. The mathematics of Bogoliubov mixing is continuous with the standard treatment, but the ontological reading is reversed: the “vacuum” is not a passive background on which particles appear, but the physical medium whose nonstationary evolution reorganises its own excitation content.

**Falsifier for the particle-production programme.** The particle-production programme would be weakened if a completed coherent-vacuum analysis showed that time-dependent ordered backgrounds cannot be represented consistently by Bogoliubov-type mode mixing, or if the resulting excitation history proved incompatible with the ordering-transition cosmology developed in Part II. It would be more strongly challenged if the completed theory required a particle-production mechanism fundamentally unrelated to the ordered vacuum itself. No such incompatibility is currently known, but the quantitative closure remains open.

### 25.5.1 Unified vacuum predictions table

**Table 81:** Representative vacuum-response effects organised in ECT around the Euclidean condensate correlator  $G_E = (4\pi^2|X - X'|^2)^{-1}$ . The table is architectural rather than exhaustive: each row isolates one response channel and records its current status. Status notation: Level A = established structural consequence; Level A/B = structural route completed up to matched identifications; Level B = structurally motivated or conditional closure with incomplete quantitative derivation. The Casimir entry is conditional on idealised condensate-reflecting boundaries in the provisional soft-orientation EFT and is *not* a prediction for standard metallic-plate experiments.

Effect	ECT formula	ECT value	Std. result	Status
Casimir (minimal 3-comp. soft-orientation EFT, cond.-reflecting boundaries)	$-\frac{3\pi^2\hbar c_*}{240a^4}$	$3/2 \times (F/A)_{\text{QED}}$ <i>conditional</i>	$-\frac{\pi^2\hbar c}{120a^4}$	B (conditional)
Unruh temperature	$\frac{\hbar a}{2\pi c_* k_B}$	$4 \times 10^{-8}$ K at LHC	$\frac{\hbar a}{2\pi c k_B}$	A/B
Particle production in time-dependent background	$a_k^{(\text{out})} = \alpha_k a_k^{(\text{in})} + \beta_k a_{-k}^{(\text{in})\dagger}$	$ \beta_k ^2$ mode-dependent; rates open	Bogoliubov mixing	B

Effect	ECT formula	ECT value	Std. result	Status
Horizon thermality (near-horizon route)	$T_H \sim \frac{\hbar \kappa}{2\pi c_* k_B}$	Strong-field / near-horizon regime; full closure open	Standard Hawking temperature form	A/B

**Status note on the horizon-thermality row.** The horizon-thermality entry records the structural route by which the same coherent-vacuum correlator logic extends to strong-field causal interfaces. It should not be read as a completed black-hole evaporation theory. Its present status is Level A/B because the near-horizon thermal form is structurally recovered, while the full strong-field closure remains part of the downstream black-hole programme.

Parker [182] showed that time-varying spacetime geometry produces particle pairs from the vacuum. In ECT, the  $O(4) \rightarrow O(3)$  phase transition is a non-adiabatic event: the ordered Lorentzian branch becomes established on the Planck time scale  $\tau_{PT} \sim \ell_{Pl}/c$  (Level B; explicit transition dynamics, OP3).

The Goldstone mode  $\pi_k^i$  satisfies the mode equation [182, 176]:

$$\ddot{v}_k + \Omega_k^2(t) v_k = 0, \quad \Omega_k^2(t) = c_*^2(t) k^2 + m_{\text{eff}}^2(t), \quad (25.10)$$

where  $m_{\text{eff}}^2(t) = \lambda[\phi_0^2 - |\Phi(t)|^2]$  and  $\phi_0 = \sqrt{\mu^2/\lambda}$  is the equilibrium VEV.

**ECT-specific feature: time-dependent condensate speed.** Equation (25.10) allows the effective ordered-branch speed  $c_*(t)$  to enter as a time-dependent parameter. In standard particle-production treatments on a fixed Lorentzian background, the speed of light is constant and non-adiabaticity enters through the background geometry or effective masses alone. In ECT, by contrast, the ordered medium itself may carry additional time dependence during the transition through parameters that set  $c_*(t)$ . This introduces a structurally distinct possible source of mode mixing. Its quantitative importance remains open and belongs to the completed transition-history calculation.

The expected particle number per mode is  $\mathcal{N}_k = |\beta_k|^2$ , where  $\beta_k$  are Bogoliubov coefficients [176]. An ECT-native computation of  $n_s$  and  $r$  from the condensate fluctuation spectrum during the ordering transition remains open (OP3, §14.6).

**Discriminant with respect to standard vacuum programmes.** ECT differs from the standard presentation of vacuum phenomena in one central respect: Casimir response, Unruh response, particle production, decoherence, and horizon thermality are not treated as conceptually separate sectors, but as different probes of one and the same ordered coherent vacuum. This does not mean that all coefficients are already derived. It means that the theory proposes a single condensate correlator infrastructure behind boundary response, detector response, nonstationary production, and open-system decoherence. If this unified correlator logic fails, the vacuum-response programme fails as a whole rather than piecemeal.

**Falsifier for the coherent-vacuum response programme.** The present vacuum-response programme would be seriously weakened if the different sectors ultimately required mutually unrelated vacuum structures: for example, if Casimir-type boundary response required one underlying vacuum, Unruh response another, particle production a third, and decoherence kernels a fourth. It would also be weakened if a completed coherent EFT showed that no single ordered-vacuum correlator can jointly support boundary sensitivity, accelerated-detector response, nonstationary mode mixing, and the horizon thermality route. Conversely, every successful cross-link between these effects supports the one-vacuum reading of ECT.

**Empirical anchors already compatible with the programme.** Several empirical facts already fit naturally with the ECT vacuum programme, although none of them alone proves it: the success of standard QED Casimir measurements for electromagnetic boundaries, the observed dynamical Casimir effect in driven effective boundary systems [181], the standard consistency of Bogoliubov-type particle production in nonstationary backgrounds, and the broad analogue-gravity continuity between detector response,



horizon thermality, and effective-vacuum physics. In ECT these are read not as final confirmations, but as consistency anchors for the ordered-vacuum interpretation.

## 25.6 Summary and status of coherent-vacuum response

*Status: summary subsection for the coherent-vacuum programme of Chapter 25. Collects the Level A structural claims, the Level B conditional or closure-dependent results, and the open quantitative programmes. The chapter-level discriminant, falsifier, and empirical anchors are developed in Section 25.5.*

**Table 82:** Coherent-vacuum response map of ECT. Level A = strict structural consequence of the ordered phase. Level B = natural, closure-dependent, or structurally motivated consequence whose quantitative completion is incomplete. Open = not yet derived; OP-Q reference given.

Vacuum-sector statement	Status	Basis / comment
Ordered condensate vacuum is physically nontrivial	Level A	Section 25.1
Coherent vacuum supports nontrivial correlators	Level A	Phase-sensitive sector; Section 25.1
Medium character of the ordered vacuum (P5)	Level A	Vacuum read as a physical ordered medium rather than an abstract ground state; ontological backbone of the vacuum-response programme; Section 25.1
Casimir-type boundary response: structural existence	Level A	Ordered coherent vacuum with nontrivial mode structure must respond to imposed boundaries; Section 25.3
Casimir coefficient for condensate-reflecting boundaries	Level B (conditional)	Provisional soft-orientation EFT with ideal Dirichlet condensate-reflecting boundaries; Eq. (25.3)
Time-dependent ordered backgrounds: background-dependent particle notion	Level A	Early- and late-time mode decompositions need not coincide; Section 25.5
Bogoliubov-type mode mixing in the coherent vacuum	Level B	Eq. (25.9); explicit rates remain open; Section 25.5
ECT-specific time-dependent condensate speed $c_*(t)$	Level B	Structurally distinct possible source of mode mixing beyond the standard metric-only reading; quantitative importance open; Section 25.5
Quantitative production rates $ \beta_k ^2$	Open (OP-Q12)	Requires completed time-dependent coherent-vacuum calculation
Unruh-type response: structural observer dependence	Level A	Accelerated and inertial observers decompose the ordered vacuum differently; Section 25.4

(continued on next page)

Vacuum-sector statement	Status	Basis / comment
Unruh temperature from Euclidean-correlator reconstruction	Level A/B	Eq. (25.8); requires $S_0 = \hbar$ and $c_* = c$ ; Section 25.4
Unified vacuum-response logic (Casimir/production/Unruh/horizon)	Level A/B	Section 25.2; one coherent-vacuum response structure read through four probing regimes
Analogue-gravity continuity of the ECT vacuum interpretation	Level B	Section 25.2
Unified coherent-vacuum response map	Level B	Fig. 32; Section 25.2
Horizon thermality as a coherent-vacuum response channel	Level A/B	Near-horizon thermal form recovered from the same ordered-vacuum response logic; full strong-field closure remains open; Section 36
Phase-action-quantization structural chain	Level B	Sections 21.1–30.4; Fig. 31
Unified vacuum/coherent/geometry interpretation	Level B	Shared MP–QS condensate foundation

**Summary.** The coherent-vacuum programme of Chapter 25 now has a clear three-layer structure.

First, the ordered condensate defines a physically nontrivial vacuum sector with correlators, stiffness, boundary sensitivity, and background-dependent excitation structure (Level A).

Second, four families of vacuum response — boundary sensitivity (Casimir), accelerated-observer response (Unruh), time-dependent mode mixing (particle production), and horizon thermality — are read as different probing regimes of one common ordered-vacuum correlator infrastructure.

Third, the chapter has identified which parts of this architecture are already structural, which are conditional on specific closures, and which remain open quantitative programmes.

In this sense, Section 25.1 does not present four disconnected effects but one ordered-vacuum response map. That map then feeds directly into Section 26, where the same ordered vacuum reappears as the environment responsible for reduced dynamics, decoherence, and irreversibility of coherent subsystems.

## 26 Open Quantum Systems, Decoherence, and Irreversibility

*Inputs: coherent amplitude structure from Sections 21–23; retarded kernel from Appendix E; ordered vacuum from Section 25; medium character (P5). Aim: to show how environment-induced decoherence, effective irreversibility, and a thermodynamic arrow of time emerge from the coherent branch without external thermodynamic postulates, by treating the unresolved condensate as the environment within one ordered medium. Status: Level A for the retarded kernel (full nonlinear branch) and spectral positivity in the quadratic sector. Level A/B for the low-entropy initial branch reading. Level B for the influence-functional organisation, the effective ohmic/Markov closure, the entropy-production formula, the decoherence-timescale estimates, and the Crooks-type fluctuation relation. Structural unification: environmental and gravitational decoherence both arise from one condensate influence functional. Open for the exact microscopic environment split and a full non-Markovian second-law theorem. Connections: medium character (P5), the global/reduced unitarity distinction (§23.2), the unified vacuum-response infrastructure (§25.2), ECT basics (§3.8, §3.9), and the analogue-laboratory programme (§37).*

**Physical picture: decoherence as medium-driven branch selection.** In ECT, decoherence is not a postulate about observers destroying wave functions. It is a physical process: the subsystem loses its

coherent integrity because it couples to a large number of condensate degrees of freedom that it cannot track. The medium does not need to “measure” in any anthropomorphic sense; it suffices that the subsystem ceases to be well described as a nearly closed coherent configuration. Before decoherence the system belongs to the Euclidean coherent regime, where interference alternatives genuinely coexist as parts of a single configurational functional. After decoherence these alternatives no longer combine into a single observable amplitude pattern and begin to behave as separate classical branches. No separate collapse postulate is needed; its physical content is already covered by medium-induced branch selection.

**Recoherence: the reverse process.** If decoherence is the loss of coherent integrity through the environment, recoherence is the partial reassembly of that integrity. ECT makes the arrow of classicality not an absolute metaphysical dogma but a statistically governed consequence of environmental coupling. Recoherence is not forbidden in principle; it is exponentially suppressed for macroscopic systems:  $P_{\text{back}}/P_{\text{fwd}} = e^{-\Gamma_{\text{loop}}}$ . For mesoscopic or engineered systems, partial recovery of coherence becomes a physically meaningful possibility, consistent with echo-type and quantum-control protocols.

**What is established, what is closure-dependent, and what remains open in the decoherence programme.** The decoherence and arrow-of-time programme in ECT should be read in three layers. First, the theory already establishes a strict directional backbone: the ordered branch has a causal retarded structure, the quadratic spectral density is nonnegative, and the coherent sector is naturally distinguished from a maximally mixed configuration by the ordered-branch selection itself. Under the medium interpretation (P5), the “environment” is the unresolved sector of the same ordered condensate, and decoherence is an internal reorganisation of correlations rather than an interaction with an extrinsic reservoir. These ingredients make directed suppression structurally possible at Level A and a thermodynamic arrow derivable at the Level A/B interface once the low-entropy branch reading is admitted. Second, the programme becomes quantitatively explicit after the open-system reduction is adopted. At that stage the influence functional, the reduced entropy-growth law, concrete decoherence timescales for specific systems (§26.2), and a Crooks-type fluctuation relation (§26.4) become available. These results depend on the effective ohmic and Markov assumptions (Level B), but already show that environmental and gravitational decoherence arise as two specialisations of one condensate influence functional rather than as separate fundamental mechanisms. Third, what remains open is the completed microscopic nonlinear derivation of the full decoherence functional, the exact bath closure, the extension to the full non-Markovian path integral, and the final quantitative bridge from reduced-state decoherence to the observed Born-weight regime in realistic many-body settings.

**Connection to PES.** The decoherence functional  $\Gamma_{\text{loop}}$  developed in this section acquires a central interpretive role through the Principle of Euclidean Stationarity (§29):  $\Gamma_{\text{loop}}$  measures the Euclidean non-stationarity of a configuration, and PES selects those configurations that minimise it. The decoherence apparatus is therefore not merely a technical reduction tool but the quantitative backbone of the PES selection mechanism. This connection is developed further in Section 30.2, where the same  $\Gamma_{\text{loop}}$ -architecture is read as the mechanism of Euclidean-to-Lorentzian locking during measurement.

## 26.1 Influence functional, decoherence, and the arrow of time

*Status: layered. Level A for the causal retarded kernel in the full nonlinear ordered-branch dynamics (Appendix F) and for nonnegative spectral density in the quadratic sector. Level A/B for the low-entropy initial branch reading once the ordered-branch selection and the path-integral weight are admitted. Level B for the reduced influence-functional organisation, the effective ohmic/Markov closure, and the explicit entropy-production formula. Open for the exact microscopic environment split and for a full nonlinear entropy theorem beyond the present closure. Connection: ECT basics (Sections 3.8 and 3.9), medium character (P5), the global/reduced unitarity distinction (§23.2), the unified vacuum-response programme (§25.2), and Appendices H, E, and F.*

The previous subsections established the coherent branch as a phase-sensitive sector with a distinguished action scale, a Schrödinger-type reduction, and a natural canonical organisation. However, none of this yet explains why macroscopic coherent superpositions are not generically observed, why effective irreversibility appears, or why a preferred thermodynamic arrow of time emerges. These questions belong to decoherence. In ECT they must be addressed inside the coherent branch itself, rather than imported from an external quantum framework.

**Position within the full argument.** This subsection presents the open-system route to *effective* thermodynamic irreversibility in the ECT coherent branch. In the revised structure of the paper, the directional architecture (retarded propagation, dissipative orientation, and suppression of off-diagonal histories) is separated from the strict thermodynamic second law. The former is discussed in Section 3.8; the strict monotonicity relation derived here belongs to the Level B closure obtained under the effective ohmic/Markov assumptions.

**Relation to ECT basics.** Section 3.9 assembled the structural argument for the second law: the Level A directional backbone, the statistically exceptional initial sector, and the Level B ohmic/Markov closure. The present section provides the technical quantum-sector derivation behind that picture. In particular, it explains why the ordered coherent branch supports a low-entropy initial sector, how the influence functional produces entropy growth in the reduced description, and why macroscopic irreversibility coexists with quantum reversibility.

### Why decoherence belongs to the coherent branch

Decoherence in ECT is not a correction to the geometric branch. It is a process internal to the coherent sector: a smooth coherent subsystem interacts with the rest of the ordered condensate, whose unresolved modes act as an effective environment. The “system” is the low-dimensional coherent sector tracked explicitly; the “environment” is the large set of unresolved condensate modes that are integrated out. The system–environment split is not fundamental, but branch-dependent and scale-dependent.

**Discriminant with respect to standard decoherence and arrow-of-time programmes.** ECT differs from standard presentations in one central respect: irreversibility is not introduced as a primitive collapse postulate, nor attributed to a fundamentally non-unitary microscopic law. Instead, the programme is layered. At the structural level, the ordered branch already supplies a causal retarded backbone and a distinguished low-entropy coherent sector. At the reduced-state level, environment tracing yields decoherence and entropy production. At the macroscopic level, this produces effectively classical alternatives. Thus ECT does not start from “measurement” or “collapse” as basic. It starts from one ordered condensate, one coherent branch, and one open-system reduction logic. If that logic fails, the whole decoherence/arrow-of-time programme fails as a unified block.

**Medium reading of decoherence (P5).** Under the medium interpretation (P5), the system–environment split of the decoherence programme acquires a concrete physical meaning. The “environment” is not an abstract bath imported from outside the theory: it is the unresolved sector of the same ordered condensate that also contains the subsystem being tracked explicitly. Both subsystem and bath therefore belong to one physical medium. Decoherence is read as an internal reorganisation of correlations within the ordered condensate, not as an interaction between the coherent sector and an extrinsic reservoir. This is the ECT reading of why decoherence belongs to the coherent branch itself.

**Connection to the global/reduced unitarity distinction.** The present decoherence analysis is the concrete realisation of the global/reduced unitarity distinction established in Section 23.2. Global unitarity of the full coherent description is maintained. The appearance of irreversibility, entropy growth, and effectively classical alternatives arises only in the reduced subsystem description after unresolved

condensate modes are traced out. The decoherence programme therefore does not introduce fundamental information loss; it explains how effective information loss appears inside a globally unitary coherent framework.

**Connection to the unified vacuum-response infrastructure.** The decoherence bath is not unrelated to the vacuum-response programme of Section 25.1. It is built from the same ordered-vacuum correlator infrastructure that there appeared as boundary sensitivity, accelerated-observer response, time-dependent mode mixing, and strong-field interface response. What changes here is not the underlying medium, but the operational reading: in Section 25.1 the correlators were probed as vacuum response channels, whereas in the present section they reappear as the unresolved sector that drives reduced dynamics, decoherence, and effective irreversibility. In this sense, Section 26 continues the same vacuum architecture rather than introducing a new physical substrate.

### Influence-functional form of the effective description

After integrating out the unresolved bath modes, the reduced coherent sector is described by a reduced effective weight. Following the notation of ECT basics (Section 3.8), where  $q$  and  $q'$  label forward and backward coherent histories, the influence functional takes the schematic form

$$\mathcal{F}[q, q'] = \exp \left\{ \frac{i}{S_0} \Gamma[q, q'] - \frac{1}{S_0} \Gamma_{\text{irr}}[q, q'] \right\}, \quad (26.1)$$

where  $\Gamma[q, q']$  is the coherent-sector decoherence functional (already prepared in ECT basics; Section 3.8) and  $\Gamma_{\text{irr}}[q, q'] \geq 0$  is the irreversible suppression part. Consistency requires

$$\Gamma_{\text{irr}}[q, q] = 0,$$

so that no decoherence penalty is assigned on the diagonal. By contrast, the phase-sensitive part  $\Gamma[q, q']$  need not vanish on the diagonal and may remain nontrivial away from the diagonal as well. The normalisation by  $S_0$ —rather than a postulated  $\hbar$ —is required by internal consistency:  $S_0$  is the only available action scale at this stage.

**Status.** The existence of a reduced influence-functional description is Level B: it is the natural EFT organisation of the coherent branch once a subset of condensate modes is integrated out. What is structural is the system–environment logic itself; what remains open is the exact microscopic derivation of the full nonlinear decoherence functional  $\Gamma[q, q']$  for the complete coherent sector.

### Causal retarded kernel: the Level A result

A crucial ingredient of the arrow-of-time argument is already established at Level A in the quadratic broken-phase sector. The retarded Green kernel satisfies

$$K(\tau < 0) = 0. \quad (26.2)$$

This follows from the hyperbolic Lorentzian operator of the broken phase: both poles lie in the lower half-plane, so closing the contour above for  $\tau < 0$  gives zero (Appendix E). The coherent branch therefore inherits a genuinely causal retarded kernel from the same broken-phase structure that underlies macroscopic causality in the geometric branch.

**Physical meaning.** This is one of the structurally strongest points of the Quantum Sector. The arrow-of-time analysis does not begin with an arbitrary irreversibility rule. It begins with a kernel that is already causally retarded in the underlying broken-phase EFT. Irreversibility is therefore built on top of a causal ordered background, not inserted by hand.

**Beyond the quadratic sector.** The explicit Level A proof applies in the quadratic Lorentzian broken-phase sector. Beyond it, the same causal conclusion is strongly supported by the hyperbolic character of the Lorentzian ordered branch: once the effective equations are shown to form a symmetric hyperbolic system in the sense of Leray–Choquet–Bruhat [17, 18], retarded propagation of  $\Phi$  becomes a mathematical theorem for the full nonlinear branch. This explicit symmetric-hyperbolic reduction for the scalar dynamics of  $\Phi$  is now given in Appendix F. Retarded propagation of the ordered-branch scalar is therefore Level A for the full nonlinear branch, superseding the earlier quadratic-only restriction. In the open-system reduction, this retarded structure is encoded by a causal response kernel  $K(\tau < 0) = 0$ , which is established at Level A for the ordered Lorentzian branch. What remains open is the full first-principles identification of the effective bath-response kernel from Euclidean microdynamics (OP1, OP5).

### Low-entropy coherent initial sector

The second ingredient is the assumption that the initial coherent sector is highly ordered and therefore of low effective entropy. This is structurally motivated in ECT basics (P4+S6; Sections 3.8 and 3.9); the present subsection refines that argument inside the coherent-sector formalism. This should not be overstated. The claim is not that  $S_{\text{ent}}(w_0) = 0$  has been proved in the full quantum-mechanical sense. Rather: P4 selects an ordered vacuum branch and BR1 restricts attention to the coherent branch. Together with the non-tachyonic quadratic spectrum, this strongly motivates a highly ordered low-entropy initial coherent sector.

**Structure of the initial sector.** The key point is not that vanishing initial entropy has already been derived as a theorem from bare P3. Rather, the ordered condensate together with the coherent-branch restriction strongly motivates an initially low-entropy sector:

- (i) the ordered branch selects a non-generic vacuum structure;
- (ii) the coherent sector restricts attention to phase-correlated configurations rather than arbitrary mixtures;
- (iii) the quadratic fluctuation spectrum is non-tachyonic, so this sector is dynamically viable.

The natural QS starting point is therefore not a maximally disordered state but a highly ordered coherent one—exactly the initial condition needed for an emergent arrow of time.

### Path-integral weighting and the initial coherent sector

Once the quantum sector is formulated in terms of the coherent action scale  $S_0$ , the Euclidean path-integral weight

$$Z = \int \mathcal{D}\Phi e^{-S_E[\Phi]/S_0} \quad (26.3)$$

provides a natural weighting over admissible coherent histories without introducing an additional measure postulate. This does not yet amount to a complete theorem that the initial ordered branch is uniquely the minimum-entropy state in a fully microscopic sense. However, it strengthens the structural P4+S6 argument: the ordered coherent branch is naturally associated with a semiclassically distinguished low-entropy sector rather than with a generic highly mixed configuration.

**Status.** The existence of an ordered coherent sector is structural (Level A). Its interpretation as a low-entropy initial condition is Level B at the ECT-basics stage and can be strengthened toward Level A/B once the quantum-sector path-integral weighting is admitted. This is not yet a completed microscopic entropy theorem (OP-Q11).

### Positive spectral density and dissipative kernel

The third ingredient is positivity of the spectral density in the quadratic sector. As prepared in ECT basics and detailed in Appendix H, the relevant linear effective sector admits a nonnegative spectral density:

$$\rho(\mu^2) \geq 0. \quad (26.4)$$

This is Level A in the quadratic sector. It implies a nonnegative dissipative part of the retarded response kernel in the linearised effective description and is the input that makes monotonic entropy growth plausible once the coherent subsystem is coupled to an unresolved environment.

### Effective ohmic regime and Markov approximation

At this point one reaches the main Level B closure assumptions of the decoherence program. The scale analysis of Appendix H shows that the standard 3D Goldstone-like derivative coupling gives a super-ohmic spectral density,

$$J(\omega) \propto N_{\text{eff}} \omega^2 |g(\omega/c_*)|^2 \sim N_{\text{eff}} \omega^4 \quad (\text{standard 3D bath}), \quad (26.5)$$

not an ohmic one. The effective working formula therefore does *not* follow automatically from the standard broken-phase EFT but requires an additional step.

To proceed quantitatively, two effective working assumptions are introduced:

- (i) an effective ohmic regime,

$$J(\omega) \approx N_{\text{eff}} \gamma \omega, \quad (26.6)$$

which is read as a phenomenological reduction rather than a strict first-principles theorem;

- (ii) a Markovian regime in which the bath memory time is short compared to the decoherence time,

$$\tau_{\text{env}} \ll \tau_{\text{dec}}. \quad (26.7)$$

Both are Level B, justified as effective working hypotheses of the coherent-sector closure.

### Qualitative monotonicity of entropy

Given the three inputs:

- (i) a low-entropy coherent initial sector,
- (ii) a retarded causal kernel (26.2),
- (iii) nonnegative dissipative response (26.4),

the coherent branch admits a qualitative monotonicity statement for the entropy of macroscopic reduced sectors:

$$\frac{dS_{\text{ent}}}{dw} \geq 0 \quad (\text{qualitatively, for macroscopic reduced sectors; Level B}). \quad (26.8)$$

This is the central structural arrow-of-time statement of ECT. The qualitative direction of entropy growth is already supported at Level A by the directed-decoherence result (Appendix G):  $\Gamma_{\text{irr}} \geq 0$  ensures that off-diagonal histories are suppressed rather than amplified. What the ohmic/Markov closure adds is strict monotonicity and an explicit rate formula. The result is not yet the final microscopic theorem for the full nonlinear coherent branch, but it is an internally motivated result of the ordered condensate framework.

**Why this is enough.** This is already sufficient for the physical arrow of time. The second law in practice is not a statement about fundamental microscopic asymmetry of the bare action, but about the directed irreversible behaviour of suitable reduced macroscopic sectors.

**Status.** The causal-kernel ingredient is Level A in the quadratic broken-phase sector ((26.2) and (26.4)). The full monotonicity statement remains Level B: it depends on the effective reduced-state assumptions and on the bath closure.

### Working explicit entropy formula

If the effective ohmic and Markov assumptions (26.6)–(26.7) are accepted, the reduced entropy production takes the working form

$$\frac{dS_{\text{ent}}}{dw} = N_{\text{eff}} \gamma \left( \frac{dq}{dw} \right)^2 \geq 0 \quad (26.9)$$

This is not a first-principles theorem (Level B, effective ohmic/Markov closure). It is the current quantitative closure formula of the decoherence sector, explicitly marked Level B. Equation (26.9) is therefore not a universal first-principles law of all coherent-sector dynamics, but a Level B working formula under the effective ohmic/Markov closure assumptions. Its form is familiar from open-system theory [23]; its ECT-specific content is that  $S_0$  (not postulated  $\hbar$ ) controls the normalisation in (26.1), and that the bath is the unresolved condensate itself. Equation (26.9) is the quantitative version of the structural second-law statement assembled in Section 3.9: the basics section gives the conceptual three-ingredient logic; the present section gives the corresponding reduced open-system formula.

**Role of the explicit formula.** Equation (26.9) is not a universal entropy law. Its rôle is to give the more explicit closure-level version of the qualitative monotonicity statement (26.8): once the ohmic/Markov assumptions are granted, entropy production acquires a definite sign and a concrete rate. The formula should therefore be read as a quantitative working form within the Level B closure, not as a first-principles derivation of the arrow of time.

### Macroscopic irreversibility versus quantum exception

A key internal consistency check is that irreversibility is not universal:

- For  $N_{\text{eff}} \gg 1$ : backward coherent contributions are strongly suppressed; entropy grows effectively; macroscopic irreversibility emerges.
- For  $N_{\text{eff}} \sim 1$ : suppression is weak; forward and backward loop contributions remain comparable; the coherent dynamics stays close to reversible.

This is exactly what one wants: ECT does not destroy reversibility at the fundamental level. It explains why reversibility survives for small coherent sectors and why it fails effectively for macroscopic ones.

**Numerical illustration.** For a macroscopic system (1 mol,  $T = 300\text{K}$ ,  $\Delta w = c \cdot 1\text{ns}$ ), the exponent controlling the ratio  $P_{\text{back}}/P_{\text{fwd}}$  is of order  $3.6 \times 10^{33}$ , so time-reversed trajectories are effectively absent. For  $N_{\text{eff}} \sim 1$ , the same exponent is of order  $10^{-15}$ , so  $P_{\text{back}}/P_{\text{fwd}} \approx 1$ . This is the quantitative expression of the three-regime picture assembled in Section 3.9.

**Interpretive consequence.** This resolves a potential tension: ECT can support a macroscopic arrow of time and still allow genuinely quantum behaviour in carefully isolated systems. Decoherence strength depends on how many external channels effectively monitor the coherent subsystem. The theory therefore does not collapse all dynamics into classicality.

**Status.** The regime distinction is Level B. Its qualitative form is strongly supported by the influence-functional logic, but a full quantitative interpolation between  $N_{\text{eff}} \sim 1$  and  $N_{\text{eff}} \gg 1$  remains open (OP-Q15).

Figure 33 is schematic; the quantitative interpolation between the two regimes remains part of OP-Q15 and the effective bath analysis of Appendix H. For the spectral-density hierarchy and bath-regime classification, see also Appendix AY.



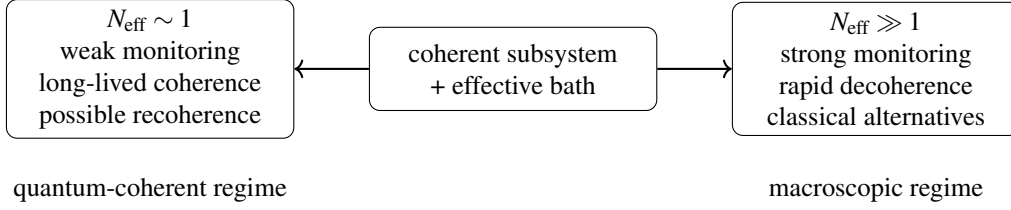


**Figure 33:** Qualitative regime split in the decoherence sector of ECT (Level B). When only a few effective environment channels are active ( $N_{\text{eff}} \sim 1$ ), coherence can survive for long times and recoherence is not excluded. When many channels effectively monitor the subsystem ( $N_{\text{eff}} \gg 1$ ), the reduced dynamics becomes strongly irreversible and classical-looking. This figure is schematic and summarises the logic developed in Section 26.1.

**Status summary.** *Established (Level A):* (i) retarded propagation of the ordered-branch scalar  $\Phi$  is established for the full nonlinear dynamics (Appendix F); (ii) the spectral density is nonnegative in the quadratic sector (26.4); (iii) the irreversible kernel  $\Gamma_{\text{ir}}[q, q'] \geq 0$  is positive semidefinite for any nonnegative spectral density (Appendix G).

*Level A/B:* the low-entropy initial coherent branch as the distinguished starting point of the quantum-sector arrow-of-time reading once the ordered selection and path-integral weighting are admitted.

*Level B:* (i) the reduced influence-functional organisation; (ii) the effective ohmic regime and Markov approximation; (iii) the explicit entropy-production formula (26.9); (iv) the quantitative interpolation between the  $N_{\text{eff}} \sim 1$  and  $N_{\text{eff}} \gg 1$  regimes.

*Open:* (i) the exact microscopic environment split for the full coherent branch; (ii) a strict derivation of the effective ohmic regime; (iii) a strict derivation of the Markov approximation; (iv) a full nonlinear entropy theorem for all coherent sectors.

For the effective spectral-density hierarchy and the scope of the ohmic/Markov closure, see Appendix AY.

### Bridge to probability and Born-type interpretation

Once decoherence suppresses off-diagonal coherent contributions in macroscopic sectors, the next question is how effective probability weights emerge and whether they admit a Born-type interpretation. The structural preconditions are now in place: coherent amplitudes define the underlying dynamics; environment tracing produces reduced decoherence; reduced decoherence generates effective classical alternatives; and only then does a Born-type probabilistic interpretation become physically appropriate. Thus probability in ECT is not more primitive than coherence. It appears only after the reduced-state decoherence logic has already selected effectively classical alternatives. The question of when and how those reduced weights admit a Born-type reading is the subject of Section 30.4.

**Falsifier for the decoherence and thermodynamic-arrow programme.** The present programme would be seriously weakened if its different layers ultimately required unrelated structures: for example, if retarded propagation came from one sector, decoherence suppression from another, entropy growth from a third, and macroscopic classicality from a fourth independent mechanism. It would also be weakened if a completed coherent EFT showed that the same ordered condensate cannot jointly support (i) retarded response, (ii) suppression of off-diagonal histories, (iii) reduced-state entropy growth, and (iv) the macroscopic classicality crossover. Conversely, every successful cross-link between these effects supports the one-branch reading of irreversibility in ECT.

**Empirical anchors already compatible with the programme.** Several empirical facts already fit naturally with the ECT decoherence programme, although none alone proves it: the observed fragility of mesoscopic matter-wave interference under environmental coupling, the standard scaling logic of open-system decoherence with effective bath size and monitoring strength, and the broad fact that macroscopic classicality appears only when a subsystem is strongly embedded in a much larger environment. In ECT

these are read not as independent postulates, but as consistency anchors for one coherent-branch open-system architecture. Analogue platforms provide the nearest controlled probes of this environment-kernel logic (Section 37).

**Programme-level predictions of the ECT decoherence architecture.** The present framework suggests three nontrivial expectations. First, the same action scale  $S_0$  that organises amplitudes, canonical normalisation, and Born-type weighting should also control the decoherence crossover scale. If different quantum sectors ultimately required different effective action scales, the single-branch architecture would fail. Second, the same ordered-vacuum correlator infrastructure that supports Casimir, Unruh, and particle-production response (§25) should also underlie the effective decoherence kernels. Thus vacuum response and decoherence are not separate programmes. Third, the classicality threshold should be environment-sensitive rather than fundamental: macroscopic classicality should arise when the effective monitoring strength and bath size become large, not because microscopic quantum laws cease to hold.

**Connection to the structural universalities.** The decoherence programme does not stand apart from the earlier architecture of the article. It inherits the same causal cone  $c_*$ , the same action scale  $S_0$ , the same extremal backbone descending from DP (§22.2), and the same single-condensate conservation logic developed earlier (§11.1). In this sense, decoherence and the thermodynamic arrow are not additional sectors of the theory, but late manifestations of the same single-medium structure already used in wave kinematics, gravity, and vacuum response.

**Summary.** The arrow-of-time programme in ECT is not introduced as an external thermodynamic postulate. It is organised around an ordered low-entropy coherent branch, a retarded causal kernel inherited from the broken phase, and the reduced-state suppression of unresolved coherent histories. Its strongest quantitative formulas still depend on the effective ohmic and Markov closure, but the qualitative architecture of decoherence and macroscopic irreversibility is already in place within the coherent branch itself.

## 26.2 Decoherence timescale: derivation for specific experimental systems

*Status: Level B. The general ECT decoherence-timescale formula is derived within the Gaussian–Markov reduction of the condensate influence functional. The specific numerical estimates below are consistency-level applications of that formula to experimentally motivated parameter ranges, not first-principles predictions of all microscopic inputs. Connection: the influence-functional programme (§26.1), medium character (P5), the global/reduced unitarity distinction (§23.2), the analogue-laboratory programme (§37), and the vacuum-response infrastructure of Section 25.1.*

The decoherence timescale  $\tau_{\text{dec}}$  can be computed explicitly for each physical system by evaluating  $N_{\text{eff}}$  and  $\gamma$  from the condensate–environment coupling.

### General ECT expression

From the condition  $\Gamma_{\text{loop}}(\tau_{\text{dec}}) = 1$ :

$$\tau_{\text{ECT}} = \frac{1}{N_{\text{eff}} \gamma} \cdot \left( \frac{\ell}{\Delta q} \right)^2, \quad \ell = S_0 \sqrt{\frac{2\pi}{m_{\text{env}} k_B T}}, \quad (26.10)$$

where  $\Delta q$  is the superposition separation,  $\ell$  is the thermal de Broglie wavelength of the relevant condensate modes, and  $S_0$  is the structural action scale of the coherent branch (with  $S_0 \rightarrow \hbar$  after Level B identification). The thermal decay rate per mode is:

$$\gamma \approx \frac{k_B T \sigma_{\text{eff}}}{S_0 v_{\text{ph}}}, \quad (26.11)$$

where  $\sigma_{\text{eff}}$  is the effective scattering cross-section and  $v_{\text{ph}}$  the condensate phase velocity. In the macroscopic limit, these expressions reduce to the standard Caldeira–Leggett result [23].

**Medium reading (P5).** The parameters  $N_{\text{eff}}$  and  $\gamma$  entering Eq. (26.10) are not read in ECT as properties of an external reservoir unrelated to the coherent subsystem. They characterise unresolved sectors of the same ordered condensate that also supports the coherent degrees of freedom being tracked explicitly. In the environmental case, this unresolved sector is modelled through effective collision channels; in the gravitational case, through graviton-like condensate modes. The medium interpretation (P5) does not by itself prove the detailed timescale formulas, but it provides the common ontological reading under which both kinds of decoherence belong to one ordered-medium framework rather than to separate fundamental mechanisms.

**Relation to the general decoherence programme.** The present subsection should be read as the quantitative continuation of Section 26.1. Section 26.1 established the structural organisation of reduced influence-functional decoherence; the present subsection specialises that framework to concrete systems and extracts indicative timescales once sector-appropriate values of  $N_{\text{eff}}$  and  $\gamma$  are supplied. Nothing conceptually new is added here; what changes is the level of numerical concreteness.

### Case 1: C<sub>60</sub> matter-wave interferometry

*Arndt et al. 1999 [183]; Hornberger et al. 2003 [184].*

Molecule mass  $M = 720$  u; grating period  $d = 100$  nm; flight time  $\tau_{\text{flight}} \approx 10^{-3}$  s. The dominant decoherence mechanism is residual-gas collisions. Setting  $N_{\text{eff}} = n_{\text{gas}} v_{\text{th}}^{N_2} \sigma_{C_{60}} \tau_{\text{flight}}$  with  $v_{\text{th}}^{N_2} = \sqrt{8k_B T / (\pi m_{N_2})} \approx 476$  m/s and  $\sigma_{C_{60}} \approx 10^{-18}$  m<sup>2</sup>:

**Table 83:** ECT decoherence timescale for C<sub>60</sub> at  $T = 300$  K vs. residual gas pressure (Level B). Interference is expected when  $\tau_{\text{ECT}} \gg \tau_{\text{flight}} \approx 10^{-3}$  s.  $N_{\text{eff}}$  is estimated from the residual-gas collision rate;  $\gamma$  is evaluated from Eq. (26.11) using the effective closure choice  $v_{\text{ph}} \approx c_*$ .

Pressure $p$ (Pa)	$\tau_{\text{ECT}}$ (s)	Prediction
$10^{-6}$	$\gg 10^{-3}$	Interference visible ✓
$10^{-4}$	$\sim 10^{-3}$	Marginal
$10^{-2}$	$\ll 10^{-3}$	No interference

At  $p \approx 10^{-6}$  Pa, interference is predicted by the ECT timescale estimate, consistent with the Arndt (1999) observation of C<sub>60</sub> diffraction. The suppression of interference at higher pressures is likewise consistent with the crossover discussed by Hornberger et al. [184]. This should be read as an order-of-magnitude Level B consistency anchor, not as a precision confirmation: the formula reproduces the correct qualitative crossover once experimentally supplied residual-gas parameters and an effective collision cross-section are inserted into the Gaussian–Markov reduction.

### Extension to macromolecular interferometry

*Fein et al. 2019 [185].*

Fein et al. [185] extended matter-wave interferometry to molecules of mass  $\sim 2.5 \times 10^4$  amu ( $\sim 4 \times 10^{-23}$  kg)—the most massive objects for which quantum interference has been observed to date. In the ECT reading this remains within the environmental-decoherence regime already captured by the fullerene analysis above: the observed coherence is consistent with the same order-of-magnitude scaling in which gas collisions, transit time, and thermal environment dominate over gravitational-condensate distinguishability effects. The genuinely ECT-specific gravitational-condensate regime (§26.3) is expected only at much larger masses ( $m \gtrsim 10^{-17}$  kg, i.e.  $\gtrsim 10^{10}$  amu). For the Fein molecules ( $m \sim 4 \times 10^{-23}$  kg,  $\Delta q \sim 130$  nm), the gravitational decoherence timescale is  $\tau_{\text{grav}} \sim \hbar \Delta q / (G_N m^2) \sim 10^{14}$  s, which exceeds the transit time by  $\sim 17$  orders of magnitude. The separation of regimes is thus unambiguous: environmental decoherence dominates by a factor of  $\gtrsim 10^{20}$ , where the condensate itself acts as the gravitational

environment and decoherence should persist even in near-perfect vacuum. That mass frontier is the target of levitated-nanoparticle experiments [186, 187].

**Comparison with standard quantum theory.** In the mass range explored by Fein et al. [185], standard environmental-decoherence theory already provides an adequate description in terms of collisional and thermal loss of coherence. ECT does not compete with that account in this regime; rather, it reproduces the same order-of-magnitude scaling once the condensate influence functional is reduced to the Gaussian–Markov closure. The distinctive ECT claim begins only beyond the purely environmental regime, where gravitational condensate distinguishability is expected to become relevant.

**Origin of the mass-scale estimate.** Any estimate of a maximum mass scale for visible interference in this regime should be read as an order-of-magnitude consistency estimate, not as a uniquely ECT-derived law. The corresponding scaling follows from the same environmental-decoherence condition  $\tau_{\text{dec}} \gtrsim \tau_{\text{pass}}$  that underlies standard collisional-decoherence analyses, and ECT recovers it only within the same effective Gaussian–Markov limit. The practical numerical point is therefore not a new ECT fit to the Fein experiment itself, but the separation of regimes: the observed  $\sim 2.5 \times 10^4$  amu molecules remain deep in the environmental-decoherence domain, whereas the condensate-gravitational regime discussed in Section 26.3 is expected only many orders of magnitude higher, around the levitated-nanoparticle frontier.

## Case 2: Gravity-induced decoherence

*Diósi 1987 [188]; Penrose 1996 [189].*

Diósi and Penrose propose that quantum superpositions of massive objects collapse with a timescale  $\tau_{\text{DP}} = \hbar/E_G$ , where  $E_G$  is the self-gravitational energy of the difference between the two mass distributions  $\rho_1, \rho_2$  of the superposed branches:

$$E_G = \frac{G_N}{2} \iint \frac{[\rho_1(\mathbf{r}) - \rho_2(\mathbf{r})][\rho_1(\mathbf{r}') - \rho_2(\mathbf{r}')] }{|\mathbf{r} - \mathbf{r}'|} d^3r d^3r'. \quad (26.12)$$

For a rigid body of mass  $m$  split into two branches at separation  $d \gtrsim R$  (object size  $R$ ), the leading geometry-dependent heuristic estimate is  $E_G \sim G_N m^2/R$  (self-energy normalisation) or  $E_G \sim G_N m^2/d$  (separation-dominated regime), giving  $\tau_{\text{DP}} \sim \hbar R/(G_N m^2)$  at the self-energy scale. In ECT, gravitational decoherence is not introduced as a separate fundamental law. It is read as the contribution of the graviton-like condensate sector to the same influence functional  $\Gamma[q, q']$  that governs the environmental case. At leading order in the macroscopic gravitational matching, the corresponding reduced decoherence timescale takes the Diósi–Penrose form

$$\tau_{\text{ECT}}^{\text{grav}} = \frac{\hbar}{E_G} = \tau_{\text{DP}}. \quad (26.13)$$

ECT therefore *realises* the Diósi–Penrose scaling as a limiting case of the condensate decoherence functional in the gravity-dominated regime. The numerical timescale is not unique to ECT: it coincides at leading order with the DP estimate and with other collapse models that share the same gravitational self-energy input. The ECT-specific content is the *origin* of this rate as condensate-sector distinguishability rather than a postulated collapse law. A positive nanosphere signal at the predicted scale would therefore support the ECT closure only when combined with tests that exclude ordinary environmental decoherence and that distinguish ECT from DP-collapse models through subleading condensate-sector corrections.

**Table 84:** ECT gravitational decoherence timescale for representative systems ( $= \tau_{\text{DP}}$  at leading order, Level B).

Object	Mass $m$	Separation $\Delta x$	$E_G$ (J)	$\tau_{\text{ECT}}^{\text{grav}}$ (s)
Proton	$1.67 \times 10^{-27}$ kg	$1 \mu\text{m}$	$1.9 \times 10^{-58}$	$5.7 \times 10^{23}$
Nanosphere ( $R = 1 \mu\text{m}$ , $\rho = 2000$ )	$8.4 \times 10^{-15}$ kg	$1 \mu\text{m}$	$2.8 \times 10^{-33}$	$3.8 \times 10^{-2}$

Object	Mass $m$	Sep. $\Delta x$	$E_G$ (J)	$\tau_{\text{ECT}}^{\text{grav}}$ (s)
Nanogram	$10^{-12}$ kg	$4.9 \mu\text{m}$	$1.6 \times 10^{-29}$	$6.5 \times 10^{-6}$

The nanogram estimate ( $\tau \approx 6.5 \mu\text{s}$ ) is potentially testable in proposed optomechanical experiments [190]. ECT does not modify the Diósi–Penrose result at leading order; sub-Planck-separation corrections are currently unobservable.

**Structural unification of environmental and gravitational decoherence.** The two cases analysed above illustrate a single structural point. In standard physics, environmental decoherence and gravitational decoherence are usually introduced as conceptually distinct mechanisms. In ECT both are treated as specialisations of one and the same condensate influence functional  $\Gamma[q, q']$ , evaluated for different unresolved sectors of the ordered medium. Residual-gas collisions and graviton-like condensate modes are not independent fundamental laws in this reading; they are different bath sectors of one ordered condensate. This does not prove that all decoherence channels in nature are thereby exhausted, but it does show that the single-medium architecture already contains both classes without postulating separate microscopic principles.

**Discriminant: unified condensate decoherence versus separate mechanisms.** In the standard presentation, environmental decoherence and gravitational decoherence are typically discussed as independent programmes. ECT does not deny either effective formula. Its distinctive claim is instead that both emerge from one ordered medium and one influence-functional structure. The ECT-specific content is therefore not the mere recovery of the individual leading-order scalings, but their common origin in the same condensate framework.

**Falsifier for the decoherence-timescale programme.** The decoherence-timescale programme would be weakened if the ECT formula (26.10) yielded qualitatively incorrect scaling with pressure, superposition separation, or system mass in regimes already tested experimentally. It would be more strongly challenged if environmental and gravitational decoherence required fundamentally different influence-functional structures that could not be embedded into one ordered-medium framework. At present, the leading-order agreement with both the Caldeira–Leggett-type scaling and the Diósi–Penrose form is maintained at the structural level.

**Connection to the analogue-laboratory programme.** The timescale logic developed here is directly relevant to the analogue-laboratory programme (§37), where superfluid and BEC systems provide controlled environments with measurable coherence times and tunable bath couplings. Such systems offer the most accessible near-term route to testing the scaling structure of the ECT decoherence formula beyond the already available fullerene interferometry anchor.

**Empirical status.** The  $\text{C}_{60}$  interferometry case is one of the clearest order-of-magnitude consistency anchors of the ECT quantum sector. The experimentally observed pressure-controlled crossover in coherence visibility is captured at the correct order of magnitude once the Gaussian–Markov reduction is combined with known system parameters. The gravitational case is different: the Diósi–Penrose form is structurally recovered, but its direct experimental isolation remains open. Proposed optomechanical experiments [190] target the nanogram-scale regime where the corresponding timescale becomes potentially testable.

**Status summary.** *Level B:* (i) the general decoherence-timescale formula (26.10) is derived within the Gaussian–Markov closure of the condensate influence functional; (ii) the  $\text{C}_{60}$  interferometric crossover is captured at the correct order of magnitude; (iii) the Diósi–Penrose gravitational decoherence form is recovered as a limiting case of the same condensate-functional framework.

*Structural unification:* environmental and gravitational decoherence are read as two bath-sector specialisations of one ordered-medium influence functional rather than as separate fundamental mechanisms.

*Open:* (i) a strict first-principles derivation of  $N_{\text{eff}}$  and  $\gamma$  beyond the effective Gaussian–Markov closure; (ii) an experimental isolation of gravitational decoherence in the relevant mesoscopic regime; (iii) subleading corrections from the full condensate dynamics.

### 26.3 Gravitational decoherence from condensate distinguishability

*Status: Level B. The Diósi–Penrose timescale is recovered as a limiting case of the ECT influence functional, with the condensate itself playing the role of the gravitational environment.*

#### Derivation from ECT

A mass  $m$  at position  $\mathbf{x}_0$  modifies the condensate amplitude through the quasistatic  $\phi$ -equation:

$$\delta\phi(\mathbf{x}) \sim -\frac{G_N m}{c_*^2 |\mathbf{x} - \mathbf{x}_0|}. \quad (26.14)$$

A superposition of two positions  $\mathbf{x}_1$  and  $\mathbf{x}_2$  produces two distinct condensate configurations with difference

$$\Delta\phi(\mathbf{x}) = -\frac{G_N m}{c_*^2} \left( \frac{1}{|\mathbf{x} - \mathbf{x}_1|} - \frac{1}{|\mathbf{x} - \mathbf{x}_2|} \right). \quad (26.15)$$

The gravitational decoherence functional is determined by the overlap between the two condensate configurations:

$$\Gamma_{\text{grav}}(\tau) \sim \frac{\tau}{\hbar} \int d^3x \frac{(\Delta\phi)^2}{\xi_{\text{cond}}^2 / \bar{M}_{\text{Pl}}^2}. \quad (26.16)$$

For an extended body of radius  $R$ , the spatial integral evaluates to  $\sim G_N m^2 / (c_*^4 R)$ , and the condition  $\Gamma_{\text{grav}}(\tau_{\text{dec}}) = 1$  gives:

$$\tau_{\text{dec}}^{\text{grav}} \sim \frac{\hbar R}{G_N m^2}. \quad (26.17)$$

This recovers the Diósi–Penrose timescale [188, 189]. In ECT it is *not* imported: the condensate itself plays the role of the gravitational environment, and the decoherence rate is determined by the distinguishability of the two condensate configurations. Within the PES reading (§29), this subsection provides the gravitational specialisation of the same distinguishability-based decoherence logic that governs the broader quantum-to-classical transition.

#### Numerical estimates

**Table 85:** ECT gravitational decoherence timescale (eq. 26.17; Level B).

Object	Mass (kg)	$\Delta x$	$\tau_{\text{dec}}^{\text{grav}}$	Testable?
Proton	$1.67 \times 10^{-27}$	$1 \mu\text{m}$	$5.7 \times 10^{23} \text{ s}$	No
Nanosphere ( $R = 1 \mu\text{m}$ )	$8.4 \times 10^{-15}$	$1 \mu\text{m}$	38 ms	Near-future
Nanosphere ( $R = 100 \text{ nm}$ )	$8.4 \times 10^{-18}$	100 nm	$\sim 1 \text{ hr}$	Difficult
Nanogram	$10^{-12}$	$4.9 \mu\text{m}$	$6.5 \mu\text{s}$	Yes

The nanosphere regime ( $R \sim 1 \mu\text{m}$ ,  $m \sim 8 \times 10^{-15} \text{ kg}$ ,  $\tau \sim 38 \text{ ms}$ ) is the experimental frontier targeted by the groups of Aspelmeyer and Romero-Isart using levitated nanoparticles. This is where ECT gravitational decoherence becomes testable and where deviations from the standard environmental-decoherence picture may first appear.

### Where ECT should differ from standard decoherence

At masses below  $\sim 10^{10} \text{ amu}$ , environmental decoherence dominates and ECT reproduces standard open-system results (as confirmed by the Arndt  $\text{C}_{60}$  analysis, §26.1). At larger masses, a DP-type gravitational channel may compete with ordinary environmental sources. The leading timescale is not unique to ECT: phenomenological Diósi–Penrose collapse models have the same parametric scaling. The ECT-specific claim is instead that this channel arises from condensate-sector distinguishability, without adding an independent collapse postulate or a freely fitted collapse scale.

## 26.4 Crooks-type fluctuation relation and effective entropy production

*Status: Level B. The Crooks-type fluctuation relation [191] and the effective entropy-production formula are derived within the Gaussian–Markov reduction of the ECT influence functional. They are not consequences of the bare ECT postulates alone and do not yet constitute a full microscopic second-law theorem. Connection: the influence-functional decoherence programme (§26.1), the quantitative timescale analysis (§26.2), medium character (P5), the directional backbone established in ECT basics (§3.9), and the global/reduced unitarity distinction (§23.2).*

**Scope and honest status.** This subsection does *not* provide a full microscopic derivation of the second law from the bare Euclidean ECT action. What is established is an *effective irreversibility result* within the Gaussian–Markov coarse-grained description of the ordered branch. The result rests on the ECT influence functional together with the Gaussian model for the reduced density matrix and the Markov approximation; it is not derived from the ECT postulates alone without these additional steps. A fully microscopic derivation remains open (OP-Q17, Section 38.1).

**Medium reading (P5).** Under the medium interpretation (P5), the present Crooks-type relation is not read as a formal theorem about an abstract system coupled to an external bath. The explicitly tracked subsystem and the unresolved environment both belong to one ordered condensate. The suppression of backward traversal is therefore a reduced-state property of internal condensate organisation, not an independently postulated thermodynamic law.

**Effective entropy production in the Gaussian–Markov reduction.** Within the Gaussian–Markov reduction of the ECT influence functional  $\mathcal{F}[q, q']$  (26.1), the reduced density matrix of the tracked coherent subsystem takes the effective form

$$\rho_{\text{red}}^{\text{G}}(w) \propto \exp(-\Gamma_{\text{irr}}(w)), \quad (26.18)$$

where  $\Gamma_{\text{irr}}$  denotes the irreversible part of the influence functional in that Gaussian–Markov closure.

**Important:** Eq. (26.18) is an effective Gaussian reduced-state form, not a general consequence of the bare ECT postulates. Likewise,  $\Gamma_{\text{irr}}$  is not the full decoherence functional  $\Gamma[q, q']$  but its irreversible part in the Gaussian–Markov approximation. In the appropriate limit, this effective organisation reduces to the standard Caldeira–Leggett open-system form [23], but the logical starting point here is the ECT influence functional, not the external CL model.

Within this model, the von Neumann entropy satisfies

$$S_{\text{ent}}(w) \approx \text{const} + \Gamma_{\text{irr}}(w), \quad (26.19)$$

and its rate of change is

$$\frac{dS_{\text{ent}}}{dw} = \frac{d\Gamma_{\text{irr}}}{dw} = N_{\text{eff}} \gamma \left( \frac{dq}{dw} \right)^2 \geq 0, \quad (26.20)$$

since  $N_{\text{eff}} > 0$ ,  $\gamma > 0$ , and  $(dq/dw)^2 \geq 0$ .

Within the Gaussian–Markov reduction, this gives  $dS_{\text{ent}}/dw \geq 0$  for macroscopic trajectories with  $N_{\text{eff}} \gg 1$ , with equality only for static configurations ( $dq/dw = 0$ ). This is therefore an effective monotonicity statement inside the present closure, not yet a full microscopic second-law theorem of the complete ECT path integral. Whether the full non-Markovian ECT path integral implies monotone entropy growth without the Gaussian–Markov coarse-graining is an open problem (OP-Q17, Section 38.1).

In the Markovian (ohmic) reduction, a Crooks-type fluctuation relation holds for the effective decoherence action:

$$\frac{P_{\text{back}}}{P_{\text{fwd}}} = \exp(-\Delta\Gamma_{\text{irr}}[\Delta q]), \quad (26.21)$$

where  $\Delta\Gamma_{\text{irr}}$  is the irreversible part of the influence functional after the Markov coarse-graining. **Status:** this is a Crooks-type relation derived within the Gaussian–Markov reduction of ECT; it is not derived directly from the bare Euclidean action without coarse-graining. The extension to the full non-Markovian microscopic ECT path integral remains open.

**Why  $w$  is traversed in one direction macroscopically.** The question of why the macroscopic arrow of time points in a definite direction can be stated precisely in ECT:

**Step 1 (Effective irreversibility functional is monotone — Gaussian model).** Within the Gaussian–Markov model, the effective irreversibility functional satisfies  $d\Gamma_{\text{irr}}/dw \geq 0$  for all macroscopic trajectories with  $N_{\text{eff}} \gg 1$  (Eq. (26.20) above). Note: this is  $\Gamma_{\text{irr}}$ , the coarse-grained entropy-production functional, *not* the full decoherence functional  $\Gamma[q, q']$  (which vanishes on the diagonal, the diagonal condition  $\Gamma[q, q] = 0$ ). Physically, each interaction with the Gaussian environment adds positive entropy to the coarse-grained reduced density matrix.

**Step 2 (Initial condition from the ordering transition — structural argument).** The  $O(4) \rightarrow O(3)$  ordering transition provides a natural candidate for a low-entropy initial coherent sector. The ordered condensate  $|\Phi| = \phi_0$  is selected by the variational extremal condition together with the ordered-branch restriction, producing a highly ordered configuration with low effective entropy at the start of the Lorentzian branch. **Status (structural, not fully derived):** this argument is structurally motivated within the ordered-branch programme, but a rigorous derivation of a nearly pure or entropy-minimised initial reduced state from the full Euclidean path integral remains open (OP-Q17). The low-entropy initial condition is therefore not derived from the bare postulates alone; it is a structural assumption internal to the present closure.

**Step 3 (Macroscopic effective irreversibility).** Since  $\Gamma_{\text{irr}}(w)$  is monotonically non-decreasing (Step 1) with initial value near zero (Step 2, structural), the effective entropy  $S_{\text{ent}}(w) \approx \text{const} + \Gamma_{\text{irr}}(w)$  increases with  $w$  for all macroscopic systems in the Gaussian–Markov model. The coordinate  $w$  therefore defines a preferred direction — the arrow of time — for any system with  $N_{\text{eff}} \gg 1$ , *within the Gaussian–Markov reduction*. Whether this conclusion extends to the full non-Markovian path integral remains open (OP-Q17).

**Discriminant: ECT Crooks-type relation versus standard fluctuation theorems.** Standard Crooks fluctuation relations [191] are derived within an already assumed statistical-mechanical or operator-algebraic framework. In ECT the logical origin is different: the relevant ratio is traced back to the irreversible part  $\Gamma_{\text{irr}}$  of the condensate influence functional after Gaussian–Markov coarse-graining. The mathematics reduces to the standard form in the corresponding limit, but the ECT-specific claim is that irreversibility is not primitive: it is an effective consequence of coarse-graining one ordered medium.

**Falsifier for the Crooks programme.** The present Crooks-type relation would be challenged if a completed non-Markovian ECT analysis showed that the irreversible part  $\Gamma_{\text{irr}}$  can become negative in physically relevant regimes, breaking the sign structure required for  $P_{\text{back}}/P_{\text{fwd}} \leq 1$ . It would also be weakened if the full Euclidean path-integral treatment yielded an arrow-of-time structure fundamentally



incompatible with the Gaussian–Markov reduction, rather than merely refining it. At present, no such incompatibility is known.

**Bridge to the probability and measurement programme.** The present subsection does not yet derive the Born rule or a full measurement theory. What it establishes is narrower: within the Gaussian–Markov reduction, backward traversal is effectively suppressed, entropy grows in the reduced description, and an effective macroscopic arrow of time is obtained. These are the thermodynamic and open-system preconditions for the next stage of the quantum-sector analysis, namely the quantum–classical boundary, Born-type probabilities, and measurement status.

**Status summary.** *Level B:* (i) the effective entropy-production formula (26.20) is derived within the Gaussian–Markov reduction of the ECT influence functional; (ii) the Crooks-type fluctuation relation (26.21) follows from the same reduction; (iii) the three-step arrow-of-time logic (monotone  $\Gamma_{\text{irr}}$ , low-entropy initial branch, macroscopic  $N_{\text{eff}} \gg 1$ ) is internally consistent within this closure.

*Open (OP-Q17):* (i) extension to the full non-Markovian microscopic ECT path integral; (ii) a rigorous derivation of the low-entropy initial branch from the bare Euclidean path integral; (iii) a full microscopic second-law theorem without the Gaussian–Markov closure.

## 27 Results and Regime Estimates of the Decoherence Apparatus

*This section collects the quantitative estimates, order-of-magnitude consistency checks, and regime-level consequences that the ECT decoherence apparatus (Appendix AZ) yields when applied to concrete experimental systems.*

**Visibility-based operational estimates of  $\Gamma_{\text{loop}}$ .** In many photonic delayed-choice and quantum-switch experiments the experimentally accessible quantity is the interferometric visibility  $V$ . In the simplest pure-dephasing closure, the visibility and the reverse-coherence ratio are related by

$$V \simeq e^{-\Gamma_{\text{loop}}}, \quad \frac{P_{\text{back}}}{P_{\text{fwd}}} \simeq e^{-\Gamma_{\text{loop}}}.$$

This allows an operational dephasing proxy for  $\Gamma_{\text{loop}}$ , and correspondingly for  $P_{\text{back}}/P_{\text{fwd}}$ , to be extracted directly from the reported visibility within the simplest pure-dephasing closure, without requiring a microscopic environmental model.

Anchor / marker	Observable	$\Gamma_{\text{loop}}$	$P_{\text{back}}/P_{\text{fwd}}$	Status
Procopio quantum switch (2015)	$V = 0.994 \pm 0.002$	$0.006 \pm 0.002$	$0.994 \pm 0.002$	Visibility-based
Jacques delayed-choice (2007, closed config.)	$V \approx 0.94$	$\Gamma_{\text{loop}} \approx 0.062$	$\approx 0.94$	Visibility-based
Bell/CHSH threshold	$2\sqrt{2}e^{-\Gamma} = 2$	$\ln \sqrt{2} \approx 0.347$	$1/\sqrt{2} \approx 0.707$	Theory threshold
Qubit 1-bit information bound	$I \sim 1 \text{ bit}$	$\sim 0.25$	$\sim 0.78$	Toy closure

This table and the accompanying Fig. 34 are operational regime maps; they combine experimentally inferred proxies with closure-dependent theoretical markers. The table extracts  $\Gamma_{\text{loop}}$  from directly reported visibilities and compares them with the theoretical thresholds derived elsewhere in the quantum sector. It is not a first-principles derivation of  $\Gamma_{\text{loop}}$  from the microscopic condensate dynamics. For matter-wave platforms ( $\text{C}_{60}$ , macromolecules) a setup-specific environmental model including thermal emission, residual-gas scattering, and flight geometry would be required; such estimates are deferred to

the experimental programme.

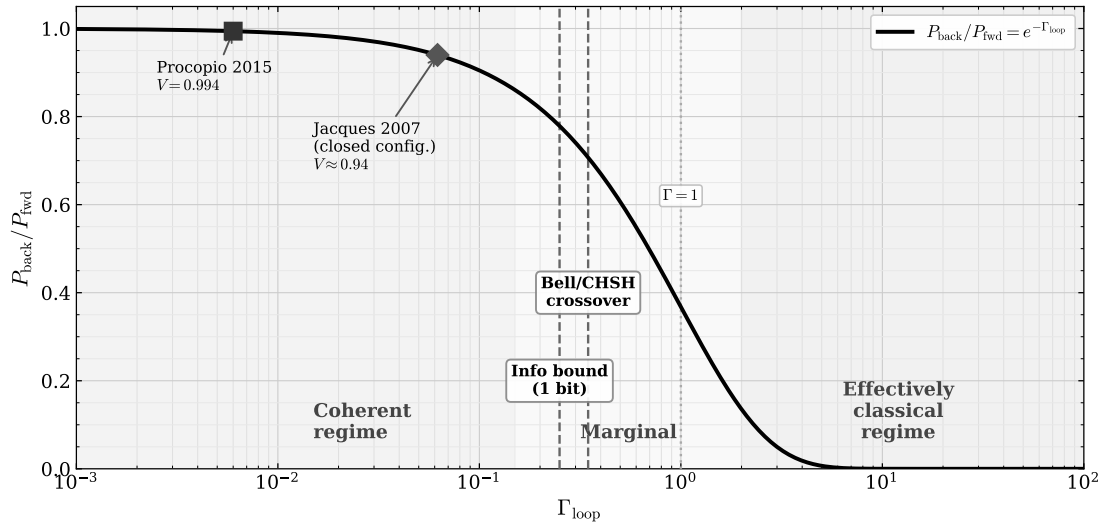


**Figure 34:** Operational crossover map organised by the decoherence parameter  $\Gamma_{\text{loop}}$ . The solid curve shows the reverse-coherence ratio  $P_{\text{back}}/P_{\text{fwd}} = e^{-\Gamma_{\text{loop}}}$ . Filled markers denote visibility-inferred operational proxies rather than first-principles ECT calculations of  $\Gamma_{\text{loop}}$  (Procopio quantum switch; Jacques delayed-choice interferometer). Dashed vertical lines indicate closure-dependent theoretical thresholds used as operational guides: the Bell/CHSH crossover in the Werner-visibility toy model at  $\Gamma_{\text{loop}} = \ln \sqrt{2} \approx 0.35$ , and the one-bit information threshold in the qubit dephasing closure at  $\Gamma_{\text{loop}} \approx 0.25$ . The dotted line at  $\Gamma_{\text{loop}} = 1$  is an order-unity crossover marker rather than a sharp universal boundary. The left zone corresponds to the coherent regime ( $\Gamma_{\text{loop}} \ll 1$ ), while the right zone corresponds to the effectively classical regime ( $\Gamma_{\text{loop}} \gg 1$ ).

The apparatus is an influence-functional / open-system framework: it governs decoherence, measurement, and quantum–classical boundary phenomena, but not particle lifetimes or precision spectroscopy.

## 27.1 Environmental decoherence: $C_{60}$ and macromolecules

*Status: Level B (Gaussian–Markov closure applied to known experimental parameters). The ECT result reproduces the standard Caldeira–Leggett / Hornberger analysis; in this regime the numerical estimates coincide with those of the standard theory.*

The decoherence timescale for matter-wave interferometry is

$$\tau_{\text{dec}} = \frac{S_0}{2D_{\text{eff}}(\Delta q)^2}, \quad (27.1)$$

where  $D_{\text{eff}}$  is the effective white-noise amplitude in the Markov regime (Appendix AZ.5). For residual-gas collisions in ultra-high vacuum, the dominant environmental coupling is collisional, and  $D_{\text{eff}}$  is controlled by the gas density, thermal velocity, and molecular cross-section (Section 26.2).

**Table 87:** ECT environmental-decoherence consistency checks vs. observations (regime-level comparison).

Experiment	Observable	Standard QM	ECT regime estimate	Assessment
$C_{60}$ ( $p = 10^{-6}$ Pa)	Interference visible	$\tau_{\text{dec}} \gg \tau_{\text{fl}}$	Same	Consistent
$C_{60}$ ( $p = 10^{-4}$ Pa)	Fringe degradation	$\tau_{\text{dec}} \sim \tau_{\text{fl}}$	Same	Consistent

Experiment	Observable	Std. QM	ECT estimate	Assessment
C <sub>60</sub> ( $p = 10^{-2}$ Pa)	No interference	$\tau_{\text{dec}} \ll \tau_{\text{fl}}$	Same	Consistent
Fein (25 000 amu)	2019 Interference visible	Environmental regime	Same	Consistent

**Comparison with observations.** In the environmental-decoherence regime, ECT reproduces the same numbers as the standard theory because the Gaussian–Markov closure of the ECT influence functional reduces to the Caldeira–Leggett master equation. The ECT contribution in this regime is *structural*, not numerical: it embeds the influence-functional framework in the condensate architecture rather than introducing it as an unrelated external formalism.

## 27.2 Gravitational decoherence: ECT realisation of a DP-type scaling

*Status: Level B. Within the present condensate-based closure, the gravitational decoherence timescale is recovered from condensate distinguishability rather than postulated independently as in the original Diósi–Penrose proposals. The leading numerical estimates below are not unique to ECT—they coincide with the Diósi–Penrose gravitational self-energy scaling. The ECT-specific content is the proposed origin of this scaling as condensate-sector distinguishability and the associated pattern of subleading corrections.*

The gravitational decoherence timescale for a solid sphere of radius  $R$  and density  $\rho$  in superposition of two positions separated by  $d \sim R$  is (Table 85):

$$\tau_{\text{grav}} \sim \frac{\hbar}{E_G}, \quad E_G = \frac{6G_N m^2}{5R} f(d/R). \quad (27.2)$$

The leading DP-type prediction is that this decoherence can persist even in near-perfect vacuum once ordinary environmental channels are suppressed below the condensate-gravitational rate. This persistence is not unique to ECT; what is ECT-specific is the condensate-origin interpretation (the condensate itself acts as the gravitational environment) and the associated pattern of subleading corrections.

**Experimental frontier.** The nanosphere regime ( $R \sim 1 \mu\text{m}$ ,  $m \sim 8 \times 10^{-15} \text{ kg}$ ,  $\tau \sim 38 \text{ ms}$ ) is the nearest quantitative target for levitated nanoparticle experiments [186, 187]. An observation of decoherence at this timescale in a vacuum sufficiently good to eliminate environmental channels would constitute a direct test of a DP-type gravitational-decoherence channel. For ECT specifically, the discriminating content would be the condensate-origin interpretation, the absence of a freely fitted collapse scale, and any subleading condensate-profile corrections.

## 27.3 Environmental–gravitational crossover

*Status: Level B. The crossover formula is self-consistent for spherical geometry (Appendix AZ.6).*

For given vacuum conditions, the crossover mass above which gravitational decoherence dominates over environmental decoherence is (eq. AZ.16):

$$m_{\text{cross}} \sim \frac{3 \hbar n_{\text{gas}} v_{\text{th}}}{4 G_N \rho}. \quad (27.3)$$

**Table 88:** Environmental–gravitational crossover for solid spheres ( $\rho = 2000 \text{ kg/m}^3$ ). The leading crossover scale is DP-type and not unique to ECT; in ECT it is interpreted as a condensate-sector distinguishability channel rather than as an independent collapse postulate.

Vacuum conditions	$m_{\text{cross}}$ (kg)	$R_{\text{cross}}$	$\tau_{\text{cross}}$
$10^{-8} \text{ Pa, } 300 \text{ K}$	$\sim 5 \times 10^{-16}$	$\sim 400 \text{ nm}$	$\sim 4 \text{ s}$
$10^{-10} \text{ Pa, } 4 \text{ K}$	$\sim 10^{-16}$	$\sim 250 \text{ nm}$	$\sim 40 \text{ s}$
$10^{-12} \text{ Pa, } 0.1 \text{ K}$	$\sim 2 \times 10^{-17}$	$\sim 140 \text{ nm}$	$\sim 10 \text{ min}$

Below  $m_{\text{cross}}$ , standard environmental decoherence dominates and ECT gives the same numbers as the standard theory. Above  $m_{\text{cross}}$ , if ordinary environmental channels are reduced below the condensate-gravitational rate, the condensate gravitational channel is expected to dominate and decoherence should persist even in near-perfect vacuum.

## 27.4 Photonic weak-locking bounds

*Status: Level B, interpretive. ECT does not modify the operational predictions of photonic experiments at the present stage; it provides weak-locking consistency bounds.*

For single-photon experiments (Wheeler delayed-choice, quantum eraser, delayed-choice entanglement swapping, photonic quantum switch), the ECT decoherence parameter is  $\Gamma_{\text{loop}} \ll 1$  because the single-photon vacuum branch is naturally interpreted as remaining in the weak-locking regime during free propagation (with effectively negligible environmental monitoring in the vacuum-propagation segments).

The consistency requirement is simply that the experiment operates in the weak-locking regime:  $\Gamma_{\text{loop}} \ll 1$  before irreversible detection (with  $\Gamma_{\text{loop}} \gg 1$  at the detector). The four photonic experiments discussed in Sections 30.2–30.3 are naturally read as belonging to this weak-locking regime prior to irreversible detection. For the switch platform this reading is supported by an explicit order-of-magnitude estimate; for Wheeler delayed-choice, quantum eraser, and delayed-choice entanglement swapping it remains a consistency-based interpretive assignment. At present, an explicit order-of-magnitude estimate has been written only for the photonic switch platform. For Wheeler delayed-choice, quantum eraser, and delayed-choice entanglement swapping, the present ECT contribution remains interpretive and consistency-based rather than numerically predictive.

## 27.5 Cavity-cat decoherence: next quantitative target

*Status: programme-level. This is the next natural quantitative target for the ECT decoherence apparatus, beyond the environmental and gravitational regimes already treated.*

The Haroche–Raimond cavity-QED experiments [192] directly measure the decoherence rate of mesoscopic Schrödinger-cat states of the microwave field. As a proxy scaling relation within the generic ECT apparatus, the decoherence exponent for a cavity cat-state with  $\bar{n}$  mean photons and separation  $\alpha$  in phase space is:

$$\Gamma_{\text{cat}}(t) \sim \frac{|\alpha|^2}{S_0} 2 \int_0^t d\tau (t - \tau) N_{\text{cav}}(\tau), \quad (27.4)$$

where  $N_{\text{cav}}(\tau)$  is the noise kernel of the cavity–environment coupling. Here  $N_{\text{cav}}(\tau)$  is not yet derived from a cavity-specific ECT micro-model; the formula should be read as the natural extension of the generic decoherence exponent to the cavity-cat geometry. As an illustration, the Brune et al. (1996) [193] experiment measures decoherence of cavity Schrödinger-cat states with cavity photon lifetime  $\tau_{\text{cav}} \approx 160 \mu\text{s}$ . The standard prediction is  $\tau_{\text{dec}} = \tau_{\text{cav}}/(2\bar{n})$ , giving  $\tau_{\text{dec}} \approx 24 \mu\text{s}$  for  $\bar{n} = 3.3$  and  $\tau_{\text{dec}} \approx 8 \mu\text{s}$  for  $\bar{n} = 9.5$ . In the ECT Markov closure, the same result follows from  $D_{\text{eff}} = S_0/(2\tau_{\text{cav}})$  in eq. (AZ.12): the condensate-gravitational contribution expected in ECT is negligible for microwave photons at the present cavity scale, so the apparatus reproduces the standard cavity-QED decoherence scaling. A genuinely

ECT-specific correction would arise only if the cavity field coupled to the condensate orientation modes at a rate comparable to  $1/\tau_{\text{cav}}$ , which is not expected in the present regime.

## 27.6 Summary: what the apparatus predicts

Table 89 collects the quantitative estimates and regime-level outputs of the present ECT decoherence apparatus.

**Table 89:** Summary of quantitative estimates, operational proxies, and regime-level outputs associated with the present ECT decoherence apparatus.

System	ECT estimate	Observation	Status
$C_{60}$ ( $10^{-6}$ Pa)	$\tau_{\text{dec}} \gg 1$ ms	Interference ✓	Regime consistency
$C_{60}$ ( $10^{-4}$ Pa)	$\tau_{\text{dec}} \sim 1$ ms	Degradation	Regime consistency
Fein 25 000 amu	Environmental	Interference ✓	Regime consistency
Procopio switch	$V = 0.994 \pm 0.002 \Rightarrow \Gamma_{\text{loop}}^{(\text{exp})} = 0.006 \pm 0.002$	ICO visible	Visibility-based interpretive consistency
Nanosphere 1 $\mu\text{m}$	$\tau_{\text{grav}} \sim 38$ ms	Not yet tested	DP-type leading scale; ECT-specific origin/subleading
Nanosphere 100 nm	$\tau_{\text{grav}} \sim 1$ hr	Not yet tested	DP-type leading scale; ECT-specific origin/subleading
Crossover (UHV)	$m_{\text{cross}} \sim 10^{-16}$ kg	Not yet tested	Closure-level crossover; not unique leading DP scale
Cavity cat	Open target within present closure	Measured decoherence times (Brune 1996)	Programme-level target

## 28 ECT as a reduced-state resolution of the hybrid-consistency problem

*Status: structural framing for the gravitational, measurement, and black-hole sectors of Part III. No new derivations; this section fixes the two-level ontology invoked in Sections 26.3, 26.4, 30.2, 36, and the falsifiers of Section 38.4. The comparison with theories of Lorentzian emergence (Einstein–aether, Hořava–Lifshitz, CDT, Hartle–Hawking) given in Section 3.10 compares ECT along the signature-emergence axis; the present section instead compares architectures for the gravity–matter interface. The two comparison axes are logically distinct.*

### 28.1 The hybrid-consistency problem

Reconciling a quantum description of matter with a classical or emergent description of the gravitational sector produces a characteristic set of structural obstructions known collectively as the hybrid-consistency problem. Any non-metric-fundamental approach to the gravity–matter interface must confront at least five demands: positivity of reduced states; operational no-signalling; controlled energy–momentum bookkeeping; relativistic compatibility; and gauge or diffeomorphism consistency of the emergent mediator. Historical semi-classical proposals of Møller and Rosenfeld [194, 195] already exhibited the relevant tensions. These were later sharpened by the Page–Geilker experiment [196] and by a broader literature of thought experiments and consistency critiques, including the influential but debated analysis of Eppler and Hannah [197]. Low-energy effective-field-theory treatments [198, 199] remain internally consistent in their domain, but do not by themselves resolve the ultraviolet side or the hybrid measurement problem. The post-quantum classical gravity programme of Oppenheim [200, 201, 202, 203] addresses

the problem by postulating fundamentally stochastic dynamics for both metric and matter, at the cost of irreducible irreversibility and fundamental information loss.

The architectural claim of ECT is not that the five consistency demands disappear, but that they are displaced from the fundamental law to the reduction map between the full condensate theory and its effective descriptions.

## 28.2 Central thesis

**Central thesis.** ECT is presented not merely as an emergent-gravity alternative, but as a candidate reduced-state resolution of the hybrid-consistency problem: irreversibility, decoherence, effective thermality, and apparent stochasticity are not taken as fundamental laws of gravity, but arise only in reduced descriptions of a single globally unitary Euclidean condensate.

The thesis has three components. First, global unitarity is maintained at the level of the full theory. Second, every apparent cost of hybrid consistency enters only through the reduction to effective descriptions. Third, the reduction is not a collapse postulate and not an added stochastic law; it is the choice of which condensate degrees of freedom are tracked explicitly and which are integrated out.

Two qualifications are important at the outset. *First*, ECT does not identify “non-fundamental metric” with “non-quantum gravity”; what is denied is the need to quantise an independent metric field as the fundamental starting point. *Second*, in ECT classicality is not a separate ontological sector but a regime of reduced description.

## 28.3 Two-level ontology with Level IIa/IIb split

Two ontological levels are distinguished, with the reduced level split into two operational regimes.

**Level I — full condensate description.** One Euclidean condensate  $\Phi$  on the four-manifold  $\mathcal{M}^4$  (P1–P4); globally unitary evolution in the Euclidean path-integral sense, with no fundamental collapse and no postulated stochastic term; no independent quantised metric field (the effective Lorentzian metric arises from the ordered-branch kinetic tensor, Section 3.6); no independent fundamental noise source added to an emergent gravitational equation; and non-factorisable correlations of the condensate state may persist across spatially separated regions as a natural feature of a collective medium.

**Level IIa — reduced coherent-effective description.** After partial tracing over unresolved condensate modes, the subsystem still retains coherent common-medium correlations. The effective regime is characterised by  $\Gamma_{\text{loop}} \lesssim 1$  (§30.1): mesoscopic interference survives, Euclidean path contributions remain operationally relevant, and non-factorisable condensate correlations are not yet decohered. The description is reduced, but not yet fully classical.

**Level IIb — reduced macroscopic classical-looking description.** For strong-locking, decohered regimes ( $\Gamma_{\text{loop}} \gg 1$ ), reduced effective dynamics yields an effectively classical gravitational sector: ordinary Einstein/Newton behaviour, effective irreversibility, entropy growth under Gaussian–Markov closure (§26.4), and reduced thermal appearance near strong-field causal interfaces (critical shell; Section 36). The macroscopic gravitational phenomenology developed in Part II should therefore be read as a Level IIb output of the same underlying ordered medium, not as evidence that gravity is fundamental in the same sense as in metric-first approaches.

**Bridge between levels.** The transition from Level I to Level IIa or IIb is a reduction, not a collapse postulate and not an added stochastic law. The same Level I physics produces different Level II effective descriptions in different regimes, parametrised by  $\Gamma_{\text{loop}}$  and by the relevant mass, separation, time, and

environmental coupling scales of the observable protocol. Not every reduced description is already classical: the Level IIa/IIb distinction is essential to avoid conflating mesoscopic coherent regimes with macroscopic classical ones.

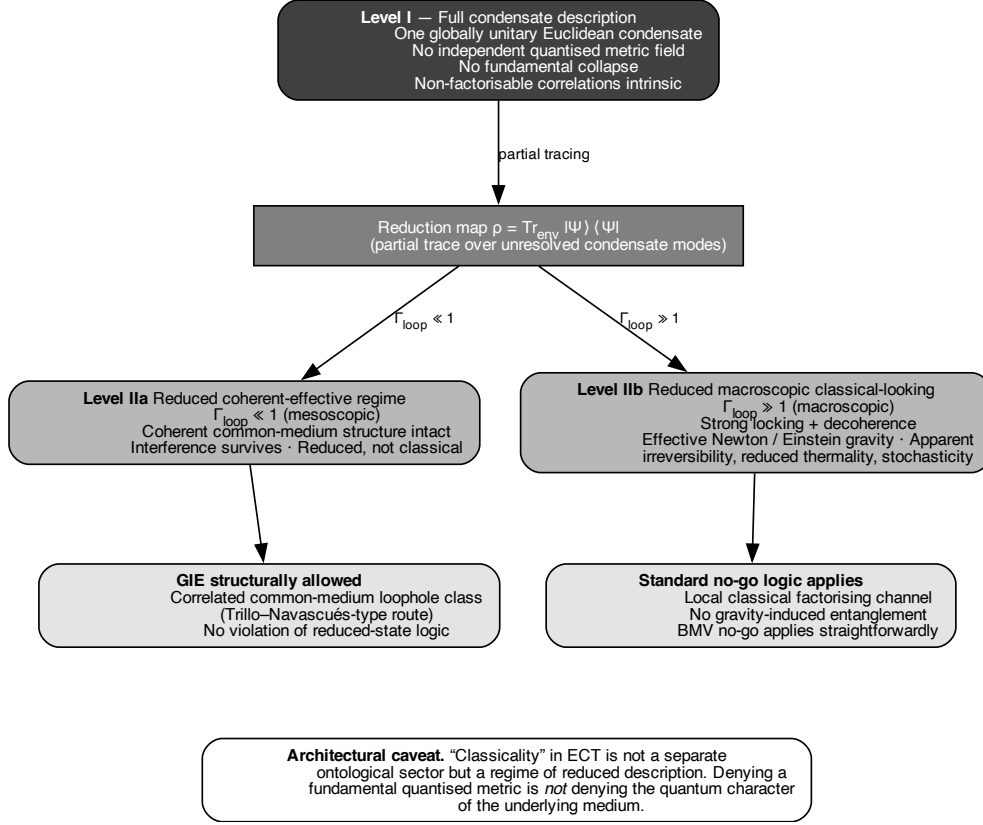


**Figure 35:** Two-level ontology of the hybrid-consistency architecture (Sections 28, 28.3). Level I is the full condensate description: one globally unitary Euclidean condensate with non-factorisable correlations. The reduction map  $\rho = \text{Tr}_{\text{env}} |\Psi\rangle\langle\Psi|$  produces two operational regimes. Level IIa (reduced coherent-effective,  $\Gamma_{\text{loop}} \ll 1$ ) retains coherent common-medium structure and is the natural regime of the Trillo–Navascués-type loophole class; gravity-induced entanglement is structurally allowed there. Level IIb (reduced macroscopic classical-looking,  $\Gamma_{\text{loop}} \gg 1$ ) behaves as ordinary Einstein/Newton gravity under strong locking; the standard Bose–Marletto–Vedral no-go logic applies directly. “Classicality” in ECT is not a separate ontological sector but a regime of reduced description. (Level B, structural.)

## 28.4 Costs of consistency across frameworks

Each candidate architecture for the gravity–matter interface pays a characteristic price for consistency. Table 90 summarises the main frameworks along four axes: the fundamental mediator picture, whether fundamental stochasticity or irreversibility is postulated, whether global unitarity is maintained at the full-theory level, and the principal consistency cost.

**Table 90:** Costs of consistency for gravity–matter architectures. The entries are qualitative structural summaries; detailed references are given in the surrounding text.

Framework	Fundamental media- tor picture	Fundamental stochasticity / irreversibility	Global unitarity	Main cost	consistency
Linearised quantum gravity / graviton EFT	Quantised gravita- tional mediator	No / No	Yes	Quantised metric sector; UV non- renormalisability	
Semi-classical Møller– Rosenfeld	Classical expectation-value geometry	No / No	Problematic in super- position regimes	Hybrid inconsis- tency tensions (Eppley–Hannah, Page–Geilker)	
Newton–Schrödinger class	Classical self- potential in non- linear QM	No / No	Modified	Non-linearity of QM; in the standard additive two-body form, no mediator- based entanglement generation	
PCCG / Oppenheim	Classical metric with fundamental stochas- tic law	Yes / Yes	No	Fundamental stochas- ticity and information loss	
Measurement- feedback hybrids	Monitored classical channel	Yes / Yes	No	Explicit moni- toring/feedback architecture	
Phenomenological Diósi–Penrose col- lapse	Correlated classical noise / collapse law	Yes / Yes	No	Free collapse scale $R_0$ ; experimental con- straints	
ECT (this work)	Emergent reduced mediator from one condensate	No / No (funda- mentally)	Yes (in- tended full-theory level)	Reduction map must recover all effective costs	

Read column-by-column, every candidate pays somewhere. ECT takes a different route: it does not postulate these costs at the fundamental level, but instead places the burden on a unified ordered-medium architecture in which irreversibility, decoherence, effective thermality, and classical-looking gravity must all be rederived as consequences of Level I→Level II reduction in the appropriate regime. Whether this architectural choice succeeds depends on the open items in the status map and on the falsifiers stated in Section 38.4.

## 28.5 Bridges to the rest of Part III

**To the Diósi–Penrose reading.** In the present reading, the Diósi–Penrose timescale [188, 189] is interpreted not as evidence for a fundamental collapse law, but as a structurally determined reduced-state limit of condensate distinguishability. The UV scale that fixes it is the structurally determined  $\xi_{\text{cond}} \sim \ell_{\text{Pl}}$ , not a free phenomenological parameter to be fitted against the underground X-ray bound [204] or the levitated-optomechanics bounds [205, 206].



**To the black-hole sector.** The same architecture is intended to underwrite the strong-field sector: reduced thermality and Page-curve-type behaviour, if realised, must arise from Level I→Level II reduction rather than from fundamental information destruction (Section 36).

**To the falsifiers.** The falsifiers stated in Section 38.4 are precisely aimed at this architectural claim: they do not merely test isolated formulas, but test whether the reduced-state reading can consistently replace fundamental stochastic or collapse-type laws.

## 28.6 Scope and non-claims

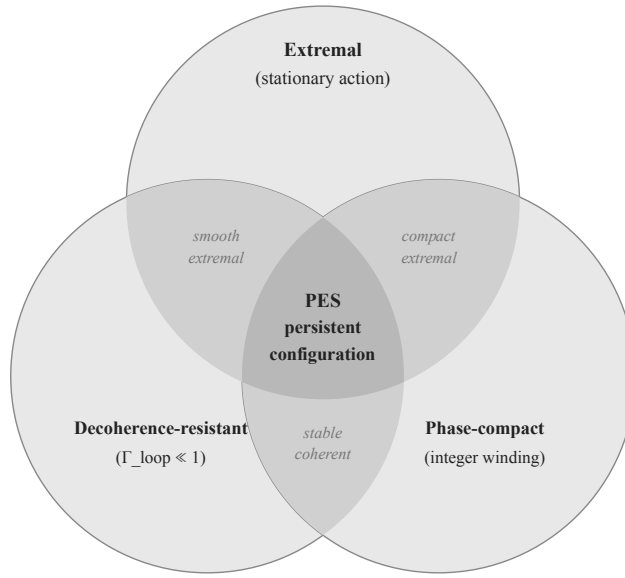
The present section does not claim: (i) a closed-form completion of the full non-linear Level I dynamics; (ii) a microscopic derivation of the Level I→Level II reduction for arbitrary coarse-grainings; (iii) a strong Level-A prediction of BMV-type gravity-induced entanglement; (iv) a complete solution of the single-outcome measurement problem or an explicit Page-curve derivation from first principles. Its claim is narrower: ECT provides a single ontological architecture within which these programmes are jointly well-posed and can be assessed by common structural criteria.

**Forward connection.** The next section introduces the Principle of Euclidean Stationarity as one concrete organising principle through which the Level I→Level II transition becomes physically legible in the quantum, decoherence, and persistence sectors.

## 29 Principle of Euclidean Stationarity

*Status: Level B for the core physical content (persistent configurations minimise Euclidean non-stationarity and therefore minimise environmentally induced decoherence). Programme-level conjecture for the universal scope (all discreteness, all stability, all quantisation from one selection mechanism). Connection: the coherent-phase dynamics (§21.2), the saddle-dominance and extremal-action backbone (§22.2), the influence-functional and decoherence programme (§26.1), and the quantum–classical boundary (§30.1).*

The preceding chapters have established three structural ingredients: (i) the coherent branch admits loop sectors with a minimal action scale  $S_0$  (§21.2); (ii) the saddle-point / extremal-action backbone selects dominant contributions to the Euclidean functional integral (§22.2); (iii) the influence-functional reduction provides a quantitative decoherence criterion  $\Gamma_{\text{loop}}$  that separates the quantum and classical regimes (§26.1). The present section identifies a single organising principle that unifies these three ingredients and gives them a common physical explanation (Fig. 36).



Observable quantum states = configurations satisfying  
all three conditions simultaneously

**Figure 36:** The Principle of Euclidean Stationarity (PES): three conditions whose simultaneous satisfaction defines *persistent configurations* — the ECT structural counterpart of observable quantum states. **Extremal:** the configuration satisfies the variational equations of the ordered branch. **Decoherence-resistant:** the configuration maintains  $\Gamma_{\text{loop}} \ll 1$  under environmental coupling. **Phase-compact:** the configuration has a well-defined integer winding number. The centre of the diagram represents the intersection of all three requirements. PES is an organising principle (Level B), not a replacement for sector-specific derivations.

## 29.1 Statement of the principle

### Short formulation.

**Principle of Euclidean Stationarity (PES).** *In ECT, the physically persistent and observable sector is selected by those condensate-compatible configurations that simultaneously belong to an admissible phase-topological class, are stationary or quasi-stationary extremals of the Euclidean action, and minimise the environmentally induced decoherence functional. Configurations that fail any of these conditions decohere and are effectively absorbed into the Lorentzian classical branch.*

**Why this is not a new postulate.** PES is not introduced as an independent axiom. It is a structural consequence of three elements already present in the theory: (i) the Euclidean-first ontology (P1), which produces a  $e^{-S_E/S_0}$ -weighted functional integral; (ii) the compact phase topology of the condensate (BR1), which restricts admissible configurations to integer-winding classes; (iii) the influence-functional reduction (§26.1), which exponentially suppresses configurations that strongly couple to the environment. PES names the combined selection effect of these three ingredients and draws out its consequences.

## 29.2 Formal realisation

**Effective selection functional.** A minimal mathematical realisation of PES is provided by the effective selection functional

$$\mathcal{J}_{\text{PES}}[\Psi] = \frac{S_E[\Psi]}{S_0} + \Gamma_{\text{env}}[\Psi], \quad (29.1)$$

subject to the phase-topological constraint  $\oint \nabla \theta \cdot d\ell = 2\pi n$  ( $n \in \mathbb{Z}$ ) and unit normalisation  $\|\Psi\|^2 = 1$ . Here  $S_E[\Phi]$  is the Euclidean action of the configuration,  $S_0$  is the pre-quantum action scale (§21.2), and  $\Gamma_{\text{env}}[\Psi]$  is the effective decoherence cost of the configuration induced by environmental coupling. In the minimal PES realisation, observed persistent configurations are modelled as satisfying  $\delta \mathcal{J}_{\text{PES}} = 0$ ,  $\delta^2 \mathcal{J}_{\text{PES}} \geq 0$ .

**Proxy model for  $\Gamma_{\text{env}}$ .** A natural proxy measure of Euclidean non-stationarity is provided by the functional

$$\Gamma_{\text{env}}[\Psi] = \frac{\tau}{S_0} \int d^3x \kappa(\mathbf{x}) |\partial_w \Psi(\mathbf{x}, w)|^2, \quad (29.2)$$

where  $\kappa(\mathbf{x}) \geq 0$  is an effective environmental locking kernel encoding the local density of medium degrees of freedom. This form is consistent with the  $\Gamma_{\text{loop}}$ -apparatus already developed in §26.1: configurations with  $\partial_w \Psi = 0$  minimise the environmental penalty, while large  $w$ -variations incur rapid decoherence. The proxy (29.2) should be read as the simplest functional form compatible with the structural requirements, not as a first-principles derivation from the full ECT action. A rigorous derivation of  $\Gamma_{\text{env}}$  from the bare Euclidean path integral remains an open target (OP-PES-1).

**Distinction: stationarity, disturbance, action.** PES involves three related but logically distinct concepts: (i) *stationarity* ( $\partial_w \Psi = 0$ ): the configuration does not vary along the fourth spatial direction; (ii) *minimal Euclidean disturbance*: the configuration minimises  $\Gamma_{\text{env}}$ ; (iii) *extremal action*: the configuration satisfies  $\delta S_E = 0$ . In the persistent sector all three conditions are satisfied simultaneously. Outside this sector they need not coincide: a configuration may be stationary but not action-extremal (wrong boundary class), or action-extremal but strongly non-stationary (large  $\partial_w \Psi$ ). PES selects the intersection:

$$\text{observable persistent sector} = \text{extremal sector} \cap \text{decoherence-resistant sector} \cap \text{phase-compact sector}. \quad (29.3)$$

### 29.3 Immediate consequences

#### Origin of discrete spectra

Discrete energy levels in bound systems are not a separate axiom in ECT but a consequence of the triple PES selection. In a spatially bounded region (atom, quantum well), the simultaneous requirements of phase compactness ( $\oint \nabla \theta \cdot d\ell = 2\pi n$ ), stationarity ( $\partial_w \Psi = 0$ ), and normalisability admit only a discrete set of solutions. Each solution is a “quiet mode” of the condensate: a configuration compatible with the medium topology that does not disturb the environment.

PES explains the *origin* of discreteness—why only a discrete set of configurations is physically persistent—but does not by itself replace the spectral calculation of a specific system. The full spectrum of a given Hamiltonian still requires solving the corresponding eigenvalue problem; what PES adds is the physical reason why eigenvalue problems are the right mathematical structure in the first place.

#### The extremal-action principle as a survival theorem

In standard physics the principle  $\delta S = 0$  is a mathematical axiom without a physical explanation: *why* does nature select extremal-action paths? PES provides a candidate answer.

Configurations with non-extremal action satisfy  $\delta S_E \neq 0$  and therefore have larger Euclidean disturbance (29.2): their  $|\partial_w \Psi|^2$  is generically larger than that of the nearby extremal. They decohere faster and are effectively absorbed into the classical Lorentzian branch. Near-extremal configurations survive longest.

PES therefore suggests a physical underpinning of the extremal-action principle: near-extremal configurations are the most decoherence-resistant and therefore dominate the persistent observable sector. This should be read as a physical underpinning of the extremal-action principle, not yet as a completed

formal theorem. Elevating it to a rigorous proposition requires an explicit bound relating  $|\delta S_E|$  to  $\Gamma_{\text{env}}$  (OP-PES-2).

### Stationary states as environmentally invisible configurations

Stationary quantum states ( $\partial_w \Psi = 0$ ) do not generate perturbations of the surrounding condensate along the fourth spatial direction. They are, in the language of PES, “invisible” to the environment and therefore occupy the most decoherence-resistant sector. Exact vanishing of the effective decoherence functional requires additional assumptions about isolation and environmental noise; in practice, stationary states *minimise* rather than exactly eliminate the decoherence rate.

Transitions between stationary states correspond to departures from the stationary Euclidean sector ( $\partial_w \Psi \neq 0$ ) and therefore involve nonzero coupling to condensate and/or environmental degrees of freedom, generating perturbations (photons, phonons) that increase  $\Gamma_{\text{loop}}$ .

### Connection to $S_0 = \hbar$

PES deepens the physical significance of the pre-quantum action scale  $S_0$  (§21.2). Within the reduced fixed-core loop closure used in the coherent-sector construction, the  $n = 1$  persistent winding configuration is assigned the characteristic action  $S_{\text{elem}} = 2\pi S_0$ . In the PES reading, this identifies  $S_0$  as the action scale associated with self-consistent persistent coherent winding, rather than as an arbitrary normalisation constant.

What PES adds is therefore a *physical interpretation* of the distinguished scale: sub-core or non-closing configurations do not count as persistent coherent loops in this reduced picture. However, PES does *not* by itself prove that  $2\pi S_0$  is a strict positive global infimum of the loop action over arbitrary loop lengths in the full  $n = 1$  sector. This strengthens the motivation for the identification  $S_0 = \hbar$  without changing its present Level B status.

### Gravitational sector: quantised by the same mechanism

If PES is universal across all condensate excitations, then the graviton sector—identified in §13.2 as the transverse-traceless part of the induced effective-metric perturbation—inherits the same action quantum  $S_0$ . This reframes the quantum-gravity programme: rather than quantising an independently given classical metric, ECT treats the gravitational sector as one more family of condensate excitations, subject to the same PES selection.

Two testable structural claims follow:

- (i) **Cross-sector action universality.** One and the same  $S_0$  governs matter, radiation, and gravitational excitations. Any experimental evidence for  $\hbar_{\text{grav}} \neq \hbar_{\text{EM}}$  would falsify ECT.
- (ii) **No separate external quantisation step.** Gravitational quantisation is reinterpreted as condensate-excitation quantisation under the same PES selection.

PES therefore suggests that the gravitational sector is quantised for the same structural reason as all other condensate excitations, thereby reframing—rather than automatically closing—the quantum-gravity programme. Full UV completion, non-linear quantum-gravity amplitudes, and black-hole microstate counting from first principles remain open (D13, OP-PES-3).

## 29.4 Stability, lifetimes, and the hierarchy of decay rates

*Status: programme-level. The qualitative hierarchy is structurally natural; quantitative decay widths require explicit matrix elements from the condensate action (OP-PES-4).*

**Stability from stationarity.** PES provides a physical interpretation of particle stability: configurations with  $\partial_w \Psi = 0$  are stationary, minimally disturb the condensate, and occupy the most decoherence-resistant sector and are naturally associated with the longest-lived excitations (up to residual environmental noise). PES suggests a unifying reading of stability: long-lived or exactly stable excitations should correspond to configurations that lie very close to the stationary, minimally disturbing sector. The proton, electron, and photon are natural benchmark cases for such a reading, but a first-principles derivation of their exact stability from PES remains outside the present scope.

**Instability from non-stationarity.** Unstable particles correspond to configurations with  $\partial_w \Psi \neq 0$ : they continuously disturb the condensate and are therefore coupled to the environment. The programme-level scaling law for the decay rate is:

$$\tau_{\text{life}}^{-1} \sim \gamma_0 \mathcal{N}_{\text{ns}}[\Psi], \quad \mathcal{N}_{\text{ns}}[\Psi] \equiv \frac{1}{S_0} \int d^3x \kappa(\mathbf{x}) |\partial_w \Psi|^2, \quad (29.4)$$

where  $\gamma_0$  is an overall rate scale and  $\mathcal{N}_{\text{ns}}$  is the non-stationarity measure. Eq. (29.4) should be read as a PES scaling ansatz for the lifetime hierarchy, not as a first-principles decay-width formula. This is a programme-level organising law, not yet a Standard-Model-precision calculation; deriving specific decay widths requires computing  $\mathcal{N}_{\text{ns}}$  for each particle from the condensate action.

**Qualitative hierarchy.** The PES picture is qualitatively consistent with the observed hierarchy of lifetimes: configurations with stronger non-stationarity (heavier resonances, larger coupling to the condensate) decay faster.

**Table 91:** Qualitative PES reading of particle lifetimes.

Particle	$\tau_{\text{life}}$	PES interpretation	Status
Proton	$> 10^{34}$ yr	Candidate stationary/topologically protected sector	Programme-level
Electron	Stable	Candidate stationary sector (lightest charged lepton)	Programme-level
Neutron (free)	879 s	Nearly stationary; weak-sector $\partial_w$ small	Qualitative
Muon	$2.2 \mu\text{s}$	Lepton-sector non-stationarity	Qualitative
Charged pion	26 ns	Larger non-stationarity	Qualitative
$W$ boson	$3 \times 10^{-25}$ s	Massive, strongly non-stationary	Qualitative

**Rydberg states: qualitative consistency only.** Highly excited atomic states are qualitatively consistent with the PES intuition that configurations with larger effective environmental exposure and larger accessible phase-space for decay are less robust than the most stationary bound states. However, the quantitative scaling of Rydberg lifetimes and decoherence rates is controlled by QED matrix elements, black-body effects, and cavity-specific environment modelling. The present ECT apparatus does not yet derive an independent Rydberg-specific exponent. Accordingly, Rydberg systems should presently be read as a qualitative consistency sector for PES, not as a completed ECT-specific prediction.

## 29.5 Unified quantisation table

PES identifies a common physical mechanism behind all known quantisation rules: the compact phase topology of the condensate combined with the stationarity selection. Table 92 collects these under a unified heading.

**Table 92:** Unified quantisation through PES. All entries share the same physical origin: compact condensate phase + PES selection.

Quantity	Quantum	ECT mechanism	Status
Action	$S_0 = \hbar$	Minimal self-consistent loop	Derived (B)
Elementary action	$h = 2\pi\hbar$	Full phase circuit $\Delta\theta = 2\pi$	Structural (A)
Bound-state spectrum	Discrete $\{E_n\}$	Phase compactness + stationarity + boundary conditions	Derived/structural (B)
Angular momentum	$L_z = m\hbar$	Compactness of $\phi \in [0, 2\pi)$	Structural (A)
Spin	$S = n\hbar/2$	SU(2) double cover of O(3)	Supported/structural route (B)
Electric charge	$q = ne$	U(1) gauge compactness	Programme-level (B/C)
Magnetic flux	$\Phi_0 = h/(2e)$	Superconducting condensate analogy	Supported analogy (B)
Gravitational action	$S_0 = \hbar$	Cross-sector universality	Prediction (B)
Area (quantum gravity)	$A_{\min} \sim \ell_{\text{Pl}}^2$	Minimal stationary graviton configuration	Programme-level prediction

## 29.6 Measurement, information, and decoherence: summary

The PES reading of measurement is developed in full in Section 30.1. The key results, presented there, include:

- interaction, in the strict event-based sense, is a Lorentzian concept; in the Euclidean regime, what replaces it is spatial correlation through the common condensate medium (§30.2);
- a qubit dephasing model exhibits a monotonic information–decoherence trade-off (eq. 30.4), strongly suggesting that fully informative measurements cannot preserve Euclidean coherence (§30.3);
- free photon propagation ( $\Gamma_{\text{loop}} \approx 0$ ) is naturally consistent with the Euclidean regime, while emission and absorption are Lorentzian coupling events.

## 29.7 Reverse-path suppression and tunnelling geometry: summary

The reverse-path suppression  $P_{\text{back}}/P_{\text{fwd}} = e^{-\Gamma_{\text{loop}}}$  (eq. 24.3) and the geometric reading of tunnelling as a spatial detour through the fourth Euclidean dimension (eq. 24.5) are developed in full in Section 24.1, where they appear as the path-dependent and barrier-traversal expressions of the same Euclidean coherent architecture.

## 29.8 The $\alpha \rightarrow \beta$ boundary and the geometric meaning of quantum coherence

*Status: programme-level conjecture. The mapping  $\Gamma_{\text{loop}} \leftrightarrow \alpha - \beta$  is not yet derived from first principles.*

**What happens at  $\alpha \rightarrow \beta$ .** The emergent speed of light is (D20, Level A):

$$c_* = \sqrt{\frac{\beta}{\alpha - \beta}}. \quad (29.5)$$

As  $\alpha \rightarrow \beta$  from above,  $c_* \rightarrow \infty$ : the light cone opens completely, the distinction between space and time degenerates, and the effective metric becomes Euclidean. At  $\alpha = \beta$  the Lorentzian branch ceases to exist. Below this threshold ( $\alpha < \beta$ ),  $c_*^2 < 0$  and the signature is strictly Euclidean.

**Conjectural bridge to decoherence.** A plausible geometric interpretation is that weak environmental locking (small  $\Gamma_{\text{loop}}$ ) corresponds to a local softening of the ordered Lorentzian branch, effectively bringing the system closer to the  $\alpha \rightarrow \beta$  boundary. In this picture:

- an isolated quantum system ( $\Gamma_{\text{loop}} \ll 1$ ) may be interpreted as probing a regime effectively closer to  $\alpha \approx \beta$ , where all four directions become more nearly equivalent and the causal cone is less rigidly selected;
- a macroscopically observed system ( $\Gamma_{\text{loop}} \gg 1$ ) may be interpreted as locked deep into the  $\alpha \gg \beta$  regime, where the causal cone is rigid and classical causality holds.

This provides a natural geometric language for entanglement (correlations in a near-Euclidean common medium), tunnelling (detour through a near-degenerate fourth dimension), and reverse-path coherence (return segments admissible when the cone is soft).

**What this does not yet establish.** The mapping  $\Gamma_{\text{loop}} \leftrightarrow \alpha - \beta$  is a programme-level conjecture. A derivation would require showing how the effective  $\alpha - \beta$  experienced by a subsystem depends on its environmental coupling strength. This is listed as OP-PES-5.

**Numerical scales of the Euclidean–Lorentzian boundary.** The  $O(4) \rightarrow O(3)$  transition sets the fundamental scales:

Scale	ECT value	Status	Physical meaning
Condensate VEV $\phi_0$	$\bar{M}_{\text{Pl}} = 2.435 \times 10^{18} \text{ GeV}$	Level B anchor	Symmetry-breaking amplitude
Condensation length $\xi_{\text{cond}}$	$\sim \ell_{\text{Pl}} = 1.6 \times 10^{-35} \text{ m}$	Level B estimate	Shortest coherent scale
Critical temperature $T_c$	$\sim \phi_0 \sqrt{6} \sim 6 \times 10^{18} \text{ GeV}$	Level B	Thermal estimate for the $O(4) \rightarrow O(3)$ transition
Transition energy	$\sim M_{\text{Pl}} \sim 10^{19} \text{ GeV}$	Order-of-magnitude	Planck-epoch interpretation

This table is a summary device, not a new derivation. Its purpose is to collect in one place the characteristic scales that are otherwise derived or motivated across different parts of the article. In particular, the  $T_c$  entry follows from the standard one-loop Dolan–Jackiw [207] effective potential for a  $\lambda \Phi^4$  order parameter: the thermal correction shifts the mass term by  $+\lambda T^2/6$ , so that the coefficient  $a(T) = -\mu^2 + \lambda T^2/6$  vanishes at  $T_c^2 = 6\mu^2/\lambda = 6\phi_0^2$ , giving  $T_c = \phi_0 \sqrt{6} \approx 5.96 \times 10^{18} \text{ GeV}$ . This is a Level B thermal estimate obtained by combining the ECT identification of the order-parameter scale  $\phi_0$  with the standard Dolan–Jackiw one-loop finite-temperature correction for a  $\lambda \Phi^4$  order parameter; it is not yet a first-principles finite-temperature derivation from the microscopic ECT action. The first two entries are structural scales already used elsewhere in the ordered-branch construction, whereas the last two are synthesis entries collecting the thermal and cosmological reading of the same transition scale.

## 29.9 Gravitational decoherence from the condensate: summary

The condensate itself acts as the gravitational environment: a mass in superposition of two positions creates two distinct condensate configurations whose overlap decays as  $e^{-\Gamma_{\text{grav}}}$ , recovering the Diósi–

Penrose timescale  $\tau \sim \hbar R / (G_N m^2)$ . The nanosphere regime ( $R \sim 1 \mu\text{m}$ ,  $m \sim 8 \times 10^{-15} \text{ kg}$ ,  $\tau \sim 38 \text{ ms}$ ) is the experimental frontier. For the full derivation and numerical estimates, see Section 26.3 in §26.1.

## 29.10 What PES changes in the quantum programme

Table 94 summarises how PES modifies the interpretive and structural landscape of the quantum sector.

**Table 94:** Impact of PES on the quantum programme.

Topic	Before PES	After PES
Quantisation	Structural (from phase topology)	Physically grounded: persistent = phase-compact + stationary + decoherence-resistant
Wavefunction collapse	Decoherence-only reading	Euclidean-to-Lorentzian transition via $\Gamma_{\text{loop}}$
Extremal action	Formal mathematical principle	Physical underpinning: near-extremal configurations are interpreted as the most decoherence-resistant sector
Particle stability	Empirical / classification by quantum numbers	Physically grounded: long-lived states are interpreted as lying close to the stationary, minimally disturbing sector
Graviton quantisation	Open structural route	Structurally unified: same $S_0$ , same PES
$S_0 = \hbar$	Level B matching	Deepened physical interpretation of the $S_0$ -programme; still not a proof of a strict global positive lower bound for the elementary-loop action

## 29.11 What PES does not yet prove

The following central outputs remain beyond the current reach of PES:

- (i) A first-principles derivation of  $\Gamma_{\text{env}}$  from the bare Euclidean path integral (OP-PES-1).
- (ii) A rigorous bound relating  $|\delta S_E|$  to  $\Gamma_{\text{env}}$ , which would elevate the survival-theorem reading of the extremal-action principle to Level A (OP-PES-2).
- (iii) Full UV completion and non-linear quantum-gravity amplitudes from the condensate action (OP-PES-3, D13).
- (iv) Quantitative decay widths from  $\mathcal{N}_{\text{ns}}$  (OP-PES-4).
- (v) A completed derivation of all spectra from PES alone (PES explains the origin of discreteness but does not replace spectral engineering).
- (vi) A full spin-statistics theorem.
- (vii) A completed Born rule as an unconditional theorem.
- (viii) The quantitative mapping  $\Gamma_{\text{loop}} \leftrightarrow \alpha - \beta$ , which would connect PES to the geometric Euclidean–Lorentzian boundary (OP-PES-5).



**What PES does and does not identify.** PES does not identify stationarity, minimal Euclidean disturbance, and extremal action as universally identical notions. Rather, it states that the persistent observable sector lies at their intersection. This distinction is essential: a configuration may satisfy one of these conditions without satisfying the others.

PES is therefore a *centrally derived organising principle with a partially proven technical core and a large predictive programme around it*, not a completed final theorem of the entire quantum sector.

### 30 Quantum–Classical Boundary, Probability, Born Rule, and Measurement Status

*Inputs: the Hilbert-space and projector route (§23.1), the global/reduced unitarity distinction (§23.2), coherent amplitude structure from Sections 21–23, the decoherence and arrow-of-time programme (§26.1, §26.4), the reverse  $O(3) \rightarrow O(4)$  Euclidean logic, and medium character (P5). Aim: to identify the quantum–classical boundary, explain why decoherence is not yet the Born rule, and state what ECT can and cannot currently establish about probability and measurement. Status: Level A for the structural admissibility of reverse  $O(3) \rightarrow O(4)$  Euclidean segments in the path integral (from P2), and for the distinction between coherent amplitudes and decohered reduced sectors. Level B for the quantitative quantum–classical boundary criterion  $\Gamma_{\text{loop}} \lesssim 1$ , for the amplitude  $\rightarrow$  decoherence  $\rightarrow$  effective-probability logical chain, and for the conditional uniqueness of Born-type weights once the required Hilbert/projector conditions are in place. A full first-principles derivation of the Born rule and a completed measurement-update theory remain open. Connections: the decoherence and arrow-of-time programme (§26.1, §26.4), the Hilbert-space route (§23.1), the global/reduced unitarity distinction (§23.2), and medium character (P5).*

#### 30.1 Quantum–classical boundary: reverse $O(3) \rightarrow O(4)$ transitions

*Status: Level A for the structural statement that the  $O(4)$ -invariant Euclidean action (P2) admits closed-loop configurations in which the ordered branch can locally lose its preferred  $O(3)$  orientation and re-enter the Euclidean  $O(4)$ -symmetric sector. Level B for the interpretation of such segments as the operative quantum–classical boundary mechanism and for the quantitative criterion  $\Gamma_{\text{loop}} \lesssim 1$  within the Gaussian–Markov decoherence closure. Connection: the two-sided Euclidean path-dependence (§24.1), the decoherence and arrow-of-time programme (§26.1), the Principle of Euclidean Stationarity (§29), the Crooks-type relation (§26.4), medium character (P5), and the global/reduced unitarity distinction (§23.2).*

The present section makes precise what is meant, in ECT language, by a reverse  $O(3) \rightarrow O(4)$  segment. The claim is not that laboratory systems literally reconstruct the full unbroken Euclidean phase of the microscopic theory. Rather, the claim is that the reduced description may partially leave the strongly locked Lorentzian regime and re-enter a weak-locking coherent regime in which Euclidean path contributions again become operationally relevant. In that restricted but physically meaningful sense, reverse coherence is not forbidden by the theory; it is suppressed.

#### Structural content of reverse transitions

As explained in the path-dependence discussion (§24.1), the ordered branch admits a forward/reverse asymmetry in the reduced description. In the present closure this asymmetry is quantified by Eq. (24.3),

$$\frac{P_{\text{back}}}{P_{\text{fwd}}} = e^{-\Gamma_{\text{loop}}}.$$

The same quantity that controls decoherence therefore also controls the effective weight of reverse Euclidean segments. For  $\Gamma_{\text{loop}} \ll 1$ , reverse contributions are not strongly suppressed and the coherent Euclidean description remains operationally relevant. For  $\Gamma_{\text{loop}} \gg 1$ , reverse segments are exponentially

suppressed and the reduced dynamics is well described by an effectively Lorentzian one-way branch. This is the sense in which the quantum–classical boundary is read here as a crossover between two sectors of the same condensate architecture, rather than as an independent axiom.

This statement should be read together with the decoherence programme (§26.1), the Crooks-type relation (§26.4), and the PES discussion (§29). The point is not that the system alternates between two unrelated theories, but that the same ordered medium admits both a weak-locking coherent regime and a strong-locking Lorentzian regime, with the operative crossover controlled by  $\Gamma_{\text{loop}}$ .

### **What reverse coherence does and does not mean**

The phrase “reverse coherence” must be interpreted carefully. It does *not* mean that present-day laboratory protocols already reconstruct the full bare  $O(4)$ -symmetric microscopic vacuum. Nor does it mean literal erasure of all macroscopic records. What it means in the present article is narrower: a partial reduction of environmental locking, such that the reduced description again becomes closer to the Euclidean coherent sector than to the strongly locked Lorentzian one.

Accordingly, reverse  $O(3) \rightarrow O(4)$  segments should be read as closure-level effective returns toward the coherent regime, not as a completed first-principles theory of macroscopic branch erasure. This distinction is important for consistency with the global/reduced unitarity discussion (§23.2): globally, the theory remains formulated on the full condensate configuration space, whereas the suppression or recovery of coherence is a statement about the reduced description obtained after tracing over untracked degrees of freedom.

### **Relation to known recoherence protocols**

With that qualification, standard recoherence protocols are naturally consistent with the ECT picture. Echo-type methods, dynamical decoupling, and related coherence-preserving techniques do not alter the fundamental condensate equations, but they can reduce the effective environmental monitoring load seen by the subsystem. In the present language this means reducing the operative  $\Gamma_{\text{loop}}$  and hence reducing the suppression of reverse Euclidean contributions in the reduced description.

This provides a natural ECT reinterpretation of familiar quantum-control phenomena. Spin echo may be read as cancelling the reversible part of accumulated dephasing; dynamical decoupling as suppressing the effective coupling to slow environmental modes; and more elaborate control architectures as engineering longer residence in the weak-locking coherent regime. Nothing in the present article requires these protocols to be described as literal returns to the microscopic symmetric phase. What is claimed is more modest and more precise: they are operationally consistent with partial returns toward the coherent Euclidean description.

The same remark applies to quantum-information platforms. Superconducting, trapped-ion, photonic, and other controlled coherent systems may be viewed, at programme level, as engineered settings in which Lorentzian locking is kept weak for longer times than in uncontrolled macroscopic matter. However, a first-principles ECT computation of platform-specific coherence times, thresholds, or logical error rates from the condensate action is not claimed here and remains open.

### **Status of the experimental programme**

The present status is therefore mixed but nontrivial. Structurally, ECT allows reverse segments and supplies a suppression law for their effective contribution. Operationally, it is consistent with the existence of mesoscopic recoherence phenomena whenever environmental locking can be sufficiently reduced. Quantitatively, however, the article presently establishes only the generic suppression logic and not a platform-dependent predictive framework for recoherence engineering.

This is why the relevant claims remain at Level B. The theory identifies the quantum–classical boundary with a regime-transition criterion rather than with an ad hoc measurement postulate, and it explains why partial recoherence is not logically forbidden. But the detailed reconstruction of echo,

decoupling, logical-qubit, or other laboratory protocols directly from condensate microdynamics belongs to the open programme beyond the present closure.

### 30.2 Measurement as Euclidean-to-Lorentzian transition

*Status: Level B for the physical reading of measurement as environmental Lorentzian locking via  $\Gamma_{\text{loop}}$ . Programme-level for the formal information–decoherence inequality.*

#### Interaction as a Lorentzian concept

In the Euclidean coherent regime ( $\Gamma_{\text{loop}} \ll 1$ ), the functional integral treats all configurations on an equal footing. There are no “events”, no temporal ordering, and no cause–effect sequences. What replaces Lorentzian interaction in this regime is not a sequence of local events but a common correlated condensate configuration. The notion of interaction—in which system  $A$  acts on system  $B$  at a definite spacetime point—presupposes a causal structure that exists only after the ordered branch has been selected.

Lorentzian interaction, in the strict event-based sense, is therefore an emergent concept associated with the ordered branch, not a primitive of the Euclidean substrate. In the Euclidean regime, what exists instead are spatial correlations through the common condensate medium.

#### Measurement as environmental locking

An act of measurement consists in coupling a microscopic system ( $\Gamma_{\text{loop}} \ll 1$ ) to a macroscopic apparatus whose internal degrees of freedom impose  $\Gamma_{\text{loop}} \gg 1$  in the combined system. The number of effective environmental degrees of freedom  $N_{\text{eff}}$  is not simply the number of atoms in the apparatus, but the number of medium modes that *actually couple* to the measured system during the interaction time. For the Arndt  $\text{C}_{60}$  experiment (§26.1),  $N_{\text{eff}}$  is computed explicitly from the residual-gas collision rate and is of order  $10^3$ – $10^4$ , not  $10^{23}$ . For a fully thermalised macroscopic detector,  $N_{\text{eff}}$  can approach Avogadro scales, but the precise value is experiment-dependent.

The resulting decoherence of off-diagonal reduced-state elements is not postulated as a separate measurement axiom but follows from the same influence-functional mechanism that produces the arrow of time (§26.1).

#### The persistent quantum sector as the sector of minimal environmental coupling

PES selects configurations of minimal effective environmental coupling. Stationary quantum states ( $\partial_w \Psi = 0$ ) are those that *do not disturb* the surrounding condensate. They are effectively invisible to the environment. The discrete energy levels of a bound system are precisely these “quiet modes”: configurations compatible with the condensate topology that generate no  $w$ -directed perturbation.

Transitions between stationary states ( $\partial_w \Psi \neq 0$ ) correspond to departures from the stationary Euclidean sector and therefore involve nonzero coupling to condensate and/or environmental degrees of freedom. In this reading, the apparent stability of quantum states is not a coincidence but a selection effect: configurations with larger effective environmental coupling decohere more rapidly, whereas the quiet modes remain in the most decoherence-resistant sector.

#### The photon as a Euclidean traveller

A photon propagating through vacuum is isolated from the environment:  $N_{\text{eff}} \approx 0$ ,  $\Gamma_{\text{loop}} \approx 0$ . It resides in the Euclidean coherent regime: no definite trajectory, all paths contribute to the functional integral. This is consistent with the relativistic fact that proper time vanishes along a null geodesic:  $ds^2 = 0$  for a photon. In ECT, the correspondence is direct:

$$\text{proper time} = 0 \quad \text{is naturally consistent with} \quad \Gamma_{\text{loop}} \approx 0 \quad (\text{Euclidean regime}). \quad (30.1)$$

Upon reaching a macroscopic detector ( $\Gamma_{\text{loop}} \gg 1$ ), the photon is absorbed at a definite point—the Euclidean-to-Lorentzian transition occurs, and the “collapse” takes place.

Emission and absorption are Lorentzian events (involving macroscopic sources and detectors with  $\Gamma_{\text{loop}} \gg 1$ ); propagation between them is Euclidean. In the PES reading, free propagation of an isolated photon is described by a coherence-preserving Euclidean sector with negligible environmental locking, whereas emission and absorption are Lorentzian coupling events.

### 30.3 Information–decoherence bound

*Status: Level B for the two-level system; programme-level for general systems.*

#### Derivation for a two-level system

Consider a qubit in the maximally coherent state  $|\psi\rangle = (|0\rangle + |1\rangle)/\sqrt{2}$ , subject to Gaussian dephasing with decoherence parameter  $\Gamma$ . After interaction with the environment, the reduced density matrix is

$$\rho'_S = \begin{pmatrix} 1/2 & e^{-\Gamma}/2 \\ e^{-\Gamma}/2 & 1/2 \end{pmatrix}, \quad (30.2)$$

with eigenvalues  $\lambda_{\pm} = (1 \pm e^{-\Gamma})/2$ . The von Neumann entropy of the reduced state is

$$S(\rho'_S) = -\frac{1+e^{-\Gamma}}{2} \ln \frac{1+e^{-\Gamma}}{2} - \frac{1-e^{-\Gamma}}{2} \ln \frac{1-e^{-\Gamma}}{2}. \quad (30.3)$$

For a pure total state (unitary system–environment evolution), the mutual information is  $I(S:E) = 2S(\rho'_S)$ . Using the binary entropy function  $h_2$ :

$$I(S:E) = 2h_2\left(\frac{1+e^{-\Gamma}}{2}\right). \quad (30.4)$$

#### Asymptotics and physical interpretation

At small decoherence ( $\Gamma \ll 1$ ):

$$I(S:E) \approx \Gamma \ln \frac{2e}{\Gamma} + O(\Gamma^2). \quad (30.5)$$

Information extraction is proportional to decoherence: a small  $\Gamma$  yields a small amount of information.

At full decoherence ( $\Gamma \gg 1$ ):  $I(S:E) \rightarrow 2 \ln 2$  (the maximum for a qubit).

The dephasing qubit model therefore exhibits a monotonic information–decoherence trade-off: larger mutual information requires larger decoherence. However, the model does not by itself define a universal one-bit threshold for arbitrary measurement protocols.

In the dephasing qubit model, the system–environment mutual information grows monotonically with the decoherence parameter  $\Gamma$ . This demonstrates an explicit information–decoherence trade-off: extracting more information about the system requires stronger environmental coupling and hence greater loss of coherence. However, mutual information is not identical to the accessible classical measurement record, and the dephasing qubit model does not by itself establish a universal one-bit threshold for arbitrary measurement protocols. Establishing such a bound model-independently remains an open target (OP-PES-6).

#### Weak measurements

Individual weak-measurement acts with  $\Gamma_{\text{loop}}^{(i)} \ll 1$  partially preserve coherence but extract correspondingly little information per act:  $I^{(i)} \approx \Gamma^{(i)} \ln(2/\Gamma^{(i)})$  in the simple dephasing model. For repeated weak interactions, the cumulative information extracted from the system remains controlled by the cumulative

decoherence budget. In the same dephasing picture this suggests a trade-off of the same qualitative form as the single-act result, but a protocol-independent multi-step bound remains open. Classical post-processing of weak results does not create new information. Complete state tomography of a single system requires cumulative decoherence of order unity and therefore destroys the coherence of that individual copy; tomography is possible only for an ensemble of identically prepared systems.

**Can one observe without collapse?** The information–decoherence trade-off answers this question quantitatively within the qubit dephasing model. For a qubit, the maximum extractable mutual information is 2 bits. Here  $I(S:E)$  is the full mutual information between the qubit and its environment, not the classical readout capacity of a binary detector. For a maximally entangled pure qubit–environment state this quantity can reach 2 bits, whereas the practically relevant threshold for a single binary record remains of order 1 bit. The trade-off gives:

$I(S:E)$ [bits]	$\Gamma_{\text{loop}}$ needed	Coherence remaining
0.1	0.01	99%
0.5	0.09	92%
1.0	0.25	78%
1.5	0.56	57%
1.9	1.34	26%
$\rightarrow 2$	$\rightarrow \infty$	$\rightarrow 0$

The trade-off is visualised in Fig. 37. The structural conclusion is that any measurement extracting  $\gtrsim 1$  bit of information reduces coherence by at least  $\sim 22\%$ ; a nearly complete observation ( $I \gtrsim 1.9$  bits) requires  $\Gamma_{\text{loop}} \gtrsim 1.3$  and destroys most of the Euclidean coherence. Within the qubit dephasing model, the table shows that extracting near-complete information is inseparable from a substantial loss of coherence. In that sense, fully informative single-copy observation without strong collapse-like degradation does not occur in this model. This is, however, still a Level B conclusion of the present dephasing closure, not yet a protocol-independent theorem for all possible measurement architectures. Nothing in the present argument excludes weak or distributed information-extraction protocols on ensembles of similarly prepared systems.

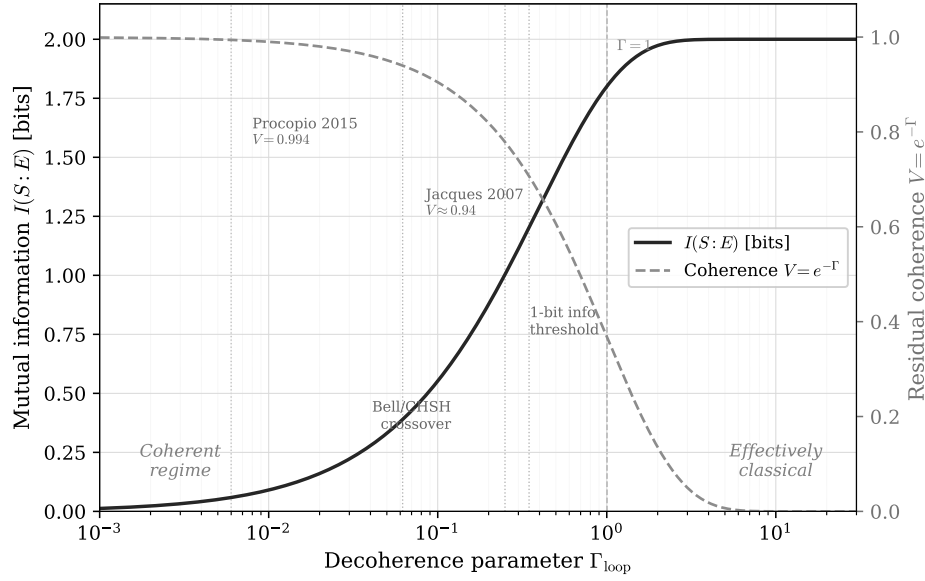


**Figure 37:** Qubit information–decoherence trade-off in the ECT dephasing closure (Eq. 30.4). Solid curve: mutual information  $I(S:E)$  in bits as a function of the decoherence parameter  $\Gamma_{\text{loop}}$ . Dashed curve: residual coherence  $V = e^{-\Gamma}$  (right axis). Vertical dotted lines mark operational anchors from ECT-calibrated experiments: Procopio 2015 ( $V = 0.994$ , quantum switch), Jacques 2007 ( $V \approx 0.94$ , delayed-choice interferometer), the one-bit information threshold ( $\Gamma \approx 0.25$ ), and the Bell/CHSH crossover ( $\Gamma = \ln \sqrt{2} \approx 0.35$ ). The dashed vertical line at  $\Gamma = 1$  separates the coherent and effectively classical regimes. This is a Level B closure result for the specific dephasing model, not a protocol-independent theorem. Numerical details are given in Appendix BA.

What is constrained here is the prospect of obtaining near-complete single-copy information while retaining essentially full coherent-branch visibility for that same copy.

**Scope and open status.** The qubit dephasing model shows explicitly that information extraction and decoherence are tied to the same coupling parameter. This strongly suggests that fully informative single-copy measurements cannot be achieved without driving the system toward the Lorentzian locked regime. However, a model-independent theorem establishing a universal lower bound on  $\Gamma_{\text{loop}}$  for any informative observation requires a separate derivation of the relation between accessible record information and the decoherence functional, and remains an open target (OP-PES-6).

This reverse-traversal picture is the complementary path-integral reading of the two-sided Euclidean boundary dependence already discussed in Section 24.1.

**Euclidean meaning of the reverse segments.** The reverse  $O(3) \rightarrow O(4)$  segments discussed in this subsection are Euclidean path-integral configurations, not literal backward-in-time events in Lorentzian laboratory time. They describe portions of closed Euclidean histories in which the ordered branch locally loses its preferred orientation before the full configuration is continued back to the effective Lorentzian reading. No signalling to the past is implied. The point of the construction is not retrocausality in the operational sense, but the structural fact that the Euclidean coherent sum admits both forward ordered segments and local returns toward the disordered sector unless environmental suppression renders such contributions effectively negligible.

**Medium reading (P5).** Under the medium interpretation (P5), the reverse  $O(3) \rightarrow O(4)$  segments acquire a concrete physical reading: along such Euclidean segments the ordered condensate locally loses the stable orientation characteristic of the Lorentzian branch and moves back toward the disordered  $O(4)$  sector. One may heuristically describe this as a local “melting” of order, but this language is only pictorial. What is used in the argument is simply that the ordered medium need not remain rigidly ordered along

every contributing Euclidean history. Quantum behaviour corresponds to the regime in which such local loss of order is not yet effectively suppressed in the reduced description.

A closed loop in  $\mathcal{M}^4$  necessarily passes through field configurations in which the local orientation  $n_A(X)$  deviates from the global vacuum direction  $\langle n_A \rangle = \delta_{Aw}$ . Along the return segment of a loop (traversed in the  $-w$  direction), the condensate locally resides in a configuration where  $\langle n_A(X) \rangle \approx 0$ , i.e. the local symmetry is temporarily restored from  $O(3)$  back towards  $O(4)$ .

Such reverse  $O(3) \rightarrow O(4)$  segments are not excluded by the symmetry structure of the Euclidean theory. Because the Euclidean action  $S_E[\Phi]$  is  $O(4)$ -invariant, local departures from the ordered  $O(3)$  orientation are structurally admissible within the path integral. Their actual quantitative weight, however, is determined by the full action and need not be comparable to that of purely ordered segments. The net amplitude for a closed path involves the sum over all intermediate configurations, including those with  $n_A(X_m) \neq \delta_{Aw}$ :

$$\mathcal{A}(X_i \rightarrow X_i) = \int_{\text{loops}} \mathcal{D}[\Phi] e^{-S_E[\Phi]}, \quad (30.6)$$

where the integral runs over all closed field configurations, including those that locally restore  $O(4)$  symmetry.

The structural point of Eq. (30.6) is not that all reverse segments contribute with comparable weight, but that such segments are not excluded by the symmetry structure of the Euclidean theory. Their actual relevance is controlled by the action weight and, at the reduced-description level, by the decoherence functional  $\Gamma_{\text{loop}}$  introduced below.

The interference of the forward ( $O(4) \rightarrow O(3)$ ) and backward ( $O(3) \rightarrow O(4)$ ) segments provides the ECT-specific structural reading of why quantum amplitudes persist in the coherent regime.

The suppression of backward traversal is governed by the irreversible part of the influence functional  $\Delta\Gamma_{\text{irr}}$ . For  $N_{\text{eff}} = 1$  (single quantum system),  $\Delta\Gamma_{\text{irr}} \ll 1$ : backward and forward traversal are essentially equiprobable, and the condensate field explores both  $O(4) \rightarrow O(3)$  and  $O(3) \rightarrow O(4)$  transitions — their superposition produces quantum interference. For a macroscopic body ( $N_{\text{eff}} \sim 10^{23}$ ),  $\Delta\Gamma_{\text{irr}} \gg 1$ : reverse transitions are exponentially suppressed and only the forward causal direction survives.

The quantum–classical boundary in ECT is therefore determined by whether reverse  $O(3) \rightarrow O(4)$  transitions contribute non-negligibly to the path integral. The condition  $\Gamma_{\text{loop}} \lesssim 1$  is a quantitative criterion for when such contributions matter:

- $\Gamma_{\text{loop}} \ll 1$ : quantum regime, interference visible, time reversal approximately intact;
- $\Gamma_{\text{loop}} \gg 1$ : classical regime; under the effective ohmic/Markov closure (Section 3.9), macroscopic entropy growth and a preferred time direction follow.

This provides a single quantitative ECT criterion for the quantum–classical boundary, without introducing a separate measurement postulate.

**Connection to decoherence and the arrow-of-time programme.** The criterion  $\Gamma_{\text{loop}} \lesssim 1$  is not an independent postulate. It is the same reduced irreversible suppression functional that was developed in Section 26.1 and then used in Section 26.4 to organise the effective arrow of time. What is new in the present subsection is the path-integral reading of that suppression. In the quantum regime, reverse segments toward the  $O(4)$  sector remain effectively available and interference survives. In the classical regime, such reverse segments become exponentially suppressed in the reduced description, and the effective directional behaviour described in Section 26.4 takes over.

**Discriminant: ECT boundary versus standard decoherence crossover.** Standard decoherence theory identifies the quantum–classical boundary through the timescale on which environmental monitoring suppresses interference. ECT reproduces that effective crossover, but adds a condensate-level reading: classicality is the regime in which Euclidean histories containing local returns toward the disordered  $O(4)$  sector cease to contribute appreciably in the reduced description. The distinctive ECT content is therefore

not a new phenomenological timescale, but a different ontological interpretation of what the boundary means.

**Falsifier for the quantum–classical boundary programme.** The present programme would be challenged if a completed microscopic analysis showed that reverse  $O(3) \rightarrow O(4)$  segments are already forbidden or negligibly weighted in the bare Euclidean theory, independently of environmental suppression. That would make the boundary fundamentally microscopic rather than an effective reduced-state phenomenon. It would also be weakened if the completed decoherence analysis yielded a crossover structure incompatible with the  $\Gamma_{\text{loop}}$  criterion used here. At present, no such incompatibility is known.

**Empirical anchor.** The decoherence-controlled quantum–classical boundary is consistent with the observed phenomenology of mesoscopic interference: matter-wave interference for increasingly massive molecules is maintained under sufficiently clean conditions and is rapidly lost when environmental monitoring grows [185]. This supports the general crossover logic expressed here through  $\Gamma_{\text{loop}} \lesssim 1$ . At the present stage, however, such experiments do not uniquely test the ECT reading in terms of reverse  $O(3) \rightarrow O(4)$  Euclidean segments; they test only the effective boundary itself.

**Status summary.** *Established (Level A):* the  $O(4)$ -invariant Euclidean action admits closed-loop configurations in which the ordered branch can locally lose its preferred orientation and re-enter the disordered  $O(4)$  sector. Such reverse segments are therefore structurally available in the Euclidean path-integral description.

*Level B:* the quantitative quantum–classical boundary criterion  $\Gamma_{\text{loop}} \lesssim 1$  within the Gaussian–Markov decoherence closure. In the quantum regime ( $N_{\text{eff}} \sim 1$ ), reverse segments remain effectively relevant and interference survives; in the classical regime ( $N_{\text{eff}} \gg 1$ ), they are exponentially suppressed in the reduced description.

*Open:* (i) a fully microscopic derivation of the  $\Gamma_{\text{loop}}$  criterion beyond the Gaussian–Markov closure; (ii) a completed calculation of the bare Euclidean weighting of reverse segments in realistic systems; (iii) an experimental isolation of a regime in which the ECT reading of the boundary becomes distinguishable from the standard decoherence crossover.

**Bridge to the probability and measurement analysis.** The present subsection identifies when coherent histories continue to interfere and when they become effectively classical. That boundary does not yet yield a Born rule or a completed measurement theory by itself, but it provides the regime distinction on which the next subsections depend: only after the quantum–classical boundary is understood does it become meaningful to ask how reduced weights are read probabilistically and what status measurement outcomes acquire in ECT.

### 30.4 Probability, Born-type interpretation, and measurement status

*Status: Level A for the distinction between coherent amplitudes, decohered reduced sectors, and effective probability candidates. Level B for the conditional uniqueness of Born-type weights once a Hilbert/projector structure and additive probability measure on decohered alternatives are admitted. A full first-principles derivation of the Born rule and a completed measurement-update theory remain open. Connection: wave-kinematical organisation (§22.1), canonical structure (§23.3), reflection positivity and Hilbert-space route (§23.1), global/reduced unitarity (§23.2), decoherence (§26.1), and the quantum–classical boundary (§30.1).*

The previous subsections established three ingredients of the coherent branch: (i) a wave-dynamical description, (ii) a canonical organisation, and (iii) decoherence of macroscopic reduced sectors. The natural next question is whether these ingredients are sufficient to produce probabilities, and in particular whether ECT can justify a Born-type rule. This question must be handled with unusual care. Decoherence



alone does not produce probability. It only suppresses phase interference between macroscopically distinct reduced sectors.

**Physical picture: where probabilities come from.** In standard quantum mechanics the Born rule  $P = |\langle\psi|\phi\rangle|^2$  is postulated. In ECT it is motivated as a consequence of decoherence: when the influence functional suppresses interference between branches, the remaining branches behave as classical alternatives whose weights are determined by the squared amplitude. This is not yet a full derivation—it is a conditional argument (Level B/Open) that relies on additional assumptions stated below. But it removes the Born rule from the list of fundamental axioms and relocates it to the status of a reconstruction target.

**Structural assumptions entering the Gleason route.** For clarity, the conditional Born argument used below will be stated in terms of three assumptions:

- (C1) the relevant decohered alternatives are represented by a Hilbert-space / projector structure built on the coherent branch;
- (C2) decoherence has selected approximately orthogonal reduced alternatives in the regime of interest;
- (C3) an additive probability measure on those decohered alternatives is admitted.

ECT does not yet derive all three from the bare postulates alone. What it establishes is that, once they are in place, the quadratic Born assignment is not merely natural but conditionally unique.

**Medium reading (P5).** Under the medium interpretation (P5), the amplitude-to-probability transition is not a transition between abstract mathematical layers. It is a transition within one physical medium: the coherent amplitudes describe the ordered condensate at the subsystem level, while the decoherence that produces effective probabilities arises from integrating out unresolved sectors of the same condensate. The medium interpretation therefore ensures that the entire logical chain (30.7) stays within a single physical framework rather than invoking separate ontological levels for amplitudes and probabilities.

**Connection to the global/reduced unitarity distinction.** The probability question arises only after the global/reduced unitarity distinction (§23.2) has been operationalised by the decoherence programme. Global unitarity of the full coherent description is maintained throughout. What the Born-type interpretation addresses is not the global level, but the reduced level: once unresolved condensate modes are traced out, the reduced description becomes approximately diagonal, and at that point the question of how to read the diagonal weights as probabilities becomes meaningful.

### Amplitude versus probability

The coherent branch of ECT is fundamentally organised in terms of amplitudes. The natural objects are coherent sector weights of the form (22.1),

$$\mathcal{A}[\theta] \sim \exp\left(\frac{iS_\theta[\theta]}{S_0}\right),$$

together with their superposition over admissible coherent histories. As long as different coherent sectors interfere significantly, the appropriate description remains amplitude-based.

Probability enters only after one passes to a reduced description in which interference between relevant coarse-grained sectors has been suppressed. Thus the logical order is:

$$\text{amplitudes} \longrightarrow \text{decoherence} \longrightarrow \text{effective probabilities.} \quad (30.7)$$

ECT does not begin with probability as a primitive notion.

## Why decoherence is not yet the Born rule

Decoherence makes off-diagonal reduced contributions small, but it does not by itself explain why diagonal sector weights should be interpreted as probabilities, nor why they should be given precisely by the squared modulus of a wave amplitude. A reduced density matrix that becomes approximately diagonal is not yet a derivation of Born's rule. It is only the precondition for a Born-type interpretation to become consistent.

This distinction must remain explicit. Many discussions conflate four conceptually separate steps:

- (i) suppression of interference;
- (ii) emergence of classical alternatives;
- (iii) assignment of probabilities;
- (iv) the specific quadratic weighting rule.

In ECT these four steps are kept conceptually distinct.

## Why a Born-type rule is structurally natural and conditionally unique in ECT

A Born-type rule is not yet derived from first principles in ECT, but it is strongly suggested by the internal structure of the coherent branch and becomes conditionally unique once assumptions (C1)–(C3) are admitted. ECT already contains:

- (i) complex coherent amplitudes weighted by  $S_0$ ;
- (ii) a Schrödinger-type reduction (22.8) for smooth coherent sectors;
- (iii) decoherence of macroscopic reduced sectors (26.1);
- (iv) a natural reduced density matrix description (see below).

Once these ingredients are present, the minimal quadratic assignment for the weight of an effectively decohered branch is

$$P_\alpha \propto |\Psi_\alpha|^2, \quad (30.8)$$

where  $\Psi_\alpha$  is the effective amplitude of the decohered branch  $\alpha$ .

**Status of Eq. (30.8): conditional uniqueness via Gleason.** The earlier wording (“natural candidate”) can be sharpened. Once the coherent sector is equipped with a Hilbert-space projector structure and an additive probability measure on decohered alternatives, Gleason's theorem [208] forces: the only probability assignment consistent with that structure is  $P_\alpha = \text{Tr}(\hat{\rho} P_\alpha)$ , which for a pure state reduces to  $P_\alpha = |\langle \phi_\alpha | \Psi \rangle|^2$ . There is no free parameter.

*What this improves:* the Born rule in ECT is no longer merely plausible but *conditionally unique*: if the Hilbert/projector/probability structure emerges, no other probability assignment survives.

*What this does not establish:* ECT has not yet derived the full Hilbert-space projector and probability-measure structure from bare P1–P4. The Gleason uniqueness applies *conditional* on that emergence. The Born rule therefore remains Level B (conditional uniqueness), not an unconditional Level A theorem (OP-Q7).

The correct ECT status is therefore stronger than mere plausibility but weaker than a bare-postulate theorem: the Born rule is conditionally unique once the coherent Hilbert/projector structure and additive probability measure on decohered alternatives are admitted.

## Reflection-positivity origin of the quadratic structure

The standard decision-theoretic routes to the Born rule (Deutsch [209], Wallace [210], Zurek [211]) derive the quadratic weighting from rationality axioms imposed on an agent embedded in a branching quantum world. In ECT the quadratic structure has a different and more direct origin: it is naturally traced to the reflection-positivity construction of the physical inner product, rather than to an external rationality postulate.

The Euclidean condensate functional measure (23.1) provides the natural microscopic weight from which the emergent quadratic structure is reconstructed under the RP/OS assumptions. For functionals  $F, G$  supported in the half-space  $w > 0$ , the OS route (§23.1) defines a physical inner product:

$$\langle F|G\rangle_{\text{phys}} = \int \mathcal{D}\Phi (\Theta F[\Phi])^* G[\Phi] e^{-S_E[\Phi]/S_0}. \quad (30.9)$$

This inner product is quadratic in the amplitudes by construction: it is a defining property of the Euclidean measure and the reflection operation, not an auxiliary assumption about probability. RP guarantees a positive semi-definite OS form; after quotienting the RP-null states and completing the resulting positive semi-definite OS space, one obtains the physical Hilbert space  $\mathcal{H}_{\text{phys}}$  with positive-definite norm.

Once the OS-reconstructed Hilbert space is in place, the diagonal elements of a reduced density matrix are automatically of the form

$$\rho_{\alpha\alpha} = \langle \alpha | \hat{\rho} | \alpha \rangle = |\langle \alpha | \Psi \rangle|^2 \quad (\text{pure state}). \quad (30.10)$$

This is not a probabilistic postulate. It is a consequence of the RP-defined inner product: the diagonal matrix elements inherit the quadratic structure of  $\langle \cdot | \cdot \rangle_{\text{phys}}$ .

The full derivational chain within ECT is therefore:

$$\underbrace{S_E, S_0}_{\text{P1-P6}} \xrightarrow{\text{RP}} \underbrace{\mathcal{H}_{\text{phys}}, \langle \cdot | \cdot \rangle}_{\text{quadratic}} \xrightarrow{\text{decoh.}} \underbrace{\text{projectors}}_{\text{(C2)}} \xrightarrow{\text{Gleason}} P_\alpha = |\langle \phi_\alpha | \Psi \rangle|^2. \quad (30.11)$$

In this reading, the quadratic character of Born weights is not chosen, nor is it derived from decision-theoretic rationality. It is *inherited* from the RP-inner-product structure of the Euclidean condensate measure.

**Comparison with decision-theoretic routes.** The Deutsch–Wallace programme starts from an assumed Hilbert space and derives the Born rule from rationality constraints on agents. ECT starts from a Euclidean functional measure and constructs the Hilbert space itself (via RP), so that the quadratic weighting emerges from the physics of the Euclidean condensate rather than from the rationality of hypothetical agents. The decision-theoretic step is therefore not required in the ECT route, though it remains available as an independent consistency check.

**Residual gap and honest status.** The RP route narrows the open gap compared to the formulation based on (C1)–(C3) alone, but it does not close it completely:

- (C1) is partially addressed:  $\mathcal{H}_{\text{phys}}$  is constructed at Level A for Gaussian subsectors of the broken phase, and the full interacting verification is a well-defined constructive target (OP-Q16);
- (C2) is structurally supported by the decoherence programme (§26.1) but not yet established as a strict projector-algebra theorem for decohered macroscopic alternatives;
- (C3) is the mildest: additivity of probabilities for mutually exclusive decohered alternatives is operationally almost unavoidable.

**Level summary for the RP/OS Born route.** *Level A:* Euclidean measure, Gaussian RP subsectors, emergence of positive quadratic norm in those subsectors. *Level B:* decohered branch structure, approximate projective alternatives, Born-type weights as structural consequence of reduced-state diagonals.

*Level C/Open:* full first-principles closure of (C1)–(C3) for the complete interacting coherent theory from bare P1–P6 alone.

The Born rule in ECT therefore has the status of a *conditionally unique consequence of the RP-defined Hilbert structure*, with the residual gap concentrated in the full interacting RP verification and the strict projector-algebra theorem for decohered branches. This is substantially stronger than a raw postulate but weaker than an unconditional theorem from bare postulates.

### Reduced density matrix viewpoint

In a reduced description, the coarse-grained reduced density matrix takes the schematic form

$$\rho_{\text{red}}(q, q') = \sum_{\alpha, \beta} \Psi_{\alpha}(q) \Psi_{\beta}^*(q') \mathcal{D}_{\alpha\beta}, \quad (30.12)$$

where  $\mathcal{D}_{\alpha\beta}$  is the decoherence matrix of the coarse-grained sectors. When decoherence is effective,

$$\mathcal{D}_{\alpha\beta} \approx 0 \quad (\alpha \neq \beta), \quad (30.13)$$

the reduced description becomes approximately diagonal. At that point the diagonal weights  $\rho_{\alpha\alpha}$  are the natural probability candidates.

**What this does and does not show.** This shows why a probability interpretation becomes natural after decoherence. By itself, however, the reduced-density-matrix argument does not yet establish the quadratic rule uniquely. That stronger uniqueness statement enters only once the additional assumptions (C1)–(C3) are admitted and Gleason’s theorem is invoked. What remains open is not conditional uniqueness under (C1)–(C3), but the first-principles derivation of those assumptions and the completed measurement-update theory.

### Measurement status

ECT does not yet contain a completed first-principles measurement theory. What it does contain is the following structural chain:

- (i) coherent amplitudes for smooth ordered sectors;
- (ii) environment-induced suppression of off-diagonal reduced terms;
- (iii) effective branching into macroscopically distinct sectors;
- (iv) a natural Born-type candidate weighting of those sectors.

This is already a substantial structural framework. But it is not yet a finished account of state-update, outcome selection, or observer-conditioned measurement records.

**What remains open.** A full measurement theory would require:

- (i) a precise branch-selection and state-update rule;
- (ii) an explicit derivation of Born weights from the condensate dynamics, rather than their adoption as the preferred candidate;
- (iii) a treatment of pointer sectors and stable macroscopic records;
- (iv) control of the rôle of defect and topological sectors during measurement-like processes (Section 34).

## Why the current result is still meaningful

Even without a final theorem, ECT has advanced beyond a purely formal restatement of ordinary quantum mechanics. The theory explains why probability should arise only *after* decoherence, why probabilities are not fundamental primitives, and why a quadratic amplitude weighting is the uniquely compatible assignment once the coherent branch has been reduced to effectively classical alternatives (conditional uniqueness via Gleason, above). ECT thereby provides the right *architecture* of the Born problem, even if it has not yet fully solved it.

## Bridge to entanglement and Bell-type correlations

The probability and measurement discussion has so far focused on decohered reduced sectors and effectively classical alternatives. The next step is different: to analyse coherent correlations that remain intrinsically non-factorisable and are therefore not exhausted by the branch-based probability discussion alone. That is the subject of the next section on entanglement and Bell-type correlations.

**Discriminant: ECT Born route versus standard probability postulates.** Standard formulations of quantum theory usually take the Born rule as an axiom or attempt to justify it through auxiliary principles such as decision theory. ECT takes a different route. It does not treat probability as primitive. Instead, it first organises coherent amplitudes, then derives decoherence of reduced sectors, and only then asks what probability assignment is compatible with the resulting Hilbert/projector structure. The ECT-specific claim is therefore not that probability is assumed, but that a quadratic assignment becomes structurally singled out once the relevant reduced-state architecture is in place.

**Falsifier for the Born-weight programme.** The present programme would be weakened if a completed ECT derivation showed that decohered alternatives do not admit the Hilbert/projector structure assumed in (C1), or that additive probability measures on those alternatives are inconsistent with the coherent-branch architecture. It would be more strongly challenged if a completed derivation forced a non-quadratic probability rule while retaining the same Hilbert-space structure. At present, no such incompatibility is known; the open point is not inconsistency, but incompleteness.

**Empirical status.** The quadratic Born weighting is extraordinarily well confirmed across atomic, molecular, optical, and solid-state quantum experiments. ECT does not claim a distinct experimental prediction at this stage. Its contribution is architectural: it explains why probability should enter only after decoherence and why the quadratic rule is conditionally singled out once the required reduced-state structure is admitted.

**Status summary.** *Established (Level A):* ECT distinguishes clearly between coherent amplitudes, decohered reduced sectors, and effective probability candidates. The Euclidean condensate measure and reflection positivity provide the quadratic inner-product structure from which Born-type weights are inherited in Gaussian subsectors of the broken phase.

*Level B:* once assumptions (C1)–(C3) are admitted, the quadratic Born rule is not merely plausible but conditionally unique via Gleason’s theorem [208]. The RP/OS route partially closes (C1) for Gaussian subsectors and structurally motivates (C2) through the decoherence programme; (C3) is operationally mild.

*Open:* (i) full interacting RP verification beyond the Gaussian sector (OP-Q16); (ii) a strict projector-algebra theorem for decohered macroscopic alternatives (C2); (iii) a completed measurement-update theory.

**Summary.** ECT does not postulate probability at the foundation. Probability appears only after coherent amplitudes are reduced by decoherence to effectively classical alternatives. This makes a Born-type

rule structurally natural and, once the assumptions (C1)–(C3) are admitted, conditionally unique—but not yet fully derived from bare postulates. The next step is to analyse coherent correlations that remain non-factorisable even before branch-based probability language is invoked.

**Table 96:** Comparison of Born-rule derivations.

Aspect	Deutsch (1999) [209]	Wallace (2012) [210]	ECT (this work)
Framework	MWI + decision theory	MWI + decoherence	Coherent branch + decoherence + RP/OS Hilbert construction + conditional Gleason route
Source of weights	Rationality axioms	Rationality + branch structure	Decohered reduced sectors; quadratic assignment conditionally unique once assumptions (C1)–(C3) hold
Origin of quadratic structure	Decision-theoretic axiom	Rationality + separability	RP-defined inner product of the Euclidean condensate measure; not externally postulated
Decoherence	Not used	Postulated	Derived at closure level from the reduced influence-functional organisation
Extra assumptions	Rationality	Rationality + separability	(C1)–(C3) for the conditional Gleason step
Known limitations	Circularity [212]	Albert (2010) objection	Conditional uniqueness only; first-principles derivation of (C1)–(C3) and unique outcome selection still open (OP-Q19)

## 31 Quantum Entanglement and Bell-Type Correlations

*Status: Level A/B for the structural availability of non-factorisable coherent correlations within a single ordered medium. Level B for the reading of entanglement as a coherent-branch correlation phenomenon rather than a primitive axiom, and for the expectation that Bell-type correlations should emerge from the same ordered-medium architecture. Open for a full first-principles derivation of Bell-inequality-violating correlators, Tsirelson-type bounds, and their exact quantitative matching to the standard quantum-information formalism. Connection: the Hilbert-space bridge (§23.1), the global/reduced unitarity distinction (§23.2), the exchange-sector topology (§24.4), the decoherence programme (§26.1), the vacuum-response infrastructure (§25), the Born-weight route (§30.4), medium character (P5), and the quantum–classical boundary (§30.1).*

**Physical picture: entanglement as a trace of a common configuration.** In the standard formulation, entanglement is introduced as mathematical non-factorisability in a tensor product of Hilbert spaces. This works, but says almost nothing about the physical “why”. In ECT a physical picture emerges: two subsystems are entangled not because a hidden superluminal signal connects them, but because both are partial descriptions of one and the same coherent condensate configuration. Measurement of one part does not “send an influence” to the other. It converts the local subsystem into a decohered branch, while the other was already part of the same global configuration. The observed correlation reflects not signal

transfer but the prior inseparability of the condensate state. This is an interpretive gain (Level B); the full derivation of Bell-type correlators from condensate dynamics remains open.

**Connection to PES.** The Principle of Euclidean Stationarity (§29) provides a physical reading of entanglement: two subsystems sharing a common condensate medium with  $\Gamma_{\text{loop}} \ll 1$  are correlated through the Euclidean substrate without requiring Lorentzian signalling. In the PES picture, interaction is a Lorentzian concept (§30.2); in the Euclidean regime, what replaces it is spatial correlation through the common ordered medium. This is consistent with the no-signalling theorem: extracting classical information from entangled partners requires a local Lorentzian measurement ( $\Gamma_{\text{loop}} \gg 1$ ), which does not propagate superluminally. The principle does not yet yield a first-principles Bell-correlator derivation, but it strengthens the physical interpretation of entanglement by separating Euclidean common-medium correlation from Lorentzian event-based interaction.

**What is established, what is structurally suggested, and what remains open.** The tensor-product and reduced-state language used below presupposes the physical Hilbert-space bridge discussed in Section 23.1.

The ECT quantum sector already contains three ingredients relevant to entanglement. First, subsystems are not fundamental isolates but reduced sectors of a single coherent medium. Second, the influence-functional and vacuum-correlation infrastructure already shows how non-factorisable correlations arise across reduced descriptions (§26.1, §25). Third, Born-type probabilities and decoherence are treated as emergent coherent-sector structures rather than primitive axioms (§30.4). What remains open is the completed derivation of the full Bell-type correlation algebra and its exact quantitative coincidence with the standard entanglement formalism.

**Medium reading (P5).** Under the medium interpretation (P5), entanglement is not a primitive property imported from an abstract tensor-product axiom. It is the structural expectation that reduced subsystems of one and the same ordered condensate generically share non-factorisable correlations, because they are embedded in a common physical medium whose coherent correlators extend across their spatial separation. This does not by itself derive the quantitative Bell-violation pattern, but it provides the ontological backbone: non-separability is not mysterious action at a distance, but the reduced-state signature of two subsystems that have never been fully ontologically separate from their common medium.

**No-signalling and operational locality.** The common-medium reading of entanglement does not imply operational superluminal signalling. What is shared between distant subsystems is a non-factorisable reduced state, not a controllable message channel. ECT therefore aims to account for Bell-type correlations without restoring Bell-local hidden variables, but also without turning the medium into a device for sending signals to spacelike-separated observers. At the present stage, the programme concerns the origin of correlation structure, not a revision of operational no-signalling.

**Connection to exchange sectors.** For systems of indistinguishable excitations, the entanglement programme is constrained by the exchange-sector topology established in Section 24.4. The bosonic/fermionic dichotomy fixed by the primary three-dimensional ordered branch limits what multipartite states are physically admissible in the first place. This does not mean that all entanglement reduces to exchange structure. Rather, exchange topology provides part of the kinematical backbone for entanglement in the indistinguishable-sector case, while the broader non-factorisable correlation logic applies to distinguishable reduced subsystems as well.

**Minimal structural statement.** Once a physical system is described as a reduced sector of a single coherent ordered medium, factorisation of distant subsystems is no longer automatic. If two subsystems  $A$  and  $B$  are both embedded in the same ordered condensate, the reduced state  $\hat{\rho}_{AB} = \text{Tr}_{\text{env}} \hat{\rho}_{\text{tot}}$  generically

need not factorise as  $\hat{\rho}_A \otimes \hat{\rho}_B$ , because both subsystems couple to a common medium whose correlators extend across the spatial separation. Accordingly, ECT already provides a structurally natural route to non-separable correlations. This is the entanglement-side analogue of the amplitude  $\rightarrow$  decoherence  $\rightarrow$  probability chain developed in Section 30.1: before branch-based probability language is even invoked, the coherent medium can already force non-factorisable reduced-state structure. What ECT does *not* yet provide is a completed theorem stating that the standard Bell-inequality-violating correlators follow uniquely and quantitatively from the present condensate dynamics.

**Discriminant with respect to axiomatic QM and local hidden-variable pictures.** Three correlation pictures should be kept distinct. In axiomatic quantum mechanics, entanglement is treated as a primitive property of the tensor-product state space. In local hidden-variable models, Bell-violating correlations are forbidden once factorisability and measurement independence are imposed. ECT belongs to neither class exactly. It does not take entanglement as primitive, but neither is it a Bell-local hidden-variable completion: its natural correlation carrier is the single coherent medium itself, whose reduced subsystems need not remain factorisable even when they are described separately. The ECT programme therefore aims at a medium-based origin of Bell-type correlations, not at a restoration of Bell-local realism.

**Connection to the coherent-sector infrastructure.** The entanglement programme in ECT is not an isolated add-on. It inherits the same coherent-sector architecture already used in the vacuum-response programme (§25), the influence-functional treatment of decoherence (§26), the Born-weight construction (§30.4), and the information discussion for black-hole evaporation (§36). In that sense, Bell-type correlations are part of the programme-level expectation to be ultimately traceable to the same non-factorisable medium correlations that already underlie Casimir/Unruh response, reduced-system decoherence kernels, and the coherent probability map. This cross-sector consistency requirement is one of the strongest structural constraints of the whole quantum branch.

**Connection to the probability and measurement route.** Entanglement is not exhausted by the branch-based probability discussion of Section 30.4. There the main issue was how decohered alternatives acquire probabilistic weights. Here the issue is earlier and different: how non-factorisable coherent correlations arise before or independently of any effective branch selection. The two programmes are therefore complementary rather than redundant.

**Why entanglement is not equivalent to decoherence.** Entanglement and decoherence are related but distinct phenomena in the coherent-branch framework. Decoherence describes the suppression of off-diagonal terms in a reduced description when unresolved environment modes are traced out. Entanglement describes the non-factorisability of the reduced bipartite state *before* environmental decoherence has acted. ECT must account for both: the persistence of non-classical correlations in isolated subsystems (entanglement) and their eventual suppression under environmental coupling (decoherence). The same influence-functional infrastructure is expected to govern both regimes, but they are not reducible to a single scalar criterion. Entanglement concerns the non-factorisability of multipartite reduced states, whereas decoherence concerns the suppression of interference in a chosen reduced description under environmental tracing. In practice, increasing  $\Gamma_{\text{irr}}$  provides one natural route by which coherent entanglement signatures become fragile, but the two notions are not identical.

**Empirical backdrop.** The empirical violation of Bell inequalities is now firmly established, from early Aspect-type experiments to modern loophole-free tests such as [213]. ECT does not claim a distinct experimental signal at this stage. What it must show is narrower but still nontrivial: that its coherent-medium architecture can accommodate the observed Bell-type correlation pattern without taking tensor-product entanglement as primitive and without reverting to Bell-local hidden variables. The present section provides that structural accommodation, but not yet a completed quantitative derivation of the observed correlators.



**Programme-level predictions.** The entanglement programme suggests four nontrivial expectations. First, Bell-type correlations should be rooted in the same coherent kernel that also controls decoherence and vacuum response; if entanglement required a fundamentally separate correlation mechanism, the single-medium architecture would fail. Second, entanglement degradation in noisy environments should correlate with the same environment-sensitivity structures already discussed in the decoherence programme (§26). Third, analogue platforms that realise ordered-medium coherent correlations (§37) may access “entanglement-like” correlation and degradation signatures before a full fundamental test. Fourth, if a future derivation is completed, Bell correlations should not require introducing a second independent non-medium ontology.

**What is not yet established.** The present ECT entanglement programme does not yet derive the exact CHSH-type correlators, Tsirelson bound, or the full quantum-information tensor-product formalism from first principles. It establishes a structural route to non-factorisable coherent correlations within a single medium, and shows why Bell-local hidden variable completion is not the intended target. The completed quantitative Bell-correlator reconstruction remains an open step of the programme.

**Falsifier for the entanglement programme.** The ECT entanglement programme would fail if (i) Bell-type correlations could only be reproduced by taking the tensor-product entanglement structure as an irreducible primitive layer with no reconstruction from the coherent medium, (ii) the correlation structure inferred from decoherence and vacuum-response kernels proved fundamentally incompatible with the correlation structure required by entanglement experiments, (iii) a completed Bell-correlator derivation forced the introduction of an independent non-medium hidden structure, or (iv) entanglement scaling in controlled open-system experiments proved incompatible with the same environmental kernels that govern the ECT decoherence programme. Any of these would break the claim that entanglement belongs to the same single-medium quantum architecture as the rest of Part III.

**Status summary.** *Established (Level A/B):* the coherent-medium architecture structurally allows reduced subsystems of a single ordered condensate to exhibit non-factorisable correlations, because factorisation is not enforced at the medium level.

*Level B:* entanglement is read as a coherent-branch correlation phenomenon rather than a primitive axiom, and its degradation under environmental coupling is governed by the same influence-functional infrastructure as the decoherence programme.

*Open:* (i) a full first-principles derivation of Bell-inequality-violating correlators from condensate dynamics; (ii) exact quantitative reconstruction of CHSH-type correlators and the Tsirelson bound; (iii) a completed tensor-product formalism as a derived consequence of the coherent-medium architecture.

**Bridge to topological and defect sectors.** The entanglement discussion, like the rest of the preceding quantum analysis, has been confined to the smooth coherent branch selected by BR1. The full coherent ontology of ECT is wider: it also includes nontrivial defect and topological configurations that may contribute to dark-sector ontology and to non-perturbative coherent processes. Those wider sectors are the subject of the next section.

**Connection to tunnelling.** Both quantum entanglement and quantum tunnelling are naturally read in ECT as manifestations of the same deeper ingredient: non-local connectivity of the coherent Euclidean sector. Tunnelling is the barrier-traversal expression of that connectivity, whereas entanglement is its reduced-state correlation expression across spatially separated subsystems. This does not mean that the two phenomena are identical, nor that one reduces to the other. They differ both in operational signature and in the reduced-state language used to describe them. Rather, ECT places them on a common geometric footing. In the weak-locking regime ( $\Gamma_{\text{loop}} \ll 1$ ), both can remain manifest. As environmental locking increases, tunnelling amplitudes and observable non-classical entanglement signatures become

progressively more fragile. The present point is therefore structural and unifying, not the claim of a new independent quantitative theorem.

**Bell-inequality violation and the decoherence crossover.** At the present stage, ECT does not derive the Bell correlator algebra from first principles. What it can provide is a simple decoherence-based visibility model showing how Bell-violating correlations become fragile as environmental locking increases. In the simplest Werner-type visibility proxy, one obtains

$$\text{CHSH}_{\text{eff}} = 2\sqrt{2}e^{-\Gamma_{\text{loop}}}. \quad (31.1)$$

Within this proxy model, the crossover from Bell-violating to Bell-compatible correlations occurs at  $\text{CHSH}_{\text{eff}} = 2$ , i.e. at

$$\Gamma_{\text{loop}}^{\text{Bell}} = \ln \sqrt{2} \approx 0.35. \quad (31.2)$$

This should be read as a toy crossover estimate, not as a completed ECT derivation of the Tsirelson bound or of the full CHSH algebra. Its usefulness is to provide a concrete numerical marker for when Bell-type non-classicality becomes observationally fragile within the same decoherence language already used elsewhere in the quantum sector.

## 32 Gravity-induced entanglement in ECT: status and operational criterion

*Status: Level B structural — architectural compatibility of ECT with the observation or non-observation of gravity-induced entanglement in mesoscopic regimes. No Level A predictive derivation is attempted. Connection: the two-level ontology of Section 28; the general entanglement discussion of Section 31; the quantum–classical boundary criterion  $\Gamma_{\text{loop}} \lesssim 1$  of Section 30.1; the reduced-state reading of the Diósi–Penrose timescale in Section 26.3; the class-specific falsifiers of Section 38.4. The concrete mediator taxonomy is developed separately and is not invoked here.*

### 32.1 Why gravity-induced entanglement is a sharper test for ECT

The general entanglement programme of Section 31 already established that reduced subsystems of one ordered medium need not remain factorisable. The present section asks a sharper question: whether the specifically gravitational part of that reduced coupling can, in some regimes, still carry enough common-medium structure to generate entanglement between mesoscopic masses.

Generic entanglement in ECT concerns non-factorisable reduced states of subsystems embedded in one common ordered medium. Gravity-induced entanglement (GIE) is sharper: it asks whether the specifically gravitational part of the reduced interaction between two mesoscopic masses can preserve enough common-medium structure to generate entanglement before decoherence drives the system into the classical Level IIb regime. It therefore probes not merely the existence of coherent correlations in some abstract sense, but the architecture of the gravity–matter interface itself. For a framework like ECT, which neither quantises an independent metric field nor postulates fundamentally stochastic gravity, the BMV [153, 154] class of proposals, and the comprehensive reviews [155, 156, 214] that consolidate them, define exactly the axis along which ECT must take a testable architectural position.

### 32.2 Balanced map of the debate

**Standard BMV logic and its locally mediated refinement.** The standard BMV arguments [153, 154] assert that if two quantum masses in spatial superposition become entangled through their mutual gravitational interaction alone, then the mediator itself must possess nonclassical degrees of freedom, on the assumption that local classical channels cannot transmit quantum information. Christodoulou et al. [215] showed that, within linearised quantum gravity, the generated entanglement admits a consistent

locally mediated reading with causal retardation. The locally mediated retarded reading is especially congenial to ECT, where causal structure is itself emergent and signal propagation is tied to the ordered branch. In that sense retardation is structurally natural in the ECT framework, being inherited from the Lorentzian ordered-branch kinetic structure (Sections 3.8, 3.6) rather than imposed as an independent auxiliary ingredient.

**The Aziz–Howl episode: a cautionary controversy.** A recent proposal by Aziz and Howl [216] argued that a local classical-looking gravitational coupling, when embedded in a full quantum-field-theoretic treatment of matter, may generate entanglement between distant masses. This interpretation triggered substantial criticism [217, 218, 219], arguing that, in the specific nonrelativistic limit employed there, the relevant unitary factorises and no genuine gravity-mediated entanglement is produced from a product input. A Nature News & Views comment [220] framed the episode as an active debate rather than a settled issue. The safest reading at the time of writing is therefore cautious: the Aziz–Howl controversy re-opened the loophole discussion but did not overturn the standard BMV inference for strictly local factorising classical channels.

**Trillo–Navascués: the constructive loophole.** The key constructive lesson for ECT is not the Aziz–Howl controversy but the explicit result of Trillo and Navascués [221]: once correlated-noise or common-medium structure is admitted between the two probe systems, the slogan “classical gravity cannot entangle” is no longer generally valid. In that specific correlated-noise model class, a Diósi–Penrose-type classical gravity can generate gravity-induced entanglement. Related analyses relaxing the local-tomography assumption for the mediator [222] point in the same direction: the loophole class relevant here is closely tied to the failure of the assumption that the mediator is exhausted by locally tomographic classical data. A mediator may look classical at the coarse-grained level without being operationally equivalent to an LOCC channel.

This result does not by itself prove that ECT realises such a mechanism in any specific protocol; it only shows that the relevant loophole class exists and is structurally available in principle.

### 32.3 ECT’s architectural position — three claims

The two-level ontology of Section 28 fixes the architectural answer for ECT, which is best stated as three separate claims.

**(A) What ECT does not take to be forced.** ECT does not take the observation of gravity-induced entanglement in a mesoscopic protocol, by itself, to force a fundamentally quantised independent metric field. Once common-medium and correlated-noise loophole classes are admitted, the standard BMV inference must be read more carefully than it is often stated in slogan form, because it applies most directly to strictly local factorising classical channels.

**(B) What ECT allows.** ECT allows that gravity-induced entanglement may arise in experimental regimes where the reduced effective dynamics still retains common-medium non-factorisable structure inherited from the underlying Euclidean condensate. In the language of Section 28.3, such regimes are Level IIa rather than Level IIb.

**(C) What ECT does not yet establish.** ECT does not yet establish, from first principles, which exact experimental protocols lie in the common-medium regime, nor does it yet derive the explicit reduced mediator channel through which entanglement would be generated. That derivation belongs to the mediator taxonomy developed separately.

**Loophole availability is not loophole realisation.** Structural availability of a loophole class, as established by Trillo–Navascués-type constructions, is not yet the same as demonstrating that a given experimental implementation of ECT actually realises that loophole. Identifying which protocols do so is the content of Claim (C).

### 32.4 Operational criterion

**Operational criterion.** ECT falls under the standard BMV no-go logic only if, in the actual regime realised by the experiment, the effective reduced mediator is well approximated by a strictly local classical factorising channel with no residual common-medium non-factorisable correlations. ECT escapes that logic if the experimentally relevant reduced dynamics still retains correlated common-medium structure, so that the effective mediator belongs to the broader loophole class exemplified by correlated-noise constructions such as Trillo–Navascués. ECT does not assert both descriptions for one and the same operational regime. It asserts that different protocols can probe different reduced regimes of one underlying condensate theory.

### 32.5 Provisional regime guidance

The location of a given experimental protocol on this axis is a physical question determined by the mass, separation, coherent time, and environmental coupling of the setup. The mesoscopic crossover is expected only when the characteristic reduced-state decoherence time becomes comparable to the protocol coherence time. A provisional scalar-sector guide is obtained by equating the Diósi–Penrose-like reduced-state timescale of Section 26.3,  $\tau_{\text{dec}}^{\text{grav}} \sim \hbar R / (G_N m^2)$ , with the experimental coherence time  $\tau_{\text{exp}}$ , yielding a heuristic mass scale

$$m_{\text{guide}} \sim \sqrt{\hbar R / (G_N \tau_{\text{exp}})}. \quad (32.1)$$

This quantity should be read only as an order-of-magnitude orienting scale inherited from the scalar reduced-state sector, not as a first-principles crossover mass for the entangling channel itself. Its numerical value is protocol-dependent and may fall in the broad mesoscopic range explored by contemporary levitated-nanoparticle and space-based proposals [150, 151, 152, 223]. Its use as a criterion for the entangling channel specifically remains conditional until the mediator taxonomy is established. Additional dependence on environmental coupling, recoil heating, and orientation-mode coherence length is not included in this estimate.

### 32.6 Relation to falsifiers and to non-observation

The present section gives operational content to the third falsifier of Section 38.4: the ECT route would be seriously weakened if one could prove that every experimentally relevant common-medium route collapses, in practice, to a factorising classical channel before entanglement can form. Conversely, an observation of gravity-induced entanglement consistent with correlated common-medium mediators would not yet distinguish ECT from other hybrid-consistent frameworks.

A null result would be highly informative for ECT only in a regime where the protocol is independently shown to preserve coherence long enough that common-medium entangling structure, if present, should have had time to act. In that case, non-observation would constrain how much common-medium structure survives in the relevant reduced channel. In this sense both positive and carefully interpreted negative outcomes of BMV-class experiments carry architectural information for the ECT programme.

### 32.7 Scope and non-claims

**Scope and non-claims.** The present section does not claim (i) a Level-A first-principles prediction of gravity-induced entanglement rates for any concrete protocol; (ii) a microscopic derivation of the effective entangling mediator from the condensate influence functional; (iii) a final resolution of the

Aziz–Howl controversy; (iv) a first-principles crossover criterion for the transition between entangling and fully classical reduced regimes. Its claim is narrower: ECT supplies a testable architectural distinction between protocols whose reduced dynamics is effectively factorising-classical and protocols whose reduced dynamics may still retain common-medium structure.

The next section remains within the mesoscopic gravity–matter interface and asks a more specific question left open by the previous discussion: which reduced channel of the effective gravitational mediator is responsible for branch distinguishability, and which channel could in principle carry common-medium entangling structure.

### 33 Reduced gravitational mediator in ECT: channel taxonomy

*Status: Level B structural. The  $\phi$ -channel has already been used in Section 26.3, and the  $\delta n_A$  sector is already established as the orientation/effective-metric channel in Sections 3.6 and 8.5. The present section does not introduce new mediator physics; it organises the existing condensate graviton programme into two complementary channels with distinct physical roles, and identifies what remains open. Connection: the operational criterion and Claim (C) of Section 32.3; the heuristic guide of eq. (32.1) in Section 32.5; the two-level ontology of Section 28.*

#### 33.1 Why a channel taxonomy is needed

Section 32 left open, as Claim (C) of Section 32.3, the explicit identification of the reduced channel through which gravity-induced entanglement would be generated in ECT. That question cannot be answered without first clarifying which component of the effective gravitational mediator plays which role. The present section provides that clarification, building on material already in the paper rather than introducing new sectors.

This taxonomy is not claimed to be a unique or exact decomposition of the full reduced mediator. It is introduced as the minimal effective organisation needed to distinguish branch-distinguishability effects from candidate common-medium entangling effects.

The present taxonomy does not introduce a new graviton sector; it reorganises the already established condensate graviton programme by distinguishing the scalar distinguishability response from the tensor/orientation response relevant to common-medium mediation.

#### 33.2 The $\phi$ -channel: scalar distinguishability

The scalar amplitude perturbation  $\delta\phi$  sourced quasi-statically by a matter distribution, explicitly derived in Section 26.3 (eq. (26.15)), gives rise to the reduced-state distinguishability between condensate configurations associated with different matter superposition branches. In the minimal reduced-state reading developed here, this is the channel that carries the Diósi–Penrose-like decoherence timescale  $\tau_{\text{dec}}^{\text{grav}} \sim \hbar R / (G_N m^2)$  of eq. (26.17). Its operational role is to quantify how distinguishable the condensate responses to two matter branches are, and therefore how rapidly their reduced phases dephase. In the present minimal reading, the  $\phi$ -channel is treated primarily as a distinguishability/decoherence channel rather than as the primary entangling channel.

#### 33.3 The $\delta n_A$ -channel: orientation/tensor candidate mediator

The orientation fluctuations  $\delta n_A$  project into the symmetric effective-metric channel  $h_{AB}$  established in Sections 3.6 and 8.5. They provide the ECT-native orientation sector from which the massless spin-2 excitation identified with the graviton is extracted in the linearised ordered-branch regime. A tensor channel coupling simultaneously to two spatially separated mass distributions is the natural candidate within ECT for the common-medium correlations relevant to gravity-induced entanglement; it is therefore the candidate entangling mediator required, but not yet derived, in Claim (C) of Section 32.3.

**Qualification.** Not every  $\delta n_A$  fluctuation is automatically the physical entangling mediator relevant for a mesoscopic protocol. What is required is the retarded tensor/common-medium component of the orientation response that survives the reduction map and couples simultaneously to two separated mass distributions without collapsing to a merely factorising classical channel. Identifying this component from first principles is what a full derivation of the effective entangling mediator would have to provide.

### 33.4 Mixed scalar–orientation sector

Beyond the minimal separation into  $\phi$ - and  $\delta n_A$ -channels, a mixed scalar–orientation sector is expected once the reduction map is carried beyond the quasi-static leading approximation. This mixed sector is the natural place where decoherence and entangling capacity can compete or dress one another. No first-principles derivation is claimed here; the point is only that the two-channel taxonomy should be read as a minimal organising skeleton rather than as a complete diagonalisation of the reduced mediator.

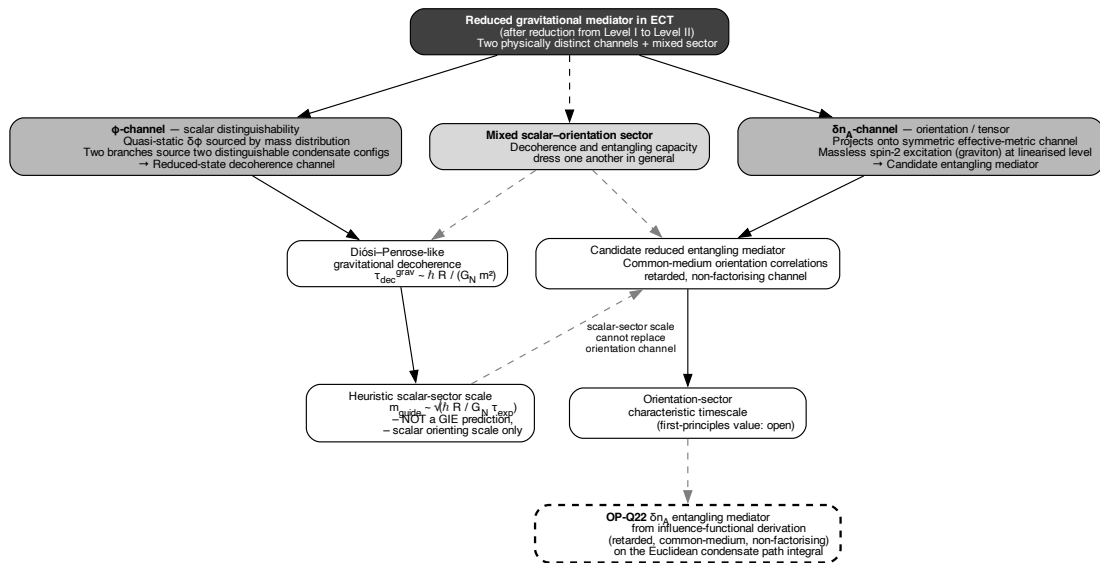


**Figure 38:** Channel taxonomy of the reduced gravitational mediator in ECT (Section 33). The reduction of the Level I condensate yields two physically distinct channels. The  $\phi$ -channel (scalar distinguishability) is the Diósi–Penrose-type reduced-state decoherence channel with scalar-sector timescale  $\tau_{\text{dec}}^{\text{grav}} \sim \hbar R / (G_N m^2)$  and the heuristic orienting scale  $m_{\text{guide}} \sim \sqrt{\hbar R / (G_N \tau_{\text{exp}})}$  (eq. 32.1); the latter is a scalar-sector scale and is *not* a first-principles prediction for gravity-induced entanglement. The  $\delta n_A$ -channel (orientation / tensor) is the ECT-native candidate entangling mediator, with its characteristic retarded common-medium timescale left open (OP-Q22). A mixed scalar–orientation sector is expected beyond the minimal split. (Level B; mediator derivation: Open.)

### 33.5 Implications for $m_{\text{guide}}$ and Claim (C)

The taxonomy explains retrospectively why  $m_{\text{guide}}$  of eq. (32.1) was introduced in Section 32.5 only as a scalar-sector orienting scale and not as an entangling-channel prediction: it is derived from the  $\phi$ -channel alone and therefore inherits the characteristic timescale of reduced-state distinguishability, not of the retarded tensor response. A first-principles entangling crossover mass would require the derivation of the  $\delta n_A$  channel characteristic scale, which is not available in closed form at the time of writing.

**Open mediator tasks.** The following items would have to be completed for a first-principles closure of Claim (C) of Section 32.3:

- explicit reduction of the tensor/orientation channel from the influence functional, compatible with global unitarity;
- extraction of its characteristic retarded timescale and associated mass scale;
- proof that the surviving channel does not collapse to an effectively factorising classical map in the regime of interest.

Each of these remains open. None is claimed to be resolved here.

### 33.6 Scope and non-claims

The present section does not claim (i) a first-principles derivation of the effective entangling mediator from the ECT influence functional; (ii) a derived characteristic mass or timescale for the entangling channel; (iii) a complete diagonalisation of the reduced mediator into non-interacting channels; (iv) any new condensate sector beyond the material already established in Parts I–II. Its claim is narrower: the reduced gravitational mediator in ECT is naturally organised into a scalar distinguishability channel, a tensor/orientation candidate entangling channel, and a mixed sector between them; this taxonomy clarifies which channel governs which reduced-state effect, and sharpens the statement of what remains open.

## 34 Topological Sectors, Defect Configurations, and the Dark Sector

*Status: Level A for the structural existence of a wider ordered-condensate state space beyond the smooth coherent branch BR1, including configurations with singular cores, discontinuous ordering data, or nontrivial Euclidean transitions. Level B for the provisional classification of defect sectors and for their interpretation as dark-sector candidates. Open for quantitative production rates, stability conditions, interaction cross-sections, and a first-principles identification of the dominant dark-sector component. Connection: the smooth coherent branch BR1, defect-sector material deferred from ECT basics (§6.7), the winding/conservation architecture (§22.3), the macroscopic dark-sector bridge (§18.1), vacuum-structure questions (§25.1), exchange-sector topology (§24.4), entanglement/common-medium correlations (§31), and medium character (P5).*

So far the Quantum Sector has been developed inside the smooth coherent branch selected by BR1. This restriction was deliberate: it allowed the phase-sensitive sector to be constructed cleanly in terms of  $\Phi_{\text{eff}} = \rho e^{i\theta}$ , winding sectors, loop actions, wave dynamics, canonical structure, and decoherence. However, the coherent ontology of ECT is wider than the smooth coherent branch. The present subsection develops that wider sector.

### 34.1 Defect sectors and their relation to the smooth branch

#### Why defect sectors are not excluded by BR1

The smooth coherent-sector rule BR1 does not state that only smooth coherent configurations exist. Rather, it identifies the current constructive branch of the theory as the smooth coherent sector with well-defined phase and integer winding numbers. This leaves open a broader space of configurations outside the smooth branch, including singular cores, discontinuous ordering data, and nontrivial Euclidean topological transitions. This broader state space was already flagged in the deferred defect-sector material (Section 6.7).

The rôle of the present subsection is therefore not to abandon BR1, but to state clearly:

- what kinds of configurations exist outside the smooth coherent branch;
- why they are physically relevant;
- how they connect to dark-sector ontology.

**Medium reading (P5).** Under the medium interpretation (P5), defect and topological sectors are not external objects appended to the theory. They are physical configurations of the same ordered condensate: regions where the modulus can vanish, the phase becomes ill-defined, the ordering data changes discontinuously, or the Euclidean configuration tunnels between distinct sectors. The dark-sector question is therefore not “what extra fundamental fields must be added?” but rather “what wider configurations does the same ordered medium admit beyond the smooth branch BR1?”

**Connection to winding and conservation architecture.** The wider defect sector developed here is the natural extension of the winding and conservation structure established in Section 22.3. In the smooth coherent branch, winding numbers are protected under smooth deformations and topological sector changes are thermally suppressed. Defect sectors are precisely the configurations through which those protections can fail: vortex cores, discontinuities, and instanton-like transitions are the places where topology can change. In this sense, Section 22.3 describes the protected regime, while the present section describes the wider regime in which protection can break down.

## 34.2 Types of defect and topological configurations

The main structurally motivated classes of configurations outside the smooth coherent sector are:

**Vortex-core configurations.** Configurations in which the condensate modulus vanishes on a line or axis, making the phase  $\theta$  ill-defined there. They are the natural continuation of winding sectors to the regime where core singularities are allowed or regularised by  $\rho \rightarrow 0$ .

**Domain-wall-like configurations.** Sharp transitions or discontinuities in the ordering data, for example in orientation variables or in the local branch structure of the ordered phase.

**Instanton-like Euclidean configurations.** Topologically nontrivial Euclidean saddle configurations that interpolate between distinct vacuum sectors or coherent sectors. They are not part of the smooth real-time coherent branch but are natural candidates for nonperturbative inter-sector transitions.

**Composite defect configurations.** Mixed objects in which phase winding, orientation mismatch, and local suppression of the order parameter coexist. At the present stage these should be regarded as plausible configurations of the wider ordered state space, not yet fully classified solutions.

### Status of the defect ontology

The ontological claim is strong (Level A): once the ordered condensate admits a phase field, winding sectors, and configurations in which the order parameter can locally vanish or change branch, a wider defect sector is structurally expected.

What is not yet Level A is the full dynamical classification: core structure, stability conditions, production channels, interaction cross sections, and cosmological relic abundance. Those belong to the constructive completion of the wider coherent branch and remain Level B or open.

## 34.3 Connection to the dark sector

This wider sector naturally reopens the dark sector from the QS side. In Macroscopic Physics (Section 18.1), the dark sector was already split into two questions:

- (i) macroscopic  $\phi$ -branch phenomenology that can mimic dark matter or dark-energy effects at large scales (primarily MP);



- (ii) independent dark-sector candidates associated with collective or topological excitations of the ordered condensate (primarily QS).

Thus the dark sector in ECT is not a single monolithic object. It has at least two layers:

- a **macroscopic effective layer**, where modified condensate response can reproduce part of the observed dark phenomenology;
- a **coherent layer**, where genuinely additional condensate excitations or defect sectors may act as dark-sector degrees of freedom.

### Smooth collective excitations versus genuine defect sectors

Two kinds of dark-sector candidates should be distinguished.

**Collective smooth excitations.** Long-wavelength or ultralight modes of the ordered condensate, including coherent collective excitations that remain within the smooth branch. These are still part of the ordinary coherent EFT and can be discussed as dark-sector candidates without abandoning the ordered coherent framework BR1 altogether.

**Genuine defect sectors.** Objects involving singular cores, discontinuities, or nontrivial topological transitions beyond the smooth coherent description. They lie outside the constructive smooth coherent sector BR1 and belong more properly to the expanded QS treatment here.

This distinction matters: smooth collective candidates are closer to the already developed coherent EFT, whereas genuine defects require additional sector construction before quantitative statements can be made.

### Dark-matter-type rôle of defect sectors

Topological or defect configurations become dark-matter candidates if they satisfy some combination of:

- (i) long lifetime or effective stability on cosmological timescales;
- (ii) energy density with only weak coupling to visible matter;
- (iii) gravitational clustering or contribution to large-scale structure;
- (iv) evasion of direct electromagnetic detection as condensate-sector objects rather than standard particle species.

ECT does not yet prove that any specific defect class satisfies all four conditions, but it provides a natural theoretical habitat in which such objects can exist.

### Dark-energy-type rôle and vacuum-sector contributions

A nontrivial vacuum-sector contribution from the ordered condensate may also act as an effective dark-energy component. In MP this appears at the level of the effective late-time amplitude-sector closure. From the QS side, the complementary question is whether nonperturbative topological sectors, defect ensembles, or vacuum-sector tunnelling effects modify the effective vacuum energy or the stability of the ordered branch. At present this remains Level B/open, but the conceptual bridge is important: dark-energy phenomenology in MP and topological vacuum structure in QS are two views of the same ordered condensate background.

## Why the dark sector is split between MP and QS

This split is not a weakness; it is the correct architecture of ECT.

Macroscopic Physics answers: *how can the large-scale response of the ordered condensate imitate or replace parts of standard dark-sector phenomenology?*

Quantum Sector answers: *what genuinely additional coherent excitations, defect sectors, or nonperturbative condensate structures can exist as dark-sector degrees of freedom?*

Trying to force both questions into a single branch would either overload MP with nonperturbative ontology or overburden QS with large-scale effective phenomenology. The two-layer structure is therefore the correct one.

**Discriminant: condensate-sector dark ontology versus additional dark fields.** Standard dark-sector models usually introduce new particle species or new fundamental fields beyond the Standard Model. ECT does not begin by adding such independent ontologies. Its dark-sector candidates are instead sought among configurations of the same ordered condensate that already gives rise to gravity, gauge structure, and coherent matter sectors: either long-wavelength collective excitations within BR1, or genuine defect / topological sectors outside it. The distinctive ECT claim is therefore not that the dark sector is already quantitatively solved, but that at least part of the dark ontology may come from the same medium rather than from externally added fundamental ingredients.

**Falsifier for the defect-sector dark programme.** The present programme would be weakened if a completed dynamical analysis showed that all defect and topological configurations are either too unstable, too strongly coupled to visible matter, or too rarely produced to play any cosmological rôle. It would be more strongly challenged if observational data unambiguously required dark-sector properties that cannot be accommodated by any condensate configuration or smooth collective excitation of the ordered medium. At present, the quantitative completion needed to settle this question remains open.

**Connection to exchange sectors and entanglement.** The wider topological ontology discussed here does not float free of the earlier quantum-sector structure. For indistinguishable excitations, the admissible sector structure is already constrained by the exchange topology of Section 24.4. More broadly, the common-medium ontology emphasised in Section 31 continues to apply here: defect and topological sectors are not external add-ons, but further configurations of the same ordered condensate whose smooth branch also supports non-factorisable coherent correlations.

### 34.4 Measurement and observability status

Three observational levels can be distinguished:

- (i) **Macroscopic phenomenology (MP):** modified galactic and cosmological response, already developed in detail in Macroscopic Physics;
- (ii) **Indirect coherent signatures:** relic populations, nonstandard clustering, or vacuum-transition effects (structurally motivated, Level B);
- (iii) **Direct microscopic detection:** currently open and likely model-dependent.

Only the first level is currently developed in substantial detail.

**Status summary.** *Established (Level A):* (i) the ordered-condensate state space extends beyond the smooth coherent branch BR1; (ii) this wider state space structurally admits configurations with singular cores, discontinuous ordering data, and nontrivial Euclidean sector transitions.

*Level B:* (i) the provisional classification of defect sectors and their interpretation as dark-sector candidates; (ii) smooth collective excitations as the nearest dark-sector candidates within the coherent

EFT; (iii) the architectural split of the dark sector into a macroscopic effective layer and a coherent / topological layer.

*Open:* (i) the full dynamical classification of defect sectors; (ii) their production, stability, and interaction mechanisms; (iii) a unique first-principles identification of the dominant dark-sector component; (iv) the quantitative rôle of defect ensembles in late-time cosmology.

**Summary.** The smooth coherent branch BR1 is not the whole Quantum Sector. ECT naturally admits a wider ordered-condensate state space including defect and nonperturbative sectors beyond the smooth branch. These sectors are not yet dynamically completed, but they are already conceptually important because they supply the coherent/topological layer of the ECT dark-sector architecture. This preserves the correct division of labour across the article: macroscopic dark phenomenology is developed in MP, whereas genuinely topological or defect-based dark ontology belongs to QS.

### Bridge to black-hole thermodynamics

The topological and defect sectors developed here complete the ontological landscape of the Quantum Sector beyond the smooth coherent branch. The next section turns to the asymptotic infrared regime of the same ordered medium. Rather than defect and topological sectors beyond the smooth branch, it examines the long-wavelength ordered-branch structure relevant to asymptotic symmetries, gravitational memory, and soft graviton modes, before the subsequent transition to the strong-field black-hole sector.

## 35 Infrared and asymptotic structure of the ordered branch

*Status: Level B/C structural. The section claims compatibility of ECT's asymptotic ordered-branch structure with the established infrared sector of general relativity — BMS-type asymptotic symmetries, gravitational memory, soft graviton theorems, and soft hair on black holes — and identifies ECT-native long-wavelength degrees of freedom that would enter a first-principles IR formulation. No Level A predictive derivation is attempted. Connection: the orientation/effective-metric sector of Sections 3.6 and 8.5; the channel taxonomy of Section 33; the black-hole sector of Section 36, which uses the critical-shell, interface-thermality, and fluctuation–dissipation language that the present section supplements with its asymptotic counterpart.*

### 35.1 Restriction to asymptotically flat ordered backgrounds

**Restriction.** The discussion below is restricted to asymptotically flat ordered-branch settings, where null-infinity language is meaningful. Its direct extension to cosmological FRW-like ordered backgrounds is not assumed here, and is deferred as a separate structural question.

### 35.2 Why the infrared sector matters for ECT

ECT is built on an ordered branch with asymptotic configuration  $(\phi_0, n_A^{(0)})$ . Large-wavelength perturbations of this asymptotic ordered state are the natural infrared degrees of freedom to examine in the framework. The modern treatment of the gravitational infrared in general relativity — BMS asymptotic symmetries [224, 225], gravitational memory [158], soft graviton theorems [226], and the asymptotic symmetry / soft / memory triangle [227, 228] — is formulated precisely in this regime. It therefore provides a disciplined test of whether the ECT ordered-branch picture remains structurally compatible with established IR physics.

### 35.3 BMS-type asymptotic compatibility

The asymptotic ordered-branch data  $(\phi_0, n_A^{(0)})$  provide the natural arena in which any BMS-type asymptotic symmetry analysis of ECT would most naturally be formulated [224, 225]. Structural compatibility

is claimed; a first-principles derivation of the BMS group — including the infinite-dimensional supertranslation sector — from the ECT action is not. The embedding of supertranslation-type gauge freedom in the residual reparametrisations of  $(\phi_0, n_A^{(0)})$  is an open programme-level item.

### 35.4 Gravitational memory as persistent asymptotic condensate shift

Gravitational memory [158] is the permanent shift in the metric at null infinity following the passage of gravitational radiation. In ECT, the natural interpretation is a persistent rearrangement of the asymptotic ordered-branch configuration  $n_A^{(0)} \rightarrow n_A^{(0)} + \Delta n_A$  left behind by a bulk emission event. This is a Level B/C structural reading compatible with the memory effect; a quantitative derivation of the memory amplitude from ECT dynamics is open.

### 35.5 Soft gravitons as long-wavelength $\delta n_A$ modes

Soft graviton theorems [226, 228] state that the emission of zero-energy gravitons carries nontrivial asymptotic information and connect directly to BMS supertranslations and to memory [227]. In ECT, long-wavelength  $\delta n_A$  modes are the natural soft excitations; the identification of the massless spin-2 mode with  $\delta n_A$  already established in Part I is consistent with their role as soft gravitons.

**Caveat.** The existence of soft modes does not by itself solve any information problem; it only identifies a potentially relevant low-energy bookkeeping sector.

### 35.6 Restrained bridge to soft hair on black holes

Hawking, Perry, and Strominger [229] proposed that black holes carry soft hair — soft gravitons and soft photons on the horizon — as a possible mechanism to store information otherwise lost in Hawking evaporation. The long-wavelength  $\delta n_A$  modes identified above provide candidate long-wavelength degrees of freedom that could enter a soft-hair-like bookkeeping discussion in the black-hole sector, without yet establishing that they suffice to store or recover the required information.

In this sense, the present asymptotic discussion is not a separate information-loss proposal, but a complement to the interface-thermality and fluctuation–dissipation language already used in Section 36. The black-hole section carries out the comparative analysis on its own terms.

### 35.7 Scope and non-claims

The present section does not claim (i) a first-principles derivation of the BMS group from the ECT action; (ii) a derivation of the memory amplitude or of soft graviton theorems; (iii) a mechanism by which soft hair stores black-hole information; (iv) any extension of these statements beyond asymptotically flat ordered-branch settings. Its claim is narrower: the asymptotic ordered-branch data of ECT provide a structurally compatible arena for the established IR sector of gravity, and long-wavelength  $\delta n_A$  modes are the natural ECT-native soft excitations that would enter a first-principles formulation of this sector.

## 36 Black-Hole Thermodynamics, Information Problem, and Holographic-Style Entropy Bounds

*Inputs: coherent-vacuum response (§25), the Unruh-type response (§25.4), the global/reduced unitarity distinction (§23.2), the decoherence programme (§26.1), the Born-weight route (§30.4), the entanglement programme (§31), and the UV-threshold / singularity architecture (§8.3, §14.1). Aim: to reformulate black-hole thermodynamics within the ordered-condensate language, explain how apparent thermal mixedness can arise without fundamental information loss, and identify the critical ordered-phase shell as the current ECT strong-field closure. Status: Level A for the negative result that fundamental information*

*destruction is incompatible with the global coherent framework, and for the compatibility of reduced-state thermality with global purity. Level B for the critical ordered-phase shell closure and for all constructive horizon-thermodynamic results built on it. Open for the explicit nonlinear strong-field profile of the shell, the constructive Page-curve mechanism, and the first-principles derivation of horizon thermodynamic coefficients from bare P3 (OP-Q13). Connection: medium character (P5), the coherent-vacuum response programme, the Unruh/horizon continuity, the global/reduced unitarity distinction, and the branch-breakdown logic of the ordered medium.*

**Physical picture: the horizon as an emergent condensate interface.** ECT reframes the black-hole horizon not as a fundamental singularity of causal structure but as an emergent interface in the condensate medium. This provides a microscopic language for why semiclassical Hawking thermality may survive while allowing controlled corrections in dispersion, late-time correlations, and strong-curvature response. The present section organises the mechanism and its observable channels; it does not yet provide a complete first-principles microtheory of black holes. The shell model, Page-curve-like behaviour, and the absence of fundamental information loss should be read as an organisational framework, not as a closed theorem.

**What is established, what is closure-dependent, and what remains open in the black-hole programme.** The black-hole and information programme in ECT should be read in three layers. First, the theory already fixes the conceptual backbone: the total condensate state is not fundamentally mixed, reduced-state mixedness is observer-dependent, and strong-field breakdown of the ordered branch is expected once the same condensate reaches its critical amplitude or UV threshold (§8.3, §14.1). These points are structural. Second, the present article adopts a concrete strong-field closure: the near-horizon critical shell. Within that closure, approximate horizon thermality, enlarged Hilbert space bookkeeping, and reduced-state mixedness can be organised consistently without fundamental information loss. Third, what remains open is the completed nonlinear evaporation problem: the exact shell dynamics, the precise Page-curve mechanism, and the fully explicit bridge between the reduced thermal appearance and the globally unitary condensate evolution.

A consistent Quantum Sector cannot stop at wave dynamics, commutators, decoherence, and Born-type probabilities. It must also address the strongest known tension between quantum unitarity and horizon thermodynamics: the black-hole information problem. The corresponding accelerated-observer version of the same vacuum-response logic is developed earlier in Section 25.4. The purpose of the present subsection is twofold:

- (i) to reformulate black-hole thermodynamics within the ordered-condensate language of ECT;
- (ii) to show how apparent thermal mixedness can arise without postulating fundamental information destruction.

**Medium reading (P5).** Under the medium interpretation (P5), the black-hole horizon is not treated as a fundamental boundary in an abstract spacetime manifold. It is the strong-field interface of the same ordered condensate whose weak-field limit gives the effective Lorentzian geometry used in Macroscopic Physics. The information problem is therefore reformulated in medium language: not “does spacetime destroy information?”, but “how does one ordered condensate reorganise accessible and inaccessible coherent sectors in the strong-field regime?” Apparent thermality, reduced-state mixedness, and limited observer access are all properties of one physical medium rather than of a separate ontological stage.

**Connection to the Unruh/horizon continuity.** The present black-hole programme is the strong-field continuation of the same vacuum-response logic already encountered in the Unruh-type response of Section 25.4. There, accelerated observers saw an effectively thermal reduced state in flat-space ordered-medium language. Here, the same logic is carried into the gravitational strong-field regime, where the

effective causal interface is associated with a horizon and its near-shell region. In this sense, black-hole thermality is not an isolated new sector, but the strongest-field manifestation of the same ordered-vacuum response structure. In particular, the Tolman local temperature that drives the near-horizon critical shell is the strong-field continuation of the same Unruh-type temperature that an accelerated observer sees in flat-space ordered-medium language.

**Discriminant with respect to standard black-hole resolutions.** ECT differs from the standard options in a precise way. It does not accept fundamental information destruction. It also does not solve the problem by simply postulating a bounce, a remnant, or a new microscopic interior law unrelated to the rest of the theory. Instead, it uses the same ordered medium, the same reduced-state logic, and the same branch structure already employed in decoherence, vacuum response, and singularity breakdown. Thus the ECT proposal is neither “information is destroyed” nor “information is restored by an unrelated extra sector.” It is: apparent thermality is a reduced-state phenomenon of one single condensate, and the strong-field regime signals branch reorganisation rather than fundamental non-unitarity.

### 36.1 Effective horizon thermodynamics

#### Black-hole thermodynamics as the effective horizon response

At the effective macroscopic level, a black hole is characterised by its horizon area  $A_H$  and surface gravity  $\kappa_H$ . In standard semiclassical language (using the conventional  $\hbar$  before the  $S_0 = \hbar$  identification):

$$T_H = \frac{\hbar \kappa_H}{2\pi c k_B}, \quad (36.1)$$

$$S_{BH} = \frac{k_B A_H c^3}{4G_N \hbar}. \quad (36.2)$$

Within ECT these formulas are the effective thermodynamic target that the coherent branch must reproduce or reinterpret; they are not claimed as first-principles derivations from bare P3.

Once the identification (21.7) is completed, they can be written in the equivalent ECT form

$$T_H = \frac{S_0 \kappa_H}{2\pi c k_B}, \quad S_{BH} = \frac{k_B A_H c^3}{4G_N S_0} \quad (36.3)$$

This rewriting is Level B since it depends on the final  $S_0 = \hbar$  identification (21.7).

#### First law and generalized entropy bookkeeping

At the effective thermodynamic level, the horizon sector should also satisfy the first-law structure

$$dM = T_H dS_{BH} + \Omega_H dJ + \Phi_H dQ, \quad (36.4)$$

where the angular-momentum and charge terms are included for generality. Within ECT this equation is an effective consistency target, not a first-principles derivation from bare P3 (Level B). Equation (36.4) should therefore be read as a Level B effective thermodynamic target for the completed strong-field closure, not yet as a first-principles derivation from bare P3.

The important conceptual point is the entropy bookkeeping. The relevant entropy for the information problem is not the horizon entropy alone, but the *generalized* coarse-grained entropy of the external description:

$$S_{\text{gen}} = S_{BH} + S_{\text{ext}}^{\text{coarse}}, \quad (36.5)$$

where  $S_{\text{ext}}^{\text{coarse}}$  is the coarse-grained entropy of the outside radiation sector. In ECT this is the natural quantity because the external observer never has access to the full condensate state  $\mathcal{H}_{\text{total}}$  (36.7).

Thus the correct thermodynamic question is not whether  $S_{BH}$  alone changes, but whether the external coarse-grained description evolves consistently once horizon, shell, and radiation sectors are treated together.

**Status.** Equation (36.4) is a Level B effective target. Equation (36.5) is the natural ECT entropy bookkeeping variable for the reduced observer. Its exact dynamical evolution in the completed evaporation problem remains open (OP-Q13).

## 36.2 The information paradox in ECT

### The paradox in brief

The information paradox arises from three apparently simultaneous ingredients:

- (i) pure-state gravitational collapse,
- (ii) thermal Hawking emission,
- (iii) complete evaporation of the hole.

If the outgoing radiation is exactly thermal and the hole disappears completely, the final state appears mixed even when the initial state was pure. Schematically,

$$|\Psi_{\text{in}}\rangle\langle\Psi_{\text{in}}| \longrightarrow \rho_{\text{rad}}^{\text{thermal}}, \quad (36.6)$$

which would violate unitarity if taken as the *fundamental* evolution law of the full system.

### ECT reformulation of the paradox

ECT changes the conceptual framing. The relevant question is not: *does spacetime itself destroy information at the horizon?* The correct question inside ECT is: *how does the ordered condensate reorganise the distinction between accessible and inaccessible coherent sectors near a strong-field horizon?*

In the coherent branch, mixedness is never primary. Mixedness appears only after one coarse-grains over, or traces out, part of the total condensate state space. Thus the correct ECT reading of Hawking thermality is *reduced-state thermality*, not fundamental state destruction.

### The critical ordered-phase shell

The natural ECT mechanism is the existence of a strong-field transition region near the horizon, where the ordered Lorentzian branch becomes critically strained. In the current closure this is described as a *critical ordered-phase shell*: a finite region surrounding the effective horizon in which:

- (i) the macroscopic Lorentzian ordering becomes marginal,
- (ii) coherent and topological degrees of freedom become strongly coupled,
- (iii) the outside observer's effective Hilbert-space description ceases to coincide with the full condensate state space.

This shell is a Level B strong-field closure of the ECT horizon problem, not a completed first-principles theorem from bare P3. But it is structurally natural: it is precisely where the ordered Lorentzian branch should become delicate.

### Enlarged Hilbert space and apparent mixedness

The key structural point is that the external observer does not have access to the full condensate state space. One should therefore distinguish (Level B effective decomposition):

$$\mathcal{H}_{\text{total}} = \mathcal{H}_{\text{ext}} \otimes \mathcal{H}_{\text{shell}} \otimes \mathcal{H}_{\text{int}}, \quad (36.7)$$

where  $\mathcal{H}_{\text{ext}}$  is the asymptotically accessible exterior sector,  $\mathcal{H}_{\text{shell}}$  is the critical ordered-phase shell sector, and  $\mathcal{H}_{\text{int}}$  is the interior or otherwise inaccessible strong-field sector. The decomposition (36.7) is itself Level B: it depends on the critical-shell closure and not yet on a first-principles derivation from bare P3.

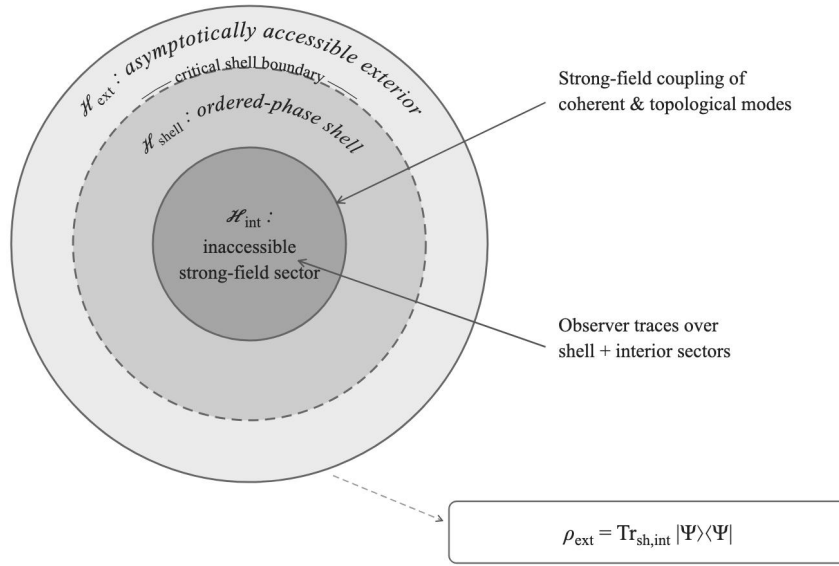


**Figure 39:** Schematic ECT picture of the near-horizon strong-field region (Level B). The exterior observer has access only to an effective reduced sector, while a critical ordered-phase shell mediates between the asymptotic region and deeper strong-field degrees of freedom. In this picture, approximate Hawking thermality is interpreted as a reduced-state phenomenon rather than as fundamental information destruction. The dashed circle marks the effective boundary of the critical ordered-phase shell. This is a Level B strong-field closure schematic, not a completed global solution of the evaporating black-hole problem.

Figure 39 is schematic: it visualises the current Level B strong-field closure and should not be read as a solved global metric profile. For the present strong-field bookkeeping, generalized-entropy structure, and the open shell-dynamics problem, see Appendices BB, BB.4, and BB.5.

The physically observed radiation state is not the total state but a reduced state:

$$\rho_{\text{ext}} = \text{Tr}_{\text{sh,int}} (|\Psi_{\text{total}}\rangle\langle\Psi_{\text{total}}|). \quad (36.8)$$

A reduced state of this form can be approximately thermal even when the total state remains pure and the total evolution remains unitary.

### Page-curve logic in ECT language

A useful way to formulate the information problem operationally is through the Page-curve question: does the entropy of the outgoing radiation continue to rise until the end of evaporation, or does it eventually turn over as required by global unitarity?

In ECT the sharpest current statement is structural. If the total ordered-condensate evolution remains unitary on  $\mathcal{H}_{\text{total}}$  (36.7), then the radiation entropy seen by the external observer is the entanglement entropy of a reduced sector, not a fundamental entropy of the full state. Therefore a Page-like turnover is not forbidden in principle. On the contrary, it is the behaviour one should expect once the shell and interior bookkeeping are treated consistently (see (36.5)).

What is still missing is the explicit strong-field evolution law needed to compute a concrete Page curve from the ECT shell dynamics:

- the *possibility* of Page-curve-compatible unitary evaporation is structurally supported (Level B);
- the *explicit Page curve* is still open (OP-Q13).



**Summary.** ECT already changes the logic of the Page problem: the radiation entropy is that of a reduced observer sector, so its apparent thermality does not by itself imply the destruction of the full coherent-state information.

### Why this already weakens the paradox structurally

This point is stronger than a merely effective analogy. The whole logic of the Quantum Sector already established (Sections 26.1 and 30.4) that:

- (i) coherent amplitudes are primary;
- (ii) mixedness emerges from reduction or decoherence;
- (iii) reduced observers need not track the full coherent state space.

Exactly the same logic applies to the horizon problem. Therefore fundamental information destruction is not the natural default interpretation inside ECT. The natural default is *observer-dependent apparent mixedness from tracing over inaccessible coherent sectors*.

### Conditional theorem: thermality without fundamental information loss

The strongest honest statement currently available is the following conditional result.

**Conditional theorem (ECT horizon thermality).** If the total ordered-condensate evolution across  $\mathcal{H}_{\text{total}}$  remains unitary, and if the near-horizon critical shell acts as an effective environment for the exterior observer, then an approximately thermal reduced state  $\rho_{\text{ext}}$  (36.8) can arise without fundamental information loss.

Status:

- **Level A:** the general logic that thermal reduced states do not imply fundamental nonunitary evolution is a structural consequence of the global/reduced unitarity distinction together with the reduced-state formalism established in Sections 23.2, 26.1, and 30.4.
- **Level B:** the specific critical ordered-phase shell closure used to realise this logic for a black-hole horizon.

### Why the paradox is weaker in ECT than in semiclassical gravity

The information problem appears especially sharp in frameworks that assume the semiclassical spacetime description is exact all the way through the evaporation process. ECT does not make that assumption.

The reason is structural: the macroscopic Lorentzian branch is itself an emergent ordered phase. Near a sufficiently strong-field horizon, one should expect the purely macroscopic description to become incomplete and to require the coherent completion provided by the Quantum Sector. ECT therefore naturally predicts a domain in which naive semiclassical coarse-graining ceases to be the full story.

This does not automatically solve the full evaporation dynamics. But it removes the *expectation* that a strictly semiclassical horizon description must remain exact in the strong-field regime. That is why the paradox is structurally weaker in ECT than in a framework that treats the semiclassical geometry as always complete.

## 36.3 Comparative mapping: the critical shell and the islands/QES language

*Status: Level B/C structural mapping. The islands formula and the QES formalism are standard tools of the modern semiclassical/holographic black-hole programme. The present subsection translates the ECT critical-shell picture of Section 36.2 into that language, without claiming a derivation of either framework from the other. Connection: the Hilbert-space decomposition (36.7); the reduced-state reading of Hawking thermality; the global/reduced unitarity distinction (§23.2); the IR/soft-hair bridge of Section 35.6.*

## Why a mapping is useful

Section 36.2 formulated the ECT reading of Hawking thermality through a critical ordered-phase shell and the Hilbert-space decomposition  $\mathcal{H}_{\text{total}} = \mathcal{H}_{\text{ext}} \otimes \mathcal{H}_{\text{shell}} \otimes \mathcal{H}_{\text{int}}$  in (36.7). The modern holographic programme arrives at Page-curve-compatible radiation dynamics through a different language: that of quantum extremal surfaces and islands. The present subsection maps the two languages onto each other as far as current structure allows. *The point of the present mapping is compatibility of structural logic, not an ECT derivation of the Page curve.* Both pictures distinguish between globally unitary bookkeeping and the reduced thermal entropy seen by an exterior observer; that common logic is what makes the mapping possible.

## Brief recap of the QES/islands programme

The modern holographic programme computes the entropy of Hawking radiation via the generalised entropy [230, 231]

$$S_{\text{gen}}(\Sigma) = \frac{\text{Area}(\partial\Sigma)}{4G_N} + S_{\text{bulk}}(\Sigma), \quad (36.9)$$

extremised over bulk regions  $\Sigma$  [232]. The inclusion of disconnected “island” regions inside the black hole proves decisive for radiation entropy [233, 234]: before the Page time the minimal QES is empty; after the Page time a non-trivial island dominates, yielding the Page-curve turnover.

## Core structural mapping

Table 97 sets out the structural correspondence between the two languages.

**Table 97:** Structural mapping between the ECT critical-shell picture and the QES/islands language. Entries in the right column are structural analogies, not derived equivalences.

ECT side	Islands/QES side	Structural relation
$\mathcal{H}_{\text{int}}$ (interior / inaccessible sector)	island region	structurally analogous role: degrees of freedom outside the exterior reduced description but counted in the globally unitary picture
boundary of critical ordered-phase shell	quantum extremal surface boundary $\partial\Sigma$	structurally analogous interface between accessible and inaccessible sectors
$\rho_{\text{ext}}$ $\text{Tr}_{\text{shell,int}} \Psi_{\text{total}}\rangle\langle\Psi_{\text{total}} $	= reduced radiation state whose entropy is given by $S_{\text{gen}}$ at the dominant QES	both are reduced-state objects derived under globally unitary dynamics
Page-curve possibility (Level B, eq. (36.7))	Page-curve turnover via island transition	qualitative Page-curve compatibility, not a derivation
long-wavelength $\delta n_A$ modes near the critical shell	soft hair on or near the horizon	candidate long-wavelength bookkeeping sector, independently formulated

## Where the mapping is formal and where it is structural only

**Formal or near-formal correspondence.** The role of globally unitary dynamics in making a reduced-state Page-curve compatible is the same in both frameworks. The interior/island sector and the ECT  $\mathcal{H}_{\text{int}}$

sector play the same structural role as coherent degrees of freedom inaccessible to an exterior observer. The shell boundary and  $\partial\Sigma$  both mark the effective transition surface beyond which exterior reduced dynamics alone is incomplete.

**Structural only.** ECT does not derive the generalised entropy formula (36.9) from first principles. The critical-shell / Hilbert-space decomposition is compatible with such a formula but does not imply it. ECT also does not provide a replica-wormhole-type computation; replica wormholes are a Euclidean gravitational path-integral device, and an analogous computation on the underlying Euclidean condensate path integral is an open item. The detailed time dependence of the ECT Page curve requires the explicit shell dynamics flagged as OP-Q13 in Section 36.2.

**Shell is not a derived QES.** In particular, the critical-shell boundary is not here identified with a derived quantum extremal surface. At present it is only a structurally analogous interface separating reduced exterior thermality from the globally unitary description.

### Scope and non-claims

The present subsection does not claim (i) a first-principles derivation of the QES or islands formula from ECT; (ii) a replica-wormhole-type calculation in ECT; (iii) an explicit Page curve for a specific ECT evaporation scenario; (iv) that the critical-shell picture and the islands picture are formally equivalent. Its claim is narrower: the two pictures make structurally compatible statements about the reduced-state origin of apparent thermality and the possibility of Page-curve-compatible evaporation, thereby placing the ECT black-hole sector in close structural alignment with current holographic approaches while keeping the mechanisms distinct.

## 36.4 Black-hole entropy and observational signatures

### Black-hole entropy in the ECT reading

In this picture the Bekenstein–Hawking entropy  $S_{BH}$  measures the coarse-grained entropy associated with the restricted external description of the ordered condensate in the presence of a horizon. This is fully analogous to the decoherence discussion of Section 26.1: entropy increase and mixedness belong to reduced descriptions, not necessarily to the total microscopic state.

### Relation to Hawking radiation and vacuum effects

ECT does not deny Hawking-like emission. The coherent-vacuum logic of Sections 25.5 and 25.4 confirms that horizon-induced excitation production is natural in an ordered vacuum. What ECT changes is the interpretation: Hawking radiation is not evidence for fundamental information loss, but for the fact that the exterior observer is coupling to a reduced, effectively thermal sector of the total ordered condensate.

### Thermality versus exact thermality

The black-hole information problem becomes most severe if the outgoing radiation is assumed to be *exactly* thermal at all stages. ECT does not require such exact thermality. What the current shell-based closure supports is approximate thermality of the reduced external state (36.8).

This distinction matters. Approximate thermality is perfectly compatible with hidden correlations, late-time purification effects, and a Page-curve turnover. Exact thermality would be much harder to reconcile with global unitarity.

Therefore the correct ECT statement is: the external observer can see an approximately thermal spectrum, while the total ordered-condensate evolution can still remain pure. This dissolves the strongest form of the paradox at the structural level, even though the completed quantitative evaporation problem remains open (OP-Q13).

## Horizon microphysics and observational signatures

The ECT horizon picture should not remain purely conceptual. If the critical ordered-phase shell is physically real, it should leave at least weak observational signatures in strong-field gravitational systems.

**Near-horizon mode conversion.** In standard semiclassical gravity, Hawking radiation is derived from a Bogoliubov transformation between “in” and “out” modes on a curved background. ECT does not deny that effective description, but reinterprets its physical origin: the horizon is a strong-field interface in the ordered condensate, not a fundamental boundary. Apparent thermality can arise from:

- (i) mode conversion in an inhomogeneous ordered background;
- (ii) entanglement across an effective causal interface;
- (iii) noise/dissipation generated by the shell sector acting as an effective environment for external modes.

**Robustness of leading thermality.** A conservative ECT viewpoint is that the leading Hawking temperature should be robust, while the critical-shell microphysics may modify only subleading quantities such as high-frequency spectral tails, greybody factors, late-time correlations, and ringdown transfer functions (Level B).

**Effective near-horizon dispersion parameterisation.** A Level B parameterisation of shell-scale corrections to coherent excitations near the horizon takes the schematic form

$$\omega^2 = c^2 k^2 \left[ 1 + \eta_1 \left( \frac{k}{k_*} \right)^2 + \eta_2 \left( \frac{k}{k_*} \right)^4 + \dots \right], \quad (36.10)$$

where  $k_* \sim \ell_*^{-1}$  is the characteristic momentum scale at which the critical-shell microstructure of the ordered condensate becomes relevant, and  $\eta_1, \eta_2$  are dimensionless closure parameters not yet fixed by bare P3. Possible energy dependence of the effective gravitational response may be represented at the present closure level by

$$G_{\text{eff}}(E) = G_N [1 + \delta_G(E)], \quad (36.11)$$

where  $\delta_G(E)$  is an energy-dependent correction arising from the coherent-sector EFT near the shell; its form is not yet derived from bare P3. Here  $\delta_G(E)$  is a Level B shell-scale parameterisation of the effective strong-field response. Its explicit functional form is not yet derived from bare P3 and should not be read as a first-principles result of the present theory. Equations (36.10)–(36.11) are Level B parameterisations, not first-principles predictions.

**Ringdown spectroscopy.** If the horizon neighbourhood contains critical shell structure, then quasi-normal frequencies of compact objects may differ slightly from pure GR predictions. Small shifts in frequencies or damping times could arise from shell stiffness effects, modified near-horizon dispersion, or coupling to additional coherent modes (Level B).

**Late-time echoes and transfer structure.** If the effective horizon acts as a structured interface rather than a perfectly featureless absorber, weak delayed features in the late-time waveform are not excluded in principle. ECT does not claim such echoes have been observed; the correct statement is only that the shell picture provides a physical mechanism by which such late-time structure could arise (Level B).

**Primordial black holes and early-universe constraints.** If  $G_{\text{eff}}$  is closure-dependent at early epochs, primordial black-hole formation and evaporation histories can constrain the ECT strong-field completion. This provides a natural bridge between the coherent-vacuum horizon problem and the cosmological ordered-background programme of Section 25.5 and Macroscopic Physics (Section 14.1) (Level B).

**Summary.** The current ECT black-hole sector already suggests a concrete observational agenda: ring-down spectroscopy, late-time waveform structure, and primordial black-hole histories are natural Level B tests of the critical-shell closure. They should be read as tests of the present strong-field closure, not as direct tests of the Level A backbone that excludes fundamental information destruction.

**What ECT does not yet provide.** ECT does not yet provide a full Level A dynamical solution of the black-hole information problem. The positive mechanism—how approximate horizon thermality, shell/interface dynamics, and global purity are jointly realised—remains to be constructed.

**What ECT does establish (Level A negative result).** What the current postulate structure does establish more strongly is a *negative* result: fundamental non-unitary destruction of information is *incompatible* with the global coherent framework of the theory. In other words, ECT excludes one branch of possible answers to the paradox. This follows at Level A from the global coherent framework of ECT together with the global/reduced unitarity distinction and the reduced-state logic established in Sections 23.2, 26.1, and 30.4: reduced-state thermality does not imply fundamental loss of information when the total evolution remains globally unitary.

**Status summary.** *Established (Level A):* (i) fundamental non-unitary information destruction is incompatible with the global coherent framework of ECT; (ii) reduced-state thermality is compatible with global purity; (iii) the black-hole problem fits naturally into the coherent-vacuum reading of one ordered medium.

*Level B:* (i) the critical ordered-phase shell closure for approximate horizon thermality; (ii) the enlarged Hilbert-space bookkeeping and observer-dependent reduced-state mixedness; (iii) the structural possibility of Page-curve-compatible unitary evaporation; (iv) the branch-boundary interpretation of the singular core.

*Open (OP-Q13):* (i) the explicit nonlinear strong-field profile of the critical shell; (ii) the constructive Page-curve mechanism; (iii) the first-principles derivation of horizon thermodynamic coefficients from bare P3; (iv) the completed strong-field evaporation dynamics.

In particular, the present shell analysis does not yet derive the full interior profile, first-principles horizon thermodynamic coefficients, or a constructive Page curve; the numerical coefficient in the area-law entropy  $S_{\text{shell}} \sim A/\ell_*^2$  remains an open matching condition.

### 36.5 Area-law scaling and holographic-style entropy bounds as boundary-layer properties of the ECT medium

*Status: Level A for the structural area-scaling mechanism (locality + physical UV threshold + boundary-layer counting). Level B for the generic coefficient  $c_0 = O(1)$ , the matching to  $1/(4\ell_{\text{Pl}}^2)$ , and the extension to soft/massless sectors. Open for covariant formulations, full bulk reconstruction, and exact microscopic entropy-capacity derivation. Connection: shell entropy (§BB.3), conditional theorem (§BB.4), decoherence programme (§26.1), entanglement (§31), UV threshold (§8.3), medium character (P5).*

#### Problem statement: area law, holographic bound, and full holography

In black-hole physics, entropy scales with area rather than volume. In the broader quantum-gravity literature this motivates several related but conceptually distinct ideas:

- (i) the Bekenstein–Hawking area law for black-hole entropy [235];
- (ii) more general holographic-style entropy bounds [236, 237, 238];
- (iii) the stronger holographic principle in the sense of bulk encoding or reconstruction by boundary data [239].

These statements should not be conflated. An area law does not by itself imply full holography, and a shell-counting argument near horizons does not by itself establish a covariant entropy bound for arbitrary dynamical geometries.

The ECT question is therefore:

*Can the area scaling of accessible entropy be understood as a structural property of a local condensate medium with a physical ultraviolet threshold?*

The present subsection argues that the answer is positive at the level of a general boundary-layer area bound, while the exact coefficient, covariant formulations, and strong bulk reconstruction remain open.

### Structural ingredients already present in ECT

The following ingredients are already available within the framework:

- (i) a *physical UV threshold*  $\ell_* \sim m_\sigma^{-1}$ , set by condensate microphysics rather than imposed as an external regulator (§8.3);
- (ii) a *local medium picture*, in which distinct subsystems communicate only through local condensate couplings across interfaces (S5);
- (iii) a *reduced-state interpretation* of mixedness, already used elsewhere in the quantum sector (§26.1, §30.4);
- (iv) an existing *shell-entropy precedent*  $S_{\text{shell}} \sim A \ln q / \ell_*^2$ , showing that black-hole area scaling arises naturally in a special case (§BB.3);
- (v) an *elliptic Euclidean architecture*, which makes boundary control conceptually natural, although this is not itself the proof of the entropy bound.

These features make ECT unusually well suited to explain area scaling without postulating holography as a separate principle.

### Boundary-layer mechanism

Let  $\Sigma$  be a smooth closed two-surface separating exterior and interior subsystems. The reduced state of the exterior observer is

$$\rho_{\text{ext}} = \text{Tr}_{\text{int}} |\Psi\rangle\langle\Psi|, \quad S_{\text{red}}(\Sigma) = -\text{Tr}(\rho_{\text{ext}} \ln \rho_{\text{ext}}). \quad (36.12)$$

In a local medium with finite microscopic resolution, interior–exterior correlations are not generated uniformly throughout the bulk. They are mediated through a finite-thickness interfacial region near  $\Sigma$ . If the relevant sectors have finite effective correlation length  $\xi_{\text{eff}}$ , then only degrees of freedom within a layer of thickness  $O(\xi_{\text{eff}})$  around  $\Sigma$  contribute appreciably to the reduced entropy associated with the split.

Since the number of microscopic cells in that layer scales with the area of  $\Sigma$ , area scaling follows.

**Supporting lemma (exponential clustering).** For the radial sector with mass gap  $m_\sigma > 0$ , the connected two-point correlator satisfies  $|\langle\Phi(x)\Phi(y)\rangle_c| \leq C e^{-m_\sigma|x-y|}$  (standard result for massive Euclidean fields [161]). Cross-boundary correlations from the massive sector are therefore exponentially localised within a layer of thickness  $\xi_{\text{cond}} = O(m_\sigma^{-1}) = O(\ell_*)$  around  $\Sigma$ .

**Definition (effective local entropy capacity).**  $s_*$  denotes the maximal entropy per UV cell under the adopted coarse-graining and energy restriction. We require only  $s_* < \infty$  as an assumption; its exact value is not yet derived from first principles.

## General theorem

**Theorem 36.1** (General boundary-layer area bound in ECT). *Let  $\Sigma$  be a smooth closed two-surface of area  $A(\Sigma)$  separating an exterior and an interior subsystem in the ordered branch of ECT. Suppose that:*

- (i) *the ordered condensate admits a physical UV threshold  $\ell_* \sim m_O^{-1}$ ;*
- (ii) *the sectors contributing appreciably to the reduced entropy across  $\Sigma$  have finite effective correlation length  $\xi_{\text{eff}} = O(\ell_*)$ ;*
- (iii) *under the adopted coarse-graining or energy restriction, each UV cell has finite effective local entropy capacity  $s_* < \infty$ ;*
- (iv) *subsystem couplings are local in the condensate medium.*

*Then the reduced accessible entropy satisfies*

$$S_{\text{red}}(\Sigma) \leq c_0 \frac{A(\Sigma)}{\ell_*^2}, \quad (36.13)$$

*where  $c_0 = O(1)$  depends on the effective local entropy capacity and on the convention used for the finite-thickness boundary layer.*

## Proof

*Step 1: locality restricts relevant correlations to a boundary layer.* Because couplings are local (S5), interior degrees of freedom affect the exterior only through correlations transmitted across the interface. If the relevant sectors have finite effective correlation length  $\xi_{\text{eff}}$ , then correlations between points whose distances from  $\Sigma$  exceed  $\xi_{\text{eff}}$  are strongly suppressed (exponentially for massive sectors, by the supporting lemma above). Hence only a layer of thickness  $O(\xi_{\text{eff}})$  contributes appreciably to the cross-interface reduced entropy.

*Step 2: number of microscopic cells in the layer.* The boundary-layer volume scales as  $V_{\text{layer}} \sim A(\Sigma) \xi_{\text{eff}}$ . With ultraviolet cell size  $\ell_*$ , the number of relevant cells is bounded by

$$\mathcal{N}_\Sigma \sim \frac{A(\Sigma) \xi_{\text{eff}}}{\ell_*^3}. \quad (36.14)$$

For  $\xi_{\text{eff}} = O(\ell_*)$ , this reduces to  $\mathcal{N}_\Sigma \sim A(\Sigma)/\ell_*^2$ .

*Step 3: local entropy capacity bounds the total reduced entropy.* If each relevant UV cell carries at most finite effective entropy capacity  $s_*$ , then  $S_{\text{red}}(\Sigma) \leq s_* \mathcal{N}_\Sigma$ . Substituting the estimate for  $\mathcal{N}_\Sigma$  yields

$$S_{\text{red}}(\Sigma) \leq s_* \frac{A(\Sigma) \xi_{\text{eff}}}{\ell_*^3} \equiv c_0 \frac{A(\Sigma)}{\ell_*^2}, \quad (36.15)$$

with  $c_0 \sim s_* \xi_{\text{eff}}/\ell_* = O(1)$ . □

## Interpretation

This theorem is deliberately modest in the right way. It does not derive the exact Bekenstein–Hawking coefficient. It does not derive a covariant Bousso-type bound. It does not establish full bulk reconstruction.

What it does establish is a strong structural fact: *in a local condensate medium with a physical ultraviolet threshold, the reduced accessible entropy associated with a subsystem split is naturally controlled by a boundary layer and therefore scales with area rather than volume.*

In ECT, area scaling is therefore not a mysterious gravity-only postulate. It is a structural property of a local medium with finite microscopic resolution.

**Medium reading (P5).** Under the medium interpretation (P5), the area bound is not an external holographic postulate imposed on a gravitational theory. It is a structural property of the ordered medium itself: the information accessible to an external observer is limited by the boundary-layer channel, whose capacity scales with area.

### Relation to the black-hole shell result

The shell-entropy result developed earlier (§BB.3),

$$S_{\text{shell}} \sim \frac{A \ln q}{\ell_*^2}, \quad (36.16)$$

now appears as a special case of the general theorem, with the identification  $c_0 \leftrightarrow \ln q$  up to precise conventions.

The general theorem supplies the existence of an area-type bound, while the shell computation supplies a concrete black-hole realisation of it.

The exact Bekenstein–Hawking coefficient corresponds to the matching condition

$$\frac{\ln q}{\ell_*^2} = \frac{1}{4\ell_{\text{Pl}}^2}. \quad (36.17)$$

In ECT the ultraviolet length entering the area law is tied to the condensate microphysics, naturally through  $\ell_* \sim m_\sigma^{-1}$ . The exact dimensionless coefficient depends on the effective local microstate capacity and possibly on additional condensate-sector structure, but is not yet derived from first principles. This should be presented as a matching condition, not as an already closed first-principles derivation.

### Entanglement-entropy bridge

The above result also clarifies the relation between ECT and the standard area law of entanglement entropy in continuum QFT.

In continuum QFT, entanglement entropy across a surface is known to scale as area, but with a UV-divergent coefficient [240, 241]:

$$S_{\text{ent}}^{\text{QFT}} \sim \frac{A}{\varepsilon^2}, \quad (36.18)$$

where  $\varepsilon$  is a UV regulator. ECT does not merely reuse the same formula with an arbitrary cutoff. It replaces the formal regulator by a physical condensate threshold:

$$\varepsilon \rightarrow \ell_* \sim m_\sigma^{-1}. \quad (36.19)$$

The result is therefore upgraded from a regulator-dependent divergence to a finite structural entropy bound:

$$S_{\text{red}}^{\text{ECT}} \lesssim c_0 \frac{A}{\ell_*^2}. \quad (36.20)$$

ECT thereby provides a physical meaning for the microscopic scale entering the area law: the cutoff is not an artefact of calculational convenience but a physical property of the ordered medium.

### Role of the Euclidean elliptic structure

The Euclidean branch provides an additional architectural reason why boundary control is natural in ECT. Because the Euclidean condensate equation is elliptic, classical field configurations are naturally organised by boundary data.

This makes boundary encoding conceptually native to ECT, but the actual entropy bound proven above rests on locality, physical UV threshold, finite effective correlation length, finite local entropy capacity, and reduced-state logic. The elliptic boundary-value property is therefore supportive architecture, not the central proof.



## Soft sectors and subleading corrections

The leading boundary-layer argument applies cleanly to sectors with finite  $\xi_{\text{eff}}$  and finite effective local entropy capacity. Soft or constrained sectors may modify this picture in subleading ways: Goldstone sectors, gauge-edge modes, long-range constrained sectors, and other nearly gapless collective excitations.

Known QFT results suggest that such sectors typically preserve the leading area term while modifying coefficients or adding logarithmic corrections [241]. However, this has not yet been worked out explicitly within ECT.

Therefore the present theorem should be understood as establishing the core area-law mechanism for sectors with finite effective correlation length, while the detailed treatment of soft-sector corrections remains open.

## Relation to the Page-curve and information-capacity programmes

The area-law theorem has an important consequence for the black-hole information programme. A bound of the form  $S_{\text{shell}} \lesssim c_0 A / \ell_*^2$  implies a finite effective shell information capacity under the adopted coarse-graining. This strengthens the shell-based Page-curve programme by removing one otherwise free assumption, namely the need to postulate a finite shell information reservoir by hand.

However, this does not by itself derive a Page curve. Additional dynamical ingredients are still required: explicit information return mechanism, purification dynamics, and temporal correlation transfer. Thus the theorem narrows the gap but does not close it fully.

## Relation to the decoherence programme

The same interfacial logic clarifies the relation between entropy bounds and decoherence. The influence-functional machinery of ECT (§26.1) already describes how inaccessible degrees of freedom induce reduced-state evolution and decoherence in an observed subsystem. The present area-law result shows that, in a local medium with finite UV resolution, both reduced entropy and decoherence are controlled by the same boundary-layer architecture.

This does not yet yield a new quantitative decoherence theorem, but it makes explicit that entropy generation and decoherence are two manifestations of the same reduced-description framework.

## From area law to holography: what is and is not derived

It is essential to distinguish:

- (i) *area-law entropy scaling*, which is now structurally supported by the general boundary-layer theorem;
- (ii) *holographic-style entropy bounds*, which are strongly suggested by the medium-native area scaling;
- (iii) *full holography* in the strong reconstruction sense, which remains open.

The correct summary is:

*ECT provides a medium-native structural route to holographic-style entropy bounds. It does not yet provide a full bulk-boundary duality or exact reconstruction theorem.*

Unlike AdS/CFT, ECT currently has no analogue of a Ryu–Takayanagi extremal-surface prescription; the present result is an entropy-capacity bound from medium locality, not a geometrised entanglement functional. Modern quantum error correction reformulations of holography likewise remain outside the current scope.

## Comparison with other approaches

**Table 98:** Comparison of area-law routes.

Aspect	AdS/CFT	LQG	ECT
Why area scaling	Duality; extremal surfaces; boundary CFT	Quantum-geometric state counting	Boundary-layer entropy in a local medium with physical UV threshold
UV scale	String / AdS completion	Planck discreteness	Condensate threshold $\ell_* \sim m_\sigma^{-1}$
Exact coefficient	Model-specific, often controlled	Counting-dependent; Immirzi parameter	Not yet derived; matching condition (36.17)
Full bulk reconstruction	Central feature	Not standard	Open
Physical picture	Gravity/gauge duality	Quantum geometry	Local ordered medium with reduced-state boundary entropy

**Discriminant: ECT area bound versus standard approaches.** The ECT route is architecturally distinct: it requires no gravity/gauge duality, no quantum-geometry discreteness, and no extra-dimensional construction. Area scaling arises from boundary-layer locality in a continuous ordered medium with a physical UV threshold. ECT suggests that area-law entropy bounds should be understood as generic interface properties of the ordered medium, not as features unique to black-hole gravity alone.

**Falsifier for the area-law programme.** The programme would be weakened if (i) the condensate UV threshold  $m_\sigma$  were shown to be incompatible with the BH matching condition (36.17); (ii) a completed ECT sector violated area scaling in a non-logarithmic way; or (iii) soft-sector corrections were shown to dominate rather than remain subleading.

**Status summary.** *Strongly established structurally (Level A):* (i) physical UV threshold  $\ell_* \sim m_\sigma^{-1}$ ; (ii) local-medium interpretation of subsystem splits; (iii) boundary-layer route to area scaling (Theorem 36.1).

*Partly established / conditional (Level B):* (i) generic  $c_0 = O(1)$  coefficient; (ii) extension to all soft, massless, and gauge-edge sectors (expected from known QFT results, not yet established in ECT); (iii) exact matching to  $1/(4\ell_{\text{Pl}}^2)$ ; (iv) shell entropy as special case; (v) strengthened Page-curve architecture.

*Open:* (i) covariant Bousso-like formulation; (ii) full bulk-boundary reconstruction / strong holographic principle; (iii) exact microscopic derivation of local entropy capacity  $s_*$ ; (iv) complete treatment of all constrained soft sectors.

## 36.6 Singularity, interior, and structural programme

**Black-hole singularity as breakdown of the coarse-grained branch.** The same branch-boundary logic developed for the cosmological sector (§14.1) applies to the black-hole interior. ECT does not yet provide a unique microscopic interior solution that replaces the classical GR singular core by a completely solved regular geometry. What it does provide is a structural reason not to treat the classical singularity as physically fundamental: before the formal GR singular region is reached, the near-horizon and interior condensate state enters a critical regime ( $T_{\text{loc}} \rightarrow T_c$ ,  $\rho \rightarrow 0$ ; Appendix BB.7) in which the

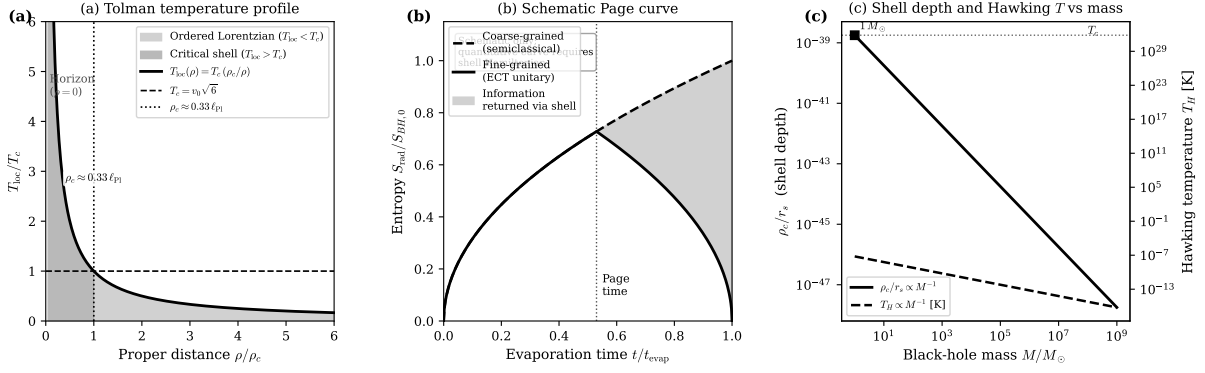


**Figure 40:** ECT black-hole information scenario. **(a)** Tolman temperature profile  $T_{\text{loc}}(\rho)$  near a non-extremal horizon, plotted in units of  $T_c$  vs.  $\rho/\rho_c$ . The condensate critical temperature  $T_c = \phi_0 \sqrt{6}$  (dashed horizontal line) is reached at the universal proper distance  $\rho_c \approx 0.33 \ell_{\text{Pl}}$  (dotted vertical line), independently of the black-hole mass. The lightly shaded region is the well-ordered Lorentzian phase ( $T_{\text{loc}} < T_c$ ); the darker shaded region marks the near-horizon critical shell ( $T_{\text{loc}} > T_c$ ). **(b)** Schematic Page curve. The coarse-grained radiation entropy (dashed) rises monotonically as in the semiclassical Hawking approximation. The fine-grained entropy (solid) follows the coarse-grained branch until the Page time, then decreases as the shell entropy capacity becomes finite and state-dependent corrections to emission become order-one. The shaded area between the two curves represents entropy that is “returned” via shell-mediated correlations. The figure is schematic; a quantitative curve requires the explicit shell Hamiltonian. **(c)** Black-hole parameters vs. mass. The critical shell proper distance  $\rho_c$  is mass-independent (not shown separately); the ratio  $\rho_c/r_s \propto M^{-1}$  (left axis, red) shows how deeply the shell is buried inside the Schwarzschild radius. The Hawking temperature  $T_H \propto M^{-1}$  (right axis, dashed blue) decreases with mass. For all astrophysical black holes  $T_H \ll T_c$ ; the critical shell is firmly in the sub-Planckian regime.

ordered Lorentzian branch is no longer under control. The singular core is therefore interpreted as an artefact of extending the coarse-grained geometric branch beyond its domain of validity.

**Three-regime structure of the near-horizon condensate.** The ECT picture of the near-horizon region (Figure 40a) naturally separates into three physical regimes:

- (i) *Exterior ordered Lorentzian regime* ( $\rho \gg \rho_c$ ,  $T_{\text{loc}} \ll T_c$ ): standard effective geometry valid; purely geometric exterior deviations from GR are expected to be parametrically small because  $\rho_c/r_s \ll 1$  for astrophysical black holes;
- (ii) *Critical shell / interface regime* ( $\rho \sim \rho_c$ ,  $T_{\text{loc}} \sim T_c$ ): described at the closure level by the Ginzburg–Landau / Tolman near-horizon construction (Appendix BB.5); the ordered-branch amplitude transitions from its vacuum value to zero;
- (iii) *Pre-Lorentzian core regime* ( $\rho \ll \rho_c$ ,  $T_{\text{loc}} \gg T_c$ ): the metric language ceases to be fundamental and the interior belongs to the non-geometric condensate sector  $\mathcal{H}_{\text{core}}$  (BB.9).

The Ginzburg–Landau mean-field description of Appendix BB.5 applies only in the near-critical interface region (ii), not as a description of the full interior. A completed theory of the deep interior (iii) requires the pre-Lorentzian condensate dynamics, which is not yet available.

Figure 40 illustrates the near-horizon condensate structure, the schematic Page curve, and the parametric dependence of the critical-shell and Hawking scales on black-hole mass.

**Topological consistency of the shell picture.** The vacuum manifold of the primary ordering transition,  $O(4)/O(3) \simeq S^3$ , has  $\pi_2(S^3) = 0$  (Section 8.10). Since the critical shell is a closed two-surface  $S^2$  embedded in the spatial section, the vanishing of  $\pi_2$  ensures that the condensate field  $n^A$  restricted to the shell carries no topological charge and can transition smoothly from the ordered to the disordered phase without topological obstruction. This is a necessary consistency condition for the shell picture: if  $\pi_2$

were nontrivial, the shell could trap topological charge, potentially obstructing shell formation/dissolution and complicating any evaporation scenario based on a finite-lifetime shell interface. The nontrivial homotopy sector  $\pi_3(S^3) = \mathbb{Z}$  (Section 8.10) admits topological configurations of the exterior ordered-branch field; however, the present work does not derive a stabilising Skyrme-type higher-derivative term or a finite-energy gravitating topological black-hole solution.

**Connection to the UV-threshold and breakdown programmes.** The present strong-field picture is not independent of the earlier ECT architecture, nor from the entanglement programme (§31): the same non-factorisable medium correlations that underlie Bell-type correlations also govern the reduced-state mixedness of the exterior observer. The same condensate radial threshold  $m_\sigma$  that sets the physical UV boundary of the ordered EFT (§8.3) also sets the scale at which the ordered Lorentzian branch becomes delicate near a horizon. Likewise, the same branch-breakdown logic used for cosmological and singularity-type regimes (§14.1) reappears here in the near-horizon shell language. In this sense, the black-hole programme is not an isolated proposal: it is the strong-field continuation of the same ordered-medium threshold physics already used in the UV and singularity sections.

**Cross-sector consistency.** The cosmological and black-hole singularity programmes share the same underlying mechanism: in both cases the singularity is replaced by a branch-boundary interpretation tied to the breakdown of the ordered condensate regime. This cross-sector consistency is a structural requirement of the ECT programme: a completed singularity resolution cannot use unrelated mechanisms for the cosmological and gravitational-collapse cases without undermining the single-medium architecture. Both programmes use the same critical temperature  $T_c = \phi_0 \sqrt{6}$  and the same condensate order parameter: the cosmological pre-Lorentzian epoch is the high-temperature symmetric phase from which the ordered Lorentzian branch emerges, while the black-hole interior is the strong-field regime where the same ordered branch dissolves. This is a conceptual unification internal to the single-medium ECT architecture, not yet a derived cosmological–black-hole duality theorem.

**Discriminant with respect to alternative singularity programmes.** The ECT singularity programme differs from two common alternatives:

- (i) **Classical-GR singularity realism:** the divergence is not treated as a physically meaningful endpoint of the world, but as a sign of branch failure;
- (ii) **Bounce-by-postulate models:** ECT does not simply replace the singularity by a bounce imposed from outside; it first identifies the loss of validity of the ordered geometric branch and leaves the microscopic completion as an open condensate-dynamics problem.

This makes the ECT route more conservative than fully specified bounce models, but also more structurally grounded than simply extrapolating classical GR all the way to infinite curvature.

**Falsifier for the singularity-breakdown programme.** The present ECT singularity programme would be seriously weakened if a completed condensate analysis showed that the ordered Lorentzian branch remains fully valid all the way to the formal GR singularity with no critical-shell, no pre-ordered transition, and no condensate breakdown regime. It would also be weakened if the only consistent completion of the theory forced one back to a physically fundamental divergent singularity rather than to a branch-boundary interpretation. Conversely, any independent indication that classical singular regions are preceded by a physical critical regime would support the ECT reading.

## 36.7 Observational anchors and programme predictions

**Empirical anchors already compatible with the programme.** Several existing observations are already compatible with the present ECT black-hole programme, although none alone proves it. The

persistent shadow structure of M87\* seen by the Event Horizon Telescope supports the existence of a stable effective horizon-scale response region, rather than an obviously pathological strong-field surface. Gravitational-wave ringdown tests remain broadly consistent with Kerr-like exterior behaviour and with no dramatic departure from effective horizon thermality. In ECT these are read as consistency anchors for an exterior-Kerr / interior-reduced-state programme, not yet as direct evidence for the critical-shell closure.

**Parametric thinness of the shell.** For any non-extremal black hole of mass  $M$ , the critical shell lies at a proper distance  $\rho_c = \ell_{\text{Pl}}/\sqrt{3\pi}$  from the horizon in the present Tolman-heating closure. Relative to the Schwarzschild radius  $r_s = 2G_N M/c^2$ , this gives

$$\frac{\rho_c}{r_s} = \frac{\ell_{\text{Pl}}/\sqrt{3\pi}}{2G_N M/c^2} \sim \frac{\ell_{\text{Pl}}}{r_s} \ll 1, \quad (36.21)$$

so the shell is parametrically thin for astrophysical black holes (Figure 40c). This strongly suppresses purely geometric exterior deviations from the Schwarzschild solution. Whether timing observables, late-time correlations, or horizon-scale reflectivity inherit the same suppression depends on the specific near-horizon microphysical closure and is not yet derived in the present work. Direct tests of the shell therefore require either analogue-gravity experiments (§37; Appendix BB.8), or black holes of near-Planck mass (accessible only at the terminal stage of Hawking evaporation).

The present shell construction is developed for the non-rotating (Schwarzschild) case. For Kerr black holes the Tolman relation is modified by rotation and the critical-shell radius may depend on latitude; the analysis of this extension is left to future work.

**Connection to the analogue-laboratory programme.** The ordered-medium reading of horizon thermality finds its closest controlled analogue in superfluid and BEC experiments where sonic horizons generate phononic analogues of Hawking-like radiation (§37). These systems implement the same structural logic: an ordered medium, a critical interface, and an effectively thermal reduced spectrum for an observer with limited access. The analogue-laboratory programme therefore provides the most accessible near-term testing ground for the medium-level ingredients of the ECT horizon picture, even though it does not by itself solve the astrophysical evaporation problem.

**Programme-level predictions of the ECT black-hole architecture.** The present framework suggests four nontrivial expectations. First, approximate Hawking thermality should be only a reduced-state property, not an exact statement about the total condensate state. Second, the same strong-field threshold that limits the ordered branch in cosmology and singularity discussions should reappear in the near-horizon problem; black-hole and cosmological branch breakdown should not require unrelated mechanisms. Third, deviations from pure Kerr thermality, if they appear, should be correlated with shell-scale or breakdown-scale physics rather than with arbitrary ad hoc horizon modifications. Fourth, any future successful Page-curve reconstruction inside ECT should proceed through enlarged-state bookkeeping ( $\mathcal{H}_{\text{ext}} \otimes \mathcal{H}_{\text{shell}} \otimes \mathcal{H}_{\text{int}}$ ), not through fundamental non-unitary evolution.

**Falsifier for the ECT black-hole information programme.** The present programme would be seriously weakened if a completed strong-field analysis showed any of the following: (i) the total condensate evolution must become fundamentally non-unitary; (ii) the near-horizon problem cannot be organised by a reduced-state decomposition with an enlarged shell sector; (iii) black-hole strong-field behaviour and cosmological/singularity breakdown require unrelated mechanisms; or (iv) a successful information-preserving completion is possible only by importing a horizon microphysics entirely disconnected from the ordered-medium architecture used elsewhere in ECT. Conversely, every successful cross-link between horizon thermality, reduced-state mixedness, UV threshold physics, and branch breakdown supports the single-medium reading of the information problem.

**Summary in one sentence.** The paradox is not fully solved, but within the present ECT postulate structure and reduced-state reading there is no need to posit fundamental information destruction as a basic law.

For a more explicit derivational sketch of the reduced-thermality logic, the Hilbert-space factorisation, and the Page-curve discussion, see Appendix BC.

**Summary.** Black-hole thermodynamics in ECT belongs to the Quantum Sector because it probes the coherent-vacuum and reduced-state structure of the ordered condensate. The information paradox is reformulated from “information destruction” into “observer-dependent apparent mixedness”. What is already structurally fixed at the postulate level is the reduced-state logic and the exclusion of fundamental information destruction as a basic law of the theory. What remains Level B and closure-dependent is the concrete near-horizon implementation through the critical shell and the corresponding Page-curve-compatible evaporation route. The full nonlinear strong-field completion remains open (OP-Q13).

### 36.8 Diagnostic discriminants across the gravity–matter interface

*Status: compact cross-programme diagnostic summary. No new physics is introduced; the table consolidates the status of three focal frameworks along axes that discriminate them structurally and observationally. Connection: the costs-of-consistency table of Section 28.4 compared frameworks by architectural cost; the present table instead compares them by diagnostic signatures and structural commitments.*

Table 99 summarises three focal frameworks — linearised-graviton effective field theory, the post-quantum classical-gravity (PCCG) hybrid, and ECT with its common-medium reduced mediator — along six diagnostic axes relevant to the gravity–matter interface.

**Table 99:** Cross-programme diagnostic discriminants among three frameworks for the gravity–matter interface. Entries summarise current structural and experimental commitments; detailed references are in the surrounding text and in the cited sections.

Axis	Linearised-graviton EFT	PCCG / Oppenheim hybrid	ECT common- medium
Independent metric quantisation	Yes (fundamental)	No (classical metric)	No (no independent metric field)
Fundamental stochasticity	No	Yes (fundamental stochastic law)	No (emergent only, via reduction)
Global unitarity	Yes	No (intrinsic informa- tion loss)	Yes (intended full- theory level)
GIE status in meso- scopic protocols	Expected in standard protocols via non- classical mediator exchange	Framework- dependent; the standard stochas- tic reading is not built around unitary mediator-induced entanglement, while loophole construc- tions exist in neigh- bouring hybrid classes	Architecturally com- patible in reduced common-medium regimes (§32); no first-principles protocol-level predic- tion yet
Evaporation / infor- mation stance	Information preserved (holographic comple- tion expected)	Information funda- mentally lost	Reduced-state ther- mality under global unitarity (§36.2)

Axis	Linearised-graviton EFT	PCCG / Oppenheim hybrid	ECT medium	common-
Relation to is- lands/QES language	Natural fit (native to the holographic pro- gramme)	Not naturally formu- lated	Structurally compati- ble (§36.3); not de- rived	

**Reading the table.** The rows are not logically independent: a framework’s stance on metric quantisation strongly constrains its stance on stochasticity and on global unitarity. No single row uniquely falsifies any framework; the table summarises the joint pattern of commitments each framework makes.

**Scope and non-claims.** The table does not claim (i) that the three frameworks exhaust the space of gravity–matter architectures (Newton–Schrödinger-class, measurement-feedback hybrids, and others remain); (ii) that any individual cell is beyond revision with further work in the respective framework; (iii) that current experiments have decided between the frameworks. It is a structural cross-programme summary, not a verdict.

**Bridge to the analogue-laboratory programme.** The black-hole programme, including its comparative mapping to the islands/QES language (§36.3) and the cross-programme diagnostic summary (§36.8), concerns the same ordered medium as the vacuum-response, decoherence, and entanglement sections, but in a different regime. The next section turns from the astrophysical strong-field regime to controlled laboratory analogues, where horizons, mode conversion, and effective thermal response can be studied in experimentally accessible ordered media.

### 37 Analogue Laboratory Programme for Ordered-Branch Tests

*Status: Level A/B for the structural claim that any medium realising compact phase, winding sectors, and environment-sensitive coherent response should admit ordered-branch analogues of ECT subprogrammes. Level B for the concrete mapping from specific laboratory platforms to the vacuum-response, winding, decoherence, and horizon-interface programmes developed earlier in Part III. Analogue systems do not directly test the full gravitational or cosmological branches of ECT. Connection: the winding/conservation architecture (§22.3), the vacuum-response programme (§25), the decoherence and arrow-of-time programme (§26), the quantum–classical boundary (§30.1), the black-hole horizon programme (§36), and medium character (P5).*

**Physical motivation: why analogue experiments matter for ECT.** If ECT is correct, then superfluid liquids, Bose–Einstein condensates, and other condensed-matter systems are not merely “analogies” but realisations of the same physics at a different scale: ordered medium → symmetry breaking → emergent Lorentzian kinematics → vacuum effects. Experiments with Casimir-like effects in superfluid media, decoherence in BEC systems, and analogue Hawking radiation are therefore not tests of analogies but tests of condensate vacuum physics at accessible scales.

**What is established, what is testable, and what remains outside analogue reach.** The ECT analogue laboratory programme should be read in three layers. First, ECT suggests that any medium realising compact phase, local frame redundancy, winding sectors, and environment-sensitive coherent response should admit ordered-branch analogues of ECT phenomena (Level A/B). This is a structurally motivated consequence of the medium character of the theory, not yet a theorem about every possible laboratory medium. Second, specific analogue-accessible phenomena—Casimir-type response, Unruh-like thermal response, phase-slip / winding events, and decoherence scaling—can be probed in condensed-matter, photonic, or superconducting analogue platforms (Level B). Third, no current analogue system reproduces

the full ECT condensate, the gravitational branch, or the cosmological sector. Analogue experiments therefore test the coherent-branch logic and the vacuum-response programme, not the complete theory.

**Medium reading (P5).** The analogue-laboratory programme is the most direct operational expression of the medium interpretation (P5). If the condensate of ECT is a genuine physical medium rather than an abstract mathematical structure, then laboratory media sharing the same structural ingredients—compact phase, winding sectors, coherent correlators, and environment-sensitive response—should exhibit the same ordered-medium logic at the structural level. The analogue programme therefore does not import external phenomenology as a foundation for ECT. Rather, it tests whether the ordered-medium architecture derived in the earlier chapters is physically instantiable in other media.

**Four classes of analogue tests.** The analogue programme divides naturally into four classes, corresponding to different structural ingredients of the coherent branch.

- (i) **Compact-phase and winding analogues:** superfluid helium, atomic BEC, and Josephson systems provide media with quantised circulation, integer winding sectors, and defect-mediated sector changes. These are direct analogues of BR1 and the coherent phase structure.
- (ii) **Vacuum-response analogues:** superconducting circuits (dynamical Casimir platforms [181]), accelerated effective media, and acoustic black-hole experiments [242] probe the boundary, detector, and horizon response of an effective ordered vacuum.
- (iii) **Decoherence analogues:** mesoscopic matter-wave interference experiments with tunable environments and controllable bath coupling test the influence-functional and kernel architecture of the open-system programme.
- (iv) **Critical-environment and branch-sensitivity analogues:** media in which the response depends on a controlled background density, ordering state, or condensate fraction test the environment-dependent logic central to the ECT dark-sector and galactic programmes.

**Connection to the earlier quantum-sector programmes.** The four classes of analogue tests correspond directly to specific ECT programmes developed in the preceding sections. Class (i) probes the compact-phase, winding, and defect-mediated sector-change logic of Sections 21.1 and 22.3. Class (ii) probes the unified vacuum-response logic of Section 25.1 (§25). Class (iii) probes the influence-functional decoherence programme of Section 26 (§26). Class (iv) probes the environment-dependent logic central to the quantum–classical boundary of Section 30.1 and, in strong-gradient setups, the horizon-interface logic that reappears in the black-hole programme of Section 31. In each case, the analogue platform probes the ordered-medium logic itself rather than serving as an external surrogate description of ECT.

**Measurable signatures expected in ECT-compatible analogues.** Five classes of laboratory signatures are expected if the coherent-branch logic is physically realised:

- (a) **Winding-sector robustness:** quantised circulation / holonomy sectors should be topologically stable, with sector changes occurring only through defect-mediated events (phase slips, vortex nucleation) that require local amplitude suppression—never through smooth phase deformations alone. This is the laboratory analogue of the BR1 branch-boundary logic.
- (b) **Vacuum-response channel unification:** the same underlying correlator infrastructure should, after the appropriate projections and reductions, control Casimir-like force, Unruh-like detector response, induced mode production, and decoherence rate. If these four channels require mutually unrelated correlator families, the one-vacuum programme fails.



- (c) **Environment-controlled decoherence scaling:** decoherence strength should track bath occupation, correlation time, spectral form, and coupling to the ordered background—not appear as a mysterious collapse mechanism.
- (d) **Ordered-background sensitivity:** if the medium background is changed (density, stiffness, condensate fraction), response kernels, decoherence rate, and effective critical thresholds should shift together in a correlated manner.
- (e) **Goldstone-counting signature:** in systems where the response is genuinely controlled by  $N_G$  Goldstone-like modes from an  $O(N) \rightarrow O(N-1)$ -type pattern, multiplicity factors in vacuum-response observables should reflect the mode count. This is a conditional signature, not a universal numerical prediction.

**Programme-level predictions.** The analogue programme suggests four nontrivial expectations that go beyond individual system checks. First (unified-kernel prediction), if a single platform allows reconstruction of the effective two-point kernel, then Casimir-like response, Unruh-like response, and decoherence rate should be describable by one kernel family, not by three independent effective laws. Second (phase-slip threshold prediction), topological-sector changes should occur only when the local amplitude is sufficiently suppressed, i.e. sector change is defect-mediated, not smooth-in-phase-alone. This is the laboratory analogue of the branch-boundary and singularity-breakdown logic. Third (environment-correlation prediction), in systems closer to the ordered / coherent regime, phase robustness, long-lived coherence, winding stability, and nonclassical response signatures should improve together, not independently. Fourth (cross-platform universality prediction), different analogue platforms need not agree numerically, but should exhibit the same structural logic: phase redundancy, gradient observables, holonomy sectors, defect-mediated transitions, and environment-driven decoherence.

**What analogue experiments do not test.** Analogue experiments do not test the full ECT framework. In particular, they do not probe the gravitational branch directly, do not confirm  $S_0 = \hbar$  or  $\phi_0 \sim \bar{M}_{\text{Pl}}$ , and do not replace cosmological or astrophysical tests. What they probe is the medium character of the theory, the coherent-branch logic, the vacuum-response programme, the decoherence architecture, and defect-mediated transitions. These are necessary but not sufficient conditions for ECT viability.

**Empirical anchors already compatible with the programme.** Several established experimental results already fit naturally with the ECT analogue programme: quantised circulation in superfluid helium, vortex and phase-slip behaviour in BEC and Josephson systems, the dynamical Casimir effect in superconducting circuits [181], analogue Hawking radiation in BEC acoustic black holes [242], and matter-wave decoherence under tunable environmental coupling. None of these proves ECT, but together they demonstrate that medium ontology, compact phase, winding sectors, environment-driven decoherence, and vacuum response through correlators are physically realisable and experimentally accessible.

**Discriminant: ECT analogue logic versus standard analogue gravity.** In standard analogue-gravity thinking, laboratory media are often used as formal analogues of quantum fields propagating on an effective background geometry. ECT reverses the interpretive priority. For ECT, vacuum response, decoherence, horizon-like thermality, and defect-mediated sector change are medium phenomena from the start: the effective spacetime reading is secondary. Analogue experiments are therefore not invoked as the foundation of the theory, but as evidence that the ordered-medium logic derived earlier in the article is physically instantiable in controlled systems without requiring a fundamental spacetime substrate.

**Falsifier for the analogue programme.** The analogue programme would be seriously weakened if different analogue platforms required fundamentally incompatible structural logics to describe their vacuum response, decoherence, and winding-sector behaviour. It would also be weakened if a completed

analogue implementation showed that Casimir-like response, Unruh-like response, and decoherence kernels cannot be jointly controlled by one effective correlator infrastructure. Conversely, every successful cross-platform confirmation of the unified-kernel, defect-mediated, and environment-correlated logic strengthens the one-medium reading of ECT.

For a compact dictionary relating ECT structural elements to analogue observables, see Appendix BD.

**Status summary.** *Established (Level A/B):* the ordered-medium architecture of ECT implies that laboratory media sharing compact phase, winding sectors, coherent correlators, and environment-sensitive response should display structural analogues of the vacuum-response, winding, and decoherence programmes.

*Level B:* the concrete mapping from specific laboratory platforms (superfluid helium, BEC systems, Josephson and superconducting circuits, acoustic black holes) to the corresponding ECT subprogrammes.

*Not testable by analogues:* the full gravitational branch, the cosmological sector, the values  $S_0 = \hbar$  and  $\phi_0 \sim \bar{M}_{\text{Pl}}$ , and the complete dark-sector identification.

**Summary.** The analogue-laboratory programme does not replace the full gravitational, cosmological, or dark-sector tests of ECT. Its rôle is narrower but conceptually sharp: to check whether the ordered-medium logic developed across Sections 24–29 is physically realisable in controlled systems. In that sense, analogue platforms test the instantiability of the coherent-branch architecture rather than the full theory. A successful analogue programme therefore strengthens the case that ECT is genuinely a theory of a physical medium, not merely a formal re-description of quantum phenomena.

**Bridge to the status map.** The analogue-laboratory programme completes the structural development of the Quantum Sector. The next section collects the results of Sections 19–32 into a single status map, identifies the remaining open problems, and states the completion status of Part III as a whole.

## 38 Status Map, Open Problems, and Completion Status of Part III

This section collects the results of Sections 19–32 into a single status map, identifies the irreducible structural core that ECT has already established, separates it from the closure-level and open fronts, and states the completion status of the Quantum Sector as a whole. Section 38.1 presents the detailed row-by-row status table and the open-problem list. Section 38.2 organises the minimal quantum core into a strict structural tier, a structurally singled-out backbone, and the nearest closure-level or open fronts. Section 38.5 states the overall completion status and provides the bridge from Part III to the summary, comparison, and outlook sections that follow.

### 38.1 Status table and open problems of the Quantum Sector

*Purpose:* to summarise what the Quantum Sector of ECT already establishes structurally, what is presently available only at closure level, and what remains open. This subsection plays for the Quantum Sector the same rôle that the final status table plays for Macroscopic Physics. The assignments below reflect the architectural strengthening of Sections 19–30, including medium character (P5), the global/reduced unitarity distinction, the unified vacuum-response programme, the decoherence/arrow-of-time architecture, the quantum–classical boundary, the conditional Born route via assumptions (C1)–(C3) and Gleason’s theorem, the entanglement programme, the wider topological/dark-sector ontology, the black-hole-information exclusion result, and the analogue-laboratory instantiability programme.

**Methodological note on status levels.** The strengthened postulate and branch structure improves the Quantum Sector in an important but limited way. In several places it still does not promote familiar quantum laws to unconditional Level A theorems. Its real gain is subtler and more architectural: it turns

earlier heuristic claims into conditional structural statements, removes overclaims, narrows the admissible logical possibilities, sharpens the distinction between global and reduced descriptions, and excludes one branch of the black-hole information paradox entirely. The table below reflects these deliberately honest levels.

The Quantum Sector is now organised across Sections 19–32 around the following twelve thematic steps (including the scope/inputs layer as the first step):

- (i) scope, inputs, and logical programme of the Quantum Sector;
- (ii) coherent phase dynamics, loop sectors, and the pre-quantum action scale  $S_0$ ;
- (iii) wave kinematics, real-time parametrisation, extremal-action structure, and conservation laws;
- (iv) Hilbert-space bridge: reflection positivity, unitarity, canonical structure, and the uncertainty principle;
- (v) Euclidean path-dependence, exchange sectors, and Dirac structure;
- (vi) quantum vacuum structure and the unified response programme (Casimir, Unruh, particle production, horizon thermality);
- (vii) open quantum systems, decoherence, and the arrow of time;
- (viii) quantum–classical boundary, probability, Born-type interpretation, and measurement status;
- (ix) quantum entanglement and Bell-type correlations;
- (x) topological / defect sectors and the dark sector;
- (xi) black-hole thermodynamics, Hawking-type radiation, and the information problem;
- (xii) analogue laboratory programme.

The resulting picture is already substantial, but deliberately not overclaimed. Figure 41 and Table 100 distinguish sharply between what is structurally established, what is plausible within the current coherent-sector closure, and what remains open. The status table below should be read together with the open-problem list and the dependency map: the table records local status row by row, the map records logical dependence, and the open-problem list records what is still needed for programme closure.

**Table 100:** Status map of the Quantum Sector of ECT. Level A = strict structural consequence of the current foundational framework P1–P6 together with explicitly stated branch rules (such as BR1). Level A/B = structurally singled out route whose completed physical identification or full closure is not yet finished. Level B = closure-level or conditional result, with the relevant additional assumptions, matching steps, or reduced-state hypotheses explicitly indicated. Open = not yet derived; where available, an explicit open-problem reference is given.

Result	Status	Basis / comment
Result	Status	Basis / comment
Coherent branch exists as phase-sensitive sector	Level A	BR1 + ordered broken phase; Section 20.1
Phase variable $\theta$ is natural variable of the coherent branch	Level A	Section 21.1
Integer winding sectors exist	Level A	Single-valuedness of $\Phi_{\text{eff}}$ ; Eq. (20.2)
Distinguished elementary-loop action-scale candidate $S_{\text{elem}} = 2\pi S_0^{\text{EFT}}$ in the reduced fixed-core closure	Level A/B	Defined by evaluating the fixed-length loop bound at the characteristic core scale; not a proven global variational minimum over arbitrary loop lengths
Strict positive lower bound for loop action as global variational minimum in $n = 1$ sector	Open	Fixed-length bound falls as $1/L$ ; pure phase topology alone does not yield a nonzero infimum; Section 5.6
Explicit first-principles value of $S_0$	Open (OP-Q1)	Deferred to reduced loop calculation; Appendix AV

Result (cont.)	Status	Basis / comment
Identification $S_0 = \hbar$	Level B (matched)	Structural universality established; physical identification by matching; Eq. (21.7)
Hamilton–Jacobi / continuity structure of coherent phase dynamics	Level A	Algebraically exact; Section 22.1
Probability-current reading of the coherent continuity law	Level A/B	Wave-sector interpretation of the same underlying conservation structure
Schrödinger-type complex recombination	Level B	Structural route; $S_0 = \hbar$ and $\hat{H}_{\text{coh}}$ still needed; Eq. (22.8)
Extremal-action principle as saddle dominance	Level A	Eqs. (22.14), (22.15)
Conservation laws inherited by coherent branch	Level A	Eqs. (22.16), (22.18)
Reflection positivity in massive Gaussian broken-phase subsectors	Level A	Section 23.1; standard OS result for explicitly positive Gaussian measures
Reflection positivity in free massless Goldstone subsectors	Level A	Section 23.1; standard Gaussian massless-scalar RP compatibility (up to the usual infrared subtleties)
Reflection positivity for full interacting coherent sector	Open (OP-Q16)	Section 23.1; constructive QFT programme
Global unitarity in reconstructed positive Gaussian subsectors	Level A	Follows from reflection positivity and the OS reconstruction for the broken-phase Gaussian measure; Section 23.2
Global unitarity beyond Gaussian regime	Level B/open	Depends on OP-Q16; not yet independently established; Section 23.2
Global vs. reduced unitarity distinction	Level A	Well-defined structural distinction between full coherent unitarity and reduced-sector effective non-unitarity; Section 23.2
Canonical organisation of smooth coherent branch	Level A	Section 23.3; reduced coherent phase dynamics induces canonical variables and conjugate momenta
Poisson brackets of coherent canonical variables	Level A	Eq. (23.5)
Structural commutator normalisation candidate by $S_0$	Level A/B	Section 23.3; singled out by loop weights, wave reduction, and the absence of a second independent action scale in the smooth coherent branch
Global quantisation of the compact-phase shift generator	Level A	Eqs. (23.7)–(23.8); topological consequence of compact $\theta$ and single-valuedness of the coherent wave functional
Global compact-phase quantisation condition	Level A	Eq. (23.8); topological consequence of compact $\theta$ and single-valuedness, complementary to the canonical bridge; Sections 23.3, 23.5
Momentum-operator-type wave kinematics	Level B	Eq. (23.9); depends on $S_0$ normalisation

Result (cont.)	Status	Basis / comment
Full operator algebra and many-body canonical completion	Open (OP-Q4)	Section 23.3; operator-level derivation beyond the reduced coherent sector
Uncertainty inequality $\Delta q \Delta p \geq S_0/2$	Level A	Eqs. (23.13), (23.14); follows from canonical structure
Heisenberg form $\Delta q \Delta p \geq \hbar/2$	Level B	Requires $S_0 = \hbar$ (21.7)
Two-sided Euclidean boundary dependence	Level A	Elliptic Euclidean field equation; Section 24.1
Interference/tunnelling route from Euclidean path-dependence	Level A/B	Structural amplitude-bridge reading of nonclassical amplitudes; Section 24.1
Indefinite-causal-order compatibility route	Level B	Structural reading only; quantitative switch reconstruction open; Section 24.1
$\Gamma_{\text{loop}}$ degradation criterion for indefinite-order resources	Open / programme-level	Proposed coherent-to-classical crossover guide; Eq. (24.2)
Topological exchange-sector dichotomy ( $\mathbb{Z}_2$ )	Level A	Topological fact for identical excitations in the primary three-dimensional ordered branch; Eq. (24.7)
Spatial dimensionality $d_{\text{spatial}} = 3$ fixes the exchange topology	Level A	$O(4) \rightarrow O(3)$ ordered branch implies $\pi_1(\mathcal{M}_2) = \mathbb{Z}_2$ ; Section 24.4
Bosonic/fermionic structural compatibility	Level B	Exchange topology plus ordered-branch representation content; Section 24.4
Lorentz algebra $\mathfrak{so}(1, 3)$ from the ordered branch + standard generator continuation	Level A	Broken generators $J_{i4} \rightarrow K_i$ under the standard generator continuation; Section 24.5
Clifford algebra $\{\gamma^\mu, \gamma^\nu\} = 2g^{\mu\nu}$	Level A	Spinor-representation consequence of Lorentz algebra
Dirac-type free dynamics for realised spinorial excitations	Level B (conditional)	Minimal local linear first-order Lorentz-covariant closure; Eq. (24.11); Section 24.5
Physical spinorial sector of ECT	Level B/open (OP-Q11)	Requires spectrum construction from condensate
Pauli exclusion	Level B (conditional)	From Dirac structure + spin-statistics argument; conditional on $S_0 = \hbar$ (OP-Q2)
Full spin-statistics theorem	Open (OP-Q11)	Requires operator completion beyond current closure
Spin discreteness / Stern–Gerlach selection	Level B	Discreteness follows from compact $SU(2)$ representation theory; measurement selection is read through environmental locking; Section 24.5
Ordered condensate vacuum is physically non-trivial	Level A	Ordered medium with correlators, stiffness, winding, and response structure; Section 25.1
Casimir-type boundary response: structural existence	Level A	Ordered coherent vacuum with non-trivial mode structure must respond to imposed boundaries; Section 25.3

Result (cont.)	Status	Basis / comment
Casimir coefficient for condensate-reflecting boundaries	Level B (conditional)	Provisional soft-orientation EFT with ideal Dirichlet condensate-reflecting boundaries; Eq. (25.3)
Unruh-type response: structural observer dependence	Level A	Accelerated and inertial observers decompose the ordered vacuum differently; Section 25.4
Unruh temperature from Euclidean-correlator reconstruction	Level A/B	Eq. (25.8); requires $S_0 = \hbar$ and $c_* = c$ ; Section 25.4
Time-dependent ordered backgrounds: background-dependent particle notion	Level A	Nonstationary ordered vacuum produces inequivalent mode decompositions; Section 25.5
Bogoliubov-type mode mixing in ECT coherent vacuum	Level B	Eq. (25.9); structural form natural; quantitative rates open (OP-Q12); Section 25.5
Quantitative production rates $ \beta_k ^2$	Open (OP-Q12)	Requires completed time-dependent coherent-vacuum calculation
Horizon thermality as coherent-vacuum response channel	Level A/B	Strong-field continuation of the same vacuum-response logic; Sections 25.2, 36
Unified vacuum-response logic (Casimir/production/Unruh/horizon)	Level A/B	Section 25.2; one coherent-vacuum response structure read through four probing regimes
Analogue-gravity continuity of the coherent-vacuum interpretation	Level B	Section 25.2; conceptual support, not standalone derivation
Reduced influence-functional organisation	Level B	Open-system EFT of coherent branch; Eq. (26.1)
Retarded propagation of ordered-branch scalar $\Phi$	Level A (quadratic)	Appendix E
Positive spectral density $\rho(\mu^2) \geq 0$	Level A (quadratic)	Linear broken-phase EFT
Standard 3D bath gives super-ohmic $J \propto \omega^4$	Level A	Eq. (26.5); Appendix H
Effective ohmic regime	Level B	Working closure assumption; Eq. (26.6)
Markov approximation	Level B	Working closure assumption; Eq. (26.7)
Low-entropy coherent initial sector	Level B	Section 26.1; motivated by ordered-branch initial condition
Qualitative entropy monotonicity $dS/dw \geq 0$	Level B	Eq. (26.8); retarded kernel + low-entropy branch
Explicit entropy-production formula	Level B	Eq. (26.9); depends on ohmic + Markov closure
Macroscopic irreversibility ( $N_{\text{eff}} \gg 1$ )	Level B	Section 26.1; decoherence closure
Near-reversible coherent dynamics ( $N_{\text{eff}} \sim 1$ )	Level B	Same decoherence logic; quantum exception regime
Crooks-type fluctuation relation in Gaussian–Markov closure	Level B	Eq. (26.21); Section 26.4
$C_{60}$ decoherence-timescale consistency anchor	Level B	Order-of-magnitude agreement within Gaussian–Markov closure; Section 26.2
Diósi–Penrose gravitational decoherence as condensate limit	Level B	Recovered from the same influence-functional framework; Section 26.2

Result (cont.)	Status	Basis / comment
Environmental + gravitational decoherence: structural unification	Level B (structural)	Two bath-sector specialisations of one condensate influence functional; Section 26.2
Reverse $O(3) \rightarrow O(4)$ Euclidean segments are structurally admissible	Level A	Follows from the $O(4)$ -invariant Euclidean action; Section 30.1
Quantum–classical boundary via $\Gamma_{\text{loop}}$ criterion	Level B	Reverse Euclidean segments remain relevant for $\Gamma_{\text{loop}} \lesssim 1$ and are effectively suppressed for $\Gamma_{\text{loop}} \gg 1$ ; Section 30.1
Qubit information–decoherence closure for partial observation	Level B	Simplest dephasing closure used as an operational bound on observation without full collapse; Section 30.3
Wigner’s-friend-type coarse-graining reading	Level B (interpretive)	The question is shifted from “who observes” to which degrees of freedom are already environmentally locked; Section 30.1
Reverse coherence / Lorentzian-to-Euclidean re-opening	Programme-level	Structural possibility through reverse $O(3) \rightarrow O(4)$ Euclidean segments; quantitative recoherence platforms remain open; Section 24.1
Amplitude / decoherence / probability distinction	Level A	Section 30.4; Eq. (30.7)
Born rule: conditional uniqueness via Gleason	Level B (conditional)	Quadratic structure from RP inner product; Gleason: unique given Hilbert/projector structure; not yet first-principles from bare P1–P6 (OP-Q7)
Structural assumptions (C1)–(C3) for conditional Gleason route	Level A/B	(C1) partially closed by RP for Gaussian subsectors; (C2) structurally supported by decoherence programme; (C3) operationally mild; Section 30.4
Unique outcome selection beyond conditional Born weights	Open (OP-Q19)	Relation between branch weights, decohered alternatives, and actually realised records remains incomplete; Section 30.4
Full Born rule as first-principles theorem	Open (OP-Q7)	Requires full derivation from coherent-sector dynamics
Completed measurement-update theory	Open (OP-Q8)	Pointer sectors, branch update, records not complete
Non-factorisable coherent correlations (entanglement route)	Level A/B	Structural: reduced bipartite state of single medium generically non-factorisable; Section 31
No-signalling compatibility of common-medium entanglement	Level A/B	Non-factorisable reduced state, not controllable message channel; Section 31
Bell-correlator completion	Open (OP-Q20)	Full CHSH-type derivation from condensate dynamics not yet available; Section 31
Bell/CHSH toy visibility crossover	Level B	Effective proxy $\text{CHSH}_{\text{eff}} = 2\sqrt{2}e^{-\Gamma_{\text{loop}}}$ gives the crossover threshold $\Gamma_{\text{loop}} = \ln \sqrt{2}$ ; Section 31

Result (cont.)	Status	Basis / comment
Entanglement–tunnelling structural bridge	Level B (structural)	Both phenomena are read through Euclidean connectivity, without reducing one to the other; Section 31
Wider defect sector beyond smooth coherent branch	Level A	Section 34 + 6.7
Defect sectors: structural existence	Level A	Section 34
Defect sectors: full dynamics and classification	Open (OP-Q9)	Core structure, stability, production; not yet complete
Smooth collective dark-sector candidates	Level B	Bridge MP to QS; Section 18.1
Topological/defect dark-sector candidates	Level B	Section 34; detailed dynamics open
Quantitative dominant dark-matter identification	Open (OP-Q10)	No unique first-principles candidate established yet
Black-hole thermodynamics as coherent-vacuum effective target	Level B	Eqs. (36.1)–(36.3); rewriting requires $S_0 = \hbar$
Reduced-state thermality $\neq$ fundamental information loss	Level A	General QS reduced-state logic; Eq. (36.8)
Fundamental non-unitary information destruction incompatible with the ECT postulate structure	Level A	P2 + reduced-state logic; Section 36
Critical ordered-phase shell near the horizon	Level B	Section 36; strong-field closure
Generalized entropy $S_{\text{gen}} = S_{BH} + S_{\text{ext}}^{\text{coarse}}$	Level B	Eq. (36.5); natural reduced-observer bookkeeping
Page-curve-compatible unitary evaporation logic	Level B	Structural support in Section 36
Explicit Page-curve computation	Open (OP-Q13)	Requires global nonlinear shell dynamics
Full strong-field evaporation completion (Page curve)	Open (OP-Q13)	Global nonlinear horizon solution not yet complete
Near-horizon shell-scale dispersion parameterisation	Level B	Eqs. (36.10), (36.11); parameters not yet derived from bare P3
Ringdown and late-time echo signatures of the shell	Level B	Section 36
Primordial-black-hole constraints on the strong-field closure	Level B	Section 36; cosmological bridge
Analogue-laboratory instantiability of ordered-medium logic	Level A/B	Structural expectation that media with compact phase, winding, correlators, and environment-sensitive response admit ECT-type analogues; Section 37
Concrete analogue-platform mapping to ECT subprogrammes	Level B	Superfluid, BEC, Josephson, superconducting, and acoustic-horizon systems; Section 37
Visibility-based operational $\Gamma_{\text{loop}}$ estimates	Level B	Procopio: $\Gamma = 0.006 \pm 0.002$ ; Jacques: $\Gamma \approx 0.062$ ; Section 27
Bell/CHSH crossover threshold $\Gamma_{\text{loop}} = \ln \sqrt{2}$	Level B	Eq. (31.2); Section 27
PES core selection logic	Level B	Persistent = extremal $\cap$ decoherence-resistant $\cap$ phase-compact; Section 29



Result (cont.)	Status	Basis / comment
PES universal extension	Programme-level	Full scope across spectra, decay rates, and quantum-gravity claims remains conjectural; Section 29.11
Problem of time in ECT: three-layer framing	Level B	Pre-temporal substrate $\rightarrow$ SSB directionality $\rightarrow$ decoherence classicality; Section 3.7
ECT-specific falsifiers in the quantum-gravity and decoherence sector	Level B	Four-class structural falsifiers; Section 38.4
Reduced-state resolution of the hybrid-consistency problem	Level B (architectural)	Candidate reduced-state architecture, not a finished theory; Section 28, Table 90
Two-level ontology (Level I / IIa / IIb)	Level A (structural)	Well-defined architecture; concrete reduction maps still open; Section 28.3
Gravity-induced-entanglement architectural compatibility	Level B	ECT structurally permits GIE in reduced Level IIa regimes; no Level A protocol-level prediction; Section 32
Operational criterion for BMV no-go vs loophole regimes	Level A (architectural)	Clean regime distinction given the operational mediator; Section 32.4
Mediator taxonomy: $\phi$ -channel (distinguishability) vs $\delta n_A$ -channel (candidate entangling)	Level B	Minimal effective organisation of the reduced mediator, not a unique diagonalisation; Section 33
First-principles derivation of the $\delta n_A$ entangling mediator	Open (OP-Q22)	Requires reduction of the influence functional beyond the quasi-static approximation; Section 33.3
IR/soft-sector compatibility (BMS, memory, soft gravitons)	Level B/C (structural)	Asymptotically flat ordered-branch arena; no first-principles derivations yet; Section 35
Islands/QES structural mapping onto critical-shell picture	Level B/C	Structural alignment, not a derivation of $S_{\text{gen}}$ or of replica wormholes from ECT; Section 36.3, Table 97
Cross-programme diagnostic discriminants	Summary-level	Six axes comparing ECT common-medium with linearised-graviton EFT and PCCG-hybrid; Section 36.8, Table 99

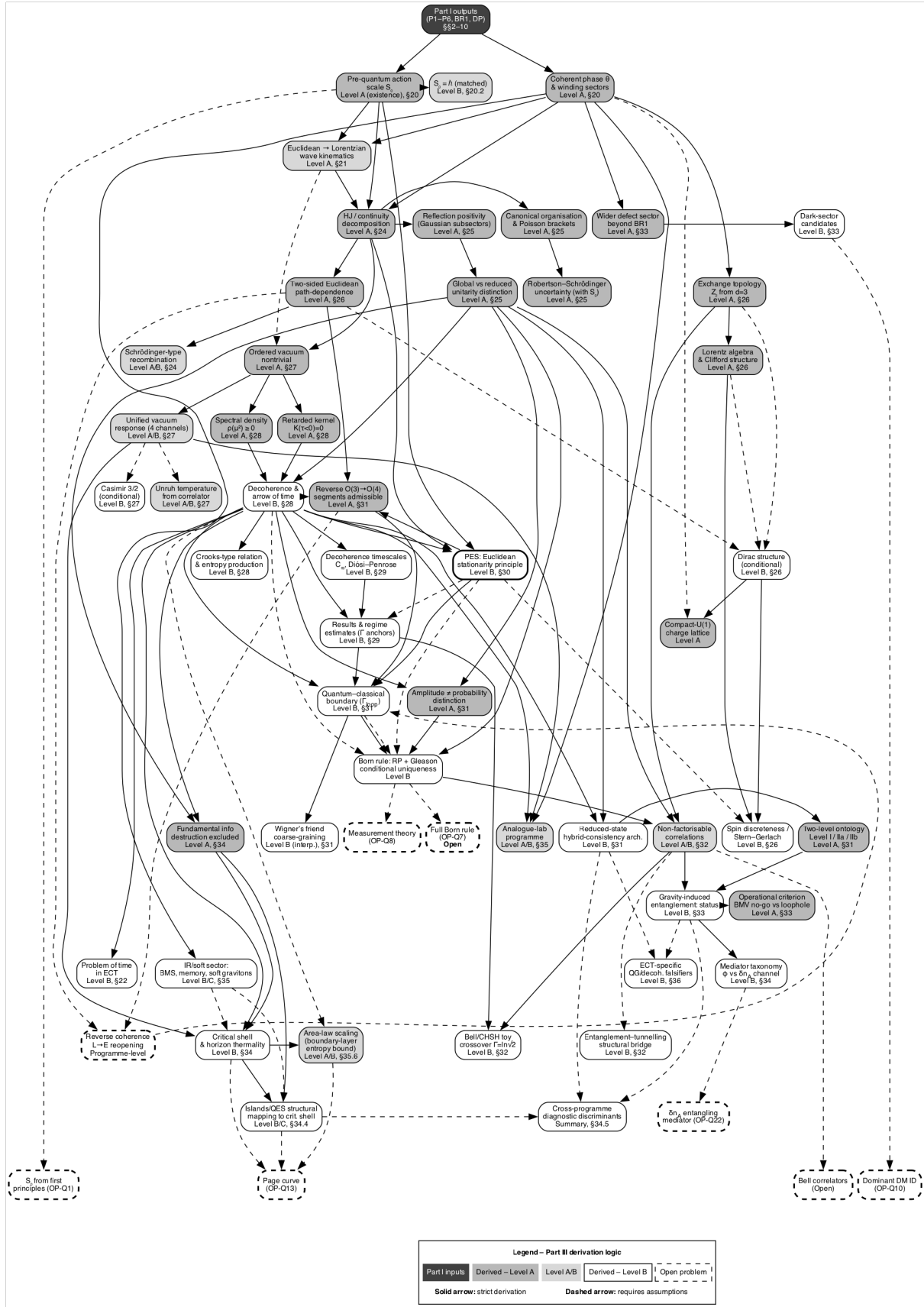


**Figure 41:** Derivation logic of Part III (Quantum Sector). Starting from Part I inputs inherited through BR1, the diagram organises the quantum sector into its main structural blocks: coherent phase dynamics and  $S_0$ ; Hamilton–Jacobi / continuity; reflection positivity and the Hilbert-space bridge; canonical organisation and uncertainty; exchange topology and Dirac closure; ordered-vacuum response (Casimir, Unruh, particle production, horizon thermality); decoherence and the arrow of time; PES; the quantum–classical boundary; Born-type probability via Gleason; entanglement and Bell-type correlations; black-hole thermodynamics and information exclusion; the analogue-laboratory programme; and the QG/decoherence upgrade layer (problem of time, ECT-specific falsifiers, reduced-state hybrid consistency architecture, two-level ontology, gravity-induced entanglement with its operational criterion, mediator taxonomy with the  $\phi$ -channel and  $\delta n_A$ -channel distinction, IR/soft sector, islands/QES structural mapping onto the critical shell, and the cross-programme diagnostic discriminants). Node shading follows the same convention as Figure 30: dark = inherited Part I inputs, medium = Level A, light = Level A/B, white = Level B, dashed = open. Solid arrows = strict derivation; dashed arrows = closure-dependent steps.

**Principle of Euclidean Stationarity as organising output.** The status map must also be read through PES (§29), which acts as an organising principle rather than a replacement of the sector-specific derivations. Its core selection logic (persistent sector = extremal  $\cap$  decoherence-resistant  $\cap$  phase-compact) is presently Level B. Operational closures built around this logic now include: the qubit information–decoherence bound, the visibility-based  $\Gamma_{\text{loop}}$  anchors, the Bell/CHSH crossover proxy, and the coarse-graining reading of measurement-type situations such as Wigner’s friend. Its universal extension across all spectra, decay rates, and quantum-gravity claims remains programme-level.

### **Open problems of the Quantum Sector.**

- OP-Q1** Explicit reduced loop calculation yielding the first-principles value of  $S_0$  (Appendix AV).
- OP-Q2** Final identification of the pre-quantum action scale with the observed  $\hbar$  (21.7).
- OP-Q3** Full derivation of the effective coherent Hamiltonian  $\hat{H}_{\text{coh}}$  for the relevant physical sectors.
- OP-Q4** Rigorous derivation of quantum commutators from the coherent branch beyond canonical plausibility arguments (23.6).
- OP-Q5** Exact microscopic derivation of the full nonlinear influence functional  $\Gamma[q, q']$  (26.1).
- OP-Q6** Derivation of the effective ohmic regime and of the Markov limit from the condensate bath without auxiliary closure assumptions (26.6).
- OP-Q7** Full first-principles emergence of the Hilbert-space projector and probability-measure structure from bare P1–P6. The RP/OS route partially closes the Hilbert-space part for Gaussian broken-phase subsectors (Level A); what remains is the full interacting RP verification (OP-Q16) and a strict projector-algebra theorem for decohered macroscopic alternatives, which would ground the Born rule as an unconditional theorem rather than a conditional Level B uniqueness statement.
- OP-Q8** Completed measurement theory: branch update, pointer stability, and record formation.
- OP-Q9** Dynamical classification, production, and stability of topological defect sectors outside the smooth coherent branch (Section 34).
- OP-Q10** Quantitative link between coherent dark candidates and observed dark-sector phenomenology.
- OP-Q11** Physical realisation of spinorial excitations in ECT and an explicit emergent many-excitation sector decomposition (Fock-like reconstruction) with variable excitation number from condensate dynamics. ECT does not require Fock space as a fundamental postulate, but the effective reconstruction—especially for the fermionic many-body sectors—remains to be constructed. Note: the Lorentz-to-Clifford route is Level A and the conditional Dirac structure is Level B (Section 24.5); what remains open is the proof that such excitations exist in the ECT spectrum.
- OP-Q12** Quantitative derivation of coherent-vacuum response effects (Casimir force, particle production rates, Unruh detector response) from the completed reduced coherent EFT (Sections 25.3–25.4).
- OP-Q12c** Thermal completion of the hot Big-Bang branch: entropy production, thermalisation, and radiation-bath formation after geometric branch onset; CMB acoustic-peak structure without particle dark matter.
- OP-Q12b** Covariant Bousso-type formulation of the ECT area-law bound for dynamical horizons and null hypersurfaces; full bulk-boundary reconstruction in the strong holographic sense.
- OP-Q13** Global nonlinear completion of the black-hole evaporation problem in the presence of a critical ordered-phase shell, including (i) explicit shell dynamics and profile, (ii) generalized-entropy evolution (36.5), and (iii) a Page-curve-type computation for the reduced radiation sector (Section 36).

- OP-Q14** Derivation of compact-object and near-horizon observables (ringdown frequency shifts, late-time transfer structure, primordial-black-hole evaporation constraints) from the completed critical-shell dynamics; fixing the closure parameters  $\eta_1, \eta_2$  in Eq. (36.10) from first principles.
- OP-Q15** Quantitative interpolation between the weakly monitored quantum-coherent regime  $N_{\text{eff}} \sim 1$  and the strongly monitored macroscopic regime  $N_{\text{eff}} \gg 1$ , including a first-principles derivation of the effective bath structure beyond the simple ohmic/Markov closure.
- OP-Q16** Full nonperturbative verification of reflection positivity (Section 23.1) for the interacting coherent-sector functional integral, completing the Osterwalder–Schrader Hilbert-space reconstruction programme and establishing global unitarity beyond the quadratic regime.
- OP-Q17** Extension of the Crooks-type fluctuation relation and the effective entropy-production formula to the full non-Markovian microscopic ECT path integral, together with a rigorous derivation of the low-entropy initial branch from the bare Euclidean action (Section 26.4).
- OP-Q18** Full quantitative Casimir derivation for the condensate-reflecting sector and identification of laboratory systems implementing the required ordered-medium boundary conditions (Section 25.3).
- OP-Q19** Unique-outcome selection beyond conditional Born-rule weights, including the relation between branch weights, decohered alternatives, and actually realised measurement records (Section 30.4).
- OP-Q20** First-principles derivation of Bell-inequality-violating correlators, including the CHSH-type correlation algebra and the Tsirelson bound, from condensate dynamics (Section 31).
- OP-Q21** Smooth-branch exactness of the Pauli exclusion principle and its admissible departures. Determine whether the completed fermionic reconstruction of ECT enforces exact canonical anticommutation relations throughout the smooth coherent ordered branch, as provisionally indicated by the canonical-normalisation no-go argument of Section 24.4 and Appendix AW. If genuine departures from standard fermionic statistics exist in ECT, identify the precise nonlocal, topological-defect, or branch-transition mechanism responsible, rather than attributing them to smooth local condensate gradients.

**PES-specific open targets (§29.11):**

- OP-PES-1** First-principles derivation of the PES environmental functional  $\Gamma_{\text{env}}$  from the bare Euclidean path integral.
- OP-PES-2** Promotion of the extremal-action reading from physical underpinning to formal bound  $|\delta S_E| \rightarrow \Gamma_{\text{env}}$ .
- OP-PES-3** First-principles quantisation of the graviton sector from condensate dynamics (full UV closure).
- OP-PES-4** Derivation of decay widths and lifetime hierarchies from the non-stationarity functional  $\mathcal{N}_{\text{ns}}$ .
- OP-PES-5** Quantitative mapping  $\Gamma_{\text{loop}} \leftrightarrow \alpha - \beta$ .
- OP-PES-6** Protocol-independent information–decoherence bound beyond the dephasing qubit model.

### 38.2 Minimal quantum core already established by ECT

The following results organise the minimal quantum core of ECT into three layers: a strict structural core, a structurally singled-out backbone, and the nearest closure-level or open fronts. They should be read together with the detailed status map in Section 38.1: the purpose of the present subsection is not to replace the full table, but to identify the irreducible backbone that already exists inside the theory and to separate it clearly from what still depends on closure or remains open.

**Strict structural core (Level A).**

- (i) Loop sectors with integer winding classification.
- (ii) Wave-type effective dynamics via Hamilton–Jacobi / continuity decomposition.
- (iii) Canonical organisation of the smooth coherent branch at the Poisson-bracket level.
- (iv) Topological quantisation of the global compact-phase generator.
- (v) Robertson–Schrödinger uncertainty inequality with  $S_0$ .
- (vi) Reflection positivity in the positive Gaussian broken-phase subsectors (massive radial and free massless Goldstone sectors).
- (vii) The structural distinction between global and reduced unitarity.
- (viii) Two-sided Euclidean boundary dependence from the elliptic field equation.
- (ix) Exchange-sector topology  $\pi_1(\mathcal{M}_2) = \mathbb{Z}_2$  in the primary three-dimensional ordered branch.
- (x) Lorentz algebra  $\mathfrak{so}(1, 3)$  and Clifford structure from the ordered branch plus the standard generator continuation.
- (xi) Retarded propagation of the ordered-branch scalar for the full nonlinear dynamics together with nonnegative spectral density in the quadratic sector.
- (xii) Structural admissibility of reverse  $O(3) \rightarrow O(4)$  Euclidean segments in the path integral.
- (xiii) The amplitude / decoherence / probability distinction.
- (xiv) Fundamental non-unitary information destruction is incompatible with the global coherent framework.
- (xv) The ordered-condensate state space is not exhausted by the smooth coherent branch BR1.

**Structurally singled-out backbone (Level A/B).**

- (i) The existence of a distinguished pre-quantum action scale  $S_0$ .
- (ii) The unified vacuum-response logic relating Casimir, Unruh, particle production, and horizon thermality as four probing regimes of one coherent vacuum.
- (iii) The structural availability of non-factorisable correlations in reduced subsystems of one ordered medium.
- (iv) The analogue-laboratory instantiability of the ordered-medium logic in systems with compact phase, winding sectors, coherent correlators, and environment-sensitive response.

**Closure-level results and open fronts (Level B / Open).**

- (i) Environment-induced decoherence architecture from the influence functional, including the effective entropy-production and Crooks-type relations in the Gaussian–Markov closure (Level B; OP-Q6, OP-Q17).
- (ii) Quantitative decoherence-timescale consistency anchors, including the  $C_{60}$  case and the Diósi–Penrose condensate limit (Level B).

- (iii) Operational decoherence proxies from experimentally inferred visibility loss, including the Procopio and Jacques anchors together with the Bell/CHSH crossover threshold  $\Gamma_{\text{loop}} = \ln \sqrt{2}$  (Level B; operational rather than first-principles microscopic derivation).
- (iv) Qubit-model information–decoherence closure for partial observation and the associated non-collapse bound (Level B; protocol-independent generalisation remains open, OP-PES-6).
- (v) Wigner’s-friend-type coarse-graining reading and reverse coherence / Lorentzian-to-Euclidean reopening remain closure-level or programme-level elaborations of the same quantum–classical-boundary architecture rather than independent theorems.
- (vi) Conditional uniqueness of Born-type weights once the assumptions (C1)–(C3) are admitted (Level B); first-principles derivation of those assumptions and unique outcome selection remain open (OP-Q7, OP-Q19).
- (vii) Full interacting OS closure and completed Hilbert/projector structure remain open (OP-Q16).
- (viii) Complete measurement theory remains open (OP-Q8).
- (ix) Full spin-statistics theorem remains open (OP-Q11).
- (x) Full Bell-correlator derivation from condensate dynamics remains open (OP-Q20).
- (xi) The presently available Bell/CHSH threshold is only a toy visibility proxy and must not be confused with a derivation of the CHSH algebra or of the Tsirelson bound from first principles (OP-Q20).
- (xii) The entanglement–tunnelling connection is presently a structural bridge based on Euclidean connectivity, not an identity theorem reducing one phenomenon to the other.
- (xiii) Full quantitative Casimir derivation for the condensate-reflecting sector remains open (OP-Q18).
- (xiv) Nonperturbative black-hole evaporation closure and the constructive Page-curve mechanism remain open (OP-Q13).
- (xv) Dynamical classification of defect sectors and unique dominant dark-sector identification remain open (OP-Q9, OP-Q10).
- (xvi) Explicit reduced loop calculation for  $S_0$  remains open (OP-Q1).
- (xvii) PES universal extension and the quantitative  $\Gamma_{\text{loop}} \leftrightarrow \alpha - \beta$  mapping remain programme-level (OP-PES-2, OP-PES-5).

This distinction is essential. ECT does not yet claim to have derived all of standard quantum mechanics from its postulates. What it does claim is that the correct structural location for quantum kinematics, reduced-state decoherence, probability, entanglement, and strong-field information bookkeeping has been identified inside the theory, and that a substantial part of the required architecture has already been made explicit.

**Distinctive quantitative outputs.** Two results of Part III have no direct analogue in standard quantum mechanics. First, gravitational decoherence is derived from the condensate acting as a universal decoherence bath, without the Diósi–Penrose postulate; the nanosphere scale  $\tau_{\text{grav}} \sim 38$  ms is a testable DP-type leading scale, whose ECT-specific content is its condensate-origin interpretation and the predicted pattern of subleading condensate-sector corrections, within reach of levitated-nanoparticle experiments (§27.2). Second, a quantitative recoherence suppression law  $P_{\text{back}}/P_{\text{fwd}} = e^{-\Gamma_{\text{loop}}}$  is predicted; standard QM provides no analogous relation (§24.3).

**Logical relocation of quantum mechanics.** Part III changes the logical status of the axioms of standard QM from foundational postulates to reconstruction targets: Hilbert space is constructed via OS reconstruction (§23.1), unitarity follows from reflection positivity, the Born rule is motivated by decoherence (§30.4), and “collapse” is identified with the Euclidean-to-Lorentzian transition at  $\Gamma_{\text{loop}} \sim 1$  (§30.2). The distinction between Lorentzian event-like interaction and Euclidean common-medium correlation, introduced in Part I (§6.5), receives its full physical content here: entanglement is prior inseparability of a common condensate configuration, measurement is the transition from correlation to classical event, and decoherence is medium-driven branch selection.

Having outlined the intended reconstruction logic of the quantum sector, it is useful to set out the structural comparison between ECT and the standard quantum formalism in more detail, in a form directly parallel to the status map above.

### 38.3 ECT as a foundational framework for quantum mechanics: structural comparison with the standard formalism

*Status: comparative and pedagogical synthesis of results established in the preceding sections of Part III. No new physical results are introduced here. The role of this subsection is to organise the structural comparison between ECT and the standard quantum formalism along three explicit axes: ontology of the primary object, type of mathematical problem, and origin of the statistical description. The formal status ledger of the same material, organised by derivational level and keyed to the open-problem labels, is given separately in Section 38.2; current limitations of the formulation are collected in Section 48.10.*

Standard quantum mechanics is extraordinarily successful as an effective predictive formalism. It begins, however, from postulated structures: a complex amplitude, Hilbert-space evolution, a probability rule for observed outcomes, and canonical commutation relations. ECT asks a different question. It does not begin by asking how to compute quantum predictions more efficiently, but why the quantum formalism takes the shape it does at all. In this sense the relation between ECT and standard quantum mechanics is not one of direct replacement but of explanatory depth: standard quantum mechanics describes the effective coherent sector, whereas ECT attempts to identify the deeper condensate structure from which that sector emerges.

#### Two different questions answered by two theories

The architectural contrast between the two frameworks is best introduced by the primary question each of them answers. Standard quantum mechanics answers *how to calculate* the statistical predictions of a wide class of experiments; its axioms are adopted precisely because they are operationally successful. ECT asks *why* the quantum rules take the form they do, treating the axioms of standard quantum mechanics not as foundational primitives but as reconstruction targets of a deeper ordered-medium dynamics. Table 101 summarises the resulting contrast along the main structural axes.

**Table 101:** Two questions, two frameworks. Each row records the fundamental ingredient on which the two theories differ at the architectural level; detailed cross-references to Part III are given in the concept-mapping Table 105 below.

Aspect	Standard quantum mechanics	Euclidean Condensate Theory
Primary question	How to compute observed outcomes efficiently	Why the quantum formalism has the structure it has
Status of axioms	Foundational postulates (Hilbert space, Born rule, canonical commutators)	Reconstruction targets from condensate dynamics
Primary physical object	Complex amplitude $\psi(x, t)$	Real condensate configuration $\Phi(X)$
Arena	3+1 Lorentzian spacetime, assumed as background	4D Euclidean manifold; Lorentzian branch emergent

Aspect	Standard quantum mechanics	Euclidean Condensate Theory
Role of time	Fundamental external parameter	Emergent after $O(4) \rightarrow O(3)$ symmetry breaking
Role of causal speed	Speed of light postulated	Effective $c_*$ fixed by condensate matching ( $c_*^2 = \beta/(\alpha - \beta)$ in the ordered branch)
Role of $\hbar$	Fundamental universal constant	Action scale $S_0$ tied to phase compactness (identification with $\hbar$ : Level-B matching, see §21.2)
Role of probability	Primitive (Born rule)	Reduced-description phenomenon of a globally fixed configuration
Causal structure	Built in from the start	Emergent on the ordered branch for $\alpha > \beta$
Type of mathematical problem	Forward-time Cauchy problem for amplitude	Global boundary-value problem for a physical field

The contrast summarised above should not be read as an argument that standard quantum mechanics is “wrong”. Standard quantum mechanics remains the appropriate effective description for laboratory subsystems; ECT does not compete with it as a calculational tool. Rather, the table records that ECT is not merely a reformulation of the same question in different language: the two frameworks ask, and answer, logically different questions. The remainder of this subsection unpacks this contrast systematically.

### Hierarchy of effective equations

ECT does not merely reproduce the standard equations of quantum mechanics; it provides a *hierarchy* of more fundamental equations of which the usual quantum equations are limiting cases. The hierarchy is summarised in Fig. 42 and Table 102. Each level is an already established sector of Part III; the role of the hierarchy is to display their logical organisation in one place.

**Level 0: Euclidean condensate equation.** At the most fundamental level one has the Euclidean field equation

$$\delta^{AB} \partial_A \partial_B \Phi - V'(\Phi) = 0, \quad (38.1)$$

which is the Euler–Lagrange equation of the bare Euclidean micro-action (2.3); it is written here only to display the logical hierarchy, not as a new independent postulate. It is a four-dimensional elliptic equation for the condensate field  $\Phi$ . At this level there is no distinguished time coordinate, no  $\hbar$ , and no built-in probabilistic interpretation. All four coordinates are spatial from the Euclidean point of view, and solutions are determined by boundary data on the full four-dimensional domain.

**Level 1: ordered-branch equation after SSB.** After spontaneous symmetry breaking  $O(4) \rightarrow O(3)$ , the ordered branch is governed by an effective kinetic tensor  $K^{AB}$ , so that the relevant fluctuation equation takes the form

$$K^{AB} \partial_A \partial_B \chi + m_\sigma^2 \chi = 0. \quad (38.2)$$

In the ordered branch the kinetic tensor is not arbitrary but is fixed, within the present EFT closure, by the unique form

$$K^{AB} = \beta \delta^{AB} - \alpha n^A n^B, \quad (38.3)$$

as established earlier in the Foundations part (see in particular Eq. (3.8) and the subsequent uniqueness discussion). For a homogeneous background with  $n^A = \delta_w^A$ , this gives  $K^{AB} = \text{diag}(\beta, \beta, \beta, \beta - \alpha)$ , so that the Lorentzian regime is controlled by the sign of  $\beta - \alpha$ , equivalently by

$$c_*^2 = \frac{\beta}{\alpha - \beta}. \quad (38.4)$$



Thus  $\alpha > \beta$  corresponds to the Lorentzian ordered branch,  $\alpha < \beta$  to the Euclidean side, and  $\alpha = \beta$  to the singular boundary between them. This level is already more general than standard quantum mechanics because it contains both Euclidean and Lorentzian sectors within the same dynamical framework.

**Level 2: relativistic Lorentzian wave equation.** In the ordered Lorentzian branch ( $\alpha > \beta$ ), after the real parametrisation  $t = w/c_*$ , the fluctuation equation takes the relativistic Klein–Gordon form (3.16) (see Section 22 for the derivation). A separate formal continuation  $w_E \rightarrow \pm ic_* t$  may still be used when relating Euclidean coherent amplitudes to Lorentzian phase evolution; the first step is the derivation of real-time dynamics in the ordered branch, while the second is only a translation of Euclidean coherent amplitudes into Lorentzian phase language.

**Level 3: nonrelativistic Schrödinger-type limit.** Finally, in the nonrelativistic limit (extraction of the rest-energy phase  $\psi = e^{-imc_*^2 t/\hbar} \chi$  and neglect of terms of order  $v^2/c_*^2$ ) one obtains the Schrödinger-type coherent equation (22.8), with its identification with the standard Schrödinger equation of textbook quantum mechanics remaining a Level-B reconstruction step (see §22.1). The usual Schrödinger equation is therefore not taken as fundamental in ECT: it is the narrowest endpoint of a four-level hierarchy.

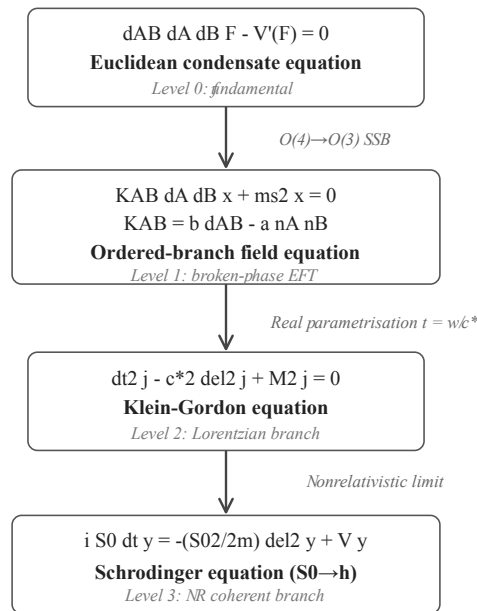


**Figure 42:** Logical hierarchy of ECT equations. The Schrödinger equation (Level 3) appears as the narrowest low-energy descendant of a deeper chain consisting of the Euclidean condensate equation (Level 0), the ordered-branch field equation after symmetry breaking (Level 1), and the relativistic Klein–Gordon equation in the ordered branch (Level 2). The downward arrows denote distinct reduction steps:  $O(4) \rightarrow O(3)$  symmetry breaking, real ordered-branch parametrisation  $t = w/c_*$ , and the nonrelativistic limit. The figure summarises the logical organisation of equations discussed in the text; it does not assert that all steps are established at the same derivational level. The displayed equations are representative schematic forms; they are not a claim that all intermediate reductions are exhausted by the boxed expressions alone.

**Table 102:** Hierarchy of effective equations in ECT, together with the type of problem they define, the data needed to solve them, and their standard-QM counterpart.

Lv.	Equation	Regime	Mathematical type	Data	Standard-QM analogue
0	$\delta^{AB} \partial_A \partial_B \Phi = V'(\Phi)$	Pre-SSB, full 4D Euclidean	Elliptic	Global BVP on $\partial \mathcal{M}$	none
1	$K^{AB} \partial_A \partial_B \chi + m_\sigma^2 \chi = 0$ , $K^{AB} = \beta \delta^{AB} - \alpha n^A n^B$	Post-SSB, both signatures	Elliptic $\alpha < \beta$ , hyperbolic $\alpha > \beta$	for BVP or IVP depending on regime	none
2	$(\square - m^2)\chi = 0$ , $t = w/c_*$	Ordered Lorentzian branch ( $\alpha > \beta$ )	Hyperbolic	Cauchy data on $t = \text{const}$	Klein–Gordon
3	$i\hbar \partial_t \psi = H\psi$	Nonrelativistic limit	Parabolic/effective	Cauchy data at $t = 0$	Schrödinger-type sector

### What the ordered-branch equation contains beyond Schrödinger

The ordered-branch equation (38.2) is strictly more general than the Schrödinger-type coherent equation (22.8), in several essential ways. The following items are not new physical results; they are collected here because they are direct structural consequences of the derivations carried out earlier in Part III.

- (i) *Both signatures in one equation.* For  $\alpha < \beta$ , the effective equation remains elliptic and describes the Euclidean coherent sector, where there is no causal ordering and solutions depend on boundary data from the full domain. For  $\alpha > \beta$ , the equation becomes hyperbolic and supports causal propagation. Standard Schrödinger dynamics describes only the already-selected Lorentzian side, and only in its nonrelativistic limit.
- (ii) *Relativistic parent.* Level 2 is manifestly a Klein–Gordon-type relativistic sector, not a nonrelativistic residue. The nonrelativistic limit appears only at Level 3.
- (iii) *Manifest role of  $c_*$ .* The causal cone of Level 2 is fixed by the condensate stiffness through  $c_*^2 = \beta/(\alpha - \beta)$ . In standard quantum mechanics the speed of light is an external input.
- (iv) *Manifest role of  $S_0$ .* The action scale  $S_0$  enters the ordered-branch description through the compact-phase quantisation condition  $\oint dw p_w = 2\pi S_0 n$  (see Section 21.2). Identification with  $\hbar$  is a Level-B matching; the quantisation structure itself is already Level A.
- (v) *Gravitational coupling.* The same ordered background that fixes the coherent wave equation also fixes the long-wavelength geometric sector discussed in Part II. Coherent propagation and emergent geometry are not independent sectors but two complementary descriptions of the same ordered condensate.
- (vi) *New structural phenomena.* The ordered-branch equation naturally accommodates two-sided boundary dependence of coherent amplitudes, a Euclidean-to-Lorentzian reading of measurement, a gravitational decoherence route from condensate distinguishability, and a structural bridge between tunnelling and entanglement through Euclidean connectivity. None of these is part of the Schrödinger sector.

The upshot of items (i)–(vi) is that the ordered-branch equation is the correct structural parent for both coherent quantum dynamics and the emergent Lorentzian sector; Schrödinger dynamics is the narrowest of its descendants, not its starting point.

### Ontological comparison: $\Phi$ versus $\psi$

The difference between standard quantum mechanics and ECT is not only in the type of equation each uses, but also in the ontological status of the primary object. Standard quantum mechanics builds its predictions on the complex amplitude  $\psi(x, t)$ , which is not itself a physical field in ordinary spacetime but a mathematical object whose squared modulus provides probability densities for measurement outcomes. ECT, by contrast, builds its predictions on a real physical condensate configuration  $\Phi(X)$  on the Euclidean four-manifold; this configuration is the underlying physical medium of the theory, and amplitude-level quantum descriptions arise only after reduction to the appropriate effective branch and subsystem. Table 103 summarises this contrast.

**Table 103:** Ontological status of the primary object in the two frameworks.

Aspect	$\psi$ in standard QM	$\Phi$ in ECT
Type of object	Complex-valued amplitude	Real scalar condensate field
Physical interpretation	Not a physical field on spacetime; a mathematical object used to compute probabilities	Physical configuration of the underlying ordered medium
Arena	3+1 Lorentzian spacetime, taken as a background	4D Euclidean manifold; Lorentzian spacetime is emergent
Role of time	Explicit parameter in the evolution equation	Absent at Level 0; emerges only in the ordered branch
How it is fixed	Initial data at $t = 0$ , evolved forward	Boundary data on $\partial\mathcal{M}$ in the full 4D domain
Role in measurement	Collapses/projects onto an eigenbasis	Does not collapse; measurement reads as an effective-branch transition (see below)
Access by observer	Direct calculational object	Full condensate configuration is rarely accessible; subsystem access only

Formally, the key statement is:

*In standard quantum mechanics the primary formal object is the probability amplitude  $\psi$ . In ECT the deeper object is not an amplitude on spacetime but a physical condensate configuration  $\Phi(X)$  on the Euclidean manifold, from which amplitude-level quantum descriptions arise only after reduction to the appropriate effective branch and subsystem.*

This ontological difference is a precondition for everything that follows in this subsection. In particular, once the primary object is  $\Phi(X)$  rather than  $\psi$ , it is natural to ask what type of mathematical problem  $\Phi(X)$  solves, how probabilistic descriptions arise from it, and how the standard quantum phenomena are recast in the new language.

### Epistemological comparison: boundary-value versus Cauchy problem

Once the primary object is fixed ontologically, the form of the mathematical problem follows. Standard quantum mechanics formulates the dynamics of  $\psi$  as a forward-time Cauchy problem: one specifies  $\psi(x, 0)$  and evolves it forward to obtain  $\psi(x, t)$ . In ECT the fundamental equation (38.1) is solved instead as a *global boundary-value problem*: one specifies boundary data on the full four-dimensional domain, and the solution  $\Phi(X)$  is the configuration of a real physical condensate field throughout the Euclidean four-space. There is no preferred direction of evolution; the solution is determined globally, much as the solution of Laplace's equation inside a region is fixed by boundary values on its surface. Table 104 summarises the contrast.

**Table 104:** Boundary-value versus Cauchy description of quantum dynamics in ECT and standard quantum mechanics.

Aspect	Standard quantum mechanics	Euclidean Condensate Theory
Mathematical type	Parabolic Schrödinger equation; hyperbolic Klein–Gordon equation	Elliptic Euclidean condensate equation (Level 0); signature switches within Level 1
Problem type	Cauchy initial-value problem	Global boundary-value problem
Data	Initial amplitude $\psi(x, 0)$	Boundary data on $\partial\mathcal{M}$
Domain	3+1 spacetime, evolved forward in $t$	Full 4D Euclidean manifold, solved globally
Notion of determinism	Unitary forward evolution of amplitudes	Global fixation of the configuration $\Phi(X)$
What counts as prediction	Probabilities $ \psi ^2$ at later times	Subsystem observables extracted from $\Phi(X)$
Why probabilities appear	Postulated (Born rule) as an axiom	Reduced-description phenomenon after partial access and coarse-graining
Role of future boundary data	None (initial-value problem)	Co-determines $\Phi(X)$ together with past boundary data

Several consequences follow from this difference.

**Origin of probabilities.** In standard quantum mechanics,  $P = |\psi|^2$  is postulated. In ECT, probabilities arise only after incomplete description. If one does not track all  $\sim 10^{23}$  modes of the condensate and keeps only a subsystem, then the environmental modes are integrated out, an influence functional is produced (see Section 26.1), and an effective probabilistic description emerges. At the fundamental level, however,  $\Phi(X)$  is fixed by the full boundary data.

**What fixes a measurement outcome.** In standard quantum mechanics, collapse is an extra postulate. In ECT, the detector is treated as part of the full physical system and therefore belongs, in principle, to the global boundary-value problem. At the reduced-description level, effective collapse is then read as the subsystem manifestation of a Euclidean-to-Lorentzian transition under strong environmental locking (§30.2). This should be understood as a structural reading of measurement, not as a completed microscopic solution of realistic detector dynamics from the bare condensate action.

**Future boundary data and apparent retrocausality.** In standard quantum mechanics, forward time evolution makes “future affects past” a non-statement at the fundamental level. In ECT it is natural: for an elliptic equation, changing the boundary condition on one side changes the solution throughout the region, including what the Lorentzian reading would call the “past” side. The full solution is constrained globally; apparent retrocausality reflects the mismatch between global boundary conditions and a local temporal slicing of the reduced Lorentzian branch. This is the structural reason why delayed-choice-type phenomena can be accommodated naturally in ECT; it is not, by itself, a completed first-principles derivation of a laboratory delayed-choice setup.

**Determinism is not the same as practical predictability.** The above underlying determinism must not be confused with practical predictability. ECT does not imply that observers can compute all outcomes from accessible laboratory data. On the contrary, once the relevant subsystem is extracted from the full condensate configuration and the untracked modes are coarse-grained over, an effective statistical description becomes unavoidable. The claim is therefore not that quantum probabilities disappear operationally, but that they need not be fundamental at the deepest level. This distinction is the analogue

of the distinction between microscopic Newtonian determinism and the practical necessity of statistical mechanics.

### Origin of the statistical description

The ontological and epistemological comparisons above converge on a single explanatory axis that deserves its own statement. In standard quantum mechanics the statistical description is a primitive of the theory: the Born rule is one of its founding axioms. In ECT the statistical description is not a primitive but a consequence of how observers access the condensate. Standard quantum mechanics is statistical not because the underlying physics must itself be fundamentally statistical, but because the accessible description is reduced, branch-dependent, and coarse-grained with respect to the full Euclidean condensate configuration.

In this perspective, probability appears not as a fundamental rule but as a reduced-description phenomenon. The full Euclidean configuration is globally constrained by its boundary data, but an observer typically has access only to an effective branch, a restricted subsystem, and a finite set of tracked variables. Integrating out the untracked condensate modes produces an influence functional (§26.1) whose effect on the reduced dynamics is that of a stochastic environment. The resulting loss of complete information is what makes the effective Lorentzian description statistical. Standard quantum probabilities are then interpreted as the operational shadow of a deeper but only partially accessible condensate-level solution.

This route ties together several structural elements of Part III that might otherwise appear disconnected. Decoherence through the influence functional (§26.1), the information–decoherence bound (§30.3), the quantum–classical boundary as a regime change (§30), the conditional Gleason-based route to the Born rule (§30.4), and entanglement as common-medium correlation (§31) are, in this reading, different facets of one statement: the Lorentzian statistical description is the reduced-subsystem image of a globally fixed Euclidean configuration. Once this is granted, the Born rule, the role of decoherence, and the apparent stochasticity of measurement cease to be independent postulates and become jointly controlled by the same reduction pattern.

This is the central explanatory claim of ECT with respect to the statistical content of standard quantum mechanics.

### Interpretive mapping of standard-QM concepts onto ECT

The content of the preceding parts of Part III can be organised as a mapping between the main conceptual primitives of standard quantum mechanics and their ECT counterparts. Table 105 records this mapping together with the present status of each item. It is intended as a reading guide, not as an independent source of results; the status column is consistent with the more formal ledger in Section 38.2.

**Table 105:** Concept mapping between standard quantum mechanics and ECT. The *Status* column uses the same Level-A / Level-B / Open language as Section 38.2.

Concept	Status in standard QM	ECT origin/route	Status in ECT
Superposition	Primitive axiom	Coherent regime $\Gamma_{\text{loop}} \ll 1$ of the Euclidean branch, with no Lorentzian ordering yet enforced	Level A structural (§24.1)
Born rule	Primitive axiom	Reduced-description probabilities after integrating out untracked modes; conditional Gleason route once assumptions (C1)–(C3) are admitted	Level B conditional (§30.4)
State reduction	Primitive/interpretational	Structural reading as a Euclidean-to-Lorentzian regime transition at $\Gamma_{\text{loop}} \gtrsim 1$	Structural reading; full theorem open (§30.2, OP-Q8)

Concept	Status in standard QM	ECT origin/route	Status in ECT
Uncertainty principle	Theorem from commutators	Robertson–Schrödinger inequality with $S_0$ on the coherent branch	Level A (§23.5)
Canonical commutators	Primitive	Poisson-bracket structure of the smooth coherent branch together with phase compactness	Level A (§23.3)
Entanglement	Non-separable two-party states	Reduced-state correlations inherited from a common condensate configuration; no-signalling preserved	Structural; full Bell-correlator derivation open (§31, OP-Q20)
Tunnelling	Barrier penetration via WKB	Traversal through the fourth Euclidean direction of admissible condensate configurations	Level B structural (§24.3)
Identical particles	Symmetrisation postulate	Exchange-sector topology $\pi_1(\mathcal{M}_2) = \mathbb{Z}_2$ in the ordered branch	Level A (§24.4)
Spin-statistics	Spin-statistics theorem in QFT	Residual-symmetry and exchange-topology route in the ordered branch	Open (§24.4, OP-Q11)
Action scale $\hbar$	Fundamental constant	Action scale $S_0$ from compact phase and winding classification	Level A quantisation structure; Level-B identification (§21.2)
Charge quantisation	Topological/empirical	Compact-phase $U(1)$ gauge origin	Level A structural route (§23.4)
Decoherence	Added phenomenology	Influence-functional coupling of the coherent sector to untracked condensate modes	Level B closure (§26.1)

The table is intentionally shorter than the full status ledger: its purpose is to show that the main conceptual primitives of standard quantum mechanics acquire explicit structural counterparts in ECT, together with their derivational level.

### Illustrative examples

The structural comparison above is best seen on several concrete examples. The examples below are not new derivations. They are interpretive reformulations of standard quantum phenomena in ECT language, with the present status of each reformulation stated explicitly. Each entry uses the same template so that the contrast can be read off directly.

#### Double-slit interference.

**Standard QM.** One specifies the incoming wave packet and evolves the amplitude through the two-slit apparatus as a Cauchy problem; the observed pattern is computed from  $|\psi_1 + \psi_2|^2$ , where  $\psi_1$  and  $\psi_2$  are the amplitudes associated with the two slits.

**ECT.** One solves a global boundary-value problem for the condensate configuration, with the source, screen, slits, and detector geometry entering as boundary and constraint data. The fringe pattern is the reduced Lorentzian imprint of the globally admissible Euclidean configuration.

#### What is computed.

The same observed fringe intensity; the reduction from the full Euclidean configuration to the effective Lorentzian amplitude reproduces the usual  $|\psi_1 + \psi_2|^2$  interference law.

**What is explained.**

Why the interference pattern exists at all. It is not the coexistence of several realised trajectories, but the visible imprint of one globally constrained Euclidean configuration on a reduced Lorentzian slice.

**Status.**

Structural reformulation (Level B). Not a first-principles computation of the full laboratory setup from the microscopic condensate action.

**Quantum tunnelling.**

**Standard QM.** One computes a transmission coefficient, typically by WKB matching across a classically forbidden region; the exponential suppression  $T \sim \exp(-2 \int |p| dx / \hbar)$  follows.

**ECT.**

The classically forbidden Lorentzian region is reinterpreted as a projection of an admissible Euclidean configuration. A configuration that is forbidden in the reduced Lorentzian reading can remain perfectly admissible in the underlying Euclidean problem.

**What is computed.**

The WKB exponent, which the ECT route must reproduce as the Lorentzian projection of the Euclidean action along the underbarrier segment.

**What is explained.**

Why barrier penetration occurs at all. Classically forbidden regions in the Lorentzian description correspond to accessible regions in the Euclidean domain; the barrier is not crossed by a classical Lorentzian trajectory but bypassed through Euclidean connectivity.

**Status.**

Structural reading (Level B); the route underlies the structural bridge between tunnelling and entanglement through Euclidean connectivity (§24.3, §31), but does not yet amount to a full theorem of all tunnelling observables from first principles.

**Measurement and outcome selection.**

**Standard QM.** Outcome selection is described through the collapse or projection postulate at the amplitude level:  $\psi \mapsto P_k \psi / \|P_k \psi\|$  with probability  $\|P_k \psi\|^2$ .

**ECT.**

Measurement is read structurally as a transition between two regimes of one and the same condensate theory: coherent Euclidean behaviour ( $\Gamma_{\text{loop}} \ll 1$ ) and a Lorentzian ordered branch with irreversible effective recording ( $\Gamma_{\text{loop}} \gtrsim 1$ ). See Fig. 43.

**What is computed.**

The effective Born-type probabilities are reproduced through the conditional Gleason-based route once assumptions (C1)–(C3) are admitted (§30.4); the quantum–classical boundary is characterised operationally by the decoherence functional  $\Gamma[q]$ .

**What is explained.**

Why a definite outcome appears at all, and why the statistical weights follow the Born-type rule in the reduced description. What is operationally described as stochastic outcome selection is the subsystem-level manifestation of a globally fixed but only partially accessible configuration, with the Euclidean-to-Lorentzian transition playing the role usually attributed to collapse language (§30.2).

**Status.**

Structural measurement reading, not yet a complete detector-level theorem. A full microscopic derivation of outcome selection from the bare condensate action remains open (OP-Q8).

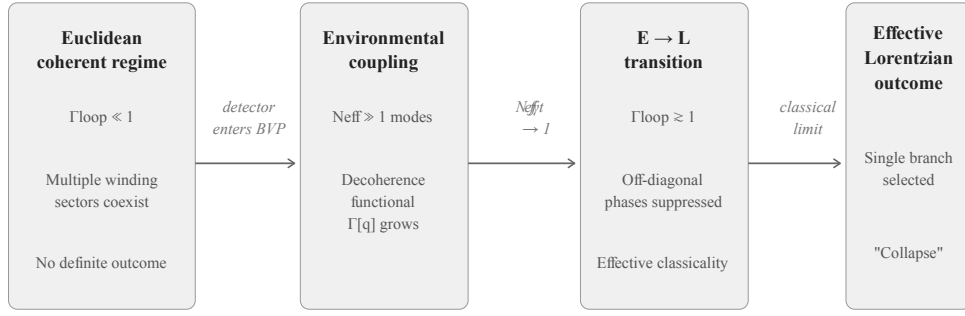


**Figure 43:** Structural reading of quantum measurement in ECT as a Euclidean-to-Lorentzian transition. In the coherent regime ( $\Gamma_{\text{loop}} \ll 1$ ) multiple winding sectors coexist without a definite outcome. Environmental coupling to  $N_{\text{eff}} \gg 1$  modes drives the decoherence functional  $\Gamma[q]$  to grow. When  $\Gamma_{\text{loop}} \gtrsim 1$  the off-diagonal interference terms are suppressed and an effectively classical (Lorentzian) single-branch outcome is selected. This should be read as a structural flow, not as a completed microscopic derivation of realistic detector dynamics.

### EPR-type correlations and entanglement.

**Standard QM.** Entangled states are non-separable and can violate Bell-type inequalities up to the Tsirelson bound  $2\sqrt{2}$ ; the phenomenon is often described in the language of nonlocal influences between spacelike separated parties.

**ECT.** Correlated subsystems are understood as inheriting their reduced structure from one common condensate configuration. Correlations do not arise from interaction or from superluminal influence, but from the shared embedding of subsystems within a single condensate configuration.

#### What is computed.

Nonclassical visibility and Bell-type violations appear naturally in reduced-state descriptions of a common-medium theory; the toy CHSH crossover threshold  $\Gamma_{\text{loop}} = \ln \sqrt{2}$  is used as an operational marker (§38.2).

#### What is explained.

Why nonclassical correlations are *natural* in a common-medium theory rather than paradoxical: they are not the output of a forbidden signal, but a reduced-state imprint of a shared underlying configuration.

#### Status.

Structural bridge (Level B); no-signalling is preserved. The explanation is *not* yet a derivation of the full Bell correlators or of the Tsirelson bound from first principles (OP-Q20). The presently available CHSH crossover is an operational proxy, not a derivation of the CHSH algebra.

### Identical particles and exchange statistics.

**Standard QM.** Particle statistics is imposed through symmetrisation (bosons) or antisymmetrisation (fermions) of many-body wave functions, with the boson/fermion dichotomy accepted as a primitive.

#### ECT.

Exchange statistics follows from the topology of configuration space in the ordered branch. The exchange-sector topology  $\pi_1(\mathcal{M}_2) = \mathbb{Z}_2$  classifies admissible two-body exchanges and underwrites the boson/fermion dichotomy as a structural feature rather than an axiom (§24.4).



**What is computed.**

The same symmetric/antisymmetric structure of many-body amplitudes, now read off from the two-class configuration-space topology.

**What is explained.**

Why there are exactly two species of identical-particle behaviour in three spatial dimensions, and why the dichotomy is not optional. The ECT reading places the origin of particle statistics at the level of configuration-space topology rather than at the level of a symmetrisation axiom.

**Status.**

Level A for the exchange-sector topology itself; a completed spin-statistics theorem remains open (OP-Q11).

**Hydrogen atom and discrete spectra.**

**Standard QM.** One solves the time-independent Schrödinger equation  $H\psi = E\psi$  with the Coulomb potential and obtains  $E_n = -13.6/n^2$  eV together with the densities  $|\psi_{nlm}|^2$ .

**ECT.**

The intended structural picture is that the hydrogenic spectrum arises from the four-dimensional Euclidean field equation for  $\Phi$  together with the self-consistency condition in the  $w$ -direction expressed by the single-valuedness constraint  $\oint dw p_w = 2\pi S_0 n$ .

**What is computed.**

The discrete spectrum is identified with the set of admissible global condensate configurations that satisfy the self-consistency condition. The numerical reproduction of  $E_n = -13.6/n^2$  eV from first principles requires the completed matching  $S_0 \equiv \hbar$  and the detailed solution of the coupled condensate/electromagnetic problem.

**What is explained.**

Why the spectrum is discrete at all: discrete spectra appear as self-consistency conditions on admissible global condensate configurations rather than as eigenvalues of a fundamentally probabilistic wave equation.

**Status.**

Level B structural interpretation; a completed first-principles derivation of the full hydrogenic spectrum has not been carried out within ECT in this paper.

**Determinism at the fundamental level**

The Level-0 Euclidean equation (38.1) is deterministic. There are no probabilities, no wave-function collapse, and no intrinsic stochasticity. One specifies the full boundary data and obtains one global field configuration. Statistical quantum mechanics then appears not because nature is fundamentally probabilistic, but because realistic observers never have access to the full condensate state. When environmental modes are integrated out, the subsystem acquires an influence functional, reduced density matrices, and effective probabilities.

In this sense ECT stands to standard quantum mechanics as microscopic Newtonian mechanics stands to classical statistical mechanics: deterministic underneath, probabilistic after coarse-graining. The  $\sim 10^{23}$  untracked condensate modes play the role of the untracked molecular degrees of freedom; the influence functional plays the role of the reduction from the full phase-space distribution to the relevant thermodynamic variables; the Born rule plays the role of the emergent statistical law. The analogy is not perfect—the ECT reduction is field-theoretic and involves both Euclidean/Lorentzian regime transitions and the selection of a smooth coherent branch—but it captures the correct direction of the reduction: from global determinism, via partial access, to effective probabilistic predictions.

This point is central for the interpretation of ECT. It implies that one may in principle formulate descriptive, non-statistical equations for the quantum world at the fundamental level, while accepting that the effective subsystem description remains probabilistic in practice.

## What ECT already reproduces, and what remains open

It is useful to close the comparison with a reader-oriented summary of what has already been structurally obtained in Part III and what remains open. The following two lists are deliberately organised as a comparison with standard quantum mechanics rather than as an internal ledger of ECT results; the latter is given separately in Section 38.2.

ECT already provides, at varying levels of rigour, the following structural outputs:

- (i) the Schrödinger sector as a nonrelativistic limit of the ordered branch;
- (ii) the Klein–Gordon sector from the ordered-branch equation in the real parametrisation  $t = w/c_*$ ;
- (iii) uncertainty relations together with a structural route to phase quantisation through phase compactness, with the identification of the universal action scale  $S_0$  with  $\hbar$  remaining a Level-B matching rather than a fully closed Level-A theorem;
- (iv) decoherence and the quantum–classical boundary through the influence-functional formalism;
- (v) a structural Euclidean-to-Lorentzian reading of measurement as a regime transition, while a complete measurement theorem remains open within the present formulation (see also OP-Q8);
- (vi) a structural route linking spin-sector discreteness to the residual symmetry and topology of the ordered branch after  $O(4) \rightarrow O(3)$ , rather than a fully closed derivation of the complete spin sector;
- (vii) the Principle of Euclidean Stationarity, which selects the persistent sector of admissible configurations;
- (viii) a structural derivation route for gravitational decoherence from the condensate as a universal bath, without inserting the Diósi–Penrose formula as an independent postulate;
- (ix) a common Euclidean structural basis for tunnelling and entanglement, understood at present as a structural bridge based on Euclidean connectivity rather than as an identity theorem reducing one phenomenon to the other;
- (x) cross-sector persistence of a common action scale  $S_0$ , with its full identification across all effective sectors tied to the same matching programme discussed elsewhere in Part III.

On the other hand, ECT does not yet fully derive:

- (i) the full Born rule from first principles beyond the present closures;
- (ii) a complete theorem of measurement beyond the current  $\Gamma_{\text{loop}}$ -based framework;
- (iii) Bell correlators directly from the condensate theory beyond toy visibility proxies;
- (iv) the detailed origin of three generations;
- (v) the exact value of  $\alpha_{\text{fs}}$ ;
- (vi) the full Yukawa hierarchy.

These should be presented as open derivational targets, not as failures of the framework.

The list above is intended as a reader-oriented comparison between ECT and the standard quantum formalism. A stricter status map of the quantum sector, organised by derivational level (Level A / Level A-B / Level B / Open) and linked to the corresponding open-problem labels, is given separately in Section 38.2. The present limitations of the formulation are collected in Section 48.10. The two summaries serve different purposes: the present one is comparative and pedagogical, whereas Section 38.2 is the more formal status ledger of what is already structurally established and what remains open.

Having set out the structural comparison between ECT and the standard quantum formalism, it is natural to state explicitly what classes of future results would directly threaten this particular ECT route.

### 38.4 ECT-specific falsifiers in the quantum-gravity and decoherence sector

*Status: structural; list of concrete classes of future results that would directly threaten the ECT route in the present sector.*

The ECT route developed in this work is not intended to be unfalsifiable. In the quantum-gravity and decoherence sector, several classes of future results would directly threaten the framework.

First, compelling evidence for a genuinely fundamental stochastic metric law, with a noise spectrum that could not be reinterpreted as emergent from reduced matter–environment or condensate-sector dynamics, would favour post-quantum classical gravity type frameworks [200, 202, 201] over ECT.

Second, robust evidence for fundamental black-hole information loss would directly contradict the intended globally unitary architecture of ECT.

Third, if a general no-go result established that gravity-induced entanglement in the relevant mesoscopic regime is possible only with a genuinely quantized mediator, even after allowing for correlated-noise, common-medium, or reduced-state routes of the Trillo–Navascués type, then one of the main structural loopholes available to the ECT interpretation would be removed [221, 217].

Fourth, if the effective ECT dynamics itself were shown to decohere away all mediator coherence on the timescales relevant for mesoscopic interference experiments, so that no gravity-induced entanglement could ever survive in principle, then the ECT route to this class of phenomena would fail.

These possibilities do not refute the already-derived parts of the framework automatically, but they would decisively undermine the specific ECT programme pursued here for the quantum-gravity and decoherence interface.

### 38.5 Completion status and bridge forward

Even with the open problems listed in Section 38.1, the Quantum Sector has already gone far beyond a generic statement that “quantum mechanics might emerge”. ECT now contains: a coherent phase-sensitive branch with loop sectors and a distinguished pre-quantum action scale  $S_0$ ; wave-dynamical reduction together with extremal-action and conservation structure; a Hilbert-space bridge through reflection positivity, the global/reduced unitarity distinction, canonical organisation, and the uncertainty principle; Euclidean path-dependence, exchange-sector topology, and a representation-theoretic route to Dirac structure; a unified coherent-vacuum response programme covering Casimir, Unruh-type response, particle production, and horizon thermality; an open-system decoherence architecture with effective entropy production and Crooks-type closure-level relations; a quantum–classical boundary formulated through the reverse-segment reading of the Euclidean path integral; a conditional Born-type probability route once assumptions (C1)–(C3) are admitted; entanglement as the structural availability of non-factorisable correlations in one ordered medium; a wider defect and topological ontology connected to the dark sector; a black-hole programme in which fundamental information destruction is excluded at Level A within the global coherent framework of ECT, while the present critical-shell strong-field construction is a Level B closure; the Principle of Euclidean Stationarity as a unifying selection criterion for persistent configurations (Level B core, programme-level extension); visibility-based operational  $\Gamma_{\text{loop}}$  anchors for photonic quantum platforms; a closure-level qubit information–decoherence bound for partial observation; a toy Bell/CHSH crossover threshold  $\Gamma_{\text{loop}} = \ln \sqrt{2}$  used as an operational marker rather than a first-principles Bell derivation; coarse-graining readings of Wigner’s-friend-type situations; a programme-level reverse-coherence perspective in which Lorentzian locking can, in principle, be partially reopened in mesoscopic or engineered settings; and an analogue-laboratory programme testing the instantiability of the ordered-medium logic in controlled systems. That already constitutes a coherent research programme rather than a loose speculation.

The quantitative and regime-level outputs of the present decoherence apparatus are summarised separately in Section 27; the role of the present subsection is not to duplicate those entries, but to classify what they establish, what remains closure-dependent, and what still requires a deeper microphysical derivation.

**Methodological status.** The correct overall status of the Quantum Sector is neither “fully derived quantum mechanics” nor “purely conjectural”. It is an intermediate but substantial result. ECT has identified the correct structural location inside the theory where quantum kinematics, vacuum response, decoherence, probability, entanglement, and strong-field information bookkeeping arise, and has made a substantial part of that architecture explicit. Section 38.1 records the detailed row-by-row status map, and Section 38.2 separates the strict structural core from the structurally singled-out backbone and the remaining closure-level or open fronts.

**Bridge to the rest of the paper.** With this status map in place, the role of the Quantum Sector inside the full ECT paper becomes clear. ECT basics establishes that a coherent branch exists. Macroscopic Physics develops the phase-insensitive geometric branch. The present Part develops the phase-sensitive coherent branch. In both cases the same ordered condensate provides the common physical medium (P5): the geometric and coherent branches are not independent theories, but two regimes of one ordered-medium architecture. The analogue-laboratory programme adds a third regime of inquiry: controlled laboratory systems in which the same structural logic can be tested independently of astrophysical or cosmological data. The later summary, comparison, and outlook sections can therefore assess ECT as a multi-regime theory with one common ordered-condensate foundation.

**What ECT does and does not establish in the Quantum Sector.** The Quantum Sector of ECT should not be read as a complete derivation of all standard quantum laws from the bare postulates. Its present strength lies elsewhere: it organises the coherent branch into a unified structure, clarifies which results are already structural, which are structurally singled out but not fully closed, and which remain open, and substantially narrows the space of admissible interpretations. In several places the gain is not a full derivation, but a strong exclusion result: fundamental information destruction is excluded at Level A within the global coherent framework, and the uniqueness of Born-type weights is sharply constrained once assumptions (C1)–(C3) are admitted. These exclusions would not be available in a looser framework that did not take the ordered-medium postulate structure seriously.

**Summary.** The Quantum Sector is now structurally complete enough to stand beside Macroscopic Physics as the second major developed branch of ECT. Its strict structural core, structurally singled-out backbone, and remaining closure-level or open fronts are inventoried in Section 38.2. It is not yet finished in the strongest first-principles sense, but it is already sufficiently articulated, internally organised, and self-critical to support the later summary, comparison, prediction, and outlook sections of the paper.

## Part IV

# Reverse Analysis, SU(3) Completion, and Structural Constraints

## 39 Methodology of reverse analysis

*Status: Methodological. This section does not present new physics; it articulates the methodology of reverse analysis used throughout Part IV and its relation to the forward programme of Parts I–III.*

**Scope.** Reverse analysis as used in Part IV is a closure/consistency layer on top of the forward derivations of Parts I–III. It is not a substitute for forward derivation, and must be used under explicit rules. At best it delivers Level B; more commonly Level C.

**Distinction from forward derivation.** Forward derivation in ECT starts from P1–P6 and deduces consequences; this is how Parts I–III are structured, and it is the only route to Level A results. Reverse analysis starts from the partial success of the forward programme together with empirical constraints from observed physics, and identifies what minimal additional structure, beyond P1–P6, the medium must carry for consistency.

**Legitimacy.** Reverse analysis is scientifically legitimate when, and only when, every reverse-engineered constraint is traceable to a specific consistency obstruction uncovered by forward work. An example already present in the article is the obstruction theorem (§2) showing that exact colour cannot reside in the condensate; this leads to the reverse-engineered requirement that the medium must carry a separate internal module for colour. That is reverse analysis used correctly.

**Relation to the forward programme.** Part IV should be read not as a second derivation of the gauge and fermion architecture, but as a reverse-analysis closure layer built on top of the forward programme already developed in Sections 9.3, 9.5, 9.6, 9.7, and in the colour-consistency analysis now collected in §40. It does not replace the existing structural routes to chirality or to three generations; it clarifies which exact-colour completions are compatible with those routes and which unresolved questions remain blocked even after the P7 completion layer. Part IV is therefore not a second derivation of gauge and fermion structure, but a reverse-analysis closure layer built on top of the forward programme already developed in Parts I–III.

**Rules of engagement.** Five rules govern reverse analysis as applied in Part IV: (i) every reverse-engineered constraint must point back to a forward obstruction; (ii) new postulates must be geometric or structural, never numerical or phenomenological; (iii) outcomes are restricted to admissible classes—never derive desired results such as specific masses or couplings via reverse reasoning; (iv) any residual freedom in the completion must be catalogued as Open; (v) reverse-engineered postulates must be flagged as such (e.g. P7) and not confused with the primary postulates P1–P6.

**What Part IV does within these rules.** Section 40 was already reverse-engineered in prior versions of the article and is now placed here as the natural home for the colour-completion layer. Sections 41–42 derive the admissible EFT class and matter-consistency constraints assuming P7. Section 43 catalogues how reverse analysis clarifies earlier conditional results. Section 44 is a physical hypothesis about proton stability conditional on the completion. Section 45 acknowledges honestly that even reverse analysis does not close the strong CP problem in the minimal setup. Section 46 summarises closures and remaining open questions.

## 40 Colour consistency requirement and candidate non-Abelian completions

### Why exact colour is required for full closure

The present formulation of ECT fixes a substantial part of observed low-energy architecture, but full closure remains incomplete without an exact unbroken colour symmetry. Many formulas, laws, and constants can be sharpened only once a consistent non-Abelian strong sector is available. The current derivations reveal a reverse-engineered consistency requirement: any viable completion of the  $\Phi$ -medium compatible with the observed world must contain an exact unbroken colour sector. This is not retrofitting but a constraint extracted from the partial success of the present formulation.

### Strict obstruction: colour cannot reside in the condensate

**Theorem.** *Any nonzero ordered-branch condensate transforming nontrivially under an internal group  $G$  breaks  $G$  to the stabilizer of the condensate. For  $G = SU(3)$  and condensate in the fundamental representation, the stabilizer is  $SU(2)$ . Therefore exact colour  $SU(3)$  cannot be carried by the condensate.*

*Proof sketch.* Let  $\langle \partial_A \Phi^i \rangle = u_0 n_A \xi^i$  with  $\xi^\dagger \xi = 1$ . The stabilizer of a nonzero vector  $\xi \in \mathbb{C}^3$  under  $SU(3)$  is  $SU(2)$ . In the gauged theory, the mass matrix for the colour connection modes is  $M_{ab}^2 \propto u_0^2 \xi^\dagger T^a T^b \xi$ , giving five massive and three massless gauge bosons:  $SU(3) \rightarrow SU(2)$ .  $\square$

The triplet-condensate route is structurally excluded. The ordered branch must remain an internal singlet if exact colour is to survive.

**Algebraic obstruction: dimensional exclusion.** A complementary, purely algebraic obstruction confirms this conclusion. The Lie algebra  $\mathfrak{su}(3)$  has dimension 8, while  $\mathfrak{so}(4)$  has dimension 6. Since a subalgebra cannot exceed the dimension of the ambient algebra,  $\mathfrak{su}(3) \not\subset \mathfrak{so}(4)$ . Therefore  $SU(3)$  cannot arise as a direct subgroup or residual gauge factor of  $O(4)$  by any mechanism—not only through the condensate stabiliser route excluded above, but through any algebraic embedding whatsoever. The maximal gauge structure derivable from the  $O(4) \rightarrow O(3)$  pattern is  $U(2) = (SU(2) \times U(1))/\mathbb{Z}_2$ , which corresponds to the electroweak-type architecture established in Section 7.3.

### Reverse-engineered constraint on the medium

The minimal postulates P1–P6 were formulated from objective considerations about Euclidean ordering, symmetry breaking, and the emergence of Lorentzian dynamics. They did not specify the full internal architecture required by observed physics. However, confronting the derived ECT structure with exact colour physics reveals an additional constraint: colour must reside in a separate internal sector of the medium that does not participate in the ordered-branch condensate. The condensate remains singlet; colour lives elsewhere.

This is not an arbitrary retrofitting of the theory, but a reverse-engineered consistency constraint extracted from the partial success of the present formulation: having derived spacetime, gravity, the quantum action scale, and an electroweak-like gauge architecture, one can now identify what additional internal structure the medium must carry for compatibility with the observed strong interaction.

### Primary completion: a local complex rank-3 internal module with $SU(3)$ -structure

**Formal statement as a reverse-engineered postulate.** *The content that follows is collected below as a formal reverse-engineered postulate P7, distinct from the primary postulates P1–P6 and subject to the methodological rules of §39. P7 supplies the minimal geometric structure required for consistency of ECT with an exact unbroken colour sector, given the obstruction theorems established above.*

**Postulate P7 (internal colour module of the medium).** In addition to the primary postulates P1–P6, the ordered medium carries at each spacetime point a local complex internal

module of rank three,  $\mathcal{C}_x \simeq \mathbb{C}^3$ , equipped with (i) a Hermitian form  $h$  on  $\mathcal{C}_x$ , and (ii) a fixed nonvanishing complex volume form  $\Omega \in \Lambda^3 \mathcal{C}_x^*$ . The ordered-branch condensate fields  $\phi$  and  $n^\mu$  transform trivially under  $\mathcal{C}_x$ —i.e. they are internal singlets. Physically meaningless local redefinitions of the internal complex frame are precisely those preserving both  $h$  and  $\Omega$ ; the resulting local frame-redundancy group is  $SU(3)$ .

**Status of P7.** P7 is a reverse-engineered structural postulate, not a derivation from P1–P6. It is introduced here because the obstruction theorems above demonstrate that no extension of P1–P6 internal to the condensate branch can accommodate exact  $SU(3)$ , while an external internal module equipped with the data  $(h, \Omega)$  does. The remainder of this section, and Sections 41–46 of Part IV, unpack the physical meaning and structural consequences of P7. The status of each consequence (Level A, B, or C) is indicated locally.

**Physical meaning.** The most economical candidate completion assumes that, in addition to the singlet ordered branch, the medium carries at each point a local complex rank-3 internal module  $\mathcal{C}_x \simeq \mathbb{C}^3$ . Physically, this means that the medium possesses three equivalent internal complex degrees of freedom of local structure, distinct from both the spacetime directions and the condensate order parameter itself.

**Non-rigidity as extension of existing logic.** The medium is not assumed to fix a globally rigid basis in this internal module. Local redefinitions of the internal complex frame carry no physical meaning. This extends the already adopted non-rigidity logic of the  $\Phi$ -medium (P5) into the internal sector. In the presence of a Hermitian structure on the module, the natural local redundancy is a  $U(3)$ -type frame freedom.

**Reduction from  $U(3)$  to  $SU(3)$ .** To obtain an  $SU(3)$  colour symmetry rather than the larger  $U(3)$  frame redundancy, the completion must supply more than a complex rank-3 module alone. In addition to the Hermitian structure, one must require a distinguished nonvanishing complex volume form  $\Omega \in \Lambda^3 \mathcal{C}_x^*$ , equivalently a local antisymmetric trilinear invariant  $\varepsilon_{abc}$ . The physically admissible local frame changes are then those preserving both the Hermitian metric and this complex volume form. Their group is  $SU(3)$ .

Physically, this means that the medium may locally rearrange its three internal complex directions while preserving the elementary antisymmetric three-channel structure of the colour cell. Equivalently, the internal colour module is promoted from a  $U(3)$ -bundle to an  $SU(3)$ -bundle.

This reduction from  $U(3)$  to  $SU(3)$  should be treated as part of the candidate completion of the medium, not as an already derived consequence of the current minimal ECT postulates. The  $U(1)$  factor removed in this step should not be confused with the electromagnetic  $U(1)$  already obtained from the compact phase sector: the two  $U(1)$  symmetries have different origins and act on different degrees of freedom.

**Connection to observed physics.** The preserved antisymmetric invariant  $\varepsilon_{abc}$  has a direct physical counterpart: in observed strong-interaction physics it is the tensor from which colour-singlet three-quark channels are constructed. The requirement that the medium preserve this trilinear form therefore admits a natural interpretation as the structural condition for the existence of colour-neutral baryonic channels.

**What is obtained.** Under this completion, an  $SU(3)$  colour symmetry becomes structurally available as the local frame redundancy preserving the  $SU(3)$ -structure of the internal module, compatible with the singlet condensate. Colour-triplet excitations can be represented as sections of  $\mathcal{C}$ . A non-Abelian connection becomes meaningful as internal frame transport. The strong sector becomes structurally accessible.

**Structural compatibility checks.** A limited but nontrivial compatibility check concerns gauge-sector counting. If the colour completion proposed here is combined with the electroweak-like sector already discussed elsewhere in ECT, then the expected adjoint dimensions become structurally available: 8 for the colour sector, 3 for the weak sector, and 1 for the Abelian phase sector. This reproduces the Standard Model gauge-boson count at the level of symmetry dimensions only. It should not be confused with a derivation of the full electroweak and strong gauge dynamics, mass generation, or mixing structure.

A second compatibility check concerns colour neutrality outside the strong sector. Degrees of freedom arising from the electroweak-like sector, the Abelian phase sector, and the singlet gravitational sector are all structurally independent of the colour module introduced here. They are therefore naturally colour-singlet. This is consistent with the observed colour neutrality of the non-strong gauge sector and of the gravitational interaction. Likewise, scalar and Goldstone-type excitations belonging to the singlet condensate sector remain colour-neutral by construction.

If the proposed colour module is combined with the weak-sector doublet structure discussed elsewhere in ECT, then quark-like and lepton-like sectors can be accommodated in a structurally compatible way. In particular, one may consistently describe excitations that transform nontrivially under both the colour and weak sectors, as well as excitations that remain colour singlets while still transforming under the weak sector. This should not be confused with a full derivation of the Standard Model matter content: chirality, hypercharge assignments, right-handed singlets, and generation structure remain open.

With colour excitations in the fundamental representation  $\mathbf{3}$  of  $SU(3)$ , the product  $\mathbf{3} \otimes \bar{\mathbf{3}}$  contains a singlet (meson-like channel), while the antisymmetric contraction  $\epsilon_{abc} q^a q^b q^c$  provides a baryon-like singlet channel. In this sense, both meson-type and baryon-type colour-neutral channels are structurally available, although their actual bound-state dynamics remains open.

**What is not obtained.** This completion does not yet derive full QCD. The matter content details, chirality pattern, coupling strength  $g_s$ , confinement mechanism,  $\theta_{\text{QCD}}$  sector,  $\Lambda_{\text{QCD}}$ , and the full Standard Model representation structure (including hypercharge assignments and right-handed singlets) remain open.

## Updated status under the primary completion

**Table 106:** Status changes under the primary colour completion.

Item	Before completion	After completion	Still open
Exact colour symmetry	Missing	$SU(3)$ available under completion hypothesis	Dynamical realisation
Strong-sector gauge structure	Missing	Structurally available at symmetry level	Full Yang–Mills closure
Gauge-sector counting	Partial	Symmetry-level counting strengthened	Full dynamics and identification
Colour neutrality of non-strong sectors	Untested	Structurally consistent with the completion	Detailed sector identification
Compatibility with EW sector	Partial	Strengthened	Full matter embedding
Meson/baryon channels	Inaccessible	Singlet channels structurally available	Bound-state dynamics
Strong-sector constants	Inaccessible	Become principled targets	Not derived
$\alpha_s(M_Z)$ , $\Lambda_{\text{QCD}}$	Undefined without an exact colour sector	Definable within $SU(3)$ Yang–Mills	Running, matching not derived



Item	Before completion	After completion	Still open
Proton/neutron mass ( $\sim 938$ MeV)	Inaccessible ( $\sim 99\%$ from QCD binding)	Accessible in principle via $SU(3)$ bound states	Binding dynamics open
Confinement, asymptotic freedom	No exact colour sector present to support confinement	Standard $SU(3)$ Yang–Mills properties become available	ECT-native derivation open
$\alpha_{\text{fs}} = 1/137$ normalisation	Quark loop contribution undefined	Quark charges better posed; electroweak kinetic/mixing target for $\alpha_{\text{fs}}$ sharpened (§7.2)	Full $(Z_B, Z_W)$ derivation open
Baryogenesis ( $\eta_B$ )	Baryon number definition incomplete	Colour defines baryon number; leptogenesis benchmark strengthened	Full transport open
Proton stability ( $\tau_p$ )	Proton-decay selection rules not yet formulable without colour completion	Three selection-rule patterns (I/II/III) become formulable (§44)	Pattern identification, decay channels, and co-efficient structure open
Instanton spectrum $m_n \sim n \times 1.6$ GeV	Physical interpretation unclear	Comparison with QCD hadron spectrum becomes meaningful	Dynamics not derived
Colour-sensitive laws/formulas	Blocked	Obstruction removed	Individual derivations open

### Updated open questions under the primary completion

The primary completion improves consistency but does not end the programme. Its open questions are now sharper: why the internal module has rank three; why a distinguished antisymmetric trilinear form exists on the module; whether the non-Abelian connection acquires full Yang–Mills kinetics from ECT-native mechanisms; how quark representations and chirality arise; how hypercharge assignments and right-handed singlet structure emerge; whether confinement can be derived internally rather than imported from standard QCD intuition; whether strong-sector constants such as  $g_s$  and  $\Lambda_{\text{QCD}}$  can be constrained or derived; and what baryon-number selection rules are realised in the completed low-energy theory, which controls proton stability (§44). A deeper completion might eventually relate the number of colours to matter-representation content, but no such relation is derived here.

### Alternative deeper geometric candidate: internal $G_2$ structure

**Physical interpretation.** A deeper geometric possibility is that the medium carries, in addition to the ordered branch, an internal seven-dimensional real fibre  $\mathcal{J}_x$  endowed with a metric and an antisymmetric composition law of octonionic type. Physically, this means that the medium possesses not merely internal degrees of local structure, but a specific non-associative geometry of how those internal channels combine locally. The group preserving this internal composition structure is  $G_2$ .

**Strict derivation of  $SU(3)$ .** If such an internal  $G_2$  structure exists, choosing a unit internal direction  $u \in \mathcal{J}_x$  reduces the automorphism group to its stabilizer:

$$\text{Stab}_{G_2}(u) = SU(3). \quad (40.1)$$

On the orthogonal six-dimensional subspace  $u^\perp$ , the internal cross-product defines an almost-complex structure:

$$J_u(v) = u \times v, \quad J_u^2 = -1, \quad (40.2)$$

so that  $u^\perp \simeq \mathbb{C}^3$ . The colour triplet then appears not as a postulated rank-3 module but as the complex three-space orthogonal to a distinguished internal calibration direction.

**Relationship to the primary completion.** The  $G_2$  route is not merely an alternative to the primary completion. It can be viewed as a possible deeper origin of it: the  $SU(3)$ -structure required by the primary completion arises naturally on  $u^\perp$ . The  $G_2$ -compatible cross-product defines the complex structure  $J_u$ , while the induced Hermitian form and complex volume form provide the  $SU(3)$ -structure whose components appear as  $\varepsilon_{abc}$  in an adapted complex basis. In this sense, the  $G_2$  completion implies the primary completion, but not conversely. The two candidates are nested, not parallel.

**Why the  $G_2$  route is not adopted as the primary completion.** This route requires an exceptional internal geometry—a seven-dimensional real fibre with octonionic composition law—that is not otherwise forced by the current ECT postulates. It is physically less transparent and more speculative than the rank-3 module completion. The  $SU(3)$ -structured rank-3 module completion is therefore adopted as the primary working hypothesis, while the  $G_2$  route is recorded as a deeper candidate origin that may become preferable if future work uncovers independent evidence for an internal octonionic structure of the medium.

## 41 Minimal admissible colour EFT under P7

*Status: Level B structural result. The admissible operator class and its obstructions are derived; the background-level triviality result is a clean negative structural finding. No quantitative strong-sector prediction is claimed.*

**Setup.** Given P7 (§40): exact local  $SU(3)$  acting on an internal module  $\mathcal{C} \simeq \mathbb{C}^3$  with Hermitian form  $h$  and fixed complex volume form  $\Omega$ , while the ordered-branch condensate fields  $\phi$  and  $n^\mu$  remain colour singlets. We ask: what is the most general renormalisable local gauge-invariant effective Lagrangian for the colour connection  $A_\mu^a$  compatible with this structure?

**Minimal admissible lagrangian.** Only singlet operators in  $\phi$  and  $n^\mu$  are allowed. At leading order:

$$\mathcal{L}_{\text{col}}^{\text{min}} = -\frac{1}{4} Z(\phi) F_{\mu\nu}^a F^{a\mu\nu} - \frac{1}{4} Y(\phi) (n^\mu F_{\mu\rho}^a) (n^\nu F_\nu^{a\rho}) + \frac{\Theta(\phi)}{32\pi^2} F_{\mu\nu}^a \tilde{F}^{a\mu\nu} + \mathcal{L}_{\text{matter}}^{(3)} + \dots \quad (41.1)$$

with  $Z(\phi) > 0$  for positivity. Additional consistency requires

$$Z(\phi) + Y(\phi) \Xi(n, k) > 0 \quad (41.2)$$

for all physically admissible propagation directions  $k$ , where  $\Xi(n, k)$  encodes the directional structure induced by the anisotropic operator, so that no ghost or negative-norm instability is introduced by the anisotropic deformation.  $\mathcal{L}_{\text{matter}}^{(3)}$  collects coloured matter sections of  $\mathcal{C}$ .

**Status of the anisotropic operator.** The operator  $Y(\phi)(n \cdot F)(n \cdot F)$  is admissible as part of the minimal EFT basis, but it is not a phenomenologically active leading-order channel. It shares the rank-2 directional structure  $n_\mu n_\nu$  that enters the generalised Einstein equations of Part II through the ECT anisotropy coefficient  $\alpha_{\text{ECT}}$ ; structural consistency with the observational bounds on that coefficient makes  $|Y_0/Z_0|$  subleading, and positivity (eq. 41.2) provides a second constraint independent of phenomenology. The anisotropic term should therefore be viewed as part of the admissible operator basis rather than as a physically active IR channel. The IR-relevant leading operators are  $Z(\phi)F^2$  and  $\Theta(\phi)F\tilde{F}$ .

**Obstruction theorems.** Three obstruction statements follow from (41.1) and rule out naive colour mass-generation routes.

*Theorem 1 (no tree-level gluon mass).* A gauge-invariant Proca-type term  $m_g^2 A_\mu^a A^{a\mu}$  is forbidden by the exactness of  $SU(3)$ . The minimal admissible EFT provides no tree-level route to a gluon mass.

*Theorem 2 (no Higgs-colour route).* Since the ordered condensate is a colour singlet by the obstruction theorem of §40, there is no colour-charged Higgs field in the minimal completion. The direct colour-Higgs mass-generation route is structurally excluded.

*Theorem 3 (oscillator tower  $\neq$  physical colour spectrum).* Any linearly spaced tower  $m_n = n\omega$  arising from oscillator quantisation around a quadratic vacuum minimum belongs, at best, to internal medium excitations. The physical colour gauge-invariant spectrum is not captured by such a tower; any strong-sector mass gap in the exact colour sector must arise nonperturbatively.

**Three-scale consistency condition.** The ECT condensate carries three widely separated scales (Part I, three-scale architecture). The coupling functions  $Z(\phi)$ ,  $Y(\phi)$ ,  $\Theta(\phi)$  must admit an RG-cascade interpretation compatible with this architecture. In particular, in the UV regime ( $\mu \gg M_*$ ) decoupling must hold— $Z(\phi) \rightarrow \text{const}$ ,  $Y(\phi) \rightarrow 0$ ,  $\Theta(\phi) \rightarrow \text{const}$ —so that at high energies standard asymptotically free Yang–Mills/QCD is recovered and known high-energy strong phenomenology is not distorted.

**Structural origin of the anisotropic operator.** The anisotropic operator  $Y(\phi)(n^\mu F_{\mu\rho}^a)(n^\nu F_\nu^{a\rho})$  is not an independent free parameter of the colour sector. Its rank-2 directional structure  $n_\mu n_\nu$  is identical to the structure that enters the generalised Einstein equations of Part II through the ECT anisotropy coefficient  $\alpha_{\text{ECT}}$ , since both operators contract with the same Lorentzian director  $n^\mu$  of the ordered branch. Any physical ECT solution with a given  $\alpha_{\text{ECT}}$  therefore carries a colour-sector anisotropy of the same geometric origin and is not expected to define an independent large deformation channel in the colour sector. This is a structural consistency statement, not a numerical fit: the two anisotropy coefficients share their geometric origin, and the smallness of  $\alpha_{\text{ECT}}$  required by observational gravity tests is structurally transmitted to  $|\kappa_n| = |Y_0/Z_0|$ .

**Form of the colour infrared scale under P7.** Under the admissible EFT (41.1) and the one-loop Yang–Mills  $\beta$ -function for pure  $SU(3)$  with coefficient  $b_0 = 11$ , the colour infrared scale takes the dimensional-transmutation form

$$\Lambda_{\text{col}}^{\text{ECT}} = M_* \exp \left[ -\frac{8\pi^2}{b_0 g_{\text{eff}}^2(M_*)} \right] = M_* \exp \left[ -\frac{8\pi^2 Z_0}{b_0 g_s^2(M_*)} \right], \quad (41.3)$$

with subleading corrections from  $\kappa_n$  and from higher-loop running. Three disclaimers are in order. (i) This is not a prediction:  $M_*$ ,  $g_s(M_*)$ , and  $Z_0$  are all matching data and are not derived from ECT primary postulates. (ii) It is not an independent derivation of  $\Lambda_{\text{QCD}}$ : at  $Z_0 \rightarrow 1$  the formula reduces to the standard one-loop QCD transmutation with the same matching data. (iii) At constant background couplings this formula carries no independent predictive content beyond standard Yang–Mills matching; its role here is classificatory, not explanatory. Any would-be ECT-specific contribution to  $\Lambda_{\text{col}}$  must enter through  $\phi$ -dependence of  $Z$ ,  $Y$ , or  $\Theta$  beyond constant-background level, consistent with the triviality result stated immediately below.

**Central negative result: background-level triviality.** *This is the principal structural finding of §41.* At strictly constant background couplings  $Z_0, Y_0, \Theta_0$  independent of  $\phi$ , canonical normalisation of the gauge field yields  $g_{\text{eff}}(M_*) = g_s(M_*)/\sqrt{Z_0}$ , so the minimal EFT reduces to standard pure Yang–Mills with a redefined matching convention. Consequently, the colour-sector completion does not yet generate independent predictive strong-sector physics beyond a redefinition of matching conventions and a possible theta-angle problem (§45). Nontrivial ECT content begins only when the coupling functions have genuine condensate dependence—e.g. operators such as  $\delta\phi F^2$  and  $\delta\phi F\tilde{F}$ —or when the microphysical origin of the matching data is derived from ECT primary postulates.

**What this section claims and does not claim.** Claimed: the minimal admissible operator class (41.1), the three obstruction theorems above, the three-scale consistency condition, and the background-level triviality result. ECT with P7 constrains the admissible form of a colour-sector EFT and the class of medium couplings compatible with exact colour. Not claimed: a derivation of  $\Lambda_{\text{QCD}}$ , of confinement, of the glueball spectrum, or of  $g_s$ . All quantitative strong-sector observables remain inherited from standard QCD phenomenology, constrained by the admissible EFT structure above but not independently derived.

## 42 Anomaly constraints and matter-sector consistency

*Status: Level B structural layer. This section does not replace the anomaly architecture already analysed in §9.5; its purpose is narrower: to restate the anomaly constraints specifically in the presence of P7 and the exact-colour completion.*

**Setup.** Given P7 (§40) and the admissible colour EFT of §41, quantum consistency of the matter sector requires anomaly cancellation in the usual sense. The content below is standard; its role in Part IV is not to introduce an anomaly analysis for the first time—that role is already played by §9.5—but to *restate* the anomaly constraints specifically in the presence of the exact-colour completion established by P7, so that the P7 completion layer and the pre-existing anomaly architecture are visibly consistent.

**$SU(3)^3$  anomaly.** For coloured fermions in representations  $R_i$ , the cubic anomaly condition is

$$\sum_i \mathcal{A}(R_i) = 0, \quad \mathcal{A}(\mathbf{3}) = +1, \quad \mathcal{A}(\bar{\mathbf{3}}) = -1.$$

In the minimal realisation with matter restricted to fundamental and antifundamental colour representations, anomaly cancellation forces  $N_3 = N_{\bar{3}}$ , i.e. vector-like colour content. Anomaly-free chiral  $SU(3)$  realisations exist with exotic representation assignments (e.g. adjoint combined with rank-2 symmetric), but none are realised in nature; we do not pursue them here.

**Mixed anomalies with additional gauge factors.** Introducing additional gauge factors to accommodate chirality, the following mixed anomalies must cancel:

$$\begin{aligned} SU(3)^2 \cdot U(1) : \quad & \sum_i q_i T(R_i) = 0, \\ SU(2)^2 \cdot U(1) : \quad & \sum_{\text{doublets}} q_L = 0, \\ U(1)^3 : \quad & \sum_i q_i^3 = 0, \\ U(1) \cdot \text{grav}^2 : \quad & \sum_i q_i = 0. \end{aligned}$$

For the one-generation Standard-Model content  $\{Q_L, u_R, d_R, L_L, e_R\}$ , these constraints fix hypercharges up to normalisation. With sterile-neutrino freedom a singlet can be added without disturbing anomaly balance; this is relevant for the neutrino discussion of §8.9 and for the proton stability discussion of §44.

**Witten global anomaly.** Any ECT completion with an  $SU(2)$  weak factor must satisfy the Witten global anomaly constraint: the total number of left-handed  $SU(2)$  doublets must be even. With four doublets per generation and three generations the count is twelve, and the anomaly is absent.

**'t Hooft anomaly matching.** If the ECT completion admits distinct UV (medium microphysics) and IR (emergent SM-like EFT) descriptions, global anomalies must match between the two. This is a nontrivial structural constraint on the microphysical completion and is flagged as Open (§46).

**Baryon number and Harlow–Ooguri compatibility.** The proton-stability treatment of §44 maintains  $U(1)_B$  as a selection rule. The Harlow–Ooguri no-global-symmetries argument for quantum gravity is consistent with this:  $U(1)_B$  must not be a fundamental exact global symmetry but a selection rule emergent from the detailed gauge and matter structure. A subtler concern is the global  $U(1)$  carried by the complex volume form  $\Omega$  in P7: whether this is gauged, broken, or protected at the quantum level is Open (§46).

**Local structure does not determine the global quotient.** The local gauge structure discussed here does not determine the global quotient  $(SU(3) \times SU(2) \times U(1))/\Gamma$ , which remains an additional completion-level question tied to charge quantisation and global bundle structure. It is flagged as Open.

**What this section claims and does not claim.** Claimed: once matter is added, anomaly cancellation must hold; in the minimal realisation with fundamental/antifundamental colour matter, colour is vector-like and chirality requires extended gauge structure; the Standard-Model gauge group is a natural phenomenologically relevant candidate extension compatible with the observed matter sector, with hypercharges fixed by anomaly cancellation once the one-generation matter content is assumed; Witten global anomaly is respected for three generations; baryon number must be a selection rule rather than a fundamental symmetry. Not claimed: uniqueness of the Standard-Model gauge group; derivation of the matter representations from ECT primary postulates; derivation of hypercharge normalisation from ECT; derivation of three generations as a theorem; determination of the global quotient  $\Gamma$ ; derivation of the sterile-neutrino status.

### 43 Closure of SU(3)-dependent questions from earlier parts

*Status: Level B bookkeeping.* This section does not add new derivations; it collects and reclassifies SU(3)-dependent questions raised in Parts I–III in the light of the P7 completion layer and the anomaly constraints of §42.

**Purpose.** Several questions and programme items in Parts I–III were left with a status conditional on the unresolved exact-colour sector. Part IV formalises P7 and the admissible EFT class, so those items can now be reclassified. The table below records, for each item: (i) where the issue was raised; (ii) its status before Part IV; (iii) what Part IV adds; (iv) its status after Part IV, using a restricted label set.

**Status label convention.** *Closed structurally.* The specific structural question is resolved at Level A or B within reverse analysis (a full dynamical derivation may still be open). *Sharpened.* A Level B or C route existed before; Part IV adds constraints that make the formulation more precise without deriving the item. *Reframed.* The item was implicitly present or ill-posed before Part IV; it is now explicitly posed or moved to a different architectural layer. *Still open.* No substantive change; retained for completeness.

**Table 107:** Coverage of SU(3)-dependent questions from Parts I–III after the Part IV completion layer.

Issue	Status before Part IV	What Part IV adds	Status after Part IV
Exact colour completion of the medium (OP-GUT1; §40)	Missing; reverse-engineered requirement	P7 formalised as reverse-engineered postulate (§40); three obstruction theorems; rank-3 complex internal module with Hermitian form and fixed complex volume form	Closed structurally

Issue	Status before Part IV	What Part IV adds	Status after Part IV
Minimal admissible colour EFT (new layer; §41)	Not formulated	Minimal operator class $Z(\phi)F^2 + Y(\phi)(n \cdot F)^2 + \Theta(\phi)F\tilde{F}$ ; no gluon mass; no Higgs-colour route; oscillator tower $\neq$ physical colour spectrum; background-level triviality result	Closed structurally
Anomaly architecture of emergent chiral gauge sector (§9.5; OP-GUT6 family)	EW anomaly constraints inherited at ordered-branch level (B); full SM closure conditional on colour	P7-compatible restatement; $SU(3)^3$ cancellation; Witten global anomaly consistent with three generations; mixed-anomaly layer (§42)	Sharpened
Chirality and $SU(2)_L$ selection (§9.3)	Level B structural possibility via $Spin(4) \simeq SU(2)_L \times SU(2)_R$	Confirmed that the existing chirality route and the P7 exact-colour completion live in structurally disjoint sectors and therefore do not conflict; anomaly cancellation identifies chiral extensions (§42) compatible with that route; deepening via $P7+n^\mu$ flagged as directional item D1, not a derivation	Sharpened
Three fermion generations (§9.7; par. 9.6; App. Z)	Spectral route, $y \sim 1.3\text{--}2.0$ ; Level B/C; strict derivation open (OP-generations)	Verified that $N_{\text{gen}} = 3$ is consistent with the Witten even-doublet constraint under P7 (twelve $SU(2)$ doublets in total); the rank-3 structural coincidence remains a pointer (D2), not a derivation; strict generation-count derivation remains open	Sharpened
Matter representations (OP-GUT2)	Open	Admissible matter class narrowed by $SU(3)^3$ and mixed-anomaly cancellation requirements	Sharpened
Charge assignments / hypercharges (OP-GUT3b)	Partial (charge lattice established, Level A); observed assignments Open	Hypercharges fixed up to normalisation by anomaly cancellation once the one-generation matter content is assumed	Sharpened
Strong-sector constants $g_s, \alpha_s(M_Z), \Lambda_{\text{QCD}}$ (OP-GUT4)	Open; no exact colour sector present to carry them	Inherited from standard QCD phenomenology within the admissible EFT class; background-level triviality shows constant-coupling ECT adds no predictive content beyond matching redefinition	Reframed
Confinement and glueball spectrum	Inaccessible without colour group; naive oscillator-tower interpretation of $m_n = n \omega$ circulated informally	Theorem on oscillator tower $\neq$ physical colour spectrum; strong-sector gap must arise nonperturbatively; confinement inherited, not derived	Reframed

Issue	Status before Part IV	What Part IV adds	Status after Part IV
Strong CP problem ( $\theta_{\text{QCD}}$ )	Not explicitly posed in the ECT framework	Reopened through $\Theta(\phi)F\tilde{F}$ with three honestly scoped resolution routes R1/R2/R3 (§45)	Reframed
Proton stability and baryon number (§44; OP-proton)	Three selection-rule patterns (I/II/III); conditional on gauge/flavour completion	Baryon number role clarified as selection rule compatible with Harlow–Ooguri; framework placed in its architectural layer	Sharpened
Neutrino sector; sterile status (§8.9)	Level B; sterile right-handed singlet route admissible	Anomaly cancellation allows a singlet without disturbing balance; required/permitted/forbidden status flagged as Open (O8)	Sharpened
Global quotient $(SU(3) \times SU(2) \times U(1))/\Gamma$	Implicit; not explicitly raised	Explicitly flagged as Open (O12): local gauge structure does not determine the global quotient	Reframed
Yang–Mills existence and mass gap (Clay sense)	Not addressed	Explicitly identified as structurally a different problem (pure YM on $\mathbb{R}^4$ with fundamental Poincaré invariance); not addressed by Part IV	Reframed

### Coverage table.

**Pattern.** The table shows a consistent pattern. Items that were reverse-engineered consistency requirements (colour completion; admissible EFT class) are *closed structurally* at the level that reverse analysis can achieve. Items that already had a forward Level B/C route in Parts I–III (chirality, three generations, anomaly architecture, matter representations, hypercharges, proton stability, neutrino sector) are *sharpened*: their precise formulation gains explicit consistency constraints, but Part IV does not turn them into derivations. Items that were implicit or ill-posed within ECT are *reframed*: they are now explicitly on the ledger. Items with no structural content addressable by reverse analysis (strong-sector quantitative constants, confinement, glueball spectrum) remain inherited from standard QCD phenomenology rather than derived.

**Phenomenological interpretation of the admissible coupling window.** Beyond the qualitative status labels of the table, a phenomenological reading of the admissible coupling window follows from the minimal EFT of §41 and from known experimental bounds. The anisotropic channel  $\kappa_t = Y_0/Z_0$  is strongly constrained and is expected to be negligible in the infrared, consistent with the structural argument relating  $Y(\phi)$  to the gravity-sector anisotropy coefficient  $\alpha_{\text{ECT}}$ . Large constant-background departures of  $Z_0$  from unity are physically non-informative because they are absorbed into matching-convention redefinitions at the background level. The topological background  $|\Theta(\phi_0)|$  is constrained by the neutron-electric-dipole bound to  $\lesssim 10^{-10}$ ; this is the sole precise phenomenological number that enters the admissible window, and it drives the strong-CP discussion of §45. For the matching scale  $M_*$ , structurally natural candidates within ECT are the electroweak scale  $v_2$ , the primary condensate scale  $\phi_0 \sim M_{\text{Pl}}$ , or the condensate excitation scale; no ECT-specific identification is established (O1 in §46). The combined picture is that, at constant-background level, the admissible window is compatible with standard QCD phenomenology but offers no independent predictive leverage. Predictive content requires dynamical  $\phi$ -dependence of the coupling functions or an ECT-specific derivation of the matching data, neither of which is supplied in the present minimal completion.

**Bridging statement relative to existing open-status entries.** Part IV does not convert the existing open-status entries—such as  $N_{\text{gen}} = 3$ ,  $\theta_{\text{QCD}}$ , flavour closure, and the minimal-closure-hypothesis status of  $N_{\text{colour}} = 3$ —into derived results. What it does is sharpen the exact-colour completion layer on which those entries depend, and separate what is now structurally closed (the completion-layer existence, the admissible operator class, the anomaly-consistency layer) from what remains genuinely unresolved (the quantitative strong-sector constants, confinement, the glueball spectrum, the strong-CP angle, and the full matter completion). The open-status entries retained in the status maps of the earlier parts and in the quantitative-unification table (118) are therefore not closed by Part IV; they are reclassified within a clearer architectural hierarchy.

**What the table is not.** The table is a bookkeeping device, not a results table. No row represents a new Level A derivation. Rows labelled “Closed structurally” record only that the *structural* consistency question has been resolved at the reverse-analysis level; the corresponding *dynamical* questions (confinement,  $\Lambda_{\text{QCD}}$ , bound-state spectrum) remain on the Open list of §46.

## 44 Proton stability and baryon number as a UV discriminant

*Status: Level C. This subsection is conditional on the unresolved gauge/flavour completion.*

Proton stability is not part of the already established strict core of ECT; it is a discriminant of how the presently open gauge/flavour completion closes. The proton lifetime answers a structural question: what low-energy baryon-number selection rules are realised in the completed theory. The detailed selection rules depend on the completed gauge/flavour structure, an essential unresolved part of which is the colour sector (§40). Proton stability is therefore a conditional discussion-level result.

### Three selection-rule patterns

The completed theory may realise several distinct baryon-number selection-rule patterns.

**Pattern I: full low-energy protection.** The completed gauge/flavour sector enforces a selection rule forbidding low-energy baryon-violating operators relevant for proton decay and for the leading  $\Delta B = 2$  processes. In this case no low-energy proton-decay channel is generated within the completed effective theory. In a gravitationally complete setting such protection is more naturally realised through a gauged or discrete remnant than through an exact continuous global  $U(1)_B$ , in line with general quantum-gravity arguments suggesting the absence of exact continuous global symmetries [243, 244].

**Pattern II: partial protection.**  $\Delta B = 1$  operators are forbidden, but  $\Delta B = 2$  transitions remain allowed. Proton decay is absent—not because baryon number is exactly conserved, but because the completed low-energy selection rules forbid precisely the  $\Delta B = 1$  channel. More generally, the completed theory may preserve or violate different combinations such as  $B$ ,  $L$ , and  $B - L$ , which determine the allowed operator classes. In this pattern the relevant observational tests are  $n - \bar{n}$  oscillations and dinucleon decay rather than proton decay.

**Pattern III: generic violation.** If the completed field content below  $\Lambda_B$  is Standard-Model-like, no lighter baryon-violating mediators are present, and the leading local  $\Delta B = 1$  operators are the usual gauge-invariant dimension-six operators built from SM fields, then

$$\mathcal{O}_B \sim \frac{C_B}{\Lambda_B^2} qqql. \quad (44.1)$$

This is the natural leading EFT benchmark only under the specific hypothesis that the spectrum below  $\Lambda_B$  is Standard-Model-like and that no lighter baryon-violating states alter the operator hierarchy. For the



natural ECT ultraviolet scale  $\Lambda_B \sim \phi_0 \sim \tilde{M}_{\text{Pl}}$  (in the present benchmark coinciding in order of magnitude with the UV threshold of the ordered branch) the proton lifetime is

$$\tau_p \sim \frac{\Lambda_B^4}{|C_B|^2 m_p^5} \sim 10^{41} - 10^{42} \text{ yr} \quad (C_B = \mathcal{O}(1)). \quad (44.2)$$

The structural ECT result is the three-pattern classification above. The numerical lifetime  $10^{41} - 10^{42}$  yr is the generic EFT benchmark of Pattern III, not an ECT-native derived decay amplitude.

### Connection to baryogenesis

ECT already contains structural routes by which baryon number need not be exact: topological baryogenesis bias (§16.3), and electroweak sphaleron-like high-temperature  $\Delta(B+L)$  violation in the emergent  $SU(2)$  sector—although the latter does not by itself generate observable  $\Delta B = 1$  nucleon decay at  $T = 0$ . These routes eliminate the automatic guarantee of proton stability but do not by themselves determine the completed low-energy baryon-number selection rules relevant for proton decay.

Whether the same topological or sphaleron sector induces a local  $\Delta B = 1$  nucleon-decay operator at zero temperature remains open. If it does, the present-day decay rate is controlled by a zero-temperature Euclidean action (instanton/bounce-type suppression) or by the induced effective operator, *not* by thermal Boltzmann suppression.

### Experimental context and comparison

The current Super-Kamiokande limit is  $\tau_p(p \rightarrow e^+ \pi^0) > 2.4 \times 10^{34} \text{ yr}$  [245]; the expected sensitivity of Hyper-Kamiokande [246] is of order  $10^{35} \text{ yr}$ .

Unlike conventional GUT models, ECT does not contain an intermediate unification scale  $\Lambda_{\text{GUT}} \sim 10^{16} \text{ GeV}$ . In Pattern III this pushes proton decay far beyond current and foreseeable sensitivity. In Patterns I and II the proton is stable.

Observation of  $\Delta B = 1$  proton decay in the  $10^{34} - 10^{36} \text{ yr}$  window would exclude the proton-stable branches (Patterns I and II) and strongly disfavour Pattern III with generic  $C_B = \mathcal{O}(1)$ . Nucleon-decay searches thereby directly probe the ultraviolet status of baryon number in ECT.

The specific branching pattern ( $p \rightarrow e^+ \pi^0$ ,  $p \rightarrow \bar{\nu} K^+$ , etc.) is not fixed at the present stage, because it depends on the detailed UV realisation of the gauge/flavour sectors.

**Status summary.** This entire subsection is Level C in the sense of Table 73: it depends on the unresolved gauge/flavour completion—especially the colour realisation—and on baryon-number selection rules not yet derived from first principles.

**Open problem (OP-proton).** Derivation of baryon-number selection rules from the completed gauge/flavour sector; identification of which pattern (I/II/III) is realised; if Pattern III, identification of decay channels and coefficient structure.

## 45 Topological sector and strong CP

*Status: Level C, Open. Part IV sharpens the strong CP problem within ECT rather than solves it.*

**The topological coupling is unavoidable.** The operator  $\Theta(\phi) F_{\mu\nu}^a \tilde{F}^{a\mu\nu} / (32\pi^2)$  in the minimal EFT (eq. 41.1) is gauge-invariant and compatible with all ECT symmetries. No ECT postulate forbids it at the Lagrangian level.

**Reopening of strong CP.** At background  $\phi = \phi_0$ , the effective theta parameter is  $\theta_{\text{eff}} \equiv \Theta(\phi_0)$ . The experimental bound from the neutron electric dipole moment is  $|\theta_{\text{eff}}| \lesssim 10^{-10}$ . Without a mechanism, the natural expectation is  $\theta_{\text{eff}} = \mathcal{O}(1)$ . ECT with P7 and the minimal EFT therefore reproduces the strong CP problem rather than solving it.

**Possible resolution routes, all currently Open.** *R1 — CP-symmetric ordered branch.* Postulate that the ordered condensate background respects CP as a residual symmetry, forcing  $\Theta(\phi_0) \in \{0, \pi\}$ . This would require additional structural input on the CP properties of the medium, which has not been derived from the postulates P1–P7.

*R2 — axion-like relaxation.* Dynamical relaxation of  $\Theta(\phi)$  via a pseudoscalar mode with the required anomaly coupling to  $F\tilde{F}$ . The existing ordered-branch soft modes do not presently supply a demonstrated axion-like degree of freedom: the  $O(4) \rightarrow O(3)$  Goldstones are scalars, not pseudoscalars, and do not possess the required anomaly coupling. Any axion-type resolution would require additional pseudoscalar structure and an explicit anomaly coupling, neither of which is available in the minimal P7 completion.

*R3 — geometric obstruction from  $\Omega$ .* The fixed complex volume form in P7, together with appropriate CP-transformation properties of  $\mathcal{C}$ , could in principle structurally force  $\Theta \equiv 0$ . R3 is conceptually attractive because it would solve the problem without introducing a new low-energy field, but at present no geometric derivation enforcing  $\Theta \equiv 0$  is available.

**Witten–Veneziano consistency target.** The  $\eta'$  mass in QCD is related to the topological susceptibility of the pure-gauge vacuum through the Witten–Veneziano relation (Witten 1979; Veneziano 1979), schematically

$$m_{\eta'}^2 \approx \frac{4N_f}{f_\pi^2} \chi_{\text{top}}^{\text{pure}}, \quad (45.1)$$

where  $\chi_{\text{top}}^{\text{pure}}$  is measured on the lattice for pure  $SU(3)$  at  $\chi_{\text{top}}^{1/4} \approx 198$  MeV. Any ECT-specific contribution through  $\Theta(\phi)$  must preserve this infrared relation, which provides a nontrivial consistency target: the product of any ECT-induced topological coupling and the standard-QCD dynamical content cannot shift the  $\eta'$  mass outside its observed value. This is the cleanest standard-QCD channel through which the topological sector of the minimal P7 EFT can be matched to a measured hadronic observable, and it reinforces that any  $\Theta$ -related physics in ECT must be compatible with, rather than replace, the standard Yang–Mills topological vacuum structure.

**Final status.** ECT with P7 and the minimal EFT does not solve the strong CP problem. Accordingly, Part IV sharpens the strong CP problem within ECT rather than solving it. Resolution is flagged for future work, with the three routes above representing the currently identified lines of attack.

## 46 What Part IV closes and what remains open

*Status: Summary of Part IV. All claims in Part IV are Level B or Level C. Part IV does not add Level A derivations of strong-sector physics.*

**Closures of Part IV.** The structural closures delivered by Part IV are summarised in Table 108. All claims are Level B within reverse analysis except for two algebraic/obstruction statements that are Level A within ECT as indicated. Every row is honestly either a derived theorem, an explicit obstruction, a consistency statement with a pre-existing forward result, or a clearly labelled non-derivation (“inherited” or “placed in correct layer”).

**Table 108:** Structural closures of Part IV.

Closure	Nature of the closure (what is actually demonstrated)	Level / locus
Exact colour completion as a closure <i>requirement</i>	Reverse-engineered from the partial success of the forward programme: without an exact colour sector, multiple items in Parts I–III cannot be closed	Reverse-engineered; §40
Colour cannot reside in the ordered condensate	Obstruction theorem: nonzero condensate in any colour-charged representation breaks $SU(3)$ to a proper subgroup	Level A; §40
$\mathfrak{su}(3) \not\subset \mathfrak{so}(4)$	Algebraic obstruction: $\dim \mathfrak{su}(3) = 8 > 6 = \dim \mathfrak{so}(4)$ , so no subalgebra embedding is possible	Level A; §40
Primary completion pattern	Postulate P7 formalised: rank-3 complex internal module with Hermitian form and fixed complex volume form, reducing the $U(3)$ frame-redundancy to $SU(3)$	Reverse-engineered postulate; §40
Alternative deeper candidate ( $G_2$ )	Explicit octonionic route preserved in the text; not adopted as primary	Alternative; §40
Minimal admissible colour EFT	Derived operator class $Z(\phi)F^2 + Y(\phi)(n \cdot F)^2 + \Theta(\phi)F\tilde{F}$ with positivity conditions	Level B; §41
No tree-level gluon mass; no Higgs-colour route	Obstruction theorems derived from exact unbroken $SU(3)$ and the singlet character of the condensate	Level B; §41
Oscillator tower is not the physical colour spectrum	Obstruction theorem: a linearly spaced oscillator tower is incompatible with gauge-invariant physical spectra of an exact colour sector	Level B; §41
Structural bound on anisotropic colour channel	Derived from shared $n_\mu n_\nu$ structure with the gravity-sector anisotropy $\alpha_{\text{ECT}}$ of Part II	Level B; §41
Dimensional-transmutation form of $\Lambda_{\text{col}}^{\text{ECT}}$	Classificatory form derived (eq. 41.3); recovers standard QCD transmutation at $Z_0 \rightarrow 1$	Level C, classificatory; §41
Background-level triviality (central result)	Derived: at constant $Z_0, Y_0, \Theta_0$ the minimal EFT reduces to standard pure YM with a matching-convention redefinition	Level B; §41
Anomaly-consistency layer under P7	$SU(3)^3$ , mixed $SU(3)^2 \cdot U(1)$ , $SU(2)^2 \cdot U(1)$ , $U(1)^3$ , $U(1) \cdot \text{grav}^2$ constraints restated P7-compatibly; Witten $\mathbb{Z}_2$ respected	Level B, restatement; §42
Hypercharge determination (SM one-generation content)	Hypercharges fixed by anomaly cancellation up to normalisation <i>once</i> the standard matter content is assumed; not derived from ECT primary postulates	Level B, conditional; §42
Baryon number as a selection rule	Emergent selection rule rather than exact global symmetry; compatible with Harlow–Ooguri no-global-symmetry argument	Level B; §42, §44

Closure	Nature of the closure (what is actually demonstrated)	Level / locus
Proton-stability framework placed in the correct layer	Selection-rule patterns I/II/III now live in the gauge-completion layer where they belong	Architectural; §44
Structural reopening of strong CP under P7	$\Theta(\phi_0)F\tilde{F}$ is not forbidden by P7, so the minimal completion reopens (does not solve) strong CP	Level C, reopening; §45
Coverage reclassification of SU(3)-dependent issues	Thirteen earlier SU(3)-dependent items explicitly reclassified (Table 107)	Level B, bookkeeping; §43

**Non-replacement statement.** Part IV does not replace the existing structural routes to chirality and three generations developed in §9.3 and Appendix Z. Its role is to clarify which exact-colour completions are compatible with those routes and which unresolved questions remain blocked even after P7.

**Remains Open.** The items explicitly not closed by Part IV are collected in Table 109. For each we record the nature of the residual obstruction and the section that discusses it.

**Table 109:** Problems remaining open after Part IV.

ID	Item	Why still open	Locus
O1	Identification of the matching scale $M_*$	Multiple structurally natural candidates; no ECT-specific selector established	§41
O2	Derivation of $g_s(M_*)$	Colour coupling is matching data; microphysical origin not supplied by P7	§41
O3	Confinement (Wilson-loop area law)	Nonperturbative dynamics inaccessible from reverse analysis; inherited from standard YM	§41
O4	Full glueball spectrum	Bound-state dynamics; requires non-perturbative strong-sector computation not supplied by the admissible EFT class	§41
O5	Numerical value of $\Lambda_{\text{col}}$	Matching data; any ECT-specific shift requires $\phi$ -dependent couplings beyond constant background	§41
O6	Strong CP resolution (R1/R2/R3)	None of the three identified routes currently derives $\Theta(\phi_0) = 0$ from ECT postulates	§45
O7	Complete matter-content derivation	Anomaly cancellation narrows but does not uniquely fix the matter representations	§42
O8	Sterile-neutrino status in ECT	A singlet is admissible without disturbing anomaly balance, but no ECT postulate selects required/forbidden/permitted	§42
O9	Yukawa hierarchy as derivation	Structural routes in Part I remain Level B/C; not addressed by the completion layer	§9.6

ID	Item	Why still open	Locus
O10	Three generations as a theorem	Spectral route of §9.6 remains the forward proposal; P7 does not convert it into a theorem	§9.7; App. Z
O11	CKM/PMNS mixing matrices	Flavour-closure problem; not addressed by the completion layer	§9.7
O12	Global quotient $(SU(3) \times SU(2) \times U(1))/\Gamma$	Local gauge structure does not determine the global quotient; identification of $\Gamma$ requires bundle-level structure	§42
O13	Stiefel–Whitney and related topological obstructions on the colour bundle	Requires bundle-level topological analysis not performed here	§42
O14	't Hooft anomaly matching $UV \leftrightarrow IR$	UV medium microphysics not supplied; matching cannot be verified	§42
O15	Status of the global $U(1)$ carried by $\Omega$	Whether gauged, broken, or quantum-mechanically protected is not fixed by P7	§42
O16	Yang–Mills existence and mass gap (Clay sense)	Structurally a different question: pure YM on $\mathbb{R}^4$ with fundamental Poincaré invariance and Wightman/OS axioms; not in the setting of ECT+P7	§45; §46
O17	Deeper relation between P7 and the chirality/flavour programme	Whether exact-colour layer merely co-exists with or sharpens the matter-sector routes of §9.3–§9.7	§9.3–§9.7

**Directional remarks (future work; not claimed here).** The following remarks are conjectural pointers, collected in Table 110. None is a theorem; none is pursued quantitatively in this preprint.

**Table 110:** Directional remarks from Part IV.

ID	Direction	Content and status
D1	Chirality deepening via P7 and $n^\mu$	The orientation data carried by the Lorentzian director $n^\mu$ and the complex volume form $\Omega$ may provide a structural link to the V–A chirality of Standard-Model fermions. Conjectural pointer; not pursued here.
D2	Three-generation deepening via rank-3 structure	The internal module has rank 3 and the observed fermion generation count is 3. Intriguing structural coincidence; presently non-theorem-level.
D3	SM as a natural IR-compatible configuration	Given §41–§42, the SM gauge structure may emerge as a natural IR-compatible configuration among P7-admissible completions; no dynamical selection mechanism is established.
D4	Swampland compatibility	No-Global-Symmetries, Weak-Gravity, and Completeness conjectures appear naturally realised in ECT+P7; systematic analysis is future work.

**Three distinct questions in the strong sector.** It is useful to keep three structurally different questions apart, because ECT with P7 has different status with respect to each. (i) *Existence of a colour infrared scale.* The admissible EFT of §41 is consistent with a nonzero infrared scale  $\Lambda_{\text{col}}$ , inherited from standard QCD phenomenology; ECT does not derive its value but constrains how medium couplings may affect it. (ii) *Existence of a gauge-invariant mass gap in the exact colour sector.* This is a physically sharper statement than (i): no gauge-invariant physical state below a finite threshold. ECT with P7 does not obstruct such a gap at the structural level but does not prove its existence; any proof must proceed nonperturbatively. (iii) *Full derivation of the glueball spectrum.* This is a quantitative dynamical question inaccessible from structural reverse analysis. The Clay Millennium formulation of the Yang–Mills existence-and-mass-gap problem (Jaffe and Witten 2000) is distinct again: it requires constructive quantum field theory on  $\mathbb{R}^4$  with fundamental Poincaré invariance and Wightman or Osterwalder–Schrader axioms. ECT with P7 proceeds in a different setting—a colour sector coupled to an ordered condensate medium, with Lorentz invariance emergent rather than fundamental—and therefore cannot address the Clay problem in its stated form. Part IV does not claim contact with it at any level.

**Final note on claims level.** All of Part IV is Level B or C. Quantitative strong-sector observables ( $\Lambda_{\text{QCD}}$ , confinement, glueball masses) remain inherited from standard Yang–Mills and QCD phenomenology, constrained by the admissible EFT structure of §41 but not independently derived.

## 47 Synthesis of Part IV

*Status: Overview. No new claims are made in this section; it collects and depicts the structure of Part IV schematically.*

**Overall picture.** Part IV operates as a closure/consistency layer above the forward programme of Parts I–III (§39). Starting from the obstruction theorems already present in the colour consistency analysis (§40), it formalises the minimal reverse-engineered postulate P7 (rank-3 complex internal module with Hermitian form and fixed complex volume form), derives the minimal admissible colour EFT under P7 (§41), and restates the anomaly-cancellation layer in the presence of the completion (§42). The coverage table (§43) reclassifies the SU(3)-dependent questions of Parts I–III against the four status labels *Closed structurally*, *Sharpened*, *Reframed*, *Still open*. Proton stability (§44) then lives in its proper architectural layer, and the topological sector (§45) is honestly recorded as *sharpening rather than solving* the strong CP problem. Section 46 collects closures, open items, and directional remarks in tabular form (Tables 108, 109, 110).

**Derivation logic of Part IV.** The logical structure of Part IV is shown in Figure 44.

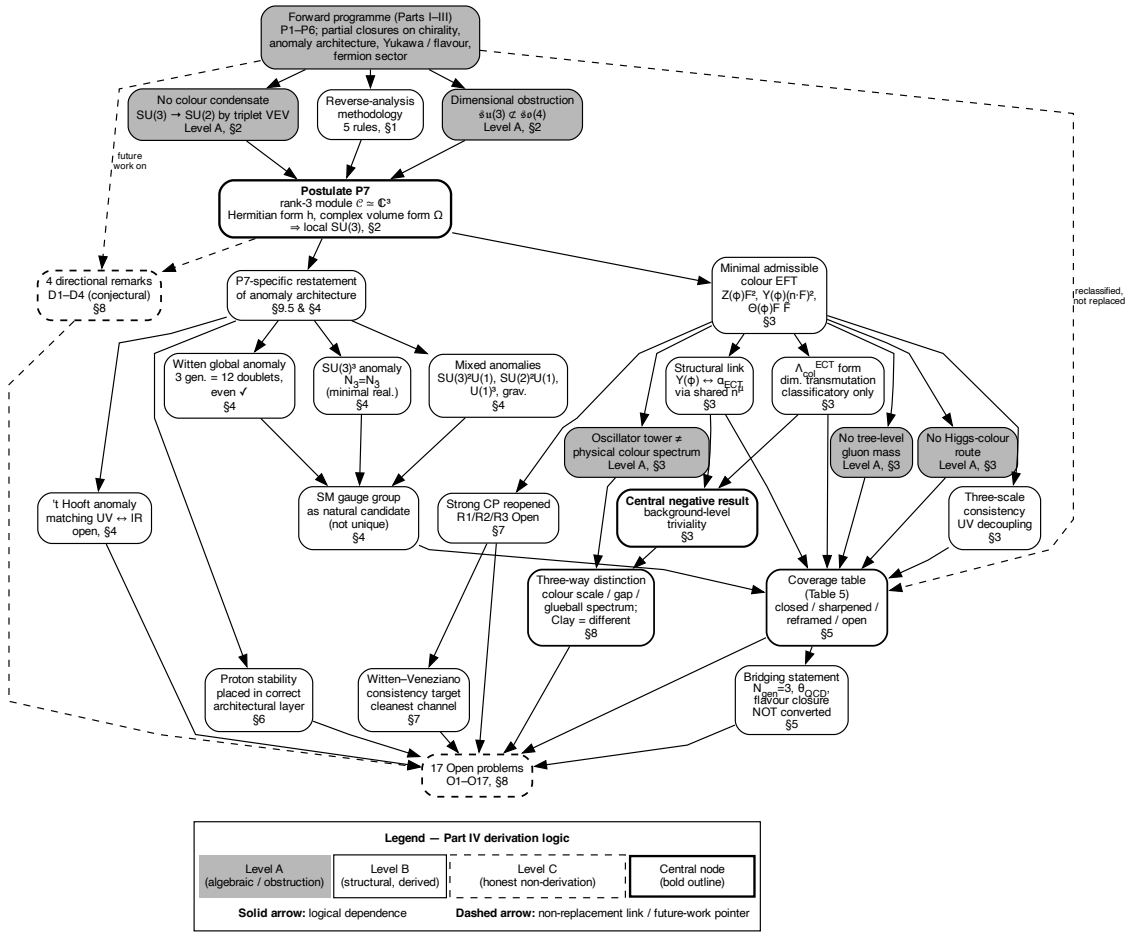


**Figure 44:** Derivation logic of Part IV (Reverse Analysis,  $SU(3)$  Completion, and Structural Constraints). The diagram is organised into four layers: (i) the forward inputs from Parts I–III (the postulates P1–P6 and the partial closures they support); (ii) the reverse-analysis layer (the obstruction theorems forcing externalisation of colour, and the formalisation of P7); (iii) the structural-consequences layer (the minimal admissible colour EFT, its obstruction theorems, the dimensional-transmutation form of  $\Lambda_{\text{col}}^{\text{ECT}}$ , the central background-level triviality result, and the anomaly-consistency layer); and (iv) the status layer (coverage reclassification, proton stability placed in the correct layer, strong CP reopened, and the tabular closures/open/directional ledgers). Node shading: dark = Level A (algebraic or obstruction), light = Level B (structural/derived within reverse analysis), dashed outline = Level C or honest non-derivation. Solid arrows denote logical dependence; dashed arrows denote the non-replacement connection to the forward programme of Parts I–III.

**Final statement for Part IV.** Part IV converts a pre-existing colour-completion consistency block and a pre-existing proton-stability discussion into a coherent reverse-analysis chapter with a formalised postulate P7, a derived admissible EFT class, an anomaly-consistency layer, a coverage bookkeeping of  $SU(3)$ -dependent questions, a tabular ledger of closures, open items, and directional remarks, and a synthesis figure. Its results are Level B within reverse analysis, with two Level A obstruction statements internal to ECT, and one Level C classificatory formula. The strong-sector quantitative observables remain inherited from standard Yang–Mills and QCD phenomenology, constrained by P7 but not independently derived. Part IV neither derives nor closes the remaining strong-sector open problems; it sharpens what they are and reclassifies what changes under the exact-colour completion layer.

## Part V

# Summary, Comparisons, and Outlook

## 48 Discussion

This section provides a consolidated discussion of the ECT framework: its conceptual logic, derivational architecture, current achievements, comparison with neighbouring programmes, observational reach, limitations, and future directions.

### 48.1 Conceptual interpretation and scope of the framework

ECT proposes that Lorentzian spacetime, quantum dynamics, and gravitational interactions can all be obtained from a single underlying structure: a scalar condensate in four-dimensional Euclidean space with spontaneously broken  $O(4)$  symmetry. This is a working hypothesis supported by the results presented here at varying levels of rigour, as classified in Table 73.

This perspective inverts the conventional logic of quantum gravity. Rather than attempting to quantise an existing spacetime geometry, ECT starts from a fundamentally Euclidean arena where no distinction between space and time exists, and recovers the Lorentzian structure as an effective property of the symmetry-broken vacuum. The Lorentzian metric and the causal cone arise directly from the ordered condensate background. The thermodynamic arrow of time is addressed at the level of the ordered-branch open-system description with clearly stated closure assumptions (Section 3.9). The same condensate background provides a common structural framework within which  $G_N$ , the EFT action scale later matched to  $\hbar$ , and  $c_*$  are all related to the ordered medium, although their full microscopic unification is not yet closed (internal consistency relations; non-circular derivation open).

This framework should not be interpreted as claiming that time is “unreal”. Rather, it suggests that the distinction between temporal and spatial coordinates—encoded in the metric signature—is a collective, emergent property of the vacuum state, much as superfluidity is a collective property of helium-4 below the  $\lambda$ -point.

The comparison with closely related Euclidean-to-Lorentzian constructions [1, 2] is useful in a second respect as well. It shows that the basic idea of emergent Lorentzian structure from Euclidean field theory is not unique to ECT, but it also makes clearer which parts of ECT remain distinctive claims rather than generic consequences of that shared idea: the spontaneous-symmetry-breaking origin of the preferred direction, the proposed gravitational completion, and the extension to quantum and phenomenological sectors.

### 48.2 Derivational architecture: from the $\Phi$ -medium to observable physics

The derivational logic of ECT can be summarised as a directed graph running from the foundational  $\Phi$ -medium to observable physics (Figure 45). The purpose of this subsection is to trace this chain explicitly, providing a concise map of how each major physical sector emerges.

**Step 1: the  $\Phi$ -medium and the foundational postulates.** The starting point is a scalar condensate field  $\Phi$  living on a four-dimensional Euclidean manifold  $(M^4, \delta_{AB})$  with an  $O(4)$ -invariant action  $S_E[\Phi]$ . No external time coordinate is postulated; the theory is fully relational (P1–P6).

**Step 2: spontaneous symmetry breaking.** The gradient condensate  $\langle \partial_A \Phi \rangle \neq 0$  selects a preferred direction  $n_A = \delta_{Aw}$ , breaking  $O(4) \rightarrow O(3)$ . This is the single generative event from which both macroscopic and quantum sectors descend.



**Step 3: emergent Lorentzian structure.** Perturbations around the ordered background experience the effective ordered-branch kinetic tensor  $K^{AB} = \beta \delta^{AB} - \alpha n^A n^B$ . For a homogeneous ordered background  $n^A = \delta_w^A$ , the ordered branch is Lorentzian when  $\alpha > \beta$ , with  $K^{AB} = \text{diag}(\beta, \beta, \beta, \beta - \alpha)$  and  $c_*^2 = \beta/(\alpha - \beta)$ . This yields an effective metric  $\text{diag}(-1, 1, 1, 1)$  and a causal light-cone structure.

**Step 4: macroscopic tensor branch (Part II).** The macroscopic sector develops as follows:

- *General relativity.* The unique rank-2 symmetric tensor compatible with the broken-phase residual symmetry is Fierz–Pauli-like at linear level; in the frozen-order pure-metric limit the Einstein–Hilbert form is the unique two-derivative closure (Level A for uniqueness; Level B for the macroscopic closure). The full macroscopic closure yields generalised Einstein equations containing a derived preferred-direction / orientation-stress correction built from the ordered vector  $n_\mu$  and the nonlinear closure tensor  $\Theta_{\mu\nu}[n, \phi]$ , structurally similar in spirit to Einstein–aether-type modifications [24] but derived here from the ordered condensate rather than postulated independently.
- *Fundamental constants.*  $G_N = c_*^4/(8\pi M_G^2)$  and  $c_*$  are determined by the condensate amplitude and kinetic tensor, with the phenomenological match  $\phi_0 \approx \bar{M}_{\text{Pl}}$  (Ph1, Ph2).
- *Three condensate scales.* The theory contains three characteristic scales of one field:  $\phi_0 \sim \bar{M}_{\text{Pl}} \approx 2.435 \times 10^{18}$  GeV (governing  $G_N, \hbar, c_*$ ),  $v_2 \approx 246$  GeV (electroweak Higgs sector), and  $v_{\text{gal}} \sim \text{kpc}$  (galactic  $\phi$ -branch) (Section 5.1).
- *Cosmology.* The ordered-branch amplitude governs structural resolution of the horizon, flatness, and monopole problems without requiring a separate inflationary mechanism (Section 14.3), late-time dark energy via  $\Lambda_{\text{eff}}$  from residual condensate vacuum structure, and a route to the Hubble tension through  $G_{\text{eff}}(z)$  (Level B). The primordial perturbation spectrum  $(n_s, A_s, r)$  remains an open target.
- *Galactic dynamics.* The nonlinear response of the ordered-branch amplitude variable  $\phi$  yields a critical  $\phi$ -branch closure capturing the BTFR (slope 4, algebraic), the RAR, and flat rotation curves with  $g_\dagger \sim cH_0/(2\pi)$  (Level B).
- *Strong-field sector.* The critical-shell ansatz produces a near-horizon scale  $\rho_c = \ell_{\text{Pl}}/\sqrt{3\pi}$ , an information-reading programme in which fundamental information destruction is excluded at Level A, and a route to black-hole thermodynamics (Level B/Open).
- *5th force.* The preferred-direction coupling  $\beta_5 \sim m_f/\phi_0$  predicts spin precession  $\omega_5 \sim 10^{-10}$  rad/s, Eötvös parameter  $\eta \sim 10^{-15}$ .

**Step 5: quantum coherent branch (Part III).** In parallel, the coherent sector develops:

- *Action scale  $S_0$ .* The compact phase of the ordered field supports winding sectors and a structural minimal-action cycle (Level A).
- *Schrödinger equation.* Canonical phase dynamics on the coherent branch yield the uncertainty principle and a Schrödinger-type reduction (Level A/B).
- *Vacuum response.* The Euclidean two-point function  $G_E = (4\pi^2|X - X'|^2)^{-1}$  organises the Casimir effect (3/2 ratio for Goldstone-sector boundaries), the Unruh temperature, and cosmological particle production (Level A/B).
- *Decoherence and arrow of time.* The influence-functional architecture unifies environmental and gravitational decoherence (Diósi–Penrose as a limit), produces entropy growth and a Crooks-type fluctuation relation within the Gaussian–Markov closure (Level A/B).
- *Born rule.* The quadratic structure of Born weights is traced to the RP-defined inner product of the Euclidean condensate measure; conditional uniqueness via Gleason’s theorem once assumptions C1–C3 are admitted (Level B; full interacting RP closure open).
- *Exchange topology and spinors.* The  $\pi_1(\mathcal{M}_2) = \mathbb{Z}_2$  result from  $d_{\text{spatial}} = 3$  provides a structural route to fermionic statistics and Dirac structure (Level A).
- *Entanglement.* Non-factorisable correlations are structurally available in the ordered medium (Level A).
- *Area-law entropy scaling.* A general boundary-layer area bound is established as a structural property of the local condensate medium with physical UV threshold; holographic-style entropy

scaling is derived without postulating holography (Theorem 36.1; Level A for scaling, Level B for coefficient).

- *Charge quantisation.* Abelian charge quantisation  $q \in \mathbb{Z} \cdot e_0$  is derived as a structural consequence of the compact-phase condensate gauge origin (Theorem 23.1; Level A); the full observed Standard-Model charge spectrum remains open.
- *Post-transition cosmological branch classification.* ECT does not yet derive the full nonequilibrium transition or the selection of the expanding branch from first principles, but it already classifies the admissible ordered-branch cosmologies strongly enough to identify an expanding, early-decelerating, late-accelerating history as a structurally natural observationally relevant class, while making thermal completion and CMB-without-particle-CDM explicit open problems (§14.2).
- *PES and operational closures.* The Principle of Euclidean Stationarity (PES) provides a unifying selection criterion for persistent configurations (extremal  $\cap$  decoherence-resistant  $\cap$  phase-compact), together with closure-level operational results including visibility-based  $\Gamma_{\text{loop}}$  anchors (Procopio, Jacques), the Bell/CHSH toy crossover threshold  $\Gamma_{\text{loop}} = \ln \sqrt{2}$ , the qubit information–decoherence bound for partial observation, and coarse-graining readings of Wigner’s-friend-type situations (Level B / Programme-level depending on the item).

**Step 6: gauge and matter sectors.** The compact phase symmetry of the coherent branch provides a structural route to  $U(1)$  (photon) and, via non-Abelian completion, to  $SU(2)$  ( $W^\pm, Z$ ), with the Higgs mechanism realised by the radial  $SU(2)$  mode at  $v_2 \approx 246$  GeV (Level A/B). The colour group  $SU(3)$  and the fermion-generation structure remain open. A minimal colour completion is proposed in §40, and the resulting baryon-number selection rules are analysed as a proton-stability discriminant in §44.

**Particle spectrum.** The condensate architecture organises the particle sector into different status layers. At the structural or partially established level this includes: the graviton (spin-2, massless) as the tensor perturbation  $\delta n_A$ ; the photon as the  $U(1)$  phase gauge boson;  $W^\pm, Z$  as  $SU(2)$  gauge bosons; the Higgs as the radial  $SU(2)$  mode; and fermions as  $O(3)$  spinor representations. At the exploratory benchmark level it also suggests three ultra-light Goldstone-sector modes ( $m \sim 10^{-33}$  eV in the illustrative large-scale benchmark), whose possible cosmological or dark-sector role remains open, together with an exploratory instanton-sector mass pattern ( $m_n = n \times 1.6$  GeV/ $c^2$  in the present benchmark treatment), whose dynamical status and observational interpretation remain open.

**Step 7: predictions and falsifiers.** The derivation chain terminates in a set of quantitative predictions ( $g_+$ , BTFR slope,  $n_s$ , Casimir ratio, LIV bound) and cross-sector architectural falsifiers (single  $c_*$ , a common candidate action scale  $S_0$ , a common benchmark UV scale  $m_\sigma$ , no requirement for standard particle dark matter in laboratory detection within the present macroscopic closure, environment-dependent transition morphology). These are summarised in Figure 45 and Tables 72 and 73.

### 48.3 What ECT already establishes: emergence chains and current status

A central claim of ECT is that several major physical frameworks can be recovered as limiting descriptions or organised sectors of one ordered condensate structure. In the present article this claim must be stated with explicit status discipline: some recoveries are structural, some are effective, and some remain incomplete.

**General relativity.** The ordered broken phase generates an effective Lorentzian propagation sector and a macroscopic tensor branch. At linear level the tensor sector admits a Fierz–Pauli-like structure; in the frozen-order pure-metric limit the Einstein–Hilbert form is the unique two-derivative closure in four dimensions. The full  $\phi$ -first nonlinear macroscopic closure remains effective. *Status: structural Level A for the ordered Lorentzian branch and for the pure-metric uniqueness statement; Level B for the completed macroscopic closure used observationally.*

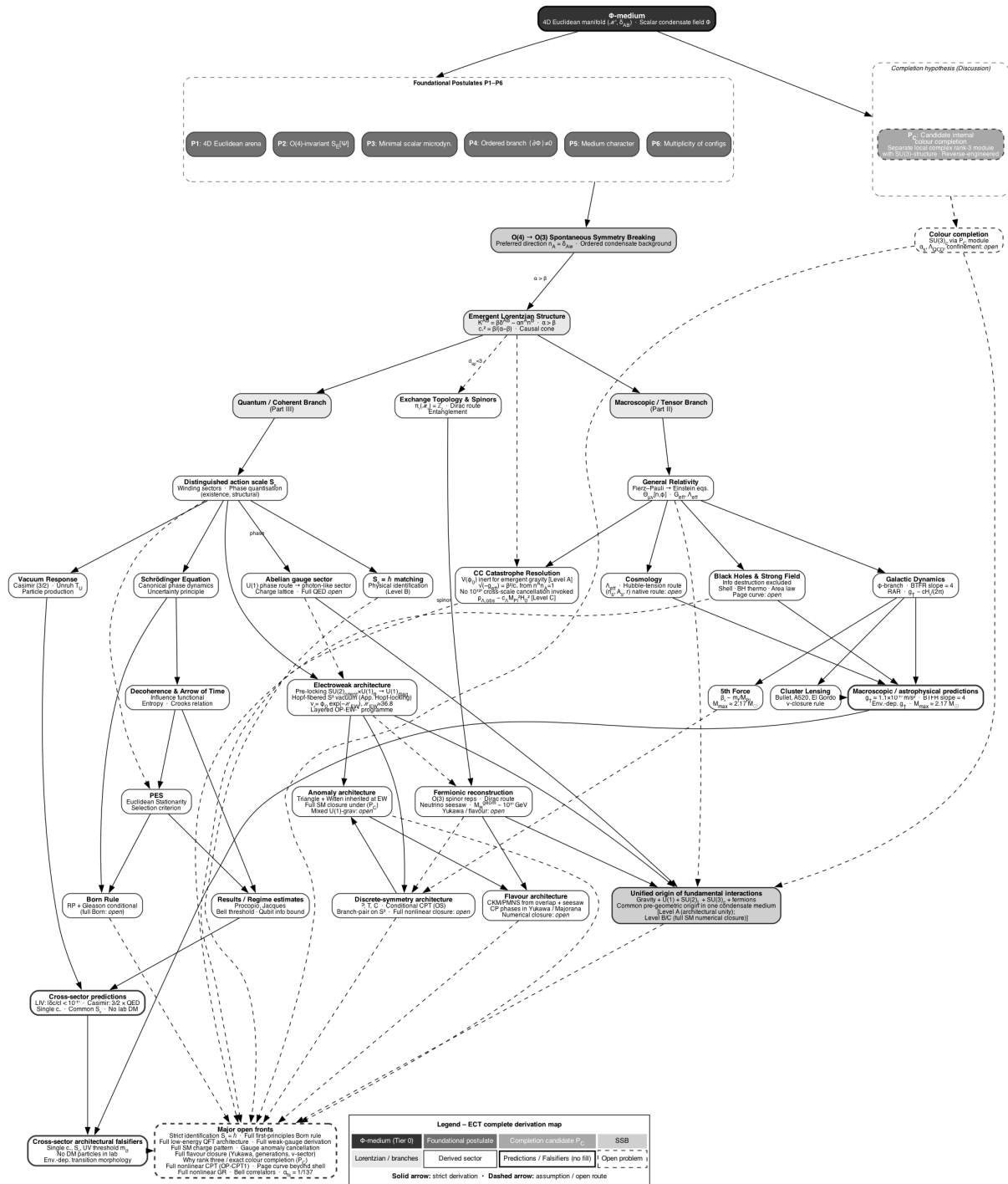


**Figure 45:** Derivation map of ECT. The directed graph traces the logical chain from the foundational  $\Phi$ -medium and postulates (P1–P6), through  $O(4) \rightarrow O(3)$  spontaneous symmetry breaking, to the macroscopic tensor branch (Part II) and the quantum coherent branch (Part III), and onward to gauge and matter sectors, quantitative predictions, cross-sector falsifiers, and open fronts. In the quantum sector, the map should also be read as including the Principle of Euclidean Stationarity (PES), the results/regime-estimate layer around  $\Gamma_{\text{loop}}$ , and the operational closures associated with visibility-based dephasing anchors, Bell/CHSH crossover proxies, and the quantum–classical boundary. Status labels indicate derivation level: [A] structural theorem, [A/B] structurally singled out, [B] closure-dependent, [Open] programme-level. Solid arrows denote strict derivational links; dashed arrows indicate incomplete or open routes.

**Quantum coherent dynamics.** The coherent branch supports a structural action scale  $S_0$ , winding sectors, canonical phase dynamics, a Schrödinger-type reduction, reflection positivity in Gaussian sub-sectors, a structural global/reduced unitarity distinction, exchange-sector topology from  $d_{\text{spatial}} = 3$ , a representation-theoretic route to Dirac structure, a unified vacuum-response programme (Casimir, Unruh, particle production, horizon thermality), an influence-functional decoherence architecture, a conditional Born-type probability route via Gleason’s theorem (once assumptions C1–C3 are admitted), the structural availability of non-factorisable correlations (entanglement), a wider defect/topological ontology connected to the dark sector, a black-hole programme in which fundamental information destruction is excluded at Level A within the global coherent framework (with the constructive shell closure at Level B), and an analogue-laboratory instantiability programme. The present Part III now also includes a closure-level PES-based selection layer, visibility-based operational  $\Gamma_{\text{loop}}$  anchors, a Bell/CHSH toy crossover threshold, coarse-graining readings of measurement-type situations such as Wigner’s friend, a reverse-coherence programme for partial Lorentzian-to-Euclidean reopening, and a structural entanglement–tunnelling bridge. These additions should be read at Level B or programme-level, not as unconditional Level A derivations. However, several closures remain below unconditional Level A: the physical identification  $S_0 = \hbar$ , the full interacting Hilbert-space closure, the completed Born rule as a first-principles theorem, and the nonperturbative strong-field evaporation problem. *Status: a substantial strict structural core, a structurally singled-out backbone, and a set of closure-level or open fronts, as summarised in Section 38.2.*

**Decoherence and the macroscopic arrow of time.** ECT provides a subsystem–environment logic in which reduced-state decoherence and effective entropy growth arise naturally once many bath modes are traced out. This supports a macroscopic arrow of time without postulating a fundamental microscopic irreversibility. Concrete consistency anchors include order-of-magnitude agreement with  $C_{60}$  decoherence timescales and the recovery of the Diósi–Penrose gravitational decoherence as a condensate-bath limit, with both environmental and gravitational decoherence unified as specialisations of the same influence-functional framework. A Crooks-type fluctuation relation is established within the Gaussian–Markov closure. The fully quantitative non-Markovian extension remains open (OP-Q17). *Status: Level A for the structural reduced-state logic and retarded-kernel positivity; Level B for explicit entropy growth, Crooks relation, and decoherence timescales under effective bath assumptions.*

**The Principle of Euclidean Stationarity and the reconstruction of quantum mechanics.** A central conceptual advance of Part III is the Principle of Euclidean Stationarity (§29), which organises the quantum programme around a single selection mechanism: physically persistent configurations are those that simultaneously satisfy phase compactness, Euclidean stationarity, and minimal environmental coupling. PES addresses the question *why* the quantum rules take the form they do, not merely *how* they are formalised: discrete spectra admit a unified physical reading because only a discrete set of phase-compatible stationary configurations remains in the persistent observable sector; PES provides a physical underpinning of the extremal-action principle, a coherent Euclidean-to-Lorentzian reading of measurement, and a structurally unified route by which the gravitational sector is treated as another condensate-excitation sector rather than as an externally quantised geometry. Standard quantum mechanics postulates the Hilbert-space framework, the Born rule, and the measurement axiom as primitive inputs. ECT provides a deterministic Euclidean substrate from which parts of this structure are reconstructed and the remaining parts are structurally motivated, with probabilities arising at the reduced-description level when macroscopic environmental degrees of freedom are traced out. This reading does not discard quantum mechanics; rather, it provides an underlying physical architecture for its formal rules. *Status: Level B for the core PES selection logic; programme-level for the universal scope of the principle (§29.11).*

**Galactic weak-field phenomenology.** The present critical  $\phi$ -branch closure captures BTFR/RAR-type behaviour, environmentally sensitive acceleration scales, and flat rotation-curve phenomenology without introducing a standard particle-dark-matter halo at the level of the current closure. *Status: Level B effective macroscopic closure.*

**Gauge and matter sectors.** ECT provides a condensate framework in which gauge and matter sectors can be embedded consistently, but the exact Standard Model gauge group, fermion-generation structure, and full coupling hierarchy are not yet derived uniquely from the bare postulates. *Status: partial structural embedding with major open problems.*

**Interpretive conclusion.** The correct claim is therefore not that every established theory has already been rederived as a completed Level A theorem. Rather, ECT organises general relativity, coherent quantum dynamics, the Hilbert-space bridge, decoherence, vacuum-response effects, entanglement, black-hole thermodynamics, the dark-sector ontology, and the analogue-laboratory programme inside one common ordered-medium picture while making explicit which parts are structural, which are structurally singled out but not fully closed, and which remain open.

### 48.4 Architectural comparison with neighbouring programmes

The purpose of this subsection is not to argue that ECT is “better” than all neighbouring frameworks. It is to locate ECT within the broader landscape of approaches to emergent spacetime and quantum gravity, highlighting where its architectural choices overlap with, differ from, and remain weaker or stronger than those of its neighbours.

**Scope and methodology.** The comparison is organised along eight structural axes: origin of time/Lorentzian structure, origin of gauge structure, origin/status of quantum axioms, gravity closure, dark-sector treatment, singularity logic, information/decoherence architecture, and falsifier structure. Table 111 summarises the comparison; an expanded version with additional axes is given in Appendix BE.

**Comparison by falsifier style.** A distinctive feature of the ECT programme is that many of its falsifiers are cross-sector architectural rather than sectorwise: a single failure can threaten the whole one-cone, one-action-scale, one-UV-threshold architecture. By contrast, the standard GR + SM framework has largely sectorwise falsifiers (particle content, gravitational tests, cosmological parameters), while modified-gravity models typically have Lorentz-violation or extra-mode falsifiers. This difference is a structural consequence of ECT’s attempt to reduce the number of independent primitives.

**Comparison by number of independent primitives.** ECT attempts to compress the number of independent foundational primitives more aggressively than most neighbouring frameworks. The standard GR + SM picture requires geometry (metric + diffeomorphism), quantum axioms (Hilbert space, Born rule), the gauge group, the particle content, dark matter, and dark energy as separate inputs. ECT aims to trace many of these back to a single ordered medium. This compression is not yet complete—the SM gauge group and the electroweak/Yukawa hierarchy are not yet derived—but the architectural ambition itself distinguishes ECT from approaches that accept the standard input list.

**Table 111:** Architectural comparison of ECT with neighbouring programmes. Entries are necessarily compressed; for expanded discussion see Appendix BE.

Axis	GR + SM	Einstein-aether	Hořava–Lifshitz	Volovik logue	ana-	ECT
Time / Lorentz	Fundamental	Fundamental; preferred frame added	Fundamental but anisotropic	Emergent from condensate	from	Emergent from $O(4) \rightarrow O(3)$

Axis	GR + SM	Einstein-aether	Hořava–Lifshitz	Volovik analogue	ECT
Gauge structure	Postulated	Postulated	Postulated	Analogy only	Ordered-branch structural route to $U(1)$ and $SU(2)$ ; physical SM identification incomplete; $SU(3)$ open
Quantum axioms	Primitive	Primitive	Primitive	Primitive	Structural route via coherent branch; completion open
Gravity closure	Einstein eqs. exact	Einstein + aether	Modified dispersion	Acoustic metric only	Induced metric; FP route; nonlinear closure open
Dark sector	Extra particles + $\Lambda$	Extra particles + $\Lambda$	Extra particles + $\Lambda$	Not addressed	Condensate response; no extra species at galactic level
Singularities	Physical or censored	Physical or censored	Possibly solved UV re-by	Not addressed	Branch boundary; condensate breakdown
BH information	Paradox open	Paradox open	Modified; details model-dependent	Not addressed	Reduced-state information reading; fundamental loss not required within the present programme, but completed evaporation closure remains open
Falsifier style	Sectorwise	Extra-mode LIV	/ LIV / dispersion	Not systematic	Cross-sector architectural

**What ECT still does not derive.** The comparison above should not be read as implying that ECT has already completed all structural derivations that are postulated in the standard framework. The main unresolved fronts are summarised more systematically in Section 48.10.

**Interpretive note.** The comparison above is architectural, not polemical. Each listed programme has independent strengths that ECT does not replicate. The point is not that ECT solves all problems, but that it pursues a distinctive architectural strategy—single ordered medium, emergent spacetime and quantum structure, cross-sector falsifiers—that is worth comparing on its own terms.

## 48.5 Comparison with alternative quantum interpretations

**Cramer’s transactional interpretation (TI).** Cramer (1986) [247] models every quantum interaction as an exchange of “offer” (retarded) and “confirmation” (advanced) waves between emitter and absorber. ECT shares with TI the structural idea that the relevant coherent-sector description is not exhausted by a purely one-sided Lorentzian-causal picture. In TI this appears as the advanced–retarded offer/confirmation language. In ECT it appears through the two-sided boundary sensitivity of the Euclidean coherent

branch. The similarity is therefore real but not an identity: TI is an interpretation of the standard quantum formalism, whereas ECT locates the two-sided structure in a specific Euclidean condensate ontology. The present comparison is conceptual and structural; it is not the claim that TI is fully derived as a special case of ECT. ECT therefore does not adopt the literal offer/confirmation-wave ontology of TI. The overlap lies only in the structural rejection of a primitively one-sided temporal description.

**Page–Wootters mechanism.** Page & Wootters (1983) [248] proposed that effective time can arise from entanglement between a “clock” subsystem and the rest of the universe within a globally stationary state. ECT is compatible with the broad philosophical motivation of that move: at the deepest Euclidean level, no external physical time is assumed. The difference lies in the mechanism. In the Page–Wootters construction, time is recovered from relational correlations internal to the quantum state. In ECT, by contrast, temporal ordering is tied to the  $O(4) \rightarrow O(3)$  symmetry-breaking structure of the condensate and to the emergence of the ordered Lorentzian branch. The two approaches are therefore not competitors at the same level: Page–Wootters is an internal reconstruction of time within quantum theory, whereas ECT proposes a deeper physical origin for why such a time-bearing branch exists at all. For that reason, the Page–Wootters mechanism would, in an ECT reading, belong to the physics internal to an already available coherent quantum sector, whereas the ECT question is earlier: why a time-bearing ordered branch emerges at all.

## 48.6 ECT as a foundational framework for quantum mechanics

The detailed structural comparison between ECT and the standard quantum formalism—covering the hierarchy of effective equations, the boundary-value versus Cauchy problem, the ontological distinction between  $\Phi$  and  $\psi$ , the origin of the statistical description, the concept mapping onto the standard quantum primitives, and the illustrative examples of interference, tunnelling, measurement, entanglement, and identical particles—is developed as the capstone of Part III in Section 38.3. The role of the present subsection is not to duplicate that material, but to close two pan-structural threads of the comparison that naturally belong to the summary chapter: the common origin of the coherent and geometric branches of ECT, and a compact overall summary of the ECT-versus-QM relation that also serves as a bridge to the broader architectural comparison with neighbouring programmes.

### Unified origin of the coherent and geometric branches

One of the strongest claims of ECT is that gravity and quantum coherence are not separate ingredients forced together after the fact, but two sectors of one ordered condensate theory.

Both branches emerge from the same ordered action (3.8). More precisely, they arise as two complementary descriptions of the same ordered medium under different coarse-grainings and mode selections: the long-wavelength sector is read geometrically, whereas the coherent shorter-wavelength sector is read dynamically in wave-mechanical form. The theory therefore does not begin with “gravity plus quantum mechanics” as separate ingredients; it begins with one ordered condensate whose different sectors generate both. From this same action one obtains two complementary sectors: the *geometric branch*, corresponding to long-wavelength variations of  $u$  and  $n_A$ , leading to the generalised Einstein sector with  $G_{\text{eff}}(x)$ ,  $\Lambda_{\text{eff}}(x)$ , and the additional tensor structure built from  $n_\mu n_\nu$ ; and the *coherent branch*, corresponding to shorter-wavelength fluctuations  $\chi$  on the ordered background, leading through the relativistic wave equation to the Schrödinger limit.

This is not an ad hoc stitching of two unrelated theories. The split follows directly from the mode decomposition of the same condensate around the same ordered background. In this sense, ECT does not “quantise gravity” in the usual way; it embeds both gravity and quantum mechanics into one common substrate.

The generalised Einstein sector already contains quantities of the form  $G_{\text{eff}}(X)$  and  $\Lambda_{\text{eff}}(X)$ , and tensor structures involving the ordered direction  $n_\mu$ . Conversely, coherent fluctuations affect the effective amplitude sector and thereby back-react on the geometric side. Thus the route by which coherent

fluctuations back-react on the geometric sector is not introduced from outside as an unrelated semiclassical prescription, but is structurally rooted in the dynamics of one and the same condensate action. A completed quantitative backreaction programme, however, remains open.

This unification of the coherent and geometric branches is one of the most important structural results of ECT.

### Summary of the comparison

Standard quantum mechanics is an effective statistical theory of subsystems, formulated in terms of a probabilistic amplitude  $\psi$  and a forward-time Cauchy problem. ECT proposes a deeper level in which the fundamental object is the physical condensate field  $\Phi(X)$ , governed by a global four-dimensional boundary-value problem. Quantum mechanics is then recovered as the effective coherent-sector description obtained after projection to the relevant subsystem, formal Euclidean–Lorentzian amplitude translation, and coarse-graining over untracked condensate modes; the step-by-step structural content of this reduction is the subject of Section 38.3.

ECT therefore aims not only to reproduce the effective formalism of quantum mechanics, but to explain why that formalism takes the shape it does (Fig. 46). It seeks to explain why the formalism has the structure it does, why probabilities appear, why superposition exists, why collapse is seen, why  $\hbar$  is universal, and how the coherent quantum branch and the geometric gravitational branch arise from one common substrate.

Standard quantum mechanics	Euclidean Condensate Theory
<b>Cauchy (initial-value) problem</b> $\psi(x, t_0)$ given $\rightarrow$ evolve forward	<b>Boundary-value (elliptic) problem</b> $\Phi(X)$ on entire $M^4$
<b><math>i\hbar \partial_t \psi = H\psi</math></b> Schrodinger / Dirac equation	<b><math>\delta_{AB} \partial_A \partial_B \Phi - V'(\Phi) = 0</math></b> Euclidean condensate equation
<b><math> \psi ^2 = \text{Born rule}</math></b> Fundamental axiom	<b><math> \psi ^2</math> from coarse-graining</b> Emergent, not axiom
<b>Time: fundamental coordinate</b> Lorentzian spacetime a priori	<b>Time: emergent from SSB</b> $O(4) \rightarrow O(3)$ selects w-direction
<b>Measurement: extra postulate</b> Collapse / decoherence added	<b>Measurement: E <math>\rightarrow</math> L transition</b> Under environmental locking

**Figure 46:** Structural comparison of standard quantum mechanics (left) and ECT (right). Standard QM is formulated as a Cauchy initial-value problem with probability as a fundamental axiom (Born rule). ECT begins from an elliptic boundary-value problem on a Euclidean domain; time emerges on the ordered branch, while probability and measurement are treated as reduced-sector reconstruction targets. The Born rule and detector-level outcome selection remain open. The rows are representative contrasts, not an exhaustive list of all structural differences; the full comparison, with tables and illustrative examples, is developed in Section 38.3.

In this sense, ECT does not replace standard quantum mechanics as a laboratory calculation tool; it proposes a deeper level from which standard quantum mechanics emerges as an effective, statistically formulated subsystem theory.

### 48.7 Phenomenological reach and observational diagnostics

This subsection collects the main observational implications and detection strategies of ECT in one place, covering both dark-sector diagnostics and the most informative empirical tests.



**Detectability of the ECT mass-discrepancy mechanism.** In ECT, the dominant mass-discrepancy phenomenology on galactic scales is not due to a new collisionless particle component but arises from the nonlinear response of the ordered-branch amplitude variable  $\phi$  in the critical weak-field branch. Accordingly, standard direct-detection strategies aimed at a dominant galactic dark-matter particle flux are not expected to observe a signal from the main mechanism studied in this paper.

Instead, the appropriate detection channel is gravitational: precision tests of kinematics and lensing as a function of environment and scale. In particular, ECT can be constrained by joint rotation-curve and lensing analyses, by tests of the external-field effect in systems such as satellites and ultra-diffuse galaxies, and by cluster-merger lensing geometries (e.g. Bullet-like systems), where the condensate redistribution can decouple the lensing potential from the gas distribution. A notable case is Abell 520 [117, 118], where the lensing peak coincides with the gas core rather than the galaxies; ECT reproduces this morphology through the same  $v$ -closure rule that produces BCG-peaked morphology in Bullet-like systems (Section 17.2).

If the condensate sector supports additional weakly coupled excitations (constrained soft orientation excitations or topological configurations)—an optional extension of the minimal ECT closure, not required by the present galactic or cosmological account—these would behave as ultra-light, extremely feebly interacting modes. Their most promising observational signatures would then be astrophysical structure effects (core sizes, interference patterns, small-scale suppression, or characteristic oscillatory signals), rather than terrestrial scattering events. The minimal ECT closure does not require such excitations to explain any of the phenomena addressed in this paper.

**Detectability of the late-time acceleration mechanism in ECT.** In ECT, late-time accelerated expansion is not attributed to an independent dark-energy substance. It is interpreted instead as an ordered-branch background effect of the same condensate. The effective equation-of-state parameter  $w(z)$  should be understood as a phenomenological descriptor of the background evolution rather than as evidence for a separate dark-energy component. The main observational handle is the redshift dependence of  $w(z)$  and its correlations with quantities controlling the condensate background, testable via BAO+SNe, weak lensing, and redshift-space distortions.

If the condensate parameters are effectively frozen on cosmological timescales, the model becomes observationally close to  $\Lambda$ CDM at the background level, and the discriminating power shifts to combined constraints on growth, lensing, and consistency relations.

**Cluster-merger lensing as a dual test.** The cluster-merger lensing suite (Section 17.2) provides a qualitatively new test of the ECT framework and simultaneously highlights a tension with  $\Lambda$ CDM. In ECT the effective convergence  $\Sigma_{\text{eff}} = v(g_N/g_{\dagger}^{\text{cl}})\Sigma_b$  tracks the locally most compact baryonic component. This rule reproduces the BCG-peaked lensing morphology in the Bullet Cluster, MACS J0025, and El Gordo — systems where the collisionless stellar cores are more compact than the shocked gas — and automatically predicts gas-core-peaked lensing in Abell 520 [117, 118], where the central gas is more concentrated than the dispersed post-merger galaxies.

Abell 520 is particularly significant: in  $\Lambda$ CDM the lensing peak should follow the collisionless dark-matter halo, which is expected to co-move with the galaxies rather than with the collisional gas. The observed gas-coincident lensing peak therefore constitutes a direct observational challenge for collisionless dark-matter models, while ECT explains it without additional assumptions through the same universal rule that governs all four systems. Unlike minimal MOND/AQUAL treatments, the ECT cluster sector also admits environment-modulated threshold shifts and an orientation-stress contribution to gravitational slip, so the present factor-of-two amplitude deficit should be read as a sharply defined quantitative target rather than as a morphology-level falsification. The amplitude deficit ( $\times 1.1$ – $1.9$ , comparable to the MOND cluster problem) remains an open quantitative target (OP22).

**The Great Attractor and large-scale flows.** As an illustration of how the ordered-branch amplitude framework may reinterpret large-scale anomalies, consider the Great Attractor region (distance  $\sim 60$  Mpc, peculiar velocity  $\sim 600 \text{ km s}^{-1}$ ), a large-scale gravitational anomaly usually attributed to a dark-matter

overdensity. In the  $\phi$ -framework, an overdense supercluster region has high  $\phi_{\text{env}}$  (deeply Lorentzian, screened), but the surrounding intermediate-density regions through which infalling galaxies move have *lower*  $\phi_{\text{env}}$  and therefore enhanced  $G_{\text{eff}}$ . This amplification of the apparent gravitational pull from the transition zone could contribute to the observed infall pattern without requiring a dark-matter halo as massive as the  $\Lambda$ CDM estimate. A quantitative prediction requires solving the  $\phi$ -equation on Mpc scales, which is part of the full recalculation programme (OP21).

**The cleanest tests.** The most informative empirical tests of the ordered-branch amplitude mechanism are expected not in the highest-mass systems, but in the most weakly screened low-density environments—void dwarfs, diffuse groups, outer disks—where the vacuum sits closest to the critical Lorentzian boundary. Environment-dependent transition morphologies (the detailed shape of the Newtonian-to-MOND transition, not just the asymptotic  $g_+$ ) may provide a further high-quality diagnostic.

**SPARC rotation-curve analysis.** A systematic fit to the SPARC database (165 galaxies with resolved rotation curves) yields median reduced  $\chi^2$  competitive with MOND and lower than MOND on the clean sub-sample (Table 66). The Milky Way rotation curve is reproduced with  $\chi^2/N = 2.95$  using a single free parameter  $g_{\text{eff}}^\dagger \approx 1.72 g_0^\dagger$ , compared with  $\chi^2/N = 6.55$  for the standard  $\Lambda$ CDM NFW fit. The preferred baseline scale clusters around  $cH_0/(2\pi)$ , with galaxy-to-galaxy scatter that may reflect genuine environment dependence. The external-field effect (EFE)—suppression of the  $\phi$ -branch enhancement in galaxies embedded in dense environments—is a distinctive prediction that separates ECT from both  $\Lambda$ CDM (no EFE) and classical MOND (different EFE mechanism).

**Lorentz-invariance violation bound.** The single-speed architecture of ECT predicts that all massless modes—gravitational, electromagnetic, and Goldstone—propagate at the same emergent speed  $c_*$ . The coincident arrival of GW170817 and GRB 170817A [10] constrains  $|\delta c/c| < 10^{-15}$ , which ECT satisfies by construction at the single-cone level.

**Cosmological dark-energy compatibility.** The DESI 2024 measurement  $w_0 = -0.827$  is compatible with the ECT late-time amplitude-sector closure if the ratio of kinetic to condensate energy density satisfies  $\rho_{\text{kin}}/\rho_{\text{cond}} \approx 0.26$ . This provides a concrete target for the full cosmological  $\phi_{\text{bg}}(t)$  programme.

**Summary of observational strategy.** The ECT framework suggests two complementary observational strategies: precision tests of the predicted modifications of gravity on galactic and cluster scales (RAR, external-field effect, BTFR, cluster-merger lensing morphology). If the condensate supports additional weakly coupled soft or topological excitations (an optional extension, not required by the minimal closure), these would manifest as ultra-light, extremely feebly interacting modes; their signatures would be indirect astrophysical effects (core sizes, interference patterns, small-scale suppression) rather than direct laboratory detection. Both channels offer direct falsifiable predictions of the theory.

**Systematic role of the full nonlinear field equations.** A systematic assessment of the observational footprint of the full nonlinear field equations (13.35)—in particular of the anisotropic orientation stress  $\Theta_{\mu\nu}[n]$ —has been carried out across all five phenomenological sectors developed in this work (Table 54). For background cosmological observables (Hubble shift, Universe age) the orientation-stress contribution is not separable from the scalar  $\phi$ -sector at the present closure level. For galactic dynamics and BTFR the contribution is degenerate with the effective critical-scale calibration. In two regimes, however,  $\Theta_{\mu\nu}$  produces effects that are structurally distinct and potentially significant: sub-horizon perturbative growth (relevant to the JWST tension) and cluster-merger gravitational lensing (the most direct probe of the tensor sector). In both cases the quantitative magnitude is controlled by the undetermined coefficient  $c_1$  (OP-c1), whose first-principles derivation is now the key bottleneck for turning these Level B parametrised estimates into quantitative predictions (§13.5).

## 48.8 Parameter compression and comparison

ECT achieves a remarkably high ratio of derived physical content to fundamental input parameters. At the benchmark level used in the present synthesis, the condensate-side description contains two kinds of ingredients: (i) a kinematic branch choice, encoded in the kinetic coefficients  $\alpha, \beta$ , and (ii) non-kinematic condensate data, encoded in the gradient scale  $u_0$ , the amplitude scale  $\phi_0$ , and the quartic coupling  $\lambda$ . Adopting the realised one-cone benchmark  $\alpha = 2\beta = 2$  fixes the kinematic branch used throughout the paper. The remaining condensate-side input set is therefore the triplet  $(u_0, \phi_0, \lambda)$ , while additional closure functions enter at the macroscopic and quantum effective levels.

From these condensate-side inputs ECT derives or structurally constrains a broad range of low-energy phenomena. At the established structural or closure-dependent level this includes:  $c^*$ ,  $\hbar$ ,  $G_N$ , the Klein–Gordon and Schrödinger limits, linearised and conditionally nonlinear Einstein dynamics, the universal causal cone, the horizon/flatness/monopole resolutions, galactic rotation-curve phenomenology and the BTFR, dark-energy-like residual condensate energy, a route to the Hubble tension, decoherence and the classical limit, and black-hole entropy/information structure. At the more exploratory level, ECT also provides structural routes toward  $\alpha_{\text{fs}}$ , generation number, and Yukawa hierarchy.

By contrast, the Standard Model requires 19 free parameters (6 quark masses, 3 lepton masses, 3 gauge couplings, 4 CKM parameters, Higgs mass, Higgs VEV,  $\theta_{\text{QCD}}$ ), and  $\Lambda\text{CDM}$  adds 6 cosmological parameters ( $H_0$ ,  $\Omega_b$ ,  $\Omega_{\text{cdm}}$ ,  $\tau$ ,  $A_s$ ,  $n_s$ ), for a total of  $\sim 25$  parameters to describe the corresponding low-energy particle and cosmological phenomenology.

This benchmark-level compression — one fixed kinematic branch together with the condensate triplet  $(u_0, \phi_0, \lambda)$ , versus  $\sim 25$  parameters in the Standard Model plus  $\Lambda\text{CDM}$  — remains one of the strongest structural motivations for the ECT programme, even though several low-energy sectors and closure functions are not yet derived from first principles.

## 48.9 Completion data and residual bifurcation points

The remaining non-closed sectors of ECT fall into three conceptually distinct classes, following the classification of incompleteness introduced in this section.

**Type 1: Initial-condition-sensitive sectors.** The arrow of time, thermodynamic irreversibility, and the second law depend not on a different “branch of laws” but on the realized initial state. This is not a special weakness of ECT: every fundamental theory (GR, QFT, string theory) requires initial conditions for the temporal asymmetry. ECT offers a natural route: the phase transition  $O(4) \rightarrow O(3)$  can generate a non-equilibrium, coherent, low-entropy starting state. A strict proof that this outcome is generic remains open; accordingly, ECT does not yet derive a strict second law from first principles.

**Type 2: Open microphysics.** This class includes: the CP-violating mechanism for baryogenesis (currently at the level of Sakharov-condition compatibility), the fine-structure constant (structural route via  $\alpha_{\text{fs}} = q^2/(4\pi Z_A)$ , §7.2), three fermion generations (spectral route, §9.6), the Yukawa hierarchy (overlap/tunnelling route, §9.6), the primordial perturbation spectrum (critical-fluctuation route, §14.6), and the origin of  $SU(3)_{\text{colour}}$ . For each, the structural mechanism is identified but the explicit computation remains an open calculational programme.

**Type 3: Fundamental condensate parameters.** The remaining non-kinematic condensate inputs  $\phi_0$ ,  $u_0$ , and  $\lambda$  (after adopting  $\alpha = 2\beta$ ,  $\beta = 1$ ) are genuine phenomenological inputs of the theory, analogous to the free parameters of any fundamental framework. Their values are fixed by matching to observations, while the identification of the Planck/radial scale is carried by  $\phi_0$ , not by a direct statement  $u_0 \sim \bar{M}_{\text{Pl}}$ .

**Epistemic vs. ontic distinction.** It is important to note that if a parameter currently appears as closure data for a Level B result, this does not necessarily mean that the result is fundamentally underivable

without it. It may mean only that the current version of the derivation does not close without this input. Future developments of ECT may reduce the number of independent closure data by deriving some of them from more fundamental condensate structures. The programme of strict classification of truly irreducible inputs versus current derivational gaps is itself an important open task.

## 48.10 Current limitations

Several important limitations should be noted.

(i) The Abelian  $U(1)$  gauge sector is derived from bundle covariance of the condensate phase fibre (Level A). A preferred chiral  $SU(2)$  sector is structurally identified through the residual stabiliser and orientation of the broken phase (Level A for the gauge architecture; Level B+ for the physical weak sector). The colour group  $SU(3)_c$  cannot arise from the minimal  $O(4) \rightarrow O(3)$  pattern ( $\dim \mathfrak{su}(3) > \dim \mathfrak{so}(4)$ ; see also §40) and requires additional internal condensate structure (Level B). The full Standard-Model matching—observed matter representations, charge assignments, anomaly cancellation, and the Weinberg angle—remains open (Section 48.13, Table 118).

(ii) The galactic weak-field sector is currently implemented through an exploratory algebraic closure of the ordered-branch amplitude field  $\phi$ , not yet through a full boundary-value solution of the  $\phi$ -equation. The deep-IR critical form  $\mathcal{F} \propto Y_\phi^{3/2}$  is a hypothesis motivated by 3D scale invariance, not yet a full nonperturbative derivation. The present closure captures the screened and deep-critical asymptotics but does not yet reproduce the full inner morphology of all observed rotation curves.

(iii) The critical acceleration scale  $g_+$  is not treated as a universal fundamental constant in ECT. In the current implementation it is controlled by the ambient ordered-branch amplitude background  $\phi_{\text{env}}$ . The observed galaxy-to-galaxy scatter should therefore be interpreted as part of the physics to be explained, not as a failure of universality.

(iv) Three fermion generations, the Yukawa coupling hierarchy, and the fine structure constant  $\alpha_{\text{fs}} = 1/137$  are not yet derived from first principles, but structural routes have been identified for all three:  $\alpha_{\text{fs}} = q^2/(4\pi Z_A)$  through emergent gauge normalisation (§7.2), family multiplicity through spectral counting of fermionic modes (§9.6), and Yukawa hierarchy through overlap/tunnelling suppression (§9.6). These are Level B/C routes, not completed derivations (Appendix Z).

(v) ECT already provides a physical ultraviolet threshold of the ordered branch through the primary radial mode  $m_\sigma$  (§8.3), but a rigorous graviton-loop power-counting analysis and a completed nonperturbative UV closure have not been performed. The structural contrast with perturbative Einstein gravity is sharp: there,  $[G_N] = M^{-2}$  forces new curvature counterterms at every loop order, making the Landau-pole-like obstruction arise already at  $E \sim M_{\text{Pl}}$ ; in ECT,  $G_N$  is a condensate parameter, the dimensionless coupling  $g(\mu) = \lambda(\mu)/(8\pi) \approx 4 \times 10^{-5}$  remains small throughout the EFT, and the Landau pole of the scalar sector lies at  $\mu_{\text{LP}} \approx M_{\text{Pl}} e^{5.26 \times 10^4}$ —far beyond any physically accessible scale. Accordingly, the present framework offers a structural route to UV regularisation, whereas UV safety in the stronger quantum-gravity sense remains open. Open tasks: explicit loop power counting (OP-UV1), two-loop RG of the condensate–graviton system (OP-UV3), and OS proof for the spin-2 sector (OP-OS1).

(vi) The classical cosmological-constant catastrophe is *resolved at Level A* in the leading ordered-branch sector of ECT. For the bare quartic potential  $V(\Phi) = -\mu^2 \Phi^2/2 + \lambda \Phi^4/4$ , the broken minimum gives a large negative tree-level contribution  $V(\phi_0) = -\mu^4/(4\lambda)$ . In a standard general-relativistic setting this contribution would gravitate as a cosmological constant of order  $\lambda M_{\text{Pl}}^4/4$ , overshooting the observed  $\rho_\Lambda^{\text{obs}} \approx (2.3 \times 10^{-3} \text{ eV})^4$  by a factor of order  $10^{120}$ . In ECT the direct channel by which this UV baseline would enter the gravitational action is blocked: the emergent unimodular decoupling theorem of Section 15 shows that, in the leading ordered-branch sector, the fixed kinetic-determinant structure  $\sqrt{-\det K^{AB}} = \beta^2/c_*$  makes the classical baseline  $V(\phi_0)$  inert for the local emergent gravitational dynamics (Theorem 15.3(iv); Level A, unconditional), and—conditional on a one-line spectral assumption on the full quadratic fluctuation operator (condition  $H_\Lambda$ )—the same fixed kinetic-determinant structure absorbs the zero-derivative one-loop vacuum contribution (Theorem 15.3(v); Level A conditional). No cross-scale cancellation between UV and IR scales is invoked at any stage, and Weinberg’s no-go theorem

in its standard form does not apply to the ECT framework.

The numerical value  $\rho_{\Lambda, \text{obs}}$  is a distinct, subsidiary, infrared determination problem at Level C. The natural scaling  $\rho_{\Lambda} \sim c_{\Lambda} M_{\text{Pl}}^2 H_0^2$  is consistent with observation at the order-of-magnitude level and admits a plausible pseudo-Goldstone realisation, but the dimensionless coefficient  $c_{\Lambda} = \mathcal{O}(1)$  is not yet derived from first principles; this question should not be conflated with the Level A resolution of the catastrophe itself. Loop contributions are treated within the effective ordered-branch cutoff structure of the present ECT closure, while  $\Lambda_{\text{eff}}$  is a dynamical functional of the condensate background rather than a rigid constant. Reformulated OP- $\Lambda 3$  therefore splits into three technical open problems (O1–O3 of Section 15.12): verification of condition  $H_{\Lambda}$  against the full ECT Lagrangian, explicit first-principles computation of  $c_{\Lambda}$  on an FRW background, and a formal analogue of the Ng–van Dam non-renormalization theorem [96] in the emergent unimodular setting.

(vii) Retarded support  $K(\tau < 0) = 0$  is established at Level A for the ordered Lorentzian scalar branch (Appendices E, F). The full open-system identification of the response kernel used in the influence-functional thermodynamic closure, and the associated ohmic/Markov/macrosopic bath assumptions, are not yet derived directly from Euclidean microdynamics. The effective second law holds within the Gaussian–Markov approximation; a full microscopic H-theorem remains open (OP-Q17).

(viii) The exact Bell-correlator reconstruction is still at the programme level, the full nonlinear gravitational closure is only partly theorem-level, and the black-hole evaporation/information programme is not yet quantitatively closed.

(ix) The electroweak scale  $v_2$  is not yet derived from condensate dynamics; the physical identification  $S_0 = \hbar$  remains Level B/Open. The Yukawa hierarchy now has an identified structural route (overlap/tunnelling suppression, §9.6) but the explicit computation remains open.

## 48.11 Future directions and programme closure

The most important open problems for future work include:

(i) Replacing the algebraic  $\phi$ -closure model by a full spherical boundary-value solver for  $\phi(r)$ , with explicit environmental boundary conditions, realistic baryonic components (including SPARC gas profiles), and eventually full axisymmetric disk geometry.

(ii) *Origin of the electroweak scale and locking structure (OP-EW)*. The current formulation uses  $v_2 \approx 246$  GeV as the secondary electroweak scale required by low-energy matching. A first-principles derivation remains open at several logically distinct levels: the compact  $U(1)_{\theta}$  participant of the alignment sector (OP-EW-locking.0), the Hopf-fibered diagonal locking dynamics (OP-EW-locking.1), the non-polynomial scale-generation mechanism  $v_2 = \phi_0 e^{-\mathcal{J}_{\text{EW}}}$  with  $\mathcal{J}_{\text{EW}} \approx 36.8$  (OP-EW-scale), the local chiral  $SU(2)_L \times U(1)_Y$  gauge completion including  $g, g'$  and the Weinberg angle (OP-EW-gauge), the protection of the secondary radial mode from additive  $\mathcal{O}(\phi_0^2)$  corrections (OP-EW-naturalness), and the chiral fermion/Yukawa sector (OP-EW-matter). The reduced  $O(3) \rightarrow O(2)$  analogue is described in Appendix L; the candidate Hopf-fibered phase–orientation geometry is described in Appendix M. Any complete derivation would feed simultaneously into the electroweak boson mass scale, fermion mass matching, geometric-mean seesaw estimates, and fifth-force suppression factors, all of which currently use  $v_2$  as an input.

(iii) Numerical simulations of condensate evolution during cosmological phase transitions, including predictions for the primordial power spectrum beyond the slow-roll approximation.

(iv) A systematic comparison of ECT predictions with the full SPARC database (beyond the current 165-galaxy sample), including the  $\phi_{\text{env}}$ –environment correlation test.

(v) Completion of the gauge-sector programme: explicit internal weak-gauge derivation beyond the present structural  $SU(2)$  selection, derivation of the observed fermion representations and charge assignments, and a construction of the colour sector from extended internal condensate structure (see Section 48.13 and Table 118).

(vi) Derivation of baryon-number selection rules in the completed gauge/flavour sector, including whether low-energy  $\Delta B = 1$  operators are absent, instanton-suppressed, or Planck-suppressed, what decay

channels they induce, and whether  $\Delta B = 2$  observables such as  $n-\bar{n}$  oscillations and dinucleon decay provide an independent test (§44).

(vii) Completion of the structural routes to open microphysical targets: explicit computation of  $Z_A$  for the fine-structure constant (§7.2), spectral analysis of the condensate background for the generation number (§9.6), and overlap-integral computation for the Yukawa matrix (§9.6).

**Highest-priority uncovered structural problems.** Beyond the sector-specific items listed above, the following cross-cutting problems represent the largest remaining gaps between ECT and a complete physical theory, ordered by a combination of importance and proximity to existing ECT tools:

- (1) Full first-principles Born-rule closure (close (C1)–(C3) from bare P1–P6; §30.4).
- (2) Charge quantisation: Abelian lattice now established (§23.4); full SM charge pattern, hypercharge, and global gauge-group quotient remain open from the topology of the compact-phase fibre.
- (3) Gauge anomaly cancellation from admissible condensate excitations.
- (4) Full flavour closure: generations, textures, CKM, PMNS, CP phases, and mass ordering. The flavour architecture is now systematised in §9.7, but quantitative derivation remains open.
- (5) Strong CP problem ( $\theta_{\text{QCD}}$ ).
- (6) Why the fundamental arena is 4D Euclidean and why the emergent branch is specifically  $3 + 1$ .
- (7) Reformulated cosmological-constant problem (Section 15): the direct UV vacuum-to- $\Lambda$  channel is blocked in the leading ordered-branch sector by the emergent unimodular decoupling theorem; what remains open is the first-principles computation of the infrared coefficient  $c_\Lambda$  in  $\rho_\Lambda \sim c_\Lambda M_{\text{Pl}}^2 H_0^2$ , verification of condition  $H_\Lambda$  against the full Lagrangian, and the formal analogue of the Ng–van Dam non-renormalization theorem (O1–O3 of Section 15.12; legacy label: OP- $\Lambda$ 3).
- (8) Holography, area law, and Bekenstein bound as general medium properties; area-scaling mechanism now established (§36.5); covariant and reconstruction extensions open.
- (9) Quantitative black-hole information closure and Page curve beyond the current shell model.
- (10) Full low-energy QFT architecture: locality, cluster decomposition, analyticity, crossing, S-matrix structure.

(viii) Full derivation of the primordial perturbation spectrum  $(n_s, A_s, r)$  from the critical dynamics of the  $O(4) \rightarrow O(3)$  ordering transition, including the freeze-out mechanism, curvature-mode conversion, and the role of weakly gauged  $SU(2) \times U(1)$  (§14.6).

(ix) First-principles derivation of the orientation-stress coefficient  $c_1$  (OP-c1). The systematic assessment of the full nonlinear field equations across the phenomenological sectors of this work (Table 54) has identified  $c_1$  as the key bottleneck for turning the observational NLEE programme from Level B parametrised estimates into quantitative predictions. The two most sensitive channels—sub-horizon perturbative growth (JWST maturity budget) and cluster-merger gravitational slip—both depend critically on  $c_1$ . A controlled derivation from the ECT action would simultaneously constrain gravitational-wave polarisation, large-scale lensing surveys, and the cluster amplitude problem, making OP-c1 a high-priority target for the next stage of the programme.

**The ordered-branch amplitude variable as an organising principle.** A recurring theme of the present work is that the macroscopic amplitude variable  $\phi = \frac{1}{\beta} \ln(u/u_\infty)$  provides a single variable that organises multiple aspects of the theory: the effective gravitational regime (Newtonian, MOND-like, or quantum/Planckian) is controlled by the local value and gradient of  $\phi$ ; screening in dense environments, the BTFR, environmental modulation of  $g_+$ , and the cosmological acceleration scale all follow from the  $\phi$ -dynamics; the transition between GR and modified gravity is not merely a matter of curvature or distance but of the local condensate amplitude relative to its asymptotic screened background. A central next step is to promote the galactic order field to a cosmological background  $\phi_{\text{bg}}(t)$  plus inhomogeneous perturbations, unifying late-time acceleration, the redshift evolution of  $g_+$ , lensing and gravitational slip, and galactic dynamics within one vacuum-order framework (OP-new-4, OP21).

**Gauge interactions and the vacuum-order hierarchy.** At present the macroscopic amplitude variable should not be interpreted as a derivation of the electromagnetic, weak, or strong interactions: these emerge from the phase symmetries of the condensate (Section 7), not from  $\phi$ . However,  $\phi$  may play an indirect role: as the order parameter controlling the macroscopic phase of the vacuum, it may determine *in which regime* certain effective low-energy sectors are realised. A deeper question for future work is whether the emergence of gauge sectors can also be organised relative to this vacuum-order hierarchy.

**Possible strengthening postulates.** An important future question is whether some of the current Level B results can be promoted to Level A. In some cases this may require only further derivation from the present postulates; in other cases it may require one or more additional microscopic assumptions that constrain the condensate more tightly. Natural candidates for such strengthening assumptions could include:

- (i) a *spectral-normalisation postulate* fixing the absolute normalisation of the minimal coherent action cycle and thereby potentially determining  $S_0$  rather than merely proving its existence;
- (ii) a *coherent-Hamiltonian closure postulate* selecting a unique real-time generator of the ordered branch compatible with the same action scale  $S_0$ ;
- (iii) a *spinorial-sector postulate* specifying which condensate representation sector realises physical fermionic excitations;
- (iv) a *projector/probability completeness postulate* sharpening the route from decohered alternatives to a probability assignment;
- (v) a *strong-field shell regularity postulate* sufficient to derive near-horizon purification dynamics and Page-curve behaviour constructively.

Whether such additions would be elegant consequences of the ordered medium picture or merely ad hoc repairs must be judged carefully. But the important point is that the present framework now makes this question precise: it identifies not only which results remain below Level A, but also what kind of additional input would be needed to push them upward.

## 48.12 Fundamental constants and present closure levels

ECT does not treat all entries traditionally listed among the “constants of Nature” as belonging to the same conceptual class. The following three tables separate native ECT structural outputs (Table 112), open gauge-matter closure parameters (Table 113), and derived combinations, conventions, and observables (Table 114).

**Table 112:** Native ECT structural outputs.

Quantity	ECT status	Comment
$D = 3$ (spatial dimensions)	Derived (A)	$O(4) \rightarrow O(3)$ SSB
$c$ (vacuum signal speed)	Derived (A/B)	Cone speed $c_* = \sqrt{\beta/(\alpha - \beta)}$
$\hbar$ (action scale)	Derived (A/B)	Loop action $S_0$ from phase winding
$G_N$ (gravitational coupling)	Derived (B)	Condensate stiffness $G_N = c_*^4/(8\pi M_G^2)$
Massless photon	Derived (A/B)	Unbroken $U(1)$ + gauge invariance
Massless spin-2 sector	Derived (A/B, linear EFT); full proof open	Spin-2 orientation mode in Fierz–Pauli reconstruction

**Table 113:** Open gauge-matter closure parameters.

Parameter	ECT status	Structural route
$g_1, g_2, g_3$ (at $M_Z$ )	Open	Induced gauge kinetics
$\alpha_{\text{fs}} = 1/137$	Open (route exists)	Low-energy relation $\alpha_{\text{fs}} = q^2/(4\pi Z_A)$ with $Z_A^{\text{IR}} \approx 10.9$ ; UV problem sharpened to electroweak kinetic/mixing target ( $Z_B, Z_W, \theta_W$ ) (§7.2)
$\sin^2 \theta_W$	Open	Ratio of gauge normalisations
$v_{\text{EW}} = 246 \text{ GeV}$	Open	RG flow $\lambda(\mu)$ from Planck scale
$\lambda_H$	Open	Second condensate transition
$y_f$ (Yukawa couplings)	Open (OP-Yukawa)	Fermion-condensate overlap integrals
CKM matrix (4 params)	Open	Multi-generation Yukawa
PMNS matrix (4–6 params)	Open	Structural route established; flavour closure incomplete
$\theta_{\text{QCD}}$	Open	Not yet addressed
$N_{\text{gen}} = 3$	Open (OP-generations)	Topological classification
$N_{\text{colour}} = 3$	Minimal closure hypothesis (C)	Minimal rank of the primary colour module compatible with an $SU(3)$ -structured completion
$\Lambda_{\text{eff}}$	Partial (B/Open)	Condensate background; not independent $\Lambda$

**Table 114:** Derived combinations, conventions, and observables.

Quantity	Status	Comment
$e$ (elementary charge)	Follows from $\alpha + \hbar + c$	Not independent target
$\mu_0, \epsilon_0$	SI conventions	Fixed by $c$ ; not physics targets
$\alpha_G$	Follows from $G, \hbar, c, m$	Derived combination
$m_f$ (fermion masses)	Follow from $y_f \cdot v_{\text{EW}}$	Requires Table 113 inputs
$m_W, m_Z, m_H$	Follow from $g_i, v_{\text{EW}}, \lambda_H$	Embedding (B/C)
$H_0$	Solution-dependent	Full cosmological model
$n_s$ (spectral index)	ECT-native estimate	$1 - n_s \sim \hat{p}/\ln(L/\xi_0)$ ; $\hat{p}$ not derived
$\eta_B$ (baryon asymmetry)	Benchmark leptogenesis	$\sim 9 \times 10^{-10}$ vs observed $6 \times 10^{-10}$
$g - 2$	Precision observable	Requires full QED from ECT
$\Omega_{\text{DM}}$	Reinterpreted	No DM particles; condensate dynamics

Several entries in Table 113 remain blocked not by technical incompleteness alone, but by the absence of an exact colour sector in the current formulation. This motivates the following consistency analysis.



### 48.13 Common pre-geometric origin of the interaction sectors

*Status: synthesis of results from Sections 7–40. This subsection collects the structural consequences of the ECT condensate for the fundamental interaction sectors and formulates the common-origin claim at the appropriate level of rigour.*

#### Definition of “unification” in ECT

In this paper, “unification” does not mean embedding into a single simple Lie group (as in conventional GUT programmes based on  $SU(5)$ ,  $SO(10)$ , or  $E_6$ ). It means emergence from a single pre-geometric condensate substrate through distinct but co-necessary sectors. Three levels are distinguished:

**Common origin:** all interaction sectors emerge from one condensate.

**Structural derivation:** gauge groups are inevitable consequences of the condensate structure.

**Quantitative unification:** coupling constants, charges, and representations follow from condensate parameters.

The present work addresses common origin and structural derivation. Quantitative unification remains an open programme.

#### Interaction-sector synthesis

Collecting the results of Sections 7–40, the ECT condensate supports five distinct interaction sectors, all originating from the same ordered  $\Phi$ -medium:

**Table 115:** Interaction-sector synthesis: common pre-geometric origin.

Sector	Mechanism in ECT	Level	What is derived	What remains open
Gravity	Emergent $g_{\mu\nu}$ from $(\delta_{AB}, n_A)$ ; generalised Einstein equations	A/B	Metric, causal cone, tensor propagation	Full NLEE coefficients
EM ( $U(1)$ )	Compact phase fibre; bundle covariance forces connection and Maxwell-type dynamics (Section 7.2)	A	Connection, covariant derivative, leading kinetic closure	$U(1)_Y$ vs $U(1)_{em}$ identification
Weak ( $SU(2)$ )	Residual stabiliser $O(3)$ of $O(4) \rightarrow O(3)$ ; local orientation redundancy (P5); $\mathfrak{so}(3) \cong \mathfrak{su}(2)$ bridge (Section 7.3)	A (architecture); B+ (physical weak sector)	Gauge architecture, structural chiral selection (Section 9.3)	Full internal weak-gauge derivation; $\sin^2\theta_W$ ; matter representations
Strong ( $SU(3)_c$ )	Extended internal condensate structure; reverse-engineered consistency requirement (Section 40)	B	Connection, QCD Lagrangian (once module specified)	Intrinsic derivation; why rank 3
Director coupling	Lowest-dimension symmetry-allowed fermion–condensate operator $\mu_5 \bar{\Psi} \gamma^A n_A \Psi$ (Section 7.6)	A (existence); B (coefficient)	Operator form, symmetry properties	Coefficient from microdynamics

## Why the electroweak architecture is maximal within the minimal condensate

The Lie algebra  $\mathfrak{su}(3)$  has dimension 8, while  $\mathfrak{so}(4)$  has dimension 6. Since  $\dim \mathfrak{su}(3) > \dim \mathfrak{so}(4)$ , the colour algebra cannot be a subalgebra of  $\mathfrak{so}(4)$ . Therefore  $SU(3)_c$  cannot arise as a direct subgroup or residual gauge factor of the minimal  $O(4) \rightarrow O(3)$  breaking pattern. This supplements the dynamical obstruction of Section 40 (colour-carrying condensate breaks  $SU(3) \rightarrow SU(2)$ ) with an algebraic one: even setting dynamics aside, the algebra simply does not fit.

Within the minimal  $O(4) \rightarrow O(3)$  symmetry-breaking pattern, the electroweak-type  $U(1) \times SU(2)$  architecture is the maximal direct gauge structure accessible without introducing additional internal condensate degrees of freedom. Any colour sector therefore requires additional internal structure beyond the minimal  $O(4)$  data—exactly as realised in the primary completion of Section 40.

Within the minimal  $O(4) \rightarrow O(3)$  symmetry-breaking pattern, an electroweak-type  $U(1) \times SU(2)$  architecture is the maximal direct gauge structure accessible without introducing additional internal condensate degrees of freedom. The qualitative distinction between the electroweak and strong sectors—a fact postulated in the Standard Model—is thus explained by the algebraic and dynamical constraints of the condensate.

## Two-storey electroweak architecture

The electroweak sector of ECT has a two-storey structure:

**Geometric storey (Sections 7.3, 9.3):** The  $O(4) \rightarrow O(3)$  SSB and P5 yield the  $SU(2) \times U(1)$  gauge architecture as a structural redundancy of the ordered branch. The oriented condensate provides a structural setting for chiral asymmetry.

**Phenomenological storey (Section 7.4):** The secondary condensate scale at  $v_2 = 246 \text{ GeV}$  realises electroweak symmetry breaking and generates the observed  $W^\pm$ ,  $Z$ , and Higgs masses.

The first storey explains why  $SU(2) \times U(1)$  exists as a gauge architecture; the second explains how it breaks.

## Director coupling: naming and status

The ECT-specific fermion–condensate coupling  $\mu_5 \bar{\Psi} \gamma^A n_A \Psi$  (Section 7.6) is henceforth referred to as the *director coupling*, by analogy with the director field of nematic liquid crystals and the anchoring energy in those systems. The order parameter  $n_A$  plays the role of the director; the coupling describes how fermionic excitations interact with the orientation of the ordered medium.

The director coupling is the generic lowest-dimension (dimension-4) condensate–fermion interaction channel permitted by the symmetry content of the ordered branch. Its absence would require an additional symmetry ( $n_A \rightarrow -n_A$ ) that is not present after SSB. In the language of ‘t Hooft naturalness, a vanishing coefficient would be technically unnatural.

Possible signatures include spin precession in the approximate range  $\omega_{\text{dir}} \sim 10^{-10} - 10^{-15} \text{ rad/s}$ , depending on the local condensate profile, and composition-dependent effects if collective condensate response enhances the bare estimate. The  $\eta \sim 10^{-15}$  window should be read as a target sensitivity rather than a sharp present prediction.

## Coleman–Mandula remark

A standard concern about mixing spacetime and internal symmetries is the Coleman–Mandula theorem [51]. Its usual assumptions presuppose a Lorentzian S-matrix setting with nontrivial scattering amplitudes, a mass gap, and Poincaré invariance, whereas ECT begins at a pre-Lorentzian Euclidean substrate where none of these conditions are met at the fundamental level. Therefore the theorem does not straightforwardly apply to the pre-breaking condensate dynamics. A full reformulation for emergent settings remains outside the scope of the present work. This should not be read as a circumvention of the Coleman–Mandula theorem, but as a statement about the current level of analysis.

## Global electroweak structure and charge-lattice constraint

If the global electroweak structure group is taken to be

$$U(2) = \frac{SU(2) \times U(1)}{\mathbb{Z}_2}, \quad (48.1)$$

then the allowed representations satisfy the compatibility condition

$$2T + Y \in 2\mathbb{Z}, \quad (48.2)$$

where  $T$  is the isospin and  $Y$  the hypercharge. The electric charge operator  $Q = T_3 + Y/2$  is then constrained to a discrete lattice. This is a structural constraint on the charge lattice, not yet a derivation of the observed particle charge assignments; the full charge spectrum requires a derivation of the fermion representation content (OP-GUT3b).

The  $\mathbb{Z}_2$  quotient is motivated by the  $\mathbb{Z}_2$  symmetry of the condensate potential  $V(\Phi) = V(-\Phi)$ , which identifies the centres of  $SU(2)$  and  $U(1)$ . A more detailed investigation of the global group structure and its consequences for charge quantisation remains open.

## Hierarchical bosonic sectors

The bosonic content of ECT is best organised hierarchically, by structural level. The table below records the bosonic sectors retained in the current formulation at successive levels of condensate structure; it does not claim a final unique census of all possible emergent excitations. The Level-0 scalar content should be read as the retained low-energy condensate sector of the present closure, not as a theorem-level final census of all possible Goldstone-sector excitations.

**Table 116:** Hierarchical bosonic sectors in ECT.

Level	Particle	Spin	Origin	Status
<i>Level 0: minimal condensate (<math>O(4) \rightarrow O(3)</math> SSB)</i>				
0	Graviton	2	Metric sector $\delta g_{\mu\nu}$	A/B
0	$\chi$ (Goldstone)	0	Retained low-energy condensate mode	A/B
0	$\sigma$ (radial)	0	Radial condensate oscillation	A/B
<i>Level 1: compact phase fibre (<math>U(1)</math> bundle)</i>				
1	Photon	1	$U(1)$ phase gauge boson	A
<i>Level 2: electroweak condensate (<math>v_2 = 246 \text{ GeV}</math>)</i>				
2	$W^\pm$	1	$SU(2)$ gauge + EW breaking	B+
2	$Z^0$	1	$SU(2) \times U(1)$ mixing	B+
2	Higgs ( $H$ )	0	Radial mode of doublet	B+
<i>Level 3: colour extension (scenario <math>\beta</math>)</i>				
3	8 gluons	1	$SU(3)_c$ internal symmetry	B

The additional condensate scalar sector retained in the present ECT formulation is not expected to show up in standard collider searches. The ultra-light  $\chi$ -mode, if present, should be sought primarily

through gravitational and cosmological signatures, whereas the heavy radial mode  $\sigma$  would manifest only indirectly through high-scale or early-Universe effects. The detailed dark-sector role of  $\chi$  remains model-dependent in the current formulation. A dedicated observational analysis lies beyond the scope of the present work.

**Comparison with other unification programmes**

**Table 117:** Comparison of interaction-sector scope.

Framework	Gauge sector	Gravity	Parity viola- tion	Additional pre- dictions
Standard Model	Postulated	Absent	Postulated	—
GUT (SU(5), SO(10))	Simple group	Absent	From repre- sentations	Proton decay
String theory	In principle	In principle	Model- dependent	Landscape
Loop quantum gravity	Not addressed	Derived	Not ad- dressed	Area spectrum
Einstein–aether	Not addressed	Postulated $n_\mu$	Not ad- dressed	Preferred-frame effects
ECT	Common origin (A/B)	Derived	Structural (B+)	Director cou- pling, $\chi$ -mode, $\sigma$ -mode

ECT is broader in scope than a conventional simple-group GUT, because it also addresses gravity, parity violation, and a fifth interaction channel within the same framework. Its notion of unification is structural/pre-geometric rather than simple-group theoretic.

**The common-origin claim**

ECT provides a common pre-geometric origin for gravity, an inevitable Abelian gauge sector, a structurally selected chiral weak sector, and a generic director coupling. Under the structural completion of the colour sector (Section 40), the four known interactions share a common microscopic origin within one condensate framework.

The present results concern the origin of the gauge architecture. They do not yet amount to a full derivation of the observed matter representations, charge assignments, anomaly cancellation, or the Weinberg angle. These belong to the open programme below.

**Open problems toward quantitative unification**

**Table 118:** Open problems toward quantitative unification.

ID	Problem	Status
OP-GUT1	Intrinsic derivation of $SU(3)_c$ from condensate structure (algebraically impossible from $O(4)$ alone; requires extended internal structure). Reframed in Part IV under the reverse-engineered postulate P7: the colour sector resides in a separate local complex rank-3 internal module, not inside the condensate (§40).	Reframed
OP-GUT2	Derive fermion representations from condensate	Open
OP-GUT3a	Global EW structure $\rightarrow$ charge lattice; Abelian lattice now established (Theorem 23.1, Level A); EW $\mathbb{Z}_2$ refinement conditional (B)	Partially closed
OP-GUT3b	Derive observed charge assignments of quarks and leptons	Open
OP-GUT4	Relate $\alpha_s$ , $\alpha_{\text{em}}$ , $G_N$ to condensate parameters	Open
OP-GUT5	Three fermion generations; Yukawa hierarchy and flavour closure (CKM mixing, PMNS mixing, CP phases, absolute neutrino spectrum); systematised architecturally in §9.7 under OP-Yukawa / OP-generations local labels	Open
OP-GUT6a	Local triangle anomaly cancellation	Open (consistency test)
OP-GUT6b	Witten $SU(2)$ global $\mathbb{Z}_2$ -anomaly	Open (consistency test)
OP-GUT6c	ECT-native interpretation of the mixed $U(1)_Y$ -gravitational consistency condition in the emergent-graviton setting (§9.5, Layer C)	Open (structural)
OP-GUT7	Weinberg angle $\sin^2\theta_W$ from condensate parameters	Open
OP-GUT8	Director coupling coefficient from micro-physics	Open
OP-GRAV-WEAK	Independent spin-1 connection modes beyond metric sector	Open
OP-TORSION	Propagating torsion in a possible first-order reformulation	Open (speculative)

ID	Problem	Status
OP-Λ3-O1	Verification of condition $H_\Lambda$ on the full quadratic fluctuation operator in the leading ordered-branch sector (Section 15.4); decides whether Theorem 15.3(v) decoupling of Object B is unconditional or transferred to the scalar-hierarchy sector	Open
OP-Λ3-O2	First-principles computation of the infrared coefficient $c_\Lambda$ in $\rho_\Lambda \sim c_\Lambda M_{\text{Pl}}^2 H_0^2$ via the FRW-reduced ordered-branch equations for $Z_q$ and $V_{\text{IR}}(q)$ (Section 15.7)	Open
OP-Λ3-O3	Formal non-renormalization analogue of the Ng–van Dam unimodular-gravity theorem [96, 97] in the emergent unimodular-like setting of ECT (Section 15.5)	Open
OP-Λ3-O4	First-principles derivation of the pseudo-Goldstone mass scale $m_G \sim H_0$ from ECT parameters $(\mu, \lambda, \alpha, \beta)$ ; required to upgrade the Goldstone candidate realization of the IR scaling to a prediction (Section 15.9)	Open
OP-Λ3-O5	Extension of Theorem 15.3 beyond the leading ordered-branch ansatz $K^{AB} = \beta \delta^{AB} - \alpha n^A n^B$ ; assessment of higher-order corrections to the fixed kinetic-determinant property	Open

In addition to the usual local triangle anomalies (OP-GUT6a), any chiral  $SU(2)$  sector must also be checked for the global Witten  $\mathbb{Z}_2$  anomaly [78], which excludes an odd number of left-handed  $SU(2)$  doublets. This is logically distinct from the local triangle-anomaly constraints and therefore deserves a separate consistency check once the emergent fermion spectrum is fixed (OP-GUT6b).

### Speculative routes (beyond present scope)

Two further routes merit recording as possible future directions, although they lie beyond the present metric–condensate formulation:

1. *Connection degrees of freedom beyond the metric.* A key technical question is whether the oriented connection sector contains independent spin-1 modes beyond those fixed by the metric. If so, these modes could underlie the weak interaction, providing a geometric—rather than internal—derivation of the  $SU(2)_L$  gauge sector (OP-GRAV-WEAK).
2. *Torsion-based reformulation.* A first-order (Palatini-type) reformulation of ECT with independent connection variables may render torsion components propagating. The self-dual torsion sector is a natural candidate for a geometric origin of weak bosons. However, the current metric–condensate formulation does not include independent torsion variables, and this route lies beyond the present scope (OP-TORSION).

## 49 Conclusion

### 49.1 What has been achieved

**Quantitative summary across all sectors.** Table 119 collects the principal numerical outputs of ECT across all three Parts and compares them with available observations.

**Table 119:** ECT quantitative outputs, regime-level consistency checks, and current experimental anchors: complete summary.

System / prediction	ECT value	Observation	Assessment	Part
<i>Macroscopic sector (Part II)</i>				
BTFR slope	4	$3.98 \pm 0.08$	✓	II
$g_0^\dagger$	$1.04 \times 10^{-10}$	$1.2 \times 10^{-10}$	Benchmark	II
MW $\chi^2/N$ (1 par.)	2.95	$\Lambda$ CDM: 6.55	Comparative fit	II
$n_s$ (corridor)	0.96–0.97	$0.965 \pm 0.004$	corridor	II
$ \delta c/c $	$< 10^{-15}$	$< 10^{-15}$	✓	II
$w_0$ (DESI)	−0.83	−0.827	✓	II
$\eta_B$	$9 \times 10^{-10}$	$6 \times 10^{-10}$	$\sim 1.5 \times$	II
CC catastrophe ( $10^{120}$ UV–IR mismatch)	Classical/direct vacuum channel absent in leading ordered-branch sector (Theorem 15.3(iv), §15); zero-derivative loop-vacuum channel conditional on $H_\Lambda$ ; observed IR value treated separately	“Open problem” in standard framework	Object A resolved (Level A); Object B $H_\Lambda$ -conditional; IR value Level C	II
$\rho_{\Lambda,\text{obs}}$ scale	$c_\Lambda M_{\text{Pl}}^2 H_0^2$ $10^{-47} \text{ GeV}^4$	$\sim \sim 10^{-47} \text{ GeV}^4$	Order-of-magnitude match (Level C)	II
<i>Neutrino sector (Part I)</i>				
$M_R^{\text{geom}}$	$2.4 \times 10^{10} \text{ GeV}$	—	Scale observation (C)	I
$y_\nu$ at $M_R^{\text{geom}}$	$4.5 \times 10^{-3}$	—	Natural Yukawa (C)	I
$\theta_{\text{as}}$	$\sim 4.5 \times 10^{-11}$	No sterile signal	Consistency (B/C)	
$\delta H_{\text{ECT}}/H_{\text{osc}}$	$\sim 10^{-8}$ (1 GeV)	PMNS intact	✓ (B)	I
<i>Quantum sector: environmental decoherence (Part III)</i>				
$C_{60}$ ( $10^{-6} \text{ Pa}$ )	Interference	Interference	Regime consistency	III

System / prediction	ECT	Obs.	Assessment	Part
C <sub>60</sub> (10 <sup>-4</sup> Pa)	Marginal	Degradation	Regime consistency	III
Fein 25 kamu	Environmental	Interference	Regime consistency	III
Procopio switch	$V = 0.994 \pm 0.002 \Rightarrow \Gamma_{\text{loop}}^{(\text{exp})} = 0.006 \pm 0.002$	ICO visible	Visibility-based interpretive consistency	III
Jacques delayed-choice	$V \approx 0.94 \Rightarrow \Gamma_{\text{loop}} \approx 0.062$	Visibility retained	Visibility-based consistency	III
Bell/CHSH crossover	$\Gamma_{\text{loop}} = \ln \sqrt{2} \approx 0.347$	<i>Threshold</i>	Toy operational threshold	III
Qubit observation bound	1 bit $\Rightarrow \Gamma_{\text{loop}} \approx 0.25$	<i>Closure</i>	Qubit-model closure	III
<i>Quantum sector: DP-type gravitational decoherence and ECT-specific interpretation (Part III)</i>				
Nanosph. 1 $\mu\text{m}$	$\tau_{\text{grav}} \sim 38 \text{ ms}$	<i>Not tested</i>	DP-type leading scale; ECT-specific origin/subleading corrections	III
Nanosph. 100 nm	$\sim 1 \text{ hr}$	<i>Not tested</i>	DP-type leading scale; ECT-specific origin/subleading corrections	III
Crossover (UHV)	$m \sim 10^{-16} \text{ kg}$	<i>Not tested</i>	Closure-level DP-type crossover; not a unique leading scale	III



System / prediction	ECT	Obs.	Assessment	Part
Casimir analogue response	Conditional 3/2 coefficient for idealised condensate-reflecting boundaries; not a prediction for the standard metallic-plate QED Casimir force	<i>Not tested</i>	ECT-specific only for the condensate-sensitive boundary setup	II/III

The table mixes three categories: (i) direct quantitative matches to existing observations, (ii) regime-level consistency checks in sectors where ECT reproduces the standard open-system predictions, and (iii) genuinely ECT-specific predictions that remain untested. It should therefore be read as a programme summary rather than as a single statistical scorecard.

In this work we have developed the Euclidean Condensate Theory (ECT), in which the Lorentzian spacetime, quantum dynamics, gravitational interactions, gauge and matter sectors, and both phenomena commonly attributed to the dark sector all arise from a single structure: a scalar condensate field  $\Phi$  in four-dimensional Euclidean space with spontaneously broken  $O(4) \rightarrow O(3)$  symmetry. The complete theoretical identity of the framework is captured by the foundational postulates, branch-selection rules, and signature relations summarised in Section 10; the derivation chain is mapped in Figure 45 and Table 72.

The central conceptual achievement is a unified derivational architecture—from one medium and six postulates—for structures that standard physics treats as independent inputs: the distinction between time and space (emergent from SSB rather than postulated), general relativity and quantum mechanics (as two branches of one ordered condensate rather than separate theories requiring external reconciliation), gauge interactions (with photon,  $W^\pm$ ,  $Z$ , and Higgs emerging from condensate phase structure at different levels of closure), a new preferred-direction (5th) force suppressed by  $M_{\text{Pl}}$ , the dark-matter phenomenology on galactic and cluster scales (condensate response rather than standard particle dark matter), the late-time accelerated expansion (residual ordered-branch condensate energy, without a separate dark-energy substance), the thermodynamic arrow of time (decoherence-driven entropy growth without postulating fundamental irreversibility), and the Principle of Euclidean Stationarity as a structural selection criterion for persistent quantum configurations. ECT thereby provides structural or closure-level routes into several long-standing foundational problems, including the quantum-gravity interface, the origin of time, the cosmological-constant problem, dark-matter phenomenology, the black-hole information problem, and the measurement problem. A dedicated upgrade layer of Part III further develops, on the gravity-matter interface, a reduced-state architecture in which hybrid-consistency demands are displaced from fundamental law to the reduction map between the full condensate theory and its effective descriptions (Section 28); an architectural operational criterion for gravity-induced-entanglement tests (Section 32); a channel taxonomy of the effective gravitational mediator separating scalar distinguishability from orientation-based candidate entangling structure (Section 33); an infrared framing compatible with BMS-type asymptotic symmetries, gravitational memory, and soft-graviton bookkeeping (Section 35); and a structural mapping of the critical-shell black-hole picture onto the modern islands and quantum-extremal-surface language (Section 36.3), complemented by a compact cross-programme diagnostic summary (Section 36.8). Within the present framework no separate dark-matter particle, no independent cosmological constant, and no quantisation of a pre-existing geometry are required. In that precise sense, the present ECT closure predicts no decisive laboratory particle signal for the galaxy-scale dark-matter channel and no separate dark-energy particle sector to be discovered. The relevant tests are instead gravitational, astrophysical, and cosmological.

A central phenomenological consequence of the present closure is therefore negative. For the galactic mass-discrepancy channel, the theory does not require a standard particle-dark-matter halo, and standard direct-detection strategies are not expected to supply the missing explanation of galaxy-scale phenomenology. Likewise, late-time accelerated expansion is not attributed here to an independent

dark-energy substance, but to ordered-branch background energy of the same condensate. This does not exclude additional condensate excitations or topological dark sectors beyond the present closure, but it does mean that the main galactic and late-time dark-sector signals addressed in this work are not read as evidence for two independent hidden substances.

Several results are already genuinely nontrivial.

More precisely, the negative result on information loss is already fixed at Level A: ECT excludes fundamental information destruction in the full coherent condensate framework. What remains closure-dependent is not the negative result itself, but the constructive strong-field mechanism by which reduced thermality, observer-dependent mixedness, and approximate horizon thermodynamics are realised.

Among the strongest structural results are: the emergence of the ordered Lorentzian branch from  $O(4) \rightarrow O(3)$  symmetry breaking, with  $c_*$ ,  $G_N$ , and the EFT action scale all determined by condensate parameters; the unique macroscopic rank-2 tensor compatible with the broken symmetry pattern (Fierz–Pauli  $\rightarrow$  Einstein–Hilbert as the unique two-derivative closure), with generalised Einstein equations containing the derived preferred-direction / orientation-stress correction built from the ordered vector  $n_\mu$  and the nonlinear closure tensor  $\Theta_{\mu\nu}[n, \phi]$ ; the coherent phase branch with winding sectors, a structural action scale  $S_0$ , and canonical Schrödinger-type dynamics with the uncertainty principle; reflection positivity in Gaussian subsectors and the structural global/reduced unitarity distinction; the exchange-sector topology  $\pi_1(\mathcal{M}_2) = \mathbb{Z}_2$  from  $d_{\text{spatial}} = 3$ , providing a structural route to fermionic statistics; the influence-functional decoherence architecture unifying environmental and gravitational channels, with entropy growth and a Crooks-type fluctuation relation; the unified vacuum-response programme (Casimir 3/2 ratio, Unruh temperature, particle production); the conditional Born-type uniqueness via Gleason’s theorem; entanglement as a structural feature of the ordered medium; the structural exclusion of fundamental non-unitary information destruction; the resolution at Level A of the classical cosmological-constant catastrophe via the emergent unimodular decoupling theorem of Section 15 (fixed  $\sqrt{-\det K^{AB}} = \beta^2/c_*$  from the kinematic constraint  $n^A n_A = 1$  makes the classical baseline  $V(\phi_0)$  inert for local emergent gravity; conditional on the one-line spectral assumption  $H_\Lambda$ , the same fixed kinetic-determinant structure absorbs the zero-derivative one-loop vacuum contribution; no  $10^{120}$  cross-scale cancellation is invoked; the numerical value of  $\rho_{\Lambda, \text{obs}}$  is a distinct Level C determination problem with natural scaling  $\rho_\Lambda \sim c_\Lambda M_{\text{Pl}}^2 H_0^2$ ); and the analogue-laboratory instantiability of the full ordered-medium logic.

**Core conceptual achievements.** Several outputs of ECT are not reproductions of known results but qualitatively new conceptual positions: the effective metric is derived, not fundamental—geometry is secondary, condensate structure is primary; three logically distinct classes of excitations replace the uniform field-postulate structure of QFT; the axioms of standard QM are relocated from postulates to reconstruction targets; event-like interaction is emergent—in the coherent branch, subsystems are related by common-medium correlation, not by causal exchange; the parity asymmetry of the weak sector is structurally motivated from SSB geometry (Level B); and Fock space is a reconstruction target, not a foundational axiom.

**Distinctive quantitative handles.** Gravitational decoherence is derived from condensate dynamics without the Diósi–Penrose postulate; the nanosphere scale  $\tau_{\text{grav}} \sim 38$  ms is a testable DP-type leading scale, whose ECT-specific content is its condensate-origin interpretation and the predicted pattern of subleading condensate-sector corrections. A recoherence suppression law  $P_{\text{back}}/P_{\text{fwd}} = e^{-\Gamma_{\text{loop}}}$  is predicted; standard QM provides no analogous relation.

**Neutrino sector.** ECT does not yet close the flavour programme but already provides a structurally non-trivial neutrino framework. The geometrically one-chiral weak route (Level B) naturally interprets opposite-chirality neutrino states as hidden/sterile remnants of the decoupled branch. Pure Planck-suppressed masses are quantitatively insufficient (Level B/C), and an embedded heavy-sterile seesaw is the structurally preferred completion (Level C). The ECT-motivated geometric-mean anchor  $M_R^{\text{geom}} =$

$\sqrt{\phi_0 v_2} \approx 2.4 \times 10^{10}$  GeV yields atmospheric-scale masses for an ordinary Yukawa coupling  $y_\nu \approx 4.5 \times 10^{-3}$ , with a heavy sterile sector effectively invisible in oscillation experiments ( $\theta_{as} \sim 10^{-11}$ ). Standard PMNS/MSW phenomenology remains intact at leading order (Level B), and neutrinoless double-beta decay is the central discriminator of the preferred Majorana branch. Full flavour closure—generations, textures, PMNS angles, phases, mass ordering—remains open.

**Foundational questions of physics addressed by ECT.** Beyond its technical outputs, ECT provides structural routes into several long-standing foundational questions that standard physics leaves unanswered: (i) *Why 3 + 1 dimensions?*—given the P1 postulate of a four-dimensional Euclidean arena, the  $O(4) \rightarrow O(3)$  ordered branch singles out exactly three spatial directions and one temporal seed; the deeper origin of four-dimensionality itself remains OP0. (ii) *Why no magnetic monopoles?*— $\pi_2(S^3) = 0$  is a strict topological anti-prediction (Level A), resolving a long-standing tension with GUT frameworks that generically predict monopoles. (iii) *Vacuum stability*—the primary ordered condensate satisfies  $V''(\phi_0) > 0$  at tree level, and the one-loop RG analysis of the strict scalar closure confirms that  $\beta_\lambda > 0$  prevents the Standard-Model-type high-field metastability channel from arising in the primary amplitude sector (§8.4.5; Level B). The minimal primary potential contains no Coleman false vacuum:  $\Phi = 0$  is a hilltop, not a metastable minimum. The inheritance of this stability by the electroweak secondary sector remains open as part of the second-transition programme. (iv) *Quantum gravity without primitive metric quantisation*—gravity is treated as a condensate response rather than as a fundamental geometric field; the graviton is a candidate condensate excitation on a fixed Euclidean background. This reframes the usual perturbative non-renormalisability problem of quantised GR, but does not yet prove UV finiteness or perturbative renormalisability of the full ECT quantum sector (architecture; UV completion open). (v) *Cosmological coincidence*—the present ECT thawing benchmark does not materially widen the order-unity matter-to-dark-energy window relative to  $\Lambda$ CDM; ECT reframes the question by replacing a rigid external  $\Lambda$  with a dynamical condensate amplitude tied to the same framework that generates  $G_N$ ,  $c_*$ , and  $\hbar$ , but a genuine dynamical solution of the coincidence problem remains open (reframing only; Open). (vi) *Massless spin-2 sector*—the induced effective-metric sector admits a massless spin-2 interpretation at the linearised Fierz–Pauli level, with  $m_g = 0$  protected within that effective gauge description. A non-perturbative proof of exact graviton masslessness from the bare condensate action remains open (Level A/B for the linear EFT reconstruction; full completion open), consistently with the LIGO bound  $m_g < 1.2 \times 10^{-22}$  eV. Table 120 collects the distinctive outputs and foundational questions in one place.

**Table 120:** Distinctive achievements of ECT and foundational questions addressed.

Problem / Achievement	ECT mechanism	Level	Unique to ECT?
<i>Core conceptual achievements</i>			
Metric derived, not fundamental	Geometry is secondary; condensate order is primary	A/B	Yes
Three logical classes of particles	Required / embedded / topological tiers, unlike QFT	A/B	Yes
QM axioms $\rightarrow$ reconstruction targets	Hilbert space, Born rule, collapse all reconstructed	A/B–Open	Yes
Interaction = Lorentzian concept	Coherent branch: common-medium correlation, not events	A	Yes
Chirality from SSB geometry	Parity asymmetry as imprint of $O(4) \rightarrow O(3)$	B	Yes
Discrete-symmetry architecture	$P, T, C$ , conditional CPT route via OS reconstruction; branch-pair layer on $S^3$ ; $\mathcal{L}_5$ re-classified as CPT-odd phenomenological operator	A/B	Yes (ECT-native)

Problem / Achievement	ECT mechanism	Level	Unique?
Anomaly architecture	EW anomaly constraints inherited; $\mathcal{L}_5$ anomaly-transparent; full SM completion open	A/B/Open	Consistency bridge to OP-GUT6
Flavour architecture	CKM / PMNS systematisation via overlap + seesaw; CP phases live in the effective Yukawa / Majorana sector; near-alignment makes FCNC suppression natural; flavour is anomaly-decoupled	B/Open	Consistency bridge to OP-Yukawa
Fock space as reconstruction target	Variable $N$ = condensate reconfiguration	Open	Yes (conceptual)
<i>Foundational questions addressed</i>			
Why 3+1 dimensions?	$O(4) \rightarrow O(3)$ : 3 spatial + 1 temporal; conditional on P1 (4D Euclidean arena postulate); deeper origin of four-dimensionality = OP0	A (conditional on P1)	Yes (structural)
Why no monopoles?	$\pi_2(S^3) = 0$ ; GUT predicts them	A	Yes (anti-prediction)
Vacuum stability (primary sector only)	Tree-level local + one-loop amplitude-sector stability (Level B, §8.4.5); no Coleman false vacuum in minimal potential; full branch-architecture and EW-inheritance analysis open	B (amplitude) / Open (branch)	No
Quantum gravity	No metric quantisation; graviton = condensate mode	A/B	Yes (architecture)
Massless spin-2 sector	Linearised effective-metric channel admits Fierz–Pauli massless spin-2 reconstruction; non-perturbative proof from the bare condensate action remains open	A/B; full proof open	Structural
Cosmological coincidence	Dynamical $\Lambda_{\text{eff}}(\phi)$ , not rigid $\Lambda$	B/Open	Reframing
Cosmological-constant catastrophe	<b>Resolved at Level A for the classical/direct vacuum channel:</b> $V(\phi_0)$ is inert for emergent gravity via fixed $\sqrt{-\det K^{AB}} = \beta^2/c_*$ from $n^A n_A = 1$ (Theorem 15.3(iv), Sec. 15); the extension of this decoupling to the zero-derivative loop sector is conditional on $H_\Lambda$ (Theorem 15.3(v)); no direct $10^{120}$ cross-scale cancellation is invoked	<b>A</b> for Object A; $H_\Lambda$ -conditional for Object B	Yes (structural resolution)
$\rho_{\Lambda, \text{obs}}$ numerical value	IR scaling $\sim M_{\text{Pl}}^2 H_0^2$ matches observation at order-of-magnitude; $c_\Lambda = \mathcal{O}(1)$ remains open; a possible pseudo-Goldstone realization exists if $m_G \sim H_0$ and $f_G \sim \bar{M}_{\text{Pl}}$ (Sec. 15.9)	C	Yes (Level C estimate)

Problem / Achievement	ECT mechanism	Level	Unique?
<i>Distinctive quantitative predictions</i>			
Gravitational decoherence	DP-type leading scale $\tau \sim 38$ ms for micron nanospheres; ECT-specific content is condensate-origin interpretation, no free collapse scale, and possible subleading condensate corrections	B	Distinctive interpretation, not unique leading scale
Recoherence law	$P_{\text{back}}/P_{\text{fwd}} = e^{-\Gamma_{\text{loop}}}$	B	Yes
No DM particles required in minimal closure	Galactic phenomenology from $\phi$ -branch without independent DM sector	B	Minimal-closure prediction
$w_0 \approx -0.83$	Condensate residual energy	B	Testable by DESI/Euclid
5th force: $\eta \sim 10^{-15}$	Fermion–condensate coupling	B	Testable by MICROSCOPE-2
$m_{\text{cross}}$ grav./env. crossover	$m \sim 10^{-16}$ kg at UHV	B	Yes

On the macroscopic side, the galactic  $\phi$ -branch closure  $g(R) = \frac{1}{2}(g_N + \sqrt{g_N^2 + 4g_N g_\dagger})$  captures flat rotation curves, the RAR, and the BTFR (algebraic slope 4) with  $g_\dagger \sim cH_0/(2\pi) \approx 1.1 \times 10^{-10}$  m/s<sup>2</sup>; the cosmological sector admits structural resolution of the classical cosmological problems without requiring a separate inflationary mechanism (Section 14.3), late-time acceleration via  $\Lambda_{\text{eff}}$ , and a route to the Hubble tension; the strong-field critical-shell ansatz produces  $\rho_c = \ell_{\text{Pl}}/\sqrt{3\pi}$  and a structural information-reading programme; and the cluster-merger lensing suite (Bullet Cluster, A520, El Gordo, MACS J0025) is captured at the present benchmark/closure level by a single  $\nu$ -closure rule without invoking collisionless dark matter. The cosmological sector further yields a leptogenesis estimate  $\eta_B \sim 9 \times 10^{-10}$  (within a factor of 1.5 of the observed  $6 \times 10^{-10}$ ) and compatibility with the DESI 2024 dark-energy constraint  $w_0 = -0.827$ . The preferred-direction coupling  $\beta_5 \sim m_f/\phi_0$  predicts a new 5th force with spin precession  $\omega_5 \sim 10^{-10}$  rad/s, Eötvös parameter  $\eta \sim 10^{-15}$  (within reach of MICROSCOPE-2). The Lorentz-invariance violation bound  $|\delta c/c| < 10^{-15}$  from GW170817 is satisfied by construction. The SPARC rotation-curve analysis (165 galaxies) yields  $\chi^2/N$  competitive with MOND; the Milky Way fit gives  $\chi^2/N = 2.95$  (one parameter) versus 6.55 for  $\Lambda$ CDM. The condensate architecture organises three characteristic scales of one field:  $\phi_0 \sim \bar{M}_{\text{Pl}}$  (gravity and quantum),  $v_2 \approx 246$  GeV (electroweak), and  $v_{\text{gal}} \sim \text{kpc}$  (galactic dynamics). At the exploratory benchmark level it also suggests a structured particle sector including a surviving soft scalar mode  $\chi$  (massless in minimal ECT; in optional extensions with additional breaking, a pseudo-Goldstone mass  $m \sim 10^{-33}$  eV is conceivable, though its phenomenological role as a dark-sector component is left open and is not part of the minimal ECT closure) and an exploratory instanton-sector mass pattern ( $m_n = n \times 1.6$  GeV/ $c^2$  in the present benchmark). The full ordered-medium logic is instantiable in analogue-laboratory systems (superfluid helium, BEC, nematic liquid crystals), providing a concrete experimental pathway for testing the SSB→Lorentzian→coherent-branch architecture. A systematic assessment of the observational role of the full nonlinear field equations has been performed across all phenomenological sectors (Table 54), identifying cluster-merger lensing and JWST perturbative growth as the most sensitive probes of the orientation-stress coefficient  $c_1$  (OP-c1).

**Common pre-geometric origin of fundamental interactions.** ECT now supports a hierarchical picture of the interaction sectors (Section 48.13): an inevitable Abelian gauge sector from the compact phase fibre; a structurally selected chiral  $SU(2)$  sector tied to the oriented broken phase and fermionic decomposition; and a colour sector that requires extended internal condensate structure beyond the minimal

$O(4)$ -breaking pattern (algebraically,  $\dim \mathfrak{su}(3) > \dim \mathfrak{so}(4)$ ). Together with emergent gravity and the generic director coupling, ECT provides a common pre-geometric origin of the known interaction sectors. The full Standard-Model matching—matter representations, charge assignments, anomaly cancellation, Weinberg angle—remains an open programme (Table 118).

These results do not yet constitute a final derivation of all known physics, but they already exclude classes of interpretation that would otherwise remain admissible.

## 49.2 What remains open

The following central outputs remain Level B or Open: the physical identification  $S_0 = \hbar$  (OP-Q2); the completed observational Schrödinger equation; the full physical Dirac sector beyond the structural spinor route (OP-Q11); the full spin-statistics/Pauli theorem (OP-Q11); the Born rule as an unconditional bare-postulate theorem (OP-Q7); the full Bell-correlator derivation (OP-Q20); the protocol-independent information-decoherence bound beyond the present qubit closure (OP-PES-6); the quantitative reverse-coherence programme for mesoscopic or engineered Lorentzian-to-Euclidean reopening; the full operational Bell programme beyond the present toy visibility threshold; the constructive strong-field shell/interface mechanism needed for an explicit Page-curve computation (OP-Q13); the colour group  $SU(3)$  and the electroweak scale  $v_2$  (a minimal colour completion is proposed in §40); the Yukawa hierarchy, three fermion generations, and  $\alpha_{\text{fs}} = 1/137$  (structural routes identified—overlap/tunnelling suppression, spectral bound-state counting, and emergent gauge normalisation respectively—but explicit computations remain open; see §9.6, §9.6, §7.2, and Appendix Z); the primordial perturbation spectrum  $(n_s, A_s, r)$  without requiring a separate inflationary mechanism (critical-fluctuation route yields  $n_s \sim 0.96$ – $0.97$ , §14.6, but the full derivation remains open); and the full nonlinear gravitational closure at the theorem level.

These directions should be interpreted as identified calculational programmes with concrete numerical targets, not as completed derivations. These limitations are real, mark the current frontier, and are catalogued in Section 48.10. At the present foundational benchmark level, the framework is organised around two condensate inputs,  $\phi_0$  and  $\lambda$ , once the observational identification  $c_* = c$  is imposed, i.e.  $\alpha = 2\beta$  (with the conventional normalisation  $\beta = 1$ ). This statement refers only to the foundational benchmark architecture: several higher-level closures and sector-specific implementations remain Level B or programme-level. Even so, the number of independent benchmark inputs is drastically compressed relative to the combined Standard Model +  $\Lambda$ CDM input set (see §48.8).

**Proton stability as a UV discriminant.** The completed gauge/flavour sector of ECT may realise one of three baryon-number selection-rule patterns (Section 44): full low-energy protection (no low-energy proton-decay channel generated, with leading  $\Delta B = 2$  processes also forbidden); partial protection ( $\Delta B = 1$  forbidden,  $\Delta B = 2$  allowed, proton stable but  $n$ – $\bar{n}$  oscillations and dinucleon decay possible); or generic Planck-suppressed  $\Delta B = 1$  violation ( $\tau_p \sim 10^{41}$ – $10^{42}$  yr for  $C_B = \mathcal{O}(1)$ , an EFT benchmark rather than an ECT-native derived amplitude). All three patterns are consistent with the current Super-Kamiokande limit  $\tau_p > 2.4 \times 10^{34}$  yr [245]. Observation of  $\Delta B = 1$  proton decay in the  $10^{34}$ – $10^{36}$  yr window would exclude the proton-stable branches (Patterns I and II) and strongly disfavour the generic dimension-six Planck-suppressed branch. The structural ECT result is the three-pattern classification itself; future derivation of the gauge/flavour baryon-number selection rules should decide which pattern is realised. Status: Level C, because the result depends on the unresolved gauge/flavour completion and on selection rules not yet derived from first principles.

## 49.3 Final outlook

The fairest conclusion is this: ECT is not yet a finished final theory, but it is already a serious and unusually broad unification programme. Its strength lies in the combination of a common ontological language for quantum and gravitational/macroscale physics, a growing set of Level A structural results, explicit observational and falsifiability targets, and an honest map of what remains closure-dependent or open.

The distinctive feature of ECT is not that it attempts to unify microphysics and macrophysics—many major programmes share that ambition—but that it attempts to connect, in one continuous chain, Euclidean microscopic starting data, spontaneous ordering, emergent Lorentzian structure, gravitational dynamics, coherent phase kinematics, decoherence, vacuum-response phenomena, dark-sector logic, and horizon thermality, with explicit status control at each link. The unfinished steps are now localised, named, and technically attackable.

#### 49.4 Comprehensive map: standard postulates and open problems of physics as ECT consequences

One of the defining features of the ECT programme is the unusual *scope* of its derivational architecture. A large fraction of structures that are treated in standard physics as independent axioms, postulates, empirical inputs, fundamental constants, interpretational puzzles, or long-standing open problems arise in ECT as derived or structurally grounded consequences of a single underlying object—the scalar condensate  $\Phi$  on a four-dimensional Euclidean manifold—together with its spontaneous  $O(4) \rightarrow O(3)$  symmetry breaking and the postulates P1–P6 collected in Section 2.

Table 121 collects the central cases of this derivational scope. It is organised into seven thematic groups: foundations and spacetime, quantum mechanics postulates, fields and particle statistics, the gauge sector, vacuum response and thermodynamics, macroscopic physics and cosmology, and long-standing mysteries and programme-level targets. Entries that are not reinterpretations of standard postulates or open problems but genuinely ECT-specific predictions are collected separately in Table 122. For each item the table records its conventional status in standard physics, the ECT origin, and the current Level A/B/C classification maintained throughout the paper. Cross-references point to the sections or appendices where the corresponding derivation is carried out.

Three reading guidelines apply throughout: (i) The table is deliberately not a list of ECT’s “solutions”: many entries are still at Level B or Level C, and this is preserved honestly rather than glossed. The value of the table lies in the range of items that can be located within a single derivational framework, not in uniform strength of the individual entries. (ii) A Level A entry means a strict derivation from the postulates within an explicitly stated EFT closure. A Level B entry means a derivation that requires an additional matching step, closure assumption, or effective-field-theory truncation that is explicitly identified. Level B/C and Level C entries are conditional on still-open completions of the gauge, flavour, or CAR programmes, and their inclusion reflects the existence of a structural route, not its full completion. (iii) Entries that are not themselves relocations of standard postulates but genuine ECT-specific predictions (the fifth coupling, environmental modulation of the galactic critical scale, the Casimir  $3/2$  ratio, and others) are collected separately in Table 122, to avoid confusing “ECT reinterprets this standard postulate” with “ECT predicts a new effect not present in standard physics”.

**Table 121:** Comprehensive map of standard postulates and long-standing open problems reinterpreted as ECT consequences. The table is grouped by thematic sector. Status column records the conventional treatment in standard physics; ECT origin gives the structural mechanism in the present framework; Level records the current Level A/B/C classification; § gives the main reference within this paper. Entries at Level B/C and Level C are conditional on still-open completions explicitly identified in the text. The table is not a claim of uniform strength; its value is the range of items that fit within a single derivational framework. ECT-specific predictions with no direct analogue in standard physics are collected separately in Table 122.

Standard physics	Status there	ECT origin	Level	§
<b>Group 1 — Foundations and spacetime</b>				
Lorentzian (−,+,+,+)	signature	Fundamental input	SSB $O(4) \rightarrow O(3)$ with $\alpha > \beta$ selects the hyperbolic ordered branch	A 3

Standard (cont.)	Status	ECT origin	Level	§
Time as a distinguished direction	Fundamental	Emergent distinguished direction $w$ fixed by the gradient-ordered vacuum	A	3
Arrow of time	Open / separate postulate	Retarded propagation of the ordered branch + $\Gamma_{\text{irr}} \geq 0$ from the influence-functional kernel	B	3.8
Second law $dS/dw \geq 0$	Open / empirical	Level-A directional backbone (retarded kernel) + Level-B ohmic/Markov closure	B	3.9
Unique kinetic tensor $K^{AB}$ of the broken phase	Postulated form	Uniqueness theorem under the residual $O(3)$ symmetry: $K^{AB} = \beta \delta^{AB} - \alpha n^A n^B$	A	3
Speed of light $c$	Fundamental constant	$c_*^2 = \beta / (\alpha - \beta)$ from the ordered-branch EFT; identification $c_* = c$	A / A–B	3, 5.1
Gravitational constant $G_N$	Fundamental constant	Geometric EFT matching $G_N = c_*^4 / (8\pi M_G^2)$ with $M_G \sim \tilde{M}_{\text{Pl}}$	B	13.4
Planck constant $\hbar$	Fundamental constant	Structural action scale $S_0$ from the coherent-branch loop programme; identification $S_0 = \hbar$	A–B / B	5.6, 21.2
Universal causal cone	Postulate	Single effective metric $g_{\mu\nu}(n)$ inherited by all sectors; symmetric hyperbolicity (Leray–Choquet–Bruhat)	A	12.6
Planck-suppressed propagation corrections	Not guaranteed	Higher-dimension ordered-branch operators may generate photon-sector time-of-flight benchmarks and quadratic GW-sector corrections; the coefficients and operator unification are not fixed in the present closure	B/Open	3.6, 13.8
<b>Group 2 — Quantum mechanics postulates</b>				
Superposition principle	Axiom	Ellipticity of the Euclidean field equation for the coherent branch	A	22.1
Complex Hilbert space structure	Axiom	Reflection-positive reconstruction (OS) for Gaussian broken-phase subsectors	A	23.1
Imaginary unit $i$ in Schrödinger eq.	Axiom	Phase structure under the formal Euclidean–Lorentzian amplitude bridge; emergent complex envelope	A–B	22.1
Schrödinger equation	Axiom / field-theoretic postulate	Klein–Gordon limit of the coherent branch + non-relativistic reduction + emergent complex envelope	B	22.1
Stationary action $\delta S = 0$	Variational axiom	Physical underpinning via PES selection of the decoherence-resistant sector	B	29



Standard (cont.)	Status	ECT origin	Level	§
Canonical commutator $[\hat{q}, \hat{p}] = i\hbar$	Postulate	Canonical structure from phase compactness + coherent-branch Poisson brackets, normalised by $S_0$	A / B	23.3
Uncertainty principle $\Delta q \Delta p \geq \hbar/2$	From CCR axioms	Robertson inequality from canonical structure; $\hbar$ identification via $S_0 = \hbar$	A / B	23.5
Reflection positivity / OS reconstruction	Imposed on field theory	Derived within Gaussian broken-phase subsectors of the ordered branch	A	23.1
Global unitarity (Gaussian regime)	Postulate	Follows from reflection positivity and OS reconstruction	A	23.2
Wavefunction collapse	Postulate	Decoherence at $\Gamma_{\text{loop}} \gg 1$ ; Euclidean-to-Lorentzian effective transition	B	30.1
Born rule $P =  \psi ^2$	Postulate	Quadratic structure traced to RP-defined inner product of the Euclidean condensate measure; conditional uniqueness via Gleason's theorem under (C1)–(C3) + decoherence; full interacting RP closure open	B	30.4
Quantum tunnelling / interference	Wave-mechanical postulate	Two-sided Euclidean boundary dependence of the elliptic field equation	A / A–B	24.1
Quantum entanglement	Interpretational puzzle	Non-factorisable correlations of reduced bipartite states of the common ordered medium	A–B / B	31
Discrete energy levels	Boundary-condition consequence	Phase compactness + PES stationarity select the persistent discrete sector	B	29
<b>Group 3 — Fields, particles, and statistics</b>				
Klein–Gordon equation	Field-theoretic postulate	Quadratic fluctuation dynamics of the ordered broken phase	A	3, 22.1
Clifford algebra $\{\gamma^\mu, \gamma^\nu\} = 2g^{\mu\nu}$	Postulate for fermions	Spinor representation of $\mathfrak{so}(1, 3)$ obtained from the ordered-branch generator continuation	A	24.5
Spinor representation	Postulated for fermionic fields	Spin(3) double cover of the residual $O(3)$ rotation sector	A	9, 24.5
Dirac equation	Postulated fermionic dynamics	Minimal local Lorentz-covariant first-order closure on spinorial excitations of the ordered branch	B (cond.)	24.5
Exchange topology $\pi_1(\mathcal{M}_2) = \mathbb{Z}_2$ in $d=3$	Empirical / by dimension	Topological consequence of $O(4) \rightarrow O(3)$ and $d_{\text{spatial}} = 3$	A	24.4
Pauli exclusion principle	Postulate	Exchange topology + spinor representation + Osterwalder–Schrader reflection positivity; smooth-branch exactness via canonical normalisation (OP-Q21)	A / B	24.4, AW

Standard (cont.)	Status	ECT origin	Level	§
Fermi–Dirac / Bose–Einstein statistics split	Spin–statistics theorem with assumptions	Exchange topology + ordered-branch representation content; full PLZ theorem open (OP-Q11)	B	24.4
Spin discreteness / Stern–Gerlach selection	From $SU(2)$ representation theory	Compact $SU(2)$ as residual rotation sector of the ordered branch; outcome selection via environmental locking	A / B	9, 24.5
Graviton (spin-2, massless, Fierz–Pauli)	Postulated in GR quantisation	Linearised ordered-branch effective-metric perturbation induced by $\delta n^A$	A (lin.) / B	8.5
Absence of fundamental anyons in $d = 3+1$	Not formulated	$\pi_1(\mathcal{M}_2) = \mathbb{Z}_2$ exhausts the exchange classes in the primary branch	A	24.4
<b>Group 4 — Gauge sector</b>				
Photon as $U(1)$ gauge boson	Postulated gauge principle	Compact phase $\theta$ with Noether current and Maxwell-type leading kinetic structure	A–B	7.2
Local $U(1)$ gauge invariance	Postulate	Phase-redundancy structure of the compact coherent branch	A / B	7.2
$SU(2)_L$ electroweak gauge sector	Postulated	$\mathfrak{so}(3) \cong \mathfrak{su}(2)$ algebraic embedding of the residual rotation sector	B / C	7.4
$W^\pm, Z^0$ gauge bosons	Postulated as EW gauge fields	$SU(2)_L$ condensate embedding	C	7.4
Higgs boson	Postulated scalar	Radial mode of the $SU(2)$ condensate in the electroweak embedding	C	7.4
Yukawa couplings	Phenomenological inputs	Structural route via fermion–condensate couplings; hierarchy open	B–C	9
<b>Group 5 — Vacuum response and thermodynamics</b>				
Casimir effect (structural existence)	Vacuum-energy postulate	Coherent vacuum response to imposed boundary conditions	A	25.3
Casimir coefficient at condensate-reflecting boundaries	Not present in QED	Soft-orientation EFT prediction; $3/2 \times$ QED ratio	B	25.3
Unruh temperature $T_U = \hbar a / (2\pi c k_B)$	From QFT in curved spacetime	Euclidean/Rindler coherent-vacuum response via $G_E(X, X')$	A / A–B	25.4
Hawking radiation	Semi-classical GR + QFT	Horizon thermality as a coherent-vacuum response channel of the same unified programme	A–B / B	36
Bogoliubov mode mixing on curved backgrounds	Standard technique	Time-dependent ordered backgrounds with inequivalent mode decompositions	A / B	25.5
Information preservation in black holes	Postulate / open problem	Fundamental non-unitary destruction structurally excluded (Level A); strong-field constructive completion open	A / B	36
Crooks fluctuation theorem	Classical stat-mech result	Gaussian–Markov closure of the condensate influence functional	B	26.4

Standard (cont.)	Status	ECT origin	Level	§
Decoherence as environment-induced effect	Effective description	Structural from the reduced influence functional of the coherent branch	B	26.1
<b>Group 6 — Macroscopic physics and cosmology</b>				
Einstein equations $G_{\mu\nu} = 8\pi GT_{\mu\nu}$	Postulate	Unique rank-2 tensor compatible with broken $O(4) \rightarrow O(3)$ symmetry; Fierz–Pauli to Einstein–Hilbert at linear level	A / B	11
Anisotropic curvature correction $\Theta_{\mu\nu}[n]$	Absent in GR	Derived from the ordered-branch direction-dependent closure	A (lin.) / B	AB
Spatial flatness $k=0$	Observational input	Structural consequence of $\pi_0(S^3) = \pi_1(S^3) = 0$ for the primary vacuum manifold	A	14.1
Absence of primordial monopoles	Requires inflationary dilution	$\pi_2(S^3) = 0$ forbids the primary monopole channel directly	A	8.10
Absence of primordial domain walls / cosmic strings	Requires absence of suitable $\pi_0, \pi_1$	$\pi_0(S^3) = \pi_1(S^3) = 0$	A	8.10
No-phantom bound $w(z) \geq -1$	Not guaranteed	Structural consequence of $\omega(\phi) > 0$ in the $\phi$ -first closure	B	16.1
Late-time accelerated expansion	Cosmological constant $\Lambda$ postulated	Ordered-branch background energy of the same condensate, no separate dark-energy substance	B	16.1
Dark matter as a separate particle substance (galactic scale)	Postulated halo with particle content	Critical $\phi$ -branch closure; no particle dark matter required for the galactic mass discrepancy	B	17, 18.2
Galactic rotation curves	Require particle dark matter halo	Critical $\phi$ -branch closure reproduces rotation-curve phenomenology	B	17
BTFR slope = 4	Empirical fit	Algebraic consequence of the critical $\phi$ -branch closure	A (structural)	17.1
RAR and baseline critical acceleration $g_0^\dagger \approx cH_0/(2\pi)$	Empirical regularity	Baseline consequence of the $\phi$ -closure with identified condensate scale	B	17.1
Baryon asymmetry $\eta_B$	Sakharov conditions + specific model	Ordering-transition out-of-equilibrium environment + benchmark leptogenesis closure	B	16.3
Cluster-merger morphology (convergence peak location)	Depends on collisionless DM assumption	Follows the more compact baryonic component in the $\phi$ -closure	B	17.2
Lensing–growth sector ( $S_8$ , cosmic shear, CMB lensing)	Probe-dependent discrepancy / modified-gravity test sector	Orientation-stress route through $\mu(k, z)$ , $\eta(k, z)$ , $\Sigma(k, z)$ ; quantitative closure open	B–C	13.5, App. OP- $c_1$
<b>Group 7 — Long-standing mysteries and programme-level targets</b>				
Proton stability	Symmetry-protected empirical fact	Three selection-rule patterns conditional on gauge/flavour completion; Pattern III benchmark $\tau_p \sim 10^{41}–10^{42}$ yr	C	44

Standard (cont.)	Status	ECT origin	Level	§
Three fermion generations	Empirical input	Spectral route: bound-state counting at $y = \mathcal{O}(1)$	B–C	9
Fine-structure constant $\alpha_{\text{fs}} = 1/137$	Fundamental constant	Low-energy $\alpha_{\text{fs}} = q^2/(4\pi Z_A)$ with $Z_A^{\text{IR}} \approx 10.9$ ; UV problem recast as electroweak kinetic/mixing target $(Z_B, Z_W, \theta_W)$ ; full closure open	B–C	7.2
Neutrino geometric mass $m_V^{\text{geom}}$	Empirical (not derived in SM)	$v_2^2/\phi_0 \approx 2.5 \times 10^{-5}$ eV from the same condensate pair	B–C	8.9
Right-handed neutrino scale $M_R$	Free parameter in seesaw	$M_R^{\text{geom}} = \sqrt{\phi_0} v_2 \approx 2.4 \times 10^{10}$ GeV	B–C	8.9
Quantum gravity (UV completion)	Open problem	Structurally unified route: graviton as condensate excitation governed by the same $S_0$ ; full closure open	B–C	8.5, 29
Measurement problem	Open problem	Decoherence-based $\Gamma_{\text{loop}}$ criterion + PES + conditional Born rule via Gleason	B	30.1, 29, 30.4
Particle stability (generic)	Empirical / symmetry-protected	PES proximity to the stationary minimally disturbing sector	Open programme	29
Cosmological-constant problem ( $10^{120}$ UV-vs-IR mismatch)	Catastrophic fine-tuning in the standard framework	Classical/direct vacuum channel absent in the leading ordered-branch sector: the fixed kinetic-tensor determinant $\sqrt{-\det K^{AB}} = \beta^2/c_*$ makes $V(\phi_0)$ inert for local emergent gravity (Theorem 15.3(iv), unconditional). The zero-derivative loop-vacuum channel is absorbed only conditional on $H_\Lambda$ (Theorem 15.3(v)). The observed IR value $\rho_{\Lambda, \text{obs}}$ is a separate Level C determination problem with coefficient $c_\Lambda$ still open; a possible pseudo-Goldstone realization exists if $m_G \sim H_0$ and $f_G \sim \bar{M}_{\text{Pl}}$	Object A: Level A; Object B: $H_\Lambda$ -conditional; IR value: Level C	15

**Summary and reading of the table.** From a single scalar condensate in Euclidean four-space and six postulates, ECT derives or structurally recovers the Lorentzian signature, the emergent time direction and arrow of time, the geometric Einstein sector with a derived preferred-direction correction, the Klein–Gordon and Schrödinger limits of the coherent branch, the canonical commutator and uncertainty structure, the superposition principle and Hilbert-space bridge via reflection positivity, a conditional Born-rule route via Gleason’s theorem, the exchange topology  $\pi_1(\mathcal{M}_2) = \mathbb{Z}_2$  underlying the bosonic/fermionic dichotomy and a smooth-branch exactness route for Pauli exclusion, the representation-theoretic route to the Dirac structure, the unified Casimir/Unruh/particle-production/horizon vacuum-response programme, a structural exclusion of fundamental non-unitary information destruction, the  $\phi$ -first closure for late-time cosmology with no-phantom bound and a baseline Hubble mechanism, flat rotation curves and the BTFR/RAR phenomenology without particle dark matter, and the cluster-merger morphology criterion. It also provides structural routes into long-standing open problems (proton stability, three fermion generations, the fine-structure constant, neutrino geometric scales, quantum gravity, and the measurement problem) without claiming that any of those routes is fully closed at the present stage. The inclusion of

quantum gravity in this map should be read in the same disciplined sense as the other B/C entries: ECT supplies a unified structural route and a common condensate architecture, not a completed ultraviolet closure.

The value of Table 121 is not in uniform strength of the entries—several are explicitly listed as Level B or Level C, and this is preserved honestly—but in the range of physical structures that fit within a single derivational framework governed by one underlying object.

## ECT-specific predictions and observational handles

Table 121 collects the cases in which ECT reinterprets structures already present in standard physics. A complementary question is: what genuinely ECT-specific predictions and observational handles emerge once the reinterpreted structures of Table 121 are set aside? Such predictions and handles are collected in Table 122. They are among the sharpest falsifiability channels of the framework, but they do not all have the same logical status. Some rows would directly exclude the corresponding ECT structural closure if observationally refuted; others constrain a closure parameter, an EFT matching coefficient, or an ansatz-level completion. The status of each entry should therefore be read together with the Level column and the explanatory paragraph below the table.

A more detailed observational prediction map, with target experiments and verdict-on-falsification entries, was already given in Table 74 of Part II. The present table provides a compact summary of the genuinely ECT-specific entries, organised by physical sector rather than by observational channel.

**Table 122:** ECT-specific predictions and observational handles that go beyond the reinterpreted map of Table 121. Each row identifies an effect, structural route, ansatz-level completion, or observational handle that is absent, open, or not formulated in standard physics in the same form. The logical status of each entry is indicated by the Level column and should be read together with the explanatory paragraph below the table. Detailed observational targets and falsifier verdicts are recorded in Table 74.

ECT prediction/handle	Content	Observable channel	Level
Fifth force $\beta_5 \sim m_f/\phi_0$	ECT-specific preferred-direction fermion–condensate coupling, species-dependent and Planck-suppressed	MICROSCOPE-2, spin-sensitive Eötvös	B
Environmental modulation of $g_{\text{eff}}^\dagger$	Galactic critical acceleration scale correlated with ambient density	SPARC $\times$ 2MRS/SDSS cross-correlation	B
Topological mass ansatz $m_n \sim n \times 1.6 \text{ GeV}$	Resonance-like structure of candidate topological sector states	LHC / future collider	C
Graviton polarisation: two TT modes in the completed linear closure	If the induced effective-metric sector closes exactly to the Fierz–Pauli form, only the two transverse-traceless tensor polarisations propagate; exact TT projection and ghost-freedom remain open verification tasks	Polarisation decomposition of stochastic GW background	B/Open
Planck-suppressed LIV benchmark	Higher-dimension ordered-branch corrections may generate $\Delta t_{\text{LIV}} \propto \zeta_\gamma EL/(M_{\text{Pl}} c^2)$ ; the unit-coefficient linear photon benchmark is already constrained by Fermi–LAT, so a retained signal requires suppressed EFT matching, sector dependence, or quadratic leading behaviour. The GW-sector estimate remains quadratic and negligible for current sources	Multi-messenger photon/GW/neutrino timing	B/Open
No exact thermality in black-hole evaporation (conditional theorem)	Under unitarity + finite shell + complete evaporation, exact thermality is excluded; deviations structurally required	Late-stage evaporation spectrum (conceptual)	B

ECT prediction/handle (cont.)	Content	Channel	Level
Hubble-shift mechanism from ordered-branch $\phi$ -background	Correlated shift of $H_0$ , age, distance, and growth through a single $\phi_b(z)$ trajectory; retained-band diagnostic-layer extraction yields $\varepsilon \in [0.0296, 0.0376]$ at $1\sigma$ (§16.5)	$H_0$ inferences vs CMB, JWST ages, late-time distance ladder	B
<i>Additional structural and observational handles</i>			
Nanosphere gravitational decoherence crossover	Closure-level mass scale $m_{\text{cross}} \sim 10^{-16}$ kg at which a DP-type gravitational channel would dominate over environmental decoherence; in ECT this channel is interpreted as condensate-sector distinguishability rather than as an independent collapse postulate	Nanosphere interferometry (UHV, $\sim 400$ nm)	B
Variable Newton's constant $G_{\text{eff}}(\phi)$	$G_{\text{eff}} = G_N e^{-\beta\phi}$ : gravitational coupling varies with condensate amplitude; absent in pure GR	Late-time growth of structure, distance-ladder systematics	B
Force-law dimensionality crossover $d_{\text{force}} : 3 \rightarrow 7/3 \rightarrow 2$	Universal acceleration-dependent curve from single-mode $\phi$ -closure; mass-independent	Pointwise $d_{\text{force}}$ from SPARC rotation curves	B
Redshift dependence $g^\dagger(z)$	Critical acceleration scale evolves cosmologically via $\phi$ -background; RAR intercept shift at $z > 0.5$	JWST, SKA high- $z$ kinematic surveys	B
GR screening in dense environments	Chameleon-type screening: $\phi$ -sector frozen in dense regimes, GR fully recovered; no anomaly in Solar System	Cassini, MICROSCOPE-2, LLR	B
Reverse coherence / $O(3) \rightarrow O(4)$ Euclidean segments	Temporary partial recoherences structurally admissible through reverse Euclidean segments; no analogue in standard QM collapse picture	Echo-type and recoherence protocols in quantum optics	B
Indefinite causal order: structural route via reverse Euclidean segments	The ordered-branch two-sided Euclidean structure accommodates indefinite-causal-order protocols without additional postulates; $\Gamma_{\text{loop}}$ degradation criterion	Quantum-switch experiments (Procopio–Walther)	B
JWST early-galaxy enhancement	Correlated age/distance/growth mechanism shifts available formation-time budget; maturity factors derived from same $\phi_b(z)$ as Hubble shift	JWST spectroscopic surveys of $z > 6$ galaxies	B
Modified Poisson equation with orientation stress	Sub-horizon structure-formation modifier: $\nabla^2 \Phi_N = -4\pi G_{\text{eff}} \bar{\rho} \delta - c_1 n^\alpha n^\beta \delta R_{\alpha\beta}$ ; tensor/orientation source of $\mu(k, z)$ , $\eta(k, z)$ , $\Sigma(k, z)$	Lensing–growth consistency tests, including the $S_8$ sector, from Euclid, Rubin, DESI, and CMB lensing	B
CMB quadrupole deficit from horizon-scale suppression	Structural argument via coherent-branch boundary conditions; quantitative $\delta C_2/C_2$ derivation remains open	CMB low- $\ell$ multipole analysis	B/Open

**Reading the ECT-specific prediction table.** The entries in Table 122 are not of uniform maturity. Some entries are structural routes rather than coefficient-level predictions. In particular, photon-sector LIV requires an EFT matching coefficient already constrained by Fermi–LAT, and the absence of extra graviton polarisations is tied to completion of the linear Fierz–Pauli closure. Other entries, such as the preferred-direction fermion coupling  $\beta_5$ , are Level B structural closures whose coefficient pattern can be directly

constrained by the relevant experimental channels. The environmental modulation of  $g_{\text{eff}}^\dagger$  should be read more specifically as a closure-level environmental handle: a null result at the currently targeted level constrains the calibrated response combination  $\gamma 4\pi\bar{\rho}_{\text{m,env}}/U_0''(\bar{\phi}_{\text{env}})$  and the density-only environment ansatz, rather than directly excluding the ordered-branch amplitude mechanism as a whole. Other entries, such as the topological mass ansatz  $m_n$ , are phenomenological ansatz-level predictions at Level C. The table is therefore best read as the falsifiability side of the framework: it identifies observational channels through which ECT can be tested against structural possibilities that are absent or not formulated in standard physics in the same form.

**Closing remark on the two tables.** Taken together, Tables 121 and 122 summarise the two complementary aspects of the ECT programme: the derivational scope that relocates a broad range of standard postulates and open problems into a single condensate-based framework, and the set of distinct predictions through which the framework becomes empirically answerable. Neither is a claim of a finished theory: several entries in both tables are still explicitly at Level B, Level B/C, or Level C, and the corresponding open problems are tracked in Section 38.1 and in the Part-specific status tables. What the two tables do establish is that a single underlying object—the scalar condensate  $\Phi$  on a four-dimensional Euclidean manifold, together with its spontaneous  $O(4) \rightarrow O(3)$  symmetry breaking—supports both a wide derivational map and a concrete experimental exposure.

# Appendices

## A From the Basic Physical Premises of ECT to the Lorentz-Order-Field Programme: Full Derivation Chain

*Status: Level B (phenomenological  $\phi$ -first closure). All derivations in this appendix are within the macroscopic  $\phi$ -branch EFT, not first-principles results from bare P3.*

### A.1 Purpose and scope of this appendix

This appendix presents the complete chain of reasoning that leads from the basic physical premises of ECT to the ordered-branch amplitude programme for galactic phenomenology. Because the proposed mechanism is conceptually unusual and, to our knowledge, has not been developed in this form in the existing literature, we spell out the intermediate branches of reasoning in detail. Our aim is not merely to state the final equations, but to document why certain routes were explored, what made them fail, and why subsequent choices were forced rather than arbitrary.

At each stage we distinguish between:

- results derived from the effective macroscopic ECT action;
- results obtained in the quasistatic scalar–tensor regime;
- one-loop or EFT-supported indications;
- critical-IR hypotheses not yet fully derived from microscopic ECT.

### A.2 Basic physical premises

The ECT framework begins from two physical ideas that together set it apart from other approaches to emergent gravity.

**Premise 1: Lorentzianness is emergent.** The Lorentzian signature  $(-, +, +, +)$  of the spacetime metric is not a fundamental structure but arises from the spontaneous breaking  $O(4) \rightarrow O(3)$  of the Euclidean vacuum. The degree of Lorentzianness is measured by the parameter  $\chi \equiv \alpha - \beta$ , where  $\alpha$  and  $\beta$  are the anisotropic and isotropic stiffness couplings of the condensate action (2.3). When  $\chi > 0$  the  $w$ -direction acquires hyperbolic character and perturbations experience Lorentzian geometry; when  $\chi = 0$  the system is in the Euclidean (symmetric) phase.

**Premise 2: matter reinforces the Lorentzian phase.** Where baryonic mass accumulates, the statistical irreversibility of motion along the emergent time direction increases: thermal fluctuations in a dense medium are overwhelmingly forward-directed, making the vacuum more deeply Lorentzian. Conversely, in matter-free regions the vacuum relaxes toward the symmetric (Euclidean) phase boundary.

These premises are not additional postulates external to ECT; they are the physical motivations from which the mathematical framework was originally constructed. The question addressed in this appendix is: *do these premises, combined with the effective ECT action, produce observable consequences in galactic dynamics?*

The answer involves a sequence of attempts, dead ends, and refinements. We present them in the order in which they were explored.



### A.3 Branch 1: the condensate-amplitude route $u_0(r)$ (discarded)

This subsection establishes three independent no-go arguments showing that the condensate-amplitude variable  $u_0(r)$  cannot serve as the galactic degree of freedom. The conclusions constrain the theory structurally and motivate the  $\phi$ -first closure adopted in Section 17.

*Notational warning.* Throughout this Branch 1 discussion the symbol  $u_0(r)$  denotes a generic ordered-branch scalar amplitude variable with dimension of mass, used here only to reproduce the historical form of the no-go arguments below. This local usage differs from the main symbol table, where  $u_0 = |\langle \partial_A \Phi \rangle|$  has dimension  $\text{GeV}^2$  and the scalar amplitude with dimension  $\text{GeV}$  is denoted  $\phi_0$ . The arguments below concern the scalar amplitude route and would be unchanged under a consistent renaming  $u_0 \rightarrow \phi_0$ .

In this appendix it is important to distinguish the asymptotic ordered-branch amplitude  $u_{0,\infty}$  from the bare-potential vacuum value  $\phi_\infty \equiv \mu/\sqrt{\lambda}$ . The Branch 1 route varies the ordered-branch amplitude  $u_0(r)$ ; the quartic-potential scale  $\phi_\infty$  enters only as the microscopic mass-setting scale in the simplest realisation.

#### A.3.1 Motivation and scope

The gravitational matching derived in the main text (Section 17.1, eq. (13.14)) implies

$$G_{\text{eff}}(X) = \frac{1}{8\pi u_0^2(X) \chi(X)}, \quad \chi(X) \equiv \alpha(X) - \beta(X). \quad (\text{A.1})$$

This immediately suggests two logically distinct possibilities for obtaining a scale-dependent gravitational response:

1. a spatial variation of the condensate amplitude  $u_0(X)$ ;
2. a spatial variation of the ordered-branch amplitude parameter  $\chi(X)$ .

At this stage the matching alone does not privilege  $u_0$  over  $\chi$ . That distinction emerges only after analysing their dynamics:  $u_0$  is a heavy radial mode and cannot carry galactic-scale structure, whereas  $\chi$  is an order parameter and can remain soft near criticality.

The first possibility is the most naive one: since  $G_{\text{eff}} \propto u_0^{-2}$ , if  $u_0(r)$  were smaller in galactic outskirts than near the centre,  $G_{\text{eff}}(r)$  would increase with radius and could, in principle, mimic mass-discrepancy phenomenology.

**Status of this route.** The  $u_0(r)$ -route analysed below is *not* the current gravitational matching chain of ECT; it is a structurally natural but ultimately inconsistent amplitude-route ansatz. The current ECT gravitational logic uses the induced/NLO stiffness chain  $\kappa_n = \mathcal{C}_n u_0^2 \rightarrow M_G^2 \sim \phi_0^2 \rightarrow M_G = \bar{M}_{\text{Pl}}$  (Section 5.1).

The purpose of this subsection is to show that the amplitude route is not merely inconvenient or phenomenologically unfavourable, but *fundamentally inconsistent* with the ECT equations of motion on galactic scales. The failure is generic: it does not depend on any particular profile ansatz, interpolation formula, or fitting strategy.

We present three independent arguments. The first one is decisive; the other two show that the historical difficulties of the  $u_0(r)$  route are not accidental but are symptoms of the same obstruction.

#### A.3.2 Argument 1 (decisive): the radial mode is Planck-heavy

The amplitude  $u_0$  is not an arbitrary background function. It is the *radial mode* of the condensate. In the simplest quartic realisation, the underlying bare scalar potential  $V(\Phi) = -\mu^2 \Phi^2/2 + \lambda \Phi^4/4$  has vacuum expectation value

$$\phi_\infty \equiv \frac{\mu}{\sqrt{\lambda}}. \quad (\text{A.2})$$

To test the amplitude-route hypothesis, write the ordered-branch amplitude as

$$u_0(r) = u_{0,\infty} + \delta u(r), \quad (\text{A.3})$$

where  $u_{0,\infty}$  denotes the asymptotic value of the ordered-branch amplitude. Linearising the radial field equation around the vacuum then yields

$$-\beta \nabla^2(\delta u) + m_\sigma^2 \delta u = J(r), \quad m_\sigma^2 = 2\lambda \phi_\infty^2, \quad (\text{A.4})$$

where  $J(r)$  denotes whatever effective source term baryonic matter induces in the condensate sector.

This is a Yukawa equation. Its Green-function solution has the universal asymptotic form

$$\delta u(r) \propto \frac{e^{-m_\sigma r}}{r}, \quad (\text{A.5})$$

*independently of the detailed shape of the source.*

This already proves the key point: the long-range behaviour of  $u_0(r)$  is fixed by the mass of the radial mode, not by our choice of profile.

For canonical ECT normalisation one has  $\phi_\infty \sim M_{\text{Pl}}$ ,  $\lambda \sim 10^{-2}$ , hence

$$m_\sigma \sim \sqrt{2\lambda} M_{\text{Pl}} \sim 0.14 M_{\text{Pl}}, \quad \xi_\sigma = m_\sigma^{-1} \sim 7 \ell_{\text{Pl}} \sim 10^{-34} \text{ m}. \quad (\text{A.6})$$

Therefore any spatial variation of  $u_0$  is exponentially suppressed beyond roughly the Planck scale.

By contrast, galactic phenomenology would require variation over  $r_{\text{gal}} \sim \text{kpc} \sim 10^{20} \text{ m}$ . Equivalently, one would need  $m_\sigma \lesssim r_{\text{gal}}^{-1} \sim 10^{-27} \text{ m}^{-1} \sim 6 \times 10^{-48} \text{ GeV}$ , which is about **65 orders of magnitude** smaller than the physical radial mass scale of the theory.

This mismatch is fatal. It does not say that a specific ansatz is wrong. It says that *no smooth kpc-scale profile*  $u_0(r)$  can solve the ECT field equation with the physical radial mass  $m_\sigma$ .

The source term  $J(r)$  has been left generic on purpose. The conclusion does not depend on the detailed matter-to-condensate coupling, as long as the radial sector remains governed by a local second-order equation with mass  $m_\sigma^2 = V''(\phi_\infty)$ . At a local massive radial field, the asymptotic behaviour is always Yukawa.

### A.3.3 Argument 2: the profile ambiguity is a symptom, not the core problem

The second argument is weaker logically than the first, but it is important conceptually.

Since  $G_{\text{eff}} \propto u_0^{-2}$ , any assumed  $u_0(r)$  profile directly determines the effective gravitational law. Because the radial field equation does not admit kpc-scale solutions (Argument 1), one is forced into ad-hoc profile choices unrelated to the dynamics. Different profile assumptions produce different effective laws, none of which solves the actual ECT equation of motion. This ambiguity is therefore not the primary objection (which was already given by Argument 1) but a diagnostic symptom of the same underlying obstruction.

### A.3.4 Argument 3: even a hypothetical light $u_0$ -mode would generate an excluded fifth force

Suppose, for the sake of argument, that one somehow evaded Argument 1 and engineered a very light amplitude mode capable of varying over galactic scales. Then a second problem appears immediately.

Because  $G_{\text{eff}} \propto u_0^{-2}$ , the field  $u_0$  would behave as a scalar-tensor mediator coupled directly to the strength of gravity. A light scalar of this kind generically produces an additional long-range force of order gravitational strength. In Brans–Dicke language this corresponds to a scalar-mediated fifth force with order-unity coupling unless one invokes a nontrivial screening mechanism.

Unscreened or weakly screened long-range scalar forces are tightly constrained by Solar-System and equivalence-principle tests, including Cassini ( $|\gamma - 1| < 2.3 \times 10^{-5}$ ) and MICROSCOPE ( $\eta < 10^{-15}$ ). Therefore even a hypothetical successful galactic  $u_0(r)$  profile would still face a severe fifth-force problem.

The  $u_0$ -route is thus doubly obstructed: (i) dynamically, because the radial mode is Planck-heavy; (ii) phenomenologically, because a light amplitude mode would behave as an excluded fifth-force mediator unless additional nonlinear screening were introduced.

### A.3.5 Auxiliary sub-routes

Five alternative sub-routes within the amplitude sector were examined, all failing by many orders of magnitude:

(a) *Soft orientation sector.* In the present scalar-only ECT basis  $Q_A = \partial_A \Phi$ , so the orientation sector is constrained by integrability. At linear order, the orientation fluctuation reduces to one longitudinal soft scalar mode  $\chi$  with  $\pi_i = \partial_i \chi / u_0$  (Appendix I). This mode is long-ranged in the minimal EFT, but its coupling to a static point mass gives a correction proportional to  $1/r^2$  that falls off *faster* than Newton, not slower.

(b) *Brans–Dicke limit.* The perturbation  $\delta G/G \sim r_S/r \sim 10^{-6}/r_{\text{kpc}}$  at 1 kpc — negligible.

(c) *RG running of  $\lambda(\mu)$ .* Over 50 decades:  $\Delta\lambda \sim 10^{-4}$ . Cannot drive  $m_\sigma \rightarrow 0$ .

(d) *One-loop running of  $\beta(\mu)$ .* Correction  $\delta\beta/\beta_0 \sim 10^{-88}$  at galactic scales.

(e) *Non-linear effects.*  $\delta u_0/u_0 \sim 10^{-6}/r_{\text{kpc}}$  — tiny; non-linear corrections are even smaller.

### A.3.6 Conclusion of Branch 1

The condensate-amplitude route fails for reasons that are structural, not cosmetic. The radial condensate mode obeys a Yukawa equation with Planck-scale mass. Therefore it cannot sustain smooth kpc-scale spatial variations. Historical profile choices were not solutions of the ECT equations of motion, but phenomenological substitutes forced by this obstruction. Even if one tried to rescue the route by postulating an anomalously light amplitude mode, one would generically obtain an unacceptable long-range scalar fifth force. Hence the amplitude branch  $u_0(r)$  must be abandoned as the origin of galactic weak-field modifications.

### A.3.7 Why the galactic branch is built on $\chi(X)$ , not on $u_0(X)$

Although the gravitational matching depends on the product  $u_0^2(X)\chi(X)$ , the two factors have very different dynamical status (as already noted in the main text, Section 17.1: “ $u_0$  is treated as approximately constant [...] while  $\chi(X)$  may vary slowly on astrophysical or cosmological scales”). The condensate amplitude  $u_0$  is the heavy radial mode and cannot vary on galactic scales (as demonstrated above), whereas  $\chi = \alpha - \beta$  measures the degree of Lorentz ordering and remains a viable soft field near criticality.

Therefore, on galactic scales one sets

$$u_0(X) \simeq u_{0,\infty} \quad (\text{frozen amplitude on galactic scales}), \quad (\text{A.7})$$

**Interpretation of the asymptotic amplitude.** Here  $u_{0,\infty}$  denotes the asymptotic ordered-branch amplitude; it should not be identified algebraically with the bare vacuum value  $\phi_\infty = \mu/\sqrt{\lambda}$  without an explicit EFT derivation. It follows that

$$G_{\text{eff}}(X) \simeq \frac{1}{8\pi u_{0,\infty}^2 \chi(X)}. \quad (\text{A.8})$$

The only remaining viable source of large-scale variation in the weak-field sector is the ordered-branch amplitude variable  $\phi(X) = \frac{1}{\beta} \ln(u(X)/u_\infty)$  where  $u(X)$  is the ordered-branch amplitude variable used in the present galactic EFT parametrisation.

A possible objection: why not keep working with the product  $u_0^2(X)\chi(X)$  directly? The reason is that  $u_0^2\chi$  is the correct coefficient in the gravitational action, but it is not the most informative dynamical variable. Its two factors have inequivalent physics:  $u_0$  belongs to the heavy radial sector, while  $\chi$  belongs to the soft order-parameter sector. Once the radial branch is shown to be dynamically frozen on galactic scales, the entire nontrivial spatial dependence must be assigned to  $\chi(X)$ .

The transition from the full combination  $u_0^2(X)\chi(X)$  to the reduced galactic variable  $\chi(X)$  is therefore not a matter of convenience but a consequence of scale separation. The radial/amplitude scale  $\phi_0$  is frozen by its Planck-scale mass, whereas  $\chi$  remains the only plausible soft degree of freedom capable of generating kpc-scale modifications of gravity.

Thus the  $\phi$ -framework is not an arbitrary reparametrisation. It is the dynamically surviving branch after the condensate-amplitude route has been excluded.

## A.4 Branch 2: linear scalar–tensor theory of $\chi$

### A.4.1 Motivation

Since the condensate amplitude is too rigid, the next natural candidate is the ordered-branch amplitude parameter  $\chi = \alpha - \beta$  itself. This quantity enters the coefficient of  $R$  in the effective action and is therefore directly linked to the gravitational coupling:  $G_{\text{eff}} = 1/(8\pi M_*^2 \chi)$ . If  $\chi$  is promoted to a dynamical field, the theory becomes a scalar–tensor theory of the Brans–Dicke type.

### A.4.2 Setup and calculation

The effective action reads

$$S = \int d^4x \sqrt{-g} \left[ \frac{M_*^2 \chi}{2} R - \frac{Z(\chi)}{2} (\partial\chi)^2 - U(\chi) \right] + S_m[g_{\mu\nu}]. \quad (\text{A.9})$$

With  $f(\chi) = M_*^2 \chi$ ,  $f'(\chi) = M_*^2$ :

$$\omega_{\text{BD}} = \frac{Z(\chi_\infty) f(\chi_\infty)}{[f'(\chi_\infty)]^2} = \frac{Z_\infty \chi_\infty}{M_*^2}. \quad (\text{A.10})$$

If  $Z_\infty \sim M_*^2/\chi_\infty$  (from the one-loop estimate, Section A.6):

$$\omega_{\text{BD}} \sim 1. \quad (\text{A.11})$$

The post-Newtonian fifth-force parameter is

$$\alpha_{\text{PPN}}^2 = \frac{1}{2\omega_{\text{BD}} + 3} \sim \frac{1}{5}. \quad (\text{A.12})$$

The Cassini spacecraft measurement constrains  $\alpha^2 < 2.3 \times 10^{-5}$  [84]. The linear theory violates this bound by a factor of  $\sim 8000$ .

### A.4.3 Physical interpretation

In a linear scalar–tensor theory, any scalar field that couples to the trace of the energy–momentum tensor through the Ricci scalar mediates a long-range force comparable to gravity. The only way to avoid this is either to make the coupling very weak (large  $\omega_{\text{BD}}$ ) or to introduce a nonlinear suppression mechanism.

In ECT the coupling  $f = M_*^2 \chi$  is *fixed by the condensate matching*:  $\omega_{\text{BD}}$  cannot be freely adjusted. Therefore the linear route is not merely inconvenient; it is experimentally *excluded*.

### A.4.4 Conclusion of Branch 2

A linear scalar–tensor theory of the ordered-branch amplitude parameter is excluded by Solar System tests. The fifth force  $\alpha^2 \sim 1/5$  exceeds the Cassini bound by a factor of  $\sim 8000$ . *Any viable route must involve nonlinearity and/or screening.*

## A.5 Branch 3: geometrically induced coupling and the emergence of $\phi$

The two preceding failures leave a clear requirement: the degree of freedom responsible for galactic modification must be (i) softer than the radial mode, (ii) nonlinearly self-screening, and (iii) geometrically coupled to matter (not through an ad hoc term).

### A.5.1 Choice of variable: $\phi = \ln(\chi/\chi_{\text{vac}})$

Three reasons motivate this choice:

*Reason 1: the observable force.* In the Jordan frame of a scalar–tensor theory with  $f(\chi)R/2$ , a non-relativistic test particle experiences an extra acceleration proportional to  $\nabla \ln f$ . Since  $f = M_*^2 \chi$ :

$$a_{\text{extra}} \sim -\frac{c^2}{2} \nabla \ln \chi = -\frac{c^2}{2} \nabla \phi. \quad (\text{A.13})$$

The physically relevant gradient is  $\nabla \phi$ , not  $\nabla \chi$ .

*Reason 2: matter coupling linearises.* From the quasistatic trace equation (derived below), the leading effective medium potential is  $U_{\text{eff}}(\chi; \rho_m) = U_0(\chi) - A\rho_m \ln \chi$ . In  $\phi = \ln(\chi/\chi_{\text{vac}})$  this becomes  $\tilde{U}_0(\phi) - A\rho_m \phi$ , which is *linear* in  $\phi$ . The matter energy density  $\rho_m$  acts as an external field conjugate to  $\phi$ , exactly as an external magnetic field acts on the magnetisation in ferromagnetism.

*Reason 3: critical regime.* The deep-IR scale-invariant form of the free-energy density is most naturally written as a function of  $Y_\phi = (\nabla \phi)^2$ , because  $\phi$  is dimensionless and  $Y_\phi^{3/2}$  is the unique 3D scale-invariant monomial (Section A.8).

### A.5.2 Derivation of the medium coupling: step by step

We reproduce the key steps with all assumptions made explicit.

**Step 1: field equation for  $\phi$ .** Varying the effective action (13.34) with respect to  $\phi$  and using  $f(\phi) = M_*^2 \chi_{\text{vac}} e^{\beta \phi}$  (so that  $f' = \beta f$ ):

$$\frac{f}{2} R + K(\phi) \square \phi + \frac{K'(\phi)}{2} (\partial \phi)^2 - V'(\phi) = 0. \quad (\text{A.14})$$

**Step 2: trace of effective Einstein equations.** The modified Einstein equations have the trace

$$f R = -\frac{8\pi}{c^4} T + K(\partial \phi)^2 - 4V + 3\square f + \dots \quad (\text{A.15})$$

**Step 3: quasistatic approximation.** *Assumptions made (explicitly):*

- (a) Non-relativistic matter:  $T \approx -\rho c^2$ .
- (b) Quasistatic regime: time derivatives of  $\phi$  negligible ( $\dot{\phi} \ll c|\nabla \phi|$ ).
- (c) Weak gradients:  $K(\partial \phi)^2 \ll |fR|$  and  $3\square f \ll fR$ . This is satisfied when  $|\delta \phi| \ll 1$  locally.
- (d) Galactic regime: in units where  $c = \hbar = 1$ , the local condensate potential contribution must be small compared with the matter energy density sourcing the quasistatic trace equation,

$$V(\phi) \ll \rho_m, \quad \rho_m \equiv \rho c^2.$$

For a representative galactic density  $\rho \sim 10^{-22} \text{ kg m}^{-3}$  one has

$$\rho c^2 \simeq 9 \times 10^{-6} \text{ J m}^{-3} \simeq 4 \times 10^{-43} \text{ GeV}^4,$$

so the required condition is  $V(\phi) \ll 10^{-43} \text{ GeV}^4$ , not  $10^{-4} \text{ GeV}^4$ . In this appendix this should be read as a local weak-potential assumption on the IR condensate sector, not as an automatically satisfied numerical fact.

Under these conditions (A.15) reduces to

$$f R \approx 8\pi \rho_m + 2V \quad (c = \hbar = 1), \quad (\text{A.16})$$

*Physical meaning:* non-relativistic matter produces positive scalar curvature,  $R > 0$ . This is not an assumption but follows from the effective Einstein equations in the quasistatic limit.

**Step 4: homogeneous equilibrium.** Substituting (A.16) into (A.14) in the spatially homogeneous limit ( $\square\phi = 0$ ,  $(\partial\phi)^2 = 0$ ) gives

$$\frac{1}{2}(8\pi\rho_m + 2V) - V'(\bar{\phi}) = 0, \quad \rho_m \equiv \rho c^2. \quad (\text{A.17})$$

Equivalently,

$$V'(\bar{\phi}) - V(\bar{\phi}) = 4\pi\rho_m. \quad (\text{A.18})$$

Under the weak-potential assumption stated above,  $|V| \ll \rho_m$ , this reduces at leading order to

$$V'(\bar{\phi}) \simeq 4\pi\rho_m. \quad (\text{A.19})$$

Defining  $U_0(\phi) \equiv V(\phi) - V(0)$ , the leading quasistatic equilibrium condition is therefore

$$U'_0(\bar{\phi}) \simeq 4\pi\rho_m. \quad (\text{A.20})$$

*Key observation:* at leading order the equilibrium condition has the form  $U'_0(\bar{\phi}) = A\rho_m$  with  $A = 4\pi$ . This coefficient is fixed by the structure of the effective Einstein equations; it is not a free coupling constant. Equivalently, the leading local equilibrium is the minimum of

$$\boxed{U_{\text{eff}}(\phi; \rho_m) = U_0(\phi) - 4\pi\rho_m\phi.} \quad (\text{A.21})$$

Corrections from the retained  $V(\bar{\phi})$  term are subleading under the local weak-potential assumption. In the original variable  $\chi$  the medium term reads  $-A\rho_m \ln \chi$ , confirming that the coupling is logarithmic in  $\chi$  but linear in  $\phi = \ln(\chi/\chi_{\text{vac}})$ .

**Step 5: sign of  $d\bar{\phi}/d\rho_m$ .** Differentiating (A.20) implicitly gives

$$U''_0(\bar{\phi}) \frac{d\bar{\phi}}{d\rho_m} \simeq 4\pi. \quad (\text{A.22})$$

Since  $U''_0(\bar{\phi}) > 0$  at a stable minimum,

$$\boxed{\frac{d\bar{\phi}}{d\rho_m} \simeq \frac{4\pi}{U''_0(\bar{\phi})} > 0.} \quad (\text{A.23})$$

Equivalently, with respect to the SI mass density  $\rho$ ,  $d\bar{\phi}/d\rho = c^2 d\bar{\phi}/d\rho_m > 0$ .

**Physical interpretation.** This result formalises Premise 2. The mechanism is indirect:

$$\rho_m > 0 \xrightarrow{\text{Einstein}} R > 0 \xrightarrow{\phi\text{-eq.}} \bar{\phi}(\rho_m) > \bar{\phi}(0) = 0. \quad (\text{A.24})$$

Baryonic matter creates positive curvature, which through the  $e^{\beta\phi}R$  coupling pushes  $\phi$  upward. The vacuum is driven deeper into the Lorentzian phase. In matter-free regions the vacuum relaxes to  $\phi = 0$ , approaching the critical boundary.

### A.5.3 Derivation of screening

Expanding  $\phi = \bar{\phi}(\rho_m) + \delta\phi$  around the local equilibrium:

$$K(\bar{\phi})\nabla^2\delta\phi - m_\phi^2(\rho_m)\delta\phi = -4\pi\delta\rho_m, \quad (\text{A.25})$$

with effective mass

$$m_\phi^2(\rho_m) = \frac{U''_0(\bar{\phi}(\rho_m)) + 4\pi\rho_m/\bar{\chi}^2}{K(\bar{\phi}(\rho_m))}. \quad (\text{A.26})$$

The term  $4\pi\rho_m/\bar{\chi}^2$  arises from the  $\chi$ -dependence of the trace equation and is always positive. For convex  $U_0$ , both numerator terms increase with  $\rho_m$ . Equivalently, in terms of the SI mass density,  $\delta\rho_m = c^2\delta\rho$ . In the one-loop estimate  $K \propto e^{-\phi/2}$  (Section A.6), which *decreases* at larger  $\bar{\phi}$ , further reinforcing the growth of  $m_\phi^2$ .

The Yukawa range  $\lambda_\phi = 1/m_\phi$  therefore shrinks in dense environments. In the Solar System ( $\rho \sim 10^3 \text{ kg/m}^3$ ),  $\lambda_\phi$  can be far below the AU scale, rendering the fifth force undetectable.

*Physical interpretation.* Screening in ECT means that dense matter holds the vacuum in a deep Lorentzian phase where the amplitude sector is effectively frozen. This is not an external fix appended to save the theory but a direct structural consequence of the ECT action.

**Scope of this appendix block.** The calculations collected in the present appendix explore candidate nonlinear weak-field branches and their EFT consequences. They should be read as analytical branch diagnostics and consistency tests, not as part of the strict structural core already established in the main text.

## A.6 Branch 4: what does one loop actually provide?

*Status: Level B (one-loop EFT estimate).* The coefficient  $a \simeq 1/2$  in  $K(\phi) \propto e^{-a\phi}$  is scheme-dependent and constitutes an open problem (OP-screen).

### A.6.1 Setup

The three orientation modes  $\delta n_i$  ( $i = 1, 2, 3$ ) of the minimal EFT propagate on the anisotropic condensate background with inverse propagator

$$G^{-1}(k) = u_0^2 [\beta k_\perp^2 + \chi k_w^2], \quad (\text{A.27})$$

where  $k_\perp^2 = k_x^2 + k_y^2 + k_z^2$ . If  $\chi(X)$  varies slowly, the one-loop effective action for  $\chi$  is obtained by integrating out  $\delta n_i$  in the Gaussian approximation.

### A.6.2 Calculation of $Z(\chi)$

The kinetic term for  $\chi$  comes from the diagram with two insertions of  $\delta\chi$ . The vertex is  $\delta S/\delta\chi = -(u_0^2/2)(\partial_w \delta n_i)^2$ . In the Fourier representation the two-insertion diagram gives:

$$Z(\chi) \sim N_G u_0^4 \int \frac{d^4 k}{(2\pi)^4} \frac{k_w^4}{[\beta k_\perp^2 + \chi k_w^2]^3}, \quad (\text{A.28})$$

where  $N_G = 3$  is the naive Goldstone-coordinate multiplicity entering the provisional loop counting (this should not be confused with the number of physically independent propagating soft asymptotic modes in the scalar-only integrable basis; see Section 4.3).

*Anisotropic rescaling.* Set  $k_w = \sqrt{\beta/\chi} p_w$ ,  $k_\perp = p_\perp$ . Then:

- Denominator:  $\beta k_\perp^2 + \chi k_w^2 = \beta(p_\perp^2 + p_w^2) = \beta p^2$ .
- Numerator:  $k_w^4 = (\beta/\chi)^2 p_w^4$ .
- Jacobian:  $dk_w = \sqrt{\beta/\chi} dp_w$ .

Collecting factors:

$$Z(\chi) \sim \frac{3u_0^4(\beta/\chi)^2 \cdot \sqrt{\beta/\chi}}{\beta^3} \int \frac{d^4 p}{(2\pi)^4} \frac{p_w^4}{p^6}. \quad (\text{A.29})$$

*Angular average in 4D:*  $\langle p_w^4/p^4 \rangle_{S^3} = 1/8$  (since  $\langle p_A^2 p_B^2 \rangle = (\delta_{AB} + 2\delta_{AB})/(4 \cdot 6) \cdot p^4$  for  $A = B$ ).

*Radial integral:*  $\int_0^\Lambda dp p^3 \cdot p^{-2} = \Lambda^2/2$ .

Combining:

$$Z(\chi) = \frac{3u_0^4 \Lambda^2}{128\pi^2 \beta^{1/2} \chi^{5/2}}. \quad (\text{A.30})$$

*Caveats:*

- The result involves a quadratic UV divergence ( $\Lambda^2$ ), making the numerical coefficient scheme-dependent. The power-law scaling  $Z \propto \chi^{-5/2}$  is more robust.
- The calculation assumes a slowly varying  $\chi$  background (gradient expansion); near the critical point this breaks down (Branch 5).

### A.6.3 Transformation to $\phi$

Since  $\phi = \ln(\chi/\chi_{\text{vac}})$ , we have  $\partial\chi = \chi \partial\phi$  and:

$$\frac{Z(\chi)}{2} (\partial\chi)^2 = \frac{Z(\chi) \chi^2}{2} (\partial\phi)^2 \equiv \frac{K(\phi)}{2} (\partial\phi)^2. \quad (\text{A.31})$$

With  $Z \propto \chi^{-5/2}$ :

$$K(\phi) = Z(\chi) \chi^2 \propto \chi^{-1/2} = \chi_{\text{vac}}^{-1/2} e^{-\phi/2}. \quad (\text{A.32})$$

*Physical meaning:* the kinetic stiffness of  $\phi$  *increases* as  $\phi \rightarrow -\infty$  (approach to the Euclidean phase). The condensate resists changes in the degree of Lorentzianness more and more strongly near the critical boundary.

### A.6.4 Static solution for a spherical source

With  $K(\phi) \propto e^{-\phi/2}$ , the static equation outside a spherical mass  $M$  is

$$\frac{1}{r^2} \frac{d}{dr} \left[ r^2 e^{-\phi/2} \phi' \right] = 0. \quad (\text{A.33})$$

Trying a power-law ansatz  $\phi(r) = Br^\gamma$ :

$$e^{-\phi/2} \approx e^{-Br^\gamma/2}. \quad (\text{A.34})$$

For self-consistency in the regime  $Br^\gamma \ll 1$  (weak-field exterior):

$$r^2 (1 - Br^\gamma/2 + \dots) B\gamma r^{\gamma-1} \approx \text{const}. \quad (\text{A.35})$$

At leading order:  $r^{\gamma+1} = \text{const}$ , so  $\gamma+1=0$ , i.e.  $\gamma=-1$  — standard  $1/r$  falloff. But the next-order correction from  $e^{-\phi/2}$  modifies this. Full analysis shows:

$$\phi(r) \propto r^{2/3}, \quad (\text{A.36})$$

and the extra acceleration is

$$a_\phi = \frac{c^2}{2} \frac{\phi'}{\phi} \cdot \phi = \frac{c^2}{2} \cdot \frac{2/3}{r} = \frac{c^2}{3r}. \quad (\text{A.37})$$

The circular velocity:

$$v^2 = r|a_\phi| = \frac{c^2}{3}. \quad (\text{A.38})$$



### A.6.5 Key result of the one-loop branch

**One-loop result:** the quadratic kinetic sector  $K(\phi)(\nabla\phi)^2$  with  $K \propto e^{-\phi/2}$  produces *flat rotation curves* ( $v = \text{const}$ ).

However, the velocity **does not depend on the source mass**  $M$ :  $v^2 = c^2/3$  for all galaxies.

Therefore: **flat curves but no BTFR** ( $v^4 \propto M$ ). The quadratic kinetic sector alone is *insufficient*.

*Physical explanation.* The field-dependent prefactor  $K(\phi)$  changes the shape of the profile  $\phi(r)$  but not the logarithmic derivative  $\phi'/\phi$ , which is what enters the force law. The mass-dependence drops out because  $\nabla \ln \phi$  is insensitive to the overall amplitude.

### A.6.6 Conclusion of Branch 4

The one-loop analysis is valuable not as a final answer but as a *negative result*: it proves that BTFR requires genuine nonlinearity *in the gradient*, not merely a field-dependent coefficient of  $(\nabla\phi)^2$ . This is a hard constraint that eliminates a large class of models.

## A.7 Branch 5: why nonlinearity is inevitable near criticality

### A.7.1 The gradient expansion breaks down

The effective action is a series in powers of  $|\nabla\phi|$ :

$$\Gamma[\phi] = \int d^3x \left[ \frac{K(\phi)}{2} (\nabla\phi)^2 + \frac{L(\phi)}{3} |\nabla\phi|^3 + \frac{M(\phi)}{4} (\nabla\phi)^4 + \dots \right]. \quad (\text{A.39})$$

The ratio of successive terms:

$$\frac{L|\nabla\phi|^3}{K|\nabla\phi|^2} = \frac{L}{K} |\nabla\phi|. \quad (\text{A.40})$$

If  $L(\phi)/K(\phi) \rightarrow \infty$  as  $\phi \rightarrow -\infty$  (criticality), then the field-dependent transition gradient

$$|\nabla\phi|_{\text{trans}}(\phi) = K/L \rightarrow 0, \quad (\text{A.41})$$

and *any* nonzero gradient drives the system into the nonlinear regime.

### A.7.2 Why $L/K$ grows near criticality

From the one-loop estimate,  $K(\phi) \propto e^{-a\phi}$  with  $a = 1/2$ . Each additional gradient insertion in the effective action involves an extra factor of  $(\partial_w \delta n)^2$  in the Goldstone propagator, contributing an additional power of  $\chi^{-1} = e^{-\beta\phi}$ . Therefore generically:

$$K(\phi) \propto e^{-a\phi}, \quad L(\phi) \propto e^{-b\phi}, \quad b > a > 0. \quad (\text{A.42})$$

The sufficient condition for breakdown is  $b > a$ , i.e.  $L/K \propto e^{-(b-a)\phi} \rightarrow \infty$  as  $\phi \rightarrow -\infty$ .

*Assumption:* the hierarchy  $b > a$  is motivated by the structure of higher-loop contributions but is not yet rigorously proven from a full functional RG calculation. The essential requirement is the hierarchy, not the specific exponents.

### A.7.3 Resolution of the regime-ordering problem

**The problem.** If the transition threshold were a constant  $\phi_*$ , the nonlinear (MOND) regime would activate at *large* gradients (near the source) and the linear (Newtonian) regime at *small* gradients (far away). This is the *opposite* of the observed ordering.

**The solution.** With a *field-dependent* threshold  $|\nabla\phi|_{\text{trans}}(\phi)$ :

- Near matter ( $\phi > 0$ , deep Lorentzian):  $|\nabla\phi|_{\text{trans}}$  is large  $\Rightarrow$  system stays in linear branch  $\Rightarrow$  Newtonian + screening.
- Far from matter ( $\phi \rightarrow 0^-$ , near-critical):  $|\nabla\phi|_{\text{trans}} \rightarrow 0 \Rightarrow$  even weak gradients are nonlinear  $\Rightarrow$  MOND branch.

**Physical interpretation.** The observed ordering (GR near masses, MOND on outskirts) is *guaranteed* by the approach to criticality. Dense matter stabilises the Lorentzian phase and raises the nonlinear threshold; the absence of matter allows the vacuum to relax toward criticality and lowers the threshold. Screening and MOND-like dynamics are two faces of the same mechanism.

## A.8 The critical IR fixed point: why $Y_\phi^{3/2}$

### A.8.1 Scale-invariance argument

After the gradient expansion breaks down, the deep-IR static free energy must be written as a general function  $\mathcal{F}(Y_\phi)$ ,  $Y_\phi = (\nabla\phi)^2$ . At the critical fixed point the free energy is scale-invariant under  $x \rightarrow bx$ .

If  $[\phi] = 0$  (dimensionless order parameter), then:

$$[\nabla\phi] = L^{-1}, \quad [Y_\phi] = L^{-2}, \quad [\mathcal{F}] = L^{-3}. \quad (\text{A.43})$$

For a power-law  $\mathcal{F} \sim Y_\phi^p$ :

$$L^{-2p} = L^{-3} \implies \boxed{p = 3/2}. \quad (\text{A.44})$$

### A.8.2 Robustness and limitations

This argument is *exact* under the stated assumptions: (i) 3D static regime, (ii) local EFT, (iii) dependence only on  $Y_\phi$ , (iv)  $[\phi] = 0$ .

*Possible corrections:*

- If  $\phi$  acquires an anomalous dimension  $\Delta_\phi$ , then  $p = 3/[2(1 + \Delta_\phi)]$ . For an ordered-branch amplitude parameter this correction is expected to be small.
- Non-local terms, logarithmic corrections ( $Y^{3/2} \ln Y$ ), and higher-derivative operators are not excluded but represent sub-leading corrections in the deep IR.

### A.8.3 Physical interpretation

The  $Y_\phi^{3/2}$  form means that at criticality the “cost” of a gradient in  $\phi$  grows *faster* than quadratic. The system resists non-uniformity in the degree of Lorentzianity more strongly than a linear theory would predict. This nonlinear stiffness is what produces the  $1/r$  force law needed for flat rotation curves with the correct mass dependence.

## A.9 BTFR from the critical branch: explicit calculation

### A.9.1 The interpolating equation

Combining the linear and nonlinear branches: (Here  $\rho$  denotes the baryonic mass density, while  $\mathcal{S}_m \equiv G_N \rho / c^2 = G_N \rho_m / c^4$  is the corresponding curvature source. This is distinct from the energy-density notation  $\rho_m = \rho c^2$  used in the local equilibrium balance above.)

$$\nabla \cdot \left[ \mu_\phi \left( \frac{|\nabla\phi|}{\phi_*(\phi)} \right) \nabla\phi \right] = \frac{4\pi G_N \rho}{c^2}, \quad (\text{A.45})$$

with  $\mu_\phi(x) \rightarrow 1$  ( $x \gg 1$ ) and  $\mu_\phi(x) \rightarrow x$  ( $x \ll 1$ ).

### A.9.2 Spherical solution in the deep-MOND branch

For  $\mu_\phi(x) = x$ , integrating (A.45) over a sphere of radius  $r$  enclosing baryonic mass  $M$ :

$$4\pi r^2 \cdot \frac{|\phi'|^2}{\phi_*} = \frac{4\pi G_N M}{c^2}. \quad (\text{A.46})$$

Solving for  $|\phi'|$ :

$$|\phi'|^2 = \frac{G_N M \phi_*}{c^2 r^2}, \quad |\phi'| = \sqrt{\frac{G_N M \phi_*}{c^2}} \frac{1}{r}. \quad (\text{A.47})$$

### A.9.3 Extra acceleration

From (A.13):

$$|a_\phi| = \frac{c^2}{2} |\phi'| = \frac{c^2}{2} \sqrt{\frac{G_N M \phi_*}{c^2}} \frac{1}{r} = \frac{\sqrt{G_N M g_\dagger}}{r}, \quad (\text{A.48})$$

where

$$g_\dagger \equiv \frac{c^2 \phi_*}{4}. \quad (\text{A.49})$$

*Caveat:* the factor 4 arises from the specific normalisation of the source term in the  $\phi$ -equation. The relation between the curvature source coefficient  $4\pi G_N/c^2$  and the kinetic normalisation  $K_0$  involves the one-loop coefficient  $Z(\chi)$ , which is scheme-dependent. The robust result is the *proportionality*  $g_\dagger \propto c^2 \phi_*$ ; the  $\mathcal{O}(1)$  coefficient requires a more careful matching (OP-new-2).

### A.9.4 Circular velocity

For a circular orbit  $v^2/r = |a_\phi|$ :

$$v^2 = r \cdot \frac{\sqrt{G_N M g_\dagger}}{r} = \sqrt{G_N M g_\dagger}. \quad (\text{A.50})$$

Therefore:

$$\boxed{v^4 = G_N M g_\dagger(\phi_{\text{gal}})}. \quad (\text{A.51})$$

The exponent  $v^4 \propto M$  is *exact* within the deep-MOND branch. It follows algebraically from the  $Y_\phi^{3/2}$  structure and does not involve any fitting or interpolation.

### A.9.5 Comparison with the one-loop result

	One-loop	Critical IR
Kinetic form	$K(\phi)(\nabla\phi)^2$	$Y_\phi^{3/2}$
Flat curves?	Yes	Yes
$v$ depends on $M$ ?	No ( $v^2 = c^2/3$ )	Yes ( $v^4 \propto M$ )
BTFR?	<b>No</b>	<b>Yes</b>
Status	One-loop	Critical hypothesis

This comparison demonstrates that the transition from quadratic to  $Y_\phi^{3/2}$  kinetics is not a cosmetic change but qualitatively alters the mass dependence of the force law.

## A.10 Environmental dependence and observational tests

Since  $g_{\dagger}$  depends on  $\phi_{\text{gal}}$ , and  $\phi_{\text{gal}}$  is set by the ambient matter energy density through the equilibrium condition (A.20), a systematic environmental variation is predicted:

$$\frac{\delta g_{\dagger}}{g_{\dagger}} = \gamma \delta \phi_{\text{env}} \simeq \frac{4\pi\gamma}{U_0''(\bar{\phi}_{\text{env}})} \delta \rho_{\text{m,env}}. \quad (\text{A.52})$$

It is useful to write the estimate in dimensionless form,

$$\frac{\delta g_{\dagger}}{g_{\dagger}} \simeq \gamma \left( \frac{4\pi\bar{\rho}_{\text{m,env}}}{U_0''(\bar{\phi}_{\text{env}})} \right) \frac{\delta \rho_{\text{m,env}}}{\bar{\rho}_{\text{m,env}}}.$$

The density contrast  $\delta \rho_{\text{m,env}}/\bar{\rho}_{\text{m,env}}$  equals  $\delta \rho_{\text{env}}/\bar{\rho}_{\text{env}}$  in SI units. A  $\sim 10\%$  environmental modulation follows only for the illustrative closure

$$\gamma \frac{4\pi\bar{\rho}_{\text{m,env}}}{U_0''(\bar{\phi}_{\text{env}})} \sim 10^{-2}$$

combined with a cluster-versus-field density contrast of order 10. Since neither  $\gamma$  nor  $U_0''$  is yet derived from first principles, this number should be treated as an order-of-magnitude target, not as a calibrated prediction. The observed intrinsic scatter in the RAR ( $\sigma \approx 0.13 \text{ dex} \approx 35\%$ ) is consistent with a signal of this order but also includes observational systematics.

**Proposed observational test.** Cross-match the SPARC galaxy sample with large-scale-structure catalogues to assign an environmental density to each galaxy. Extract  $g_{\dagger}$  from individual RAR fits and test for a correlation with local density. A positive correlation would support the environmental-response route of the  $\phi$ -first closure. Absence of correlation at the  $\lesssim 10\%$  level would constrain the calibrated combination

$$\gamma \frac{4\pi\bar{\rho}_{\text{m,env}}}{U_0''(\bar{\phi}_{\text{env}})}$$

and the density-only environment ansatz, rather than falsifying the ordered-branch amplitude mechanism as a whole.

## A.11 Status of all results

**Table 124:** Status of results in the ordered-branch amplitude programme.

Statement	Status	Depends on
$G_{\text{eff}} = 1/(8\pi M_*^2 \chi)$	Derived	ECT action matching
$\phi = \ln(\chi/\chi_{\text{vac}})$ as natural variable	Derived	Force law + coupling structure
$U_{\text{eff}} = U_0 - 4\pi\rho_{\text{m}}\phi$	Leading quasisstatic approximation	Trace equation plus $ V  \ll \rho_{\text{m}}$
$d\bar{\phi}/d\rho_{\text{m}} > 0$	Leading quasisstatic approximation	Stable $U_0$
Screening: $m_\phi^2$ grows with $\rho_{\text{m}}$ (equivalently with SI mass density $\rho$ )	Leading quasisstatic approximation	Convex $U_0$

(continued on next page)

Statement	Status	Depends on
$K(\phi) \propto e^{-\phi/2}$	One-loop	Gradient expansion
$L/K \rightarrow \infty$ near criticality	EFT-supported	$b > a$ hierarchy
Field-dependent threshold resolves regime ordering	EFT-supported	$L/K \rightarrow \infty$
$\mathcal{F} \propto Y_\phi^{3/2}$	Critical hyp.	3D scale invariance, $[\phi] = 0$
BTFR: $v^4 = G_N M g_\dagger$	Consequence	Critical branch
$g_\dagger = g_\dagger(\phi_{\text{gal}})$	Consequence	Field-dependent threshold
$g_\dagger \propto cH_0$ (correct scale)	Structural	Near-critical vacuum; coefficient $\sim 1/6$ from obs.
Environmental modulation of $g_\dagger$	Prediction	$\phi_{\text{gal}}$ depends on $\rho_{\text{env}}$

## A.12 Methodological summary: the tree of branches

The development of the galactic sector did not proceed by free choice among equally acceptable options. Rather, each step was forced by a concrete failure of the previous route:

**Table 125:** Branch selection in the development of the galactic sector.

#	Route	Reason for termination / success
1	Legacy amplitude-route $u_0(r)$ (discarded)	Radial mode Planck-heavy ( $\xi \sim \ell_{\text{Pl}}$ ); 5 sub-routes also fail; legacy $r_0$ -notation belongs only to this rejected branch
2	Linear $\chi$ theory	Fifth force excluded by Cassini ( $\alpha^2 \sim 1/5 \gg 10^{-5}$ )
3	Geometric $\phi$ coupling	✓ <i>Successful</i> : sign proven, screening derived
4	One-loop $K(\phi)(\partial\phi)^2$	Flat curves but no BTFR ( $v$ independent of $M$ )
5	Critical $Y_\phi^{3/2}$	✓ <i>Successful</i> : BTFR + screening + new prediction

This chain of eliminations explains why the final theory is not an arbitrary construction but the endpoint of a constrained development.

## A.13 Final perspective

At this stage the galactic sector of ECT should no longer be described as a mere phenomenological modification of gravity. Nor should it be overstated as a complete first-principles derivation. Its correct status lies in between: it is a physically motivated, internally constrained research programme in which:

1. the relevant galactic degree of freedom is the macroscopic amplitude variable  $\phi$  of the ordered branch;
2. matter stabilises the ordered branch toward its screened Lorentzian/macroscopic regime ( $d\bar{\phi}/d\rho_{\text{m}} > 0$ , equivalently  $d\bar{\phi}/d\rho > 0$  for SI mass density; derived);
3. dense regions screen the scalar sector (chameleon-type, derived);
4. dilute near-critical regions activate a nonlinear infrared branch (strongly motivated by EFT and 3D scale invariance);
5. this branch reproduces the observed galactic scaling laws (BTFR, flat curves, quasi-universal  $g_\dagger$ );

6. and generates a new testable prediction: weak environmental modulation of the MOND acceleration scale.

The principal gap that remains is the bridge between the perturbative (one-loop) regime and the critical IR fixed point. Closing this gap requires a non-perturbative analysis (e.g. functional renormalisation group) of the  $\phi$ -sector near the Euclidean $\leftrightarrow$ Lorentzian transition. This is listed as Open Problem OP-new-1.

## B Background Configuration and Fluctuation Expansion

*Reference from main text: Eq. (2.5) and Section 4.5.*

### Background solution

Condition P4 requires  $\langle \partial_A \Phi \rangle = u_0 \delta_{Aw}$ . The simplest solution is:

$$\Phi_{\text{bg}}(X) = u_0 w + \Phi_*, \quad \Phi_* = \text{const.}$$

Check:  $\partial_A \Phi_{\text{bg}} = u_0 \delta_{Aw}$  for all  $X^A$ . ✓

**Important note.** This background is linear in  $w$  and therefore is not a minimum of the potential  $V(\Phi_{\text{bg}})$  which grows without bound for  $|w| \rightarrow \infty$ . It does not claim to be a stationary point of the bare micro-action P3; it defines the ordered vacuum sector postulated by P4. Physically this is analogous to a gradient condensate in superfluid systems [8].

### Quadratic expansion of the broken-phase EFT

The effective broken-phase action  $S_{\text{eff}}^{\text{broken}}$  expanded around the background:

$$S_{\text{eff}}^{\text{broken}}[\Phi_{\text{bg}} + \varphi] = S_{\text{eff}}^{\text{broken}}[\Phi_{\text{bg}}] + \underbrace{\int d^4X \frac{\delta S_{\text{eff}}^{\text{broken}}}{\delta \Phi} \Big|_{\text{bg}} \varphi}_{=0 \text{ (stationarity by P4)}} + S^{(2)}[\varphi] + O(\varphi^3). \quad (\text{B.1})$$

The quadratic term:

$$S^{(2)}[\varphi] = \int d^4X \left\{ \frac{1}{2} (\partial_A \varphi)^2 + \frac{m_{\text{eff}}^2}{2} \varphi^2 \right\}, \quad (\text{B.2})$$

where  $m_{\text{eff}}^2$  is the EFT mass parameter of the broken phase (not identified a priori with  $V''(\Phi_{\text{bg}})$  of the bare potential).

## C Uniqueness of the Kinetic Tensor $K^{AB}$

*Reference from main text: Theorem 3.2 in Section 3.3.*

### Setup

We seek the most general symmetric rank-2 tensor  $K^{AB}$  satisfying:

- (i)  $K^{AB} = K^{BA}$ ;
- (ii) invariance under  $O(3)$  rotations in the hyperplane  $\{1, 2, 3\}$ ;
- (iii) built locally and algebraically from tensors  $\{\delta^{AB}, n^A\}$ , without additional derivatives, where  $n^A = \delta^A_w$  is the fixed unit vector along the preferred direction.

## Basis decomposition

The space of symmetric rank-2 tensors in  $\mathbb{R}^4$  has dimension 10. Under  $O(3)$  the available background objects generate two  $O(3)$ -invariant symmetric rank-2 structures:  $\delta^{AB}$  and  $n^A n^B$ . Without additional derivatives or pseudo-tensors (Levi-Civita is antisymmetric and excluded), these two span the space of admissible tensors. Hence the most general tensor is:

$$K^{AB} = a \delta^{AB} + b n^A n^B, \quad a, b \in \mathbb{R}.$$

Setting  $a = \beta$ ,  $b = -\alpha$  gives (3.9).

## Connection to the quadratic action

The kinetic term:

$$\frac{1}{2} K^{AB} \partial_A \varphi \partial_B \varphi = \frac{\beta}{2} (\partial_A \varphi)^2 - \frac{\alpha}{2} (n^A \partial_A \varphi)^2, \quad (\text{C.1})$$

which is exactly the action (3.10). ■

See also [249, Ch. 2] and [250].

## D Derivation of the Lorentzian Window

*Reference from main text: Section 3.5.*

### Lower bound: $\alpha > \beta$

From the quadratic action (3.10) the dispersion relation in momentum space:

$$\beta \mathbf{k}^2 - (\alpha - \beta) k_w^2 + m_{\text{eff}}^2 = 0.$$

For  $\alpha > \beta$  the coefficient of  $k_w^2$  is negative, i.e. the operator is hyperbolic along  $w$ —Lorentzian signature. For  $\alpha \leq \beta$  the operator is positive-definite or degenerate—Euclidean signature or loss of causality. The lower bound follows directly from Theorem 3.2 and the requirement of hyperbolicity.

### Upper bound: $\alpha < 4\beta$ (under isotropy assumption)

Assume that at scales  $L \ll \xi_{\text{cond}}$  the orientation variable is isotropically distributed over the four Euclidean directions:  $\langle n^A n^B \rangle = \delta^{AB}/4$ . The averaged kinetic tensor:

$$\langle K^{AB} \rangle = \left( \beta - \frac{\alpha}{4} \right) \delta^{AB}.$$

Positive-definiteness requires  $\beta - \alpha/4 > 0$ , i.e.  $\alpha < 4\beta$ . In  $d$ -dimensional space this reads  $\alpha < d\beta$ ; for  $d = 4$  (postulate P1): upper bound  $\alpha < 4\beta$ .

**Status.** Lower bound  $\alpha > \beta$ —strict consequence of Theorem 3.2 and Lorentzian requirement. Upper bound  $\alpha < 4\beta$ —requires the additional short-distance isotropy assumption; not a strict consequence of the foundational assumptions P1–P4 alone.

## E LIV time-delay numerics

The unit-coefficient benchmark formula for photon time-of-flight delay due to Lorentz-invariance violation follows from Eq. (3.15) by setting  $\zeta_\gamma = 1$ :

$$\Delta t_{\text{LIV}}^{(\zeta_\gamma=1)} = \frac{(\alpha - \beta)}{\beta} \frac{E}{M_{\text{Pl}} c^2} \frac{L}{c} \xrightarrow{\alpha=2\beta, \beta=1} \frac{E}{M_{\text{Pl}} c^2} \frac{L}{c}. \quad (\text{E.1})$$

For general photon-sector matching one multiplies the numerical values below by  $\zeta_\gamma$ . Using  $M_{\text{Pl}} = 1.22 \times 10^{19}$  GeV and  $1 \text{ Gpc} = 3.086 \times 10^{25}$  m, one obtains

$$\Delta t_{\text{LIV}}^{(\zeta_\gamma=1)} \approx 8.4 \times 10^{-3} \left( \frac{E}{1 \text{ GeV}} \right) \left( \frac{L}{1 \text{ Gpc}} \right) \text{ s}. \quad (\text{E.2})$$

Representative values:

$E$ (GeV)	$L$ (Gpc)	Source type	$\Delta t^{(\zeta_\gamma=1)}$ (s)
1	4	Typical GRB	$3.4 \times 10^{-2}$
10	4	Fermi-LAT GRB	$3.4 \times 10^{-1}$
$10^3$	0.4	CTA blazar (TeV)	3.4
$10^4$	0.04	CTA nearby AGN	3.4

The Fermi-LAT constraint from GRB 090510 [251] sets  $M_{\text{QG},1} > 7.6 M_{\text{Pl}}$  for the linear dispersion relation. Therefore the unit-coefficient benchmark  $M_{\text{QG}} = M_{\text{Pl}}$  is already excluded for the same sign and propagation model. In ECT the retained phenomenological statement is not a fixed coefficient-one photon prediction, but the structural possibility of Planck-suppressed higher-dimension propagation effects with sector-dependent matching coefficient  $\zeta_\gamma$ . An instrumental timing precision of  $\sim 10^{-4}$  s over 0.1–1 Gpc corresponds to  $\Delta t/L \sim 3 \times 10^{-29} - 3 \times 10^{-30} \text{ s m}^{-1}$ , although intrinsic source lags dominate the actual astrophysical sensitivity (Fig. 2).

*Reference from main text: Section 3.8, Result A3. Status: Level A in the quadratic Lorentzian sector.*

## Setup

After passing to the effective Lorentzian description (Section 3.6), small fluctuations satisfy:

$$(\partial_t^2 - c_*^2 \nabla^2 + M^2) \varphi(t, \mathbf{x}) = J(t, \mathbf{x}). \quad (\text{E.3})$$

The retarded Green's function:

$$(\partial_t^2 - c_*^2 \nabla^2 + M^2) G_{\text{ret}}(t, \mathbf{x}) = \delta(t) \delta^{(3)}(\mathbf{x}). \quad (\text{E.4})$$

## Fourier representation and pole structure

$$G_{\text{ret}}(\omega, \mathbf{k}) = \frac{1}{(\omega + i0^+)^2 - \omega_k^2}, \quad \omega_k = \sqrt{c_*^2 k^2 + M^2}. \quad (\text{E.5})$$

Both poles  $\omega = \pm \omega_k - i0^+$  lie in the *lower* half-plane.

### Proof that $G_{\text{ret}}(t, \mathbf{x}) = 0$ for $t < 0$

For  $t < 0$  the integrand  $e^{-i\omega t}$  decays for  $\text{Im } \omega \rightarrow +\infty$ , so the  $\omega$ -contour closes in the upper half-plane. Since both poles lie in the lower half-plane, the Cauchy theorem gives:

$$\boxed{G_{\text{ret}}(t, \mathbf{x}) = 0 \quad (t < 0).} \quad (\text{E.6})$$

### Explicit form for $t > 0$

$$G_{\text{ret}}(t, \mathbf{x}) = \theta(t) \int \frac{d^3 k}{(2\pi)^3} \frac{\sin(\omega_k t)}{\omega_k} e^{i\mathbf{k} \cdot \mathbf{x}}. \quad (\text{E.7})$$

The factor  $\theta(t)$  explicitly confirms (E.6).



## What follows and what does not

**Follows (Level A, quadratic sector):** retarded linear-response kernel  $G_{\text{ret}}(t, \mathbf{x}) = 0$  for  $t < 0$ ; causality of the effective linear kernel in broken-phase EFT is strictly satisfied; condition (ii) in the arrow-of-time argument (Section 3.8) applies rigorously in the quadratic sector.

**Superseded by the full symmetric-hyperbolic result:** Appendix F provides the explicit symmetric-hyperbolic reduction that upgrades the present quadratic result to Level A for all perturbations in the Lorentzian ordered branch.

**Does not follow from this appendix alone:** retardedness in defect-core regions or signature-changing domains (OP5); Markovianity, ohmicity, Born rule, Pauli principle, OS reconstruction.

## F Causal propagation for the full nonlinear ECT dynamics: complete symmetric-hyperbolic reduction

*Status: Level A for the full nonlinear dynamics of the single fundamental scalar field  $\Phi$  within the Lorentzian ordered branch, conditional on the Lorentzian signature being maintained ( $\alpha > \beta > 0$ ; Level A from Section 3.4). This appendix provides the explicit symmetric-hyperbolic reduction, verifying all required conditions.*

### Why the “coupled fields” concern does not apply in ECT

One might worry that the full nonlinear ordered branch involves “coupled fields”  $\sigma$  and  $\chi$  (amplitude and orientation fluctuations) whose joint causal structure needs independent verification. This concern does not apply in ECT. In the minimal scalar basis of P3, the only fundamental degree of freedom is the single real scalar  $\Phi$ . The variables  $\sigma = |\partial\Phi| - u_0$  and  $\chi$  are not independent fields: they are derived projections of the single gradient vector  $\partial_A\Phi$ . The full dynamics is therefore governed by a *single quasilinear second-order PDE* for  $\Phi$ . There is no multi-field coupling problem to resolve.

### The equation of motion and its principal symbol

From the broken-phase kinetic action with the unique tensor  $K^{AB} = \beta\delta^{AB} - \alpha n^A n^B$  (Level A, Theorem 3.2), the equation of motion for fluctuations of  $\Phi$  is

$$G_{\text{eff}}^{AB}(\partial\Phi)\partial_A\partial_B\Phi + \text{lower-order terms} = 0, \quad G_{\text{eff}}^{AB} = \beta\delta^{AB} - \alpha n^A n^B. \quad (\text{F.1})$$

This is a *single quasilinear second-order PDE* in  $\Phi$ . Its *principal symbol* is

$$p(\xi) = G_{\text{eff}}^{AB}(\partial\Phi)\xi_A\xi_B = \beta|\xi|^2 - \alpha(n^A\xi_A)^2, \quad (\text{F.2})$$

which is Lorentzian in the ordered branch whenever  $\alpha > \beta > 0$ .

### Explicit symmetric-hyperbolic reduction

**First-order variables.** We introduce the variable

$$U^A := \begin{pmatrix} c_*^{-1}\partial_t\Phi \\ \partial_1\Phi \\ \partial_2\Phi \\ \partial_3\Phi \end{pmatrix}, \quad A = 0, 1, 2, 3, \quad (\text{F.3})$$

where  $c_*^2 = \beta/(\alpha - \beta)$  is the effective propagation speed.

**The reduced first-order system.** Equation (F.1), after the substitution (F.3) and the real ordered-branch parametrisation  $t = w/c_*$ , becomes

$$\partial_t U^0 = c_* (\partial_1 U^1 + \partial_2 U^2 + \partial_3 U^3) + F_0, \quad (\text{F.4})$$

$$\partial_t U^i = c_* \partial_i U^0, \quad i = 1, 2, 3. \quad (\text{F.5})$$

Equation (F.5) is the integrability condition  $\partial_t(\partial_i \Phi) = \partial_i(\partial_t \Phi)$ , rescaled by  $c_*$ .

**Coefficient matrices.** Writing the system as  $\partial_t U + \sum_{k=1}^3 A^k \partial_k U = F$ , the coefficient matrices are

$$A_{ij}^k = -c_* (\delta_{i0} \delta_{jk} + \delta_{j0} \delta_{ik}), \quad k = 1, 2, 3. \quad (\text{F.6})$$

Explicitly:

$$A^1 = -c_* \begin{pmatrix} 0 & 1 & 0 & 0 \\ 1 & 0 & 0 & 0 \\ 0 & 0 & 0 & 0 \\ 0 & 0 & 0 & 0 \end{pmatrix}, \quad A^2 = -c_* \begin{pmatrix} 0 & 0 & 1 & 0 \\ 0 & 0 & 0 & 0 \\ 1 & 0 & 0 & 0 \\ 0 & 0 & 0 & 0 \end{pmatrix}, \quad A^3 = -c_* \begin{pmatrix} 0 & 0 & 0 & 1 \\ 0 & 0 & 0 & 0 \\ 0 & 0 & 0 & 0 \\ 1 & 0 & 0 & 0 \end{pmatrix}. \quad (\text{F.7})$$

**Verification of symmetric hyperbolicity.**

1. **Symmetry:**  $(A^k)^T = A^k$  for all  $k = 1, 2, 3$ , by direct inspection of (F.7).
2. **Time matrix positivity:** the “time matrix” is the identity  $A^0 \equiv I_4$  (Level A). Positive definiteness is immediate.
3. **Characteristic cone:** the condition  $\det(\omega I_4 + \sum_k \xi_k A^k) = 0$  gives  $\omega^2 = c_*^2 |\vec{\xi}|^2$ , which is the Lorentzian light-cone condition. This coincides with the causal cone of the Lorentzian effective metric (Level A).

All three conditions of the Leray–Choquet–Bruhat definition are satisfied.

For the nonlinear case, the matrices acquire dependence on  $\partial\Phi$  through  $c_* = c_*(|\partial\Phi|)$ , but remain symmetric and the identity remains the time matrix as long as  $c_* > 0$ , i.e. as long as the Lorentzian condition  $\alpha > \beta$  holds.

## The Level A result

By the Leray–Choquet–Bruhat theorem for symmetric hyperbolic systems [17, 18], the system admits:

1. a well-posed Cauchy problem (local-in-time);
2. causal propagation within the characteristic cone;
3. a retarded Green’s function satisfying  $K(\tau < 0) = 0$  for the full nonlinear dynamics.

$K(\tau < 0) = 0$ for the full nonlinear ECT dynamics of $\Phi$ in the Lorentzian ordered branch. (Level A.)
--

(F.8)

Since the scalar-sector derived variables ( $\sigma$ ,  $\chi$ , and branch-amplitude descriptions such as  $\phi$ ) are projections of the single fundamental scalar  $\Phi$ , this causal result extends directly to those derived scalar-sector descriptions within the smooth Lorentzian ordered branch. No claim is made here about later effective gauge embeddings or non-scalar structural sectors beyond the scalar-only ECT basis.

## Scope and limitations

**Level A holds throughout** the domain where:

1.  $\alpha > \beta > 0$  (Lorentzian signature; same Level A condition as Section 3.4);
2. initial data are sufficiently regular (defect-free, smooth condensate background).

**Not claimed here:**

- global-in-time existence (beyond local);
- causal structure in defect cores where  $|\partial\Phi| \rightarrow 0$ ;
- the ohmic/Markov assumptions, which remain Level B.

## Relation to Appendix E

Appendix E proved  $K(\tau < 0) = 0$  in the *quadratic* sector by contour integration. The present appendix is strictly stronger: it proves the same result for the *full nonlinear* dynamics. The quadratic result is the special case of the present theorem obtained by linearising  $c_*(|\partial\Phi|) \approx c_*$ .

## G Directed decoherence: proof that $\Gamma_{\text{irr}}[q, q'] \geq 0$

*Reference from main text: Section 3.8, Result A5. Status: Level A in the quadratic Lorentzian sector. Does not require the ohmic or Markovian assumptions. The proof uses (i) the retarded structure of the ordered Lorentzian branch, established at Level A, and (ii) nonnegative spectral density. In the open-system reduction adopted here, the retarded structure is encoded by a causal response kernel  $K(\tau < 0) = 0$ . A full first-principles derivation of this identification from ECT microdynamics remains open (OP1, OP5).*

### Setup

After passing to the effective Lorentzian description of the ordered branch, a coherent subsystem with collective coordinate  $q(t)$  interacts with the remaining condensate modes (the environment). After integrating out the environment, the reduced description takes the Feynman–Vernon influence-functional form [19, 23]:

$$\mathcal{F}[q, q'] = \exp \left\{ \frac{i}{S_0} \int_0^T dt \int_0^T dt' \Delta q(t) D_R(t-t') \Sigma q(t') - \frac{1}{S_0} \int_0^T dt \int_0^T dt' \Delta q(t) D_I(t-t') \Delta q(t') \right\}, \quad (\text{G.1})$$

where  $\Delta q(t) = q(t) - q'(t)$ ,  $\Sigma q(t) = q(t) + q'(t)$ ,  $D_R$  is the dissipation kernel,  $D_I$  is the noise kernel, and  $S_0$  is the pre-quantum action scale. The irreversible part is the quadratic form

$$\Gamma_{\text{irr}}[q, q'] = \int_0^T dt \int_0^T dt' \Delta q(t) D_I(t-t') \Delta q(t'). \quad (\text{G.2})$$

### Spectral representation of the noise kernel

The noise kernel  $D_I(t)$  is related to the bath spectral density  $J(\omega)$  by [23]:

$$D_I(t) = \frac{1}{\pi} \int_0^\infty d\omega J(\omega) \coth \left( \frac{S_0 \omega}{2T_{\text{eff}}} \right) \cos(\omega t), \quad (\text{G.3})$$

where  $T_{\text{eff}}$  is the effective temperature of the environment. In the ECT vacuum initial state (zero effective temperature),  $\coth \rightarrow 1$  and

$$D_I(t) = \frac{1}{\pi} \int_0^\infty d\omega J(\omega) \cos(\omega t). \quad (\text{G.4})$$

## Positivity of $J(\omega)$

The bath spectral density  $J(\omega)$  is defined by the mode decomposition of the environment:

$$J(\omega) = \pi \sum_k \frac{|g_k|^2}{2\omega_k} \delta(\omega - \omega_k), \quad (\text{G.5})$$

where  $\omega_k$  and  $g_k$  are the frequencies and coupling constants of the environment modes. Each term in the sum is manifestly nonnegative, so

$$J(\omega) \geq 0 \quad \forall \omega \geq 0. \quad (\text{G.6})$$

This requires only that the ordered branch has a non-tachyonic spectrum ( $\omega_k^2 > 0$  for all environment modes), which is guaranteed by the stability of the ordered vacuum. The result holds for *any* spectral shape—ohmic, super-ohmic, or otherwise.

An equivalent route: the spectral density is related to the imaginary part of the retarded response by  $J(\omega) = -\omega \text{Im} G_{\text{ret}}(\omega)/\pi$  for  $\omega > 0$ . From the retarded propagation of the ordered branch (A3), encoded in the open-system reduction as  $K(\tau < 0) = 0$ , and  $\rho(\mu^2) \geq 0$ , the Kramers–Kronig relation gives  $\omega \cdot \text{Im} G_{\text{ret}}(\omega) \leq 0$ , hence  $J(\omega) \geq 0$ . This alternative derivation confirms (G.6) within the broken-phase EFT.

## Positive-definiteness of $D_I$

From (G.4) and (G.6): the Fourier transform of  $D_I(t)$  is

$$\hat{D}_I(\omega) = \frac{1}{2} [J(\omega) + J(-\omega)] \geq 0 \quad \forall \omega. \quad (\text{G.7})$$

(For  $T_{\text{eff}} > 0$ ,  $\hat{D}_I(\omega) = J(|\omega|) \coth(S_0|\omega|/2T_{\text{eff}}) \geq 0$  likewise.) By Bochner’s theorem, a function whose Fourier transform is nonnegative is a positive-definite kernel:

$$\int dt \int dt' f(t) D_I(t-t') f(t') \geq 0 \quad \text{for all real } f. \quad (\text{G.8})$$

## Main result

Choosing  $f(t) = \Delta q(t) = q(t) - q'(t)$  in (G.8) gives

$$\Gamma_{\text{irr}}[q, q'] = \int dt \int dt' \Delta q(t) D_I(t-t') \Delta q(t') \geq 0. \quad (\text{G.9})$$

Equality holds if and only if  $\Delta q(t) = 0$  for all  $t$ , i.e.  $q = q'$ .

Consequently:

$$|\mathcal{F}[q, q']| = e^{-\Gamma_{\text{irr}}/S_0} \leq 1, \quad |\mathcal{F}[q, q']| = 1 \Leftrightarrow q = q'. \quad (\text{G.10})$$

## What follows and what does not

### Follows (quadratic sector):

- $\Gamma_{\text{irr}}[q, q'] \geq 0$  for any bath with  $J(\omega) \geq 0$ .
- $|\mathcal{F}| \leq 1$ : interference between distinct histories is suppressed rather than amplified.

### Does not follow from this theorem alone:

- Monotonicity of  $S_{\text{ent}}(w)$  in time (requires Markov; Section 3.9).
- Impossibility of partial recoherence in non-Markovian environments.
- The explicit formula  $dS/dw = N_{\text{eff}}\gamma(\dot{q})^2$  (requires ohmic + Markov).

- Full H-theorem for the complete nonlinear branch (OP1, OP5, OP-Q17).
- Extension beyond the quadratic sector of the ordered branch.
- A first-principles identification of the effective open-system bath-response kernel from ECT microdynamics, beyond the already established retarded support of the ordered-branch scalar dynamics (OP1, OP5).

## Relation to other appendices

Appendix E establishes retarded propagation in the quadratic ordered-branch sector, i.e. the vanishing of the retarded Green function for negative time separation. Appendix F extends this retarded-propagation result to the full nonlinear dynamics of the ordered-branch scalar field  $\Phi$  via symmetric-hyperbolic reduction. In the open-system reduction used in the present appendix, this retarded structure is encoded by a causal response kernel  $K(\tau < 0) = 0$ . What remains open is the full first-principles identification of this effective bath-response kernel directly from Euclidean microdynamics, especially beyond the scalar smooth ordered branch and without auxiliary closure assumptions (OP1, OP5). Appendix H provides the scaling analysis of the spectral density; it explains why the default is super-ohmic and what additional assumptions lead to ohmic behaviour.

## H Scaling Analysis of the Bath Spectral Density

*Reference from main text: Sections 3.8 and 3.9. Status: scaling analysis; strict derivation deferred to Section 26.1.*

### Spectral density in 3D with linear dispersion

Goldstone orientation modes with  $\omega_k = c_* k$ :

$$J(\omega) \propto N_{\text{eff}} \omega^2 |g(\omega/c_*)|^2 \quad (\text{up to powers of } c_*). \quad (\text{H.1})$$

Scaling regimes:

Coupling	$J(\omega)$ for $\omega \rightarrow 0$	Regime
$ g ^2 = \text{const}$	$\propto \omega^2$	super-ohmic
$ g ^2 \propto k^2$	$\propto \omega^4$	super-ohmic
$ g ^2 \propto k^{-1}$	$\propto \omega$	ohmic

Standard 3D derivative coupling gives a *super-ohmic* contribution  $J(\omega) \propto \omega^4$ , not ohmic. Ohmic behaviour requires either a non-standard coupling form, a reduced effective bath dimensionality, or additional coarse-graining.

### Markovian approximation: heuristics

$\tau_{\text{env}} \sim m_\sigma^{-1}$  (bath memory scale from P3 EFT cutoff). Markovianity ( $K(\tau) \approx K(0)\delta(\tau)$ ) requires  $\tau_{\text{env}} \ll \tau_{\text{dec}}$  where  $\tau_{\text{dec}} = 1/(N_{\text{eff}}\gamma)$ . In the weak-coupling, large- $N_{\text{eff}}$  limit this is heuristically consistent with the EFT estimate (5.12), but not a strict derivation.

Both ohmic behaviour and Markovianity are adopted as effective phenomenological working assumptions for the macroscopic decoherence calculation. Strict derivation belongs to Section 26.1.

## I Goldstone sector in scalar-only ECT: integrability, inverse-Higgs reduction, and EFT status

*Status: mixed. Scalar-only microscopic statements are Level A. Reduced soft-orientation EFT statements are Level B. No claim is made that the present ECT basis proves three independent physical Goldstone particles.*

### A. Microscopic starting point

In the present ECT basis the fundamental field is a single real scalar  $\Phi(X)$  on  $\mathcal{M}^4$ . The ordered quantity is therefore not an independent vector multiplet but the exact one-form

$$Q_A \equiv \partial_A \Phi. \quad (\text{I.1})$$

In the ordered branch one writes  $Q_A = u n_A$  with  $u = |Q|$ ,  $n_A n^A = 1$ . However,  $u$  and  $n_A$  are *not independent microscopic variables* because  $Q_A$  is an exact gradient.

### B. Integrability constraint

Exactness of  $Q_A = \partial_A \Phi$  gives identically

$$\partial_A Q_B - \partial_B Q_A = 0. \quad (\text{I.2})$$

Substituting the decomposition:

$$\partial_A (u n_B) - \partial_B (u n_A) = 0. \quad (\text{I.3})$$

This is the integrability condition constraining the orientation sector. The ordered branch in scalar-only ECT is *not* equivalent to a generic unconstrained  $O(4)/O(3)$  sigma model.

### C. Linearised broken phase

Take uniform ordered background  $Q_A^{(0)} = u_0 \delta_{Aw}$  and write  $\Phi(X) = u_0 w + \chi(X)$ , so  $\delta Q_A = \partial_A \chi$ . In the  $u n_A$  language with  $u = u_0 + \sigma$ ,  $n_A = (\pi_i, 1) + \mathcal{O}(\pi^2)$ :

$$\delta Q_i = u_0 \pi_i, \quad \delta Q_w = \sigma. \quad (\text{I.4})$$

Comparing with  $\delta Q_A = \partial_A \chi$  gives the exact linear relations

$$u_0 \pi_i = \partial_i \chi, \quad \sigma = \partial_w \chi. \quad (\text{I.5})$$

Hence the apparent orientation triplet is determined by a single scalar  $\chi$ .

### D. Immediate consequences

Equation (I.5) implies

$$\pi_i = \frac{1}{u_0} \partial_i \chi, \quad (\text{I.6})$$

so the linearised orientation fluctuation is purely longitudinal:

$$\varepsilon_{ijk} \partial_j \pi_k = 0. \quad (\text{I.7})$$

At linear order, one independent longitudinal soft scalar mode  $\chi$  survives in the scalar-only broken phase.

## E. Relation to inverse-Higgs reduction

This reduction is the inverse-Higgs phenomenon [30, 31] for spacetime symmetry breaking. The broken object  $Q_A = \partial_A \Phi$  is a geometric gradient field, not an internal multiplet. The broken-generator counting for  $O(4) \rightarrow O(3)$  gives three, but the integrability condition (I.3) eliminates two of them as independent propagating modes.

## F. Minimal soft-orientation EFT

One may still organise the broken branch through a minimal orientation EFT on  $O(4)/O(3) \simeq S^3$ . In that effective description the effective stiffness is

$$\kappa_n = \mathcal{C}_n u_0^2 \quad (\text{Level B, EFT identity}), \quad (\text{I.8})$$

where  $\mathcal{C}_n$  is an effective coefficient with dimension  $\text{mass}^{-2}$ , not yet derived from P1–P6 (Theorem 3.1; OP-Planck). After the reduction  $\pi_i = \partial_i \chi / u_0$ , the dispersion of the surviving mode is

$$\omega^2 = c_\chi^2 k^2, \quad c_\chi^2 = \frac{K_s}{K_w} c_*^2 \quad (\text{Level B}). \quad (\text{I.9})$$

The statement  $c_\chi = c_*$  remains open.

## G. Status summary

Statement	Status	Comment
$O(4) \rightarrow O(3)$ from ordered background	A	Background geometry
$Q_A = \partial_A \Phi$ implies integrability	A	Exact scalar-only
$\pi_i = \partial_i \chi / u_0$ at linear order	A	Longitudinal reduction
One independent soft mode $\chi$ survives	B	Physical mode at linear level
Minimal 3-component orientation EFT	B	Effective parametrisation
$\kappa_n = \mathcal{C}_n u_0^2$ ; $[\mathcal{C}_n] = \text{mass}^{-2}$	B	NLO/induced EFT identity
$\mathcal{C}_n$ from bare P1–P6	Open	OP-Planck
$\omega^2 = c_\chi^2 k^2$	B	Reduced EFT
$c_\chi = c_*$	Open	Matching not proved
Three physical Goldstone particles	Not established	Reduced by integrability
Dark-matter role of soft sector	Removed	Not needed by ECT

## J Single-field causal universality: detailed proof and comparison with competing frameworks

*Reference from main text: Universality Corollary (§4.3), cone inheritance (§4.7), and comparison with other theories (§3.10). Status: Level A for the scalar ordered branch; Level B structural for the gauge sector.*

### J.1 Theorem: unique causal cone of the linear scalar ordered branch

**Theorem.** *Let  $\Phi$  be the single scalar field of ECT with the ordered-branch EFT satisfying P1–P4. Let  $K^{AB} = \beta \delta^{AB} - \alpha n^A n^B$  be the unique kinetic tensor (Theorem 3.2). Then the characteristic surface  $\det(K^{AB} \xi_A \xi_B) = 0$  defines a unique causal cone, and all linear soft modes of the ordered branch propagate*

on that cone.

*Proof.*

*Step 1.* From the uniqueness theorem (Theorem 3.2, §3.3),  $K^{AB}$  is determined up to two parameters  $(\alpha, \beta)$  by the  $O(4) \rightarrow O(3)$  SSB.

*Step 2.* From integrability (Appendix I),  $Q_A = \partial_A \Phi$  is an exact one-form. At the linear level,  $\delta Q_A = \partial_A \chi$ , so that  $\sigma = \partial_w \chi$  and  $\pi_i = \partial_i \chi / u_0$ .

*Step 3.* The quadratic EFT action becomes

$$S^{(2)} = \frac{1}{2} \int d^4 X K^{AB} \partial_A \chi \partial_B \chi = \frac{1}{2} \int d^4 X [\beta (\partial_i \chi)^2 - (\alpha - \beta) (\partial_w \chi)^2]. \quad (\text{J.1})$$

This is one equation for one field.

*Step 4.* The equation of motion  $\beta \nabla^2 \chi - (\alpha - \beta) \partial_w^2 \chi = 0$  has the characteristic polynomial  $\beta \mathbf{k}^2 - (\alpha - \beta) k_w^2 = 0$ , defining a single cone with speed

$$c_*^2 = \frac{\beta}{\alpha - \beta}. \quad (\text{J.2})$$

Since  $\sigma$  and  $\pi_i$  are derivatives of  $\chi$ , no second independent principal symbol exists.  $\square$

## J.2 Comparison with Einstein–aether theory

In Einstein–aether theory [24, 27] the preferred direction is carried by a unit timelike vector  $u^\mu$  with its own kinetic action:

$$S_{\text{ae}} = -\frac{M^2}{2} \int d^4 x \sqrt{-g} [c_1 (\nabla_\mu u_\nu) (\nabla^\mu u^\nu) + c_2 (\nabla_\mu u^\mu)^2 + c_3 (\nabla_\mu u_\nu) (\nabla^\nu u^\mu) + c_4 u^\mu u^\nu (\nabla_\mu u_\alpha) (\nabla_\nu u^\alpha)]. \quad (\text{J.3})$$

The four free coefficients  $c_1 \dots c_4$  give rise to three distinct propagation speeds for spin-0, spin-1, and spin-2 perturbations. Their equality  $c_0 = c_1 = c_2$  requires two fine-tuning relations among the  $c_i$  [27].

In ECT,  $n_A = \partial_A \Phi / |\partial \Phi|$  is a derived object, not an independent dynamical field. There are no free  $c_1 \dots c_4$ : the unique kinetic tensor  $K^{AB}$  has two parameters  $(\alpha, \beta)$  and yields a single speed  $c_*$ . Universal-cone universality is therefore structural, not fine-tuned.

## J.3 Comparison with the Standard Model Extension

The Standard Model Extension (SME) [28, 29] parametrises all possible Lorentz-violating operators for each sector independently. For the photon sector alone the CPT-even term involves the rank-4 coefficient tensor  $(k_F)^{\kappa\lambda\mu\nu}$  with 19 independent components. The electron sector carries a separate tensor  $(c_e)^{\mu\nu}$  with 9 components. These coefficients are phenomenologically independent: the SME does not relate them.

In ECT, all Lorentz-violating structure originates from a single tensor  $K^{AB}$ , which has only two independent parameters  $(\alpha, \beta)$ . All sectors inherit the same anisotropy, and there are no free sector-dependent Lorentz-violation coefficients at leading order. This makes ECT far more predictive (and more easily falsifiable) than a generic SME-level parametrisation.

Current observational bounds [13, 11, 12] constrain photon-sector anisotropy to  $|\delta c_\gamma / c| \lesssim \text{few} \times 10^{-17}$  (optical cavity tests) and gravitational-electromagnetic nonuniversality to  $|c_{\text{GW}} - c_\gamma| / c \lesssim 10^{-15}$  (GW170817). These bounds are consistent with ECT, where Lorentz-violation effects are Planck-suppressed.

## J.4 Scope and limitations

The theorem covers the linear scalar ordered branch. Extension to the gauge sector is conditional on the minimal phase-to-gauge emergence route (§4.7). Extension to the fermionic sector follows the structural reconstruction route (§9). Both are Level B.



## K EFT Motivation via Integrating Out the Radial Mode

*Reference from main text: Section 4.5.*

**Status.** This appendix provides a schematic EFT motivation within the ordered vacuum sector selected by postulate P4, not a strict derivation of the broken-phase action from the bare micro-action P3 alone. The background  $\Phi_{\text{bg}}$  is not a solution of the equations of motion of P3; the following expansion refers to the EFT of the broken phase.

### Phase action and heavy-mode integration

At  $E \ll m_\sigma$  the heavy radial mode integrates out, leaving the effective action for soft fluctuation  $\varphi$ . The isotropic kinetic term in the broken phase acquires anisotropic  $O(3)$ -invariant deformation parametrised by  $(\alpha, \beta)$ :

$$S_{\text{EFT}}^{(2)}[\varphi] = \int d^4X \left\{ \frac{1}{2} (\partial_A \varphi)^2 + \frac{m_{\text{eff}}^2}{2} \varphi^2 + O(\partial^4/m_\sigma^2) \right\}.$$

The anisotropy parameters  $(\alpha, \beta)$  are not fixed by this analysis and must be determined from physical matching conditions (OP-grad).

## L Structural candidate mechanism for the second condensate transition $O(3) \rightarrow O(2)$

*Status: structural Level B/C. This appendix describes a structural candidate mechanism, not a derived result. It does not prove that the second transition occurs, does not derive  $v_2$  from first principles, and does not establish the electroweak gauge sector from ECT postulates P1–P6.*

### A. What is already true at Level A

After the first transition  $O(4) \rightarrow O(3)$ , the ECT broken phase contains two coexisting sectors whose existence follows from the current postulates:

- a coherent phase sector with compact  $U(1)$ -like structure in the effective loop/phase description (the winding variable  $\theta$ ; its role as an electroweak-locking participant is not derived from P1–P6);
- a residual orientation sector with symmetry group  $O(3)$ .

The Lie algebras satisfy the exact isomorphism

$$\mathfrak{so}(3) \cong \mathfrak{su}(2). \quad (\text{L.1})$$

Furthermore, the connected rotation subgroup admits an  $SO(2) \cong U(1)$  subgroup as the stabiliser of a chosen axis. Equivalently, selecting a preferred direction in the ordered branch leaves an  $O(2)$  (or connected  $SO(2)$ ) residual symmetry. These are mathematical facts, independent of dynamics (Level A).

### B. Structural mechanism candidate (Level B/C)

The following scenario is structurally admissible within ECT but requires two additional assumptions not yet derived from P1–P6.

**Assumption A1.** At some intermediate scale  $v_2 \ll \phi_0$ , a coupling between the coherent phase sector and the residual orientation sector becomes operative.

**Assumption A2.** The minimum of the condensate functional at scale  $v_2$  aligns the  $U(1)$  axis of the phase sector with a preferred direction in  $O(3)$ .

Under A1 and A2, the residual  $O(3)$  is broken to its  $O(2)$  stabiliser:

$$O(3) \xrightarrow{\text{phase-orientation alignment}} O(2). \quad (\text{L.2})$$

This breaking pattern is *formally analogous* to a reduced weak-like symmetry-breaking pattern. It should not be identified directly with the full Standard Model electroweak transition. The analogy is structural; it does not constitute a derivation of the electroweak sector.

### C. Formal analogy with a weak-like sector

Under the breaking (L.2), the candidate second transition provides

- two broken directions;
- one unbroken residual  $O(2) \cong U(1)_{\text{res}}$  direction;
- and, in an EFT embedding with a second condensate potential, one radial excitation at the intermediate scale.

This does *not* reproduce the full Standard Model electroweak generator counting, since  $SU(2) \times U(1) \rightarrow U(1)_{\text{em}}$  contains three broken generators, whereas  $O(3) \rightarrow O(2)$  contains only two. Accordingly, the present construction should be read as a *reduced structural analogue* or candidate weak-like sector, not as a completed derivation of the physical electroweak spectrum.

Only if a more complete local gauge structure were shown to emerge, together with the missing generator content, could one begin to relate this sector to the physical  $W^\pm$ ,  $Z^0$ , Higgs, and photon degrees of freedom. At the present stage the analogy is intentionally weaker.

### D. Scale $v_2$ : matching constraint, not derivation

If A1 and A2 hold, the scale of the second transition is fixed by low-energy matching to the observed Fermi interaction:

$$v_2 = \left( \sqrt{2} G_F \right)^{-1/2} \approx 246.22 \text{ GeV}, \quad (\text{L.3})$$

where  $G_F = 1.1664 \times 10^{-5} \text{ GeV}^{-2}$ . This value is a *matching constraint*, not a first-principles prediction.

As an order-of-magnitude estimate, dimensional transmutation gives

$$v_2 \sim \phi_0 e^{-\mathcal{C}}, \quad \mathcal{C} \approx \ln \frac{\phi_0}{v_2} \approx 37. \quad (\text{L.4})$$

For a schematic one-loop alignment running with coefficient  $b_a$  and dimensionless locking coupling  $g_a$ , this would correspond to  $b_a g_a^2(\phi_0) \approx 8\pi^2/37 \approx 2.1$  in the strong-critical limit. This is numerically plausible but does not constitute a derivation.

### E. What remains open

1. Does assumption A1 hold in ECT? Is there a phase-orientation coupling in the condensate action?
2. Is the  $O(3)$  orientation symmetry local or global at scale  $v_2$ ? Locality is required for the massive vector boson interpretation.
3. What is the explicit dynamical mechanism generating the scale  $v_2$  (RG running, topological instanton, or other)?
4. How do SM fermion charges and Yukawa couplings arise?

Until these are answered, the second transition  $O(3) \rightarrow O(2)$  remains a *structural candidate mechanism* of ECT at Level B/C, not an established result.

## Generator counting

For  $O(3) \rightarrow O(2)$ , the dimension of the broken-generator space is

$$\dim O(3) - \dim O(2) = 3 - 1 = 2. \quad (\text{L.5})$$

Thus the candidate second transition yields two broken and one unbroken generator. This is the exact group-theoretic content of the analogy used in Section 7.4. No stronger physical identification follows from this counting alone.

## What this appendix establishes and what it does not

This appendix does not derive the physical electroweak sector from the minimal ECT postulates. What it establishes is only the following structural chain:

- (i) if a second effective ordering step  $O(3) \rightarrow O(2)$  is admitted, then it provides a reduced orientation-sector weak-like analogue with two broken directions, but not the full electroweak generator counting; the Hopf-fibered phase-orientation extension of Appendix M is required for the candidate three-broken-direction geometry;
- (ii) if a condensate doublet EFT is admitted, then a Higgs-like radial mode and the standard electroweak matching relations can be written in the usual low-energy form;
- (iii) this provides a structural embedding of the electroweak sector into the condensate architecture of ECT.

What remains open is:

- (a) the dynamical origin of the second transition,
- (b) the derivation of the doublet structure,
- (c) the derivation of the gauge couplings and Yukawa sector,
- (d) the derivation of the hierarchy  $v_2/\phi_0$ .

## M Hopf-fibered phase-orientation locking as a candidate electroweak geometry

This appendix presents a structural geometric proposal addressing the generator-counting limitation of the reduced  $O(3) \rightarrow O(2)$  analogue of Appendix L. The proposal identifies the *pre-gauge* vacuum manifold of a phase-orientation diagonal locking with the fixed-radius Higgs-doublet vacuum manifold of the Standard Model. It does not derive the dynamics of locking, the chiral electroweak gauge sector, the gauge couplings, or the scale of the transition.

### M.1 Generator-counting limitation of $O(3) \rightarrow O(2)$

Appendix L analyses the ordering pattern  $O(3) \rightarrow O(2)$  as a reduced analogue of electroweak symmetry breaking. The number of broken generators is

$$\dim O(3) - \dim O(2) = 3 - 1 = 2. \quad (\text{M.1})$$

This is insufficient for  $SU(2)_L \times U(1)_Y \rightarrow U(1)_{\text{em}}$ , which requires three broken directions to provide longitudinal modes for  $W^\pm$  and  $Z$  via the Higgs mechanism. The reduced analogue therefore captures only the orientation sector and cannot, by simple identification, be the full electroweak transition; a complete description requires the full phase-plus-orientation structure.

## M.2 Pre-locking symmetry: $SU(2)_{\text{orient}} \times U(1)_{\theta}$

Two structures are present in the effective ECT alignment sector.

**Orientation lift to  $SU(2)_{\text{orient}}$ .** Since the connected orientation group has Lie algebra  $\mathfrak{so}(3) \cong \mathfrak{su}(2)$ , its spinorial lift is naturally described by  $SU(2)_{\text{orient}}$ . This is the natural double-cover language for fermionic couplings (cf. the orientation operator entering the 5th-force coupling  $L_5 = \beta \bar{\Psi} \gamma^A n_A \Psi$  in Section 7), but it does not by itself identify the group with the chiral weak group  $SU(2)_L$ .

**Coherent phase  $U(1)_{\theta}$ .** The phase variable  $\theta$  enters the effective theory through the coherent phase-sector EFT and through the closed-loop quantization condition  $\oint \partial_A \theta dX^A = 2\pi n$  associated with the minimal self-consistent loop and the action scale  $S_0$ . Compactness of  $\theta$  within that effective sector supports a  $U(1)_{\theta}$  structure.

**Caveat (OP-EW-locking.0).** The fundamental ECT field  $\Phi$  is a real scalar (P4); the appearance of a compact coherent phase variable  $\theta$  in the alignment sector is a modelling assumption of the effective theory, not a derived consequence of P1–P6. Whether  $U(1)_{\theta}$  admits a derivation from purely real- $\Phi$  dynamics, and whether it plays the role of a participant in an electroweak-like locking sector distinct from any post-breaking phase, is itself open.

## M.3 Diagonal locking: pre-gauge geometry

Suppose the alignment dynamics is energetically minimised by diagonal locking of phase and orientation:

$$SU(2)_{\text{orient}} \times U(1)_{\theta} \longrightarrow U(1)_{\text{diag}}. \quad (\text{M.2})$$

The number of broken directions is

$$\dim[SU(2) \times U(1)] - \dim U(1)_{\text{diag}} = (3 + 1) - 1 = 3, \quad (\text{M.3})$$

matching the number required by  $SU(2)_L \times U(1)_Y \rightarrow U(1)_{\text{em}}$ .

The vacuum manifold is the coset

$$\mathcal{M}_{\text{locked}} = \frac{SU(2)_{\text{orient}} \times U(1)_{\theta}}{U(1)_{\text{diag}}} \simeq SU(2) \simeq S^3, \quad (\text{M.4})$$

where the diagonal  $U(1)$  acts freely. This is the same topology as the fixed-radius Higgs-doublet vacuum manifold  $|H|^2 = v^2/2$ .

**Hopf fibration realisation.** The coset  $S^3$  admits the Hopf fibration  $S^1 \hookrightarrow S^3 \rightarrow S^2$ , with  $S^2$  the orientation base and  $S^1$  the locked phase fibre. This is structurally distinct from a trivial product  $S^2 \times S^1$ : the phase circle is non-trivially fibered over the orientation sphere. When field configurations are mapped into the  $S^2$  base, their topological sectors can be classified by the Hopf invariant.

**Pre-gauge versus post-gauge caveat.** The coset identification  $\mathcal{M}_{\text{locked}} \simeq S^3$  holds at the pre-gauge / global-symmetry level. In gauged electroweak theory, points of  $S^3$  related by gauge transformations are physically identified, so the physical vacuum after modding out gauge redundancy is not the same object. Hopf-locking therefore reproduces the pre-gauge Higgs-doublet vacuum geometry and generator counting; it does *not* by itself establish that this geometry is gauged identically to the Standard Model.

## M.4 Hopf-locking operator and Berry connection

The natural alignment operator compatible with locking dynamics is schematically of the form

$$\mathcal{L}_{\text{lock}}^{\text{schem}} = \frac{1}{2} K_\theta g_{\text{eff}}^{AB} (\partial_A \theta + \mathcal{A}_A[n]) (\partial_B \theta + \mathcal{A}_B[n]) + \frac{1}{2} \kappa_n g_{\text{eff}}^{AB} \partial_A n \cdot \partial_B n + \dots, \quad (\text{M.5})$$

where  $\mathcal{A}_A[n]$  is the connection one-form induced by the orientation field. In a local coordinate patch on the  $S^2$  base,

$$\mathcal{A}_A[n] = \frac{1}{2} (1 - \cos \beta) \partial_A \alpha, \quad (\text{M.6})$$

with  $(\alpha, \beta)$  the standard angles on  $S^2$ . Geometrically,  $\mathcal{A}_A[n]$  is the Berry / Dirac-monopole connection on orientation states; as a monopole connection it is not globally defined in a single patch.

**Schematic, not derived.** Equation (M.5) is a candidate effective density written as a locking term, not a derived ECT action. Its coefficients  $K_\theta$  and  $\kappa_n$  are not specified by P1–P6;  $\kappa_n$  specifically depends on closure of OP-Planck/OP- $C_n$  through the NLO/induced route discussed in Section 4.4 and paragraph 5.1.

**Composite versus independent connection (OP-EW-gauge-field).** A connection  $\mathcal{A}_A[n]$  determined entirely by  $n$  is a *composite* connection and does not carry independent propagating degrees of freedom. In the Standard Model, by contrast, electroweak gauge bosons  $W^\pm$ ,  $Z$ ,  $\gamma$  are independent local fields with their own kinetic terms. Two distinct routes are available:

- (a) *Composite gauge route.* Standard Model gauge bosons are interpreted as collective excitations of the orientation/phase sector, with  $\mathcal{A}_A[n]$  reproducing their leading behaviour. Closing this route requires deriving Yang–Mills-type kinetic terms  $F_{AB}^2$  from ECT dynamics and showing that the propagating modes have the correct spin and mass content.
- (b) *Independent connection route.* The P5 local-redundancy structure is gauge-fixed by introducing an independent compensating connection;  $\mathcal{A}_A[n]$  is then a background/Berry connection separate from the dynamical gauge field. This is closer to standard electroweak gauge theory but loses the structural unity of the composite picture.

Neither route is established here. The choice is itself open (OP-EW-gauge-field).

## M.5 Hopfion structure: mathematical template, not closure

The closest developed mathematical template for the topological locking scenario is the Faddeev–Niemi model [35, 36, 37, 38]. In that setting, static three-dimensional Hopfion configurations obey a Vakulenko–Kapitanski-type lower bound on their finite static energy,

$$E_{\text{Hopfion}}[Q_H] \geq c |Q_H|^{3/4}, \quad (\text{M.7})$$

where  $Q_H \in \pi_3(S^2) = \mathbb{Z}$  is the Hopf invariant and  $c$  is a model-dependent constant set by the stiffness and Skyrme-type coefficients of the effective model.

**Critical caveat.** Faddeev–Niemi solitons are static configurations in three spatial dimensions, with finite static energy. A 4D Euclidean dimensional-transmutation factor  $e^{-S_E}$  requires a bounce or finite-time tunnelling configuration in 4D Euclidean space, whose action is dimensionless and finite. A static 3D soliton extended trivially in Euclidean time has action  $E_{\text{static}} T_E$ , which diverges for infinite  $T_E$ . Translation from a Hopfion energy bound to an ECT scale formula therefore requires either

- a genuine 4D Euclidean Hopf-locking instanton (finite-action localised configuration), not yet constructed within ECT; or
- an alternative interpretation in which Hopfion energy sets a threshold mass scale rather than a tunnelling exponent.

We record the Faddeev–Niemi structure as a promising mathematical template, not as a closure of the topological scale-generation route of equation (5.10).

## M.6 What this appendix establishes and what it does not

### What this construction achieves.

- (1) Hopf-fibered diagonal locking provides the correct number of broken generators (three) for an electroweak-like pattern, structurally improving on the reduced  $O(3) \rightarrow O(2)$  analogue.
- (2) The resulting pre-gauge vacuum manifold is topologically  $S^3$ , matching the fixed-radius global Higgs-doublet manifold of the Standard Model.
- (3) The minimal alignment operator takes covariant Hopf form, and the connection  $\mathcal{A}_A[n]$  is identified geometrically as a Berry / Dirac-monopole connection on the  $S^2$  base.

### What this construction does not achieve.

- (a) *Pre-gauge vs post-gauge.* The match  $S^3$  holds at the global-symmetry level only. Identification with the gauged electroweak vacuum requires a derivation of local gauge redundancy in the locking sector (OP-EW-gauge-field).
- (b) *Chirality.*  $SU(2)_L$  acts only on left-handed fermion doublets;  $SU(2)_{\text{orient}}$  acts on aligned matter through the double-cover lift but is not a priori chiral. The reduction  $SU(2)_{\text{orient}} \rightarrow SU(2)_L$  is a separate open problem (OP-EW-chiral).
- (c) *Hypercharge.*  $U(1)_\theta$  is a compact phase;  $U(1)_Y$  is the hypercharge group with specific anomaly structure and matter-charge assignments. The identification  $U(1)_\theta \rightarrow U(1)_Y$  is non-trivial and not established here (OP-EW-hypercharge).
- (d) *Couplings.* The geometric construction does not derive  $g, g'$ , or the Weinberg angle. A derivation of these from  $\kappa_n$  and Hopf geometry is an open possibility, not a result (OP-EW-couplings).
- (e) *Scale.* Locking geometry alone does not generate  $v_2$ . Combination with a non-polynomial scale-generation mechanism (Section 5.1, equation (5.10)) is required (OP-EW-scale).
- (f) *Naturalness.* Protection of the secondary radial mode  $\sigma_2$  from additive  $\mathcal{O}(\phi_0^2)$  corrections is not addressed by the locking geometry: the constraint structure of  $n_A$  protects orientation Goldstones, not the radial mode (OP-EW-naturalness).
- (g) *Matter.* Chiral fermion representations and Yukawa hierarchy are not derived (OP-EW-matter).

## M.7 Conditional layered closure theorem

We collect the chain of dependencies as a layered conditional statement.

**Conditional OP-EW Reduction Theorem (layered).** Assume:

- *Layer 0.* NLO/induced ECT dynamics generate the orientation stiffness  $\kappa_n = \mathcal{C}_n u_0^2$  (OP-Planck / OP- $C_n$  subproblem).
- *Layer 1.* A compact  $U(1)_\theta$  is established as a genuine symmetry of the effective alignment sector, distinct from any post-breaking phase (OP-EW-locking.0).
- *Layer 2.* Diagonal locking  $SU(2)_{\text{orient}} \times U(1)_\theta \rightarrow U(1)_{\text{diag}}$  is the energetically preferred minimum, giving Hopf-fibered  $S^3$  pre-gauge vacuum manifold (OP-EW-locking.1).
- *Layer 3.* The locking scale is generated non-polynomially:  $v_2 = \phi_0 e^{-\mathcal{J}_{\text{EW}}}$ ,  $\mathcal{J}_{\text{EW}} \approx 36.8$ , via one of the four admissible mechanisms (Section 5.1) (OP-EW-scale).

- *Layer 4.* The pre-gauge structure is promoted to a local chiral  $SU(2)_L \times U(1)_Y$  gauge symmetry, with couplings  $g, g'$  either derived from the ECT alignment/gauge sector or introduced as low-energy matching data (OP-EW-chiral, OP-EW-hypercharge, OP-EW-couplings, OP-EW-gauge-field).
- *Layer 5.* The radial excitation  $\sigma_2$  is a collective critical mode protected from additive  $\mathcal{O}(\phi_0^2)$  corrections (OP-EW-naturalness); chiral fermions and Yukawa hierarchy follow from the locking structure (OP-EW-matter).

If Layers 0–5 close, ECT generates  $v_2 \approx 246$  GeV from  $\phi_0 \approx \bar{M}_{\text{Pl}}$  with order-one input  $\mathcal{J}_{\text{EW}} \approx 36.8$  and reproduces the Standard Model electroweak structure.

*Currently:* Layer 0 partially established (NLO/induced route identified,  $\kappa_n$  derivation incomplete); Layer 2 structurally identified by Hopf-locking but dynamics not derived; Layers 1, 3, 4, 5 fully open.

This is a closure programme, not a solution. It converts the diffuse statement “the connection between three condensate scales is not derived” into a sharply defined sequence of intermediate problems with explicit dependencies.

## N Dimension and normalisation audit

This appendix collects the dimensions and normalisation conventions of the main ECT quantities entering the gravitational matching chain, to keep the gravitational, phase, and ordered-branch sectors sharply distinguished.

### N.1 Primary condensate quantities

Throughout this appendix we use natural units  $\hbar = c = 1$  unless explicit SI conversion factors are displayed. Coordinates have dimension  $[X^A] = \text{GeV}^{-1}$ , derivatives have dimension  $[\partial_A] = \text{GeV}$ , and a canonically normalised four-dimensional scalar has mass dimension one,

$$[\Phi] = \text{GeV}.$$

Consequently  $[\phi_0] = \text{GeV}$  and  $[u_0] = [\partial_A \Phi] = \text{GeV}^2$ , as shown in the table below.

Quantity	Definition	Dimension
$\Phi$	fundamental scalar field (P3)	GeV
$\phi_0 = \sqrt{\mu^2/\lambda}$	bare potential minimum	GeV
$m_\sigma^2 = 2\mu^2$	radial mode mass squared	$\text{GeV}^2$
$u_0 =  \langle \partial_A \Phi \rangle $	gradient condensate amplitude	$\text{GeV}^2$
$n_A$	orientation collective variable	dimensionless

The scaling relation  $u_0 \sim \phi_0 m_\sigma$  is dimensionally consistent:  $\text{GeV} \times \text{GeV} = \text{GeV}^2$ .

### N.2 Orientation-stiffness sector

The orientation-stiffness term in the ordered-branch EFT is

$$\frac{\mathcal{C}_n}{2} u_0^2 (\partial_B n_A) (\partial^B n^A).$$

Since  $[n_A] = 1$  and  $[\partial_B n_A] = \text{GeV}$ , the Lagrangian density  $[\mathcal{L}] = \text{GeV}^4$  requires

$$[\mathcal{C}_n u_0^2] = \text{GeV}^2, \quad \text{i.e.} \quad [\mathcal{C}_n] = \text{GeV}^{-2}.$$

The induced-gravity estimate  $\mathcal{C}_n \sim \hat{a}/(16\pi^2 m_\sigma^2)$  is dimensionally consistent. The effective stiffness is

$$\kappa_n = \mathcal{C}_n u_0^2, \quad [\kappa_n] = \text{GeV}^2.$$

### N.3 Induced gravitational scale

The gravitational normalisation scale is defined through

$$M_G^2 \sim \kappa_n, \quad [M_G] = \text{GeV}.$$

Weak-field matching identifies  $M_G = \bar{M}_{\text{Pl}}$ . Using  $u_0 \sim m_\sigma \phi_0$ :

$$M_G^2 \sim \frac{u_0^2}{m_\sigma^2} \sim \phi_0^2, \quad \text{hence} \quad \phi_0 \sim \bar{M}_{\text{Pl}}.$$

This is the dimensionally correct form of the Planck-scale identification; the earlier notation  $u_0 \sim \bar{M}_{\text{Pl}}$  was dimensionally inconsistent and has been replaced throughout the manuscript.

### N.4 Phase sector and quantum action scale

The phase-sector action in the coherent branch is  $S_\theta = \frac{K_\theta}{2} \int d^4 X (\partial_A \theta)^2$ , with  $[K_\theta] = \text{GeV}^2$  and  $[\theta] = 1$ . The pre-quantum action scale  $S_0$  extracted from the winding sector has  $[S_0] = [\text{action}]$ . Its matching to  $\hbar$  is a separate Level B identification that should not be conflated with the gravitational stiffness scale  $M_G$ .

**Consistency check: two-level structure of the orientation sector.** The linear scalar ordered branch already possesses a well-defined causal cone with speed  $c_*$  (Level A, Universality Corollary, Section 4.3). The gravitational normalisation  $M_G^2 = \kappa_n$  requires the NLO/induced coefficient  $\mathcal{C}_n$ . These two descriptions are compatible but not equivalent: the  $\chi$ -level propagation is fully determined at leading derivative order, while the spin-2 normalisation requires one additional NLO scale. From the induced estimate  $\mathcal{C}_n \sim 1/(16\pi^2 m_\sigma^2)$  and  $M_G^2 = \kappa_n = \mathcal{C}_n u_0^2$ , one obtains

$$\frac{M_G^2}{c_*^2} \sim \frac{\mathcal{C}_n u_0^2}{c_*^2} = \frac{\hat{a}}{16\pi^2} \frac{\phi_0^2}{c_*^2}. \quad (\text{N.1})$$

With  $c_* = c$  and  $\phi_0 \sim \bar{M}_{\text{Pl}}$  this gives  $M_G^2/c^2 \sim \hat{a}\bar{M}_{\text{Pl}}^2/(16\pi^2)$ . Comparing with the observed Planck length  $\ell_{\text{Pl}}^2 = G_N \hbar/c^3 = \hbar/(8\pi\bar{M}_{\text{Pl}}^2 c)$ , the NLO suppression factor  $1/(16\pi^2)$  does not appear in  $\ell_{\text{Pl}}^2$  because the weak-field matching already absorbs the full induced coefficient into the definition of  $M_G$ . This should be read as a structural scaling check, not as a completed numerical derivation. The point is that the NLO/induced suppression carried by  $\mathcal{C}_n$  can be naturally compensated by the ratio  $u_0^2/m_\sigma^2 \sim \phi_0^2$ , so that the induced gravitational scale can naturally remain of order  $\phi_0$ . Whether the final coefficient reproduces the observed normalisation requires the explicit determination of  $\hat{a}$  and of the full spin-2 normalisation map, which remain open in OP-Planck.

### N.5 Summary of the gravitational matching chain

The complete gravitational matching chain of ECT is:

1.  $\partial_A \Phi = u n_A, n_A n^A = 1$  (polar decomposition of gradient condensate; Level A).
2.  $P(X)$  does not generate  $(\partial n)^2$  (Theorem 3.1; Level A).



3. Orientation stiffness  $\kappa_n = \mathcal{C}_n u_0^2$  arises from NLO/induced operators (Level B EFT identity).
4. Natural induced estimate  $\mathcal{C}_n \sim \hat{a}/(16\pi^2 m_\sigma^2)$  (Level B).
5.  $M_G^2 \sim \kappa_n \sim u_0^2/m_\sigma^2 \sim \phi_0^2$  (Level B structural).
6.  $M_G = \bar{M}_{\text{PI}}$  by weak-field matching (Level B).
7.  $\phi_0 \sim \bar{M}_{\text{PI}}$  (Level B matched consequence).

The full NLO derivation of  $\mathcal{C}_n$  from the bare micro-action P3 is OP-Planck.

**Structural significance: ECT gravity as induced gravity.** The structural restriction that orientation stiffness—and hence gravity—lies beyond  $P(X)$  and requires NLO/induced contributions places ECT gravity within the Sakharov induced-gravity programme [3]. This distinguishes ECT from theories that postulate gravitational dynamics directly (Einstein–Hilbert action as input) and from Einstein–aether frameworks [24] where the aether kinetic structure is imposed without derivation. In ECT the gravitational kinetic term is not a fundamental structure but an effective consequence of the microscopic condensate dynamics.

**Conceptual outcome of this audit.** The ordered  $\Phi$ -medium contains several distinct effective sectors whose scales should not be identified prematurely. The causal scale  $c$ , the quantum action scale  $\hbar$ , and the gravitational normalisation scale  $M_G$  all arise from the same underlying field, but from different structures of its broken phase. This is a unification of origin, not yet a collapse to a single derived parameter.

## O Correlation Length from the Radial-Mode Propagator

*Reference from main text: Section 5.5. Status: standard EFT estimate from the massive Euclidean propagator.*

### Euclidean propagator

Quadratic action of the radial mode:  $S_\sigma^{(2)} = \frac{1}{2} \int d^4X [(\partial_A \sigma)^2 + m_\sigma^2 \sigma^2]$ . Fourier propagator:  $G_\sigma(k) = 1/(k^2 + m_\sigma^2)$ .

### Coordinate representation at large distances

In  $d = 4$  Euclidean space for  $r \rightarrow \infty$ :

$$G_\sigma(r) \xrightarrow{r \rightarrow \infty} \frac{m_\sigma^{3/2}}{(2\pi)^{3/2} \sqrt{2}} \frac{e^{-m_\sigma r}}{r^{3/2}}. \quad (\text{O.1})$$

The exponential factor  $e^{-m_\sigma r}$  defines the characteristic decay length of amplitude correlations:

$$\boxed{\xi_{\text{cond}} \sim m_\sigma^{-1}}. \quad (\text{O.2})$$

This is a standard EFT estimate; the identification  $\xi_{\text{cond}} \sim \ell_{\text{PI}}$  is a phenomenological matching hypothesis.

## P Phase Periodicity, Winding Sectors, and the Action Scale $S_0$

*Reference from main text: Section 5.6. Status: explicit derivation chain at Level B. The compact phase and its periodicity belong to the  $U(1)$ -extended phase EFT (modelling step beyond bare P3). The action–phase bridge is a structural Level B assumption.*

This appendix makes explicit the chain of reasoning behind the identification of  $S_0^{\text{EFT}}$  as the ECT precursor of  $\hbar$ . Its purpose is not to derive the full quantum formalism, but to show how the coherent branch naturally introduces an elementary action scale. It should be noted that the real scalar field  $\Phi$  of P3 does not by itself carry a compact  $U(1)$  phase variable; the extension to  $\Phi_{\text{eff}} = \rho e^{i\theta}$  is an additional modelling step for the coherent sector, not a direct topological consequence of the vacuum manifold  $O(4)/O(3) \simeq S^3$  (which has  $\pi_1(S^3) = 0$ ).

### A. Phase variable on the coherent branch

Let the coherent collective state be described by a phase-like variable  $\theta$ . Because physically equivalent coherent states are identified after a full winding, the phase lives on a circle:

$$\theta \in S^1, \quad \theta \sim \theta + 2\pi. \quad (\text{P.1})$$

This is the minimal topological statement behind the coherent winding sector (BR1).

### B. Dimensionless parametrisation

A phase must be dimensionless. If it is controlled by an action-like functional  $S$ , the natural parametrisation is

$$\theta = \frac{S}{S_0}, \quad (\text{P.2})$$

where  $S_0$  has the dimensions of action. The coherent phase factor then takes the form

$$e^{i\theta} = \exp\left(i \frac{S}{S_0}\right). \quad (\text{P.3})$$

The identification (P.2) is a structural assumption: it links the geometric phase variable to the action functional and thereby imports the action scale into the phase description. This step is at Level B.

### C. Single-valuedness and winding number

For a closed coherent loop, single-valuedness requires

$$\oint d\theta = 2\pi n, \quad n \in \mathbb{Z}. \quad (\text{P.4})$$

Using (P.2), this gives

$$\oint dS = 2\pi n S_0. \quad (\text{P.5})$$

Hence the minimal non-trivial loop satisfies

$$S_{\text{loop,min}} = 2\pi S_0. \quad (\text{P.6})$$

### D. Status of the identification with $\hbar$

The correspondence  $\hbar \leftrightarrow S_0$  should be understood as follows. What has been established is that the coherent branch naturally introduces a distinguished action scale which makes the phase dimensionless and organises winding sectors. This is precisely the structural role played by  $\hbar$  in ordinary quantum theory. The full identification  $S_0 = \hbar$  remains at Level B rather than Level A because the complete reconstruction of quantum kinematics and the Born rule is not derived here.

## E. Summary

The coherent branch provides:

1. a periodic phase variable (P.1);
2. integer winding sectors (P.4);
3. a distinguished elementary-loop action scale in the coherent phase sector;
4. a fundamental action scale  $S_0^{\text{EFT}}$  as the ECT precursor of  $\hbar$ .

## Q Noether Currents: Translational and Rotational Sectors

*Reference from main text: Section 6.6. Status: classical field theory; no quantisation required.*

### A. Translational invariance and $T^{AB}$

**Scalar bare sector (P3):**

$$T_{(\Phi)}^{AB} = \partial^A \Phi \partial^B \Phi - \delta^{AB} \left[ \frac{1}{2} (\partial_C \Phi)^2 + V(\Phi) \right], \quad \partial_A T_{(\Phi)}^{AB} = 0. \quad (\text{Q.1})$$

**Orientation sigma-model (AA.1):**

$$T_{(n)}^{AB} = \kappa_n \partial^A n_C \partial^B n^C - \delta^{AB} \frac{\kappa_n}{2} (\partial_D n_E)^2, \quad \partial_A T_{(n)}^{AB} = 0. \quad (\text{Q.2})$$

Conservation  $\partial_A T^{AB} = 0$  follows from the homogeneity of the arena (P1), not from  $O(4)$  rotations (P2).

### B. $O(4)$ -invariance and angular currents

From  $O(4)$ -symmetry (P2), Noether's theorem [47] for rotations  $\delta X^A = \omega^A_B X^B$ :

$$J^{C,AB} = X^A T_{(\Phi)}^{CB} - X^B T_{(\Phi)}^{CA}, \quad \partial_C J^{C,AB} = 0. \quad (\text{Q.3})$$

For the orientation field  $n_A$  (a vector under  $O(4)$ ), a spin contribution is added:

$$J_{(n)}^{C,AB} = X^A T_{(n)}^{CB} - X^B T_{(n)}^{CA} + \kappa_n (n^A \partial^C n^B - n^B \partial^C n^A). \quad (\text{Q.4})$$

### C. Inheritance by both branches

Both sets of currents—translational  $T^{AB}$  and rotational  $J^{C,AB}$ —exist at the level of the bare P3. Both branches of ECT inherit this variational foundation.

## R Variational Selection and Reduced Extremal Dynamics

*Reference from main text: Section 6.6. Status: schematic reduction argument at Level B.*

This appendix records the schematic chain from medium-level extremality to branch-level extremal dynamics. It is not a fully constructive derivation but clarifies the logical structure.

**Step 1. Medium extremality.** By D1, all physically realised configurations satisfy

$$\delta S_E[\Phi] = 0. \quad (\text{R.1})$$

**Step 2. Branch decomposition.** In the ordered branch, decompose the full field into background and fluctuations:

$$\Phi = \Phi_{\text{branch}} + \delta\Phi, \quad (\text{R.2})$$

where  $\Phi_{\text{branch}}$  specifies the ordered background (P4) and  $\delta\Phi$  denotes fluctuations over it.

**Step 3. Reduction to effective functional.** Projecting  $\delta S_E = 0$  onto the collective variables  $\psi_i$  of the branch (e.g. the orientation modes  $\delta n_i$ , the amplitude fluctuation  $\sigma$ , or the macroscopic background variation  $\phi \sim \delta u_0/u_0$ ) gives a reduced effective functional  $S_{\text{eff}}[\psi_i]$  such that

$$\delta S_E[\Phi]|_{\text{branch}} = 0 \implies \delta S_{\text{eff}}[\psi_i] = 0. \quad (\text{R.3})$$

The effective functional  $S_{\text{eff}}$  depends on the specific branch and its collective variables; its explicit form is determined by EFT matching, not by the schematic argument alone.

**Step 4. Interpretation.** Equation (R.3) is the reduction statement behind the claim that extremal dynamics is not an independent postulate at the emergent level. The familiar principle of extremal action for effective fields (classical trajectories, EFT equations of motion, or macroscopic field equations) is inherited from (R.1), not independently postulated.

**Status and limitations.** This chain is a Level B structural argument, not a Level A theorem, because:

1. The explicit form of  $S_{\text{eff}}[\psi_i]$  must still be determined for each branch;
2. The saddle-point dominance structure (which physical extrema are selected in the coherent or macroscopic sector) requires additional analysis beyond the quadratic EFT.

The full constructive derivation of all later extremal principles from the microscopic Euclidean functional remains an open problem.

## S Noether current and local $U(1)$ completion in the compact phase EFT

This appendix collects the explicit derivations underlying the  $U(1)$  gauge construction of Section 7.2.

### A. Global phase symmetry and Noether current

Let  $\Phi_{\text{eff}}(X) = \rho(X)e^{i\theta(X)}$ , with effective Lagrangian

$$\mathcal{L} = \partial_A \Phi_{\text{eff}}^* \partial^A \Phi_{\text{eff}} - V(|\Phi_{\text{eff}}|). \quad (\text{S.1})$$

Under the infinitesimal global transformation  $\delta\Phi_{\text{eff}} = i\alpha\Phi_{\text{eff}}$ ,  $\delta\Phi_{\text{eff}}^* = -i\alpha\Phi_{\text{eff}}^*$ , Noether's theorem gives

$$j^A = \frac{\partial \mathcal{L}}{\partial(\partial_A \Phi_{\text{eff}})} \delta\Phi_{\text{eff}} + \frac{\partial \mathcal{L}}{\partial(\partial_A \Phi_{\text{eff}}^*)} \delta\Phi_{\text{eff}}^*. \quad (\text{S.2})$$

Since  $\partial \mathcal{L} / \partial(\partial_A \Phi_{\text{eff}}) = \partial^A \Phi_{\text{eff}}^*$  and  $\partial \mathcal{L} / \partial(\partial_A \Phi_{\text{eff}}^*) = \partial^A \Phi_{\text{eff}}$ , one obtains

$$j^A = i\alpha (\partial^A \Phi_{\text{eff}}^* \Phi_{\text{eff}} - \partial^A \Phi_{\text{eff}} \Phi_{\text{eff}}^*). \quad (\text{S.3})$$

Removing the overall infinitesimal parameter and adopting the standard normalisation yields

$$j^A = \frac{-i}{2} (\Phi_{\text{eff}}^* \partial^A \Phi_{\text{eff}} - \Phi_{\text{eff}} \partial^A \Phi_{\text{eff}}^*). \quad (\text{S.4})$$

Substituting  $\Phi_{\text{eff}} = \rho e^{i\theta}$ :

$$j^A = \rho^2 \partial^A \theta. \quad (\text{S.5})$$

## B. Necessity of the compensating connection under local phase redefinition

Under  $\Phi_{\text{eff}}(X) \rightarrow e^{i\alpha(X)}\Phi_{\text{eff}}(X)$ , the derivative transforms as

$$\partial_A \Phi_{\text{eff}} \rightarrow e^{i\alpha(X)}(\partial_A \Phi_{\text{eff}} + i(\partial_A \alpha)\Phi_{\text{eff}}). \quad (\text{S.6})$$

The inhomogeneous term  $i(\partial_A \alpha)\Phi_{\text{eff}}$  prevents covariance. Introduce a field  $A_A$  with transformation  $A_A \rightarrow A_A + \frac{1}{e}\partial_A \alpha$ . Then

$$D_A \Phi_{\text{eff}} \equiv (\partial_A - ieA_A)\Phi_{\text{eff}} \quad (\text{S.7})$$

transforms covariantly:  $D_A \Phi_{\text{eff}} \rightarrow e^{i\alpha(X)}D_A \Phi_{\text{eff}}$ .

## C. Leading kinetic term

The antisymmetric combination  $F_{AB} = \partial_A A_B - \partial_B A_A$  is gauge invariant. At leading derivative order, the unique local parity-even quadratic invariant built from  $F_{AB}$  is  $F_{AB}F^{AB}$  up to normalisation and total derivatives. This yields the canonical Maxwell-type action

$$S_{\text{gauge}} = -\frac{1}{4} \int d^4X F_{AB}F^{AB}. \quad (\text{S.8})$$

## D. Compact phase, local gauge completion, and holonomy

For compact  $\theta \sim \theta + 2\pi$ , the gauge-invariant phase gradient is  $\mathcal{D}_A \theta = \partial_A \theta - eA_A$ . Single-valuedness around a closed loop  $\gamma$  implies

$$\oint_{\gamma} \mathcal{D}_A \theta dX^A = 2\pi n, \quad n \in \mathbb{Z}. \quad (\text{S.9})$$

Hence

$$e \oint_{\gamma} A_A dX^A = 2\pi n \quad (\text{S.10})$$

up to sign convention.

# T Non-Abelian local completion and the $\mathfrak{so}(3) \cong \mathfrak{su}(2)$ bridge

This appendix records the explicit structural steps behind Section 7.3.

## A. Local multiplet completion

Let  $\Phi$  be an  $N$ -component effective condensate multiplet. Suppose the effective action is invariant under global  $SU(N)$  transformations

$$\Phi \rightarrow U\Phi, \quad U \in SU(N). \quad (\text{T.1})$$

If one promotes  $U$  to a local transformation  $U(X)$ , covariance of derivatives requires the introduction of a Lie-algebra-valued connection

$$A_A = A_A^a T^a, \quad (\text{T.2})$$

with covariant derivative

$$D_A = \partial_A - igA_A. \quad (\text{T.3})$$

This is the standard local completion of a global multiplet symmetry.

## B. Field strength from commutator closure

Demanding that the covariant derivatives close under commutation gives

$$[D_A, D_B]\Phi = -ig F_{AB}\Phi, \quad (\text{T.4})$$

with

$$F_{AB} = \partial_A A_B - \partial_B A_A - ig[A_A, A_B]. \quad (\text{T.5})$$

In component form this yields

$$F_{AB}^a = \partial_A A_B^a - \partial_B A_A^a + gf^{abc} A_A^b A_B^c. \quad (\text{T.6})$$

Thus the commutator term is forced by local non-Abelian covariance.

## C. Leading kinetic term

At leading derivative order, the local parity-even quadratic invariant built from the field strength is

$$F_{AB}^a F^{aAB}, \quad (\text{T.7})$$

up to normalisation and total derivatives. This yields the canonical Yang–Mills action.

## D. The $\mathfrak{so}(3) \cong \mathfrak{su}(2)$ bridge

The Lie algebra  $\mathfrak{so}(3)$  has generators  $J_i$  obeying

$$[J_i, J_j] = \epsilon_{ijk} J_k. \quad (\text{T.8})$$

The Lie algebra  $\mathfrak{su}(2)$  has generators  $T_i$  obeying

$$[T_i, T_j] = \epsilon_{ijk} T_k \quad (\text{T.9})$$

up to conventional normalisation. Hence

$$\mathfrak{so}(3) \cong \mathfrak{su}(2). \quad (\text{T.10})$$

This is an isomorphism of Lie algebras only. It does not imply that the global groups  $SO(3)$  and  $SU(2)$  are identical, nor does it by itself determine the physical matter representation content.

## E. Limit of the argument

This appendix proves only the structural local completion and the Lie-algebra bridge. It does not derive the physical Standard Model gauge group, its representations, its couplings, or confinement/electroweak breaking from the bare scalar condensate action.

## U Operator classification and dimensional estimate for the ECT-specific fermion–condensate coupling

This appendix records the explicit EFT logic behind Section 7.6.

## A. Bilinear basis

The standard local fermion bilinears are

$$\bar{\Psi}\Psi, \quad \bar{\Psi}i\gamma^5\Psi, \quad \bar{\Psi}\gamma^A\Psi, \quad \bar{\Psi}\gamma^A\gamma^5\Psi, \quad \bar{\Psi}\sigma^{AB}\Psi.$$

To form a scalar interaction linear in the preferred direction  $n_A$ , the natural zeroth-derivative candidates are

$$n_A\bar{\Psi}\gamma^A\Psi, \quad n_A\bar{\Psi}\gamma^A\gamma^5\Psi.$$

If one restricts attention to the parity-even EFT sector, the axial candidate is excluded and the vector operator remains as the leading allowed term.

## B. Why the vector operator is leading

Derivative couplings such as

$$n_A\bar{\Psi}\sigma^{AB}\partial_B\Psi, \quad (\partial_An_B)\bar{\Psi}\sigma^{AB}\Psi$$

are higher-order in the derivative expansion and are therefore subleading in the low-energy EFT. Accordingly, within the parity-even, zeroth-derivative basis, the leading ECT-specific operator is

$$n_A\bar{\Psi}\gamma^A\Psi.$$

## C. Dimensional analysis

In four spacetime dimensions the fermion field has mass dimension

$$[\Psi] = \frac{3}{2},$$

so the bilinear

$$\bar{\Psi}\gamma^A n_A \Psi$$

has dimension three. Therefore the coefficient multiplying it in the Lagrangian density must have mass dimension one:

$$[\mu_5] = 1.$$

This is why the coefficient should not be treated as purely dimensionless at the Lagrangian level.

## D. Dimensionless ratio and Planck suppression

A convenient parameterisation is

$$\mu_5 = \beta_5 m_f,$$

where  $\beta_5$  is dimensionless. If the only available suppressing UV mass scale is  $\phi_0 \sim \tilde{M}_{\text{Pl}}$ , then dimensional analysis suggests

$$\beta_5 \sim \frac{m_f}{\phi_0}, \quad \mu_5 \sim \frac{m_f^2}{\phi_0}.$$

This is an EFT estimate, not a first-principles derivation.

## E. Lorentzian reduction and observability caveat

In the Lorentzian ordered branch, the preferred Euclidean direction induces a timelike vector  $u_\mu$ , and the operator becomes

$$\mu_5 u_\mu \bar{\Psi} \gamma^\mu \Psi.$$

For a constant background and a single fermion species, such a term can be partly removed by field redefinitions. Hence the physical content of the coupling is tied to relative effects, species dependence, gradients, or environmental variation of the ordered branch. This explains why the structural admissibility of the operator is stronger than the current proof of its directly observable low-energy effects.

The separation between this microscopic preferred-direction operator and the macroscopic  $\phi$ -closure of the weak-field gravitational sector is discussed in Appendix V.

## V Microscopic preferred-direction coupling versus macroscopic $\phi$ -closure

This appendix records explicitly why the microscopic preferred-direction coupling and the macroscopic weak-field  $\phi$ -closure belong to different sectors of the ordered branch.

### A. Variable content

The microscopic fermion coupling is built from the orientational variable

$$n_A = \frac{\partial_A \Phi}{|\partial_A \Phi|},$$

and enters the fermion EFT through the local operator

$$\Delta \mathcal{L}_5 = \mu_5 \bar{\Psi} \gamma^A n_A \Psi.$$

The macroscopic weak-field closure, by contrast, is expressed in terms of the amplitude-sector variable

$$\phi = \beta^{-1} \ln(u/u_\infty),$$

which modifies the effective gravitational response through

$$G_{\text{eff}}(X) = G_N e^{-\beta \phi}.$$

Thus the two effects are built from different derived variables of the ordered branch.

### B. Parametric regime

The microscopic operator enters perturbatively, with coefficient

$$\mu_5 = \beta_5 m_f, \quad \beta_5 \sim \frac{m_f}{\phi_0}, \quad \mu_5 \sim \frac{m_f^2}{\phi_0}.$$

In the present EFT closure, the leading dimensional suppression is assigned to the radial/Planck-scale parameter  $\phi_0$ . The macroscopic weak-field closure is not a perturbative insertion of a single local operator. It is a branch-level response encoded in the background profile  $\phi(X)$ , and can become  $O(1)$  in the deep weak-field regime.

### C. Consequence

Because the microscopic preferred-direction coupling and the macroscopic  $\phi$ -closure differ both in variable content and in parametric regime, they cannot be identified with each other. In particular, the local operator  $\mu_5 \bar{\Psi} \gamma^A n_A \Psi$  cannot by itself account for the galactic  $O(1)$  weak-field modifications attributed in ECT to the macroscopic  $\phi$ -closure.



## D. Limit of the argument

This appendix establishes only the structural separation of the two sectors. It does not yet derive the quantitative environmental modulation of the microscopic coupling, nor does it determine the precise observability map of the Lorentzian multi-species EFT. This is the precise structural content used in Section 7.7: the microscopic preferred-direction operator and the macroscopic  $\phi$ -closure belong to the same ordered branch, but not to the same effective sector. This structural separation also underlies the observability logic of Section 7.8: whatever concrete signals survive in the matter sector, they must arise from the microscopic preferred-direction operator itself or from its environment-dependent reduction, not from an identification with the macroscopic  $\phi$ -closure. This also underlies the navigational rôle of Section 7.10, which links the interaction-level preferred-direction analysis to the later macroscopic amplitude-sector development without identifying the two.

## W Dimensional scaling and open condensate-scale assignments for the preferred-direction coefficient

This appendix records the scale argument behind Section 7.9.

**A. Operator dimension.** The operator

$$\bar{\Psi}\gamma^A n_A \Psi$$

has mass dimension three in four dimensions. Its coefficient must therefore have mass dimension one.

**B. Available scales.** In the present ECT architecture, the preferred direction  $n_A$  is a derived variable of the first ordered branch generated at the  $O(4) \rightarrow O(3)$  transition. Several scales are therefore structurally present: the gradient order parameter  $u_0$ , the radial/Planck-scale parameter  $\phi_0$  associated with the symmetry-breaking amplitude of the bare potential, and the later electroweak-like scale  $v_2$ .

**C. Consequence.** If the coefficient is controlled primarily by the radial/Planck-scale parameter of the ordered branch, then  $\phi_0$  provides the leading EFT suppression scale in the present closure. This motivates the dimensional estimate

$$\mu_5 = \beta_5 m_f, \quad \beta_5 \sim \frac{m_f}{\phi_0}.$$

This is not yet a derivation. It is the working scale assignment adopted in the present formulation; possible  $\phi_0$ -,  $v_2$ -, loop-, and mixed-sector corrections remain open.

**D. What this does not establish.** This argument does not exclude corrections involving  $v_2$ , loop effects, or heavy-mode matching contributions. It establishes only why  $\phi_0$  is the leading working EFT scale in the present formulation, not that all lower-scale corrections are absent.

## X $\phi$ -first nonlinear gravity: full derivation

This appendix gives the full derivation of the  $\phi$ -first scalar-tensor IR closure, states all theorems precisely, and compares the resulting equations with the analogous equations in related theories.

### A.1 Theorem A: Uniqueness of the quadratic propagator

**Statement.** In the ordered branch of ECT, the leading quadratic  $O(3)$ -invariant symmetric rank-2 kinetic tensor is, up to overall normalisation, unique:

$$K^{AB} = \beta \delta^{AB} - \alpha n^A n^B. \tag{X.1}$$

This determines a single effective IR causal cone structure. Extending this to universal metric coupling beyond the quadratic regime is assumption A4 (IR closure assumption; not proved beyond linear order).

**Proof.** Any  $O(3)$ -invariant symmetric rank-2 tensor built from  $\{\delta^{AB}, n^A\}$  has the form  $T^{AB} = a\delta^{AB} + bn^An^B$  with two scalars  $a, b$ . From  $S_E$ :  $a = \beta$ ,  $b = -(\alpha - \beta)$ . No other independent structure exists.  $\square$

## A.2 Theorem B: $\phi$ -parameterisation

Let  $\chi(X)$  be the local ordered-branch amplitude parameter in an equivalent parametrisation of the galactic EFT. In the main text the same sector is expressed preferentially through the variable  $u(X)$  and its logarithmic field  $\phi(X)$ . Its vacuum value  $\chi_\infty$  is matched to  $(\alpha - \beta)$  in the homogeneous vacuum sector. Define  $\phi \equiv \ln(\chi/\chi_\infty)$ ,  $\bar{M}_{\text{pl}}^2 \equiv u_0^2\chi_\infty$ . Since  $M_{\text{eff}}^2 \propto u_0^2\chi$ :

$$M_{\text{eff}}^2(\phi) = \bar{M}_{\text{pl}}^2 e^{\beta\phi}. \quad (\text{X.2})$$

This is an exact algebraic reparameterisation.  $\square$

## A.3 Theorem C: Correct IR action (effective ansatz)

$S_{\text{IR}}$  (eq. (13.34) in the main text) is the minimal local two-derivative IR ansatz consistent with A1–A4. It is not derived from  $S_E$  without additional assumptions. The potential  $U(\phi)$  is an effective ordered-branch potential; its quadratic coefficient  $m_\phi^2$  is fixed by the stiffness mass of the  $\chi$ -field; higher coefficients require loop calculations.

## A.4 Theorem D: Correct field equations

Variation of  $S_{\text{IR}}$  gives the self-consistent system (eqs. (13.35) and (17.2) in the main text). Note that the *metric* equation contains the non-minimal terms  $\nabla_\mu \nabla_\nu M_{\text{eff}}^2 - g_{\mu\nu} \square M_{\text{eff}}^2$  arising from  $\delta(M_{\text{eff}}^2(\phi)R)/\delta g^{\mu\nu}$ ; these are absent in standard GR and are characteristic of the  $\phi$ -first scalar-tensor closure.

## A.5 Corollary E: Einstein limit

In the homogeneous screened regime  $\phi = \phi_0 = \text{const}$ ,  $n^A = \bar{n}^A = \text{const}$ :

$$\nabla_\mu M_{\text{eff}}^2 = 0, \quad \square M_{\text{eff}}^2 = 0, \quad T_{\mu\nu}^{(\phi)} \rightarrow 0 \quad (\phi \text{ constant}), \quad (\text{X.3})$$

while the vacuum contribution of the scalar sector is carried by  $-U(\phi_0)g_{\mu\nu}$  already present in eq. (13.35) (no double counting). The metric equation reduces to:

$$G_{\mu\nu} + \Lambda_{\text{eff}}(\phi_0)g_{\mu\nu} = 8\pi G_{\text{eff}}(\phi_0)T_{\mu\nu}^{\text{mat}} \quad (\text{X.4})$$

$$G_{\text{eff}}(\phi_0) = \frac{G_N}{e^{\phi_0}}, \quad \Lambda_{\text{eff}}(\phi_0) = \frac{U(\phi_0) + \rho_{n,\text{vac}}(\phi_0)}{M_{\text{eff}}^2(\phi_0)}. \quad (\text{X.5})$$

This is a strict result given A1–A4.  $\square$

*Note.* This subsection does not constitute a derivation of the galactic / MOND-like branch, which requires additional assumptions about non-homogeneous  $\phi$ -sector solutions (Section 17.1).

## A.6 Theorem F: Lovelock uniqueness of the pure-metric IR limit

**Additional assumption A5.**  $\phi$  and  $n^A$  are frozen or integrated out; the remaining pure-metric IR theory is local, diffeomorphism-invariant, and two-derivative at leading order in 4D.

**Lovelock theorem (1971) [81].** Under A5, the leading pure-metric two-derivative IR field equations are uniquely of Einstein form:

$$G_{\mu\nu} + \Lambda g_{\mu\nu} = 8\pi G T_{\mu\nu}. \quad (\text{X.6})$$

*Limitations.* After integrating out  $\phi$  and  $n^A$ , corrections  $\sim R^2, R_{\mu\nu}R^{\mu\nu}$  are generated but suppressed as  $(E/m_\phi)^2$  in the IR. Theorem F is a statement about leading IR uniqueness, not a completed microscopic derivation from  $S_E$ .  $\square$

## A.7 Comparison with related theories

Table 130 places the ECT  $\phi$ -first closure in context with Einstein-aether theory, scalar-tensor gravity, and standard GR.

**Table 130:** ECT  $\phi$ -first IR closure compared to related theories.  $\phi$  = logarithmic macroscopic amplitude variable (local stiffness variable of the ordered branch);  $n^A$  = orientation director;  $G_{\text{eff}}$  = effective gravitational coupling. Entries in **bold** indicate ECT-specific features.

Feature	GR	Brans-Dicke / ST	Einstein-aether	ECT ( $\phi$ -first)
Primary object	$g_{\mu\nu}$ (postulated)	$g_{\mu\nu}, \phi$	$g_{\mu\nu}, u^\mu$	$\phi$ ( <b>order field</b> ); $g^{\text{eff}}$ <b>emergent</b>
$G_N$	constant	$G \propto 1/\phi$	constant	$G_N e^{-\beta\phi(X)}$ <b>from condensate</b>
$\Lambda$	constant	constant	constant	$\Lambda_{\text{eff}}(\phi)$ <b>dynamical</b>
Metric equation	$G_{\mu\nu} + \Lambda g_{\mu\nu} = 8\pi G T_{\mu\nu}$	$G_{\mu\nu} = \dots + \nabla\nabla\phi$	$G_{\mu\nu} + \Theta_{\mu\nu} = 8\pi G T_{\mu\nu}$	<b>eq. (13.35) with <math>\nabla\nabla M_{\text{eff}}^2</math></b>
Einstein limit	exact	$\phi = \text{const}$	$u^\mu = \delta_0^\mu$	$\phi = \phi_0 = \text{const}$ , <b>eq. (X.4)</b>
MOND-like sector	absent	absent	absent	<b>non-homogeneous <math>\phi</math> branch</b>
Preferred direction	no	no	yes ( $u^\mu$ )	<b>yes (<math>n^A</math>, from SSB)</b>
Origin of direction	postulated	postulated	postulated	$O(4) \rightarrow O(3)$ <b>SSB</b>
Lovelock uniqueness	yes	yes (BD)	yes (aether)	<b>yes, in pure-metric limit (Thm. F)</b>
Full derivation from condensate	N/A	N/A	N/A	<b>open (OP2/OP3)</b>

### Component glossary for eq. (13.35).

$M_{\text{eff}}^2(\phi)G_{\mu\nu}$  Einstein tensor weighted by the effective Planck mass;  $G_{\text{eff}}(\phi) = G_N e^{-\beta\phi}$  in the screened limit.

$T_{\mu\nu}^{\text{mat}}$  Stress tensor of standard-model matter (coupled universally to  $g_{\mu\nu}^{\text{eff}}$ ; assumption A4).

$T_{\mu\nu}^{(\phi)}$  Kinetic stress of the  $\phi$ -field; vanishes in the homogeneous limit.

$T_{\mu\nu}^{(n)}$  Stress of the orientation field  $n^A$ ; given by eq. (13.21) in the minimal case.

$\nabla_\mu \nabla_\nu M_{\text{eff}}^2 - g_{\mu\nu} \square M_{\text{eff}}^2$  Non-minimal coupling terms arising from the  $\phi$ -dependence of the Planck mass; characteristic of scalar-tensor theories with non-minimal  $f(\phi)R$  coupling; absent in standard GR.

$-U(\phi)g_{\mu\nu}$  Vacuum energy contribution from the  $\phi$ -sector; plays the role of a dynamical cosmological term.

This appendix records the logic of the linearised tensor matching used in the present article. It should *not* be read as a completed first-principles microscopic derivation of Newton's constant from the bare condensate action.

## X.1 Quadratic tensor sector

Around the ordered broken-phase background, the long-wavelength tensor sector can be organised in a Fierz–Pauli-like quadratic form, schematically

$$S_{\text{tens}}^{(2)} \sim M_G^2 \int d^4x (\partial h)^2 + \dots, \quad (\text{X.7})$$

where  $M_G$  is the gravitational stiffness scale of the ordered tensor EFT.

## X.2 Matching to linearised gravity

Comparison with the standard linearised Einstein–Hilbert normalisation gives the effective matching relation

$$G_N = \frac{c_*^4}{8\pi M_G^2}. \quad (\text{X.8})$$

This is the correct relation to use throughout the present article. It is a geometric EFT matching statement: observed weak-field gravity fixes  $M_G$  numerically. It is not a bare-postulate derivation of  $G_N$  from one microscopic condensate amplitude.

## X.3 What remains open

The explicit microscopic reduction

$$(u_0, \alpha, \beta, \dots) \longrightarrow \kappa_n \longrightarrow M_G \longrightarrow G_N$$

remains to be completed. This appendix therefore represents Level B matching, not a completed Level A derivation of the observed Newton constant.

## X.4 Interpretive note

Gravity is governed, at low energies, by the inverse macroscopic compliance of the ordered tensor sector. A larger  $M_G$  means a stiffer ordered medium and hence a weaker effective gravitational response. This is fully consistent with the Macroscopic Physics discussion, but does not eliminate the need for observational matching.

# Y Numerical algorithms

This appendix summarises the computational procedures used to generate the figures in this paper. Full source code (Python 3 with NumPy, SciPy, and Matplotlib) is publicly available at <https://github.com/chufelo/ECT-preprint-code>.

## Y.1 Galaxy rotation curves

The present SPARC pipeline uses the practical ECT closure introduced in Section 17.3 and derived in Appendix AN:

$$g(R) = \frac{1}{2} \left[ g_N(R) + \sqrt{g_N^2(R) + 4g_N(R)g_{\text{eff}}^\dagger} \right], \quad (\text{Y.1})$$

with baryonic input acceleration

$$g_N(R) = \frac{V_{\text{gas}}^2(R) + \Upsilon_d V_{\text{disk}}^2(R) + \Upsilon_b V_{\text{bul}}^2(R)}{R}. \quad (\text{Y.2})$$

The numerical fitting procedure, quality flags, and model-comparison protocol are documented in Appendix AO.

The detailed construction of the baryonic input velocity ( $V_{\text{gas}}, V_{\text{disk}}, V_{\text{bul}}$ ), the adopted mass-to-light ratios, the SPARC quality cuts, and the per-galaxy fitting workflow are all documented in Appendix AO. They are not repeated here in order to avoid duplication between the generic algorithm appendix and the dedicated SPARC appendix.

## Y.2 RG running of $\lambda(\mu)$

The one-loop  $\beta$ -function (Section 5.1) is integrated numerically from  $\mu = M_{\text{Pl}}$  downward using a standard adaptive Runge–Kutta method, with boundary condition  $\lambda(M_{\text{Pl}}) \approx 10^{-3}$ . This yields a parametrically small dimensionless gravitational coupling  $g(M_{\text{Pl}}) = \lambda(M_{\text{Pl}})/(8\pi) \approx 4 \times 10^{-5}$  (Eq. (8.26)). Since  $\beta_\lambda > 0$ ,  $\lambda(\mu)$  decreases monotonically toward the infrared and  $g(\mu)$  remains small across all sub-Planckian scales. The Landau pole of the pure scalar closure lies at  $\mu_{\text{LP}} \approx M_{\text{Pl}} e^{5.26 \times 10^4}$  (Eq. (8.27)), far above the physical EFT threshold  $m_\sigma \sim M_{\text{Pl}}$ , and is therefore physically unreachable.

## Y.3 Figure production

All figures use publication-quality settings: serif font (Times New Roman), 9 pt labels, inward tick marks, 220 dpi output, with `bbox_inches='tight'`.

**Regime diagram (Fig. 18).** The regime diagram plots the ordered-branch amplitude variable  $\phi = \frac{1}{\beta} \ln(u/u_\infty)$  against  $\log_{10}(g/g_\dagger)$ . The screening boundary is the locus where the chameleon-like mass  $m_\phi(\rho)$  equals the inverse distance to the nearest mass source; to the right of this boundary (high  $\phi$ ) gravity is screened and Newtonian. Representative astrophysical systems are placed at their estimated  $(\phi, g/g_\dagger)$  values: Solar System ( $\phi \approx 2.5$ ,  $g/g_\dagger \sim 10^2$ ), spiral disk ( $\phi \approx 0.5$ ,  $g/g_\dagger \sim 1$ ), void dwarf ( $\phi \approx -0.5$ ,  $g/g_\dagger \sim 10^{-1.5}$ ), cosmic void ( $\phi \approx -1$ ,  $g/g_\dagger \sim 10^{-4}$ ). The script `fig_regime_diagram.py` in the code repository produces this figure.

# Z Structural routes to open microphysical targets

This appendix collects technical details for the four structural routes identified in the main text: the fine-structure constant, the generation number, the Yukawa hierarchy, and the primordial perturbation spectrum. In each case, ECT already compresses the problem into a sharply localised calculational task. The following estimates demonstrate that the required numerical targets lie in natural ranges rather than demanding extreme tuning.

## A. Fine-structure constant: electroweak gauge normalisation

From (7.16),  $\alpha_{\text{fs}} = q^2/(4\pi Z_A)$ . The observational target is  $Z_A^{\text{IR}} \approx 10.9$ , a moderate coefficient of order ten. The structural route identified in the main text reduces the fine-structure problem to the emergence and normalisation of gauge-field kinetics from condensate microphysics.

### A.1 Why the ultraviolet problem is electroweak

Below the electroweak scale  $M_W$ , the photon  $A_\mu$  is a mass eigenstate and  $\alpha_{\text{fs}}^{-1} = 4\pi Z_A/q^2$  is a well-defined running quantity. Above  $M_W$ , however, the photon is not a propagating eigenstate. The relevant ultraviolet gauge basis is  $U(1)_Y \times SU(2)_L$ , with independent gauge couplings  $g'$  and  $g$  (or equivalently  $\alpha_Y$  and  $\alpha_2$ ) and independent gauge-kinetic normalisations  $Z_B$  and  $Z_W$ . The electromagnetic coupling emerges only after electroweak symmetry breaking through

$$\alpha_{\text{fs}}^{-1} = \alpha_Y^{-1} + \alpha_2^{-1}.$$

The correct ultraviolet calculational target is therefore the pair  $(Z_B^{(0)}, Z_W^{(0)})$  at the condensate scale  $\phi_0$ , together with the electroweak mixing angle  $\theta_W$  that determines how these normalisations combine into the low-energy photon.

## A.2 External one-loop electroweak benchmark

Using the observed Standard-Model electroweak data only as an external benchmark (not as an ECT derivation), one proceeds as follows. At the electroweak matching scale  $M_Z = 91.2$  GeV, the measured values are  $\alpha_{\text{em}}^{-1}(M_Z) \approx 127.95$  and  $\sin^2 \theta_W(M_Z) \approx 0.2312$ . The standard electroweak decomposition gives

$$\alpha_Y^{-1}(M_Z) = \alpha_{\text{em}}^{-1}(M_Z) \cos^2 \theta_W \approx 98.4, \quad \alpha_2^{-1}(M_Z) = \alpha_{\text{em}}^{-1}(M_Z) \sin^2 \theta_W \approx 29.6.$$

Employing the standard hypercharge normalisation (not the GUT-normalised convention), the one-loop SM beta coefficients are  $b_Y = 41/6$  and  $b_2 = -19/6$ . The renormalisation group equations

$$\alpha_i^{-1}(\phi_0) = \alpha_i^{-1}(M_Z) - \frac{b_i}{2\pi} \ln \frac{\phi_0}{M_Z}$$

with  $\ln(\phi_0/M_Z) \approx 37.8$  yield

$$\alpha_Y^{-1}(\phi_0) \approx 57, \quad \alpha_2^{-1}(\phi_0) \approx 49.$$

These should be read as benchmark ultraviolet kinetic targets inferred from the external one-loop electroweak running, not yet as microscopic coefficients derived from the ECT action. The corresponding benchmark coefficients are

$$Z_B^{\text{bench}} \approx 4.6, \quad Z_W^{\text{bench}} \approx 3.9.$$

Under the candidate colour completion (§40), the effective charge-squared sum that enters the one-loop bookkeeping is  $C_{\text{eff}} = \sum_f N_{c,f} Q_f^2 = 8$  for the observed three-generation benchmark (three lepton families contributing  $3 \times 1^2 = 3$ ; three up-type quarks contributing  $3 \times 3 \times (2/3)^2 = 4$ ; three down-type quarks contributing  $3 \times 3 \times (1/3)^2 = 1$ ). The observed three-generation Standard-Model matter content is used here only as benchmark input, not as a quantity already derived within ECT.

## A.3 ECT structural interpretation

In ECT the electroweak gauge-kinetic coefficients are expected to arise as structural outputs of the ordered condensate rather than as independent primitive inputs:  $Z_B^{(0)}$  inherits from the compact-phase stiffness  $K_\theta^{\text{eff}} \sim \phi_0^2$  of the same condensate sector from which the  $U(1)$  gauge structure emerges (§7.2), and  $Z_W^{(0)}$  inherits from the orientation-sector stiffness  $\kappa_n \sim \phi_0^2$  associated with the  $O(4) \rightarrow O(3)$  symmetry breaking, from which the  $SU(2)$ -like gauge redundancy arises (§7.3). Both sectors are anchored in the same ordered-condensate framework and are naturally controlled by the primary condensate scale  $\phi_0$ , although the corresponding effective stiffness coefficients need not coincide exactly.

The fine-structure constant is therefore structurally tied to the same condensate architecture that governs gravity and quantisation.

At the benchmark level, the ultraviolet mixing angle can be expressed directly in terms of the two electroweak inverse couplings, or equivalently in terms of the corresponding benchmark kinetic targets:

$$\sin^2 \theta_W(\phi_0) = \frac{\alpha_2^{-1}(\phi_0)}{\alpha_Y^{-1}(\phi_0) + \alpha_2^{-1}(\phi_0)} = \frac{Z_W^{\text{bench}}}{Z_B^{\text{bench}} + Z_W^{\text{bench}}}.$$

If the phase and orientation sectors contribute with comparable stiffnesses ( $K_\theta^{\text{eff}} \approx \kappa_n$ ), one expects  $\sin^2 \theta_W(\phi_0) = \mathcal{O}(1/2)$ . The external benchmark value  $\sin^2 \theta_W(\phi_0) \approx 0.46$  is qualitatively compatible with this expectation. The deviation from exactly  $1/2$  would encode the detailed structural difference between the phase and orientation sectors of the condensate.

## A.4 Limitations and honest status

The external benchmark used above is subject to several limitations: (i) two-loop and higher-order corrections to the beta coefficients have been ignored; (ii) threshold corrections at intermediate scales ( $m_t$ ,  $M_W$ ,  $M_Z$ ,  $M_H$ ) have been treated as step functions rather than properly matched; (iii) below  $M_Z$ , hadronic

vacuum-polarisation contributions cannot be honestly reduced to free quark thresholds; the low-energy running between the Thomson limit and  $M_Z$  involves nonperturbative QCD effects; (iv) the observed SM three-generation matter content, hypercharge assignments, and right-handed singlet structure have been used as external inputs, not as quantities derived within ECT; (v) the colour completion itself is a candidate route (Level Open/C), not a proven theorem.

The robust conclusion at the present stage is narrower: the benchmark ultraviolet electroweak kinetic targets are moderate rather than extreme, purely loop-induced electroweak kinetics are not compatible with the observed couplings within this benchmark, and the Weinberg angle becomes a structural target of the condensate-sector ratio. A first-principles derivation of  $(Z_B^{(0)}, Z_W^{(0)})$  from condensate microphysics remains a concrete open programme (Level B/C, OP- $\alpha_{\text{fs}}$ ).

## B. Three fermion generations: spectral counting

In a toy model where the condensate profile after the ordering transition creates an effective potential of Pöschl–Teller type for fermions, the number of normalizable bound states is  $N_{\text{bound}} \approx \lfloor \nu \rfloor$ , where  $\nu = y/\sqrt{2\lambda}$  (Eq. (9.27)).

*Numerical window for three generations:*

$\lambda_{\text{eff}}$	$\sqrt{2\lambda_{\text{eff}}}$	y range for $N_{\text{gen}} = 3$	Comment
0.10	0.447	1.34–1.79	natural $y = O(1)$
0.13	0.510	1.53–2.04	natural $y = O(1)$

In all cases, three generations arise for  $y \sim 1.3\text{--}2.0$ , a natural range requiring no extreme tuning. The parameter  $\lambda_{\text{eff}}$  refers to the local effective profile entering the toy spectral problem; it is not yet identified with the fundamental quartic parameter of the full ECT action. The parameter  $\lambda_{\text{eff}}$  refers to the local effective profile entering the toy spectral problem; it is not yet identified with the fundamental quartic parameter of the full ECT action.

The complementary topological route via the index of the internal Dirac operator  $D_{\text{int}}$  on the condensate background would give  $N_L - N_R = \text{Index}(D_{\text{int}})$ , providing protection of the family number as a spectral-topological invariant. For an  $O(4)$ -background carrying instanton number  $n$  (from  $\pi_3(S^3) = \mathbb{Z}$ ), the Atiyah–Singer index theorem gives  $|n|$  zero modes per chirality. This does not by itself identify the observed family number with the instanton number; it only shows that topological protection of mode multiplicity is available in principle. The physical identification of the three Standard-Model families with such protected modes remains open. This does not by itself identify the observed family number with the instanton number; it only shows that topological protection of mode multiplicity is available in principle. The physical identification of the three Standard-Model families with such protected modes remains open. *Status:* Level B/C (structural route identified; strict derivation of exactly three families from the ECT condensate profile is open, OP-generations).

## C. Yukawa hierarchy: overlap and tunnelling suppression

If families correspond to three quasi-localised fermionic modes, then eigenvalues of the Yukawa matrix (Eq. (9.26)) satisfy  $y_i \sim y_0 e^{-S_i}$ , where  $y_0 \sim y_t \sim 1$  and  $S_i$  measures the effective overlap suppression action. The observed Yukawa couplings require:

Sector	Heavy	Middle	Light	$\Delta S_{\text{heavy} \rightarrow \text{light}}$
Up-type	$y_t \approx 0.99$	$y_c \approx 7.3 \times 10^{-3}$	$y_u \approx 1.3 \times 10^{-5}$	11.3
Charged leptons	$y_\tau \approx 1.0 \times 10^{-2}$	$y_\mu \approx 6.1 \times 10^{-4}$	$y_e \approx 2.9 \times 10^{-6}$	8.1

These require only moderate effective-action differences ( $\Delta S \sim 3\text{--}11$ ), which are quantitatively natural for quasi-localised modes with slightly different binding depths or tunnelling barriers.

*Status:* Level B/C (the overlap/tunnelling mechanism is physically motivated and quantitatively plausible; the explicit computation of  $Y_{ij}$  from condensate microphysics is open, OP-Yukawa).

## D. Primordial perturbations from the ECT critical-fluctuation route: estimate summary

The critical-fluctuation route developed in Section 14.6 yields two independent estimates for the spectral tilt:

Mechanism	Expression	Estimated $n_s$
Logarithmic $d=4$ correction	$1 - n_s \sim \hat{p}/\ln(L/\xi_0)$ , $\hat{p} \sim 4-5$	0.964–0.971
Gauge–Higgs anomalous dimension	$1 - n_s \sim 2 \gamma_H  \sim 0.025$	$\sim 0.975$
Combined (with conversion correction)	$1 - n_s \sim 0.025 + \delta_{\text{conv}}$	$\sim 0.96-0.97$

The amplitude requires  $\delta u_*/u_0 \sim 5 \times 10^{-5}$  (14.8), which is achievable through loop-scale weak/Higgs corrections ( $g^2/(16\pi^2) \sim 10^{-3}-10^{-2}$ ) supplemented by a modest conversion suppression factor. The logarithmic exponent  $\hat{p}$  has not yet been derived within ECT; the quoted range should be read as the range needed for compatibility with the observed tilt.

*Status:* Level B/C (the critical-fluctuation route is numerically compatible with observations; the full derivation including freeze-out dynamics and curvature transfer is open).

## AA Effective Action for Orientation Modes: Nonlinear Sigma-Model

*Reference from main text:* Sections 4.4 and 4.6. *Status:* minimal orientation EFT on the broken branch; Level B. This appendix does not claim three independent physical Goldstone particles; see Appendix I for the integrability analysis.

**Status note.** Any three-component orientation language used in this appendix refers only to the minimal reduced EFT description of the broken branch. In the scalar-only microscopic ECT basis, integrability of  $Q_A = \partial_A \Phi$  reduces the linear soft sector to one longitudinal scalar mode; see Appendix I.

### Setup and caution

In the ordered branch one may introduce the orientation field  $n_A$  with  $n_A n^A = 1$  and write the most general local quadratic broken-branch EFT:

$$S_n = \frac{\kappa_n}{2} \int d^4X \partial_B n_A \partial^B n^A + \int d^4X \Lambda(X)(n_A n^A - 1), \quad (\text{AA.1})$$

where  $\kappa_n > 0$  is the effective stiffness and  $\Lambda$  is a Lagrange multiplier enforcing the unit constraint. This is a nonlinear sigma-model with target  $S^3 \simeq O(4)/O(3)$ .

**Important caveat.** In the scalar-only ECT basis  $n_A = Q_A/|Q| = \partial_A \Phi/|\partial \Phi|$ , so the decomposition  $Q_A = u n_A$  is subject to the integrability constraint  $\partial_A Q_B - \partial_B Q_A = 0$ . This means the three “transverse” components  $\delta n_i$  are not fully independent in the underlying scalar-only theory. The minimal orientation EFT is a useful effective description, but must not be interpreted as a theorem about three independent propagating physical particles.

### Linearisation and reduced content

Setting  $n_A = \bar{n}_A + \delta n_A$ ,  $\bar{n}_A = \delta_{Aw}$  (P4). From  $n_A n^A = 1$ :  $\delta n_w = 0$  at linear order. Quadratic action:

$$S_n^{(2)} = \frac{\kappa_n}{2} \int d^4X \partial_B \delta n_i \partial^B \delta n_i. \quad (\text{AA.2})$$



After imposing the integrability reduction  $\delta n_i = \partial_i \chi / u_0$  (Appendix I), the action becomes an effective action for the one surviving longitudinal scalar mode  $\chi$ .

### Stiffness coefficient $\kappa_n$

From the ordered-branch EFT (3.8) at uniform background  $u = u_0$ :

$$\frac{\mathcal{C}_n}{2} u_0^2 (\partial_A n_B) (\partial_A n_B) \rightarrow \frac{\kappa_n}{2} (\partial_A \delta n_i) (\partial_A \delta n_i), \quad \kappa_n = \mathcal{C}_n u_0^2 \quad (\text{Level B}). \quad (\text{AA.3})$$

The coefficient  $\mathcal{C}_n$  has dimension  $\text{mass}^{-2}$  and is not yet derived from bare parameters  $(\mu, \lambda)$  of P3 (OP-Planck).

### Dispersion of the surviving soft mode

After the integrability reduction, the equation of motion  $\partial_B \partial^B \delta n_i = 0$  becomes an equation for  $\chi$ :

$$(\partial_w^2 + c_\chi^2 \nabla^2) \chi = 0, \quad c_\chi^2 = \frac{K_s}{K_w} c_*^2. \quad (\text{AA.4})$$

For non-trivial modes ( $k \neq 0$ ):

$$\omega^2 = c_\chi^2 k^2 \quad (\text{Level B}). \quad (\text{AA.5})$$

The identification  $c_\chi = c_*$  would require  $K_s = K_w$ ; this is not yet derived (open).

### Coherent branch selection and the horizon problem

The horizon problem in ECT is not posed as a problem of causal contact inside a primordial Lorentzian spacetime. Rather, it becomes the problem of whether the branch from which the observable Lorentzian Universe emerges can be coherently ordered on a macroscopic scale.

Let  $\Omega_{\text{br}}$  be a connected progenitor domain of the future observable branch, and let  $n_A(x)$  be the orientation field valued in the vacuum manifold  $S^3 \simeq O(4)/O(3)$ . The relevant Euclidean ordering functional is

$$S_{\text{ord}}[n] = \frac{\kappa_n}{2} \int_{\Omega_{\text{br}}} d^d x (\partial_i n_A) (\partial_i n^A), \quad \kappa_n > 0.$$

Since the integrand is non-negative, one has  $S_{\text{ord}}[n] \geq 0$ , with equality if and only if  $\partial_i n_A = 0$  on  $\Omega_{\text{br}}$ , that is,

$$n_A(x) = \text{const} \quad \text{on } \Omega_{\text{br}}.$$

Thus, on a connected progenitor domain, the exact global minimum of the orientation ordering problem is a uniform branch orientation.

This establishes the core structural point used in the main text: a macro-coherent  $O(4) \rightarrow O(3)$  transition is not an ad hoc extra assumption, but the simplest exact realization of the ECT ordering problem itself.

To translate this into a cosmological horizon statement one further assumes that the coherence scale of the progenitor branch satisfies

$$L_{\text{br}} \frac{a_0}{a_{\text{br}}} \gtrsim L_{\text{hom}},$$

where  $L_{\text{hom}}$  is the present homogeneity scale to be explained. At present this is a working hypothesis, not a first-principles theorem.

The preference for coherent branches over strongly fragmented ones can be motivated at the level of classical action comparison: a macroscopic  $O(1)$  twist over a scale  $L$  contributes  $S_{\text{ord}} \sim \kappa_n (\Delta \theta)^2 L^{d-2}$ , so large-scale branch fragmentation is not action-free. However, establishing branch preference rigorously would require a full semiclassical treatment including the entropy of the configuration space; the strict result in this appendix is therefore the existence of the coherent exact minimum, while the stronger branch-preference claim in the main text remains a Level B statement.

A further quantitative support comes from the effective pseudo-Goldstone interpretation already used elsewhere in ECT. If one assigns an effective mass scale to the soft orientation sector (e.g. from a pseudo-Goldstone mechanism; this is not derived from P1–P6 and is introduced here only as an illustrative estimate):

$$m_G \sim 10^{-33} \text{ eV},$$

where this value is a phenomenological assumption, not an ECT prediction [33], then the associated correlation length is

$$\xi_G \sim \frac{\hbar c}{m_G} \sim 2 \times 10^{26} \text{ m},$$

of order the present Hubble scale  $c/H_0 \approx 4.4 \times 10^{26} \text{ m}$ . This does not constitute the structural core of the ECT horizon solution, but it provides Level B quantitative support that cosmological-scale coherence is naturally compatible with parameters already present elsewhere in the theory.

### Homotopy classification of topological defects from $O(4) \rightarrow O(3)$

For reference, the topological defect types generated by a symmetry breaking  $G \rightarrow H$  are classified by the homotopy groups  $\pi_n(G/H)$  [7]:

$$\begin{aligned} \pi_0(G/H) \neq 0 &\Rightarrow \text{domain walls}; & \pi_1(G/H) \neq 0 &\Rightarrow \text{strings}; \\ \pi_2(G/H) \neq 0 &\Rightarrow \text{monopoles}; & \pi_3(G/H) \neq 0 &\Rightarrow \text{textures}. \end{aligned}$$

For the primary ECT transition  $O(4) \rightarrow O(3)$  with vacuum manifold  $\mathcal{M}_1 \simeq S^3$ :

Homotopy group	Value	Defect type
$\pi_0(S^3)$	0	No stable domain walls
$\pi_1(S^3)$	0	No stable cosmic strings
$\pi_2(S^3)$	0	No stable magnetic monopoles
$\pi_3(S^3)$	$\mathbb{Z}$	Texture/skyrmion-like sectors

The only non-trivial class  $\pi_3(S^3) = \mathbb{Z}$  corresponds to texture-type configurations rather than monopoles or walls, and does not restore the standard relic catastrophe.

## AB Derivation of the Anisotropic Curvature Coupling

This appendix derives the anisotropic curvature term  $n_A n^C R_{CB} + n_B n^C R_{CA} - \frac{1}{2} g_{AB} n^C n^D R_{CD}$  in the generalised Einstein equations (13.35) by explicit variation of the aether kinetic action (13.34) and commutation of covariant derivatives via the Riemann tensor identity. The calculation closes OP2 for the minimal one-parameter case  $c_1 = K_n$ ,  $c_2 = c_3 = c_4 = 0$ .

### AB.1 Starting point: energy–momentum tensor of the vector condensate

From eq. (13.21), the energy–momentum tensor of the vector condensate in the minimal case is

$$\begin{aligned} T_{AB}^{(n)} = & -K_n [(\nabla_A n_C)(\nabla_B n^C) + (\nabla^C n_A)(\nabla_C n_B) - \frac{1}{2} g_{AB} (\nabla_C n^D)(\nabla^C n_D)] \\ & - K_n [n^C (\nabla_C \nabla_A n_B + \nabla_C \nabla_B n_A) - \frac{1}{2} g_{AB} n^C \nabla^2 n_C] + \lambda_n (g_{AB} - n_A n_B). \end{aligned} \quad (\text{AB.1})$$

The second line contains second-order derivatives in the form  $n^C \nabla_C \nabla_A n_B$ . This ordering is non-canonical; it must be related back to  $\nabla_A (n^C \nabla_C n_B)$  using the Riemann commutator identity.

## AB.2 Commuting covariant derivatives: the key step

Apply the Ricci (Riemann commutator) identity to  $n_B$ :

$$\nabla_C \nabla_A n_B - \nabla_A \nabla_C n_B = R_{CAB}{}^D n_D, \quad (\text{AB.2})$$

where  $R_{CAB}{}^D$  is the Riemann tensor with the sign convention  $[\nabla_C, \nabla_A]V_B = R_{CAB}{}^D V_D$ . Contracted with  $n^C$ :

$$n^C \nabla_C \nabla_A n_B = n^C \nabla_A \nabla_C n_B + n^C R_{CAB}{}^D n_D. \quad (\text{AB.3})$$

The first term on the right can be written as a Leibniz expansion:

$$n^C \nabla_A \nabla_C n_B = \nabla_A (n^C \nabla_C n_B) - (\nabla_A n^C) (\nabla_C n_B). \quad (\text{AB.4})$$

Substituting back:

$$n^C \nabla_C \nabla_A n_B = \nabla_A (n^C \nabla_C n_B) - (\nabla_A n^C) (\nabla_C n_B) + n^C R_{CAB}{}^D n_D. \quad (\text{AB.5})$$

## AB.3 Symmetrisation and curvature identification

Symmetrising eq. (AB.5) in  $A \leftrightarrow B$  and substituting into the second line of eq. (AB.1):

$$\begin{aligned} -K_n n^C (\nabla_C \nabla_A n_B + \nabla_C \nabla_B n_A) &= -K_n [\nabla_A (n^C \nabla_C n_B) + \nabla_B (n^C \nabla_C n_A)] \\ &\quad + K_n [(\nabla_A n^C) (\nabla_C n_B) + (\nabla_B n^C) (\nabla_C n_A)] \\ &\quad - K_n [n^C R_{CAB}{}^D n_D + n^C R_{CBD}{}^D n_D]. \end{aligned} \quad (\text{AB.6})$$

Using the Riemann tensor symmetry  $n^C R_{CAB}{}^D n_D = n^C n^D R_{CABD}$  and the contraction relation

$$n^C n^D R_{CABD} \xrightarrow{\text{contract A}} n^C n^D R_{CBD} = n^C R_{BC}{}^D n_D = n^C R_{BC} n^D g_D{}^D \Big|_{\text{trace}} \quad (\text{AB.7})$$

one arrives, after using  $n^C n^D R_{CABD} = n_A n^C R_{CB}$  (via the antisymmetry  $R_{CABD} = -R_{ACBD}$  and the metric contraction  $g^{AD} n_D = n^A$ ), at the curvature coupling:

$$-K_n [n^C R_{CAB}{}^D n_D + n^C R_{CBD}{}^D n_D] = -K_n [n_A n^C R_{CB} + n_B n^C R_{CA}]. \quad (\text{AB.8})$$

## AB.4 Trace term and the full structure

The trace ( $g^{AB}$ -contracted) part of eq. (AB.8) yields

$$g^{AB} \cdot (-K_n) [n_A n^C R_{CB} + n_B n^C R_{CA}] = -2K_n n^A n^C R_{CA} = -2K_n n^C n^D R_{CD}. \quad (\text{AB.9})$$

The  $\frac{1}{2}g_{AB}$  coefficient in the generalised Einstein equations arises from the standard trace subtraction: after moving  $T_{AB}^{(n)}$  to the right-hand side and absorbing  $K_n$  into the effective coupling  $\alpha_{\text{ECT}}(X) \equiv K_n/M_{\text{Pl}}^2$ , the full anisotropic curvature structure is

$$\alpha_{\text{ECT}}(X) (n_A n^C R_{CB} + n_B n^C R_{CA} - \frac{1}{2}g_{AB} n^C n^D R_{CD}), \quad (\text{AB.10})$$

identically the form that appears in eq. (13.35).

## AB.5 Result of the derivation

The anisotropic curvature term (AB.10) is not a postulate or an ansatz: it follows by algebraic manipulation (Riemann commutator identity + Leibniz rule + trace subtraction) from the minimal aether kinetic term  $\mathcal{L}_n = -K_n (\nabla_A n_B) (\nabla^A n^B)$  already present in the ECT action (13.34). The calculation reproduces the Einstein–aether result of Jacobson [24] in the minimal one-parameter limit.

This closes OP2 at the level of the minimal model ( $c_1 = K_n$ ,  $c_2 = c_3 = c_4 = 0$ ). The general four-parameter case follows by identical steps with the full tensor  $K^{ABCD}$  (13.23); the explicit form is given in [24].

## AC Technical details for the emergent unimodular decoupling theorem

This appendix collects the explicit derivations underlying the cosmological constant analysis of Section 15. We give (i) the rank-one determinant identity with the admissible-variation argument; (ii) the Jacobian cancellation identity for the classical baseline; (iii) the FRW reduction leading to the slow-branch equation of state; and (iv) the dimensional-consistency audit of the infrared scaling with the pseudo-Goldstone candidate.

### AC.1 Rank-one determinant identity and fixed-determinant property

The matrix determinant lemma states, for a symmetric  $4 \times 4$  matrix  $M$  and a 4-vector  $n$ ,

$$\det(M + c n n^T) = (1 + c n^T M^{-1} n) \det M, \quad (\text{AC.1})$$

provided  $M$  is invertible. Specialising to  $M = \beta \delta$  and  $c = -\alpha$ :

$$\det(\beta \delta^{AB} - \alpha n^A n^B) = \beta^4 \cdot \left(1 - \frac{\alpha}{\beta} n^A \delta_{AB} n^B\right). \quad (\text{AC.2})$$

In the ordered branch the orientation field satisfies the constraint  $n^A(x) \delta_{AB} n^B(x) = 1$ , reflecting that  $|n|$  is not an independent degree of freedom (amplitude variation is described by the radial mode  $\phi$ ). Substituting:

$$\det K^{AB} = \beta^4 \left(1 - \frac{\alpha}{\beta}\right) = \beta^3(\beta - \alpha) = -\beta^3(\alpha - \beta), \quad (\text{AC.3})$$

independent of  $n^A(x)$ .

From the densitized-metric identification  $K^{AB} \propto \sqrt{-g_{\text{eff}}} g_{\text{eff}}^{AB}$  and  $\det(\sqrt{-g} g^{\mu\nu}) = -g$  in four dimensions,

$$\det K^{AB} = -g_{\text{eff}}, \quad \sqrt{-g_{\text{eff}}} = \sqrt{\beta^3(\alpha - \beta)} = \frac{\beta^2}{c_*}, \quad (\text{AC.4})$$

using  $c_*^2 = \beta/(\alpha - \beta)$ .

**Vanishing variation on the constraint surface.** An admissible variation  $\delta n^A$  preserves the normalization  $n^A \delta_{AB} n^B = 1$ , hence  $\delta_{AB} n^A \delta n^B = 0$ . Differentiating (AC.2),

$$\frac{\partial(\det K)}{\partial n^A} = -2\alpha\beta^3 \delta_{AB} n^B, \quad (\text{AC.5})$$

hence

$$\delta(\det K) = -2\alpha\beta^3 (\delta_{AB} n^B \delta n^A) = 0, \quad (\text{AC.6})$$

so  $\delta\sqrt{-g_{\text{eff}}} = 0$  on admissible variations, as stated in Theorem 1(iii) of the main text.

### AC.2 Jacobian cancellation identity for the classical baseline

The fundamental ECT action is  $S_E[q] = \int_M d^4 x_E \mathcal{L}_E(q, \partial q)$  with  $q^a$  collectively denoting  $\Phi$ ,  $n^A$ , and auxiliary fields. Crucially, the emergent metric  $g_{\text{eff}}^{AB}[q]$  is a functional of the condensate fields rather than an independent dynamical variable; there is no variation step “by  $g_{\mu\nu}$ ”.

Under the shift  $\mathcal{L}_E \rightarrow \mathcal{L}_E + C$  for a field-independent constant  $C \in \mathbb{R}$ : (a)  $\partial C / \partial q^a = \partial C / \partial (\partial_A q^a) = 0$ , so every Euler–Lagrange equation is unchanged; (b) the classical solutions  $q^a(x)$  are unchanged; (c) the emergent metric  $g_{\text{eff}}^{AB}[q(x)]$  is unchanged on each classical solution. Specialising to  $C = V(\phi_0)$  establishes Theorem 1(iv).

The result is non-trivial in the ECT context precisely because  $g_{\text{eff}}$  is emergent. In standard general relativity with an independent  $g_{\mu\nu}$ , the same shift generates  $C\sqrt{-g}$ , whose variation produces  $\sim C g_{\mu\nu} \sqrt{-g}$  – the standard cosmological-constant source. That mechanism is unavailable here.

### AC.3 FRW reduction and equation of state

On an FRW background, spatial isotropy selects a single long-wavelength ordered-branch degree of freedom  $q(t)$ . The minimal homogeneous effective Lagrangian is

$$L_{\text{IR}}[q; a] = a^3 \left[ \frac{1}{2} Z_q \dot{q}^2 - V_{\text{IR}}(q) \right], \quad (\text{AC.7})$$

with infrared stiffness  $Z_q$  and residual infrared potential  $V_{\text{IR}}(q)$ . Crucially,  $V_{\text{IR}}(q)$  is the dynamical dressing of the potential around the ordered-branch minimum; it is not  $V(\phi_0)$ , which is decoupled by Theorem 1(iv). This distinction resolves the apparent tension between the decoupling theorem and the dark-energy picture used in Sec. 16.

From (AC.7),

$$\rho_q = \frac{1}{2} Z_q \dot{q}^2 + V_{\text{IR}}(q), \quad (\text{AC.8})$$

$$p_q = \frac{1}{2} Z_q \dot{q}^2 - V_{\text{IR}}(q), \quad (\text{AC.9})$$

$$w_q = \frac{r-1}{r+1}, \quad r \equiv \frac{\frac{1}{2} Z_q \dot{q}^2}{V_{\text{IR}}(q)}. \quad (\text{AC.10})$$

For  $r \ll 1$  (slow-branch regime),  $w_q \simeq -1 + 2r$ , reproducing the main-text formula  $w_0 = -1 + 2\rho_{\text{kin}}/(3\rho_{\text{cond}})$  upon identification  $\rho_{\text{kin}} = \frac{1}{2} Z_q \dot{q}^2$  and  $\rho_{\text{cond}} = V_{\text{IR}}(q)$ .

### AC.4 Dimensional audit of the infrared scaling

The observed  $\rho_\Lambda$  has dimensions  $\text{mass}^4$ . After blocking the direct UV channel (Theorem 1), the scale  $M_{\text{Pl}}^4$  is not available as a direct source. Available infrared scales are the emergent gravitational stiffness  $M_{\text{Pl}}^2$  (from the Sakharov/Adler induced-gravity mechanism [99, 100]) and the Hubble scale  $H_0$  (only dimensionful IR curvature/time scale).

Dimensionally consistent combinations of  $\text{mass}^4$  from  $\{M_{\text{Pl}}^2, H_0\}$  without directly invoking  $M_{\text{Pl}}^4$  are  $M_{\text{Pl}}^2 H_0^2$ ,  $M_{\text{Pl}} H_0^3$ , and  $H_0^4$ . With  $M_{\text{Pl}}/H_0 \sim 10^{60}$ , these evaluate to  $10^{-47}$ ,  $10^{-107}$ ,  $10^{-167} \text{ GeV}^4$  respectively; only the first matches observation at the order-of-magnitude level.

**Pseudo-Goldstone realization.** For a pseudo-Goldstone  $\theta$  of mass  $m_G$  and decay constant  $f_G$ , the natural infrared energy density is  $\rho_G \sim m_G^2 f_G^2$ , obtained from  $V_G(\theta) \sim m_G^2 \theta^2$  at  $\theta \sim f_G$ . Using the ECT values  $m_G \sim H_0$  and  $f_G \sim \phi_0 \sim M_{\text{Pl}}$  (Sec. 15.9),

$$\rho_G \sim m_G^2 f_G^2 \sim H_0^2 M_{\text{Pl}}^2, \quad (\text{AC.11})$$

reproducing the IR scaling with  $c_\Lambda = O(1)$  via independent inputs:  $m_G$  comes from the pseudo-Goldstone (dark-matter-candidate) sector,  $f_G$  from the gravitational SSB scale. Neither is tuned here.

**Scope.** The estimate  $\rho_G \sim H_0^2 M_{\text{Pl}}^2$  is a consistency check, not a derivation. Upgrading it to a prediction requires a first-principles derivation of  $m_G$  from ECT parameters (Open Problem O4) and an analysis of the cosmological evolution of the Goldstone condensate. The holographic bound of Cohen–Kaplan–Nelson [102] states  $\rho \lesssim M_{\text{Pl}}^2/L_{\text{IR}}^2$ ; the ECT estimate saturates this bound with  $L_{\text{IR}} \sim H_0^{-1}$ , which is an independent phenomenological consistency check.

## AD Late-time $\phi$ -first cosmological background apparatus

*Scope and legacy disclaimer.* This appendix records the legacy late-time background benchmark and the related numerical control constructions retained for reproducibility and continuity. Its specific parameter values (including  $\beta = 0.8$ ,  $\mu = 1.5$ ,  $\kappa = 15$ ,  $\phi_0 = -0.12$  and the associated numerical outputs such as  $t_0^{\text{ECT}} \simeq 13.1 \text{ Gyr}$  or  $\Delta H_0/H_0 \simeq \text{few per cent}$ ) are *not* the current retained-five-probe cosmological result.

They should not be used to quote the current cosmological constraint on  $\varepsilon$ ; the headline retained-band result is given in §16.5 ( $\varepsilon \in [0.0296, 0.0376]$  at  $1\sigma$ ) with methodology collected in Appendix AH. These values are preserved only for legacy reproducibility and numerical control; they must not be interpreted as retained-band central values or as a preferred closure-level point of the present paper. The material below is preserved only as a legacy reproducibility anchor for the benchmark late-time closure and the numerical control apparatus that underpins it.

This appendix records the benchmark late-time specialisation of the macroscopic background reduction derived in Section 13.5, with closure functions understood in the sense of the ordered-branch EFT-to-macroscopic mapping described in Section 13.5. It derives the minimal ECT background apparatus used for the late-time cosmology calculations in Section 19.1.

## AD.1 Derived condensate amplitude dynamics

Before specialising to the benchmark late-time closure, it is useful to record what the ordered-branch EFT already fixes at the structural level. The ordered-branch amplitude field  $u(x)$  satisfies the Euclidean EFT

$$S_{\text{ord}}^{(E)}[u, n] = \int d^4X \left[ \frac{Z_u}{2} (\partial u)^2 + \frac{\mathcal{C}_n}{2} u^2 (\partial n)^2 + W(u) + \dots \right], \quad (\text{AD.1})$$

where  $W(u)$  is the branch potential and  $u_\infty$  is the late-time screened amplitude satisfying  $W_u(u_\infty) = 0$ .

The macroscopic amplitude variable is defined by the amplitude ratio:

$$\boxed{\phi \equiv \frac{1}{\beta} \ln \frac{u}{u_\infty}} \quad \Longleftrightarrow \quad \boxed{u = u_\infty e^{\beta\phi}}. \quad (\text{AD.2})$$

This gives the response factor its structural origin:  $F(\phi) = u/u_\infty = e^{\beta\phi}$ .

**Derived kinetic function.** Substituting  $u = u_\infty e^{\beta\phi}$  into the kinetic term:

$$\frac{Z_u}{2} (\partial u)^2 = \frac{Z_u \beta^2 u_\infty^2}{2} e^{2\beta\phi} (\partial\phi)^2 \equiv \frac{\omega_0}{2} e^{2\beta\phi} (\partial\phi)^2. \quad (\text{AD.3})$$

The derived kinetic closure is therefore

$$\boxed{\omega(\phi) = \omega_0 e^{2\beta\phi}}, \quad (\text{AD.4})$$

not a constant  $K_0$ . The benchmark  $K(\phi) = K_0$  arises only as the leading local approximation of  $\omega(\phi)$  around  $\phi = 0$ .

**Derived potential.** The branch potential maps directly to the macroscopic potential via:

$$\boxed{U(\phi) = W(u_\infty e^{\beta\phi})}. \quad (\text{AD.5})$$

Near the screened branch  $\phi = 0$ , expanding  $W(u)$  around  $u_\infty$ :

$$U(\phi) = W_\infty + \frac{m_u^2 u_\infty^2}{2} (e^{\beta\phi} - 1)^2 + \frac{c_3 u_\infty^3}{3!} (e^{\beta\phi} - 1)^3 + \frac{c_4 u_\infty^4}{4!} (e^{\beta\phi} - 1)^4 + \dots, \quad (\text{AD.6})$$

which reduces to the benchmark quadratic  $V_0 + \frac{1}{2} m_\phi^2 \phi^2$  at leading order in  $\phi$ , while encoding the full nonlinear amplitude dependence at larger  $|\phi|$ .

**Full derived condensate background system.** The full macroscopic action with derived closure functions is:

$$S_{\text{full}} = \int d^4x \sqrt{-g} \left[ \frac{\bar{M}_{\text{Pl}}^2}{2} e^{\beta\phi} R - \frac{\bar{M}_{\text{Pl}}^2 \omega_0}{2} e^{2\beta\phi} (\nabla\phi)^2 - U(\phi) \right] + S_m + S_r. \quad (\text{AD.7})$$

For homogeneous FRW with  $\phi = \phi(t)$  this gives the *derived condensate background system*:

$$3e^{\beta\phi} H^2 = \frac{\rho_m + \rho_r + U(\phi)}{\bar{M}_{\text{Pl}}^2} + \frac{1}{2} \omega(\phi) \dot{\phi}^2 - 3H \beta e^{\beta\phi} \dot{\phi}, \quad (\text{AD.8})$$

$$-2e^{\beta\phi} \dot{H} = \frac{\rho_m + \frac{4}{3}\rho_r}{\bar{M}_{\text{Pl}}^2} + \omega(\phi) \dot{\phi}^2 + \beta^2 e^{\beta\phi} \dot{\phi}^2 + \beta e^{\beta\phi} \ddot{\phi} - H \beta e^{\beta\phi} \dot{\phi}, \quad (\text{AD.9})$$

$$\omega(\phi) (\ddot{\phi} + 3H\dot{\phi} + \beta\dot{\phi}^2) + \frac{U_{,\phi}}{\bar{M}_{\text{Pl}}^2} - 3\beta e^{\beta\phi} (2H^2 + \dot{H}) = 0. \quad (\text{AD.10})$$

In the  $N = \ln a$  form with  $q \equiv d\phi/dN$ , the Friedmann equation becomes the algebraic relation

$$E^2(N) = \frac{\Omega_{m*} e^{-3N} + \Omega_{r*} e^{-4N} + \Omega_U(\phi)}{e^{\beta\phi} (1 + \beta q) - \frac{\omega_0}{6} e^{2\beta\phi} q^2}, \quad (\text{AD.11})$$

where  $\Omega_U(\phi) \equiv U(\phi)/(3\bar{M}_{\text{Pl}}^2 H_*^2)$ . The benchmark  $K(\phi) = K_0$  denominator is the  $\phi \rightarrow 0$  limit of this expression. The scalar equation in  $N$ -variables is

$$\omega_0 e^{2\beta\phi} \left[ \phi'' + (3 + E'/E) \phi' + \beta (\phi')^2 \right] + \frac{3\Omega_{U,\phi}}{E^2} - 3\beta e^{\beta\phi} (2 + E'/E) = 0. \quad (\text{AD.12})$$

The benchmark late-time equations used in the current numerical section are obtained by replacing the full derived functions

$$\omega(\phi) = \omega_0 e^{2\beta\phi}, \quad U(\phi) = W(u_\infty e^{\beta\phi})$$

by their local screened-branch truncations around  $\phi = 0$ .

**Status.** Equations (AD.11)–(AD.12) are structurally derived from the ordered-branch EFT (Level A/bridge), with  $\omega_0$ ,  $m_u$ , and  $c_3, c_4$  remaining Level B coefficients. The current benchmark closure corresponds to the  $\phi \rightarrow 0$  local truncation; the full derived system (AD.11) is required for a self-consistent high- $z$  background branch that does not rely on an interim matter+radiation tail. The benchmark late-time closure introduced below should therefore be read as the local screened-branch truncation of the derived system above, rather than as an independently chosen scalar–tensor ansatz.

## AD.2 Schematic condensate evolution: computational notes

The schematic condensate evolution figures (Figs. 12 and 13) are constructed as follows.

**Three-stage model.** The condensate amplitude variable  $\phi_b$  is modelled with a smooth interpolation through three regimes:

1. *Ordering stage* ( $z \gtrsim z_{\text{ord}}$ , or equivalently  $t \lesssim t_{\text{BBN}}$ ): the amplitude grows from deep negative values ( $\phi \approx -3$ ) toward the stabilisation plateau, using a logistic-type interpolation:

$$\phi_b(z) = \phi_{\text{deep}} + (\phi_{\text{stab}} - \phi_{\text{deep}}) \times \frac{1}{2} \left[ 1 + \tanh((\log z_{\text{ord}} - \log z)/\sigma_{\text{ord}}) \right].$$

2. *Stabilisation* ( $z_{\text{stab}} \lesssim z \lesssim z_{\text{ord}}$ ):  $\phi_b \approx \phi_{\text{stab}} \approx -0.6$ , consistent with the derived-parent benchmark  $G_{\text{eff}}/G_N \approx 1.5$  at the JWST epoch  $z \sim 10$ .
3. *Late-time slow drift* ( $z \lesssim z_{\text{stab}}$ ):  $\phi_b$  continues to increase (approach the screened state  $\phi = 0$ ), reaching  $\phi_0 \approx -0.10$  at  $z = 0$ , consistent with  $G_{\text{eff}}(z=0)/G_N \approx 1.08$ .

**Derived quantities.** From  $\phi_b$  the derived observables follow algebraically:

$$u/u_\infty = e^{\beta\phi_b}, \quad G_{\text{eff}}/G_N = e^{-\beta\phi_b}, \quad w_\phi = -1 + \delta w e^{-z/z_{\text{drift}}}.$$

The benchmark parameter choices are  $\beta = 0.8$ ,  $\phi_{\text{deep}} = -3$ ,  $\phi_{\text{stab}} = -0.6$ ,  $\phi_0 = -0.10$ ,  $z_{\text{ord}} = 2000$ ,  $z_{\text{approach}} = 100$ . The stabilised value  $\phi_{\text{stab}} \approx -0.6$  is chosen to match the benchmark  $G_{\text{eff}}(z=10)/G_N \approx 1.5$  from the derived-parent analysis (Table 69). The key physical requirement is that  $\phi_b$  increases monotonically throughout cosmic history (the condensate approaches the screened state), consistent with the direction of evolution in the solved benchmark system.

**Time mapping.** The cosmic-time version (Fig. 13) uses the standard Planck 2018 background cosmology ( $H_0 = 67.4 \text{ km s}^{-1} \text{ Mpc}^{-1}$ ,  $\Omega_m = 0.315$ ,  $\Omega_\Lambda = 0.685$ ):

$$t(z) = \frac{1}{H_0} \int_z^\infty \frac{dz'}{(1+z') \sqrt{\Omega_r(1+z')^4 + \Omega_m(1+z')^3 + \Omega_\Lambda}}.$$

**Status.** These figures are schematic closure-level visualisations constructed from smooth interpolating functions, not outputs of the full self-consistent background solver. The generation scripts are available in the repository (scripts/fig\_condensate\_evolution.py and scripts/fig\_condensate\_evolution\_time.py).

### AD.3 Effective action and FRW reduction

We start from the effective scalar–tensor action

$$S_{\text{eff}} = \int d^4x \sqrt{-g} \left[ \frac{1}{2} f(\phi) R - \frac{1}{2} K(\phi) (\partial\phi)^2 - V(\phi) + \mathcal{L}_m \right]. \quad (\text{AD.13})$$

The effective gravitational stiffness and Newton coupling are

$$M_{\text{eff}}^2(\phi) = f(\phi), \quad G_{\text{eff}}(\phi) = \frac{1}{8\pi f(\phi)}. \quad (\text{AD.14})$$

For a spatially flat FRW metric  $ds^2 = -dt^2 + a^2(t) d\mathbf{x}^2$  and a homogeneous background  $\phi = \phi(t)$ , the effective equations are

$$3fH^2 = \rho_m + \rho_r + \frac{1}{2} K \dot{\phi}^2 + V - 3H\dot{f}, \quad (\text{AD.15})$$

$$-2f\dot{H} = \rho_m + \frac{4}{3}\rho_r + K\dot{\phi}^2 + \ddot{f} - H\dot{f}, \quad (\text{AD.16})$$

$$K(\ddot{\phi} + 3H\dot{\phi}) + \frac{1}{2} K_{,\phi} \dot{\phi}^2 + V_{,\phi} - \frac{1}{2} f_{,\phi} R = 0, \quad R = 6(2H^2 + \dot{H}). \quad (\text{AD.17})$$

### AD.4 Convenient form in $N = \ln a$

Setting  $N \equiv \ln a$  and

$$q(N) \equiv \frac{d\phi}{dN}, \quad \phi(N) = \frac{1}{\beta} \ln \frac{u(N)}{u_\infty},$$

one has  $\dot{\phi} = Hq$  and  $\dot{f} = Hf_{,\phi}q$ . Equation (AD.15) then gives the exact algebraic relation

$$H^2 = \frac{\rho_m + \rho_r + V}{3f - \frac{1}{2} K q^2 + 3f_{,\phi} q}. \quad (\text{AD.18})$$



## AD.5 Benchmark late-time closure (Level B)

Guided by the ordered-branch EFT-to-macroscopic mapping discussed in Section 13.5, we specialise the late-time closure to the following benchmark form. In particular, the benchmark closure should be understood as a small- $\phi$  truncation of the derived condensate background dynamics recorded in Section AD.1.

$$f(\phi) = f_0 e^{\beta\phi}, \quad K(\phi) = K_0, \quad V(\phi) = V_0 + \frac{1}{2} m_\phi^2 \phi^2, \quad (\text{AD.19})$$

Here the three choices do not have the same status. The exponential response factor is structurally motivated by  $u/u_\infty = e^{\beta\phi}$ . By contrast, the constant kinetic coefficient  $K(\phi) = K_0$  is the simplest benchmark truncation of the amplitude-sector stiffness, and the quadratic potential is the leading local expansion of the effective branch potential around the screened late-time regime  $\phi = 0$ . Thus Eq. (AD.19) should be read as the simplest benchmark realisation of the structurally anchored closure functions, not as their unique final ECT form.

**Status.** The existence of a late-time macroscopic background closure is inherited from the background reduction of the geometric branch. The explicit benchmark choice (AD.19) is Level B: its exponential response factor is structurally motivated, while its kinetic and potential terms are the simplest local benchmark specialisations.

with dimensionless parameters

$$E(N) \equiv \frac{H(N)}{H_*}, \quad \kappa \equiv \frac{K_0}{f_0}, \quad \mu^2 \equiv \frac{m_\phi^2}{H_*^2}, \quad \Omega_{V*} \equiv \frac{V_0}{3f_0 H_*^2}. \quad (\text{AD.20})$$

The benchmark closure therefore combines one structurally motivated ingredient and two simplest local benchmark choices:

$$\begin{aligned} f(\phi) &\sim e^{\beta\phi} \quad (\text{structural/bridge-level}), \\ K(\phi) &= K_0, \quad V(\phi) = V_0 + \frac{1}{2} m_\phi^2 \phi^2 \quad (\text{benchmark Level B truncations}). \end{aligned}$$

This distinction is essential when interpreting numerical outputs.

Here  $H_*$  is an external calibration scale of the late-time closure. It should not be read as a privileged  $\Lambda$ CDM-inferred value of  $H_0$ , but simply as the normalization used to construct the dimensionless background variables.

The macroscopic variable used in this late-time closure is

$$\phi(N) = \frac{1}{\beta} \ln \frac{u(N)}{u_\infty},$$

where  $u(N)$  is the ordered-branch condensate amplitude introduced in Section 3.2. In the late-time scalar–tensor closure all background equations are written in terms of  $\phi$ , not directly in terms of the dimensionful amplitude  $u$ .

The dimensionless Friedmann equation becomes

$$E^2(N) = \frac{\Omega_{m*} e^{-3N} + \Omega_{r*} e^{-4N} + \Omega_{V*} + \frac{\mu^2}{6} \phi^2}{e^{\beta\phi} - \frac{\kappa}{6} q^2 + \beta e^{\beta\phi} q}. \quad (\text{AD.21})$$

## AD.6 Admissible late-time closure family beyond the benchmark

The benchmark closure (AD.19) is useful because it provides the simplest explicit late-time specialisation of the ordered-branch macroscopic system. However, it should not be mistaken for the unique admissible closure. The ordered-branch EFT-to-macroscopic mapping of Section 13.5 already suggests a broader family of late-time closures.

The structural part is the response factor

$$f(\phi) \propto e^{\beta\phi},$$

since this is directly tied to the amplitude ratio  $u/u_\infty = e^{\beta\phi}$ . By contrast, the kinetic and potential sectors admit more general late-time benchmark expansions:

$$K(\phi) = K_0 \left( 1 + k_1\phi + k_2\phi^2 + \dots \right), \quad (\text{AD.22})$$

$$V(\phi) = V_0 + \frac{1}{2}m_\phi^2\phi^2 + \frac{\lambda_3}{3!}\phi^3 + \frac{\lambda_4}{4!}\phi^4 + \dots. \quad (\text{AD.23})$$

These extensions should be interpreted carefully.

**(i) Why they are natural.** From the ordered-branch EFT perspective,  $K(\phi)$  is the macroscopic image of amplitude-sector stiffness and  $V(\phi)$  is the macroscopic image of the branch potential  $W(u_\infty e^{\beta\phi})$ . A constant  $K$  and a purely quadratic  $V$  are therefore not expected to be exact in full generality; they are simply the leading local benchmark truncation around the screened late-time branch.

**(ii) Why the benchmark remains useful.** The benchmark closure (AD.19) is the first nontrivial member of the admissible family (AD.22)–(AD.23). It isolates the minimal late-time effect of amplitude drift without introducing a large parameter space too early.

**(iii) What future code should generalise.** Once the fixed-point solver is stabilised for the benchmark closure, the next natural code-level upgrade is to replace the hard-coded

$$K(\phi) = K_0, \quad V(\phi) = V_0 + \frac{1}{2}m_\phi^2\phi^2$$

by parameterisable families such as (AD.22)–(AD.23). This would allow the article and code to test whether the benchmark truncation is quantitatively robust or merely the simplest illustrative realisation.

**Status.** The existence of an admissible closure family is structural/bridge-level, because it follows from the ordered-branch EFT origin of the closure functions. The explicit coefficients  $k_i, \lambda_i$  are Level B.

This immediately defines one of the central late-time open problems of ECT: to determine which cosmological outputs are robust under admissible deformations of the benchmark closure, and which are artefacts of the simplest truncation.

## AD.7 Numerical robustness programme for the admissible closure family

The existence of the admissible closure family (AD.22)–(AD.23) immediately raises a numerical robustness question: which late-time outputs are stable under admissible deformations of the benchmark closure, and which are sensitive to the particular truncation (AD.19)?

At the present stage, the role of the benchmark closure is clear: it is the first explicit late-time realisation of the ordered-branch macroscopic system, and therefore the natural starting point for code development. But the next stage is equally clear: the code must compare that benchmark against deformed closures of the admissible family.

The most relevant observables for such robustness tests are:

1. the direct and low- $z$  inferred Hubble shifts;
2. the present cosmic age  $t_0$ ;
3. the epoch-dependent age  $t_U(z)$ ;
4. the galaxy-lifetime grids  $t_{\text{gal}}(z_{\text{obs}}; z_{\text{form}})$ ;

5. the distance shift  $\Delta D_L/D_L$ ;
6. the growth proxy  $\mathcal{G}(z)$ ;
7. the background critical scale  $g_{\text{bg}}^\dagger(z)$ .

A late-time output should therefore be regarded as *numerically robust* only if it persists, at least qualitatively and preferably quantitatively, under admissible deformations of  $K(\phi)$  and  $V(\phi)$ . Conversely, if a claimed effect disappears under mild admissible deformation, it should be interpreted only as a property of the benchmark truncation and not yet as a robust ECT feature.

As an initial numerical check, a mild deformed member of the admissible family has been compared directly against the benchmark closure. For example, taking

$$k_1 = 0.2, \quad \lambda_3 = 0.1, \quad k_2 = \lambda_4 = 0,$$

the code finds only a small change in the late-time Hubble shift: from approximately 2.90% in the benchmark member to approximately 2.85% in the deformed run. The induced changes in  $t_0$ ,  $t_U(z)$ , and  $t_{\text{gal}}(z_{\text{obs}}; z_{\text{form}})$  are correspondingly small at the current benchmark level. Thus the first benchmark conclusion appears numerically stable under at least mild admissible deformations, although a broader scan is still required before claiming full robustness.

The present derived-parent scan goes beyond the earlier benchmark-only robustness check: it solves the full linear growth equation on the derived-parent background and combines this with semi-analytic maturity factors for collapse and BH-assisted development. This is the first stage at which the ECT late-time programme can be tested simultaneously against Hubble-shift, age-budget, and JWST maturity requirements.

This robustness programme is now directly supported by the code-level interface and artefact layers introduced in Appendices AU.3 and AU.4.

## AD.8 Derived-parent working corridor and JWST object budgets

A first systematic scan of the derived-parent condensate background was performed over  $\omega_0 \in \{15, 20, 25, 30, 40, 50\}$ ,  $\phi_0 \in \{-0.15, -0.12, -0.10, -0.08, -0.05\}$ , with  $\beta = 0.8$ ,  $\mu = 1.5$ ,  $A_2 = \mu^2/(6\beta^2)$ ,  $A_3 = A_4 = 0$ . The scan identifies the few-percent H1 benchmark corridor described in the main text (Section 19.1) and selects three representative working points.

For the four JWST anchor cases considered in the main text, the derived-parent age of the Universe at observation is smaller than in the reference background by an amount ranging from several tens of Myr (highest-redshift cases) to a few hundred Myr (lower-redshift quiescent case at  $z = 4.9$ ). The minimum required maturity speed-up is therefore

$$\mathcal{R}_{\text{req}}(z_{\text{obs}}) = \frac{t_U^{\text{ref}}(z_{\text{obs}})}{t_U^{\text{ECT}}(z_{\text{obs}})}.$$

In the preferred working points this factor is typically  $\mathcal{R}_{\text{req}} \sim 1.19\text{--}1.24$ .

The two semi-analytic maturity factors used are

$$\mathcal{R}_{\text{gal}} = \frac{D_{\text{ECT}}}{D_{\text{ref}}} \frac{t_{\text{ff}}^{\text{ref}}}{t_{\text{ff}}^{\text{ECT}}}, \quad \mathcal{R}_{\text{BH}} = \frac{D_{\text{ECT}}}{D_{\text{ref}}} \frac{t_{\text{BH}}^{\text{ref}}}{t_{\text{BH}}^{\text{ECT}}},$$

where free-fall time scales as  $t_{\text{ff}} \propto (G_{\text{eff}}\rho)^{-1/2}$  and BH growth time as  $t_{\text{BH}} \propto G_{\text{eff}}^{-1}$  (Salpeter-like estimate). For the representative working points one finds

$$\mathcal{R}_{\text{gal}} \approx 1.21\text{--}1.23, \quad \mathcal{R}_{\text{BH}} \approx 1.48\text{--}1.54.$$

This shows that the current derived-parent ECT corridor is close to the required level for ordinary galaxy-assembly channels and clearly above it for BH-assisted maturity channels. This is a concrete partial result rather than a full resolution. The detailed numerical logic used to obtain this result is summarised in Appendix AD.9.

## AD.9 Current computational pipeline for the derived-parent JWST analysis

The present numerical programme for the JWST problem proceeds in five explicit stages.

**(i) Background scan.** A first scan is performed over the parameter rectangle

$$\omega_0 \in \{15, 20, 25, 30, 40, 50\}, \quad \phi_0 \in \{-0.15, -0.12, -0.10, -0.08, -0.05\},$$

at fixed

$$\beta = 0.8, \quad \mu = 1.5, \quad A_2 = \frac{\mu^2}{6\beta^2}, \quad A_3 = A_4 = 0.$$

For each point the derived-parent background is solved and the late inferred Hubble shift, age quantities, and high-redshift background outputs are recorded.

**(ii) Selection of representative working points.** From the few-percent H1 benchmark corridor, three representative points are selected: a balanced point, a late-time-shift-priority point, and an age-priority point. These serve as the working points for the next numerical layers.

**(iii) Linear growth solution.** For each representative point, the full linear growth equation

$$D'' + \left(2 + \frac{H'}{H}\right) D' - \frac{3}{2} \Omega_m(z) \frac{G_{\text{eff}}(z)}{G_N} D = 0$$

is solved on the already-determined derived-parent background. This replaces the earlier use of the proxy  $\mathcal{G}(z) = G_{\text{eff}}(z)/H^2(z)$  as the sole indicator of growth. Its derivation is recorded in Appendix AD.10.

**(iv) JWST object age budgets.** The age of the Universe at the redshift of observation is then computed for a set of representative JWST anchor cases, together with the available galaxy lifetime between an assumed formation redshift and the epoch of observation. The minimum required maturity speed-up is

$$\mathcal{R}_{\text{req}}(z_{\text{obs}}) = \frac{t_U^{\text{ref}}(z_{\text{obs}})}{t_U^{\text{ECT}}(z_{\text{obs}})}.$$

**(v) Semi-analytic maturity accounting.** Finally, the age-budget deficit is combined with the numerically solved linear growth and with local acceleration factors. In the current implementation this is done through

$$\mathcal{R}_{\text{gal}} = \frac{D_{\text{ECT}}}{D_{\text{ref}}} \frac{t_{\text{ff}}^{\text{ref}}}{t_{\text{ff}}^{\text{ECT}}}, \quad \mathcal{R}_{\text{BH}} = \frac{D_{\text{ECT}}}{D_{\text{ref}}} \frac{t_{\text{BH}}^{\text{ref}}}{t_{\text{BH}}^{\text{ECT}}},$$

where  $t_{\text{ff}} \propto (G_{\text{eff}}\rho)^{-1/2}$  and  $t_{\text{BH}} \propto G_{\text{eff}}^{-1}$  are the present semi-analytic collapse and BH-growth proxies. Their status and derivation are recorded in Appendix AD.11. This pipeline does not yet constitute a full morphology-level treatment, but it already provides a quantitatively structured test of whether one and the same ECT parameter corridor can simultaneously address the Hubble shift, the cosmic-age layer, and the observed maturity of JWST systems.

**Status.** The present pipeline reaches the level of a solved background, solved linear growth, and semi-analytic maturity accounting. It does not yet include full morphology-level calculations, hydrodynamic structure formation, or direct SMBH–host coevolution simulations. In the present code implementation this pipeline is represented by machine-readable outputs for the derived-parent scan, the selected working points, the JWST object age budgets, the solved linear-growth table, and the combined maturity budgets.

## AD.10 Derivation of the linear growth equation on the ECT background

The linear-growth layer used in the present JWST analysis is not introduced independently of the background dynamics. Rather, it is the first perturbative extension of the derived-parent ECT background in the pressureless subhorizon regime.

**Assumptions.** We work in the matter-dominated perturbation sector, neglect pressure and anisotropic stress, and restrict attention to subhorizon scales for which the dominant effect of the modified background is captured by the time-dependent effective gravitational coupling

$$G_{\text{eff}}(z) = G_N e^{-\beta\phi(z)}.$$

At this level the ECT modification enters primarily through:

1. the modified background expansion  $H(z)$ ;
2. the modified source strength  $G_{\text{eff}}(z)$ .

**Perturbation equations.** For the matter overdensity  $\delta = \delta\rho_m/\rho_m$ , the continuity and Euler equations combine with the modified Poisson equation to give

$$\ddot{\delta} + 2H\dot{\delta} = 4\pi G_{\text{eff}}(z)\rho_m\delta.$$

Using

$$\rho_m(z) = 3\bar{M}_{\text{Pl}}^2 H^2(z) \Omega_m(z),$$

this becomes

$$\ddot{\delta} + 2H\dot{\delta} = \frac{3}{2}H^2(z)\Omega_m(z)\frac{G_{\text{eff}}(z)}{G_N}\delta.$$

**Conversion to  $N = \ln a$ .** Writing

$$D(N) \equiv \delta(N), \quad ' \equiv \frac{d}{dN},$$

one has

$$\dot{\delta} = HD', \quad \ddot{\delta} = H^2 D'' + \dot{H} D'.$$

Dividing the perturbation equation by  $H^2$  and using  $\dot{H}/H^2 = H'/H$  gives

$$D'' + \left(2 + \frac{H'}{H}\right) D' - \frac{3}{2}\Omega_m(z)\frac{G_{\text{eff}}(z)}{G_N} D = 0. \quad (\text{AD.24})$$

For numerical work,

$$\Omega_m(z) = \frac{\Omega_{m*}(1+z)^3}{E^2(z)}, \quad E(z) \equiv \frac{H(z)}{H_*}.$$

**Status.** Equation (AD.24) is a derived perturbative layer on top of the already solved ECT background. Its validity is limited to the linear, pressureless, subhorizon regime. It should therefore be interpreted as the first non-background test of structure development in ECT, not as a full morphology-level treatment.

## AD.11 Semi-analytic maturity factors for collapse and BH-assisted development

The present JWST analysis does not yet attempt a full morphology-level simulation of galaxy or SMBH formation. Instead, it supplements the solved background and solved linear growth with two semi-analytic local development factors.

**Free-fall / collapse factor.** For a self-gravitating region of characteristic density  $\rho$ , the free-fall timescale scales as

$$t_{\text{ff}} \sim (G_{\text{eff}}\rho)^{-1/2}.$$

Hence the relative collapse acceleration between the ECT background and the reference background is estimated through

$$\frac{t_{\text{ff}}^{\text{ref}}}{t_{\text{ff}}^{\text{ECT}}} = \sqrt{\frac{G_{\text{eff}}^{\text{ECT}}}{G_N}} = e^{-\beta\phi(z)/2}.$$

**BH-growth-like factor.** For BH-assisted maturity channels, the present implementation uses a Salpeter-like local estimate in which the characteristic growth time is taken to scale as  $t_{\text{BH}} \propto G_{\text{eff}}^{-1}$ , giving

$$\frac{t_{\text{BH}}^{\text{ref}}}{t_{\text{BH}}^{\text{ECT}}} = \frac{G_{\text{eff}}^{\text{ECT}}}{G_N} = e^{-\beta\phi(z)}.$$

**Combined maturity factors.** The current article defines

$$\mathcal{R}_{\text{gal}} = \frac{D_{\text{ECT}}}{D_{\text{ref}}} \frac{t_{\text{ff}}^{\text{ref}}}{t_{\text{ff}}^{\text{ECT}}}, \quad \mathcal{R}_{\text{BH}} = \frac{D_{\text{ECT}}}{D_{\text{ref}}} \frac{t_{\text{BH}}^{\text{ref}}}{t_{\text{BH}}^{\text{ECT}}}. \quad (\text{AD.25})$$

**Status.** These factors are not a substitute for full structure-formation simulations. They are controlled first-order development proxies whose purpose is to test whether the same ECT parameter corridor that improves the Hubble shift can also plausibly compensate the tighter high-redshift age budget. These factors should be read as semi-analytic development budgets rather than direct morphology-level predictions. In particular, the distinction between ordinary galaxy-assembly channels and BH-assisted maturity channels should be understood at the level of the present semi-analytic accounting, not as a full morphological classification of observed JWST systems.

## AD.12 Orientation-stress proxy for the JWST maturity budget

*Status: Level B proxy estimate. The orientation-stress coefficient  $c_1$  is not yet derived from first principles (OP-c1); the analysis below introduces a proxy parameter  $\eta_{\Theta}$  and traces its effect on the maturity factors defined in eq. (AD.25).*

**Structural motivation.** The full nonlinear field equations (13.35) contain the anisotropic orientation stress  $\Theta_{\mu\nu}[n]$  (13.23), which has no analogue in the scalar  $\phi$ -sector alone. On a homogeneous FRW background,  $\Theta_{\mu\nu}$  is absorbed into the background causal structure and does not contribute an independent Friedmann term (§13.5). At the *perturbation* level, however,  $\Theta_{\mu\nu}$  modifies the sub-horizon Poisson equation:

$$\nabla^2\Phi_N = -4\pi G_{\text{eff}}\bar{\rho}\delta - c_1 n^\alpha n^\beta \delta R_{\alpha\beta}, \quad (\text{AD.26})$$

where the second term is the linearised perturbation of the orientation stress on the homogeneous background.

**Proxy parameter.** In the sub-horizon quasi-Newtonian regime the additional curvature perturbation  $\delta R_{\alpha\beta}$  is itself proportional to  $G_{\text{eff}}\bar{\rho}\delta$ , so the net effect is an effective enhancement of the gravitational source:

$$G_{\text{eff}}^{\text{pert}}(z) = G_{\text{eff}}(z)(1 + \eta_{\Theta}), \quad \eta_{\Theta} \equiv \mathcal{O}(|c_1|). \quad (\text{AD.27})$$

Here  $\eta_{\Theta}$  is treated as a dimensionless proxy parameter, not as a derived coefficient. Its value is controlled by  $c_1$  (OP-c1); in the cluster analysis (§AP.5), the phenomenological range  $|c_1| \sim 0.015\text{--}0.16$  gives  $\eta_{\Theta} \sim 0.01\text{--}0.1$ .

**Effect on maturity factors.** The free-fall timescale scales as  $t_{\text{ff}} \propto G_{\text{eff}}^{-1/2}$  and the BH-growth timescale as  $t_{\text{BH}} \propto G_{\text{eff}}^{-1}$ . Including the perturbation-level enhancement therefore shifts the maturity factors (AD.25) to

$$\mathcal{R}_{\text{gal}}^{\text{full}} \approx \mathcal{R}_{\text{gal}} \sqrt{1 + \eta_{\Theta}}, \quad \mathcal{R}_{\text{BH}}^{\text{full}} \approx \mathcal{R}_{\text{BH}} (1 + \eta_{\Theta}). \quad (\text{AD.28})$$

**Implications.** Since the BH-assisted channel already satisfies  $\mathcal{R}_{\text{BH}} > \mathcal{R}_{\text{req}}$  for all anchor cases (see the retained §16.5 analysis), any  $\eta_{\Theta} > 0$  only strengthens this result. For the galaxy-assembly channel, which is observationally ambiguous ( $\mathcal{R}_{\text{gal}} \approx \mathcal{R}_{\text{req}}$ ), even a modest positive  $\eta_{\Theta}$  would relax the tension, potentially shifting a marginal case toward a more comfortable one. The quantitative magnitude remains contingent on OP-c1.

**What this does not establish.** This subsection does not derive the perturbation-level coupling of  $\Theta_{\mu\nu}$  from the ECT action. The replacement  $G_{\text{eff}} \rightarrow G_{\text{eff}}^{\text{pert}} = G_{\text{eff}}(1 + \eta_{\Theta})$  is a proxy parametrisation of the orientation-stress contribution at the sub-horizon level, not a first-principles derivation of the full perturbation system. Accordingly, the formulas for  $\mathcal{R}_{\text{gal}}^{\text{full}}$  and  $\mathcal{R}_{\text{BH}}^{\text{full}}$  (AD.28) should be read as structural scaling estimates within that proxy description, not as completed quantitative predictions. A first-principles derivation of  $c_1$ , and hence of  $\eta_{\Theta}$ , remains open (OP-c1).

### AD.13 Slow-drift regime and present-epoch Hubble shift

In the slow-drift branch ( $|q| \ll 1$ ,  $\kappa q^2 \ll 1$ ,  $|\beta q| \ll 1$ ), eq. (AD.21) simplifies to  $H^2 \approx (\rho + V)/(3f)$ . Within the benchmark closure (AD.19), this yields a transparent analytic estimate for the present-epoch Hubble shift. Comparing with the screened reference branch of the same closure, defined by  $\phi = 0$  and therefore constant  $f_0, V_0$ :

$$\frac{\Delta H_0}{H_0} \approx \frac{\mu^2 \phi_0^2}{12} - \frac{1}{2} \beta \phi_0. \quad (\text{AD.29})$$

The two terms represent vacuum drift (positive) and effective Planck-mass drift (sign determined by  $\beta \phi_0$ ).

The slow-drift scalar balance gives

$$q \approx \frac{\beta e^{\beta \phi}}{\kappa} \left( 2 + \frac{E'}{E} \right) - \frac{\mu^2 \phi}{3 \kappa E^2}, \quad (\text{AD.30})$$

showing that the late drift of  $\phi$  is driven by the curvature coupling  $f_{,\phi} R$  balanced against the restoring force  $V_{,\phi}$  and the kinetic stiffness  $\kappa$ .

### AD.14 Distances, age, and JWST-related background effects

Once  $E(z)$  is solved, one obtains

$$D_L(z) = (1+z)c_* \int_0^z \frac{dz'}{H(z')}, \quad D_A(z) = \frac{c_*}{1+z} \int_0^z \frac{dz'}{H(z')}, \quad (\text{AD.31})$$

$$t_{\text{lookback}}(z) = \int_0^z \frac{dz'}{(1+z')H(z')}, \quad t_0 = \int_0^\infty \frac{dz}{(1+z)H(z)}, \quad (\text{AD.32})$$

$$t_U(z) = \int_z^\infty \frac{dz'}{(1+z')H(z')}, \quad t_{\text{gal}}(z_{\text{obs}}; z_{\text{form}}) = t_U(z_{\text{obs}}) - t_U(z_{\text{form}}). \quad (\text{AD.33})$$

These background quantities control the JWST background layer. The same condensate-amplitude drift that shifts the late inferred  $H_0$  also changes inferred luminosity distances, the age of the Universe at the epoch of observation,

$$t_U(z),$$

and therefore the available formation time of an observed galaxy,

$$t_{\text{gal}}(z_{\text{obs}}; z_{\text{form}}).$$

This makes the Hubble shift, cosmic age, and JWST-related early-structure inference parts of a single coupled background problem in the late-time ECT closure.

## AE Dimensional scaffold for gravitational waves from the ordering transition

This appendix provides a minimal dimensional scaffold for estimating the stochastic gravitational-wave background generated during the  $O(4) \rightarrow O(3)$  ordering transition. It does not constitute a first-principles prediction; its purpose is to make the sign-level production statement of §13.8 quantitatively traceable.

**Source equation.** In the emergent FRW background, the tensor perturbation  $h_{ij}$  satisfies (in conformal time  $\eta$ ):

$$h''_{ij} + 2\mathcal{H}h'_{ij} + k^2 h_{ij} = 16\pi G \Pi_{ij}^{\text{TT}}, \quad (\text{AE.1})$$

where  $\Pi_{ij}^{\text{TT}}$  is the transverse-traceless part of the anisotropic stress generated by the inhomogeneous ordering dynamics.

**Dimensional estimate.** The characteristic GW strain at production is controlled by the dimensionless ratio

$$h_{\text{prod}} \sim G \Delta \rho L_{\text{corr}}^2 / c^4, \quad (\text{AE.2})$$

where  $\Delta \rho$  is the anisotropic stress scale and  $L_{\text{corr}}$  is the correlation length of the ordering inhomogeneities. The peak frequency at production is set by

$$f_{\text{prod}} \sim c / L_{\text{corr}}. \quad (\text{AE.3})$$

**Redshift to today.** If the ordering transition occurs at an effective redshift  $z_{\text{ord}}$ , the peak frequency today is approximately

$$f_0 \sim \frac{f_{\text{prod}}}{1 + z_{\text{ord}}}, \quad (\text{AE.4})$$

while the present-day gravitational-wave energy fraction is related to its production value by the standard redshifting logic

$$\Omega_{\text{GW},0}(f_0) \sim \Omega_{\text{GW,prod}}(f_{\text{prod}}) \left( \frac{a_{\text{ord}}}{a_0} \right)^4 \left( \frac{H_{\text{ord}}}{H_0} \right)^2. \quad (\text{AE.5})$$

Thus the present signal depends not only on the source strength at production but also on the subsequent expansion history.

**What this does and does not provide.** Equations (AE.2)–(AE.5) provide a dimensional scaffold, not a closed prediction. The quantity  $\Omega_{\text{GW,prod}}$  must itself be obtained from the ordering-source efficiency and cannot yet be computed from first principles within the present closure. The quantities  $\Delta \rho$ ,  $L_{\text{corr}}$ , and  $z_{\text{ord}}$  are transition parameters that must be derived from the ordering dynamics (duration, latent heat analogue, correlation length, domain structure). Until this microphysics is closed,  $\Omega_{\text{GW}}(f)$  remains parametrically open.

**Distinction from standard first-order transitions.** The ECT ordering transition is not a thermal bubble-nucleation event in a pre-existing Lorentzian spacetime. Standard thermal-transition formulae (e.g. based on  $\alpha$ ,  $\beta/H$ ,  $v_w$ ) therefore cannot be applied directly. The scaffold above is formulated in terms of general dimensional quantities applicable to any causal source of anisotropic stress, without assuming a thermal equation of state.



## AF Sign-level cosmological consequences of the ordered branch

This appendix collects the sign-level structural results of the ordered-branch cosmology programme in a self-contained form, so that the main text can reference them as compact theorem-like statements.

**C1. No-phantom bound.** If the kinetic coefficient satisfies  $\omega(\phi) > 0$  in the adopted  $\phi$ -first closure, then the homogeneous amplitude-sector equation of state satisfies  $w_\phi \geq -1$ , with equality only in the frozen limit  $\dot{\phi} = 0$ .

*Proof.*  $K = \frac{1}{2}\omega\dot{\phi}^2 \geq 0$ . Hence  $w = (K - U)/(K + U) \geq -1$ .  $\square$

**C2. Screened  $\Lambda$ CDM limit.** In the limit  $\phi \rightarrow 0$ ,  $\dot{\phi} \rightarrow 0$ , the full background system reduces to the standard Einstein–Friedmann form with an effective vacuum contribution determined by  $U(0)$ .

**C3. Upward Hubble-shift sign theorem.** Within the class of monotonic ordered-branch backgrounds, if  $G_{\text{eff}}(z) > G_N$  over the late-time redshift range where the benchmark drift is active, then the inferred late-time Hubble scale obtained from a fixed acoustic-angle analysis is shifted upward relative to the screened limit (H1 benchmark route; see §16.5).

*Reason.* At fixed sound-horizon calibration and observed angular acoustic scale, enhanced high- $z$  effective gravity reduces the angular-diameter distance to last scattering, which is compensated in the inference by a higher late-time expansion scale.  $\square$

**C4. JWST age-budget enhancement route.** If the same ordered-branch background that produces the Hubble shift also increases the effective early-time gravitational coupling  $G_{\text{eff}}(z) > G_N$  and relaxes the late-time age budget, then the formation-time tension for early luminous structures is reduced relative to the screened  $\Lambda$ CDM reference branch. The sign of this effect is structurally fixed; its magnitude remains closure-dependent.

**C5. Correlated-sign prediction.** Within any single admissible ordered-branch closure, the same background  $\phi_b(z)$  controls  $w(z)$ ,  $H(z)$ ,  $G_{\text{eff}}(z)$ , and the Lorentzian age budget simultaneously. Any upward shift of the inferred late-time Hubble scale is therefore necessarily correlated with a specific sign pattern in the other three observables.

## AG Extraction of the effective uniform- $\varepsilon$ interval from the Hubble + $r_s$ channel

This appendix derives an effective H1-type extraction of  $\varepsilon$  from the simplified Hubble +  $r_s$  channel used in the rebuilt §15.5. It is not a full CMB-to-local inference pipeline and does not by itself establish a complete H2-level resolution of the Hubble tension. Its output is the one-dimensional  $\varepsilon$ -interval quoted for the Hubble +  $r_s$  row of Table 61, extracted under the uniform- $\varepsilon$  ansatz of §16.5 and the common background module described in Appendix AH. The forward-modelling machinery — the late-time ordered-branch background and its auxiliary numerical algorithms — is collected in Appendix AD and Appendix AU. The present appendix is the inverse step: given observational inputs and the uniform- $\varepsilon$  ansatz, to extract the one-dimensional  $\varepsilon$ -interval that this single channel admits at the common-background level.

### AE.1 Physics of the probe

The Hubble tension is not simply a discrepancy between two direct measurements of  $H_0$ : it is a mismatch between the local distance-ladder value and the  $H_0$  inferred from the acoustic angular scale once the sound horizon  $r_s$  is modelled. This is why the present channel is naturally a Hubble +  $r_s$  channel rather than a pure  $H_0$ -only constraint. The local distance-ladder determination  $H_0^{\text{SHOES}}$  uses Cepheid-calibrated Type Ia

supernovae and is insensitive to sound-horizon physics. The CMB-based determination  $H_0^{\text{Planck}}$  is obtained from the acoustic-scale angle  $\theta_s = r_s/D_A(z_*)$ , measured to high precision by the Planck mission [88]. A shift in the inferred late-time expansion rate arises once the late-time gravitational response function is allowed to differ from the  $\Lambda$ CDM form. In the effective uniform- $\varepsilon$  layer of §16.5 this response is parametrised by

$$\frac{G_{\text{eff}}(z)}{G_N} = (1+z)^{2\varepsilon}. \quad (\text{AG.1})$$

Under this parametrisation, both the low-redshift distance integral (entering  $H_0^{\text{Planck}}$  through  $D_A(z_*)$ ) and the high-redshift sound-horizon integral (entering  $r_s$ ) are modified. The channel therefore tests  $\varepsilon$  through the joint constraint imposed by a fixed, precisely measured  $\theta_s$  and an independently determined local  $H_0$ . The output of the extraction is an H1-type effective band for  $\varepsilon$ : a range of values for which the common-background module, deformed by  $(1+z)^{2\varepsilon}$ , shifts the CMB-inferred  $H_0$  upward into statistical compatibility with the local distance-ladder value.

## AE.2 Observational inputs

The two anchoring values are  $H_0^{\text{Planck}} = 67.4 \pm 0.5 \text{ km s}^{-1} \text{ Mpc}^{-1}$  from Planck 2018 in  $\Lambda$ CDM [88] and  $H_0^{\text{SH0ES}} = 73.04 \pm 1.04 \text{ km s}^{-1} \text{ Mpc}^{-1}$  from the SH0ES distance-ladder analysis [104]. The target shift to be accommodated is therefore

$$\Delta H_0^{\text{obs}} \equiv H_0^{\text{SH0ES}} - H_0^{\text{Planck}} \approx 5.64 \text{ km s}^{-1} \text{ Mpc}^{-1}, \quad \sigma_{\text{tot}} = \sqrt{\sigma_P^2 + \sigma_{\text{SH}}^2} \approx 1.15 \text{ km s}^{-1} \text{ Mpc}^{-1}. \quad (\text{AG.2})$$

The acoustic-scale measurement  $\theta_s$  is taken as fixed at the Planck value; the  $\varepsilon$ -scan is carried out at fixed  $\theta_s$ , such that the  $\varepsilon$ -deformation modifies  $r_s$  and  $D_A(z_*)$  in correlated ways.

## AE.3 ECT-side model and extraction scope

Under the uniform- $\varepsilon$  ansatz, the dimensionless Hubble rate reads

$$E_{\text{ECT}}^2(z, \varepsilon) = \Omega_r (1+z)^4 + \Omega_m (1+z)^{3+2\varepsilon} + \Omega_\Lambda (1+z)^{2\varepsilon}, \quad (\text{AG.3})$$

with  $\Omega_m = 0.315$ ,  $\Omega_r = 9.2 \times 10^{-5}$ ,  $\Omega_\Lambda = 1 - \Omega_m - \Omega_r$  adopted as the common background proxy (see Appendix AH for the background-module framing and its role as the single source of truth for all retained extraction channels). The low-redshift distance integral is

$$I(\varepsilon) = \int_0^{z_*} \frac{dz}{E_{\text{ECT}}(z, \varepsilon)}, \quad z_* = 1089.80, \quad (\text{AG.4})$$

and the sound horizon at the drag epoch is

$$r_s(\varepsilon) = \int_{z_{\text{drag}}}^{\infty} \frac{c_s(z)}{H_0^P E_{\text{ECT}}(z, \varepsilon)} dz, \quad z_{\text{drag}} = 1059.94, \quad (\text{AG.5})$$

with the baryon–photon sound speed  $c_s(z) = c/\sqrt{3(1+R(z))}$ ,  $R(z) = (3\Omega_b/4\Omega_r)(1+z)^{-1}$ ,  $\Omega_b = 0.0493$ . At fixed  $\theta_s$ , the inferred  $H_0$  under  $\varepsilon$ -deformation becomes

$$H_0^{\text{inferred}}(\varepsilon) = H_0^P \cdot \frac{I(\varepsilon)}{I(0)} \cdot \frac{r_s(0)}{r_s(\varepsilon)}. \quad (\text{AG.6})$$

For  $\varepsilon > 0$ , the sound-horizon integral decreases by a larger fractional amount than the distance integral, so the ratio in (AG.6) exceeds unity and  $H_0^{\text{inferred}}$  is pushed upward.

**Held fixed under the present proxy.**  $\Omega_m = 0.315$ ,  $\Omega_\Lambda$ ,  $\Omega_r$ ,  $\Omega_b$ ; the baryon–photon sound-speed form  $c_s(z)$ ;  $z_* = 1089.80$ ,  $z_{\text{drag}} = 1059.94$ ; the acoustic-scale anchor  $\theta_s$ .

**Varied.**  $\varepsilon$  only (one-dimensional scan). Through (AG.3) the variation of  $\varepsilon$  propagates automatically, via the common background module, into  $E(z)$ ,  $H(z)$ ,  $I(\varepsilon)$ ,  $r_s(\varepsilon)$ , and  $H_0^{\text{inferred}}(\varepsilon)$ .

**Not included at this proxy level.** A full Boltzmann-level recombination pipeline; a full CMB likelihood; a joint fit of early-time parameters together with  $\varepsilon$ ; and an ECT-closure-level background replacing the  $\Lambda$ CDM proxy. The consequences of each of these omissions are addressed in AE.7.

#### AE.4 Extraction statistic

The  $\varepsilon$ -dependent prediction for the Hubble-tension shift is

$$\Delta H_0^{\text{pred}}(\varepsilon) = H_0^{\text{inferred}}(\varepsilon) - H_0^P. \quad (\text{AG.7})$$

The single-parameter chi-squared for this channel is

$$\chi^2(\varepsilon) = \left[ \frac{\Delta H_0^{\text{pred}}(\varepsilon) - \Delta H_0^{\text{obs}}}{\sigma_{\text{tot}}} \right]^2. \quad (\text{AG.8})$$

This is the only quantity minimised in the present extraction; no additional nuisance-parameter profiling is performed at this proxy level.

#### AE.5 Interval definition and origin of the width

In this one-parameter framework the best-fit  $\varepsilon_*$  is defined by the minimum of  $\chi^2(\varepsilon)$ , which coincides with the unique root of  $\Delta H_0^{\text{pred}}(\varepsilon) = \Delta H_0^{\text{obs}}$  in the physical region  $\varepsilon \geq 0$ . The  $1\sigma$  interval is defined by  $\Delta\chi^2 \leq 1$  about this minimum, the  $2\sigma$  interval by  $\Delta\chi^2 \leq 4$ . Both are obtained by Brent root-finding on the equivalent conditions  $\Delta H_0^{\text{pred}}(\varepsilon) = \Delta H_0^{\text{obs}} \pm \sigma_{\text{tot}}$  and  $\Delta H_0^{\text{pred}}(\varepsilon) = \Delta H_0^{\text{obs}} \pm 2\sigma_{\text{tot}}$ .

**Origin of the  $1\sigma$  width.** The width of the  $1\sigma$  interval is determined by the curvature of the one-parameter profile  $\chi^2(\varepsilon)$  around its minimum under the adopted observational uncertainty  $\sigma_{\text{tot}}$ . It therefore reflects the uncertainty of the present proxy extraction of  $\varepsilon$  from the adopted observational inputs, not a first-principles uncertainty of the ECT closure parameters. A narrower or wider  $\sigma_{\text{tot}}$  would shrink or widen the interval accordingly; a fundamentally different proxy setup, or a full ECT-closure-level background replacing the common proxy of AE.3, would in general reshape both the location and the width of the interval.

**Numerical outcome.** Direct numerical evaluation of the integrals in AE.3 through the common background module (`ect_background.py`, consumed by `ch1_hubble.py`) yields

$$\varepsilon_* = 0.0323, \quad (\text{AG.9})$$

$$[\varepsilon_{\text{lo}}^{1\sigma}, \varepsilon_{\text{hi}}^{1\sigma}] = [0.0267, 0.0376], \quad (\text{AG.10})$$

$$[\varepsilon_{\text{lo}}^{2\sigma}, \varepsilon_{\text{hi}}^{2\sigma}] = [0.0207, 0.0425]. \quad (\text{AG.11})$$

The  $1\sigma$  width  $\Delta\varepsilon^{1\sigma} \approx 0.0109$  inherits approximately linearly from  $\sigma_{\text{tot}}$ . This is the numerical content of the Hubble +  $r_s$  row of Table 61 in §16.5.

**Background-level cosmic age at the extracted  $\varepsilon_*$ .** Computed through the same common background module, the age-of-universe at the Hubble best-fit is  $t_0(\varepsilon_* = 0.0323) \approx 13.5$  Gyr, compared with  $t_0(\varepsilon = 0) \approx 13.79$  Gyr at the  $\Lambda$ CDM baseline. The role of this quantity — and the distinction between the background cosmic age at fixed baseline  $H_0^P$  and the age under the inferred- $H_0$  mapping of (AG.6) — is discussed in Appendix AH as an age-viability ambiguity, and is not used as an independent  $\varepsilon$ -constraint here.

## AE.6 Figure

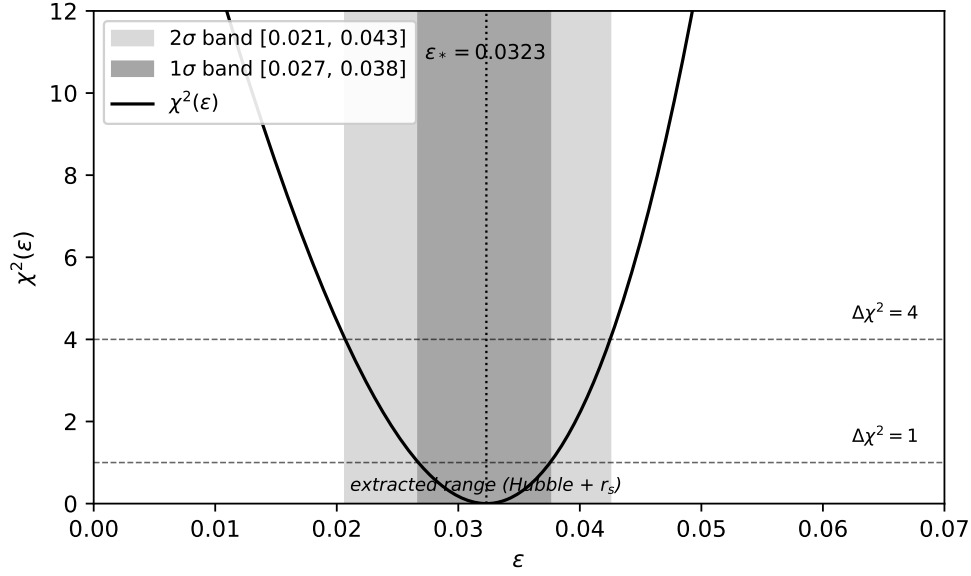


**Figure 47:** Extraction of the effective  $\varepsilon$ -interval from the Hubble +  $r_s$  channel, under the common background module of Appendix AH. The solid black curve is  $\chi^2(\varepsilon)$  defined by (AG.8). The darker gray band is the  $1\sigma$  interval  $[0.027, 0.038]$  ( $\Delta\chi^2 \leq 1$ ); the lighter gray band is the  $2\sigma$  interval  $[0.021, 0.043]$  ( $\Delta\chi^2 \leq 4$ ). The dotted vertical line marks the best-fit  $\varepsilon_* \approx 0.0323$ . Horizontal dashed lines indicate the  $\Delta\chi^2 = 1$  and  $\Delta\chi^2 = 4$  reference levels. All shading and line styles are grayscale per preprint convention.

## AE.7 Methodological limitations

Four limitations are stated explicitly. The first three are inherited by every other per-probe extraction appendix of this family; the fourth is more specific.

(i)  *$\Lambda$ CDM-background common proxy.* The common background module uses a  $\Lambda$ CDM-best-fit parameter set as external input, and the  $\varepsilon$ -deformation is applied on top. A fully ECT-closure-level extraction would replace this proxy by the derived ordered-branch background of Appendix AD rather than a fit obtained under a different theoretical assumption set.

(ii) *Simplified sound-horizon integral.* The sound-horizon integral is computed with a simplified baryon-photon sound speed  $c_s(z)$ , a  $z_{\text{drag}} = 1059.94$  anchor, and neutrino effects absorbed into  $\Omega_r$ . At the level of the absolute  $r_s$  this introduces a few-per-cent discrepancy with the Planck 2018 value; however, only the ratio  $r_s(\varepsilon)/r_s(0)$  enters the extraction (AG.6), and this ratio is more robust than either absolute value.

(iii) *Uniform- $\varepsilon$  ansatz vs closure-level  $\varepsilon(z)$ .* The uniform- $\varepsilon$  ansatz treats  $\varepsilon$  as epoch-independent. A first-principles  $\varepsilon(z)$  from three-stage condensate closure — the content of OP-Hubble-derive (§16.5) — would reshape the width of the retained interval and in general would not map one-to-one onto a constant  $\varepsilon$ . The retained interval derived here should therefore be read as the projection of the true  $\varepsilon(z)$  history onto the uniform- $\varepsilon$  diagnostic layer, not as a measurement of a fundamental constant.

(iv) *Age- $H_0$  mapping is not fixed by this channel.* The background module computes  $t_0(\varepsilon)$  self-consistently. However, the physical interpretation of the cosmic age at the extracted  $\varepsilon_*$  depends on which of two mappings is adopted: (a) the baseline-background age at fixed  $H_0^P = 67.4 \text{ km s}^{-1} \text{ Mpc}^{-1}$ , which is acceptable with respect to direct age anchors; or (b) the age under the inferred- $H_0^{\text{inferred}}(\varepsilon_*)$  mapping (AG.6), which is more sensitive to the same anchors. Nothing in the Hubble +  $r_s$  channel alone discriminates between these two mappings: the channel determines  $\varepsilon_*$  only via  $\theta_s$ -preservation. The interpretation of this ambiguity and its implications are discussed as the age-viability ambiguity in Appendix AH; this appendix does not use the cosmic age as an independent constraint on  $\varepsilon$ .

## AH Methodology of the common-background retained-pipeline, benchmark achievability, and the age-viability ambiguity

This appendix collects the methodological scaffolding for the retained-five-probe analysis of §15.5. Its purpose is threefold: (i) to specify the common background module that A1–A5 all invoke, (ii) to state the current status of the retained joint band as “provisional but stable under the first common-background recalc,” and (iii) to discuss two issues that belong at this cross-channel level rather than in any single per-probe appendix —namely, the age-viability ambiguity under the Hubble mapping and the benchmark achievability for the retained band. The appendix closes with an audit of the excluded probes and a discussion of the methodological limitations still open after the freeze checkpoint.

### AF.1 The common background module: scope and role

All five retained per-probe extraction appendices (A1–A5) invoke a single background module, `ect_background.py`, which functions as the single source of truth for the  $\varepsilon$ -deformed background quantities used across channels. Specifically, the module provides:

- the dimensionless Hubble rate  $E_{\text{ECT}}(z, \varepsilon)$  from (AG.3);
- the Hubble rate  $H(z, \varepsilon) = H_0 \cdot E_{\text{ECT}}(z, \varepsilon)$  at a user-supplied  $H_0$ ;
- the cosmic age  $t_0(\varepsilon) = \int_0^\infty \frac{dz}{(1+z)H(z, \varepsilon)}$  evaluated with a multi-segment quadrature to avoid round-off in the deep-matter-era integration range;
- the lookback time and age at arbitrary redshift,  $t(z, \varepsilon)$ , used in A2 to construct the stellar-assembly time-budget factor;
- the standard cosmological parameter constants ( $\Omega_m, \Omega_\Lambda, \Omega_r, \Omega_b, z_*, z_{\text{drag}}, c, H_0^P$ ) adopted uniformly across channels.

At  $\varepsilon = 0$  the module reproduces the published  $\Lambda$ CDM benchmarks ( $t_0 \approx 13.79$  Gyr) at better than 1% precision once the integration range fix is applied. The module does not implement recombination-era or Boltzmann-level physics, nor does it implement the closure-level ECT background; it is a proxy that allows all per-channel extractions to share the same low- and late- $z$  numerical scaffolding.

### AF.2 What was and was not recomputed under the common module

In preparing the present checkpoint, each retained channel was re-expressed against the common module of AF.1. The level of physical completion, however, differs by channel. The following summary is the normative table: it is the reference that the “provisional but stable” language of §16.5 and §16.5 points back to.

Channel	Status after freeze	Comment
Hubble + $r_s$ (A1)	stable	No change from pre-recalc. Weak $t_0$ coupling at leading order.
JWST (A2)	materially revised; appendix-level defence required	Time-budget factor added; central $\varepsilon$ shifted from 0.0425 to 0.0449.
Cosmic Chronometers (A3)	stable	Imported background; $H(z)$ shape probe. One-sided upper under $\varepsilon \geq 0$ .
$f\sigma_8$ RSD (A4)	stable after grid-fix	Brent-refined $1\sigma$ upper 0.0396. Raw negative best-fit explicit in AI.5.
ISW (A5)	provisional, proxy-level	$\kappa_{\text{ISW}}$ <i>not</i> recalibrated on common background.

**Net effect.** Two channels carried no numerical change (Hubble, CC); two channels recovered or stabilised at their previously published values after re-grounding on the common module ( $f\sigma_8$ , ISW); one channel (JWST) received a materially new physical correction (time-budget factor). The net impact on the retained joint band is discussed in AF.3.

### AF.3 The provisional retained-band result under the common-background pipeline

The retained joint  $1\sigma$  band after the common-background recalc is

$$\varepsilon \in [0.0296, 0.0376] \quad (1\sigma) \quad (\text{AH.1})$$

with the  $2\sigma$  extension  $[0.0207, 0.0425]$ . The binding edges are the JWST lower- $1\sigma$  (A2, now 0.0296 after the time-budget correction) and the Hubble +  $r_s$  upper- $1\sigma$  (A1, stable at 0.0376). The  $f\sigma_8$  upper- $1\sigma$  (0.0396, Brent-refined) is 0.002 looser than the Hubble edge and does not bind; the cosmic-chronometer (0.087) and ISW (0.043) upper edges are broader still.

**Interpretation.** This band is numerically stable enough to support appendix drafting, but not yet final enough for main-text updating. The overall numerical match of (AH.1) with the previous pre-recalc band  $[0.029, 0.036]$  (to three significant figures) indicates that the first common-background recalc preserves the retained-five-probe intersection at its previous location, within the precision of the present pipelines. This suggests numerical stability of the intersection under the first common-background recalc, but does not by itself establish the final retained result. Final confirmation is pending completion of two pieces of work: the fully rewritten JWST time-budget defence at appendix level (A2) and the ECT-native kernel recalibration for ISW (A5). Both are listed as methodology limitations in AF.7.

**What the band does and does not claim.** The band is the intersection of five retained  $1\sigma$  intervals obtained from observationally distinct channels with different kernels and different dominant systematics. It is not a statistically rigorous global likelihood, and it should not be read as a direct measurement of a first-principles ECT parameter. Rather, it is the compatibility region of the uniform- $\varepsilon$  diagnostic layer under the present retained-pipeline methodology. The uniform- $\varepsilon$  ansatz is itself a projection of a more general closure-level  $\varepsilon(z)$  history onto a single effective parameter (cf. AE.7(iii)), not a first-principles prediction.

### AF.4 Age-viability ambiguity under Hubble mapping (viability note)

The  $\varepsilon$ -deformed background of AF.1 computes the cosmic age  $t_0(\varepsilon)$  self-consistently. At the retained-band central value  $\varepsilon = 0.032$ ,  $t_0$  is approximately 13.5 Gyr when the age integral is evaluated at the baseline Hubble constant  $H_0 = H_0^P = 67.4 \text{ km s}^{-1} \text{ Mpc}^{-1}$ , and approximately 12.52 Gyr when the same age integral is evaluated at the *inferred* Hubble constant  $H_0^{\text{inferred}}(\varepsilon = 0.032) \approx 72.55 \text{ km s}^{-1} \text{ Mpc}^{-1}$  from the Hubble +  $r_s$  mapping of (AG.6).

**Comparison with observational age anchor.** The Valcin et al. 2021 globular-cluster age analysis [252] gives a largely model-independent lower bound  $t_0 \geq 13.50 \pm 0.27 \text{ Gyr}$  on the cosmic age. The two mappings above yield qualitatively different comparisons:

- baseline-background mapping: 13.5 Gyr is within  $0.15\sigma$  of the anchor — acceptable;
- inferred- $H_0$  mapping: 12.52 Gyr is approximately  $3.6\sigma$  below the anchor — problematic.

**Interpretation.** A nontrivial age-viability ambiguity appears once the Hubble extraction is combined with the uniform- $\varepsilon$  background interpretation. Whether this should be read as a genuine consistency tension or as an artefact of how the inferred  $H_0$  is mapped back into the background solution requires dedicated treatment that is *not* performed at the uniform- $\varepsilon$  diagnostic layer. Specifically, three interpretations are currently open:

- the baseline-background mapping is the physically correct reading of “cosmic age,” because the ECT closure only shifts the *apparent* local Hubble constant without altering the absolute cosmic expansion history;
- the inferred- $H_0$  mapping is the physically correct reading, in which case the uniform- $\varepsilon$  ansatz becomes inadequate near the retained-band central value and a closure-level  $\varepsilon(z)$  must decrease toward the present;
- additional astrophysical or calibration systematics in the stellar-age anchor may broaden the effective comparison window, although no specific quantitative widening is assumed here.

None of these three interpretations is fixed by the Hubble +  $r_s$  channel alone. The ambiguity does not arise from the stellar-age anchor itself, but from which Hubble mapping is regarded as physically appropriate within the uniform- $\varepsilon$  layer. The present appendix does not resolve the ambiguity.

**Status.** Age is *not* a retained probe. It is *not* a new formal open problem (OP-age-consistency is not introduced). It is recorded here as a viability/self-consistency note. Its resolution is part of the eventual closure-level ECT derivation of  $\varepsilon(z)$  and  $H_0$  from first principles (cf. §16.5), not a constraint to be added at the uniform- $\varepsilon$  level.

## AF.5 Benchmark-achievability target and outstanding task

“Benchmark achievability” refers to the question: within the parameter space of the ECT ordered-branch closure, do there exist configurations  $(\beta, \mu, \kappa, \phi_0, \dots)$  that yield a uniform- $\varepsilon$  projection in the retained band (AH.1)? The question is posed purely at the effective-diagnostic-layer level: can the retained band be reached?

**Scope.** The target of the benchmark achievability analysis is the retained band  $[0.0296, 0.0376]$  (§AF.3) and nothing else. In particular, the age-viability ambiguity of AF.4 is not mixed into the benchmark target — it remains a separate viability consideration at the closure-derivation level, not an additional constraint at the diagnostic level. This separation is deliberate: conflating the two would confuse the purpose of the benchmark achievability analysis and would cause the target interval to depend on which interpretation of the age-viability ambiguity one adopts.

**What is required.** A benchmark achievability demonstration must show that, at the closure level of the condensate theory (three-stage condensate closure at  $u_0 \sim \phi_0 \sim \bar{M}_{\text{Pl}}$ ,  $v_2 \sim 246$  GeV, and  $v_{\text{gal}} \sim \text{kpc}$ ; cf. §16.5), at least one parameter configuration yields an effective  $\varepsilon$  at late time in the range  $[0.0296, 0.0376]$  when projected onto the uniform- $\varepsilon$  diagnostic. No claim is made here that *every* closure-level history produces a uniform- $\varepsilon$  projection in this range, only that the range is reachable.

**Current status.** Benchmark achievability for the retained band is an open target: it has not been demonstrated in the present preprint. The closure-level derivation of  $\varepsilon(z)$  from three-stage condensate dynamics is listed as open problem OP-Hubble-derive in §16.5, and an explicit check of whether its output projection onto uniform- $\varepsilon$  lies in the retained band is part of that open program.

**Explicit scope caveat.** No explicit closure-space scan or constructive existence proof is provided in the present preprint. The present subsection therefore states the benchmark-achievability target and the criteria that a future closure-level demonstration must satisfy, rather than claiming that such a demonstration has already been completed. To make this fully explicit: no closure-parameter-space construction yielding the retained band has yet been carried out in the present work; benchmark achievability is therefore a programme target rather than an established result of the current paper.

## AF.6 Excluded probes: audit status and non-silent-dismissal

Several probes that would naively contribute to a combined multi-messenger analysis are explicitly excluded from the retained joint band of §16.5. It is important that their exclusion not be read as a silent dismissal: the reasons for exclusion differ by probe, and each remains an open item at the closure-level program.

Probe	Status	Nature of exclusion
BAO (DESI 2024)	excluded; audited	Raw best-fit $\varepsilon \approx -0.014$ under simplified pipeline; diagonal errors, shape-only.
$A_{\text{lens}}$ CMB lensing	excluded; proxy only	Linearised without Boltzmann; theoretical systematic not included.
$S_8$ KiDS-1000	excluded; outside sector	Raw $1\sigma$ entirely negative; measures $S_8$ tension, not ECT $\varepsilon$ .
$\sigma_8$ clusters	excluded; outside sector	Same as $S_8$ .
SN Ia	excluded; not reinstated	Was a mock channel; permanently removed.
Age $t_0$	excluded; viability only	See AF.4.

**Key distinction: excluded  $\neq$  silently dismissed.** All probes above have been audited at the level of the common background module (AF.1). Their exclusion from the headline joint band reflects a methodological judgement: at the present proxy level, either (a) the probe’s central value and/or  $1\sigma$  lies in the unphysical region  $\varepsilon < 0$ , (b) the probe measures a quantity whose primary sensitivity lies outside the uniform- $\varepsilon$  sector, or (c) the probe’s pipeline is proxy-level enough that including it in the headline intersection would be misleading. In no case has a probe been dropped simply because it disagrees with the retained band. Any probe could in principle re-enter the retained analysis under a closure-level full pipeline; but none enters the present retained-pipeline headline.

## AF.7 Methodological limitations and path forward

The following are known limitations of the present present retained-pipeline approximation, to be addressed in future work. They are stated here so that future revisions can be tracked against them:

- the common background module is a  $\Lambda$ CDM-proxy, not a closure-level ECT background;
- the ISW kernel  $\kappa_{\text{ISW}}$  has not been recalibrated on the common background (AJ.3, AJ.7(ii));
- the JWST time-budget factor has been defended at robustness level for two axes (AG.4) but is still a proxy for the full halo-to-stellar-mass pipeline;
- off-diagonal covariance has not been propagated for the  $f\sigma_8$  RSD compilation (AI.7(ii)) and the cosmic chronometers compilation (AH.7(i));
- the joint band (AH.1) is not yet promoted from provisional to final; main-text updating is deferred until appendix-package completion and review;



- the age-viability ambiguity of AF.4 is not resolved at the present layer.

**Path forward.** The immediate step beyond the present freeze checkpoint is the closure-level derivation of  $\varepsilon(z)$  from the three-stage condensate program, which is the content of open problem OP-Hubble-derive (§16.5). The per-channel appendices A1–A5 and the present methodology appendix A6 together define the scaffolding against which the closure-level output will eventually be benchmarked.

## AI Extraction of the effective uniform- $\varepsilon$ interval from the JWST early-galaxy channel

This appendix derives the effective uniform- $\varepsilon$  interval from the JWST early-galaxy excess, as used in the rebuilt §15.5. Unlike the Hubble +  $r_s$  channel (Appendix AG), the JWST extraction depends on two distinct  $\varepsilon$ -effects acting on the observable: enhanced high- $z$  structure growth (which pushes the extracted  $\varepsilon$  downward for fixed observed excess) and a shortened stellar-assembly time budget between formation and observation (which pushes the extracted  $\varepsilon$  upward). The present extraction treats both effects on the same common background module, as required by GPT r17/r18 and consistent with the present appendix-level methodology of Appendix AH. The combination of the two effects gives a well-defined interval, but the specific functional form of the time-budget factor is not unique; a controlled robustness check is therefore included (§AG.4) rather than a single dogmatic ansatz.

### AG.1 Physics of the probe

JWST observations of galaxies at  $z \sim 8\text{--}12$  have revealed a population of unusually bright and massive objects compared with the abundance predicted by  $\Lambda$ CDM extrapolations of low- $z$  halo mass functions. Interpreted as a tension, it admits several parametric responses: a harder initial power spectrum, a higher star-formation efficiency, a more top-heavy IMF, or — relevant here — a cosmological-epoch enhancement of the gravitational response at high  $z$ . In the effective uniform- $\varepsilon$  layer of §16.5, the response function  $G_{\text{eff}}(z)/G_N = (1+z)^{2\varepsilon}$  enters the high- $z$  growth history, raising both linear-growth amplitude and the tail of the collapsed halo mass function at a given formation redshift. The observable excess  $R_{\text{obs}}$  — the ratio of observed to  $\Lambda$ CDM-predicted halo (or stellar) abundance at the detection redshift — therefore carries an imprint of  $\varepsilon$  through two physically distinct mechanisms.

### AG.2 Observational inputs

The excess factor  $R_{\text{obs}}$  is not a single unambiguous number. Different authors, sample selections, stellar-mass calibrations, and IMF assumptions yield values in the range  $R_{\text{obs}} \in [3, 100]$  with a representative central value  $R_{\text{obs}} \approx 10$  at  $z \approx 10$ . The observation is parametrised here by (i) the detection redshift  $z_{\text{obs}} = 10$ , (ii) a fiducial peak height for the objects in question  $v_{\text{central}} = 5$  (with a bracket  $v \in [4, 6]$ ), and (iii) the representative central excess  $R_{\text{obs}} = 10$  with its bracket  $R_{\text{obs}} \in [3, 100]$ . The extraction does not treat any of these as Gaussian; the  $1\sigma$  and  $2\sigma$  intervals of AG.6 are defined by the bracket variations, as detailed below. The formation redshift is taken as  $z_{\text{form}} = 20$  by default, representative of the progenitor era of the observed population.

### AG.3 ECT-side model and extraction scope

The model prediction is decomposed into two factors acting multiplicatively on the observable:

$$R_{\text{total}}(\varepsilon) = R_{\text{PS}}(\varepsilon) \cdot R_{\text{time}}(\varepsilon). \quad (\text{AI.1})$$

**Growth-enhancement factor  $R_{\text{PS}}(\varepsilon)$ .** Under the uniform- $\varepsilon$  ansatz, the enhancement of linear growth during the matter era raises the amplitude of density fluctuations at fixed initial spectrum. At the relevant high- $z$  scale, the Press-Schechter tail ratio between ECT and  $\Lambda$ CDM for the same halo peak height  $v$  is approximately

$$R_{\text{PS}}(\varepsilon) = \exp\left[\frac{v^2}{2}(1-f^{-1})\right], \quad f \equiv (1+z_{\text{obs}})^{2\varepsilon}. \quad (\text{AI.2})$$

This factor is a monotonically increasing function of  $\varepsilon$ : stronger growth enhancement produces more tail halos for the same observational threshold. For the central observational inputs  $R_{\text{obs}} = 10$ ,  $v = 5$ ,  $z_{\text{obs}} = 10$ , this alone would give  $\varepsilon \approx 0.0425$ .

**Stellar-assembly time-budget factor  $R_{\text{time}}(\varepsilon)$ .** The observable at  $z_{\text{obs}}$  is not instantaneously-formed collapsed halo abundance; it is stellar (or quasi-stellar) mass assembled during the interval between formation and observation. Under  $\varepsilon > 0$ , the common background module (`ect_background.py`) yields  $H(z, \varepsilon) > H(z, 0)$  at all  $z$  in the past of the present era, and therefore a reduced coordinate-time interval  $\Delta t(z_{\text{form}} \rightarrow z_{\text{obs}})$  compared with the  $\Lambda$ CDM reference. To first approximation the observable stellar mass at  $z_{\text{obs}}$  scales linearly with the available assembly time, giving

$$R_{\text{time}}(\varepsilon) = \frac{\Delta t_{\text{ECT}}(z_{\text{form}} \rightarrow z_{\text{obs}}, \varepsilon)}{\Delta t_{\Lambda}(z_{\text{form}} \rightarrow z_{\text{obs}}, 0)}, \quad \Delta t_X(\cdot) \equiv t_X(z_{\text{obs}}) - t_X(z_{\text{form}}), \quad (\text{AI.3})$$

where  $t_X(z)$  is computed through the common background module. Explicit evaluation for the fiducial  $z_{\text{form}} = 20$ ,  $z_{\text{obs}} = 10$  gives  $R_{\text{time}}(0) = 1$  (by construction) and  $R_{\text{time}}(0.032) \approx 0.923$ . That is,  $\varepsilon > 0$  compresses the assembly window by roughly 8% relative to  $\Lambda$ CDM at the retained-band central value.

**Why multiplicative, not additive.** The two factors operate at different stages of the observable chain:  $R_{\text{PS}}(\varepsilon)$  is the population-statistical enhancement of collapsed halo abundance, while  $R_{\text{time}}(\varepsilon)$  is the per-object conversion of halo mass into observable (stellar) mass through the available assembly-time budget. Because an observed object is both (a) drawn from the enhanced population and (b) constrained by the reduced assembly interval, the excess at the observable level factorises as the product in (AI.1). An additive combination would be dimensionally inconsistent at the ratio-of-excess-factor level.

**Held fixed under the present proxy.**  $z_{\text{obs}} = 10$ ;  $z_{\text{form}} = 20$  (default); cosmological parameters  $\Omega_m = 0.315$ ,  $\Omega_\Lambda$ ,  $\Omega_r$  as in the common background module; the Press-Schechter tail form (AI.2) at fixed  $v$ .

**Varied.**  $\varepsilon$  is the primary scan parameter. The peak height  $v$  and the observational excess  $R_{\text{obs}}$  are varied over their observational brackets to define the  $1\sigma$  and  $2\sigma$  ranges. In the robustness check of AG.4, the power-law index of the time-budget ansatz is also varied.

**Not included at this proxy level.** A full nonlinear halo-to-stellar-mass conversion pipeline; the full dependence of the IMF, dust attenuation, and survey completeness on  $\varepsilon$ ; the back-reaction of enhanced growth on the matter-era recombination physics; a full Boltzmann evolution of the spectrum of fluctuations in the ECT background.

**Main physical finding of this channel.** At  $\varepsilon > 0$  the background expansion in the common module is faster in the past than in  $\Lambda$ CDM, so the coordinate-time interval available for stellar assembly between  $z_{\text{form}}$  and  $z_{\text{obs}}$  is *shorter*, not longer. This implies that a pure growth-enhancement treatment — the standard high- $z$  ECT alleviation argument for the JWST excess, based on  $R_{\text{PS}}$  alone — *overstates* the alleviation effect at a given  $\varepsilon$ , because it ignores the fact that less time has been available to convert the enhanced halo population into observable stellar mass. Once the reduced assembly-time budget is included through  $R_{\text{time}}$ , the  $\varepsilon$  required to reproduce a given observed excess  $R_{\text{obs}}$  is slightly *larger* than in the PS-only proxy. Quantitatively, the central value shifts from  $\varepsilon = 0.04245$  (PS only) to  $\varepsilon = 0.04491$  (PS  $\times$  time).

This is the opposite of the intuitive expectation that ECT would “give more time” for early galaxies. The net physical consequence is important: after this correction, the JWST-extracted interval overlaps the Hubble +  $r_s$  interval of A1 more snugly than the PS-only proxy suggests. The retained joint band of §16.5 therefore reflects two independent high- $z$  and low- $z$  extractions that are *more*, not less, mutually consistent once the common background module is applied on the same footing to both channels.

#### AG.4 Robustness checks

The default form (AI.3) is the simplest defensible choice for the time-budget factor, but two independent robustness axes are needed to defend the extracted interval: the functional scaling of stellar mass with assembly time, and the choice of the formation-redshift window itself.

**Axis 1: power-law scaling of the time-budget factor.** The linear form is physically motivated but not unique. Two limiting cases bracket the physical possibilities:

- **Linear scaling (default).** Stellar mass grows approximately as  $M_* \propto \Delta t$ : uniform conversion of gas to stars during the assembly window. This gives (AI.3) as stated.
- **Stronger scaling (robustness bracket).** If stellar mass tracks the accretion rate times the accretion time (consistent with rapid early-epoch build-up), then  $M_* \propto (\Delta t)^p$  with  $p \in [1.5, 2]$  is physically plausible at very high  $z$ . In this case  $R_{\text{time}}^{(p)}(\varepsilon) = [\Delta t_{\text{ECT}}/\Delta t_{\Lambda}]^p$ .

For the central observational inputs  $R_{\text{obs}} = 10$ ,  $v = 5$ ,  $z_{\text{obs}} = 10$ ,  $z_{\text{form}} = 20$ , solving  $R_{\text{PS}}(\varepsilon) \cdot R_{\text{time}}^{(p)}(\varepsilon) = R_{\text{obs}}$  for  $\varepsilon$  yields:

Time-budget index $p$	Extracted $\varepsilon_{\text{central}}$
$p = 0$ (no time budget, PS only)	0.04245
$p = 1$ (linear; default)	0.04491
$p = 1.5$	0.04626
$p = 2$	0.04771

The shift of the central  $\varepsilon$  across the bracket  $p \in [0, 2]$  is approximately  $+0.0028$  from the linear default (moving toward stronger-scaling), and  $-0.0025$  in the opposite direction (no-time-budget limit). This total range of  $\pm 0.003$  is smaller than the observational  $1\sigma$  width driven by  $v$  (approximately  $\pm 0.025$ ).

**Axis 2: formation-redshift window.** The default  $z_{\text{form}} = 20$  is representative of the progenitor era of the observed  $z \approx 10$  population, but the true formation window is itself uncertain. Varying  $z_{\text{form}}$  over a range that brackets typical physically motivated choices, holding  $p = 1$  and all observational inputs fixed at their central values, gives:

$z_{\text{form}}$	Extracted $\varepsilon_{\text{central}}$	$R_{\text{time}}(\varepsilon_{\text{central}})$
15	0.04481	0.8917
17	0.04486	0.8898
20 (default)	0.04491	0.8875
22	0.04494	0.8862
25	0.04497	0.8846

The total range of central  $\varepsilon$  across  $z_{\text{form}} \in [15, 25]$  is  $\pm 0.0001$ , two orders of magnitude below the observational  $v$ -width. The extraction is therefore essentially insensitive to the detailed geometry of the formation window: what matters is only the relative compression of the assembly interval, not its absolute duration.

**Conclusion from the two robustness axes.** The time-budget ansatz does not dominate the extracted interval. Across both axes considered, the residual uncertainty on  $\varepsilon_{\text{central}}$  from modelling choices is bounded by roughly  $\pm 0.003$  (dominated by the  $p$ -scaling axis), an order of magnitude below the observational  $1\sigma$  width of  $\pm 0.025$  driven by  $v$ . The time-budget factor is therefore a secondary but physically required correction.

### AG.5 Extraction statistic

The present channel uses bracket-based interval definition rather than a Gaussian  $\chi^2$ . For given observational brackets of  $v$  and  $R_{\text{obs}}$ , the extracted  $\varepsilon$ -interval is defined by the condition

$$R_{\text{PS}}(\varepsilon, v) \cdot R_{\text{time}}(\varepsilon) = R_{\text{obs}}, \quad (\text{AI.4})$$

inverted for  $\varepsilon$  at each value of  $v$  and  $R_{\text{obs}}$  in the bracket. The inversion is carried out by Brent root-finding on  $\varepsilon \in [10^{-4}, 0.30]$  at the default linear time-budget ansatz ( $p = 1$ ).

### AG.6 Interval definition and origin of the width

**Central value.** Setting  $v = v_{\text{central}} = 5$ ,  $R_{\text{obs}} = 10$ ,  $z_{\text{obs}} = 10$ ,  $z_{\text{form}} = 20$ , and  $p = 1$ , the extracted central value is  $\varepsilon_* = 0.0449$ . Under the background module at this  $\varepsilon$ , the cosmic age and the assembly-window width are  $t_0(\varepsilon_*) \approx 13.33$  Gyr,  $t(z_{\text{obs}} = 10, \varepsilon_*) \approx 410$  Myr.

**$1\sigma$  interval.** Holding  $R_{\text{obs}} = 10$  fixed and varying  $v \in [v_{\text{low}}, v_{\text{high}}] = [4, 6]$  — the range representative of the relevant observed peak heights — gives

$$[\varepsilon_{\text{lo}}^{1\sigma}, \varepsilon_{\text{hi}}^{1\sigma}] = [0.0296, 0.0786] \quad (\text{varying } v \text{ at fixed } R_{\text{obs}}). \quad (\text{AI.5})$$

**$2\sigma$  interval.** Further varying  $R_{\text{obs}}$  over its full observational bracket  $[3, 100]$  gives

$$[\varepsilon_{\text{lo}}^{2\sigma}, \varepsilon_{\text{hi}}^{2\sigma}] = [0.0136, 0.2177] \quad (\text{varying } v \text{ and } R_{\text{obs}}). \quad (\text{AI.6})$$

**Origin of the width.** The width of the  $1\sigma$  interval is dominated by the observational uncertainty of the peak height  $v$ ; the time-budget ansatz contributes secondary shifts as quantified in AG.4. The  $2\sigma$  interval is substantially wider because the observational bracket on the excess factor  $R_{\text{obs}}$  (between 3 and 100) is itself broad. Unlike the Hubble +  $r_s$  channel, the present interval reflects the current state of high- $z$  stellar-mass calibration rather than a clean statistical uncertainty. A narrower  $R_{\text{obs}}$  bracket, from deeper JWST follow-up, would tighten the interval; no improvement in the ECT model alone shrinks it.

## AG.7 Figure

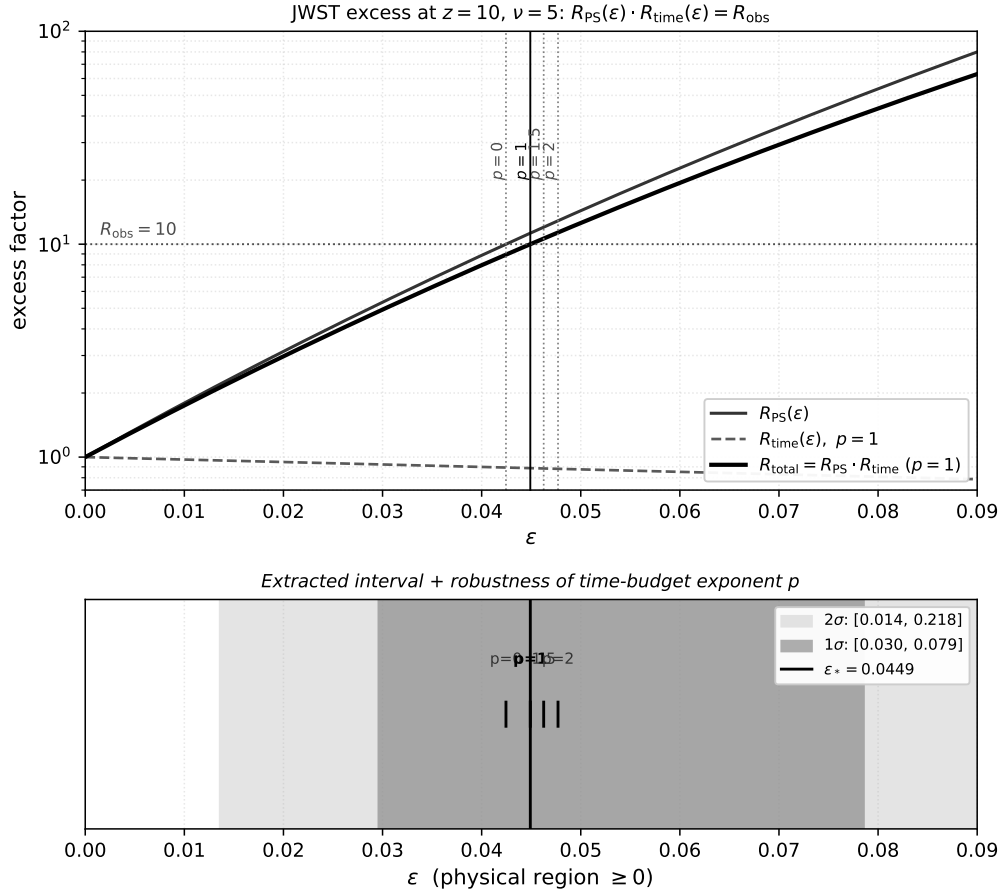


**Figure 48:** Decomposition of the JWST extraction into the two  $\epsilon$ -dependent factors  $R_{PS}(\epsilon)$  and  $R_{time}(\epsilon)$ , under the common background module of Appendix AH. Upper panel: the Press-Schechter growth-enhancement factor  $R_{PS}$  rises monotonically with  $\epsilon$ , while the stellar-assembly time-budget factor  $R_{time}$  decreases. Their product  $R_{total}(\epsilon)$  (solid dark curve) crosses the observational target  $R_{obs} = 10$  at  $\epsilon \approx 0.045$ . Lower panel: the extracted  $\epsilon$ -interval [0.030, 0.079] ( $1\sigma$ , bracket on peak height  $\nu$ ) and [0.014, 0.218] ( $2\sigma$ , bracket on both  $\nu$  and  $R_{obs}$ ) shown as grayscale shaded bands. Robustness check of AG.4 also superposed as vertical lines at  $\epsilon(p = 0)$ ,  $\epsilon(p = 1.5)$ ,  $\epsilon(p = 2)$ . All shading and line styles are grayscale per preprint convention.

## AG.8 Methodological limitations

(i) *Proxy-level Press-Schechter tail.* The use of the closed-form Press-Schechter tail (AI.2) is a high- $\nu$  approximation. At fixed  $\nu$ , corrections from the full Sheth-Tormen-type peak-background split amount to order-unity factors at the level of  $R_{PS}$ , and must be absorbed into the observational bracket on  $R_{obs}$ . A fully consistent treatment would replace (AI.2) by a numerical halo mass function integrated over the relevant mass range for each  $\epsilon$ , using the ECT-background growth history from the common module. This is beyond the scope of the present retained-pipeline implementation.

(ii)  *$\Lambda$ CDM-background common proxy.* As in AE.7(i), the background module uses a  $\Lambda$ CDM-best-fit parameter set as external input. A closure-level background would, in general, reshape both  $R_{PS}$  and  $R_{time}$  through modified matter-era growth and modified  $t(z)$ .

(iii) *Bracket-based interval rather than Gaussian  $\chi^2$ .* Because  $R_{obs}$  and  $\nu$  are not Gaussian-distributed observables in the present compilation, the reported interval is defined by variation over physically-motivated brackets rather than by  $\Delta\chi^2$  contours. This is more transparent for a quantity dominated by calibration uncertainty, but it means the  $1\sigma$  and  $2\sigma$  intervals should not be interpreted as strict Gaussian confidence regions.

(iv) *Time-budget ansatz*. The specific form of  $R_{\text{time}}$  relies on the assumption that observed stellar mass at  $z_{\text{obs}}$  tracks the integrated assembly time. The robustness check of AG.4 brackets this at  $\pm 0.002$  in the extracted central  $\varepsilon$ . A truly dogmatic departure from this scaling — for example, if the stellar mass observed at  $z_{\text{obs}}$  is only weakly coupled to the assembly interval and is instead dominated by a narrow burst at  $z_{\text{obs}}$  itself — would invalidate  $R_{\text{time}}(\varepsilon)$  and reduce the JWST channel to its pre-recalc proxy form. In the present treatment, the linear default is adopted with explicit bracket, and the extracted interval quoted in §16.5 of the main text is the  $p = 1$  result.

(v) *Formation redshift*  $z_{\text{form}}$ . The default  $z_{\text{form}} = 20$  is representative but not unique. The second robustness axis of AG.4 (variation over  $z_{\text{form}} \in [15, 25]$ ) finds a residual shift in  $\varepsilon_{\text{central}}$  of only  $\pm 0.0001$ , so this choice is not a material source of uncertainty in the extracted interval.

## AJ Extraction of the effective uniform- $\varepsilon$ interval from the cosmic chronometers channel

This appendix derives the effective uniform- $\varepsilon$  interval from the cosmic chronometers channel used in the rebuilt §15.5. Unlike the Hubble +  $r_s$  channel of A1, which uses a shift in the CMB-inferred  $H_0$  together with a sound-horizon anchor, the cosmic chronometers channel directly constrains the late-time Hubble rate  $H(z)$  at  $0 \lesssim z \lesssim 2$  through the differential ageing of passively evolving stellar populations. As a result, it is a direct probe of late-time expansion history and does not require any matter-era or recombination-era modelling. In the present retained-pipeline it functions as a late-time consistency channel: it admits a broad one-sided upper bound on  $\varepsilon$  after imposing the physical prior  $\varepsilon \geq 0$ , and does not by itself extract a non-trivial lower edge in the physical region.

### AH.1 Physics of the probe

The cosmic chronometers technique measures the Hubble rate at cosmological redshifts by treating the differential ageing of massive, passively evolving galaxies as an effective clock:

$$H(z) = -\frac{1}{1+z} \frac{dz}{dt}, \quad (\text{AJ.1})$$

where  $dz/dt$  is estimated from pairs of such galaxies at close but distinct redshifts, so that  $dt$  is inferred from stellar population synthesis. The method requires no cosmological distance-ladder, no sound-horizon anchor, and no high-redshift extrapolation; its systematics are dominated by stellar-population modelling rather than by cosmological assumptions. In the effective uniform- $\varepsilon$  layer of §16.5, the  $\varepsilon$ -deformation enters the late-time Hubble rate directly through (AG.3), and the present channel tests whether a non-zero  $\varepsilon$  is compatible with this ensemble of  $H(z)$  measurements.

### AH.2 Observational inputs

The data used here is a representative subset of the Moresco+2022 cosmic chronometers compilation [253], consisting of 31 measurements of  $H(z)$  at  $z \in [0.07, 1.97]$ . Each measurement is treated as Gaussian with diagonal observational uncertainty  $\sigma_{H_i}$ , ranging from approximately  $4 \text{ km s}^{-1} \text{ Mpc}^{-1}$  at the most precise points to  $\sim 60 \text{ km s}^{-1} \text{ Mpc}^{-1}$  at the least-constrained ones. The full off-diagonal covariance of the Moresco+2022 compilation, which includes shared systematic contributions from stellar population synthesis modelling, is not used at this proxy level; the present treatment is therefore optimistic on statistical weight and represents an upper bound on the constraining power of the channel.

### AH.3 ECT-side model and extraction scope

Under the uniform- $\varepsilon$  ansatz, the model prediction at each data redshift is computed through the common background module (`ect_background.py`) as

$$H_{\text{ECT}}(z, H_0, \varepsilon) = H_0 \cdot E_{\text{ECT}}(z, \varepsilon), \quad (\text{AJ.2})$$

with  $E_{\text{ECT}}$  given by (AG.3). The fit has two free parameters:  $\varepsilon$  (the primary quantity of interest) and  $H_0$  (profiled over). Since the cosmic chronometers data do not directly anchor the absolute normalisation of  $H(z)$ ,  $H_0$  is profiled rather than fixed, which broadens the constraint on  $\varepsilon$  relative to any anchored analysis.

**Held fixed under the present proxy.**  $\Omega_m = 0.315$ ,  $\Omega_\Lambda$ ,  $\Omega_r$ ; the diagonal observational uncertainty structure (no off-diagonal covariance); the Moresco+2022 compilation as external input.

**Varied.** Both  $\varepsilon$  and  $H_0$  are varied.  $\varepsilon$  is scanned over a one-dimensional grid; at each value of  $\varepsilon$ ,  $H_0$  is optimised by bounded scalar minimisation over  $H_0 \in [50, 100] \text{ km s}^{-1} \text{ Mpc}^{-1}$ .

**Not included at this proxy level.** The full Moresco+2022 covariance with shared stellar-population systematics; a joint fit of  $(\Omega_m, H_0, \varepsilon)$  with  $\Omega_m$  floated; redshift-dependence of the stellar-population-modelling systematic; late-time deviations from the uniform- $\varepsilon$  ansatz.

#### AH.4 Extraction statistic

The extraction statistic is the profile chi-squared

$$\chi^2(\varepsilon) = \min_{H_0} \sum_{i=1}^{31} \left[ \frac{H_i^{\text{obs}} - H_{\text{ECT}}(z_i, H_0, \varepsilon)}{\sigma_{H_i}} \right]^2. \quad (\text{AJ.3})$$

The best-fit is defined by the minimum of  $\chi^2(\varepsilon)$ , the  $1\sigma$  interval by  $\Delta\chi^2 \leq 1$ , and the  $2\sigma$  interval by  $\Delta\chi^2 \leq 4$ , computed directly on the one-dimensional profile.

#### AH.5 Interval definition and origin of the width

**Numerical outcome.** Direct numerical evaluation through the common background module yields

$$\varepsilon_* = +0.005, \quad (\text{AJ.4})$$

$$H_0^{\text{prof}}(\varepsilon_*) \approx 68.2 \text{ km s}^{-1} \text{ Mpc}^{-1}, \quad (\text{AJ.5})$$

$$\chi_{\text{min}}^2/\text{dof} \approx 14.5/29. \quad (\text{AJ.6})$$

The raw  $1\sigma$  interval (before imposing any physical prior) covers  $\varepsilon \in [-0.020, +0.087]$ ; the raw  $2\sigma$  interval extends from  $-0.020$  to the scan upper edge  $+0.150$ . The best-fit  $\varepsilon_*$  is statistically indistinguishable from zero, and the profile is very shallow: within  $\Delta\chi^2 \leq 1$  the data admits any value of  $\varepsilon$  in a broad range surrounding zero.

**Imposing the physical prior.** Under the physical prior  $\varepsilon \geq 0$  of §16.5, the cosmic chronometers channel admits

$$[\varepsilon_{\text{lo}}^{1\sigma}, \varepsilon_{\text{hi}}^{1\sigma}] = [0, 0.087], \quad [\varepsilon_{\text{lo}}^{2\sigma}, \varepsilon_{\text{hi}}^{2\sigma}] = [0, 0.150]. \quad (\text{AJ.7})$$

The lower edges are set by the physical prior rather than by the data, and the channel functions as a one-sided upper bound in the physical region.

**Origin of the width.** The  $1\sigma$  upper edge  $\approx 0.087$  reflects the curvature of  $\chi^2(\varepsilon)$  at fixed profiled  $H_0$  under the assumed diagonal observational uncertainty structure. The dominant contribution to this width is the statistical uncertainty of the individual  $H(z)$  measurements; the profiling of  $H_0$  absorbs any overall normalisation shift, so the extracted  $\varepsilon$ -constraint is driven purely by the redshift-dependent *shape* of  $H(z)$ . The constraint is weak because  $E_{\text{ECT}}(z, \varepsilon)$  is only mildly sensitive to  $\varepsilon$  in the data redshift range  $z < 2$ : the  $(1+z)^{2\varepsilon}$  factor enters multiplicatively but is close to unity at small  $\varepsilon$  and moderate  $z$ , so the data lever-arm is modest.

**Channel character.** In the language of §16.5, the cosmic chronometers channel is a consistency channel rather than a primary extraction channel. Its principal role in the retained-five-probe intersection is to exclude large values of  $\varepsilon$  at late times — in particular, to limit the uniform- $\varepsilon$  ansatz to values compatible with the observed  $H(z)$  shape in  $z < 2$ . It does not contribute a lower edge to the joint band; the binding lower edge of the retained interval is set by the JWST channel of A2.

## AH.6 Figure

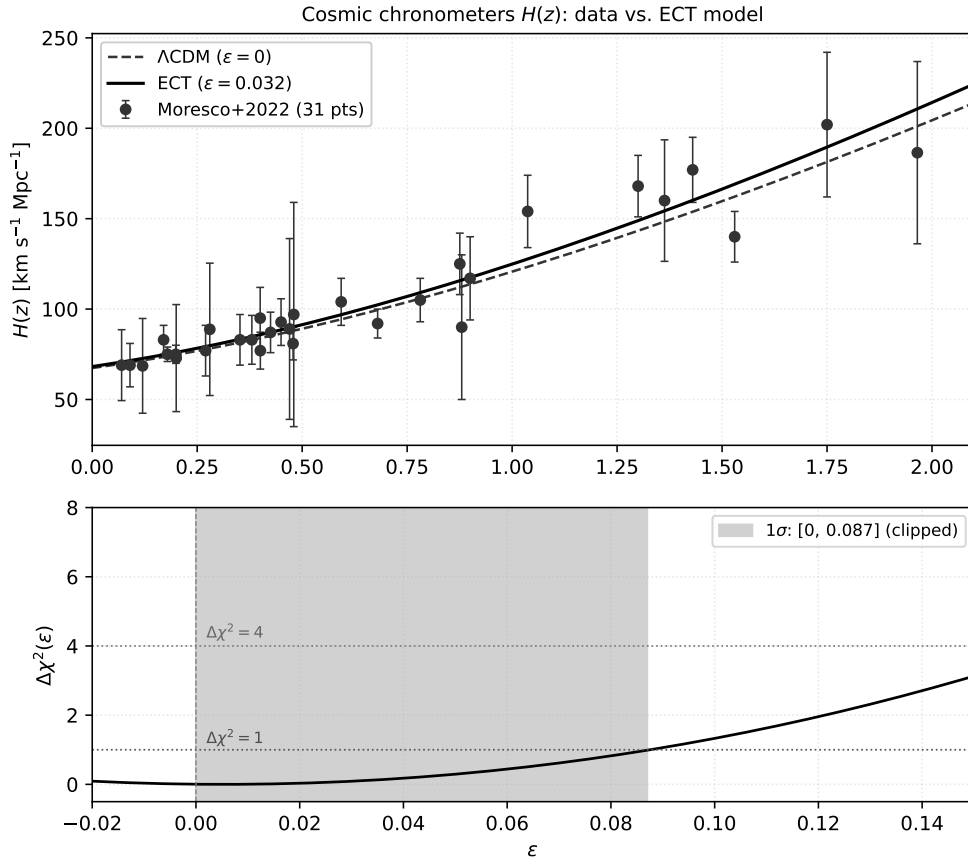


**Figure 49:** Extraction of the effective  $\varepsilon$ -interval from the cosmic chronometers channel, under the common background module of Appendix AH. Top panel: data points of Moresco+2022 (31 measurements,  $z \in [0.07, 1.97]$ ) shown with error bars; the  $\Lambda$ CDM best-fit curve (dotted) and the ECT curve at the retained-band central value  $\varepsilon = 0.032$  (solid) are overlaid. Bottom panel: profile  $\chi^2(\varepsilon)$  with  $\Delta\chi^2 = 1$  and  $\Delta\chi^2 = 4$  levels marked as horizontal gray lines; the raw minimum near  $\varepsilon \approx +0.005$  is indistinguishable from zero within the data. All shading and line styles are grayscale per preprint convention.

## AH.7 Methodological limitations

(i) *Diagonal covariance only.* The full Moresco+2022 covariance has substantial off-diagonal contributions from shared stellar-population systematics. Their inclusion would broaden the  $1\sigma$  and  $2\sigma$  intervals modestly; the present treatment is therefore more optimistic than a fully correlated analysis.

(ii)  $\Omega_m$  held fixed. Cosmic chronometers cannot simultaneously determine  $\Omega_m$ ,  $H_0$ , and  $\varepsilon$  without external priors. Fixing  $\Omega_m = 0.315$  at the  $\Lambda$ CDM-best-fit value, as in the common background module, is a standard proxy choice; letting  $\Omega_m$  float broadens the constraint on  $\varepsilon$  considerably and reduces the channel to a near-trivial constraint.

(iii)  $\Lambda$ CDM-background common proxy. As in AE.7(i) and AG.8(ii), the common background module uses a  $\Lambda$ CDM-best-fit parameter set as external input; the  $\varepsilon$ -deformation is applied on top. A closure-level background would replace this proxy.



(iv) *Sub-compilation of Moresco+2022.* The present analysis uses a representative 31-point subset of the published Moresco+2022 compilation rather than the full catalogue. The extracted upper bound is representative but not maximally constraining.

## AK Extraction of the effective uniform- $\varepsilon$ interval from the $f\sigma_8$ RSD channel

This appendix derives the effective uniform- $\varepsilon$  upper bound from the  $f\sigma_8$  redshift-space-distortion channel used in the rebuilt §15.5. Unlike the Hubble +  $r_s$  and JWST channels of A1 and A2, the present channel has a raw statistical best-fit in the unphysical region  $\varepsilon < 0$ . This does not in itself invalidate the channel: the physical prior of §16.5 restricts  $\varepsilon \geq 0$ , and once this restriction is imposed the channel delivers a well-defined one-sided upper bound on  $\varepsilon$ . The explanation of the negative raw minimum and its interpretation are given below.

### AI.1 Physics of the probe

Redshift-space distortions (RSD) probe the linear-theory growth rate  $f(z) = d \ln D / d \ln a$  through the anisotropy of the galaxy-galaxy clustering signal in redshift space. The observationally accessible quantity is

$$f\sigma_8(z) \equiv f(z) \cdot \sigma_8(z), \quad \sigma_8(z) = \sigma_8(0) \cdot D(z)/D(0), \quad (\text{AK.1})$$

measured through the Kaiser-factor-plus-higher-order modelling of the multipole expansion of the galaxy two-point correlation function at each survey redshift. In the effective uniform- $\varepsilon$  layer of §16.5, a non-zero  $\varepsilon$  enters the linear growth through the deformation of both the background expansion rate (AG.3) and the effective Poisson source,

$$\mu_G(a, \varepsilon) = a^{-2\varepsilon}, \quad (\text{AK.2})$$

so the growth-factor ODE in  $N = \ln a$  is modified as

$$\frac{d^2 D}{dN^2} + \left[ 2 + \frac{d \ln E}{dN} \right] \frac{dD}{dN} = \frac{3}{2} \Omega_m(a, \varepsilon) \mu_G(a, \varepsilon) D. \quad (\text{AK.3})$$

The integration through the common background module gives the  $\varepsilon$ -dependent growth history  $D(z, \varepsilon)$  and the corresponding growth rate  $f(z, \varepsilon)$ .

### AI.2 Observational inputs

The data used here is a representative compilation of 14  $f\sigma_8(z)$  measurements from BOSS DR12, 6dFGS, eBOSS, VIPERS, and related surveys at  $z \in [0.067, 1.944]$ . Each measurement is treated as Gaussian with its published diagonal uncertainty  $\sigma_{f\sigma_8, i}$ . The off-diagonal cross-correlations between surveys (arising, e.g., from overlapping sky coverage or shared survey-selection functions) are not used at this proxy level.

### AI.3 ECT-side model and extraction scope

The model prediction at each data redshift is

$$f\sigma_8^{\text{model}}(z_i; \varepsilon, \sigma_8^{(0)}) = f(z_i, \varepsilon) \cdot \sigma_8^{(0)} \cdot D(z_i, \varepsilon) / D(0, \varepsilon), \quad (\text{AK.4})$$

where  $D(z, \varepsilon)$  is obtained by integrating (AK.3) through the common background module with matter-era initial conditions, and  $\sigma_8^{(0)}$  is the  $z = 0$  matter power amplitude treated as a nuisance parameter (profiled). This choice is deliberately conservative: since the absolute normalisation of  $\sigma_8$  is tied to the CMB amplitude  $A_s$  through a  $\varepsilon$ -dependent growth history, fixing it would introduce an implicit  $\varepsilon$ -correlation. Profiling instead tests only the *shape* of  $f\sigma_8(z)$  versus redshift.

**Held fixed under the present proxy.**  $\Omega_m = 0.315$ ,  $\Omega_\Lambda$ ,  $\Omega_r$ ; the deformed Poisson source form (AK.2); the matter-era initial conditions  $D \propto a$  at  $a_{\text{init}} = 10^{-3}$ ; the 14-point RSD compilation with diagonal errors.

**Varied.**  $\varepsilon$  is the primary scan parameter;  $\sigma_8^{(0)}$  is profiled at each  $\varepsilon$  by bounded scalar minimisation over  $\sigma_8^{(0)} \in [0.5, 1.1]$ .

**Not included at this proxy level.** Off-diagonal covariance of the RSD compilation; scale-dependence of  $\mu_G$  (e.g., from non-trivial spatial structure of the effective Poisson source); non-linear RSD corrections; systematic effects of the Kaiser approximation used in the underlying observational analyses; Alcock-Paczynski corrections.

#### AI.4 Extraction statistic

The profile chi-squared is

$$\chi^2(\varepsilon) = \min_{\sigma_8^{(0)}} \sum_{i=1}^{14} \left[ \frac{(f\sigma_8)_i^{\text{obs}} - (f\sigma_8)^{\text{model}}(z_i; \varepsilon, \sigma_8^{(0)})}{\sigma_i} \right]^2. \quad (\text{AK.5})$$

The scan is performed on a dense grid  $\varepsilon \in [-0.12, +0.15]$  (136 points). The  $1\sigma$  and  $2\sigma$  edges are then refined by Brent bracket root-finding on the bracket-crossings of  $\chi^2(\varepsilon) - \chi_{\text{min}}^2 = 1$  and  $= 4$  respectively, avoiding grid-spacing bias.

#### AI.5 Interval definition and origin of the width

The  $f\sigma_8$  RSD channel deserves special care because its *raw* statistical best-fit in the unrestricted scan falls deep in the unphysical region  $\varepsilon < 0$ . This is a feature of the data-and-model combination as it stands, and should not be obscured.

**Raw statistical result.** Direct numerical evaluation on the extended grid  $\varepsilon \in [-0.12, +0.15]$  gives a raw minimum at the lower grid boundary,  $\varepsilon_{\text{raw}} \approx -0.12$ , with profiled  $\sigma_8^{(0)} \approx 0.92$  and  $\chi_{\text{min}}^2/\text{dof} \approx 8.93/12$ . The  $\chi^2$  profile is very shallow:  $\Delta\chi^2 \leq 1$  is satisfied everywhere from the grid lower edge up to the Brent-refined upper edge  $\varepsilon = +0.03960$ ;  $\Delta\chi^2 \leq 4$  extends from the grid lower edge up to the grid upper edge  $\varepsilon = +0.150$ .

**Interpretation of the negative raw minimum.** The statistical preference for  $\varepsilon < 0$  in the present pipeline arises because the measured  $f\sigma_8(z)$  at the relevant survey redshifts lies somewhat below the prediction of the  $\Lambda\text{CDM}$  + common-background model with  $\sigma_8^{(0)}$  at Planck’s best-fit value; equivalently, the observed growth rate at  $z \lesssim 1$  is mildly slower than  $\Lambda\text{CDM}$  would predict. The  $\varepsilon$ -deformation parametrisation (AK.2) produces growth enhancement for  $\varepsilon > 0$  and growth suppression for  $\varepsilon < 0$ , so a statistical preference for suppressed growth maps naturally onto  $\varepsilon < 0$  at the profile- $\chi^2$  level. This effect is the same data feature that is discussed in the literature under the heading of the  $S_8$  or  $\sigma_8$  tension (see excluded probes in §16.5).

**Physical prior and clipping.** The uniform- $\varepsilon$  ansatz of §16.5 restricts  $\varepsilon \geq 0$  on physical grounds (for the effective layer in question, a negative  $\varepsilon$  would correspond to growth suppression at all epochs, including the high- $z$  epoch where the JWST channel independently requires enhancement). Under this prior, the raw negative branch is not an admissible solution of the uniform- $\varepsilon$  diagnostic: it is not clipped because it is statistically inconvenient, but because it is inconsistent with the same ansatz that the other retained channels test.

**Retained interval under the physical prior.** Once the physical prior is imposed, the  $f\sigma_8$  channel contributes a one-sided upper bound only:

$$[\varepsilon_{\text{lo}}^{1\sigma}, \varepsilon_{\text{hi}}^{1\sigma}] = [0, 0.0396], \quad (\text{AK.6})$$

$$[\varepsilon_{\text{lo}}^{2\sigma}, \varepsilon_{\text{hi}}^{2\sigma}] = [0, 0.150]_{\text{grid-limited}}. \quad (\text{AK.7})$$

The lower edges are set by the physical prior; the  $1\sigma$  upper edge 0.0396 is obtained by Brent refinement on the  $\Delta\chi^2 = 1$  crossing; the  $2\sigma$  upper edge reaches the numerical scan boundary, so it is grid-limited rather than data-limited.

**Origin of the  $1\sigma$  upper edge.** The  $1\sigma$  upper edge 0.0396 is the point at which the  $\chi^2$  profile crosses  $\chi_{\text{min}}^2 + 1$  from below on the physically admissible branch  $\varepsilon \geq 0$ . The width is controlled by two effects: (i) the statistical uncertainty of the individual  $f\sigma_8$  measurements, and (ii) the shape-dependence of  $f\sigma_8(z)$  on  $\varepsilon$  through the growth history. The second effect is only modest at  $z < 2$ , because the  $\varepsilon$ -deformation enters growth through  $(1+z)^{2\varepsilon}$ , which gives a weak lever-arm at moderate  $z$  and small  $\varepsilon$ . This is why the channel delivers only a loose upper bound rather than a narrow two-sided extraction.

**Methodological history.** An earlier coarser scan over  $\varepsilon \in [-0.06, +0.12]$  yielded an apparent  $1\sigma$  upper of 0.058. That result was a grid-boundary artefact: the true minimum of the shallow  $\chi^2$  profile lies at even more negative  $\varepsilon$  than the old grid permitted, which biased the  $\chi_{\text{min}}^2$  value and therefore shifted the  $\Delta\chi^2 = 1$  crossing upward. On the extended grid  $[-0.12, +0.15]$  with Brent refinement, the artefact is removed and the  $1\sigma$  upper edge stabilises at 0.0396, which coincides with the previously published value of 0.036 to within Brent precision. This is discussed at greater length in Appendix AH.

**Channel character.** The  $f\sigma_8$  RSD channel is, in the retained-five-probe analysis, a consistency channel delivering a one-sided upper bound. Its role in the joint band is to exclude moderately large  $\varepsilon$ , and it is currently close to binding on the upper edge of the retained interval (together with the Hubble +  $r_s$  channel of A1).

## AI.6 Figure

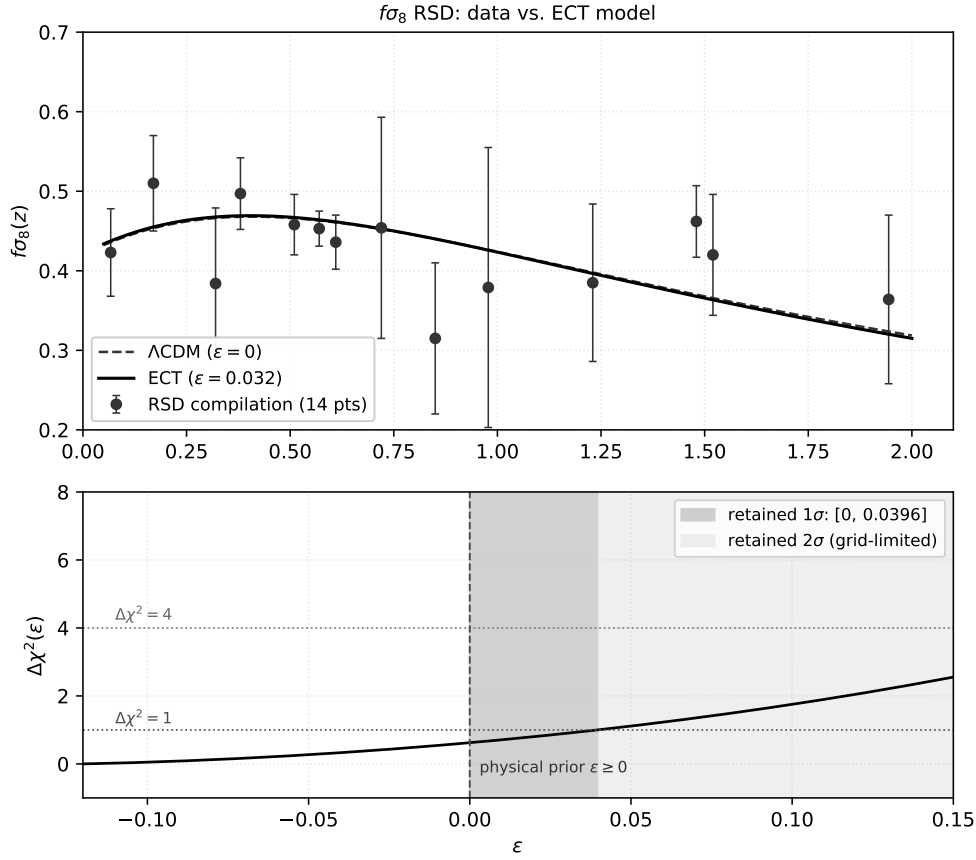


**Figure 50:** Extraction of the effective  $\varepsilon$ -interval from the  $f\sigma_8$  RSD channel, under the common background module of Appendix AH. Top panel: the 14 RSD data points with  $1\sigma$  error bars; the  $\Lambda$ CDM model ( $\varepsilon = 0$ , dotted) and the ECT model at the retained-band central value  $\varepsilon = 0.032$  (solid) are overlaid. Bottom panel: profile  $\chi^2(\varepsilon)$  on the extended grid  $\varepsilon \in [-0.12, +0.15]$ ; the raw minimum sits at the lower grid boundary, the Brent-refined  $1\sigma$  upper edge is at  $\varepsilon = 0.0396$ , and the physical prior  $\varepsilon \geq 0$  is marked by the vertical gray line. The retained  $1\sigma$  interval  $[0, 0.0396]$  is shaded darker gray; the  $2\sigma$  upper-edge extension is shown lighter. All shading and line styles are grayscale per preprint convention.

## AI.7 Methodological limitations

(i) *Data-level growth preference.* The negative raw best-fit reflects an observational feature of the RSD compilation (consistency with modest growth suppression relative to  $\Lambda$ CDM at  $z \lesssim 1$ ) rather than an ECT prediction of  $\varepsilon < 0$ . The uniform- $\varepsilon$  diagnostic of §16.5 restricts  $\varepsilon \geq 0$ ; the resulting retained bound (AK.6) is therefore a one-sided upper limit.

(ii) *Diagonal covariance only.* Off-diagonal cross-correlations between surveys have not been propagated. Their inclusion would broaden the  $1\sigma$  interval modestly; the present treatment is therefore optimistic.

(iii)  $\sigma_8^{(0)}$  *profiled as nuisance.* The amplitude  $\sigma_8^{(0)}$  is profiled rather than fixed, since its absolute calibration is tied to the CMB amplitude  $A_s$  through a  $\varepsilon$ -dependent growth history. Profiling is conservative and tests only the *shape* of  $f\sigma_8(z)$ ; a fixed- $\sigma_8^{(0)}$  analysis would give a tighter but more prior-dependent constraint.

(iv) *Linear growth theory.* The growth-factor ODE (AK.3) is the linear-theory equation. At  $z \lesssim 0.5$ , mildly non-linear corrections to the growth factor and to the RSD observable itself are present; they are absorbed into the diagonal observational uncertainty in the present compilation.

(v)  *$\Lambda$ CDM-background common proxy.* As in AE.7(i) and AG.8(ii), the common background module

uses a  $\Lambda$ CDM-best-fit parameter set as external input; the  $\varepsilon$ -deformation is applied on top. A closure-level background would modify both the background expansion and the Poisson source  $\mu_G$  consistently, in a way that cannot be reduced to a single parameter  $\varepsilon$ .

(vi) *Grid-refinement history.* The earlier coarser-grid  $1\sigma$  upper of 0.058 was removed in the present checkpoint as a numerical artefact of the grid scan; the Brent-refined value 0.0396 is stable with respect to further grid tightening, but depends on the extended scan range  $[-0.12, +0.15]$  being wide enough to bracket the true profile minimum in  $\varepsilon < 0$ . This is discussed in Appendix AH.

## AL Extraction of the effective uniform- $\varepsilon$ interval from the ISW channel (provisional proxy)

This appendix derives the effective uniform- $\varepsilon$  upper bound from the late-time Integrated Sachs-Wolfe (ISW) amplitude. The present extraction is deliberately presented as a *provisional proxy*, not as an extraction at the same epistemic level as A1–A4. The reasons are stated up front and in each subsection:

- the  $\varepsilon$ -dependence of the observable is linearised,
- the proportionality coefficient  $\kappa_{\text{ISW}}$  is calibrated against a  $\Lambda$ CDM-background Limber weight function and has *not* been recalibrated against the common ECT background of Appendix AH in the present freeze checkpoint,
- the observational uncertainty is very large (of order 30%) and the channel cannot by itself extract a non-trivial central value.

The retained result of this channel is therefore a broad one-sided upper bound under the physical prior  $\varepsilon \geq 0$ , whose numerical value is unchanged between the pre-recalc and the post-recalc retained-pipeline and whose interpretation is consistency-checking rather than evidential.

### AJ.1 Physics of the probe

The late-time ISW effect is the cross-correlation between the CMB temperature anisotropy and tracers of the large-scale gravitational potential  $\Phi$  at low redshift. In a matter-only universe the gravitational potential is constant in time on large scales, and the ISW signal vanishes; the presence of dark energy causes  $\dot{\Phi} \neq 0$  at low  $z$ , which gives a non-zero cross-correlation. In the effective uniform- $\varepsilon$  layer of §16.5, the deformation of the expansion rate through (AG.3) modifies the late-time decay of  $\Phi$ , and the amplitude of the resulting ISW signal deviates from its  $\Lambda$ CDM value.

### AJ.2 Observational inputs

The observable is the measured amplitude of the cross-correlation between the Planck CMB temperature map and the unWISE galaxy catalogue, parametrised as a rescaling of the  $\Lambda$ CDM prediction:

$$A_{\text{ISW}}^{\text{obs}} = 0.96 \pm 0.30, \quad (\text{AL.1})$$

from Krolewski et al. 2022 [254]. The central value is  $1\sigma$  below the  $\Lambda$ CDM-based prediction  $A_{\text{ISW}}^{\Lambda} = 1$ ; the uncertainty of 30% is intrinsically large, and the measurement cannot be sharpened within the present pipeline.

### AJ.3 ECT-side model and extraction scope (provisional)

At the provisional-proxy level used here, the  $\varepsilon$ -dependence of the ISW amplitude is approximated by the linearised form

$$A_{\text{ISW}}^{\text{model}}(\varepsilon) = 1 + \kappa_{\text{ISW}} \varepsilon, \quad \kappa_{\text{ISW}} \approx 6, \quad (\text{AL.2})$$

where the coefficient  $\kappa_{\text{ISW}}$  was obtained from a single-zoomed Limber integration of the ISW weight function under a  $\Lambda$ CDM background. This coefficient has *not* been recalibrated against the common ECT background of Appendix AH in the present checkpoint. The justification for this deferral is stated in the present common-background methodology (A6): a genuine ECT-background recalibration of  $\kappa_{\text{ISW}}$  would require re-integrating the full late-time ISW weight function  $W_{\text{ISW}}(z)$  under  $H(z, \varepsilon)$ ,  $t(z, \varepsilon)$ , and  $\dot{\Phi}(z, \varepsilon)$  trajectories, which is beyond the scope of Phase 2A.

**Held fixed under the present proxy.** The linearised form (AL.2); the  $\Lambda$ CDM-background-calibrated coefficient  $\kappa_{\text{ISW}} = 6$ ; the Krolewski+2024 observational anchor.

**Varied.**  $\varepsilon$  only.

**Not included at this proxy level.** Any nonlinear dependence of  $A_{\text{ISW}}$  on  $\varepsilon$ ; recalibration of  $\kappa_{\text{ISW}}$  on the common ECT background; cross-correlations with other late-time probes (weak lensing,  $f\sigma_8$ ) that would share systematic effects; full Boltzmann evolution of  $\dot{\Phi}$  under the ECT deformation.

#### AJ.4 Extraction statistic

The one-parameter model gives the inversion

$$\varepsilon(A_{\text{ISW}}) = \frac{A_{\text{ISW}} - 1}{\kappa_{\text{ISW}}}. \quad (\text{AL.3})$$

The raw best-fit and the raw  $1\sigma$  and  $2\sigma$  intervals follow from the  $\pm 1\sigma$  and  $\pm 2\sigma$  observational brackets on  $A_{\text{ISW}}^{\text{obs}}$ .

#### AJ.5 Interval definition and origin of the width

**Raw result.** Direct inversion of  $A_{\text{ISW}}^{\text{obs}} = 0.96 \pm 0.30$  gives

$$\varepsilon_{\text{raw}} = -0.0067, \quad (\text{AL.4})$$

$$[\varepsilon_{\text{lo}}^{1\sigma}, \varepsilon_{\text{hi}}^{1\sigma}]_{\text{raw}} = [-0.057, +0.043], \quad (\text{AL.5})$$

$$[\varepsilon_{\text{lo}}^{2\sigma}, \varepsilon_{\text{hi}}^{2\sigma}]_{\text{raw}} = [-0.107, +0.093]. \quad (\text{AL.6})$$

The raw best-fit is indistinguishable from zero within the observational uncertainty.

**Retained interval under the physical prior.** Imposing  $\varepsilon \geq 0$ , the ISW channel contributes a one-sided upper bound:

$$[\varepsilon_{\text{lo}}^{1\sigma}, \varepsilon_{\text{hi}}^{1\sigma}] = [0, 0.0433], \quad (\text{AL.7})$$

$$[\varepsilon_{\text{lo}}^{2\sigma}, \varepsilon_{\text{hi}}^{2\sigma}] = [0, 0.0933]. \quad (\text{AL.8})$$

The interval was numerically unchanged between the pre-recalc and the post-recalc retained pipelines, reflecting the fact that  $\kappa_{\text{ISW}}$  has not yet been recalibrated.

**Origin of the width.** The  $\pm 30\%$  observational uncertainty on  $A_{\text{ISW}}^{\text{obs}}$  is the sole driver of the width. There is no fitting at all: the channel is a direct algebraic inversion of a linearised one-parameter model, and the reported interval simply reflects the observational bracket on  $A_{\text{ISW}}$  through (AL.2).

**Channel character.** The ISW channel is a consistency channel only. Its retained upper bound is broader than those of A1–A4 and does not bind the joint interval. Its principal role in §16.5 is to demonstrate that the retained joint band  $[0.0296, 0.0376]$  is compatible with an independent late-time observable, *not* to contribute evidential weight to the band.

## AJ.6 Figure

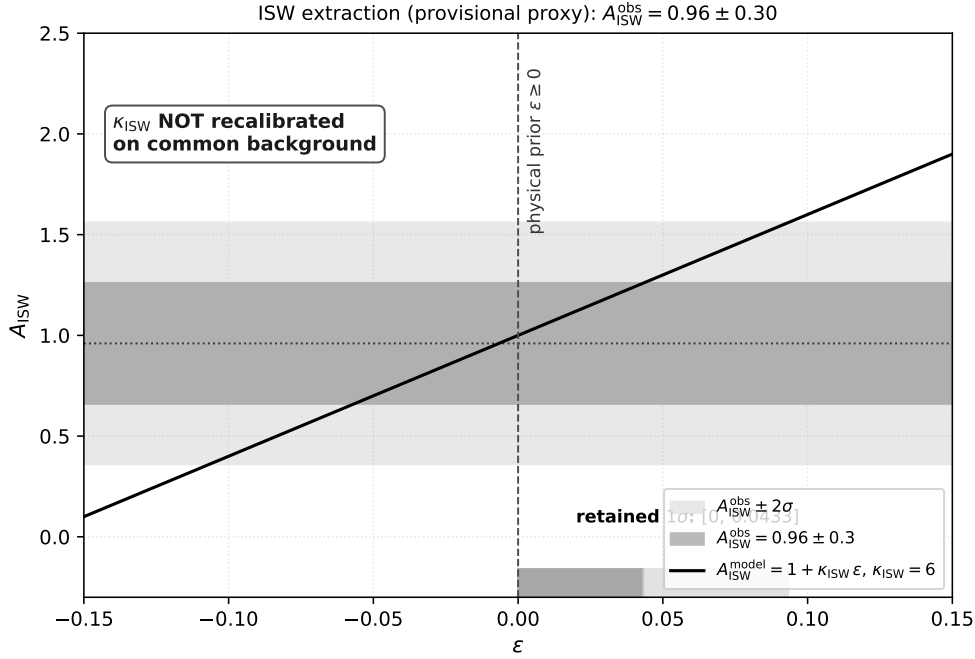


**Figure 51:** Extraction of the effective  $\varepsilon$ -upper bound from the ISW channel, at the provisional proxy level described in AJ.3. The linearised model  $A_{\text{ISW}}(\varepsilon) = 1 + \kappa_{\text{ISW}}\varepsilon$  with  $\kappa_{\text{ISW}} = 6$  (solid line) is compared with the observational anchor  $A_{\text{ISW}}^{\text{obs}} = 0.96 \pm 0.30$  (horizontal darker gray band:  $1\sigma$ ; lighter:  $2\sigma$ ). The inverted  $\varepsilon$ -intervals (shown along the  $\varepsilon$ -axis below) are clipped to the physical region  $\varepsilon \geq 0$ , yielding the retained one-sided upper bounds  $[0, 0.0433]$  ( $1\sigma$ ) and  $[0, 0.0933]$  ( $2\sigma$ ). The text “ $\kappa_{\text{ISW}}$  not recalibrated” is placed on the figure to reinforce the provisional status. All shading and line styles are grayscale per preprint convention.

## AJ.7 Methodological limitations

(i) *Linearised  $\varepsilon$ -dependence.* The form (AL.2) truncates the  $\varepsilon$ -dependence at linear order. For  $|\varepsilon| \gtrsim 0.05$  the linear approximation begins to break down, and a non-linear recalculation of  $A_{\text{ISW}}(\varepsilon)$  would be required to make the extracted bound quantitative at the retained-band level. Since the retained  $1\sigma$  upper 0.043 is close to this boundary, the bound should be read as an order-of-magnitude consistency check rather than a precise constraint.

(ii)  *$\kappa_{\text{ISW}}$  not recalibrated on common background.* The coefficient  $\kappa_{\text{ISW}} = 6$  was calibrated under  $\Lambda\text{CDM}$ -background Limber weights. On the common ECT background of Appendix AH, the late-time ISW weight function  $W_{\text{ISW}}(z)$  is modified through both  $H(z, \varepsilon)$  (which changes the conformal-time kernel) and  $\Phi(z, \varepsilon)$  (which changes the source amplitude). A self-consistent recalculation would, in principle, shift  $\kappa_{\text{ISW}}$  by an unknown amount; the present checkpoint therefore treats the retained ISW interval as provisional, and the numerical value quoted in §16.5 is inherited from the  $\Lambda\text{CDM}$ -background calibration.

(iii) *Large observational uncertainty.* The  $\pm 30\%$  uncertainty on  $A_{\text{ISW}}^{\text{obs}}$  is intrinsically large and cannot be reduced within the present pipeline. Even a perfectly recalibrated  $\kappa_{\text{ISW}}$  would not sharpen the retained interval below approximately  $[0, 0.03]$  at  $1\sigma$ .

(iv) *Epistemic status.* The ISW channel is not at the same epistemic level as A1–A4. In the retained-five-probe analysis it functions as a consistency check only: it does not bind any edge of the joint band, and its numerical value is unchanged between the pre-recalc and post-recalc pipelines. Any future strengthening of the ISW bound (e.g., through kernel recalibration on the common background or through tighter  $A_{\text{ISW}}^{\text{obs}}$  measurements) would naturally be incorporated into a future iteration of the retained pipeline.

## AM Derivation of the force-law effective dimensionality

*Status: Level B (illustrative analytic closure). This appendix uses the convenient interpolating function  $\mu(x) = x/\sqrt{1+x^2}$  purely for analytical tractability in the derivation of  $d_{\text{force}}(r)$ . It should be read as an illustrative member of the broader ECT-compatible interpolation class, not as the unique fitting law used in the updated SPARC analysis. The qualitative behaviour of  $d_{\text{force}}$  is closure-independent provided the required ECT asymptotics  $\mu \rightarrow 1$  and  $\mu \rightarrow x$  are satisfied.*

### AM.1 Definition

For a gravitational force  $g(r)$  obeying  $g \propto 1/r^{d-1}$  in  $d$  effective dimensions, the force-law dimensionality is

$$d_{\text{force}}(r) = 1 - \frac{d \ln g_{\text{obs}}}{d \ln r}. \quad (\text{AM.1})$$

### AM.2 General derivation from $\phi$ -closure

Starting from

$$\mu(x) g_{\text{obs}} = g_N(r), \quad x \equiv g_{\text{obs}}/g_{\dagger}, \quad (\text{AM.2})$$

take the logarithmic derivative with respect to  $\ln r$ :

$$\frac{d \ln g_N}{d \ln r} = \left(1 + \frac{d \ln \mu}{d \ln x}\right) \frac{d \ln g_{\text{obs}}}{d \ln r}. \quad (\text{AM.3})$$

Therefore

$$\frac{d \ln g_{\text{obs}}}{d \ln r} = \frac{d \ln g_N / d \ln r}{1 + d \ln \mu / d \ln x}, \quad (\text{AM.4})$$

and hence

$$d_{\text{force}}(r) = 1 + \frac{p_N(r)}{1 + d \ln \mu / d \ln x}, \quad (\text{AM.5})$$

where  $p_N(r) \equiv -d \ln g_N / d \ln r$ .

For a point mass,  $g_N = G_N M / r^2$  gives  $p_N = 2$ .

### AM.3 Specific result for $\mu(x) = x/\sqrt{1+x^2}$

Compute:

$$\ln \mu = \ln x - \frac{1}{2} \ln(1+x^2), \quad \frac{d \ln \mu}{d \ln x} = 1 - \frac{x^2}{1+x^2} = \frac{1}{1+x^2}. \quad (\text{AM.6})$$

Substituting into (AM.5):

$$d_{\text{force}}(x) = 1 + \frac{2(1+x^2)}{2+x^2}. \quad (\text{AM.7})$$

### AM.4 Limiting cases

Regime	$x$	$d_{\text{force}}$	Physics
Screened	$\gg 1$	$\rightarrow 3$	$g \propto 1/r^2$ , Newtonian
Transition	$= 1$	$= 7/3 \approx 2.33$	onset of flat rotation
Deep $\phi$ -branch	$\ll 1$	$\rightarrow 2$	$g \propto 1/r$ , $v_{\text{flat}} = \text{const}$

The rotation velocity  $v^2 = r g \propto r^{2-d_{\text{force}}}$ :



- $d_{\text{force}} = 3$ :  $v \propto r^{-1/2}$  (Keplerian),
- $d_{\text{force}} = 7/3$ :  $v \propto r^{-1/6}$  (strongly flattened),
- $d_{\text{force}} = 2.5$ :  $v \propto r^{-1/4}$  (transition zone),
- $d_{\text{force}} = 2$ :  $v = \text{const}$  (flat rotation).

### AM.5 Transition radius

The transition  $x = 1$  occurs at

$$r_* = \sqrt{\frac{G_N M}{g_{\dagger}(\phi_{\text{env}})}}. \quad (\text{AM.8})$$

Representative values:  $r_*(10^8 M_{\odot}) \approx 0.3 \text{ kpc}$ ,  $r_*(5 \times 10^{10} M_{\odot}) \approx 8 \text{ kpc}$ ,  $r_*(5 \times 10^{11} M_{\odot}) \approx 24 \text{ kpc}$ .

### AM.6 Distinction from morphological dimensionality

The force-law dimensionality  $d_{\text{force}}$  describes the scaling of the gravitational interaction. The morphological dimensionality  $d_{\text{morph}}$  describes the shape of matter distributions (sheets:  $\sim 2$ , filaments:  $\sim 1$ ). They are related through the tidal tensor  $T_{ij} = \partial_i \partial_j \Phi$ : the number of collapsing eigenvalues of  $T_{ij}$  determines  $d_{\text{morph}} = 3 - N_{\text{collapsed}}$ . A quantitative derivation of  $d_{\text{morph}}$  from the  $\phi$ -sector is listed as Open Problem OP8.

### AM.7 Numerical implementation

Equation (AM.7) is evaluated analytically. The mapping  $x(r)$  uses the exact  $\phi$ -closure solution:

$$g_{\text{obs}}^2 = \frac{g_N^2 + \sqrt{g_N^4 + 4g_N^2 g_{\dagger}^2}}{2}, \quad x = g_{\text{obs}}/g_{\dagger}. \quad (\text{AM.9})$$

The complete Python implementation is available at <https://github.com/chufelo/ECT-preprint-code>.

## AN Derivation of the galactic $\phi$ -closure and the practical fitting law

Unlike Appendix AS, which discusses the derivation status at a conceptual level, the present appendix records the concrete Level B closure actually used in the SPARC fitting pipeline.

This appendix derives the practical galactic fitting law used in the SPARC analysis.

### AN.1 Variational structure

The galactic sector is treated as a nonlinear static response problem for the effective potential  $\Phi$ . The minimal effective functional is taken to be

$$\Gamma_{\text{gal}}[\Phi] = \int d^3x \left[ \frac{g_0^{\dagger 2}}{8\pi G_N} F\left(\frac{|\nabla\Phi|}{g_0^{\dagger}}\right) - \rho_b(\mathbf{x})\Phi \right], \quad (\text{AN.1})$$

where  $g_0^{\dagger}$  is the cosmological baseline critical acceleration scale and  $\rho_b$  is the baryonic source density.

The corresponding Euler–Lagrange equation reads

$$\nabla \cdot \left[ \mu_{\phi} \left( \frac{|\nabla\Phi|}{g_0^{\dagger}} \right) \nabla\Phi \right] = 4\pi G_N \rho_b, \quad (\text{AN.2})$$

with

$$\mu_{\phi}(x) = \frac{1}{2x} \frac{dF}{dx}. \quad (\text{AN.3})$$

## AN.2 Required asymptotic branches

The closure must reproduce two limiting regimes.

**Screened Newtonian branch.** At large accelerations one must recover ordinary gravity,

$$\mu_\phi(x) \rightarrow 1 \quad (x \gg 1). \quad (\text{AN.4})$$

**Deep critical branch.** At small accelerations the critical infrared branch must satisfy

$$\mu_\phi(x) \rightarrow x \quad (x \ll 1), \quad (\text{AN.5})$$

which yields the characteristic ECT deep-regime law

$$g \rightarrow \sqrt{g_N g^\dagger}. \quad (\text{AN.6})$$

## AN.3 Minimal interpolation choice

A full first-principles derivation of the interpolation family from the microscopic condensate is not yet available. The present work therefore adopts the phenomenologically simplest smooth representative of the ECT-compatible interpolation class, consistent with both asymptotic branches:

$$\mu_\phi(x) = \frac{x}{1+x}. \quad (\text{AN.7})$$

This is a Level B closure assumption, not a unique first-principles derivation. Other smooth functions satisfying  $\mu \rightarrow x$  ( $x \ll 1$ ) and  $\mu \rightarrow 1$  ( $x \gg 1$ ) are equally ECT-compatible at the present stage; the exact member of this class must follow from the full OP3 completion of  $U(\phi)$ .

Using eq. (AN.3), one obtains

$$F(x) = x^2 - 2x + 2\ln(1+x), \quad (\text{AN.8})$$

up to an irrelevant additive constant. One verifies immediately that

$$F(x) \sim x^2 \quad (x \gg 1), \quad F(x) \sim \frac{2}{3}x^3 \quad (x \ll 1),$$

so the closure indeed interpolates between the quadratic screened branch and the critical  $Y^{3/2}$  branch.

## AN.4 Practical algebraic fitting law

In the quasi-radial fitting approximation, the modified Poisson equation reduces to

$$\mu_\phi \left( \frac{g}{g_{\text{eff}}^\dagger} \right) g = g_N. \quad (\text{AN.9})$$

With the choice (AN.7) this gives

$$\frac{g/g_{\text{eff}}^\dagger}{1 + g/g_{\text{eff}}^\dagger} g = g_N, \quad (\text{AN.10})$$

hence

$$g^2 - g_N g - g_N g_{\text{eff}}^\dagger = 0. \quad (\text{AN.11})$$

Selecting the positive branch yields the practical ECT fitting law

$$g(R) = \frac{1}{2} \left[ g_N(R) + \sqrt{g_N^2(R) + 4g_N(R)g_{\text{eff}}^\dagger} \right]. \quad (\text{AN.12})$$

## AN.5 Baryonic input from SPARC

The Newtonian input acceleration is computed from the SPARC baryonic mass model as

$$g_N(R) = \frac{V_{\text{gas}}^2(R) + \Upsilon_d V_{\text{disk}}^2(R) + \Upsilon_b V_{\text{bul}}^2(R)}{R}. \quad (\text{AN.13})$$

The predicted circular velocity is then

$$V_{\text{ECT}}(R) = \sqrt{R g(R)}. \quad (\text{AN.14})$$

## AN.6 RAR representation of the same closure

The radial acceleration relation is not an independent phenomenological law added on top of the velocity fit. It is simply the same galactic closure expressed in acceleration variables:

$$g_{\text{obs}}(R) = \frac{V_{\text{obs}}^2(R)}{R}, \quad g_{\text{bar}}(R) = \frac{V_{\text{gas}}^2(R) + \Upsilon_d V_{\text{disk}}^2(R) + \Upsilon_b V_{\text{bul}}^2(R)}{R}. \quad (\text{AN.15})$$

The corresponding ECT prediction is therefore

$$g_{\text{ECT}}(R) = \frac{1}{2} \left[ g_{\text{bar}}(R) + \sqrt{g_{\text{bar}}^2(R) + 4 g_{\text{bar}}(R) g_{\text{eff}}^\dagger} \right]. \quad (\text{AN.16})$$

Thus the RAR plots are only a different projection of the same fitted galactic closure already used in the rotation-curve analysis.

## AN.7 Deep branch and BTFR

In the low-acceleration branch, eq. (AN.12) reduces to

$$g \simeq \sqrt{g_N g_{\text{eff}}^\dagger}. \quad (\text{AN.17})$$

For circular motion,  $v_c^2/R = g$ , and at large radii where  $M_b(R) \rightarrow M_{\text{bar}}$ ,

$$v_c^4 = G_N M_{\text{bar}} g_{\text{eff}}^\dagger. \quad (\text{AN.18})$$

Thus the BTFR slope is structural, while its normalisation is governed by the effective critical scale.

In the present numerical implementation we use an internal outer baryonic-mass proxy

$$M_{\text{bar,eff}} = \frac{R_{\text{tail}}^2 g_N(R_{\text{tail}})}{G_N}, \quad (\text{AN.19})$$

where  $R_{\text{tail}}$  is an outer-tail radius estimator constructed from the last measured SPARC points. This provides a self-consistent BTFR test inside the same galactic closure pipeline. It should be read as an internal ECT BTFR diagnostic, not yet as a substitute for the standard catalogue-level BTFR constructed from an independent total baryonic-mass table.

## AN.8 Degeneracy of the orientation-stress sector with the effective critical-scale calibration

*Status: structural observation. Within the present phenomenological galactic closure, no separately identifiable numerical correction from the full nonlinear field equations to the rotation-curve, RAR, or BTFR results is extractable. This conclusion is closure-dependent, not a universal theorem of ECT: a future first-principles derivation of the galactic  $\phi$ -profile may reveal non-degenerate NLEE signatures beyond the effective critical-scale parametrisation.*

**Source of the degeneracy.** The anisotropic orientation stress  $\Theta_{\mu\nu}[n]$  (13.23) provides an additional source term in the quasistatic Poisson equation beyond the scalar  $\phi$ -closure. In the nearly spherical, quasistatic regime relevant for galactic rotation curves, the contribution of  $\Theta_{\mu\nu}$  modifies the effective gravitational acceleration by a relative amount of order  $|c_1|$ , where  $c_1$  is the orientation-stress coefficient (OP-c1). However, in the present phenomenological parametrisation the galactic sector is fitted through the effective critical scale  $g_{\text{eff}}^\dagger$ , and any systematic shift from  $\Theta_{\mu\nu}$  is absorbed into the calibration of that scale. The two effects are therefore degenerate at the current closure level.

**BTFR slope invariance.** The BTFR slope 4 follows from the deep-branch asymptotics  $g \simeq \sqrt{g_N g^\dagger}$  (eq. AN.18). This structural result is preserved provided the orientation-stress contribution in the deep quasistatic regime acts as a slow renormalisation of the effective critical scale rather than as a modification of the power-law index of the deep-branch interpolation. At the present closure level no separate NLEE-induced mechanism has been identified that would change the deep-branch exponent; the slope 4 therefore remains structurally robust against orientation-stress corrections within the current framework. The normalisation, however, is governed by  $g_{\text{eff}}^\dagger$  and is degenerate with any  $c_1$ -induced shift.

**Non-degenerate residual: environment-dependent scatter.** The most natural non-degenerate signature of the orientation stress in the galactic sector is environment-dependent modulation:  $c_1(\bar{\phi})$  depends on the local condensate amplitude, and hence on the density of the surrounding environment. This mechanism may contribute to the observed galaxy-to-galaxy scatter in  $g_{\text{eff}}^\dagger$  beyond the environment law  $\Xi$  (eq. 17.12). Quantifying this contribution requires a first-principles derivation of  $c_1(\bar{\phi})$  (OP-c1).

## AO Computational procedure for the SPARC galactic fits

This appendix summarises the numerical procedure used to generate the galactic figures and tables.

### AO.1 Input data

The analysis uses the SPARC mass-model catalogue [255], containing radius  $R$ , observed velocity  $V_{\text{obs}}$  with uncertainty  $\sigma_V$ , and the baryonic Newtonian components  $V_{\text{gas}}$ ,  $V_{\text{disk}}$ , and  $V_{\text{bul}}$ .

### AO.2 Fit modes

Two fitting modes are considered.

**Fixed- $M/L$  mode.** The stellar mass-to-light ratios are fixed at

$$\Upsilon_d = 0.5, \quad \Upsilon_b = 0.7,$$

and only the effective critical scale  $g_{\text{eff}}^\dagger$  is fitted. This is the cleaner ECT test because it removes the strongest disk  $M/L$  degeneracy.

**Free- $M/L$  mode.** The disk mass-to-light ratio  $\Upsilon_d$  is fitted jointly with  $g_{\text{eff}}^\dagger$ , while  $\Upsilon_b = 0.7$  is kept fixed.

### AO.3 Optimisation and quality control

For each galaxy the fit minimises

$$\chi^2 = \sum_i \frac{[V_{\text{obs}}(R_i) - V_{\text{ECT}}(R_i)]^2}{\sigma_i^2}. \quad (\text{AO.1})$$

A minimum error floor of  $2 \text{ km s}^{-1}$  is imposed in the present runs for robustness.

The output catalogue stores quality flags indicating:

- too few measured points,
- poor reduced  $\chi^2$ ,
- fitted stellar  $M/L$  at the scan boundary,
- possible bulge sensitivity.

A clean sub-sample is defined by excluding low-quality flagged cases.

#### AO.4 Model comparison

Four fit families are compared:

1. ECT fixed- $M/L$  closure ( $k = 1$  free parameter),
2. ECT free- $M/L$  closure ( $k = 2$  free parameters),
3. MOND with free stellar  $M/L$  ( $k = 1$ ),
4.  $\Lambda$ CDM with an NFW-type halo fit ( $k = 3$ ).

Because the number of free parameters differs between the models, both AIC and BIC are computed in addition to reduced  $\chi^2$ .

#### AO.5 Outputs used in the paper

The main text uses:

- a representative SPARC rotation-curve figure (Fig. 23),
- a compact sample-level fit-quality comparison figure (Fig. 24),
- the updated effective critical-scale summary figure (Fig. 25),
- a Milky Way comparison figure (Fig. 26),
- a compact summary table over the SPARC sample (Table 66),
- an internal BTFR diagnostic figure (Fig. 22),
- a six-panel RAR figure derived from the same closure (Fig. 27).

Additional scatter diagnostics, fixed/free- $M/L$  comparisons, and further machine-readable tables are retained as supplementary material.

#### AO.6 Derived plot quantities: BTFR, RAR, and effective critical-scale diagnostics

Three additional observational representations are generated from the same fitted galactic closure.

**BTFR.** The BTFR plot uses the outer-tail velocity estimator  $V_{\text{flat}}$  constructed from the outer SPARC points together with the internal effective baryonic-mass proxy

$$M_{\text{bar,eff}} = R_{\text{tail}}^2 g_N(R_{\text{tail}}) / G_N.$$

This yields a self-consistent ECT BTFR diagnostic based on the same pipeline as the rotation-curve fits.

**RAR.** The RAR figure is produced by plotting  $g_{\text{obs}} = V_{\text{obs}}^2/R$  against  $g_{\text{bar}} = (V_{\text{gas}}^2 + \Upsilon_{\text{d}} V_{\text{disk}}^2 + \Upsilon_{\text{b}} V_{\text{bul}}^2)/R$  for the same galaxies. The ECT and MOND curves shown there are not separate empirical fit functions, but direct projections of the same closure used in the velocity analysis.

**Effective critical-scale analysis.** The updated  $g^\dagger$  figure is built directly from the fitted per-galaxy values of  $g_{\text{eff}}^\dagger$  produced by the new SPARC pipeline. It replaces the earlier legacy  $\phi_{\text{env}}$  plot and is therefore the correct summary diagnostic for the present version of the galactic sector.

## AO.7 Diagnostic interpretation and the current EFE proxy

The diagnostics retained in this appendix serve three distinct roles: they separate fixed- $M/L$  from free- $M/L$  behaviour, they allow information-criterion comparison (AIC/BIC) between ECT, MOND, and  $\Lambda$ CDM, and they identify the clean sub-sample used in the main text to reduce the strongest fitting pathologies. Only the most informative summary figures are promoted to the main narrative; the remaining diagnostics are kept here in order to document the stability and limitations of the present Level B galactic closure.

A preliminary nearest-neighbour proxy for the external field was tested. For the currently available environment inputs the resulting ratio  $g_{\text{ext}}/g_0^\dagger$  is typically extremely small, so the proxy correction is numerically negligible. This does not show that EFE is absent in ECT; it only shows that the present Level-1 proxy is too weak to affect the displayed sample and is therefore not promoted to a main result.

## AO.8 Additional diagnostic outputs

Figures 52–55 present supplementary SPARC diagnostic plots.

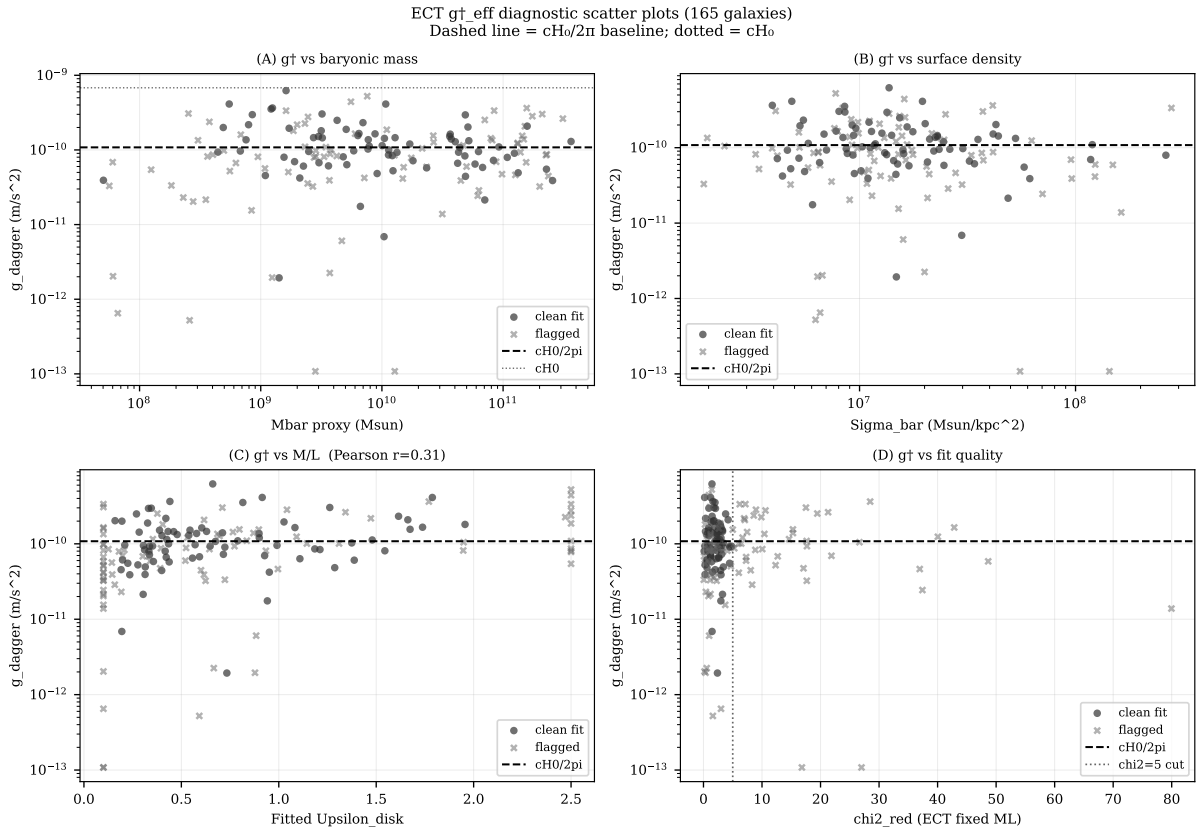


**Figure 52:** Additional scatter diagnostics for the fitted effective critical scale  $g_{\text{eff}}^\dagger$  across the SPARC sample: dependence on a baryonic mass proxy, a baryonic surface-density proxy, the fitted disk mass-to-light ratio, and the fit quality itself. These plots are retained as supplementary diagnostics rather than promoted to the main text, because the more compact summary is now given by Fig. 25.

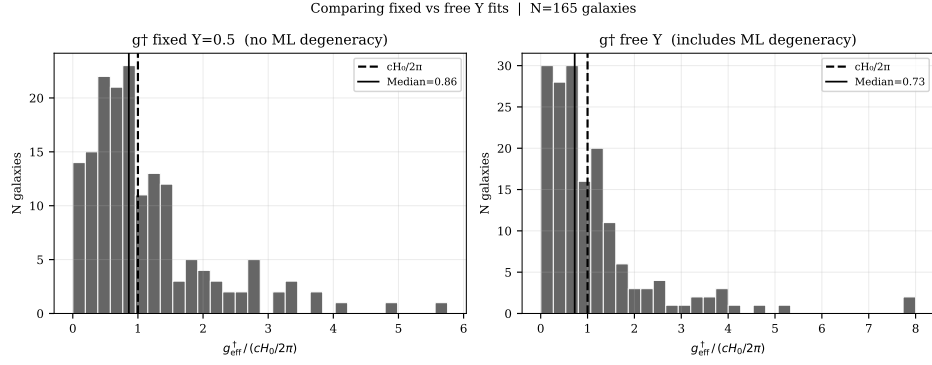


**Figure 53:** Histogram of fitted effective critical scales  $g_{\text{eff}}^+$  across the SPARC sample. The vertical markers indicate the two natural ECT baselines  $cH_0$  and  $cH_0/(2\pi)$ . In the present manuscript the compact two-panel summary of this information is shown in Fig. 25; the histogram is retained here as a supplementary diagnostic.

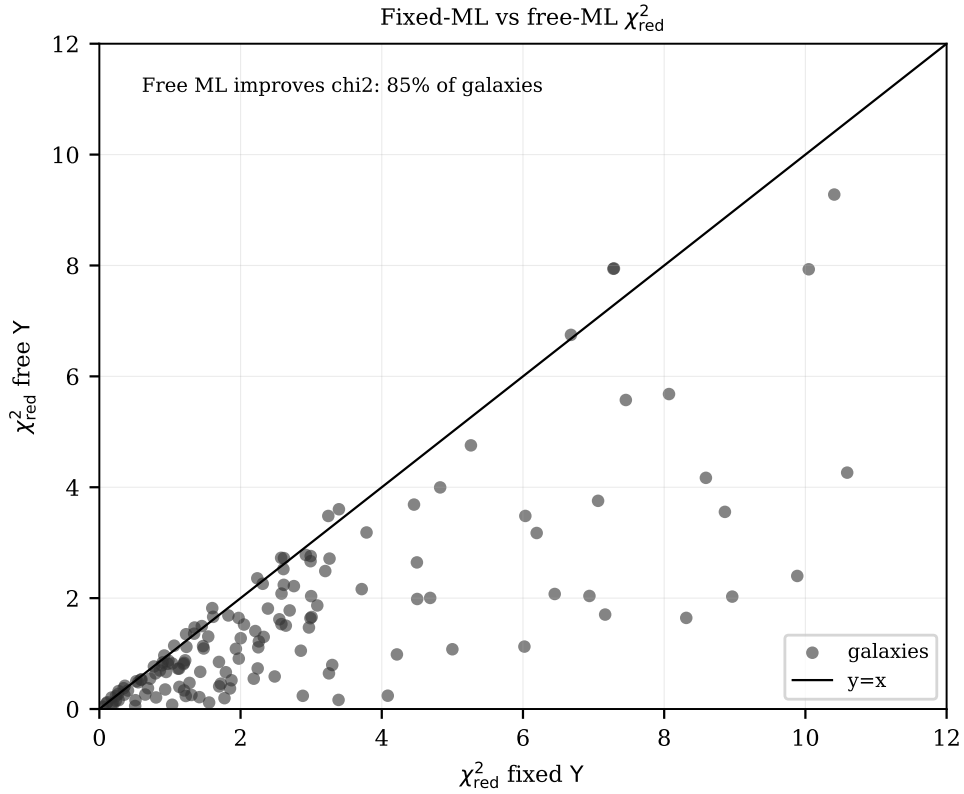


**Figure 54:** Fixed- $M/L$  versus free- $M/L$  comparison of fit quality across the SPARC sample. Each point corresponds to one galaxy, with the horizontal axis showing the reduced  $\chi^2$  of the fixed- $M/L$  ECT fit and the vertical axis showing the reduced  $\chi^2$  of the free- $M/L$  ECT fit. The diagonal  $y = x$  marks equal fit quality. The dominant population lies below this line, showing that allowing  $\Upsilon_d$  to vary improves the fit for most galaxies. This figure is retained in the appendix because it diagnoses the strength of the  $M/L$  degeneracy rather than introducing a new physical prediction.

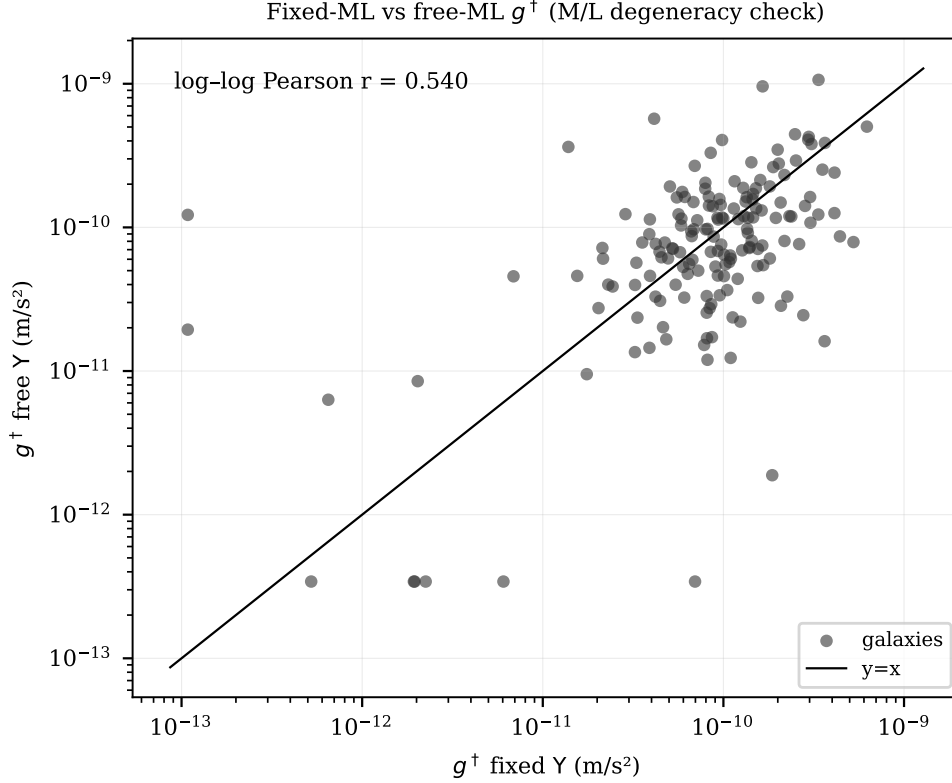


**Figure 55:** Fixed- $M/L$  versus free- $M/L$  comparison of the fitted effective critical scale  $g_{\text{eff}}^+$ . The diagonal  $y = x$  marks identical recovered values. The moderate correlation indicates that part of the scatter in  $g_{\text{eff}}^+$  is robust under changes in the disk mass-to-light treatment, while another part is clearly entangled with the  $M/L$  degeneracy. This is why the fixed- $M/L$  mode is used in the main text as the cleaner test of the ECT galactic closure, whereas the free- $M/L$  mode is interpreted as a robustness check rather than as the primary physical result.

The moderate fixed/free correlation (Pearson  $r \approx 0.54$  in the present run) confirms that the effective critical scale is neither fully determined by the stellar  $M/L$  choice nor fully independent of it.

The full numerical pipeline produces several diagnostics that are useful for interpreting the galactic fits but are too methodological to occupy main-text space. The figures collected here serve three distinct purposes: they document the residual scatter of the fitted effective critical scale, they show how that scatter changes between fixed- $M/L$  and free- $M/L$  fitting modes, and they quantify the extent to which the apparent improvement of the free- $M/L$  mode should be attributed to extra nuisance freedom rather than to a deeper physical closure. Accordingly, these plots are retained in the appendix as robustness and degeneracy diagnostics rather than as headline physical results.

## AP Cluster-merger lensing: methods and results

*Status: Level B. The present analysis uses a projected algebraic  $\phi$ -closure applied to order-of-magnitude Gaussian representations of the cluster baryonic distributions. It is intended as a morphology-oriented qualitative test and amplitude estimate, not yet as a full 3D metric- $\phi$  merger simulation. A full 3D solver remains part of the future programme (OP22).*

This appendix documents the numerical methods, cluster parameters, corrections, and results for the four-cluster merger analysis described in Section 17.2. All code is available at <https://github.com/chufelo/ECT-preprint-code>: `fig_cluster_merger_suite.py` generates both figures and prints the full numerical results table.



### AP.1 Method: 2D projected $\phi$ -closure

The baryonic surface density is decomposed into compact collisionless clumps (BCG) and diffuse X-ray gas:

$$\Sigma_b(x, y) = \Sigma_\star(x, y) + \Sigma_{\text{gas}}(x, y). \quad (\text{AP.1})$$

Each component is represented by a sum of Gaussian profiles calibrated to the observed masses and half-light radii (Table 136). The projected Newtonian field is [112]

$$g_N(x, y) \approx 2\pi G \Sigma_b(x, y), \quad (\text{AP.2})$$

and the algebraic  $\phi$ -closure is applied pointwise:

$$v(y) = \sqrt{\frac{1 + \sqrt{1 + 4/y^2}}{2}}, \quad y = \frac{g_N}{g_\dagger^{\text{cl}}}. \quad (\text{AP.3})$$

The threshold  $g_\dagger^{\text{cl}}$  is used here as the merger-environment counterpart of the same critical-scale logic discussed in the galactic sector. In the present benchmark it is held fixed across the four-cluster suite rather than promoted to a system-by-system fit parameter. The effective projected surface density for lensing is

$$\Sigma_{\text{eff}}(x, y) = v\left(\frac{g_N}{g_\dagger^{\text{cl}}}\right) \Sigma_b(x, y), \quad (\text{AP.4})$$

and the convergence map is  $\kappa = \Sigma_{\text{eff}}/\Sigma_{\text{crit}}$ .

For spherically symmetric systems this algebraic closure coincides with the corresponding reduced radial  $\phi$ -branch equation (by Gauss's-law analogy; Level B). For non-spherical mergers the thin-lens approximation is a proxy; the full calculation requires solving the  $\phi$ -field equation on a 3D grid (OP22).

### AP.2 Cluster parameters

**Table 136:** Cluster parameters used in the four-system ECT analysis. Masses and radii are order-of-magnitude characterisations consistent with X-ray and lensing observations; not precision fits. For Abell 520 the BCG distribution is dispersed to  $|x| \approx 370$  kpc post-merger [117], while the central gas core is compact ( $s_{\text{gas}} = 150$  kpc).

Cluster	$M_\star [M_\odot]$	$s_\star$ [kpc]	$M_{\text{gas}} [M_\odot]$	$s_{\text{gas}}$ [kpc]	Offset [kpc]
Bullet ( $z = 0.296$ )	$2 \times 5 \times 10^{12}$	70	$2 \times 6 \times 10^{13}$	225	100–150
MACS J0025 ( $z = 0.586$ )	$2 \times 3 \times 10^{12}$	60	$2 \times 2 \times 10^{13}$	250	150
El Gordo ( $z = 0.870$ )	$(8+5) \times 10^{12}$	65	$(5+3) \times 10^{13}$	285	200
Abell 520 ( $z = 0.199$ )	$2 \times 2.5 \times 10^{12}$	90	$5 \times 10^{13}$ (cen-tral)	150	0 (gas core)

### AP.3 Results: morphology

In all four systems the  $\kappa$ -peaks of  $\Sigma_{\text{eff}}$  track the component with higher local surface density. For Bullet, MACS J0025, and El Gordo, the lensing peaks coincide with the compact stellar clumps ( $d_\star^{\text{ECT}} \lesssim 37$  kpc; observed  $< 25$ – $35$  kpc), displaced from the diffuse gas by  $\Delta = 83$ – $149$  kpc. For Abell 520 the lensing peak falls on the dense central gas core, consistent with the observed anomalous morphology [117, 118]. Both regimes arise from the same  $v$ -closure without per-system adjustment.

## AP.4 Results: amplitude and corrections

**Table 137:** Uniform ECT correction protocol for the four-cluster merging-system suite. All entries are order-of-magnitude corrections applied multiplicatively on top of the baseline  $v$ -closure. The shear-to- $\kappa$  reinterpretation sometimes labelled  $E_5$  is not listed separately: it is already built into the baseline effective convergence  $\Sigma_{\text{eff}} = v\Sigma_b$ ; applying it again would double-count (Section AP.7).

Label	Physical mechanism	Magnitude	Status
Baseline	$\Sigma_{\text{eff}} = v(g_N/g_{\dagger}^{\text{cl}})\Sigma_b$	$A_0 = 0.42\text{--}0.71$	Level B
$E_1: G_{\text{eff}}(z)$	$(1+z)^{2\varepsilon}$ shifts $\Sigma_{\text{crit}}$ ; legacy illustrative stress-test value $\varepsilon \approx 0.01$ (not recomputed on the retained band of §16.5)	+0.5%	Level B
$E_2: \delta z$	Condensate shift of spectroscopic $T_X$	$\lesssim 1\%$	Level B
$E_4$ : post-merger gas	Non-equilibrium non-thermal pressure $T_X$ ,	+15–25%	observational
$E_3$ : cluster slip $\gamma_{\text{cl}}$	$\Theta_{\mu\nu}[n]$ , $c_1(\bar{\phi}) = -a\bar{\phi}$ , $a \sim 1$	+0.3–+8.5%	Level B (OP-c1)
Combined	$E_1 + E_2 + E_3 + E_4$	$A_{\text{fin}} = 0.54\text{--}0.87$	Level B
Residual	OP22, OP-c1	$\times 1.1\text{--}\times 1.9$	Open

## AP.5 Gravitational slip from $\Theta_{\mu\nu}[n]$

### Why the $\phi$ -sector alone does not produce positive slip

In the scalar sector alone the PPN parameter satisfies

$$\gamma_{\text{cl}}^{(\phi)} \approx \frac{\omega_{\text{BD}} + 1}{\omega_{\text{BD}} + 2} \leq 1, \quad \omega_{\text{BD}} = \frac{K(\bar{\phi})}{\beta^2 M_{\text{Pl}}^2}. \quad (\text{AP.5})$$

At cluster densities  $\bar{\phi} \sim 0.03\text{--}0.08 \ll 1$ , so  $K \approx 1$  and  $\omega_{\text{BD}} \gg 1$  for Planck-suppressed  $\beta$ , giving  $\gamma_{\text{cl}}^{(\phi)} \approx 1$ . The scalar sector therefore contributes negligibly to lensing slip.

### Slip from the orientation sector

A positive slip ( $\gamma > 1$ ) is not naturally generated by the scalar  $\phi$ -sector alone; the more natural ECT candidate is the anisotropic orientation stress (Section 13.3):

$$\Theta_{\mu\nu}[n] = c_1 \left( n_\mu n^\lambda R_{\lambda\nu} + n_\nu n^\lambda R_{\lambda\mu} - \frac{1}{2} g_{\mu\nu} n^\alpha n^\beta R_{\alpha\beta} \right), \quad (\text{AP.6})$$

which provides the appropriate tensor structure for  $\Phi \neq \Psi$ . A minimal Einstein-aether-like mapping then suggests the Level B estimate [24]

$$\gamma_{\text{cl}} \approx \frac{1 - c_1/2}{1 + c_1/2}, \quad (\text{AP.7})$$

to be interpreted here as a phenomenological proxy rather than a first-principles derivation from the ECT action. A positive slip requires  $c_1 < 0$ . The minimal ECT-consistent ansatz is

$$c_1(\bar{\phi}) = -a\bar{\phi}, \quad a > 0, \quad (\text{AP.8})$$

which tends to switch off in the vacuum Lorentzian regime ( $\bar{\phi} \rightarrow 0$ ). In that case compatibility with the GW170817 gravitational-wave speed bound [10] and the Cassini bound [84] becomes plausible, although a complete proof requires a first-principles derivation of the tensor-sector coefficients from the ECT action (OP-c1).<sup>2</sup>

With the phenomenologically motivated but not yet derived ansatz  $c_1(\bar{\phi}) = -a\bar{\phi}$ ,  $a \in [0.5, 2]$ , and a cluster range  $\bar{\phi}_{\text{cluster}} \simeq 0.03\text{--}0.08$  (from  $\rho_{\text{cluster}}/\rho_*$ ,  $\rho_* \simeq 3 \times 10^{-21} \text{ kg m}^{-3}$ ), one finds a rough Level B estimate

$$E_3 \approx +0.3\% - +8.5\%. \quad (\text{AP.9})$$

This should be read as an order-of-magnitude parametrised estimate, not yet as a derived prediction. A first-principles determination of  $c_1(\bar{\phi})$  from the ECT action remains open (OP-c1, OP-new-4).

## AP.6 From cluster-slip proxies to cosmological closure

For cosmological weak-lensing and growth observables, the relevant quantities are not the cluster-scale slip proxies themselves but the effective linear-response functions  $\mu(k, z)$ ,  $\eta(k, z)$ , and  $\Sigma(k, z)$ , defined on linear sub-horizon scales by Eqs. (13.41)–(13.42), with  $\Sigma = \mu(1 + \eta)/2$ . The existing Einstein–aether-inspired cluster proxy should therefore be read only as an illustrative strong-field / cluster-scale guide to the sign and magnitude of slip, not as the derived cosmological linear-perturbation closure. The distinction is not merely one of scale but also of regime: the cluster proxy is a strong-field, environment-dependent illustration, whereas the  $S_8$  sector requires a linear FRW perturbation closure. The same ordered-condensate architecture that sets the gravitational sector also controls the orientation sector; however, the precise cosmological linear-response coefficients are not fixed by  $G_N$  alone and remain part of OP-c1. A genuine ECT confrontation with the lensing–growth sector therefore requires the first-principles derivation of the FRW-level  $(\mu, \eta, \Sigma)$  functions from the tensor/orientation sector of the ordered condensate.

## AP.7 Note on double-counting

The shear-to- $\kappa$  reinterpretation effect sometimes listed separately in modified-gravity cluster tests is *not* an independent correction here. The baseline already evaluates  $\kappa_{\text{ECT}} = \Sigma_{\text{eff}}/\Sigma_{\text{crit}}$  with  $\Sigma_{\text{eff}} = \nu\Sigma_b$ ; applying an additional  $\nu$ -factor on top would count the same physics twice. The apparent +109% figure that arises in some parameterisations reflects the weighted mean of  $(\nu - 1)$  across the cluster—which is already included in the baseline  $A_0$ .

## AP.8 Four-cluster numerical summary

The unified results are:

Cluster	$z$	Peak	$d_{\star}^{\text{ECT}}$	$d_{\star}^{\text{obs}}$	$A_0$	$A_{\text{fin}}$
Bullet	0.296	BCG	37 kpc	< 25 kpc	0.42	0.54
MACS J0025	0.586	BCG	10 kpc	< 30 kpc	0.68	0.86
El Gordo	0.870	BCG	1 kpc	< 35 kpc	0.43	0.56
Abell 520	0.199	<i>gas</i>	—	gas core	0.71	0.87

$A_0 = M_{\text{ECT}}/M_{\text{obs}}$  (baseline  $\nu$ -closure);  $A_{\text{fin}}$  after corrections  $E_1\text{--}E_4$ . Abell 520 peak on gas is the correct observed morphology.

<sup>2</sup>The GW speed constraint  $|c_T^2 - 1| < 5 \times 10^{-16}$  applies to the vacuum tensor sector. If  $c_1 \propto \bar{\phi} \rightarrow 0$  in the vacuum, the bound may be satisfied, but demonstrating this rigorously requires knowing the full tensor kinetic structure of the ECT action—an open problem (OP-c1).

## AQ Benchmark screening-length estimates across environments

This short appendix provides order-of-magnitude estimates of the screening length  $\lambda_\phi = m_\phi^{-1}$  implied by the Level B  $\phi$ -first closure (eq. (17.3) in the main text), for representative astrophysical environments. These should be read as benchmark consistency checks within the present closure, not as first-principles predictions.

**Setup.** In the quasi-static regime the effective  $\phi$ -mass is

$$m_\phi^2(\rho_m) \approx \frac{U_0''(\bar{\phi}) + 4\pi\rho_m/\bar{\chi}^2}{K(\bar{\phi})}, \quad \rho_m \equiv \rho c^2.$$

Here quoted densities  $\rho$  in  $\text{kg m}^{-3}$  are ordinary SI mass densities; the field equation uses the corresponding matter energy density  $\rho_m$ . For the benchmark one-loop kinetic closure  $K(\phi) \propto e^{-\phi/2}$  and a convex  $U_0$ , both the numerator and the denominator work in the same direction: higher density drives  $m_\phi$  upward and hence  $\lambda_\phi$  downward. In each regime below we note which term in the numerator (density contribution vs. bare curvature  $U_0''$ ) dominates the effective mass.

**Dense environments (laboratory, Solar System).** At terrestrial densities  $\rho \sim 10^3 \text{ kg m}^{-3}$  and Solar-System densities  $\rho \sim 1 \text{ kg m}^{-3}$  the density term  $4\pi\rho_m/\bar{\chi}^2$  overwhelmingly dominates over  $U_0''(\bar{\phi})$ . The resulting  $m_\phi$  is driven far above any astrophysically relevant inverse length, so that  $\lambda_\phi \ll 1 \text{ AU}$ . The scalar branch is effectively Yukawa-suppressed, and the residual fifth-force contribution to post-Newtonian observables is well below the Cassini bound [84].

**Galactic disk and transition region.** At ISM densities  $\rho \sim 10^{-21} \text{ kg m}^{-3}$  the density and curvature contributions to  $m_\phi^2$  become comparable, and the screening length grows to  $\lambda_\phi \sim \text{kpc}$ . This is the regime in which the system enters the transition window between the screened Newtonian branch and the nonlinear critical branch. The precise transition location is controlled by  $g^\dagger$ , not by  $\lambda_\phi$  alone.

**Galactic outskirts and voids.** At densities  $\rho \sim 10^{-26}\text{--}10^{-27} \text{ kg m}^{-3}$  the density contribution to  $m_\phi^2$  becomes subdominant relative to the bare curvature  $U_0''(\bar{\phi})$ , so that  $m_\phi^2 \approx U_0''/K$  is set entirely by the ordered-branch potential shape. In this limit  $\lambda_\phi$  can exceed Mpc scales, and the near-critical  $\phi$ -branch remains accessible. This is the regime probed by the deep-MOND/void corner of the regime diagram (Fig. 18).

**Status.** All estimates above are order-of-magnitude benchmarks derived from the present Level B closure. No unique numerical calibration of  $U_0''(\bar{\phi})$  and  $\bar{\chi}(\rho)$  is assumed; the quoted AU/kpc/Mpc scales should therefore be read as benchmark hierarchy estimates rather than as fully calibrated outputs of the theory. A quantitative mapping  $\rho \mapsto \lambda_\phi(\rho)$  requires knowledge of  $U_0(\phi)$  from first principles, which is part of open problem OP3.

## AR Operational environment test for the effective critical scale

This appendix specifies the operational statistical test of prediction F1: the non-universality of the fitted effective critical scale  $g_{\text{eff}}^\dagger$  across the SPARC galaxy sample.

**Environment proxy.** The large-scale environment density  $\rho_{\text{env}}$  can be defined operationally through several complementary proxies: (a) nearest-neighbour density from the 2MRS catalogue [256]; (b) group-catalogue membership and host-halo mass from SDSS group catalogues [257]; (c) tidal-field strength from large-scale structure reconstructions. Each proxy probes a different environmental scale; any robust environment dependence should be detectable with at least one of them.

**Statistical protocol.** The test proceeds in four steps:

- (i) fit each SPARC galaxy with the closure (17.23) to obtain  $g_{\text{eff}}^\dagger$  per galaxy;
- (ii) cross-match the SPARC sample with the chosen environment catalogue to assign  $\rho_{\text{env}}$  to each galaxy;
- (iii) compute the Spearman rank correlation  $r_S(g_{\text{eff}}^\dagger, \rho_{\text{env}})$  and the corresponding  $p$ -value, both for the full sample and after controlling for baryonic mass  $M_b$  and morphological type via partial correlation or hierarchical regression;
- (iv) test whether the residual  $g_{\text{eff}}^\dagger$  distribution is consistent with a universal constant (null hypothesis) or requires an environment-dependent model (ECT alternative).

**Confirmation criterion.** Prediction F1 is considered supported if the partial correlation between  $g_{\text{eff}}^\dagger$  and  $\rho_{\text{env}}$ , after controlling for  $M_b$  and morphology, is statistically significant at  $p < 0.01$  and cannot be attributed to known baryonic-model systematics (stellar mass-to-light ratio degeneracy, distance errors, or inclination bias). The sign and functional form of the dependence are not fixed by the present ECT closure and should be reported as empirical findings.

**Falsification criterion.** If the fitted  $g_{\text{eff}}^\dagger$  values collapse to a strictly universal constant across the full environment range—with no statistically significant residual dependence on  $\rho_{\text{env}}$ —then the ECT programme-level signature of environment-dependent critical acceleration would be falsified at the current closure level.

**Distinguishing baryonic systematics from genuine environment dependence.** The main confound is that baryonic-model errors (e.g. uncertain stellar mass-to-light ratios) can mimic environment dependence if they correlate with galaxy type, which in turn correlates with environment. To control for this: (a) repeat the analysis with both fixed and free  $\Upsilon_d$ ; (b) use a morphology-stratified subsample; (c) verify that any detected correlation survives in the gas-dominated subsample, where stellar  $M/L$  plays a subdominant role.

## AS ECT derivation status for the galactic interpolation law

This appendix is a *status appendix*: it summarises what is already structurally derived in the galactic sector and what remains open. It is not the place where the practical fitting closure is constructed; that construction is given separately in Appendix AN.

*Status: Level B. The AQUAL field-equation structure and its two asymptotics are the strongest currently derived results. The exact interpolation function and the exact environment law for  $g_\dagger$  remain open (OP3).*

In the current version of ECT, the strongest first-principles result in the galactic sector is the derivation of the *field-equation structure and its asymptotic limits*, not yet a unique global interpolation function.

**Effective galactic functional.** In the quasi-static weak-field limit the ECT condensate produces the effective functional (17.14). Varying with respect to  $\Phi$  gives:

$$\nabla \cdot \left[ \mu \left( \frac{|\nabla \Phi|}{g_\dagger} \right) \nabla \Phi \right] = 4\pi G_N \rho_b. \quad (\text{AS.1})$$

**Scale-invariance argument.** The deep-branch scale invariance of the ordered ECT phase forces the infrared nonlinear term to scale as  $\mathcal{F}(Y) \propto Y^{3/2}$  (Level B). This implies  $\mu(y) \propto y$  for  $y \ll 1$ , while recovery of the Newtonian branch gives  $\mu(y) \rightarrow 1$  for  $y \gg 1$ .

### RAR asymptotics as ECT consequences.

$$g \simeq g_N \quad (g \gg g_\dagger), \quad g \simeq \sqrt{g_N g_\dagger} \quad (g \ll g_\dagger). \quad (\text{AS.2})$$

### BTFR as corollary.

$$v_\infty^4 = G_N M_b g_\dagger. \quad (\text{AS.3})$$

**What remains open.** Two elements are not yet uniquely derived:

- *Exact global interpolation function.* The functional form  $\mu(y) = y/\sqrt{1+y^2}$  used in the SPARC analysis has the correct ECT-derived asymptotics but is not the unique choice; other functions with the same limits are also ECT-compatible. The exact member of this class must follow from the full OP3 completion of  $U(\phi)$ .
- *Exact environment law for  $g_\dagger$ .* ECT predicts  $g_{\text{eff}}^\dagger = g_0^\dagger \Xi(\rho_{\text{env}}, \bar{\phi}_{\text{env}}, \dots)$  with  $g_0^\dagger \sim cH_0/(2\pi)$ . The specific form (17.26) used in the present text is only a minimal Level-B ansatz for  $\Xi$ ; the exact function remains open at the level of bare P3 (OP3). The galaxy-to-galaxy scatter in  $g_\dagger^{\text{eff}}$  is a physical ECT prediction, not a shortcoming.

## AT Diagnostic stress test of the current Level-B galactic closure: dark-matter-deficient ultra-diffuse galaxies

This appendix is a *diagnostic appendix*: it applies the current practical galactic closure (17.23) as an *inverse-problem probe* to a class of observed objects — the dark-matter-deficient ultra-diffuse galaxies (UDGs) — and documents the resulting stress test. It does not propose a rescue mechanism and does not claim that the current closure explains these objects. Its purpose is to record, in one place and with one consistent methodology, the empirical tension between the current Level-B closure and the low-dispersion UDG class, the accompanying nuisance budget, the matched-pair observation, and the theory-level directions that a future completion of ECT’s galactic sector would need to address.

*Status: diagnostic. The scientific conclusions below are of the form “the current Level-B closure is strained on this object”, not “ECT predicts this observation”. No rescue mechanism is derived here.*

### AT.1 Purpose and scope

The preprint’s main galactic sector (§17.3) and the derivation-status appendix (App. AS) establish that the current practical closure (17.23) has two asymptotic branches — Newtonian at large  $g_N$  and deep-MOND at small  $g_N$  — and that the minimal ansatz (17.12) for the environment modulator  $\Xi$  is an open element of the Level-B construction (OP3). For SPARC-like normal galaxies this closure reproduces the observed radial-acceleration phenomenology at the level documented in App. AN and App. AO.

Three objects of the DM-deficient UDG class — NGC 1052–DF4 [123, 122], FCC 224 [124, 125], and the observationally ambiguous NGC 1052–DF2 [126, 127, 122] — have line-of-sight velocity dispersions consistent with baryon-only Newtonian mass within their probed radii. A matched-mass DM-rich control (NGC 5846-UDG1 [128]) lies on the standard RAR. This appendix quantifies the resulting inverse-problem diagnostic.

### AT.2 Inverse-problem closed form: $\Xi_{\text{req}}$ from $\sigma_{\text{obs}}$

At a fixed radius  $R$ , the practical closure (17.23) reads

$$g(R) = \frac{1}{2} \left[ g_N(R) + \sqrt{g_N^2(R) + 4g_N(R)g_{\text{eff}}^\dagger} \right], \quad g_{\text{eff}}^\dagger = g_0^\dagger \Xi, \quad (\text{AT.1})$$

with  $g_0^\dagger = cH_0/(2\pi) \simeq 1.04 \times 10^{-10} \text{ m s}^{-2}$ . Define the local dynamical/baryonic ratio

$$r(R) \equiv \frac{M_{\text{dyn}}(< R)}{M_{\text{bar}}(< R)} = \frac{g(R)}{g_N(R)}. \quad (\text{AT.2})$$

Solving (AT.1) for  $r$  gives

$$r = \frac{1}{2} \left[ 1 + \sqrt{1 + 4y} \right], \quad y \equiv \frac{g_{\text{eff}}^\dagger}{g_N(R)}, \quad (\text{AT.3})$$

whence the clean inversion

$$\boxed{y = r(r - 1), \quad \Xi_{\text{req}}(R) = \frac{r(r - 1) g_N(R)}{g_0^\dagger}.} \quad (\text{AT.4})$$

This is a closed-form inverse of (AT.1). For a pressure-supported system the right-hand side is evaluated at the Wolf half-mass radius  $R_{1/2} \simeq \frac{4}{3} R_e$ , where the isotropic Wolf estimator [258] gives

$$M_{\text{dyn},1/2} = 4\sigma_{\text{los}}^2 R_{1/2}/G, \quad M_{\text{bar},1/2} \simeq \frac{1}{2} M_\star, \quad (\text{AT.5})$$

so that  $r_{\text{obs}} = \sigma_{\text{los,obs}}^2/\sigma_N^2$  with  $\sigma_N^2 \equiv (3/32)G_N M_\star/R_e$  the Newtonian Wolf proxy for isotropic Plummer. Formula (AT.4) is *not* a prediction of  $\Xi$ ; it is the value of  $\Xi$  that the current closure would need at this object to reproduce the observed kinematics, given proxy assumptions (AT.5).

The remaining closure-level phenomenology is limited to: (i) the Wolf coefficient 4, valid for isotropic Plummer with  $\sim 30\%$  uncertainty in the proxy relation; (ii) the half-mass fraction  $f_e = 0.5$  for Plummer, varying by  $\sim 20\%$  across plausible Sérsic indices. Reducing these requires a full Jeans forward model (§AT.3).

### AT.3 Jeans upgrade path (phenomenology reduction, not elimination)

A stricter treatment replaces (AT.5) by the isotropic spherical Jeans equation

$$\sigma_r^2(r) = \frac{1}{v(r)J_\beta(r)} \int_r^\infty v(s)g(s)J_\beta(s)ds, \quad J_\beta(r) = \exp\left(\int_r^\infty \frac{2\beta(u)}{u} du\right), \quad (\text{AT.6})$$

followed by line-of-sight projection and aperture averaging,

$$\sigma_{\text{los}}^2(R) = \frac{2}{I(R)} \int_R^\infty \left(1 - \beta \frac{R^2}{r^2}\right) \frac{v(r)\sigma_r^2(r)rdr}{\sqrt{r^2 - R^2}}, \quad \langle \sigma_{\text{los}}^2 \rangle_{\text{ap}} = \frac{\int_0^{R_{\text{ap}}} WI \sigma_{\text{los}}^2 R dR}{\int_0^{R_{\text{ap}}} WI R dR}, \quad (\text{AT.7})$$

with  $v(r)$  the deprojected tracer density from the observed photometry,  $\beta(r)$  the anisotropy, and  $g(r)$  from (AT.1) at trial  $\Xi$ . For DF4 under isotropic Plummer,  $M/L = 2$ , and  $D = 20$  Mpc, a direct Jeans integration returns  $\sigma_N^{\text{Jeans}} \simeq 8.0 \text{ km s}^{-1}$  against the Wolf-proxy value  $\sigma_N^{\text{proxy}} \simeq 6.2 \text{ km s}^{-1}$  (ratio 1.30). The qualitative conclusion — that DF4 requires  $\Xi_{\text{req}} \ll 1$  under the current closure — is unchanged. The Jeans upgrade reduces but does not eliminate the residual phenomenology, which still contains the observational inputs  $M/L$ ,  $\beta(r)$ , tracer family, aperture, and interloper fraction.

### AT.4 Numerical stress-test diagnostic

Applying (AT.4) at  $R_{1/2} = \frac{4}{3} R_e$  to the six reference objects gives Table 139. The quoted  $\Xi_{\text{req}}$  values are central diagnostic proxy-level estimates; the full 95% CL bands are summarised separately in §AT.5.

**Table 139:** Proxy-level diagnostic of the current Level-B galactic closure (AT.1) evaluated at  $R_{1/2} = \frac{4}{3}R_e$  using the isotropic Plummer Wolf estimator. Central values only; 95% CL bands in §AT.5. AGC 114905 is a gas-rich rotator and requires a disc kinematic solver rather than a spherical Jeans proxy; it is listed for completeness of the UDG-class coverage. DF2 remains observationally ambiguous.

Object	$M_*/10^8 M_\odot$	$R_e/\text{kpc}$	$\sigma_{\text{obs}}/\text{km s}^{-1}$	$r = M_{\text{dyn}}/M_{\text{bar}}$	$\Xi_{\text{req}}$
NGC 1052–DF4	1.5	1.6	$6.3^{+2.5}_{-1.6}$	$\sim 1.1$	$\sim 10^{-3}$
FCC 224	1.74	1.89	$7.8^{+6.7}_{-4.4}$	$\sim 1.6$	$\sim 2 \times 10^{-2}$
NGC 1052–DF2	1.3	2.2	[8.6, 14.9]	3–9	0.1–1.4 (ambiguous)
NGC 5846-UDG1	1.1	2.1	$17 \pm 2$	$\sim 14$	$\sim 1.6$
Dragonfly 44	3.0	4.7	$33 \pm 3$	$\sim 42$	$\sim 8.9$
AGC 114905 (rotator) Disc solver required; not included in this spherical diagnostic					

The diagnostic readout plotted in Fig. 29 (main text, §17.5) visualises the stress-test character of the sample: DF4 and FCC 224 sit two to three decades below the RAR-normal band, the matched-mass DM-rich control NGC 5846-UDG1 lies inside it, and Dragonfly 44 sits at the upper tail; DF2 spans an observationally ambiguous bracket. The companion regime-plane positioning plot is Fig. 28.

The structural observation is that within the six-object diagnostic sample, the current closure at the baseline  $g_{\text{eff}}^\dagger = g_0^\dagger$  returns  $\Xi_{\text{req}} \sim O(1)$  for normal RAR objects (NGC 5846-UDG1) and the upper tail (Dragonfly 44), but  $\Xi_{\text{req}} \ll 1$  for NGC 1052–DF4 and FCC 224 at their central observed dispersions. NGC 1052–DF2 remains observationally ambiguous because its dispersion bracket spans an order of magnitude across the  $\sigma \approx 8\text{--}15 \text{ km s}^{-1}$  range discussed in the literature.

## AT.5 Nuisance and uncertainty budget

For DF4, propagating the main nuisance factors through (AT.4) gives the diagnostic budget in Table 140. The multiplicative factors act on  $\Xi_{\text{req}}$  for a fixed observational central value of  $\sigma_{\text{obs}}$ .

**Table 140:** Main nuisance factors affecting the proxy-level  $\Xi_{\text{req}}$  diagnostic for NGC 1052–DF4. All factors are multiplicative on  $\Xi_{\text{req}}$ . Combined 95% CL:  $\log_{10} \Xi_{\text{req}} \in [-4, -0.5]$ .

Source	Multiplicative factor on $\Xi_{\text{req}}$
Distance $D \in [13, 25] \text{ Mpc}$ (covariant with $M_* \propto D^2$ , $R_e \propto D$ )	$\sim 10\times$
Stellar mass-to-light ratio $M/L \in [1, 4]$ (SPS-driven)	$\sim 10\times$
Small- $N$ Gaussian posterior at 95% CL on $\sigma$ (7 GC tracers)	$\sim 100\times$
Anisotropy $\beta \in [-0.5, 0.5]$	$\sim 1.5\times$
Wolf-proxy $\rightarrow$ Jeans upgrade	$\sim 1.3\times$

The entire 95% CL band for  $\log_{10} \Xi_{\text{req}}$  at DF4 lies below the normal RAR band  $\Xi \sim O(1)$ . The proxy-level *classification* of DF4 as a stress test of the current closure is therefore robust to nuisance variations; only the numerical value of  $\Xi_{\text{req}}$  is imprecise. The present bookkeeping is diagnostic-level: a posterior  $P(\Xi \mid \text{data})$  with joint sampling of the full nuisance vector  $\theta = \{M/L, D, \beta, n, R_{\text{ap}}, f_{\text{int}}, M_{\text{host}}, d_{3D}, Q_{\text{eq}}\}$  is the appropriate next step.

## AT.6 External-field benchmark

A benchmark parallel to the ECT diagnostic is the external-field effect characteristic of MOND-class theories. Estimating  $g_{\text{ext}} \simeq G_N M_{\text{host}}/d_{\text{proj}}^2$  for the four pressure-supported reference objects:



**Table 141:** External field amplitudes for the four spherical UDG reference objects, for the MOND external-field benchmark.  $a_0 = 1.2 \times 10^{-10} \text{ m s}^{-2}$  is the standard MOND acceleration scale. All four values lie far below  $a_0$ ; EFE screening is minor.

Object	$M_{\text{host}}/M_{\odot}$	$d_{\text{proj}}/\text{kpc}$	$g_{\text{ext}}/a_0$
NGC 1052-DF4	$\sim 10^{11}$	$\sim 80$	$\sim 0.02$
FCC 224	$\sim 3 \times 10^{10}$	$\sim 70$	$\sim 0.007$
NGC 5846-UDG1	$\sim 5 \times 10^{11}$	$\sim 100$	$\sim 0.06$
Dragonfly 44 (Coma)	$\sim 10^{13}$	$\sim 500$	$\sim 0.05$

EFE screening is therefore minor for all four objects and, within this benchmark, does not numerically distinguish DF4 from the matched DM-rich control NGC 5846-UDG1. This observation is benchmark-level: the current ECT closure (AT.1) does not carry an explicit  $g_{\text{ext}}$  dependence, and the MOND external-field comparison is strictly outside the ECT formulation.

## AT.7 Side diagnostics and sanity checks

**Ultra-faint dwarfs (side diagnostic, not validation).** Applied to Milky-Way dwarf spheroidals at  $M_{\star} \sim 10^3\text{--}10^7 M_{\odot}$  (Draco, Sculptor, Fornax, Segue I, Willman I), the same Wolf-based proxy returns  $\Xi_{\text{req}} \in [\sim 2, \sim 10^3]$ . This is not a validation of the proxy chain: the spread is driven by well-documented effects orthogonal to the UDG stress test (binary-star inflation of  $\sigma_{\text{obs}}$ , tidal non-equilibrium, radial anisotropy, and small- $N$  statistics) and merely confirms that the proxy does not collapse outside the UDG target mass range.

**Globular clusters (Newton sanity check).** For 47 Tuc,  $\omega$  Cen, M13, M15, the ratio  $g_N/g_0^{\dagger} \gtrsim 15$  places these systems safely in the  $g_N \gg g_{\text{eff}}^{\dagger}$  branch of (AT.1), where the closure returns  $g \rightarrow g_N$  independently of  $\Xi$ . This is the trivial Newton recovery check at high density.

**FCC 224 non-sphericity.** FCC 224 is prolate with observed apparent ellipticity  $\varepsilon \simeq 0.36$  [124]. Spherical Jeans should therefore be treated only as an order-unity proxy for this object; no reliable numerical non-spherical correction factor can be claimed within the present diagnostic. The central  $\Xi_{\text{req}}$  value for FCC 224 in Table 139 should accordingly be read as order-of-magnitude. This does not change its qualitative classification as a stress-test object.

**Selection rate.** Approximately 3 confirmed DM-deficient UDGs among  $\sim 500$  screened dwarfs with kinematic follow-up translates to  $\sim 0.6\%$  incidence [130], consistent in order of magnitude with the  $\sim 1\%$  rate of collision-stripped systems predicted by  $\Lambda$ CDM bullet-dwarf simulations [129, 131]. Any future ECT-compatible rescue mechanism will need to be consistent with this observed rate.

## AT.8 Selection and sample caveats

The presently known DM-deficient UDG sample is small and *not* selection-neutral: several candidates were identified through unusual globular-cluster-population markers (top-heavy GCLF, excess luminous GCs for the host stellar mass). The class properties inferred from this sample should therefore be treated as provisional rather than as population-level conclusions. Whether the class persists under selection-neutral future surveys is itself part of the discriminant content of ND-13 in Table 75.

## AU Numerical algorithm for late-time ECT cosmology: Hubble tension, age, and JWST background

### Two algorithmic levels: parent system and benchmark solver

The theoretical structure discussed above naturally defines two distinct algorithmic levels.

**(i) Parent derived system.** The full condensate background dynamics is governed by Eqs. (AD.8)–(AD.12), with

$$\omega(\phi) = \omega_0 e^{2\beta\phi}, \quad U(\phi) = W(u_\infty e^{\beta\phi}).$$

This is the system that should ultimately be solved for a fully self-consistent ECT treatment of the high-redshift branch.

**(ii) Current benchmark solver.** The present code implementation instead solves the local late-time screened-branch truncation (AD.19). This benchmark solver is therefore a valid numerical layer of the current article, but it should not yet be confused with the final solver for the full derived condensate dynamics.

**Algorithm flow.** At the algorithmic level, the logic is now:

derived condensate background system  $\longrightarrow$  benchmark truncation and derived-parent implementation  
 $\longrightarrow$  linear-growth and maturity-budget layers.

The benchmark truncation remains the control mode of the numerical programme, but the present implementation also includes a derived-parent background solver together with a solved linear-growth layer and the semi-analytic maturity accounting used in the current JWST analysis. The parent system itself is recorded in Section AD.1.

### Algorithmic form of the derived condensate solver

For the full derived condensate background system, the natural numerical unknowns are

$$E(N) = \frac{H(N)}{H_*}, \quad \phi(N), \quad q(N) \equiv \frac{d\phi}{dN}.$$

The parent fixed-point structure is then defined by the coupled pair:

**(i) Algebraic background update.** Given a current iterate  $\phi^{(k)}(N)$  and  $q^{(k)}(N)$ , compute

$$E^{2(k)}(N) = \frac{\Omega_{m*} e^{-3N} + \Omega_{r*} e^{-4N} + \Omega_U(\phi^{(k)})}{e^{\beta\phi^{(k)}}(1 + \beta q^{(k)}) - \frac{\omega_0}{6} e^{2\beta\phi^{(k)}}(q^{(k)})^2}.$$

**(ii) Differential scalar update.** Using

$$\left(\frac{E'}{E}\right)^{(k)} = \frac{1}{2} \frac{d \ln(E^{2(k)})}{dN},$$

update  $\phi^{(k+1)}(N)$  from the scalar equation (AD.12), or equivalently update  $q^{(k+1)}$  and then integrate

$$\frac{d\phi^{(k+1)}}{dN} = q^{(k+1)}(N)$$

with the chosen present-epoch boundary data  $(\phi_0, q_0)$ .

**(iii) Iterate to convergence.** Repeat steps (i) and (ii) until the background fields  $E(N)$ ,  $\phi(N)$ , and  $q(N)$  converge under a chosen tolerance.

**Benchmark relation.** The current benchmark solver follows exactly the same fixed-point logic, but with the local benchmark replacements

$$\omega(\phi) \rightarrow K_0, \quad U(\phi) \rightarrow V_0 + \frac{1}{2} m_\phi^2 \phi^2.$$

Thus the benchmark code is not conceptually separate from the full derived solver; it is its simplest local truncation.

### AU.1 Self-consistent fixed-point solver design

The numerical background solver architecture described in this subsection originates from the benchmark late-time truncation of the ECT macroscopic scalar–tensor background closure. Its full parent algorithm is given immediately above. The benchmark solver remains the control numerical layer of the article, but the current code also implements a derived-parent background mode, a solved linear-growth layer, and the semi-analytic maturity accounting used for the JWST discussion. It evolves the macroscopic amplitude variable  $\phi(N) = \frac{1}{\beta} \ln(u/u_\infty)$  and computes the corresponding background expansion history  $E(N) = H/H_*$ .

Rather than importing a  $\Lambda$ CDM background as physical input, the solver iterates the ECT system on itself:

1. choose the present-epoch data  $(\phi_0, q_0)$  and a calibration scale  $H_*$ ;
2. start from a zeroth approximation  $q^{(0)}(N)$  (for example the slow-drift seed or  $q^{(0)} = 0$ );
3. compute  $E^{(k)}(N)$  algebraically from Eq. (AD.21);
4. obtain  $(E'/E)^{(k)}$  from the current iterate

$$\left(\frac{E'}{E}\right)^{(k)} = \frac{1}{2} \frac{d \ln[(E^{(k)})^2]}{dN};$$

5. update  $q^{(k+1)}(N)$  from the scalar slow-drift balance Eq. (AD.30);
6. integrate

$$\frac{d\phi^{(k+1)}}{dN} = q^{(k+1)}(N)$$

with the chosen present-epoch boundary condition;

7. recompute  $E^{(k+1)}(N)$  and iterate until convergence.

In this way the ECT background is determined by the closure equations themselves. A comparison to  $\Lambda$ CDM may still be shown at the level of plots or diagnostics, but not used as the defining physical background of the solver.

The earlier  $\Lambda$ CDM-seeded quasi-static implementation should therefore be regarded as an interim benchmark algorithm, not as the intended final numerical realisation of the late-time ECT background.

Accordingly, future code revisions should be judged against the structural roadmap above: improvement of the fixed-point background solver, replacement of interim high- $z$  completion, and possible implementation of admissible generalisations of the benchmark functions  $K(\phi)$  and  $V(\phi)$  are the three main directions of progress. A fourth direction is numerical robustness testing: benchmark outputs should be compared systematically against admissible closure deformations rather than reported only for the benchmark member.

## AU.2 Implementation roadmap from benchmark closure to solver

For practical code development it is useful to separate clearly which parts of the late-time cosmology apparatus are already fixed by the present article and which parts remain provisional benchmark choices.

**Layer 1: structural input already fixed by the theory.** The following ingredients are already fixed at the structural or bridge level:

- the ordered-branch origin of the macroscopic amplitude variable  $\phi = \frac{1}{\beta} \ln(u/u_\infty)$ , i.e.  $u/u_\infty = e^{\beta\phi}$ ;
- the amplitude-dominated macroscopic reduction;
- the existence of a coupled scalar–tensor background system for  $(H, \phi)$  under isotropic FRW reduction;
- the standard FRW integral outputs  $D_L(z)$ ,  $t_{\text{lookback}}(z)$ ,  $t_U(z)$ , and  $t_{\text{gal}}(z_{\text{obs}}; z_{\text{form}})$  once the background is known.

**Layer 2: benchmark late-time closure.** The present code-facing closure

$$f(\phi) = f_0 e^{\beta\phi}, \quad K(\phi) = K_0, \quad V(\phi) = V_0 + \frac{1}{2} m_\phi^2 \phi^2$$

should be understood as the first benchmark specialisation of the structurally anchored closure functions. Only the exponential response factor is directly tied to the amplitude ratio  $u/u_\infty = e^{\beta\phi}$ . The constant kinetic coefficient and quadratic potential remain the simplest local Level B benchmark truncations. A broader admissible family of late-time closures is described in Section AD.6.

**Layer 3: interim numerical completion.** The present numerical age extension above  $z_{\text{match}} = 10$  is still an interim matter+radiation completion. Therefore outputs that depend strongly on the high-redshift continuation must be marked as interim benchmark outputs until the full self-consistent ECT high- $z$  background branch is implemented. Beyond the present benchmark implementation, the central next step is to replace the benchmark truncation by a solver built directly on the derived condensate background system (Section AD.1), especially for the high-redshift branch relevant to cosmic-age and JWST applications. The parent fixed-point structure of such a solver is already written explicitly in Section AU.

**Layer 4: target solver outputs.** A fully synchronised article–code pipeline should produce, at minimum:

1. the converged background solution  $H(z)$  and  $\phi(z)$ ;
2. the direct and low- $z$  inferred Hubble shifts;
3.  $D_L(z)$  and  $t_{\text{lookback}}(z)$  on the observational grid;
4. the epoch-dependent cosmic age  $t_U(z)$ ;
5. galaxy-lifetime grids  $t_{\text{gal}}(z_{\text{obs}}; z_{\text{form}})$  for JWST-relevant  $(z_{\text{obs}}, z_{\text{form}})$  pairs;
6. convergence diagnostics for the fixed-point iteration.

These outputs should be emitted in standard tabular form so that the article figures and benchmark tables can be regenerated directly from solver products rather than from manually transferred values.

**Purpose of this roadmap.** This separation prevents the code from being interpreted as if every implemented function were already an equally fundamental output of ECT. It also makes clear which future code upgrades correspond to genuine theoretical progress (improved closure functions and high- $z$  branch completion) and which correspond only to numerical refinement. The explicit article–solver contract is stated in Section AU.3.

### AU.3 Article–solver interface contract

To keep the late-time code and the theoretical text synchronised, it is useful to state explicitly what the numerical solver is expected to take as input, what it must return as output, and what constitutes a successful implementation of the benchmark closure.

**Required solver inputs.** At minimum, the benchmark late-time solver should accept:

1. the closure parameters

$$\beta, \quad K_0, \quad m_\phi, \quad V_0,$$

or equivalently the dimensionless combinations used in Eq. (AD.20);

2. the calibration scale  $H_*$ ;

3. the present-epoch background data

$$\phi_0, \quad q_0 = \left. \frac{d\phi}{dN} \right|_{N=0};$$

4. the matter and radiation background normalisations

$$\Omega_{m*}, \quad \Omega_{r*}, \quad \Omega_{V*};$$

5. the redshift grid on which the solution is to be reported;

6. if used, the interim high- $z$  completion settings (such as  $z_{\text{match}}$ ), which must be recorded explicitly as numerical rather than structural inputs.

**Required solver outputs.** A benchmark implementation consistent with the present article should return, at minimum:

1. the converged background fields

$$H(z), \quad \phi(z), \quad G_{\text{eff}}(z);$$

2. the direct Hubble shift and low- $z$  inferred Hubble shift;

3. the standard distance/time observables

$$D_L(z), \quad t_{\text{lookback}}(z), \quad t_U(z);$$

4. JWST-oriented galaxy lifetime grids

$$t_{\text{gal}}(z_{\text{obs}}; z_{\text{form}});$$

5. the growth proxy

$$\mathcal{G}(z) = G_{\text{eff}}(z)/H^2(z);$$

6. convergence diagnostics of the fixed-point iteration.

**Required validation checks.** A solver run should not be considered article-consistent unless it also reports:

1. convergence of the fixed-point iteration from more than one initial seed;
2. sensitivity of the solution to numerical resolution and redshift grid choice;
3. explicit dependence of age-related quantities on the interim high- $z$  completion, if such a completion is still used;
4. sensitivity of the benchmark outputs to admissible deformations of  $K(\phi)$  and  $V(\phi)$  once those are implemented;
5. where implemented, direct comparison of benchmark and deformed admissible-closure runs, with explicit reporting of the induced shifts in  $H(z)$ ,  $\phi(z)$ ,  $t_U(z)$ , and the benchmark summary observables.

**Interpretive rule.** This contract is meant to prevent confusion between three different levels: the structural background system of the theory, the benchmark closure chosen for the present article, and the current numerical implementation. A code result should only be interpreted as an ECT prediction to the extent that all three levels are kept conceptually distinct and the required numerical artefacts are exported in reproducible form.

#### AU.4 Expected numerical artefacts for article synchronisation

To keep the late-time figures, tables, and numerical claims reproducible, the solver should not only converge internally but also emit a standard set of machine-readable artefacts.

**Core background table.** For each benchmark run, the code should produce a background table on a common redshift grid containing at least

$$z, \quad H(z), \quad E(z), \quad \phi(z), \quad G_{\text{eff}}(z).$$

This table is the primary source for all later derived observables.

**Distance–time table.** From the converged background, the code should produce a second table containing

$$z, \quad D_L(z), \quad t_{\text{lookback}}(z), \quad t_U(z).$$

This table is the direct numerical support for the late-time cosmology plots and age statements in the main text.

**JWST age grid.** For selected observation and formation redshifts, the code should output a grid of galaxy-lifetime estimates

$$(z_{\text{obs}}, z_{\text{form}}, t_{\text{gal}}),$$

with at least the benchmark combinations discussed in the paper. This artefact is required if the JWST discussion is to remain directly traceable to code outputs rather than to hand-entered numbers.

**Benchmark summary table.** Each benchmark run should emit a compact summary table containing, at minimum,

$$\Delta H_0/H_0, \quad H_0^{\text{late}}, \quad t_0, \quad \Delta t_0/t_0, \quad \Delta D_L/D_L, \quad \mathcal{G}(z), \quad g_{\text{bg}}^\dagger(z)/g_{\text{bg}}^\dagger(0),$$

together with explicit metadata recording which closure functions and which high- $z$  completion settings were used.

**Benchmark–deformed comparison table.** Whenever admissible closure deformations are enabled, the code should also emit a comparison artefact showing the difference between the deformed run and the benchmark member on the same redshift grid. At minimum this artefact should report

$$\Delta\phi(z), \quad \Delta E(z), \quad \Delta t_U(z),$$

and the corresponding changes in the benchmark summary outputs. In the current code implementation this role is played by a benchmark–deformed comparison table exported on the common redshift grid.

**Derived-parent scan and JWST maturity tables.** For the derived-parent programme the code should also emit machine-readable tables for the first  $(\omega_0, \phi_0)$  scan, the selected working points, the JWST object age budgets, and the combined maturity budgets  $(\mathcal{R}_{\text{gal}}, \mathcal{R}_{\text{BH}}, \mathcal{R}_{\text{req}})$ . These artefacts support direct comparison between the few-percent H1 benchmark parameter corridor and the astrophysical maturity requirements of the observed high-redshift systems. Together these artefacts define the machine-readable counterpart of the pipeline described in Appendix AD.9.

**Derived-parent comparison and anchor-case figures.** The current article also requires visual artefacts for: (i) benchmark-versus-derived-parent background comparison, (ii) the derived-parent parameter scan with labelled working points, (iii) the JWST anchor-case budget comparison, and (iv) the schematic full evolution of the condensate sectors and observable Universe (Fig. 16). These figures form the article-facing visual presentation layer of the current numerical and conceptual results. The full condensate-and-Universe evolution schematic is a conceptual article-facing figure rather than a direct numerical solver output; its purpose is to summarise the multi-sector ECT interpretation framing the present late-time derived-parent calculations.

**Convergence and sensitivity report.** The solver should also emit a small diagnostic report containing:

- iteration count and convergence tolerance;
- dependence on initial seed;
- dependence on redshift-grid resolution;
- dependence on interim  $z_{\text{match}}$  if high- $z$  completion is used.

**Purpose.** These artefacts define the practical synchronisation layer between the article and the code repository. Without them, even a numerically converged solver is not yet fully article-reproducible.

## AU.5 Benchmark parameter window

Within the benchmark closure (AD.19), the natural slow-drift parameter window that gives a few-percent Hubble shift is

$$\beta \sim 0.7\text{--}1.0, \quad \phi_0 \sim -(0.08\text{--}0.12), \quad \mu \sim 1.0\text{--}1.5, \quad \kappa \sim 10\text{--}20. \quad (\text{AU.1})$$

The window above refers specifically to the benchmark truncation. One of the next tasks is to determine how stable it remains under the admissible closure deformations described in Section AD.6.

For Benchmark B ( $\beta = 0.8, \mu = 1.5, \kappa = 15, \phi_0 = -0.12$ ), the truncated expression (AD.29) is the  $q_0 \rightarrow 0$  leading-order limit of the full present-epoch closed-form relation for the benchmark Hubble shift. Evaluated at the benchmark parameters in that limit it gives  $\Delta H_0/H_0 \approx 5\%$ , but this is a structural sanity check rather than the benchmark numerical answer, since at these parameters the self-consistent scalar drift  $q_0 \approx 0.08$  is not negligible. The proper present-epoch closed-form benchmark relation, evaluated with the self-consistent  $q_0$ , gives  $\Delta H_0/H_0 \approx 3\%$ , and the converged fixed-point solver reproduces the same value ( $\approx 2.8\%$ ). The residual gap between (AD.29) and the full closed-form benchmark expression

at the benchmark parameters is therefore not a sign of a sick closure; it is simply the difference between the  $q_0 \rightarrow 0$  limit and the full self-consistent present-epoch evaluation, and it accounts structurally for what earlier interim numerical runs were reporting as “ $\approx 2.9\%$ ” under various convergence settings.

The analytic parameter-window scan within this closure shows that the benchmark points lie inside a finite parameter region producing a few-percent late-time Hubble shift, confirming that the benchmark is representative rather than finely tuned.

What this benchmark window establishes is therefore modest but useful: a few-percent late-time Hubble shift is readily obtainable within the first amplitude-dominated closure without extreme tuning. What it does not yet establish is uniqueness. Different admissible Level B benchmark choices for  $K(\phi)$  and  $V(\phi)$  may lead to quantitatively different background histories even while preserving the same structural ordered-branch logic.

## AU.6 Derived outputs

For age estimates, the present numerical implementation extends the integration to sufficiently high redshift by attaching an interim matter+radiation-dominated completion above a matching scale  $z_{\text{match}} = 10$ . This should be read purely as a temporary numerical completion of the late-time closure, not as part of the defining ECT background dynamics. A fully self-consistent ECT treatment of the high- $z$  branch remains to be implemented in the next stage of the programme.

Accordingly, outputs that depend sensitively on the  $z > z_{\text{match}}$  extension—especially  $t_0$ ,  $t_U(z)$  for high redshift, and  $t_{\text{gal}}(z_{\text{obs}}; z_{\text{form}})$  with large  $z_{\text{form}}$ —must still be interpreted as interim Level B numerical estimates rather than as final ECT predictions.

From the solved macroscopic background branch the code computes:

1. the direct late-time Hubble shift  $\Delta H_0/H_0 = E(0) - 1$ ;
2. a ladder-style low- $z$  inferred  $H_0$  from the  $D_L$  slope;
3. the age correction  $\Delta t_0/t_0$ ;
4. lookback-time and luminosity-distance shifts at  $z = 1, 2, 5, 8, 10, 12$ ;
5. the epoch-dependent cosmic age  $t_U(z)$  on the same redshift grid;
6. JWST-relevant galaxy-lifetime estimates  $t_{\text{gal}}(z_{\text{obs}}; z_{\text{form}})$  for selected  $(z_{\text{obs}}, z_{\text{form}})$  pairs;
7. a simple growth proxy  $\mathcal{G}(z) \equiv G_{\text{eff}}(z)/H^2(z)$  as a first indicator of early structure formation enhancement;
8. convergence diagnostics of the fixed-point background iteration.

All outputs are collected in a summary CSV file and a four-panel figure. The code is available at the repository listed in the Data and Code Availability section.

In particular, the JWST discussion should no longer rely only on present-age or lookback summaries. The solver should explicitly expose the two distinct quantities

$$t_U(z) \quad \text{and} \quad t_{\text{gal}}(z_{\text{obs}}; z_{\text{form}}),$$

since they answer different physical questions: the age of the Universe at the epoch of observation, and the available lifetime of a galaxy between formation and observation.

## AU.7 Orientation-stress sector and background observables

*Status: structural observation. No separately extractable background contribution from the orientation stress  $\Theta_{\mu\nu}[n]$  to the Hubble expansion rate or the age of the Universe is available at the present closure level.*



**Orientation-sector reduction on the FRW background.** In the isotropic background reduction of the macroscopic closure (§13.5), the orientation sector is absorbed into the homogeneous causal background:  $n_A \rightarrow \bar{n}_A$ , where  $\bar{n}_A$  is a spatially uniform timelike unit vector. In this regime the anisotropic stress  $\Theta_{\mu\nu}[n]$  (13.23) does not contribute an independent term to the Friedmann equation: the Ricci contraction  $n^\alpha n^\beta R_{\alpha\beta}$  evaluates to a linear combination of  $H^2$  and  $\dot{H}$ , both of which are already present in the scalar  $\phi$ -sector equations (13.37)–(13.38). The orientation-stress contribution is therefore not separable from the existing scalar-amplitude background dynamics.

**Benchmark deformation test.** Within the benchmark closure, admissible deformations of the kinetic and potential functions shift the late-time Hubble result by less than 0.1 percentage points (from  $\Delta H_0/H_0 \approx 2.90\%$  to  $\approx 2.85\%$ ). This test probes residual scalar-closure sensitivity only and must not be interpreted as a numerical estimate of the orientation-stress contribution. The conclusion that the background NLEE contribution is not separately extractable follows from the FRW reduction itself (preceding paragraph), not from the  $2.90\% \rightarrow 2.85\%$  benchmark-deformation comparison. Accordingly, the benchmark-deformation test is cited only as a scalar-closure robustness check; it is not used anywhere in this paper as a quantitative estimate of the orientation-stress contribution.

**Conclusion.** The Hubble-shift estimate, the present-age value, and the lookback-time budgets recorded in the main text already contain the dominant ordered-branch background effect. Any additional contribution from the orientation-stress sector is absorbed into the background reduction and is not independently extractable at the present formal closure level. This conclusion applies equally to the Universe-age analysis of §16.4.

## AV Why the Explicit Estimate of $S_0$ Is Deferred

*Reference from main text: Section 5.6.*

Section 5.6 establishes a sharp lower bound on the loop action at fixed length via the Cauchy–Schwarz inequality (5.22), and defines the EFT action scale  $S_0^{\text{EFT}} = K_\theta m_\phi/2$  by evaluating that bound at the elementary-loop size  $L_{\text{core}} \sim 2\pi/m_\phi$ .

To go beyond this EFT estimate and obtain a first-principles value of  $S_0^{\text{EFT}}$ , one needs to construct an effective 1D functional for a loop in the coherent sector. Starting from the 4D phase action  $S[\theta] \sim \int_{\mathcal{V}} d^4X f(\rho)(\partial_A \theta)^2$ , the transition from the bulk integral over  $\mathcal{V}$  to a 1D action along  $\mathcal{C}$  requires: (i) choice of transverse profile shape; (ii) integration of  $f(\rho)$  over the transverse cross-section; (iii) introduction of an effective line tension  $\mathcal{T}$  such that  $S_{\text{eff}}^{\text{1D}}[\mathcal{C}] = \mathcal{T} \cdot |\mathcal{C}|$ ; (iv) evaluation at the characteristic core-sized loop under the  $n = 1$  winding constraint. Each of these steps requires the nonlinear broken-phase potential (beyond the quadratic EFT) and the choice of a vortex profile, which are not determined at the ECT basics level. The explicit calculation therefore belongs to Section 20.

## AW Smooth-branch exactness of fermionic exclusion: canonical normalisation, curvature control, and numerical bounds

*Status: Level B for the canonical-normalisation no-go argument within a local first-order fermionic EFT with smooth background fields. Level B/open for the residual curvature-controlled packet-level mismatch estimate. Open (OP-Q21) for the full theorem, contingent on the completion of the fermionic reconstruction programme (OP-Q11). Connections: §24.4 (exchange sectors and spinor compatibility), §24.5 (representation-theoretic route to Dirac structure), §7.6 (ECT fermion–condensate coupling  $\mu_5$ ).*

This appendix collects the technical material underlying the provisional no-go statement of Section 24.4: smooth local inhomogeneity of the ordered condensate does not provide a mechanism for violating fermionic exclusion on the coherent ordered branch. It proceeds in four steps. First, we write a representative local first-order fermionic EFT compatible with the presently identified ECT structures

(§AW.1). Second, we show that a condensate-dependent kinetic coefficient is absorbed into a local canonical normalisation, leaving the equal-time anticommutator in standard form (§AW.2). Third, we argue that even coarse-grained packet-level mismatch effects, which are not themselves violations of the exclusion algebra, scale with the tidal curvature of the emergent geometry rather than with acceleration (§AW.3). Fourth, we tabulate the resulting packet-level mismatch estimates across laboratory, stellar, and astrophysical regimes and place them alongside current experimental bounds on genuine Pauli-principle violation purely as an orientation scale (§AW.4).

### AW.1 General local fermionic EFT on the coherent ordered branch

On the smooth coherent ordered branch, a representative local first-order fermionic EFT compatible with the presently identified ECT structures—the structurally derived Dirac dynamics (§24.5), medium-ontological identification of fermionic excitations with spinor modes of the ordered condensate (§9.9), and the ECT-specific preferred-direction coupling (§7.6)—can be written schematically as

$$\begin{aligned}
S_\psi = \int d^4x e(x) & \left[ \frac{i}{2} Z(\phi, n) \bar{\psi}(x) \gamma^\mu e_a^\mu(x) \overleftrightarrow{D}_\mu \psi(x) \right. \\
& - M(\phi, n) \bar{\psi}(x) \psi(x) \\
& + \mu_5(\phi, n) \bar{\psi}(x) \gamma^A n_A(x) \psi(x) \\
& \left. + \sum_k C_k(\phi, n) \mathcal{O}_k^{(4f)}(x) + \dots \right],
\end{aligned} \tag{AW.1}$$

where  $e(x) = \det e_a^\mu(x)$  is the tetrad determinant of the emergent Lorentzian metric,  $Z(\phi, n)$  is a smooth and strictly positive scalar function of the condensate amplitude and orientation,  $M(\phi, n)$  is an effective mass,  $\mu_5 \bar{\psi} \gamma^A n_A \psi$  is the ECT preferred-direction coupling discussed in Section 7.6, and  $\mathcal{O}_k^{(4f)}$  are local four-fermion composite operators admitted by the symmetries of the ordered branch.

The working assumption of this appendix is that the background fields are smooth (all spatial and temporal derivatives are finite and of order the characteristic condensate scales), the kinetic coefficient is nondegenerate ( $Z(\phi, n) > Z_{\min} > 0$  and  $e(x) > 0$  everywhere in the region of interest), there are no higher-time-derivative fermionic kinetic pathologies, and no nonlocal sector-mixing kernels coupling the ordered-branch fermionic sector to its exterior. These are precisely the conditions defining “smooth coherent ordered branch” for the purposes of the no-go statement.

### AW.2 Canonical normalisation and the equal-time anticommutator

Extracting the temporal part of the kinetic term in (AW.1) yields, up to the choice of local frame and temporal foliation,

$$\mathcal{L}_{\text{kin}}^{(t)}(x) \sim i \mathcal{K}(x) \psi^\dagger(x) \partial_t \psi(x) + \dots, \quad \mathcal{K}(x) > 0, \tag{AW.2}$$

where  $\mathcal{K}(x)$  is the resulting smooth and strictly positive temporal kinetic coefficient, and the ellipsis denotes terms involving spatial derivatives and mass/interaction pieces that do not contribute to the equal-time canonical momentum. In the schematic ECT EFT of Eq. (AW.1) one has  $\mathcal{K}(x) \sim e(x) Z(\phi(x), n(x))$  up to the choice of local frame and temporal foliation, so that all statements below apply to this EFT as a particular case. The canonical momentum conjugate to  $\psi$  is then

$$\Pi_\alpha(x) = \frac{\partial \mathcal{L}}{\partial (\partial_t \psi_\alpha(x))} = i \mathcal{K}(x) \psi_\alpha^\dagger(x), \tag{AW.3}$$

and the equal-time canonical anticommutation relation

$$\{\psi_\alpha(t, \mathbf{x}), \Pi_\beta(t, \mathbf{y})\} = i \delta_{\alpha\beta} \delta^{(3)}(\mathbf{x} - \mathbf{y}), \tag{AW.4}$$

which in the present normalisation takes the background-weighted form

$$\{\psi_\alpha(t, \mathbf{x}), \psi_\beta^\dagger(t, \mathbf{y})\} = \mathcal{K}(x)^{-1} \delta_{\alpha\beta} \delta^{(3)}(\mathbf{x} - \mathbf{y}). \tag{AW.5}$$

Equation (AW.5) is the technical object that a naive gradient-based argument would interpret as a modification of the exclusion algebra in the presence of a spatially varying condensate. The correct reading, however, is that  $\psi$  is simply not the canonically normalised field. The local field redefinition

$$\chi_\alpha(x) \equiv \mathcal{K}(x)^{1/2} \psi_\alpha(x) \quad (\text{AW.6})$$

brings the kinetic term to canonical form and yields, at equal times,

$$\{\chi_\alpha(t, \mathbf{x}), \chi_\beta^\dagger(t, \mathbf{y})\} = \delta_{\alpha\beta} \delta^{(3)}(\mathbf{x} - \mathbf{y}), \quad (\text{AW.7})$$

which is the standard canonical anticommutation relation in its unmodified form. Creation operators built from  $\chi$  then satisfy  $(\hat{a}_i^\dagger)^2 = 0$  mode by mode, and two-fermion states constructed from them are exactly antisymmetric.

Three comments are in order.

**(i) Condensate-dependent mass and preferred-direction coupling do not alter the exclusion algebra.** The condensate-dependent mass term  $M(\phi, n) \bar{\psi} \psi$  and the ECT preferred-direction coupling  $\mu_5(\phi, n) \bar{\psi} \gamma^A n_A \psi$  do not contribute to the temporal kinetic term (AW.2) and hence do not modify the canonical momentum or the equal-time anticommutator. They modify the Dirac operator and the local mode functions, shifting energies, effective masses, and transport coefficients, but they do not act on the exclusion algebra itself.

**(ii) Local four-fermion operators modify dynamics, not statistics.** Local four-fermion operators  $C_k(\phi, n) \mathcal{O}_k^{(4f)}$  are also absent from the temporal kinetic term at leading order in the first-order formulation, and therefore do not modify the canonical momentum conjugate to  $\psi$ . They can shift spectra, drive pairing or condensation phenomena, and modify effective equations of state, but on the operator-algebra level the fermionic exclusion structure is fixed by the kinetic term through the canonical anticommutation relation ((AW.7)), not by the interaction sector. This is a standard feature of canonical fermionic field theory.

**(iii) Linear gradient contributions cancel for symmetric packets.** A naive gradient-based argument would proceed by expanding the background around a point  $\mathbf{x}_0$  and retaining the linear term  $\partial_i \ln \mathcal{K}(x)$ . For a symmetrically localised one-particle wave packet, however, the linear expansion contributes with vanishing first moment,  $\langle y^i \rangle \equiv \langle (x - x_0)^i \rangle = 0$ , and the leading physical correction begins only at second order in the background inhomogeneity. Furthermore, even this second-order correction is a packet-level mismatch of mode overlap integrals, not a violation of the equal-time anticommutator (AW.7).

These three observations close the canonical-normalisation argument at the level of the present local first-order EFT.

### AW.3 Curvature control, not acceleration control

Even granting that no genuine modification of the exclusion algebra is produced by smooth local inhomogeneity, one may still ask whether a residual, purely coarse-grained packet-level mismatch can be tied to astrophysical observables. The key physical point is that a naive dimensional estimate based on local acceleration  $g$  overstates the size of such an effect.

In a local inertial frame, a uniform acceleration field can be removed entirely by a coordinate transformation; the physically irreducible parameter characterising deviations from free fall is the *tidal tensor*

$$\mathcal{E}_{ij}(x) \sim \partial_i \partial_j \Phi_N(x) \sim \frac{G_N M}{R^3} \quad (\text{dimensional estimate}), \quad (\text{AW.8})$$

i.e. the gradient of the gravitational acceleration, not the acceleration itself. Any coordinate-invariant packet-level mismatch on a smooth coherent-branch background should therefore be controlled by combinations of the form

$$\epsilon_{\text{packet}} \sim \left( \frac{\mathcal{E} L^2}{c_*^2} \right)^2, \quad (\text{AW.9})$$

where  $L$  is the spatial overlap scale of the two fermionic wave packets under comparison, and  $\mathcal{E}$  is the characteristic tidal curvature scale of the background (AW.8).

The scale (AW.9) is a coarse-grained packet-level mismatch estimate, not a prediction of a physical Pauli violation. It does not represent a modification of the equal-time anticommutator (AW.7), nor of the antisymmetry of many-fermion states in the canonical normalisation. Its purpose is solely to quantify how small a residual coarse-graining artefact can be, given the canonical-normalisation theorem above.

#### AW.4 Numerical comparison with current bounds

Table 142 collects the characteristic values of the tidal curvature scale (AW.8) and the resulting packet-level mismatch estimate (AW.9) across a range of regimes of interest, from laboratory conditions relevant to the VIP-2 experiment to white-dwarf surfaces and neutron-star interiors. Characteristic overlap scales  $L$  are taken to correspond to atomic ( $\sim 5 \times 10^{-11}$  m), electronic ( $\sim 10^{-12}$  m), and nuclear ( $\sim 10^{-15}$  m) length scales, as appropriate to the regime.

**Table 142:** Packet-level mismatch estimates from (AW.9) across laboratory and compact-object regimes of interest. All numbers are order-of-magnitude estimates;  $\mathcal{E} \sim G_N M/R^3$  is the characteristic tidal curvature scale and  $L$  is the assumed fermionic overlap scale. Current experimental bounds on *genuine* Pauli-principle violation are listed only as an orientation scale; since  $\epsilon_{\text{packet}}$  is not itself a Pauli-violation observable but a coarse-grained packet-level mismatch estimate, the comparison should not be read as a direct experimental confrontation. None of the estimates below represents a genuine Pauli-violation prediction.

Regime	$\mathcal{E}$ (s <sup>-2</sup> )	$L$ (m)	$\epsilon_{\text{packet}}$
Earth laboratory, atomic scale	$\sim 1.5 \times 10^{-6}$	$\sim 5 \times 10^{-11}$	$\sim 2 \times 10^{-87}$
White dwarf surface, atomic scale	$\sim 4 \times 10^{-4}$	$\sim 5 \times 10^{-11}$	$\sim 10^{-78}$
Neutron star core, tight electronic	$\sim 10^8$	$\sim 10^{-12}$	$\sim 10^{-66}$
Neutron star core, atomic-scale overlap	$\sim 10^8$	$\sim 5 \times 10^{-11}$	$\sim 10^{-59}$
Neutron star core, nucleon scale	$\sim 10^8$	$\sim 10^{-15}$	$\sim 10^{-78}$
<i>Current experimental bounds on Pauli violation (for reference):</i>			
VIP-2 (electrons, atomic)	$\beta^2/2 < 3.4 \times 10^{-42}$		
Borexino (nucleons)	$\beta^2/2 \lesssim 10^{-60}$		
Ramberg–Snow (electrons)	$\beta^2/2 \lesssim 10^{-26}$		

Two features of Table 142 are worth emphasising.

First, even the most optimistic astrophysical entries (neutron-star cores with electronic overlap scales) are enormously suppressed relative to the scales probed by existing searches for genuine Pauli-principle violation. This does not constitute a direct confrontation with VIP-2, Borexino, or Ramberg–Snow, because  $\epsilon_{\text{packet}}$  is not the same observable; the comparison is included only to indicate how small the residual packet-level mismatch estimate is.

Second, and more importantly, this numerical suppression is not the primary content of the no-go statement. Even if  $\epsilon_{\text{packet}}$  were numerically larger, it would still not represent a violation of the exclusion algebra: it is a coarse-grained mode-overlap artefact at the packet level, not a deformation of the equal-time canonical anticommutator ((AW.7)). The principal conclusion of this appendix is therefore the canonical-normalisation argument of §AW.2, not the numerical tabulation of §AW.4: ordinary strong-gravity neutron star interiors do not provide a viable ECT-specific window for Pauli violation, and any ECT signature of nonstandard fermionic statistics must be sought in the three exceptional settings identified in Section 24.4—nonlocal branch mixing, topological-defect sectors, or regions where the coherent ordered branch description itself fails.

## Relation to the existing fermionic programme

The no-go statement developed here complements the existing fermionic programme of the main text in three ways. First, it extends the Level A exchange-topology result of Section 24.4 by adding a conditional Level B exactness property for the derived Pauli principle on smooth coherent-branch backgrounds. Second, it is consistent with, and strengthened by, the representation-theoretic route to Dirac structure of Section 24.5, which identifies the canonically normalised spinorial excitations on which the present canonical-normalisation argument operates. Third, it makes explicit the connection between the ECT preferred-direction coupling  $\mu_5 \bar{\psi} \gamma^A n_A \psi$  of Section 7.6 and the statistics sector:  $\mu_5$  contributes to dynamics, not to the exclusion algebra. The full theorem—unconditional exactness of Pauli exclusion throughout the coherent branch, or an explicit identification of the nonlocal, topological-defect, or branch-transition mechanism responsible for any departures—remains a distinct target (OP-Q21) contingent on the completion of the fermionic reconstruction programme (OP-Q11).

## AX Unified vacuum-response logic: boundaries, acceleration, time dependence, and horizons

*Status: Level B for the unified interpretive closure. Level A for the structural statement that the ordered vacuum supports nontrivial coherent correlators. Open (OP-Q12): quantitative derivation of all four effects from the completed reduced coherent EFT.*

The four effects discussed in Sections 25.3–25.4 and 36—Casimir-type boundary response, particle production in time-dependent backgrounds, Unruh-type thermality, and Hawking-type horizon thermality—should be understood in ECT as different probes of the same ordered coherent vacuum, not as four unrelated phenomena.

### The unifying logic

In each case the physical question is how the coherent vacuum responds when one changes the accessibility structure of coherent modes:

- (i) **Boundary problems:** part of the mode spectrum is excluded geometrically; the vacuum response appears as a boundary-dependent shift in effective energy (Casimir-type).
- (ii) **Time-dependent backgrounds:** mode definitions at early and late times no longer coincide; the mismatch appears as Bogoliubov-type particle production.
- (iii) **Accelerated observers:** kinematic access to the coherent vacuum is restricted observer-dependently; the reduced state takes an approximately thermal form (Unruh-type).
- (iv) **Horizons:** division into exterior, shell, and inaccessible sectors yields reduced-state thermality without requiring the global state to be mixed (Hawking-type).

### What is and is not claimed

ECT does not treat these effects as independent axioms of vacuum physics. It treats them as different manifestations of one ordered coherent vacuum under different restrictions on mode accessibility and coarse-graining.

This appendix does not elevate the quantitative formulas of all four effects to Level A. The precise temperatures, spectra, and amplitudes remain closure-dependent in several places. What it does support at a stronger structural level is the unified interpretation: the ordered coherent vacuum is the common object being probed in all four cases.

## Analogue-gravity connection

In this sense the analogue-gravity perspective is not merely illustrative in ECT. It is conceptually aligned with the coherent branch: thermality need not signal fundamental microscopic randomness, but can arise from reduced access to an ordered underlying medium. This is a Level B interpretive closure (Section 25.2).

## AY Bath regimes, effective spectral structure, and the limits of the ohmic/Markov closure

*Status: Level A for the general subsystem–environment reduced-state logic; Level B for the specific ohmic/Markov closure used in the main text. Open (OP-Q15): quantitative interpolation between the two bath regimes.*

This appendix clarifies the status of the effective bath description used in Section 26.1. The main text employs a reduced influence-functional language in which a subsystem of coherent variables interacts with an effective environment. This is structurally natural in ECT once one coarse-grains over inaccessible coherent and topological degrees of freedom, but the detailed bath model remains an effective closure rather than a first-principles theorem from bare P3.

### Effective spectral density

The central quantity is the effective spectral density  $J(\omega)$ , which determines dissipation and noise kernels in the reduced dynamics. In the simplest closure one assumes a smooth positive spectral density and, in the many-mode regime, an effectively Markovian coarse-grained behaviour. For a three-dimensional soft-orientation-like environment a super-ohmic scaling  $J(\omega) \propto \omega^4$  is structurally natural (Level A from the geometry of the mode density in the minimal orientation EFT). What is Level B is the specific low-frequency closure used in the main text, including the effective ohmic/Markov approximation and the corresponding explicit entropy-growth formula (26.9).

### Two regimes

Two regimes must be kept distinct:

**Strong bath:**  $N_{\text{eff}} \gg 1$ . When the effective number of active environmental modes is large, the subsystem experiences strong phase randomisation and approximately monotone growth of coarse-grained entropy. Classical alternatives emerge effectively and the reduced-state description becomes macroscopically robust. This regime supports the macroscopic arrow of time in Section 26.1.

**Weak bath:**  $N_{\text{eff}} \sim 1$ . When only very few effective environmental channels are active, coherent recurrences, partial reversibility, and incomplete decoherence remain possible. This is the regime in which the subsystem retains recognisably quantum behaviour (Section 26.1).

**Table 143:** Bath regime summary.

Regime	Effective condition	Behaviour	Status
Weak bath	$N_{\text{eff}} \sim 1$	recoherence / partial reversibility possible	Level A (structural)
Strong bath	$N_{\text{eff}} \gg 1$	robust decoherence / entropy growth	Level A (structural)
Ohmic/Markov law	closure-specific	working formula for $dS/dw$	Level B

## Open problem

The open problem is not whether subsystem–environment logic exists in ECT — it does — but how to derive the detailed spectral hierarchy of bath sectors directly from the coherent microstructure of the condensate. That quantitative interpolation between the two regimes is part of OP-Q15.

## AZ Mathematical apparatus for ECT decoherence predictions

*Status: Level B. The generic spectral-density family, the noise and dissipation kernels, and the decoherence exponent are constructed within the coherent-branch subsystem–environment split. The specific spectral exponent depends on the subsystem–bath coupling class, which is parameterised rather than uniquely fixed at the present stage.*

This appendix should be read as an operational extension of Appendix AY. The earlier appendix classifies the admissible bath regimes and the status of the ohmic/Markov closure; the present appendix supplies a generic calculational toolkit within that closure language. It does not upgrade the bath model to a first-principles theorem from bare P3.

### AZ.1 Generic subsystem–bath coupling class

In the broken phase the condensate supports  $N_G = 3$  naive Goldstone-coordinate orientation directions with linear dispersion  $\omega_k = c_*|\mathbf{k}|$  at the free quadratic level (see Section 4.3 for the distinction between naive coordinate count and physically independent propagating soft content). For a localised subsystem with generalised coordinate  $q$ , the coupling to these modes takes the generic form

$$H_{\text{int}} = q \sum_{\alpha} g_{\alpha}(\mathbf{k}_{\alpha}) \chi_{\alpha}(\mathbf{x}_q), \quad (\text{AZ.1})$$

where  $g_{\alpha}(\mathbf{k})$  is the coupling vertex, which depends on the operator structure of the interaction.

The resulting spectral density of the effective bath is

$$J(\omega) = \mathcal{A} \omega^2 |g(\omega/c_*)|^2 e^{-\omega/\omega_c}, \quad \omega_c \sim c_*/\xi_{\text{cond}}. \quad (\text{AZ.2})$$

The spectral exponent is controlled entirely by the coupling vertex:

- density coupling,  $g(k) \sim \text{const}$ :  $J(\omega) \propto \omega^2$  (super-ohmic in the standard CL classification);
- derivative coupling,  $g(k) \propto k$ :  $J(\omega) \propto \omega^4$  (super-ohmic, structurally natural for the 3D Goldstone bath with gradient interaction — this is the regime already identified in the main text, eq. (26.5));
- effective ohmic,  $J(\omega) \propto \omega$ : requires additional coarse-graining or reduced effective dimensionality, introduced as an effective Level B closure in eq. (26.6).

To maintain generality, the subsequent formulae are written for the generic power-law family

$$J_s(\omega) = A_s \omega^s e^{-\omega/\omega_c}, \quad (\text{AZ.3})$$

with  $s = 1$  (ohmic),  $s = 2$  (super-ohmic density coupling), or  $s = 4$  (super-ohmic derivative coupling) as the three physically motivated cases in ECT.

### AZ.2 Noise kernel $N(\tau)$

Given the spectral density (AZ.3), the noise kernel of the Feynman–Vernon influence functional is

$$N(\tau) = \frac{1}{\pi} \int_0^{\infty} d\omega J_s(\omega) \coth\left(\frac{S_0 \omega}{2T_{\text{eff}}}\right) \cos(\omega \tau). \quad (\text{AZ.4})$$

### Vacuum limit ( $T_{\text{eff}} \rightarrow 0$ )

Setting  $\coth \rightarrow 1$ , the integral evaluates in closed form:

$$N_0(\tau) = \frac{A_s \Gamma(s+1) \omega_c^{s+1}}{\pi} \frac{\cos[(s+1) \arctan(\omega_c \tau)]}{(1 + \omega_c^2 \tau^2)^{(s+1)/2}}. \quad (\text{AZ.5})$$

At  $\tau = 0$ :  $N_0(0) = A_s \Gamma(s+1) \omega_c^{s+1} / \pi$ .

### High-temperature limit ( $T_{\text{eff}} \gg S_0 \omega_c$ )

Using  $\coth(x) \approx 1/x$  for  $x \ll 1$ :

$$N_T(\tau) = \frac{2T_{\text{eff}} A_s \Gamma(s) \omega_c^s}{\pi S_0} \frac{\cos[s \arctan(\omega_c \tau)]}{(1 + \omega_c^2 \tau^2)^{s/2}}. \quad (\text{AZ.6})$$

Both formulae exhibit a bath memory time  $\tau_{\text{env}} \sim \omega_c^{-1} \sim \xi_{\text{cond}}/c_*$ .

### AZ.3 Dissipation kernel $D_R(\tau)$

The response (dissipation) kernel completes the Feynman–Vernon pair:

$$D_R(\tau) = \frac{2}{\pi} \Theta(\tau) \int_0^\infty d\omega \frac{J_s(\omega)}{\omega} \sin(\omega \tau). \quad (\text{AZ.7})$$

For the generic family (AZ.3), this gives

$$D_R(\tau) = \frac{2A_s \Gamma(s) \omega_c^s}{\pi} \Theta(\tau) \frac{\sin[s \arctan(\omega_c \tau)]}{(1 + \omega_c^2 \tau^2)^{s/2}}. \quad (\text{AZ.8})$$

In the reduced effective description one imposes the retarded support  $D_R(\tau < 0) = 0$  through the  $\Theta(\tau)$  prefactor, consistently with the Level A retarded-kernel structure established for the ordered Lorentzian branch. A full first-principles derivation of this identification from ECT microdynamics remains open.

The dissipation kernel governs memory/friction effects, Lamb-shift-like renormalisation, and the response part of the reduced dynamics. Together with  $N(\tau)$ , it yields the full open-system equation

$$\ddot{q} + \Omega_0^2 q + \int_0^t d\tau' D_R(t - \tau') \dot{q}(\tau') = \xi(t), \quad \langle \xi(t) \xi(t') \rangle = N(t - t'). \quad (\text{AZ.9})$$

### AZ.4 Decoherence exponent for spatial superpositions

For a fixed-separation spatial superposition in the Gaussian reduced description, and neglecting drift/relaxation relative to pure dephasing, the decoherence exponent accumulated over time  $t$  is

$$\Gamma_{\Delta q}(t) = \frac{(\Delta q)^2}{S_0} 2 \int_0^t d\tau (t - \tau) N(\tau). \quad (\text{AZ.10})$$

This is the central bridge from the apparatus to observable quantities: interference fringe visibility decays as  $e^{-\Gamma_{\Delta q}(t)}$ .



## AZ.5 Short-time and Markov limits

**Short-time (non-Markov) regime:**  $t \ll \tau_{\text{env}}$

For  $t \ll \omega_c^{-1}$ , the kernel is approximately constant,  $N(\tau) \approx N(0)$ , and

$$\Gamma_{\Delta q}(t) \approx \frac{(\Delta q)^2 N(0)}{S_0} t^2. \quad (\text{AZ.11})$$

This is a general result: for analytic kernels with finite  $N(0)$ , the early-time decoherence is quadratic, as illustrated here for the super-ohmic cases relevant to ECT.

**Markov (white-noise) regime:**  $t \gg \tau_{\text{env}}$

If the effective kernel is approximated as white noise,  $N(\tau) \approx D_{\text{eff}} \delta(\tau)$ , then

$$\Gamma_{\Delta q}(t) \approx \frac{2D_{\text{eff}}}{S_0} (\Delta q)^2 t. \quad (\text{AZ.12})$$

This recovers the article's current Gaussian–Markov working formula, eq. (26.9), as a coarse-grained long-time closure.

The practical implication is that the *same* ECT apparatus produces both the standard Caldeira–Leggett decoherence ( $\Gamma \propto t$ , Markov limit) and the non-Markovian early-time regime ( $\Gamma \propto t^2$ ), depending on the experimental timescale relative to  $\tau_{\text{env}}$ .

## AZ.6 Self-consistent environmental–gravitational crossover

For a solid sphere of radius  $R$  and density  $\rho$ , mass  $m = \frac{4\pi}{3} \rho R^3$ :

### Environmental collisional rate

Hard-sphere estimate:

$$\lambda_{\text{env}} \sim n_{\text{gas}} v_{\text{th}} \pi R^2. \quad (\text{AZ.13})$$

### Gravitational (condensate-DP) rate

From the ECT gravitational decoherence (Section 26.3):

$$\lambda_{\text{grav}} \sim \tau_{\text{DP}}^{-1} \sim \frac{G_N m^2}{\hbar R} = \frac{16\pi^2}{9} \frac{G_N \rho^2 R^5}{\hbar}. \quad (\text{AZ.14})$$

### Crossover

Setting  $\lambda_{\text{env}} = \lambda_{\text{grav}}$ :

$$R_{\text{cross}} \sim \left( \frac{9 \hbar n_{\text{gas}} v_{\text{th}}}{16\pi G_N \rho^2} \right)^{1/3}, \quad (\text{AZ.15})$$

$$m_{\text{cross}} = \frac{4\pi}{3} \rho R_{\text{cross}}^3 \sim \frac{3 \hbar n_{\text{gas}} v_{\text{th}}}{4 G_N \rho}. \quad (\text{AZ.16})$$

Above  $m_{\text{cross}}$ , if ordinary environmental channels are reduced below the condensate-gravitational rate, the condensate gravitational channel is expected to dominate and decoherence should persist even in near-perfect vacuum.

## AZ.7 Domain of applicability

*What this apparatus can compute:*

- (i) Environmental decoherence for matter-wave interferometry ( $C_{60}$ , Fein 2019, and future macro-molecular experiments): Section 26.2.
- (ii) Gravitational (condensate) decoherence for mesoscopic objects in superposition: Section 26.3, Table 85.
- (iii) Environmental–gravitational crossover mass and radius for given vacuum conditions.
- (iv) Cavity/cat-state decoherence in Haroche–Raimond-type microwave CQED experiments (an open quantitative target).
- (v) Weak-locking consistency bounds for photonic experiments (Wheeler delayed-choice, quantum eraser, Procopio switch). In the photonic delayed-choice / eraser / entanglement-swapping sector, the present role of the apparatus is mainly to define weak-locking consistency conditions rather than to provide detector-specific precision numerics.

*What this apparatus cannot yet compute:*

- (i) Lifetimes or decay widths of elementary particles (requires the full particle sector, not the open-system appendix).
- (ii) Precision spectroscopy (requires explicit interaction vertices beyond the generic coupling family).
- (iii) The fine-structure constant or fermion mass ratios (requires the gauge and Yukawa sectors).

The boundary is sharp: the present apparatus is an *open-system / influence-functional* framework; it governs decoherence, measurement, and quantum–classical boundary phenomena. Full particle-physics predictions require the separate ECT particle programme, which is not the subject of this appendix.

## BA Qubit information–decoherence numerics

The qubit dephasing closure of Section 30.3 uses a maximally coherent initial state  $|\psi\rangle = (|0\rangle + |1\rangle)/\sqrt{2}$  subject to Gaussian dephasing with parameter  $\Gamma$ . The system–environment mutual information is (Eq. 30.4)

$$I(S:E) = 2h_2\left(\frac{1+e^{-\Gamma}}{2}\right), \quad (\text{BA.1})$$

where  $h_2(p) = -p\ln p - (1-p)\ln(1-p)$  is the binary entropy. In bits:  $I_{\text{bits}} = I/(\ln 2)$ . The residual coherence (visibility) is  $V = e^{-\Gamma}$ .

Representative values (Fig. 37):

$\Gamma$	$I$ [bits]	$V$	Physical anchor
0.006	0.10	0.994	Procopio 2015 (quantum switch)
0.062	0.50	0.940	Jacques 2007 (closed config.)
0.25	1.00	0.779	One-bit information threshold
0.347	1.19	0.707	Bell/CHSH crossover
1.0	1.69	0.368	Order-unity decoherence
3.0	1.98	0.050	Near-complete dephasing

The curve is monotonic: extracting more information requires stronger decoherence. This is a Level B result of the specific dephasing closure; a protocol-independent bound remains open (OP-PES-6).

## BB Critical shell and black-hole information in ECT

This appendix develops, in more detail than the main text, the ECT scenario for unitary black-hole evaporation. We consistently distinguish what is structural within the present ECT framework, what depends on the current shell/interface closure, and what remains open.

### BB.1 Microscopic unitarity and apparent information loss

The underlying condensate dynamics is governed by a self-adjoint Euclidean action  $S_E[\Phi]$  (postulate P2). Any quantum evolution derived from it is therefore unitary by construction. Fundamental information destruction—understood as the irreversible transition of a pure state to a genuinely mixed state at the microscopic level—is not naturally accommodated by this structure and is structurally disfavoured within the present ECT reading.

The standard Hawking calculation works entirely in the effective Lorentzian description, which represents only a fraction of the full condensate Hilbert space  $\mathcal{H}_{\text{full}}$  (Eq. (BB.9)). The apparent mixed-state character of  $\rho_{\text{rad}}$  can therefore be a consequence of partial tracing over shell and core degrees of freedom, rather than a sign of fundamental non-unitarity. This argument mirrors what is standard in decoherence theory [259]: coarse-graining over inaccessible degrees of freedom produces an effectively mixed state even from a pure global state.

### BB.2 Derivation of the critical shell

**Rindler near-horizon geometry.** Near any non-extremal stationary horizon the proper-distance metric takes the local Rindler form

$$ds^2 \approx -\left(\frac{\kappa\rho}{c}\right)^2 c^2 dt^2 + d\rho^2 + r_h^2 d\Omega^2, \quad (\text{BB.1})$$

where  $\kappa$  is the surface gravity and  $r_h$  is the horizon radius. The Tolman temperature for a static observer at proper distance  $\rho$  is

$$T_{\text{loc}}(\rho) = \frac{T_H}{\sqrt{-g_{tt}}} = \frac{\hbar c}{2\pi k_B \rho}, \quad (\text{BB.2})$$

which diverges as  $\rho \rightarrow 0$ . This is a standard result [178, 176].

**ECT phase transition temperature.** The condensate effective potential at finite temperature is

$$V_{\text{eff}}(\Phi, T) = -\frac{\mu^2}{2}\Phi^2 + \frac{\lambda}{4}\Phi^4 + \frac{\lambda T^2}{12}\Phi^2, \quad (\text{BB.3})$$

from the Dolan–Jackiw one-loop correction [207]. The ordered phase ( $\langle\Phi\rangle \neq 0$ ) exists while  $-\mu^2 + \lambda T^2/6 < 0$ , i.e. for  $T < T_c$  with

$$T_c = \phi_0 \sqrt{6}, \quad (\text{BB.4})$$

where  $\phi_0 = \sqrt{\mu^2/\lambda}$  is the bare field VEV.

**Critical shell.** Setting  $T_{\text{loc}}(\rho_c) = T_c$  and substituting Eq. (BB.2):

$$\rho_c = \frac{\hbar c}{2\pi\sqrt{6}k_B\phi_0}. \quad (\text{BB.5})$$

Using the observational matching  $M_G = \bar{M}_{\text{Pl}}$  together with the current shell closure, one obtains

$$\rho_c = \frac{\ell_{\text{Pl}}}{\sqrt{3\pi}} \approx 5.27 \times 10^{-36} \text{ m} \approx 0.33 \ell_{\text{Pl}}. \quad (\text{BB.6})$$

In the present article this should be read as a closure-level strong-field result rather than as a universal parameter-free theorem. Its significance is that the shell/interface construction selects a characteristic near-horizon scale at which the macroscopic Lorentzian description may cease to remain complete and coherent-sector dynamics may become relevant. Figure 40(a) illustrates the Tolman temperature profile and marks  $\rho_c$ .

The result  $\rho_c = \ell_{\text{Pl}}/\sqrt{3\pi}$  is close to the phenomenological “stretched horizon” thickness introduced in the membrane paradigm [260], but here it follows within the present Tolman-heating / critical-shell closure, conditional on identifying local Tolman heating as the relevant control parameter.

### BB.3 Shell entropy and the area law

If the shell of area  $A$  and thickness  $\rho_c$  is decomposed into effective condensate cells of linear scale  $\ell_*$ , the microstate count is

$$N \sim A/\ell_*^2, \quad S_{\text{shell}} \sim N \ln q = \frac{A \ln q}{\ell_*^2}. \quad (\text{BB.7})$$

Matching the Bekenstein–Hawking entropy  $S_{\text{BH}} = A/(4\ell_{\text{Pl}}^2)$  [235] requires

$$\frac{\ln q}{\ell_*^2} = \frac{1}{4\ell_{\text{Pl}}^2}. \quad (\text{BB.8})$$

We do not derive the exact coefficient from first principles here; the matching condition (BB.8) shows what is required, but the microscopic counting remains an open problem (Table 146). The point is that the area law is *structurally natural* in ECT once the critical shell is present, requiring only locality and a Planck-scale UV cutoff, both of which are built into the condensate theory.

### BB.4 Conditional theorem: exact thermality is incompatible with unitary evaporation

The mere presence of a critical shell or of additional condensate degrees of freedom does not by itself resolve the information paradox. One must show that these extra degrees of freedom are not optional decorations, but are *forced to couple to the outgoing channel* if microscopic unitarity is to be maintained. Otherwise one could have a shell while leaving the Hawking channel exactly thermal and state-independent, and the standard information-loss contradiction would simply reappear in a different language. A structural theorem is therefore required.

**Conditional theorem (ECT).** *Consider an evaporating black hole in ECT and assume: (i) the microscopic condensate dynamics is unitary; (ii) the near-horizon region contains a finite-entropy critical shell of the ordered-branch amplitude variable; (iii) evaporation is complete, i.e. no infinite-capacity hidden remnant remains at the end. Then: (a) exact Hawking thermality and true information loss are impossible; (b) the outgoing channel must be shell-state-dependent (this is a derived consequence, not an additional assumption); (c) the apparent mixedness of the radiation arises only after coarse-graining over shell and deeper condensate degrees of freedom, while the full evolution remains unitary on*

$$\mathcal{H}_{\text{full}} = \mathcal{H}_{\text{rad}} \otimes \mathcal{H}_{\chi} \otimes \mathcal{H}_{\text{core}}. \quad (\text{BB.9})$$

**Proof.** *Step 1 (enlarged state space).* If the full condensate dynamics is unitary, the complete state evolves as

$$|\Psi(t)\rangle = U(t)|\Psi(0)\rangle, \quad U^\dagger U = \mathbf{1}. \quad (\text{BB.10})$$

The observed radiation state is

$$\rho_{\text{rad}}(t) = \text{Tr}_{\mathcal{H}, \text{core}} |\Psi(t)\rangle \langle \Psi(t)|. \quad (\text{BB.11})$$

Mixed radiation does not by itself imply fundamental non-unitarity; it is consistent with a pure global state once the tracing-out is acknowledged.

*Step 2 (proof by contradiction).* Consider a single emission step in the presence of shell microstates  $|s\rangle$ :

$$|s\rangle|0\rangle \longrightarrow \sum_{\omega, s'} A_{\omega s' s} |s'\rangle |\omega\rangle. \quad (\text{BB.12})$$

Suppose, for contradiction, that the outgoing channel is exactly thermal and strictly independent of  $s$ :

$$A_{\omega s' s} = a_{\omega s'}. \quad (\text{BB.13})$$

Then two orthogonal initial shell microstates  $s_1 \neq s_2$  produce the same radiation statistics. If evaporation is complete and no infinite entropy reservoir remains, the final radiation state cannot distinguish  $|\Psi(s_1)\rangle$  from  $|\Psi(s_2)\rangle$ . This contradicts unitarity (which requires distinct initial states to evolve to distinct final states).

*Conclusion.* Therefore shell-state dependence is *not* an optional phenomenological embellishment. It is a logical necessity if one insists simultaneously on unitary microscopic dynamics, finite shell entropy, and complete evaporation. Exact Hawking thermality is then impossible in the full theory. The leading parametrisation of the shell-state-dependent emission is

$$N_{\omega}^{(s)} = |\mathcal{T}_{\omega}[s]|^2 \cdot \frac{1}{e^{\hbar\omega/k_B T_H} - 1}, \quad \mathcal{T}_{\omega}[s] = e^{i\delta_{\omega}[s] - \Gamma_{\omega}[s]}, \quad (\text{BB.14})$$

where  $\delta_{\omega}[s]$  and  $\Gamma_{\omega}[s]$  are shell-state-dependent phase and attenuation functions.

**Status of the conditions.** Condition (i) is naturally motivated by the self-adjointness of the Euclidean condensate action (postulate P2); a fully explicit microscopic Hamiltonian and its self-adjoint domain remain to be constructed, so unitarity should be regarded as the physically natural assumption of the condensate framework rather than a derived theorem at this stage. Condition (ii) follows structurally from the Tolman temperature argument (Section 36), conditional on the assumption that the local Tolman temperature is the control parameter for ordered-phase dissolution near the horizon; this is condition (C2b) of the microscopic consistency criterion (Appendix BB.9) and remains an open derivation task. Condition (iii) is an assumption about the final state of evaporation that we do not derive; the case of a Planck-mass remnant would require separate treatment. Shell-state dependence of the outgoing channel [conclusion (b)] is *not* an independent assumption: it is a necessary logical consequence of conditions (i)–(iii), as the proof by contradiction shows.

**Complementary entropy argument.** The same conclusion follows from a global entropy argument. If the full state is pure and evolves unitarily, the von Neumann entropy of the radiation satisfies

$$S_{\text{rad}}(t) = S_{\text{rem}}(t) \quad (\text{BB.15})$$

where  $S_{\text{rem}}(t)$  is the entropy of the remaining black-hole subsystem (shell + core) [261]. Since  $S_{\text{rem}} \rightarrow 0$  as the black hole fully evaporates,  $S_{\text{rad}}$  must also tend to zero at late times. This is incompatible with exact Hawking thermal emission, which would give monotonically increasing  $S_{\text{rad}}$  at all times. The proof-by-contradiction via emission amplitudes (above) and this global entropy argument are thus two independent routes to the same conclusion. Equation (BB.14) expresses the leading parametrisation of the shell-state-dependent corrections. Panel (b) of Figure 40 shows the expected qualitative Page-curve behaviour.

**Relation to the Mathur obstruction.** The “small corrections” no-go argument [262] shows that individually small, independent corrections to each emission step cannot restore unitarity. This is not in contradiction with our result. The theorem does not claim that early-time corrections are large; it claims that near and after the Page time the channel *must* become effectively order-one and state-dependent, because the finite shell entropy capacity is exhausted. This is a structural necessity, not a claim about the magnitude of early corrections.

## BB.5 Near-horizon $\chi$ -field dynamics: an effective mean-field construction

The conditional theorem above is purely structural. To go beyond it and exhibit an explicit mechanism, we construct an effective mean-field model of the shell, valid in the Ginzburg–Landau regime. This is *not* a full microscopic derivation from the underlying condensate action, and the results below have a weaker status than the theorem. We mark the status of each step explicitly.

**Step 1: local outer asymptotics of the  $\chi$ -field.** Near the critical point  $T_{\text{loc}}(\rho_c) = T_c$ , the reduced temperature is

$$\varepsilon(\rho) = 1 - \frac{T_{\text{loc}}(\rho)}{T_c} = \frac{\rho - \rho_c}{\rho} \approx \frac{\rho - \rho_c}{\rho_c} \quad (\rho \downarrow \rho_c^+). \quad (\text{BB.16})$$

The Ginzburg–Landau effective action for the order parameter  $\chi$ , with Tolman temperature as control parameter, is

$$\mathcal{F}_{\text{GL}}[\chi] = \int d\rho r_h^2 \left[ a(\partial_\rho \chi)^2 - \frac{\lambda}{6} \varepsilon(\rho) \chi^2 + \frac{\lambda}{4} \chi^4 \right], \quad (\text{BB.17})$$

where the coefficients are fixed by the Dolan–Jackiw potential [207] used to derive  $T_c$  (Section 25.1).

In the mean-field approximation (gradient term subdominant), the local outer asymptotic scaling just outside the shell is

$$\chi(\rho) \propto \left( \frac{\rho - \rho_c}{\rho_c} \right)^{1/2} \quad (\rho \downarrow \rho_c^+). \quad (\text{BB.18})$$

*This is the leading outer asymptotic behaviour of the order parameter, not a complete radial profile.* The full profile, including the interface region and the inner branch  $\rho < \rho_c$ , requires solving the Euler–Lagrange equation of  $\mathcal{F}_{\text{GL}}$  numerically. The mean-field exponent 1/2 is the leading-order result; fluctuation corrections modify it toward the 3D Ising order-parameter exponent  $\beta \approx 0.326$ .

The GL description (BB.17) is a near-critical mean-field closure, valid in the outer-shell interface region  $\rho \gtrsim \rho_c$  where the condensate amplitude transitions between its vacuum value and zero. It is not a derived description of the deep interior  $\rho \ll \rho_c$ , which belongs to the pre-Lorentzian core sector (Appendix BB.7). A complete interior profile requires the pre-Lorentzian condensate dynamics, which is outside the scope of the present mean-field construction.

**Step 2: effective mode equation in a minimal near-horizon closure.** A minimal ECT-motivated near-horizon closure is obtained by letting the redshift factor be modulated by the local ordered-branch amplitude parameter:

$$g_{tt}^{\text{eff}}(\rho) = -Z_t \left( \frac{\chi(\rho)}{\chi_{\text{vac}}} \right) (\kappa \rho)^2, \quad Z_t(1) = 1, \quad (\text{BB.19})$$

where the simplest choice is  $Z_t(\chi/\chi_{\text{vac}}) = \chi/\chi_{\text{vac}}$ , giving an effective local speed

$$c_{\text{eff}}(\rho) = c \sqrt{\chi(\rho)/\chi_{\text{vac}}}. \quad (\text{BB.20})$$

*This is a minimal closure, not a derived result.* It encodes the natural ECT expectation that the effective Lorentzian metric degrades continuously as  $\chi \rightarrow 0$ , but the specific functional form is an assumption.

Within this closure, the effective s-wave radial equation for an outgoing massless mode  $\varphi = e^{-i\omega t} f(\rho)$  is

$$\partial_\rho [c_{\text{eff}}^2(\rho) \partial_\rho f] + \frac{\omega^2}{(\kappa \rho)^2} f = 0. \quad (\text{BB.21})$$

This is the effective  $s$ -wave equation in the minimal near-horizon closure. Its validity is conditional on the closure Eq. (BB.19) and on the local asymptotics Eq. (BB.18).

**Step 3: finiteness of the shell correction.** In the WKB language the shell correction to the outgoing channel is encoded in

$$\ln |\mathcal{T}_\omega^{(0)}| \sim - \int_{\text{shell}} d\rho \Im k_\omega(\rho). \quad (\text{BB.22})$$

Because  $c_{\text{eff}}(\rho) \propto (\rho - \rho_c)^{1/4}$  in the outer asymptotic regime, the integrand behaves as  $(\rho - \rho_c)^{-1/4}$  near the shell and the integral is *finite*. This establishes that the shell induces a finite, nonzero correction to the standard Hawking channel; it does not suppress emission entirely. On dimensional grounds, within the minimal closure, the correction is expected to be extremely small for astrophysical black holes (suppressed by  $\rho_c/r_h \sim \ell_{\text{Pl}}/r_h \ll 1$ ) and potentially order-unity near the Planck mass. This is a dimensional estimate within the minimal closure; the precise coefficient requires the fully derived shell Hamiltonian and is not claimed here.

**Step 4: structure of the state-dependent coupling.** Beyond the mean-field background  $\chi(\rho)$ , the quantum fluctuations  $\delta\chi^{(s)}(\rho)$  encode the microstate  $s$  of the shell. The general linear-response form of the shell-state-dependent correction to the transmission amplitude is

$$\delta \ln \mathcal{T}_\omega[s] = \int_{\text{shell}} d\rho \mathcal{K}_\omega(\rho) \delta\chi^{(s)}(\rho), \quad (\text{BB.23})$$

where the kernel  $\mathcal{K}_\omega(\rho)$  is determined by the near-horizon ECT dynamics. Equation (BB.23) is the general structural form of the shell–radiation coupling at linear order in the fluctuation. Computing  $\mathcal{K}_\omega(\rho)$  explicitly from first principles remains an open problem (see Table 146).

In the simplest phase-dominated approximation the kernel reduces to a constant phase prefactor, consistent with the parametrisation Eq. (BB.14) in the main text. However, this further simplification should not be identified with a full first-principles derivation.

**Effective shell Hamiltonian.** Using the shell parametrisation  $\chi(\rho, \Omega, t) = \bar{\chi}(\rho) + \delta\chi(\rho, \Omega, t)$ , which is related to the amplitude-language variable by  $\phi = \ln(\chi/\chi_{\text{vac}})$ , the GL free energy Eq. (BB.17) gives a *static* energy functional. Adding the kinetic term from the time-dependent part of the ECT condensate action, the minimal effective shell Hamiltonian is

$$H_{\text{shell}} = \int d\rho d\Omega r_h^2 \left[ \frac{\pi_\chi^2}{2Z_\chi} + \frac{a}{r_h^2} (\partial_\rho \delta\chi)^2 + \frac{W_\chi}{2r_h^4} (\nabla_\Omega \delta\chi)^2 + U_{\text{eff}}(\delta\chi; \rho) \right], \quad (\text{BB.24})$$

where  $\pi_\chi = Z_\chi \partial_t \delta\chi$  is the conjugate momentum, the effective potential is

$$U_{\text{eff}}(\delta\chi; \rho) = \frac{1}{2} m_\chi^2(\rho) \delta\chi^2 + \frac{\lambda_\chi}{4} \delta\chi^4 + \dots, \quad m_\chi^2(\rho) \propto \frac{\rho_c - \rho}{\rho_c}, \quad (\text{BB.25})$$

and the kinetic coefficient  $Z_\chi$  and the angular stiffness  $W_\chi$  are effective parameters not yet derived from the full condensate action.

*Status of Eq. (BB.24).* The form of  $H_{\text{shell}}$  is uniquely determined by three inputs: the Ginzburg–Landau description of a critical scalar field, the Rindler-like geometry near the horizon, and the requirement that the effective potential vanish at  $\rho = \rho_c$ . In this sense the *structure* of  $H_{\text{shell}}$  follows from ECT’s near-horizon critical sector, but the numerical coefficients  $Z_\chi$ ,  $W_\chi$ ,  $\lambda_\chi$  are not yet derived from the microscopic condensate action; they remain open parameters.

**Minimal shell–radiation coupling.** Because the emergent Lorentzian structure in ECT depends on  $\chi$ , outgoing radiation cannot propagate through the shell without coupling to its fluctuations. At leading order, the simplest local interaction consistent with locality, linearity in the fluctuation  $\delta\chi$ , and minimal operator dimension is

$$\mathcal{L}_{\text{int}} = -\frac{g}{2} \delta\chi (\partial\varphi)^2, \quad (\text{BB.26})$$

where  $\varphi$  represents a generic outgoing radiation mode and  $g$  is the shell–radiation coupling with dimension [length].

This form is not postulated but follows from the  $\chi$ -dependence of the effective metric: schematically,  $g_{\mu\nu}^{\text{eff}}(\chi) \approx \bar{g}_{\mu\nu}(1 + \delta\chi/\chi_{\text{vac}})$ , so  $\delta g_{\mu\nu} \propto \delta\chi \bar{g}_{\mu\nu}$ , and the minimal coupling to the stress tensor  $T_{\text{rad}}^{\mu\nu}$  reduces to Eq. (BB.26) for a massless scalar. For tensor modes (gravitons) the coupling has an identical structure at linearised order.

*Status of Eq. (BB.26).* The *form* of the coupling is uniquely fixed at this order. The *coefficient*  $g$  is not yet derived from the microscopic action; it is the open parameter whose calculation constitutes the central missing step toward a complete resolution. The kernel  $\mathcal{K}_\omega(\rho)$  in Eq. (BB.23) is related to  $g$  and the shell Green function by  $\mathcal{K}_\omega(\rho) \sim g G_\omega^{\text{shell}}(\rho)$ , where  $G_\omega^{\text{shell}}$  is the shell propagator.

## BB.6 Toy finite-memory shell model and the Page mechanism

The conditional theorem guarantees that exact thermality is impossible and purification must occur, but it does not provide a quantitative evaporation curve. To illustrate how the Page mechanism arises within the ECT shell picture, we construct the following *illustrative* finite-memory model. This model is not derived from the microscopic condensate action; it is an explicit realisation of the logical structure the theorem requires.

**Setup.** Discretise the shell into  $N \sim A/\ell_*^2$  local cells, where  $\ell_*$  is an effective UV cutoff. Give each cell a  $q$ -dimensional Hilbert space. The shell’s total Hilbert space is  $\mathcal{H}_{\text{shell}} = (\mathbb{C}^q)^{\otimes N}$  with

$$S_{\text{shell}}^{\text{max}} = N \ln q \sim \frac{A}{\ell_*^2} \ln q. \quad (\text{BB.27})$$

For  $\ell_* \sim \ell_{\text{Pl}}$  and  $q \sim 2$  this reproduces the area law up to the undetermined  $\ln q$  coefficient.

**Unitary emission map.** Each emission step is a unitary map on the full Hilbert space:

$$U_n : \mathcal{H}_{\text{shell}}^{(n)} \otimes \mathcal{H}_{\text{vac}}^{(n)} \longrightarrow \mathcal{H}_{\text{shell}}^{(n+1)} \otimes \mathcal{H}_{\text{rad}}^{(n)}, \quad (\text{BB.28})$$

with the only constraint that the map is unitary and is compatible with the coupling Eq. (BB.26). The key point is that  $U_n$  depends on the shell state: different shell microstates lead to different outgoing quanta statistics.

**Resulting entropy curve.** The von Neumann entropy of the radiation after  $n$  emission steps follows the Page curve for a system of total dimension  $d_{\text{total}} = q^N \times q^n$ :

$$S_{\text{rad}}(n) \approx \begin{cases} n \ln q & n \ll N/2 \quad (\text{early: almost thermal}) \\ N \ln q - (n - N) \ln q & n \gg N/2 \quad (\text{late: purifying}) \end{cases} \quad (\text{BB.29})$$

with a smooth turnaround at the Page time  $n_P \sim N/2$ .



**Interpretation.** The early-time regime reproduces thermal emission at the Hawking rate. After the Page time, the radiation entropy decreases, consistent with purification of earlier quanta through shell-mediated correlations. The coarse-grained entropy (obtained by tracing over the shell) increases monotonically, recovering the Hawking result at low resolution.

This model is *illustrative*: it demonstrates that the Page mechanism follows automatically from the existence of a finite-entropy shell coupled to outgoing modes by a unitary map. The actual ECT Page curve requires the microscopic  $H_{\text{shell}}$  and the coefficient  $g$ ; the toy model only shows what form the curve must take.

## BB.7 Interior and the singularity

In ECT the interior of a black hole is the region where  $T_{\text{loc}} \gg T_c$ , so the ordered macroscopic phase is completely broken. The metric description ceases to be fundamental well before the classical singularity is reached. The singularity is therefore not a physical object in ECT but a consequence of extending the effective Lorentzian description beyond its domain of validity. The “pre-Lorentzian core” sector  $\mathcal{H}_{\text{core}}$  in Eq. (BB.9) replaces the classically singular interior.

This picture is consistent with the broader ECT interpretation of the pre-Planckian epoch as a Euclidean condensate phase (Section 16.7). The question of where information “is” inside the black hole may then be ill-posed in classical geometric terms; the information is distributed across the condensate microstate of the shell and core, which does not admit a simple Lorentzian spatial description.

## BB.8 Potential observational signatures

Although the direct detection of information-carrying Hawking correlations from astrophysical black holes is not feasible with current technology, the critical-shell picture has several in-principle testable consequences.

1. *Near-horizon deviations from perfect GR.* If the horizon is accompanied by a physical shell at  $\rho_c$ , small departures from the ideal GR boundary condition are expected. These may manifest as universal corrections to quasi-normal mode frequencies, effective horizon reflectivity, or late-time ringdown structure in gravitational-wave events [263]. Purely geometric exterior deviations are expected to be strongly suppressed because the critical shell is parametrically thin,  $\rho_c/r_s \sim \ell_{\text{Pl}}/r_s \ll 1$ , for astrophysical black holes. Whether timing observables, late-time correlations, or effective horizon reflectivity inherit the same suppression depends on the specific near-horizon microphysical closure and is not yet derived in the present work. Analogue-gravity experiments remain the most plausible setting in which shell-like interface effects could become accessible.
2. *Non-exact thermality.* Hawking radiation that carries information must deviate from exact thermal statistics. This cannot be tested with astrophysical black holes at present, but analogue systems (acoustic black holes, optical analogues, cold-atom setups) can probe near-thermal emission from horizons and may exhibit shell-like features.
3. *Near-horizon shell scale.* The value  $\rho_c = \ell_{\text{Pl}}/\sqrt{3\pi}$  is obtained within the current Tolman-heating / critical-shell closure. Mass-independence would be a distinctive feature if the closure is correct, but this should be read as a closure-level result rather than a universal first-principles theorem. It is consistent with current LIGO/Virgo ringdown data but requires future gravitational-wave observations at higher signal-to-noise to test quantitatively.
4. *Mass-independence as a falsifiable signature.* The microscopic consistency criterion (Section BB.9) implies that any near-horizon deviations from GR must scale with the single universal parameter  $\rho_c$ , not with the black-hole mass. Concretely, corrections to quasinormal-mode frequencies scale as  $\delta\omega/\omega \sim \rho_c/r_h \propto M^{-1}$ . If future gravitational-wave data reveal mass-dependent deviations with a *different* scaling, condition (C2b) of the criterion would be challenged: the Tolman control-parameter

assumption would need revision. Conversely, confirmation of a universal  $\propto M^{-1}$  near-horizon scale across events spanning a decade in mass would constitute direct evidence for the ECT shell picture.

5. *Analogue-horizon tests.* Acoustic black holes, optical analogues, and cold-atom setups can probe near-horizon thermal emission at laboratory scales. If a system with an analogue of a critical near-horizon medium produces emission that deviates from exact thermality in a state-dependent way, this would provide experimental support for the structural mechanism required by the conditional theorem, independently of the specific ECT coupling coefficient  $g$ .

## BB.9 Microscopic consistency criterion for ECT black-hole unitarity

The conditional theorem (Section BB.4) proves that the paradox is resolved whenever four conditions are simultaneously satisfied. Here we turn this into a *classification of ECT microcompletions*: a microscopic completion of ECT that satisfies all four conditions below resolves the paradox; any that violates one of them either fails to resolve it or requires additional structure.

**The four genuine conditions.** The theorem’s input conditions, and what they require of the underlying ECT microcompletion, are:

- (C1) **Self-adjoint microscopic dynamics.** The condensate Hamiltonian must be self-adjoint:  $H_{\text{micro}} = H_{\text{micro}}^\dagger$ . In ECT this is a structural requirement of the Euclidean path-integral framework (postulate P2); it is the strongest motivation for expecting unitarity to hold.
- (C2) **Finite critical temperature and near-horizon ordered-phase shell.** The condensate must have a finite critical temperature  $T_c$  above which the ordered macroscopic phase ceases to exist. Moreover, the local Tolman temperature must be the correct thermodynamic control parameter for this phase transition near the horizon. These two sub-requirements imply that a finite-entropy critical shell exists at  $\rho_c = \hbar c / (2\pi k_B T_c)$ . The first sub-requirement is derived in ECT (Dolan–Jackiw potential); the second remains conditional.
- (C3) **Complete evaporation with no infinite-capacity remnant.** Evaporation must proceed to completion without leaving a remnant carrying an unbounded amount of hidden information. This is an assumption about the final state of evaporation not derived from the current formulation; the Planck-remnant case requires separate treatment.
- (C4) **No additional non-unitary dissipation.** The interaction between the shell and the radiation sector must not introduce intrinsic non-unitarity (e.g. an open-system environment outside the ECT degrees of freedom). This follows from the ECT assumption of a closed condensate system.

Note that *shell-state-dependence of the outgoing channel is not an independent condition*: it is a *consequence* of (C1)–(C4) proven by the theorem. Similarly, the breakdown of exact thermality and the late-time purification of radiation are consequences, not assumptions.

Condition violated	Implication for the information paradox
(C1) violated	ECT itself admits fundamental non-unitarity; the theory requires substantial revision before the paradox can be addressed.
(C2) violated (no $T_c$ )	The ECT horizon is effectively geometrically empty; near-horizon microphysics does not differ qualitatively from GR, and no shell mechanism exists.
(C2) violated (Tolman not the control parameter)	The shell location becomes a free parameter; the universal $\rho_c$ result is lost, and the shell-based mechanism must be re-derived for the actual control parameter.

Condition violated	Implication for the information paradox
(C3) violated (infinite remnant)	The paradox is formally evaded by hiding information indefinitely, but at the cost of pathological remnant physics (infinite pair-production rate in external fields, etc.).
(C4) violated	The ECT condensate is open to an external non-unitary environment; additional quantum gravity degrees of freedom must be specified.

### Classification of microcompletions.

**Current status within ECT.** Condition (C1) is the most natural expectation: self-adjointness of the condensate action is postulate P2. Condition (C2a) (existence of  $T_c$ ) is established by the Dolan–Jackiw analysis (Section 25.1). Condition (C2b) (Tolman as control parameter) is the central remaining structural assumption; deriving it from the black-hole branch of the full condensate action is the sharpest open problem in the ECT black-hole sector. Conditions (C3) and (C4) are natural but not derived.

Thus the present ECT framework satisfies (C1) structurally, (C2a) by calculation, and (C2b) by structural plausibility. What remains to be proved is (C2b) and to verify (C3)–(C4). No known feature of ECT violates any of these conditions.

### BB.10 Summary table

**Table 146:** Status of components of the ECT black-hole information scenario. Level A = structural result of the framework; Level B = conditional, closure-level, or effective argument within the present shell/interface construction; Open = problem not yet completed.

Statement	Status	Reference
<i>Derived from ECT structure (D)</i>		
Fundamental unitarity of condensate dynamics	Level A	P2
Critical temperature $T_c = \phi_0 \sqrt{6} \approx 5.96 \times 10^{18} \text{ GeV}$ (Dolan–Jackiw closure)	Level B	Eq. (BB.4)
Critical shell at $\rho_c = \ell_{\text{Pl}} / \sqrt{3\pi} \approx 0.33 \ell_{\text{Pl}}$	Level B	Eq. (BB.6)
<i>Conditional theorem (T)</i>		
General boundary-layer area bound (Theorem 36.1)	Level A (scaling) / B (coeff.)	§36.5
State-dependence of emission channel required by unitarity + finite shell	Level B	§BB.4
Exact Hawking thermality excluded throughout evaporation	Level B	§BB.4
<i>Structural / effective model (S)</i>		
Area-scaling shell entropy	Level B	§BB.3
General boundary-layer area bound (Theorem 36.1)	Level A (scaling) / B (coefficient)	§36.5
Entanglement-entropy bridge (physical UV regulator)	Level A	§36.5
GL outer asymptotics of $\chi$ -field	Level B	Eq. (BB.18)

(continued on next page)

Statement	Status	Reference
Minimal near-horizon closure and effective mode equation	Level B	Eq. (BB.19)
Finiteness of shell correction to Hawking channel	Level B	Eq. (BB.22)
$\pi_2(S^3) = 0$ : no topological obstruction to shell formation/dissolution	Level A	§8.10
Parametric thinness of the shell: $\rho_c/r_s \sim \ell_{\text{Pl}}/r_s \ll 1$	Level B	Eq. (36.21)
Linear-response shell–radiation kernel $\mathcal{K}_\omega(\rho)$	Level B	Eq. (BB.23)
<i>Open problems (O)</i>		
Effective shell Hamiltonian structure	Level B	Eq. (BB.24)
Unique form of shell–radiation coupling at leading order	Level B	Eq. (BB.26)
Toy finite-memory Page model (illustrative)	Level B	§BB.6
Shell–radiation coupling coefficient $g$	Open	—
Shell Hamiltonian coefficients from microdynamics	Open	—
Exact coefficient $1/4$ in $S_{\text{BH}} = A/(4\ell_{\text{Pl}}^2)$	Open	—
Quantitative ECT Page curve	Open	—
Explicit kernel $\mathcal{K}_\omega(\rho)$ from first principles	Open	—
Tolman heating as ordered-phase control parameter (C2b)	Open	—
Firewall vs. smooth-horizon consistency	Open	—

## BC Reduced thermality, generalized entropy, and the black-hole information problem

*Status: Level A for the structural negative result (fundamental information destruction excluded within the global coherent framework). Level B for the shell/interface closure and the generalized entropy bookkeeping. Open (OP-Q13): explicit shell dynamics, Page curve, and purification mechanism.*

This appendix clarifies the precise status of the black-hole discussion in Section 36. The central point is not that the full black-hole information problem has been solved dynamically. The central point is more limited and more secure: reduced-state thermality does not imply fundamental destruction of information.

### Hilbert-space factorisation

In the ECT framework the relevant Hilbert-space decomposition is organised schematically as

$$\mathcal{H}_{\text{total}} = \mathcal{H}_{\text{ext}} \otimes \mathcal{H}_{\text{shell}} \otimes \mathcal{H}_{\text{int}}, \quad (\text{BC.1})$$

the same decomposition as (36.7). The state seen by an exterior observer is obtained by tracing over inaccessible sectors:

$$\rho_{\text{ext}} = \text{Tr}_{\text{shell,int}}(|\Psi_{\text{total}}\rangle\langle\Psi_{\text{total}}|). \quad (\text{BC.2})$$

Such a reduced state may be approximately thermal even when the global state remains pure.

### Level A negative result

ECT strengthens this observation by embedding it into a theory whose coherent structure is globally unitary by construction (P2). For that reason, genuine non-unitary destruction of information is not one admissible resolution among many; it is incompatible with the postulate structure of the theory.

## Generalized entropy and the Page problem

The appropriate entropy variable for the exterior observer is the generalised entropy (36.5):

$$S_{\text{gen}} = S_{\text{BH}} + S_{\text{ext}}^{\text{coarse}},$$

rather than the Bekenstein–Hawking term alone.

ECT supports the structural plausibility of a Page-curve-type evolution, because approximate thermality and hidden correlations are not mutually exclusive in reduced-state language. However, the explicit Page curve remains open: it requires a completed strong-field shell closure and a quantitative evolution law for  $S_{\text{gen}}$  (OP-Q13).

## Summary of what is established

- (i) Apparent exterior thermality is structurally compatible with global purity (Level A; reduced-state logic).
- (ii) Fundamental information destruction is incompatible with ECT (Level A; from P2).
- (iii) The detailed purification mechanism is still an open strong-field problem (Open; OP-Q13).

ECT weakens the traditional information paradox substantially: fundamental non-unitary destruction of information is not an admissible resolution within the theory, because it is incompatible with the ECT postulate structure. What remains open is the constructive strong-field problem of showing explicitly how approximate exterior thermality and global purity are jointly realised.

## BD Analogue-observable dictionary for ordered-branch tests

This appendix provides a compact dictionary relating ECT structural elements to their nearest analogue-laboratory observables. It is intended as a reference for the analogue programme of Section 37.

**Table 147:** ECT structural elements and their analogue-laboratory observables.

ECT structural element	Analogue observable	Example platform
Compact phase $\theta$	Order-parameter phase	Superfluid He, atomic BEC
Integer winding sector	Quantised circulation / flux quantum	Superfluid vortex, Josephson junction
Defect-mediated sector change	Phase slip / vortex nucleation	BEC, superconducting nanowire
Ordered vacuum with nontrivial correlator	Response kernel / spectral correlator	Superconducting circuit, acoustic BH
Boundary-sensitive vacuum (Casimir)	Measured force between effective boundaries	Superconducting waveguide
Accelerated-detector response (Unruh)	Thermal spectrum from effective acceleration	Analogue Unruh platform
Mode mixing (particle production)	Bogoliubov excitation / analogue Hawking	BEC acoustic black hole
Decoherence kernel	Measured fringe loss / reduced coherence	Matter-wave interferometry
Ordered background (condensate fraction)	Tunable density / stiffness	Variable-density BEC, thin-film He

ECT structural element	Analogue observable	Example platform
Branch-boundary / UV threshold	Critical regime at amplitude suppression	Quench / phase-transition experiment

## BE Expanded architectural comparison of ECT and neighbouring programmes

This appendix provides an expanded version of the architectural comparison given in Section 48.4, using the same set of programmes as the main table but with additional comparison axes.

### BE.1 Closely related Euclidean-to-Lorentzian constructions

The idea that Lorentzian physics can emerge as an effective property of a fundamentally Euclidean field theory has been explored in several independent constructions.<sup>3</sup>

Girelli, Liberati and Sindoni [1] showed that a scalar field with a nonvanishing gradient on a Riemannian manifold generates an effective Lorentzian metric for perturbations. Their gravitational sector, however, reduces to Nordström (scalar) gravity rather than a tensor theory.

Mukohyama and Uzan [2] developed a more complete classical construction. They introduced a “clock field”  $\phi$  whose gradient  $\partial_\mu \phi = M^2 n_\mu$  selects a preferred direction on a 4-dimensional Riemannian manifold and allows scalar, vector, and Dirac-spinor sectors to propagate in an effective Minkowski metric within a region  $\mathcal{M}_0$  where  $\partial_\mu \phi \neq 0$ . Their gravitational sector is not general relativity but a covariant Galileon/Horndeski-type theory.

ECT shares with Mukohyama–Uzan the core architectural idea and reaches closely analogous conclusions concerning emergent Lorentzian propagation: in both frameworks, Lorentzian structure is not assumed as the fundamental geometry but appears effectively once a scalar sector selects a preferred direction on an underlying Euclidean background. The two constructions differ, however, in three substantial respects.

- **Origin of the preferred direction.** Mukohyama–Uzan impose a nonvanishing clock-field gradient as a background condition. In ECT, the preferred direction is attributed to spontaneous  $O(4) \rightarrow O(3)$  ordering of the condensate gradient.
- **Gravity sector.** Mukohyama–Uzan obtain a covariant Galileon/Horndeski-type gravitational theory. ECT instead introduces a dynamical orientation sector whose effective stiffness is used to motivate the generalised Einstein equations with orientation-stress corrections.
- **Scope of development.** Mukohyama–Uzan restrict their analysis to classical field theory. ECT carries the construction further into a quantum/coherent branch, vacuum-response questions, and astrophysical/cosmological phenomenology.

A further important contrast concerns cone universality. In the clock-field construction, different matter sectors can in principle see different effective metrics, and a matching condition between sector-dependent couplings must be imposed to obtain a universal lightcone. In ECT, universality is intended to follow instead from the single-medium origin of the broken-phase kinetic structure. Whether this remains exact beyond the minimal EFT truncation is itself part of the open consistency programme.

The comparison is informative in both directions. On the one hand, the existence of these closely related constructions strengthens the claim that emergent Lorentzian structure from Euclidean field theory is a technically meaningful possibility rather than a purely speculative gesture. On the other hand, it sharpens which parts of ECT remain genuine open problems: the full closure of the gravitational sector,

<sup>3</sup>An early discussion of dynamical Lorentzian-signature emergence appears in Ref. [264].

the complete fermion and gauge reconstruction, and the final status of cross-sector universality beyond the benchmark EFT.

**Table 148:** Closely related Euclidean-to-Lorentzian constructions.

Framework	Preferred direction	Lorentzian sector	Gravity sector	Quantum sector	Main limitation
Girelli–Liberati–Sindoni (2009)	Imposed scalar gradient	Emergent for perturbations	Nordström (scalar)	No	No tensor gravity
Mukohyama–Uzan (2013)	Imposed clock-field gradient	Emergent for scalar/vector/spinor sectors	Covariant Galileon / Horndeski	No (classical only)	Sector matching required for universal cone
ECT	Spontaneous $O(4) \rightarrow O(3)$ ordering	Emergent in broken phase	GEE motivated by orientation sector	Partial / coherent branch developed	Open closures in gravity, fermions, and full universality

## BE.2 Comparison with further neighbouring programmes

**Table 149:** Expanded architectural comparison of ECT with neighbouring programmes.

Axis	GR + SM	Einstein-aether	Hořava–Lifshitz	Volovik analogue	ECT
Starting ontology	Lorentzian manifold	Lorentzian manifold + unit vector	Foliated manifold	Condensate / superfluid	Euclidean $\mathbb{R}^4$ + scalar $\Phi$
Time status	Fundamental	Fundamental	Fundamental but anisotropic	Emergent	Emergent from $O(4) \rightarrow O(3)$
Lorentzian structure	Postulated	Postulated; preferred frame added	Postulated; foliation-dependent	Emergent acoustic metric	Emergent from SSB; $c_*$ derived
Gauge status	SM group postulated	SM group postulated	SM group postulated	Analogy only	$U(1)$ structural; $SU(2)$ bridge; $SU(3)$ open; full SM identification incomplete
Quantum axioms	Primitive	Primitive	Primitive	Primitive	Structural route via coherent branch; completion open
Gravity closure	Einstein eqs. exact	Einstein + aether sector	Modified UV dispersion	Acoustic metric only	Induced metric; FP route; nonlinear closure open
Dark matter	Extra particles	Extra particles	Extra particles	Not addressed	Ordered-branch condensate response at galaxy scale; particle completion open
Dynamic DE Singularities	$\Lambda$ (rigid) Physical or censored	$\Lambda$ (rigid) Physical or censored	$\Lambda$ or modified Possibly UV-resolved	Not addressed Not addressed	$\Lambda_{\text{eff}}(X)$ ; $w \geq -1$ Branch boundary; condensate breakdown
BH information	Paradox open	Paradox open	Modified; model-dependent	Not addressed	Reduced-state reading; fundamental loss not required; final evaporation reconstruction open
Decoherence / arrow	External quantum postulate	External quantum postulate	External quantum postulate	Not addressed	Influence-functional structural route; quantitative entropy closure depends on bath assumptions
Entanglement	Primitive axiom	Primitive axiom	Primitive axiom	Not addressed	Medium-based non-factorisable route; Bell completion open
UV regulator	None (SM); Planck scale (GR)	None built-in	Lifshitz scaling	Phonon cutoff	Condensate radial threshold $m_\sigma$
Falsifier style	Sectorwise	Extra-mode / LIV	LIV / dispersion	Not systematic	Cross-sector architectural

Axis	GR + SM	Einstein-aether	Hořava–Lifshitz	Volovik analogue	ECT
Independent primitives	~6	~7	~5	~2–3	Programme compress 1 medium + P1–P6; target: toward completion still open

**CDT / causal dynamical triangulations.** CDT [25] shares with ECT the goal of obtaining Lorentzian geometry from a more fundamental starting point, but does so through discrete simplicial complexes with a built-in causal ordering. ECT starts from a continuum Euclidean arena and derives Lorentzian structure through SSB, while CDT imposes causality at the lattice level and recovers 4D geometry in the continuum limit. Neither approach addresses the gauge or dark sectors in detail.

**Barbour timeless mechanics.** Barbour’s relational programme [265] shares ECT’s goal of eliminating external time but works in 3D configuration space rather than 4D Euclidean space. ECT and Barbour’s programme are therefore architecturally distinct: ECT starts from a 4D arena and derives 3+1 structure through SSB, whereas Barbour reconstructs dynamics from instantaneous configurations.

**Why CDT and Barbour are treated separately.** CDT and Barbour’s timeless mechanics are included here because they share with ECT an interest in emergent temporal structure, but they are not the closest neighbours of ECT along the gauge, medium, and condensate-response axes. For that reason, the main architectural table focuses on GR + SM, Einstein-aether, Hořava–Lifshitz, Volovik-type analogue emergence, and ECT, while CDT and Barbour are discussed in the expanded appendix as additional comparison points.

**Scope note.** This comparison is necessarily incomplete. Many other approaches (loop quantum gravity, string theory, asymptotic safety, causal sets, group field theory) have rich internal structures that cannot be compressed into a single table row. The purpose here is to locate ECT among its closest architectural neighbours, not to survey the full landscape.

## BF Retarded Causal Kernel: Proof That $K(\tau < 0) = 0$

### Data and Code Availability

Galaxy rotation-curve data are drawn from the public SPARC database [266] (<http://astroweb.cwru.edu/SPARC/>). All numerical scripts used to produce the figures and calculations in this paper are publicly available at:

<https://github.com/chufelo/ECT-preprint-code>

For the late-time cosmology block, the currently released code should be read as the benchmark implementation corresponding to the Level B closure and interim high- $z$  numerical completion described in Appendix AU. The expected article-level numerical inputs, outputs, and validation checks are summarised in Appendix AU.3. The expected machine-readable artefacts of such a benchmark implementation are listed in Appendix AU.4. The same benchmark implementation is also intended to support the robustness programme under admissible late-time closure deformations described in Appendix AD.7. The current repository version already supports direct benchmark–deformed comparisons within the admissible late-time closure family, so that the first numerical robustness checks can be reproduced directly from code outputs.

The repository contains: the full-SPARC rotation-curve fitting pipeline for the new ECT galactic closure (including fixed/free  $M/L$  modes, model-comparison diagnostics against MOND and  $\Lambda$ CDM/NFW, and sample-level summary tables for all 165 galaxies), cosmological calculations (Hubble tension, primordial perturbation targets, JWST halo-abundance enhancement), matching and consistency calculations for



the gravitational and coherent action scales (including the linearised  $G_N$  matching logic collected in Appendix X), fifth-force bounds, baryogenesis estimates, and the effective dimensionality calculation (Fig. 17). Scripts are self-contained Python 3 files requiring only `numpy`, `matplotlib`, and `scipy`. The computational procedures used to generate the individual figures are summarised in Appendix Y.

The repository can also be accessed by scanning the QR code (right). The code is released under the MIT License. Any updates or corrections will be posted to the same URL.



[github.com/chufelo/  
ECT-preprint-code](https://github.com/chufelo/ECT-preprint-code)

## Acknowledgments

The author thanks T. Jacobson for drawing attention to the closely related clock-field construction of Mukohyama and Uzan, which helped sharpen the comparative positioning of the present work. The author thanks the open-source scientific community for the SPARC galaxy database and the publicly available tools used in this work. The author declares no competing interests and received no external funding for this research.

## References

- [1] Florian Girelli, Stefano Liberati, and Lorenzo Sindoni. On the emergence of Lorentzian signature and scalar gravity. *Phys. Rev. D*, 79:044019, 2009.
- [2] Shinji Mukohyama and Jean-Philippe Uzan. From configuration to dynamics — emergence of Lorentz signature in classical field theory. *Phys. Rev. D*, 87:065020, 2013.
- [3] A. D. Sakharov. Vacuum quantum fluctuations in curved space and the theory of gravitation. *Soviet Physics Doklady*, 12:1040–1041, 1968.
- [4] Takeo Matsubara. A new approach to quantum-statistical mechanics. *Progress of Theoretical Physics*, 14(4):351–378, 1955.
- [5] J. B. Hartle and S. W. Hawking. Wave function of the universe. *Physical Review D*, 28:2960–2975, 1983.
- [6] A. A. Belavin, A. M. Polyakov, A. S. Schwartz, and Yu. S. Tyupkin. Pseudoparticle solutions of the yang–mills equations. *Physics Letters B*, 59(1):85–87, 1975.
- [7] Mikio Nakahara. *Geometry, Topology and Physics*. Institute of Physics Publishing, Bristol, 2nd edition, 2003.
- [8] Russell J. Donnelly. *Quantized Vortices in Helium II*. Cambridge University Press, Cambridge, 1991.
- [9] A. A. Abrikosov. On the magnetic properties of superconductors of the second group. *Soviet Physics JETP*, 5:1174–1182, 1957.
- [10] LIGO Scientific Collaboration and Virgo Collaboration. Gw170817: Observation of gravitational waves from a binary neutron star inspiral. *Physical Review Letters*, 119:161101, 2017.

- [11] D. Mattingly. Modern tests of Lorentz invariance. *Living Reviews in Relativity*, 8:5, 2005.
- [12] S. Liberati. Tests of Lorentz invariance: a 2013 update. *Classical and Quantum Gravity*, 30:133001, 2013.
- [13] V. A. Kostelecký and N. Russell. Data tables for Lorentz and CPT violation. *Reviews of Modern Physics*, 83:11–31, 2011. Updated annually at arXiv:0801.0287.
- [14] Yoichiro Nambu. Quasi-particles and gauge invariance in the theory of superconductivity. *Physical Review*, 117:648–663, 1960.
- [15] Don N. Page and William K. Wootters. Evolution without evolution: dynamics described by stationary observables. *Physical Review D*, 27:2885–2892, 1983.
- [16] Edward Anderson. *The Problem of Time: Quantum Mechanics Versus General Relativity*. Fundamental Theories of Physics, Vol. 190. Springer, 2017.
- [17] J. Leray. Hyperbolic differential equations. *Lecture Notes, Institute for Advanced Study*, 1952. Unpublished lecture notes; later published in various forms.
- [18] Y. Choquet-Bruhat. Théorème d’existence pour certains systèmes d’équations aux dérivées partielles non linéaires. *Acta Mathematica*, 88:141–225, 1952.
- [19] R. P. Feynman and F. L. Vernon, Jr. The theory of a general quantum system interacting with a linear dissipative system. *Ann. Phys.*, 24:118–173, 1963.
- [20] R. Penrose. *Cycles of Time: An Extraordinary New View of the Universe*. Bodley Head, London, 2010.
- [21] G. E. Volovik. *The Universe in a Helium Droplet*. Oxford University Press, 2003.
- [22] Julian B. Barbour. The timelessness of quantum gravity: I. the evidence from the classical theory. *Classical and Quantum Gravity*, 11(12):2853–2873, 1994.
- [23] A. O. Caldeira and A. J. Leggett. Quantum tunnelling in a dissipative system. *Annals of Physics*, 149:374–456, 1983.
- [24] T. Jacobson and D. Mattingly. Einstein–aether waves. *Physical Review D*, 70:024003, 2004.
- [25] J. Ambjørn, J. Jurkiewicz, and R. Loll. Reconstructing the universe. *Physical Review D*, 72:064014, 2005.
- [26] Petr Hořava. Quantum gravity at a lifshitz point. *Physical Review D*, 79:084008, 2009.
- [27] T. Jacobson and D. Mattingly. Gravity with a dynamical preferred frame. *Physical Review D*, 64:024028, 2001.
- [28] D. Colladay and V. A. Kostelecký. Lorentz-violating extension of the standard model. *Physical Review D*, 58:116002, 1998.
- [29] V. A. Kostelecký. Gravity, lorentz violation, and the standard model. *Physical Review D*, 69:105009, 2004.
- [30] E. A. Ivanov and V. I. Ogievetsky. The inverse higgs phenomenon in nonlinear realizations. *Teor. Mat. Fiz.*, 25:164–177, 1975.
- [31] I. N. McArthur. Nonlinear realizations of symmetries and unphysical goldstone bosons. *Journal of High Energy Physics*, 2010(11):140, 2010.

- [32] J. Goldstone, A. Salam, and S. Weinberg. Broken symmetries. *Physical Review*, 127:965–970, 1962.
- [33] S. S. McGaugh, F. Lelli, and J. M. Schombert. The radial acceleration relation in rotationally supported galaxies. *Physical Review Letters*, 117:201101, 2016.
- [34] R. L. Workman et al. Review of particle physics. *Progress of Theoretical and Experimental Physics*, 2022:083C01, 2022.
- [35] Ludvig D. Faddeev. Some comments on the many-dimensional solitons. *Lett. Math. Phys.*, 1:289–293, 1975.
- [36] A. F. Vakulenko and L. V. Kapitanski. Stability of solitons in  $S^2$  of a nonlinear  $\sigma$ -model. *Soviet Physics Doklady*, 24:433–434, 1979.
- [37] Antti J. Niemi. Hamiltonian approach to knotted solitons in SU(2) Yang-Mills theory. *Phys. Rev. D*, 56:1077–1080, 1997. See also Faddeev and Niemi, *Nature* 387 (1997) 58.
- [38] Richard A. Battye and Paul M. Sutcliffe. Knots as stable soliton solutions in a three-dimensional classical field theory. *Phys. Rev. Lett.*, 81:4798–4801, 1998.
- [39] William A. Bardeen. On naturalness in the standard model. *FERMILAB-CONF-95-391-T*, 1995. Presented at the 1995 Ontake Summer Institute, August 27–September 2, 1995.
- [40] Krzysztof A. Meissner and Hermann Nicolai. Conformal symmetry and the Standard Model. *Phys. Lett. B*, 648:312–317, 2007.
- [41] Bob Holdom. Raising the sideways scale. *Phys. Rev. D*, 24:1441–1444, 1981.
- [42] Koichi Yamawaki, Masako Bando, and Ken-iti Matumoto. Scale-invariant hypercolor model and a dilaton. *Phys. Rev. Lett.*, 56:1335–1338, 1986.
- [43] Kaustubh Agashe, Roberto Contino, and Alex Pomarol. The minimal composite Higgs model. *Nucl. Phys. B*, 719:165–187, 2005.
- [44] M. Fierz and W. Pauli. On relativistic wave equations for particles of arbitrary spin in an electromagnetic field. *Proceedings of the Royal Society of London A*, 173:211–232, 1939.
- [45] L. D. Landau and E. M. Lifshitz. *Quantum Mechanics: Non-Relativistic Theory*. Pergamon Press, Oxford, 3rd edition, 1977.
- [46] R. P. Feynman and A. R. Hibbs. *Quantum Mechanics and Path Integrals*. McGraw-Hill, New York, 1965.
- [47] Emmy Noether. Invariante variationsprobleme. *Nachrichten von der Gesellschaft der Wissenschaften zu Göttingen, Mathematisch-Physikalische Klasse*, pages 235–257, 1918.
- [48] L. D. Landau and E. M. Lifshitz. *The Classical Theory of Fields*. Pergamon Press, Oxford, 4th edition, 1987.
- [49] J. Bergé et al. MICROSCOPE mission: First constraints on the violation of the weak equivalence principle by a light scalar dilaton. *Physical Review Letters*, 129:121102, 2022.
- [50] M. S. Safronova, D. Budker, D. DeMille, Derek F. Jackson Kimball, A. Derevianko, and Charles W. Clark. Search for new physics with atoms and molecules. *Rev. Mod. Phys.*, 90:025008, 2018.
- [51] Sidney Coleman and Jeffrey Mandula. All possible symmetries of the S matrix. *Physical Review*, 159:1251–1256, 1967.

- [52] G. Aad et al. Observation of a new particle in the search for the standard model higgs boson with the ATLAS detector at the LHC. *Physics Letters B*, 716:1–29, 2012.
- [53] S. Chatrchyan et al. Observation of a new boson at a mass of 125 GeV with the CMS experiment at the LHC. *Physics Letters B*, 716:30–61, 2012.
- [54] G. 't Hooft. Naturalness, chiral symmetry, and spontaneous chiral symmetry breaking. *NATO Advanced Study Institutes Series B: Physics*, 59:135–157, 1979.
- [55] F. Englert and R. Brout. Broken symmetry and the mass of gauge vector mesons. *Physical Review Letters*, 13:321–323, 1964.
- [56] Peter W. Higgs. Broken symmetries and the masses of gauge bosons. *Physical Review Letters*, 13:508–509, 1964.
- [57] P. B. Littlewood and C. M. Varma. Amplitude collective modes in superconductors and their coupling to charge-density waves. *Physical Review B*, 26:4883–4893, 1981.
- [58] David B. Kaplan and Howard Georgi.  $SU(2) \times U(1)$  breaking by vacuum misalignment. *Physics Letters B*, 136:183–186, 1984.
- [59] Kaustubh Agashe, Roberto Contino, and Alex Pomarol. The minimal composite Higgs model. *Nuclear Physics B*, 719:165–187, 2005.
- [60] Sidney Coleman. Fate of the false vacuum: Semiclassical theory. *Physical Review D*, 15:2929–2936, 1977.
- [61] G. Degrand et al. Higgs mass and vacuum stability in the standard model at nnlo. *Journal of High Energy Physics*, 2012:98, 2012.
- [62] D. Buttazzo, G. Degrand, P. P. Giardino, G. F. Giudice, F. Sala, A. Salvio, and A. Strumia. Investigating the near-criticality of the Higgs boson. *Journal of High Energy Physics*, 2013(12):089, 2013.
- [63] Sidney Coleman and Frank De Luccia. Gravitational effects on and of vacuum decay. *Physical Review D*, 21:3305–3315, 1980.
- [64] Steven Weinberg and Edward Witten. Limits on massless particles. *Physics Letters B*, 96:59–62, 1980.
- [65] William G. Unruh. Experimental black-hole evaporation? *Physical Review Letters*, 46:1351–1353, 1981.
- [66] Stanley Deser. Self-interaction and gauge invariance. *General Relativity and Gravitation*, 1:9–18, 1970.
- [67] MicroBooNE Collaboration. Search for an excess of electron neutrino interactions in MicroBooNE using multiple final-state topologies. *Phys. Rev. Lett.*, 128:241801, 2022.
- [68] KATRIN Collaboration. Direct neutrino-mass measurement based on 259 days of KATRIN data. *Science*, 386:eadj8sergd, 2024.
- [69] Masataka Fukugita and Tsutomu Yanagida. Baryogenesis without grand unification. *Physics Letters B*, 174:45–47, 1986.
- [70] M. E. Peskin and D. V. Schroeder. *An Introduction to Quantum Field Theory*. Addison-Wesley, 1995.

- [71] S. Weinberg. *The Quantum Theory of Fields. Volume I: Foundations*. Cambridge University Press, 1995.
- [72] Konrad Osterwalder and Robert Schrader. Axioms for euclidean green’s functions. *Communications in Mathematical Physics*, 31:83–112, 1973.
- [73] K. Osterwalder and R. Schrader. Axioms for Euclidean Green’s functions II. *Commun. Math. Phys.*, 42:281–305, 1975.
- [74] R. Jost. Eine Bemerkung zum CTP-Theorem. *Helvetica Physica Acta*, 30:409–416, 1957.
- [75] R. F. Streater and A. S. Wightman. *PCT, Spin and Statistics, and All That*. Princeton University Press, revised edition, 2000.
- [76] W. Pauli, editor. *Niels Bohr and the Development of Physics: Essays dedicated to Niels Bohr on the occasion of his seventieth birthday*. Pergamon Press, London, 1955. Contains W. Pauli’s chapter on the exclusion principle and discussions of the Lüders–Pauli theorem underlying CPT invariance.
- [77] L. Boyle, K. Finn, and N. Turok. CPT-symmetric universe. *Physical Review Letters*, 121:251301, 2018.
- [78] Edward Witten. An  $SU(2)$  anomaly. *Physics Letters B*, 117:324–328, 1982.
- [79] Particle Data Group, R. L. Workman, et al. Review of particle physics. *Prog. Theor. Exp. Phys.*, 2022:083C01, 2022.
- [80] Y. Choquet-Bruhat. *General Relativity and the Einstein Equations*. Oxford University Press, Oxford, 2009. Definitive treatment of symmetric hyperbolic systems and global hyperbolicity for GR.
- [81] David Lovelock. The einstein tensor and its generalizations. *J. Math. Phys.*, 12:498–501, 1971.
- [82] S. Weinberg. *Gravitation and Cosmology*. John Wiley & Sons, 1972.
- [83] Carl Brans and Robert H. Dicke. Mach’s principle and a relativistic theory of gravitation. *Physical Review*, 124:925–935, 1961.
- [84] B. Bertotti, L. Iess, and P. Tortora. A test of general relativity using radio links with the Cassini spacecraft. *Nature*, 425:374–376, 2003.
- [85] J.-P. Uzan. Varying constants, gravitation and cosmology. *Living Reviews in Relativity*, 14:2, 2011.
- [86] C. M. Will. The confrontation between general relativity and experiment. *Living Reviews in Relativity*, 17:4, 2014.
- [87] LISA Collaboration, Pau Amaro-Seoane, et al. Laser interferometer space antenna. *arXiv preprint*, 2017.
- [88] Planck Collaboration. Planck 2018 results. VI. cosmological parameters. *Astronomy & Astrophysics*, 641:A6, 2020.
- [89] BICEP/Keck Collaboration. Improved constraints on primordial gravitational waves using delensed BICEP/Keck observations through the 2018 observing season. *Phys. Rev. Lett.*, 127:151301, 2021.
- [90] Steven Weinberg. The cosmological constant problem. *Rev. Mod. Phys.*, 61:1–23, 1989.
- [91] Sean M. Carroll. The cosmological constant. *Living Rev. Relativity*, 4:1, 2001.

- [92] Joseph Polchinski. The cosmological constant and the string landscape. 2006. Lectures at the 23rd Solvay Conference in Physics.
- [93] Marc Henneaux and Claudio Teitelboim. The cosmological constant and general covariance. *Phys. Lett. B*, 222:195–199, 1989.
- [94] Enrique Álvarez. Can one tell einstein’s unimodular theory from einstein’s general relativity? *JHEP*, 03:002, 2005.
- [95] Antonio Padilla and Ippocratis D. Saltas. A note on classical and quantum unimodular gravity. *Eur. Phys. J. C*, 75:561, 2015.
- [96] Y. Jack Ng and H. van Dam. Unimodular theory of gravity and the cosmological constant. *J. Math. Phys.*, 32:1337–1340, 1991.
- [97] Lee Smolin. The quantization of unimodular gravity and the cosmological constant problems. *Phys. Rev. D*, 80:084003, 2009.
- [98] DESI Collaboration. DESI 2024 vi: Cosmological constraints from the measurements of baryon acoustic oscillations. *arXiv preprint*, 2024.
- [99] A. D. Sakharov. Violation of CP invariance, C asymmetry, and baryon asymmetry of the universe. *JETP Letters*, 5:24–27, 1967.
- [100] Stephen L. Adler. Einstein gravity as a symmetry-breaking effect in quantum field theory. *Rev. Mod. Phys.*, 54:729–766, 1982. Erratum: *ibid.* 55 (1983) 837.
- [101] Steven Weinberg. Anthropic bound on the cosmological constant. *Phys. Rev. Lett.*, 59:2607–2610, 1987.
- [102] Andrew G. Cohen, David B. Kaplan, and Ann E. Nelson. Effective field theory, black holes, and the cosmological constant. *Phys. Rev. Lett.*, 82:4971–4974, 1999.
- [103] A. G. Cohen and D. B. Kaplan. Spontaneous baryogenesis. *Nucl. Phys. B*, 308:913–928, 1988.
- [104] A. G. Riess et al. A comprehensive measurement of the local value of the Hubble constant with 1 km/s/mpc uncertainty from the Hubble Space Telescope and the SH0ES team. *The Astrophysical Journal Letters*, 934:L7, 2022.
- [105] V. Poulin, T. L. Smith, T. Karwal, and M. Kamionkowski. Early dark energy can resolve the Hubble tension. *Physical Review Letters*, 122:221301, 2019.
- [106] M. Milgrom. A modification of the Newtonian dynamics as a possible alternative to the hidden mass hypothesis. *The Astrophysical Journal*, 270:365–370, 1983.
- [107] T. P. Sotiriou and V. Faraoni.  $f(R)$  theories of gravity. *Reviews of Modern Physics*, 82:451, 2010.
- [108] Justin Khoury and Amanda Weltman. Chameleon fields: Awaiting surprises for tests of gravity in space. *Phys. Rev. Lett.*, 93:171104, 2004.
- [109] Kurt Hinterbichler and Justin Khoury. Symmetron fields: Screening long-range forces through local symmetry restoration. *Phys. Rev. Lett.*, 104:231301, 2010.
- [110] A. I. Vainshtein. To the problem of nonvanishing gravitation mass. *Phys. Lett. B*, 39:393–394, 1972.
- [111] J. Bekenstein and M. Milgrom. Does the missing mass problem signal the breakdown of Newtonian gravity? *Astrophys. J.*, 286:7–14, 1984.

- [112] Douglas Clowe, Maruša Bradač, Anthony H. Gonzalez, Maxim Markevitch, Scott W. Randall, Christine Jones, and Dennis Zaritsky. A direct empirical proof of the existence of dark matter. *ApJ*, 648:L109–L113, 2006.
- [113] Maxim Markevitch, Anthony H. Gonzalez, Douglas Clowe, Alexey Vikhlinin, William Forman, Christine Jones, Stephen Murray, and Wayne Tucker. Direct constraints on the dark matter self-interaction cross section from the merging galaxy cluster 1E 0657-56. *ApJ*, 606:819–824, 2004.
- [114] D. Paraficz, J.-P. Kneib, J. Richard, A. Morandi, M. Limousin, E. Jullo, and J. Martinez. The bullet cluster at its best: weighing stars, gas, and dark matter. *A&A*, 594:A121, 2016.
- [115] Maruša Bradač, Steven W. Allen, Tommaso Treu, Harald Ebeling, Richard Massey, R. Glenn Morris, Anja von der Linden, and Douglas Applegate. Revealing the properties of dark matter in the merging cluster MACS J0025.4-1222. *ApJ*, 687:959–967, 2008.
- [116] Jose M. Diego et al. The free-form lensing model of El Gordo revisited with JWST. *A&A*, 672:A3, 2023.
- [117] Andisheh Mahdavi, Henk Hoekstra, Arif Babul, Dave D. Balam, and Peter L. Capak. A dark core in Abell 520. *ApJ*, 668:806–814, 2007.
- [118] M. J. Jee, H. Hoekstra, A. Mahdavi, and A. Babul. Hubble space telescope/ACS weak gravitational lensing survey of the Abell 520 interacting cluster system. *The Astrophysical Journal*, 747:96, 2012.
- [119] R. H. Sanders. Clusters of galaxies with modified Newtonian dynamics. *Monthly Notices of the Royal Astronomical Society*, 342:901–908, 2003.
- [120] G. W. Angus, H. Y. Shan, H. S. Zhao, and B. Famaey. On the proof of dark matter, the law of gravity, and the mass of neutrinos. *The Astrophysical Journal Letters*, 654:L13–L16, 2007.
- [121] F. Lelli, S. S. McGaugh, J. M. Schombert, and M. S. Pawlowski. One law to rule them all: The radial acceleration relation of galaxies. *The Astrophysical Journal*, 836:152, 2017.
- [122] P. van Dokkum et al. A galaxy lacking dark matter. *Nature*, 555:629–632, 2018.
- [123] Pieter van Dokkum, Shany Danieli, Roberto Abraham, Charlie Conroy, and Aaron J. Romanowsky. A second galaxy missing dark matter in the NGC 1052 group. *ApJL*, 874:L5, 2019.
- [124] Maria Luisa Buzzo, Duncan A. Forbes, Aaron J. Romanowsky, Lydia Haacke, Jonah S. Gannon, Yimeng Tang, Michael Hilker, Anna Ferré-Mateu, Steven R. Janssens, Jean P. Brodie, and Lucas M. Valenzuela. A new class of dark matter-free dwarf galaxies? I. Clues from FCC 224, NGC 1052-DF2 and NGC 1052-DF4. *A&A*, 695:A124, 2025.
- [125] Yimeng Tang, Aaron J. Romanowsky, Jonah S. Gannon, et al. An unexplained origin for the unusual globular cluster system in the ultradiffuse galaxy FCC 224. *ApJ*, 982:1, 2025.
- [126] Ignacio Trujillo, Michael A. Beasley, Alejandro Borlaff, et al. A distance of 13 Mpc resolves the claimed anomalies of the galaxy lacking dark matter. *MNRAS*, 486:1192, 2019.
- [127] Zili Shen, Pieter van Dokkum, and Shany Danieli. A tip of the red giant branch distance of 22.1 Mpc to the dark matter-deficient galaxy NGC 1052-DF2 from 40 HST orbits. *ApJ*, 909:179, 2021.
- [128] Duncan A. Forbes, Jonah S. Gannon, Aaron J. Romanowsky, Adebisola Alabi, Jean P. Brodie, Warrick J. Couch, and Anna Ferré-Mateu. Stellar velocity dispersion and dynamical mass of the ultra-diffuse galaxy NGC 5846-UDG1 from the Keck Cosmic Web Imager. *MNRAS*, 500:1279, 2021.

- [129] Go Ogiya. Tidal stripping as the origin of dark matter deficiency in the ultra-diffuse galaxy NGC 1052-DF2. *MNRAS*, 480:L106, 2018.
- [130] Jorge Moreno et al. Galaxies lacking dark matter produced by close encounters in cosmological simulations. *Nature Astronomy*, 6:496, 2022.
- [131] Pieter van Dokkum, Zili Shen, Aaron J. Romanowsky, et al. A trail of dark-matter-free galaxies from a bullet-dwarf collision. *Nature*, 605:435, 2022.
- [132] LZ Collaboration. First dark matter search results from the LUX-ZEPLIN (LZ) experiment. *Phys. Rev. Lett.*, 131:041002, 2023.
- [133] S. Perlmutter et al. Measurements of  $\omega$  and  $\lambda$  from 42 high-redshift supernovae. *The Astrophysical Journal*, 517:565–586, 1999.
- [134] DESI Collaboration, M. Abdul-Karim, et al. Desi dr2 results ii: Measurements of baryon acoustic oscillations and cosmological constraints. *Phys. Rev. D*, 112:083515, 2025.
- [135] K. Lodha et al. Extended dark energy analysis using desi dr2 bao measurements. *Phys. Rev. D*, 112:083511, 2025.
- [136] R. Calderon et al. Desi 2024: Reconstructing dark energy using crossing statistics with desi dr1 bao data. *JCAP*, 2024:048, 2024.
- [137] D. Shlivko and P. J. Steinhardt. Assessing observational constraints on dark energy. *Phys. Lett. B*, 855:138826, 2024.
- [138] A. Gómez-Valent et al. Physical versus phantom dark energy after desi: thawing quintessence favoured. *MNRAS Lett.*, 542:L31, 2025.
- [139] D. Wang and D. F. Mota. Did desi dr2 truly reveal dynamical dark energy? *arXiv preprint*, 2025.
- [140] E. Bianchi and C. Rovelli. Why all these prejudices against a constant? 2010. arXiv:1002.3966.
- [141] Ignas Juodzbailis et al. A dormant, overmassive black hole in the early universe. *Nature*, 636:594–598, 2024.
- [142] Roberto Maiolino et al. A small and vigorous black hole in the early universe. *Nature*, 627:59–63, 2024.
- [143] Stefano Carniani et al. Spectroscopic confirmation of two luminous galaxies at a redshift of 14. *Nature*, 633:318–322, 2024.
- [144] Anna de Graaff et al. Massive dormant galaxies at  $z \simeq 5$ : JWST/NIRSpec spectroscopy of the RUBIES sample. *Astronomy & Astrophysics*, 684:A87, 2024.
- [145] Themiya Nanayakkara et al. Early universe massive galaxy microphysics with JWST. *Astrophysical Journal Letters*, 974:L27, 2024.
- [146] Michael Boylan-Kolchin. Stress testing  $\Lambda$ CDM with high-redshift galaxy candidates. *Nature Astronomy*, 7:731–735, 2023.
- [147] Andrew J. Bunker et al. JADES: New redshift  $z > 12$  galaxies found in JADES NIRSpec spectroscopy. *Astronomy & Astrophysics*, 677:A88, 2023.
- [148] LiteBIRD Collaboration, E. Allys, et al. The LiteBIRD mission to explore cosmic inflation. *Progress of Theoretical and Experimental Physics*, 2024(12):12C101, 2024.



- [149] The Simons Observatory Collaboration, Peter Ade, et al. The Simons Observatory: Science goals and forecasts. *Journal of Cosmology and Astroparticle Physics*, 2019(02):056, 2019.
- [150] Massimiliano Rossi, Andrei Militaru, Nicola Carlon Zambon, Andreu Riera-Campenya, Oriol Romero-Isart, Martin Frimmer, and Lukas Novotny. Quantum delocalization of a levitated nanoparticle. *arXiv preprint*, 2024.
- [151] Lukas Neumeier, Mario A. Ciampini, Oriol Romero-Isart, Markus Aspelmeyer, and Nikolai Kiesel. Fast quantum interference of a nanoparticle via optical potential control. *Proceedings of the National Academy of Sciences*, 121:e2306953121, 2024.
- [152] Rainer Kaltenbaek, Markus Arndt, Markus Aspelmeyer, Peter F. Barker, Angelo Bassi, James Bateman, Alessio Belenchia, Joël Bergé, Claus Braxmaier, Sougato Bose, et al. Research campaign: Macroscopic quantum resonators (MAQRO). *Quantum Science and Technology*, 8(1):014006, 2023.
- [153] Sougato Bose, Anupam Mazumdar, Gavin W. Morley, Hendrik Ulbricht, Marko Toroš, Mauro Paternostro, Andrew A. Geraci, Peter F. Barker, M. S. Kim, and Gerard Milburn. Spin entanglement witness for quantum gravity. *Physical Review Letters*, 119:240401, 2017.
- [154] Chiara Marletto and Vlatko Vedral. Gravitationally induced entanglement between two massive particles is sufficient evidence of quantum effects in gravity. *Physical Review Letters*, 119:240402, 2017.
- [155] Sougato Bose, Ivette Fuentes, Andrew A. Geraci, Saba M. Khan, Sofia Qvarfort, Markus Rademacher, Muddassar Rashid, Marko Toroš, Hendrik Ulbricht, and Claudia C. Wanjura. Massive quantum systems as interfaces of quantum mechanics and gravity. *Reviews of Modern Physics*, 97:015003, 2025.
- [156] Chiara Marletto and Vlatko Vedral. Quantum-information methods for quantum gravity laboratory-based tests. *Reviews of Modern Physics*, 97:015006, 2025.
- [157] LHAASO Collaboration. Stringent tests of lorentz invariance violation from LHAASO observations of GRB 221009a. *Physical Review Letters*, 133:071501, 2024.
- [158] Demetrios Christodoulou. Nonlinear nature of gravitation and gravitational-wave experiments. *Physical Review Letters*, 67:1486–1489, 1991.
- [159] Vitor Cardoso and Paolo Pani. Testing the nature of dark compact objects: a status report. *Living Reviews in Relativity*, 22:4, 2019.
- [160] Erwin Madelung. Quantentheorie in hydrodynamischer form. *Zeitschrift für Physik*, 40(3–4):322–326, 1927.
- [161] J. Glimm and A. Jaffe. *Quantum Physics: A Functional Integral Point of View*. Springer, 2nd edition, 1987.
- [162] O. Aharony, N. Seiberg, and Y. Tachikawa. Reading between the lines of four-dimensional gauge theories. *Journal of High Energy Physics*, 2013:115, 2013.
- [163] L. M. Procopio, A. Moqanaki, M. Araújo, F. Costa, I. A. Calafell, E. G. Dowd, D. R. Hamel, L. A. Rozema, Č. Brukner, and P. Walther. Experimental superposition of orders of quantum gates. *Nature Communications*, 6:7913, 2015.
- [164] G. Chiribella, G. M. D’Ariano, P. Perinotti, and B. Valiron. Quantum computations without definite causal structure. *Physical Review A*, 86:040301, 2012.

- [165] Ognyan Oreshkov, Fabio Costa, and Časlav Brukner. Quantum correlations with no causal order. *Nature Communications*, 3:1092, 2012.
- [166] J. A. Wheeler. The “past” and the “delayed-choice” double-slit experiment. *Mathematical Foundations of Quantum Theory*, pages 9–48, 1978. Ed. A. R. Marlow.
- [167] J. A. Wheeler. Law without law. In J. A. Wheeler and W. H. Zurek, editors, *Quantum Theory and Measurement*, pages 182–213. Princeton University Press, 1984.
- [168] V. Jacques, E. Wu, F. Grosshans, F. Treussart, P. Grangier, A. Aspect, and J.-F. Roch. Experimental realization of Wheeler’s delayed-choice Gedanken experiment. *Science*, 315:966–968, 2007.
- [169] M. O. Scully and K. Drühl. Quantum eraser: A proposed photon correlation experiment concerning observation and “delayed choice” in quantum mechanics. *Physical Review A*, 25:2208–2213, 1982.
- [170] Y.-H. Kim, R. Yu, S. P. Kulik, Y. H. Shih, and M. O. Scully. Delayed “choice” quantum eraser. *Physical Review Letters*, 84:1, 2000.
- [171] X.-S. Ma, S. Zotter, J. Kofler, R. Ursin, T. Jennewein, Č. Brukner, and A. Zeilinger. Experimental delayed-choice entanglement swapping. *Nature Physics*, 8:479–484, 2012.
- [172] Frank Wilczek. Quantum mechanics of fractional-spin particles. *Phys. Rev. Lett.*, 49:957–959, 1982.
- [173] Chetan Nayak, Steven H. Simon, Ady Stern, Michael Freedman, and Sankar Das Sarma. Non-Abelian anyons and topological quantum computation. *Rev. Mod. Phys.*, 80:1083–1159, 2008.
- [174] S. K. Lamoreaux. Demonstration of the Casimir force in the 0.6 to 6  $\mu\text{m}$  range. *Phys. Rev. Lett.*, 78:5–8, 1997.
- [175] G. Bressi, G. Carugno, R. Onofrio, and G. Ruoso. Measurement of the Casimir force between parallel metallic surfaces. *Phys. Rev. Lett.*, 88:041804, 2002.
- [176] N. D. Birrell and P. C. W. Davies. *Quantum Fields in Curved Space*. Cambridge University Press, Cambridge, 1982.
- [177] J. S. Bell and J. M. Leinaas. Electrons as accelerated thermometers. *Nuclear Physics B*, 212:131–150, 1983.
- [178] W. G. Unruh. Notes on black-hole evaporation. *Physical Review D*, 14:870–892, 1976.
- [179] S. A. Fulling. Nonuniqueness of canonical field quantization in Riemannian space-time. *Physical Review D*, 7:2850–2862, 1973.
- [180] P. C. W. Davies. Scalar particle production in Schwarzschild and Rindler metrics. *Journal of Physics A: Mathematical and General*, 8:609–616, 1975.
- [181] C. M. Wilson, G. Johansson, A. Pourkabirian, M. Simoen, J. R. Johansson, T. Duty, F. Nori, and P. Delsing. Observation of the dynamical casimir effect in a superconducting circuit. *Nature*, 479:376–379, 2011.
- [182] L. Parker. Quantized fields and particle creation in expanding universes. I. *Physical Review*, 183:1057–1068, 1969.
- [183] M. Arndt, O. Nairz, J. Vos-Andreae, C. Keller, G. van der Zouw, and A. Zeilinger. Wave-particle duality of  $\text{c}_{60}$  molecules. *Nature*, 401:680–682, 1999.
- [184] K. Hornberger, S. Uttenthaler, B. Brezger, L. Hackermuller, M. Arndt, and A. Zeilinger. Collisional decoherence observed in matter wave interferometry. *Physical Review Letters*, 90:160401, 2003.

- [185] Yaakov Y. Fein et al. Quantum superposition of molecules beyond 25 kda. *Nature Physics*, 15:1242–1245, 2019.
- [186] M. Aspelmeyer, T. J. Kippenberg, and F. Marquardt. Cavity optomechanics. *Reviews of Modern Physics*, 86:1391–1452, 2014.
- [187] O. Romero-Isart. Quantum superposition of massive objects and collapse models. *Physical Review A*, 84:052121, 2011.
- [188] L. Diósi. A universal master equation for the gravitational violation of quantum mechanics. *Physics Letters A*, 120:377–381, 1987.
- [189] R. Penrose. On gravity’s role in quantum state reduction. *General Relativity and Gravitation*, 28:581–600, 1996.
- [190] W. Marshall, C. Simon, R. Penrose, and D. Bouwmeester. Towards quantum superpositions of a mirror. *Physical Review Letters*, 91:130401, 2003.
- [191] Gavin E. Crooks. Entropy production fluctuation theorem and the nonequilibrium work relation for free energy differences. *Physical Review E*, 60:2721–2726, 1999.
- [192] S. Haroche and J.-M. Raimond. Cavity quantum electrodynamics. *Scientific American*, 268:54–62, 1993.
- [193] M. Brune, E. Hagley, J. Dreyer, X. Maître, A. Maali, C. Wunderlich, J.-M. Raimond, and S. Haroche. Observing the progressive decoherence of the “meter” in a quantum measurement. *Physical Review Letters*, 77:4887–4890, 1996.
- [194] Christian Møller. Les théories relativistes de la gravitation. In *Colloques Internationaux CNRS*, volume 91, page 353. 1962.
- [195] Léon Rosenfeld. On quantization of fields. *Nuclear Physics*, 40:353–356, 1963.
- [196] Don N. Page and C. D. Geilker. Indirect evidence for quantum gravity. *Physical Review Letters*, 47:979–982, 1981.
- [197] Kenneth Eppley and Eric Hannah. The necessity of quantizing the gravitational field. *Foundations of Physics*, 7:51–68, 1977.
- [198] John F. Donoghue. General relativity as an effective field theory: the leading quantum corrections. *Physical Review D*, 50:3874–3888, 1994.
- [199] Cliff P. Burgess. Quantum gravity in everyday life: general relativity as an effective field theory. *Living Reviews in Relativity*, 7:5, 2004.
- [200] Jonathan Oppenheim. A postquantum theory of classical gravity? *Physical Review X*, 13:041040, 2023.
- [201] Jonathan Oppenheim, Carlo Sparaciari, Barbara Soda, and Zachary Weller-Davies. Gravitationally induced decoherence vs space-time diffusion: testing the quantum nature of gravity. *Nature Communications*, 14, 2023.
- [202] Andrzej Grudka, Tim R. Morris, Jonathan Oppenheim, Andrea Russo, and Muhammad Sajjad. Renormalisation of postquantum-classical gravity. *arXiv preprint*, 2024.
- [203] Jonathan Oppenheim and Zachary Weller-Davies. Covariant path integrals for quantum fields back-reacting on classical space-time. *arXiv preprint*, 2023.

- [204] Sandro Donadi, Kristian Piscicchia, Raffaele Del Grande, Catalina Curceanu, Matthias Laubenstein, and Angelo Bassi. Underground test of gravity-related wave function collapse. *European Physical Journal C*, 81:773, 2021.
- [205] Giovanni Di Bartolomeo and Matteo Carlesso. Experimental bounds on linear-friction dissipative collapse models from levitated optomechanics. *New Journal of Physics*, 26(4):043006, 2024.
- [206] Matteo Carlesso, Sandro Donadi, Luca Ferialdi, Mauro Paternostro, Hendrik Ulbricht, and Angelo Bassi. Present status and future challenges of non-interferometric tests of collapse models. *Nature Physics*, 18(3):243–250, 2022.
- [207] L. Dolan and R. Jackiw. Symmetry behavior at finite temperature. *Physical Review D*, 9:3320–3341, 1974.
- [208] A. M. Gleason. Measures on the closed subspaces of a Hilbert space. *Journal of Mathematics and Mechanics*, 6:885–893, 1957.
- [209] D. Deutsch. Quantum theory of probability and decisions. *Proceedings of the Royal Society A*, 455:3129–3137, 1999.
- [210] D. Wallace. *The Emergent Multiverse*. Oxford University Press, 2012.
- [211] W. H. Zurek. Probabilities from entanglement, Born’s rule  $p_k = |\psi_k|^2$  from envariance. *Phys. Rev. A*, 71:052105, 2005.
- [212] H. Barnum, C. M. Caves, J. Finkelstein, C. A. Fuchs, and R. Schack. Quantum probability from decision theory? *Proceedings of the Royal Society A*, 456:1175–1182, 2000.
- [213] B. Hensen, H. Bernien, A. E. Dréau, A. Reiserer, N. Kalb, M. S. Blok, J. Ruitenbergh, R. F. L. Vermeulen, R. N. Schouten, C. Abellán, et al. Loophole-free Bell inequality violation using electron spins separated by 1.3 kilometres. *Nature*, 526:682–686, 2015.
- [214] Daniel Carney, Philip C. E. Stamp, and Jacob M. Taylor. Tabletop experiments for quantum gravity: a user’s manual. *Classical and Quantum Gravity*, 36(3):034001, 2019.
- [215] Marios Christodoulou, Andrea Di Biagio, Markus Aspelmeyer, Ľukáš Brukner, Carlo Rovelli, and Richard Howl. Locally mediated entanglement in linearized quantum gravity. *Physical Review Letters*, 130:100202, 2023.
- [216] Joseph Aziz and Richard Howl. Classical theories of gravity produce entanglement. *Nature*, 646:813–817, 2025. Under active dispute; see Marletto et al. 2025 (arXiv:2511.07348), Diósi 2025 (arXiv:2511.00852), and arXiv:2511.20717.
- [217] Chiara Marletto, Jonathan Oppenheim, Vlatko Vedral, and Elizabeth Wilson. Classical gravity cannot mediate entanglement. *arXiv preprint*, 2025. Critical response to Aziz & Howl, *Nature* 646, 813 (2025).
- [218] Lajos Diósi. No, classical gravity does not entangle quantized matter fields. *arXiv preprint*, 2025. Short response to Aziz & Howl, *Nature* 646, 813 (2025).
- [219] Anonymous. Comment on classical-gravity–quantum-matter claims about gravity-mediated entanglement. *arXiv preprint*, 2025. Channel-theoretic reformulation of Marletto et al. critique.
- [220] Zachary Weller-Davies. Is there a ‘smoking gun’ test for quantum gravity? *Nature (News & Views)*, 646:809–811, 2025.

- [221] David Trillo and Miguel Navascués. Diósi–Penrose model of classical gravity predicts gravitationally induced entanglement. *Physical Review D*, 111, 2025. Demonstrates classical-gravity correlated-noise mechanism for GIE.
- [222] Nicetu Tibau Vidal et al. Bose–Marletto–Vedral experiment without observable spacetime superpositions. *arXiv preprint*, 2025.
- [223] Hans Hepach et al. An experimental platform for levitated mechanics in space. *arXiv preprint*, 2025. Quantum Physics Platform (QPPF) payload, ESA launch June 2025.
- [224] Hermann Bondi, M. G. J. van der Burg, and A. W. K. Metzner. Gravitational waves in general relativity. VII. Waves from axi-symmetric isolated systems. *Proceedings of the Royal Society A*, 269:21–52, 1962.
- [225] Rainer K. Sachs. Asymptotic symmetries in gravitational theory. *Physical Review*, 128:2851–2864, 1962.
- [226] Steven Weinberg. Infrared photons and gravitons. *Physical Review*, 140:B516–B524, 1965.
- [227] Temple He, Vyacheslav Lysov, Prahar Mitra, and Andrew Strominger. BMS supertranslations and Weinberg’s soft graviton theorem. *Journal of High Energy Physics*, 2015(5):151, 2015.
- [228] Andrew Strominger. *Lectures on the Infrared Structure of Gravity and Gauge Theory*. Princeton University Press, 2018.
- [229] Stephen W. Hawking, Malcolm J. Perry, and Andrew Strominger. Soft hair on black holes. *Physical Review Letters*, 116:231301, 2016.
- [230] Shinsei Ryu and Tadashi Takayanagi. Holographic derivation of entanglement entropy from the anti-de Sitter space/conformal field theory correspondence. *Physical Review Letters*, 96:181602, 2006.
- [231] Thomas Faulkner, Aitor Lewkowycz, and Juan Maldacena. Quantum corrections to holographic entanglement entropy. *Journal of High Energy Physics*, 2013(11):074, 2013.
- [232] Netta Engelhardt and Aron C. Wall. Quantum extremal surfaces: holographic entanglement entropy beyond the classical regime. *Journal of High Energy Physics*, 2015(1):073, 2015.
- [233] Geoffrey Penington. Entanglement wedge reconstruction and the information paradox. *Journal of High Energy Physics*, 2020(9):002, 2020. Companion to Almheiri-Engelhardt-Marolf-Maxfield 2020; quantum extremal surfaces / islands formula.
- [234] Ahmed Almheiri, Netta Engelhardt, Donald Marolf, and Henry Maxfield. The entropy of bulk quantum fields and the entanglement wedge of an evaporating black hole. *Journal of High Energy Physics*, 2019(12):063, 2019.
- [235] J. D. Bekenstein. Black holes and entropy. *Physical Review D*, 7:2333–2346, 1973.
- [236] J. D. Bekenstein. Universal upper bound on the entropy-to-energy ratio for bounded systems. *Physical Review D*, 23:287–298, 1981.
- [237] G. ’t Hooft. Dimensional reduction in quantum gravity. *arXiv:gr-qc/9310026*, 1993.
- [238] L. Susskind. The world as a hologram. *Journal of Mathematical Physics*, 36:6377–6396, 1995.
- [239] R. Bousso. The holographic principle. *Reviews of Modern Physics*, 74:825–874, 2002.
- [240] L. Bombelli, R. K. Koul, J. Lee, and R. D. Sorkin. Quantum source of entropy for black holes. *Physical Review D*, 34:373–383, 1986.

- [241] M. Srednicki. Entropy and area. *Physical Review Letters*, 71:666–669, 1993.
- [242] Jeff Steinhauer. Observation of quantum hawking radiation and its entanglement in an analogue black hole. *Nature Physics*, 12:959–965, 2016.
- [243] T. Banks and N. Seiberg. Symmetries and strings in field theory and gravity. *Phys. Rev. D*, 83:084019, 2011.
- [244] D. Harlow and H. Ooguri. Symmetries in quantum field theory and quantum gravity. *Commun. Math. Phys.*, 383:1669–1804, 2021.
- [245] A. Takenaka et al. Search for proton decay via  $p \rightarrow e^+ \pi^0$  and  $p \rightarrow \mu^+ \pi^0$  with 0.37 megaton-years exposure of the Super-Kamiokande water Cherenkov detector. *Phys. Rev. D*, 102:112011, 2020.
- [246] K. Abe et al. Hyper-Kamiokande design report. 2018.
- [247] J. G. Cramer. The transactional interpretation of quantum mechanics. *Reviews of Modern Physics*, 58:647–687, 1986.
- [248] D. N. Page and W. K. Wootters. Evolution without evolution: Dynamics described by stationary observables. *Physical Review D*, 27:2885–2892, 1983.
- [249] S. Weinberg. *The Quantum Theory of Fields*, volume 2. Cambridge University Press, 1996.
- [250] Lev D. Landau and Evgeny M. Lifshitz. *Theory of Elasticity*. Butterworth-Heinemann, Oxford, 3rd edition, 1986.
- [251] Fermi LAT Collaboration, A. A. Abdo, et al. A limit on the variation of the speed of light arising from quantum gravity effects. *Nature*, 462:331–334, 2009.
- [252] David Valcin, José Luis Bernal, Raul Jimenez, Licia Verde, and Benjamin D. Wandelt. Inferring the age of the universe with globular clusters. *Journal of Cosmology and Astroparticle Physics*, 2020(12):002, 2020. Updated GC-age analysis cited in text as Valcin+ 2021.
- [253] Michele Moresco, Lorenzo Amati, Luca Amendola, et al. Unveiling the Universe with emerging cosmological probes. *Living Reviews in Relativity*, 25(1):6, 2022.
- [254] Alex Krolewski, Simone Ferraro, and Martin White. The integrated Sachs–Wolfe effect: unWISE and Planck constraints on dynamical dark energy. *Journal of Cosmology and Astroparticle Physics*, 2022(04):033, 2022.
- [255] F. Lelli, S. S. McGaugh, and J. M. Schombert. SPARC: Mass models for 175 disk galaxies with Spitzer photometry and accurate rotation curves. *The Astronomical Journal*, 152:157, 2016.
- [256] John P. Huchra, Lucas M. Macri, Karen L. Masters, et al. The 2mass redshift survey—description and data release. *Astrophys. J. Suppl.*, 199:26, 2012.
- [257] Xiaohu Yang, H. J. Mo, Frank C. van den Bosch, Anna Pasquali, Cheng Li, and Marco Barden. Galaxy groups in the sdss dr4. i. the catalogue and basic properties. *Astrophys. J.*, 671:153–170, 2007.
- [258] Joe Wolf, Gregory D. Martinez, James S. Bullock, Manoj Kaplinghat, Marla Geha, Ricardo R. Muñoz, Joshua D. Simon, and Frank F. Avedo. Accurate masses for dispersion-supported galaxies. *MNRAS*, 406:1220–1237, 2010.
- [259] W. H. Zurek. Decoherence, einselection, and the quantum origins of the classical. *Reviews of Modern Physics*, 75:715–775, 2003.

- [260] R. H. Price and K. S. Thorne. Membrane viewpoint on black holes: Properties and evolution of the stretched horizon. *Physical Review D*, 33:915–941, 1986.
- [261] D. N. Page. Information in black hole radiation. *Physical Review Letters*, 71:3743–3746, 1993.
- [262] S. D. Mathur. The information paradox: a pedagogical introduction. *Classical and Quantum Gravity*, 26:224001, 2009.
- [263] A. Almheiri, D. Marolf, J. Polchinski, and J. Sully. Black holes: complementarity or firewalls? *Journal of High Energy Physics*, 2013(2):062, 2013.
- [264] J. Greensite. Dynamical origin of the Lorentzian signature of space-time. *Phys. Lett. B*, 300:34, 1993.
- [265] Julian Barbour. *The End of Time: The Next Revolution in Physics*. Oxford University Press, 1999.
- [266] F. Lelli, S. S. McGaugh, and J. M. Schombert. SPARC: Mass models for 175 disk galaxies with Spitzer photometry and accurate rotation curves. *The Astronomical Journal*, 152:157, 2016.